QC
851
.G73
v.11

Air Ministry
Meteorological Research Committee
MRP 1002-1054 (non-inclusive)

MRP No.	Title	Author
1002 AD 141021	An Atmosphere Model for Numerical Integration Including the Tropopause Effects.	E. Knighting
1003 AD 141022	A Non-geostrophic Extension of the Sawyer-Bushby Model of the Atmosphere Suitable for Numerical Integration.	E. Knighting
1005 AD 141023	Heat Sources and Sinks at the Earth's Surface.	D.M. Houghton
1006 AD 223120	Measurements of Short Range Diffusion of Airborne Particles at a Height of a Few Hundred Feet in the Atmosphere (Porton Technical Paper No. 561).	J.S. Hay F. Pasquill
1009 AD 141025	A Survey of the Facilities and Research Programme of the Radar Research Station.	W.G. Harper
1010 AD 141024	Wind Recording Apparatus for the New Ballistic Range at Shoeburyness.	G.E.W. Hartley
1012 AD 141029	Atmospheric Nuclei. An Estimate of the Value and Practicability of Routine Measurements.	B.C.V. Oddie
1014 AD 147509	A Note on the Published Results of Studies in Atmospheric Chemistry.	B.C.V. Oddie
1015 AD 223121	The Air Flow Over a Ridge - the Effects of the Upper Boundary and High-level Conditions.	G.A. Corby J.S. Sawyer
1016 AD 223128	Numerical Forecasts Based on Objectively Analysed Data.	V.M. Huckle
1017 AD 139538	Analysis of Reports of Ice Accretion on Aircraft.	R.F. Jones
1018	Numerical Experiments in the Integration of the Meteorological Equations of Motion.	E. Knighting D.E. Jones M.K. Hinds
1019	Preliminary Report on Cumulus Investigations, East Hill, June-August, 1956 and on Plans for Future Similar Work.	W.G. Harper F.H. Ludlam P. Saunders
1020 AD 139539	Average Height of the Standard Isobaric Surfaces Over the Area From the North Pole to 55 deg. N in April and October.	H. Heastie

MRP No.	Title	Author
1021 AD 139540	Radio Refraction in the Free Atmosphere.	A.H. Hooper A.P. Taylor
1022 AD 216263	The Movement of Precipitation Belts as Observed by Radar.	W.G. Harper J.G.D. Beimers
1023	The Serial Correlations of Daily Mean Temperatures at Kew Observatory.	J.M. Craddock
1024	Observations of Humidity, Temperature and Wind at Idris 23rd May - 2nd June, 1956.	N.C. Helliwell J.K. Mackenzie
1025 AD 223131	A Numerical Study of the Wavelength and Amplitude of Lee Waves.	C.E. Wallington J. Portnall
1032 AD 141027	Response Characteristics of the Sensitive Cup Anemometer Type IV.	A.G.A. Rae
1033 AD 141026	Photo-electric Visibility Meter Mk. II.	J.R. Bibby
1038	Studies of Eddy Structure in the First Few Thousand Feet of the Atmosphere. Part 1. Measurements of the Vertical and Horizontal (Longitudinal) Components. (Porton Technical Paper No. 574).	J.I.P. Jones H.E. Butler
1039	A Study of the Average Distribution of Pollution Around Staythorpe.	P.J. Meade F. Pasquill
1040 AD 139541	The Representation of Circumpolar 500 mb Charts by a Series of Spherical Harmonics.	A. Gilchrist
1041 AD 223132	Numerical Calculations of the Airflow Over a Ridge for Small Amplitudes.	J.S. Sawyer M.K. Hinds
1043	Report on Flight Tests of a Prototype Conical Head Aircraft Thermometer.	C.H. Hinkel
1044	Studies of Eddy Structure in the First Few Thousand Feet of the Atmosphere. Part 2. A Preliminary Examination of the Spectrum and Scale of the Vertical Component at 2000 Feet. (Porton Technical Paper No. 588).	R.A. Jones
1045	Average Height of the Standard Isobaric Surfaces Over the Temperate and Tropical Regions in January.	H. Heastie
1046 AD 216262	An Approximate Relation Between Slant Visibility and Horizontal Visibility at Ground Level.	K.H. Stewart
1047 AD 208932	A Method for Assessing the Frequency of Dangerous Visibility Conditions.	K.H. Stewart

MRP No.	Title	Author
1048 AD 216261	Convection - Diffusion Processes Below a Stable Layer. (Porton Technical Paper No. 584).	F.B. Smith
1049 AD 223144	Problems of Surface Air-flow and Related Phenomena in Agriculture, Horticulture and Forestry.	R.W. Gloyne
1050	Recent Developments in the Measurement of Precipitation Elements From Aircraft.	M.P. Garrod
1051	A Contribution to the Study of Meteorological Time Series.	J.M. Craddock
1052 AD 223145	An Analysis of Humidity Measurements in the Upper Troposphere and Lower Stratosphere Over Southern England.	G.B. Tucker
1054	Index of M.R.P.'s Approved for General Distribution.	

Mats

M.R.P. 1002

S.C.11/216

17th September, 1956.

AD141021

An atmospheric model for numerical integration including the tropopause effects

by

E. Knighting.

(Meteorological Office)

AIR MINISTRY

METEOROLOGICAL RESEARCH COMMITTEE

57-74

In order to specify the form of the functions α and β we assume that there is a linear change of isobaric divergence with pressure in both the troposphere and the stratosphere, vanishing at the upper level p_1. The thermal wind shear is taken to be linear in the troposphere, and in the stratosphere if predictions are to be extended to levels above the tropopause. The equations written here will apply to the troposphere but the extension to the stratosphere is clear. It will be observed that once again we are making the crudest assumptions which fit the general observations, following the practice of taking the simplest models possible in a first examination of the problem.

3. The variation of vertical velocity and wind with pressure

Equation (1) is sufficient for our purpose, but with the assumption of a linear distribution of isobaric divergence with pressure we have

$$\omega = \omega_T\left(\frac{p-p_1}{p_T-p_1}\right)^2, \qquad p_1 \leq p \leq p_T$$

$$= \omega_T\left[2\left(\frac{1}{p_T-p_0} - \frac{1}{p_T-p_1}\right)(p-p_0) + \left(\frac{2(p_T-p_0)}{p_T-p_1} - 1\right)\left(\frac{p-p_0}{p_T-p_0}\right)^2\right] \qquad p_T \leq p \leq p_0$$

..... (2)

If we take p_0 = 1000 mb, p_1 = 0 mb, then from equation (2)

$\omega_T = (9/25)\,\omega_m \qquad p_T$ = 200 mb

$= \frac{3}{4}\,\omega_m \qquad p_T$ = 500 mb

where ω_m is the maximum value of ω, showing that in dealing with ω_T we are not dealing with a quantity which is an order of magnitude less than the maximum or mean vertical velocity.

The variation of wind with pressure is expressed in terms of the thermal wind between two fixed levels p_0, P below the tropopause

$$V = V_0 + \frac{p-p_0}{P-p_0}V' \qquad p_T \leq p \leq p_0 \qquad ..... (3)$$

$$\left.\begin{aligned} V' &= k \wedge \frac{g}{f}\nabla h' \\ V_0 &= k \wedge \frac{g}{f}\nabla h_0 \end{aligned}\right\} \qquad ..... (4)$$

with similar vorticity equations.

/4.

At the time of issue this report has not been published. Any author desiring to quote this paper should refer to it as "A paper of the Meteorological Research Committee (London). M.R.P. No.1002 by Mr. E. Knighting A copy is available in the Library of the Meteorological Office."

M.R.P. 1002
S.C.II/216
17th September, 1956

AIR MINISTRY

METEOROLOGICAL RESEARCH COMMITTEE

An atmospheric model for numerical integration including the tropopause effects

by

E. Knighting (Meteorological Office)

1. Introduction

The atmospheric models which have been used for the numerical integration of the equations of motion have divided the atmosphere into slices bounded by isobaric surfaces and these models may be regarded as either ignoring the tropopause or having a fixed tropopause. It is very convenient mathematically to use such divisions since the equations used for forecasting are expressed in terms of pressure rather than of height; they are obtained either by direct expression in finite differences, as in the Charney-Phillips (1953) hierarchy of models, or by averaging in the vertical between two fixed pressure levels, as in the Sawyer-Bushby (1953) and similar models. Physically, however, it is clear that the atmosphere is divided into two parts with different physical characteristics, and especially with different stabilities, above and below the tropopause which varies in pressure from about 100 mb to 500 mb. The effect of the stable upper layer will be to reduce the intensity of the disturbances which are found in the lower layers and it is reasonable to think that the height of the boundary will aid in determining the reduction.

The following analysis is concerned with a simple model including a variable pressure surface which is identified with the tropopause. It is assumed that the vertical velocity has a parabolic profile with pressure in both the troposphere and stratosphere; this profile is determined by two parameters, the pressure and vertical velocity at the tropopause. The divergence is thus a linear function of pressure in both stratosphere and troposphere and its pressure derivative has a discontinuity at the tropopause, consistent with the jet stream and a change in static stability. This simple assumption about the vertical velocity shows some of the major requirements of a physical definition of a tropopause. The thermal wind is taken as a linear function of pressure and constant in direction, so that the results of time integrations should then be comparable with the results obtained by using the Sawyer-Bushby model.

2. The model

The model is represented pictorially in Fig.1 which explains the notation. H_0, H_1 and H represent heights above the mean sea level; p_0 and p_1 are two pressure levels at which dp/dt vanishes, while P is a fixed pressure surface; h' is the thickness between p_0 and P. The tropopause pressure is p_T and at that pressure $dp/dt = \omega_T$; it is assumed that $\omega \equiv dp/dt$ at any given level p is given by

$$\begin{aligned} \omega &= \omega_T\,\alpha(p, p_T)\,, & p_1 \leq p \leq p_T \\ &= \omega_T\,\beta(p, p_T)\,, & p_T \leq p \leq p_0 \end{aligned} \qquad \ldots\ldots(1)$$

/In

G.9364/PN/9/56/50

$$\frac{\partial \zeta'}{\partial t} + V_0.\nabla\zeta' + V'.\nabla(\zeta_0 + \zeta' + f) =$$

$$\omega_T(2\zeta_0 + \zeta' + 2f)\left(\frac{p - p_0}{p_T - p_0}\right)^2\left(\frac{2(p_T - p_0)}{p_T - p_1} - 1\right) \qquad \text{.....} \ (9)$$

where ω and derivatives have been expressed in terms of ω_T. If we now assume that the winds are sufficiently geostrophic

$$\zeta' = \frac{g}{f}\nabla^2 h'$$

so that combining equations (7) and (9)

$$\frac{KR}{g}\nabla^2(G\omega_T) - \frac{f\omega_T}{g}(2\zeta_0 + \zeta' + 2f)\left(\frac{p - p_0}{p_T - p_0}\right)^2\left(2\frac{p_T - p_0}{p_T - p_1} - 1\right) =$$

$$\nabla^2(V\nabla h') - \frac{f}{g}V'.\nabla(\zeta_0 + \zeta' + f) - \frac{f}{g}V_0.\nabla\zeta' \qquad \text{.....} \ (10)$$

Having eliminated the time variable, equation (10) is diagnostic in ω_T and can be solved either by integration or by finite difference methods.

6. Forecast of thickness and height of an isobaric surface

The thickness tendency equation to the level P is

$$\frac{\partial h'}{\partial t} + V.\nabla h' = \frac{R}{g}KG\omega_T \qquad \text{.....} \ (11)$$

and this equation is used as a prognostic equation in h' since ω_T has already been obtained from equation (10). It remains to obtain a forecasting equation for H_0 or for H. Owing to the proximity to the surface it is possible that the vorticity equation

$$\frac{\partial}{\partial t}\frac{g}{f}\nabla^2 H_0 + V_0.\nabla\left(\frac{g}{f}\nabla^2 H_0 + f\right)$$

$$= 2\left(\frac{g}{f}\nabla^2 H_0 + f\right)\left(\frac{1}{p_T - p_0} - \frac{1}{p_T - p_1}\right)\omega_T \qquad \text{.....} \ (12)$$

/is

4. The adiabatic equation

We assume that the motion is adiabatic, although non-adiabatic effects can be allowed for. The equation for the thickness h' between the levels p_o and P is

$$\frac{\partial h'}{\partial t} + V.\nabla h' = -\frac{R}{g}\int_{p_o}^{P} \omega \left(\frac{\gamma}{g\rho} - \frac{\partial T}{\partial p}\right)\frac{dp}{p} \qquad \text{..... (5)}$$

where γ is the suitable adiabatic lapse rate and ρ the density. We require an assumption about the integrand and take $\frac{\gamma}{g\rho} - \frac{\partial T}{\partial p} = -K$ where K is a constant evaluated from the mean values obtained by observation. Then,

$$\frac{\partial h'}{\partial t} + V.\nabla h' = \frac{R}{g} K \omega_T \, G(p_o, P, p_T, p_1) \qquad \text{..... (6)}$$

where

$$G = \int_{p_o}^{P} \frac{dp}{p}\left[2\left(\frac{1}{p_T - p_o} - \frac{1}{p_T - p_1}\right)(p - p_o) + \left\{2\frac{(p_T - p_o)}{p_T - p_1} - 1\right\}\left(\frac{p - p_o}{p_T - p_o}\right)^2\right]$$

and is easily evaluated. Taking the Laplacian of (6)

$$\frac{\partial}{\partial t}\nabla^2 h' + \nabla^2(V.\nabla h') = \frac{KR}{g}\nabla^2(G\omega_T) \qquad \text{..... (7)}$$

and allowance could be made in this equation for space variations of K.

5. The diagnostic equation for ω_T

Neglecting the twisting terms the vorticity equation is

$$\frac{\partial \zeta}{\partial t} + V\,\nabla(\zeta + f) + \omega\frac{\partial \zeta}{\partial p} = (\zeta + f)\frac{\partial \omega}{\partial p} \qquad \text{..... (8)}$$

and subtracting that at the level p_o from that at the level P

is unsuitable although it should be tried. Otherwise we solve the corresponding vorticity equation at the level P for H and subtract the thickness to obtain H_0 .

7. Forecast of tropopause pressure

We note that

$$\omega_T = \frac{dp_T}{dt} = \frac{\partial p_T}{\partial t} + V_T . \nabla p_T$$

so that

$$\frac{\partial p}{\partial t} = \omega_T - \left(V_0 + \frac{p_T - p_0}{P - p_0} V' \right) . \nabla p_T \qquad \text{..... (13)}$$

which is the prognostic equation for p_T .

References

(1) Charney, J.C. and Phillips, N. 1953 J.Met., 10, p. 71.

(2) Sawyer, J.S. and Bushby, F.H. 1953 J.Met., 10, p. 54.

Pictorial representation of the model

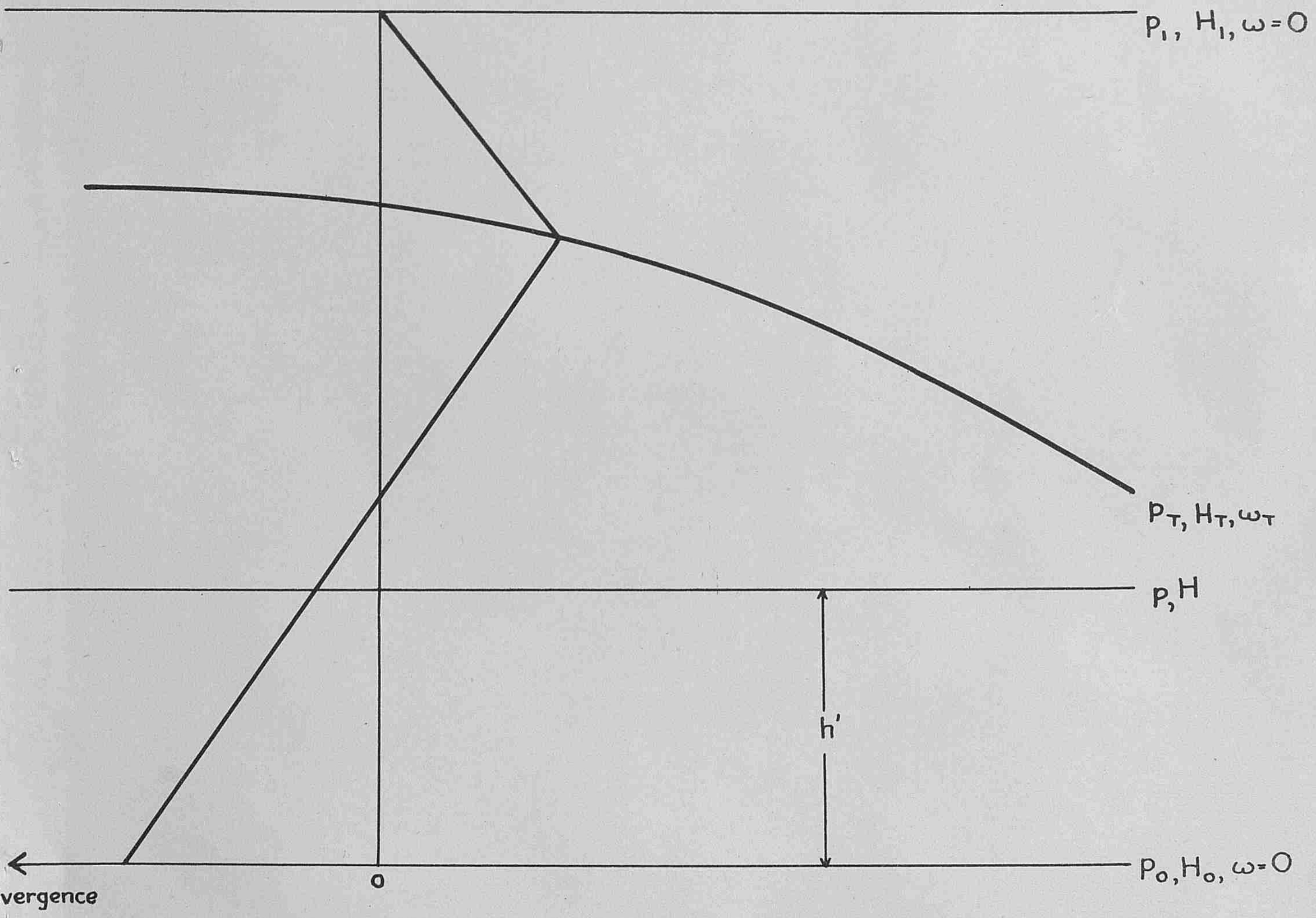
$p_1, H_1, \omega = 0$
p_T, H_T, ω_T
p, H
h'
$p_0, H_0, \omega = 0$
0
ivergence

Fig. 1

Mats

yb

M.R.P. 1003
S.C.11/217
17th September, 1956.

AD141022

A non-geostrophic extension of the Sawyer-Bushby model of the atmosphere suitable for numerical integration

by

E. Knighting.

(Meteorological Office)

AIR MINISTRY

METEOROLOGICAL RESEARCH COMMITTEE

57-81

with suffix m referring to values at $\alpha = 0$, and with V' the thermal wind between $\alpha = -1$ and $\alpha = 0$ (or $\alpha = 0$, $\alpha = +1$) the following equations are direct consequences of the assumptions

$$V = V_m + \alpha V' \tag{2}$$

$$\zeta = \zeta_m + \alpha \zeta' \tag{3}$$

$$\operatorname{div} V = \operatorname{div} V_m + \alpha \operatorname{div} V' \tag{4}$$

$$\frac{dp}{dt} = \omega = \omega_m (1 - \alpha^2) \tag{5}$$

where V is the wind corresponding to the vertical co-ordinate α and ζ, ζ_m and ζ' are the vorticities corresponding to the velocities V, V_m and V'.

3. Prognostic equations for ζ_m, ζ' and h'

Integrating the vorticity equation between $\alpha = \pm 1$, neglecting the twisting term, gives

$$\frac{\partial \zeta_m}{\partial t} + V_m . \nabla (\zeta_m + f) + \frac{1}{3} V' . \nabla \zeta' = \frac{8 \omega_m \zeta'}{3(p_0 - p_1)} \tag{6}$$

The difference between the vorticity equation at $\alpha = \pm 1$ gives

$$\frac{\partial \zeta'}{\partial t} + V_m . \nabla \zeta' + V' . \nabla (\zeta_m + f) = \frac{1}{2} \Big[(\zeta_m + f) \Big\{ \Big(\frac{\partial \omega}{\partial p} \Big)_1 - \Big(\frac{\partial \omega}{\partial p} \Big)_0 \Big\} + \zeta' \Big\{ \Big(\frac{\partial \omega}{\partial p} \Big)_1 + \Big(\frac{\partial \omega}{\partial p} \Big)_0 \Big\} \Big] \tag{7}$$

and using equation (5) gives

$$\frac{\partial \zeta'}{\partial t} + V_m . \nabla \zeta' + V' . \nabla (\zeta_m + f) = \frac{4 \omega_m}{p_0 - p_1} (\zeta_m + f) \tag{8}$$

If ϕ is the height of a pressure surface, ϕ' the thickness between the surfaces $\alpha = -1, 0$, the adiabatic equation gives

$$\int_{-1}^{0} \Big(\frac{\partial}{\partial t} + V . \nabla \Big) \frac{\partial \phi}{\partial \alpha} \, d\alpha + \frac{2}{p_0 - p_1} \int_{-1}^{0} \omega \frac{\partial \phi}{\partial p} \frac{\partial \log \theta}{\partial p} \, d\alpha = 0 \tag{9}$$

In the second integral we use equation (5) to replace ω and take values of $\partial \phi / \partial p$ and $\partial \log \theta / \partial p$ which are given by some standard atmosphere. The

At the time of issue this report has not
been published. Any author desiring to
quote this paper should refer to it as "A
paper of the Meteorological Research
Committee (London).
M.R.P. No.1003 by Mr. E. Knighting
A copy is available in the Library of
the Meteorological Office."

M.R.P. 1003
S.C.II/217
17th September, 1956

AIR MINISTRY
METEOROLOGICAL RESEARCH COMMITTEE

A non-geostrophic extension of the Sawyer-Bushby model of the atmosphere suitable for numerical integration

by

E. Knighting (Meteorological Office)

1. Introduction

The atmospheric models that have been used for the numerical prediction of the pressure field have used the quasi-geostrophic assumption, that the velocity and vorticity can be obtained from the geopotential field. The success obtained in forecasting at 500 mb with all such models has been rather similar and is characterised by correlation coefficients somewhat similar to those obtained by using the orthodox forecasting methods. Means have been sought to relax the quasi-geostrophic assumption and have led several people (see Bushby (1956)) to examine the effect of using a stream function to define the velocity and relating it to the geopotential by the ordinary equations of motion. In effect one has to obtain the stream function from the geopotential using the balance equation, carry forward the time integrations as usual and finally recover the geopotential from the forecast stream function. The motion is, of course, non-divergent and it is the purpose of this note to examine the effect of introducing a divergent component of the velocity in accordance with Helmholtz's theorem for a plane vector. An extensive treatment of this problem has recently been given by Thompson (1956).

In keeping with the general practice at the Meteorological Office, Dunstable, of examining the simplest models first, the equations have been written down for the simplest two-level model in which the divergence near the surface is not taken to be zero, while that at 500 mb is taken as zero. The method of solution is rather different from that normally used, in that the vertical velocity is first determined as the key to the development.

A simplification, which is made in section 4, reduces the difficulty of solving the equations at the expense of making a physical assumption which is not easy to understand and which involves rather high derivatives. The implication of the physical assumption is clear and shows that we have retained the quasi-geostrophic assumption in calculating the local rates of change of thermal vorticity. Among the other alternative simplifications, we could take as zero the Jacobian on the left hand side of equation (14), taking the stream function as the geopotential at 1000 mb. These simplifications should be explored in turn when numerical experiments are made using this model.

2. The assumptions

The model is bounded by two constant pressure surfaces p_0 and p_1, which will be taken for practical calculations as 1000 and 200 mb. The vertical velocity dp/dt has a parabolic distribution with height and vanishes at p_0 and p_1. The thermal wind is unidirectional and is linear with pressure. Writing suffixes zero and one to refer to the levels p_0 and p_1, and using the vertical co-ordinate

$$\alpha = \frac{p_0 + p_1 - 2p}{p_0 - p_1} \qquad (1)$$

$p = 1000; \alpha = -1$
$p = 600; \alpha = 0$
$p = 200; \alpha = +1$

G.9365/PMW/9/56/50

$$\frac{\partial}{\partial t}\nabla^2\psi' + J(\psi_m, \nabla^2\psi') + J_1(\psi', \chi', \nabla^2\psi_m + f) = \frac{4\omega_m \nabla^2(\psi_m) + f}{p_0 - p_1} \tag{16}$$

$$\frac{\partial\phi'}{\partial t} + J(\psi_m, \phi') - \frac{1}{2} J_1(\psi', \chi', \phi') = K\omega_m \tag{17}$$

where $$J_1(\psi, \chi, \lambda) = \frac{\partial\psi}{\partial x}\frac{\partial\lambda}{\partial y} - \frac{\partial\psi}{\partial y}\frac{\partial\lambda}{\partial x} + \frac{\partial\chi}{\partial x}\frac{\partial\lambda}{\partial x} + \frac{\partial\chi}{\partial y}\frac{\partial\lambda}{\partial y} \tag{18}$$

Equations (12b) to (17) are six equations with unknowns ψ_m, ψ_0, ω_m, ϕ_m, ϕ_0, χ_0 and form a closed set.

5. Some simplifications

The equations have already been simplified by the omission in equation (14) of the terms in $\partial\nabla^2\chi_0/\partial t$ and $\nabla^2\chi_0$ which could have been retained without affecting the number of equations and variables. Even with this simplification the equations are difficult to solve. The suggestion is that

$$\frac{\partial}{\partial t} J\left(\frac{\partial\phi_m}{\partial x}, \frac{\partial\psi_m}{\partial y}\right) \simeq \frac{\partial}{\partial t} J\left(\frac{\partial\phi_0}{\partial x}, \frac{\partial\phi_0}{\partial y}\right) \tag{19}$$

which is true in areas where the geostrophic approximation is fairly good and implies a linkage in the curvature of the ϕ_m and ϕ_0 surfaces. From (13) and (14) we have

$$\nabla^2 \frac{\partial\phi'}{\partial t} = f\,\nabla^2 \frac{\partial\psi'}{\partial t}$$

which implies that the local rate of change of thermal vorticity can be calculated from the thickness pattern, as is done in geostrophic motion. Then taking ∇^2 of equation (17) and subtracting (16) we have

$$K\nabla^2\omega_m + \omega_m\nabla^2 K + 2\nabla\omega_m\cdot\nabla K - \frac{4\nabla^2\psi_m + f}{p_0 - p_1} = F \tag{20}$$

where F is a known function of x, y. We solve equation (20) as a boundary value problem, and hence (12b), (15), (16) and (17), a series of Poisson equations except for the very simple (17).

References

(1) Bushby, F. H. and Huckle, V. M. 1956 Meteorological Research Papers, Air Ministry, London, No. 956.

(2) Thompson, P. D. 1956 J. Met., 13, p. 251.

G.9365/PMW/9/56/50

first integral is

$$\int_{-1}^{0}\left(\frac{\partial}{\partial t}+V_m.\nabla\right)\frac{\partial\phi}{\partial\alpha}d\alpha+\int_{-1}^{0}V'.\nabla\left(\alpha\frac{\partial\phi}{\partial\alpha}\right)d\alpha$$

and we must approximate to the second integral. For example we may take $\phi = \phi_m+\phi'\alpha$, which yields

$$\frac{\partial\phi'}{\partial t}+V_m.\nabla\phi'-\frac{1}{2}V'.\nabla\phi'=K\omega_m \tag{10}$$

where K is determined by the standard atmosphere.

4. Introduction of stream and potential function

We now have three equations (6), (8) and (10) with the unknowns $\zeta_m, V_m, \zeta', V', \phi', \omega_m$. Making the geostrophic assumption relates both ζ_m and V_m with ϕ_m, ζ' and V' with ϕ', leaving three equations and three unknowns. More generally we must write

$$V = K\wedge\nabla\psi+\nabla\chi \tag{11}$$

and substituting these expressions in equations (6), (8) and (10) leads to variables $\psi_m, \chi_m, \psi', \chi', \phi', \omega_m$. The original data will give ϕ' and ϕ_m. In this simple model we have

$$\nabla^2\chi_m = -\left(\frac{\partial\omega}{\partial p}\right)_m = 0 \tag{12a}$$

$$\nabla^2\chi' = \left(\frac{\partial\omega}{\partial p}\right)_0 = -\frac{4\omega_m}{p_0-p_1} \tag{12b}$$

so that χ_m may be taken as zero at all times. Using a suffix zero to represent values at $\alpha = -1$, i.e. at p_0 then $V_0 = V_m-V'$ and $\psi_0=\psi_m-\psi'$ and the balance equation suffices to give ψ_m and ψ_0 originally,

$$2J\left(\frac{\partial\psi_m}{\partial x},\frac{\partial\psi_m}{\partial y}\right)+f\nabla^2\psi_m = \nabla^2\phi_m \tag{13}$$

$$2J\left(\frac{\partial\psi_0}{\partial x},\frac{\partial\psi_0}{\partial y}\right)+f\nabla^2\psi_0 = \nabla^2\phi_0 \tag{14}$$

where J denotes the usual Jacobian.

The predictive equations are now

$$\frac{\partial}{\partial t}\nabla^2\psi_m+J(\psi_m,\nabla^2\psi_m+f)+\frac{1}{3}J_1(\psi',\chi',\nabla^2\psi') = \frac{8\omega_m\nabla^2\psi'}{3(p_0-p_1)} \tag{15}$$

M.R.P. 1005
S.C.11/218
26th September, 1956.

AD141023

Heat Sources and Sinks at the Earth's Surface

by

D.M. Houghton

(Meteorological Office)

AIR MINISTRY

METEOROLOGICAL RESEARCH COMMITTEE

may be affected by variation in the supply of either sensible or latent heat to the atmosphere. There is however the important difference that the modification to the temperature field resulting from variations in supply of latent heat will take place when condensation occurs and this may be at a distance of several hundred kilometres from the source of evaporation.

2. THE OCEANS

Of all the heat stored and released by the earth's surface during the course of the annual temperature cycle 86 per cent. is due to the oceans (Schumann and Burdecki (1953)). Most of this is released in winter months and at a rate which depends upon the temperature difference between the sea and the air above. As far as the sea itself is concerned the determining factors in its heat output are its surface temperature and whether or not it is frozen.

2(a) Sea surface temperature

When the sea surface is warmer than the air above it, heat is transferred upwards by convection and long wave radiation. Convective processes are also set up in the sea itself so that the sea surface temperature changes little.

When the sea surface is colder than the air above it, stable conditions are established in both media and heat is transferred downwards by long wave radiation and turbulent diffusion. Cloudy conditions are likely and there will be net downward radiation from the cloud base, but even for a cloud-sea temperature difference of 5°C (which is rare) this is only about 25 cal cm^{-2} day^{-1}.

A relationship between the flux of heat and water vapour to the atmosphere and the air-sea temperature difference has been suggested by Jacobs (1942) but is applicable only to mean values over a period of about a season. Special cases covering shorter periods have also been analysed from time to time and provide some indication of the variation in intensity of convective heat transfer over the oceans.

(i) The long term heat budget

Jacobs gives the empirical relation

$$Q_e = 0.143\ (e_w - e_a)W_a$$

where Q_e = heat equivalent of evaporated water (cal)

W_a = wind speed ($m.sec^{-1}$)

e_W = saturation vapour pressure at sea surface temperature (mb)

e_a = vapour pressure of the air at deck level (mb).

The associated transfer of sensible heat (Q_c) is then found using Bowen's ratio. No difference is made between rough and smooth conditions.

Jacobs' charts showing the mean seasonal values of Q_c and Q_e over the N. Pacific and N. Atlantic Oceans give winter values for Q_c of 20 to 80 cal cm^{-2} day^{-1} to the west of Ireland rising to over 200 cal cm^{-2} day^{-1} off the east coast of North America. The annual means for Q_c are 20 and 100 cal cm-2 day^{-1} respectively. Corresponding values for Q_e are about $2\frac{1}{2}$ times Q_c and the annual means for $(Q_c + Q_e)$ rise from about 70 cal cm^{-2} day^{-1} off western Ireland to 350 cal cm^{-2} day^{-1} off eastern America.

/The

At the time of issue this report has not been published. Any author desiring to quote this paper should refer to it as "A paper of the Meteorological Research Committee (London). M.R.P. No. 1005 by Mr. D.M. Houghton A copy is available in the Library of the Meteorological Office."

M.R.P.1005
S.C.II/218
26th September, 1956

AIR MINISTRY

METEOROLOGICAL RESEARCH COMMITTEE

Heat Sources and Sinks at the Earth's Surface

by

D.M. Houghton (Meteorological Office)

Summary

A study has been made of the spatial and temporal variations in the surface character of the earth which can result in increases or decreases in the heat supply to the atmosphere. For the sea areas the changes in surface temperature and in the ice limits are considered and for the land the changes in albedo, evaporation and evapotranspiration, state of surface, heat-storage capacity and conductivity are dealt with. Some of these factors are found to be unimportant, while others can exert an appreciable and sometimes long-term influence upon the heat supply to the atmosphere.

---

1. INTRODUCTION

The solar radiation received at the outside of the atmosphere is 800 to 900 cal cm^{-2} day^{-1} throughout the year at the equator and at the poles it is 1070 cal cm^{-2} day^{-1} in midsummer, falling to nil in winter. If we take a long period average covering the northern hemisphere then approximately 47 per cent. of this radiation reaches the earth's surface and about 19 per cent. is directly absorbed by the atmosphere and clouds (Houghton, 1954). Some of the radiation received at the earth's surface is reflected back to space, some is absorbed and stored and some is passed to the atmosphere by convection and radiation. All of these processes are affected by the physical character of the surface, with the result that the amount of heat reaching the atmosphere either immediately or by the subsequent transfer of stored heat from the surface may be significantly affected. Here we are concerned with those effects which may be sufficient to affect the circulation of the atmosphere over a substantial area for a period of days. Such effects must occur over a substantial area and persist for a few days at least. We therefore limit the study to changes which can affect an area of a minimum of 10^4 Km^2 for 5 days at least.

The magnitudes of the variations in heat supply to the atmosphere may be compared with the outgoing long wave radiation to space (500 cal cm^{-2} day^{-1} in low latitudes, 380 cal cm^{-2} day^{-1} in high latitudes), or with the change in the heat reflected to space (and consequently lost to the atmosphere) due to a change in cloudiness from nil to 8/8 (100 to 200 cal cm^{-2} day^{-1} in low latitudes). However, it is probably safer to compare the variations with one another and see which are the most important.

The energy of the atmospheric circulation is derived primarily from horizontal differences of temperature. These horizontal temperature gradients

/may

anomaly of ± 1°C in air-sea temperature difference will give ± 30 cal cm^{-2} day^{-1} in sensible heat, and ± 60 cal cm^{-2} day^{-1} in latent heat available to the atmosphere. A relationship based on Craddock's analysis suggests values up to ± 80 cal cm^{-2} day^{-1} for the increase in the supply of sensible heat corresponding to ± 1°C in strongly convective situations, while the latent heat supply will change by ± 160 cal cm^{-2} day^{-1}.

Now a change in the temperature of the sea surface is always accompanied by a change in the temperature of the air immediately above it. It is reasonable to suppose that in the case of off-shore advection of comparable air masses over sea areas close to continents an anomaly of 1°C in sea surface temperature will correspond to an anomaly of 1°C in air-sea temperature difference. The above figures can then be applied as they stand and they may be assumed to indicate the maximum effect on the heat input to the atmosphere of a 1°C sea temperature anomaly. In all other cases the air-sea temperature difference anomaly will be some fraction of the sea temperature anomaly. An independent estimate of the size of this fraction may be obtained by considering the change in heat storage capacity of the sea itself. Anomalies in sea surface temperature are sometimes observed to last for several months. If, as is reasonable, a positive anomaly of 1°C extends to 50 metres depth and disappears after 5 months then the atmosphere has received an additional 50 cal cm^{-2} day^{-1} (corrected for approximately 5 cal cm^{-2} day^{-1} lost as additional long wave radiation). This suggests that the mean effect of a 1°C anomaly is appreciable over quite a long period and somewhere near half the maximum effect indicated by the empirical equations.

2(b) Ice

(i) Freezing

When the sea freezes the transfer of heat from the sea to the air is very much reduced. This is demonstrated most markedly in observations of the modification of polar continental air over Hudson Bay before and after freezing (Burbidge, 1951). The daily input of heat to the air crossing the Bay before the surface freezes is at least 344 cal cm^{-2} (see para. 2(a)). After the Bay freezes in December hardly any modification can be observed.

(ii) Conduction

If the temperature of the water underlying the ice is 0°C and the air temperature well below this value, the rate of heat transport through the ice may be estimated for various thicknesses of ice. For ice 1 metre thick and a temperature difference across the ice of 10°C, assuming a thermal conductivity of 0.005 cal $(sec\ cm\ ^{\circ}C)^{-1}$, it is about 20 cal cm^{-2} day^{-1}. In areas where the sea freezes the atmosphere loses heat by long wave radiation at the rate of about 380 cal cm^{-2} day^{-1}. Hence any heat received by conduction through the ice is negligible in comparison with the loss of heat by radiation.

(iii) Albedo

Changes in the albedo of the sea through freezing need not be considered, as the incident solar radiation in the areas concerned is either nil or too small to matter.

2(c) Ocean Currents

The subject of ocean currents is beyond the scope of this paper, but it must be noted that it is these currents which largely determine the latitudinal and longitudinal distribution of sea temperatures. A sea temperature anomaly is normally due to either an anomaly in absorbed radiation or an anomaly in the direction or rate of flow of ocean currents. Also, as a result of ocean currents the areas of anomalous radiation and resulting anomalous sea temperature may become far removed from one another. The time lapse is important. For instance a large sea temperature anomaly in the Caribbean Sea and off the coast of Florida

/may

The observed annual amplitudes of sea surface temperature at the weather ship stations 'I' and 'J' support these figures. The mean amplitude through the top 100 metres is about 4.5°C, so that the heat given up by the sea over the 6 winter months is about 45,000 cal cm^{-2}, an average of about 250 cal cm^{-2} day^{-1}. Of this about half is accounted for by long wave radiation. Sverdrup (1940) quotes similar figures for the Bay of Biscay. Over these areas of the eastern Atlantic the annual mean of the air-sea temperature difference is between -1°C and -2°C.

(ii) Shallow convection

Riehl (1951) has studied the atmospheric heat balance over a period of a few days in the trade wind regions of the North Pacific Ocean. His data satisfy the empirical equation $Q_c = 0.036 \ (T_W - T_a) \ W_a$, with values of Q_c ranging from 10 to 30 cal cm^{-2} day^{-1} for an air-sea temperature difference of 0.5 to 1.0°C.

Data for the Baltic are contained in a paper by Hela (1951) who studied the heat exchange at Finngrundet (a lightship). He gives the mean input of sensible heat to the atmosphere during winter months as about 50 cal cm^{-2} day-1. It is probable that shallow convection obtained on the majority of occasions, so that this figure is applicable here. He suggests the equation $Q_c = 0.032 \ (W_a + 0.3)^{\frac{1}{2}} \ (T_W - T_a) \, \Theta_w$ to fit his data, where Θ_w is the sea surface temperature in degrees absolute.

For cases of shallow convection over the North Sea but with a much larger temperature difference (about 10°C) the author has found the sensible heat input to be about 40 to 80 cal cm^{-2} day-1. The data used were for very cold easterlies circulating around a Scandinavian anticyclone.

(iii) Strong convection

Craddock's (1951) paper on the modification of polar airstreams contains useful data. He shows that the sensible heat input to the atmosphere can reach values as high as 1400 cal cm^{-2} day^{-1}, while 300-500 cal cm^{-2} day^{-1} is probably quite normal in direct airstreams from the north. These figures are not strictly comparable with those already given, as an unknown proportion of the observed heating is due to release of latent heat in the shower precipitation during the passage of the air over the sea. The equations $Q_c = 0.064 \ (T_W - T_a)$ and $Q_e = 0.017 \ L \ (T_W - T_a)$ fit his graphs relating the sensible heat and water vapour transfer to the air-sea temperature difference.

A similar type of air mass is studied by Burbidge (1951). Using his data for the modification of continental polar air crossing the Hudson Bay in the late autumn the input of sensible heat is at least 344 cal cm^{-2} day-1.

No account has been taken by Craddock or Burbidge of the long wave radiational cooling of the atmosphere for which the relevant figure is of the order of 150 cal cm^{-2} day-1.

Winston (1954) relates intense cyclogenesis in the Gulf of Alaska with areas of rapid heating from the sea surface. He finds the non-adiabatic component of heating in the five cases of cold air masses studied to lie between 400 and 2210 cal cm^{-2} day^{-1}. Unfortunately values of sea and air temperature are not given.

(iv) Estimation of the effect of an anomaly of 1°C in sea temperature on the heat transport to the atmosphere

Several relationships have been suggested which give some indication of the dependence of the supply of sensible and latent heat to the atmosphere upon the sea surface temperature. For the mean effect over a period of months the partly empirical equations derived by Jacobs and Hela indicate that an

/anomaly

Little of the heat which is received by a land surface from the sun is stored in the ground for more than 24 hours. Some of it is returned to space by reflection, and radiation, some passes to the atmosphere by long wave radiation or convection and some is used in evaporation in the melting of snow etc. Any increase in the amount of heat reflected or in the amount used in evaporation will reduce the amount of sensible heat made available to the atmosphere and it is therefore convenient to think of the increase of heat dissipation by any such process as a potential local loss to the atmosphere.

3(a) Heat conduction and storage

(i) Unfrozen ground

Heat flow to and from the surface depends upon the thermal conductivity of the materials in the surface layers, on the seepage of water downwards associated with rainfall and on the temperature gradients which are established primarily as a result of incoming and outgoing radiation. All these are very variable but the purpose of this study will be achieved if extreme values can be estimated.

Using known values of thermometric conductivity (K) density (ρ) and thermal capacity (c), the following values of heat flux are calculated assuming a temperature gradient of 10°C per metre.

Table 1

	ρc	$K \times 10^{-2}$	Flux cal cm^{-2} day^{-1}
Wet sand	0.53	0.60	28
Moist sand	0.34	0.56	16
Dry sand	0.30	0.16	4
Sandy soil	0.35	0.62	19
Dry loam	0.4	0.2	7
Marsh	1.00	0.12	10
Light soil with roots	0.1	0.3	3
Uncultivated soil	0.52	0.34	15
Clay	1.4	0.2	24
Rock	0.5	1.2	52
Snow	0.12	0.2	2
Ice	0.45	0.78	30

Temperature gradients of the order of 10°C per metre are only found in conditions of strong insolation, or radiation under clear sky at night, but for short periods they may be considerably greater in the top few centimetres. On a hot summer's day at Dresden, Schreiber (1912) found the maximum mid-day heat flux into the sandy soil to be about 70 cal cm^{-2} day^{-1}. Roach (1955) using a flux plate at 6 cm depth at Kew measured a maximum flux of 5 mw (100 cal cm^{-2} day^{-1}) which lasted for about 3 hours on a hot June day. With the

/same

may be expected to be transferred northeastwards in the Gulf Stream and to reach the northeastern Atlantic in the course of a year. The maximum flow which is found off Chesapeake Bay is about 3 knots, while over most of its course the Gulf Stream transports water at about 1/3 to ½ knot (Sverdrup, 1940).

2(d) Other aspects

Other aspects of energy transformation over and in the oceans may be mentioned but are unimportant. Flow of heat through the ocean bottom is about 0·18 cal cm^{-2} day^{-1} (Helland-Hansen, 1930). Frictional energy of the wind on the sea surface is estimated at 10^{-4} times the radiation received at the surface (Sverdrup, 1940). Tidal dissipation of energy over shallow coastal waters is about 2·9 cal cm^{-2} day^{-1} (Taylor, 1919).

2(e) Heat exchange between atmosphere and ocean - summary

The exchange of heat (sensible and latent) between the sea and the atmosphere is negligible when the sea is frozen, and small ($\sim$20 cal cm^{-2} day^{-1}) when it is colder than the air. It is significant ($\sim$ 50 cal cm^{-2} day^{-1}) when mechanical turbulence and shallow convection pass heat to the air and it is very large (up to 1200 cal cm^{-2} day^{-1}) in strongly convective situations. Downward long wave radiation may supplement the small turbulent heat flux when the sea is colder than the air but is normally much smaller than 25 cal cm^{-2} day^{-1}.

The maximum change in heat supply to the atmosphere over the open ocean resulting from an anomaly of ± 1°C in sea surface temperature is estimated at ± 15 cal cm^{-2} day^{-1} for sensible heat and ± 45 cal cm^{-2} day^{-1} when latent heat is included. This applies to conditions averaged over a period of months. The latter figure is confirmed by an estimate based upon maximum observed sea temperature changes. In strongly convective situations these values may be increased to ± 40 and ± 120 cal cm^{-2} day^{-1} respectively.

Observed sea temperature anomalies of the order 1 to 3°C and the corresponding increase or decrease in energy made available to the atmosphere must have some effect on subsequent synoptic developments.

The freezing of the sea surface, although it has been shown to be important, only occurs on a comparatively small scale. The freezing of large areas of partially enclosed seas which is an annual occurrence in high latitudes is most important in connection with the modification of local air masses. It is possible that the late freezing of areas such as Hudson Bay might also hinder the establishment of the semipermanent continental cold troughs in the troposphere, and the abnormal freezing of any such area should also have an observable effect on the subsequent thickness pattern in the troposphere. However there are few areas in which the dates of freezing of substantial areas of the sea have significant variations. For instance the Baltic Sea is subject to a certain amount of freezing every winter, but it seems improbable that a variation of 20 to 50 miles in the freezing limit can exert any appreciable large scale control on the atmospheric circulation.

3. THE CONTINENTS

The non-uniformity of the land surface and its comparative inability to store and conduct heat necessitate a different approach to the question of whether any changes in its character can appreciably change the heat supply to the atmosphere.

/Little

Bare ground wet	8 - 10
Sand	20 - 25
Rock	12 - 15
Snow new	70 - 80
Snow old	55
Water	5 - 50 (depending on solar elevation)
Desert	24 - 30

In order to estimate the maximum effect of a change in albedo on the heat supply to the atmosphere it is reasonable to assume that all the radiation absorbed at the ground is redistributed to the atmosphere during 24 hours.

The largest albedo change is from a normal grass or earth surface (15 to 20 per cent.) to a snow covered surface (70 to 80 per cent.). Much winter snowfall occurs when the incoming solar radiation is so small that a change in albedo is insignificant in its effect on the heat supply to the atmosphere. However some areas as far south as 50°N, notably the southern shores of Hudson Bay (Thomson (1954)) and parts of central Siberia receive their first snowfall towards the end of September, when the mean sun and sky radiation is 180 cal cm^{-2} day^{-1} (Black (1956)). In this case the 60 per cent. increase in albedo consequent on snowfall will reduce the heat supplied to the atmosphere by 108 cal cm^{-2} day^{-1}. These same areas are the last to lose their snow cover in such southern latitudes and substantial areas of snow covered ground may persist until late April when the mean incident sun and sky radiation is as much as 300 cal cm^{-2} day^{-1}; 180 cal cm^{-2} day^{-1} is then denied to the atmosphere. Between these extremes the importance of snow cover decreases with increasing latitude and increasing proximity to the winter solstice. Snow cover in Scandinavia for instance will only be important before the end of October or after the end of February.

Of other possible changes in albedo the most important is from 15 per cent. with green grass to 25 per cent. with parched earth. This may occur in areas where the incident radiation is 500 cal cm^{-2} day^{-1}, when the 10 per cent. change in surface reflectivity will increase or decrease the heat available to the atmosphere by 50 cal cm^{-2} day^{-1}.

3(c) Snow

The change in albedo due to snowfall has already been discussed. There remains the effect of the absorption of latent heat on melting. A maximum rate of melting is about 5 cm of snow per day (about 0·5 gm) and the corresponding absorption of latent heat is 40 cal cm^{-2}. As in the case of thawing earth this is a loss to the atmosphere.

3(d) Evaporation and evapotranspiration

The thermal effects on a land surface as a result of evaporation and evapotranspiration are substantially different from the corresponding effects on a sea surface. By means of convection in the sea surface the temperature remains almost constant throughout the evaporation process. Over land the latent heat of evaporation must be supplied either by the sun, by the atmosphere or by conduction through the surface. As we have seen, the heat made available by conduction from that stored in the soil is negligible and the heat required for evaporation can be regarded either as a direct loss to the atmosphere

/or

same instrument he measured a maximum upward flux of 1 mw during a very cold easterly outbreak in January, 1954. This flux persisted for at least 24 hours. Confirmatory evidence is obtained by examining earth temperature records for Berlin and Dublin which show that the maximum 24-hour temperature changes recorded with warm air flowing over cold land or vice versa are about 3°C in the top half metre which correspond to a maximum heat flux of 30 cal cm^{-2} day^{-1}. For a long period average the total change in the heat content of the soil at Berlin between October and March gives a value of about 1700 cal cm^{-2}. This may be compared with the corresponding figure for the eastern North Atlantic which is about 45,000 cal cm^{-2} (see para. 2(a)). Thus we see that the modification of air masses by sensible heat stored in the ground is not an important process in the general circulation.

(ii) Frozen ground

Normally the ground is moist before winter freezing takes place and the soil is maintained for a period at 0°C while heat is abstracted from or communicated to it during freezing or thawing. Higher temperature gradients than are normally observed may thus be established above a frozen layer of soil and may persist for considerable periods.

Let us consider a square centimetre of earth 10 cm in depth which contains 4 gm of liquid water. The heat liberated during the freezing process is about 320 calories and the normal time taken to freeze to this depth is 4 to 10 days, giving a maximum heat flux over 4 days of 80 cal cm^{-2} day^{-1}. Thawing may proceed rather more rapidly as solar heating of the soil surface gives higher temperature gradients. At Berlin 10 cm are observed to thaw in as little as 2 days and 25 cm in 7 days. The heat absorbed is a maximum of about 150 cal cm^{-2} day^{-1}, some of which is directly removed from the atmosphere and the rest would otherwise have been transmitted to the atmosphere by convection from the heated ground. Thawing by the advection of a warm cloudy airstream proceeds at about half this rate and the maximum heat lost from the atmosphere by radiation and diffusion is about 80 cal cm^{-2} day^{-1}.

These fairly high values of heat flux are important because of the length of time for which they may persist. They suggest that frozen ground could prevent normal atmospheric heating to a significant extent, so that variations in the semi-permanent limits of frozen ground could be important.

3(b) Radiative properties

(i) Albedo

Reasonably accurate measurements of albedo are available for most types of vegetation and bare earth surfaces, though the dryness of the vegetation or earth can give quite wide variations. The following values are to be found in the literature (Budyko (1954), Fritz (1948), Houghton (1954), Smithsonian Meteorological Tables, Sutton (1953), Sverdrup (1940)).

Table 2

Percentage of incident radiation which is reflected

Forest	3 - 10
Snow covered forest	10 - 25
Grass fields dry	20 - 30
Grass fields wet	8 - 20
Bushes	10
Bare ground dry	10 - 25

/Bare

atmosphere in the area of evaporation and a corresponding abnormal heat source in some other region. The net world wide effect over a period will always be nil.

3(c) Summary

The probable maximum effects of variations in land surface conditions on the heat supply to the atmosphere are as follows:-

Table 4

Method	Source	Magnitude cal cm^{-2} day^{-1}
Conduction	Calculated - wet sand; temp-grad 10°C per metre	± 28
	Observed - Berlin; glacial ~~and~~ sand and gravel	± 30
Freezing	Latent heat liberated: calculated: water content 0.4 gm per c.c.	± 80
Thawing ground (sunny conditions)	Latent heat absorbed: same water content	- 150
Thawing ground (cloudy conditions)	"	- 80
Thawing snow	Latent heat absorbed in melting 5 cm per day	- 40
Albedo	Change due to snow: middle latitudes late autumn and early spring	- 180
	Change due to drought on green vegetation	- 50
Evaporation	Possible change due to drought or vegetation on desert	± 200

4. CONCLUSION

Before reviewing the ability of the earth's surface to modify through various means the working of the atmospheric heat engine, mention must be made of the solar constant. For many years it has been suggested that variations in the solar constant can give rise to large scale climatic changes and that small variations due to sunspot cycles are responsible for shorter fluctuations in world weather. Krivsky (1954) purports to find a definite relationship between sunspot cycles and the position of the jet stream. The most useful summary of the present state of this subject is by Wexler (1953). Although he is probably more disposed than many to advocate a relationship between sunspot cycles and the subsequent weather he states that there is as yet no proof of one and, what is more, that no proof can be readily produced. Correlations between random factors have been found which are equal to those found between weather phenomena and sunspot cycles.

The foregoing survey has covered the principal ways in which variations in the state of the earth's surface can change the energy available to the atmosphere. The following appear to be the most important:-

/(i)

or deducted from the solar energy which would otherwise have been communicated to the air by convection.

Numerous measurements indicate that the normal daily evaporation varies from 0·6 cm per day from a moist surface in the tropics to 0·05 cm per day from a dry surface in high latitudes. Table 3 gives a selection of values from the literature for evaporation and evapotranspiration.

Table 3

Surface and vegetation	Evaporation cm per day	Source
Grass-Toronto-November	0·05	Mather (1954)
Very dry soil - California	0.06	Veihmeyer (1954)
Bare soil - Toronto - November	0.07	Mather (1954)
Dry soil with vegetation - Florida	0.2	"
Bahia grass - Belgian Congo	0.3	"
Bare soil - Toronto - July	0.4	"
Moist soil with vegetation - Florida	0.5	"
Grass - Toronto - July	0.5	"
Moist sand - California	0.63	"
Grass - British Isles (Annual Mean)	0.14	Penman (1949)
	cm/year	
Savanna - tropics	92.5	Mather (1954)
Sugar cane	124.5	"
Very wet rain forest	152.9	"
Sawgrass	171.5	"

If all the latent heat of evaporation is considered to be a loss for the atmosphere then the deficit can be as much as 260 cal cm^{-2} day^{-1}. This deficit will vary according to the vegetation or crops growing and the moisture available. After a prolonged drought the heat available to the atmosphere may be as much as 200 cal cm^{-2} day^{-1} more than after a prolonged wet spell. This is partly offset by the increase in the albedo; but even so the net result should be evident in a much greater heating of the atmosphere over deserts in sub-tropical regions than over areas covered in green vegetation. The temporary formation of a new desert or vegetation over a normally desert area should be significant.

It has been assumed in the foregoing paragraphs that the heat used in evaporation is not returned to the atmosphere by recondensation in the same region. If showers occur this will not be true nor if the evaporation is balanced by deposition of dew. However in many circumstances the air will be transported hundreds of kilometres before the latent heat is released in some region of generally ascending air such as the frontal system of a depression. Under these circumstances any variation in the evaporation in a particular area may be regarded as providing an abnormal heat sink for the

/atmosphere

Albedo	Change due to snow: middle latitudes late autumn and early spring	- 180
	Change due to drought on green vegetation	- 50
Evaporation	Possible change due to drought or vegetation on desert	± 200

4. CONCLUSION

Before reviewing the ability of the earth's surface to modify through various means the working of the atmospheric heat engine, mention must be made of the solar constant. For many years it has been suggested that variations in the solar constant can give rise to large scale climatic changes and that small variations due to sunspot cycles are responsible for shorter fluctuations in world weather. Krivsky (1954) purports to find a definite relationship between sunspot cycles and the position of the jet stream. The most useful summary of the present state of this subject is by Wexler (1953). Although he is probably more disposed than many to advocate a relationship between sunspot cycles and the subsequent weather he states that there is as yet no proof of one and, what is more, that no proof can be readily produced. Correlations between random factors have been found which are equal to those found between weather phenomena and sunspot cycles.

The foregoing survey has covered the principal ways in which variations in the state of the earth's surface can change the energy available to the atmosphere. The following appear to be the most important:-

/(i)

(i) An anomaly in sea surface temperature.

(ii) Variations in the limits of frozen land and sea.

(iii) Early and late snowfall in middle latitudes.

(iv) Change from moist land or land covered in green vegetation to desert and vice versa.

A natural sequel to the present investigation is to seek evidence in the behaviour of the atmosphere of the effect on subsequent weather of anomalies of surface conditions of the kind listed above. The effects of the limits of arctic ice have already been considered by Schell (1940) and Walker (1947) but the relations with subsequent weather have been found to be weak. Possibly this might be expected from the very limited variations in the boundary of arctic ice.

A summary of other attempts to find associations between sea surface temperature, sea ice anomalies and subsequent weather has been made by Baur (1951). In particular Sandstrom suggested that a warm Gulf Stream should result in a warm winter over Europe. However the winter which followed a peak in the Gulf Stream in 1939 was the coldest in Europe for 110 years and the above-normal sea temperatures of 1955 were also followed by an abnormally cold February. Thus the search for such relations will not be easy and the effect of anomalous heat sources and sinks may be found more easily in anomalies of the atmospheric circulation over a wide area rather than in direct effects on local temperature.

Krivsky, V.	1954	Variation of the frontal zone in relation to solar activity. Czeck. Acad. Sci.
Mather, J.D.	1954	Micrometeorology of the surface layers of the atmosphere. Johns Hopkins Univ., Pub. in Climatology, 7, No. 2.
Montgomery, R.B.	1940	Observations of the vertical humidity distribution over the ocean surface and their relation to evaporation. Pap. Phys. Ocean Meteor., Mass. Inst. Tech., 7, No. 4.
Nagayama, M.	1954	On the forecasting of the rate of development of cyclones generated in the southern part of the East China Sea in winter. Ocean and Met., Japan, 6, p. 119.
Penman, H.L.	1949	Survey of Meteorology in Agriculture. Q.J.R. Met.S., 75, p. 293.
Raethjen, P.	1950	Kurzer Abriss der Meteorologie dynamisch gesehen II: Warmehaushalt der Atmosphäre, Hamburg, 1950.
Riehl, H., Yeh, T.C., Malkus, J.S. and La Seur, N.E.	1951	The northeast trade of the Pacific Ocean. Q.J.R. Met. S., 77, p. 334.
Roach, W.T.	1955	Measurements of atmospheric radiation and the heat balance at the ground at Kew. Meteorological Research Papers, Air Ministry, London, No. 936.
Robinson, G.D.	1955	The energy balance of the surface and atmosphere at Kew, May, 1953 to April, 1954. Meteorological Research Papers, Air Ministry, London, No. 929.

Schell, I.I.	1940	Polar ice as a factor in seasonal weather. M.W.R. Supp. 39, p. 27.
Schreiber, P.	1912	Micrometeorology. See Sutton (1953).
Schumann and Burdecki	1953	The seasonal storage of heat in the surface layers of the earth. Notos, 2, p. 4.
Smithsonian Institution	1952	Meteorological Tables.
Sutton, O.G.	1953	Micrometeorology, McGraw-Hill.
Sverdrup, H.U.	1940	The Ocean, Prentice-Hall.
Taylor, G.I.	1919	See Sverdrup (1940), The Oceans.
Thomson, A.	1954	The climate of the Hudson Bay region. Trans. Roy. Soc., Canada, 48, Ser. III, p.1.
Veihmeyer, F.J. and Brooks, F.A.	1954	Measurements of cumulative evaporation from bare soil. Trans. Amer. Geoph. Union, 35, p. 601.
Walker, Sir Gilbert	1947	Arctic conditions and World Weather. Q.J.R. Met. Soc., 73, p. 226.
Wexler, H.	1953	Radiation balance in climatic change - Harlow Shapely (ed.).
Winston, J.S.	1955	Tellus, Vol. 7, No. 4, p. 481.

M.R P. 1006
S.C. III/218
24th August, 1956

AD 223 120

Measurements of the short range diffusion of airborne particles at a height of a few hundred feet in the atmosphere

by

J. S. Hay and F. Pasquill

(Meteorological Office)

AIR MINISTRY

METEOROLOGICAL RESEARCH COMMITTEE

At the time of issue this report has not
been published. Any author desiring to
quote this paper should refer to it as "A
paper of the Meteorological Research
Committee (London),
M.R.P. No. 1006 by Mr. J.S. Hay and
Dr. F. Pasquill.
A copy is available in the Library of
the Meteorological Office."

M.R.P.1006
S.C.III/218
24th August, 1956

AIR MINISTRY
METEOROLOGICAL RESEARCH COMMITTEE

Measurements of the short range diffusion of airborne particles at a height of a few hundred feet in the atmosphere

by

J.S. Hay and F. Pasquill (Meteorological Office)

SUMMARY

The results of measurements of the vertical distribution of airborne particles, released usually at a height of 500 feet, and sampled for periods of about 30 minutes at downwind distances of 100, 300 and 500 metres, are presented and discussed.

At all distances the frequency distributions of the particle elevation with respect to the site of release are closely similar in shape and size to the frequency distribution of wind inclination at the site of release. This is interpreted as indicating that the diffusion of particles released successively from a fixed point in the atmosphere clear of the ground is dominated by a scale of turbulence for which one can recognise a Lagrangian correlation coefficient (R_ξ) which is maintained close to unity for periods of 1 minute or more.

In contrast to this result the wind observations show that the Eulerian auto-correlation coefficient (R_t) falls to about 0.2 in 10 seconds. Since the present experiments do not reach the condition $R_\xi \leqslant 1$ it is not possible, for example, exactly to compare the respective times T which lead to identity in the quantities

$\frac{1}{T^2}\int_0^T\int_0^t R_\xi \, d\xi \, dt$ and $\frac{1}{T^2}\int_0^T\int_0^t R_{t'} \, dt' dt$.. However it is clear that such an identity will occur with T(Lagrangian) of the order of 10 times T(Eulerian), a result which is qualitatively in keeping with wind tunnel observations by Mickelsen (1955) and with Gifford's (1955) examination of Eulerian and Lagrangian energy spectra at a height of about 300 feet in the atmosphere.

INTRODUCTION

The diffusion of particles released at a fixed point in steady, homogeneous turbulence, conditions which may often occur approximately in the atmosphere clear of the ground, is completely specified by the well known Taylor (1921) expression which may be written in the form:-

$$\overline{z^2} = 2\,\overline{w'^2}\int_0^T\int_0^t R_\xi \, d\xi \, dt \qquad \ldots\ldots\ldots\ldots (1)$$

Here z is the vertical displacement of particles from their mean vertical position after travelling time T, w' is the vertical component of eddy velocity, and R_ξ is the correlation coefficient between the vertical velocity of a particle at one instant and the velocity of the same particle a time ξ later. R_ξ is usually referred to as the Lagrangian correlation coefficient. In practice R_ξ is very difficult, if not impossible, to measure effectively and in applying equation (1) progress has depended (see Sutton 1932, 1934) on specifying intuitively or empirically some relation between R_ξ and measurable quantities. One empirical approach, however, which does not seem to have been exploited to any extent is to use experimental measurements of diffusion to obtain some indications of the

/properties

properties of the Lagrangian correlation coefficient in comparison with those of the corresponding, measurable, Eulerian coefficient $R_{t'}$, i.e. the correlation between the velocity of the air at a point at one instant and that at the same point time t' later. The simplest possible type of comparison would be to evaluate

$$\frac{1}{T^2}\int_0^T\int_0^t R_{t'}\, dt'\, dt$$ and to compare with the corresponding double integral

from (1), as a function of T. After commencing the present investigation the writers' attention was drawn to some recent work by Mickelsen (1955) in which precisely this line of approach has been followed in studying diffusion in homogeneous turbulence in a wind tunnel.

The present paper describes experiments in which the vertical distribution of airborne particles released in the atmosphere at a position remote from the ground was examined at various distances downwind up to 500 m. The height of release was usually 500 ft. A description of the technique, which uses apparatus carried on the cables of captive balloons, has been given recently (Hay and Pasquill 1955) and will not be repeated here. Simultaneously, measurements were made of the inclination of the wind at the site of release, in order effectively to specify w' and $R_{t'}$, using a balloon-borne gustiness recorder described previously by Jones (1956).

EQUIPMENT AND TECHNIQUE

In the experiments which are the subject of this paper, the releases of Lycopodium powder lasted normally for 30 min. and the sampling was carried out during the whole period of release. The sampling cylinders were positioned 100 m. downwind of the dispenser in the earlier of these experiments, but as experience was gained this range was extended to 300 and 500 m. The number of heights at which samples were taken was at first 11 but was progressively increased to a maximum of 27. At the central position, four cylinders were exposed to provide data on the reliability of the sampling. During the later experiments, an additional cylinder was exposed at 100 ft., at which height it could normally be expected to be outside the cloud of particles emitted by the dispenser and so give a sample of particles naturally present in the atmosphere.

In addition to wind inclination, measurements of mean horizontal wind speed were made with a vane anemometer incorporated in the gustiness instrument. The temperature difference between the level of the dispenser and a point 200 ft. below was measured using thermistors mounted on the balloon cable and connected to recording apparatus on the ground. The temperature difference between 23 ft. and 4 ft. above the ground was indicated by permanent apparatus located nearby.

To allow correction to be applied for the movement of both balloons, theodolite observations of the elevations of the dispenser and the central sampling position were made at regular intervals. The positioning of the "sampling" balloon downwind of the "source" balloon was directed by an observer stationed about mid-way between the balloons and viewing, in a horizontal mirror, pennants flying from the balloon cables near the central sampling position and dispenser. The former balloon was moved as necessary to keep the pennants in line.

In the assessment of the particle samples, twenty sections of each cylinder were examined by microscope. The instrument used had a magnification of 80 and was masked to give a field of view about 0.12 cm. square, slightly different from that used in the preliminary experiments. The microscopic examination was undertaken by two observers to minimise any personal bias in counting, as the spores sometimes formed only a relatively small proportion of the particles adhering to the cylinders. The mean number of particles counted per 0.12 cm. section of sampling cylinder by each observer was first obtained and the overall mean taken. At the central sampling position, the results from all four sampling cylinders were used in finding the mean. A discussion of the statistics of sampling is given in Appendix I. It is confirmed therein that the size of sampling cylinder used, and the method of examination adopted, yielded reasonable estimates of particle deposit, that the Lycopodium spores could be distinguished reliably from other particles and that there were no similar spores naturally present in the atmosphere during the experiments.

REDUCTION AND PRESENTATION OF OBSERVATIONS

(a) Particle distributions

The particle deposits observed in each of the 19 experiments were first plotted against height. In 9 cases it was evident that the cloud of particles had not been adequately sampled, due to insufficient spacing of the sampling cylinders or incorrect positioning of the sampling balloon, and these cases were not considered further. The deposits obtained in the remaining 10 experiments are given in Table I and those for experiment 17 are plotted in Figure 1 as an example.

To facilitate comparison with the measured wind inclinations at the site of release, the vertical distribution of particles was expressed in terms of their angular elevations with respect to the dispenser. It may be noted that the sampling cylinders were actually spaced at equal height intervals but these were so small relative to the distance from the dispenser that they approximated closely to equal elevation intervals. The particle deposit at each level was then expressed as a percentage of the total for all levels in the particular experiment and "cumulative percentage" deposits obtained by addition of successive individual values, commencing with that for the lowest level. For subsequent discussion, the data so derived are presented on probability graph paper in Figures 2 and 3, the "cumulative percentage" deposits being plotted against the elevation mid-way between the level to which they refer and the next higher level. This assumes that the deposit on any cylinder is representative of the interval centred on the cylinder and extending mid-way to the adjacent sampling levels.

In addition to atmospheric diffusion, the relative vertical motion of the dispenser and sampling array due to balloon movement contributes to the observed spread of particles. This contribution actually depends on the difference, ΔH, between the height of a datum point on the sampling array at time T and the height of the dispenser at a time T-t, where t is the time of travel of the particle. It seems unlikely that there will be a high degree of correlation between ΔH and the true vertical displacement of the particle with respect to its point of origin, and an approximate test of this can be made by examining the relation between ΔH and ϕ, where ϕ is the wind inclination at the dispenser position at time T - t. This test was carried out for experiment No.8, which represents the worst case in the sense that the variations of ΔH relative to the apparent vertical displacements of particles were largest, and the above supposition was confirmed. The usual statistical rule for deriving the variance of the difference of two independent quantities may therefore be applied. If σ_s^2 and σ_a^2 are respectively the variances of ΔH and the apparent vertical displacements of the particles, then σ_p^2, the variance of the true vertical displacements, is given by $\sigma_p^2 = \sigma_a^2 - \sigma_s^2$. In practice, these quantities will be expressed as elevations with respect to the dispenser. Values of ΔH were obtained from the theodolite observations, the time t being estimated from the wind speed measured over periods of a few minutes.

(b) Distributions of wind inclination

From the gustiness records, values of the wind inclination ϕ were read off to the nearest 0.5° at $2\frac{1}{2}$ sec. intervals. This proved to be a simple matter when the charts were driven at 3 in./min., but at 1 in./min., the usual speed, it was frequently only possible to estimate upper and lower limits for the value of ϕ because of the cramped nature of the record.

/In

In such cases, the mean of these limits was taken as the appropriate value. Once again, to reduce personal bias as far as possible, the data were extracted independently by two individuals and some compromise reached with readings which differed. Corrections were then applied in the following manner for deflections of the wind-inclination vane which arose from the movement of the supporting balloon rather than from the turbulent motion of the air.

If the elevation α of the vane as observed by the theodolite is small, and changes by an amount $\Delta\alpha$ in a time Δt (usually 10 sec.), the spurious component of wind inclination is $\phi_1 = -\frac{l\Delta\alpha}{u\Delta t}$ where l is the horizontal distance from the theodolite to the point directly under the vane and u is the horizontal wind speed over the interval Δt. The elevation in fact never exceeded 5°, so that the approximation made in deriving this expression was valid. The distance l was usually within the range 8900 ± 100 ft. but was assumed to have a constant value of 8900 ft. in evaluating ϕ_1, and u was actually meaned over a period of 2 or 3 min. and assumed to apply to the component intervals Δt. It is considered unlikely that this procedure gave rise to an error of more than a few per cent in calculating mean values of ϕ_1. Instantaneous values of ϕ_1 at times corresponding to the readings of ϕ were then estimated by graphical interpolation and used to correct the latter. It will be appreciated that the values of ϕ_1 derived in this way are subject to some uncertainty, especially when they are changing rapidly. They can be accepted with some confidence, however, in eight of the experiments considered here, where ϕ_1 was only 2° or more for 12 per cent or less of the time. In the exceptional cases, ϕ_1 was of this magnitude for 20 and 30 per cent of the time in experiments 8 and 19 respectively.

The corrected values of wind inclination, i.e. $\phi - \phi_1$, from each experiment were formed into a frequency distribution based on class intervals one degree wide and centred on integral values of inclination, the frequencies of the intermediate half-degree values being divided equally between adjacent intervals. These are given in Table II. For comparison with the particle distributions, cumulative frequency distributions were formed for the range of elevations covered by the sampling cylinders. This procedure necessarily excluded the occasional extreme values of inclination which were mainly positive in sign, i.e. indicative of upward moving currents. These distributions are shown together with the corresponding particle distributions in Figures 2 and 3, the cumulative frequencies being plotted against the upper limits of the respective class intervals.

(c) Meteorological and other conditions

The dates and times of the various experiments, and the distances and heights involved, are given in Table III together with wind speed and local and surface temperature gradient measurements. Mean wind speeds at the height of release ranged from 6.1 to 9.5 m./sec. and temperature gradient in the lower layers ranged from slight lapse to slight inversion.

DISCUSSION OF RESULTS

(a) The observed relation between the distributions of particle elevation and wind inclination

The frequency distributions of particle elevation and wind inclination collected in Figures 2 and 3 show three features of interest. Firstly there is the relation between the median values of the two distributions. For seven of the experiments there is agreement to within 1°, in one experiment the particle elevation is higher by 3°, while in the remaining two it is lower by 2°. The mean of the differences in median values, in the sense wind inclination minus particle elevation, is + 0.2° with a standard deviation of 1.5°, in other words there is no significant indication of a declination of the trajectories of the particles with respect to the initial air flow. However, it is noteworthy that this value of

/+ 0.2°

+ 0.2° is very close to that which would follow from the expected terminal velocity of 2 cm./sec. in a wind of about 7 m./sec. In individual experiments the gravitational fall is evidently negligible in comparison with the unknown effects of incomplete sampling (in a statistical sense), and of systematic features such as topographical control on the general flow pattern or variations of eddy structure with height. Nevertheless, the present results indicate that the resultant effect is frequently small and that to a close approximation the median values of particle elevation are equal to the median values of wind inclination at the site of release.

A second feature is that the graphs in Figures 2 and 3 are roughly linear, indicating an approximation to Gaussian form in the distributions of both wind inclination and particle elevation. This is not of particularly novel interest in the case of the wind data, except in so far as they refer to wind inclination at an unusually elevated site, for it is widely thought that turbulent components will usually be so distributed, apart from anistropic motions associated with well developed convective action. In this latter respect it is to be borne in mind that the restriction of our comparison of wind and particle distributions to the height range covered by the sampling apparatus has necessarily excluded the occasional extreme inclinations, most of which are a reflection of this anistropic feature. The main interest is rather in the approximation to Gaussian form in the particle distributions, for here it is to be remembered that the measurements are not made at a single level of say 500 ft., but over a layer which may extend between 200 and 800 ft. and which will contain some systematic variations of wind and eddy structure with height. Inspection of the individual distributions does not suggest any consistent departure from Gaussian form and it is interesting to note that there is no outstanding difference in this respect between results obtained at different distances from the source. In order to give an overall representation of the results the distributions have been normalised to give zero inclination or elevation at 50 per cent and the mean inclinations and elevations at other cumulative frequencies derived. The results are shown in Figure 3 from which it is seen that, on average, the inclination distribution is actually skew with large positive (upwards) values, though the same feature is not evident in the particle distribution.

The third and most interesting feature is the similarity in the dimensions of the wind and particle distributions, though before any realistic comparison can be made it is necessary to correct for the relative vertical displacements of the dispenser and the sampling array, as discussed previously. Values of σ_a, the standard deviation of the apparent elevations of the particles, were extracted from the distributions in Figures 2 and 3 by reading off the elevations at 2 and 98 per cent, i.e. those enclosing 4.12 times the standard deviation in a Gaussian distribution. A similar process was used to obtain σ_W, the standard deviation of the wind inclinations. The standard deviations, σ_s, of the elevations due to the relative vertical displacements, were computed directly. The values of σ_a and σ_s, the resulting values of σ_p, and the corresponding values of σ_W, are collected in Table IV below. Examination of the statistics of sampling (see Appendix I) show that the standard error of σ is of the order of 3 per cent.

/TABLE IV

TABLE IV

Comparison of standard deviations of particle elevation and wind inclination

Expt. No.	Dist. of travel (metres)	Particle elevation			Wind inclination σ_ω (degrees)	σ_p/σ_ω	$\bar{u}$ (m/sec.)	ΔT °F (23ft.-4ft.)
		σ_s	σ_a (degrees)	σ_p				
4	100	1.2	2.1	1.7	3.1	0.55	6.7	-0.6
7	100	1.3	3.9	3.7	3.0	1.23	8.0	+0.2
8	100	2.2	4.1	3.5	2.8	1.25	7.4	0
12	300	0.7	5.0	4.9	4.6	1.07	7.7	-0.4
13	300	0.5	3.9	3.9	3.8	1.03	7.3	+0.6
14	300	1.0	4.2	4.1	4.0	1.03	6.3	-0.4
15	300	0.2	4.9	4.9	4.9	1.00	6.1	-0.6
16	500	0.5	3.0	3.0	3.2	0.94	7.3	-0.7
17	500	0.3	2.9	2.9	2.7	1.07	6.8	-0.3
19	300	0.9	6.1	6.0	4.0	1.50	9.5	+0.2

With the exception of Nos. 4 and 19 there is a remarkable degree of similarity between the values of σ_p and σ_W, irrespective of the distance of travel and the conditions of wind and atmospheric stability prevailing. Taking all experiments σ_p/σ_W has a mean value of 1.07 and a standard deviation of 0.23. The odd result in the case of No.19 is clearly associated with certain subsidiary peaks in the particle distribution, which occur at a height well below the main peak and for which there appear to be insufficient corresponding large negative values of wind inclination. No. 4 was carried out in pre-frontal conditions with drizzle setting in, and is a special case in that an abrupt reduction in gustiness occurred about half way through the experiment. The observation of a distribution of particles which is narrow relative to the distribution of wind inclination could be due to unrepresentative sampling, since the positioning of the sampling array with respect to the cloud of particles was probably controlled more successfully in the second half of the experiment than in the first. This idea is supported by the very high particle deposits which were observed over a sampling time of only 16 min.

The original data have also been independently examined by a statistician. The approximation to Gaussian distribution was confirmed in one case which appeared doubtful by the application of a formal test. In the subsequent treatment, therefore, the data were assumed to be of Gaussian form. Variances of apparent particle elevation (σ_a^2) and of wind inclination (σ_ω^2) were calculated directly from the observations in Tables I and II. The values of σ_a^2 were then corrected as before to give σ_p^2.* Owing to the large number of degrees of freedom involved, the equality of σ_p^2 and σ_ω^2 could not conveniently be tested from the available statistical tables of variance ratio. Instead, a form of "t" test was applied to the differences of the variances. Of the ten experiments, six (Nos. 12, 13, 14, 15, 16, 17) showed no significant difference, while for the remaining four (Nos. 4, 7, 8, 19) the differences were found to be highly significant. However, only in No. 4 is the difference substantial and in the direction of σ_p less than σ_W, and this is the experiment which has already been discussed as possibly anomalous.

/(b)

---

*The values of σ_p and σ_ω obtained in this fashion differed only slightly from those presented in Table IV.

(b) Interpretation of the results in relation to the Lagrangian and Eulerian correlations in the eddy structure

As stated in the introduction to this paper, the fundamental object of the present investigation was to obtain indirectly some insight into the Lagrangian features of the eddy structure, that is, variations which are related to time in the sense of following the motion, in comparison with Eulerian features, which are related to time at fixed points in space. From Taylor's expression for the scattering of particles (equation 1), it immediately and necessarily follows that a linear variation of standard deviation with time (i.e. in our notation $\sigma_p = \sigma_w$) is held as long as the Lagrangian correlation coefficient remains close to unity. In the simplest possible terms the particles travel for such a time in straight lines, with the velocity imparted to them at the moment of release.

The present results, in showing equality between σ_w and σ_p for distances up to 500 m., imply that the diffusive spread of the particles may be described by equation 1 with R_ξ maintained equal to unity for at least 1 min. This period of maintenance of Lagrangian correlation is considerably longer than that which is required to explain the vertical diffusion of a smoke cloud at ground level. In the latter case (see Sutton, 1949, p.349) the required value of R_ξ falls to about 0.5 in 1 sec. Furthermore, it is very soon obvious from an examination of the wind inclination variation that the apparent persistence of Lagrangian correlation is not associated with a similar feature in the Eulerian correlation. On the contrary, the Eulerian or auto-correlation coefficient computed from corrected values of the wind inclination[*] at $2\frac{1}{2}$ sec. intervals falls off rapidly, as can be seen from the two cases quoted below in Table V. These figures are the means of three values obtained from analysis of three separate 8 min. periods in each of the two experiments.

TABLE V

Values of auto-correlation coefficient for wind inclination

Time lag (seconds)		$2\frac{1}{2}$	5	$7\frac{1}{2}$	10	15	20	30
Correlation coefficient	Expt. No. 13	0.69	0.40	0.19	0.09	-0.01	0.01	0.02
	Expt. No. 17	0.61	0.40	0.29	0.23	0.20	0.14	0.04

---

[*] For the purpose of the arguments which are ultimately developed in the present paper it is probably unnecessary to give detailed consideration to the differences between the auto-correlation for inclination ($R_{t'}(\phi)$) and that for the vertical component of eddy velocity ($R_{t'}(w)$). However, an analysis of this feature has been carried out (see Appendix II) to confirm that small values of $R_{t'}(\phi)$ of the order of 0.1 are necessarily associated with similarly small values of $R_{t'}(w)$.

The simplest possible interpretation of the present results is that, despite the rapid **Eulerian** variations, the particles actually travel in straight lines for substantial periods. It is clear, however, from practical experience, that this interpretation cannot be correct. Indeed, it is obvious from visual observations of a puff of smoke moving with the wind that the trajectories of individual smoke particles are far from linear, and are in fact rapidly distorted mainly by turbulent motions on a scale smaller than that of the puff itself. Furthermore, we have the evidence of Edinger's (1951) photographic measurements of the trajectories of individual soap bubbles in an isothermal layer at a height of 1000 ft. These provided data for the direct evaluation of the Lagrangian correlation coefficient and showed this falling to 0.5 in about 7 sec.

The real explanation of the present results is thought to be along the following lines. If we consider the particles released over some short time interval, we have in effect the case of a small puff of smoke which moves off downwind, increasing in size as it does so. A continuous release of particles may then be considered equivalent to a series of puffs, each puff leaving the release point with a different vertical velocity (or inclination in the present context) and subsequently growing with downwind travel. At any given distance downwind the vertical distribution of particles, averaged over a period of time, will be a resultant of the growth of the individual puffs and the scattering of their centres of mass. The vertical distributions of particles observed in the present experiments are then entirely explained if, firstly, the puffs travel in straight lines and, secondly, the dimensions of the puff are not more than about half the spread of the centres of mass. For example, if we assume Gaussian distributions, with σ_ω^2 and σ_d^2 respectively the variances of the centres of mass of the puffs (i.e. effectively of the wind inclination) and of the particles within the puff, then for σ_d/σ_ω equal to $\frac{1}{2}$, $\frac{1}{3}$ and $\frac{1}{4}$ the resultant σ_p (given by $\sigma_p^2 = \sigma_\omega^2 + \sigma_d^2$) is equal to $1.12\,\sigma_\omega$, $1.05\,\sigma_\omega$ and $1.03\,\sigma_\omega$ respectively.

Independent qualitative evidence for a scattering process of this nature is frequently apparent in the form of the familiar plume of smoke from an industrial chimney. In this case, the plume is usually of somewhat irregular sinuous shape with amplitudes frequently greater than the actual visible width of smoke, but if attention is fixed on some outstanding "element" near the lower or higher points of the instantaneous plume, it will be seen that the element does not trace out the sinuous form, but continues in an apparently straight path inclined downward or upward, for as long as it can be recognised as a coherent puff of smoke. This behaviour has also been observed quantitatively, by one of the writers (F.P.) and J. Crabtree, in the trajectories of smoke puffs emitted successively at a few hundred feet above ground and followed by theodolite over a distance of about 125 m. In the terms of the present measurements the standard deviations of the elevations of the puff centres were constant with distance within a matter of 5 per cent, while the overall vertical spread of the puff centres was certainly greater than the vertical dimensions of the individual puffs by a factor of two or more.

While, on the one hand, it is clearly not enough to consider the Lagrangian correlation coefficient for a particle, and on the other hand it is not physically acceptable to refer to a mass of air, for our elementary puff is in fact not a given mass of air, the features discussed above imply a kind of Lagrangian correlation which is maintained for much longer than the familiar Eulerian correlation at a point. It is as if there is a relatively large scale pattern in the eddy structure which develops and changes quite slowly, but which gives the impression of fairly rapid change merely by virtue of being swept rapidly past an observing instrument. Within this persistent pattern, going up the frequency scale of the spectrum of eddy energ , we have less correlated motions which are responsible for the growth of the elementary puff. The interesting point which has yet to be clarified is the length of time for which such a situation can be recognised and how this time is related to the physical conditions.

The greater persistence of Lagrangian as compared with Eulerian correlation has previously been observed in wind tunnel turbulence, and indeed, in an investigation similar in some respects to the present one, Mickelsen (1955) has recently compared the diffusive spread of a gas emitted from a point in wind tunnel flow with that calculated from equation (1), with the Lagrangian correlation coefficient replaced by measured Eulerian values. From this comparison Mickelsen draws certain conclusions regarding the relation between the shapes of the decay curves of the Lagrangian and Eulerian correlation coefficients, though here the argument is rather involved and our impression is that an error has occurred in the transformation from the correlation coefficient to its double integral with respect to time.

In the present discussion we will therefore restrict our attention to a comparison of the forms

$$\frac{1}{T^2}\int_0^T \int_0^t R_\xi \, d\xi \, dt \quad \text{(Lagrangian) and} \quad \frac{1}{T^2}\int_0^T \int_0^t R_{t'} dt' dt \quad \text{(Eulerian)*,}$$

when the first of these is given, through equation (1), by the observed value of $\sigma^2/2v^2T^2$, and the second may be evaluated from the measurement of the cross-stream component of eddy velocity, v. Equality in the two forms is found to occur when T (Lagrangian) is approximately 3 times T (Eulerian), for a range of values of $\sigma^2/\overline{v^2}T^2$ from 1 to 0.4. The data do not permit evaluation at lower values of $\sigma^2/\overline{v^2}T^2$ but the trend appears to be in the direction of a rapid increase in the ratio of the "Lagrangian" and "Eulerian" times.

In contrast to Mickelsen's experiments, ours do not extend into the region of non-linear relation between σ^2 and t^2, and a similar evaluation of the ratio of the "Lagrangian" and "Eulerian" times for equality in the above forms is accordingly not possible. However, substitution in equation (1) of the auto-correlation data given in Table V leads to a σ, t relation which begins to depart significantly from linearity (i.e. $\sigma^2/\overline{\omega'^2}t^2 \simeq 0.8$) for t between 5 and 10 sec., whereas in the observed values a similar order of departure from linearity is not evident even at 70 sec. In other words, this suggests that for equal values in $\sigma^2/\overline{\omega'^2}\,t^2$ the "Lagrangian" and "Eulerian" times are in the ratio of about 10 to 1, which is at any rate qualitatively similar to the result obtained in a wind tunnel flow by Mickelsen.

In the observational study of atmospheric turbulence there have recently been some quite novel measurements made by Gifford (1955), in an attempt to compare the Lagrangian and Eulerian characteristics directly at a height of 300 ft. Gifford uses the trajectories of "no-lift" balloons from which to extract vertical velocities of a Lagrangian nature, and compares these on an energy spectrum basis with Eulerian values from a fixed installation. The interesting feature of these results is the suggestion that the Lagrangian spectrum is generally displaced to the low frequency side of the Eulerian spectrum, with the respective frequencies of peak energy in the ratio of 1 to 3 approximately.

---

* The notation is that used in the Introduction and differs from that used by Mickelsen.

It seems clear, therefore, that our conclusion regarding the difference in Lagrangian and Eulerian persistence of eddy velocity is supported independently, not only in the sign, but also in the order of magnitude of the difference which we are able to estimate. A more definite evaluation of this difference would certainly be useful in understanding the process of diffusion and it is proposed to continue the work in this direction.

REFERENCES

Edinger, J.G.	1951	Report on Diffusion in the Free Atmosphere, Department of Meteorology, University of California, Los Angeles.
Gifford, F.	1955	Mon. Weath. Rev., U.S.W.B., 83, 293.
Hay, J.S. and Pasquill, F.	1955	Meteorological Research Papers, Air Ministry, London, No. 961.
Jones, J.I.P.	1956	Meteorological Research Papers, Air Ministry, London, No. 974.
Mickelsen, W.R.	1955	N.A.C.A., Technical Note 3570.
Sutton, O.G.	1932	Proc. Roy. Soc., A, 135, 143.
	1934	Proc. Roy. Soc., A, 146, 701.
	1949	Quart. J.R. Met. Soc., 75, 335.
Taylor, G.I.	1921	Proc. London Math. Soc., 20, 196.

APPENDIX I TO M.R.P. 1006

DISCUSSION OF SAMPLING TECHNIQUE

In developing the present sampling technique, the first factors to be decided on were the diameter and length of the sampling cylinders. An external diameter of about $\frac{1}{4}$ in. was preferred since glass tubes of this size are fairly robust and their collection efficiency is reasonably high. According to Gregory (Ann. App. Bio., 38, No. 2, 357-376, 1951), it exceeds 40 per cent and does not vary markedly with wind speeds above 3.3 m/sec. As regards length of cylinder, an upper limit is set by the height variation of particle concentration, if the sample is to be representative of a particular level. Assuming the vertical distribution of particle concentration to be Gaussian in form, with standard deviation σ_a, it can be shown that systematic variations in particle deposit along a cylinder of length l will at no point exceed 1 per cent if $l \leqslant \sigma_a/100$. This requirement was certainly fulfilled here with l approximately 4 cm., since the minimum value of σ_a observed was about 5 m. (The cylinders were actually about 5 cm. in length but a section of only 4 cm. was covered with adhesive. The remaining 1 cm. length was covered with sellotape for ease of handling, with an identifying number beneath). To confirm that cylinders of the above dimensions did yield reasonable estimates of particle concentration, four cylinders were exposed 7.5 cm. apart at the central sampling position.

It was of course impracticable to count the total number of particles deposited on a cylinder in one traverse by the microscope, as only a limited (constant) length of cylinder could be viewed. The number of sections scanned on each cylinder was, however, optional up to a maximum of about 34. Assuming the number of particles per section on any cylinder to follow a Poisson distribution (see Gregory, p.363), the standard error of the mean number m from n sections is given simply by $\sqrt{\frac{m}{n}}$ or $\frac{100}{\sqrt{mn}}$ when expressed as a percentage of the mean. For a constant degree of accuracy of assessment therefore, the number of sections examined should be increased as the deposit decreases. For simplicity, a fixed number of sections, n = 20, was actually used, so that the mean deposit m per section may be expected to have a standard error of 20 per cent of m or less for $m \geqslant 1$. In each experiment, smaller deposits were in fact observed on several cylinders at the top and bottom of the sampling array. It was also necessary to consider how far the estimate of the deposit on a cylinder was affected by personal bias, as it was not possible to identify every spore with absolute certainty. The precaution was therefore taken of having each set of sampling cylinders scrutinized by two individuals.

Selecting at random a number of sampling cylinders, the standard errors of the mean deposits m were calculated in the usual manner and compared with the values of $\sqrt{\frac{m}{20}}$ using a form of "chi-square" test. For cylinders with m ranging up to 30, these tests showed that the values were in good agreement, confirming that, in these cases, the particles were distributed along each cylinder according to a Poisson distribution. In two cases, however, in which m was much larger, namely 70.60 and 94.35, there was a significant difference, $\sqrt{\frac{m}{20}}$ giving an underestimate of the true standard error by a factor of about 2. To reduce the computational work in subsequent comparisons, the standard error of m was assumed to be $\sqrt{\frac{m}{20}}$ in all cases.

Considering the cylinders exposed 7.5 cm. apart at the same level, there were only three cases in which the deposit on an individual cylinder differed significantly (at the 5 per cent level) from the overall mean for the level in the same experiment. In these instances the discrepancy was within 15 per cent so it may be concluded that cylinders of the size used and examined in the manner described yield reasonable estimates of the particle deposit. Comparing now the results obtained by different observers, there were only about 2 per cent of cases in which the two estimates of deposit differed at the 5 per cent level of significance. This would appear to indicate that the spores could usually be distinguished reliably from other particles adhering to the cylinders.

As indicated above, the mean deposit m on some cylinders was less than unity so that the standard error of m would exceed 20 per cent of m in these instances. Such errors, however, are unlikely to have been in the same sense for all cylinders in one experiment so that a smaller error in the standard deviation σ_a, of the vertical distribution of particles might be anticipated. This was actually confirmed for experiments 8, 13 and 17. Assuming the standard error of each m to be $\frac{\sqrt{m}}{\sqrt{20}}$, the standard error of σ_a was computed and, in the worst case, was found to be only about 3 per cent of σ_a. It is unlikely that this figure would have been greatly exceeded, if at all, in any of the other experiments.

Finally, reference may be made to the cylinders which were exposed at 100 ft. in seven of the experiments in order to give samples of particles naturally present in the atmosphere. In four experiments, no spores were observed and there were no deflections of the wind vane corresponding to the elevation of the cylinder. In the other three experiments, however, a few spores were observed but the wind inclination records in these cases showed occasional values corresponding to the elevation of the cylinder. There seems little doubt, therefore, that there were no spores naturally present in the atmosphere during these experiments, and that the observed distributions were in fact of particles emitted by the dispenser.

THE EULERIAN AUTO-CORRELATION COEFFICIENT OF THE VERTICAL COMPONENT OF EDDY VELOCITY

In the present experiments the vertical gustiness recorder gives wind inclination $\phi = \tan^{-1}\frac{w}{u} \simeq \frac{w}{u}$,* where w is the vertical component of velocity and u the horizontal component in the direction of the mean wind. The purpose of the present analysis is to investigate the error involved in calculating the auto-correlation coefficient directly from the fluctuations $\phi' (= \phi - \overline{\phi})$ instead of from the values of w', for the derivation of which corresponding values of u' (as distinct from $\overline{u}$) would be required,

since
$$\phi \simeq \frac{w}{u} = \frac{\overline{w} + w'}{\overline{u} + u'} . \tag{1}$$

Using suffixes r and $s = r + t$ to denote values at two instants of time t apart,

$$\phi_r = \frac{w_r}{u_r} , \qquad \phi_s = \frac{w_s}{u_s}$$

and
$$w_r w_s = u_r \phi_r u_s \phi_s$$

Taking mean values and expanding, it follows that

$$\overline{w'_r w'_s} = \overline{u}^2 \, \overline{\phi_r \phi_s} \, (1 + \alpha) - \overline{w}^2$$

where
$$\alpha = \frac{\overline{u'_r \phi_r \phi_s}}{\overline{u} \, \overline{\phi_r \phi_s}} + \frac{\overline{u'_s \phi_r \phi_s}}{\overline{u} \, \overline{\phi_r \phi_s}} + \frac{\overline{u'_r u'_s \phi_r \phi_s}}{\overline{u}^2 \, \overline{\phi_r \phi_s}} \tag{2}$$

and similarly, in steady conditions,

$$\overline{w'^2_r} = \overline{w'^2_s} = \overline{u}^2 \, \overline{\phi^2} \, (1 + \beta) - \overline{w}^2$$

where
$$\beta = \frac{\overline{2 u' \phi^2}}{\overline{u} \, \overline{\phi^2}} + \frac{\overline{u'^2 \phi^2}}{\overline{u}^2 \, \overline{\phi^2}} \tag{3}$$

The Eulerian auto-correlation coefficient, R(w), for the vertical component is therefore,

$$\frac{\overline{w'_r w'_s}}{\overline{w'^2}} = \frac{\overline{\phi_r \phi_s}}{\overline{\phi^2}} \, \frac{\left(1 + \alpha - \frac{\overline{w}^2}{\overline{u}^2 \, \overline{\phi_r \phi_s}}\right)}{\left(1 + \beta - \frac{\overline{w}^2}{\overline{u}^2 \, \overline{\phi^2}}\right)} \tag{4}$$

---

* The ϕ used here is true wind inclination and hence corresponds to $\phi - \phi_1$ in the text.

The corresponding correlation coefficient, $R(\phi)$, for wind inclination, is

$$\frac{\overline{\phi'_r\phi'_s}}{\overline{\phi'^2}} = \frac{\left(\dfrac{\overline{\phi_r\phi_s}}{\overline{\phi^2}} - \dfrac{\bar{\phi}^2}{\overline{\phi^2}}\right)}{\left(1 - \dfrac{\bar{\phi}^2}{\overline{\phi^2}}\right)}$$

and for the values of $\dfrac{\bar{\phi}^2}{\overline{\phi^2}}$ which obtained for the data discussed in Table V of the text (i.e. approximately 0.01 and 0.001 in Nos. 13 and 17 respectively)

$$\frac{\overline{\phi_r\phi_s}}{\overline{\phi^2}} = R(\phi) .$$

The terms α and β in equation (4) involve correlations between the u and w components which are unobtainable from the present data and we are only able to assign limits to α and β, as follows. For the term $\overline{u'_r\phi_r\phi_s}$ we may write

$$\left|\overline{u'_r\phi_r\phi_s}\right| \leq \overline{\left|u'_r\phi_r\phi_s\right|} \leq \overline{\left|u'_r\right|\left|\phi_r\phi_s\right|} .$$

If now we assume that the maximum numerical value of u'_r is three times its standard deviation

$$\left|\overline{u'_r\phi_r\phi_s}\right| \leqslant 3\sqrt{\overline{u'^2}}\ \overline{\left|\phi_r\phi_s\right|} .$$

For small values of $r-s = t$, ϕ_r and ϕ_s will usually be of the same sign and as a further approximation the modulus on the R.H.S. may be omitted and we may write

$$\left|\frac{\overline{u'_r\phi_r\phi_s}}{\bar{u}\ \overline{\phi_r\phi_s}}\right| \leq \frac{3\sqrt{\overline{u'^2}}}{\bar{u}} ,$$

and similarly for

$$\frac{\overline{u'_s\phi_r\phi_s}}{\bar{u}\ \overline{\phi_r\phi_s}} \quad \text{and} \quad \frac{\overline{u'\phi^2}}{\bar{u}\ \overline{\phi^2}} . \tag{5}$$

We are unable to specify the variation of a term of the form $\overline{u'_r\phi_r\phi_s}$ with increasing time-lag t, but since we have no reason to expect it to increase, we will assume the inequality in (5) to apply to all values of t. By the same general argument we write

$$\left|\overline{u'_r u'_s \phi_r \phi_s}\right| \leqslant 9\ \overline{u'^2}\ \ \overline{\phi_r \phi_s} \ ,$$

hence

$$\left|\frac{\overline{u'_r u'_s \phi_r \phi_s}}{\overline{u}^2\ \ \overline{\phi_r \phi_s}}\right| \leqslant \frac{9\,\overline{u'^2}}{\overline{u}^2}$$

and similarly for $\dfrac{\overline{u'^2 \phi^2}}{\overline{u}^2\,\overline{\phi^2}}$ (6)

For the present experiments we may take

$$\frac{\overline{u'^2}}{\overline{u}^2} \simeq \frac{\overline{w'^2}}{\overline{u}^2} \simeq .0005$$

so that from (2), (3), (5), and (6)

$$|\alpha| \leqslant 0.47$$

and $|\beta| \leqslant 0.47$

In (4) the term $\dfrac{\overline{w}^2}{\overline{u}^2\,\overline{\phi_r \phi_s}} \simeq \dfrac{\overline{\phi}^2}{R(\phi)\,\overline{\phi^2}}$

$\simeq \dfrac{0.01}{R(\phi)}$ for No. 13

and $\simeq \dfrac{0.001}{R(\phi)}$ for No. 17

Similarly $\dfrac{\overline{w}^2}{\overline{u}^2\,\overline{\phi^2}} \simeq 0.01$ for No. 13

$\simeq 0.001$ for No. 17

and may be neglected.

When $R(\phi) \simeq 1$ (i.e. $r-s = t$ small) the terms α and β must be of the same sign and equal in magnitude and then from (4) we have the obvious result that $R(w) = R(\phi)$. Otherwise we can only specify outside limits to $R(w)$ and, for example, when $R(\phi) = 0.1$ it follows from (4) and the quantities evaluated above that

$$0.03 \leqslant R(w) \leqslant 0.26.$$

Although this process does not allow us to specify precise magnitudes for $R(w)$ it does mean that small values of $R(\phi)$ of the order of 0.1 can be taken to imply similarly small values of $R(w)$.

TABLE I

Particle deposits on sampling cylinders

Height above central sampling cylinder (metres)	No. of particles per 0.12 cm. section of sampling cylinder			Height above central sampling cylinder (metres)	No. of particles per 0.12 cm. section of sampling cylinder						
	Experiment No.				Experiment No.						
	4	7	8		12	13	14	15	16	17	19
+ 26	–	1.90	2.35	+ 78	0.60	0.55	0.15	0.45	–	0.05	–
+ 24	–	2.15*	4.10*	+ 72	0.65	0.45	0.25	1.00	0.25	0.15	0.45
+ 22	–	2.45	5.85	+ 66	0.80	0.75	0.25	0.80	1.10	0.15	1.40
+ 20	0	4.95*	10.00*	+ 60	0.65	0.35	0.30	2.05	0.55	0.15	1.10
+ 18	–	7.45	14.15	+ 54	0.90	0.65	0.75	4.55	1.00	0.05	1.25
+ 16	0.30	10.80*	16.35*	+ 48	1.30	0.95	0.65	5.40	0.55	0.35	1.85
+ 14	–	14.15	18.50	+ 42	2.30	2.15	1.05	5.65	0.80	0.55	1.35
+ 12	0.90	23.55	31.55	+ 36	2.00	1.45	0.85	6.50	0.85	0.85	1.55
+ 10	–	16.65	30.55	+ 30	1.60	1.45	1.15	5.15	0.75	1.15	3.60
+ 8	9.65	20.35	24.50	+ 24	3.50	4.60	1.85	6.20	1.25	0.85	6.10
+ 6	–	10.90	24.20	+ 18	4.50	12.95	5.25	6.80	1.05	2.05	9.35
+ 4	93.70	6.70	18.30	+ 12	8.05	13.25	7.65	6.20	2.90	3.60	9.95
+ 2	–	7.05	14.60	+ 6	6.10	23.45	7.80	4.10	3.35	2.70	11.60
0	74.15	3.55	7.10	0	7.80	22.15	11.10	8.30	5.30	4.45	11.90
- 2	–	5.20	4.00	- 6	6.90	14.05	3.85	7.00	4.95	6.65	14.75
- 4	10.80	4.30	3.90	-12	5.50	8.05	2.95	4.85	6.65	7.45	12.70
- 6	–	0.35	3.00	-18	3.65	2.85	8.45	3.85	5.45	5.85	8.75
- 8	4.60	0.80	1.70	-24	7.30	5.85	6.05	2.90	3.60	4.65	6.70
-10	–	0.80	1.25	-30	3.30	4.90	4.85	2.25	3.35	4.45	5.50
-12	0.70	0.35	0.20	-36	2.45	0.95	0.45	2.55	3.70	2.05	1.35
-14	–	0.05	0.20	-42	0.75	0.10	1.25	1.60	0.50	2.30	0.80
-16	0.30	0*	0.20*	-48	0.35	0.45	0.35	0.20	0.15	2.65	1.65
-18	–	0	0.15	-54	0.30	0.10	0.05	0.30	0.20	1.65	2.90
-20	0	0*	0.10*	-60	0.20	0.05	0	0.10	0.20	1.25	1.20
-22	–	0	0.05	-66	0.05	0.05	0	0.35	0.20	0.85	0.45
-24	–	0*	0*	-72	0.10	0.05	0	0.10	0.15	0.35	3.60
-26	–	0	0	-78	0	0	0	0	0.10	0.25	2.45

* Interpolated values.

TABLE II

Frequency distributions of wind inclination

Corrected inclination (degrees)	Frequency of occurrence Experiment No.									
	4	7	8	12	13	14	15	16	17	19
+ 29	1.0	–	–	–	–	–	–	–	–	–
+ 28	–	–	–	–	–	–	–	–	–	–
+ 27	–	–	–	–	–	–	–	–	–	–
+ 26	–	–	–	–	–	–	1.0	1.0	–	–
+ 25	–	–	–	–	–	–	1.5	1.0	–	–
+ 24	–	–	–	1.0	–	–	1.5	–	–	–
+ 23	–	–	–	–	–	–	–	–	–	–
+ 22	–	–	–	–	0.5	–	–	1.5	–	–
+ 21	–	–	–	–	0.5	–	2.0	0.5	–	–
+ 20	–	–	–	1.0	–	–	1.5	0.5	–	–
+ 19	–	–	–	1.5	–	–	1.5	1.0	–	–
+ 18	–	–	–	3.5	0.5	0.5	4.5	0.5	1.0	–
+ 17	–	–	–	1.5	0.5	0.5	4.0	2.0	1.0	–
+ 16	1.0	–	–	5.5	–	0.5	8.0	4.5	–	–
+ 15	3.0	–	–	3.0	–	0.5	7.5	3.0	1.5	1.0
+ 14	–	–	–	6.5	–	0.5	5.0	4.5	0.5	–
+ 13	0.5	–	–	7.0	1.5	4.0	11.0	7.0	0.5	1.5
+ 12	3.0	–	–	13.0	2.5	5.0	7.0	12.5	1.0	1.5
+ 11	2.5	1.5	1.0	15.5	4.5	3.0	10.0	13.0	1.0	–
+ 10	3.0	2.0	2.0	25.5	5.0	5.5	15.5	15.5	2.5	1.5
+ 9	4.0	5.0	2.5	16.0	15.5	6.0	9.0	15.0	5.0	3.0
+ 8	4.5	4.5	2.5	28.5	22.5	13.0	15.5	11.0	3.0	6.0
+ 7	12.0	4.0	4.5	25.5	23.0	10.0	13.5	11.0	3.5	7.0
+ 6	12.5	7.5	16.5	23.0	21.5	10.0	24.5	14.5	6.0	6.0
+ 5	13.0	11.5	32.5	22.0	24.0	10.5	28.0	20.5	18.5	6.5
+ 4	19.5	27.0	41.5	35.0	47.0	26.5	32.0	15.5	23.0	17.5
+ 3	23.5	41.5	68.5	54.0	65.0	36.0	47.5	22.5	37.5	25.0
+ 2	41.5	49.0	101.5	71.5	97.0	49.0	44.0	28.0	90.0	37.5
+ 1	55.5	99.5	129.0	81.0	129.5	68.5	68.0	56.0	116.0	54.5
0	82.5	121.0	113.5	106.0	154.0	91.0	45.0	70.0	114.0	61.0
– 1	53.0	140.0	79.0	100.0	118.0	102.0	57.0	88.5	106.0	70.0
– 2	12.5	102.5	53.0	87.0	75.5	87.5	69.0	104.5	78.0	96.0
– 3	5.0	44.0	35.5	84.5	56.5	51.5	52.0	72.5	57.5	106.0
– 4	2.0	32.0	17.0	49.5	37.5	50.5	40.0	56.0	24.0	101.5
– 5	3.5	13.5	8.5	44.0	21.5	26.0	25.5	31.5	13.0	75.0
– 6	1.5	7.0	8.0	21.5	9.5	17.0	24.0	15.5	9.5	54.5
– 7	1.0	2.0	1.5	9.0	11.0	13.0	11.5	15.5	4.0	36.0
– 8	–	1.0	1.0	6.5	4.0	4.0	8.5	3.0	2.0	21.5
– 9	–	1.0	1.0	3.5	3.0	2.0	7.0	1.0	0.5	12.0
– 10	–	0.5	–	2.0	2.0	1.0	5.0	–	–	12.0
– 11	–	1.5	–	1.5	–	–	3.0	–	–	4.0
– 12	–	–	–	–	0.5	–	–	–	–	–
– 13	–	–	–	–	1.5	–	–	–	–	–
– 14	–	–	–	–	–	–	3.5	–	–	–
– 15	–	–	–	–	–	–	1.5	–	–	–

TABLE III

Summary of meteorological and other conditions

Experimental Number	4	7	8	12	13	14	15	16	17	19
Date	16 September	26 September	26 September	4 October	4 October	13 October	14 October	17 October	17 October	28 October
Time G.M.T.	0828–0844	1436–1506	1606–1636	1521–1601	1636–1716	1522–1552	1425–1455	1151–1221	1430–1500	1517–1557
Distance of sampling (metres)	100	100	100	300	300	300	300	500	500	300
Height of dispenser above ground (metres)	143	147	255	140	143	145	154	150	151	129
Height of central sampling cylinder relative to dispenser (metres)	−0.2	−6.2	−9.0	−0.6	−4.3	−11.7	−14.4	−13.2	−8.2	−5.4
Wind speed (m./sec.)	6.7	8.0	7.4	7.7	7.3	6.3	6.1	7.3	6.8	9.5
Local temperature gradient*	–	0.90 Γ	–	0.66 Γ	0.62 Γ	0.82 Γ	0.86 Γ	0.87 Γ	0.76 Γ	–
Surface temperature gradient (23ft. - 4ft.) (°F)	−0.6	+ 0.2	0	−0.4	+ 0.6	−0.4	−0.6	−0.7	−0.3	+ 0.2
Cloud amount and height (feet)	8/8 As. 3/8 Sc 2500	3/8 Sc.5000 2/8 Cu.3000	5/8–7/8 Sc.3500	5/8 Sc.5000 2/8 Cu.3000	6/8 Sc.5000 2/8 Cu.3000	2/8 Ci.Cs. 1/8–3/8 Cu.2500	4/8 Sc.2500	6/8 Ac.As. 2/8–3/8 Cu.Sc.3000	3/8 Cu.Sc. 3000	2/8–4/8 Sc.3000

* Obtained from measurements over a height interval of 200 feet near the dispenser. Γ = dry adiabatic lapse rate.

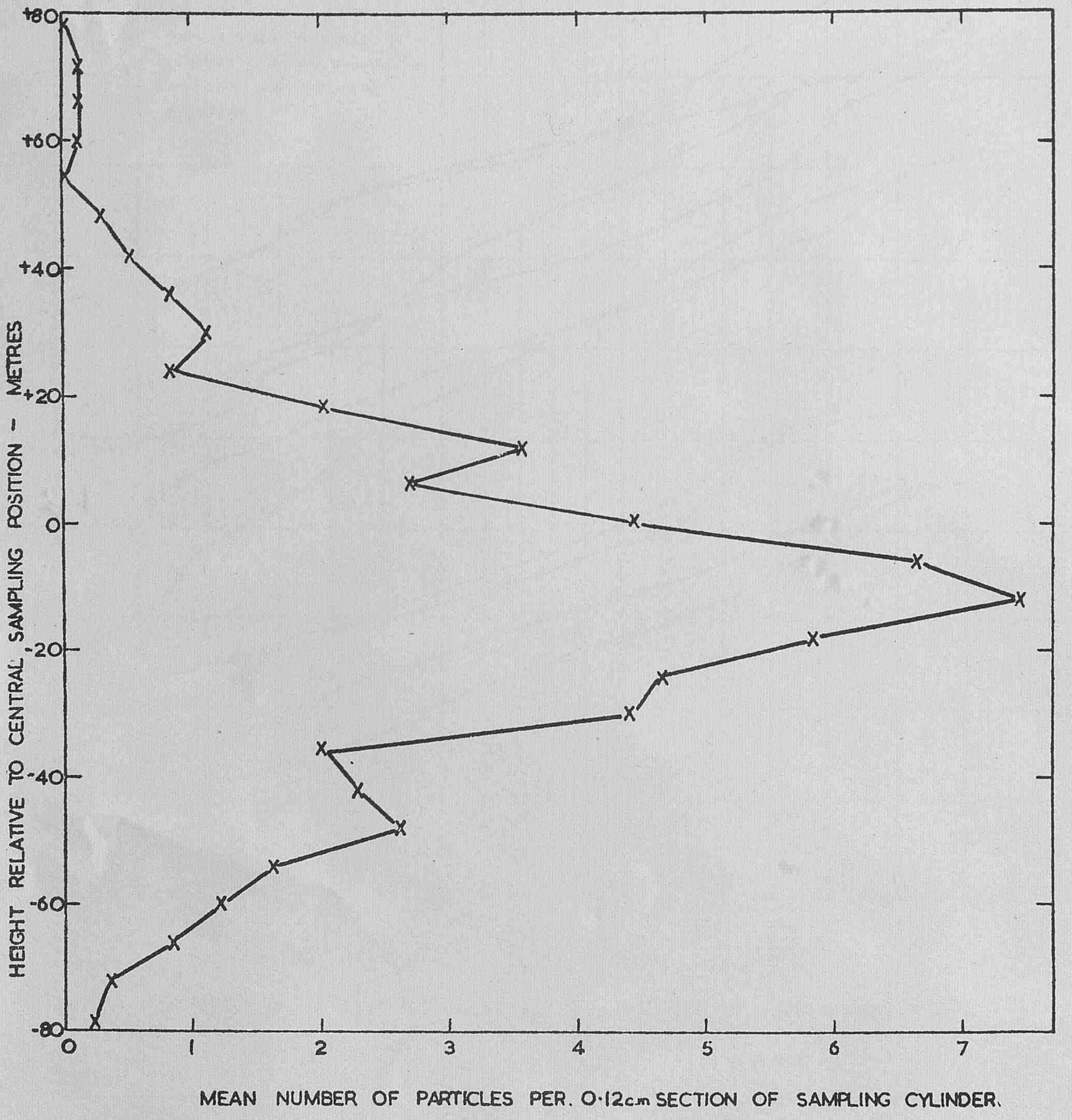

FIG. 1 VERTICAL DISTRIBUTION OF PARTICLES IN EXPERIMENT 17.

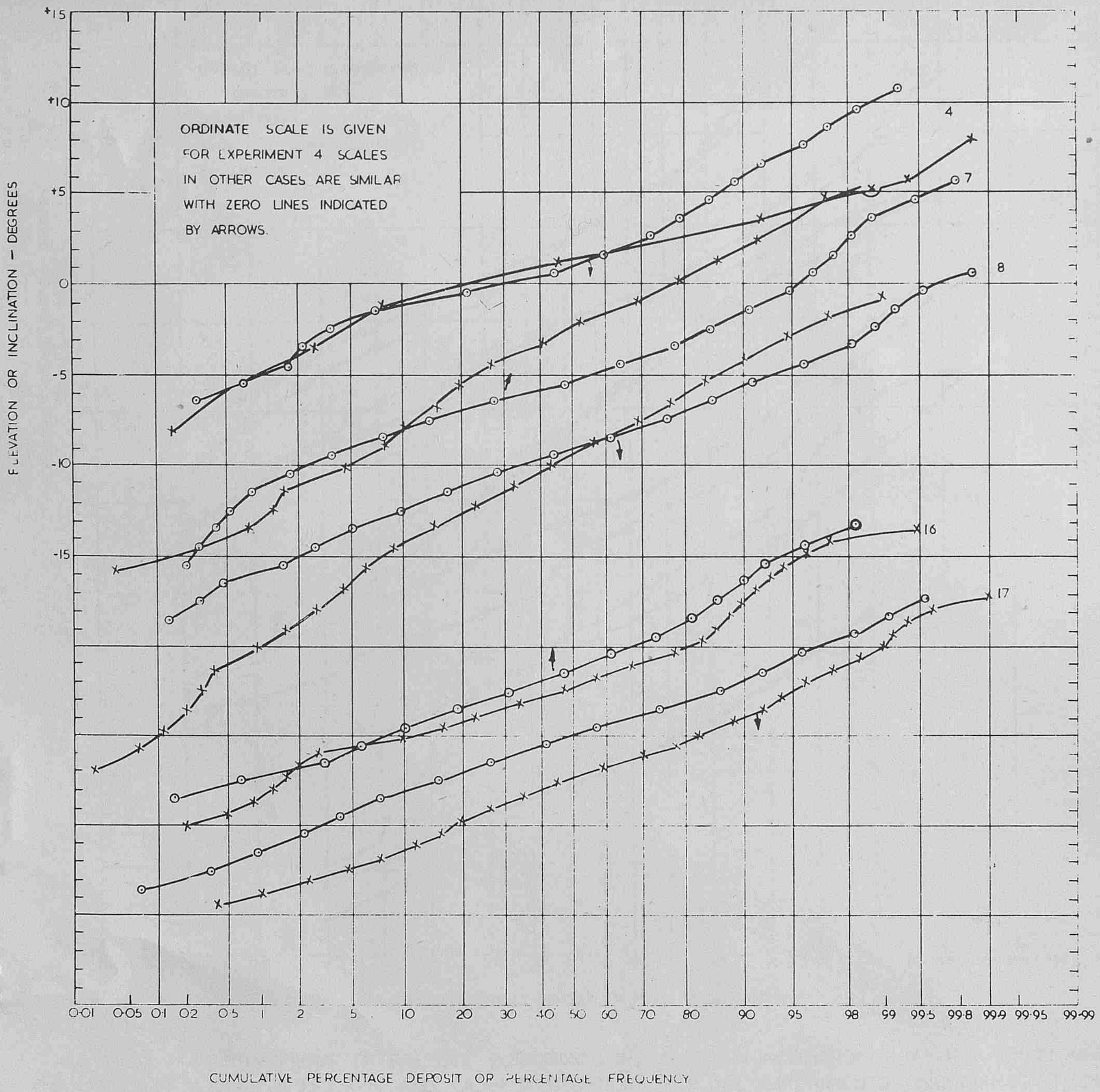

FIG 2. DISTRIBUTIONS OF PARTICLE ELEVATION (✱) AND WIND INCLINATION (⊖) FOR EXPERIMENTS 4, 7, 8, 16 AND 17

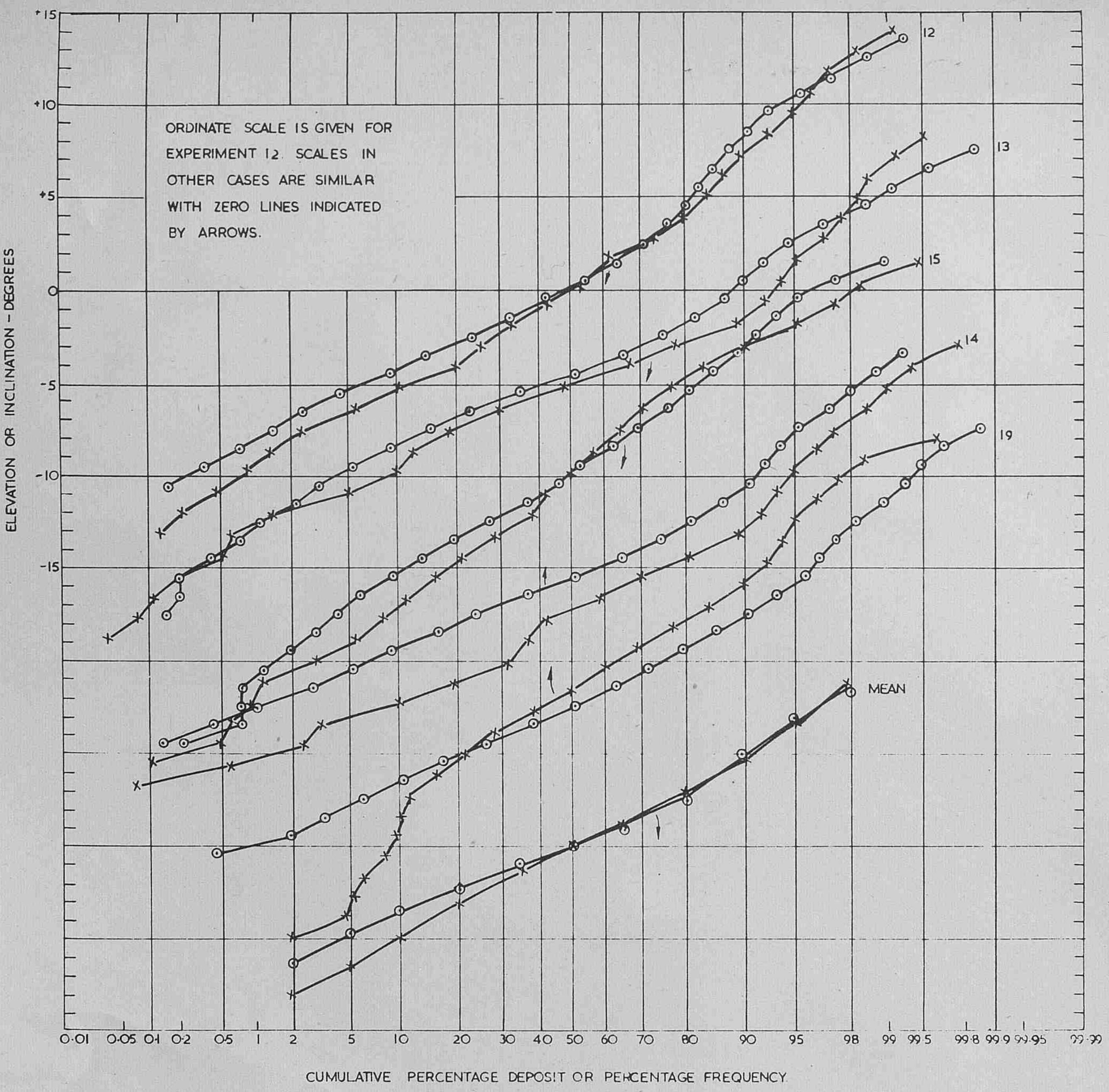

FIG. 3 DISTRIBUTIONS OF PARTICLE ELEVATION (-✱-) AND WIND INCLINATION (-⊙-) FOR EXPERIMENTS 12, 13, 14, 15 AND 19 AND MEAN DISTRIBUTIONS FOR ALL EXPERIMENTS INCLUDING THOSE IN FIG. 2.

M.R.P. 1009
S.C.111/220
29th October 1956.
A D 141025

A survey of the facilities and research programme of the Radar Research Station

by

W.G. Harper

(Meteorological Office)

AIR MINISTRY

METEOROLOGICAL RESEARCH COMMITTEE

At the time of issue this report has not been published. Any author desiring to quote this paper should refer to it as "A paper of the Meteorological Research Committee (London), M.R.P. No. 1009 by Mr. W.G. Harper. A copy is available in the Library of the Meteorological Office."

M.R.P. 1009
S.C.III/220
29th October, 1956

AIR MINISTRY
METEOROLOGICAL RESEARCH COMMITTEE

A survey of the facilities and research programme of the Radar Research Station

by

W. G. Harper (Meteorological Office)

Contents

1. Introduction
2. Brief history
3. Present equipment and site
4. Outline of work already done
5. Problems to which it is proposed to devote priority attention in the next year or two using existing equipment
6. Other problems to which attention can be given as circumstances permit
7. New equipment and site
8. Investigations using 8-mm radar
9. Conclusions
10. Reference

Appendix. List of papers.

1. Introduction

A survey of the facilities and research programme of the Radar Research Station at East Hill is particularly desirable at the present time for two reasons, first that tentative proposals for building development in the area suggest that East Hill will become untenable as a radar site within three to four years, and second that the existing 10-cm radar equipment, which has been in continuous operation for almost 10 years, cannot be expected to have a further useful working life of more than a few years, and would probably not stand transfer to a new site.

2. Brief history

The importance of radar in meteorological research was realised during the Second World War, and at its conclusion the easing of defence requirements enabled the Meteorological Office to take over the R.A.F. radar station at East Hill (2 miles northeast of the Central Forecasting Office, Dunstable) for meteorological research. A small staff was appointed and radar records commenced in 1947.

3. Present equipment and site

3.1. Equipment in use since 1947

The equipment taken over from the R.A.F. in 1947 is Radar A.M.E.S. type 21 Mk 1. It was designed for the detection and tracking of aircraft, but gives good responses from precipitation. Of high power and operating on 10-cm wavelength, it comprises two separate equipments, one designed for plan-position display, the other for range-height display. Essential characteristics of this equipment are given below:-

/3.1.1.

3.1.1. 10-cm plan-position radar (type 14)

(a) Characteristics

Peak power (nominal)	500 kw
Beam widths to half-power points	$1\frac{1}{4}^\circ$ in horizontal 6° in vertical
Pulse length	1.9 μ sec
Pulse recurrence frequency	500 sec^{-1}
Rotation frequency up to	4 rev min^{-1}
Display ranges	30, 60, 120 mi
Cathode ray tube	12 in. diam.

(b) The aerial is adjustable in elevation from 0° to 9°, but adjustment involves heavy manual labour, and the aerial is normally rotated with the centre of the beam 2° above the horizontal. This is a compromise relating to the obstructions in the vicinity of East Hill, and to the average height of the melting level of precipitation, for this usually gives the strongest echo and the best chance of detection.

(c) An upper aerial of the same horizontal beam width, but 12° wide in the vertical, is inclined $3\frac{1}{2}^\circ$ above the lower aerial. This gives a higher cover, which is of value when working with aircraft in the East Hill area.

(d) Slight modifications have been introduced to improve the performance of the equipment in precipitation, but the basic instrumentation is unchanged. Despite careful maintenance it is deteriorating with age. Its further useful life cannot be put at more than a few years.

3.1.2. 10-cm range-height radar (type 13)

(a) Characteristics

Peak power (nominal)	500 kw
Beam widths to half-power points	$1\frac{1}{2}^\circ$ in vertical $7\frac{1}{2}^\circ$ in horizontal
Pulse length	1.9 μ sec
Pulse recurrence frequency	500 sec^{-1}
Display ranges	75, 150 mi
Cathode ray tube	12 in. diam.

Sweeps continuously in elevation over the arc -1° to 20°, covering one complete cycle in 10 sec. Manual control in azimuth from the display panel.

(b) An alternative range-amplitude display (A-scope) is available on the type 13, but signal generator test equipment is not held, and neither the type 13 nor the type 14 can be calibrated absolutely.

(c) The remarks of 3.1.1.(d) apply equally to this equipment, and like the type 14 its further useful life cannot be put at more than a few years.

3.2. Equipment in use since 1949

3.2.1. 3-cm range-height radar (type AN/TPS-10)

(a) Characteristics

Peak power (nominal)	65 kw
Beam widths to half-power points	0.7° in vertical 2° in horizontal
Pulse length	1 μ sec
Pulse recurrence frequency	1000 sec^{-1}
Display range	60 mi
Cathode ray tube	12 in. diam.

Sweeps continuously in elevation over the arc -2° to 22°, covering one complete cycle in 1 sec. Manual control in azimuth from the display panel.

(b) A separate range-amplitude display is available, and with signal generator test set TS-263 echo intensities can be calibrated absolutely. This is a valuable feature of this equipment. More complete details have been given in M.R.P. 984.

(c) This radar is of American construction and is on indefinite loan to us from the Radar Research Establishment, Great Malvern.

(d) Replacements for electrical components are generally available, but spares are not held for all mechanical components and it is doubtful if some could be obtained. Thus breakdown of mechanical components will probably determine the life of this equipment.

(e) Spare equipment is at present mounted as a fixed vertical-looking aerial on amplitude display.

3.3. Equipment in use since 1953

3.3.1. 10-cm precision radar (type GL3)

(a) This type of radar is in general use in the Meteorological Office for upper wind measurement. It uses a split beam technique for the accurate measurement of azimuth and elevation of discrete targets such as corner reflectors, aircraft or "window" packets, and achieves considerable accuracy in range measurement by using a short pulse length, but is not suitable for use on extended diffuse targets such as precipitation echoes.

(b) Characteristics

Peak power (nominal)	250 kw
Beam width to half-power points	6° conical
Pulse length	1 μ sec
Pulse recurrence frequency	420 $\sec^{-1}$

Effective range up to 50 miles on a good corner reflector. Control is manual on range, elevation and azimuth, covering elevations 0° to 90° on any azimuth.

(c) Accuracy is about 20 yd in range, and 0.1° in elevation and azimuth on a good corner reflector.

3.4. Auxiliary equipment

3.4.1. Radio telephone (VHF)

Comprises duplicate transmitters BC-640C and receivers R1392D working on fixed frequency 105.48 Mc/s. Essential in aircraft co-operation flights.

3.4.2. C.R.D.F. equipment Mk 2

This equipment has been replaced at the stations of the "Sferics" network by the Mk 3 C.R.D.F., and the Mk 2 set formerly in use at Irvinestown has been acquired for studies of occurrence of lightning in relation to growth of cumulonimbus (see 5.2).

3.4.3. Camera obscura. For tracking smoke puffs fired from aircraft (see 5.5).

3.5. Present site

As propagation at radar wavelengths is essentially straight line propagation, modified only by refraction, an important range limitation is

/set

set by the curvature of the earth. Because of this curvature much of the distant precipitation to be studied is at very low elevations, and in meteorological research by radar a very open site is essential.

East Hill is a good site, but is not ideal. Its main limitations are as follows:-

(a) The escarpment of the Chilterns 2 miles SSE rises 250 ft above the station and presents a maximum obstruction of 1.3° in elevation. This means that all precipitation below 4,000 ft at a range of 30 miles, and below 9,000 ft at 60 miles in this sector is hidden from radar view.

(b) Isolated trees within $\frac{1}{2}$ mile of the station cast significant shadows when observing at low elevations on westerly bearings.

(c) East Hill is in an airway, and is just inside the London Air Traffic Control Area. This makes co-operation with aircraft difficult, and with tightening aircraft control regulations has latterly prevented all flight in cloud in the East Hill area. There are restrictions also on visual flight when cloud is present.

4. Outline of work already done

A list of papers originating from East Hill is given in the Appendix.

The unique properties of the radar in demonstrating accurately the vertical and horizontal extent of precipitation occurring simultaneously over a wide area have been used in a number of studies. In particular considerable effort has been devoted to the study of shower and thunderstorm clouds. It has been possible to direct instrumented aircraft into the most active parts of such clouds and important relationships have been established between the radar echo characteristics of the cloud and the turbulence encountered within the cloud. This has made it possible to assert with confidence that an aircraft fitted with radar would be able, by avoiding the echoing volumes of cloud, to avoid the most severe turbulence encountered in these clouds. Airborne radar for this purpose is now coming increasingly into use while ground radar is also being used with success for giving advice to pilots taking-off or about to land. Detailed examination of the records from the instrumented aircraft have also thrown light on the distribution and magnitude of the vertical currents within the clouds.

Information on the horizontal extent of cumulonimbus clouds (from P.P.I. records and controlled aircraft flights) has also been obtained and used in an assessment of the distances over which aircraft may be exposed to severe icing. This has proved of value in the design of aircraft de-icing systems.

The development of new thunderstorm cells in relation to existing ones was the subject of one study and further work is desirable, while observations of lightning discharges on radar throw some light on the mechanism of the generation of electric charge within thunderstorms.

The examination of the vertical extent of weather echoes gave the first positive information of the heights at which large precipitation particles exist and led to conclusions regarding the different methods of formation of raindrops in layer and convective clouds.

The fact that radar echoes can also be received from volumes of the atmosphere containing large gradients of refractive index has been demonstrated and provided an explanation of some unusual echoes ("angels") which have been troublesome to aircraft controllers.

Investigation of the movement of showers and precipitation belts demonstrated the feasibility of short period forecasts of precipitation using radar and the results are now being applied in the London area.

The variation with height of rainfall has also been studied and is of value in assessing the contribution of coalescence between raindrops to the rate of rainfall. Information on the variation of rainfall with height is also required in rain erosion problems.

Drop-size distributions at different rainfall rates have been measured and used to deduce an empirical relationship between radar echo intensity and rate of rainfall, but an experimental check of the relationship by measuring echo intensity above recording raingauges encountered many difficulties (see, however, Section 5(i) below).

5. Problems to which it is proposed to devote priority attention in the next year or two using existing equipment

(i) The relation between radar echo intensity and rate of rainfall

Empirical relationships between echo intensity and rate of rainfall have been established in various parts of the world on the basis of mean drop-size distributions in rainfall determined by various techniques. A direct check of this relationship by measuring rainfall intensity at the same time as echo intensity has been attempted here in the past but has failed principally because of the lack of knowledge of how typical rainfall measured at one raingauge was of the whole large volume from which the radar echo was received. The establishment of a close network of recording raingauges at Cardington only 13 miles away and the ability to make intensity measurements with the narrow beam-width 3-cm equipment above this network makes possible a new assessment. A successful outcome of this experiment would enable an assessment of the potentialities of radar for measuring rainfall intensities over wide and small areas and may have application, for example, to the vexed question of measuring rainfall at sea.

(ii) Movement of belts of precipitation

Successive P.P.I. pictures of belts of precipitation associated with cold fronts, occlusions and troughs enable a very accurate determination of the speed of movement and orientation of these belts. The accuracy of measurement is greatly in excess of that which can be achieved using synoptic charts. Correlating the movements so determined with the upper winds measured at neighbouring radiosonde stations will determine the level governing the movement of these belts. A large amount of work has already been done on these lines and the results so far are encouraging. A high correlation, for example, between the movement of precipitation belts and the component of the wind at 700 mb normal to the belt would be of great forecasting significance.

(iii) Movement and life of showers and thunderstorms, development of new thunderstorm cells in relation to existing ones. The pattern of shower activity and its relation to synoptic developments

Only radar can give an accurate picture of the distribution, movement, development and decay of showers and thunderstorms.

It is common experience to find that on occasions when occasional showers are forecast over a wide area the actual occurrence of showers is by no means as random as the forecast implies. There is usually some order in the development and occurrence of showers although the reasons may be obscure. Any advance in the ability to forecast the occurrence of showers at a particular place would be welcomed. Similarly for thunderstorms.

Radar is also coming into use at aerodromes for the guidance of pilots and controllers in the avoidance of turbulent cloud at the crtiical times of take-off and landing. If a thunderstorm is near to an aerodrome it is important to know at what place relative to this storm new cells are most likely to develop.

Theodolite and radar studies of convective cloud should give a measurement of the location of the first precipitation within a cloud in relation to the total vertical extent and life of the cloud. This should throw light on the detailed mechanism and growth of shower clouds.

(iv) Short period forecasting

This involves examination of the reliability of short period forecasts of precipitation made by extrapolation of the movements of the radar echoes associated with precipitation. (At present being investigated by M.O.21 on the basis of information supplied from East Hill sets and from the Decca Type 41 set on Victory House).

6. Other problems to which attention can be given as circumstances permit

Brief outlines only of these problems are given.

(i) Measurements of the variability of wind with time and distance. Measurement of entrainment into cumulus cloud. Using "window" and precision G.L.III radar.

(ii) The development of lightning in cumulonimbus clouds. The stage of development of the cloud when lightning first occurs. Using C.R.D.F. and radar as lightning indicator. May throw light on the mechanism of generation of charge.

(iii) "Angel" echoes. These have proved troublesome at times on aircraft control radars and it would be valuable to know more precisely the reasons why, and the conditions under which, they occur.

(iv) Variation of rainfall in frontal precipitation, possible orographic effects. By relative intensity measurements on P.P.I. presentations. Cross-sections through fronts using synoptic data would be of value here.

(v) Variation in the "bright band" height as a guide to variation of melting level in precipitation.

(vi) Growth of drops and snowflakes during their fall. By measurements of signal intensity changes in the vertical.

(vii) Radar watch on "seeding" experiments, either small-scale by M.R.F. or large-scale by Porton.

7. New equipment and site

It is necessary to make some assumptions as to the probable future equipment of the Radar Research Station and of its future site insofar as they affect the future research programme. For this reason some of the more important factors relating to equipment operating on the various wavelengths are given below:-

7.1. Millimetric radar

(a) Research at millimetric wavelengths is included in the Meteorological Research Committee's programme, and it is hoped that progress will soon be possible on this item. Estimates for the construction of an 8.6 mm set have recently been asked for from various manufacturers.

(b) The choice of 8.6 mm wavelength is determined by the position of the absorption bands due to water vapour and atmospheric oxygen. Those for water vapour fall at 13.5 and 1.6 mm, but of equal importance are those due to oxygen at 5.0 and 2.5 mm. Minimum attenuation of about 0.11 db mi^{-1} occurs at about 8.6 mm. A secondary minimum (at 3.75 mm) of about 0.26 db mi^{-1}

between the oxygen absorption bands presents interesting possibilities, but the technical problems of contructing equipment at this short wavelength are very great.

(c) The reduction to millimetric wavelengths makes possible the detection of clouds containing large droplets or ice crystals, as distinct from precipitation particles of raindrop size, but attenuation limits the range of observation to about 10 mi. For this reason the main recording equipment should be vertical-looking, but through-the-zenith scanning would be a valuable additional feature.

(d) Lines of possible research with 8.6-mm radar are suggested in Section 8.

7.2. Centimetric radar

Centimetric radar is essential if studies of precipitation processes are to be continued. The range of possible wavelengths is from 3 to 10 cm, for beyond 10 cm the cost of equipment increases rapidly due to the very large aerials and the very heavy rotation gear involved. The possible wavelengths in the range 3 to 10 cm are discussed below:-

7.2.1. 3-cm radar

(a) No high-power all-purpose British 3-cm radar suitable for weather radar research is on the market, but a specially designed set has been in use for about two years in America, the AN/CPS-9, details of which have been published. It is of exceptionally high power for a 3-cm radar, with a peak transmitted power of 250 kw, and has a 1° conical beam. This permits good discrimination of weather echoes to considerable ranges. It can be rotated to give a plan-position display or scanned to give a range-height display, and can be switched from one type of rotation to the other in a few seconds. It has complete calibration equipment, a separate range-amplitude display, and special features such as an off-centre plan-position display. It seems to be ideally suited for meteorological research. The present cost of the CPS-9 is understood to be about $180,000 (£65,000). It is unlikely that a comparable British set could be designed and built for less, because the American cost is based on quantity production. (It is understood that three CPS-9s are to be installed in Europe by the U.S.A.F., including one at Sculthorpe in Norfolk.)

(b) Rain attenuation is more serious on 3 cm than on 10 cm, but this is balanced by the improved discrimination given by the narrower beam of the 3-cm equipment.

(c) An important consideration may be that aircraft are more difficult to detect on 3 cm than on 10 cm, and are easily lost from a narrow beam. This would hamper co-operation with the Meteorological Research Flight.

7.2.2. 6-cm radar

Proposals for using 6-cm radar as the best compromise between 3 and 10 cm have received much publicity, but it must be stressed that this is for airborne radar, where aerial size is strictly limited. 6-cm equipment has no merit over 10-cm equipment when aerial size is not prohibitive.

7.2.3. 10-cm radar

(a) This wavelength has been proved to be well-suited to both detection of precipitation and to accurate control of aircraft. It is probably the ideal for precipitation studies in co-operation with aircraft.

(b) Rain attenuation at 10 cm is negligible.

/(c)

(c) Equipment may be available from R.A.F. sources at considerably less cost than a specially designed 3-cm radar, though installation costs would be high. It would be more up-to-date than the 10-cm equipment now in use at East Hill, but like it would comprise separate plan-position and range-height radars. This is especially valuable when rapid development is taking place or when time-lapse photography of the displays is necessary. Separate sets also act as a valuable performance check on each other. One is not always conscious of loss of sensitivity on a single set.

(d) Some types of echo, e.g. layer-type "angel" echoes, and some faint echoes apparently from cumulus clouds, which have not by any means been completely investigated, are detectable on 10-cm radar but not on comparable 3-cm radar.

7.3. These factors suggest that the most valuable solution would be the acquisition of new 10-cm radar equipment, to be supplemented by our existing 3-cm range-height radar, which can be expected to have some further years of useful life, and by an 8-mm radar for cloud studies.

If new 10-cm equipment cannot be obtained, every effort must be made to transfer the present 10-cm sets to a new site and to prolong their life as much as possible by rigorous maintenance.

7.4. New site

The requirements of the research programme, involving co-operation with aircraft, and a low-level unobstructed radar beam for precipitation studies, severely limit the choice of a new site. It is clearly desirable that it should improve on the old if new and expensive radar equipment is to be acquired.

The most important present restriction is that on flying in cloudy conditions. When this involves short runs in cloud, with frequent changes of altitude, as is usually the case in this type of co-operation, the flights can at present only be made under full safety control within the radar coverage area of Farnborough. This precludes all such investigations with East Hill.

It is desirable that a new radar station should have the following features:-

(a) a very open site with unobstructed horizon

(b) a site within 40 miles either of Farnborough or of an area prohibited to other aircraft

(c) a site clear of airways, aircraft control zones and flight restrictions

(d) close contact with other research departments of the Meteorological Office.

The possibility of siting at Farborough itself is excluded because of the multiplicity of existing radars there, and the severe restrictions that the airfield controller would have to place on the use of meteorological research radar in bad weather conditions. From most other aspects such an amalgamation would be wholly beneficial.

A site near Basingstoke would qualify under (b) and (c). The sector clear of airways is here some 25 miles wide, but is still within 20 miles of Farnborough, and roughly 25 miles from Bracknell.

It is doubtful whether an area prohibited to other aircraft could be allocated to the Meteorological Research Flight. If one were it would probably be in a remote part of Britain with serious objections under (d) and possibly inconveniently far from Farnborough. However, the question is still under examination.

Some compromise on requirements is necessary, and a site at Bracknell has much claim to consideration. It would have ideal contacts under (d). It is about 10 miles north of Farnborough, and could work closely with controlled aircraft over and to the west of Farnborough in a restricted sector. The principal difficulty is that every change of course of the aircraft would have to be agreed, over radio-telephone, between three authorities - the Controller, the aircraft, and the meteorological radar station. Moreover Bracknell lies within the London Control Zone and within the Western Airway leading out of London, and is only 14 miles WSW of London Airport itself. The possibility of obtaining an unobstructed site in the Bracknell area is nevertheless being explored.

8. Investigations using 8-mm radar

(a) Basic survey of frequency of detection of various cloud types, and determination of factors which affect detection. Assessment of 8-mm radar as a cloud base and top indicator. It will be important to know in which clouds echo bases are a reliable guide to cloud base, and those in which the droplet distributions at cloud base are not detectable. Cloud photography and possibly a zenith cloud camera might be used with advantage, with a cloud searchlight for cloud-base measurement. Independent measurement of cloud tops is essential and no doubt M.R.F. could assist in this.

(b) Studies of the mechanism of development, maintenance and decay of cloud systems. It should be particularly useful in the case of non precipitating cloud, but the simultaneous study of precipitating clouds with 8-mm and centimetric radar should also yield results of very great interest.

(c) Interpretation of measured signal intensities in terms of drop-size distribution, preferably with simultaneous cloud-droplet sampling by M.R.F. The distribution of water particles and ice crystals in clouds and its relation to growth processes.

(d) 8-mm radar can be expected to make a valuable contribution to some of the studies already outlined, for example

6(iv) Frontal cross-section studies

5(iii) Early stages of cumulus growth up to the onset of precipitation

6(iii) "Angels" and other unexplained echoes on 3 and 10 cm may be more easily resolvable at 8 mm.

9. Conclusions

Useful research can be undertaken from the existing radar records and with the present and proposed radar equipment. It is suggested that while the Radar Research Station remains at East Hill, probably a period of three years, and while in-cloud flying in the East Hill area is restricted, special attention should be paid to the problems outlined in Section 5.

The research programme after this can be only tentative, but on the assumptions that a good site can be found at Bracknell, that high-power 10-cm equipment will be available, and that an 8-mm radar will be acquired, it is suggested that emphasis should be placed on (a) 8-mm radar studies, and (b) cloud and precipitation studies in co-operation with M.R.F.

10. Reference

Ryde, J.W. The attenuation and radar echoes produced at centimetre wavelengths by various meteorological phenomena. Meteorological factors in radio-wave propagation. Phys. Soc. and R. Met. Soc., London, 1946.

/Appendix

Appendix

Scientific papers originating from East Hill

A. Meteorological Research Papers

J.M.R.P. 99.	Relation between radar echo intensity and rate of rainfall.
M.R.P. 453.	Size distribution of raindrops.
M.R.P. 458.	Heights and temperatures at the tops of radar echoes associated with various cloud systems.
M.R.P. 482.	Detection of icing conditions by radar.
M.R.P. 484.	Relation between radar echoes from cumulus and cumulonimbus clouds and the turbulence within those clouds, Pt. 1.
M.R.P. 535.	Horizontal dimensions of cumulonimbus clouds at various heights.
M.R.P. 564.	Distance over which an aircraft flying on a constant heading may experience severe icing in convective cloud conditions.
M.R.P. 593.	Relation between radar echoes from cumulus and cumulonimbus clouds and the turbulence within those clouds, Pt. 2.
M.R.P. 613.	Thunderstorms of 5th June, 1950 as seen by radar.
M.R.P. 683.	Aircraft observations of radar-reflecting particles above the freezing level.
M.R.P. 741.	Radar echoes from atmospheric inhomogeneities.
M.R.P. 784.	Observations of smoke puffs at heights up to 40,000 ft.
M.R.P. 820.	Five flights through a thunderstorm belt.
M.R.P. 984.	Variation with height of rainfall below the melting level.

B. Other papers and reports

(a) Radar weather echoes, Pts. I-IV. Met. Mag., Apr.-July, 1950.

(b) Thunderstorm tracks by radar. Weather, June, 1950.

(c) Turbulence in relation to the radar echoes from cumulonimbus cloud. Proc. Third Radar Weather Conf., McGill, 1952.

(d) Radar echoes from precipitation. Mar. Obs., Jan., 1954.

(e) Radar echoes from lightning. Q.J., 80, 1954, 579.

(f) Radar echoes from and turbulence within cumulus and cumulonimbus clouds. Prof. Note No. 109, 1954.

(g) Weather radar in research and operations. Met. Mag., Feb., 1955.

Note. Where a paper appeared as an M.R.P. and was later published in another journal only the M.R.P. entry is listed.

Mets RU

M.R.P. 1010
S.C.I/119
23rd October 1956.

AD141024

~~1080179~~

Wind recording apparatus for the new Ballistic Range at Shoeburyness.

by

G.E.W. Hartley.

(Meteorological Office)

AWSSS
ROUTING SLIP

FILE	INFO	ACTION				
	2					
	1		TRSD		RCU	
				✓	SEC TSD	
			SDD			
X	3		TIPD		TECH INFO	
					SEC	

AIR MINISTRY

METEOROLOGICAL RESEARCH COMMITTEE

57-378

At the time of issue this report has not
been published. Any author desiring to
quote this paper should refer to it as "A
paper of the Meteorological Research
Committee (London),
M.R.P. No. 1010 by Mr. G.E.W. Hartley
A copy is available in the Library of
the Meteorological Office".

M.R.P. 1010
S.C.I/119
23rd October, 1956

AIR MINISTRY

METEOROLOGICAL RESEARCH COMMITTEE

Wind recording apparatus for the new Ballistic Range at Shoeburyness

by

G.E.W. Hartley (Meteorological Office)

Foreword

Item I.3. (b) was placed on the M.R.C. Programme to meet a requirement at Shoeburyness for measurements of head and side components of wind experienced by a shell along a 3,000 ft trajectory. The required accuracy of measurement, for the average wind over the whole 3,000 ft range, was 1 ft per second.

This accuracy requirement could not be met. It was not practicable to site the anemometer heads nearer than 30 ft horizontally from the trajectory, and, moreover, the height of the trajectory varies. Furthermore, only five towers were available to cover the length of the range. Sampling errors were therefore bound to be quite large. It was considered that something could be done to reduce sampling errors by using 10-15 second mean winds at each measuring point rather than 'instantaneous' (about one second mean) winds.

The anemometer

There are five sets of wind recording apparatus. Each set consists of a wind transmitter, mounted on a 30 ft steel tower, and a wind recorder, housed in a hut at the foot of the tower.

A wind transmitter is shown in Fig. 1. A five-bladed windmill is mounted at the rear end of a horizontal shaft, carried in ball bearings inside a horizontal tube. At the front end of the tube is a hemispherical nosed cylindrical housing containing a Type E.2. SYL Magslip, whose spindle is connected to the front end of the windmill shaft by a flexible coupling.

The tube and housing are mounted on a hollow vertical shaft carried in tufnol bushes, with a thrust ball bearing to take the weight. The vertical shaft is continued downwards to connect with the tubular steel direction rod to the direction recorder.

On the horizontal tube just upstream of the windmill is a vertical fin which holds the windmill into wind. The windmill is mounted at the rear of the horizontal tube so that rain will not blow into the horizontal shaft rear ball bearing.

The five wires from the Magslip are brought down through the hollow vertical shaft to slip rings carried in a housing at the foot of the shaft; brushes pressing on the slip rings are connected to a terminal block on the base of the instrument inside the housing. Below the housing is a 2-inch B.S.P. screwed T-piece, the side opening of which gives access to the direction rod coupling sleeve, and the lower opening provides a method of attachment to a 2-inch gas pipe carried on the tower; this pipe is brought down the tower to the hut below, and forms an enclosure for the direction rod as well as a support for the wind transmitter.

At the foot of the direction rod above the recorder is a flexible coupling, and below it a special clutch which enables the direction rod to be disconnected from the recorder, and replaced without losing orientation.

Wind recorder

This is shown in Figs. 2, 3, 4 and 5. It consists of a run-of-wind recorder, a cosine-of-wind direction recorder, and a synchronous motor driven strip chart mechanism with a chart width of 8 inches and chart speed of 6 inches per minute; the chart is marked with cross-lines at 1/10 inch (i.e., 1 second) intervals.

The chart after use is wound on to a receiving spool.

The run-of-wind recorder

The run-of-wind recorder will be seen at the left-hand side of Fig.3 and close-up in Fig.4. It consists of a Type E.2. SYL Magslip which reproduces the movements of the transmitting Magslip and drives, through a 100:1 worm reduction gear, a vertical spindle at the top of which is a heart-shaped cam. There are two diametrically opposite cam followers, connected together by a light tension spring, and both mounted on vertical spindles; one of these vertical spindles has at its upper end a special pen stirrup, in which rests a tubular pen 5 inches long. The purpose of the second cam follower and spring is to hold the pen-carrying cam follower in contact with the cam. Both followers have rollers to reduce friction.

The cam is so shaped that in 1 revolution the pen moves two inches across the chart and back again; and by means of a special pivoted pen stirrup the circular movement of the pen is converted into a linear movement. The pivoted end of the tubular pen dips into an inkwell carried on a bracket above the top of the stirrup spindle (see Fig.4.). The windmill is designed to make 100 r.p.m. per 10 m.p.h. wind speed, so that 1 inch of pen movement across the chart corresponds to 220 ft of wind flowing past the head.

Assuming a 1-minute chart run, 10 m.p.h. (= 880 ft per min.) will be shown by the pen moving across the chart and back again during a chart movement of 6 inches. The trace will not, of course, be a straight line because of changes in wind speed; but the total distance travelled by the pen across the chart from its starting point will give the run of wind.

Wind direction component recorder

This is shown in Figs.3 and 5. The direction rod from the transmitter is connected, through the clutch already described, to a system of sprockets and chain, cranks, slotted connecting rod and a sliding pen carriage. This is arranged to move the direction pen 2 inches across the chart and back for one complete revolution of the wind vane; but, due to the crank mechanism, the pen movement is not linear with direction but is proportional to the cosine of the angle between the wind direction and the line of the range. Thus when the wind is exactly along the range, the pen is at one end of its travel, i.e., 1 inch to, say, right of centre. When the wind is at right angles to the line of the range the pen is at its central position; when the wind is exactly against range, the pen is at the other end of its travel, i.e., 1 inch left of centre.

Suppose that the angle between wind direction and firing direction is 30°, the pen will be 0.866 inches ($\cos 30^\circ = 0.866$) from its central position and on the positive (say right) side of it.

Backlash in the mechanism is reduced by the chain-tensioning jockey pulley which will be seen in Fig.3.

Chart mechanism and pens

The chart mechanism is a standard double-width chart mechanism made by Everett, Edgcumbe and Co. Ltd., and has a chart speed of 6 inches per minute;

charts are about 60 ft long. The chart is driven by a 230V. A.C. synchronous motor. The pens are made by the same makers, and consist of a length of small-bore tubing bent at right-angles at each end; the writing end carries a screw-on fine-bore writing nozzle; the other end has a cross-bar with knife edges which rest in V-notches in the pen stirrup, and balance weights to adjust the pressure of the pen on the chart; below the cross-bar is an inkwell; the downward-bent pen tube goes through a hole in the centre of the inkwell top cover to dip in the ink. These pens are started by suction. When not in use during intervals between recording they are taken from the instrument and kept in writing order by allowing them to write on a 'storage drum' which consists of a slowly moving chart mounted on a drum driven by a daily clock; this prevents their drying up, and makes it unnecessary to empty and clean them out whenever recording stops. The pens and inkwells are clearly shown in Figs.2 and 4.

Fig.6 shows a chart-reading desk made at Shoeburyness.

Summary

An anemometer and a recording mechanism were developed to meet a special requirement which arose at Shoeburyness. The apparatus has been in use at Shoeburyness for about a year and, apart from minor snags, has worked satisfactorily.

G.9906/JB/10/56/50

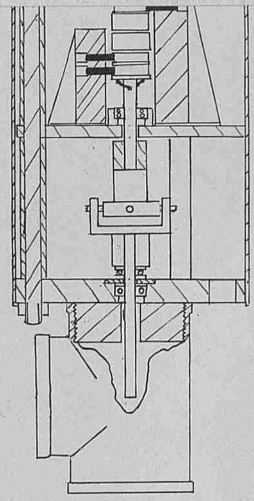

SHOEBURYNESS BALLISTIC RANGE

WIND SPEED AND DIRECTION TRANSMITTER

SCALE:— 0 1 2 3 4 5 6 INCHES.

FIG. 1.

of the stirrup spindle (see Fig.4.). The windmill is designed to make 100 r.p.m. per 10 m.p.h. wind speed, so that 1 inch of pen movement across the chart corresponds to 220 ft of wind flowing past the head.

Assuming a 1-minute chart run, 10 m.p.h. (= 880 ft per min.) will be shown by the pen moving across the chart and back again during a chart movement of 6 inches. The trace will not, of course, be a straight line because of changes in wind speed; but the total distance travelled by the pen across the chart from its starting point will give the run of wind.

Wind direction component recorder

This is shown in Figs.3 and 5. The direction rod from the transmitter is connected, through the clutch already described, to a system of sprockets and chain, cranks, slotted connecting rod and a sliding pen carriage. This is arranged to move the direction pen 2 inches across the chart and back for one complete revolution of the wind vane; but, due to the crank mechanism, the pen movement is not linear with direction but is proportional to the cosine of the angle between the wind direction and the line of the range. Thus when the wind is exactly along the range, the pen is at one end of its travel, i.e., 1 inch to, say, right of centre. When the wind is at right angles to the line of the range the pen is at its central position; when the wind is exactly against range, the pen is at the other end of its travel, i.e., 1 inch left of centre.

Suppose that the angle between wind direction and firing direction is 30°, the pen will be 0.866 inches (cos 30° = 0.866) from its central position and on the positive (say right) side of it.

Backlash in the mechanism is reduced by the chain-tensioning jockey pulley which will be seen in Fig.3.

Chart mechanism and pens

The chart mechanism is a standard double-width chart mechanism made by Everett, Edgcumbe and Co. Ltd., and has a chart speed of 6 inches per minute;

/charts

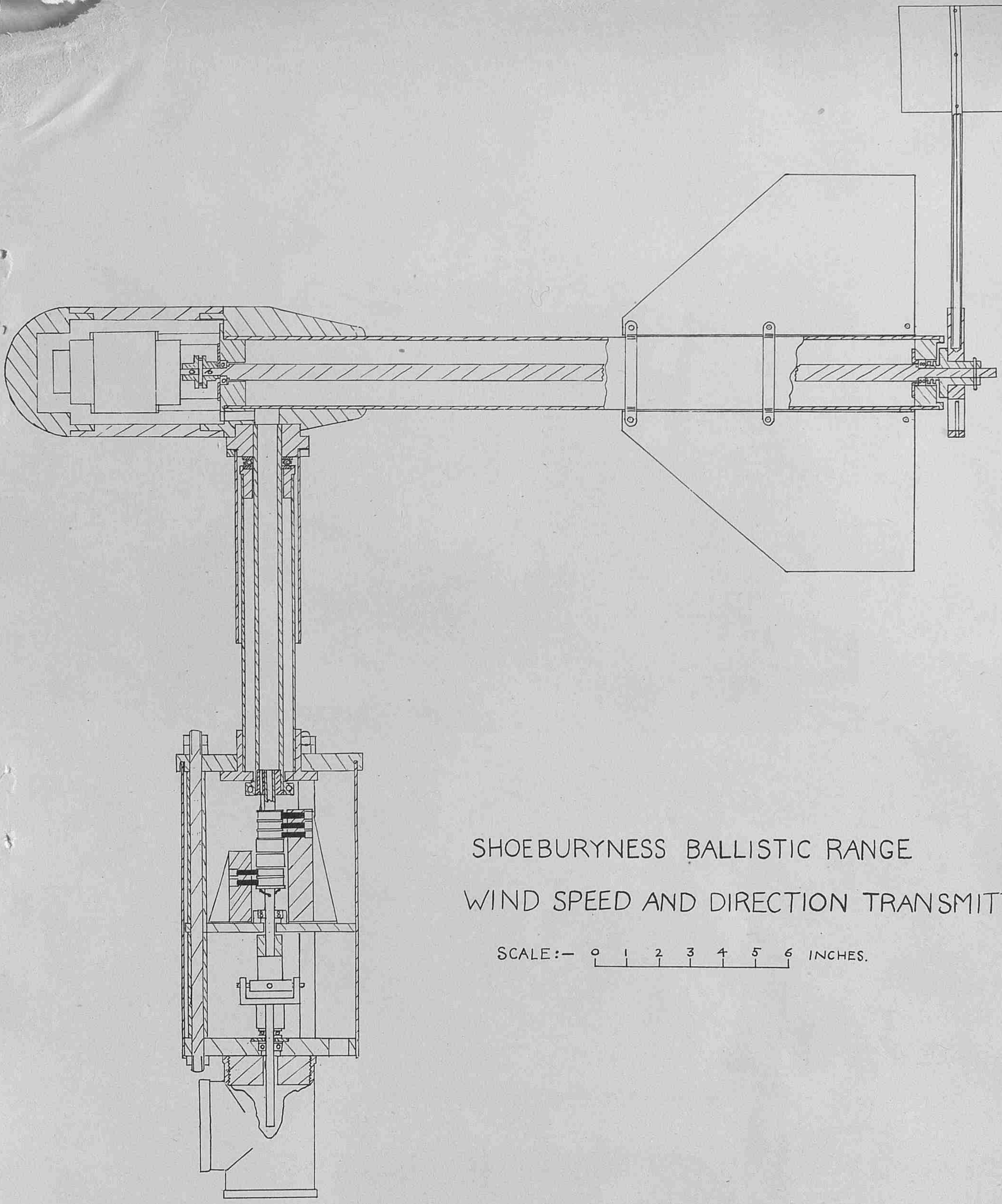

SHOEBURYNESS BALLISTIC RANGE

WIND SPEED AND DIRECTION TRANSMITTER

SCALE:— 0 1 2 3 4 5 6 INCHES.

FIG. 1.

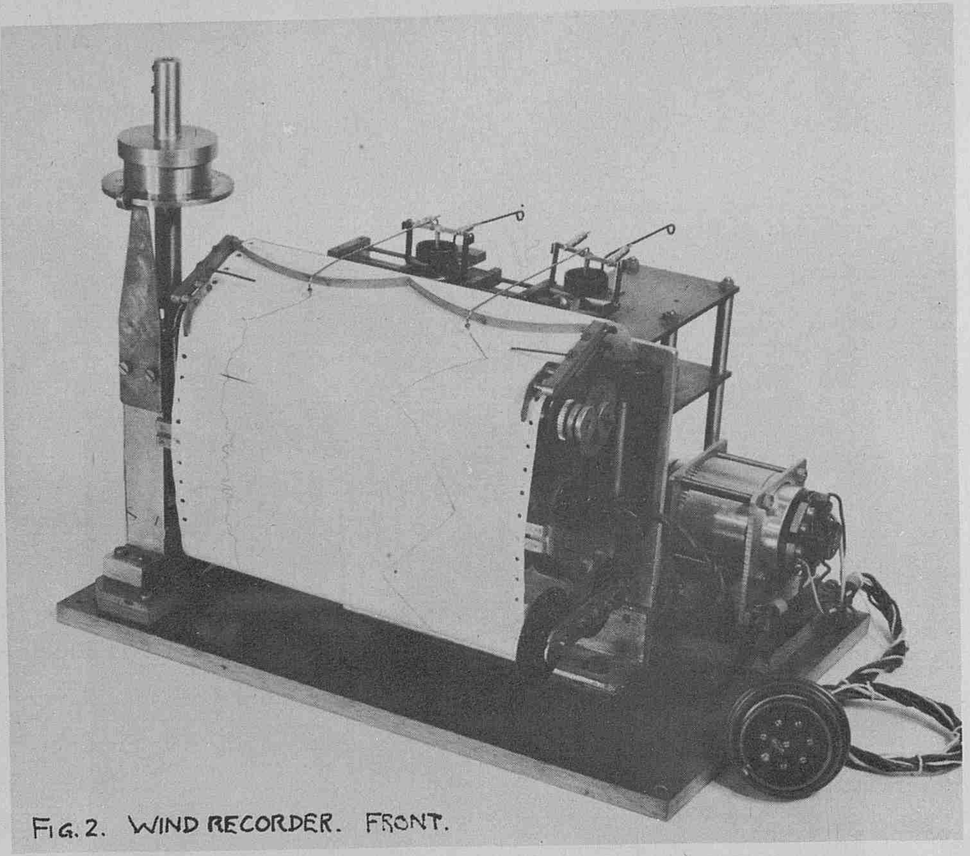

FIG. 2. WIND RECORDER. FRONT.

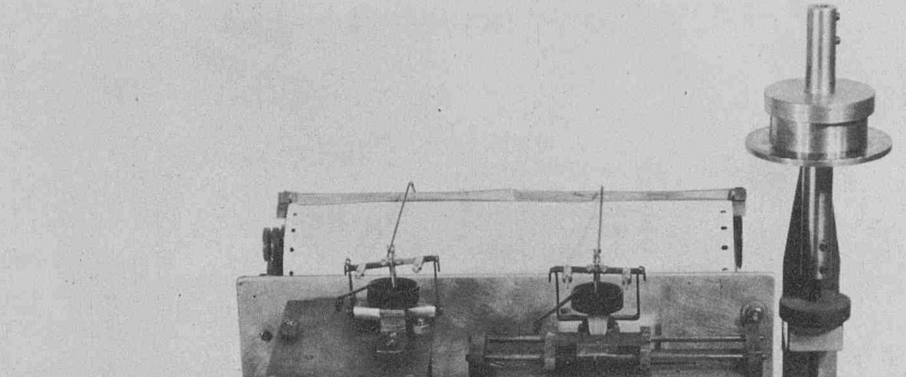

FIG. 3. WIND RECORDER. REAR.

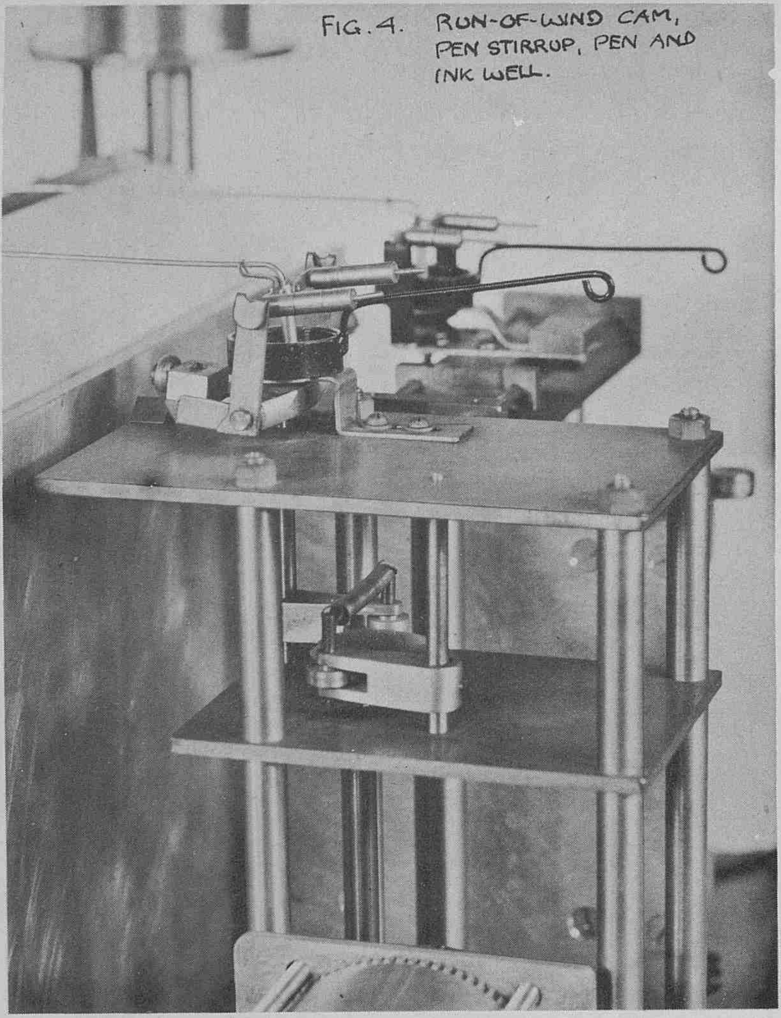

FIG. 4. RUN-OF-WIND CAM, PEN STIRRUP, PEN AND INK WELL.

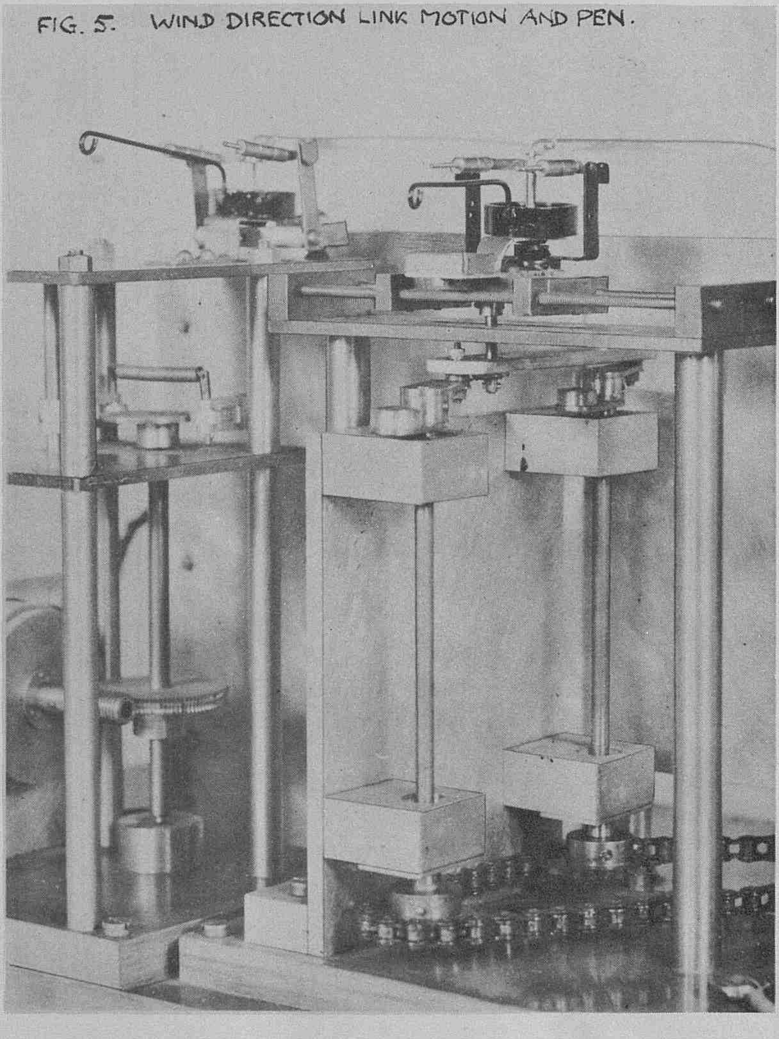

FIG. 5. WIND DIRECTION LINK MOTION AND PEN.

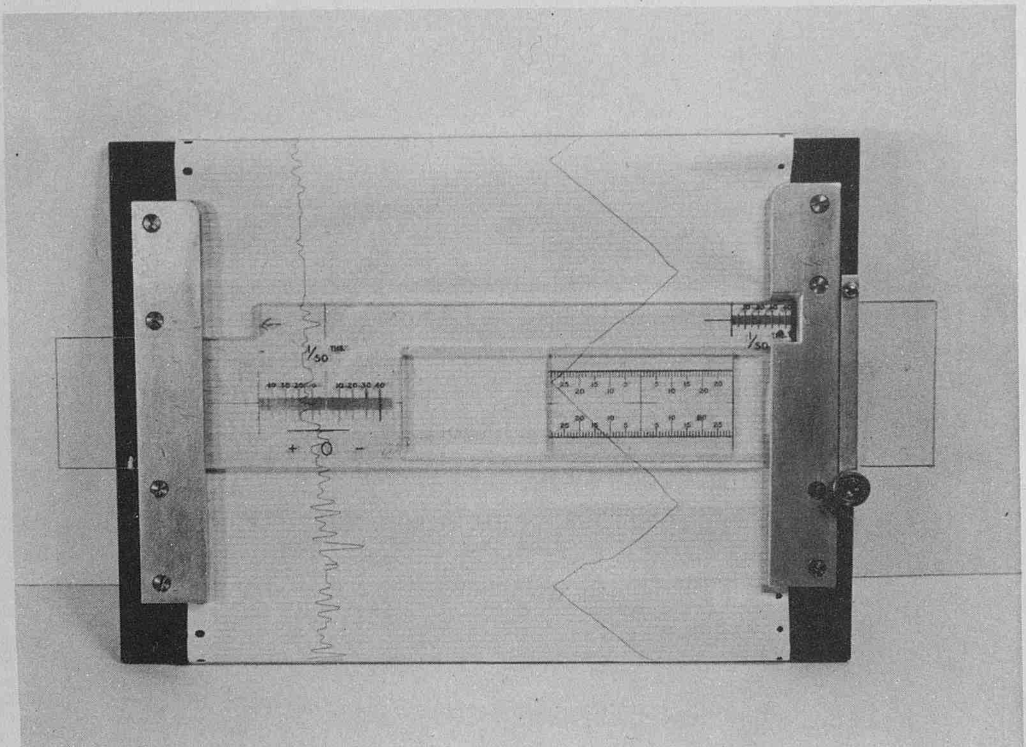
1/50 ins
40 30 20 0 10 20 30 40
+
0
−
1/50

FIG. 6. CHART READING DESK.

M.R.P. 1012
S.C.111/221
31st October 1956.

AD 141029

Atmospheric Nuclei.

An estimate of the value and practicability of routine measurements

by

B.C.V. Oddie.

(Meteorological Office)

AIR MINISTRY

METEOROLOGICAL RESEARCH COMMITTEE

At the time of issue this report has not been published. Any author desiring to quote this paper should refer to it as "A paper of the Meteorological Research Committee (London), M.R.P. No. 1012 by Mr. B.C.V. Oddie. A copy is available in the Library of the Meteorological Office."

M.R.P. 1012
S.C.III/221
31st October, 1956

AIR MINISTRY
METEOROLOGICAL RESEARCH COMMITTEE

Atmospheric Nuclei.
An estimate of the value and practicability of routine measurements

by
B.C.V. Oddie (Meteorological Office)

1. Introduction

At the 35th meeting of the Physical Sub-Committee of the Meteorological Research Committee, held on December 8th 1955, it was recommended that the value of regular ground level counts of freezing nuclei at selected stations should be considered. It was decided, therefore, to write a brief review of the position and, in view of an earlier recommendation of the Sub-Committee (29th meeting, April 2nd 1954), to consider also condensation nuclei and dust particles.

2. Dust particles

2.1. Dust is most usually collected for examination by directing a jet of dust-containing air onto a glass plate. Sometimes, as in the Owens counter, the air is first moistened to assist adhesion, but this seems not to be necessary if the speed of air through the jet is high. The deposit can afterwards be examined in various ways. If it is not too heavy, it can be examined under a microscope and the particles counted: but it is evident that the result of the count depends mainly on the resolving power of the microscope and has, therefore, little meteorological or physical significance.

2.2. F. Teichert (11) has very recently published a detailed study of methods of sampling and measuring dust, and he dismisses counting as a useless procedure. He shows by photographs how every increase in resolution of the microscope shows a very large proportional increase in the number of particles. To obtain a significant result, he says "one would have to observe the number of particles of each size and shape, so that the counting of a single dust-sample would be a whole day's work".

2.3. Even a simple count, it appears, is a fairly difficult task. Unfortunately, it has not been possible to consult anyone who has personal experience, but Teichert, after remarking that any apparatus, to be satisfactory, must be manageable by "average meteorological personnel" adds "counting of the particles, therefore, is out of the question".

2.4. It is certainly true that, although counts of dust particles have been made for many years, they have not been a very productive field of meteorological study. They have some relevance to problems of visibility, though even here the mere number of particles is not very useful unless the size-distribution is known, but they are of very little interest in the study of condensation and precipitation.

2.5. If it were decided to make observations of this character, the Owens dust counter would be the most readily available instrument. It is simple and robust, and the cost of equipment would not be great - probably less than £100 per station. But in view of the small meteorological interest of the results and the practical difficulties of counting, it is doubtful whether the attempt would be justified.

/3.

3. Condensation nuclei

The condensation nuclei of direct interest in meteorology are those which are responsible for the formation of cloud and fog. Since, so far as is known, relative humidities appreciably exceeding 100 per cent never occur in the atmosphere, the only nuclei of significance in meteorology are those which act at, or not much above, saturation.

3.1. The nuclei most commonly studied, however, have been the Aitken nuclei - nuclei activated by an instantaneous expansion resulting in supersaturations of anything from 10 per cent to 300 per cent according to the type of instrument. These Aitken nuclei are far more numerous than the true condensation nuclei, their concentrations ranging from a few thousand to a few hundred thousand per cc, whereas there are usually only one or two hundreds of cloud droplets per cc. So far, there is no evidence of any useful relationship between the number of Aitken nuclei and the number of the true condensation nuclei.

3.2. H. Dessens remarked (1) of the Aitken nuclei - "The majority .... are instrumental nuclei, defined, and perhaps created, by a particular type of apparatus: their influence on clouds and precipitation remains hypothetical".

3.3. This is a somewhat harsh judgment: the nuclei are certainly not created by the instrument, since filtered air gives no nuclei. Moreover, provided a supersaturation exceeding 10 per cent is employed, the count is almost independent of the supersaturation until very high values are reached. It can fairly be inferred that expansion instruments of the Aitken type do count everything that could be described either as a droplet or a solid particle and that they measure a real property of the air. Nevertheless, Dessens' final sentence is certainly justified, and the study of Aitken nuclei, though of some interest in itself, seems unlikely to contribute very greatly to other branches of meteorology. A glance at the titles of the papers read at the first Symposium on Condensation Nuclei (3) held in Dublin in 1955 immediately reveals the isolation of the subject. Moreover, a study which is primarily concerned with the number of nuclei, only indirectly with their size-distribution, and hardly at all with their constitution, seems a very incomplete one. One may foresee that it will eventually be linked closely with the rapidly developing subject of atmospheric chemistry, and that results of much greater scientific interest will emerge when the constitution of the particles is studied in relation to their size and number.

3.4. It might, nevertheless, be worth while to make regular measurements of Aitken nuclei at a few points in order to obtain some preliminary information on their dependence on synoptic conditions or other meteorological parameters. Similar work is being carried out at several places in Europe, and there should be opportunities for interesting comparisons. Such studies, however, entail a great deal of laborious statistical work and it is unlikely that any progress would be made unless at least one officer could devote a substantial proportion of his time to it.

3.5. The original Aitken counter, and others which resemble it in principle and method of observation, are very difficult to use, and not suited to routine observations. Pollak (2) has developed a photoelectric nucleus counter which is easy to manipulate and which can readily be made completely automatic. In this instrument a beam of light passes down a long tubular chamber, the walls of which are kept moist, and falls on a photocell at the far end. A sample of air is admitted, and a quantity of filtered air is pumped in to produce an over pressure. When sufficient time has elapsed for the air to become saturated, the over pressure is released and a cloud forms, the extinction coefficient of which is measured by the photocell. The concentration is then determined by an empirical calibration based on a comparison with an Aitken-type instrument.

3.6. All the operations of this measurement can be carried out by automatic valves and switches, and the results recorded on, for example, a recording milliammeter. Components would cost something under £100, and the apparatus could be assembled in the workshops at Kew Observatory, only about two weeks' work being required per instrument.

3.7. Hourly observations would be convenient for most purposes: for fog studies or other special purposes it would be easy to increase the rate to six per hour.

3.8. Sites which are not very liable to pollution from local fires, etc. are desirable. Lerwick, Eskdalemuir, Aberporth and St. Eval suggest themselves: the first two are not quite free from local pollution in the direction of the prevailing wind, but on the other hand they have Scientific Officer staff, which may be advantageous since one can hardly expect a newly-designed apparatus to give no trouble.

3.9. It might be thought more realistic to study, not the Aitken nuclei, but those which are active at rates of cooling comparable with those occurring in nature. The number of nuclei activated, however, increases rapidly as the rate of cooling is increased, so that the properties of the air-sample could only be represented by a table or curve relating these two quantities. This is not impossible, but the experiment is necessarily long and complicated, and would be unsuitable for performance as routine.

4. Freezing nuclei

It is generally accepted that freezing nuclei play an important part in the formation of precipitation, and it has been widely assumed that their presence or absence exercises an important degree of control over rainfall. Measurements of their availability must therefore be of great interest and importance; it is only necessary to decide (a) what quantity should be measured and (b) how the measurement should be made.

4.1. In considering a sample of air containing freezing nuclei, we require to know the number of nuclei which will induce freezing at any given temperature, as the sample is progressively cooled. Superficially, this appears to be a simple problem; it should only be necessary to take a sample of air, induce a cloud of droplets to form in it, and then cool it: the measurement would consist in noting from time to time the temperature which had been reached and the number of ice-crystals which had been formed.

4.2. Many such experiments have been carried out, and the results of some of them, including the best-known ones, are shown in Fig. 1 (reproduced from (4)). The enormous discrepancies, which are obvious at a glance, are certainly not real for the most part, but represent faults in the instruments. These have never been very fully or satisfactorily analysed: but the following are believed to be among the principal reasons for the lack of agreement.

4.2.1. The principal source of discrepancies, and the one of greatest theoretical interest, is concerned with the manner in which the droplet-cloud is formed. A freezing nucleus can only act if it is within a droplet - in other words, before it can act as a freezing nucleus, it must already have acted as a condensation nucleus.

4.2.2. If, then, the cloud is formed by gradually cooling the air-sample, either by external refrigeration or by expansion, droplets will form only on the particles which are active (as condensation nuclei) at low values of supersaturation. The result will be a cloud consisting of a comparatively small number of large droplets, formed on a particular class of particle. If a greater rate of cooling is employed, a higher degree of supersaturation will be momentarily produced, condensation will take place on more particles and therefore more will be able, if they have the right crystalline structure, to act as freezing nuclei.

/4.2.3.

4.2.3. The importance of the effect has, apparently, never been studied in detail. It is evident that a high supersaturation should lead to a greater total number of active nuclei, but its effect on the form of the freezing-nucleus spectrum - (that is the curve relating the number of crystals present to temperature) cannot be judged a priori. Findeisen and Schulz (5) used two different rates of expansion, equivalent to rates of ascent in the free atmosphere of 5 m/sec and 20 m/sec, and obtained two completely different spectra (Fig.2). In particular, ice crystals appeared at much higher temperatures when a low rate of expansion was used.

4.2.4. The tendency observed by Findeisen and Schulz is confirmed by the observations of Cwilong (6), who used a Wilson type of cloud chamber and almost instantaneous cooling: and found that no ice crystals appeared at temperatures higher than -27 to -32°C.

4.2.5. It appears from this discussion that the nucleating properties of a sample of air could only be satisfactorily described by a set of freezing-nucleus spectra, each one corresponding to a different rate of expansion - the relevant rate of expansion being of course that occurring at the moment when the cloud is formed.

4.2.6. A second possible source of discrepancy is the phenomenon of regeneration. Palmer (7) and others have demonstrated that ice crystals, once formed, have a certain power of regeneration by splintering. Findeisen and Schulz (5) noticed a phenomenon which may well be related to this -

"In many experiments, in which only moderately low temperatures are reached and therefore the number of ice crystals is in general still small, there appear occasional swarms of ice-particles, about 10-20 fragments, which are concentrated in a relatively small volume".

4.2.7. This suggests a possibility that the number of ice-crystals present may exceed considerably the number of nuclei present before freezing begins. It is evident that the longer we keep a growing ice-crystal under observation the more likely we are to see one of these explosions, if indeed they occur, and it may not be only chance that Findeisen and Schulz, who used an unusually deep chamber, are apparently the only experimenters to observe the phenomenon. Two things follow:-

(a) if one wishes to know the number of freezing nuclei present, one should use a fairly shallow cloud-chamber so as to reduce the risk of regeneration;

(b) the number of ice-crystals observed in a sample of air in a cold chamber may bear very little relationship to the number which would appear in the same air under natural conditions, even at the same temperature and with the same rate of cooling. On the whole the phenomenon seems unlikely to produce major discrepancies between the results of different instruments, although it may create serious difficulties in the application of the results to natural conditions.

4.2.8. Bigg (8) has shown that, at least in the case of pure water, there is not a definite temperature at which a given drop will freeze. There is only (in the case of a continuously cooled drop) a certain probability that the drop will freeze at any selected temperature below 0°C, and this probability depends upon the rate of cooling. It is probable, though so far as is known it has not been demonstrated, that the same rule holds for droplets containing freezing nuclei. If so, the form of the freezing-nucleus spectrum will be considerably affected by the rate of cooling of the sample at all stages of the experiment.

4.3. The difficulties which have been mentioned so far are fundamental to the problem - they would arise even if one could observe the behaviour of freezing nuclei in a natural cloud. In addition there are many instrumental problems.

4.3.1. Perhaps the most important is the settling both of droplets and of ice-crystals. If one operates with a chamber which is gradually cooled a great many drops, and especially the larger ones, settle-out and are lost before they crystallise. Again crystals are constantly settling-out, and if the quantity observed is, as usually, the number of crystals in suspension, this is the result of a balance between the rate of formation and the rate of settling, and there is no satisfactory way of relating this to the total number which has been formed. E.K. Bigg (private communication) has recently found a satisfactory means of overcoming this difficulty. He allows the crystals to fall to the bottom of the chamber, where they are caught in a shallow layer of a concentrated solution of sugar in water at a temperature of about -12°C. The crystals grow rapidly in this solution, each one developing within a few minutes into a perfect hexagon several millimetres across: these can be very easily photographed or counted. The method, evidently, is satisfactory only at low crystal-concentrations - one per cc at most - but these are in fact the concentrations of greatest interest. The problem of the settling-out of ice-crystals can, therefore, be regarded as solved: the settling-out of water droplets remains.

4.3.2. Even more important is the condensation of water on the walls of the chamber. This is bound to occur in any chamber where cooling is produced by cooling the walls, and takes place on a very large scale. Indeed, all such cloud chambers have to be constantly supplied with additional water, in the form of steam, in order to maintain the cloud - and this is in addition to the water released by cooling. This condensation must remove very large numbers of freezing nuclei from the air. Indeed, H. Cauer (9) has used the deposition of moisture on a polished metal surface as a particularly efficient method of collecting condensation nuclei.

4.3.3. When the cloud chamber is used for the study of freezing nuclei, periods of twenty minutes or more may elapse between the formation of the fog and some of the measurements. In this time the mass of water deposited will usually be comparable with, and may even exceed, the whole mass originally present, and the result of the experiment may be profoundly modified as a result of the loss of condensation nuclei. (Findeisen and Schulz appear not to have recognised this danger, perhaps because they believed that they were dealing with sublimation nuclei: at all events, in some experiments they deliberately dried the air by passing it through narrow tubes immersed in a cooling fluid.)

4.3.4. There are usually very large temperature differences between different parts of the experimental chamber - differences quite comparable with the whole range of temperature under investigation - and it is difficult to know what temperature to assign to a particular observation of crystal-concentration. Usually both temperature and concentration are measured near the centre of the chamber: but the air is in constant movement, and it is quite likely that the crystals one sees in the centre were formed close to the walls, where the temperature was several degrees lower.

4.4. It may be useful now to consider, in the light of what has so far been said, what sort of observation would be necessary and adequate for routine use.

4.4.1. The observation would need to yield a complete nucleus spectrum for a specified rate of expansion - a single constant rate of expansion throughout the experiment would probably be adequate.

4.4.2. Such an observation would be sufficient only if means can be found to adjust the nucleus spectrum for other rates of expansion.

4.4.3. The cloud chamber would need to be free from large internal temperature differences and designed so as to eliminate or correct for settling-out, deposition on the walls, and regeneration.

4.4.4. The means of counting crystals should be objective.

4.5. Without going into details, one may say at once that none of the methods of which accounts have yet been published approaches this specification. In particular, the only equipment of which the Meteorological Office has any experience, the "cold box" described in Ref. (1), has every one of the defects described in paras. 4.2. and 4.3. and it is impossible to feel much confidence in the significance of the variations registered by it.

/4.6.

4.6. Since the complete problem appears so intractable, it is natural to seek some simpler and more easily measured, but still useful, quantity. Thus Schaefer (10) has for some years made regular counts on Mount Washington of the nucleus concentration at a particular temperature (-18°C). The quantity thus measured is not a very useful one, being merely one point on the freezing-nucleus spectrum, the whole of which is needed for any useful application to the physics of precipitation. The Mount Washington count can be shown to vary from day to day, but the significance of the variations cannot be estimated.

4.7. Much more promising is the threshold temperature originally proposed by Cwilong (5). This is simply the highest temperature at which freezing nuclei are active. Many freezing-nucleus spectra show an increase in concentration from zero to several hundred per litre occurring within a few degrees Centigrade: and it is evident that if this were the general rule the threshold temperature would be the only important parameter; one would be sure that the whole of a natural cloud above the level of the threshold temperature was completely glaciated, and that all precipitation elements (or at least all those due to the Bergeron-Findeisen process) were derived from this level.

4.8. The value of the threshold temperature is unfortunately suspect for two reasons.

4.8.1. There is reason to think that it may vary considerably with the rate of cooling used to form the cloud. Some evidence on this question has already been presented in para. 4.2.1.- 4.2.4.

4.8.2. It is not certain that a considerable concentration of ice-crystals does in general develop immediately below the threshold temperature. In the observations made by the Meteorological Research Flight in January 1956 (4), for example, it was generally found that a few crystals, about $20/m^3$, were observed at relatively high temperatures, -5°C to -12°C. The number fluctuated irregularly but showed no systematic increase until a temperature of about -20°C was reached, when there was a rapid increase to a concentration of about 1 per litre or more. A third sharp increase, to a value of $10^4 - 10^5$ per litre, occurred at about -26°C. It is not suggested that the results of the M.R.F. are any more reliable than any of the others presented in Fig. 1: they have been examined in detail only because they happened to be readily accessible. Nevertheless, if taken at their face value, they suggest that the concentration increases in a slow and irregular (though by no means unsystematic) manner, and that there is in many cases no definite and clear-cut threshold temperature. The value of threshold temperature measured is, in these circumstances, likely to depend on the volume of air examined. If the instrument holds, say, only 200 cc of air, concentration of less than one particle per litre will generally be missed. This means that, taking the M.R.F.'s measurements as reliable, the observed threshold temperature is likely to be around -26°F and that the crystals formed at higher temperatures will be unnoticed. Yet these crystals may well be highly important, for in fact clouds are generally completely glaciated at temperatures of -16°C and often at considerably higher temperatures.

4.9. But in spite of these doubts, the threshold temperature is evidently deserving of further study, if only because of the great difficulty of finding any other manageable parameter. The principal objection, stated in para. 4.8.1., would vanish if it could be shown that there were a law connecting the threshold temperature with supersaturation.

4.10. Very recently E.K. Bigg (unpublished) has introduced a most interesting type of cloud chamber. It consists of a cylindrical vessel of ten litres capacity, maintained by external refrigeration at a temperature of -11°C. The bottom is entirely covered by a shallow dish containing sugar solution. The air to be sampled is admitted to the vessel, suitably compressed, and allowed to take up the temperature of the vessel. The pressure is then released, causing adiabatic cooling to some predetermined temperature, and a cloud, containing some ice-crystals, results. The crystals fall into the sugar solution. After a few minutes the cover is removed from the instrument and the crystals, now grown to an easily-visible size, are counted.

4.10.1. This instrument fulfils an unusually high proportion of the conditions set out in para. 4.4. above. It yields a complete nucleus spectrum for a given rate of expansion (i.e., for instantaneous expansion). Internal temperature differences are small because no observation windows are necessary, and therefore the chamber can be completely surrounded by the coolant. No error arises from settling-out of crystals; nor even from the deposition of moisture provided the air is originally dry enough to be cooled to -12°C without condensation occurring (it will therefore be most reliable when used in an aircraft or on a mountain where the temperature is low). The chamber is large enough to ensure detection at concentrations of one per litre or even less but small enough to make it probable that regeneration is negligible. In fact, only two doubts - both very serious ones certainly - remain. These are

(a) Can results obtained with instantaneous expansion be corrected in some way to make them applicable to rates of expansion comparable with those occurring in nature?

(b) Are serious errors introduced because the minimum temperature attained as a result of expansion is held for an instant only, as Bigg's researches (8) suggest may be the case?

4.10.2. Evidently some research on these two problems is desirable. Meanwhile, it can only be said that of all the instruments which have been employed hitherto, this appears by far the most promising. Dr. E.G. Bowen (C.S.I.R.O.) has kindly offered to supply an instrument for use in this country, probably early in 1957, and it will then be possible to form a better idea of the instrument's capabilities.

5. Conclusions

5.1. Counts of dust particles by means of the Owens dust counter appear to have no significant applications to general meteorology, and it is doubtful whether they would justify the expense and time which they would demand.

5.2. Counts of Aitken nuclei likewise seem to have no significant applications unless supplemented by information on their size and nature. The subject is however developing rapidly and is receiving a great deal of attention in many counties. It is moreover possible that interesting relationships with other meteorological parameters will reveal themselves. Provided, therefore, that sufficient time can be allocated to the search for and study of such relationships, it is considered that it would be reasonable to begin regular counts at one or two places which are relatively free from man-made pollution. The counting can be done automatically and takes up little time.

5.3. Counts of condensation nuclei active at rates of cooling comparable with those occurring in the free air would probably be of greater interest than counts of Aitken nuclei, but the problem would necessarily be extremely complex and has not yet been attacked at all systematically.

5.4. Counts of freezing nuclei would undoubtedly be of very great interest, if they could be made under natural conditions. This however presents an extremely difficult practical problem, largely because the count is a function of so many variables.

/5.5.

5.5. The most readily measurable quantities appear to be

(a) the threshold temperature

(b) the complete nucleus spectrum for instantaneous adiabatic cooling.

Neither of these quantities can be applied with confidence to problems of precipitation, but it is possible that further research may reveal laws which will enable them to be so applied, or interesting relationships with other meteorological parameters.

5.6. No satisfactory instrument for measuring threshold temperature as routine has yet been designed - indeed there is not even a clear and accepted definition of threshold temperature - but the problem does not appear intractable.

5.7. Bigg's apparatus for measuring the nucleus spectrum for instantaneous cooling is not entirely unsuited to routine use, but is rather slow to use (about 15 minutes for each point on the curve) and moreover would need skilful operators.

5.8. In view of these difficulties, it is suggested that

(a) the Bigg cloud chamber which has been promised us by C.S.I.R.O. should be installed and operated as routine in some suitable station - again Lerwick or Eskdalemuir seems to be indicated.

(b) an instrument on the same principle should be designed and fitted in the M.R.F. Hastings or Varsity.

5.9. Experiments of the kind just indicated, however, can by themselves amount to little more than groping hopefully in the dark: the significance of their results cannot be assessed unless they are supported by fundamental researches on the behaviour of both condensation and freezing nuclei, particularly on the variations in the number of nuclei with variations in the rate of cooling. Such researches are likely to be difficult and to require somewhat complex apparatus: they would require the full attention of one Scientific Officer for at least two years. In addition, of course, the study of the results of freezing-nucleus measurements, which would necessarily consist of statistical comparisons with other parameters, would require a great deal of time.

References

(1) H. Dessens 1956 Bull. de l'O. du Puy de Dome.

(2) T.C. O'Connor and L.W. Pollak 1955 Geofisica pura e applicata, Vol. 32, p.139.

(3) Geofisica pura e applicata, Vol. 31.

(4) R.J. Murgatroyd and M.P. Garrod 1956 Meteorological Research Papers, Air Ministry, London, No. 998.

(5) W. Findeisen and G. Schulz 1944 Forsch. Erfshr. Ber. Reichs. Wetterd, Reiche A, No. 27.

(6) B.M. Cwilong 1947 Proc. Roy. Soc., A, 190.

(7) H.P. Palmer 1952 Meteorological Research Papers, Air Ministry, London, No. 702.

(8) E.K. Bigg 1953 Q.J. Roy. Met. Soc., Vol. 79, No. 342.

(9) H. Cauer Some problems of Atmospheric Chemistry. Compendium of Meteorology.

(10) V.J. Schaefer "Project Cirrus", Twentieth Occasional Report.

(11) F. Teichert Zeit. für Met. June, 1956.

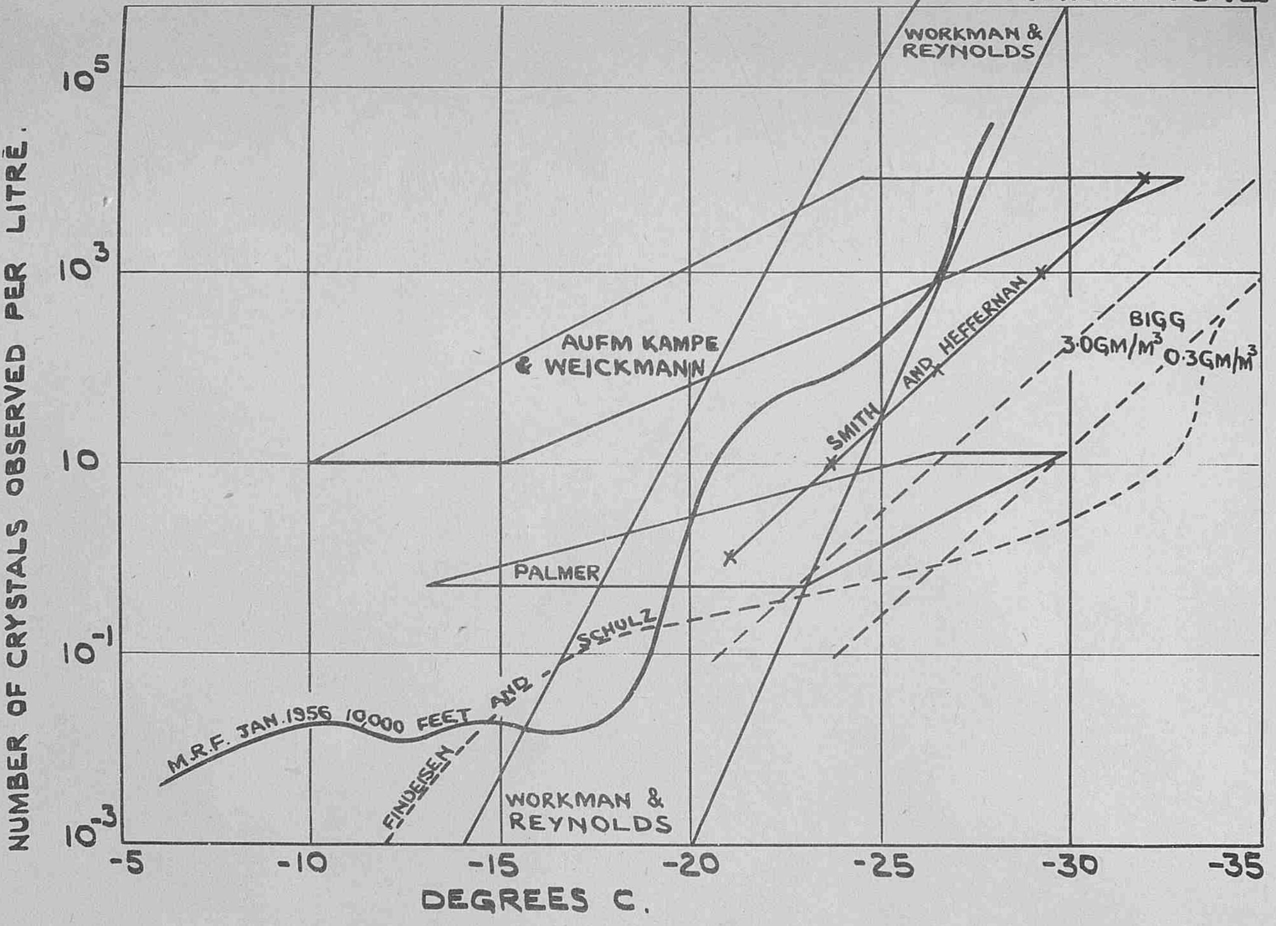

FIG.1. Concentration of freezing nuclei in air. Comparison of various measurements.

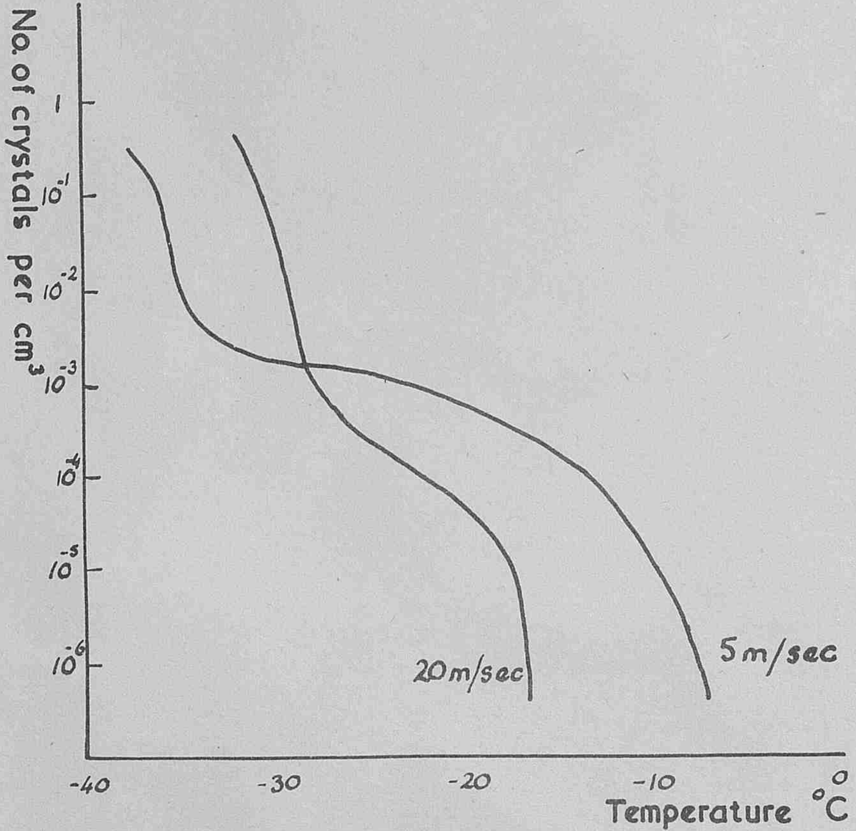

FIG.2. Average ice nucleus spectrum for surface air at Prague, obtained with rates of expansion corresponding to vertical speeds of 5m/sec and 20 m/sec. (after Findeisen and Schulz).

M.R.P. 1014
S.C. 111/222
12th November 1956.

AD 147509

A note on the published results of studies in atmospheric chemistry

by

B.C.V Oddie

(Meteorological Office)

AIR MINISTRY

METEOROLOGICAL RESEARCH COMMITTEE

At the time of issue this report has not been published. Any author desiring to quote this paper should refer to it as "A paper of the Meteorological Research Committee (London).
M.R.P. No. 1014 by Mr. B.C.V. Oddie
A copy is available in the Library of the Meteorological Office."

M.R.P. 1014
S.C.III/222
12th November, 1956

AIR MINISTRY

METEOROLOGICAL RESEARCH COMMITTEE

A note on the published results of studies in atmospheric chemistry

by

B.C.V. Oddie (Meteorological Office)

Introduction

1. M.R.P. 993 (1) recommended that the Meteorological Office should participate 'if only for the period of the Geophysical Year' in the programme of chemical sampling of the atmosphere which is now being followed by most countries of north-west Europe under the direction of Professor C. G. Rossby. M.R.P. 993 also stated that 'the value of this work to Meteorology was not yet proved,' and did not express any view as to whether it was desirable or not to maintain sampling stations in normal times.

2. The paper which follows is intended as a basis for a general discussion of policy with respect to chemical sampling. It is evident that sampling is most likely to yield interesting and useful results if it is carried out as a part of a widespread organisation, and therefore especial attention is given to the method now in general use in Professor Rossby's organisation. Other methods which have been, or might be, used are also briefly considered.

3. The technique of sampling now in general use in north-west Europe is an extremely simple one: the rainfall is collected in a funnel, while air is bubbled through a suitable absorbent solution. Both rainwater and solution are subsequently analysed for sodium, potassium, calcium, magnesium, sulphur, chlorine and ammonia, while the rainwater is also analysed for carbonate and nitrate: pH and conductivity are also measured.

4. Such observations are evidently not sufficient for a truly comprehensive study of the chemistry of the atmosphere. None of the major constituents is examined, nor are any chemical processes except those occurring in the lower atmosphere. There are even some known variables in the constitution of the lower atmosphere which are not considered, of which ozone is probably the most important.

5. The somewhat curious range of the subject is a consequence of its history. In the middle of the nineteenth century the scientific basis of plant feeding began to be understood and it was realised that nitrogen compounds were of great importance. It was natural then to enquire whether the plant could be adequately supplied either directly from the air or by salts brought down by the rain. For many years Liebig maintained that a plant could obtain all the ammonia it needed from the air, but his view was not universally accepted and much of the work done in the latter part of the nineteenth century, particularly at the Rothamsted Experimental Station, was concerned with this controversy. Once it was settled, interest in the subject declined: but it has remained, until very recently, the province of the agricultural research worker. Until the 1950s it was concerned almost exclusively with the inorganic chemistry of rainwater: and although the ions present in the free air are now also studied, the literature

/of

of the subject still deals principally with the analysis of rainwater. A comprehensive account of the chemistry of rainwater and a very full list of references is given by Eriksson (2).

6. Meteorologists first began to pay serious attention to atmospheric chemistry because of its evident importance in the study of condensation nuclei. Whereas the agriculturalists had been principally interested in nitrogen compounds, the meteorologists were principally interested in salt. But as soon as the distribution of sodium and chlorine ions in rainfall came to be studied, a very curious fact emerged. The ratio, mass of chlorine to mass of sodium, found in rainwater is (save at one or two places on very exposed coasts) usually substantially less than that found either in pure sodium chloride (1.5) or in sea water (1.8). Moreover, the farther one goes inland, the less the ratio becomes: typically, it is about 1.3 on the west coast of Scandinavia - the only region for which there is yet a substantial body of data - and diminishes to 0.6 or less in the east of Sweden.

7. This was a very unexpected result. That the total mass of salt brought down would decrease as distance from the windward coast increased was evident enough: but it had hitherto been assumed that, at whatever distance, it would still possess its original constitution. It is true that the result might have been explained if, as the salt was washed out of the air, some other sodium salt was progressively added. But there is no obvious source of this other salt in such quantities: moreover, the analyses show no trace of its anion. The only other explanation possible is that the salt removed from the sea is dissociated in some way, in itself a remarkable fact considering the stability of the material. Cauer (3) put forward the hypothesis that the sodium chloride was oxidised by the ozone present in the lower atmosphere, giving first free chlorine and then, by combination with water vapour, hydrochloric acid.

8. Cauer supposed that the hydrochloric acid remained in the air either as a gas or in the form of droplets of solution so small that they did not serve as effective condensation nuclei. Neither of these alternatives appears very attractive at first sight: but one or the other seemed essential to explain the fact that a great deal of the sodium is precipitated within two hundred miles or so of the coast, while the corresponding chlorine is not.

9. Rossby and Egnér (4) followed up the idea. Since the chlorine content of the atmosphere is certainly not increasing steadily, all this excess chlorine must return to earth at some stage. This might occur by direct absorption by the soil or plants: and there is also a possibility that it is precipitated as chlorates or hypochlorates which the sampling technique misses. But the authors dismissed these mechanisms and argued that, since rain in winds straight off the sea brought down excess of sodium, winds from some other direction, or in some other part of the world, must bring down excess of chlorine. They therefore sought for such occasions and found in fact that with southerly winds, which had had a land track of several hundred miles, the Cl : Na ratio was very high, reaching 3.5 at times. On the basis of his results, Rossby distinguishes four zones of chemical climate which are successively farther from the windward coast. These are

(a) A coastal zone where unaltered sea-salt predominates and the Cl : Na ratio in precipitation approaches 1.8.

(b) A zone where the salt is largely dissociated, and little chloride deposited: the Cl : Na ratio is low.

(c) A zone where little sodium remains, and the chloride, in forms other than NaCl, becomes the principal condensation nucleus: the Cl : Na ratio is high.

(d) A zone where most of the ions originating in the sea have already been lost: Cl and Na present are derived from the ground, where sodium is the commoner: the Cl : Na ratio is low, but the amounts of both are very small.

There is solid evidence for the existence of zones (a), (b) and (d) but the evidence for zone (c) is much less good, and the explanation which Rossby advances is largely hypothetical.

10. Meanwhile Junge (5) in America has worked on rather different lines. He has hitherto used only single observing posts, but his analyses have been more penetrating. Two classes of nuclei were separated out by a cascade impactor and analysed separately. These were 'giant nuclei' (0.8 to 8μ diameter) and 'large nuclei' (0.08 to 0.8μ diameter). At the same time, air from which virtually all particles had been removed by a millipore filter was analysed. Junge found that in the maritime air the Cl : Na ratio for giant nuclei was always substantially the same as in sea water, whereas in the large nuclei the ratio is much lower - about 0.5. Evidently, if we assume that the giant particles are precipitated earlier than the large particles, Junge's results go some way towards explaining the variable Cl : Na ratio without the necessity to assume dissociation at all. However, they do not provide a complete explanation because the total amount of Cl and Na in the large particles, per cubic metre of air, is far too small. Even more remarkable is Junge's discovery that the amounts of NH_3, SO_3 and SO_4 ions present in gaseous form are about ten times greater than the amounts present as nuclei, while the amounts of chlorine are about the same in the two forms. Evidently there are possibilities here of quite complex interactions and it is unsafe to interpret results in terms of water and salt, even dissociated salt, only. Junge also found very high concentrations of Cl, SO_4, NO_3 and NH_4 in the air near Frankfurt: but in this case they were mainly in the large nuclei. Junge concludes indeed that 'Almost all the large ions are of continental origin, even over the oceans' - a remarkable generalization. He remarks further, 'A real step forward in the understanding of the basic processes of air chemistry can be gained only if aerosols and gases are measured simultaneously but separately and if the aerosols, in turn, are separated according to size.'

11. One other conclusion of Junge's has a special interest: he believes that almost all the NO_3 in the atmosphere originates on the coast-line, which thus constitutes a 'line source'. The analysis of concentrations at various heights, using isolated mountains as sampling stations, might make useful contributions to the study of long range diffusion.

Discussion

12. A system of chemical analysis of the air should aim at the elucidation of at least the following questions -

(a) How and where are the 'chemical constituents' - using the term in the narrow and arbitrary sense discussed in paragraphs 3 to 5 - introduced into, or formed in, the air?

(b) How do they react, both chemically and physically, with each other and with the major constituents - oxygen, nitrogen, carbon dioxide and water in all its phases?

(c) How are they removed from the atmosphere?

(d) What are the effects of their variations on the other meteorological processes, particularly those of cloud-formation and precipitation?

13. A consideration of these requirements, particularly (a) and (c), at once suggests the absolute necessity of an extensive network of observing stations; there can be no other satisfactory means of identifying either the 'sources' or 'sinks' of material. Moreover, since there can be little doubt that rainfall is the most important 'sink' a study of the constitution of rain water is a necessary part of the investigation. In these respects, Rossby's methods have the advantage over Junge's. On the other hand, Junge's methods are probably the more powerful in the study of chemical processes in the atmosphere.

/14.

14. It is evident that there would be very great advantages in a combination of the two procedures, provided that the cost and problems of sampling were not prohibitive. A network such as this, yielding analyses of air, rain, and two sorts of aerosol would be in some danger of providing unmanageably large amounts of data: yet it would be by no means exhaustive. There are a number of additional quantities which could be measured, or additional refinements which could be made in the procedure and which may well be essential to the solution of the problem. The following are all theoretically possible extensions of the technique and, indeed, useful work has already been done on most of these lines of investigation.

(a) The period of sampling might be reduced, so that results for a particular synoptic type could be more readily isolated.

(b) The variations of chemical constituents in the vertical might be measured, e.g. by the systematic use of mountain stations, by balloons or aircraft.

(c) Ozone, carbon dioxide and possibly other gases now outside the scope of the investigation (e.g. methane) might be determined. (Measurements of ozone and CO_2 are of course made but they are not integrated into this investigation, although ozone is generally considered to play a vital role in atmospheric chemistry.)

(d) It is possible that useful additional information on the gaseous components could be obtained by spectroscopic methods.

(e) Junge's division of the aerosols into two size-classes and the point of division are somewhat arbitrary. It would appear desirable to discover how many chemically distinct classes there are and the best points of division: and to base further routine observations on this classification.

(f) Electrical conductivity of the atmosphere and ionic mobilities might be measured.

(g) The chemical content of rainfall might be studied in relation to drop-size, somewhat in the manner of Turner's work (6). Indeed, some study on these lines appears to be essential before any estimate can be made of the relationship between the mass of matter in suspension in the air and the rate at which it is brought down by rainfall. Turner did not measure the quantities in suspension, but his results clearly indicate that the relationship is not a simple one. Some improvement of his analytical technique would be necessary, since his assumption of a constant Na : Cl ratio is, as already shown in earlier paragraphs, no longer tenable.

15. The discussion of the last two paragraphs has related to questions (a), (b) and (c) of paragraph 12. With regard to question (d) - what are the effects of the chemical constituents on general meteorological processes? - it seems probable that ideas on the nature of condensation nuclei and perhaps of freezing nuclei will be profoundly influenced by the results of these chemical studies, and it is possible that the methods of atmospheric chemistry will have important applications in the study of long range diffusion. At all events, no theory of long range diffusion would be acceptable unless it were compatible with the observed phenomena of atmospheric chemistry. It is difficult to see how the influence of the subject could extend much farther than this in other fields of pure meteorology, although it is no doubt important in studies of meteorology applied to such subjects as agriculture, the deterioration of materials, and perhaps public health.

/16.

16. Any elaborations of the sampling technique, such as those discussed in paragraph 14, would be most productive if they were adopted by a selection of stations throughout the whole international observing network. It does not follow, however, that it is useless to discuss their application at British stations acting independently: indeed, since any of them would be fairly expensive, the international organisation would probably be reluctant to adopt them unless they had been tried out and shown to be essential or at any rate very valuable.

It would therefore be possible for valuable work to be done within the Meteorological Office on the subject of atmospheric chemistry, quite apart from any participation in the international system. But some expense would be entailed and, more important, at least one scientific officer would have to be directed to this work. Mere participation in the existing system of observation, on the other hand, entails little outlay either in money or time.

Summary

The studies in atmospheric chemistry which have been made in the last few years have led to a number of discoveries of great intrinsic interest, and have set a number of attractive problems. Most of these belong to the subject itself, but they have a limited importance in other branches of meteorology.

It would be possible for the Meteorological Office to participate in the existing network of observing stations in north-west Europe without any important outlay in money or time. This network has made great contributions to the subject, and its usefulness is certainly not yet exhausted; but the sampling technique is rather crude, since it does not permit the contribution to the sample of the gaseous ions and of the various classes of particle to be distinguished. It is likely that the need for an improved technique will be felt more and more in the next few years and there is scope here for much useful work, if the time could be found for it.

References

(1) R.M. Goody and P.A. Sheppard. Chemical sampling of air and rainwater. Meteorological Research Papers, Air Ministry, London, No.993.

(2) E. Eriksson. Composition of atmospheric precipitation. Tellus, Vol. 4, Nos. 3 and 4.

(3) H. Cauer. Ergebnisse chemisch-meteorologischer Forschung. Archiv für Meteorologie, Geophysik und Bioklimatologie. Serie B, Band I, pp. 221-256.

(4) C.G. Rossby and H. Egnér. On the chemical climate and its variation with the atmospheric circulation pattern. Tellus, Vol. 7, No.1.

(5) C.E. Junge. Recent investigations in air chemistry. Tellus, Vol. 8, No. 2.

(6) J.S. Turner. The salinity of rainfall as a function of drop-size. Q.J. Roy. Met. Soc., 81, No. 349.

M.R.P. 1015
S.C. 11/220
30th November, 1956

AD 223121

The air flow over a ridge - the effects of the upper boundary and high - level conditions

by

G. A. Corby and J. S. Sawyer

(Meteorological Office)

AIR MINISTRY

METEOROLOGICAL RESEARCH COMMITTEE

At the time of issue this report has not been published. Any author desiring to quote this paper should refer to it as "A paper of the Meteorological Research Committee (London).
M.R.P. No. 1015 by Messrs. G.A. Corby and J.S. Sawyer
A copy is available in the Library of the Meteorological Office."

M.R.P. 1015
S.C.II/220
30th November, 1956

AIR MINISTRY
METEOROLOGICAL RESEARCH COMMITTEE

The air flow over a ridge - the effects of the upper boundary and high-level conditions

by

G. A. Corby and J.S. Sawyer (Meteorological Office)

(In this paper the symbol ≒ is used to denote "equals the real part of".)

Introduction

A differential equation can be derived to represent the flow of air over a ridge. If attention is confined to the two-dimensional problem and small perturbations only are considered, the equation can be linearised and takes on a simple form.

The problem of obtaining the flow over a particular ground profile consists of determining the solution of the equation subject to suitable boundary conditions. The boundary condition at the ground is imposed directly by the requirement that the velocity there should be everywhere parallel to the ground, but additional conditions are also required to be applied either at some artificial boundaries introduced to limit the problem in the vertical and horizontal or at great heights and large horizontal distances. Only if adequate conditions of this nature are imposed does the problem become mathematically determinate.

It is usual to provide adequate boundary conditions at large horizontal distances by requiring that the disturbance to the flow should tend to zero for large distances upstream and should remain finite for large distances downstream. These requirements are based on an appeal to physical realism.

In the present paper we consider what boundary conditions should be applied at great heights and whether the introduction of an arbitrary upper boundary gives a justifiable approximation to the flow. The results of some computations using model airstreams including the stratosphere are presented to illustrate the effect on the flow of different characteristics in the airstream at high levels.

The physical problem

In the treatment of the problem by Scorer (1949), the flow is defined by ψ which is the departure of the stream function from its value in the undisturbed stream, and the differential equation obtained for small perturbations in two-dimensional flow takes the form:

$$\frac{\partial^2\psi}{\partial z^2} - \left(\frac{g}{c^2} + \beta\right)\frac{\partial\psi}{\partial z} + \left(l^2 - k^2\right)\psi = 0 \qquad 1$$

where z = height measured upwards

g = gravity

G.1337/MWW/11/56/50

where c = velocity of sound

β = static stability in the form $\theta^{-1}\partial\theta/\partial z$, θ being the potential temperature

$\ell^2 = \frac{g\beta}{U^2} - \frac{1}{U}\frac{\partial^2 U}{\partial z^2}$, a function of the stability and wind profiles in the undisturbed stream

U = undisturbed horizontal wind speed

k = 2π / (wavelength of the disturbance).

We wish to consider the behaviour of this equation for large values of z under conditions typical of the stratosphere. For simplicity we shall assume that in the stratosphere U and T are constant.

Then $\left(\frac{g}{c^2} + \beta\right) = -\frac{1}{\rho}\frac{\partial\rho}{\partial z} = \frac{g}{RT}$ 2

Also $\ell^2 = \frac{g\beta}{U^2} = \frac{\gamma-1}{\gamma}\,\frac{g}{RTU^2}$ 3

Hence in a uniform stratosphere Eq. 1 becomes

$$\frac{\partial^2\psi}{\partial z^2} - \frac{g}{RT}\frac{\partial\psi}{\partial z} + \left(\frac{\gamma-1}{\gamma}\,\frac{g^2}{RTU^2} - k^2\right)\psi = 0 \qquad 4$$

The solutions, corresponding to a known harmonic corrugation in the lower boundary of wavelength $2\pi/k$, have the form $\psi \doteq e^{mz}.e^{ikx}$

where $m = \frac{1}{2}\frac{g}{RT}\left\{1 \pm \sqrt{1-4M}\right\}$ 5

and $M = \frac{R^2T^2}{g^2}\left(\frac{\gamma-1}{\gamma}\,\frac{g^2}{RTU^2} - k^2\right)$ 6

As m may be real or complex these solutions represent waves whose amplitude increases or decreases exponentially (or is constant) with height or which vary harmonically in the vertical with increasing or decreasing (or constant) amplitude. In any given case the types of solutions which appear will depend on k, T and U.

Wholly real values of m

We first consider the case of real roots for m. This occurs when $4M \leq 1$, or, in terms of the wavelength, when $k^2 \geq g^2/R^2T^2\left(\frac{\gamma-1}{\gamma}\,\frac{RT}{U^2} - \frac{1}{4}\right)$

The solution $\psi \doteq e^{mz}e^{ikx}$ represents a wave which increases in amplitude with increasing height if $m > 0$ and the wave will decrease with height if $m < 0$. The wave fronts will necessarily be vertical.

There are thus three possibilities:

(i) If $M > 0$, both solutions represent waves which increase in amplitude with height.

(ii) If $M < 0$, one solution increases with height and the other decreases.

(iii) If $M = 0$, one solution has constant amplitude with height and the other increases.

In terms of k , the condition $M \gtrless 0$ becomes

$$k^2 \lesseqgtr \frac{\gamma-1}{\gamma} \frac{g^2}{RTU^2} \qquad 7$$

Before deciding, however, which solutions are relevant to our problem, we must note that as the density of the air decreases with height, the energy of the wave disturbance may decrease with height even when the amplitude increases with height. It would seem more appropriate to exercise discrimination in terms of the energy of the disturbance than in terms of the amplitude.

The kinetic energy of the wave motion is proportional to $\rho(u^2+w^2)$, where u and w are the perturbation velocities in the x and z directions

i.e., $$K.E. \propto \rho\left(\left(\frac{\partial\psi}{\partial z}\right)^2+\left(\frac{\partial\psi}{\partial x}\right)^2\right)$$

$$\propto \rho e^{2mz}$$

$$\propto e^{(2m-g/RT)z}$$

Thus the kinetic energy of the disturbance decreases with height provided $m < \frac{1}{2} g/RT$. Hence of those solutions under consideration, viz., real values of m , each pair comprises one solution having energy increasing with height and one solution with energy decreasing with height. The amplitude of the latter solution will itself decrease with height only if $M < 0$. There is, therefore, a narrow band of wavelengths corresponding to $0 < M < \frac{1}{4}$, for which one of the solutions, although having increasing amplitude with height, nevertheless has decreasing energy; but this band proves to involve only a very small range of wavelengths. For solutions within this band of wavelengths the amplitude will become so great at some heights that the basic assumption of perturbation theory (namely small amplitude) will become invalid. Nevertheless there is no reason to expect that, if the complete non-linear equations could be solved for these high levels, the order of magnitude of the energy would be altered. Consequently we accept as appropriate to our problem all solutions of Eq. 1 having energy decreasing with height. This is achieved by selecting the negative sign in the expression for m given in Eq. 5.

Complex values of m

If $4M > 1$, that is for wavelengths longer than a critical limit, m will be complex and the solutions take the form

$$\psi = e^{gz/2RT} \cdot e^{i(kx \pm Nz)}$$

$$\propto p^{-\frac{1}{2}} e^{i(kx \pm Nz)} \qquad 8$$

where $N = \frac{1}{2} g/RT \left\{4M-1\right\}^{\frac{1}{2}}$

$$= \left(l^2 - k^2 - \frac{1}{4} g^2/R^2T^2\right)^{\frac{1}{2}}$$

Hence

$$u = \frac{\partial\psi}{\partial z} \propto -\tfrac{1}{2} P^{-3/2} \frac{\partial P}{\partial z} \propto P^{-\frac{1}{2}}$$

$$w = \frac{\partial\psi}{\partial x} \propto P^{-\frac{1}{2}}$$

The kinetic energy of the disturbance is proportional to $\rho(u^2+w^2)$ i.e., to ρP^{-1} = constant. The kinetic energy does not, therefore, decrease with height for any wavelength in the range under consideration and the total kinetic energy above any level would appear to be infinite. However, such solutions occur only for the flow over an infinite series of sinusoidal troughs and ridges, and it can be demonstrated that for the flow over a ridge extending only a finite distance up - or down - stream the energy above any level is finite and tends to zero as that level is raised indefinitely. This difference arises because, as the energy is proportional to the square of the velocity, the energy at the various wavelengths in the range is not additive and the interference between waves of different wavelengths prevents the appearance of infinite energy.

The above discussion indicates that it is not possible to devise an adequate upper boundary condition for this range of wavelengths on the basis of energy considerations. The problem remains as to which of the two solutions given by Eq. 8, or what mixture of the two solutions, should be adopted.

We now consider the flow when a rigid upper boundary exists. This eliminates any ambiguity and renders the flow fully determinate. We shall then examine the flow as the rigid lid is removed towards infinity. If the flow at finite heights tends to a limit under these circumstances, the inference would be very strong that this limit is the appropriate choice for the unbounded atmosphere in nature.

Suppose our two-dimensional ridge is specified by the Fourier Integral:

$$\zeta_0 = \int_0^\infty e^{ikx} . F(k)\,dk \qquad 9$$

where $F(k)$ is real and necessarily bounded for all positive k, and let us assume that a rigid lid exists at $z = h$.

The general solution of our differential equation, as applied to a uniform airstream, is

$$\psi = e^{\frac{1}{2}\frac{g}{RT}z}\left(A e^{iNz} + B e^{-iNz}\right) e^{ikx} \qquad 10$$

where $N = \left(\ell^2 - k^2 - \tfrac{1}{4} g^2/R^2T^2\right)^{\frac{1}{2}}$

and A, B are constants which may be complex.

Put $\ell^2 - \frac{1}{4} g^2/R^2T^2 = L^2$. We are only concerned with the case of $L^2 > 0$, since otherwise m would not be complex for any real value of k.

By introducing the upper and lower boundary conditions into Eq. 10 we derive as the expression for the displacement of a streamline at height z in the undisturbed stream:

$$\zeta_z = \int_0^\infty e^{\frac{1}{2}\frac{g}{RT}z}\left(\cos Nz - \sin Nz \,.\, \cot Nh\right) e^{ikx} . F(k)\,dk$$

The part of the integral over the range $k > L$ corresponds to wholly real values of m, for which the upper boundary condition has been shown to be determinate from energy considerations. We need only consider, therefore, the range $k < L$.

We note that if $Lh > \pi$ the integrand has one or more poles in this range of k and as h becomes large, the number of poles increases. Thus the effect of the lid is to introduce lee waves, which become infinite in number as $h \to \infty$. It can be shown that individually they become infinitesimal in amplitude for large h except for the special case of $k = 0$ and $Lh = n\pi$, when the amplitude is indeterminate. However the shape of the mountain ridge is not sensibly altered by defining it as $\int_{\epsilon}^{\infty} e^{ikx} . F(k)\,dk$, where ϵ is small and positive, and this avoids the singularity.

Following the method established by Lamb (1932) for similar lee wave problems, we integrate by deforming the contour in the complex plane of k, noting that the integrand has no poles off the axes (see Fig. 1). That part of the displacement arising from the range $0 < k < L$ is thus given by:

$$\zeta'_z \dashv \Big\{ e^{\frac{1}{2}\frac{g}{RT}z} \int_{C_1} (\cos Nz - \sin Nz . \cot Nh)\, e^{ikx} . F(k)\,dk$$

$$+ \pi i \,(\textstyle\sum \text{residues at the poles}) \Big\} \quad \text{for } x > 0 \qquad 11$$

$$\text{and} \dashv \Big\{ e^{\frac{1}{2}\frac{g}{RT}z} \int_{C_2} (\cos Nz - \sin Nz . \cot Nh)\, e^{ikx} . F(k)\,dk$$

$$- \pi i \,(\textstyle\sum \text{residues at the poles}) \Big\} \quad \text{for } x < 0 \qquad 12$$

We now appeal to physical realism and annul the waves upstream by adding $\pi i\,(\sum$ residues) on both sides of the mountain, so obtaining as the practical solution in our problem:

$$\zeta'_z \dashv \Big\{ e^{\frac{1}{2}\frac{g}{RT}z} \int_{C_1} (\cos Nz - \sin Nz . \cot Nh)\, e^{ikx} . F(k)\,dk$$

$$+ 2\pi i \,(\textstyle\sum \text{residues at the poles}) \Big\} \quad \text{for } x > 0 \qquad 13$$

$$\text{and} \dashv \Big\{ e^{\frac{1}{2}\frac{g}{RT}z} \int_{C_2} (\cos Nz - \sin Nz . \cot Nh)\, e^{ikx} . F(k)\,dk$$

$$\text{for } x < 0 \qquad 14$$

We must now consider whether this integral tends to a finite limit as $h \to \infty$. Let $k = k_1 + i k_2$ along contour C_1

i.e., $\sqrt{L^2 - (k_1 + ik_2)^2} = N = N_1 + iN_2$, say,

or $N_1^2 - N_2^2 = L^2 - k_1^2 + k_2^2$

and $N_1 N_2 = -k_1 k_2$.

Now $N = +L$ when $k_1 = k_2 = 0$ and N_1 and N_2 must be of opposite sign. Thus in the first quadrant N_1 is +ve and N_2 is -ve. Hence $\cot Nh$ is of the form $\cot(N_1 - iN_2)h$ along C_1.

It can be shown that

$$\lim_{h \to \infty} \left\{ \cot(N_1 - iN_2)h \right\} = i$$

≠ Hence

$$\lim_{h\to\infty}\int_{C_1}(\cos Nz - \sin Nz \,.\cot Nh)\, e^{ikx} . F(k)\,dk$$

$$= \int_0^L e^{-iNz+ikx} F(k)\,dk$$

We now require to evaluate $\lim_{h\to\infty}$ $(2\pi i \sum$ residues).

The residue at a pole where $k = k'$, $N = N'$ is:

$$\frac{N'}{hk'}\,(\sin N'z)\, e^{ik'x} . F(k')$$

The poles occur where $Nh = 0, \pi, 2\pi, \text{-----} n\pi$

i.e., where $k = \left(L^2 - r^2\pi^2/h^2\right)^{\frac{1}{2}}$

$r = 0, 1, 2, \text{------} n$

Put $Lh = \pi\,(n + \alpha)$ where $0 \leq \alpha < 1$

Then the poles occur where $k = L\left[1 - r^2/(n+\alpha)^2\right]^{\frac{1}{2}}$

Hence $\lim_{h\to\infty} \sum$residues =

$$\lim_{n\to\infty}\left\{e^{\frac{1}{2}\frac{g}{RT}z}\sum_{r=0}^{n} e^{ik'x} F(k')(\sin N'z)\left(\frac{+L}{\pi(n+\alpha)^2\left\{1 - r^2/(n+\alpha)^2\right\}^{\frac{1}{2}}}\right)\right\}$$

$$= \frac{1}{\pi}\, e^{\frac{1}{2}\frac{g}{RT}z}\int_0^L e^{ikx} . F(k) \sin Nz \;\, dk$$

Thus $2\pi i$ ($\sum$ residues) $= 2i\, e^{\frac{1}{2}\frac{g}{RT}z}\int_0^L e^{ikx} F(k) \sin Nz \, dk$

Substituting in Eqs. 13 and 14 we see that

$$\int_z \varphi' = e^{\frac{1}{2}\frac{g}{RT}z}\int_0^L e^{+iNz+ikx} . F(k)\,dk \qquad 15$$

It would appear, therefore, that the proper solution is obtained by taking B = 0 in the general solution of Eq. 10. The same conclusion was reached by different methods by other authors, e.g., Queney (1947), Palm (1952), although Scorer (1949) adopted the choice A = 0. Scorer discusses the difficulties attendant upon this choice in a later paper (Scorer, 1954).

≠ It is easily verified that it is here justified to take $\lim_{h\to\infty}$ inside the integral sign.

The present treatment can be interpreted physically as follows. If there is a rigid upper boundary, then the flow of a uniform airstream over a ridge comprises a symmetrical disturbance over the ridge plus a large number of lee waves having wavelengths in the range $2\pi/L$ to ∞. The waves tend to interfere away from the ridge and as the lid is removed to infinity they annul completely for large x. They contribute, however, a finite disturbance in the neighbourhood of the ridge for positive x and the whole flow tends to a limit which is asymmetrical. It seems inescapable that this must be the solution appropriate to the unbounded atmosphere.

It is of interest to consider briefly the nature of the solutions obtained for a two-layer model in which the value of L is constant in the lower layer and zero in the upper layer. Under these conditions m is not complex in the upper layer for any value of k; accordingly there is no indeterminacy at high levels. As the depth of the lower layer is increased, more and more lee waves appear for values of k in the range $0 < k < L$ and these become infinite in number as the interface is removed to infinity. Once again the flow at finite heights tends to the asymmetrical limit corresponding to the choice $B = 0$ in Eq. 10. The proof is somewhat more lengthy but the artificiality of a rigid upper boundary is avoided.

The characteristics of certain model airstreams

In studying the character of the flow with specific model airstreams we shall use the simpler form of Eq. 1 as employed by Scorer (1949), who shows that that the character of the solution is not affected by omission of the central term in Eq. 1. The equation then becomes

$$\frac{\partial^2\psi}{\partial z^2} + \left(l^2 - k^2\right)\psi = 0 \qquad 16$$

If we wished we could allow approximately for the neglected middle term by multiplying the displacements of the streamlines deduced from Eq. 16 by the factor $(\rho_0/\rho)^{\frac{1}{2}}$, where ρ is the density and suffix 0 refers to the ground.

Suppose our model airstream comprises layers of depth a_1, a_2, ------ in each of which l is constant, the values of l being l_1, l_2, ------ and the suffixes being numbered from the ground upwards.

Then, if we adopt the upper boundary condition established above, the flow over the mountain profile given by

$$\zeta_0 \fallingdotseq \int_0^\infty e^{ikx} F(k)\,dk$$

takes the form:

$$\zeta_z \fallingdotseq \int_0^\infty \left(\cos \nu_1 z + f(k)\sin \nu_1 z\right) e^{ikx} F(k)\,dk \qquad 17$$

$$\text{where} \quad \nu_1 = +\left(l_1^2 - k^2\right)^{\frac{1}{2}}$$

The flow specified by Eq. 17 applies to the lower layer and for convenience we have assumed that the undisturbed wind speed U is constant with height, i.e., that the variations of l with height arise solely due to variations of static stability. The function $f(k)$ takes the following forms for two, three and four-layer models:

2 layers

$$f(k) = \frac{f_1}{f_2} = \frac{\nu_1 t_1 + i\nu_2}{\nu_1 - i\nu_2 t_1} \qquad 18$$

3 layers

$$f(k) = \frac{f_1}{f_2} = \frac{\nu_2(\nu_1 t_1 + \nu_2 t_2) + i\nu_3(\nu_2 - \nu_1 t_1 t_2)}{\nu_2(\nu_1 - \nu_2 t_1 t_2) - i\nu_3(\nu_1 t_2 + \nu_2 t_1)} \qquad 19$$

4 layers

$$f(k) = \frac{f_1}{f_2} = \frac{\nu_2(\nu_3 - i\nu_4 t_3)(\nu_1 t_1 + \nu_2 t_2) + \nu_3(i\nu_4 + \nu_3 t_3)(\nu_2 - \nu_1 t_1 t_2)}{\nu_2(\nu_3 - i\nu_4 t_3)(\nu_1 - \nu_2 t_1 t_2) - \nu_3(i\nu_4 + \nu_3 t_3)(\nu_1 t_2 + \nu_2 t_1)} \qquad 20$$

where $\nu_r = +(l_r^2 - k^2)^{\frac{1}{2}}$

and $t_r = \tan(\nu_r a_r)$

The values of k giving rise to lee waves are the roots of the equations $f_2 = 0$ and, in the lower layer, that part of the displacement of a streamline due to the lee waves appropriate to a root $k = k^*$ is given by:

$$\zeta_z \rightrightarrows 2\pi i \left[\frac{f_1}{\partial/\partial k(f_2)} \sin \nu_1 z \; e^{ikx} . F(k) \right]_{k=k^*} \qquad 21$$

Similar expressions can be derived for a multilayer model in which a lid exists at any specified level.

Eqs. 18-21 can be used to compute the properties of the lee waves which arise in any two, three or four-layer model airstream, the awkward quantity $\partial/\partial k(f_2)$ being obtained numerically in the course of the computations. The behaviour in the vertical of the lee waves in the layers above the lowest is obtained by applying considerations of continuity at the interfaces.

(i) Two-layer airstream

We shall first consider a simple two-layer airstream of the type which can contain lee waves and then examine how these lee wave characteristics are modified as different conditions are specified at high levels. We take a lower stable layer, 1 km deep, in which $l^2 = 4.0\ \text{km}^{-2}$ and suppose that in the upper layer which extends to infinity $l^2 = 0.3\ \text{km}^{-2}$. The appropriate lee wave equation has only one real root viz: $k = 0.76\ \text{km}^{-1}$, corresponding to a lee wavelength of 8.3 km.

In order to assign an absolute magnitude to the amplitude we specify the mountain profile as that given by

$$\zeta_0 \rightrightarrows h b \int_0^\infty e^{ikx - kb} \, dk$$

and we take the height of the ridge, h, as 0.1 km. The amplitude of the lee wave will vary with b, the so-called "half-width" parameter, and to particularise we take $b = k^{-1}$ being the value which excites the largest amplitude lee waves. In a discussion of the amplitude of lee waves, Corby and Wallington (1956) regarded the mountain having $b = k^{-1}$ as the optimum width for the particular lee wavelength, and likened the effect near this value to resonance.

Under these conditions the variation with height of the lee wave amplitude as determined from Eq. 21 is that illustrated in Fig. 2(a). The variation of amplitude with height follows the usual pattern for such an airstream in that a maximum amplitude is attained in the lower layer, where the amplitude variation in the vertical is sinusoidal; in the upper layer the amplitude falls off exponentially. For convenience, the value of the lee wave amplitude at the level where the maximum is achieved is illustrated for other values of b in Fig. 2(b).

It is of interest to consider here the effect of introducing a rigid lid at, say, 10 km above the interface or roughly at tropopause level. It is found that the lee wave at $k = 0.76\ \text{km}^{-1}$ still appears, without sensible change in its properties, but that there is an additional lee wave at $k = 0.415\ \text{km}^{-1}$. The variation with height of the two waves is indicated in Fig. 3(a) where the amplitude of each is depicted for its own optimum-width mountain. Fig. 3(b) enables the amplitudes for any particular mountain to be compared. The second wave, due to the presence of the lid, is noteworthy in that it has its maximum amplitude in the upper layer. This and several other computations suggest that, although the imposition of a lid at great height is theoretically a useful artifice, it would not give a good approximation to the flow of an unbounded atmosphere unless imposed at very great height indeed. In the present case, with the lid at height 11 km, only one additional lee wave is induced and clearly we should require a sufficiently large number to annul almost completely by interference away from the mountain. The point would be relevant if one considered using a rigid lid as an upper boundary condition when treating the problem by numerical integration of the differential equation for the flow, or when considering model experiments.

(ii) Four-layer airstream

We now consider a four-layer airstream in which the two lower layers of depth 1 and 10 km have the same values of ℓ^2 used in the two-layer example. They are surmounted by a third layer of depth 30 km in which $\ell^2 = 6.0\ \text{km}^{-2}$; this is intended to represent a stable stratosphere. Above this we assume the lapse rate to be adiabatic ($\ell^2 = 0$). Such a model is not completely unrealistic, for the upper half of the ozonosphere is believed to be a region of active convection (see Scorer, 1953). Furthermore, the presence of the upper layer with $\ell^2 = 0$ means that the disturbance necessarily decreases with height in that layer over the whole range of wavelengths.

As the terms involving tan $\nu_3 a_3$ in Eq. 20 oscillate rapidly for changing values of k, the wavelength equation $f_2 = 0$ has a large number of roots. Indeed, it is found that there are 26 nodal surfaces in the solution for $k = 0$, indicating the existence of 26 lee wavelengths. These can be conveniently put into three groups, viz., those in the ranges $0 < k < \ell_2$, $\ell_2 < k < \ell_1$ and $\ell_1 < k < \ell_3$. No lee waves occur for $k > \ell_3$. All the lee waves have sinusoidal variation of amplitude through the stable stratosphere and exponential decrease of amplitude in the uppermost layer.

There are two lee waves in the first group ($0 < k < \ell_2$). These are of appreciable amplitude at low levels and have even larger amplitude in the upper troposphere and stratosphere especially if we bear in mind the additional factor $(\rho_0/\rho)^{\frac{1}{2}}$ which for simplicity has been omitted at this stage. Formally the solutions of the equation $f_2 = 0$ corresponding to these lee waves arise because of the decrease in stability between the second and upper layers and they would not appear, for example, if we made $\ell_4 = \ell_2$. However, some similarity will be noted between these waves and the solution which was introduced into the two-layer model by the rigid lid at 11 km, and it can be shown that the form of these solutions in the lower layers is largely determined by the large increase of stability in passing from the second to the third layer, corresponding to the increase in stability at the tropopause. Although, if no less stable layer is introduced at great heights no infinite trains of lee waves appear as solutions, nevertheless $|f(k)|$ in Eq. 17 becomes large for values of k near that corresponding to lee waves with a lid and it can be shown that oscillations of the same type appear in the solution down-stream of the obstacle but that these die away slowly down-stream.

The first root in the second group, viz., that having the smallest k, occurs very nearly at $k = 0.76\ \text{km}^{-1}$ and the amplitude variation through the troposphere is very closely similar to that of the wave obtained from the two-layer model; indeed for practical purposes the waves can be regarded as identical. The next wave of the group has an amplitude in the lower layer only about 1/1000 of that at $k = 0.76\ \text{km}^{-1}$ and subsequent waves have even smaller amplitudes. The waves in the third group are also of negligible amplitude. Many of these additional waves do, however, attain their maximum amplitude in the stratosphere although even there the absolute values are negligible.

The amplitude and its variation with height are illustrated for the three main waves in Fig. 4(a). As before, the absolute magnitude of the amplitude is depicted in each case for the appropriate optimum-width mountain, and Fig. 4(b) may be used to compare the amplitudes in the lower layer for any other specific mountain width.

If the upper layer is omitted and a lid is imposed at the top of the stratosphere, once again the main lee wave near $k = 0.76\ \text{km}^{-1}$ appears without significant change in its properties. There are also two lee waves of longer wavelength (smaller k) having similar properties to those with the four-layer model, whilst all the other lee waves have negligible amplitude at all heights.

For most purposes the lee waves having the greatest interest are those which attain their maximum amplitude in the lower troposphere and which die away upwards. The unbounded two-layer airstream first considered had one lee wavelength of this type and the subsequent computations suggest that, provided the same tropospheric conditions are maintained, this lee wave appears without perceptible change in its properties whatever conditions are assumed at high levels. Thus lee waves of this type do not appear to be at all sensitive to changes in the wind or stability profiles at high levels. That this is not a fortuitous result arising because of the particular ℓ^2 profile adopted, but is true in general, can be deduced by a study of Eq. 20. It also appears that lee waves may arise as a result of the change of stability in the region of the tropopause. These are similar to the solutions obtained if a rigid lid is imposed at a level corresponding to the tropopause but for proper representation of these the stability at greater heights must be considered. The introduction of a layer of neutral stability or a lid at a very high level is a useful artifice to make these lee waves appear as infinite wave trains rather than wave trains of finite extent, thereby making the mathematical treatment easier.

The solution obtained for $k = 0$

The device of using the number of nodal surfaces in the solution for $k = 0$ as a means of determining the number of lee wavelengths was referred to earlier. We will mention another possible application of this solution.

In a problem such as that of orographic rainfall we are not concerned with the smaller scale gravity waves with wavelengths of the order of 10 km or less, but with those comparable in length with the horizontal scale of a barrier such as the Welsh mountains. On the other hand such a barrier is still small enough to allow the neglect of oscillations about the geostrophic flow without changing the nature of the problem. Accordingly, the main features of the flow will be adequately represented by Eq. 16. Here ℓ^2 varies from 0 to 10 km^{-2} or more; zero values occur when the atmosphere has neutral static stability, and the more commonly occurring lapse rates above the surface layers usually lead to values of $\ell^2 > 0.25\ \text{km}^{-2}$.

If we consider the mountain ridge whose profile is represented by Eq. 22, then clearly the amplitude of the Fourier components becomes small (e.g., $< 1/12$ of the maximum) for $k > 2.5/b$. Thus for a mountain half-width of 20 km the contribution of components with $k > 0.12$ is small and we are primarily concerned with k^2 in the range 0 to 0.015. It follows that a general idea of the large scale flow can be obtained by putting $k = 0$ in Eq. 16 and solving it in the form

$$\frac{\partial^2 \psi}{\partial z^2} + l^2 \psi = 0 \qquad 23$$

where l is now a function of z.

Since the solution near the ground must be independent of the value of l at great heights we consider a case in which l is constant above a specified upper level.

We require a solution of the form

$$\psi = F(z).e^{ikx} \qquad 24$$

where $F(z)$ is a complex function of $z \{ F(z) = F_1(z) + iF_2(z) \}$ and in order that this should have the correct form in the upper layer with constant l, we require that at any level in that layer, $\partial F/\partial z = ilF$. This provides the upper boundary condition.

The solution (24) may be assumed to hold approximately throughout the range of k in which we are interested. Then the flow at level z over a mountain with profile:

$$\zeta_0 = hb \int_0^\infty e^{ikx - kb}\, dk$$

is given by

$$\zeta_z = hb \int_0^\infty (F_1 + iF_2).e^{ikx - kb}\, dk$$

or

$$\zeta_x = \frac{hb}{b^2 + x^2} (bF_1 - xF_2) \qquad 25$$

The approximation implied by putting $k = 0$ in this way, was used by Scorer (1949) when obtaining the part of the flow above the hill (as distinct from the lee waves). The point being made here is that it is a satisfactory and realistic approximation when studying the large-scale character of the flow over a barrier such as the Welsh mountains or the Pennines in connection with orographic rainfall. In the case of l constant with height, both the symmetric and asymmetric components in the displacement (Eq. 25) have a vertical wavelength of $2\pi/l$. We, therefore, require a small value of l if the upslope motion on the windward slope is to continue as an upslope motion to considerable heights. If the air mass is very stable (statically) l will be large and we would expect to find descending air at no very great height above the windward slope. These aspects bear intimately on the problem of what conditions favour heavy orographic rain.

Although only approximate, Eq. 25 gives a specific indication of the vertical variation and asymmetry of the flow over a barrier such as the Pennines or the Welsh mountains. In layers with static stability a measurable disturbance of the temperature field would be expected and some observable effects should be apparent in the distribution of cloud layers.

Horizontal flights by aircraft well above such a barrier might therefore produce direct evidence of the validity of the treatment and in particular of the appropriateness of the upper boundary condition which has been deduced and adopted here.

Conclusions

In the theory of the airflow over mountains, further light is thrown on the problem of what choice of upper boundary condition should be adopted by studying the limit to which the flow tends as a rigid lid, or some other upper condition which renders the problem fully determinate, is removed to infinity. This device strongly suggests that, provided we are right in assuming that a stationary solution does exist, then in the uppermost layer and over the range of wavelengths for which solutions with inclined wave fronts occur, the proper procedure is to reject the solutions giving wave fronts inclined in the downstream direction and to retain those inclined in the upstream direction. This conclusion is consistent with that reached by including small friction to achieve determinacy or by obtaining the asymptotic limit of a time-varying solution.

When calculating the character of the flow in actual cases, the familiar type of lee wave which has a maximum amplitude in the lower troposphere and which dies away above, is not at all sensitive to the conditions assumed at high levels. It would appear, however, that lee waves which have their largest amplitude in the upper troposphere and stratosphere can occur in certain airstreams depending primarily on the change of stability near the tropopause; these are of somewhat longer wavelength, and for their proper study require consideration of stability and wind in the stratosphere.

REFERENCES

Lamb, Sir H.	1932	Hydrodynamics, 6th Edn. Arts 242-246.
Queney, P.	1947	Theory of perturbations in stratified currents with applications to airflow over mountain barriers. Chicago Univ. D. Misc. Rep. No. 23.
Scorer, R. S.	1949	Theory of waves in the lee of mountains. Quart. J.R. Met. Soc., 75, p.41.
Palm, E.	1952	On the formation of surface waves in a fluid flowing over a corrugated bed and on the development of mountain waves. Astrophys. Norvegica, 5, No. 3.
Scorer, R. S.	1953	Air motion in the upper atmosphere. Nature, 172, p.138.
Corby, G. A. and Wallington, C. E.	1956	Airflow over mountains - the lee wave amplitude. Quart. J.R. Met. Soc., 82, p.266.
Scorer, R.S.	1954	Theory of airflow over mountains III - Airstream characteristics. Quart. J.R. Met. Soc., 80, p.417.

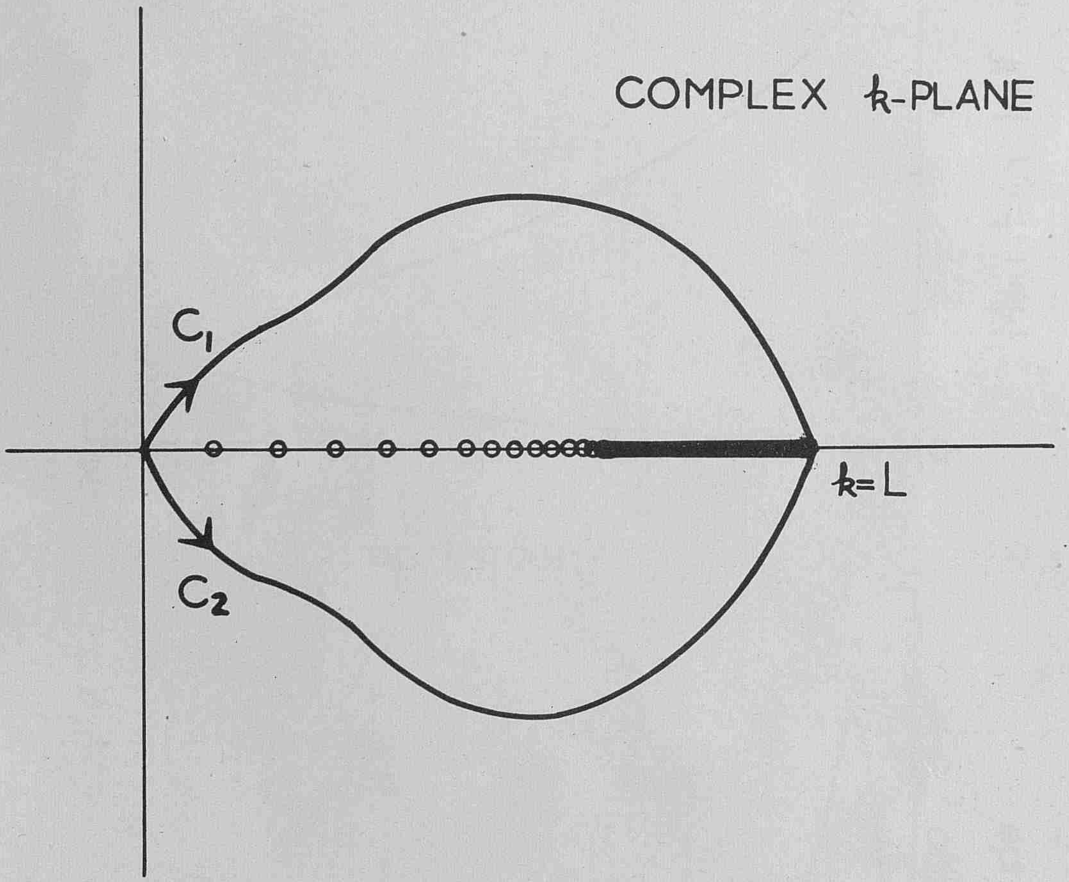
COMPLEX k-PLANE
C_1
C_2
$k = L$

Fig. 1. Contours used for contour integration.

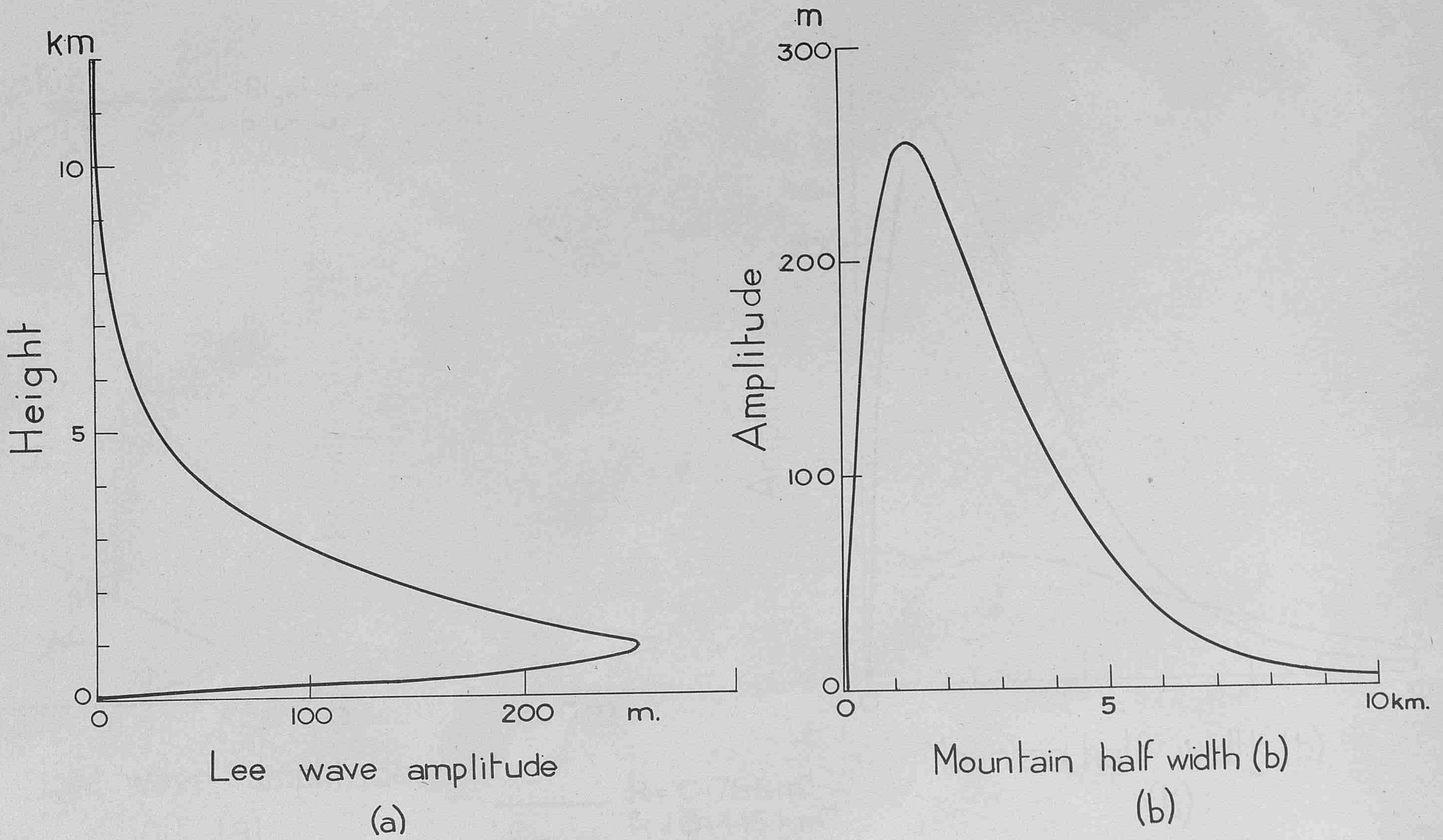

Fig. 2. The properties of the lee-wave ($k = 0{\cdot}76\ \mathrm{km}^{-1}$) for a two-layer airstream extending to infinity and flowing over a ridge of height 100 m. In (a) is depicted the variation of amplitude with height for the optimum-width ridge, and in (b) the variation with mountain width of the maximum amplitude in the lower layer.

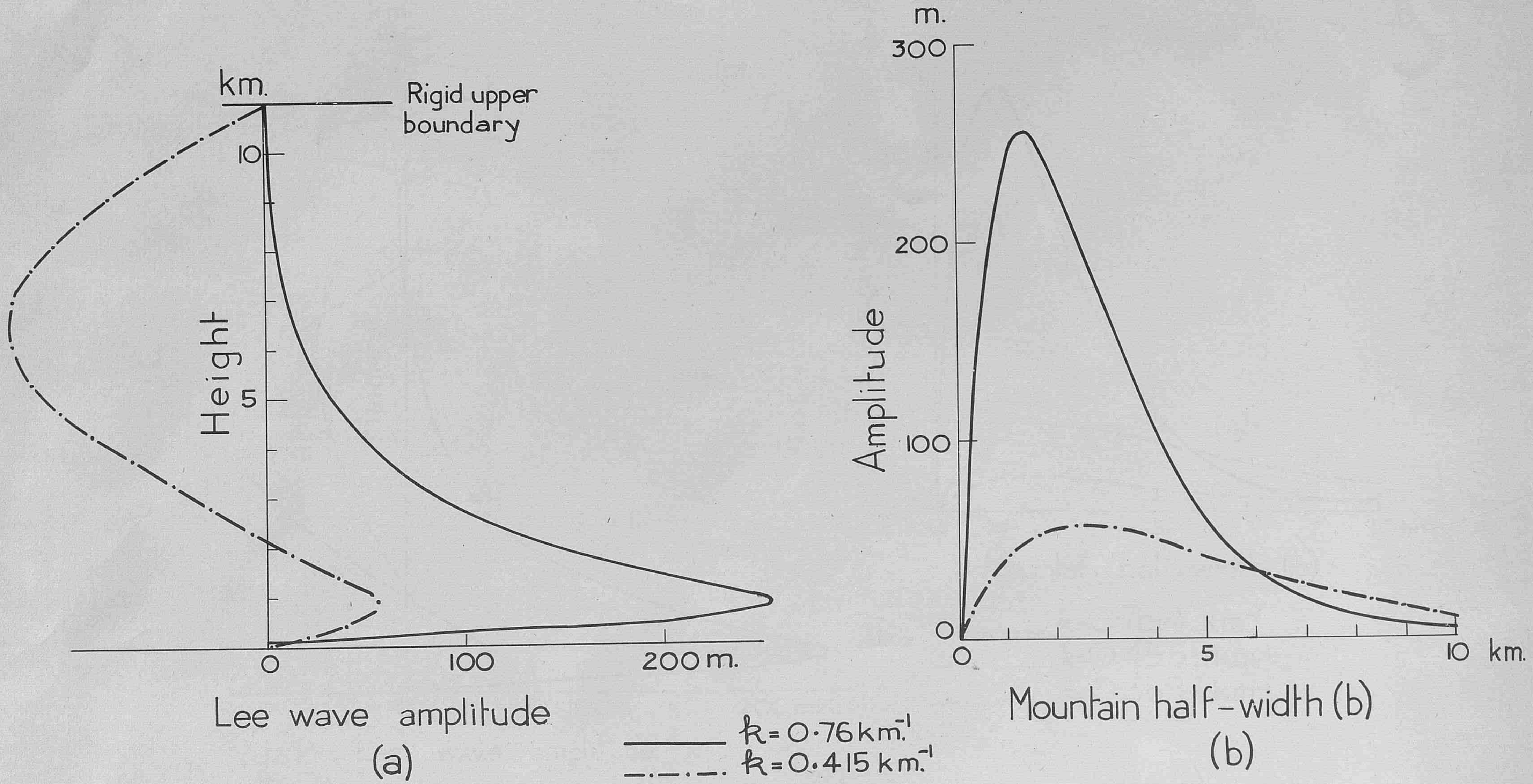

Fig. 3. The properties of the two lee-waves for a two-layer airstream bounded by a rigid lid and flowing over a ridge of height 100 m. In (a) is depicted the variation of amplitude with height, each lee-wave being associated with its optimum-width ridge, and in (b) the variation with mountain width of the maximum amplitude in the lower layer.

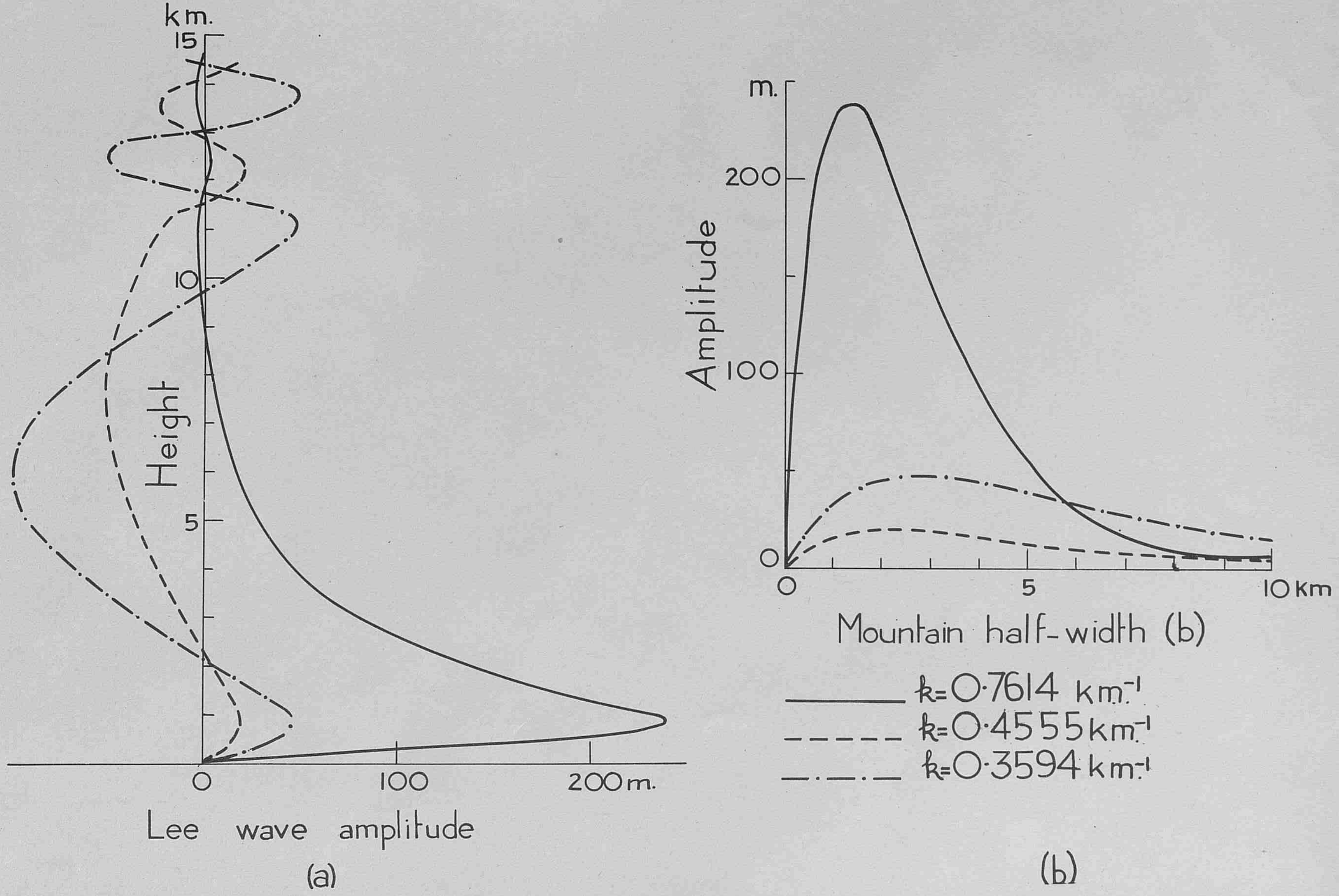

(a)

(b)

Fig. 4. The properties of the three principal lee-waves for a four-layer airstream extending to infinity and flowing over a ridge of height 100 m. In (a) is depicted the variation of amplitude with height, each lee-wave being associated with its optimum-width ridge, and in (b) the variation with mountain width of the amplitude in the lower layer.

M.R.P. 1016
S.C. 11/221
30th November 1956.

AD 223128

Numerical forecasts based on objectively analysed data

by

Vera M. Huckle

(Meteorological Office)

AIR MINISTRY

METEOROLOGICAL RESEARCH COMMITTEE

At the time of issue this report has not been published. Any author desiring to quote this paper should refer to it as "A paper of the Meteorological Research Committee (London), M.R.P. No. 1016 by Miss Vera M. Huckle A copy is available in the Library of the Meteorological Office."

M.R.P. 1016
S.C.II/221
30th November, 1956

AIR MINISTRY
METEOROLOGICAL RESEARCH COMMITTEE

Numerical forecasts based on objectively analysed data

by

Vera M. Huckle (Meteorological Office)

1. Introduction

Four numerical forecasts have been calculated on data objectively analysed by the technique explained by Bushby (1956). The data for the 500 mb level and the 1000-500 mb thickness were analysed using the quadratic surface method with $p = p_2$, $q = \frac{1}{16} p_2$ and $T^2 = 16 \text{ sec}^2$. The object in doing these calculations was to discover whether or not the standard of the forecast charts would be seriously affected by using objectively analysed data instead of data analysed by the normal methods.

Forecasts for twenty-four hours were computed based on the two sets of data for each situation and each was compared with the actual chart for that time, analysed subjectively. For interest, the surface prebaratic prepared in the Forecast Division, Dunstable was also compared with the actual chart, although it is not the purpose of this paper to compare conventional forecasts with those produced by numerical methods. The three dates chosen were 1500 G.M.T. for 12th September, 15th October, 31st October, 1955 and 30th January, 1952. The two-parameter model of the atmosphere used was that which incorporates the sea surface heating effect and uses the actual boundary values.

2. Results

(a) 12th September, 1955.

On the actual 500 mb chart for 12.9.55 (Fig.1a) there was the suggestion of a double trough, the northern one to the west of the British Isles and the southern one over the British Isles. Twenty-four hours later (Fig.1c) there was a very broad irregular trough from Scotland across Europe to Italy, with still a slight suggestion of a double trough. There was a very strong flow down from Greenland to the British Isles . The computation (Fig.1e) based on subjectively analysed data gives a trough east of the actual position and not broad enough. There is a strong flow across the Atlantic from Greenland to the British Isles but it continues **round** the trough whereas there was actually a diffluence. The values of the contours are too high in the south-west of the area and over Ireland. The computation based on objectively analysed data also gives the heights too high, those over Ireland being higher than in the previous computation. As a result of this, the flow in the Atlantic is not strong enough. The trough is in the right position and is very broad, but due to the height error it appears as a shallow trough and the double trough is over-emphasised.

On the actual 1000-500 mb thickness charts (Figs.1b and 1d), a broad trough just west of the British Isles became stronger and moved to the east of the British Isles, a ridge forming in the Atlantic, south of Greenland. The computation (Fig.1f) based on subjective analysis gives a ridge over southern Greenland and a broad trough over the British Isles with small scale oscillations superimposed on it. These may be due to computational instability. The values of the height agree fairly well with the actual chart. The chart (Fig.1h) produced from objectively analysed data is very similar to the one mentioned above. The irregularities are more marked and the thickness is about 200 feet out over the British Isles.

On the 1000 mb charts (Fig.1b and 1d) there was an almost stationary anticyclone in the Atlantic with a depression moving south-east from Iceland. There were two troughs associated with the depression, one being a frontal trough and one connected with the thickness trough. The computation (Fig.1f) based on subjectively analysed data gave an anticyclone of the right intensity in the right position and a depression of the right intensity but this was moved too far east. Two troughs appeared but they were not emphasized enough. The objective analysis produced a similar chart (Fig.1h). The frontal trough was correctly placed and there was a more pronounced ridge over the Low Countries. The values were too high over the British Isles in both computations, that based on objectively analysed data giving the higher values.

(b) 15th October, 1955.

At the 500 mb level (Fig.2a) there was a cut-off high cell centred about 49°N 22°W with a ridge extending up to Greenland and one in an easterly direction into France. There was a strong flow from Greenland over Iceland to the British Isles with a trough from Norway to the British Isles. During the following twenty-four hours (Fig. 2c) the high cell declined leaving a weak ridge. The low and associated trough from Norway broadened out and the flow slackened. The computation (Fig.2c) based on a subjective analysis of the data did not show the weakening of the Atlantic cut-off high and ridge but kept the ridge in approximately the right position. There was a broad trough over Europe but it was distorted by small scale disturbances. The low over the Baltic was computed to be too deep. The computation (Fig.2g) based on data analysed objectively had similar faults, although the distortions on the European trough were not so pronounced. The thickness chart (Fig.2b) had originally a ridge over the south-west Atlantic with a confluent trough over the east of the British Isles. By the next day (Fig.2d) the thermal gradients round the trough had become more uniform and the trough had broadened. Both the computed charts suffered from computational instability to a marked extent. Both forecasts gave a broad trough but the small scale disturbances make comparisons very difficult. The computed 1000 mb charts do not show marked instability and are very similar.

The instability produced could have been caused by the specification of vorticity on the boundary at points where fluid is leaving the region, or by the time step chosen being too long in relation to the grid length and the wind speed. To gain more information, the computation was repeated using subjectively analysed data and half-hourly time steps instead of hourly ones. The charts produced were practically identical with those produced previously. Therefore, the instability, if it is computational, must be due to the boundary conditions imposed. Since there is a very strong flow across the north-east boundary, this is very probable.

(c) 31st October, 1955.

On the original 500 mb chart (Fig.3a) there was a trough over the Atlantic extending SSW. from Iceland with an irregular flow round it. A second trough was situated over the Baltic with a low latitude trough over the Pyrenees. Twenty-four hours later (Fig.3c) the Atlantic trough was in two sections, a progressive trough in the north with a slack gradient in the centre, and a stationary one in the south, west of the Azores. The Baltic trough moved out of the area and the one over Spain filled and moved a little eastwards. The computation (Fig.3a) based on subjectively analysed data gave only one trough in the Atlantic with slack central gradient. The trough over Spain was smoothed out. Values of the 500 mb contour height were in good agreement with the actual values but the 18200 feet contour was placed too far north over Europe. The computation (Fig.3g) based on objectively analysed data gave two troughs in the Atlantic, one progressive and one not, but the progressive one had no slack gradient at the centre. A trough was left over Europe, but it had the wrong orientation. The contour heights were in good agreement with the actual values but the low over Iceland was not made quite deep enough.

The original thickness chart (Fig.3b) had a trough extending from Iceland to the south-west with another one over the Baltic, and the suggestion of one over England, these two being in higher latitudes - the lower latitudes having one broad trough. Twenty-four hours later (Fig.3d) there was a stronger trough slightly east of the original one and another one over England going down through Biscay to Spain. The computation based on subjectively analysed data (Fig.3f) gave a trough in the Atlantic in approximately the right position but wrongly orientated. There was a very pronounced ridge over England with a slight trough in the 18000 feet contour. The objectively analysed data resulted in a chart (Fig.3h) giving a trough in the Atlantic in the right position but of wrong shape. The ridge that was west of Iceland has been moved too far east placing it over the British Isles and the trough, which in this computation is in the 17800 feet contour, is also too far east. In both computations the thickness is too high in the region of the British Isles.

The 1000 mb contour chart had two depressions on the Atlantic, one south of Iceland and one west of the Azores, with an anticyclone over England and a depression over the east coast of Spain. During the following twenty-four hours, the two Atlantic depressions became important, the southern one moving and the northern one remaining stationary. They both deepened considerably, the one near Iceland becoming a vigorous one with a central closed contour of -600 feet. The anticyclone over England moved eastwards and the low over Spain remained the same. The computation based on subjectively analysed (Fig.3g) data did not move either of the Atlantic depressions and did not deepen either of them sufficiently, although the one near Iceland was deepened by 300 feet. The anticyclone over England was moved eastwards correctly but intensified as well. The low over Spain was not substantially altered, the area of low pressure becoming greater. The second computation (Fig.3h) was very similar to the first. The depression south of Iceland was made slightly deeper than in the previous computation but was still not deep enough and it was also placed too far east.

(d) 30th January, 1952.

This case has been computed using several variations of the basic two-parameter method. The computation based on subjectively analysed data using the same method as was used for the other three cases mentioned in this report is reported by Bushby and Huckle (1956). The computation has now been performed on objectively analysed data. At 500 mb the computation based on subjectively analysed data (Fig.4e) has a strong jet stream terminating in a diffluent trough that is much too far east. The jet stream is not intense enough and is too far north. Over Southern England, the heights are 1200 feet too high. When the computation was repeated on objectively analysed data (Fig.4g) the diffluent trough was placed much nearer its actual position. The jet stream is still not intense enough and too far north, the height over Southern England in this case being 1000 feet too high. In the computation based on subjectively analysed data (Fig.4f), the axis of the thickness trough was computed to be too far north and east and not curving enough and the ridge near it was also wrongly situated and shaped. In the computation based on objectively analysed data (Fig.4h) the position and shape of the trough and ridge are very near the actual position and shape. The values are only 400 feet too high over the British Isles.

The computation based on subjectively analysed data for 1000 mb (Fig.4d) gave a series of ridges and troughs right across the Atlantic, with the main trough over Europe and the ridge over the North Sea, instead of an almost straight flow across the Atlantic with a ridge west of Ireland and a trough over the North Sea. In the computation based on objective analysis of the data (Fig.4h) there was a much smoother flow across the Atlantic with a ridge over Ireland and a trough down the North Sea.

The earlier paper described the improvements in the forecast charts made by using a stream function. The improvements by this method and by the use of objective analysis were of different natures. It may be therefore that by using the stream function method on the objectively analysed data further improvements to the forecast would be made.

(e) Correlation coefficients.

Table 1. Correlation and regression coefficients.

Date 1500 GMT	Method of analysis	500 mb			1000- 500 mb			1000 mb		
		r	a	b	r	a	b	r	a	b
12.9.55	Subjective	0.95	0.96	-3.40	0.91	1.10	0.70	0.87	0.72	-3.50
	Objective	0.92	0.71	-4.30	0.85	1.04	-1.14	0.89	0.92	-3.50
15.10.55	Subjective	0.82	0.98	-6.9	0.90	0.77	-5.4	0.81	0.90	-3.60
	Objective	0.90	0.99	-8.4	0.88	0.74	-4.2	0.81	0.92	-6.60
31.10.55	Subjective	0.93	1.21	-8.1	0.83	1.01	-5.37	0.86	1.29	1.65
	Objective	0.92	1.14	2.09	0.85	0.91	-3.80	0.85	1.30	8.56
30.1.52	Subjective	0.47	0.40	-28.20	0.72	0.69	-5.5	0.58	0.63	-26.9
	Objective	0.60	0.69	-35.20	0.86	0.72	-5.4	0.76	0.80	-31.6

r = correlation coefficient; a, b are the regression coefficients of the best fitting straight line giving the actual change (Y tens of feet) in terms of the forecast change (X tens of feet) in the form

$$Y = aX + b$$

where b is in tens of feet.

The correlation coefficients show little difference between the computations based on subjectively or objectively analysed data in three of the four cases considered. The fourth case however, 30.1.52, has noticeable improvements both as regards the actual charts and the correlation coefficients when the objectively analysed data are used instead of subjectively analysed data. In this case, the objective analysis method has given a forecast for 1000 mb comparable with that produced by the Forecast Division whereas the other numerical computation based on subjectively analysed data was not as good as the conventional one.

3. Conclusion

Four cases are obviously not enough on which to judge the success or failure of objectively analysed data as a basis for time integrations. They do show that it is a practical method which is quicker than a subjective analysis when the results are needed for numerical time integrations. The results indicate that small scale features tend to be lost with objective analysis although the main features remain. On one occasion the objective analysis of the data has resulted in better forecast charts. This may be due to the difficulty in drawing the lines accurately and in reading off the values accurately in regions of strong gradients.

It appears from these four cases that objectively analysing data for time integration work only slightly affects the resulting charts unless there are very strong gradients in the area, when the objective analysis technique may well provide a necessary degree of smoothing and thus produce better results as the final product.

References

Bushby, F.H.	1956	Meteorological Research Papers, Air Ministry, London, No. 986.
Bushby, F.H. and Huckle, V.M.	1956	Quart. J.R. Met. Soc., p.409.

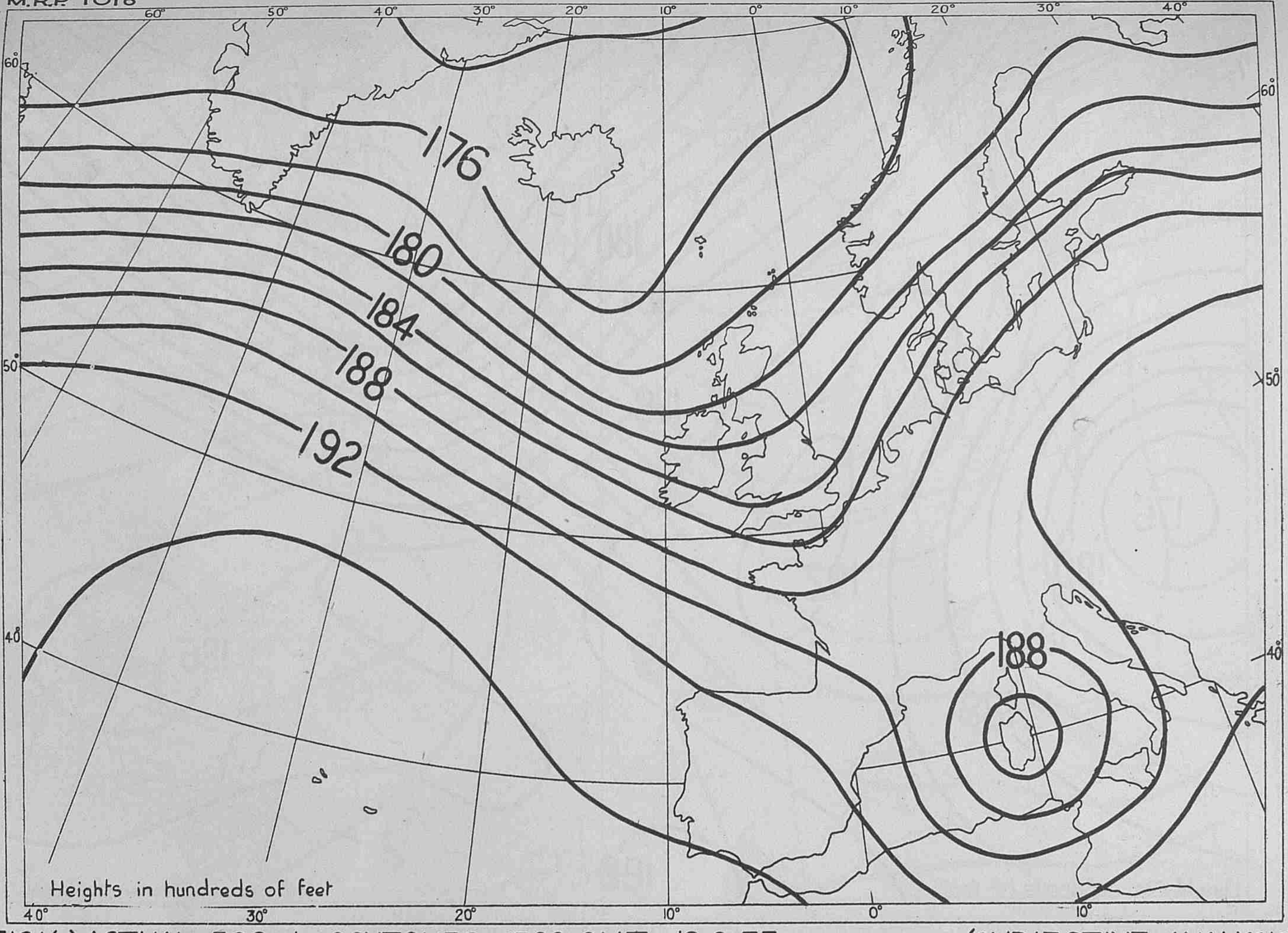
176
180
184
188
192
188
Heights in hundreds of feet
60°
50°
40°
30°
20°
10°
0°
10°
20°
30°
40°
60°
50°
40°

FIG.1(a) ACTUAL 500mb. CONTOURS, 1500 G.M.T. 12:9:55 (SUBJECTIVE ANALYSIS)

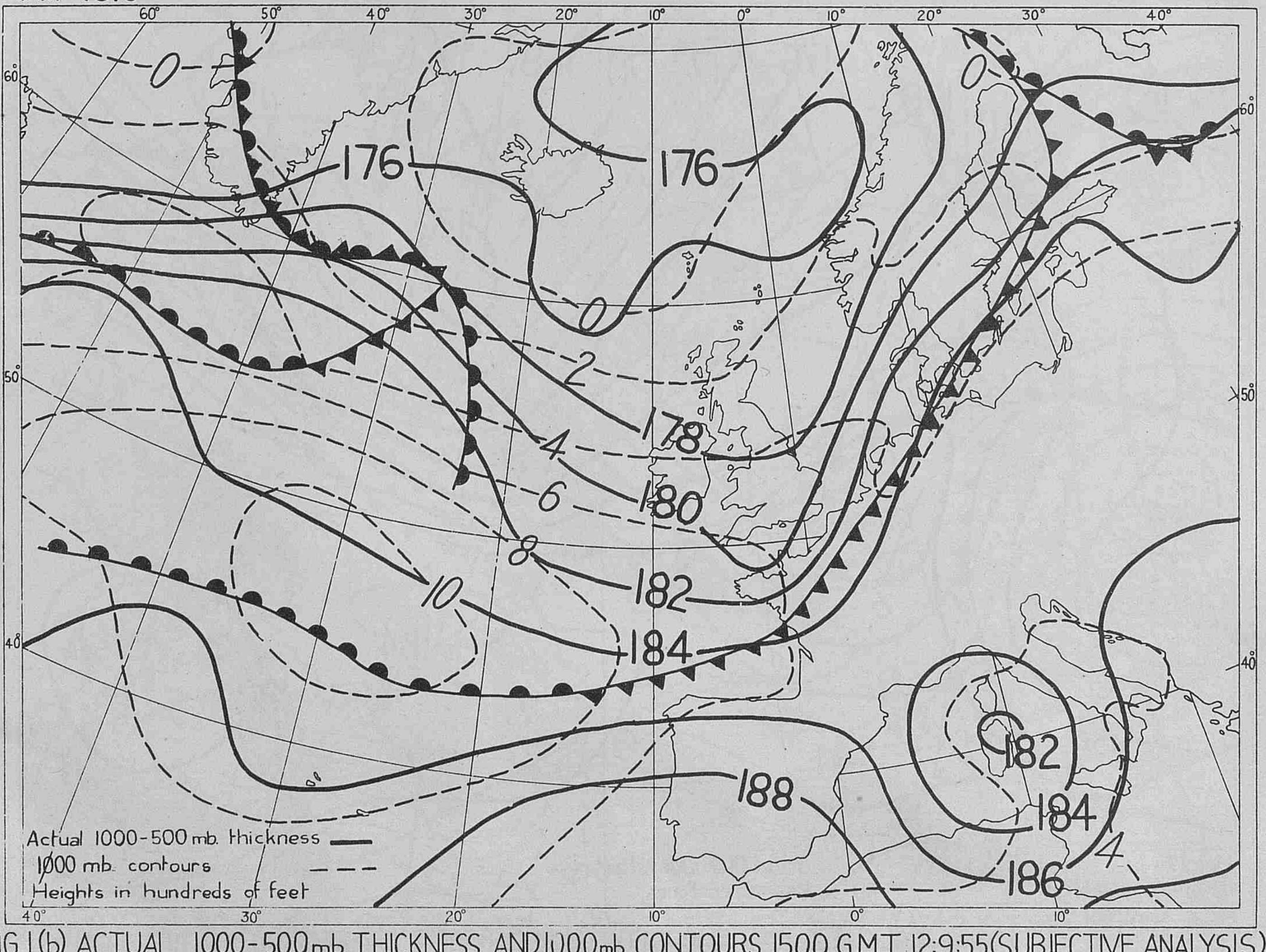
0
176
176
0
0
2
178
4
6
180
8
10
182
184
188
182
184
186
4
Actual 1000-500 mb. thickness
1000 mb. contours
Heights in hundreds of feet
60°
50°
40°
30°
20°
10°
0°
10°
20°
30°
40°

FIG 1(b) ACTUAL 1000-500mb. THICKNESS AND 1000mb. CONTOURS, 1500 G.M.T. 12:9:55 (SUBJECTIVE ANALYSIS)

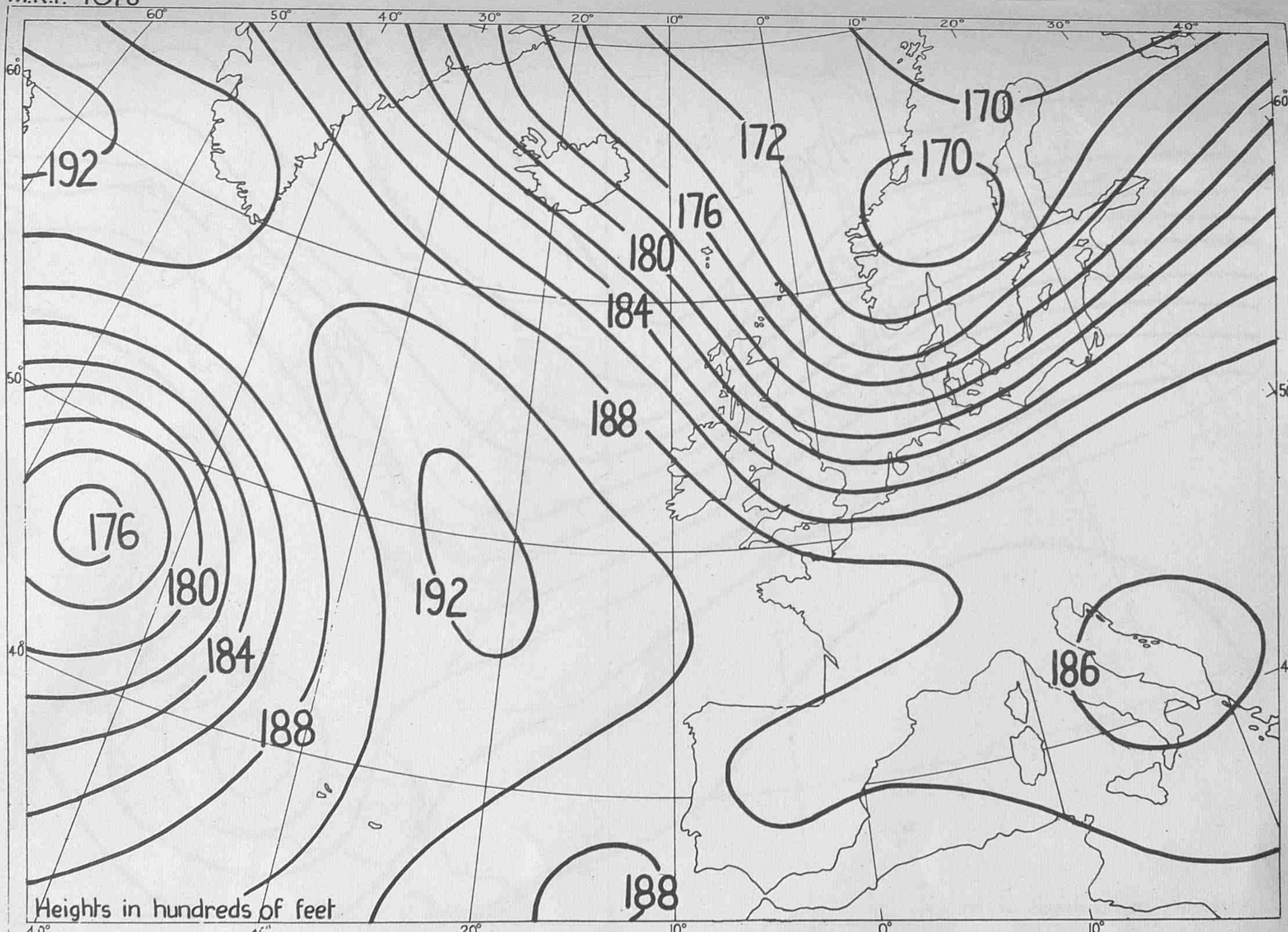
60°
50°
40°
30°
20°
10°
0°
10°
20°
30°
40°
192
170
172
170
176
180
184
188
176
180
184
188
192
186
188
Heights in hundreds of feet

FIG. 2(a) ACTUAL 500mb CONTOURS FOR 1500 G.M.T. 15:10:55 (SUBJECTIVE ANALYSIS)

M.R.P. 1016

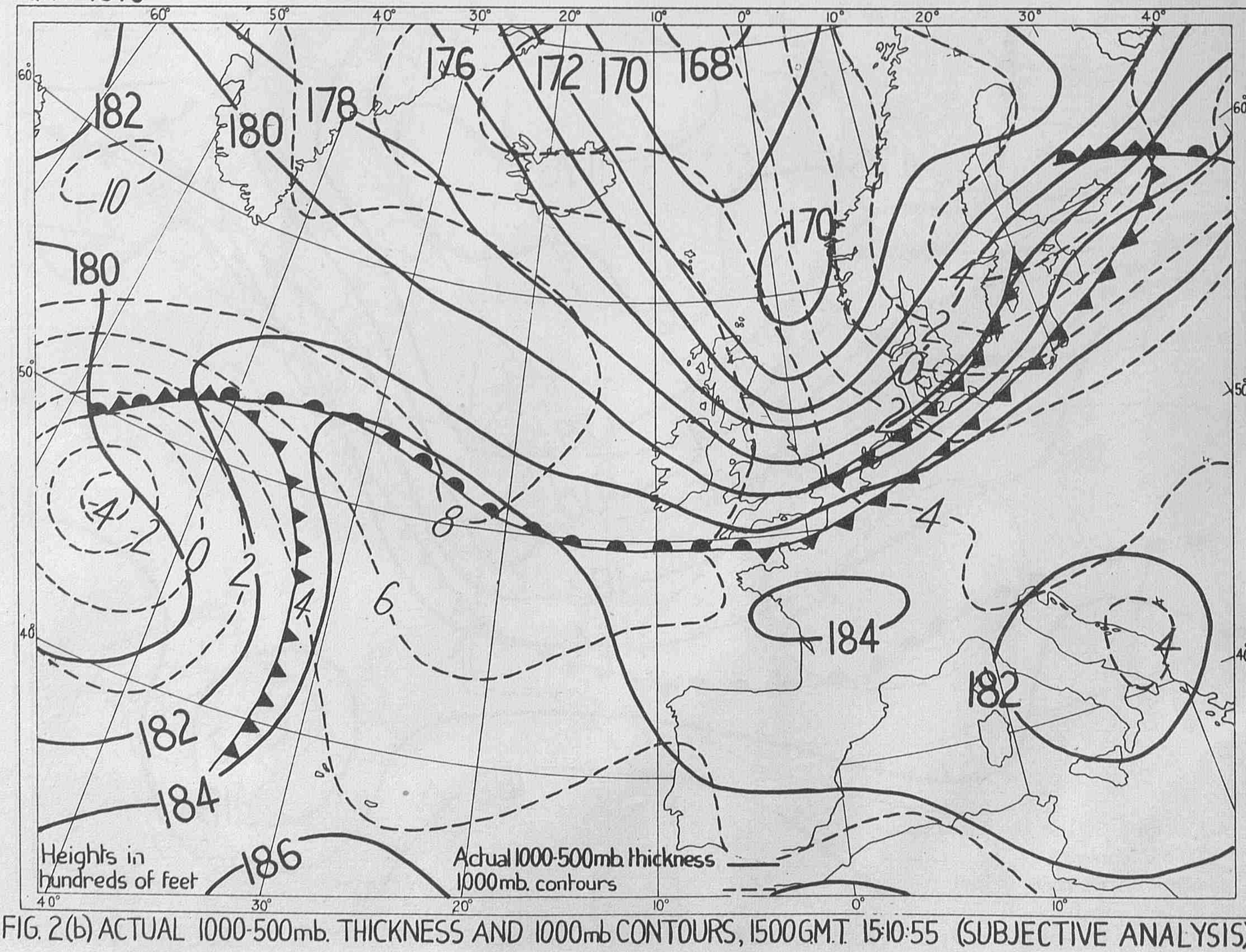
176
172
170
168
182
10
180
178
180
170
4
2
0
2
-4
-2
0
2
4
6
8
4
184
4
182
182
184
186
Heights in hundreds of feet
Actual 1000-500mb. thickness
1000mb. contours

FIG. 2(b) ACTUAL 1000-500mb. THICKNESS AND 1000mb CONTOURS, 1500 G.M.T. 15:10:55 (SUBJECTIVE ANALYSIS)

M.R.P. 1016

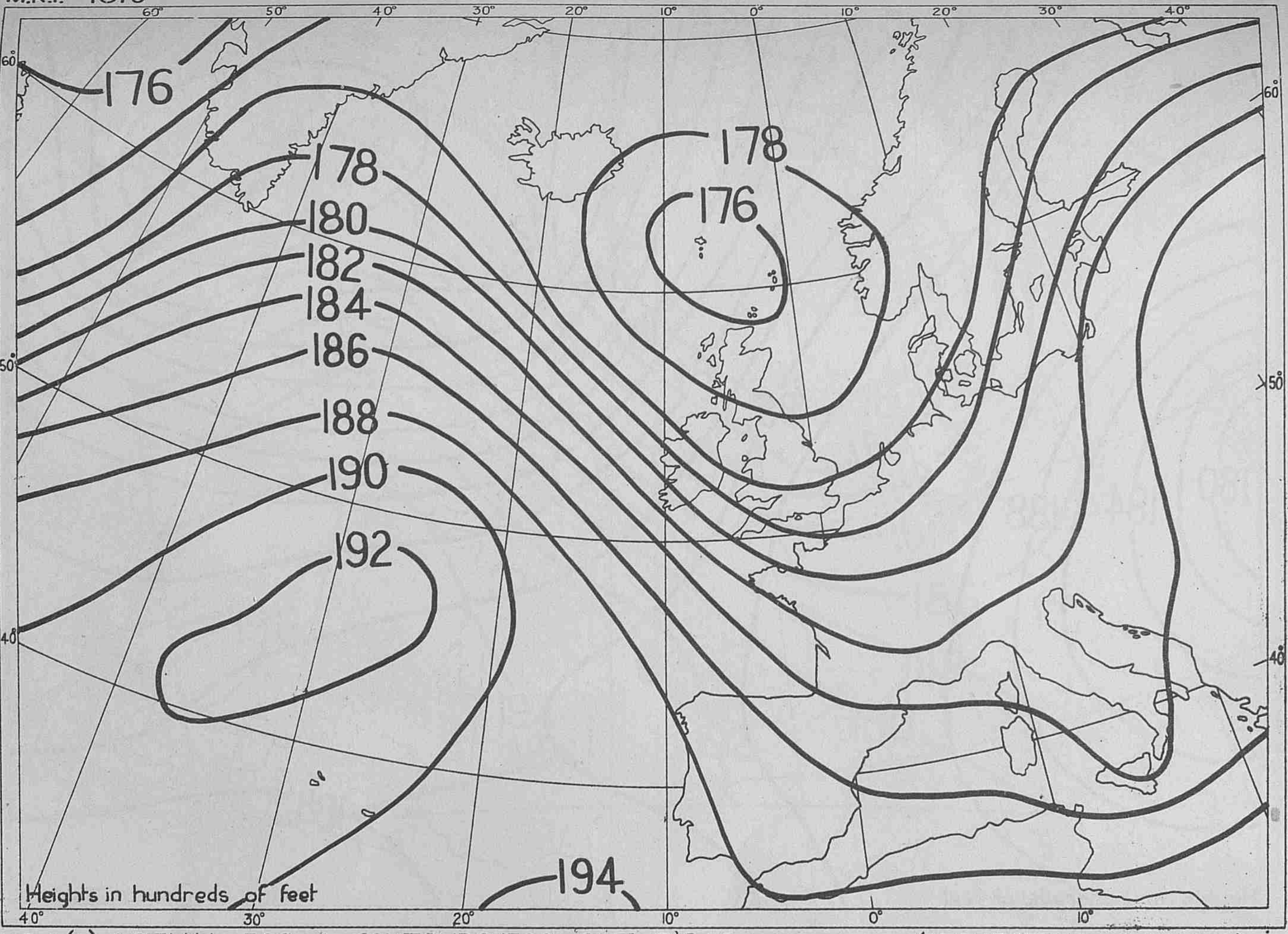
60°
50°
40°
30°
20°
10°
0°
10°
20°
30°
40°
176
178
180
182
184
186
188
190
192
194
178
176
Heights in hundreds of feet

FIG. 1 (c). ACTUAL 500 mb. CONTOURS, 1500 GMT. 13:9:55 (SUBJECTIVE ANALYSIS)

M.R.P. 1016

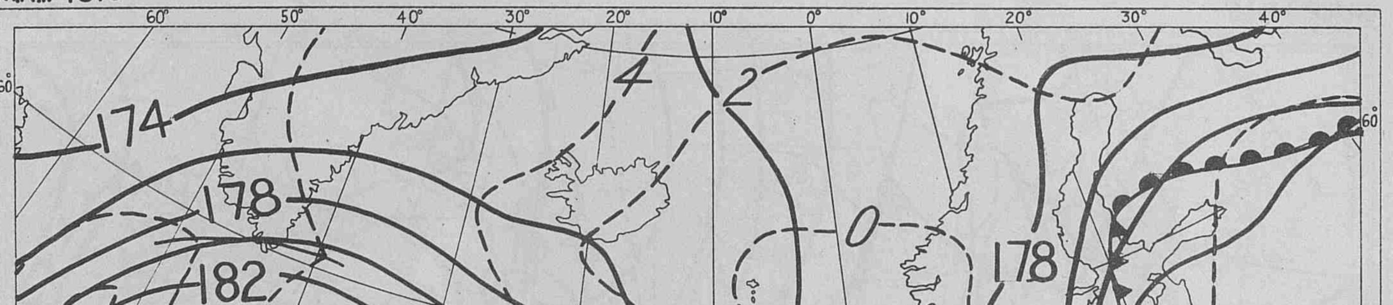
174
178
182
186
178
182
186
184
2
4
0
2
10
8
6
4
Heights in hundreds of feet
Actual 1000-500mb thickness
1000mb. contours

FIG.1(d) ACTUAL 1000-500mb. THICKNESS AND 1000mb CONTOURS 1500 GMT. 13:9:55 (SUBJECTIVE ANALYSIS)

M.R.P. 1016

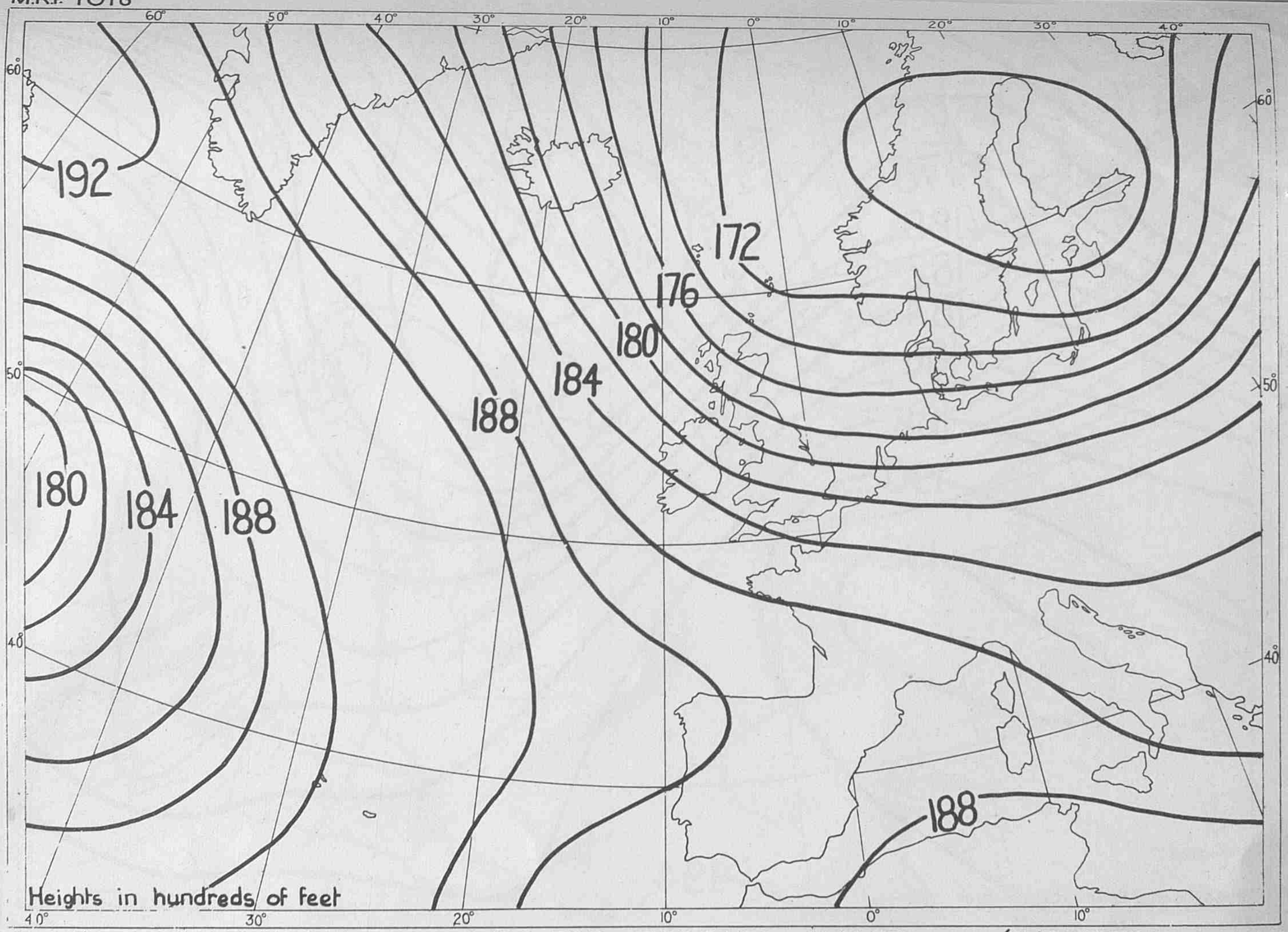
60°
50°
40°
30°
20°
10°
0°
10°
20°
30°
40°
192
172
176
180
184
188
180
184
188
188
Heights in hundreds of feet
40°
30°
20°
10°
0°
10°
60°
50°
40°

FIG 2(c) ACTUAL 500mb. CONTOURS FOR 1500 G.M.T. 16:10:55 (SUBJECTIVE ANALYSIS)

M.R.P. 1016

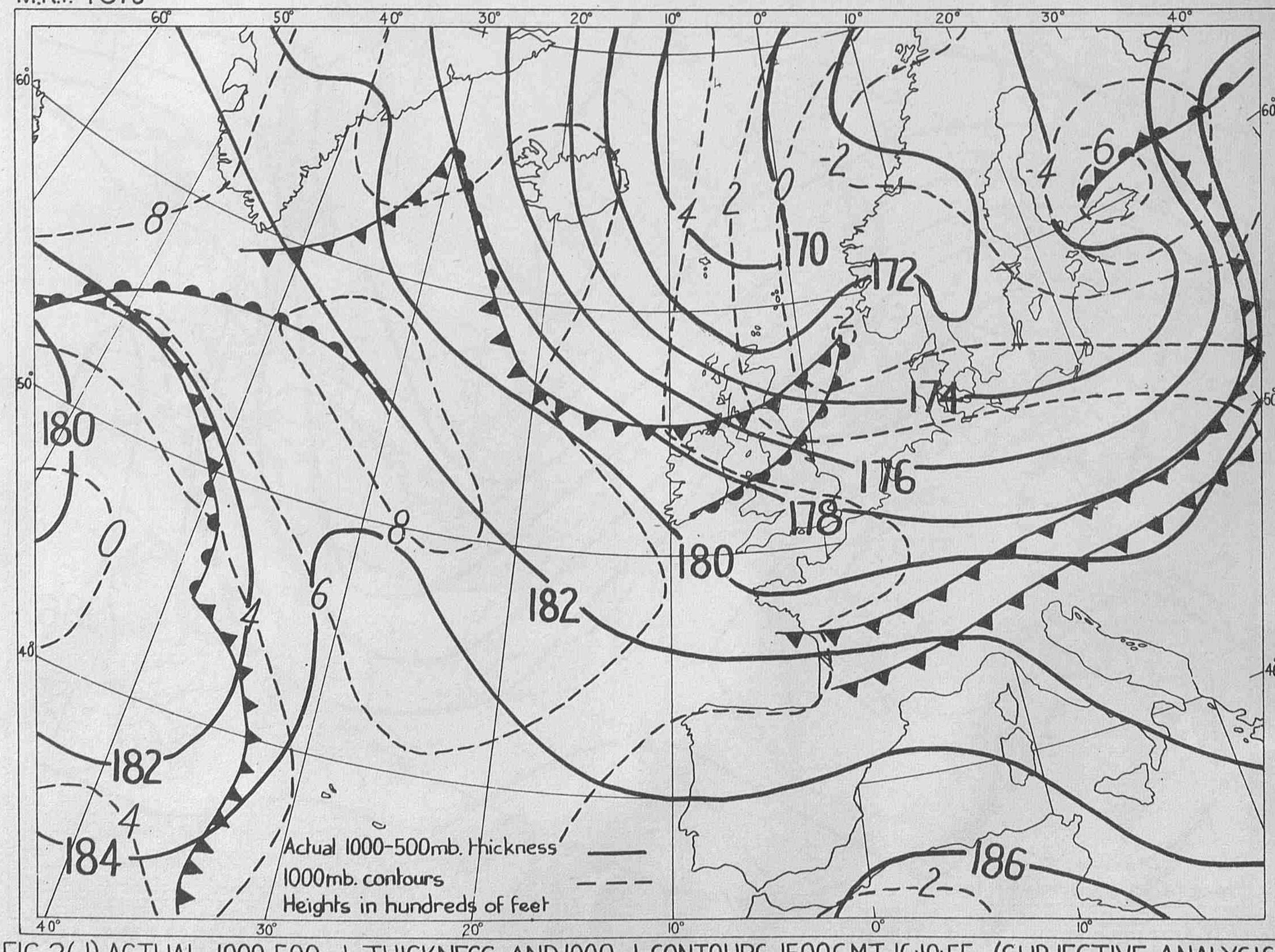
8
4
2
0
-2
-4
-6
170
172
174
176
178
180
182
180
0
8
6
4
182
4
184
-2
186
Actual 1000-500mb. thickness
1000mb. contours
Heights in hundreds of feet

FIG. 2(d) ACTUAL 1000-500mb. THICKNESS AND 1000mb CONTOURS, 1500 G.M.T. 16:10:55 (SUBJECTIVE ANALYSIS)

M.R.P. 1016

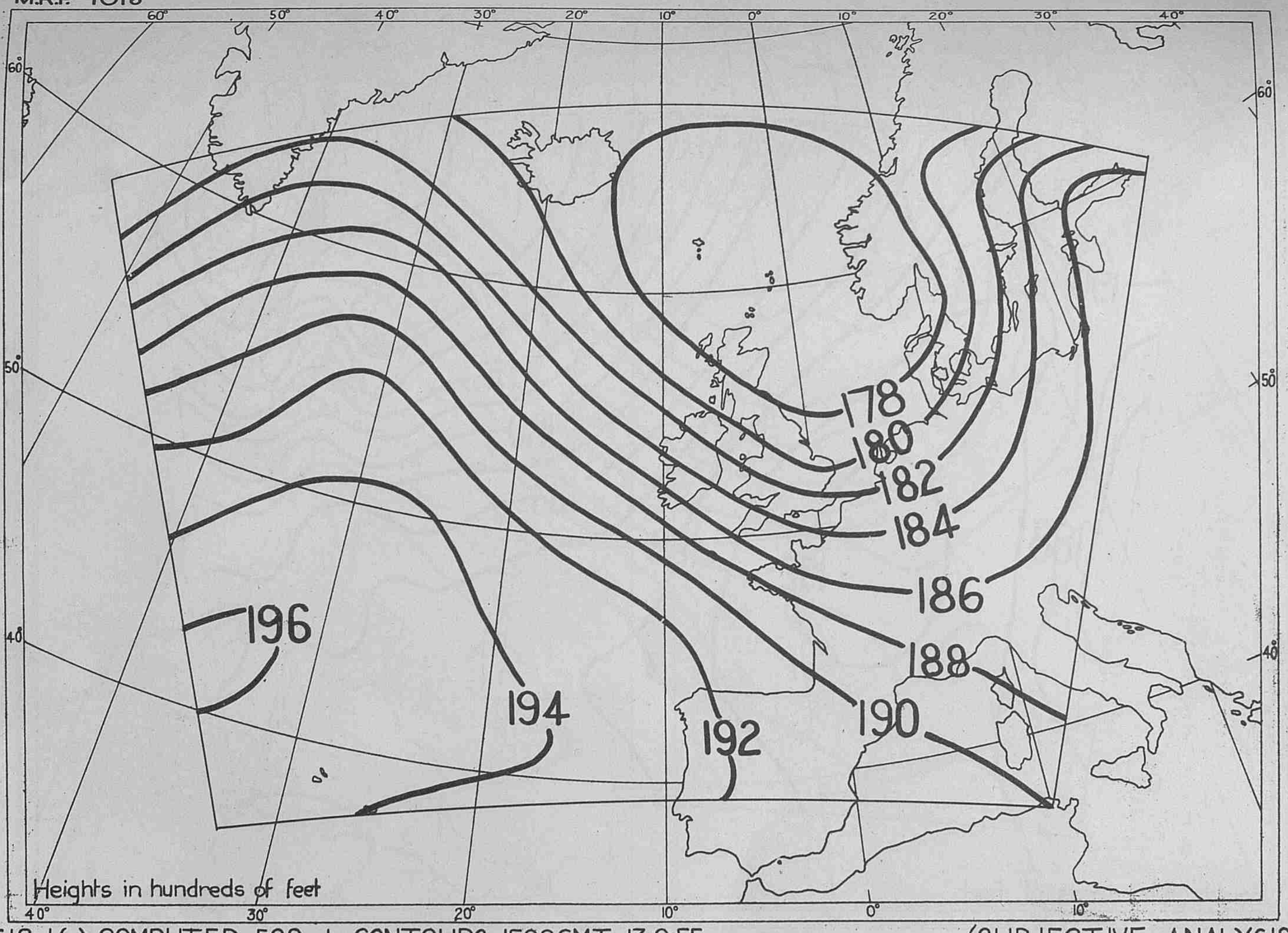
60°
50°
40°
30°
20°
10°
0°
10°
20°
30°
40°
60°
50°
40°
60°
50°
40°
178
180
182
184
186
188
190
192
194
196
Heights in hundreds of feet
40°
30°
20°
10°
0°
10°

FIG. 1(e) COMPUTED 500 mb. CONTOURS, 1500 G.M.T. 13·9·55 (SUBJECTIVE ANALYSIS)

MRP 1016

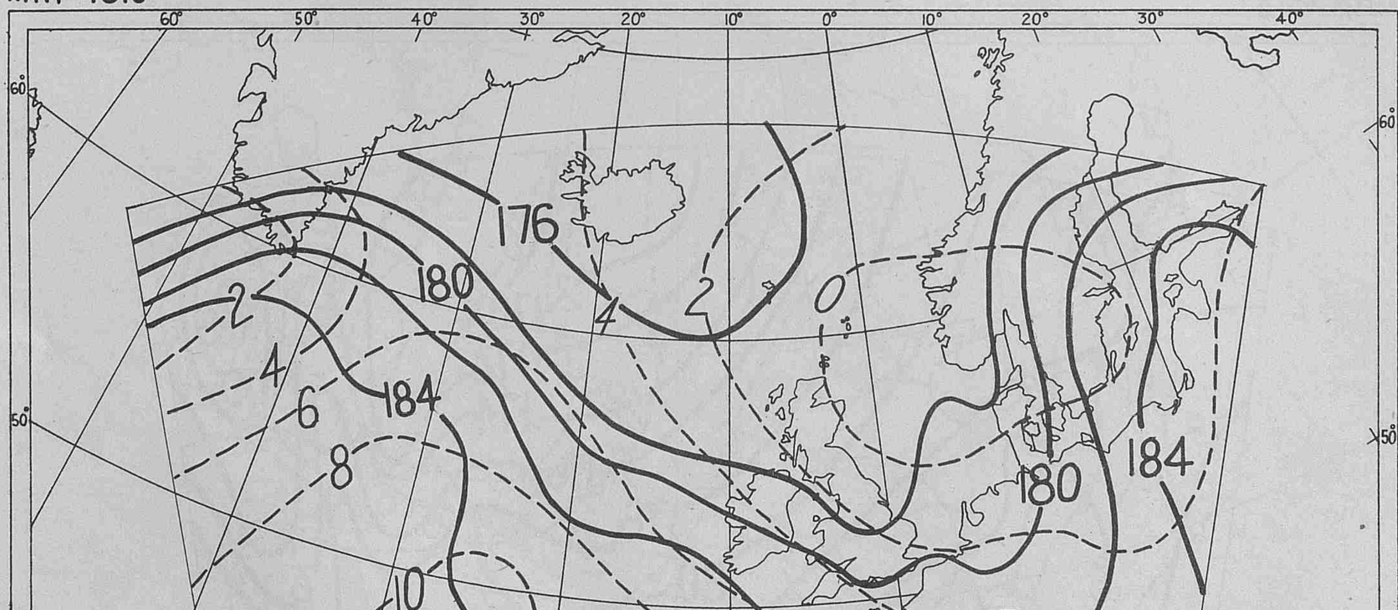
60°
50°
40°
30°
20°
10°
0°
10°
20°
30°
40°
60°
50°
40°
60°
50°
40°
176
180
184
180
184
186
2
4
6
8
10
10
2
4
0
Heights in hundreds of feet
Computed 1000-500 mb. thickness
1000 mb. contours
40°
30°
20°
10°
0°
10°

FIG. 1(f) COMPUTED 1000-500 mb. THICKNESS AND 1000 mb. CONTOURS 1500 G.M.T. 13·9·55 (SUBJECTIVE ANALYSIS)

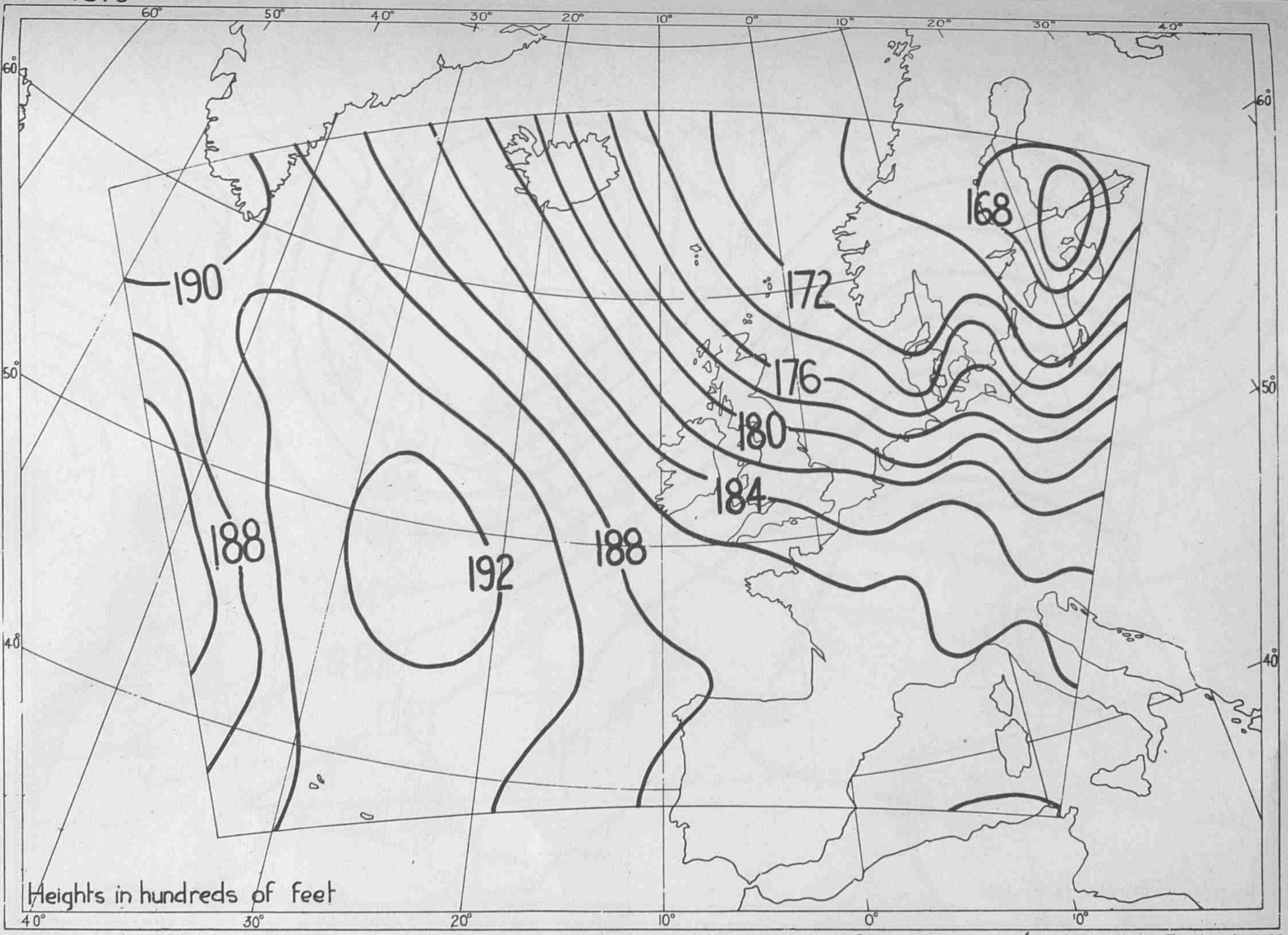
60°
50°
40°
30°
20°
10°
0°
10°
20°
30°
40°
190
188
192
188
168
172
176
180
184
Heights in hundreds of feet

FIG.2(e) COMPUTED 500 mb. CONTOURS FOR 1500 G.M.T. 16:10:55 (SUBJECTIVE ANALYSIS)

M.R.P. 1016

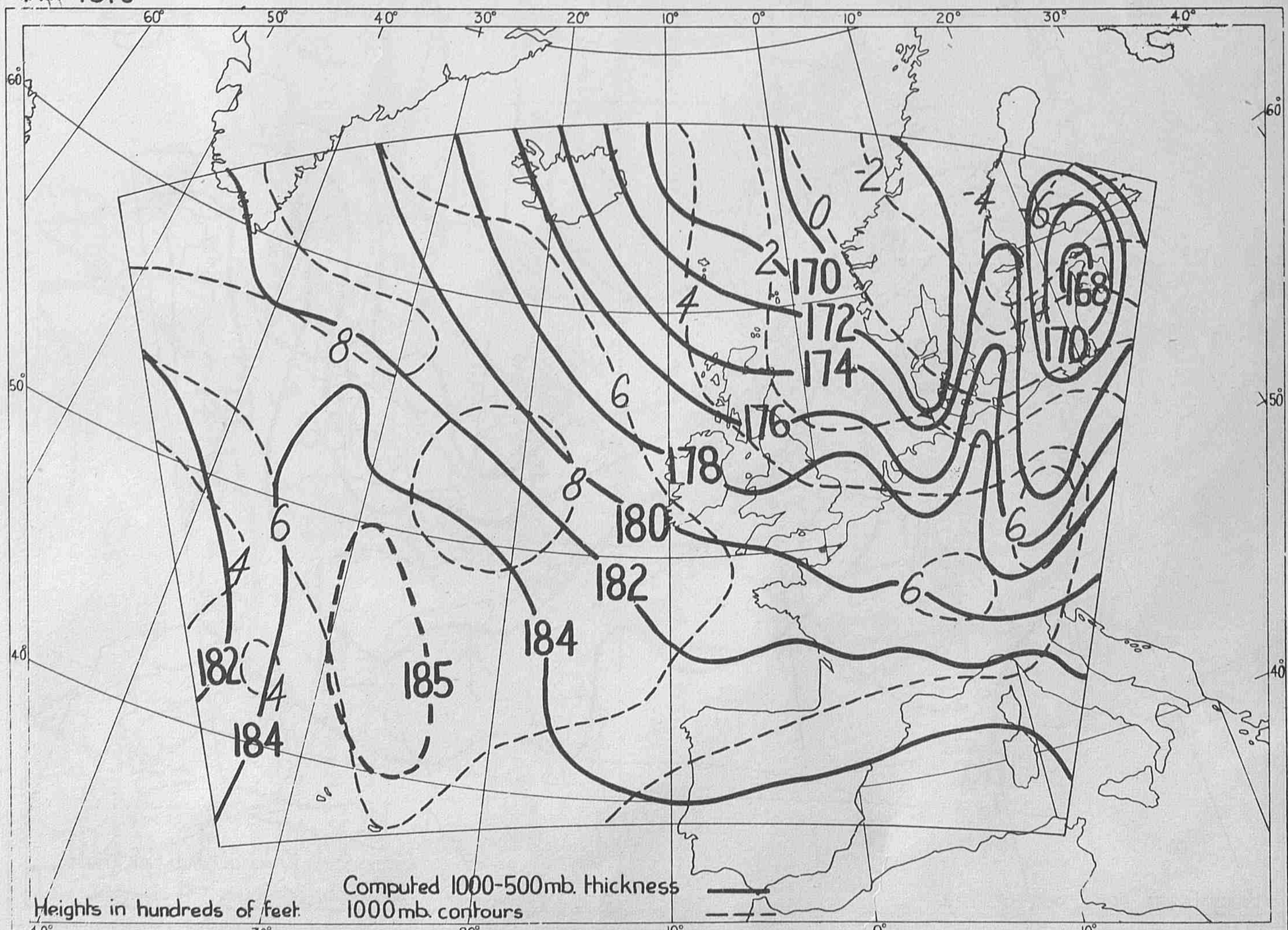
60°
50°
40°
30°
20°
10°
0°
10°
20°
30°
40°
8
6
4
6
8
4
2
0
-2
-4
6
170
172
174
176
178
180
182
184
185
182
184
4
168
170
6
6
Heights in hundreds of feet
Computed 1000-500 mb. thickness
1000 mb. contours

FIG2(F) COMPUTED 1000-500mb THICKNESS AND 1000mb. CONTOURS, 1500GMT. 16:10:55 (SUBJECTIVE ANALYSIS)

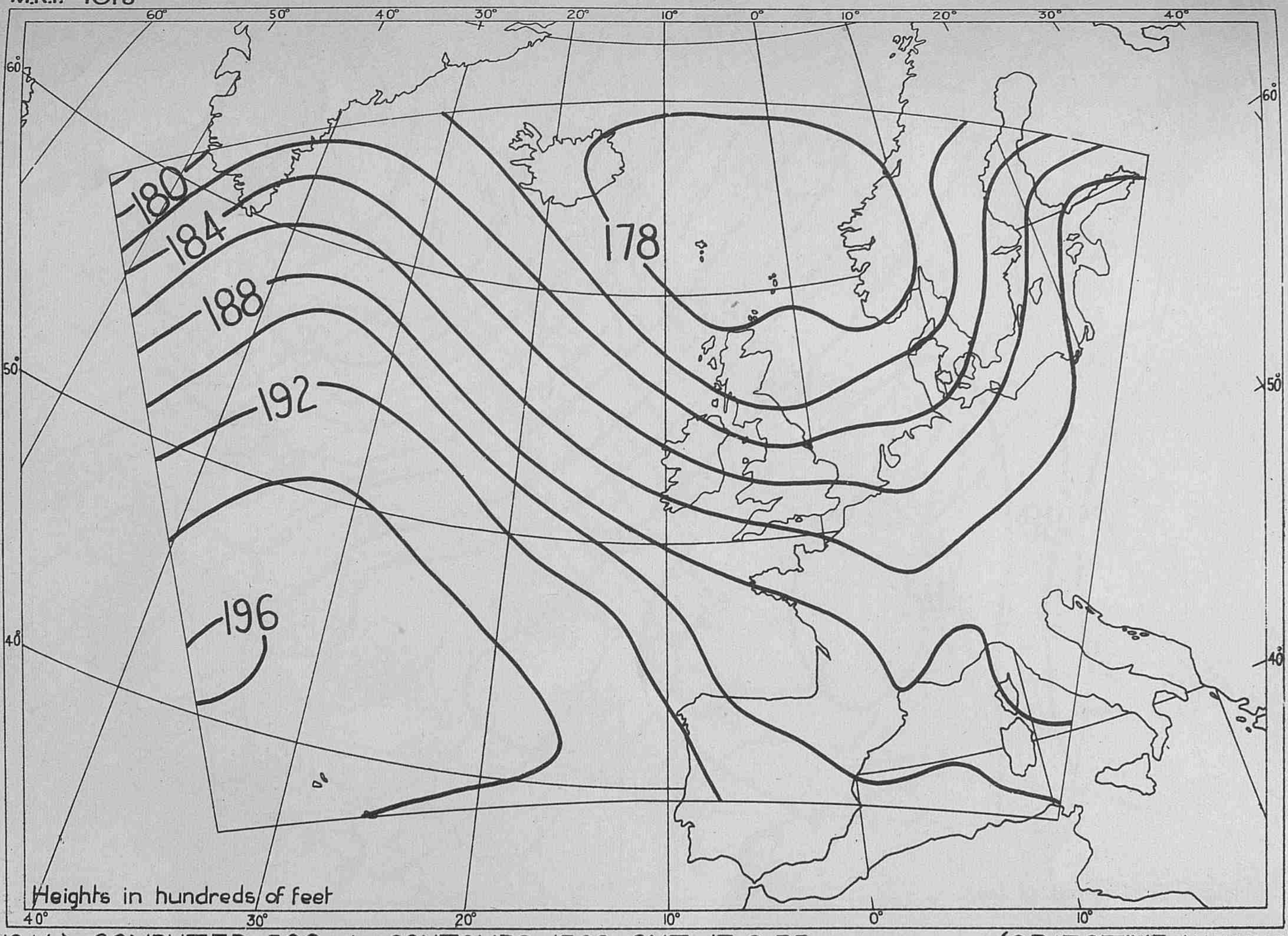
60°
50°
40°
30°
20°
10°
0°
10°
20°
30°
40°
60°
50°
40°
180
184
188
192
196
178
Heights in hundreds of feet
40°
30°
20°
10°
0°
10°

FIG.1(g) COMPUTED 500 mb. CONTOURS, 1500 G.M.T. 13:9:55 (OBJECTIVE ANALYSIS).

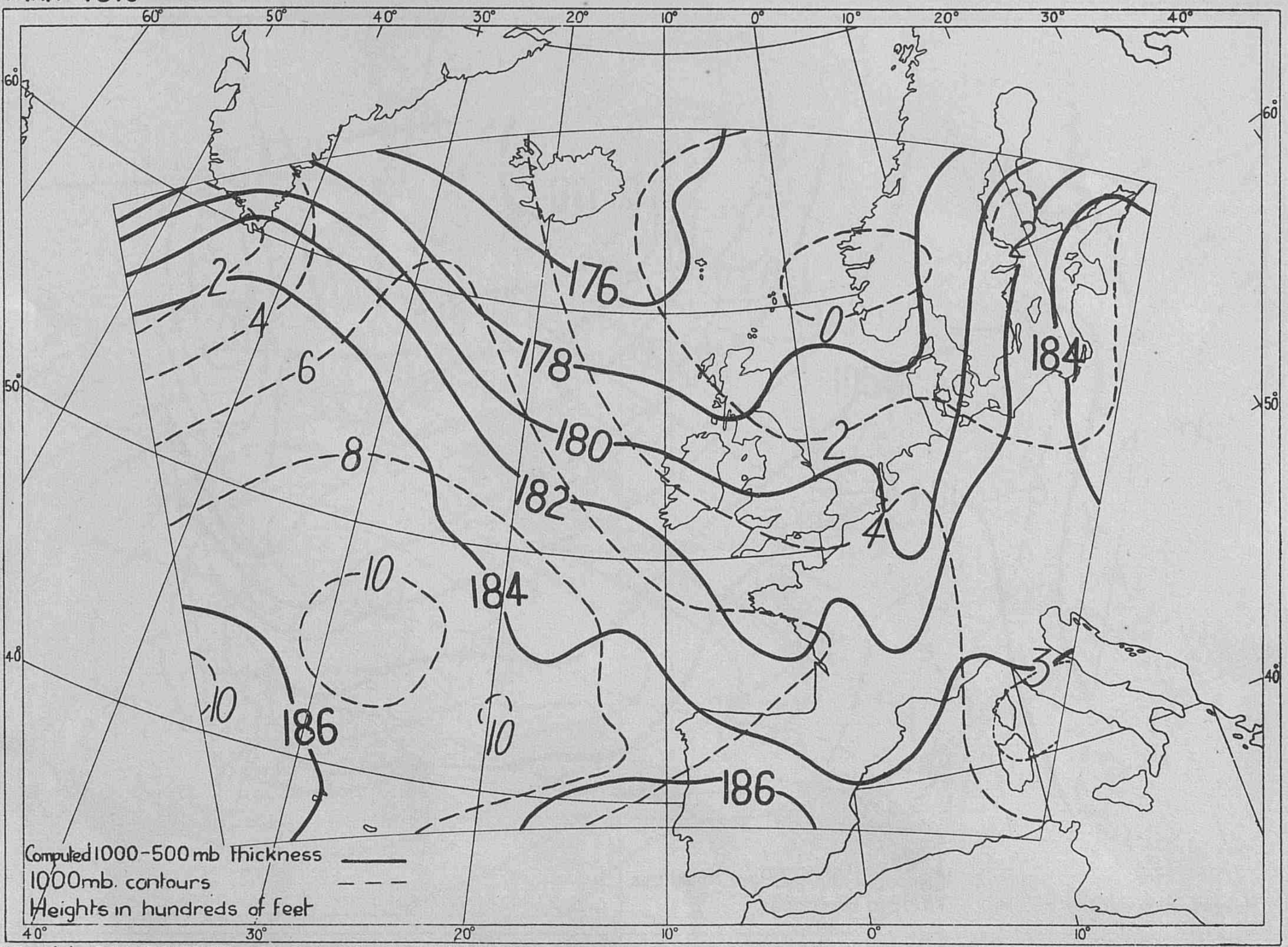
60°
50°
40°
30°
20°
10°
0°
10°
20°
30°
40°
60°
50°
40°
2
4
6
8
10
10
10
176
178
180
182
184
186
186
0
2
4
3
184
Computed 1000-500 mb thickness
1000 mb. contours
Heights in hundreds of feet
40°
30°
20°
10°
0°
10°

FIG. 1(h) COMPUTED 1000-500 mb. THICKNESS AND 1000 mb. CONTOURS, 1500 G.M.T. 13:9:55 (OBJECTIVE ANALYSIS)

M.R.P. 1016

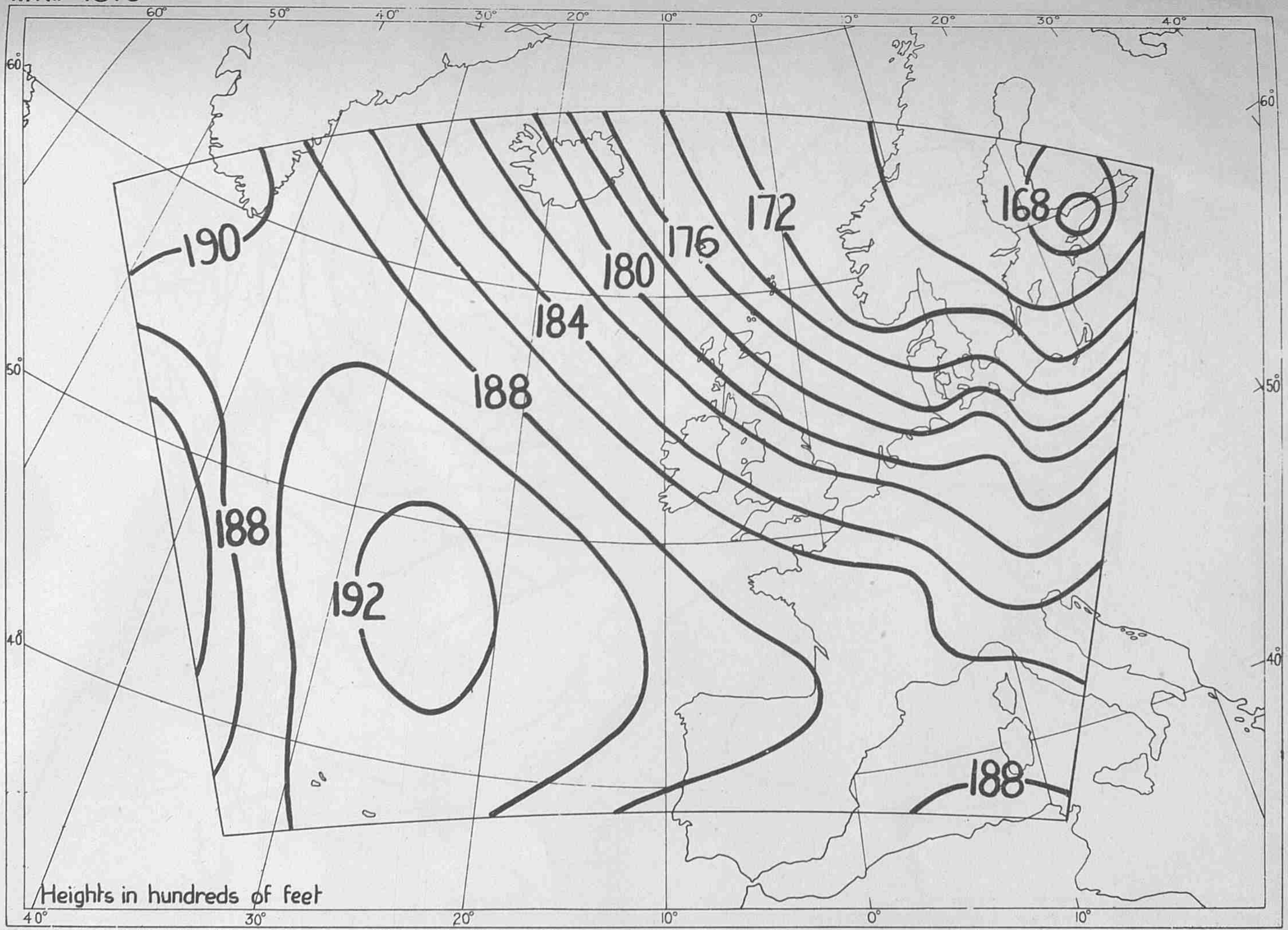
60°
50°
40°
30°
20°
10°
0°
10°
20°
30°
40°
60°
50°
40°
190
188
192
188
184
180
176
172
168
188
Heights in hundreds of feet
40°
30°
20°
10°
0°
10°

FIG 2(g) COMPUTED 500mb CONTOURS, 1500 G.M.T. 16:10:55 (OBJECTIVE ANALYSIS)

M.R.P. 1016

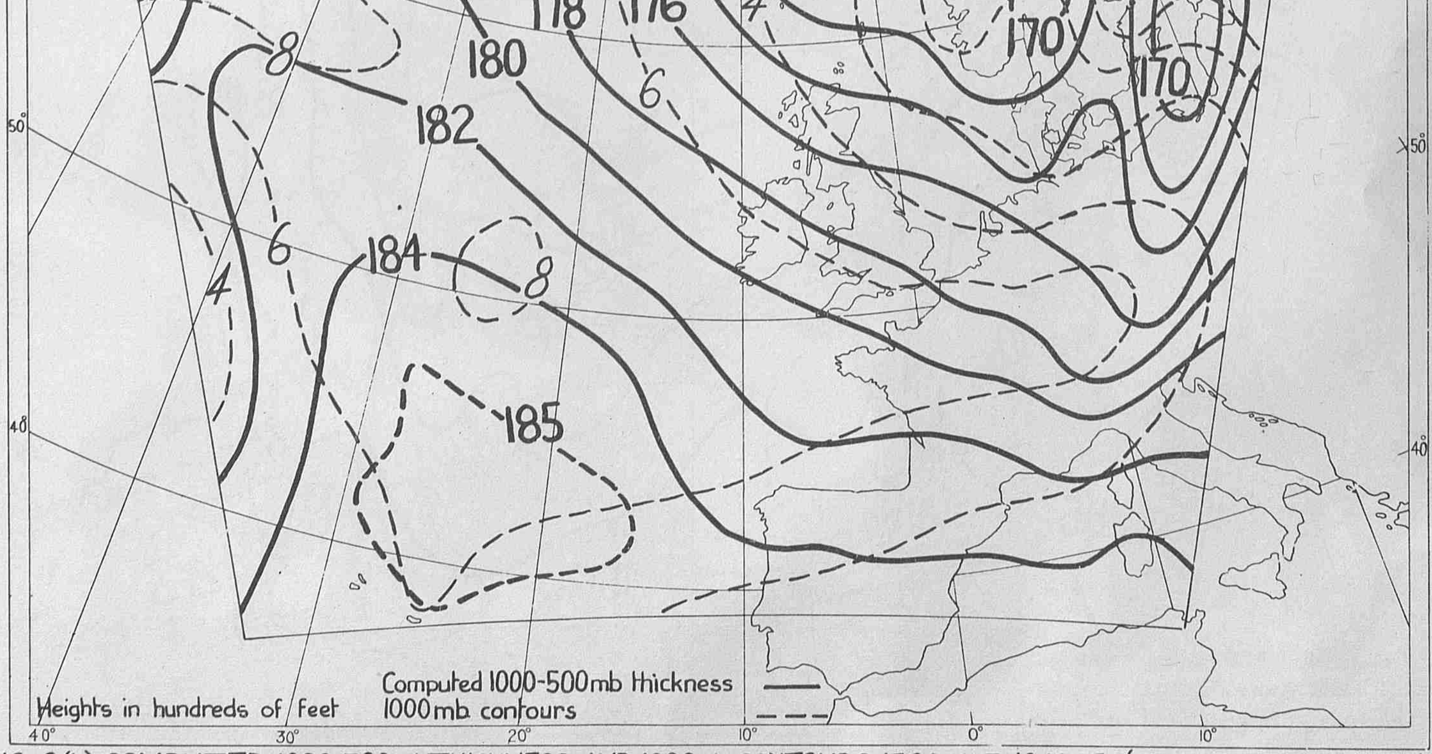
60°
50°
40°
30°
20°
10°
0°
10°
20°
30°
40°
60°
50°
40°
182
8
6
4
184
8
185
180
182
178
176
174
172
170
6
4
2
0
-2
-4
-6
170
170
Computed 1000-500mb thickness
1000mb contours
Heights in hundreds of feet
40°
30°
20°
10°
0°
10°

FIG. 2(h) COMPUTED 1000-500mb THICKNESS AND 1000mb. CONTOURS, 1500G.M.T. 16:10:55 (OBJECTIVE ANALYSIS)

M.R.P. 1016

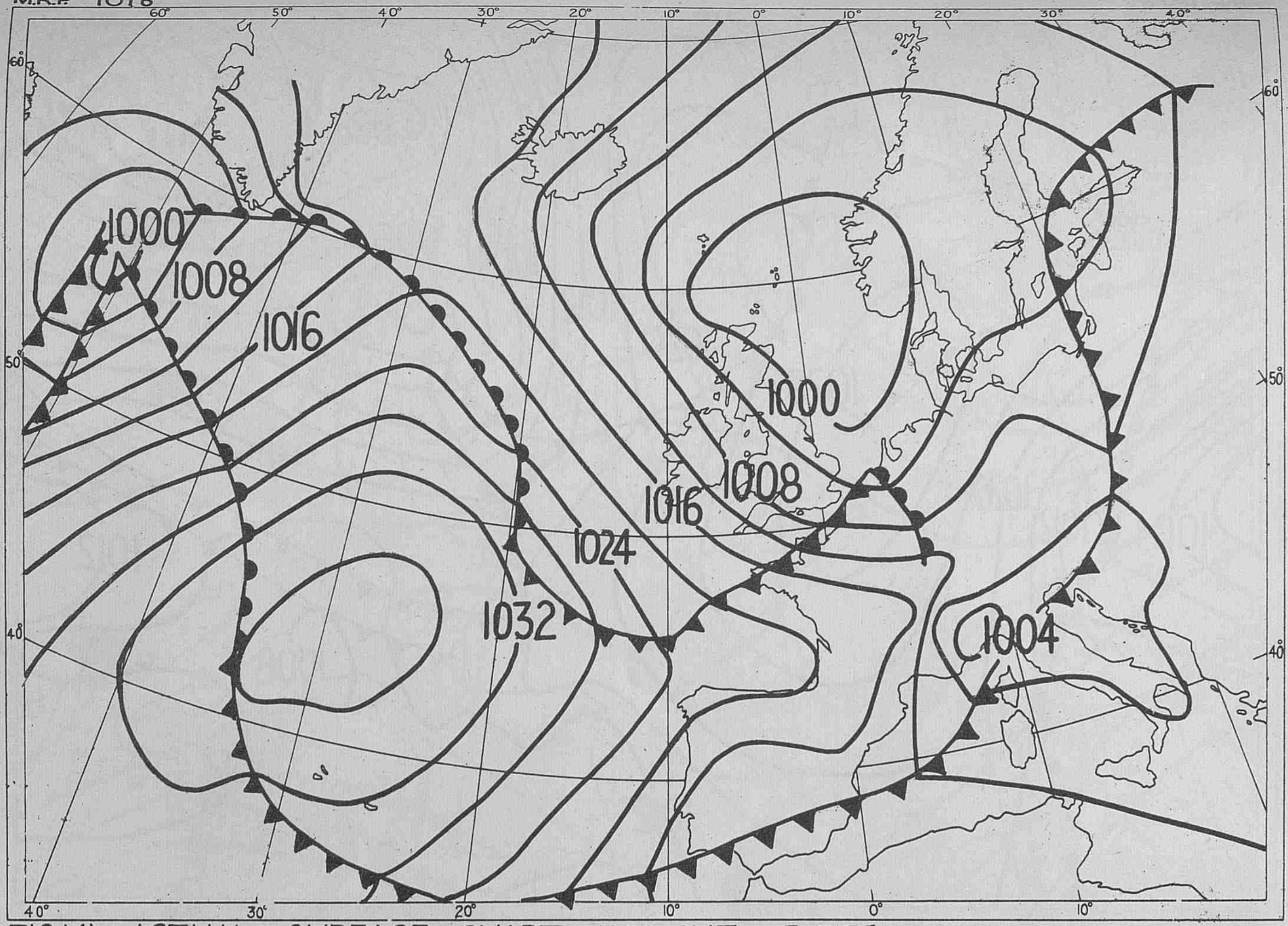

60°
50°
40°
30°
20°
10°
0°
10°
20°
30°
40°
60°
50°
40°
1000
1008
1016
1000
1008
1016
1024
1032
1004
40°
30°
20°
10°
0°
10°

FIG.1(i) ACTUAL SURFACE CHART 1800 G.M.T. 13:9:55

M.R.P. 1016

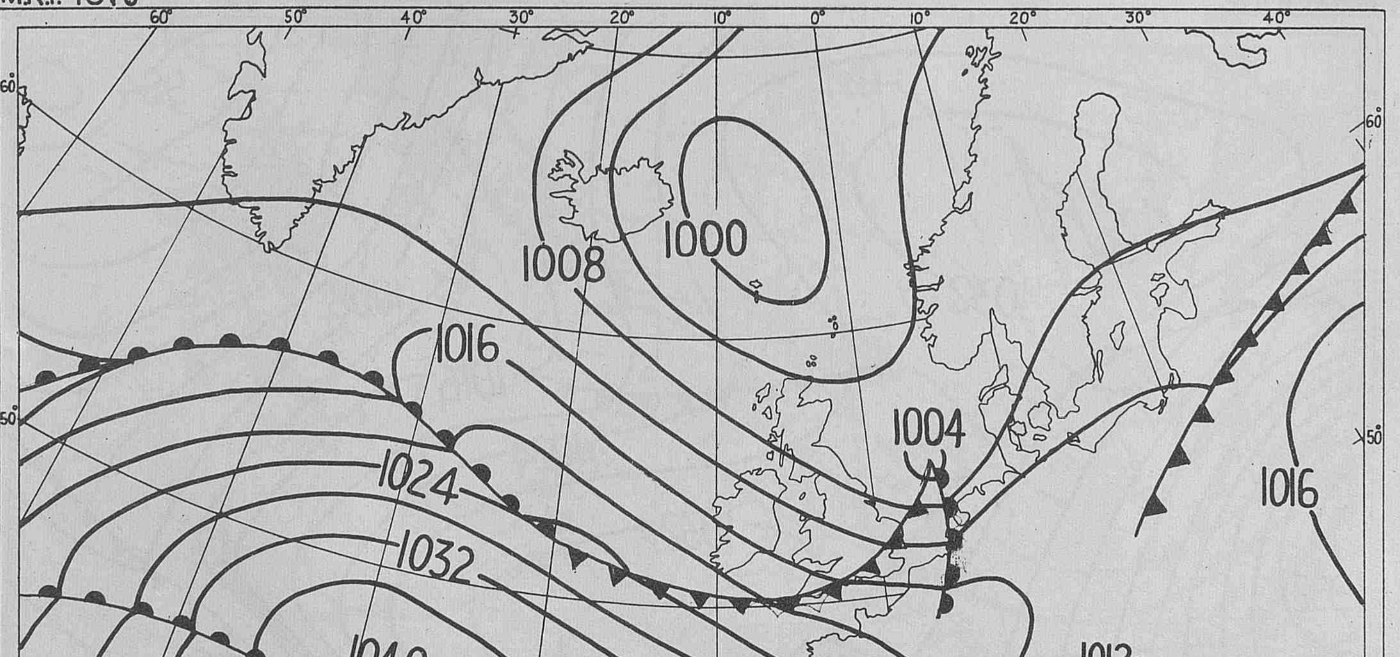

60°
50°
40°
30°
20°
10°
0°
10°
20°
30°
40°
60°
50°
40°
1000
1008
1016
1024
1032
1040
1004
1012
1016
40°
30°
20°
10°
0°
10°

FIG. 1(j) CONVENTIONAL SURFACE FORECAST 1800 G.M.T. 13:9:55

M.R.P. 1016

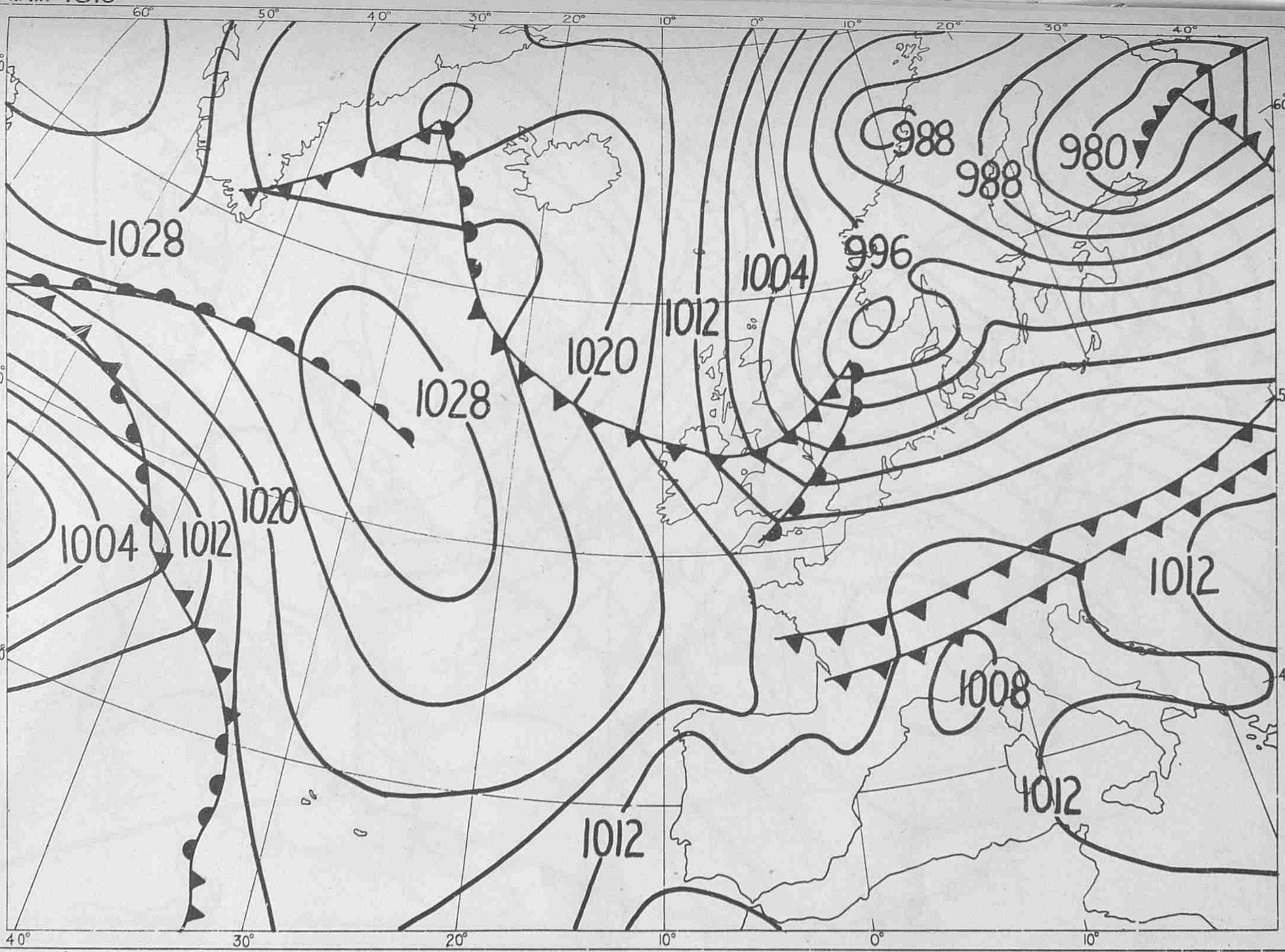
60°
50°
40°
30°
20°
10°
0°
10°
20°
30°
40°
1028
1028
1020
1012
1004
996
988
988
980
1004
1012
1020
1012
1008
1012
1012
50°
40°
60°

FIG. 2(i) ACTUAL SURFACE CHART, 1800 G.M.T. 16:10:55

M.R.P. 1016

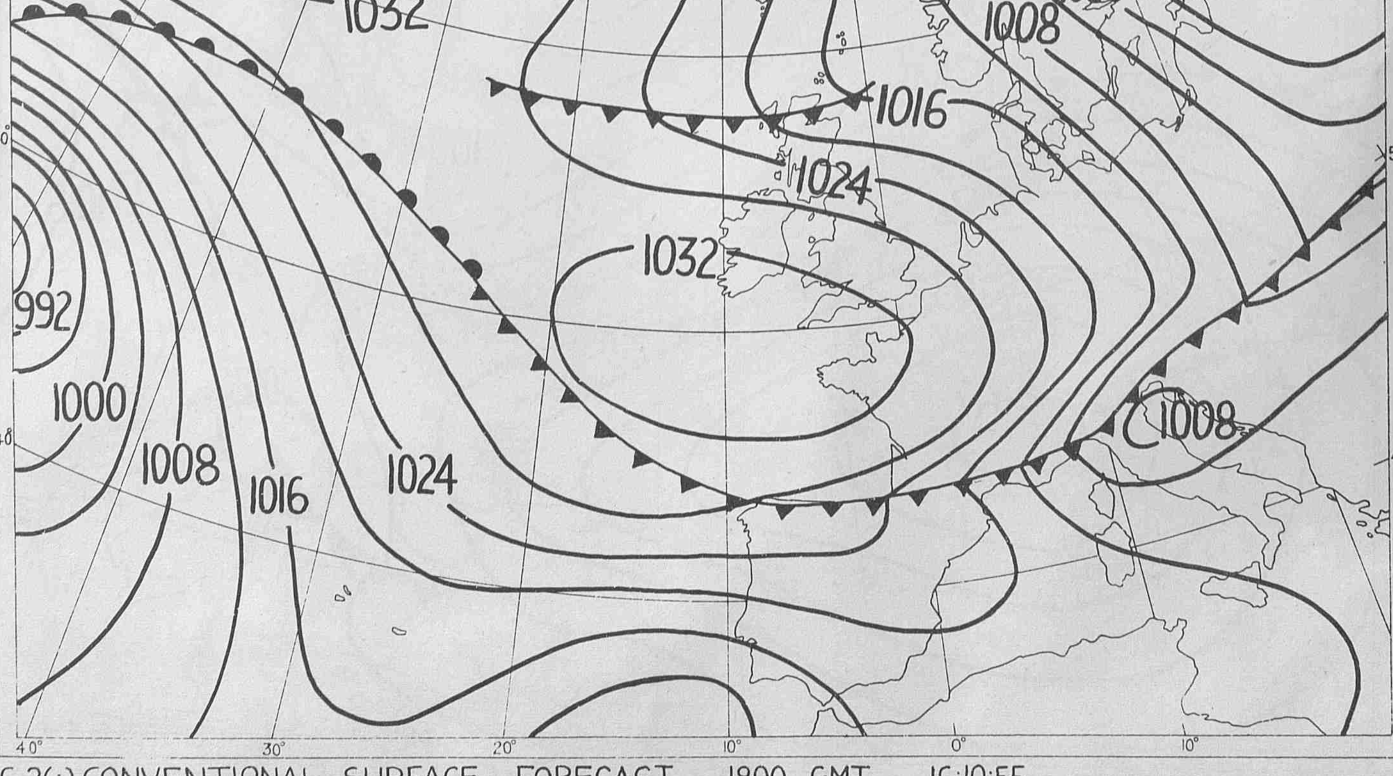
60°
50°
40°
30°
20°
10°
0°
10°
20°
30°
40°
1032
984
992
1000
1008
1016
1024
1032
992
1000
1008
1016
1024
1008
60°
50°
40°

FIG. 2(j) CONVENTIONAL SURFACE FORECAST, 1800 G.M.T. 16:10:55

M.R.P. 1016

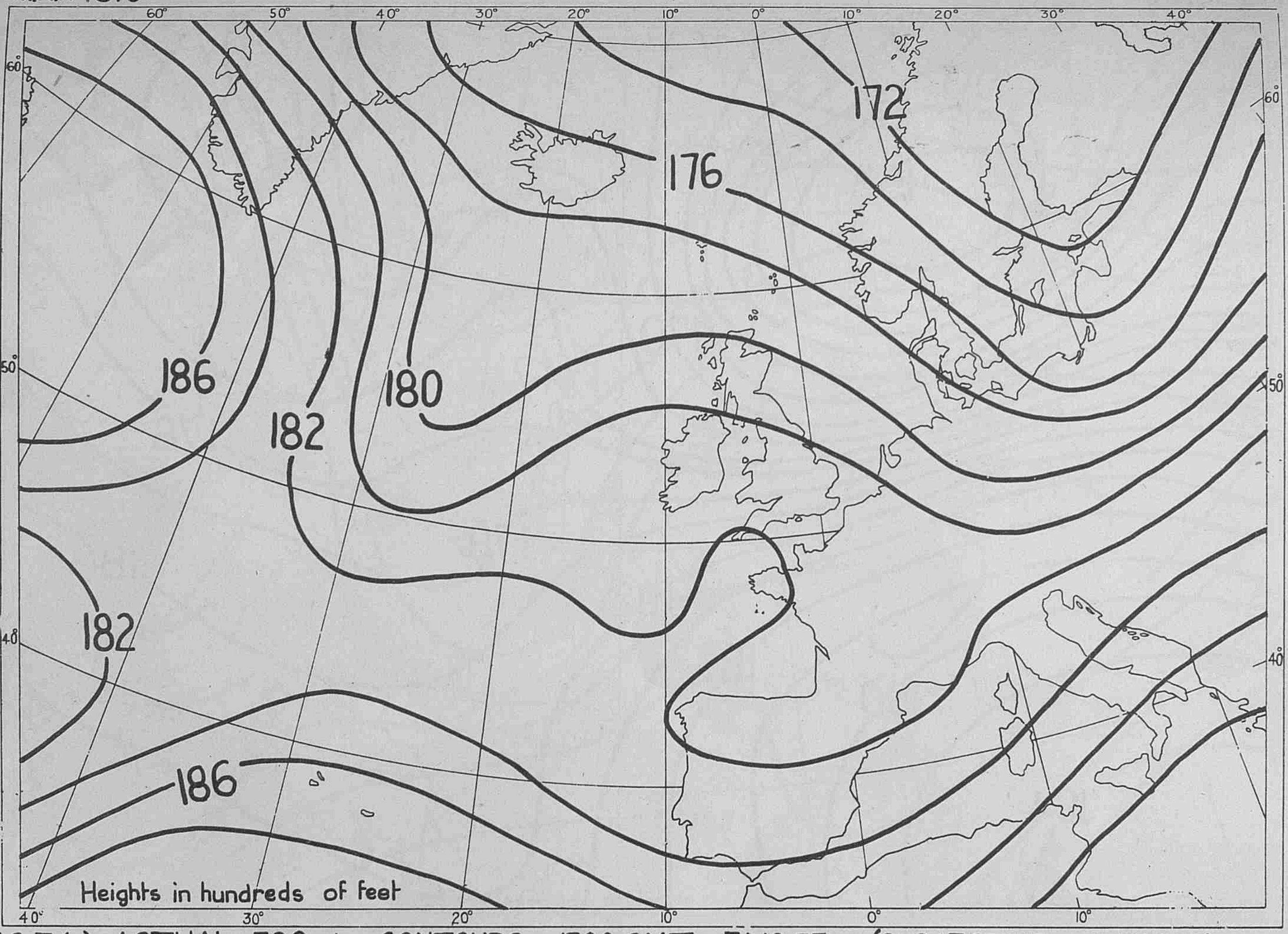
60°
50°
40°
30°
20°
10°
0°
10°
20°
30°
40°
60°
60°
50°
50°
40°
40°
172
176
186
182
180
182
186
Heights in hundreds of feet
40°
30°
20°
10°
0°
10°

FIG. 3(a) ACTUAL 500mb. CONTOURS, 1500 G.M.T. 31:10:55 (SUBJECTIVE ANALYSIS)

M.R.P. 1016

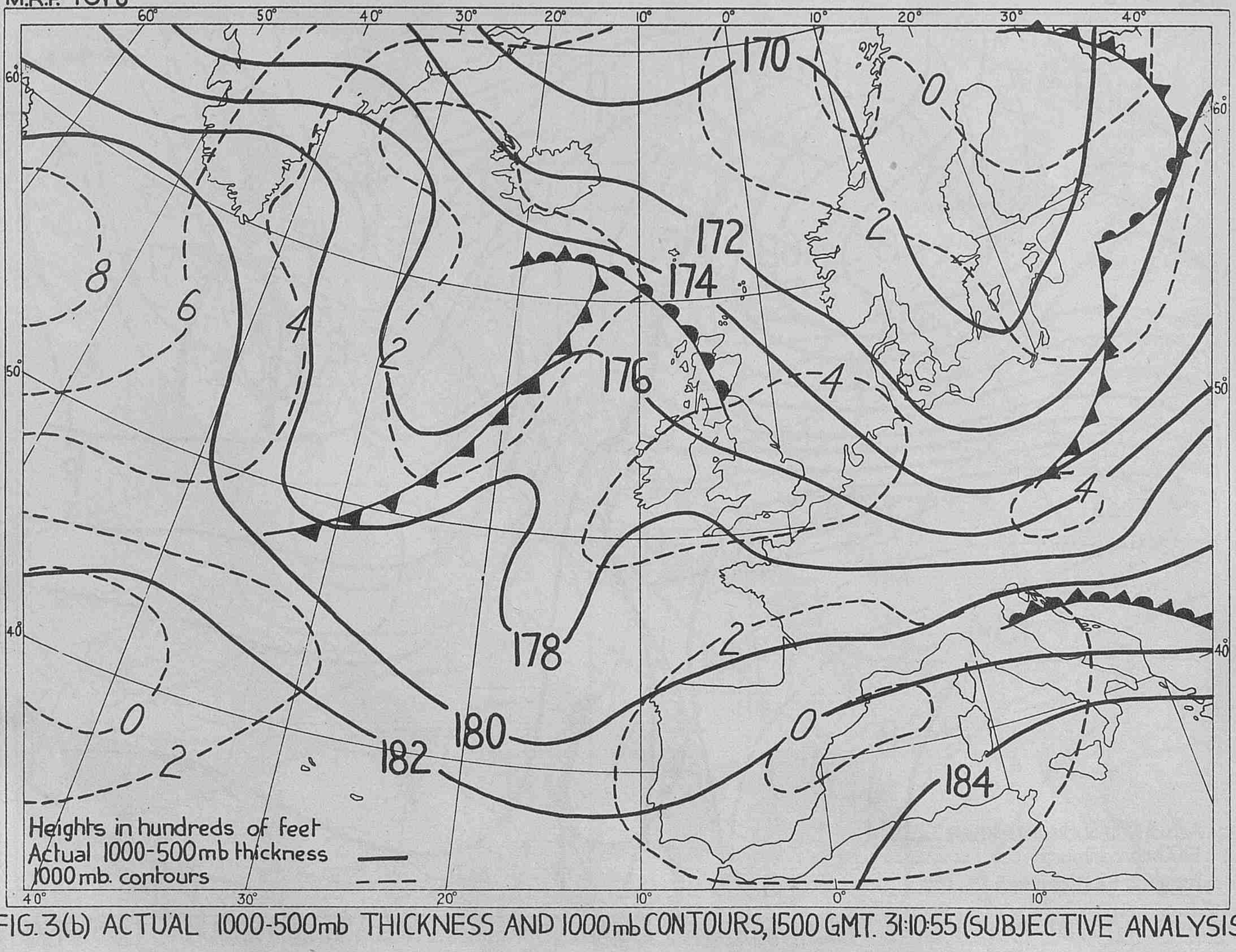
60°
50°
40°
30°
20°
10°
0°
10°
20°
30°
40°
60°
60°
50°
50°
40°
40°
170
0
172
2
174
8
6
4
2
176
4
4
178
2
0
180
0
2
182
184
Heights in hundreds of feet
Actual 1000-500mb thickness
1000 mb. contours
40°
30°
20°
10°
0°
10°

FIG. 3(b) ACTUAL 1000-500mb THICKNESS AND 1000mb CONTOURS, 1500 GMT. 31:10:55 (SUBJECTIVE ANALYSIS)

M.R.P. 1016

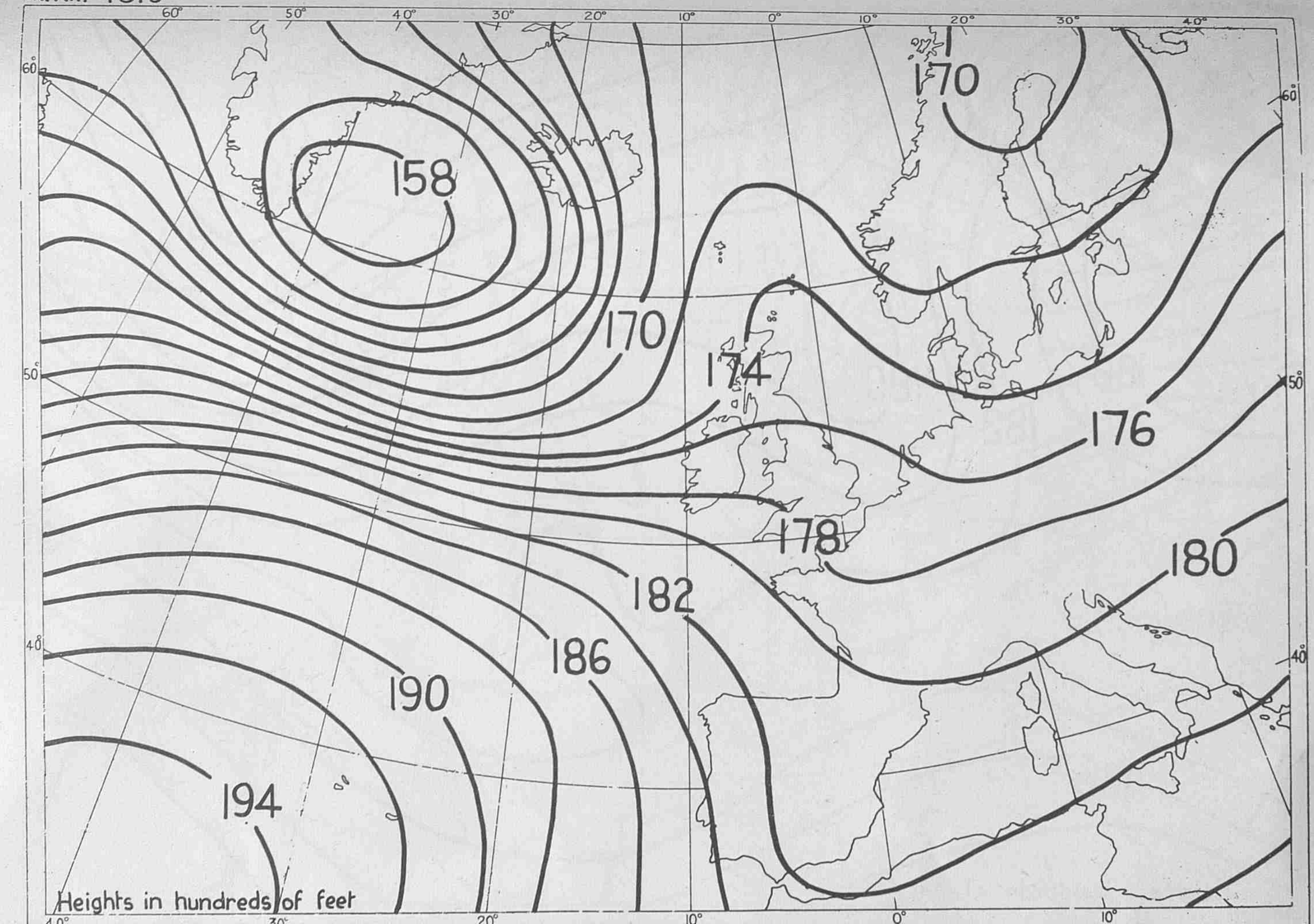

60°
50°
40°
30°
20°
10°
0°
10°
20°
30°
40°
60°
50°
40°
158
170
170
174
176
178
180
182
186
190
194
Heights in hundreds of feet
40°
30°
20°
10°
0°
10°

FIG.4(a) ACTUAL 500mb. CONTOURS, 1500 G.M.T. 30:1:52 (SUBJECTIVE ANALYSIS)

M.R.P. 1016

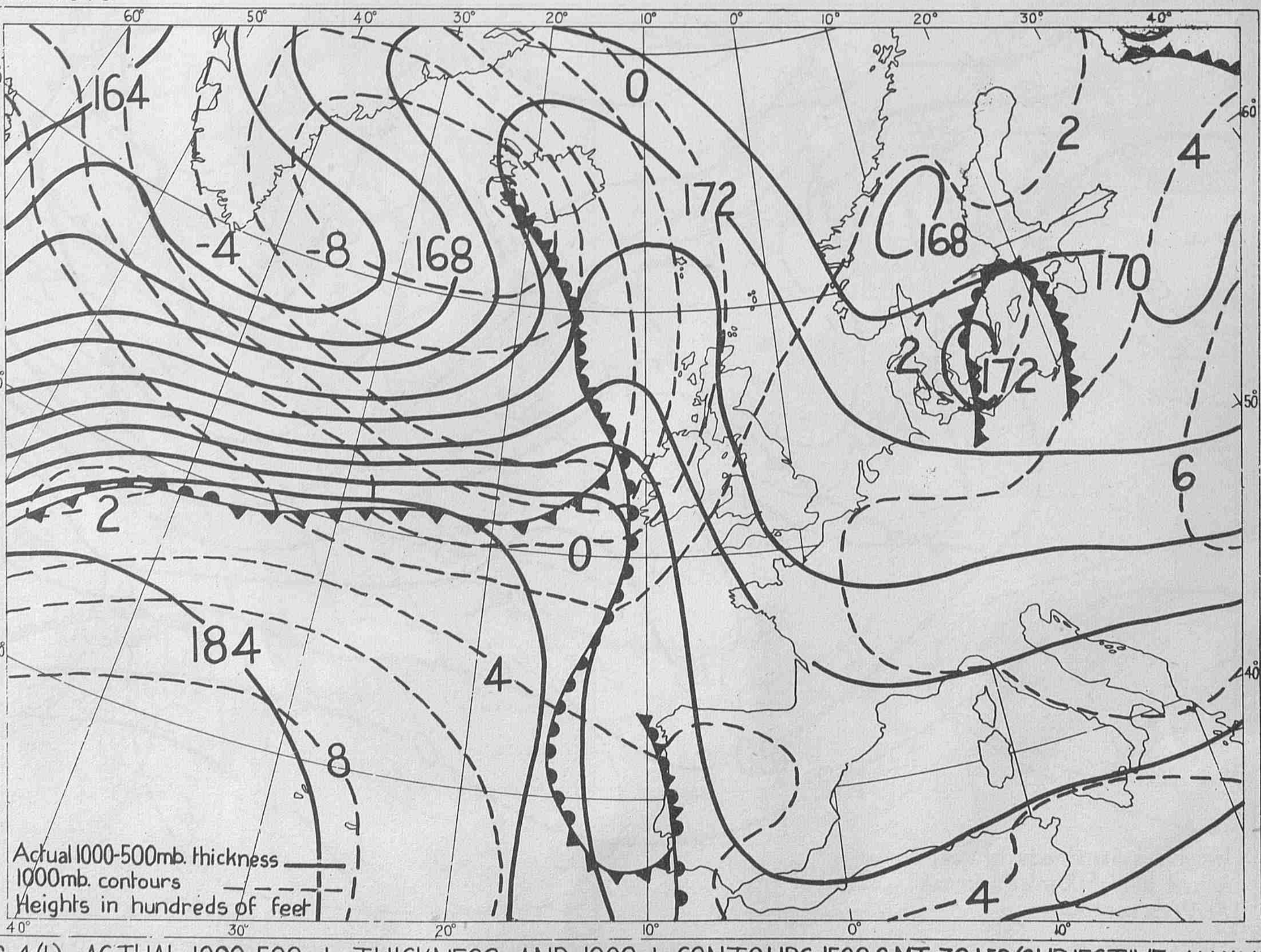

60°
50°
40°
30°
20°
10°
0°
10°
20°
30°
40°
60°
50°
40°
164
-4
-8
168
0
172
168
2
4
170
2
172
6
2
0
184
4
8
-4
Actual 1000-500mb. thickness
1000mb. contours
Heights in hundreds of feet
40°
30°
20°
10°
0°
10°

FIG. 4(b) ACTUAL 1000-500mb. THICKNESS AND 1000mb. CONTOURS, 1500 G.M.T. 30:1:52 (SUBJECTIVE ANALYSIS)

M.R.P. 1016

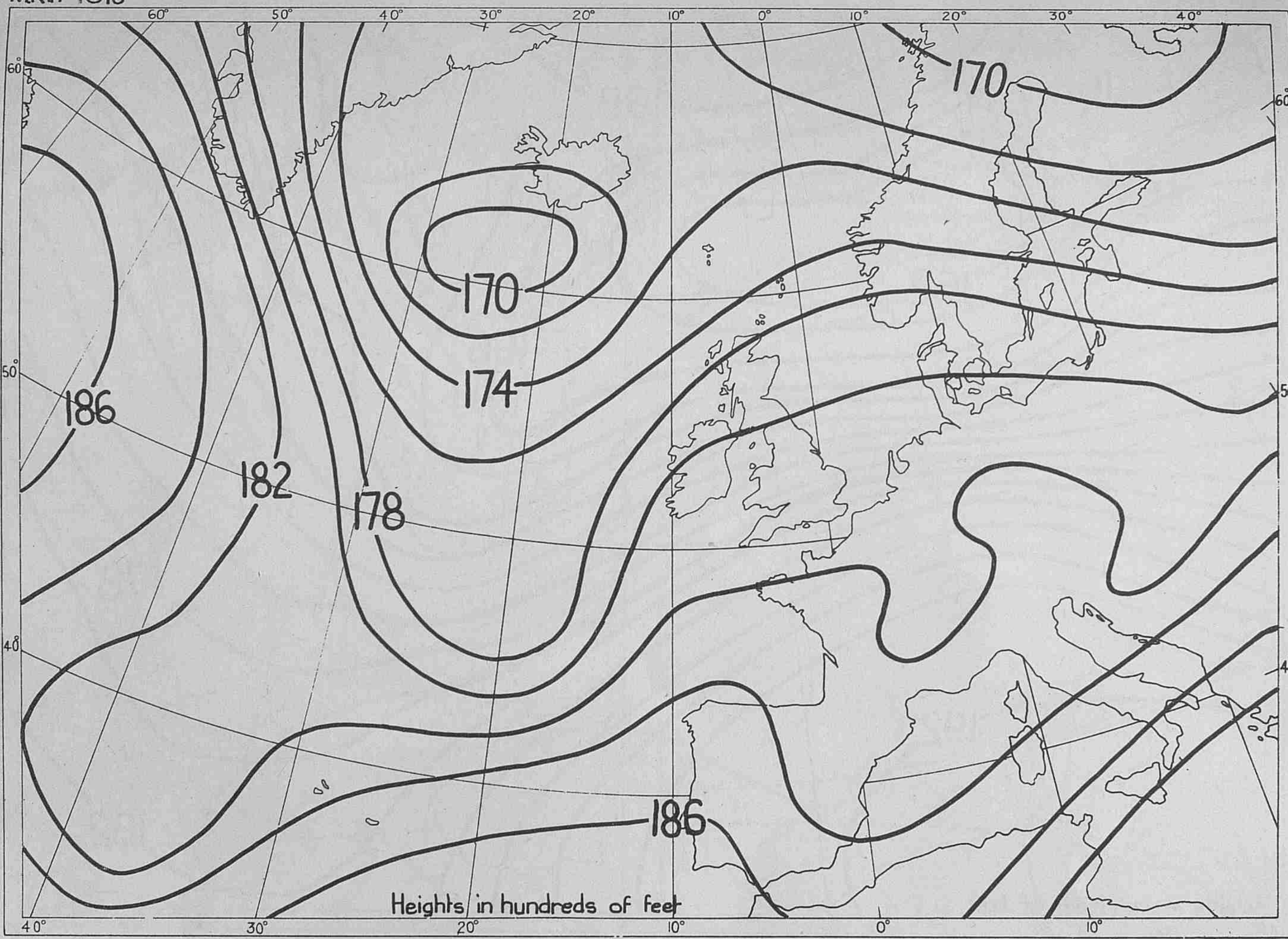
60°
50°
40°
30°
20°
10°
0°
10°
20°
30°
40°
60°
50°
40°
60°
50°
40°
170
170
174
178
182
186
186
Heights in hundreds of feet
40°
30°
20°
10°
0°
10°

FIG. 3(c) ACTUAL 500mb. CONTOURS, 1500 G.M.T. 1:11:55 (SUBJECTIVE ANALYSIS)

M.R.P. 1016

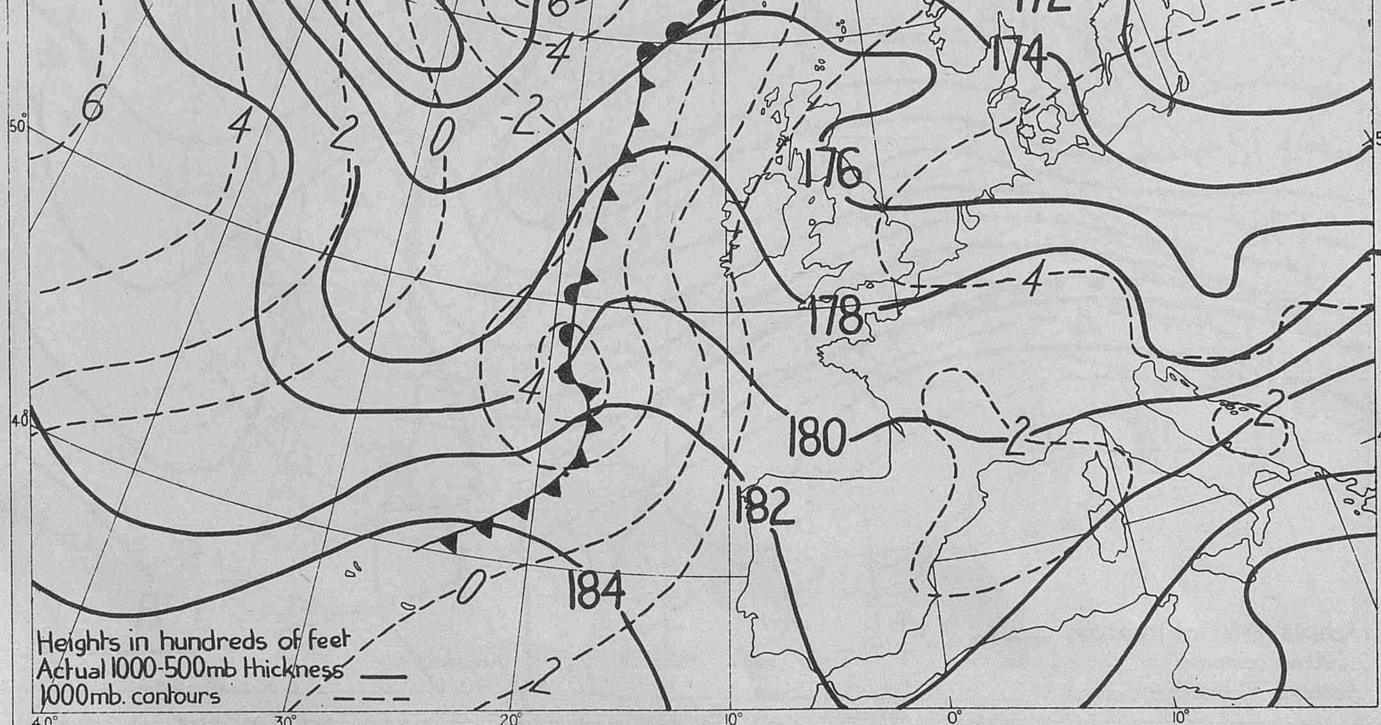
60°
50°
40°
30°
20°
10°
0°
10°
20°
30°
40°
60°
50°
40°
60°
50°
40°
168
170
172
174
176
178
180
182
184
6
6
4
2
0
-2
-4
-6
-4
0
-2
0
2
2
4
2
Heights in hundreds of feet
Actual 1000-500mb thickness ——
1000mb. contours - - -
40°
30°
20°
10°
0°
10°

FIG. 3 (d) ACTUAL 1000-500mb. THICKNESS AND 1000mb. CONTOURS, 1500 G.M.T. 1:11:55

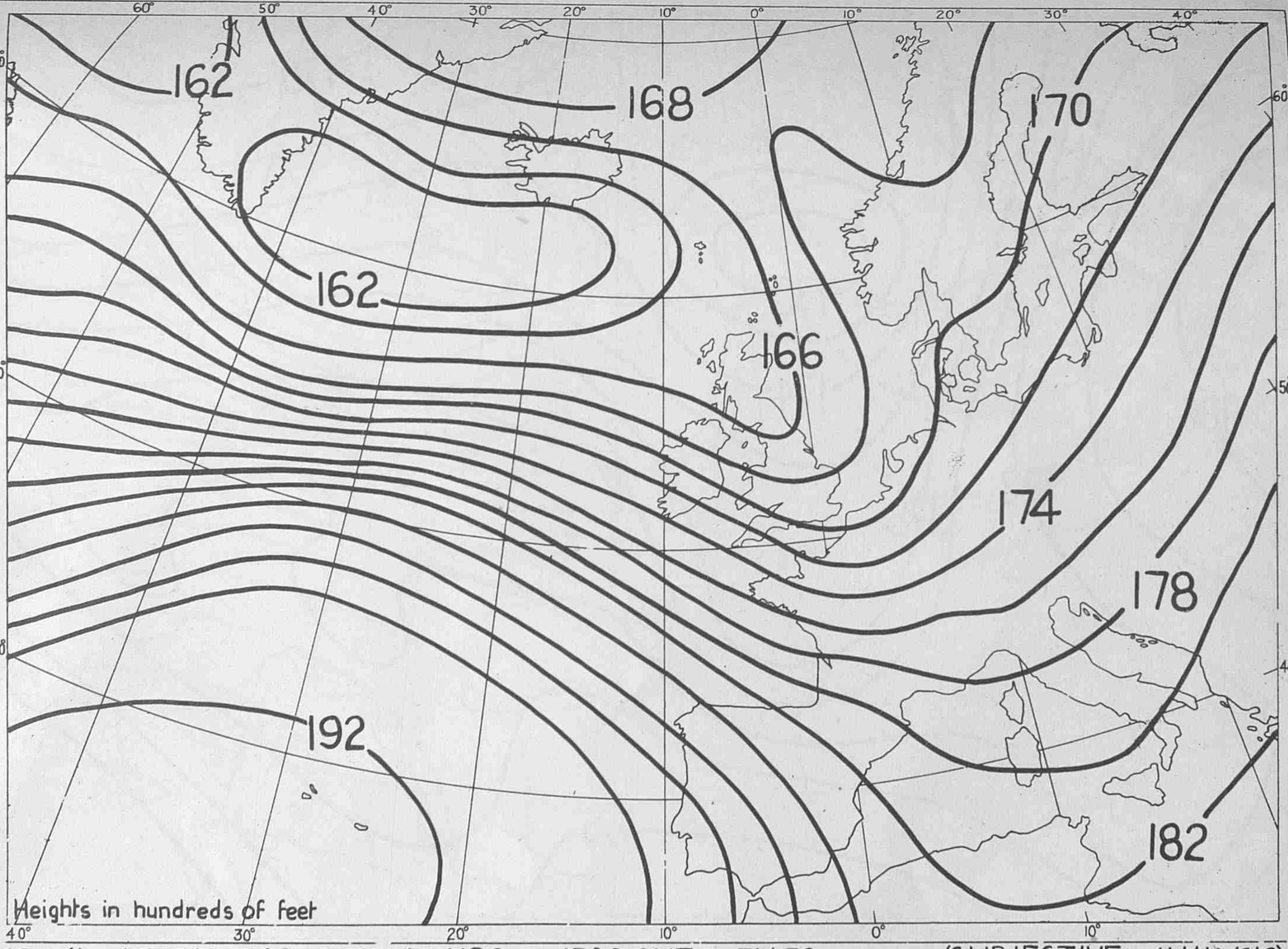
60°
50°
40°
30°
20°
10°
0°
10°
20°
30°
40°
60°
50°
40°
162
168
170
162
166
174
178
192
182
Heights in hundreds of feet
40°
30°
20°
10°
0°
10°

FIG. 4(c) ACTUAL 500 mb. CONTOURS 1500 G.M.T. 31.1.52 (SUBJECTIVE ANALYSIS)

M.R.P. 1016

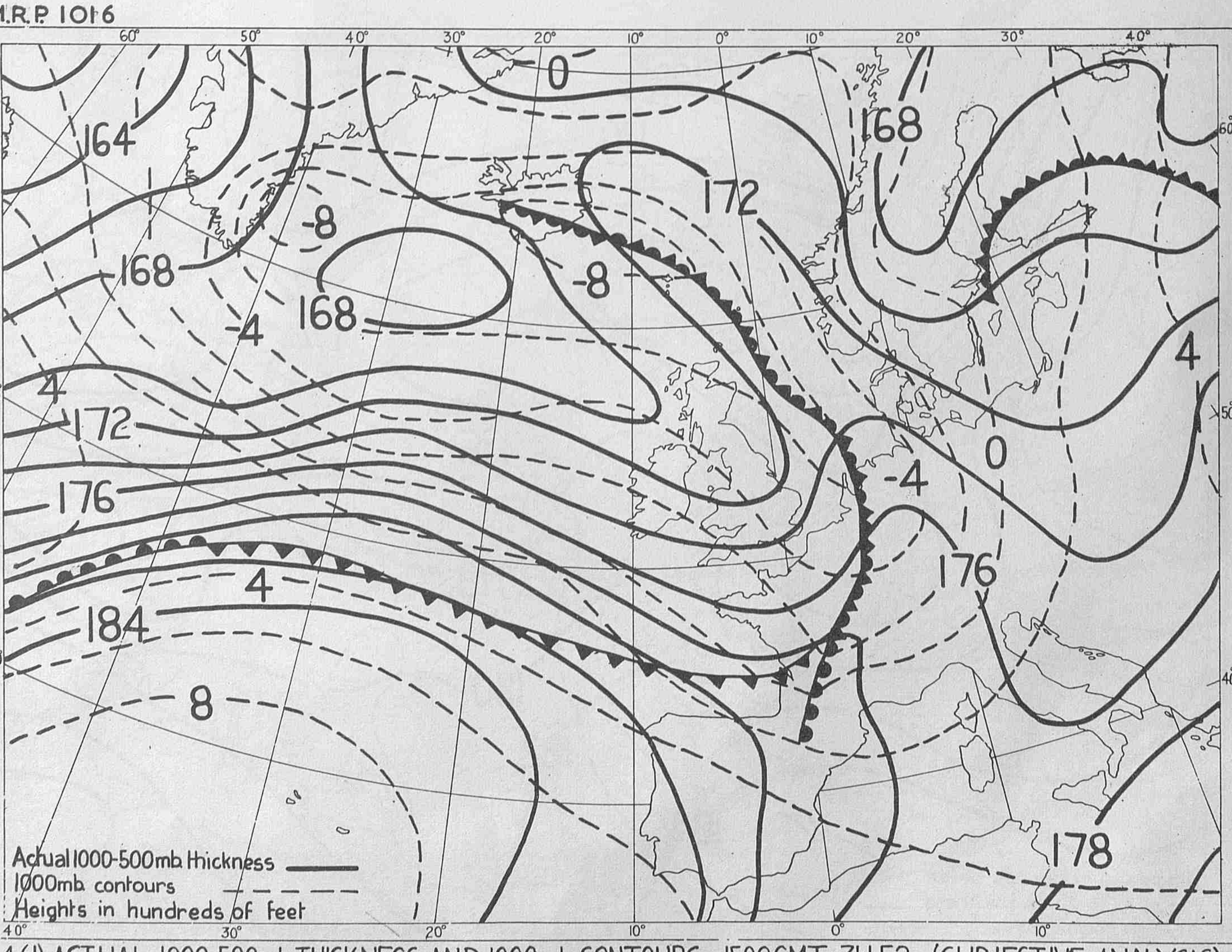
60°
50°
40°
30°
20°
10°
0°
10°
20°
30°
40°
60°
50°
40°
0
164
168
172
-8
-8
168
-4
168
4
172
4
0
-4
176
176
4
184
8
178
Actual 1000-500 mb. thickness
1000 mb. contours
Heights in hundreds of feet
30°
20°
10°
0°
10°

FIG. 4(d) ACTUAL 1000-500 mb. THICKNESS AND 1000 mb. CONTOURS 1500 GMT. 31.1.52 (SUBJECTIVE ANALYSIS)

M.R.P. 1016

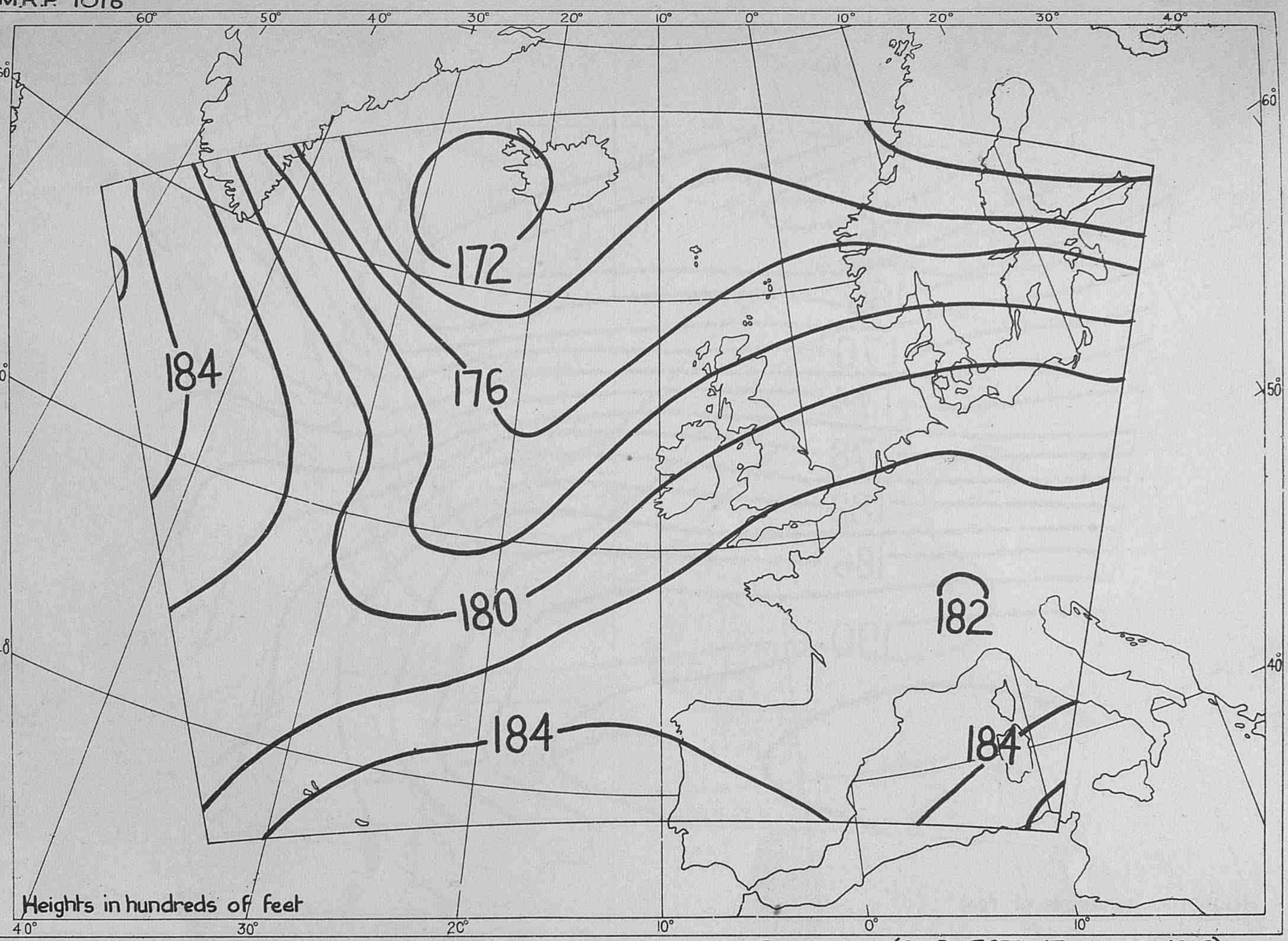

60°
50°
40°
30°
20°
10°
0°
10°
20°
30°
40°
60°
50°
40°
172
176
180
184
184
184
182
Heights in hundreds of feet
40°
30°
20°
10°
0°
10°

FIG. 3(e) COMPUTED 500 mb. CONTOURS 1500 G.M.T. 1:11:55 (SUBJECTIVE ANALYSIS)

M.R.P. 1016

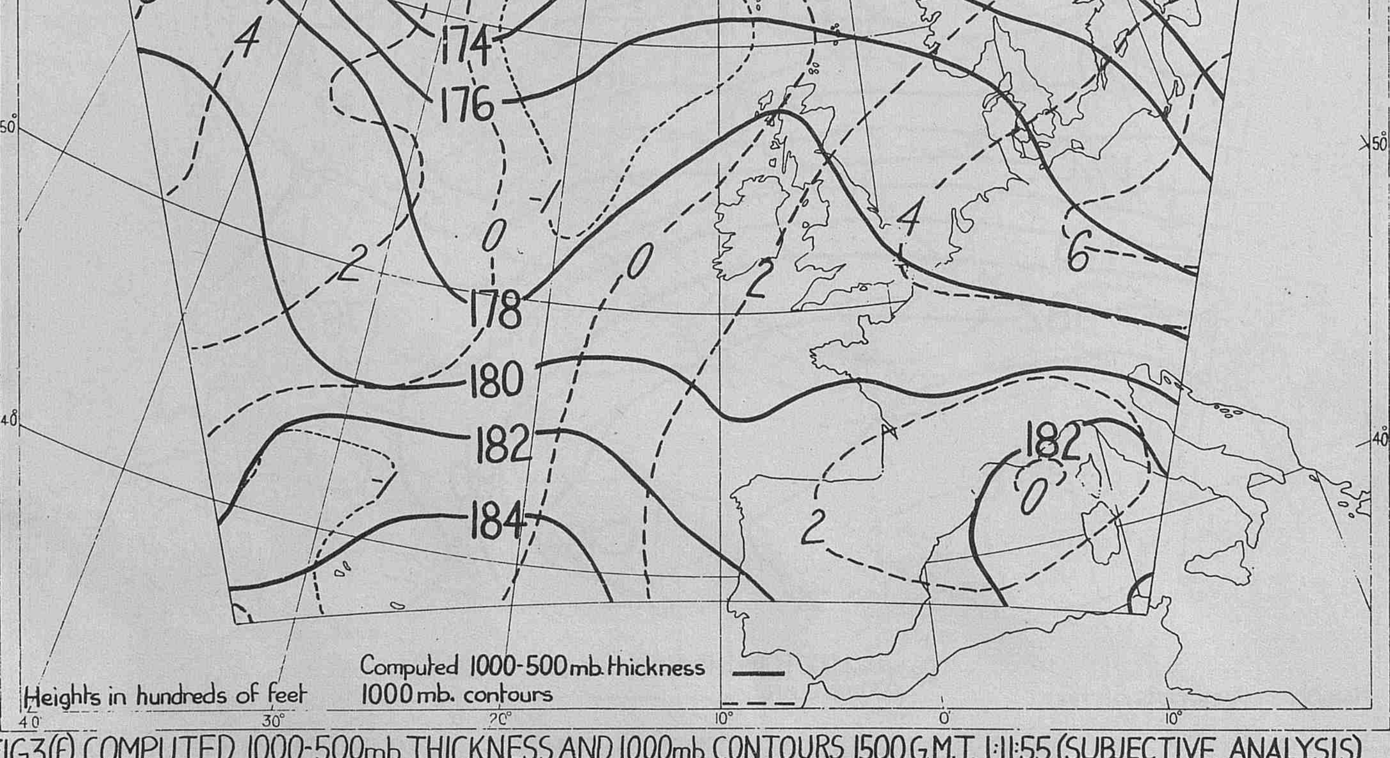

60°
50°
40°
30°
20°
10°
0°
10°
20°
30°
40°
60°
50°
40°
168
170
172
174
176
178
180
182
184
170
182
2
6
4
2
0
-1
0
2
4
6
2
0
Computed 1000-500 mb. thickness
1000 mb. contours
Heights in hundreds of feet
40°
30°
20°
10°
0°
10°

FIG. 3(f) COMPUTED 1000-500 mb. THICKNESS AND 1000 mb. CONTOURS 1500 G.M.T. 1:11:55 (SUBJECTIVE ANALYSIS)

M.R.P. 1016

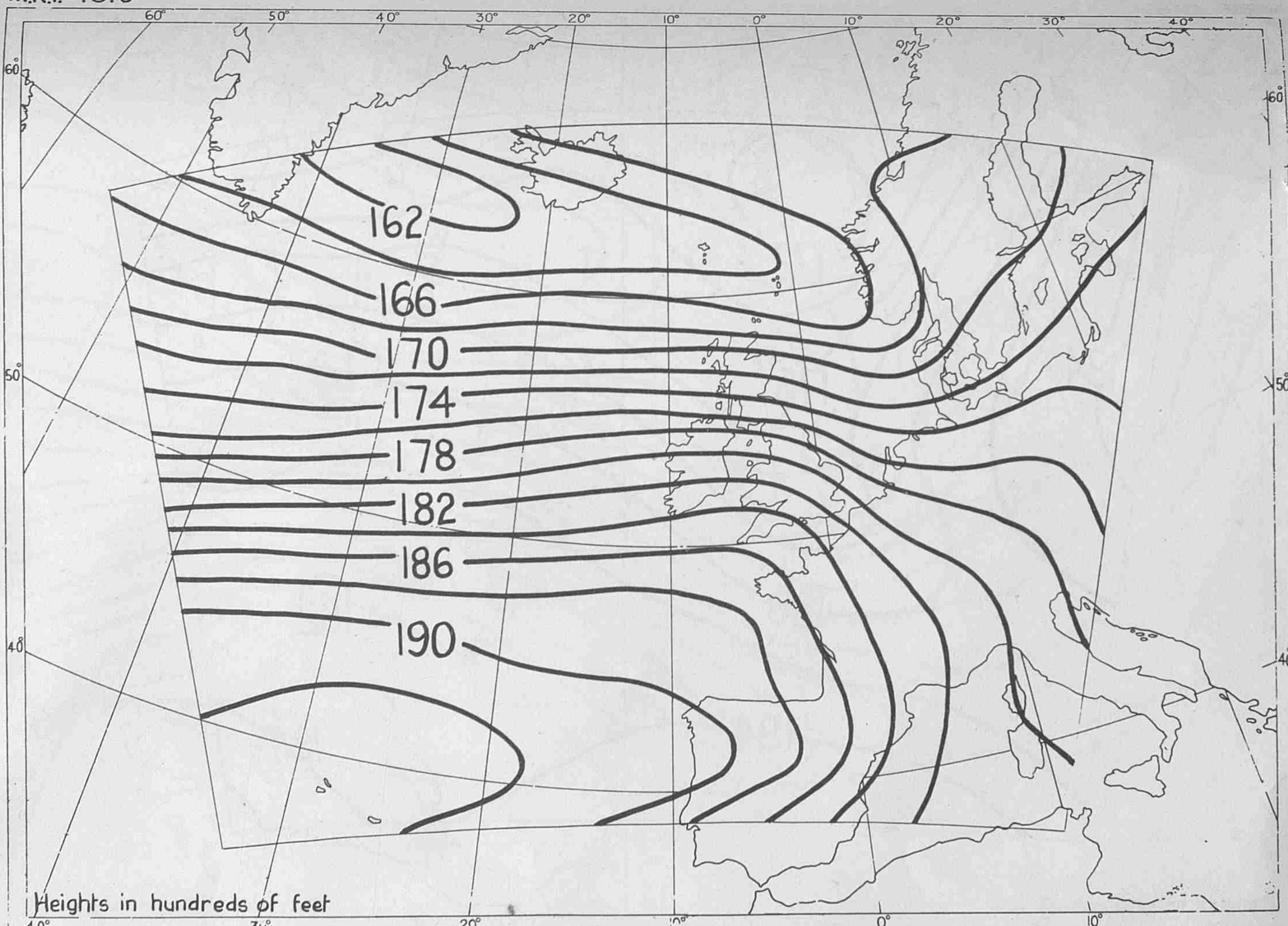
162
166
170
174
178
182
186
190
60°
50°
40°
30°
20°
10°
0°
Heights in hundreds of feet

FIG. 4 (e) COMPUTED 500mb CONTOURS 1500 G.M.T., 31:1:52 (SUBJECTIVE ANALYSIS)

M.R.P. 1016

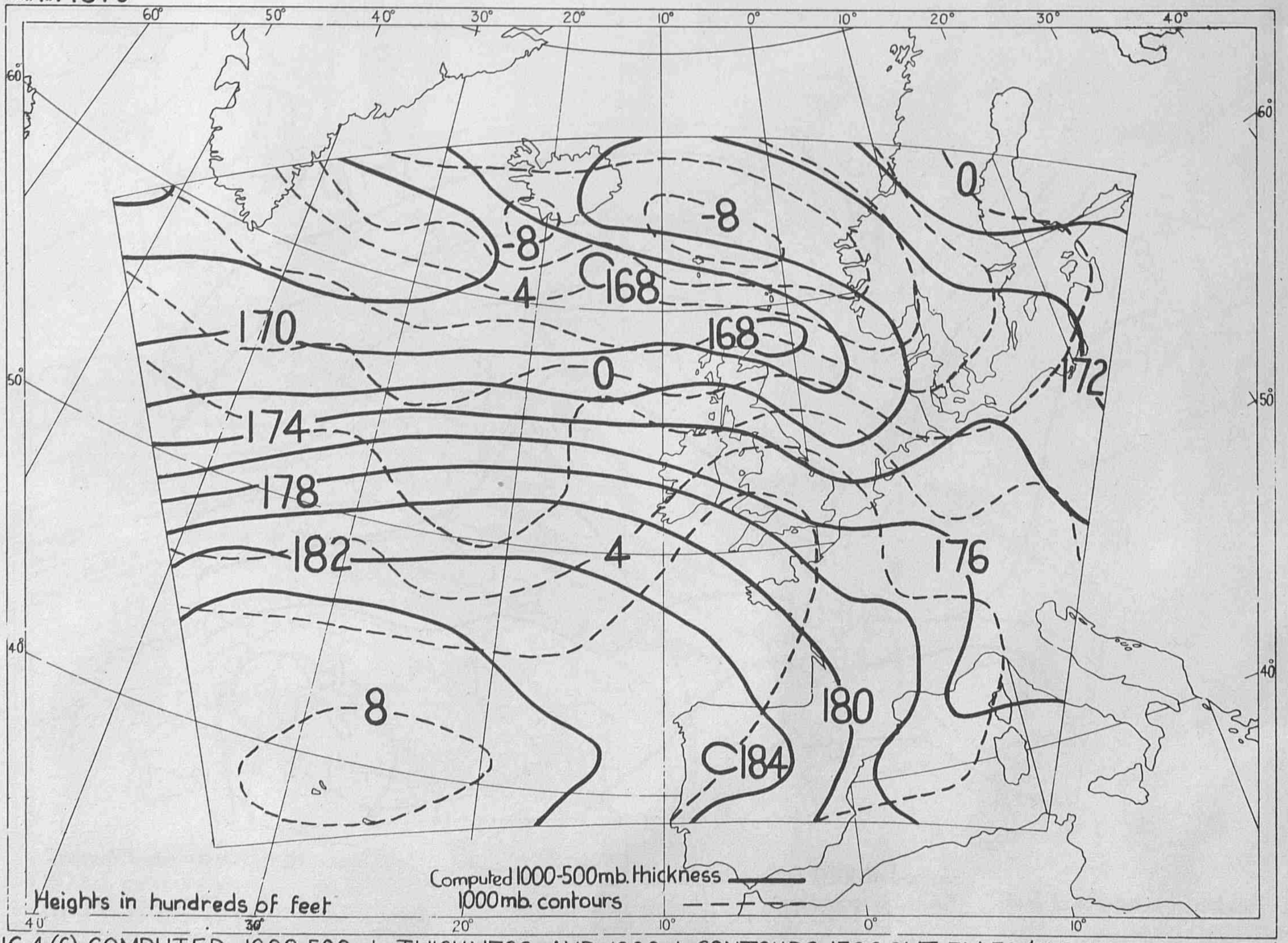
0
-8
-8
4
168
168
170
0
172
174
178
182
4
176
8
180
184
60°
50°
40°
30°
20°
10°
0°
Computed 1000-500mb. thickness
1000mb. contours
Heights in hundreds of feet

FIG.4(f) COMPUTED 1000-500mb. THICKNESS AND 1000mb. CONTOURS 1500 G.M.T. 31:1:52 (SUBJECTIVE ANALYSIS)

M.R.P. 1016

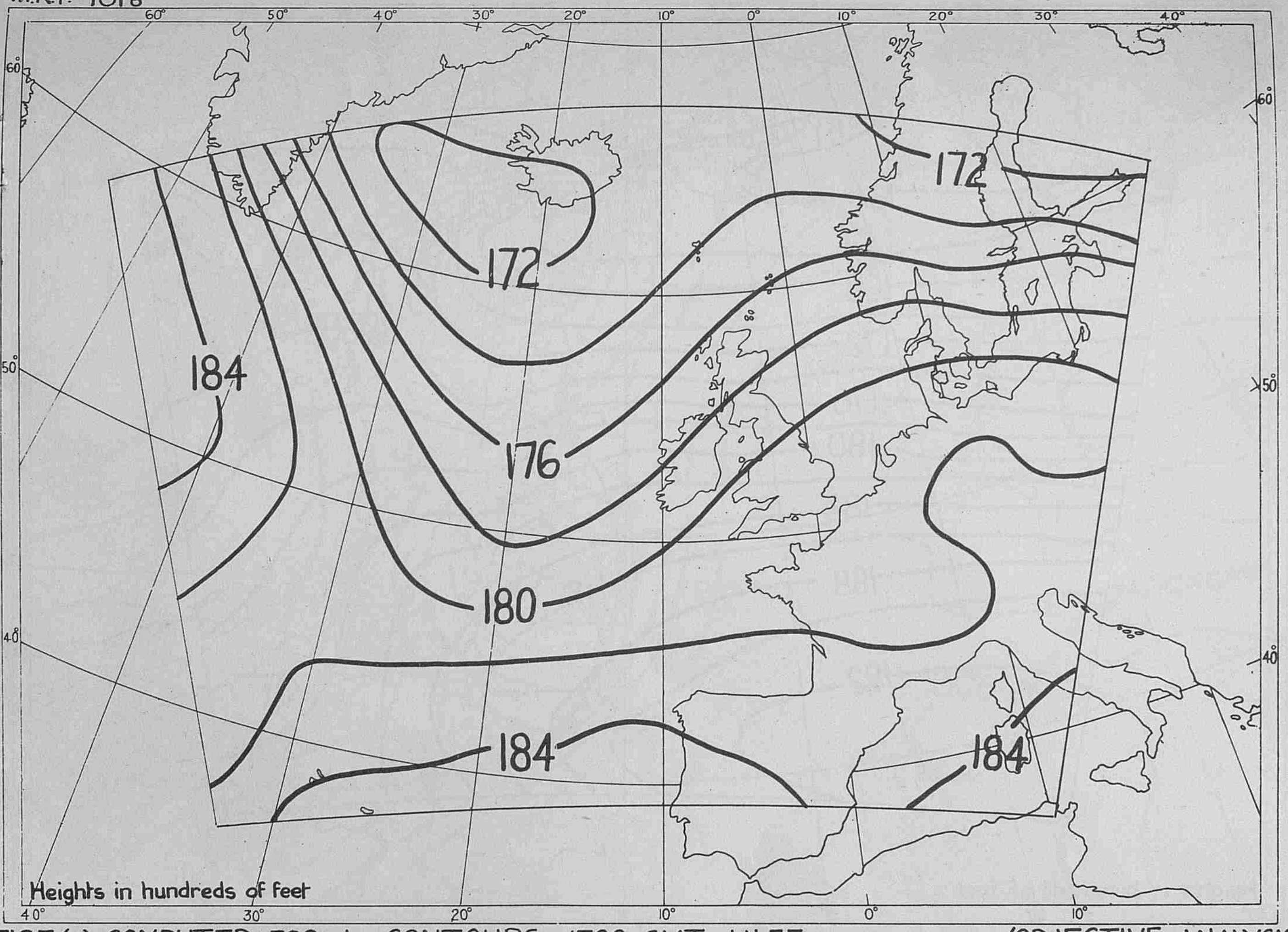

60°
50°
40°
30°
20°
10°
0°
10°
20°
30°
40°
60°
50°
40°
172
172
176
180
184
184
184
Heights in hundreds of feet
40°
30°
20°
10°
0°
10°

FIG 3(g) COMPUTED 500 mb. CONTOURS 1500 G.M.T. 1:11:55 (OBJECTIVE ANALYSIS)

M.R.P. 1016

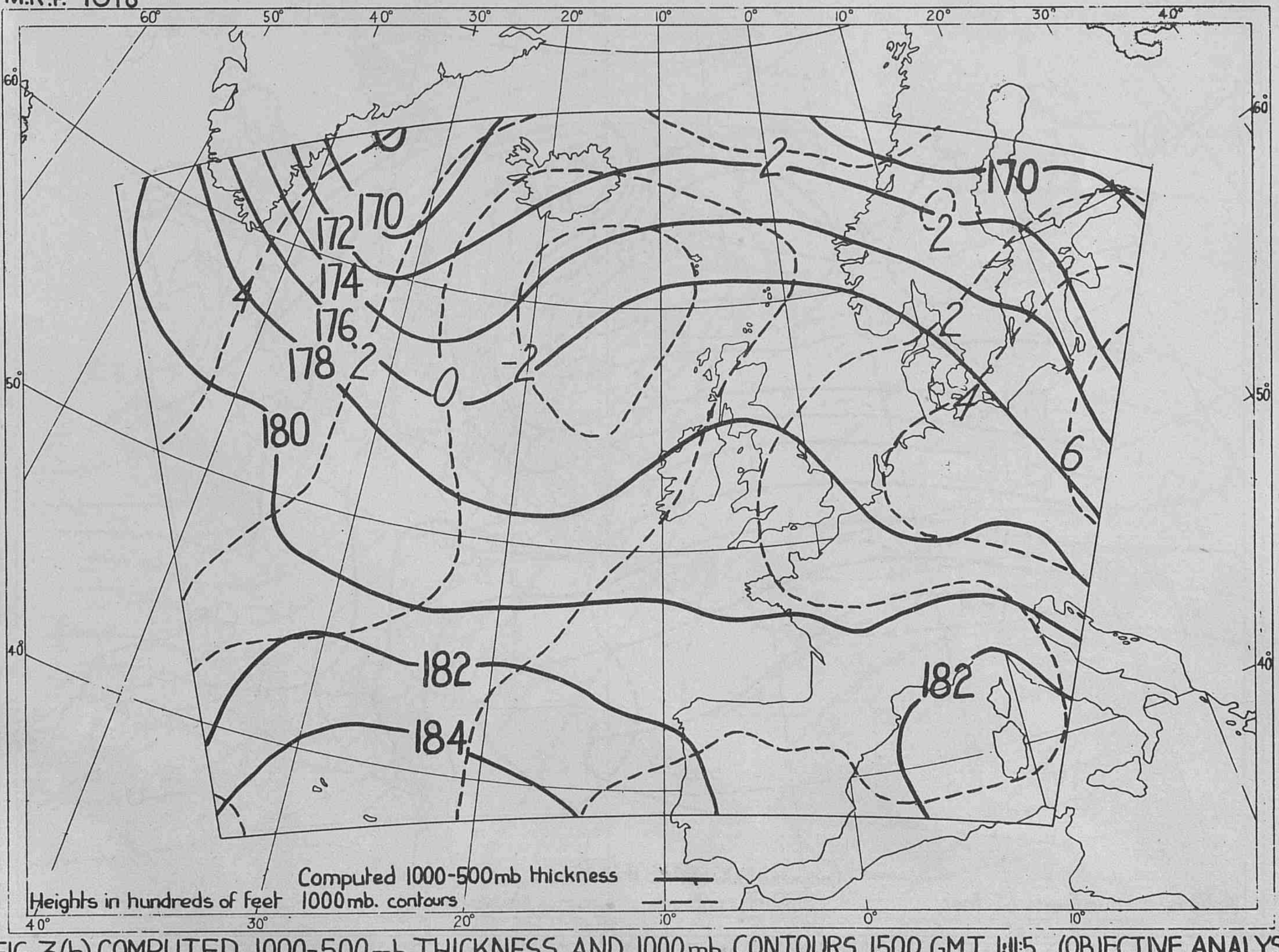

60°
50°
40°
30°
20°
10°
0°
10°
20°
30°
40°
60°
50°
40°
170
172
174
176
178
180
182
182
184
170
2
2
2
2
4
4
6
0
-2
Computed 1000-500mb thickness
1000 mb. contours
Heights in hundreds of feet
40°
30°
20°
10°
0°
10°

FIG. 3(h) COMPUTED 1000-500 mb THICKNESS AND 1000 mb. CONTOURS 1500 GMT. 1:11:5 (OBJECTIVE ANALYSIS)

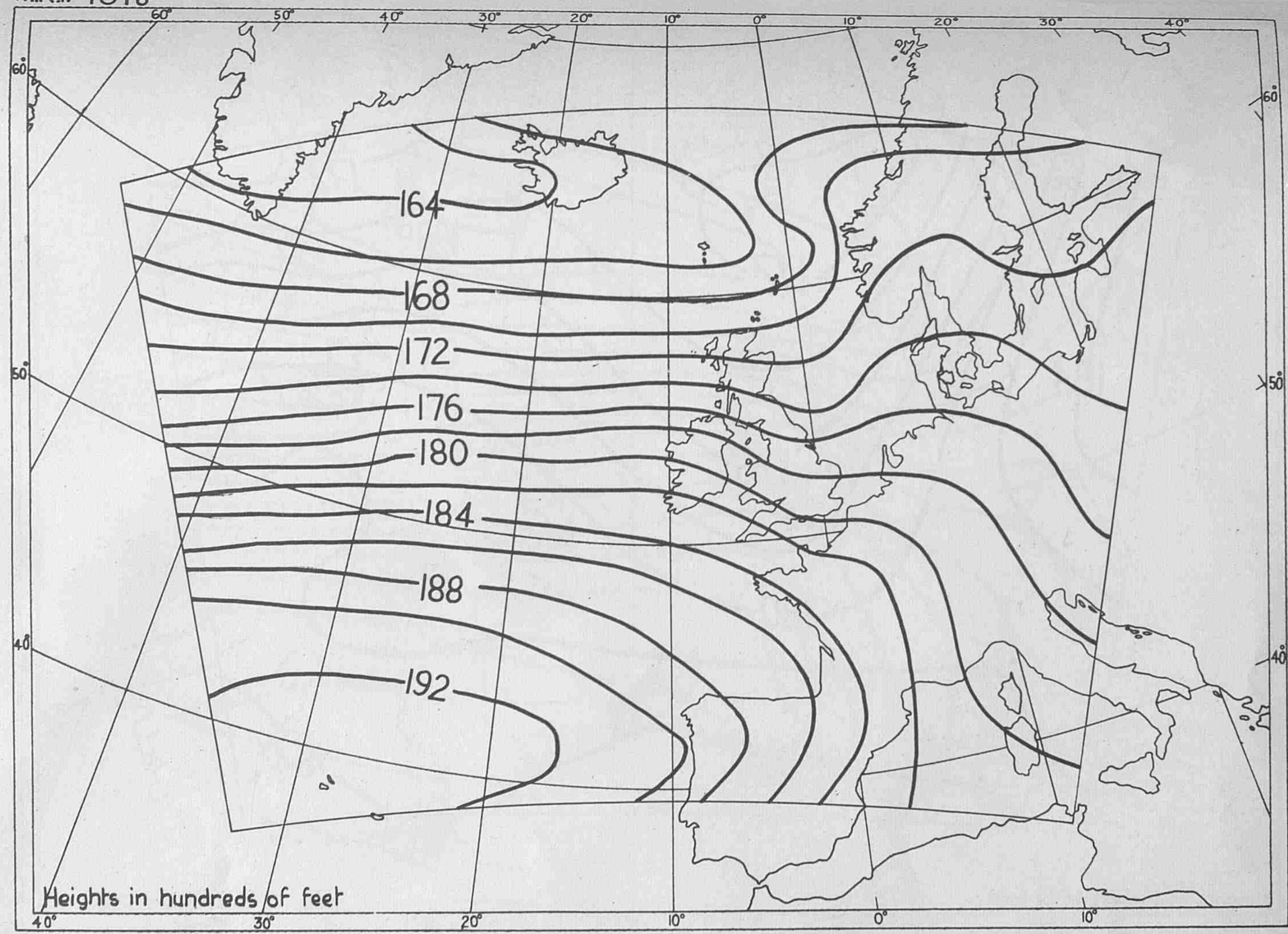
60°
50°
40°
30°
20°
10°
0°
10°
20°
30°
40°
164
168
172
176
180
184
188
192
Heights in hundreds of feet
40°
30°
20°
10°
0°
10°

FIG.4(g) COMPUTED 500mb. CONTOURS 1500 G.M.T. 31:1:52 (OBJECTIVE ANALYSIS)

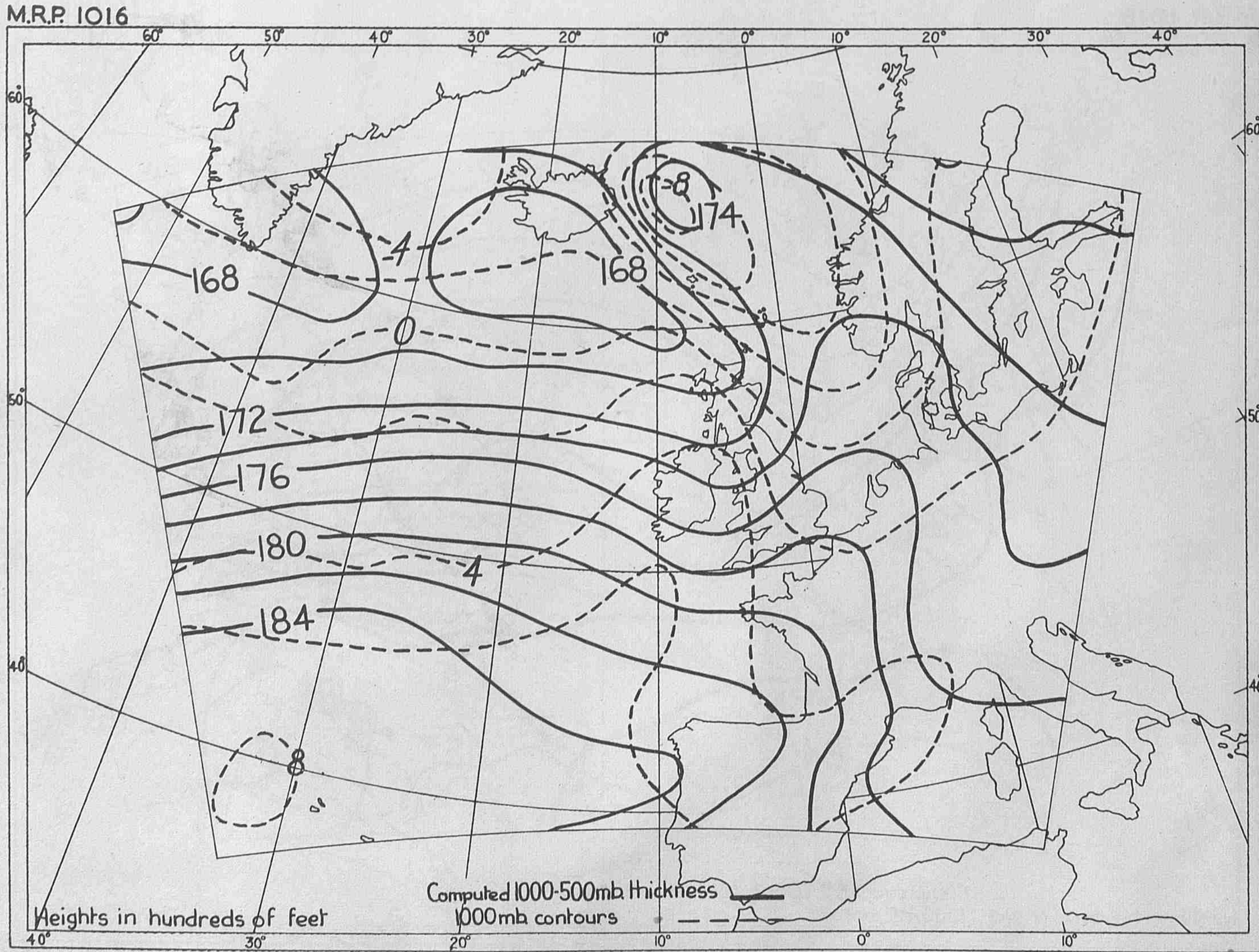
60°
50°
40°
30°
20°
10°
0°
10°
20°
30°
40°
-8
174
4
168
168
0
172
176
180
4
184
8
Computed 1000-500mb. thickness
1000mb. contours
Heights in hundreds of feet
40°
30°
20°
10°
0°
10°

FIG. 4(h) COMPUTED 1000-500mb. THICKNESS AND 1000mb. CONTOURS 1500 GMT. 31:1:52 (OBJECTIVE ANALYSIS)

M.R.P. 1016

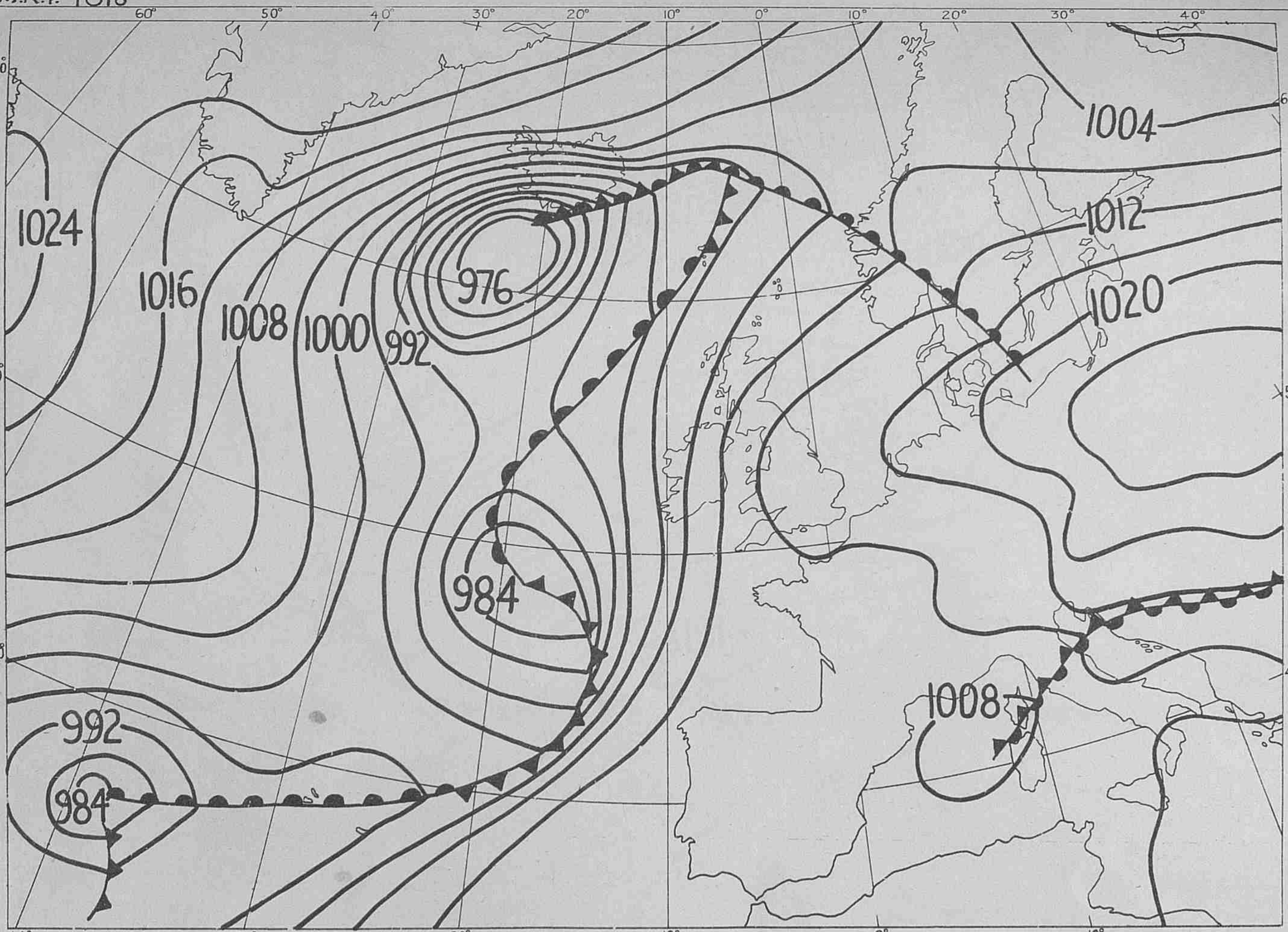
60°
50°
40°
30°
20°
10°
0°
10°
20°
30°
40°
60°
50°
40°
1024
1016
1008
1000
992
976
984
992
984
1004
1012
1020
1008
40°
30°
20°
10°
0°
10°

FIG3(i) ACTUAL SURFACE CHART, 1800 G.M.T. 1:11:55

M.R.P. 1016

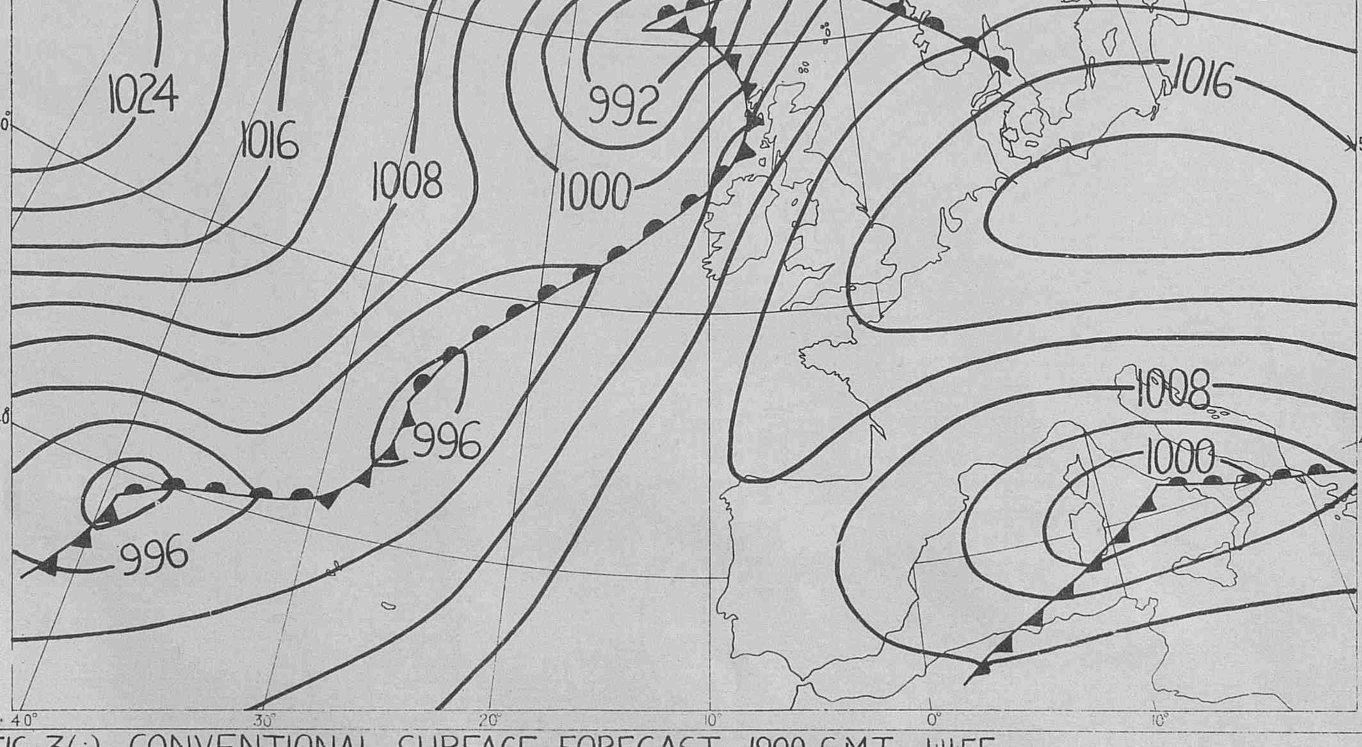
60°
50°
40°
30°
20°
10°
0°
10°
20°
30°
40°
60°
50°
40°
1024
1016
1008
1000
992
996
996
1000
1008
1016
1008
1000
40°
30°
20°
10°
0°
10°

FIG. 3(j) CONVENTIONAL SURFACE FORECAST, 1800 G.M.T. 1:11:55

M.R.P. 1016

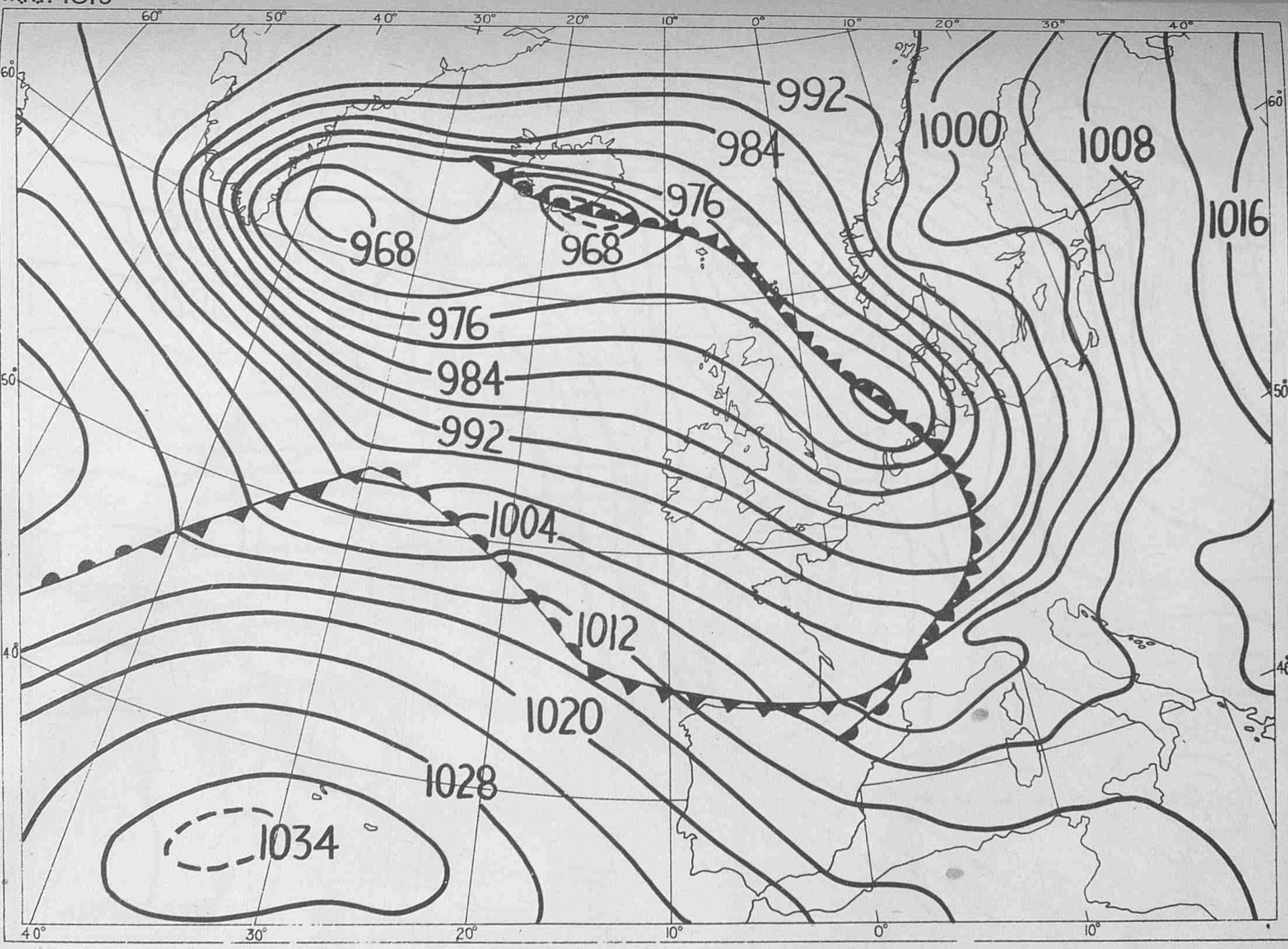
60°
50°
40°
30°
20°
10°
0°
10°
20°
30°
40°
60°
50°
40°
992
984
1000
1008
1016
976
968
968
976
984
992
1004
1012
1020
1028
1034
40°
30°
20°
10°
0°
10°

FIG. 4(i) ACTUAL SURFACE CHART 1800 G.M.T. 31:1:52

M.R.P. 1016

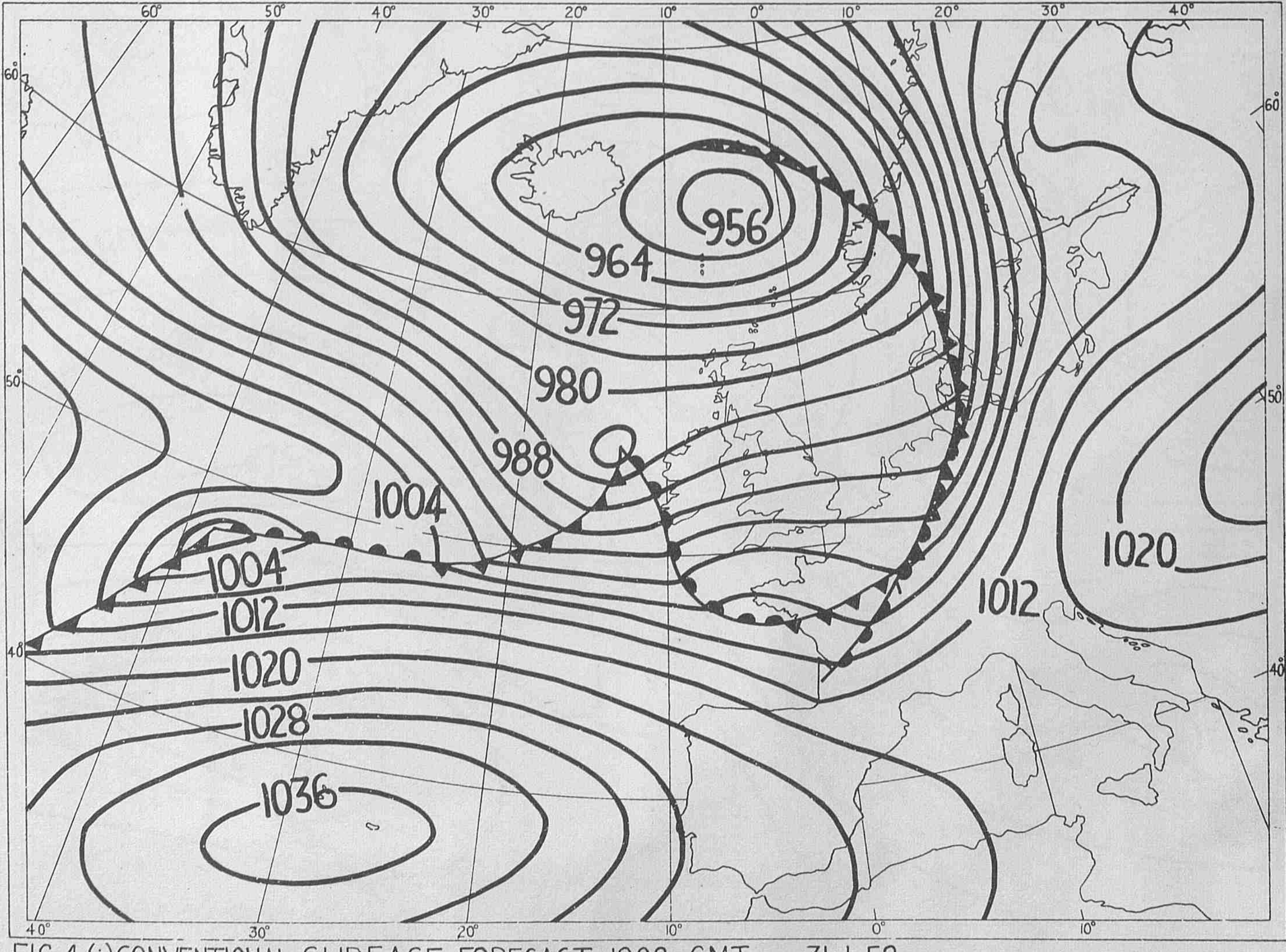
60°
50°
40°
30°
20°
10°
0°
10°
20°
30°
40°
60°
50°
40°
956
964
972
980
988
1004
1004
1012
1020
1028
1036
1020
1012
40°
30°
20°
10°
0°
10°

FIG. 4 (j) CONVENTIONAL SURFACE FORECAST 1800 G.M.T. 31:1:52

AD 139538

M.R.P. 1017
S.C. 111/223
23rd November 1956.

AD 139538

Analysis of reports of ice accretion on aircraft

by

R.F. Jones

(Meteorological Office)

AIR MINISTRY

METEOROLOGICAL RESEARCH COMMITTEE

At the time of issue this report has not been published. Any author desiring to quote this paper should refer to it as "A paper of the Meteorological Research Committee (London),
M.R.P. No. 1017 by Mr. R.F. Jones
A copy is available in the Library of the Meteorological Office."

M.R.P. 1017
S.C.III/223
23rd November, 1956

AIR MINISTRY
METEOROLOGICAL RESEARCH COMMITTEE

Analysis of reports of ice accretion on aircraft

by
R. F. Jones (Meteorological Office)

1. Introduction

During the past four years some 800 reports of icing encounters by R.A.F. and civil aircraft have been received in the Meteorological Office and have been analysed for this report. Because no reliable icing intensity meter existed suitable for fitting to operational aircraft the reports of icing severity are necessarily of a qualitative and subjective nature, although in some reports the pilot has estimated the rate of build up of ice on parts of the aircraft within his sight, e.g., windscreen, leading edge, propeller boss. As data from which useful statistical relationships can be obtained the observations are clearly of no value since we have no means of knowing the frequencies with which various levels (temperature or height) were traversed nor the frequency of clouds at those levels. Nevertheless some useful information on the occurrence of icing in various cloud types at different temperatures can be extracted. The great majority of the reports refer to conditions over the British Isles and any deductions made should only be regarded as referring to that area.

2. Qualitative reports of icing severity

(a) Reliability

Three categories of icing severity were used - "low", "moderate" and "high" - but because there was no yardstick by which to assess icing severity the reports were highly subjective, depending on the pilot's experience and probably the amount of trouble caused to him by the icing. In general terms one would expect the rate of build-up of ice on a part of the aircraft visible to the pilot to have been the principal factor in the assessment, but even this is not easy to assess and there would be a natural tendency to assess icing severity from the total build-up of ice over the variable period throughout which the aircraft was subject to icing. The rate of accumulation of ice is, of course, also a function of aircraft speed so that "light" icing to a slow aircraft might be "moderate" or "severe" to a fast aircraft.

The reliance to be placed on the pilot's estimates of severity can be checked, for there were 337 occasions when as well as making a qualitative assessment of icing rate the pilot estimated the accumulation of ice on the aircraft in terms of inches of ice and the time over which the icing occurred. Table I shows the distribution of icing rates so determined with the pilots' qualitative assessments.

Thus, if we defined a "high" icing rate as one leading to an accumulation of ice on the aircraft at 10 in./hr or more, 25 per cent of "moderate" reports and even 14 per cent of "low" reports should really be re-graded as "high" while 34 per cent of the "high" reports would require re-grading as "moderate" or "low".

/The

The subjective element in the qualitative reports is, therefore, very marked and this requires to be borne in mind in the subsequent discussion.

(b) Distribution with cloud type

The percentage distribution of reports of "high", "moderate" and "low" icing rates within each cloud type is shown in Table II.

It is immediately obvious from Table II, in accordance with general expectations, that the type of cloud in which icing is most likely to be regarded as severe is the cumulus or cumulonimbus type. There is nevertheless a significant percentage of "high" icing rates associated with layer types of cloud which, because of their greater horizontal extent, may constitute a greater total icing hazard than the convection type, and there has been at least one report of "high" icing rate in every cloud type.

(c) Distribution with temperature

On many of the occasions when icing was reported it was possible to determine the ambient temperature by making corrections to the indicated readings of the aircraft thermometer or by estimation from appropriate radiosonde ascents. Temperatures determined in this way may not be more accurate than about ±2°C but the distribution of icing experiences with these temperatures will give a useful indication of the temperature zones within which the various icing severities may occur.

The distribution of icing severities in the three qualitative groups "low", "moderate" and "high" with temperature and cloud type is shown in Table III.

It will be seen that, taking all the reports together, there is no significant difference in the distribution with temperature of "low", "moderate" and "high" icing rates. In many types the frequencies may reflect no more than the relative frequencies with which cloud of that type occurred at the temperature shown, e.g., 9.5 per cent of all reports of "low" icing rates experienced in Sc cloud occurred at temperatures between from -11°C to -15°C (Table III). This may be because 9.5 per cent of all flights in Sc cloud at temperatures below 0°C were in the temperature band from -11°C to -15°C or because there is a decreased risk of icing in the temperature band -11°C to -15°C. Without knowing how often an aircraft flew in Sc cloud in this temperature band without experiencing icing it is impossible to separate the two effects. "Nil" reports were asked for on the same form as used for icing reports but it is very unlikely that "Nil" reports received the same attention as positive reports - a total of 74 Nil reports was received compared with 786 icing reports. These are discussed in Section 8 below and it will be seen that there was only one reported occasion of horizontal flight in Sc which gave no icing, at a temperature of -7°C.

3. "Quantitative" reports

On a number of reports an estimate was given of the rate of accumulation of ice on portions of the aircraft visible to the pilot. These reports give more information than the purely qualitative reports dealt with in the previous section but although referred to as "quantitative" reports it is clear that they must be subject to very considerable errors, particularly when the accumulation, as in convection type clouds, occurs over a very short period. However, since there is as yet no suitable instrument for operational aircraft to measure rate of ice accumulation accurately an attempt is made in this section to use this additional information while bearing in mind the large errors to which it may be subject.

If an aircraft is travelling at speed v cm/sec through a cloud of super-

/cooled

cooled water content w g/m^3 the rate of accumulation of ice, d, in terms of the thickness of ice deposited on an exposed part of the aircraft, will depend on the efficiency of catch (E) of the supercooled droplets by this part of the aircraft, and the density of the ice deposited, ρ g/cm^3.

The rate of accumulation of ice would be given by:

$$d = \frac{E.v.w}{10^6 \rho} \cdot 3600 \text{ cm/hr} \qquad (1)$$

In the aircraft reports the indicated airspeed is reported in knots and can be converted into true air speed V kt while d is reported by the pilot in inches.

$$V = \frac{v}{51.5} \quad (1 \text{ kt} = 51.5 \text{ cm/sec})$$

and so $d = 7.3 \times 10^{-2} \dfrac{E}{\rho}.V.w$ in./hr from (1)

We can then obtain the water content of the air provided we know or can estimate ρ/E since

$$w = 13.7 \frac{d}{V} \cdot \frac{\rho}{E} \text{ g/m}^3 \quad (d \text{ in inches, V in kt}) \qquad (2)$$

E will depend on the shape of the collecting surface, the drop-size distribution of the droplets and the speed of the aircraft while ρ will also depend on the drop-size distribution and the temperature. If the drops are large and the temperature not greatly below 0°C the drops will tend to flow on the surface before freezing completely, leading to a deposit of clear ice of high density. If, however, the drops are small or the temperature is very low the drops will freeze on impact, leading to the formation of rime which, because of the air trapped between the frozen droplets, will have a low density. A part of the aircraft with a large radius of curvature will so deform the airflow past it that, although a high proportion of the large drops having sufficient momentum to overcome the deformation of the air track will impinge on the surface, only a small proportion of the smaller drops will be caught. On the other hand a part having a small radius of curvature will deform the airflow so little that a very much higher proportion of all the drops will be caught. Once ice has begun to form, the shape of the collecting surface will be modified and the efficiency of catch, E, will change accordingly. Thus, even if we know E initially for a particular part of the aircraft we would expect E to increase as ice accumulated since the effect of ice accumulation would usually lead to a reduced radius of curvature of the collecting surface.

On most of the flights reported here the ice formation was reported as being on the leading edge of the wing of the aircraft. If we assume a radius of curvature of the leading edge of 15 cm and a true airspeed of 200 mph then the efficiency of catch of the leading edge (ref. 1) is about 0.1 to 0.2 for drops of 10 μ radius, about 0.4 for drops of 20 μ radius and about 0.6 for drops of 30 μ radius. The mean droplet radius measured in clouds of all types in the United States (ref. 2) ranges between 5 μ and 10 μ and only a small proportion of droplets measured exceeded 15 μ in radius. It seems likely, therefore, that the efficiency of catch of the leading edge of most aircraft is likely to be of the order of 0.2 in most clouds but the efficiency will rise considerably when the droplet size is large as in freezing drizzle or rain. In such circumstances the type of ice formation is likely to be clear ice. The density of rime ice which forms on an aircraft is not known with any accuracy but may be about 0.1 to 0.2 g/cm^3 while the density of clear ice is probably about 0.8 to 0.9 g/cm^3. We see, therefore, that the ratio ρ/E

in equation (2) may be about unity for both rime ice and clear ice and as a rough approximation we may re-write equation (2) in the form

$$w = 13.7 \frac{d}{V} \text{ g/m}^3 \qquad (3)$$

At low temperatures when even quite large drops may be expected to give rapid formation of rime ice equation (3) may considerably over-estimate the value of w while at temperatures close to the freezing point in clouds of high water content with normal mean droplet radius, giving clear ice formation, w may be under-estimated. Variations in w, however, caused by the departure of ρ/E from unity may be no greater than those caused by the large errors inherent in the method of estimating rate of ice formation. For example, a typical statement from a pilot that $\frac{1}{4}$ in. of ice formed in one minute (d = 15) cannot reasonably be expected to be better than $\frac{1}{8}$ to $\frac{3}{8}$ inch in 1 - 2 min. which gives values of d varying between 3.75 and 22.5 with corresponding variability in w from equation (3).

With these inadequacies of the data in mind the "quantitative" icing reports have been analysed using equation (3) to give rough values of w. 235 reports were available for analysis in this way.

4. Type of icing

Three main types of icing were generally reported by the pilot, namely "clear", "rime" and "mixed". Included in "mixed" were reports of "cloudy" ice and two reports of packed snow.

The distribution of these types of icing with w is shown in Table IV while the distribution with temperature is shown in Table V. The three main types of icing are dealt with in detail in Sections 5, 6 and 7 below.

5. Clear ice formation

(a) Water content and temperature of formation

It will be seen from Table IV that there is a maximum frequency of occurrence of water content leading to clear ice formation in the range 0.21 to 0.30 g/m^3 which is a reasonable value for the water content of many icing clouds (ref. 2) and suggests that the method used may give reasonable estimates of water content. The method, however, leads also to an apparently surprisingly large number of high water contents (22 in excess of 1 g/m^3 with a maximum value of 5.48 g/m^3) and the question arises as to how accurate these derived values may be. Assessments of water content by the rotating cylinder method have led to the conclusion that water contents of this order are very infrequent, if they exist at all, but further examination (ref. 3) has shown that this method becomes unreliable when water contents are high especially when the temperature is also relatively high. At temperatures above about -15°C the method used was unlikely to be effective at water contents greater than 1 - 2 g/m^3. As Table V shows, all but three of the clear ice occasions occurred at temperatures above -15°C so that for similar reasons derived water contents in excess of 1 - 2 g/m^3 are unlikely to be accurate.

As indicated in Section 3 above the water contents w associated with clear ice are unlikely to be over-estimated because of the value of unity ascribed to ρ/E in equation (2) and, since the true airspeed of the aircraft (V) is known with reasonable accuracy, the only significant source of error in the values of water content in Table IV for clear ice, leading to an over-estimation, would be in the pilot's estimate of rate of accretion d. The accuracy of the pilot's estimation is impossible to assess but most of these occasions called for special comment and were undoubtedly noteworthy in the pilot's experience. On one occasion (w = 1.12) the aircraft was struck by lightning and on another (w = 1.26), although the aircraft was only in cloud for eight minutes, part of the propeller broke off. In addition on three occasions (w = 1.37, 1.14, 2.29) the observations were made over the Atlantic by trained observers of the Meteorological Reconnaissance Flight, while three occasions (w = 2.14, 2.74, 3.00) were separate reports from three aircraft flying in the same cloud mass. There seems reason, therefore, to believe that the true water contents in excess of 1 g/m^3 occurred although the derived values of water contents greater than 2 g/m^3 are probably not reliable. Table V, however, suggests that these water contents are very unlikely at temperatures below -15°C and this is more clearly brought out in Table VI where the occurrences of different water contents with temperature are tabulated for clear ice occasions only. There is, however, a definite risk of severe clear ice formation in suitable clouds at any temperature between 0°C and -15°C.

(b) Cloud type

Having established by the analysis of Section 5(a) above that clear ice formation is very unlikely with any appreciable severity at temperatures lower than -15°C it is of interest to see whether the range of conditions under which clear ice formation can occur can be further narrowed. The 84 occasions of clear ice formation have, therefore, been analysed with respect to cloud type with the results shown in Tables VII and VIII.

It is clear that little narrowing of the range of conditions can be achieved from these tables since conditions favourable for clear ice formation can occur, even leading to severe accumulation, in all the types of cloud which may be expected at temperatures higher than -15°C. The only slight gain is that the three occasions of clear ice formation in precipitation below cloud all occurred at temperatures higher than -5°C (two at a temperature of -1°C). It is perhaps surprising to find so many occasions in thick layer cloud, some of great severity, since in this type of cloud normally associated with widespread precipitation it had been anticipated that at temperatures below 0°C little supercooled water would be present once precipitation had commenced. Nevertheless precipitation was reported on 20 of the 26 occasions of icing in St, Ns, As. Eight of these 26 occasions were reports from Meteorological Reconnaissance aircraft where, since a trained observer was carried, the accuracy of reports should be high. It is noteworthy that these eight occasions gave derived cloud water contents between 0.23 and 0.69 g/m^3 and five of these were in precipitation, although in three the precipitation was reported as drizzle. Two high derived values (2.77, 3.03 g/m^3) occurred in conditions when orographic uplift may have been expected to lead to higher water contents in the cloud; in one case the aircraft had been in cloud for three hours with only light rime icing and only encountered heavy clear ice over the Cheviot Hills. A similar occasion occurred, however, in mid-Channel (derived water content 2.14 g/m^3) when with no apparent change in cloud appearance there was a sudden onset of clear ice formation after three hours in cloud with rime icing. In this case as in the other two cases the aircraft was in frontal precipitation and it appears therefore that frontal cloud may on occasions contain limited volumes of high water concentration, possibly associated with embedded convection cells. These cells may be initiated by forced uplift over high ground or by other less obvious effects. A noteworthy occasion, when the trigger effect may have been convergence in a trough of low pressure associated with a depression over North France, occurred on 1st January, 1953. On this occasion 23 reports of icing on aircraft were received - the majority of them reported severe icing - and an analysis of three of these occasions gave derived values of water content - included in the tables above - of 2.14, 2.74 and 3.00 g/m^3. Cloud tops were about 10,000 ft and the cloud base temperature about 1°C at 1,200 ft. The icing was experienced at heights between 2,500 and 3,000 ft and no precipitation was reported. The type of icing reported, "clear with rough or nobbly surface", suggested the presence of large drops. Ascent of air from cloud base to about 4,000 ft would only make available about 1 g/m^3 of free water so that if the derived water contents are true it seems likely that the water content at 2,500 - 3,000 ft had been reinforced by the descent of water to these levels from higher in the cloud. With a cloud top temperature in the region of -15°C it seems possible that the absence of precipitation could be ascribed to a deficiency of ice crystals in the cloud with consequent growth of large cloud particles by coalescence in the liquid phase. The large droplets, approaching drizzle drop size, with a rate of fall in still air of 1 - 2 m/sec, may then have fallen from above into the layer between 2,500 and 3,000 ft, where the temperature was still 1 - 2°C below freezing. Intermittent slight drizzle was reported at the ground in the neighbourhood of these reports.

(c) Distances over which clear ice formation occurred

From a knowledge of the time over which clear icing was experienced and the true air speed of the aircraft it is possible to determine the distances over which the various derived water contents were experienced for the 84 clear ice occasions. The distribution is shown in Fig. 1. In interpreting this figure it must be borne in mind that a pilot will not willingly suffer severe icing without taking remedial measures, e.g., change of course or change of altitude or use of de-icers when fitted. Thus, although Fig. 1 suggests that high water contents only occur over horizontal distances less than 20 nautical miles, this straightforward interpretation may not always be true. It is, of course, possible that the volumes of cloud in which the supercooled water content is high are always of limited horizontal extent and some of the reports suggest this. It is clearly true of convection clouds and it may be that something akin to a convection cell existed in all clouds (see Section 5(b) above) in which high water contents were found but on present information it is unsafe to draw this conclusion. Of the 22 occasions when derived water contents were greater than 1 g/m^3 the aircraft on 15 occasions was in cloud for at least seven minutes longer than the period for which the high rate of icing was reported. On eight of these 15 occasions, however, the aircraft changed height; twice being forced down by weight of ice, and on another occasion de-icing equipment was successfully used.

On Fig. 1 are shown two curves, the first of which indicates possible extreme values of water content for various distances, one point only lying outside the curve and the second a more probable curve of extreme values on the assumption that five readings of the 84 over-estimated the water content. This latter curve would suggest that peak values of water content of 5 - 6 g/m^3 may occur over very short distances and that even over a distance of 10 nautical miles water contents of 2 to 3 g/m^3 may be encountered but it must be remembered that derived water contents in excess of 2 g/m^3 are particularly unreliable. For distances in excess of 40 miles, however, it would appear improbable that mean water contents in excess of 0.6 g/m^3 would occur over the British Isles.

6. "Mixed" ice formation

There were 60 occasions when "mixed" ice formation was reported. This type of ice formation may be regarded as occurring in conditions when water concentrations are variable so that on some occasions immediate freezing of the water droplets occurs while for higher water concentrations some flow of water on the surface occurs leading to a mixture of clear and rime ice. "Mixed" ice would also be expected to occur when ice crystals and supercooled water are present simultaneously so that the supercooled droplets act as the cement holding the ice crystals which also impinge on the surface. It is to be expected, therefore, that the density of the deposit on the surface will be variable according to the relative concentrations of clear and rime ice and deduced water contents will accordingly be subject to wider errors than for the clear ice occasions.

(a) Water content and temperature of formation

The distribution of derived water contents with temperature is shown in Table IX. This table has many points of similarity with that given for clear ice occasions (Table VI) showing a maximum frequency of water contents in the range 0.21 to 0.30 g/m^3 but with a large number in excess of 1 g/m^3. The distribution with temperature shows a shift of maximum frequency to the -6 to -10°C band and there are few occasions at temperatures lower than -15°C. Two occasions of derived water content greater than 1 g/m^3 occurred, however, at temperatures below -25°C. Both of these were in thick frontal cloud over Scotland and it is possible that the deposits were mainly of rime of low density. Both aircraft were high-speed aircraft for which the efficiency of catch of the droplets would be high so that the factor ρ/E in equation (2) may well have been considerably less than unity on these occasions leading to a considerable over-estimate of the derived water content.

The maximum derived water content was 20.56 g/m^3. This was experienced on a Dove aircraft in cumulus cloud at 7,000 ft, temperature -8°C, and was described as one inch of a mixture of rime and clear ice, the whole semi-transparent, forming in $\frac{1}{4}$ min. The time interval is so short that the derived water content, apart from consideration of the density of the deposit, cannot be considered reliable.

The remaining six reports when derived water contents were greater than 3 g/m^3 all resulted in special comments by the crew and two of the reports are given here in detail.

(i) Derived water content 4.57 g/m^3 in Ns cloud over Lincoln. Two inches of white rough ice were reported forming in two minutes on all windows round the cockpit, aerials, and also on mainplanes despite de-icing fluid. "There was only slight rime on climb up to 14,000 ft then high icing began when rain began. Unable to see out without opening windows since ice covered side windows as well as windscreen. Engine boost fell off due to ice on air intakes, though using hot air. Had to abandon details and return. De-icing fluid caused ice to break away from mainplanes in irregular patches. Disturbed airflow caused loud moaning sound clearly audible inside cabin". An advancing warm front was about 100 miles away to the SSW. The estimated temperature at 14,000 ft was -12°C but the precipitation was described as sleety rain.

(ii) Derived water content 3.42 g/m^3 in Cu, 40 miles north of Glasgow. Three inches of opaque hard ice were reported to have formed in five minutes on the propeller domes and leading edges of a Pionair aircraft. "Light icing was experienced at 7,000 ft, temperature -9°C, followed by a sudden heavy accretion. Indicated airspeed fell from 130 to 95 kt in level flight ..... There was no turbulence and little tendency for sheets of ice to form on the windscreen or on the wings apart from the leading edge". There was an unstable N-NE airstream over the Highlands leading to 8/8 Cu type cloud. A little light drizzle occurred prior to icing.

Such reports suggest that on these occasions at least the water contents were exceptionally high and may well have been greater than 2 g/m^3.

/(b)

(b) Cloud type

Tables X and XI show respectively the distribution of derived water contents with cloud type and the temperature at which icing occurred with cloud type.

As in the cases of clear ice formation the large number of reports of icing in frontal cloud (St, Ns, As, Cs) is noteworthy; it includes a number of severe occasions.

The temperature distribution is also interesting in showing a greater likelihood of icing in frontal cloud at very low temperatures (below -20°C) than in convection cloud. This may be because of the greater frequency and horizontal extent of frontal cloud at these temperatures and the reluctance of pilots to enter well developed convection cloud when they have a good opportunity of observing it sufficiently far ahead to make a detour. At heights corresponding to temperatures below -20°C cumulus tops would be expected to be usually clearly defined and visibility unhampered by intervening layer cloud. Tables VIII and XI would appear to suggest that icing is unlikely in convection cloud at temperatures below -20°C but it may be dangerous to draw this conclusion. The presence of supercooled water on some occasions in frontal cloud at temperatures well below -20°C is, however, certainly to be inferred from these tables.

(c) Distances over which "mixed" ice formation occurred

With the same restrictions as discussed under para. 5(c) a curve, Fig. II, can be drawn showing the distance over which the various water contents were derived.

The curve indicated for extreme values is very similar to the most probable curve in Fig. I (shown dotted in Fig. II) giving added weight to that curve as an indication of the extreme values of water content likely to be encountered over various distances in cloud.

7. Rime ice formation

There were 88 occasions when rime ice was reported. At temperatures close to the freezing point this type of icing occurs when the droplet size is small and each droplet freezes instantaneously on impact. At low temperatures quite large drops, if present, may also freeze instantaneously. Because of the great variation in density of the deposit combined with the variation of efficiency of catch with droplet size, water contents derived from rime ice occasions may be substantially in error, particularly at low temperatures if large drops are likely to have been present (e.g., in some convection clouds). High values of water content derived from observations at low temperatures must, therefore, be regarded with great reserve.

(a) Derived water content and temperature of formation

The distribution of derived water contents with temperature is shown in Table XII. There is a clear distinction between Table XII and the similar Tables VI and IX for clear and "mixed" ice. In the latter tables there is a marked decrease in frequency of ice reported at temperatures lower than -15°C but in Table XII 27 per cent of all incidents occurred at these low temperatures, the lowest being -34°C (two occasions). This is, of course, in accordance with expectation indicating the presence of supercooled water in cloud but little flow of water after impinging on the aircraft surface at temperatures below -15°C. It is interesting, however, to note that the greatest frequency of reports is in the -1°C to -5°C band, just as it is in the clear ice occasions, indicating presumably that at these temperatures in cloud the free water content may sometimes be predominantly in the form of very small droplets (rime ice) and sometimes many larger droplets must be present (clear ice). The high frequency of reports in both conditions, however, may merely be a reflection of the relative frequency with which aircraft encountered cloud in this temperature band rather than an indication of increased risk of icing in this band compared with other temperatures.

Once again there is a significant number of derived water contents greater than 1 g/m^3 although the considerations outlined above cause less reliance to be placed on these values than in the case of clear ice. The maximum derived water content was 23.02 g/m^3 and there was also one value of 9.15 g/m^3. On both occasions, one (23.02 g/m^3) in the top of a large cumulus at a temperature of -19°C accompanied by severe turbulence and the other (9.15 g/m^3) in snow below Ns at a temperature of -6°C, it would be reasonable to assume a high efficiency of catch of water drops or snowflakes accompanied by water drops and hence as explained previously a considerable over-estimation of water content.

The two occasions of high derived water content at a temperature of -34°C (1.14 and 1.37 g/m^3) call for special attention. The first occurred in the As sheet ahead of a warm front and the other in cumulonimbus associated with AcAs near to the centre of a depression. On the first occasion icing occurred on a Meteor 8 aircraft in a narrow height band between 22,000 and 26,000 ft 20 miles north of Leuchars. Cloud base was at 8,000 ft at which height sleet was reported (temperature -7°C) but there was stated to be no precipitation above this height. The fact that the aircraft speed was 360 kt would undoubtedly increase the efficiency of catch of any droplets present leading to some overestimation of water content but there must nevertheless have been appreciable liquid water present in cloud at this temperature. On the second occasion the aircraft speed was also high, 450 kt, and this combined with the reported presence of cumulonimbus (supported by the moderate to severe turbulence encountered) makes it likely that the efficiency of catch of the droplets present was high and the value of 1.37 g/m^3 may well be a considerable over-estimate.

Similar considerations may apply to some, if not all, of the high water contents derived and the observations are perhaps better regarded merely as evidence of the presence of supercooled water in significant amounts than true quantitative evidence.

(b) Cloud type

The distribution of derived water contents with cloud type and icing temperatures with cloud type are shown in Tables XIII and XIV respectively.

High values of derived water content were found in all the types of cloud, frontal cloud, non-frontal layer cloud and convective cloud but there was only one icing occasion (discussed in para.7(a)) in convective cloud at a temperature below -20°C. Once again this probably reflects the ease with which a pilot can avoid convective cloud tops rather than an absence of icing at low temperatures in convective cloud. This is supported by the occurrence reported in Section 7(a) above of a high icing rate at a temperature of -34°C when the cumulonimbus cloud was hidden by a layer of AcAs.

As for the cases of "mixed" and "clear" ice, the inference that liquid water is present in frontal cloud at temperatures lower than -20°C can certainly be made.

(c) Distance over which rime ice formation occurred

Fig. III, analogous to Figs. I and II for clear and "mixed" ice formation, shows the distance over which the various water contents were derived. Because of the greater doubt associated with these derived water contents the curve drawn, which excludes 10 of the 88 observations, can only be regarded as giving likely values of extreme water contents leading to rime ice formation over various distances. As is to be expected it lies below the curves for clear and "mixed" ice also shown on Fig. III.

8. Reports of no icing in cloud at temperatures below 0°C

74 reports were received specifically mentioning no ice formation in cloud at temperatures below 0°C. 33 of these reports were received from aircraft of the Meteorological Reconnaissance Squadron operating over the Atlantic.

From consideration of the true airspeed of the aircraft it is apparent that in a number of cases (18) although the air temperature was below 0°C the parts of the aircraft most prone to ice formation were probably at a temperature above 0°C so that noticeable icing of the aircraft would be unlikely. If we also exclude those cases (7) in which the aircraft was in cloud for a period of 2 minutes or less and those for which there is insufficient detail (7), 42 reports remain for consideration. More than half (23) of these remaining reports were made when aircraft were ascending or descending, sometimes at considerable speed, through cloud extensive in the vertical so that the time spent in any layer which might have given ice formation may well have been short. Nevertheless the fact that aircraft could, on occasions, ascend through 25,000 ft or more of frontal cloud without experiencing any noticeable ice formation is of interest, particularly as similar ascents on other occasions have led to considerable ice accumulation. The position becomes even more confusing when it is noted that on a number of occasions the precipitation at temperatures well below freezing point was reported as rain. Thus, after a descent in Ns cloud over the Atlantic from 17,860 ft (temperature -18°C) to cloud base at 7,000 ft (temperature -2°C) it was reported that the aircraft was in continuous slight rain while in cloud but with no icing. Whether the rain in reality only occurred very close to, or even below, cloud base can only be conjectured but it was not uncommon to have reports of drizzle, rain or sleet in these clouds with no icing. It is significant, however, that in nine of the ten occasions of horizontal flight in frontal cloud without icing it was stated that there was no precipitation in cloud and the remaining report, of sleet, referred to only the first part of the flight and may have reflected the conditions on climb to cruising height. On four of these ten occasions there was precipitation at ground level.

The temperatures on nine of the ten flights in frontal cloud ranged from -5°C to -15°C (-28°C on the other) which is also the range within which a large number of icing reports was received (Table III). It would appear, therefore, that on a few occasions at least the frontal cloud above the freezing level in this temperature band must be composed entirely of dry ice crystals but that more often the ice crystals are wet and/or exist in association with large numbers of supercooled water droplets. The deduction (ref. 1) that, because most frontal rain is assumed to originate from the melting of ice crystals or snowflakes, there is little risk of appreciable ice formation above the freezing level except in a narrow layer close to the 0°C level appears to be invalid.

Of the other nine occasions of no icing in horizontal flight, five were in convection cloud at temperatures between -7°C and -44°C, three in altocumulus at temperatures of -5°C, -16°C and -17°C and one in Sc at -7°C. All the convection cloud occurrences were in conditions under which frequent showers were occurring and it seems likely that the flights were through parts of the clouds in the decaying stage in which the cloud particles were either dry ice crystals or soft hail - this was reported on three occasions. Altocumulus and stratocumulus are regarded as predominantly water clouds and lack of icing on these occasions might reflect an unusually small droplet size but on one occasion (Ac, temperature -5°C) the cloud was described as "mammatus" and was very turbulent with precipitation within cloud in the form of snow.

/9.

9. Synoptic conditions where high values of cloud water content ($\underline{w} > 1.0$ g/m^3) were deduced

Table IV indicates that there were 56 occasions when a value of water content greater than 1.0 g/m^3 was deduced, 22 from clear ice occasions, 18 from reports of mixed ice and 16 from reports of rime ice. As indicated previously the clear ice reports are probably the most reliable while the rime ice occasions in particular may have led to a considerable over-estimate of $\underline{w}$.

The synoptic conditions associated with these high values of $\underline{w}$ have been examined and are discussed in paragraphs (a), (b) and (c) below for clear ice, mixed ice and rime ice occasions respectively.

(a) Clear ice occasions

The 22 occasions divide up into 9 occasions of unstable air (4 on the same day), 3 associated with cold fronts, 3 with quasi-stationary fronts, 1 with a warm front, 1 with an occlusion, 3 with the thick cloud to the north and west of a depression centre where the fronts are ill-marked, 1 with anticyclonic Sc and 1 in precipitation below cloud.

These situations, of course, describe almost all the conditions which can lead to extensive cloud formations but some narrowing of the limits can be achieved. Thus of the occasions of unstable air all were associated with situations giving widespread convective activity, presumably because the pilot found it impossible to avoid the cloud as he could do if isolated convection clouds were forming. The type of situation was, therefore, that in which the instability cloud was formed by the passage of cold air over a warmer sea although it may have spread inland (7 occasions) or by orographic lifting of direct polar air over high ground (1 occasion) or by convergence in a polar trough (1 occasion). The one occasion in anticyclonic Sc also occurred over the sea and since the airflow was from NNE the cloud was presumably also of convective origin.

In the warm front and occlusion cases the severe icing occurred within 100 miles of the position of the surface front and there was continuous precipitation at the ground; in one case there was some possibility that orographic uplift had contributed materially to the icing. In the cold front and quasi-stationary front cases the severe icing occurred within 50 miles of the surface position of the front except on one occasion when the distance was 100 miles. There was precipitation on two of the occasions but not on the remaining three.

The three occasions of extensive cloud near to a depression centre were all within about 250 miles of the centre; on one of these occasions, when there was an ENE'ly airstream across the North Sea in November, convection over the sea was probably a contributory factor.

Although orographic lifting may have been a contributory factor on five occasions there were also five occasions when the severe icing was experienced over the open sea.

(b) "Mixed" ice occasions

The 18 occasions may be divided into 8 occasions of unstable air, 5 associated with warm fronts, 1 with a cold front, 1 with an occlusion, 1 with a quasi-stationary front, 1 with anticyclonic Sc and 1 close to the centre of a depression.

Of the 8 occasions of unstable air two were associated with convection over the sea and two with widespread convection cloud over the mountains of Scotland. The remainder would appear to be associated with more isolated convection within 400-500 miles of the centre of a depression.

Of the five warm front occasions all were within 200 miles of the surface position of the front, two within 50 miles. Four of the five fronts were active giving continuous precipitation at the position where icing occurred and quickly moving but the fifth was weak and slow moving without precipitation. In this latter case however it is probable that orographic uplift was an important factor.

In the remaining three frontal cases the aircraft was very close to (certainly within 50 miles of) the surface position of the front, but only the cold front gave general precipitation.

As in the clear ice occasion the icing in anticyclonic Sc occurred over the sea in winter (both in February).

(c) Rime ice occasions

The 16 occasions comprised 3 occasions of unstable air, 3 associated with warm fronts, 2 with quasi-stationary fronts, 2 with occlusions, 5 in the thick cloud close to a depression centre and 1 below cloud.

Two of the unstable air occasions were associated with thunderstorms, one over the Mediterranean and the other in the Middle East, where orographic effects contributed to widespread activity. The third occasion was in the top of a cumulus cloud over the North Sea.

In the frontal cases the icing occurred on five of the occasions (out of seven) 100 miles or less away from the surface position of the front. There was continuous precipitation at the ground on four of these occasions. On the remaining two occasions the icing occurred in the altostratus sheet 160 and 300 miles from the surface position of the front before precipitation had commenced.

Of the five occasions in the thick cloud associated with the centre of a depression three were 100 miles or less from the centre and the remaining two within 250 miles.

The occasion of icing below cloud is of interest. This occurred in snow beneath the Ns sheet of a quickly advancing active warm front and indicates clearly the possibility of co-existence of ice and supercooled water in warm front precipitation.

10. Forecasting ice formation

The foregoing analysis has made very clear the variable nature of icing experiences in cloud and gives little hope that accurate forecasting of the degree of icing severity can be achieved. On many occasions the volume of cloud containing appreciable supercooled water must be very limited in either horizontal or vertical extent so that chance alone decides how severe the icing experience of a particular aircraft may be.

Nevertheless the analysis does indicate some considerations which should be taken into account in making forecasts and the conclusions of this paper may be summarised in the following forecasting "rules". Severe icing has been arbitrarily defined as that leading to a derived water content w greater than 1.0 g/m^3.

(i) At temperatures below -15°C the most likely type of ice formation is rime ice. (Table V).

(ii) Icing of any type is very unlikely at temperatures below -35°C. (Table V).

(iii) Clear and "mixed" ice formation may be severe in all types of cloud at temperatures between -1°C and -15°C inclusive. (Tables VI, VII, IX and X).

(iv) Severe clear and "mixed" ice formations are very unlikely at temperatures below -15°C but heavy rime ice may occur. (Tables VI, IX and XII).

(v) Conditions favourable for severe clear and "mixed" ice formations will probably be of limited horizontal extent - perhaps not more than 30 nautical miles (Figs. I and II).

(vi) Heavy rime ice formation will probably not occur frequently over horizontal distances in excess of about 20 nautical miles (Fig. III).

(vii) Forecasts of no ice formation at temperatures between 0°C and -35°C are unlikely to be successful, although occasions of no ice formation will probably occur, unless consideration is given to the particular aircraft type and speed for which the forecast is given.

(viii) Severe ice formation, usually clear or "mixed", should be forecast in conditions likely to lead to widespread convective activity if the flight is to be made within the temperature limits indicated above and cloud is expected to reach to the flight level.
In particular, instability over the sea and in direct polar air traversing high ground are situations liable to give occurrences of severe icing.

(ix) The possibility of severe icing, usually clear or "mixed", should be indicated within 100 miles of the surface position of a warm front, when the front is active and quickly moving. In particularly active warm fronts the distance may be up to 200 miles and the icing in weak or slow moving warm fronts may be intensified over high ground. Heavy rime ice may be experienced in the altostratus sheet as much as 300 miles ahead of the surface position of the warm front and ahead of the associated rain belt.

(x) Severe icing may occur within 50-100 miles of the surface position of cold fronts, quasi-stationary fronts and occlusions.

(xi) In the thick cloud associated with the centre of a depression where the fronts are poorly defined, particularly to the north and west of the centre, severe icing may occur within 250 miles of the centre. In many areas, of course, these conditions will be covered by those described under (viii) above.

References:

(1) Ice accretion on aircraft. Meteorological Report No. 9. Meteorological Office, 1951, pp.10, 11.

(2) Lewis, W. Meteorological aspects of aircraft icing. Compendium of Meteorology. Boston, 1951, p.1201.

(3) Ludlam, F.H. Quart. J.R.Met.Soc., 77, p.663, 1951.

TABLE I

Pilots' estimate of severity	Percentage no. of occasions when icing rate greater than or equal to value shown (in./hr on observable part of aircraft - usually leading edge of wing)												Total no. of reports
	0.0	1.0	2.0	3.0	4.0	5.0	6.0	7.0	8.0	9.0	10.0	20.0	
Low	100	81	64	50	31	30	27	21	16	15	14	3	105
Moderate	100	96	85	73	55	49	42	33	28	28	25	8	150
High	100	99	98	94	87	84	82	73	67	67	66	41	82

TABLE II

Cloud type	Percentage no. of icing severities in the categories shown			Total no. of reports
	"High"	"Moderate"	"Low"	
Stratocumulus (Sc)	12	44	44	185
Cumulus (Cu) Cumulonimbus (Cb) sometimes with Sc	25	40.5	34.5	182
Nimbostratus (Ns) and Stratus (St)	20	33	47	165
Altostratus (As)	13	30	57	107
Altocumulus (Ac)	7	25	68	71
Altocumulus and Altostratus mixed (AcAs)	19	29	52	31
Layer cloud (As,Ns,St) mixed with Cu	18	45.5	36.5	22
Cirrus (Ci) Cirrostratus (Cs) Cirrocumulus (Cc)	(14)	(43)	(43)	7
Out of cloud	(33)	(0)	(67)	12
All reports	17	36	47	782

/TABLE III

TABLE III

Temperatures at which icing was reported - percentage frequency

Temperature range (°C)

Cloud type	Pilots' estimate of severity	≥ 0	-1 to -5	-6 to -10	-11 to -15	-16 to -20	-21 to -25	-26 to -30	-31 to -35	-36 to -40	≤ -41	Total no. of reports
Sc	Low	6.8	55.4	27.0	9.5	1.3	0	0	0	0	0	74
	Moderate	1.5	52.3	29.2	13.9	1.5	1.5	0	0	0	0	65
	High	0	55.5	44.5	0	0	0	0	0	0	0	18
Cu, Cb	Low	11.1	29.6	29.6	16.7	3.7	3.7	1.9	0	0	3.7	54
	Moderate	1.8	40.3	38.6	8.8	7.0	1.8	1.8	0	0	0	57
	High	3.3	30.0	43.3	20.0	3.3	0	0	0	0	0	30
St, Ns	Low	4.2	56.3	21.1	15.5	0	0	2.8	0	0	0	71
	Moderate	7.7	46.1	33.4	12.8	0	0	0	0	0	0	39
	High	0.0	65.2	21.7	8.7	4.3	0	0	0	0	0	23
As	Low	0.0	25.9	37.0	11.1	14.8	9.3	1.9	0	0	0	54
	Moderate	10.0	15.0	30.0	10.0	20.0	15.0	0	0	0	0	20
	High	0.0	0.0	25.0	37.5	12.5	0	12.5	12.5	0	0	8
Ac	Low	0.0	18.2	27.3	25.0	9.1	9.1	11.3	0	0	0	44
	Moderate	7.7	7.7	23.0	38.5	23.0	0	0	0	0	0	13
	High	0.0	40.0	20.0	20.0	20.0	0	0	0	0	0	5
Ac, As	Low	0.0	25.0	0.0	25.0	0.0	37.5	12.5	0	0	0	8
	Moderate	0.0	42.9	14.3	14.3	14.3	0	0	14.3	0	0	7
	High	0.0	0.0	66.7	33.3	0	0	0	0	0	0	3
Layer cloud mixed with Cu	Low	0.0	37.5	12.5	25.0	0.0	25.0	0	0	0	0	8
	Moderate	11.1	44.4	33.3	0.0	11.1	0	0	0	0	0	9
	High	0.0	50.0	50.0	0.0	0.0	0.0	0	0	0	0	2
Ci, Cs, Cc	Low	0.0	0.0	0.0	0.0	0.0	50.0	0	0	0	50.0	2
	Moderate	0.0	0.0	0.0	100.0	0.0	0.0	0	0	0	0	1
	High	0	0	0	0	0	0	0	100.0	0	0	1
Out of cloud	Low	0.0	33.3	33.3	0	0	0	0	0	0	33.3	3
	Moderate	0	0	0	0	0	0	0	0	0	0	0
	High	0	75.0	25.0	0	0	0	0	0	0	0	4
All reports	Low	4.4	39.3	26.7	15.1	4.7	5.3	3.1	0	0	1.2	318
	Moderate	4.3	40.8	31.8	13.3	6.6	2.4	0.5	0.5	0	0	211
	High	1.6	42.5	35.1	13.8	4.3	0.0	1.1	2.1	0	0	94

/TABLE IV

TABLE IV

Type of icing associated with different values of derived water content

w (g/m³)

Type of icing	0 to 0.10	0.11 to 0.20	0.21 to 0.30	0.31 to 0.40	0.41 to 0.50	0.51 to 0.60	0.61 to 0.70	0.71 to 0.80	0.81 to 0.90	0.91 to 1.00	1.01 to 2.00	2.01 to 3.00	>3.0	Total
Clear	3	7	20	6	5	8	5	6	2	0	9	8	5	84
Mixed	3	8	12	4	3	5	3	2	2	0	10	1	7	60
Rime	20	12	11	10	5	7	2	2	2	1	11	2	3	88
Not reported	1	0	1	0	0	1	0	0	0	0	0	0	0	3
Total:	27	27	44	20	13	21	10	10	6	1	30	11	15	235

TABLE V

Type of icing associated with different temperatures

Temperature (°C)

Type of icing	⩾0	-1 to -5	-6 to -10	-11 to -15	-16 to -20	-21 to -25	-26 to -30	-31 to -35	-36 to -40	<-40	Not reported	Total
Clear	2	37	27	15	2	1	0	0	0	0	0	84
Mixed	1	17	25	10	2	1	2	1	0	1	0	60
Rime	2	27	18	16	13	6	3	2	0	0	1	88
Not reported	1	2	0	0	0	0	0	0	0	0	0	3
Total:	6	83	70	41	17	8	5	3	0	1	1	235

/TABLE VI

TABLE VI

84 occasions of clear ice formation: water content and temperature

w (g/m^3)

Temp. °C	0 to 0.10	0.11 to 0.20	0.21 to 0.30	0.31 to 0.40	0.41 to 0.50	0.51 to 0.60	0.61 to 0.70	0.71 to 0.80	0.81 to 0.90	0.91 to 1.00	1.01 to 2.00	2.01 to 3.00	>3.0	Total
⩾ 0	0	0	1	0	0	0	1	0	0	0	0	0	0	2
-1 to -5	2	4	6	4	2	4	2	2	1	0	4	4	2	37.
-6 to -10	1	1	7	2	1	3	2	3	1	0	3	3	0	27
-11 to -15	0	1	4	0	2	1	0	1	0	0	2	1	3	15
-16 to -20	0	1	1	0	0	0	0	0	0	0	0	0	0	2
-21 to -25	0	0	1	0	0	0	0	0	0	0	0	0	0	1
Total:	3	7	20	6	5	8	5	6	2	0	9	8	5	84

TABLE VII

84 occasions of clear ice formation: water content and cloud type

w (g/m^3)

Cloud type	0 to 0.10	0.11 to 0.20	0.21 to 0.30	0.31 to 0.40	0.41 to 0.50	0.51 to 0.60	0.61 to 0.70	0.71 to 0.80	0.81 to 0.90	0.91 to 1.00	1.01 to 2.00	2.01 to 3.00	>3.00	Total
Cu, Cb, Cu and Sc	0	1	6	2	2	1	2	1	2	0	2	2	2	23
Sc	1	0	7	3	1	2	2	3	0	0	5	1	1	26
St, Ns, As	1	2	7	1	2	4	1	1	0	0	1	5	1	26
Ac, AcAs	0	3	0	0	0	1	0	1	0	0	1	0	0	6
Below cloud	1	1	0	0	0	0	0	0	0	0	0	0	1	3
Total:	3	7	20	6	5	8	5	6	2	0	9	8	5	84

/TABLE VIII

TABLE VIII

84 occasions of clear ice formation:
temperature and cloud type

Cloud type	Temperature (°C) ⩾0	-1 to -5	-6 to -10	-11 to -15	-16 to -20	-21 to -25	Total
Cu, Cb, Cu and Sc	0	7	9	6	1	0	23
Sc	2	13	8	3	0	0	26
St, Ns, As	0	13	8	3	1	1	26
Ac, AcAs	0	1	2	3	0	0	6
Below cloud	0	3	0	0	0	0	3
Total:	2	37	27	15	2	1	84

TABLE IX

60 occasions of "mixed" ice formation:
derived water content and temperature
w (g/m³)

Temp °C	0 to 0.10	0.11 to 0.20	0.21 to 0.30	0.31 to 0.40	0.41 to 0.50	0.51 to 0.60	0.61 to 0.70	0.71 to 0.80	0.81 to 0.90	0.91 to 1.00	1.01 to 2.00	2.01 to 3.00	>3.00	Total
⩾ 0	0	0	1	0	0	0	0	0	0	0	0	0	0	1
-1 to -5	0	3	3	2	0	3	1	0	0	0	4	0	1	17
-6 to -10	2	2	2	2	1	2	2	1	2	0	4	1	4	25
-11 to -15	0	1	5	0	1	0	0	1	0	0	0	0	2	10
-16 to -20	0	0	1	0	1	0	0	0	0	0	0	0	0	2
-21 to -25	1	0	0	0	0	0	0	0	0	0	0	0	0	1
-26 to -30	0	1	0	0	0	0	0	0	0	0	1	0	0	2
-31 to -35	0	0	0	0	0	0	0	0	0	0	1	0	0	1
< -35	0	1	0	0	0	0	0	0	0	0	0	0	0	1
Total:	3	8	12	4	3	5	3	2	2	0	10	1	7	60

/TABLE X

TABLE X

60 occasions of "mixed" ice formation: derived water content and cloud type

w (g/m³)

Cloud type	0 to 0.10	0.11 to 0.20	0.21 to 0.30	0.31 to 0.40	0.41 to 0.50	0.51 to 0.60	0.61 to 0.70	0.71 to 0.80	0.81 to 0.90	0.91 to 1.00	1.01 to 2.00	2.01 to 3.00	>3.00	Total
Cu, Cb, Cu and Sc	0	2	4	0	3	2	2	0	2	0	3	1	4	23
Sc	1	0	3	2	0	2	1	1	0	0	2	0	0	12
St, Ns, As	2	4	4	2	0	1	0	1	0	0	4	0	3	21
Ac, AcAs	0	2	1	0	0	0	0	0	0	0	0	0	0	3
Cs	0	0	0	0	0	0	0	0	0	0	1	0	0	1
Total:	3	8	12	4	3	5	3	2	2	0	10	1	7	60

TABLE XI

60 occasions of "mixed" ice formation: temperature and cloud type

Temperature (°C)

Cloud type	0	-1 to -5	-6 to -10	-11 to -15	-16 to -20	-21 to -25	-26 to -30	-31 to -35	< -35	Total
Cu, Cb, Cu and Sc	0	6	14	2	1	0	0	0	0	23
Sc	0	5	5	2	0	0	0	0	0	12
St, Ns, As	1	6	5	4	1	1	2	0	1	21
Ac, AcAs	0	0	1	2	0	0	0	0	0	3
Cs	0	0	0	0	0	0	0	1	0	1
Total:	1	17	25	10	2	1	2	1	1	60

/TABLE XII

TABLE XII

88 occasions of rime ice formation: derived water content and temperature

w (g/m³)

Temp °C	0 to 0.10	0.11 to 0.20	0.21 to 0.30	0.31 to 0.40	0.41 to 0.50	0.51 to 0.60	0.61 to 0.70	0.71 to 0.80	0.81 to 0.90	0.91 to 1.00	1.01 to 2.00	2.01 to 3.00	>3.00	Total
⩾ 0	0	0	0	0	0	0	1	1	0	0	0	0	0	2
-1 to -5	9	3	4	2	1	3	1	0	0	0	2	2	0	27
-6 to -10	2	2	4	3	1	1	0	0	2	0	1	0	2	18
-11 to -15	6	2	2	2	1	2	0	1	0	0	0	0	0	16
-16 to -20	0	4	0	1	2	0	0	0	0	1	4	0	1	13
-21 to -25	2	1	0	2	0	0	0	0	0	0	1	0	0	6
-26 to -30	1	0	1	0	0	1	0	0	0	0	0	0	0	3
-31 to -35	0	0	0	0	0	0	0	0	0	0	2	0	0	2
Not reported	0	0	0	0	0	0	0	0	0	0	1	0	0	1
Total:	20	12	11	10	5	7	2	2	2	1	11	2	3	88

TABLE XIII

88 occasions of rime ice formation: water content and cloud type

w (g/m³)

Cloud type	0 to 0.10	0.11 to 0.20	0.21 to 0.30	0.31 to 0.40	0.41 to 0.50	0.51 to 0.60	0.61 to 0.70	0.71 to 0.80	0.81 to 0.90	0.91 to 1.00	1.01 to 2.00	2.01 to 3.00	>3.00	Total
Cu, Cb, Cu and Sc	1	3	2	1	0	1	0	1	0	1	3	1	2	16
Sc	5	2	3	1	1	2	1	0	0	0	1	1	0	17
St, Ns, As	11	4	5	4	3	1	0	1	1	0	5	0	0	35
Ac, AcAs	3	3	1	4	1	3	0	0	1	0	2	0	0	18
Below cloud	0	0	0	0	0	0	1	0	0	0	0	0	1	2
Total:	20	12	11	10	5	7	2	2	2	1	11	2	3	88

/TABLE XIV

TABLE XIV

88 occasions of rime ice formation: temperature and cloud type

Temperature (°C)

Cloud type	⩾ 0	-1 to -5	-6 to -10	-11 to -15	-16 to -20	-21 to -25	-26 to -30	-31 to -35	Not reported	Total
Cu, Cb, Cu and Sc	1	3	5	1	4	0	0	1	1	16
Sc	0	13	1	2	1	0	0	0	0	17
St, Ns, As	0	10	6	9	4	4	1	1	0	35
Ac, AcAs	0	1	5	4	4	2	2	0	0	18
Below cloud	1	0	1	0	0	0	0	0	0	2
Total:	2	27	18	16	13	6	3	2	1	88

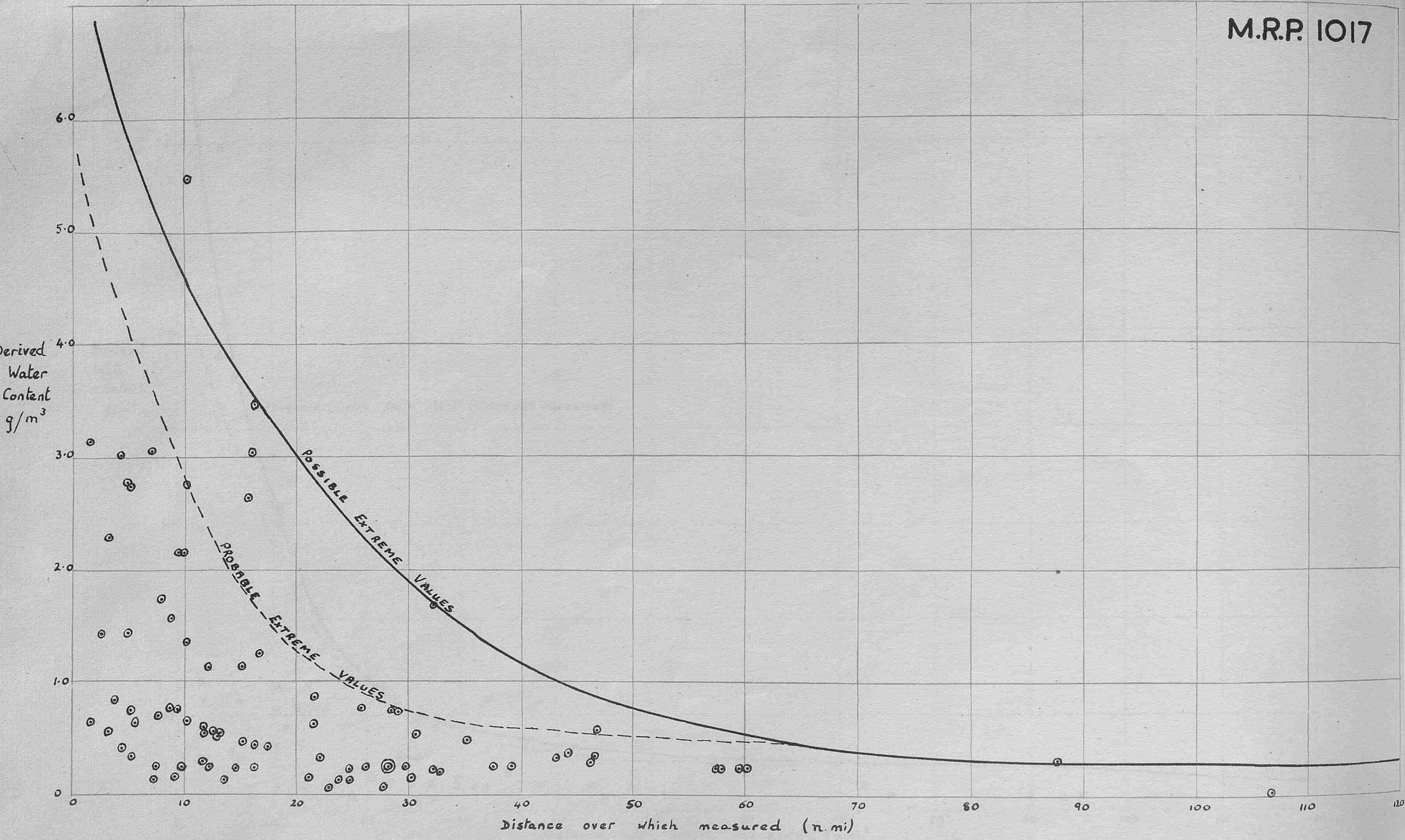

FIG. I Distances over which different values of water content were derived — Clear ice conditions only (84 occasions)

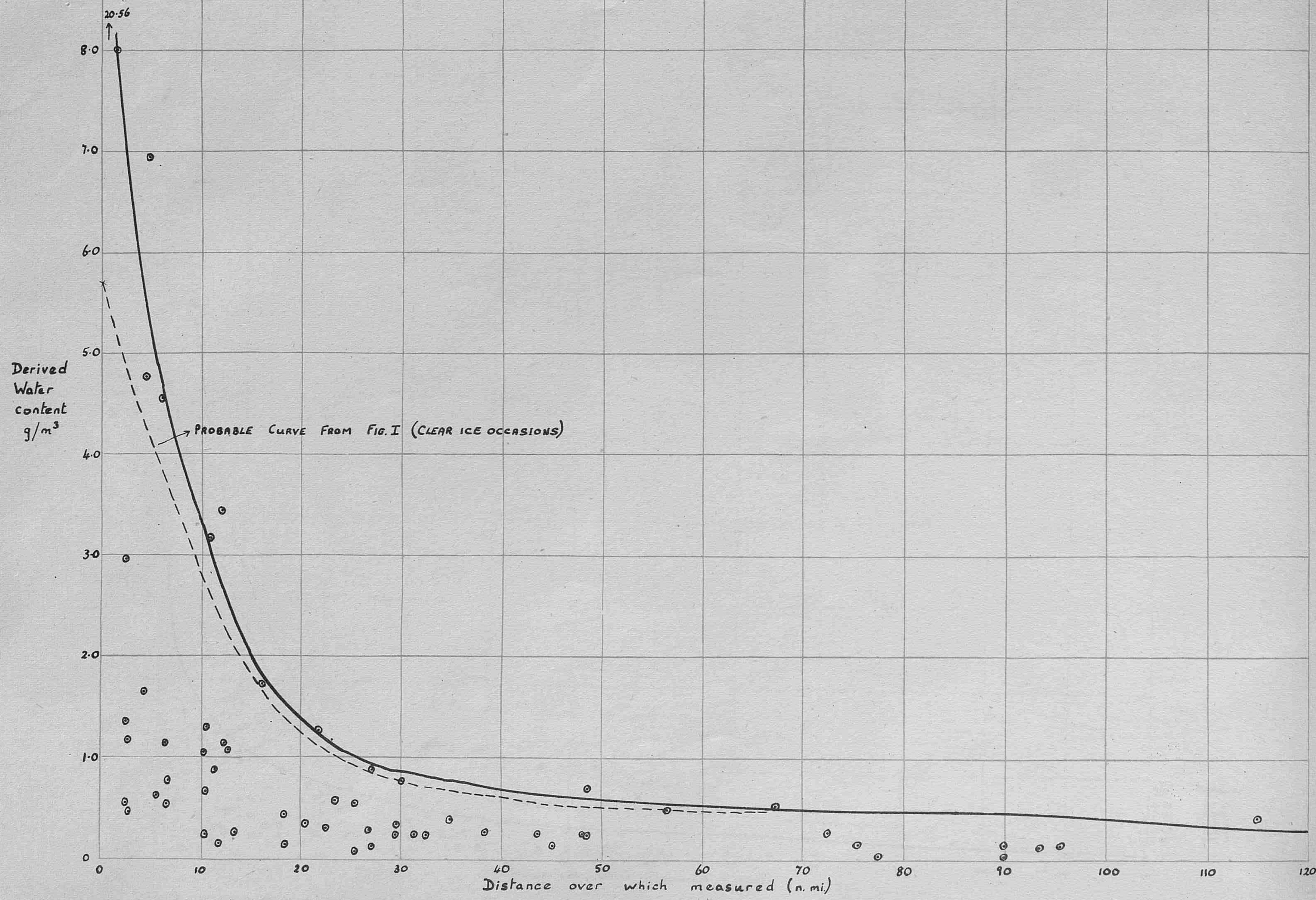

FIG. II Distances over which different values of water content were derived — "Mixed" ice conditions only (60 occasions)

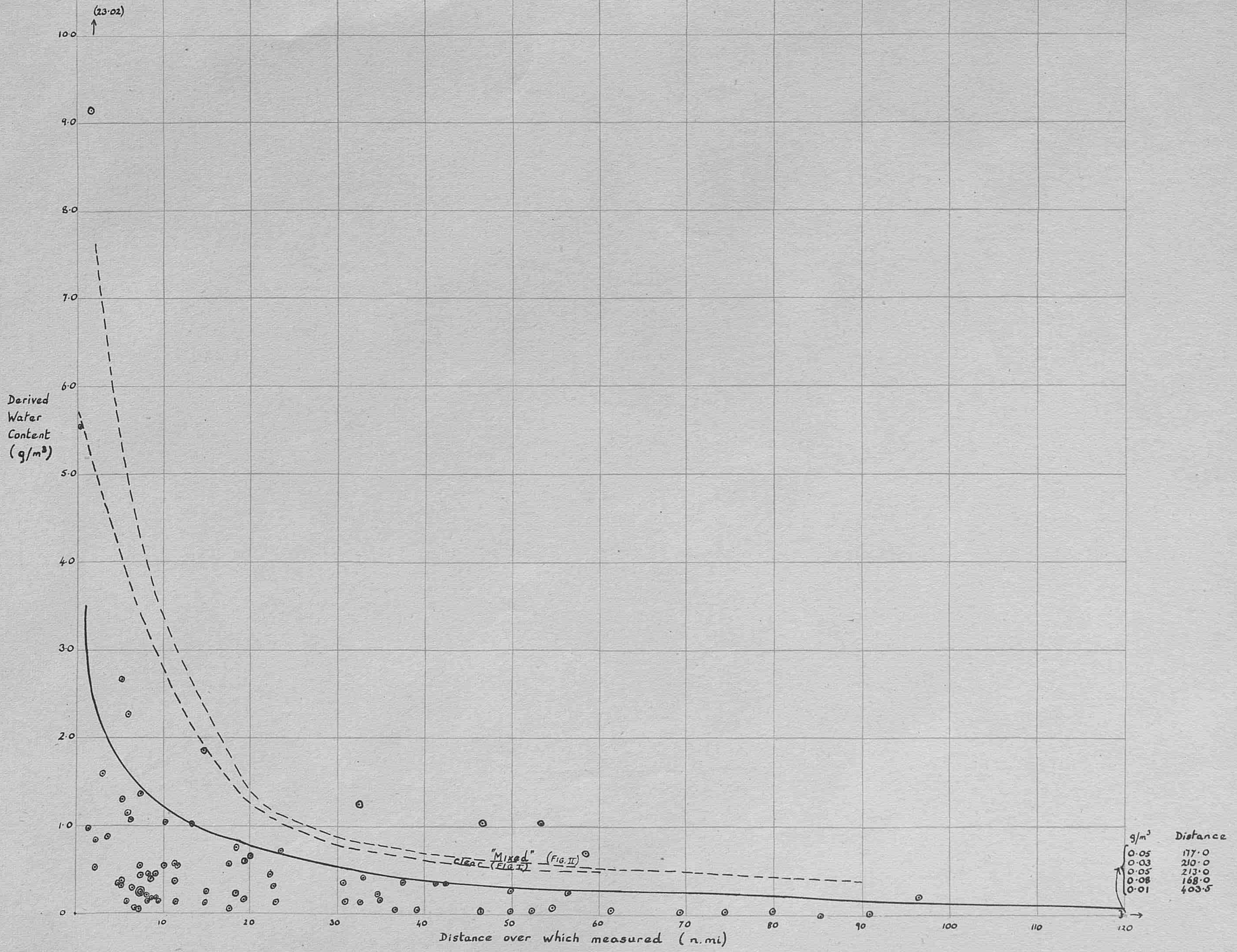

FIG. III Distances over which different values of water content were derived — Rime ice conditions only (88 occasions)

M.R.P. 1018

S.C. 11/222

7th December, 1956

[redacted]

Numerical experiments in the integration of the meteorological equations of motion

by

E. Knighting, D. E. Jones and Mavis K. Hinds

(Meteorological Office)

AIR MINISTRY

METEOROLOGICAL RESEARCH COMMITTEE

At the time of issue this report has not been published. Any author desiring to quote this paper should refer to it as "A paper of the Meteorological Research Committee (London), M.R.P. No. 1018 by E. Knighting, D.E. Jones and Mavis K. Hinds. A copy is available in the Library of the Meteorological Office."

M.R.P. 1018
S.C. II/222
7th December, 1956

AIR MINISTRY
METEOROLOGICAL RESEARCH COMMITTEE

Numerical experiments in the integration of the meteorological equations of motion

by

E. Knighting, D.E. Jones and Mavis K. Hinds (Meteorological Office)

Summary

It is usual to use finite difference methods in carrying out the time integration of the equations of motion as adapted to the prediction of the large scale atmospheric pattern, and this implies a choice of the mesh length and time increment to be used. The effect of changing the size and orientation of the mesh upon the computed values of the vorticities and their advection is examined, and the resulting differences between 24-hour predictions are shown to be important.

1. Introduction

The so-called "vorticity equation" relating changes of the vertical component of vorticity to the advection and divergence forms the basis of all practical methods of numerical weather prediction so far developed. In particular the barotropic equation used in the simplest system of practical value is merely an expression of the conservation of absolute vorticity.

Hence in the numerical calculations involved in predicting the synoptic-scale flow pattern over a period of a day or so we have to deal with expressions of the form

$$\frac{\partial \zeta}{\partial t} + V.\nabla\zeta$$

where ζ is the vertical component of vorticity. Further it has been found necessary to make use of the quasi-geostrophic character of the motion and assume that the velocity, but not its divergence, can be derived from the geopotential

$$V = \frac{g}{f} k \wedge \nabla h \qquad \text{........(1)}$$

where V is the velocity, h the height of an isobaric surface, g the acceleration due to gravity and f the Coriolis parameter; the gradient is taken in the isobaric surface. The vorticity ζ, is then given by

$$\zeta = \frac{g}{f} \nabla^2 h \qquad \text{........(2)}$$

The term $V.\nabla\zeta$ may be written, in view of equation (1) as

$$V.\nabla\zeta = \frac{g}{f} J(h,\zeta) \quad \text{........(3)}$$

J denoting, as usual, the Jacobian so that the typical equation with which we deal is

$$\nabla^2 \frac{\partial h}{\partial t} + J(h,\zeta) = F(h,\zeta,f) \quad \text{........(4)}$$

Explicit solutions of such equations cannot be obtained and the integration is carried out by replacing the equations by their finite difference analogues in terms of the height of a pressure surface (or the thickness between two pressure surfaces) at the grid points of a square mesh. The initial values of h at the grid points are not observed but are interpolated and even extrapolated values obtained from observations which are irregularly distributed. The finite difference approximations to ∇^2 and J will depend upon both the length and orientation of the mesh, although the differential operators themselves are symmetrical. The object of this investigation is to compare the finite difference approximations to ∇^2 and J using different mesh lengths and orientations and to find their effect upon the time integrations.

2. The basis of the computations

One finite difference approximation to $\nabla^2 h$ is

$$\mathbb{V}^2 h = \frac{h_1 + h_2 + h_3 + h_4 - 4h_0}{a^2} \quad \text{........(5)}$$

where the symbol $\mathbb{V}^2$ indicates a finite difference approximation, and h_i is the value of h at the grid point numbered i in Fig. 1, a being the mesh length. A similar formula applies if we consider the points numbered 5, 6, 7, 8 instead of those numbered 1, 2, 3, 4 since ∇^2 is a symmetric operator. Thus another approximation is

$$\mathbb{V}^2 h = \frac{h_5 + h_6 + h_7 + h_8 - 4h_0}{2a^2} \quad \text{........(6)}$$

The factor 2 occurs in the denominator because we are now considering a mesh of side $\sqrt{2}\,a$ making an angle $\pi/4$ with the previous mesh. We have denoted quantities such as ζ calculated in these two ways by ζ^+ and $\zeta^\times$, ζ^+ being calculated from the cross formed by the points 0, 1, 2, 3, 4 and $\zeta^\times$ from the St. Andrew's cross formed by the points 0, 5, 6, 7, 8. ζ^+ is the finite difference approximation which is usually used.

The definition of the operator J is

$$J(h,\psi) = \frac{\partial h}{\partial x}\frac{\partial \psi}{\partial y} - \frac{\partial h}{\partial y}\frac{\partial \psi}{\partial x} \quad \text{........(7)}$$

and the approximation to J is

$$J(h,\psi) = \frac{(h_1-h_3)(\psi_2-\psi_4)-(h_2-h_4)(\psi_1-\psi_3)}{4a^2} \qquad \text{........(8)}$$

the numbering being as in Fig. 1, so that J is a function of the values of h and ψ at the corners of a square. We may compute J from the values at the corners of any other square; thus an alternative approximation is

$$J(h,\psi) = \frac{(h_5-h_7)(\psi_6-\psi_8)-(h_6-h_8)(\psi_5-\psi_7)}{8a^2} \qquad \text{........(9)}$$

and again we distinguish between these two finite difference approximations by writing the first as J^+, the second as J^x. When ψ is ζ + f we already have two alternative finite difference approximations to it, ζ^+ + f and ζ^x + f, and there are four possible Jacobians

$$J^+(h,\zeta^+ + f),\quad J^+(h,\zeta^x + f),\quad J^x(h,\zeta^+ + f),\quad J^x(h,\zeta^x + f)$$

and we denote these by J^{++}, J^{+x}, J^{x+}, J^{xx} respectively.
The usual methods of integration of the dynamical equations use J^{++}.

3. The calculations

The values of the vorticities and the Jacobians were calculated from the heights of the 500 mb surface over the mesh of 18 x 14 points in current use in the Forecast Research Division (shown in Fig. 4). This is a square grid on a polar stereographic projection with a grid length of approximately 160 miles in the latitude of the British Isles. This gives vorticities over a mesh of 16 x 12 points and Jacobians over a mesh of 14 x 10 points for ζ^+ and J^+, and with points missing in the other fields at the corners of the mesh owing to the methods of calculation. The values which have been computed and which are presented in Tables III and IV are

$$\zeta = \frac{\beta^2 g}{f} \nabla^2 h \qquad \text{........(10)}$$

and are expressed in 10^2 hr^{-1}, β being the map magnification factor on this projection, so that a vorticity given as 064 is 0.64 hr^{-1}. The computed values of the Jacobians are

$$J_{comp} = a^2 J\left(h, \frac{\beta^2 g}{f} \nabla^2 h + f\right) \qquad \text{........(11)}$$

the results being expressed in ft hr^{-1} in Table VII etc. These are the expressions used in the time integrations.

The calculations of vorticities and Jacobians were carried out for 18 cases which had been used to test the Sawyer-Bushby forecasting equations (Sawyer, J.S. and Bushby, F.H. 1953); these cases were used because the data required were readily available in a punched form for use in the electronic computer. It is impracticable to reproduce all the results and in the tables we have given the results for a simple case which appeared to show wider divergences than the average, and which has been used as a test case in several modifications of the Sawyer-Bushby model.

/4.

4. Results of the vorticity calculations

It is the absolute vorticity $\zeta + f$, which enters into the forecasting equations, where f is the Coriolis parameter. In some integration schemes the equations are linearised by setting $f+\zeta = f$ where the former occurs as a multiplying factor, so that for some purposes it is better to compare $\zeta^{+} - \zeta^{\times}$ with f in order to estimate the importance of the difference. For comparison f is given in Table I in the same units as ζ. On the other hand, in anticyclonic regions where ζ is negative it is better to retain $f + \zeta$ as the comparison with $\zeta^{+} - \zeta^{\times}$.

The result which is most apparent is that the field of $\zeta^{\times}$ is generally smoother than that of ζ^{+} in regions where ζ is large i.e., $|\zeta|$ is of the order of 0.4 hr^{-1}. The patterns are often similar, in that maxima of ζ^{+} occur in the same regions as maxima of $\zeta^{\times}$, often at the same grid point, but the maxima of $\zeta^{\times}$ are usually less than those of ζ^{+}. The minima, often small negative values of the order 0.05 hr^{-1}, are more difficult to correlate and are probably of less importance. Occasionally ζ^{+}, or both ζ^{+} and $\zeta^{\times}$ were negative and large so that $f + \zeta$ at a grid point was less than zero, and some suspicion must be attached to the analysis near such points, the absolute vorticity being negative; in the time integration negative values of $\zeta + f$ are made zero.

If the height h at a grid point was changed by an amount ε, then the resulting change ε' in the field of $\zeta^{\times} - \zeta^{+}$ would have the pattern shown in Fig. 2. A difference of ε = 200 ft leads to a value of ε' of 0.40 hr^{-1}. In several cases a pattern very similar to that of Fig. 2 was clearly discernible suggesting that perhaps an error had been made in reading off the value of h from the synoptic chart and in one case where both $\zeta^{+} + f$, and $\zeta^{\times} + f$ were negative it was found that an error of 200 ft had in fact been made in the height. This property of the field of $\zeta^{+} - \zeta^{\times}$ is now used to test the initial data for use in a time integration to detect errors in interpolation. $\zeta^{+} - \zeta^{\times}$ is formed and tested to see if it exceeds 0.30 hr^{-1}.

The computations based upon the data at 1500Z 30.1.52 serve as an example of large vorticities and differences which are typical of the results found. The 500 mb height field is given in Table II, and the corresponding contour chart in Fig. 5a while ζ^{+}, $\zeta^{\times}$ and their differences are given in Tables III, IV and V. The region in which both $\zeta^{+} + f$ and $\zeta^{\times} + f$ are negative is not typical but these negative values have been closely examined and there would be no justification for redrawing the contour charts to produce positive values of $f + \zeta$, although this could easily be done. The smoothness of the $\zeta^{\times}$ field compared with the ζ^{+} field in the region of the jet stream shown in Fig. 5a is typical, as are the rather small differences in regions of weak vorticity.

There is a field h' with the same boundary values as h and such that ζ^{+} as calculated from h' is the same as $\zeta^{\times}$ calculated from h. We calculated the values of $\zeta^{\times}$, integrated the Poisson equation to give the field h' and formed the difference $h-h'$. Table VI gives the difference $h-h'$ for the data of Table II. Originally we intended to carry out the integration for all 18 cases but the first 10 integrations referred to those cases in which the differences $\zeta^{\times} - \zeta^{+}$ were most marked, so that $h-h'$ would be expected to be greatest. We found in these 10 cases that the maximum value of $h-h'$ was 70 ft over the ocean and this difference was suspect since a change of 200 ft in the height of the 500 mb surface at one grid point over the ocean would have almost cancelled the difference. A closer examination showed that an error of 200 ft had been made in reading the contour height at this point. Apart from this extreme value, the maximum value of $h-h'$ was 50 ft and this was an isolated case (occurring in Table VI). At the 1880 grid points considered the difference $h-h'$ exceeded 20 ft on only 123 occasions and exceeded 40 ft on only 10 occasions, three of which were suspect. We therefore assumed that the differences arising between ζ^{+} and $\zeta^{\times}$ were no more than could arise from differences between two analyses of the 500 mb chart.

5. The results of the Jacobian calculations

The calculation of J ($\underline{h}, \zeta$) involves the height $\underline{h}$ at a number of grid points and the patterns of points used are shown in Fig. 3; we cannot indicate the weight attached to any given point because the Jacobian is a function of two fields. Of these J^{++} uses points which are nearest the origin while J^{xx} uses the most widespread. J^{+x} and J^{xx} have no points in common so that a combination of them will use a compact system with more points than J^{++}, which is also compact.

The Jacobian is formed from first and third derivatives of the height field and is naturally rather rough; however, well marked features in one Jacobian field were generally discernible in the other three fields, although the features were often displaced and of different emphasis. These marked features correspond to some marked feature in the height field such as the presence of a strong jet stream or strongly curved motion.

The maximum absolute value of the Jacobian was 181 ft hr^{-1} and values of 70 ft hr^{-1} were quite common. The differences between the computed values at a given point were often as great as the values themselves, but these large differences were often associated with large differences of the opposite sign in the immediate neighbourhood, there being often a relative displacement of the maxima and minima of the two Jacobian fields. Owing to this relative displacement it is difficult to associate even the sign of the Jacobian with some particular feature in the height field e.g., it is not possible to say that the Jacobian has a particular sign in the rear of a depression, although on general grounds we should expect it to be negative in this region. In straight flow the Jacobian is usually rather small and of indeterminate sign suggesting that there is little change in these regions; the differences were also rather small and of indeterminate sign. There were occasional large Jacobians in flow of a rather indefinite character and these may have been occasioned by small inaccuracies in reading the 500 mb heights at some grid point.

Table VII gives the values of J^{++} calculated for 1500Z 30.1.52 and Tables VIII to X give the differences between the other Jacobians and J^{++}. The eastern and southern parts of the chart have fairly small values of the Jacobians and their difference, and in this region the vorticities and their differences were also small. In the north-west where there is a strong jet stream the differences in the Jacobians are quite marked e.g., at the grid point 5 columns and 5 rows from the north-west corner the following values occur.

J^{++}	$J^{x+} - J^{++}$	$J^{+x} - J^{++}$	$J^{xx} - J^{++}$
181	- 246	-70	- 215

Since the Jacobian has a high negative correlation with the height tendency it is clear that in this region there is a possibility of the different Jacobians leading to different signs of the calculated tendency. The values given in Tables VII to X are fairly representative of the other calculations made.

The J^{xx} field is usually the smoothest, and J^{++} the roughest field; changing the method of calculating the Jacobian makes a greater difference than changing the method of calculating the Laplacian so that the fields J^{++}, J^{+x} were akin as were those of J^{x+} and J^{xx}. The mean of J^{xx} and J^{+x} was found and proved on a whole to be smoother fields than that of any of the other Jacobians. Examination showed that the mean Jacobian fields could be associated with large scale features on the synoptic chart and it may be better to use some mean Jacobian in the time integration.

When considering the vorticity fields we were able to reconstruct the height field corresponding to a given vorticity field and given boundary values; we are unable similarly to reconstruct the height field from the Jacobian field because the differential equation to be solved is not elliptic.

/6.

6. The time integrations

It has been shown above that changing the finite difference scheme can make large differences to the calculated Jacobians. These differences may lead to forecast heights which are quite different; in the example which we have chosen to illustrate the differences it is evident that in some regions the sign of the height tendency will depend upon the finite difference Jacobian used. In order to obtain the height tendency from the Jacobian field a double integration has to be performed and it is possible that this will have a smoothing effect which will remove the differences and lead to much the same values of $\partial h/\partial t$ whatever approximation is used; this is improbable owing to the large differences observed between the Jacobians. It was decided to investigate the effect of using the different vorticities and Jacobians in a 24-hour time integration. The barotropic model affords the simplest computation which involves the vorticities and Jacobians and which leads to results which agree in a fair measure with the development which takes place in the atmosphere. There would be no difficulty in carrying out a baroclinic forecast but it was felt that the extra complication would not help in deciding the effect of using the various finite difference approximations. A programme was therefore written for the solution of

$$\nabla^2 \frac{\partial h}{\partial t} = -J\left(h, \frac{g\nabla^2 h}{f} + f\right) \qquad \text{........(12)}$$

in which one of four finite difference analogues of the Jacobian can be inserted (at will) on the right hand side. The height h was taken to be the height of the 500 mb surface, f being the Coriolis parameter. The forecasts were made on the usual grid used at Dunstable (shown in Fig. 4), the time steps being of one hour; at the boundary we assumed a knowledge of h at $t = 0$, 12 hr and 24 hr and $\partial h/\partial t$ was taken as a constant in each 12-hour period. Values of the Jacobians, tendencies and height fields could be printed out at intermediate times. We chose as the first case for study that which gave the largest differences in the Jacobian fields, the data being those for 1500Z 30.1.52 as in Table I. Two integrations were first carried out using J^{++} and J^{x+} which showed the greatest differences at time $t = 0$; the differences in the 24-hour forecast were sufficiently large to make it worthwhile to carry out the integrations using J^{+x} and J^{xx} also.

Table IX gives the predicted height of the 500 mb surface at the inner 140 points using the four methods of calculating the Jacobian and two of the corresponding contour charts are shown in Fig. 5. The forecast made using J^{++} and that made using J^{+x} are almost identical; the greatest difference is 150 ft with 7 differences of over 100 ft and 103 of 50 ft or less. Similarly the forecasts using J^{x} are almost identical, with a greatest difference of 150 ft, 6 differences of 100 ft or more and 111 of 50 ft or less. On the other hand the greatest difference between the forecast made using J^{++} and that made using J^{x+} is 720 ft, with 49 differences of 100 ft or more and only 51 of 50 ft or less. Table X gives the root mean square differences between the different forecasts. The large differences in the forecasts arise between those using a J^{+} and those using a J^{x} and we need consider only the differences between J^{++} and J^{x+}, the differences between J^{+x} and J^{xx} being similar, while those between J^{++} and J^{+x} are small.

The height field was printed out at each 3-hour interval, the vorticity, Jacobian and the tendency fields being printed at each 6-hour interval. The maximum differences between J^{++} and J^{x+}, which were initially large, decreased, the largest difference falling from -246 at $t = 0$ to 155 at $t = 12$ hr and -157 at $t = 24$ hr. The root mean square differences over the 140 points considered decreased at first but increased again, showing that the differences were increasing over most of the chart. The R.M.S. differences between J^{++} and J^{x+} were 45 ft hr^{-1} at $t = 0$, 33 ft hr^{-1} at $t = 12$ hr and 46 ft hr^{-1} at $t = 24$ hr.

The computed initial fields of $\partial h/\partial t$ using J^{++} and J^{x+} are given in Table XI. The double integration has considerably smoothed out the roughness of the original Jacobian fields and the bottom four rows of each table are very much the same. The calculated rises in the rear of the depression are larger when J^{++} is used than when J^{x+} is used by the order of 10 ft hr^{-1} and the maximum rise is displaced further south by a grid length. The falls ahead of the low towards Scotland are also larger by about the same amount so that even at this stage it will not be surprising if the final forecasts differ considerably. The 6-hour forecasts of the height of the 500 mb surface are very similar, since the differences in $\partial h/\partial t$ can lead only to differences in height of 50-100 ft ahead of and behind the low; there is a slight but noticeable difference in the trough position.

The fields of $\partial h/\partial t$ after 6 hr are given in Table XII and at this stage the difference in the isopleths in the upper central part of the field is quite marked, with the forecast using J^{++} moving the trough more rapidly eastwards with a greater surge of pressure behind.

The 12-hour forecasts are given in Table XIII and show the trough further east and north when J^{++} is used, the jet being almost west to east. The forecast made with J^{x+} holds the trough further back, extending it southward. At this stage we are effectively starting a 12-hour forecast with different initial charts using different methods of calculation and the divergence continues to grow.

The computed values of the tendency field after 24 hr are given in Table XIV; that computed using J^{++} is out of phase with that computed using J^{x+}, the centres having been moved further east and now appearing less intense. The differences between the fields have increased, the R.M.S. values being 11, 17 and 22 ft hr^{-1} at times $\underline{t}$ = 0, 12, 24 hr respectively, and the difference field is as great as the fields themselves. It is clear that further time integration would lead to more widely divergent forecasts.

The height field of the 500 mb surface at 1500Z 30.1.52 has been given in Table II, as has the height field 24 hr later. The forecast height fields have been given in Table IX; the fields are shown in chart form in Fig. 5(a), (b), (c), (d). The differences between the forecast and actual height values show that the forecast made using J^{x+} was superior to that made using J^{++}, the maximum errors being 970 ft and 1290 ft respectively. The differences between the forecast values are not quite as great as the difference between the better forecast values and the actual final values, but are of the same order in the vicinity of the trough; near the boundaries in the north-west both forecast values are similar and differ from the actual values by several hundred feet.

In the region of the trough the differences between the forecast values are large; the maximum difference is 730 ft and at eight grid points the difference exceeds 400 ft. These large differences occur because the forecast made using J^{++} moved the trough too far east without sufficient deepening and failed to predict the south-eastward extension. The forecast made using J^{x+} predicted part of the south-eastward extension and moved the trough more slowly in accordance with the actual development, the failure being mainly in the failure to forecast the considerable deepening in the region of the British Isles. The increasing difference between the two forecasts is borne out by the R.M.S. differences between them, which are 103 ft after 12 hr and 177 ft after 24 hr.

In order to compare the two forecasts with one another and also with forecasts made from the same initial data using other methods of computation, the actual and forecast height changes have been correlated over the inner grid of 12 x 8 points, and the resulting correlation coefficients are given in Table XV. There is marked difference in the correlation coefficients indicating that the forecast made using J^{x+} was superior to that made using J^{++} and this is borne out synoptically by the charts shown in Fig. 5. The improvement made by using J^{x+} instead of J^{++} is as marked as is that made by any of the changes made in the method of use of the Sawyer-Bushby model.

/7.

7. Some further results

The synoptic situation of 30.1.52 is characterized by a strong jet stream; the existence of a jet is common although perhaps that occurring in this situation is stronger than usual. Similar experiments with two quite different synoptic situations and developments were carried out.

The initial chart used in the first of these refers to 1500Z 27.1.52 and is given with the chart 24 hr later at 1500Z 28.1.52 in Fig.6(a) and (b). Initially there was a low to the west of Iceland with its attendant trough stretching SSE. The ridge ahead of it was to the west of Ireland with a deep trough extending down the North Sea, through the Low Countries and curving backward into Spain. In the next 24 hr the trough extending from the Iceland low developed and lay down the Irish Sea, while the deep trough over the North Sea moved eastward and relaxed. The ridge between these two troughs moved off the eastern coasts of Great Britain and also relaxed so that the amplitude of the pattern was reduced. The 24-hour changes in the height of the 500 mb surface were generally less than those which occurred in the 24 hr following 1500Z 31.1.52.

The 24-hour forecasts made with the use of J^{++} and J^{x+} are given in Fig.6 (c) and (d). The 24-hour changes in height of the 500 mb surface over and to the west of Great Britain were not more than about 300 ft so that minor differences in the forecast changes could lead to large differences in the positions of the relaxing trough and ridge; the pattern of height changes, a slight fall to the west of Great Britain and a rise to the east was well forecast by both the numerical methods. Table XVI, which gives a statistical summary of the three time integrations, shows the high correlation between observed and forecast changes. The difference between the forecast height changes increased with time and was in the mean about 40 per cent of the actual change. Thus, although there appears to be little difference in the success of the two methods of forecasting as judged by the correlation coefficients, the forecast height changes at many points on the chart are different in magnitude and the troughs and ridge are relatively displaced.

The last synoptic situation chosen for examination refers to 1500Z 30.1.53. On the night of 31.1.53 strong NW. winds in the North Sea caused disastrous flooding on the east coast of Great Britain and on the coasts of Holland and Denmark. Numerical forecasts had already been made using the data of 1500Z 30.1.53 and we chose to make two barotropic forecasts from the same data. At this time a deep trough with strong NW. winds stretched almost due south from Iceland with a ridge ahead over the North Sea, Great Britain being in a SW. airstream of about 50 knots. In 24 hr the trough developed rapidly, and advanced with a closed centre over the southern North Sea and very strong N. and NW. winds over Great Britain, reaching 119 knots at Larkhill, while a strong ridge almost replaced the trough.

The synoptic situations at 1500Z 30.1.53 and 1500Z 31.1.53 are shown in Fig.7(a) and (b), the numerical forecasts using J^{++} and J^{x+} being given in Fig.7(c) and (d). The pattern of changes, a rapid fall in the region of Great Britain and the North Sea with a rapid rise to the west, was well forecast, giving a high correlation coefficient between the forecast and actual changes in each case. As in Table XVI however, the resulting forecast charts showed the trough too far west and under-emphasized both the depth and the very strong northerly winds which were the most important feature of the synoptic situation. The R.M.S. of the difference between the forecast height changes again increased almost linearly with time, but were only about 10 per cent of the actual changes after 24 hr. The forecast made using J^{++} was, from a synoptic point of view, more successful than that made using J^{x+} since it moved the trough further east and gave a lower pressure within it; neither forecast gave the closed low that actually existed after 24 hr.

/8.

8. Conclusion

In the experiment which has been described above two sets of forecasts have been made from the same data using the same method, the only difference introduced being in the orientation and length of the mesh. The 24-hour forecast on two of the three occasions differed considerably in an area near the centre of the mesh which is usually supposed to be the most free from errors which arise because of the boundary conditions. The difference between the two forecast values of the changes in the height field of the 500 mb surface increased with time and was about 40 per cent of the actual change in two cases and about 10 per cent in the third. The implication is grave, that upon some occasions the choice of mesh size and orientation in the field has a decisive effect upon the forecast that is made. There can be little doubt that the differences depend very largely upon the computed Jacobians and the remedy may lie in a more accurate determination of derivatives by taking into account values at more grid points in computing them. Further experiments will be carried out to point to a solution of the difficulty.

LIST OF TABLES

TABLE I Values of the Coriolis parameter, f, at the grid points of Fig.4 ($10^{-2}hr^{-1}$).

II(a) Contour heights of 500 mb surface at 1500Z 30.1.52 at grid points of Fig.4 (tens of feet, the initial unit figure omitted).

II(b) Contour heights of 500 mb surface at 1500Z 31.1.52 corresponding to those in the inner rectangle above.

III Relative vorticity ζ^{+} 1500Z 30.1.52 ($10^{-2}hr^{-1}$) for the grid of Fig.3 calculated from points 0, 1, 2, 3, 4 of Fig.1.

IV Relative vorticity ζ^{x} 1500Z 30.1.52 ($10^{-2}hr^{-1}$) for the same grid as Table III calculated from points 0, 5, 6, 7, 8 of Fig.1.

V Relative vorticity differences $\zeta^{x} - \zeta^{+}$ 30.1.52 ($10^{-2}hr^{-1}$).

VI Height differences in feet calculated from relaxation of Table V, 1500Z 30.1.52.

VII Computed Jacobian J^{++} (ft hr^{-1}) 1500Z 30.1.52.

VIII(a) The difference $J^{X+} - J^{++}$ (ft hr^{-1}) 1500Z 30.1.52.

VIII(b) The difference $J^{+X} - J^{++}$ (ft hr^{-1}) 1500Z 30.1.52.

VIII(c) The difference $J^{XX} - J^{++}$ (ft hr^{-1}) 1500Z 30.1.52.

IX(a) Predicted heights of 500 mb surface at 1500Z 31.1.52 at the 14 x 10 inner grid points using J^{++} (tens of feet, the initial unit figure being omitted).

IX(b) Predicted heights of 500 mb surface at 1500Z 31.1.52 at the 14 x 10 inner grid points using J^{X+} (tens of feet, the initial unit figure being omitted).

IX(c) Predicted heights of 500 mb surface at 1500Z 31.1.52 at the 14 x 10 inner grid points using J^{+X} (tens of feet, the initial unit figure being omitted).

IX(d) Predicted heights of the 500 mb surface at 1500Z 31.1.52 at the 14 x 10 inner grid points using J^{XX} (tens of feet, the initial unit figure being omitted).

X The R.M.S. difference between 24-hour forecasts using different Jacobians.

XI(a) Values of $\partial h/\partial t$ computed using J^{++} 1500Z 30.1.52 (ft hr^{-1}).

XI(b) Values of $\partial h/\partial t$ computed using J^{X+} 1500Z 30.1.52 (ft hr^{-1}).

XII(a) Values of $\partial h/\partial t$ computed using J^{++} 2100Z 30.1.52 (ft hr^{-1}).

XII(b) Values of $\partial h/\partial t$ computed using J^{X+} 2100Z 31.1.52 (ft hr^{-1}).

XIII(a) Predicted heights of 500 mb surface at 0300Z 31.1.52 using J^{++} (tens of feet).

XIII(b) Predicted heights of 500 mb surface at 0300Z 31.1.52 using J^{X+} (tens of feet).

XIV(a) Values of $\partial h/\partial t$ computed at 1500Z 31.1.52 using J^{++} (ft hr^{-1}).

XIV(b) Values of $\partial h/\partial t$ computed at 1500Z 31.1.52 using J^{X+} (ft hr^{-1}).

XV Correlation of forecast height change with actual height change.

XVI Statistical summary.

TABLE I

Values of the Coriolis parameter, f, at the grid points of Fig. 4 ($10^{-2}hr^{-1}$)

045	045	046	047	047	048	048	048	048	048	048	048	047	047	046	045
044	044	045	046	046	047	047	047	047	047	047	047	046	046	045	044
043	043	044	045	045	046	046	046	046	046	046	046	045	045	044	043
041	042	043	044	044	044	045	045	045	045	045	044	044	044	043	042
040	041	042	042	043	043	044	044	044	044	044	043	043	042	042	041
039	040	040	041	041	042	042	042	043	042	042	042	041	041	040	040
038	038	039	040	040	040	041	041	041	041	041	040	040	040	039	038
036	037	038	038	039	039	039	039	039	039	039	039	039	038	038	037
035	036	036	037	037	037	038	038	038	038	038	037	037	037	036	036
033	034	035	035	035	036	036	036	036	036	036	036	036	035	035	034
032	033	033	034	034	034	035	035	035	035	035	034	034	034	033	033
030	031	032	032	032	033	033	033	033	033	033	033	032	032	032	031

TABLE II (a)

Contour heights of 500 mb surface at 1500Z 30.1.52 at grid points of Fig.4 (tens of feet, the initial unit figure omitted)

662	648	624	613	609	619	641	670	691	704	704	704	704	697	697	706	716	730
682	668	629	602	575	587	603	642	686	704	706	706	704	699	699	709	721	735
706	692	640	600	570	570	587	615	670	705	719	715	708	705	709	716	728	743
735	718	684	632	594	584	592	618	669	711	730	728	717	716	722	726	733	751
774	765	735	695	654	630	630	648	687	718	737	743	732	730	730	734	740	760
817	816	798	760	722	691	678	686	706	727	743	753	748	743	739	746	758	772
850	849	843	826	803	778	749	738	743	757	766	766	762	757	758	766	774	784
885	878	870	859	846	831	815	803	795	790	785	777	770	770	775	781	786	794
912	908	897	887	876	864	851	839	822	810	802	788	779	781	787	791	797	803
926	922	915	905	894	883	871	859	840	824	812	801	792	791	795	799	804	810
937	931	927	919	909	897	885	870	852	835	819	810	804	801	803	806	811	814
943	939	932	925	916	905	892	876	859	840	825	815	809	807	810	813	818	822
946	942	936	928	920	909	891	876	862	845	827	817	812	813	816	819	824	829
948	943	937	928	921	909	891	875	862	848	832	818	817	818	821	825	830	836

TABLE II (b)

Contour heights of 500 mb surface at 1500Z 31.1.52 corresponding to those in the inner rectangle above

654	622	610	615	621	633	636	649	666	682	682	682	695	711
674	640	621	615	613	614	618	634	653	672	687	693	699	713
708	675	654	644	639	636	637	643	650	664	681	695	708	721
749	730	713	702	694	682	670	661	655	658	677	695	711	728
815	810	792	773	752	732	716	699	679	669	679	698	719	736
866	865	855	837	821	791	760	742	725	698	696	713	733	750
902	901	893	876	856	835	812	785	759	743	734	740	753	764
914	911	909	905	889	870	846	825	801	776	771	773	772	777
921	921	917	911	906	898	878	853	834	816	805	796	789	788
923	922	921	918	913	906	897	880	855	838	821	811	802	800

TABLE III

Relative vorticity ζ^{+} 1500Z 30.1.1952 ($10^{-2}hr^{-1}$) at the grid points of Fig. 3 calculated from grid points 0, 1, 2, 3, 4, of Fig. 1

-021	017	008	062	017	039	005	-032	-013	008	004	001	008	016	006	004
-037	045	043	056	044	029	051	-004	-014	-018	001	008	011	006	008	001
004	-012	046	064	049	049	049	009	-021	-023	-007	015	010	-007	001	014
-019	002	001	026	040	028	029	-007	-010	-014	-022	010	001	005	006	028
-042	-044	001	022	047	047	027	020	017	011	-013	-002	002	023	015	000
-012	-036	-047	-047	-044	015	032	027	-002	-014	-007	-008	006	006	-006	-002
000	-004	-009	-019	-026	-031	-030	-026	-015	-006	001	010	004	-005	-008	003
-034	-011	-015	-017	-020	-019	-027	-005	-003	-016	009	019	004	-008	000	-006
-013	-014	-007	-004	-008	-008	-022	-004	001	-003	-003	010	007	000	000	002
002	-018	-016	-016	-009	-015	-012	-006	-007	009	-001	-006	002	000	003	-003
-015	-002	-009	-008	-010	-018	-011	-010	006	002	002	003	008	-002	002	-004
-008	-010	-006	-011	-020	007	-004	-010	-005	019	007	014	002	-002	004	000

Note that vorticities are given on a grid of 16 x 12 points formed from the grid of Fig. 3 by omitting the outer ring of points.

TABLE IV

Relative vorticity $\zeta^{\times}$ 1500Z 30.1.1952 ($10^{-2}hr^{-1}$) for the same grid points as Table III calculated from grid points 0, 5, 6, 7, 8 of Fig.1

	018	016	046	026	027	009	-021	-014	002	005	002	010	013	007	005
-020	030	040	059	039	038	040	-002	-013	-012	-001	008	010	007	005	005
-009	008	036	059	051	045	048	005	-014	-018	-008	012	007	-001	002	011
-015	-008	010	027	034	030	026	-003	-012	-014	-017	006	003	006	009	019
-038	-033	-003	023	039	043	034	019	013	006	-008	002	005	017	010	007
-017	-037	-041	-042	-029	008	023	019	001	-009	-010	-003	002	005	-004	-002
-007	-007	-011	-018	-027	-025	-028	-021	-016	-011	001	007	004	-003	-005	000
-026	-017	-016	-017	-020	-018	-022	-008	-005	-010	004	015	005	-005	-003	-003
-012	-011	-008	-006	-008	-010	-018	-004	-001	-003	000	008	006	-001	001	-002
-007	-014	-015	-014	-011	-013	-013	-007	-003	003	-001	-001	002	-002	002	000
-009	-007	-007	-009	-012	-013	-011	-008	000	006	002	004	006	-001	002	-004
-008	-009	-006	-012	-014	-001	000	-010	-002	011	013	009	005	-001	003	

TABLE V

Relative vorticity differences $\zeta^{\times} - \zeta^{+}$ 30.1.1952 ($10^{-2}hr^{-1}$)

	000	008	-015	009	-012	004	010	-001	-006	000	001	002	-004	001	001
018	-015	-003	003	-006	009	-011	002	001	006	-002	-000	-001	001	-002	004
-014	020	-010	-004	002	-003	-001	-005	006	005	-001	-003	-002	005	001	-003
005	-010	009	001	-006	002	-002	004	-002	-000	005	-004	002	001	002	-008
005	011	-004	001	-009	-003	007	-001	-004	-005	005	004	003	-006	-005	007
-005	-001	006	005	014	-006	-009	-008	003	005	-003	005	-003	-001	002	001
-007	-003	-002	001	-002	007	002	005	-001	-005	-001	-002	000	002	003	-003
007	-006	-001	000	000	001	004	-003	-003	006	-004	-005	001	003	-003	003
001	002	-001	-002	001	-001	004	000	-002	001	003	-001	-001	-001	001	-003
-009	004	001	002	-002	002	-001	-001	-004	006	000	004	000	-002	-001	003
006	-005	002	-001	-002	005	000	002	-006	004	000	001	-002	001	000	000
000	001	000	-001	005	-008	004	001	003	-008	006	-005	003	001	-001	

TABLE VI

Height differences in feet calculated from relaxation of Table V 1500Z 30.1.1952

	004	-001	050	003	037	-002	-036	-011	007	-002	-004	-003	008	-001	-006
-034	030	029	027	031	009	034	-011	-024	-030	-004	002	003	-002	003	-007
012	-030	029	035	026	028	024	007	-030	-034	-010	008	004	-014	-001	009
-012	001	-012	013	036	022	018	-002	-002	-012	-022	000	-007	-002	002	019
-020	-033	-010	-002	026	023	004	012	014	007	-019	-020	-009	015	011	-008
006	-010	-027	-031	-033	013	029	028	005	-004	002	-012	004	005	-004	-004
014	007	-004	-016	-017	-021	-007	-002	008	015	012	010	002	-006	-007	001
-007	010	001	-006	-012	-018	-018	001	008	-001	016	017	002	-007	000	-004
-001	-002	000	000	-007	-010	-017	-002	007	006	003	007	003	000	-002	002
011	-004	-004	-004	-002	-011	-006	-002	-001	012	002	-006	001	003	000	-005
-004	005	-002	-001	-001	-010	-006	-003	009	001	-001	-001	003	-001	000	-001
-001	-001	-001	-001	-006	006	-006	-003	-001	010	-005	005	-002	-002	-000	

TABLE VII

Computed Jacobian J^{++} (ft hr^{-1}) 1500Z 30.1.52

041	071	001	-011	-010	-067	-060	010	018	011	006	-001	004	001
005	083	-031	-021	004	016	-018	-014	006	019	009	-013	-004	009
001	-015	056	006	-021	-024	-049	-046	-024	014	011	-004	-001	008
064	126	046	000	-060	-060	-046	-013	-019	-009	006	017	008	-013
-039	-037	-039	116	181	027	-053	-044	-001	005	009	009	-004	002
000	-003	-010	-009	-034	-016	018	026	013	013	005	-009	-004	003
016	-006	003	008	003	024	041	-003	008	018	-004	-015	-003	-001
001	006	-001	002	-010	013	014	-005	011	000	-001	-005	-004	000
-004	000	000	-002	-010	010	-006	008	003	-005	-001	002	001	-001
004	002	001	-011	014	006	-003	002	003	003	004	-002	-002	-001

Note that Jacobians are given on a grid of 14 x 10 points formed from the grid of Fig. 3 by omitting the two outer rings of points, and correspond to the points inside the rectangle shown in Table II(a).

TABLE VIII (a)

The difference $J^{x+} - J^{++}$ (ft hr^{-1}) 1500Z 30.1.52

051	-043	027	008	-028	040	038	-013	-009	-006	-003	-001	-006	004
076	-114	042	001	006	-034	011	011	000	-006	-004	011	006	-010
038	151	-018	-004	006	-028	-001	009	013	-006	-004	005	002	-011
-106	-189	-066	064	147	031	-016	-026	009	019	007	-015	-010	023
089	099	033	-151	-246	-050	074	066	-004	-005	-003	-006	006	-003
-009	010	033	071	099	031	-031	-063	-009	004	-003	004	-001	-002
-020	004	-008	-007	-008	-005	-014	018	-002	-010	006	008	-003	003
006	-009	003	-002	013	-004	-003	012	-012	004	-001	000	004	-001
006	002	-003	-008	008	-015	018	-008	-003	006	004	-005	-003	002
-006	000	-003	020	-016	-002	004	003	000	000	-004	000	003	001

TABLE VIII (b)

The difference $J^{+x} - J^{++}$ (ft hr^{-1}) 1500Z 30.1.52

017	-018	007	003	-009	014	029	-008	-005	-004	-001	001	-003	001
021	-032	022	002	003	-017	-001	008	-001	-004	-002	006	001	-004
-004	045	-039	-004	-008	-007	-007	011	009	-002	000	003	001	-003
-011	-039	-009	009	045	010	-003	-009	003	006	001	-008	-005	011
013	017	026	-031	-070	-005	023	018	-006	-001	-002	-005	003	-001
004	001	-004	002	014	002	-003	-014	001	001	-001	002	001	-001
-006	007	-001	003	001	-003	-011	007	001	-005	004	004	-001	000
003	-003	002	-001	003	-003	-003	005	-005	002	000	001	002	-001
002	000	-001	-002	005	-004	004	-006	002	003	001	-003	000	002
-003	001	-003	007	-008	004	000	000	001	002	-003	000	001	000

TABLE VIII (c)

The difference $J^{xx} - J^{++}$ (ft hr^{-1}) 1500Z 30.1.52

	-034	019	005	-020	043	036	-011	-011	-005	-004	000	-006	003
056	-079	031	006	003	-031	009	014	000	-009	-003	012	005	-009
053	094	-011	-006	019	-030	-001	014	015	-006	-003	004	000	-009
-093	-152	-064	046	119	038	-005	-018	010	019	004	-016	-008	019
081	082	031	-143	-215	-049	060	053	000	-001	-004	-008	004	001
-006	016	032	061	078	028	-026	-047	-014	-001	-001	005	000	-003
-016	004	-006	-006	-002	-009	-019	013	001	-008	006	009	-001	001
004	-006	002	000	013	-006	-003	009	-011	003	001	001	003	000
006	000	-003	-003	007	-013	012	-005	-003	006	003	-005	-002	001
-004	-002	-001	015	-011	-005	007	001	002	-001	-004	000	002	-

TABLE IX (a)

Predicted heights of 500 mb surface at 1500Z 31.1.52 at the 14 x 10 inner grid points using J^{++} (tens of feet, the initial unit figure being omitted)

663	656	640	625	623	620	649	657	664	671	675	681	695	708
680	673	659	647	644	639	640	639	639	656	668	684	702	715
719	710	699	692	682	681	675	672	672	672	671	688	713	726
752	747	747	745	733	731	735	737	731	730	715	716	725	742
810	800	800	798	788	781	785	792	789	791	766	761	751	762
859	850	848	841	830	824	824	824	823	827	806	795	778	776
899	893	887	878	867	861	859	857	858	852	834	818	799	787
913	912	910	901	895	886	884	883	882	869	850	831	808	794
923	926	922	919	913	901	899	895	890	880	861	830	809	800
925	925	926	922	921	918	915	906	896	886	862	835	818	808

TABLE IX (b)

Predicted heights of 500 mb surface at 1500Z 31.1.52 at the 14 x 10 inner grid points using J^{X+} (tens of feet, the initial unit figure being omitted)

671	650	638	622	617	616	636	651	665	672	676	683	697	715
691	674	664	651	632	614	618	625	643	658	675	690	708	719
718	714	701	695	677	658	641	633	638	654	677	700	716	721
761	753	755	739	731	726	708	692	671	671	691	715	728	733
810	810	794	788	782	778	782	767	743	718	719	738	744	750
856	856	849	832	823	832	831	825	807	779	763	761	761	766
889	891	883	868	863	869	872	865	856	830	800	784	775	776
912	909	910	894	886	894	901	894	883	856	832	803	789	785
923	922	914	908	903	907	914	910	893	866	841	818	802	794
924	925	922	922	919	923	925	918	899	872	850	828	811	802

TABLE IX (c)

Predicted heights of 500 mb surface at 1500Z 31.1.52 at the 14 x 10 inner grid points using J^{+x} (tens of feet, the initial unit figure being omitted)

662	644	631	629	629	622	641	655	665	671	677	684	699	710
681	667	667	662	654	640	628	631	638	656	672	689	706	717
718	706	706	701	686	673	663	662	658	663	676	703	718	726
764	754	743	742	737	738	731	728	729	717	708	727	736	741
807	809	802	794	781	785	785	783	794	783	761	761	759	764
855	852	850	837	827	823	821	823	834	827	803	792	779	777
896	892	887	876	867	859	859	861	865	854	833	814	796	787
913	913	908	902	893	885	887	889	886	874	851	826	805	795
924	925	923	918	909	903	902	900	893	879	854	828	810	802
924	926	926	922	921	920	918	908	896	879	855	834	818	808

TABLE IX (d)

Predicted heights of the 500 mb surface at 1500Z 31.1.52 at the 14 x 10 inner grid points using J^{xx} (tens of feet, the initial unit figure being omitted)

669	651	636	620	617	616	639	654	669	676	680	687	700	713
691	677	671	643	627	616	621	631	649	666	682	696	711	719
718	711	708	695	677	660	645	636	643	666	689	708	719	723
761	761	753	737	725	729	712	693	674	682	706	726	730	735
808	805	801	798	785	780	776	765	740	723	733	747	749	753
859	857	840	832	833	832	836	827	809	779	766	767	766	768
890	890	881	867	866	872	875	873	861	828	800	787	779	779
915	911	904	892	891	900	908	905	887	856	826	804	792	788
923	922	915	907	908	913	918	913	893	864	839	816	802	795
924	926	923	922	922	925	926	916	898	871	848	828	812	803

TABLE X

The R.M.S. difference between 24-hour forecasts using different Jacobians

Forecasts using	J^{x+}, J^{++}	J^{+x}, J^{++}	J^{x+}, J^{xx}
R.M.S. difference (ft)	177	54	47

TABLE XI (a)

Values of $\partial h/\partial t$ computed using J^{++} 1500Z 30.1.52 (ft hr^{-1})

029	055	034	011	-011	-043	-050	-029	-015	-008	-007	-006	-003	001
028	064	034	010	-010	-034	-054	-046	-026	-008	-003	-007	-002	006
029	055	060	027	-011	-043	-066	-062	-041	-013	-003	-002	001	006
041	081	069	043	002	-036	-057	-050	-036	-016	-001	005	003	-001
011	031	036	071	073	014	-029	-033	-016	-004	003	003	-002	-003
009	019	025	037	031	019	013	009	008	009	004	-003	-005	-004
011	016	023	030	031	036	036	021	018	016	003	-006	-008	-007
010	016	019	023	024	033	033	024	021	014	004	-004	-008	-008
008	013	015	017	019	027	024	024	020	013	006	-001	-007	-009
008	011	012	011	020	021	019	020	021	016	009	-003	-009	-011

TABLE XI (b)

Values of $\partial h/\partial t$ computed using J^{x+} 1500Z 30.1.52 (ft hr^{-1})

044	045	041	015	-014	-030	-034	-026	-016	-011	-008	-006	-004	001
049	045	041	014	-008	-037	-044	-037	-021	-008	-004	-004	-001	003
041	076	054	027	-005	-047	-062	-053	-031	-009	-001	-001	001	003
014	029	034	041	023	-029	-053	-046	-026	-007	003	001	001	004
028	045	033	022	003	-011	-014	-014	-011	-002	003	001	-001	-002
015	032	038	046	040	020	003	-007	001	008	004	-001	-005	-004
009	021	026	033	031	032	027	018	013	011	004	-003	-007	-006
011	016	021	024	027	030	029	023	016	013	004	-004	-006	-008
010	013	015	016	020	023	027	021	018	013	006	-003	-008	-008
006	011	012	016	016	019	020	021	020	016	008	-003	-009	-010

TABLE XII (a)

Values of $\partial h/\partial t$ computed using J^{++} 2100Z 30.1.52 (ft hr^{-1})

015	028	043	031	005	-017	-030	-032	-024	-015	-009	-008	-004	001
-014	025	069	048	014	-007	-039	-061	-054	-026	-009	-007	-006	003
-018	022	068	040	030	011	-036	-064	-066	-039	-011	-003	000	002
-019	019	043	058	089	056	006	-036	-048	-038	-013	001	006	002
-016	-004	019	046	052	053	063	009	-021	-014	-002	005	001	001
-008	-003	011	021	029	048	044	018	013	015	014	005	-002	-004
-001	006	010	017	028	035	041	039	032	031	020	004	-004	-006
006	011	013	019	024	029	044	041	037	031	016	003	-005	-008
008	011	013	019	018	027	036	035	033	024	011	002	-004	-008
006	009	012	014	019	026	028	029	026	019	009	-001	-008	-010

TABLE XII (b)

Values of $\partial h/\partial t$ computed using J^{x+} 2100Z 31.1.52 (ft hr^{-1})

017	038	048	026	004	-013	-027	-031	-024	-016	-011	-008	-005	001
-001	048	057	031	014	-014	-042	-053	-041	-022	-009	-005	-002	001
-007	019	047	043	028	-004	-051	-069	-054	-027	-008	-002	-001	001
-029	029	066	049	033	008	-027	-047	-044	-023	-005	001	001	001
-016	-018	021	044	043	031	000	-023	-032	-015	-001	002	-001	-003
-010	006	023	031	029	015	009	-001	-003	002	004	001	-004	-003
-004	001	016	027	032	031	028	020	011	013	008	-001	-006	-006
004	007	014	021	028	031	036	032	022	015	008	-001	-006	-008
007	009	011	016	021	026	033	030	024	015	009	-001	-006	-009
006	010	011	016	018	024	026	025	021	015	011	-001	-009	-011

TABLE XIII (a)

Predicted heights of 500 mb surface at 0300Z 31.1.52 using J^{++} (tens of feet)

659	642	616	601	592	593	633	668	690	697	696	696	704	716
682	670	650	631	609	607	624	646	671	698	705	707	716	728
734	714	702	685	661	648	649	655	668	697	716	725	730	736
788	775	771	760	739	724	711	699	698	712	730	743	745	748
830	822	818	818	812	793	783	768	754	752	759	762	759	767
864	857	853	852	847	839	833	819	803	793	785	776	773	777
897	892	886	882	877	872	866	852	836	821	803	786	783	784
921	917	908	902	895	889	886	868	853	836	812	795	790	791
936	931	923	916	904	898	890	873	856	840	819	804	798	797
940	936	930	920	913	904	890	873	856	838	820	807	801	801

TABLE XIII (b)

Predicted heights of 500 mb surface at 0300Z 31.1.52 using J^{X+} (tens of feet)

661	641	624	599	590	598	639	670	691	696	695	696	704	717
690	677	653	620	605	600	622	651	684	701	706	710	720	728
732	725	711	679	656	638	632	644	676	710	721	727	729	735
781	782	774	745	718	695	678	676	692	723	740	742	739	747
834	817	822	816	790	767	745	736	732	747	759	758	756	762
867	866	859	865	853	827	809	791	782	777	773	770	770	777
894	891	890	890	887	877	854	835	817	802	788	780	780	784
921	913	908	904	902	895	881	861	838	819	802	790	789	790
935	930	921	914	908	900	889	870	848	829	815	800	795	796
939	936	928	923	913	904	890	870	851	834	821	806	800	800

TABLE XIV (a)

Values of $\partial h/\partial t$ computed at 1500Z 31.1.52 using J^{++} (ft hr^{-1})

-001	001	016	019	019	026	022	001	-012	-019	-020	-016	-009	-008
-004	-001	012	004	011	025	022	009	-008	-019	-029	-031	-018	-010
-010	-006	-006	002	007	009	019	009	011	019	-009	-040	-035	-011
-024	-039	-043	-003	008	-023	-026	004	014	029	029	-005	-031	-012
-009	-014	-036	-004	016	-012	-043	-021	-003	031	031	011	-011	-006
007	-003	-011	015	016	-007	-018	-014	-023	009	023	020	004	006
004	006	011	022	014	-002	-009	-016	-014	015	021	024	017	013
-006	-003	008	013	010	006	-006	-009	005	021	021	038	032	014
-012	-005	004	007	015	010	001	006	015	024	029	034	019	008
-013	-009	-001	004	011	012	015	023	034	056	060	036	018	010

TABLE XIV (b)

Values of $\partial h/\partial t$ computed at 1500Z 31.1.52 using J^{x+} (ft hr^{-1})

010	009	009	016	022	014	-002	-012	-016	-018	-018	-014	-008	-002
-001	012	011	021	019	009	-002	-011	-020	-031	-031	-024	-017	-008
-014	-012	-003	016	009	005	001	001	-008	-033	-043	-036	-020	-012
-031	-010	000	-006	009	-008	-008	006	015	-011	-046	-042	-018	-014
-029	-032	-001	018	-032	-030	000	018	038	004	-031	-031	-018	-011
-023	-011	016	-003	-028	-048	-025	014	039	041	-002	-014	-011	-009
-009	-009	014	018	-028	-048	-021	004	036	038	026	011	-003	-004
-009	-003	012	009	-015	-029	-014	012	034	048	041	021	006	-001
-011	-006	-001	003	-008	-011	004	022	033	041	033	028	011	002
-013	-009	-003	000	002	006	020	038	051	051	043	030	016	004

TABLE XV

Correlation of forecast height change with actual height change

	Method of forecast		Correlation coefficients
(a)	Barotropic using J^+		+0.48
(b)	" " J^x		+0.72
(c)	Sawyer-Bushby model	500 mb zero boundary changes	+0.61
(d)	" " "	600 mb zero boundary changes	+0.59
(e)	" " "	500 mb zero boundary changes heating effect	+0.62
(f)	" " "	600 mb actual boundary changes heating effect	+0.47
(g)	Stream function	600 mb actual boundary changes heating effect	+0.76

TABLE XVI

Statistical summary

		Forecast commencing at 1500Z		
		30.1.52	27.1.52	30.1.53
Correlation of forecast and actual 24-hour height changes at 500 mb	J^{++}	0.48	0.94	0.95
	J^{x+}	0.72	0.91	0.92
Using Sawyer-Bushby model*		0.47	0.93	0.96
R.M.S. of forecast height differences using J^{++} and J^{x+}	12 hr	103 ft	37 ft	59 ft
	24 hr	177 ft	73 ft	96 ft
R.M.S. actual change	24 hr	401 ft	256 ft	624 ft
Ratio $\frac{\text{R.M.S. (difference between 24-hour forecasts)}}{\text{R.M.S. (actual 24-hour change)}}$		0.44	0.39	0.12
$\frac{\sigma\ \text{(forecast 24-hour change)}}{\sigma\ \text{(actual 24-hour change)}}$	J^{++}	1.08	0.91	0.89
	J^{x+}	1.23	0.96	0.82

---

* Time integration at 600 mb.

LIST OF FIGURES

Fig. 1. The numbering of the mesh points.

2. Error distribution of $\zeta^{x} - \zeta^{+}$.

3. Mesh points used in the calculations of Jacobians.

4. Mesh of 18 x 14 points.

5a 500 mb contours 1500Z 30.1.52.
5b 500 mb contours 1500Z 31.1.52.
5c Forecast 500 mb contours 1500Z 31.1.52 using J^{++}.
5d Forecast 500 mb contours 1500Z 31.1.52 using J^{x+}.

6a 500 mb contours 1500Z 27.1.52.
6b 500 mb contours 1500Z 28.1.52.
6c Forecast 500 mb contours 1500Z 28.1.52 using J^{++}.
6d Forecast 500 mb contours 1500Z 28.1.52 using J^{x+}.

7a 500 mb contours 1500Z 30.1.53.
7b 500 mb contours 1500Z 31.1.53.
7c Forecast 500 mb contours 1500Z 31.1.53 using J^{++}.
7d Forecast 500 mb contours 1500Z 31.1.53 using J^{x+}.

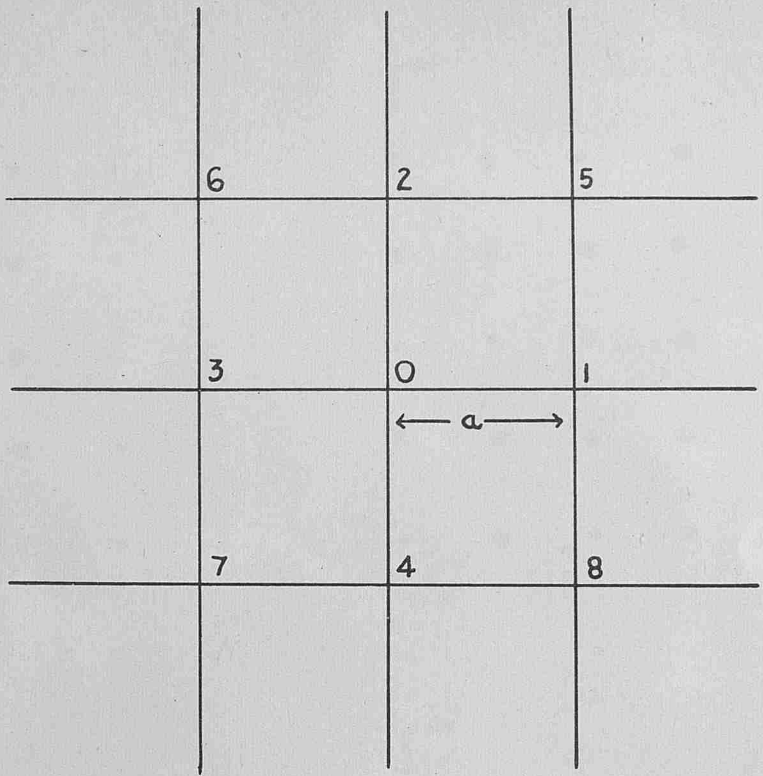
6
2
5
3
0
1
a
7
4
8

The numbering of the mesh points
Fig. 1

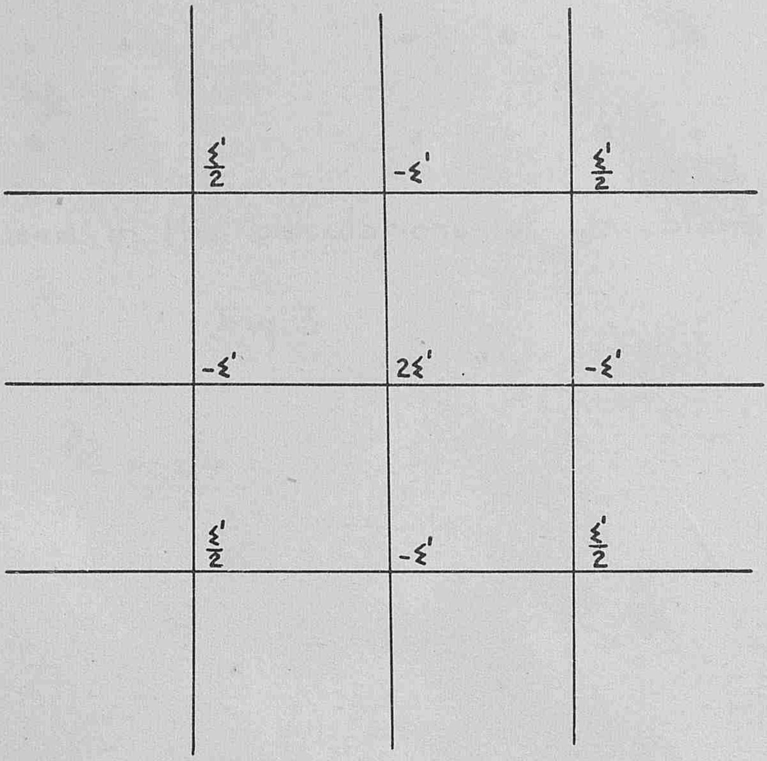
$\frac{\xi'}{2}$
$-\xi'$
$\frac{\xi'}{2}$
$-\xi'$
$2\xi'$
$-\xi'$
$\frac{\xi'}{2}$
$-\xi'$
$\frac{\xi'}{2}$

Error distribution of $\zeta^{x} - \zeta^{+}$
Fig. 2

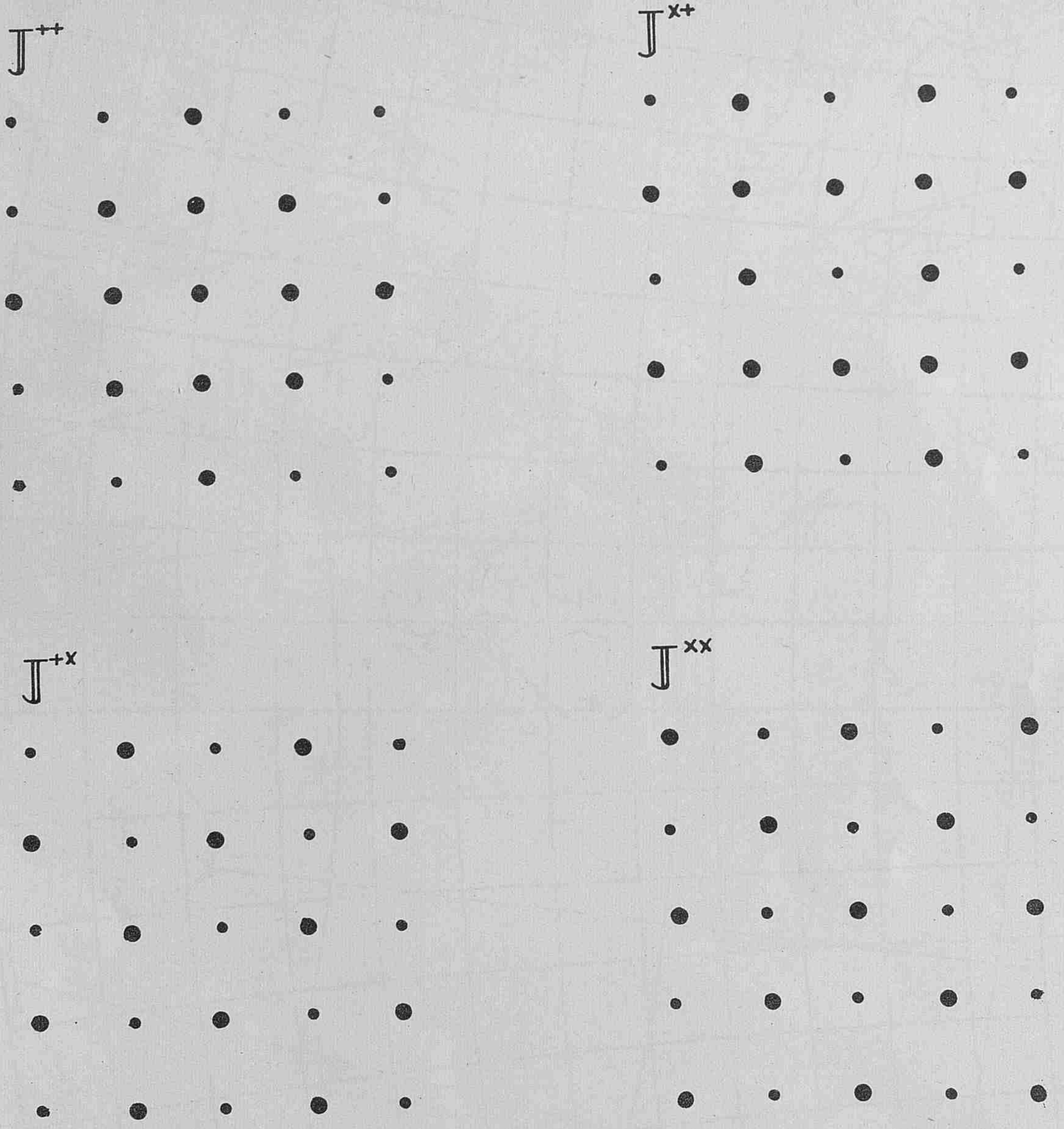
$\mathbb{J}^{++}$
$\mathbb{J}^{x+}$
$\mathbb{J}^{+x}$
$\mathbb{J}^{xx}$

Mesh points used in the calculations of Jacobians

Fig. 3

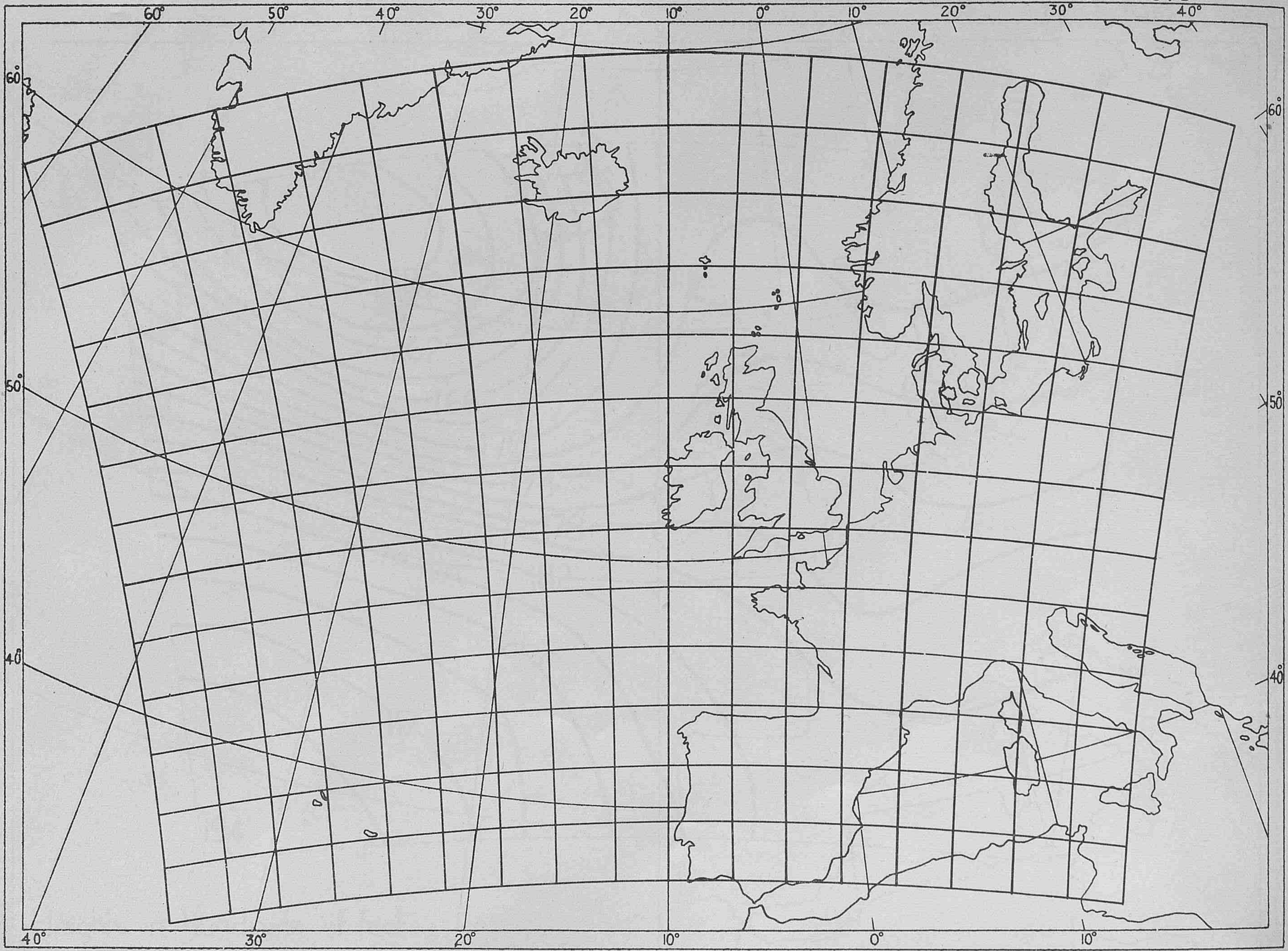
60°
50°
40°
30°
20°
10°
0°
10°
20°
30°
40°
60°
50°
40°
60°
50°
40°
40°
30°
20°
10°
0°
10°

FIG. 4

MESH OF 18×14 POINTS

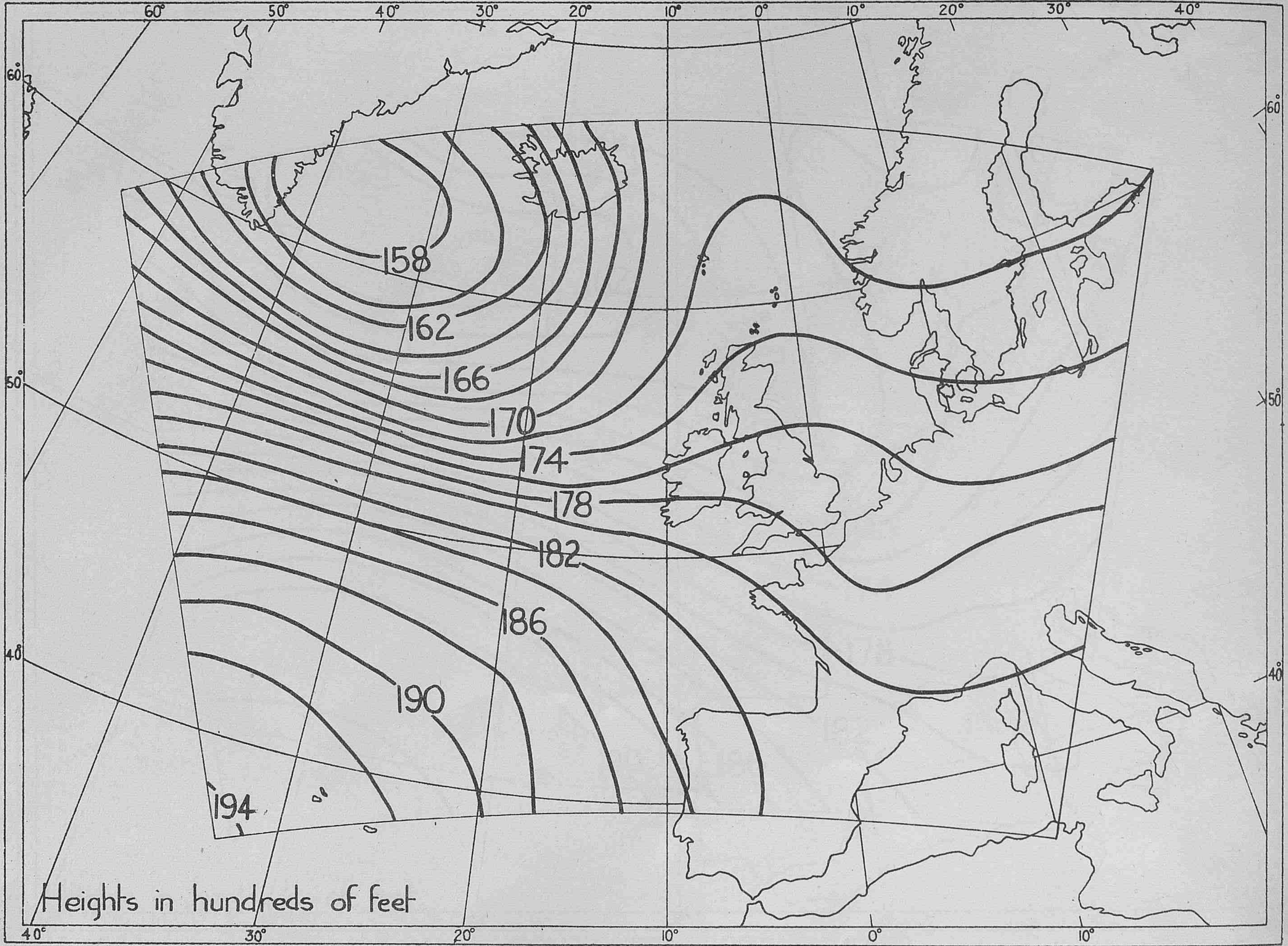
60°
50°
40°
30°
20°
10°
0°
10°
20°
30°
40°
60°
50°
40°
158
162
166
170
174
178
182
186
190
194
40°
30°
20°
10°
0°
10°

Heights in hundreds of feet

FIG.5(a) 500 mb. CONTOURS 1500Z 30:1:52

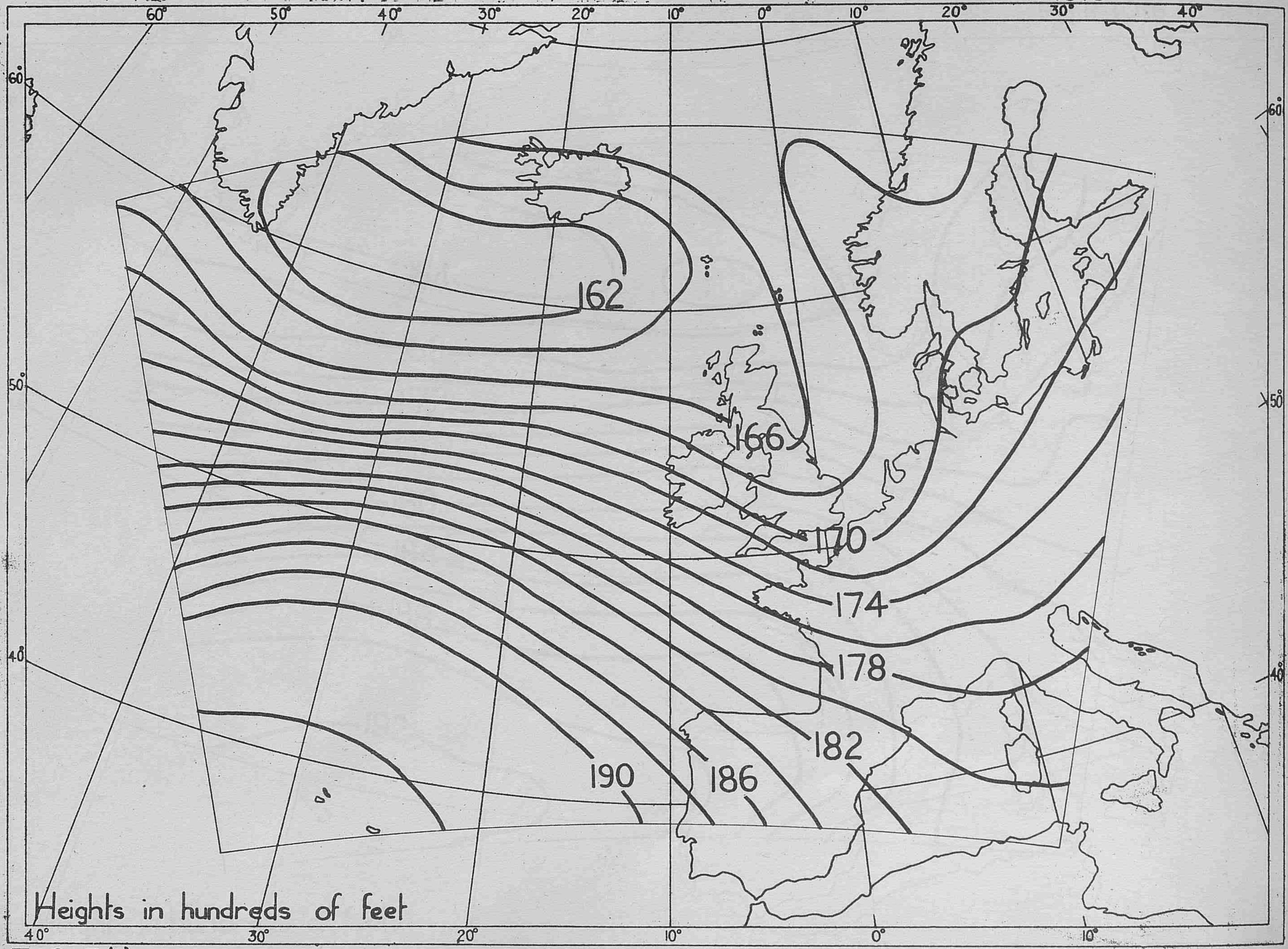
Heights in hundreds of feet
162
166
170
174
178
182
186
190
60°
50°
40°
30°
20°
10°
0°

FIG. 5(b) 500mb. CONTOURS 1500Z 31:1:52

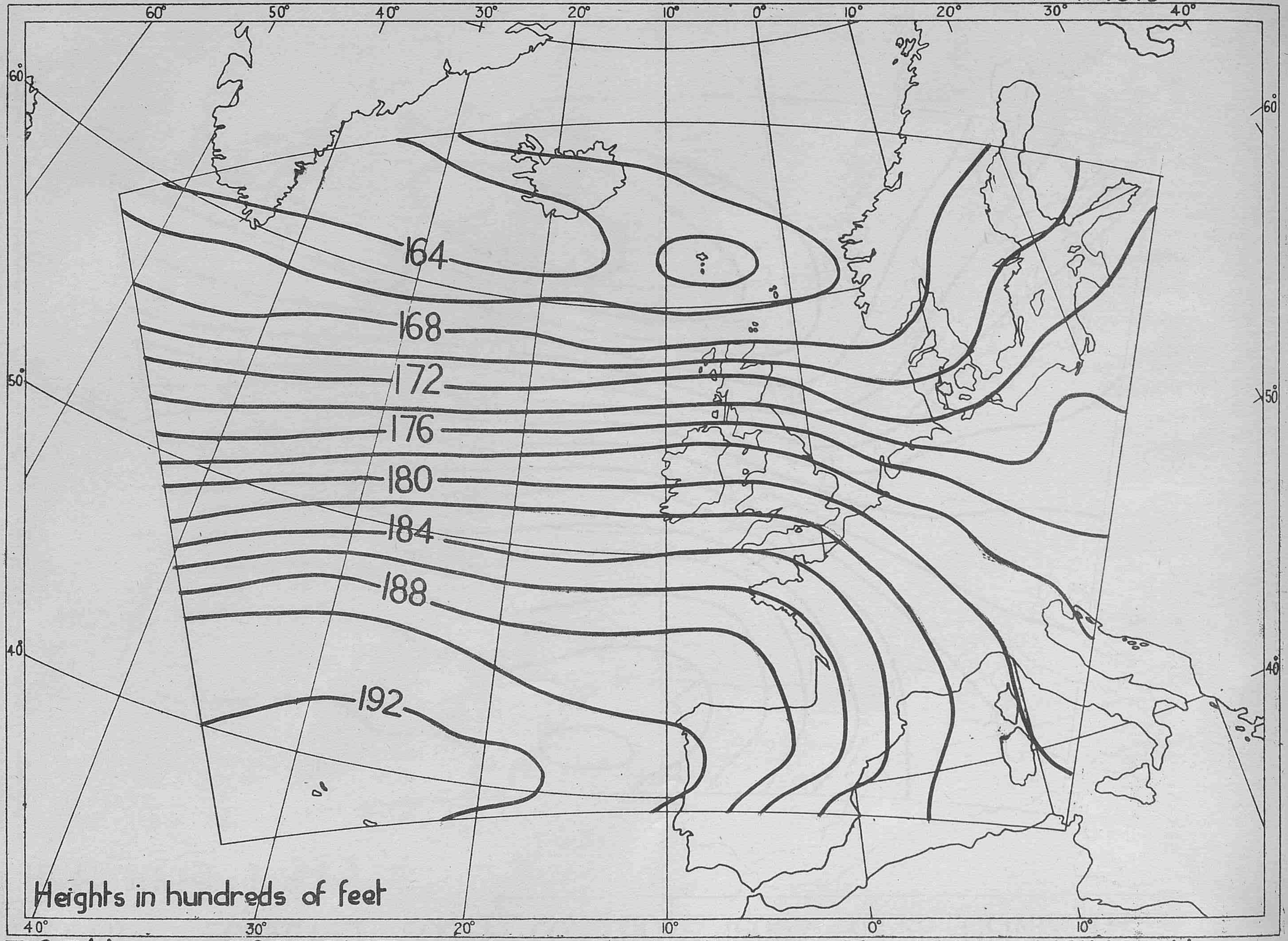
60°
50°
40°
30°
20°
10°
0°
10°
20°
30°
40°
60°
50°
40°
164
168
172
176
180
184
188
192
40°
30°
20°
10°
0°
10°

Heights in hundreds of feet

FIG.5(c) FORECAST 500mb. CONTOURS 1500Z 31:1:52 USING J^{++}

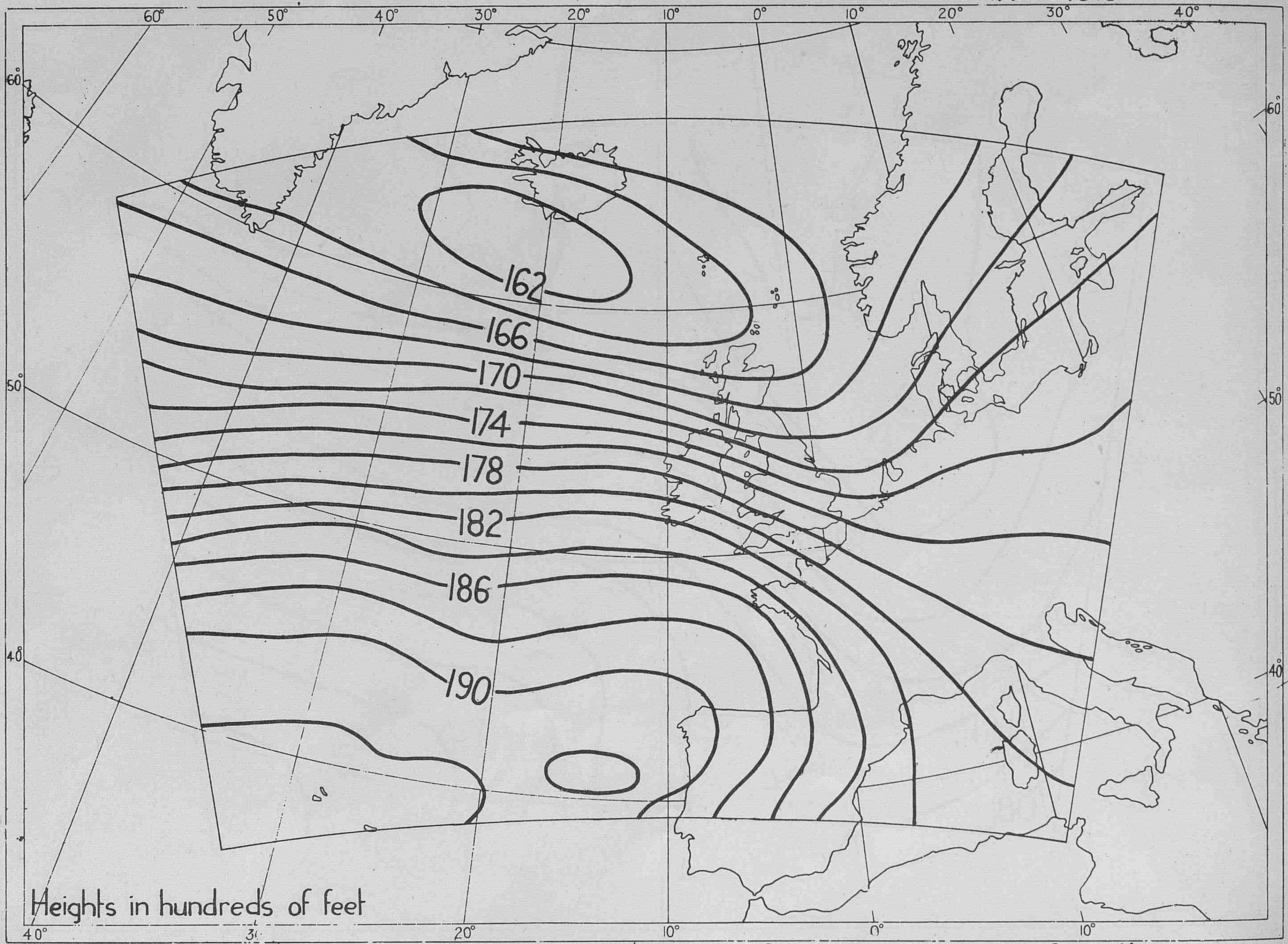
60°
50°
40°
30°
20°
10°
0°
10°
20°
30°
40°
60°
50°
40°
162
166
170
174
178
182
186
190
40°
31
20°
10°
0°
10°

Heights in hundreds of feet

FIG.5 (d) FORECAST 500mb. CONTOURS 1500Z 31:1:52 USING J^{x+}

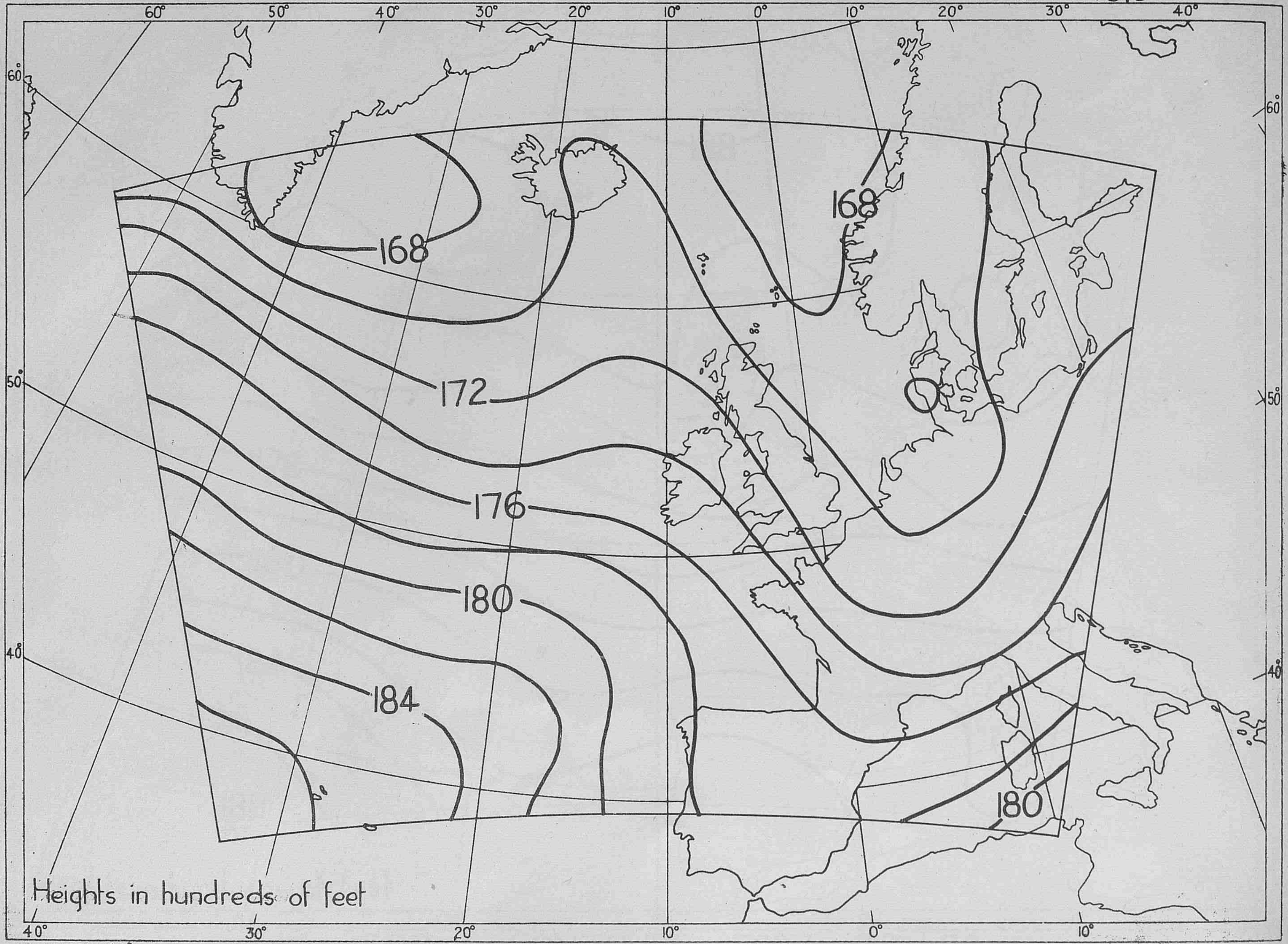
60°
50°
40°
30°
20°
10°
0°
10°
20°
30°
40°
60°
50°
40°
168
168
172
176
180
184
180
40°
30°
20°
10°
0°
10°

Heights in hundreds of feet

FIG. 6(a) 500mb. CONTOURS 1500Z 27:1:52

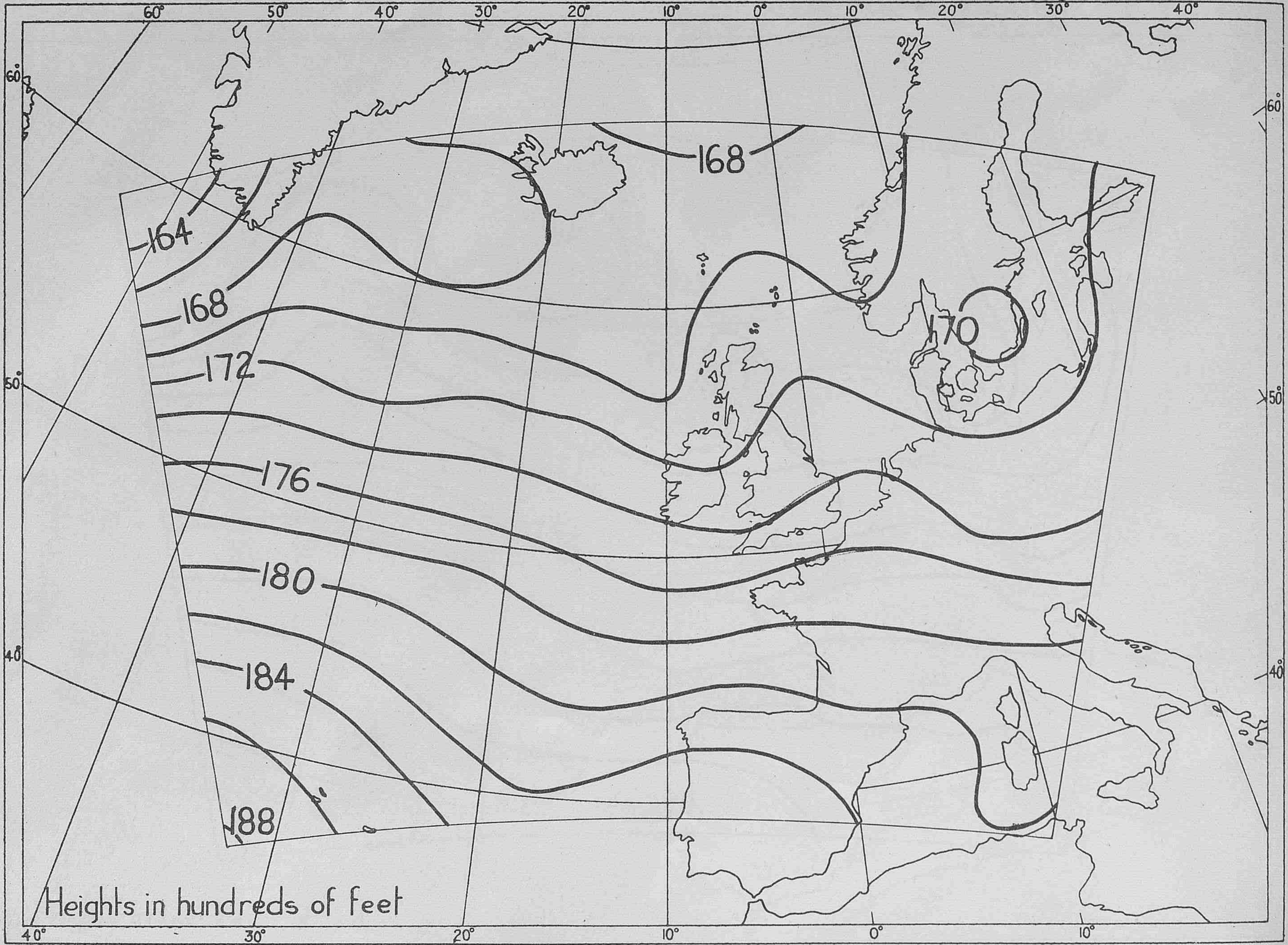
164
168
168
170
172
176
180
184
188
Heights in hundreds of feet
60°
50°
40°
30°
20°
10°
0°
10°
20°
30°
40°
60°
50°
40°
60°
50°
40°
40°
30°
20°
10°
0°
10°

FIG. 6(b) 500 mb. CONTOURS 1500Z 28:1:52

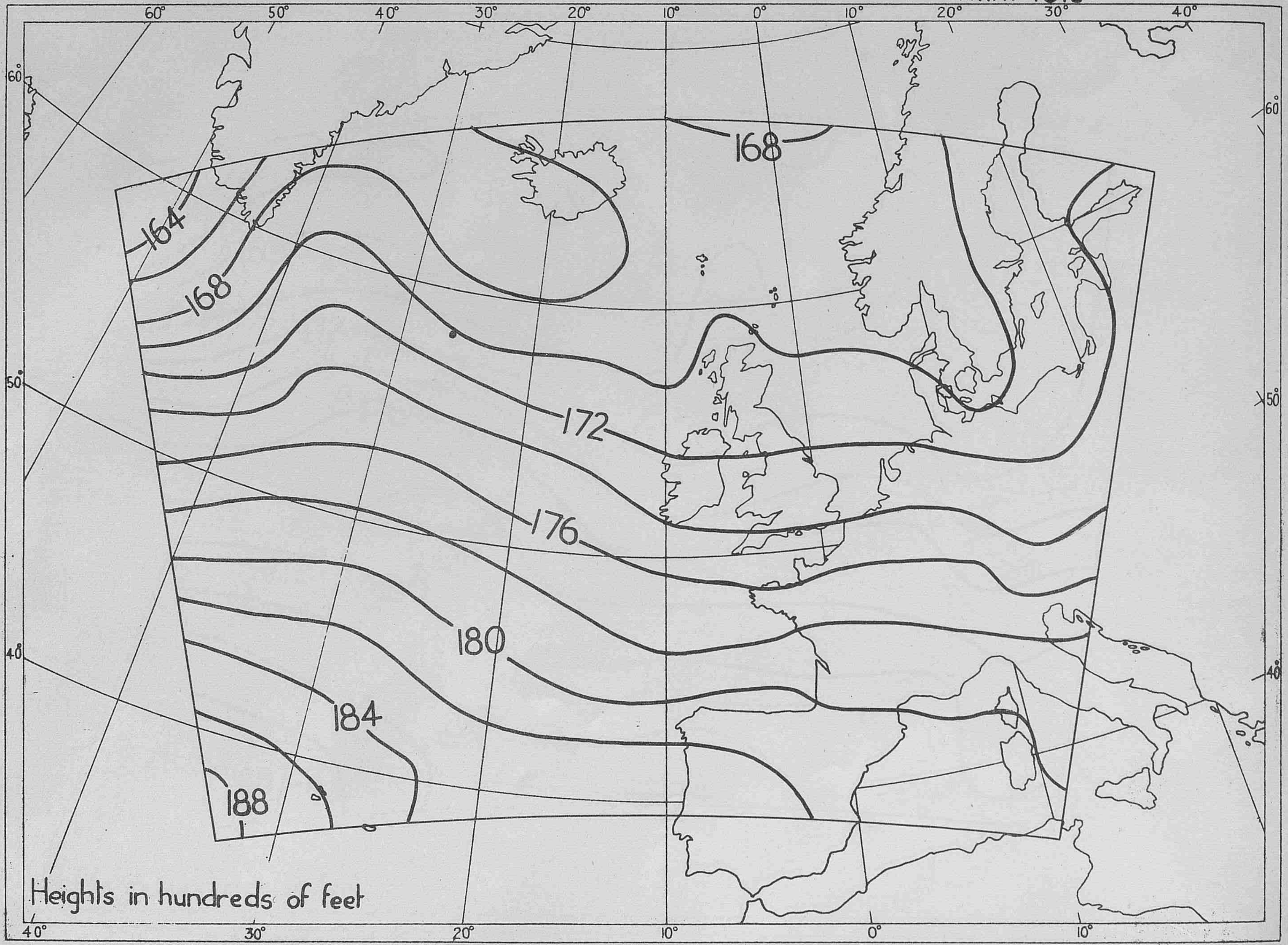
60°
50°
40°
30°
20°
10°
0°
10°
20°
30°
40°
60°
50°
40°
164
168
168
172
176
180
184
188
Heights in hundreds of feet
40°
30°
20°
10°
0°
10°

FIG. 6(c) FORECAST 500mb. CONTOURS 1500Z 28:1:52 USING J^{++}

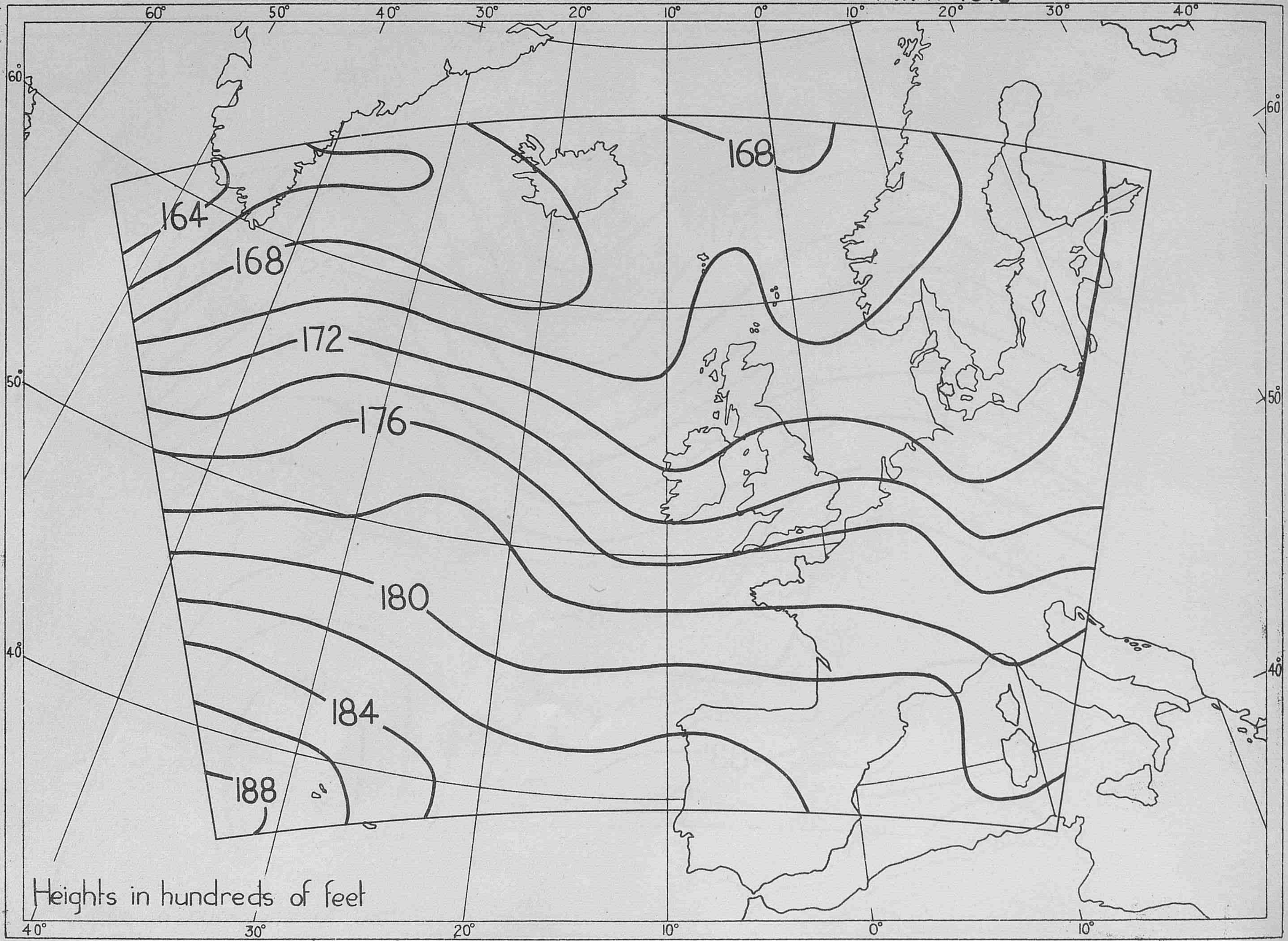
60°
50°
40°
30°
20°
10°
0°
10°
20°
30°
40°
60°
50°
40°
60°
50°
40°
164
168
168
172
176
180
184
188
Heights in hundreds of feet
40°
30°
20°
10°
0°
10°

FIG. 6(d) FORECAST 500 mb. CONTOURS 1500Z 28:1:52 USING J^{x+}

M.R.P. 1018

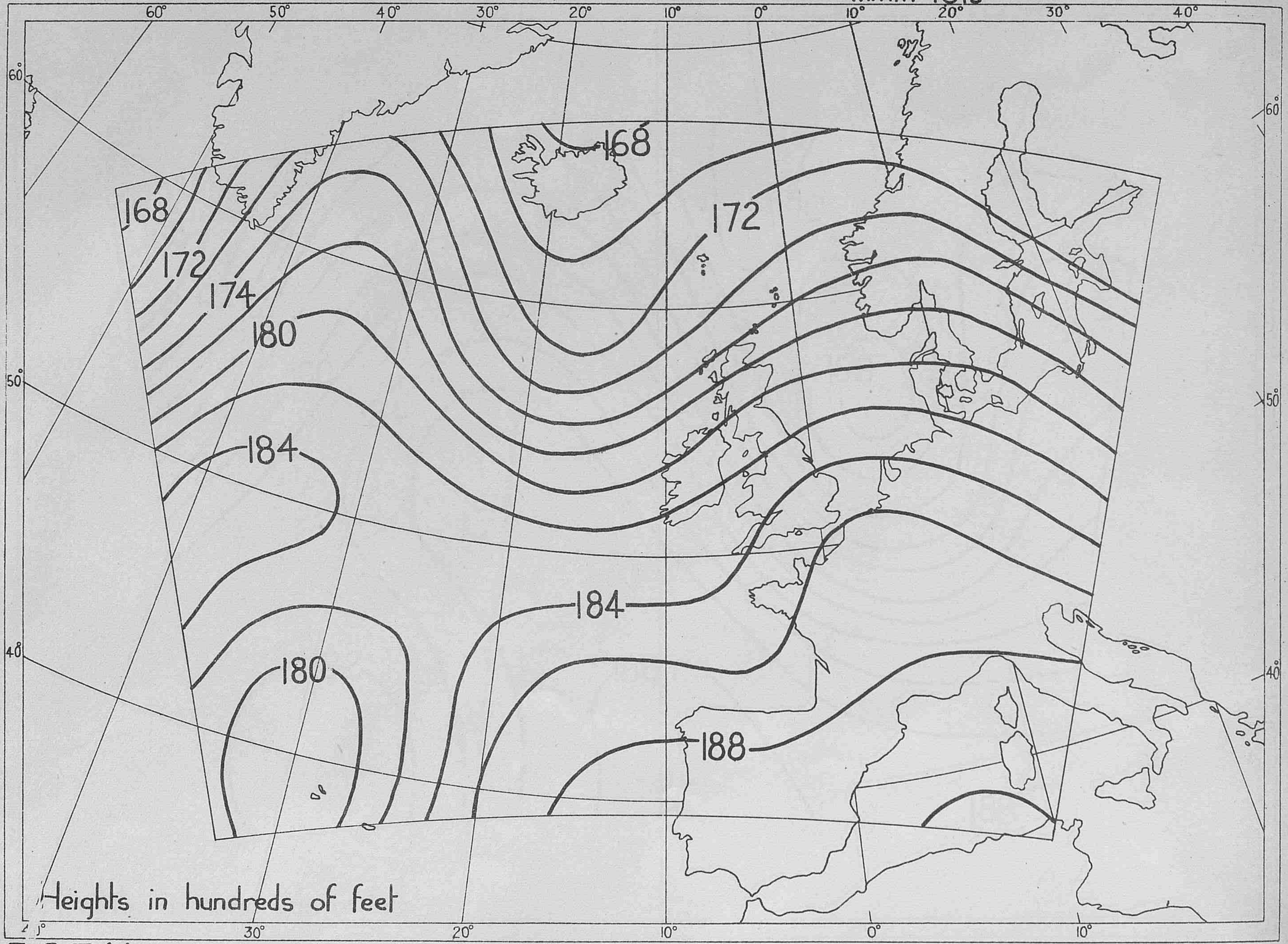
60°
50°
40°
30°
20°
10°
0°
10°
20°
30°
40°
60°
50°
40°
168
168
172
172
174
180
184
184
180
188
Heights in hundreds of feet
30°
20°
10°
0°
10°

FIG. 7 (a) 500mb. CONTOURS 1500Z 30:1:53

M.R.P. 1018

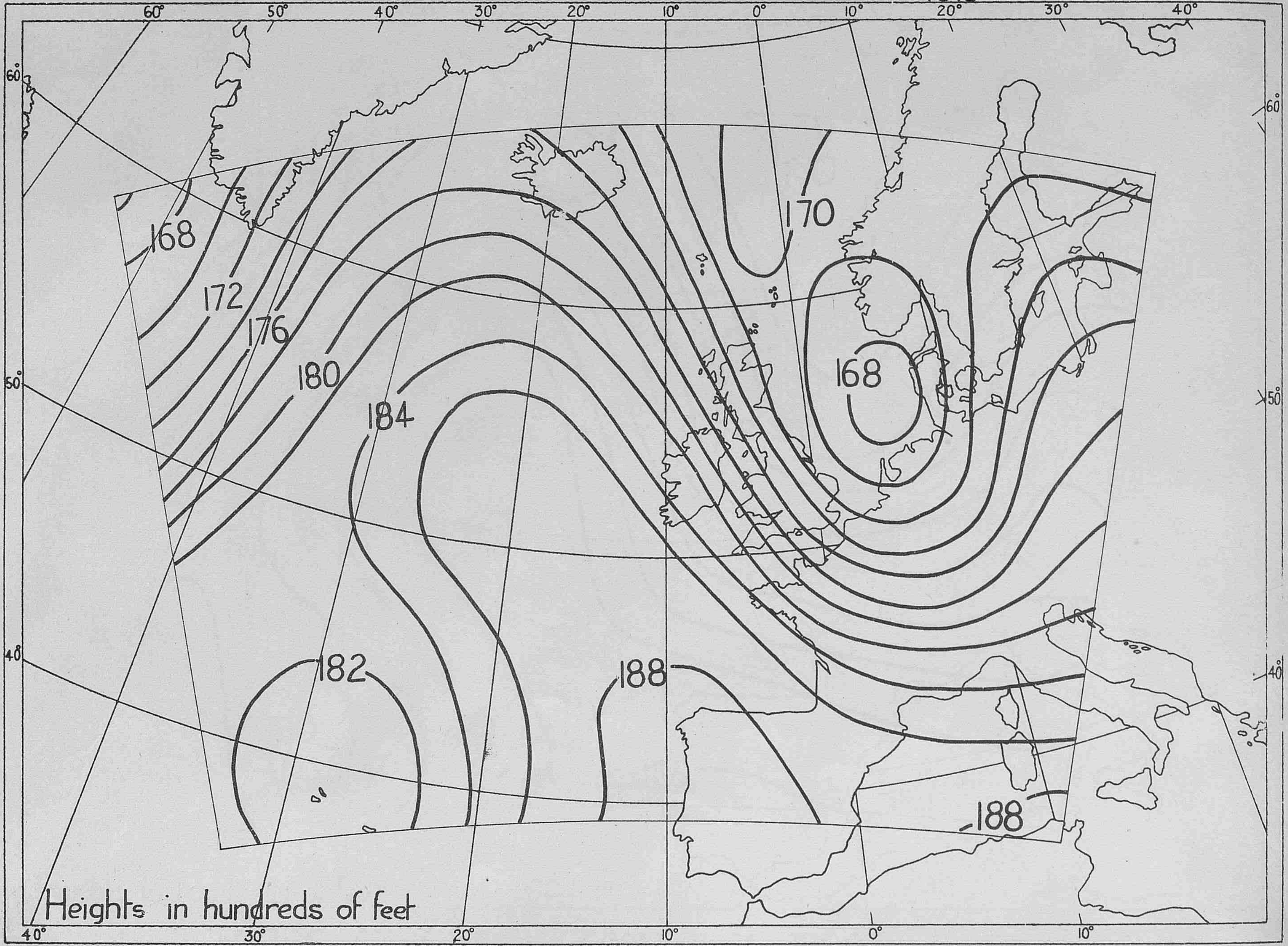
60°
50°
40°
30°
20°
10°
0°
10°
20°
30°
40°
60°
50°
40°
60°
50°
40°
40°
30°
20°
10°
0°
10°
168
172
176
180
184
182
188
170
168
188
Heights in hundreds of feet

FIG.7(b) 500 mb. CONTOURS 1500Z 31:1:53

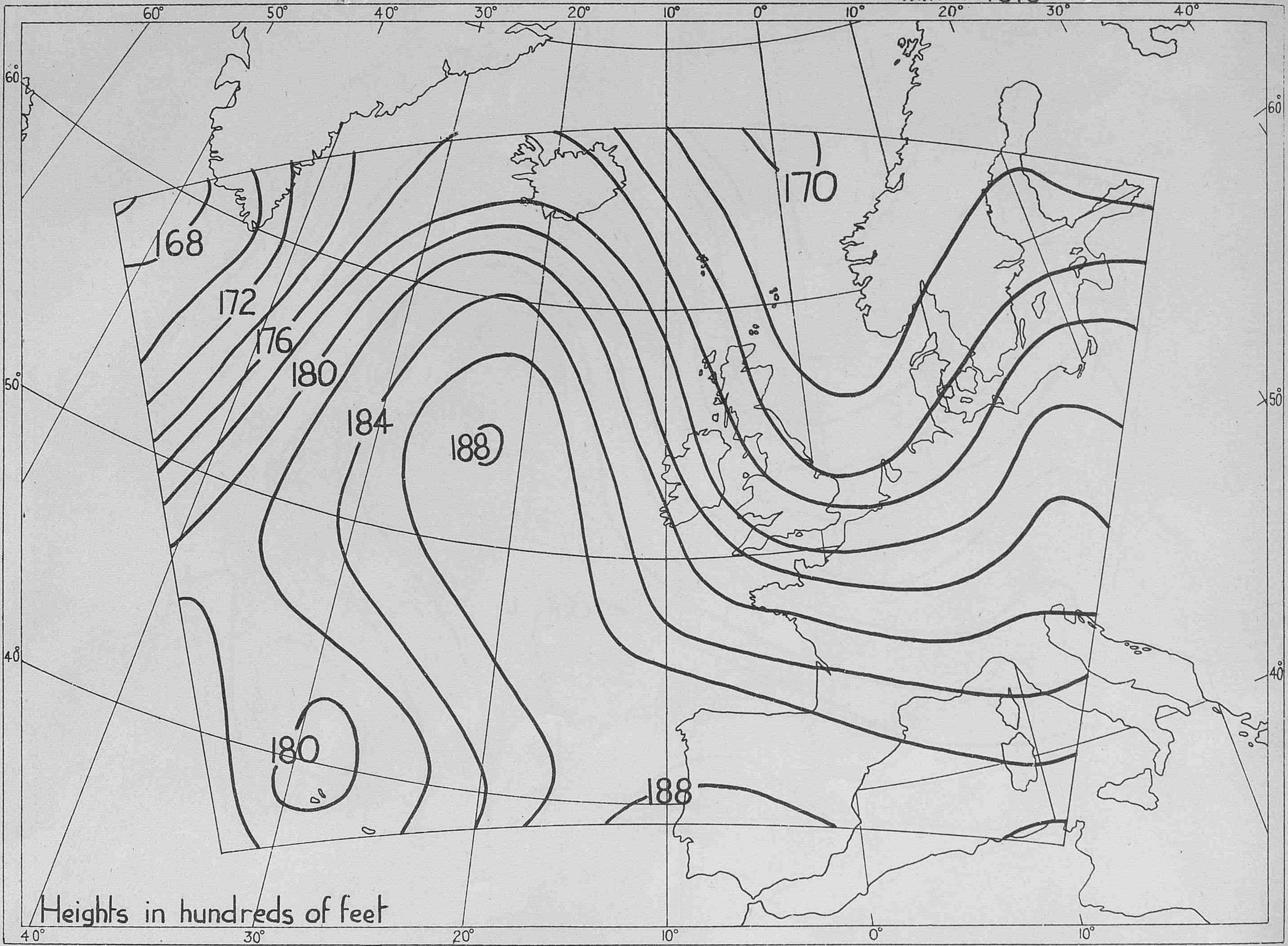
60°
50°
40°
30°
20°
10°
0°
10°
20°
30°
40°
60°
50°
40°
170
168
172
176
180
184
188
180
188
Heights in hundreds of feet
40°
30°
20°
10°
0°
10°

FIG.7 (c) FORECAST 500 mb. CONTOURS 1500Z 31:1:53 USING J^{++}

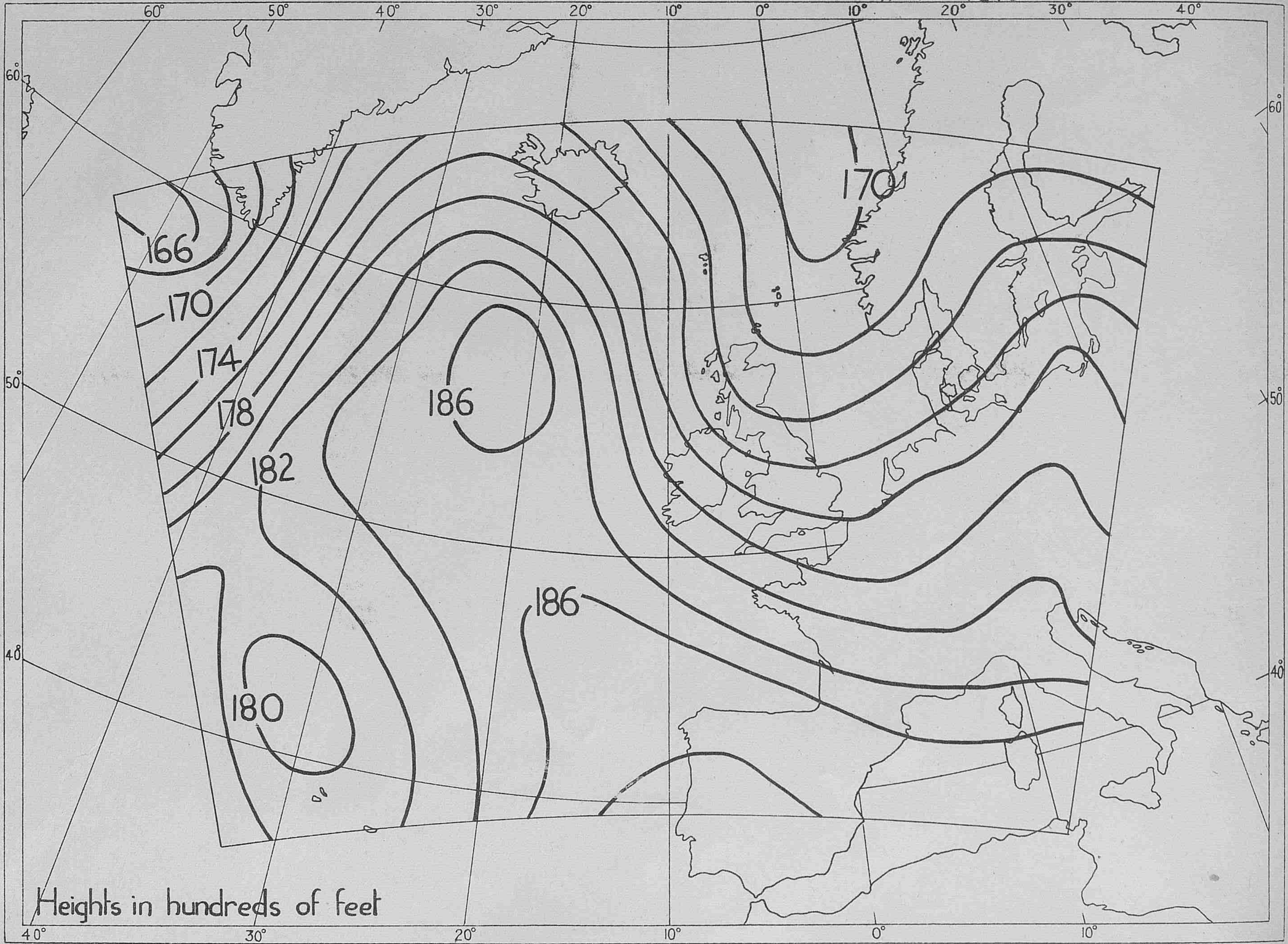
60°
50°
40°
30°
20°
10°
0°
10°
20°
30°
40°
60°
50°
40°
166
170
174
178
182
186
186
180
170
Heights in hundreds of feet
40°
30°
20°
10°
0°
10°

FIG. 7(d) FORECAST 500 mb. CONTOURS 1500Z 31:1:53 USING J^{x+}

AD 141028

M.R.P. 1019
S.C. 111/224
22nd November 1956.

Preliminary report on cumulus investigations, East Hill, June - August, 1956, and on plans for future similar work

by

W.G. Harper, F.H. Ludlam and P. Saunders

(Meteorological Office)

AIR MINISTRY

METEOROLOGICAL RESEARCH COMMITTEE

At the time of issue this report has not
been published. Any author desiring to
quote this paper should refer to it as "A
paper of the Meteorological Research
Committee (London),
M.R.P. No. 1019 by Messrs. W.G. Harper, F.H. Ludlam, P. Saunders
A copy is available in the Library of
the Meteorological Office."

M.R.P.1019
S.C.III/224
22nd November, 1956

AIR MINISTRY

METEOROLOGICAL RESEARCH COMMITTEE

Preliminary report on cumulus investigations, East Hill, June - August, 1956, and on plans for future similar work

by

W.G. Harper, F.H. Ludlam and P. Saunders

1. Introduction

These investigations were made at the Meteorological Office Radar Unit, East Hill (near Dunstable), by the local staff, in co-operation with members of the Department of Meteorology, Imperial College. The principal aim of the work was the co-ordination of visual and radar observations of developing shower clouds, and hence the elucidation of the processes of rain formation in cumulus. On suitable days the evolution of cumulus clouds was followed quantitatively, using a double-theodolite technique for visual measurements, and radar equipment with wave-lengths of 10 cm (PPI and RHI presentation) and 3 cm (RHI presentation). Co-ordinated observations and soundings were made by aircraft of the M.R.F., and by a light aircraft operated for Imperial College from a base at Kenley.

The observations were made on a number of days during the period 14 June to 10 August, 1956. A considerable amount of data was assembled, whose analysis is now being undertaken at Imperial College. The following paragraphs are a provisional summary of the results of the work, a final analysis of which will be prepared under the joint authorship of Meteorological Office and Imperial College staff.

2. Radar echoes in convective weather, not due to precipitation

Ordinarily a swept gain reduction is operated on the receiver of the 10 cm radar, which diminishes the confusing glare on the display tubes produced by permanent echoes from ground obstructions within 10 miles. When we concentrated attention on cumulus at short ranges we removed the swept gain. Although as a result greater difficulty was experienced in distinguishing and photographing non-permanent echoes, we then observed in greater frequency and intensity a kind of echo which had previously been noticed occasionally on the RHI display, but too faintly and rarely to be clearly related to particular clouds, and which as far as we know has not previously been described by radar meteorologists. We found that these echoes are commonly associated with non-precipitating cumulus. They were detectable only on the 10 cm radar, and although carefully sought were not seen on the 3 cm radar, which has a comparable performance in the detection of precipitation. We call them 'mantle echoes'.

A mantle echo is typically a persistent, diffuse, weak echo seen on the RHI presentation in the form of an inverted U or V. Occasionally the echoes appear in the form of a layer with shallow undulations. From simultaneous theodolite measurements we established that the echo is received from the sides of a cumulus or stratocumulus cumulogenitus cloud where they are intercepted by the radar beam, the lower parts of the echo lying near or a

/little

G.1312(a)/JB/11/56/50

little above the level of the cloud base, and its top corresponding to the cloud summits. With our equipment such echoes were detectable at ranges up to 15 miles. The echo has a fluctuating character, rather like that of precipitation echoes, and is quite unlike the well-known 'angel' echoes which have been reported by R.F. Jones (M.R.P.741) as occasionally observable in great numbers with clear skies. A kind of angel is also seen, however, which usually is received from levels below that of the cumulus bases, and which seems to be associated with convection from the ground. These echoes are seen as compact 'blips' on the radar screen, and give signals of a somewhat steadier character than mantle or precipitation echoes. Sometimes they do not appear on every successive sweep, although an identifiable echo can often be followed for several minutes. With our radar equipment they are observed at ranges of up to about 20 miles.

We first considered that the mantle echoes might be caused by small concentrations of drizzle-size drops within the cumulus, distributed mainly near the walls of the clouds, partly because on some occasions echoes appeared to develop as the clouds aged. This interpretation was hard to maintain when echoes were found in cumulus only two or three thousand feet thick, and also in patches of even shallower stratocumulus cumulogenitus, and had to be abandoned when mantle echoes were found on one day to be well developed in a cloudless sky. On this day convection was occurring, but was limited by an inversion which lay just below the condensation level of the surface air. We now regard the mantle echoes as refractive effects, associated with abrupt gradients of vapour pressure at the edges of clouds, and at the edges of thermals which penetrate into dry layers but do not necessarily reach their condensation level.

The echoes may originate at cloud surfaces which lie across the radar beam, or parts of the beam may enter the cloud before returning to the radar - we have considered effects which might arise because of the shape of thermal and cloud tower caps, and have devised a tentative theory of the echo production in these terms.

The existence of mantle echoes is a help in measuring cumulus, for given the range of a prominent cloud a single-theodolite measurement can be used to determine the height of cloud base; assuming this to be constant within the range of vision estimates can then be made of the range and summit-levels of cumulus too far to be detected by the radar. Mantle echoes rarely extend above 10,000 ft, perhaps because the number of larger clouds which come within radar range is comparatively small, but possibly also because the vapour pressure differences between cloud and clear air become substantially reduced as the temperature falls, so that refractive effects become weaker.

Interesting observations were made on the behaviour of the angel-type echoes. Often these appeared as enhanced ground echoes, extending up to 1,000 to 2,000 ft above the ground in the form of sloping columns. Such echoes may persist for several hours in particular places. Occasionally small blobs of echo become detached from such columns or appear independently at heights of about 2,000 ft, and can be observed for several minutes, apparently moving with the wind. During this period they may ascend by as much as 1,000 to 1,500 ft, but sometimes, especially before disappearing, they seem to descend. On more than one occasion the blips at the up-wind end of a line of angels were at ground level (or at least at zero elevation on the display), but those at the down-wind end of the line were at about 2,000 ft, and on one occasion a weak precipitation echo was noted just beyond this end of the line. We noticed on a few occasions that several ascending angels were located near or beneath rapidly building congestus clouds, and that they may then be followed to levels near the cloud base, or even above it: once we succeeded in photographing the rise of an angel into the centre of a mantle echo above it. We tentatively associate the angels with refractive effects at strong temperature gradients at the caps of rising thermals, and are developing a theory to explain the essential difference in character between the signals from these angel echoes and the mantle echoes.

It may be remarked that curved lines of angels, up to about 20 miles long, are sometimes observed lying roughly parallel to the edges of shower echoes, but separated from them by about 2 miles. Such lines are almost certainly associated with the micro-fronts produced by cumulonimbus downdraughts, and with the organised growth of new cumulus at the edges of intense showers. More intensive examination of angels may provide new insight into the role of thermals and micro-fronts in the release and organisation of convection.

3. Droplet spectra in cumulus

For the examination of the progress of coalescence in cumulus further information on the droplet spectra is needed, particularly of the occurrence near the bases of droplets of radius exceeding 20-30μ. These may be present in concentrations (up to several per litre) too small to be conveniently sampled by conventional techniques, but nevertheless significant for rain formation. Qualitative observations from the light aircraft, and previous experience, suggest that even small cumulus sometimes contain appreciable concentrations of drizzle-size drops, and the M.R.F., using impaction on silver paper, found droplets of radius about 50μ in concentrations of several per litre inside cumulus of moderate size, 2-3,000 ft above the base. At present it is difficult to account for the growth of such droplets, and further investigation of their true size and concentration is desirable.

4. The formation of showers; the initial radar echo

In recent years much attention has been given to the height at which radar echoes first appear during the formation of showers. It has been found that a developing echo is usually straddled across or even mainly below the 0° C level, and it has been inferred that the precipitation has formed by the coalescence of droplets rather than by the growth of ice crystals. In general the radar observations have not been carefully co-ordinated with the visual appearance of the shower clouds and the impression has spread that precipitation, and hence the radar echo, forms within the central parts of clouds whose tops extend above the 0° C level, often by many thousand feet.

On the other hand, Ludlam and Saunders (Tellus, in press) demonstrated in Sweden the existence of a critical and well-defined level (the fibrillation level) where evanescent traces of precipitation, capable of causing a brief, faint radar echo, for the first time appear in the decaying towers of cumulus summits; when the summits reach above this level showers develop, and, if the temperature there is below 0° C, the cloud tops become glaciated. The height of the fibrillation level varies substantially from occasion to occasion, and, because its height above the cloud base is proportional to the speed of the updraughts in the cloud, it is supposed to be the level at which the coalescence process, active amongst the droplets as they are lifted from the base of the cloud in growing cumulus towers, first leads to the appearance of significant concentrations of raindrops. In the visual observations from which these features were established, no systematic use was made of radar, partly because in the clear Swedish air traces of precipitation in the tops and below the bases of cumulus could be recognised visually at ranges exceeding 30 miles more readily than with the low-power radar available. It seemed clear, however, that the first traces of echo should in general be faint and transient, and would appear consistently at or near a particular level. On the other hand, because of the rapid glaciation which spreads throughout the cloud tops following the initial formation of precipitation, in later towers of the same cloud precipitation develops more copiously and practically simultaneously over a considerable range of heights near and above the 0° C level. Accordingly, it was supposed that the true initial radar echoes are usually small, feeble and short-lived, and practically impossible to detect except by directing the radar towards growing clouds visually recognised as likely to become shower clouds. On the other hand, only these echoes provide information on the process by which precipitation forms, as distinct from the more involved processes by which it develops after it has formed at sub-zero temperatures.

At East Hill we found visual observation of clouds to be much more difficult than in Sweden; whereas there the horizontal visibility was rarely less than 40 miles here it hardly ever exceeded 8 miles, and usually only clouds whose range lay between about 5 and 20 miles could be studied. The radar frequently showed columnar echoes extending down to the ground from cumulus within 10 miles, amongst whose summits no signs of fibrillation could be seen, and beneath whose bases was no visible evidence of a shower. Often it was impossible to see cumulus tops beyond 20 miles, and at this range it was sometimes difficult to decide even whether or not they were glaciated. Consequently the opportunities for co-ordinating visual and radar observations were much more restricted than in clean air masses. Nevertheless we were able to make some interesting comparisons, and several times succeeded in making continuous observations of growing cumulus in which initially there was no detectable echo, but in which an echo formed.

We found, in agreement with our previous experience, that radar echoes developed in clouds whose visible towers exceeded a rather well-defined level. If the towers barely reach this level only weak showers are formed, and the radar echo first appears as a narrow upright streak, half a mile or less in width. The streak is usually displayed with a length of 2,000 ft or more, with a top below the peak height attained by the cloud tower by up to about 2,000 ft. If no succeeding towers intervene both the top and the base of the echo descend; the base descends the more rapidly, at a speed of about 1000 ft/min, comparable with the fall-speed of raindrops. Where succeeding towers reach similar heights the echo column broadens; its top remains at about the same level but its base extends down to the ground within a few minutes.

Visual observations show that when the towers of a growing cumulus reach some 2,000 ft or more above the level associated with shower formation, and when, as is usual in our climate, the temperature there is below 0° C, the development of the shower is accompanied by a glaciation of the cloud tops, which within a few minutes spreads throughout the cloud sideways, and downwards to the 0° C level. At the end of this period large parts of the cloud above this level contain significant concentrations of crystals ($>$ 1/litre), probably of very various sizes, including snowflakes and small soft hail pellets. This rapid transformation was in Sweden observed to occur at minimum cloud temperatures varying between about -4° C and -23° C, and is thought to be due, not primarily to the freezing of cloud droplets containing ice nuclei, but mainly to processes of crystal multiplication which are efficiently begun when precipitation-size solid particles, commonly produced by the freezing of some of the large drops grown by coalescence, appear in the cloud tops. According to this view, the glaciation is not usually the cause of shower formation; rather, both are due to the coalescence process reaching an advanced stage at sub-zero temperatures.

5. The development of shower clouds and shower echoes

Once shower formation has begun large droplets and, if glaciation occurs, also large crystals, become spread throughout the cloud. Succeeding towers which rise through the cloud become infected with these large particles, which then grow into precipitation elements over a range of heights much below the level at which the initial elements were formed. Consequently the radar echo from maturing shower clouds is observed to broaden and intensify throughout its height.

Moreover, the concentrations of crystals which infect freshly-rising towers when they reach above the 0° C level are commonly so great that a large part of their liquid content is quickly frozen. The increase in buoyancy produced by the accompanying release of latent heat, together with an increase due to the subsequent settling-out of some of this water as precipitation, provides new energy for cloud growth. In Sweden we observed that there is often a new surge in the growth of cumulus soon after glaciation, during which the summits rise at speeds two or three times greater than previously, from heights of around 15,000 ft to near the tropopause, forming massive anvils. Craddock has reported what is clearly the same phenomenon from Malaya, and we now regard this development as a characteristic second phase in the growth of shower clouds. On the radar display it leads to the appearance of very tall and broad (5-10 miles or more) echoes, whose upper parts, corresponding to the anvils, are often mainly diffuse and rather weak, but which contain stronger columns associated with newly-rising towers. At East Hill we found that the tops of these echoes corresponded very closely (within 1,000 ft) to the highest visible tops.

By directing the 10 cm RHI beam into these large echoes with the aerial stationary, and using an amplitude display as a function of range, we were able to observe the occasional momentary increases of echo intensity which occur when lightning discharges pass through the beam (as described and discussed by Jones, Quart. J.R.Met.Soc., 80, 1954, p.579). These momentary increases are found to be coincident with VHF-receiver crackles and the flashes on Sferic direction-indicators, and their observation is a valuable way of exploring particular clouds for electrical activity. We noticed, for example, that lightning occurred only in second-phase clouds, seemed more characteristic of the diffuse rather than the stronger columnar parts of the echo, and sometimes was confined to regions near the cloud tops.

By reducing the gain of the radar we observed that the most intense parts of the precipitation echo usually remain near or below the level of shower formation. The impressive anvil structures may therefore have only an indirect effect on the intensity of shower rains. We suspect that the formation of large hail cannot proceed in second-phase clouds, because of the abundance of crystals, nor in clouds in which the strongest echoes remain below the 0° C level, because the coalescence process then precipitates most of the cloud water before it becomes supercooled. Probably large hail forms only in young clouds containing strong updraughts, so that the temperature at the level of shower formation is well below 0° C. We attempted to confirm these views by relating our observations to reports of hail made by a network of volunteers. Unfortunately the results are unlikely to be conclusive; the network so far used is too thin, and notable hailstorms were rare, except on one or two occasions which fell on week-ends or public holidays.

We regard the small hail which forms within second-phase clouds as a generator of thunderstorm electricity, and stimulated by the observations mentioned above, have devised a theory to account for the failure of clouds with base-temperatures below 0° C to produce thunderstorms.

6. The relation between cumulus properties and screen-level observations

According to the simple parcel theory of convection, the air within cumulus formed by convection from the ground has the wet-bulb potential temperature of the air near the ground. Although there are large departures from the adiabatic processes assumed in the theory, the wet-bulb potential temperature at the cloud base is still fundamental in the discussion of cumulus behaviour. Since it can in principle be obtained on many occasions from ground observations, measurements at the level of the cloud base were made during our aircraft soundings for a comparison between the actual wet-bulb potential temperature at cumulus base and the value obtained from the field of wet-bulb potential temperature shown by the screen-level observations made at synoptic stations. A preliminary inspection suggests that the values are remarkably close - within 1° C. The synoptic observations can therefore be used, when carefully analysed in conjunction with the temperature fields found on upper-level charts, to examine the distribution across the country of some important features of cumulus populations, such as the maximum internal buoyancy and the maximum height of the cloud tops. It is hoped that studies along these lines will lead to techniques for improving the forecasting of these features.

7. Plans for future work

(a) Limitations of existing knowledge

The field work already carried out in Sweden and both before and since at East Hill in our opinion points almost conclusively to the importance of the coalescence process in shower formation, and of processes involving the ice phase in shower development. Both kinds of processes can be modified artificially. Before use can be made of the new theories (e.g., in improving thunderstorm forecasts) and before scientific experiments can be made in modification (e.g., the suppression of severe hail - and thunderstorms), the theories must be refined and strengthened by more quantitative expression.

Gaps and weak points exist in our knowledge of both the physical and the meteorological laws operating within the assemblies of water particles which are called cumulus and cumulonimbus. Ultimately the evolution of a cumulonimbus will be described by specifying the particle spectrum as a function of space co-ordinates and time, and accounting for the changes in terms of the predominating physical and dynamical processes. Further, the properties of cloud populations and the meteorological laws controlling them will be elaborated. The task of drawing up these descriptions is immense, and the limited facilities and, more especially, the limited numbers of workers available lead us to concentrate on a few aspects whose clarification seems likely to promote most quickly our powers of prediction and control. These particular aspects are listed below.

(b) Pressing problems

I. Particle size spectra in cumulus

The extensive data already available on drop-size spectra in cumulus unfortunately are not much help in revealing the laws which control the growth of droplets into raindrops. There are two reasons:

(i) the sampling has so far been restricted to volumes of up to 100 cm^3, whereas the largest droplets which are present in concentrations of $1/10^3$ to 10^4 cm^3 are critically important;

(ii) the spectra obtained have not been related to position in the cloud and the cloud history. Showers form within volumes of the order of 1/100 of the volume of an individual cloud. Spectra representative of the other parts are an important property of the cloud but are not representative of the region involved in shower formation.

The first difficulty can be overcome by modifying sampling techniques, but the second can be satisfactorily solved only by making the samples in clouds whose complete history is followed by ground observers.

The droplet spectra must be related to condensation nucleus spectra, the important features of which can be obtained by existing techniques.

II. Processes of crystal multiplication

According to our views the overwhelming majority of crystals in mature cumulonimbus arise from multiplication processes set up by the freezing of large drops, and not primarily from the action of freezing nuclei in small droplets. Experiments are being planned at Imperial College to examine the production of crystalline fragments during the freezing of drops. Apart from such laboratory work systematic sampling of shower clouds for their crystal content is needed; this, like the droplet sampling, is best done in co-ordination with ground observers.

III Cumulus dynamics

Our present knowledge of the nature of the air motions in cumulus, of the factors which determine their scale and of the way in which they are influenced by the cloud particles (e.g., by the release of latent heat), are very rudimentary. Considerable advance will be needed before we understand what governs the size attained by an individual cloud. Model experiments aimed at improving the theory of convective motions are in progress at Imperial College.

As the theory is improved it should become possible to make use of aircraft measurements of cloud-air properties, such as condensed water concentration and temperature. Undoubtedly, however, a new series of measurements, including information on the history of the explored cloud and the exact position of the aircraft in the cloud, will be needed. Eventually the theory will uncover relations between internal cloud properties and external and perhaps more readily measurable features, such as the clear air sounding, the intensity of ground heating, and so on. The behaviour of individual clouds will never become completely predictable, but we may hope that understanding of and ability to forecast the statistical behaviour of populations of cumulus will be greatly improved. Such understanding will be needed to resolve such questions as

"How many clouds will reach a certain size?"

"What total amount of shower rain will fall?" and

"If some clouds are modified, what is the effect on the remainder of the population?"

It is therefore desirable to begin the study of cumulus populations; information for this study can be obtained by ground observers equipped with such facilities as theodolites, radar, and time-lapse cameras, whose observations are co-ordinated with clear-air soundings by radio-sonde or aircraft and with aerial reconnaissance over a wide area, and examined in conjunction with analyses of conditions on the meso- (see next section) and synoptic-scales.

IV. Efficiency of shower clouds

The efficiency of cumulonimbus as precipitation mechanisms, defined, say, as the ratio between the water reaching the ground and that condensed in the cloud throughout its history, seems to vary considerably. Some clouds only 2 or 3 kilometres thick produce intense showers, while others several kilometres thick fail to form precipitation, or their precipitation evaporates before reaching the ground. A knowledge of the precipitation efficiency and the factors which control it would be useful in forecasting practice, and a comparison with the efficiency of artificially modified clouds is essential for a realistic appraisal of techniques of seeding cumulus to produce rain. As a first step in the quantitative study of shower rain, observations of the amount of rain which falls from individual cumulus and populations of cumulus should be included in the field studies mentioned above. Although useful estimates can be made from detailed radar observations, their evaluation is laborious and the results are very sensitive to variations in the drop-size distribution. Moreover the computed rainfall is that within the beam, which at some distance is well above ground level. The radar evidence would therefore need to be supplemented by records from raingauges, some preferably autographic but for the rest of a simpler pattern than the conventional gauges, disposed within a radius of about 30 mi of the radar station with an average separation of 2-3 mi. Such a network would require several hundred gauges and the recruitment of voluntary observers. Experience in Sweden shows that this is possible, but of course such a network could be maintained only for rather short periods. The British Rainfall Organisation already has comparable networks in well-populated areas, which would provide a splendid basis for the dense network.

It would be very desirable to include in this network stations observing other meteorological elements, so that on selected occasions meso-scale analyses of the convective weather systems could be made. Much attention is being paid to this kind of analysis in U.S.A. (see, e.g., Res.Pap.39, U.S. Weather Bureau). There special networks have been organised with an average station separation of about 30 miles. Such a network could more easily be established in England, where the separation of stations making synoptic reports is already about this value, or is in some districts even less.

V. Seeding experiments

As the quantitative observation and theory of cumulus progress, it will become possible to plan seedings aimed at modifying their behaviour, and to measure the effect of the seedings by quantitative comparison of the observed and the predicted natural behaviour. All evaluations of seeding experiments are based upon such a comparison, with an accuracy which depends upon the errors in both the observed and predicted behaviour. The accuracy of the former depends only upon the suitability of the observing technique, while that of the latter depends also on the design of the experiment. In the absence of spectacular events, such as the explosion of treated clouds, and in view of the great variability in the natural behaviour, a sound theory must be used to design the details of an experiment, aimed at producing a predictable and detectable effect. For example, in Sweden the recognition and interpretation of the fibrillation level led to the dry-ice seeding of a cumulus whose summits were at all times below the fibrillation level; following the seeding, the cloud produced a shower, so that its behaviour was demonstrably different from that of all other clouds present, some of which were producing showers naturally. This is the first time such a difference has been established. Only by improved and repeated experiments of such a nature can we realise the possibilities of usefully modifying clouds and precipitation.

8. Facilities for future investigations

It seems clear to us that material progress with the difficult problems mentioned above can be made only by field investigations in which very detailed and comprehensive observations are made by the careful co-ordination of ground observers, using visual and radar techniques, and aircraft observers. In the recent work aircraft participated, but did not enter clouds. We are very conscious of the benefits of co-ordinating the visual and radar observations, and would like to continue this work with the added co-operation of aircraft, in order to examine selected clouds by all three techniques.

Unfortunately this is not possible at East Hill owing to restrictions on flying in and near clouds. Since another field site may need to be chosen, we summarise the desirable conditions as follows:

(a) unpolluted air, for clarity of vision and freedom from disturbed nucleus spectra;

(b) good radar and visual horizons;

/(c)

(c) freedom from restrictions on flying in cloud;

(d) proximity to radio-sonde station and other meteorological facilities;

(e) frequent occurrence, at least in some season, of well-developed cumuliform clouds.

These conditions are not all easily fulfilled anywhere in the British Isles. It must be borne in mind, however, that field studies of the kind envisaged can accumulate in one favourable month material requiring a year for its digestion. It is therefore suggested that they could be made at a site not permanently occupied, either in Britain or abroad. (It is not unlikely that sufficient progress could then be made to remove the need for flight through clouds in future work, so that it could continue without much hindrance at a more convenient place.) Since the aircraft and the ground observers are readily mobile the main difficulties in establishing a temporary site are providing staff accommodation and radar. The radar should comprise a range-height set and a plan-position set, the latter not necessarily under direct control of the ground observers but equipped with an automatic camera. It might prove possible to solve all problems by finding an RAF base well away from busy airways but not too remote (e.g., in S.W. England), with suitable accommodation, with facilities for communicating to aircraft, with a plan-position radar on the airfield or nearby whose display could be repeated at a meteorological control, and to which a 3-cm height-range radar could be taken for the duration of the field work. While the prospects of such a solution are explored it is recommended that field work should be continued at East Hill, with whatever aircraft co-operation is practicable.

AD 139539

M.R.P. 1020
S.C. 11/223
7th December, 1956

AD 139539

Average height of the standard isobaric surfaces over the area from the North Pole to 55°N. in April and October

by

H. Heastie

(Meteorological Office)

MASTER FILE COPY
NOT TO BE REMOVED
FROM AWS TECH FILES

AIR MINISTRY

METEOROLOGICAL RESEARCH COMMITTEE

At the time of issue this report has not been published. Any author desiring to quote this paper should refer to it as "A paper of the Meteorological Research Committee (London), M.R.P. No. 1020 by Mr. H. Heastie A copy is available in the Library of the Meteorological Office".

M.R.P.1020
S.C.II/223
7th December, 1956

AIR MINISTRY
METEOROLOGICAL RESEARCH COMMITTEE

Average height of the standard isobaric surfaces over the area from the North Pole to 55°N. in April and October

by

H. Heastie (Meteorological Office)

1. Introduction

This paper is a continuation of M.R.P.918(1) and M.R.P.981(2). In (1), the decision to start the revision of Geophysical Memoir 85 - Upper Winds over the World - by constructing circumpolar charts of the standard isobaric surfaces was explained and the present paper together with the two earlier papers completes this section of the revision.

2. The data

Data for the same fixed period 1949-53 were used and the sources are listed in the earlier papers.

3. Method of constructing the charts

(1) General. The method employed was the same as that used for the July charts. Again the data from Siberia were very sparse both in April and October, 1949 and the charts for these months were drawn up to the 300 mb level by means of the correlation method described in (2).

(2) Effect of solar radiation. It was not possible to use data from night time ascents only. 0300 G.M.T. data were used generally, but 1500 G.M.T. data were available from the Aleutian and Alaskan stations and were used when the 0300 G.M.T. ascents were made in daylight. At 0300 G.M.T., daylight covers most of the U.S.S.R. in April and all of Siberia in October, and no Russian data for 1500 G.M.T. were available. Guterman (3) discusses the radiation correction of the comb radiosonde used in the U.S.S.R. and suggests that for solar elevations below 15° the error is negligible. For solar elevations of 50-60° he quotes an error of 0.5°C at 10,000 metres and 1.9°C at 15,000 metres. Over that part of the U.S.S.R. north of 55°N., for the months of April and October, the solar elevation varies up to a maximum of 40°. An error of 0.5°C in the 300 mb temperature would lead to an error of 3-4 metres in the 500-300 mb thickness and this error has been ignored. Errors of 0.5°C and 1.9°C in the 300 mb and 100 mb temperatures respectively would produce an error of the order of 30-35 metres in the thickness between 300 and 100 mb. However, no Russian data above 300 mb were available and use was made of the temperature lapses from the memoir on upper air temperature (4). In the preparation of this memoir data at both 0300 and 1500 G.M.T. were used and, it is reasonable to suppose, any error due to radiation halved in consequence. Further, the maximum elevation of the sun for the area and period considered is 10° or more below that to which the radiation corrections quoted are applicable. It was assumed, therefore, that the maximum error due

/to

to radiation in the 300-100 mb thickness (and consequently in the 100 mb contours) was less than 20 metres. As, however, the variation of radiation correction with solar elevation was unknown, no attempt was made to assess the actual error.

4. The charts

The April charts show two interesting differences from those for the other mid-season months. The first concerns the centre of the main circulation. In January, July and October, at all levels above 700 mb, this centre lies between 75° and 90°W. and 67° and 87°N. In April it lies at 84°N., 50°E. at 700 mb and shifts to 84°N., 35°W. at 300 mb and to 82°N., 10°W. at 100 mb. It is possible to attribute the centre at 700 mb to the persistence of a secondary centre at about 80°N., 70°E. on the January 700 mb chart. Changes from a winter to a summer regime take place very rapidly in the spring and not necessarily at the same time in different regions of the chart (though detailed evidence from the Russian Arctic is lacking) and it is doubtful whether the April or any other monthly chart represents a true "mid-season" circulation pattern. The second peculiarity of the April charts is a departure from the normal association between features of the tropopause pressure and stratospheric thickness patterns shown generally on the charts for the other three months. This occurs at about 20°E. where the tropopause pressure chart (5) shows a marked ridge which is almost immediately below troughs in the three thickness charts 300-200 mb, 200-150 mb and 150-100 mb i.e., relatively low stratospheric temperatures above a relatively low tropopause. These thickness patterns are consistent with the patterns shown on the relevant average temperature charts (4).

An apparently similar peculiarity occurs on the October charts over the Aleutians where high stratospheric thickness is shown over high tropopause (5). The average temperature charts (4) agree with this thickness pattern. No data from the Aleutians were used in drawing the tropopause pressure chart and this chart could probably be redrawn largely to remove this peculiarity.

Both the April and October charts show a westerly circulation at all levels with main troughs at 60-80°W. and 160-180°W., though there appears to be a weak secondary circulation at 700 mb in the Bering Sea in October. The main centre of the circulation lies between Franz Josef Land and NE. Greenland in April and over Ellesmere Island in October. The April charts show a further main trough about 0°W. and a rather indeterminate trough over Siberia, while in October there are troughs between Iceland and Greenland and over western Siberia.

The stratospheric thickness charts in both months are extremely flat, the thermal winds being generally of the order of 3 kt or less. Relatively high values of thickness are shown over Siberia and northern Canada, corresponding to the two main centres of low tropopause (5).

References

(1) Heastie, H. Average height of the standard isobaric surfaces over the area from the North Pole to 55°N. in January. Meteorological Research Papers, Air Ministry, London, No.918, 1955.

(2) Heastie, H. Average height of the standard isobaric surfaces over the area from the North Pole to 55°N. in July. Meteorological Research Papers, Air Ministry, London, No. 981, 1956.

(3) Guterman, I.G. Radiation error of the comb radiosonde. Trans. by A.I. Trans. (Org.)(T) of: Leningrad, Met. Hydr., 1955, No.5, pp. 49-52. London, 1956.

(4) Goldie, N., Moore, J.G. and Austin, E.E. Upper air temperature over the world. Geophys. Mem. No.101, London (in the press).

(5) Moore, J.G. Average pressure and temperature of the tropopause. Meteorological Research Papers, Air Ministry, London, No.874, 1954.

M.R.P. 1020

AVERAGE 700 mb. CONTOURS

APRIL 1949-53

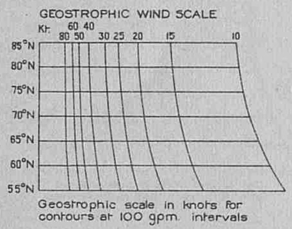

Geostrophic scale in knots for contours at 100 gpm. intervals

▨ Land over 3,000 metres

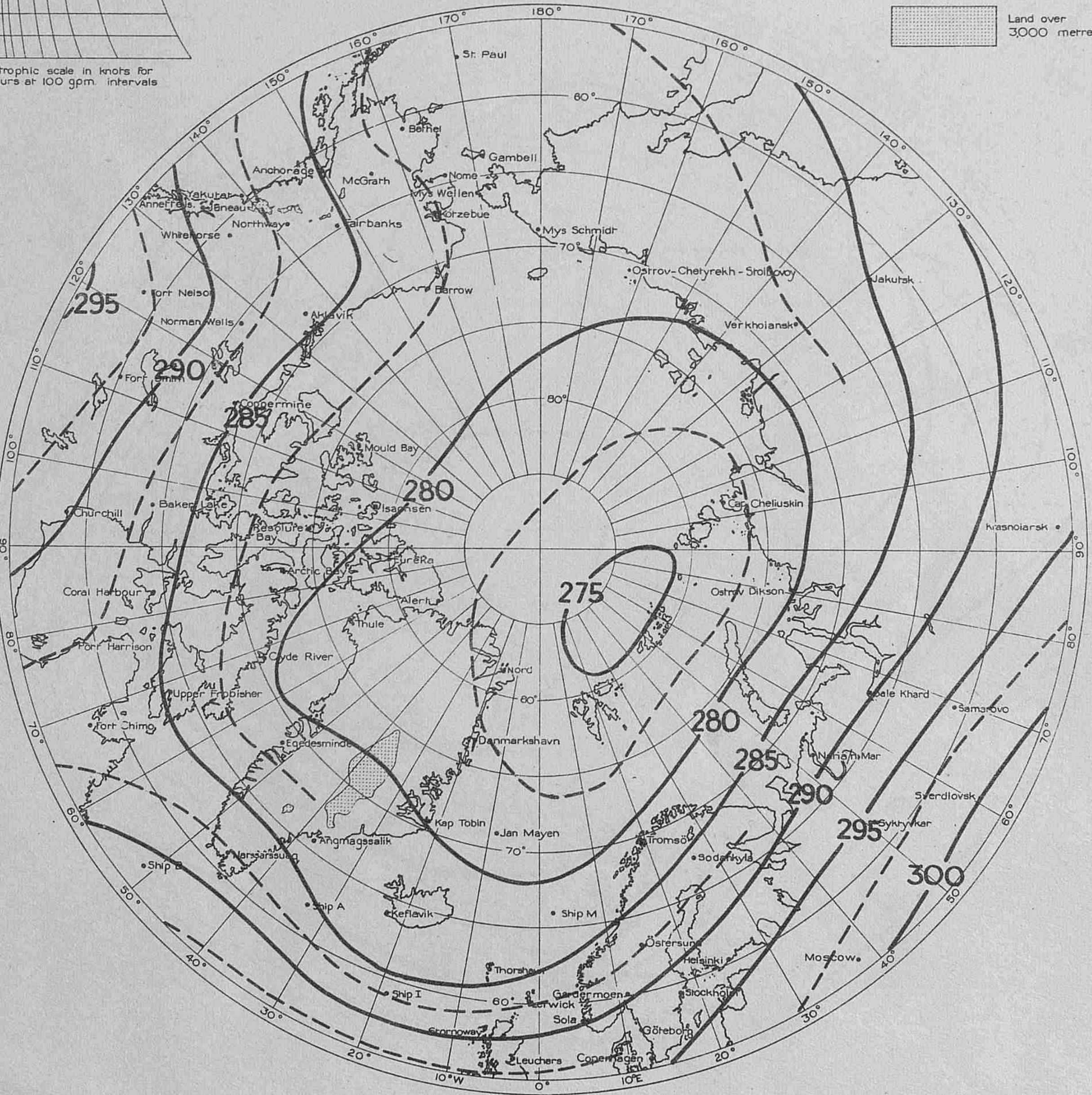
180°
170°
170°
160°
160°
150°
150°
140°
140°
130°
130°
120°
120°
110°
110°
100°
100°
90°
90°
80°
80°
70°
70°
60°
60°
50°
50°
40°
40°
30°
30°
20°
20°
10°W
0°
10°E
60°
70°
80°
80°
70°
60°
St. Paul
Bethel
Gambell
Anchorage
McGrath
Nome
Mys Wellen
Kotzebue
Yakutat
Annette Is.
Juneau
Northway
Fairbanks
Whitehorse
Mys Schmidt
Ostrov-Chetyrekh-Stolbovoy
Barrow
Jakutsk
Fort Nelson
Norman Wells
Aklavik
Verkhoiansk
Fort Smith
Coppermine
Mould Bay
Baker Lake
Isachsen
Churchill
Resolute Bay
Eureka
Arctic Bay
Alert
Cap Cheliuskin
Krasnoiarsk
Coral Harbour
Thule
Ostrov Dikson
Fort Harrison
Clyde River
Nord
Upper Frobisher
Fort Chimo
Egedesminde
Danmarkshavn
Sale Khard
Samarovo
Narian Mar
Sverdlovsk
Kap Tobin
Jan Mayen
Tromsö
Sykryvkar
Narssarssuaq
Angmagssalik
Sodankyla
Ship B
Ship A
Keflavik
Ship M
Ostersund
Moscow
Thorshavn
Helsinki
Ship I
Gardermoen
Lerwick
Stockholm
Sola
Stornoway
Göteborg
Leuchars
Copenhagen
275
280
280
280
285
285
290
290
295
295
300

Height in dekametres

Upper Air Branch (M.O.23)

M.R.P. 1020

AVERAGE 700-500mb. THICKNESS

APRIL 1949-53

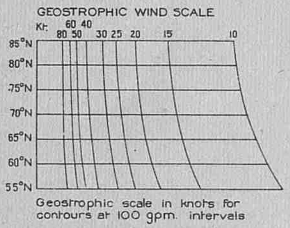

Geostrophic scale in knots for contours at 100 gpm. intervals

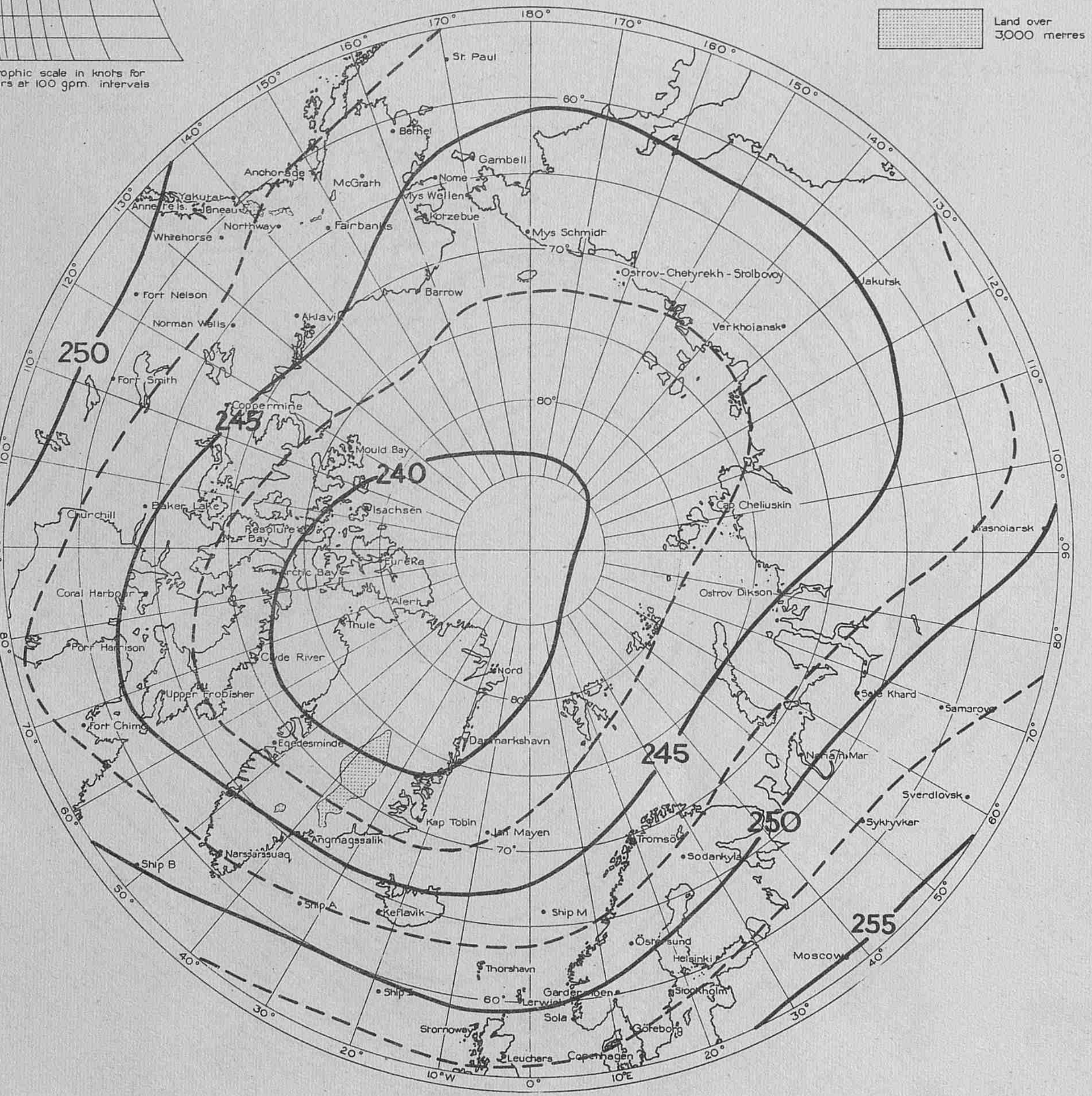
Land over 3,000 metres
180°
170°
160°
150°
140°
130°
120°
110°
100°
90°
80°
70°
60°
50°
40°
30°
20°
10°W
0°
10°E
60°
70°
80°
240
245
250
255
St. Paul
Bethel
Gambell
Nome
Mys Wellen
Korzebue
Anchorage
McGrath
Yakutat
Annette Is.
Juneau
Northway
Fairbanks
Whitehorse
Mys Schmidt
Ostrov-Chetyrekh-Stolbovoy
Jakutsk
Verkhoiansk
Barrow
Aklavik
Fort Nelson
Norman Wells
Fort Smith
Coppermine
Mould Bay
Isachsen
Eureka
Resolute Bay
Arctic Bay
Alert
Thule
Baker Lake
Churchill
Coral Harbour
Port Harrison
Clyde River
Upper Frobisher
Fort Chimo
Egedesminde
Nord
Danmarkshavn
Cap Cheliuskin
Krasnoiarsk
Ostrov Dikson
Sale Khard
Samarova
Narian Mar
Sverdlovsk
Sykryvkar
Kap Tobin
Jan Mayen
Angmagssalik
Narssarssuaq
Ship B
Ship A
Keflavik
Ship M
Tromsö
Sodankyla
Östersund
Helsinki
Moscow
Thorshavn
Ship I
Lerwick
Gardermoen
Stockholm
Sola
Göteborg
Stornoway
Leuchars
Copenhagen

Height in dekametres

Upper Air Branch (M.O.23)

AVERAGE 500 mb. CONTOURS

APRIL 1949-53

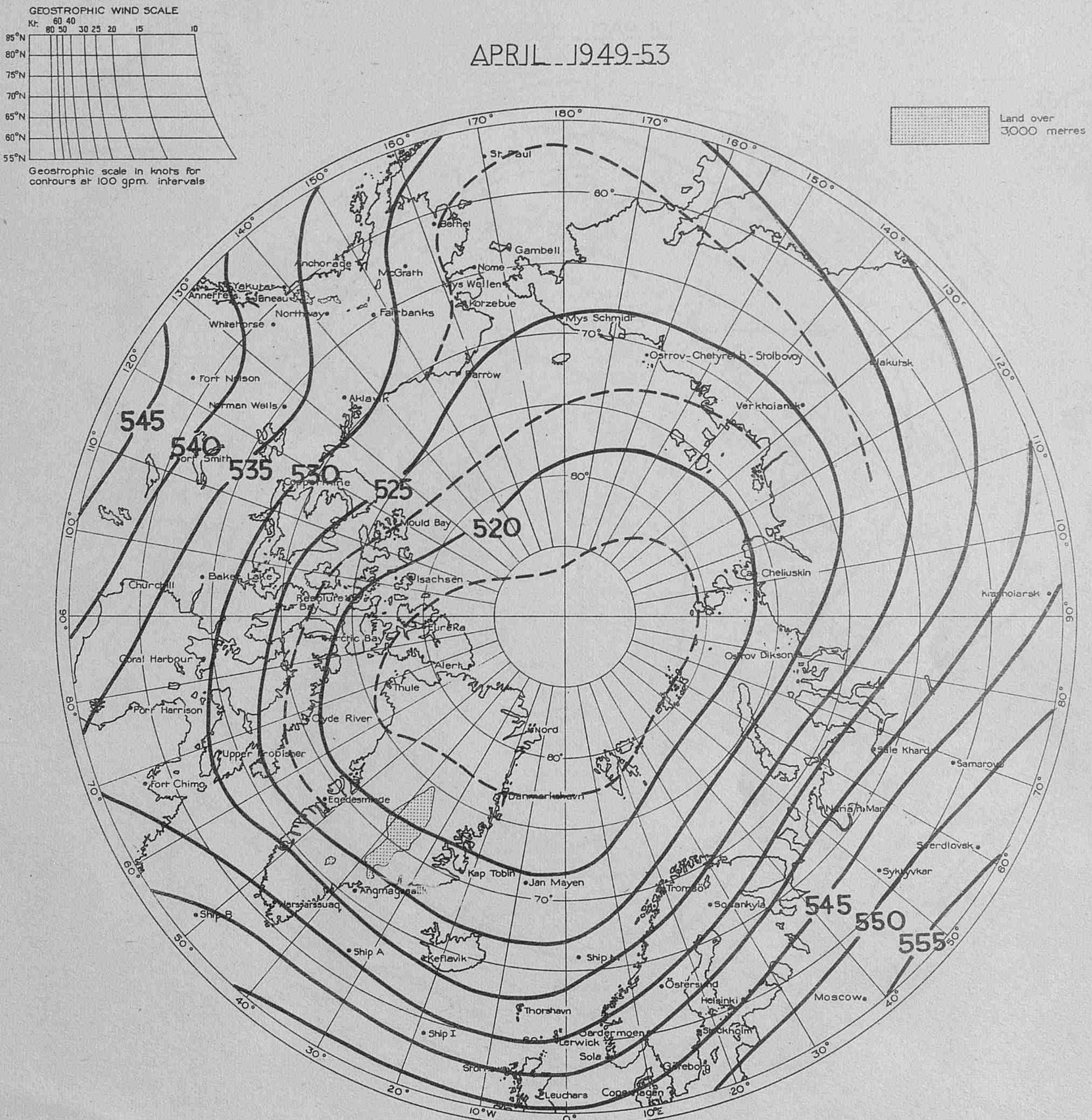
GEOSTROPHIC WIND SCALE
Kt. 80 60 50 40 30 25 20 15 10
85°N
80°N
75°N
70°N
65°N
60°N
55°N
Geostrophic scale in knots for contours at 100 gpm. intervals
Land over 3000 metres
545
540
535
530
525
520
545
550
555
180°
170°
160°
150°
140°
130°
120°
110°
100°
90°
80°
70°
60°
50°
40°
30°
20°
10°W
0°
10°E
60°
70°
80°
St. Paul
Bethel
Gambell
Nome
Mys Wellen
Kotzebue
McGrath
Anchorage
Yakutat
Annette
Juneau
Northway
Fairbanks
Whitehorse
Fort Nelson
Norman Wells
Aklavik
Barrow
Mys Schmidt
Ostrov-Chetyrekh-Stolbovoy
Verkhoiansk
Jakutsk
Fort Smith
Coppermine
Mould Bay
Isachsen
Resolute Bay
Eureka
Arctic Bay
Alert
Thule
Clyde River
Baker Lake
Churchill
Coral Harbour
Port Harrison
Upper Frobisher
Fort Chimo
Egedesminde
Nord
Danmarkshavn
Kap Tobin
Jan Mayen
Angmagssalik
Narssarssuaq
Ship B
Ship A
Keflavik
Ship M
Ship I
Thorshavn
Lerwick
Stornoway
Sola
Gardermoen
Leuchars
Copenhagen
Göteborg
Stockholm
Helsinki
Östersund
Sodankylä
Tromsø
Moscow
Sverdlovsk
Syktyvkar
Narian Mar
Salekhard
Samarovo
Ostrov Dikson
Cap Cheliuskin
Krasnoiarsk

Height in dekametres

Upper Air Branch (M.O.23)

M.R.P. 1020

AVERAGE 500-300 mb. THICKNESS

APRIL 1949-53

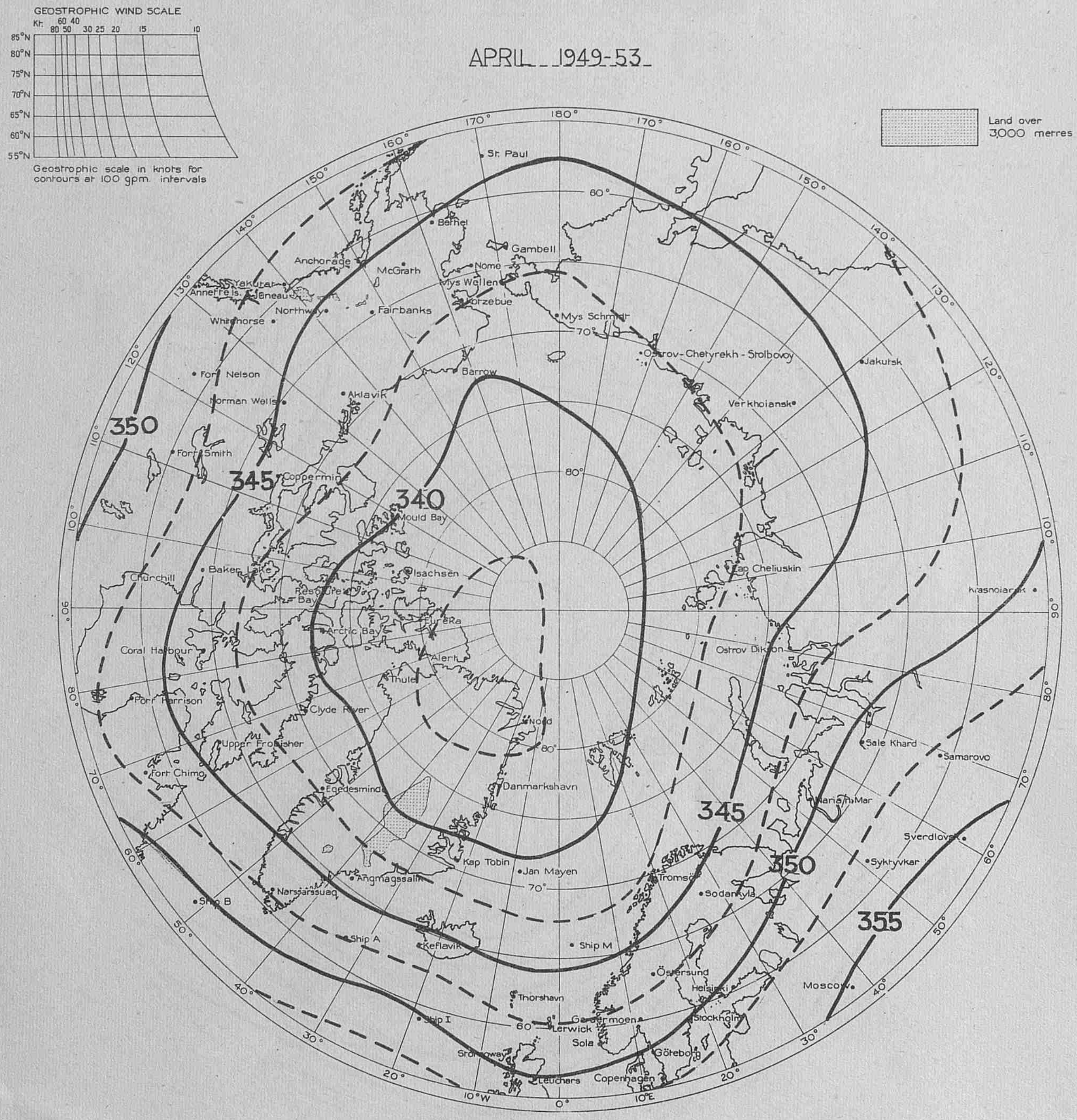
GEOSTROPHIC WIND SCALE
Kt. 60 40
80 50 30 25 20 15 10
85°N
80°N
75°N
70°N
65°N
60°N
55°N
Geostrophic scale in knots for contours at 100 gpm. intervals
Land over 3,000 metres
180°
170°
160°
150°
140°
130°
120°
110°
100°
90°
80°
70°
60°
50°
40°
30°
20°
10°W
0°
10°E
350
345
340
355
St. Paul
Bethel
Gambell
Anchorage
McGrath
Nome
Mys Wellen
Kotzebue
Yakutat
Annette Is.
Juneau
Northway
Fairbanks
Whitehorse
Mys Schmidt
Ostrov-Chetyrekh-Stolbovoy
Jakutsk
Fort Nelson
Barrow
Aklavik
Norman Wells
Verkhoiansk
Fort Smith
Coppermine
Mould Bay
Isachsen
Baker Lake
Churchill
Resolute Bay
Eureka
Cap Cheliuskin
Krasnoiarsk
Arctic Bay
Alert
Coral Harbour
Ostrov Dikson
Thule
Port Harrison
Clyde River
Nord
Upper Frobisher
Sale Khard
Samarovo
Fort Chimo
Egedesminde
Danmarkshavn
Narian Mar
Sverdlovsk
Syktyvkar
Kap Tobin
Jan Mayen
Angmagssalik
Tromsö
Narssarssuaq
Sodankyla
Ship B
Ship A
Keflavik
Ship M
Östersund
Helsinki
Moscow
Thorshavn
Ship I
Gardermoen
Lerwick
Stockholm
Sola
Stornoway
Göteborg
Leuchars
Copenhagen

Height in dekametres

Upper Air Branch (M.O.23)

AVERAGE 300 mb. CONTOURS

APRIL 1949-53

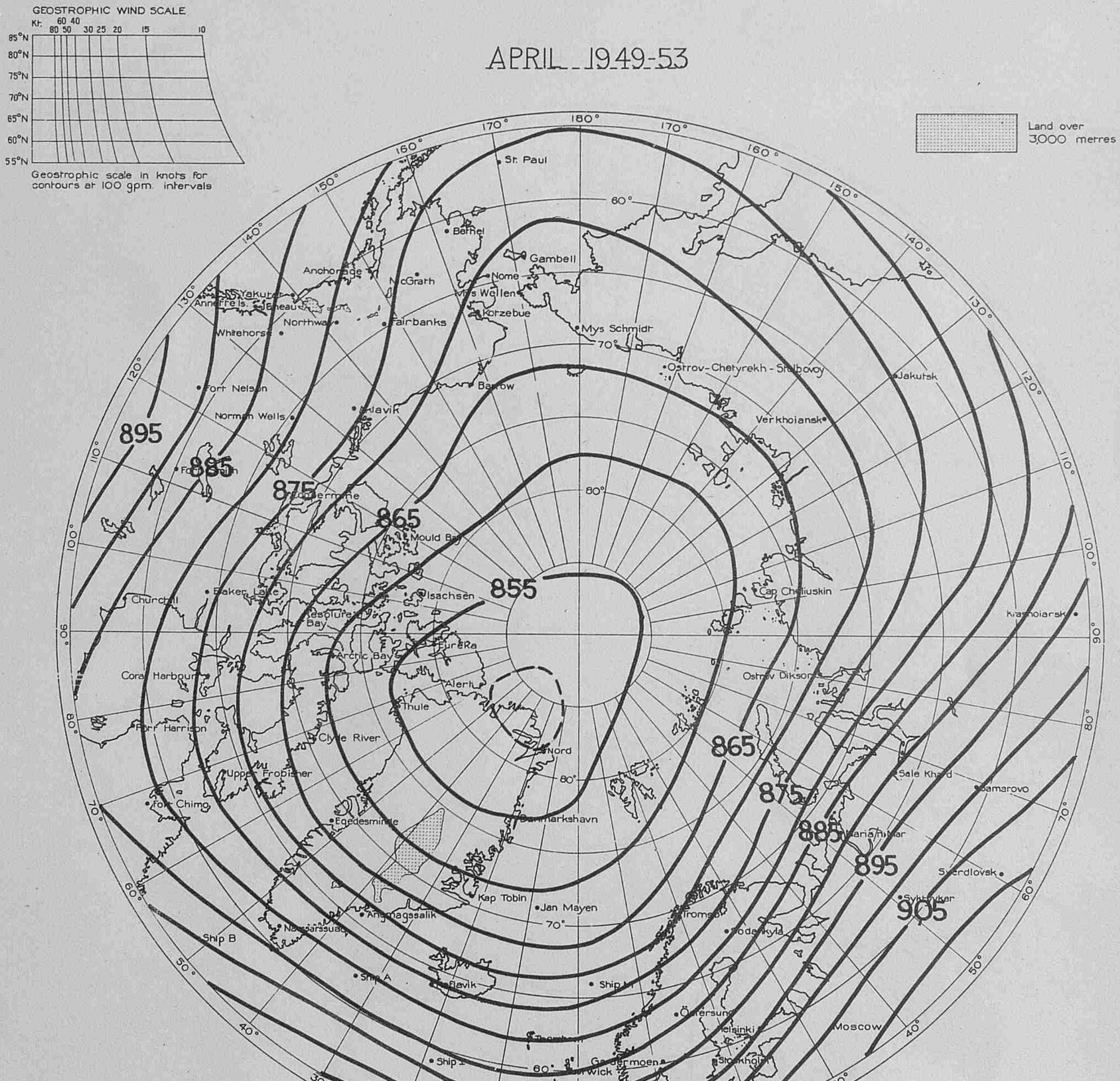
GEOSTROPHIC WIND SCALE
Kt. 60 40
80 50 30 25 20 15 10
85°N
80°N
75°N
70°N
65°N
60°N
55°N
Geostrophic scale in knots for contours at 100 gpm. intervals
Land over 3,000 metres
855
865
875
885
895
905
180°
170°
160°
150°
140°
130°
120°
110°
100°
90°
80°
70°
60°
50°
40°
30°
20°
10°W
0°
10°E
St. Paul
Bethel
Gambell
Nome
Mys Wellen
Kotzebue
Mys Schmidt
McGrath
Anchorage
Fairbanks
Northway
Yakutat
Annette Is.
Juneau
Whitehorse
Fort Nelson
Norman Wells
Aklavik
Barrow
Fort Smith
Coppermine
Mould Bay
Isachsen
Resolute Bay
Eureka
Arctic Bay
Alert
Thule
Baker Lake
Churchill
Coral Harbour
Port Harrison
Clyde River
Upper Frobisher
Fort Chimo
Egedesminde
Nord
Danmarkshavn
Angmagssalik
Narsarssuaq
Kap Tobin
Jan Mayen
Ship B
Ship A
Ship M
Ship I
Keflavik
Thorshavn
Stornoway
Leuchars
Gardermoen
Sola
Copenhagen
Orebro
Stockholm
Helsinki
Ostersund
Tromso
Sodankyla
Moscow
Syktyvkar
Sverdlovsk
Salehard
Samarovo
Narian Mar
Ostrov Dikson
Cap Cheliuskin
Krasnoiarsk
Verkhoiansk
Jakutsk
Ostrov-Chetyrekh-Stolbovoy
60°
70°
80°

Height in dekametres

Upper Air Branch (M.O.23)

M.R.P. 1020

AVERAGE 300-200 mb. THICKNESS

APRIL 1949-53

GEOSTROPHIC WIND SCALE

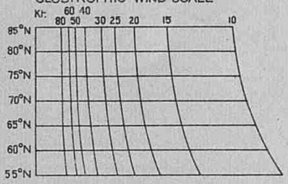

Geostrophic scale in knots for contours at 100 gpm. intervals

▨ Land over 3,000 metres

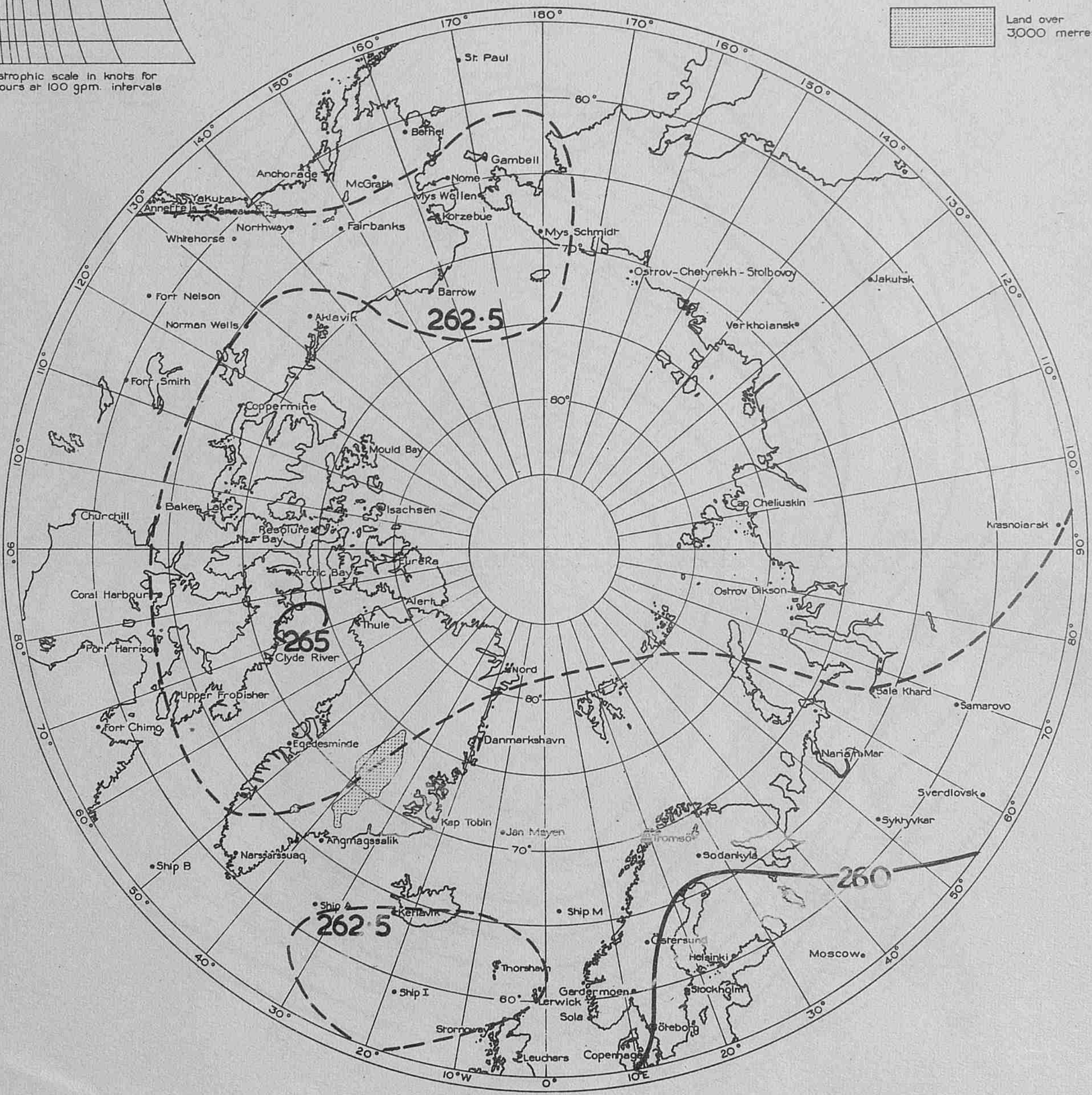
180°
170°
160°
150°
140°
130°
120°
110°
100°
90°
80°
70°
60°
50°
40°
30°
20°
10°W
0°
10°E
60°
70°
80°
262·5
265
262·5
260
St. Paul
Bethel
Gambell
Nome
Mys Wellen
Kotzebue
Mys Schmidt
Anchorage
McGrath
Yakutat
Annette Is.
Northway
Fairbanks
Whitehorse
Barrow
Ostrov-Chetyrekh-Stolbovoy
Jakutsk
Fort Nelson
Norman Wells
Aklavik
Verkhoiansk
Fort Smith
Coppermine
Mould Bay
Cap Cheliuskin
Churchill
Baker Lake
Isachsen
Resolute Bay
Krasnoiarsk
Eureka
Arctic Bay
Ostrov Dikson
Coral Harbour
Alert
Thule
Clyde River
Fort Harrison
Nord
Sale Khard
Samarovo
Upper Frobisher
Fort Chimo
Egedesminde
Danmarkshavn
Narian Mar
Sverdlovsk
Sykhyvkar
Kap Tobin
Jan Mayen
Tromsø
Sodankyla
Angmagssalik
Narssarssuaq
Ship B
Ship A
Keflavik
Ship M
Ostersund
Helsinki
Moscow
Thorshavn
Ship I
Gardermoen
Lerwick
Sola
Stockholm
Stornoway
Göteborg
Leuchars
Copenhagen

Height in dekametres

Upper Air Branch (M.O.23)

AVERAGE 200 mb. CONTOURS

APRIL 1949-53

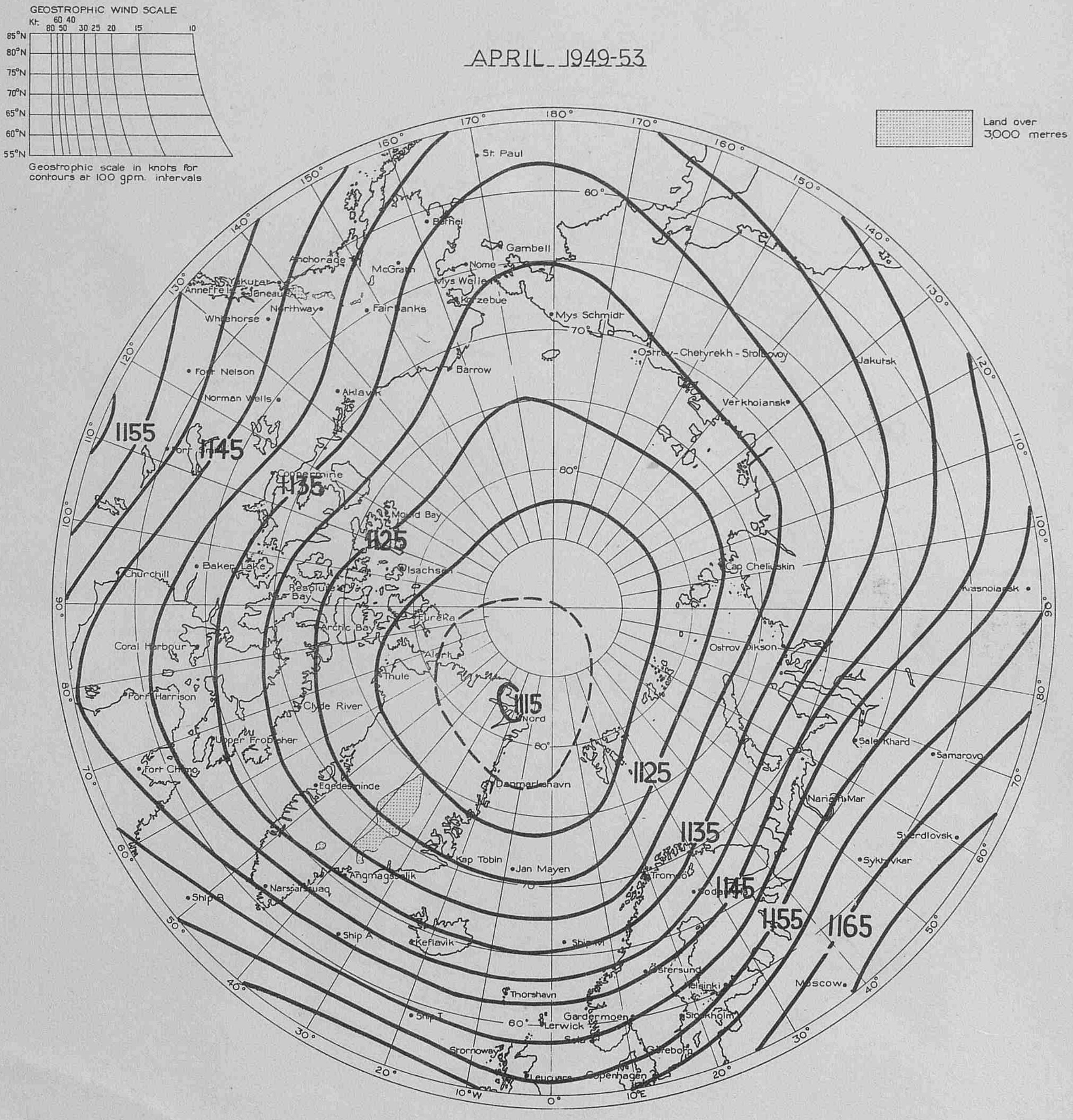
GEOSTROPHIC WIND SCALE
Kt. 80 60 50 40 30 25 20 15 10
85°N
80°N
75°N
70°N
65°N
60°N
55°N
Geostrophic scale in knots for contours at 100 gpm. intervals
Land over 3,000 metres
1155
1145
1135
1125
1115
1165
180°
170°
160°
150°
140°
130°
120°
110°
100°
90°
80°
70°
60°
50°
40°
30°
20°
10°W
0°
10°E
St. Paul
Bethel
Gambell
Nome
McGrath
Anchorage
Yakutat
Annette Is.
Juneau
Northway
Fairbanks
Whitehorse
Mys Wellen
Kotzebue
Mys Schmidt
Barrow
Ostrov-Chetyrekh-Stolbovoy
Jakutsk
Verkhoiansk
Fort Nelson
Norman Wells
Aklavik
Fort Smith
Coppermine
Mould Bay
Isachsen
Cap Cheliuskin
Krasnoiarsk
Churchill
Baker Lake
Resolute Bay
Eureka
Arctic Bay
Alert
Ostrov Dikson
Coral Harbour
Thule
Nord
Port Harrison
Clyde River
Upper Frobisher
Fort Chimo
Egedesminde
Danmarkshavn
Sale Khard
Samarovo
Narian Mar
Sverdlovsk
Syktyvkar
Kap Tobin
Jan Mayen
Angmagssalik
Narssarssuaq
Tromsø
Bodø
Ship B
Ship A
Keflavik
Ship M
Östersund
Helsinki
Moscow
Thorshavn
Ship I
Gardermoen
Lerwick
Sola
Stockholm
Stornoway
Göteborg
Leuchars
Copenhagen

Height in dekametres

Upper Air Branch (M.O.23)

AVERAGE 200-150mb. THICKNESS

APRIL 1949-53

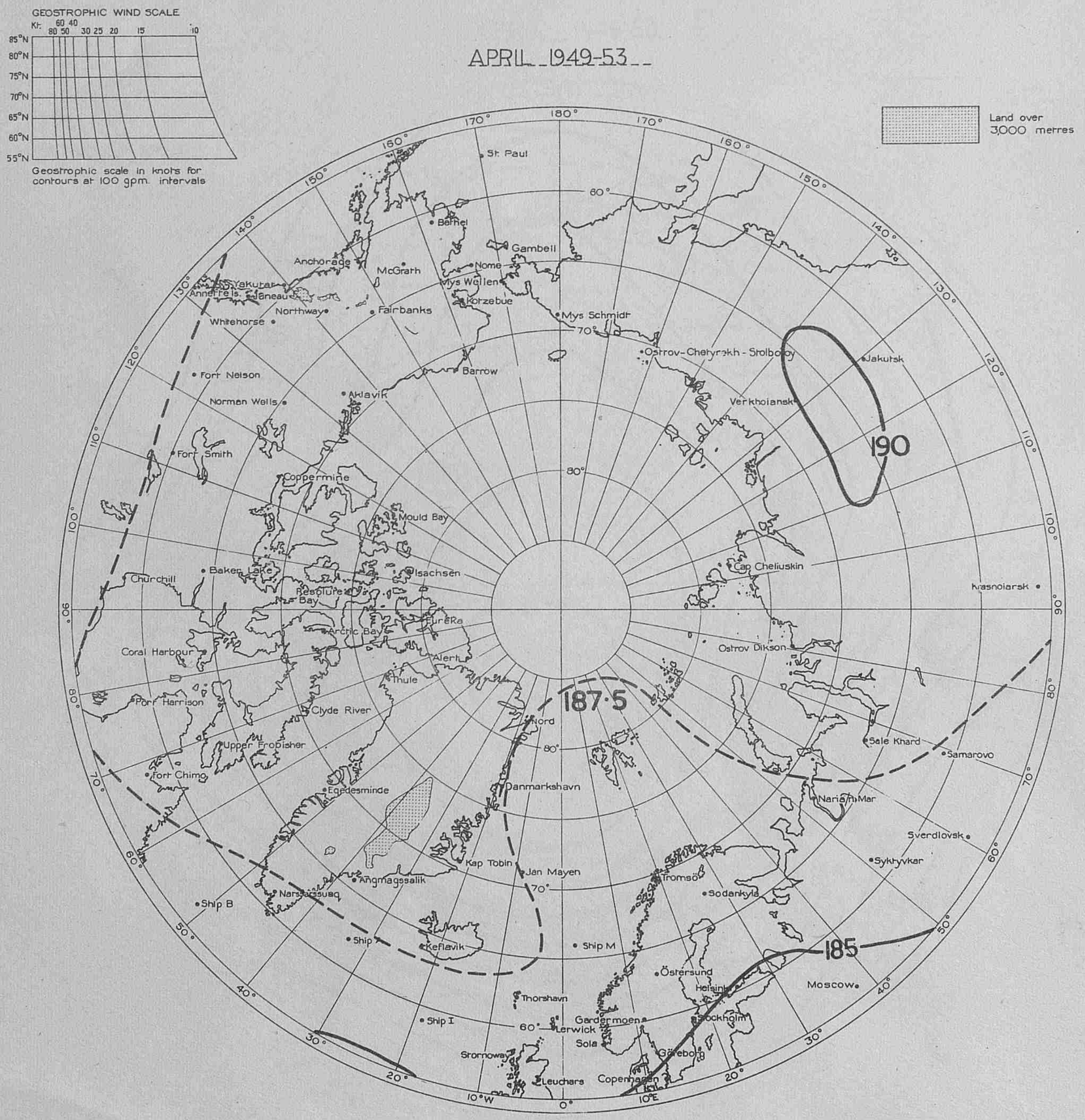
GEOSTROPHIC WIND SCALE
Kt. 80 60 50 40 30 25 20 15 10
85°N
80°N
75°N
70°N
65°N
60°N
55°N
Geostrophic scale in knots for contours at 100 gpm. intervals
Land over 3,000 metres
190
187·5
185
180°
170°
160°
150°
140°
130°
120°
110°
100°
90°
80°
70°
60°
50°
40°
30°
20°
10°W
0°
10°E
St. Paul
Bethel
Gambell
Nome
Mys Wellen
Kotzebue
Mys Schmidt
Anchorage
McGrath
Fairbanks
Yakutat
Annette Is.
Juneau
Northway
Whitehorse
Barrow
Ostrov-Chetyrekh-Stolbovoy
Jakutsk
Verkhoiansk
Fort Nelson
Norman Wells
Aklavik
Fort Smith
Coppermine
Mould Bay
Isachsen
Baker Lake
Churchill
Resolute Bay
Eureka
Arctic Bay
Alert
Thule
Coral Harbour
Fort Harrison
Clyde River
Upper Frobisher
Fort Chimo
Egedesminde
Nord
Danmarkshavn
Cap Cheliuskin
Krasnoiarsk
Ostrov Dikson
Sale Khard
Samarovo
Narian Mar
Sverdlovsk
Sykryvkar
Kap Tobin
Jan Mayen
Angmagssalik
Narssarssuaq
Ship B
Ship A
Keflavik
Ship M
Tromsö
Sodankyla
Östersund
Helsinki
Stockholm
Moscow
Thorshavn
Ship I
Lerwick
Gardermoen
Sola
Göteborg
Stornoway
Leuchars
Copenhagen

Height in dekametres

Upper Air Branch (M.O.23)

AVERAGE 150 mb. CONTOURS

APRIL 1949-53

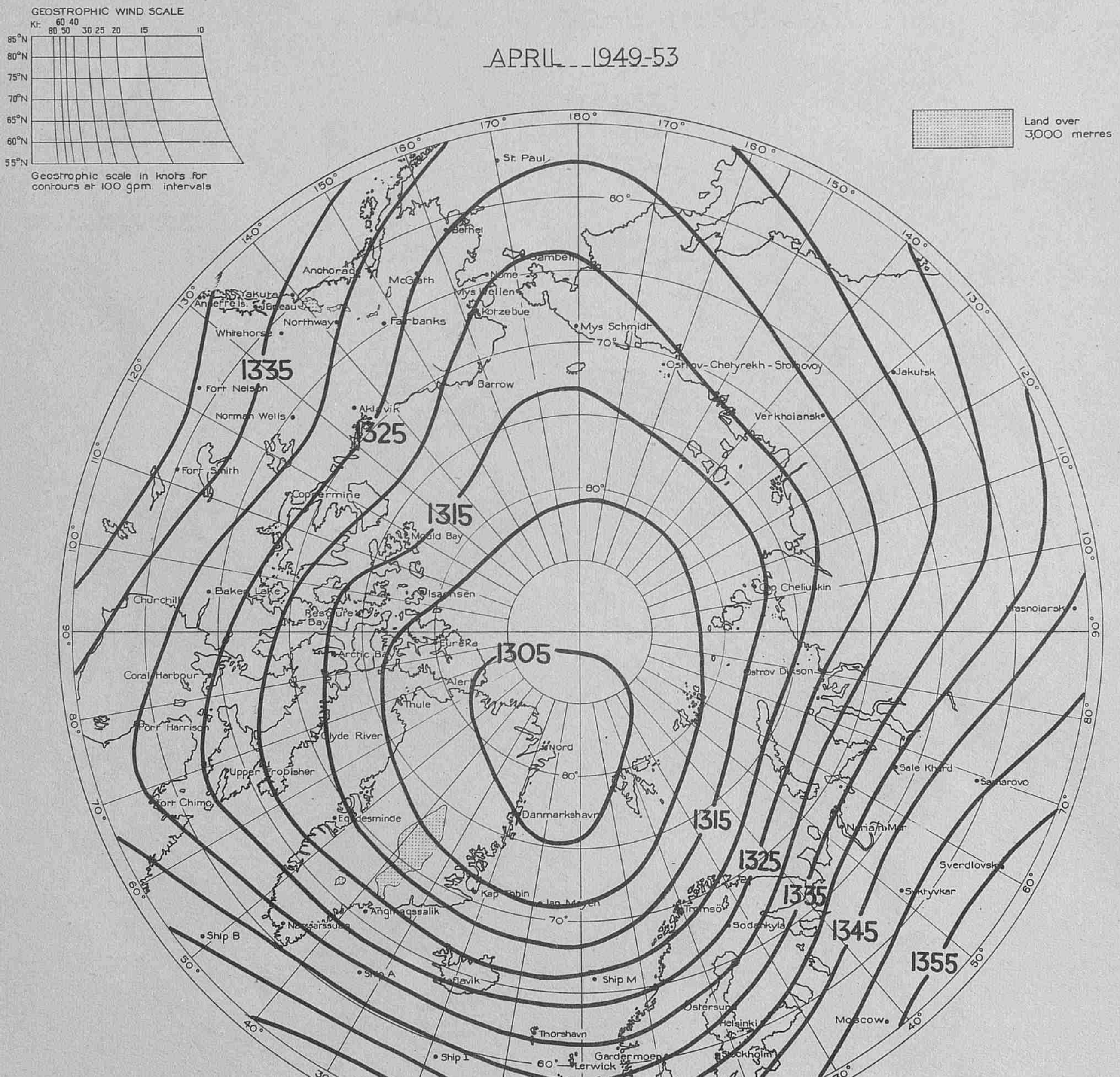
GEOSTROPHIC WIND SCALE
Kt. 60 40
80 50 30 25 20 15 10
85°N
80°N
75°N
70°N
65°N
60°N
55°N
Geostrophic scale in knots for contours at 100 gpm. intervals
Land over 3000 metres
180°
170°
160°
150°
140°
130°
120°
110°
100°
90°
80°
70°
60°
50°
40°
30°
20°
10°W
0°
10°E
1305
1315
1325
1335
1345
1355
St. Paul
Bethel
Anchorage
McGrath
Gambell
Nome
Mys Wellen
Kotzebue
Yakutat
Annette Is.
Juneau
Northway
Fairbanks
Whitehorse
Mys Schmidt
Ostrov-Chetyrekh-Stolbovoy
Jakutsk
Barrow
Fort Nelson
Aklavik
Norman Wells
Verkhoiansk
Fort Smith
Coppermine
Mould Bay
Isachsen
Cap Cheliuskin
Krasnoiarsk
Churchill
Baker Lake
Resolute Bay
Eureka
Arctic Bay
Alert
Ostrov Dikson
Coral Harbour
Thule
Port Harrison
Clyde River
Nord
Sale Khard
Samarovo
Upper Frobisher
Fort Chimo
Egedesminde
Danmarkshavn
Narian Mar
Sverdlovsk
Syktyvkar
Kap Tobin
Jan Mayen
Tromsö
Angmagssalik
Narssarssuak
Sodankylä
Ship B
Ship A
Keflavik
Ship M
Östersund
Helsinki
Moscow
Thorshavn
Ship I
Gardermoen
Lerwick
Stockholm
Sola
Göteborg
Stornoway
Leuchars
Copenhagen

Height in dekametres

Upper Air Branch (M.O.23)

M.R.P. 1020

AVERAGE 150-100mb. THICKNESS

APRIL 1949-53

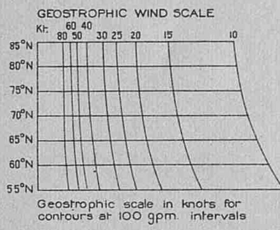

Geostrophic scale in knots for contours at 100 gpm. intervals

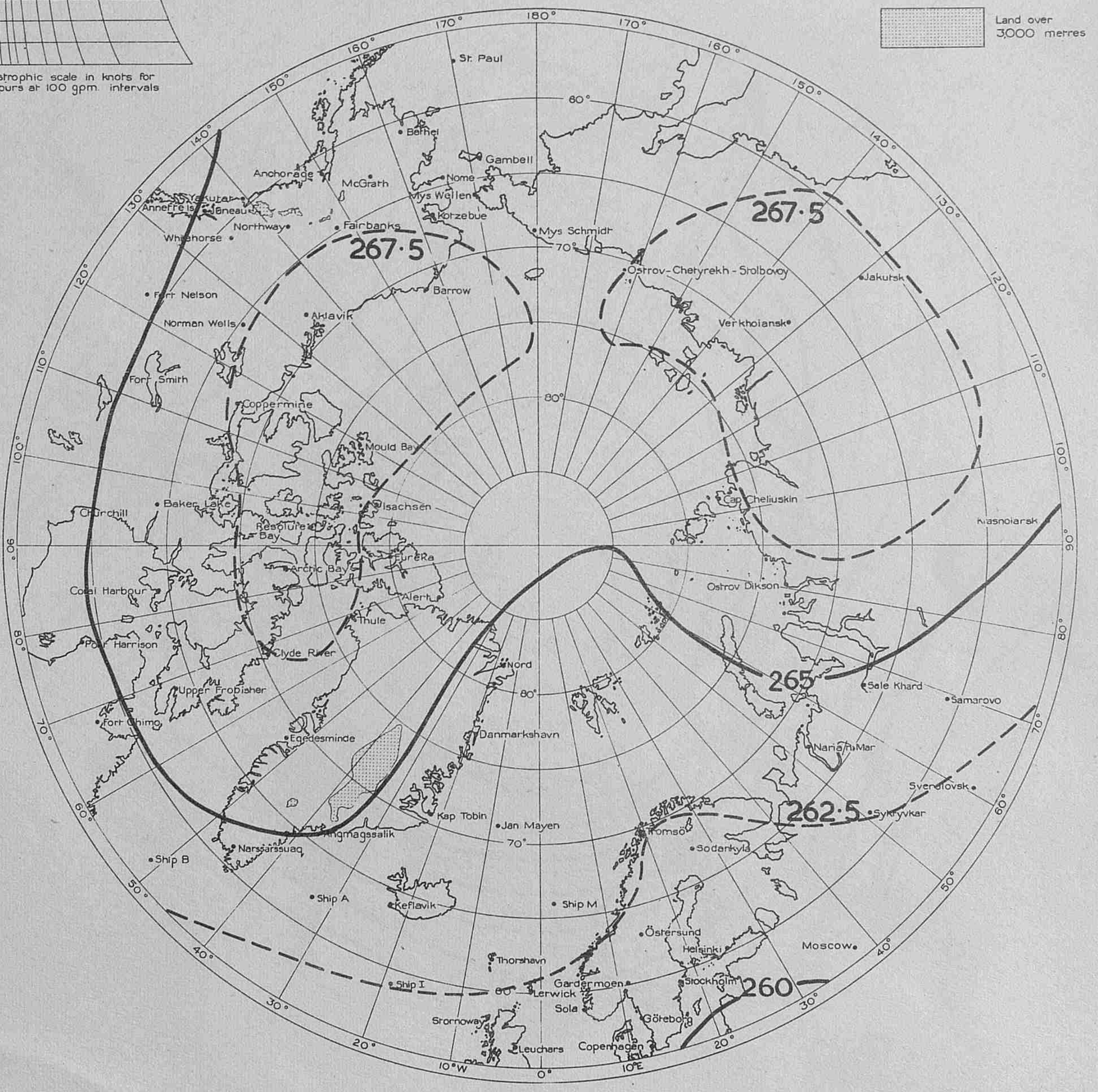
Land over 3,000 metres
267·5
267·5
265
262·5
260
180°
170°
160°
150°
140°
130°
120°
110°
100°
90°
80°
70°
60°
50°
40°
30°
20°
10°W
0°
10°E
60°
70°
80°
St. Paul
Bethel
Gambell
Nome
Mys Wellen
Kotzebue
Anchorage
McGrath
Yakutat
Annette Is.
Juneau
Northway
Fairbanks
Whitehorse
Mys Schmidt
Barrow
Aklavik
Fort Nelson
Norman Wells
Fort Smith
Coppermine
Mould Bay
Isachsen
Churchill
Baker Lake
Resolute Bay
Arctic Bay
Eureka
Alert
Thule
Coral Harbour
Port Harrison
Clyde River
Upper Frobisher
Fort Chimo
Egedesminde
Nord
Danmarkshavn
Narssarssuaq
Angmagssalik
Kap Tobin
Jan Mayen
Ship B
Ship A
Keflavik
Ship M
Thorshavn
Ship I
Stornoway
Lerwick
Gardermoen
Sola
Leuchars
Copenhagen
Göteborg
Stockholm
Östersund
Helsinki
Moscow
Tromsö
Sodankylä
Sykyvkar
Sverdlovsk
Naryan Mar
Samarovo
Sale Khard
Ostrov Dikson
Krasnoiarsk
Cap Cheliuskin
Verkhoiansk
Jakutsk
Ostrov-Chetyrekh-Stolbovoy

Height in dekametres

Upper Air Branch (M.O.23)

AVERAGE 100 mb. CONTOURS

APRIL 1949-53

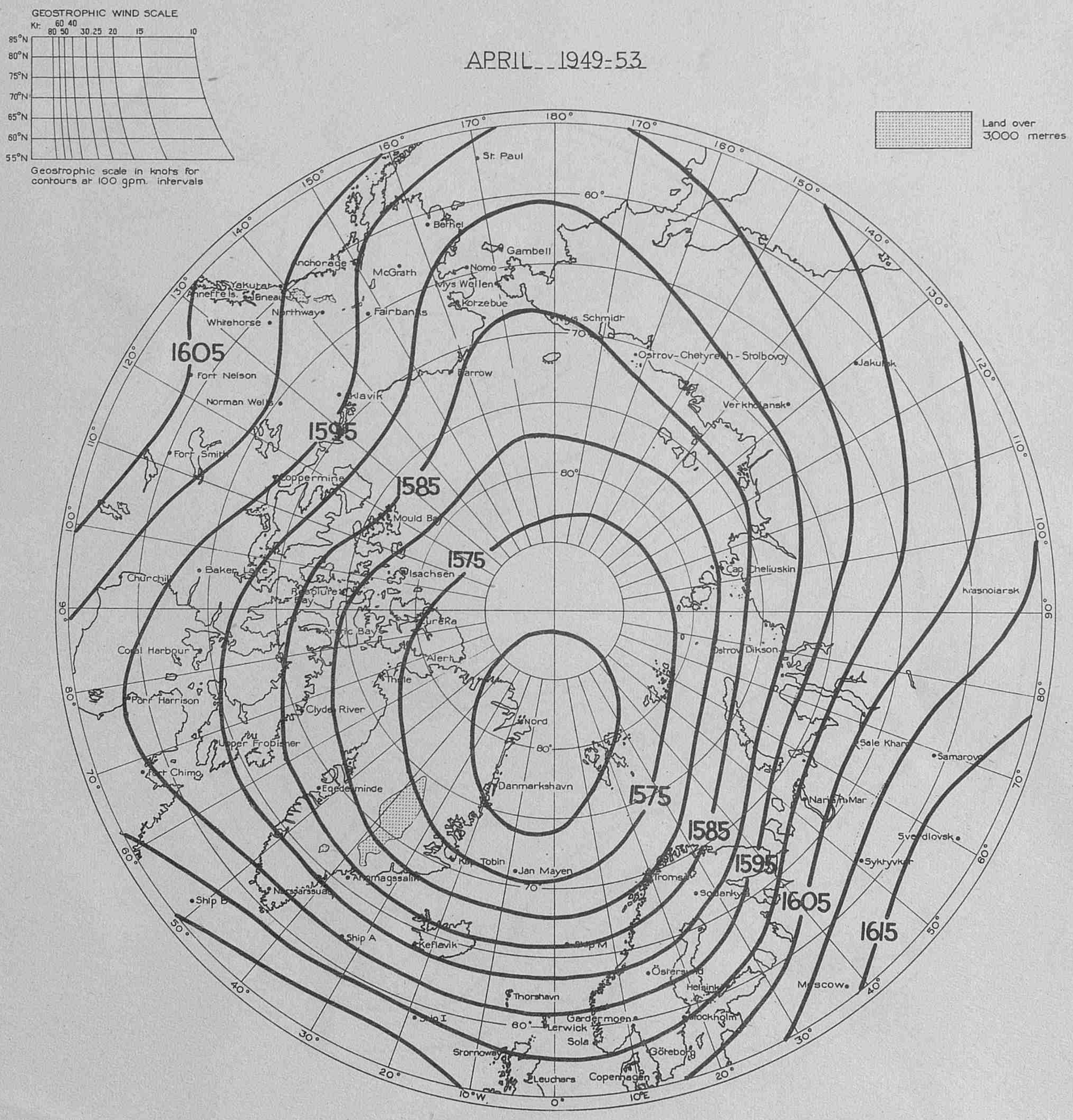
GEOSTROPHIC WIND SCALE
Kt. 80 60 50 40 30 25 20 15 10
85°N
80°N
75°N
70°N
65°N
60°N
55°N
Geostrophic scale in knots for contours at 100 gpm. intervals
Land over 3,000 metres
180°
170°
160°
150°
140°
130°
120°
110°
100°
90°
80°
70°
60°
50°
40°
30°
20°
10°W.
0°
10°E
1605
1595
1585
1575
1575
1585
1595
1605
1615
St. Paul
Bethel
Gambell
Nome
Mys Wellen
Kotzebue
McGrath
Anchorage
Yakutat
Annette Is.
Juneau
Northway
Fairbanks
Whitehorse
Mys Schmidt
Ostrov-Chetyrekh-Stolbovoy
Jakutsk
Verkhoyansk
Barrow
Aklavik
Fort Nelson
Norman Wells
Fort Smith
Coppermine
Mould Bay
Isachsen
Resolute Bay
Eureka
Arctic Bay
Alert
Thule
Baker Lake
Churchill
Coral Harbour
Port Harrison
Clyde River
Upper Frobisher
Fort Chimo
Egedesminde
Nord
Danmarkshavn
Cap Cheliuskin
Krasnoiarsk
Ostrov Dikson
Sale Khard
Samarovo
Narian Mar
Sverdlovsk
Sykryvkar
Moscow
Tromsø
Sodankylä
Jan Mayen
Kap Tobin
Angmagssalik
Narssarssuaq
Ship B
Ship A
Keflavik
Ship M
Östersund
Helsinki
Thorshavn
Ship I
Lerwick
Gardermoen
Stockholm
Sola
Stornoway
Göteborg
Leuchars
Copenhagen

Height in dekametres

Upper Air Branch (M.O.23)

AVERAGE 700 mb. CONTOURS

OCTOBER 1949-53

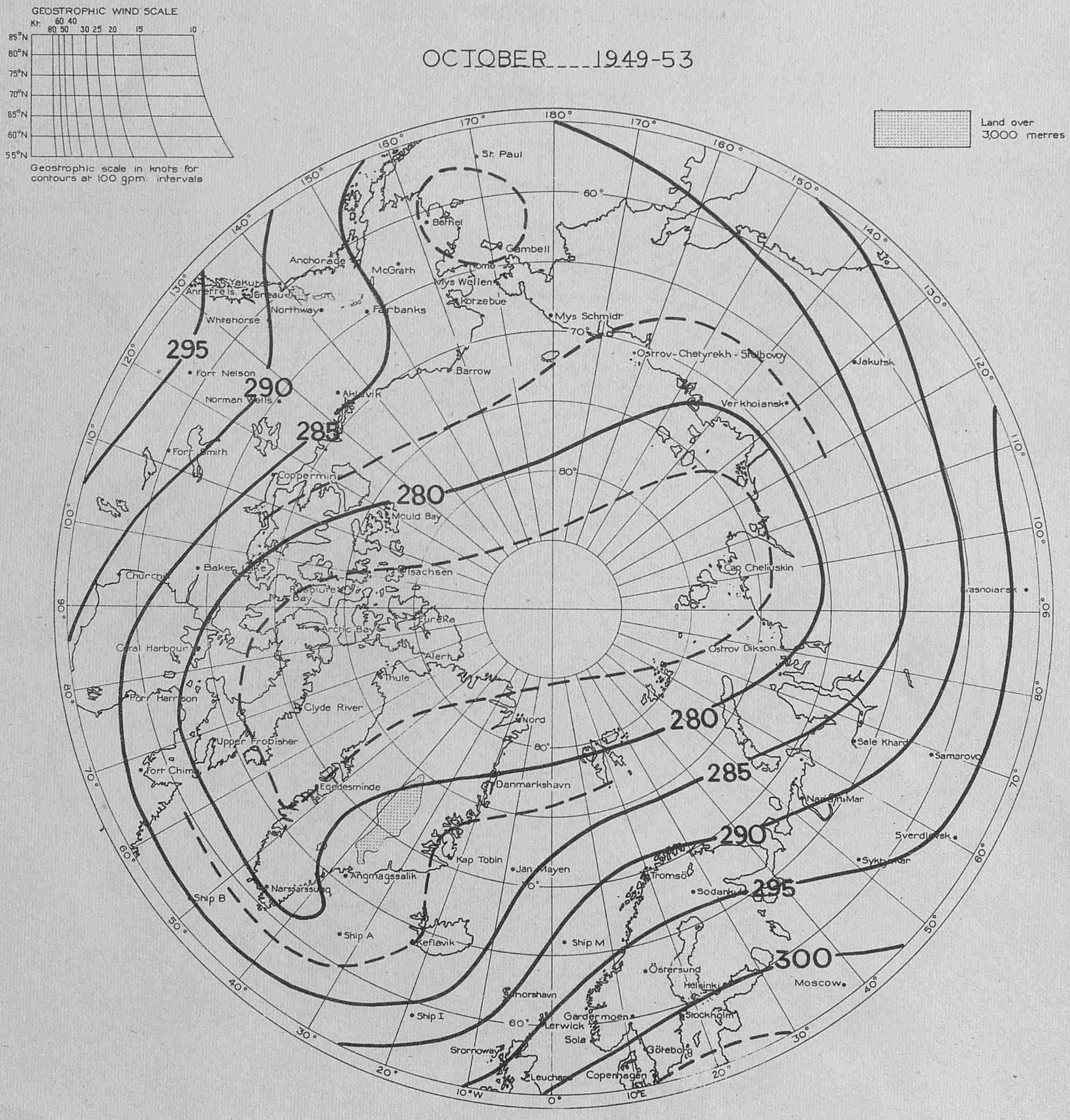
GEOSTROPHIC WIND SCALE
Kt. 60 40
80 50 30 25 20 15 10
85°N
80°N
75°N
70°N
65°N
60°N
55°N
Geostrophic scale in knots for contours at 100 gpm. intervals
Land over 3,000 metres
295
290
285
280
280
285
290
295
300
180°
170°
160°
150°
140°
130°
120°
110°
100°
90°
80°
70°
60°
50°
40°
30°
20°
10°W
0°
10°E
St. Paul
Bethel
Gambell
Nome
Mys Wellen
Kotzebue
McGrath
Anchorage
Fairbanks
Northway
Yakutat
Annette Is.
Juneau
Whitehorse
Fort Nelson
Norman Wells
Aklavik
Fort Smith
Coppermine
Barrow
Mys Schmidt
Ostrov-Chetyrekh-Stolbovoy
Verkhoiansk
Jakutsk
Mould Bay
Isachsen
Resolute Bay
Eureka
Arctic Bay
Alert
Thule
Baker Lake
Churchill
Coral Harbour
Port Harrison
Clyde River
Upper Frobisher
Fort Chimo
Egedesminde
Nord
Danmarkshavn
Cap Cheliuskin
Ostrov Dikson
Krasnoiarsk
Sale Khard
Samarovo
Narjan Mar
Sverdlovsk
Sykhyvkar
Kap Tobin
Jan Mayen
Angmagssalik
Narssarssuaq
Ship B
Ship A
Keflavik
Tromsö
Sodanky
Ship M
Östersund
Helsinki
Moscow
Thorshavn
Ship I
Gardermoen
Lerwick
Sola
Stockholm
Göteborg
Stornoway
Leuchars
Copenhagen

Height in dekametres

Upper Air Branch (M.O.23)

700-500 mb. THICKNESS

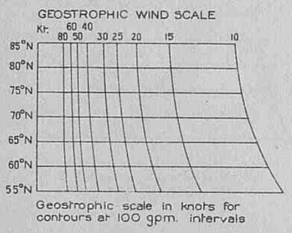

Geostrophic scale in knots for contours at 100 gpm. intervals

OCTOBER 1949-53

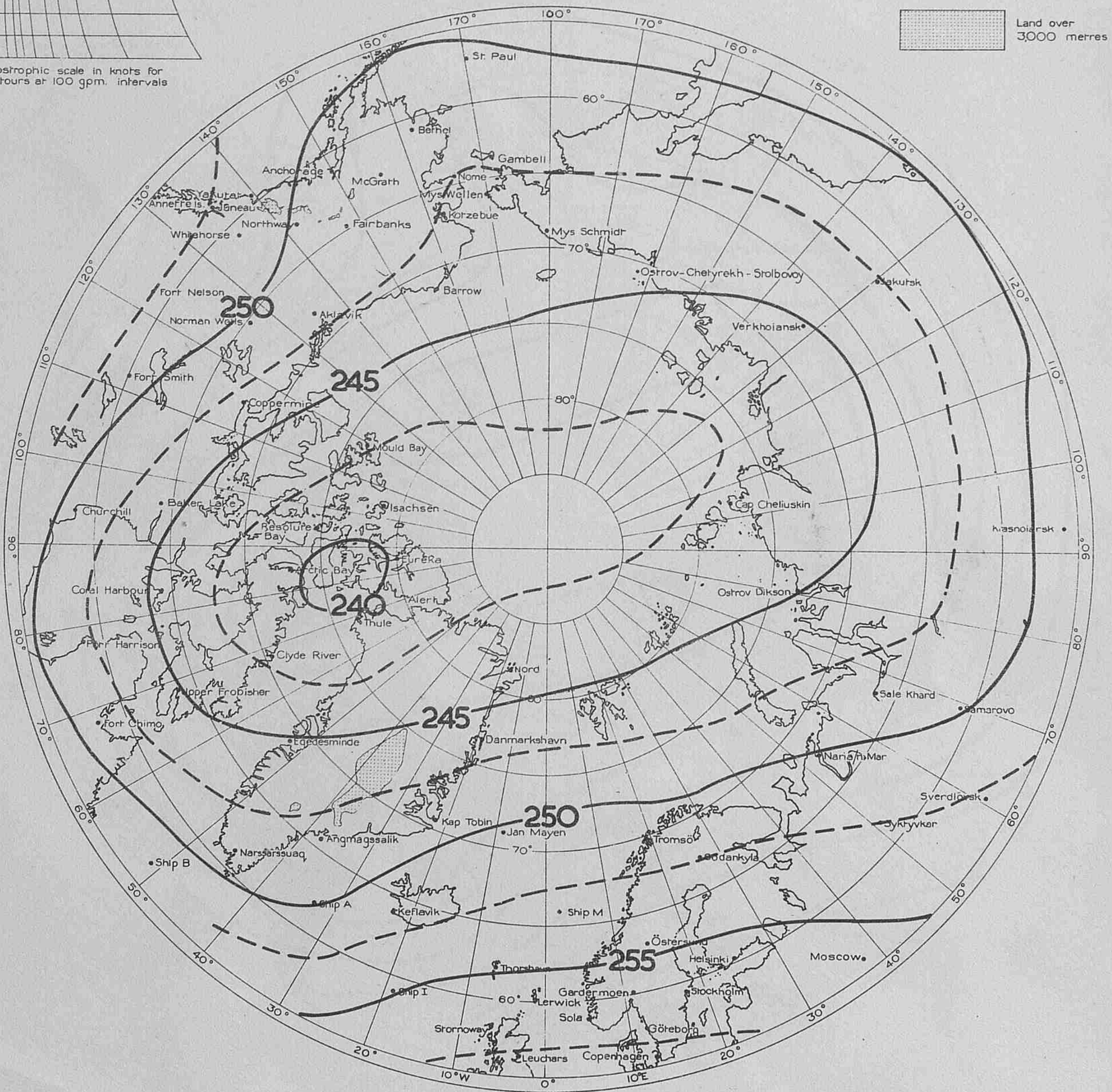
Land over 3,000 metres
250
245
240
245
250
255
St. Paul
Bethel
Gambell
Anchorage
McGrath
Nome
Mys Wellen
Kotzebue
Yakutat
Annette Is.
Juneau
Northway
Fairbanks
Whitehorse
Mys Schmidt
Ostrov-Chetyrekh-Stolbovoy
Jakutsk
Barrow
Fort Nelson
Norman Wells
Aklavik
Verkhoiansk
Fort Smith
Coppermine
Mould Bay
Isachsen
Cap Cheliuskin
Churchill
Baker Lake
Resolute Bay
Eureka
Krasnoiarsk
Arctic Bay
Coral Harbour
Alert
Thule
Ostrov Dikson
Port Harrison
Clyde River
Nord
Upper Frobisher
Sale Khard
Samarovo
Fort Chimo
Egedesminde
Danmarkshavn
Narian Mar
Sverdlovsk
Kap Tobin
Jan Mayen
Syktyvkar
Tromsø
Sodankyla
Narssarssuaq
Angmagssalik
Ship B
Ship A
Keflavik
Ship M
Östersund
Moscow
Thorshavn
Helsinki
Ship I
Gardermoen
Lerwick
Stockholm
Sola
Stornoway
Göteborg
Leuchars
Copenhagen
60°
70°
80°
170°
160°
150°
140°
130°
120°
110°
100°
90°
80°
70°
60°
50°
40°
30°
20°
10°W
0°
10°E

Height in dekametres

Upper Air Branch (M.O.23)

AVERAGE 500 mb. CONTOURS

OCTOBER 1949-53

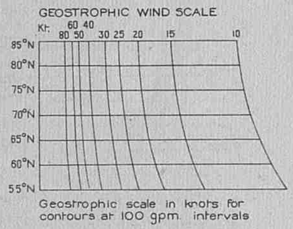

Geostrophic scale in knots for contours at 100 gpm. intervals

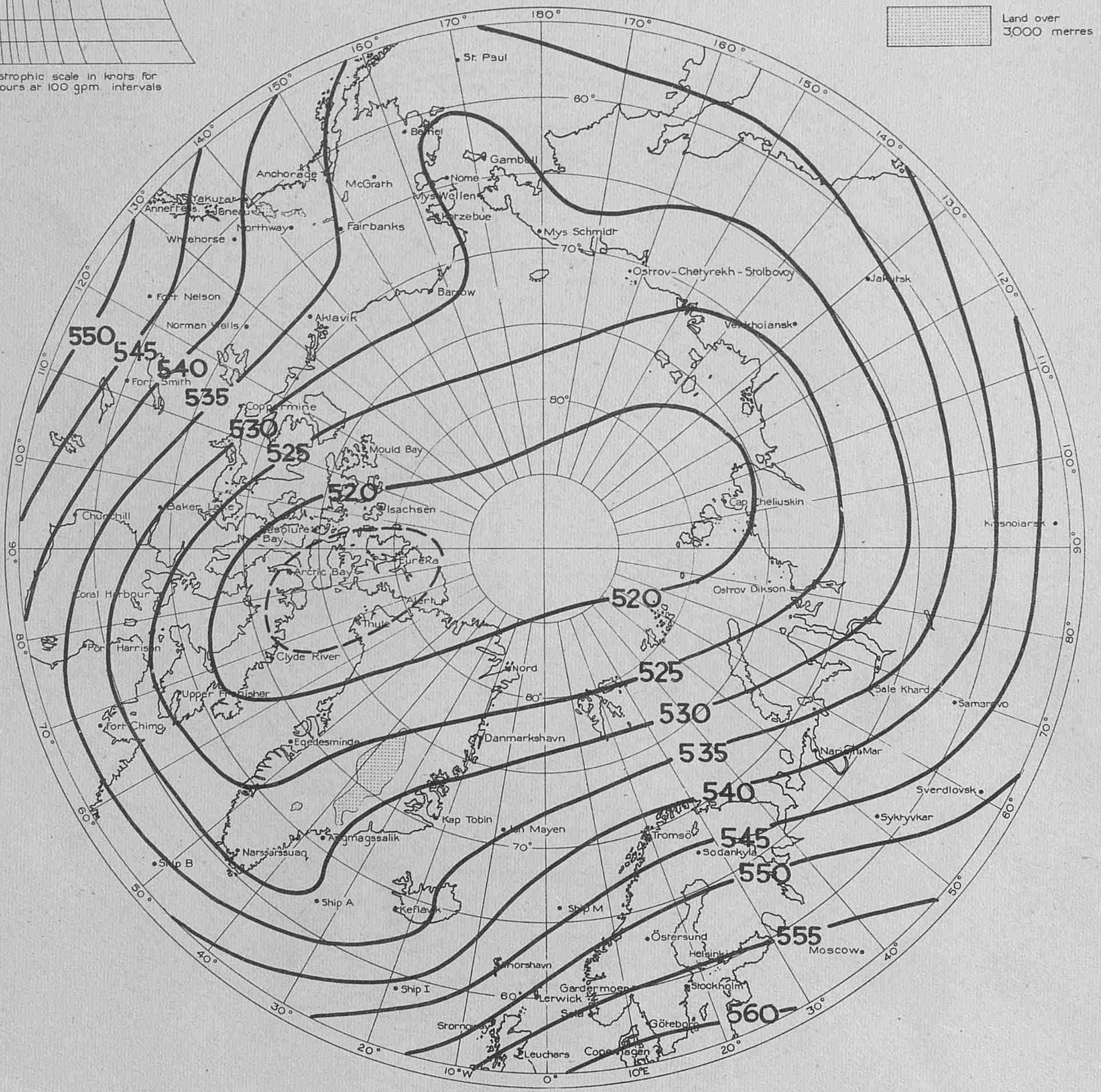
Land over 3,000 metres
180°
170°
170°
160°
160°
150°
150°
140°
140°
130°
130°
120°
120°
110°
110°
100°
100°
90°
90°
80°
80°
70°
70°
60°
60°
50°
50°
40°
40°
30°
30°
20°
20°
10°W
0°
10°E
80°
70°
60°
St. Paul
Bethel
Gambell
Nome
Mys Wellen
Kotzebue
Anchorage
McGrath
Fairbanks
Yakutat
Annette
Juneau
Northway
Whitehorse
Mys Schmidt
Ostrov-Chetyrekh-Stolbovoy
Jakutsk
Barrow
Verkhoiansk
Fort Nelson
Norman Wells
Aklavik
Fort Smith
Coppermine
Mould Bay
Isachsen
Resolute Bay
Eureka
Arctic Bay
Alert
Thule
Clyde River
Baker Lake
Churchill
Cap Cheliuskin
Krasnoiarsk
Ostrov Dikson
Coral Harbour
Port Harrison
Upper Frobisher
Fort Chimo
Egedesminde
Nord
Danmarkshavn
Sale Khard
Samarovo
Narian Mar
Sverdlovsk
Sykhyvkar
Kap Tobin
Jan Mayen
Angmagssalik
Narssarssuaq
Ship B
Ship A
Keflavik
Ship M
Tromsö
Sodankylä
Östersund
Helsinki
Moscow
Thorshavn
Ship I
Gardermoen
Lerwick
Sola
Stockholm
Stornoway
Göteborg
Leuchars
Copenhagen
550
545
540
535
530
525
520
520
525
530
535
540
545
550
555
560

Height in dekametres

Upper Air Branch (M.O.23)

500-300 mb. THICKNESS

OCTOBER 1949-53

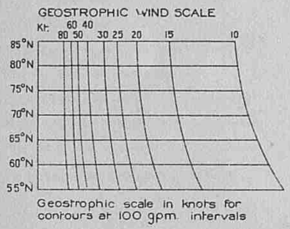

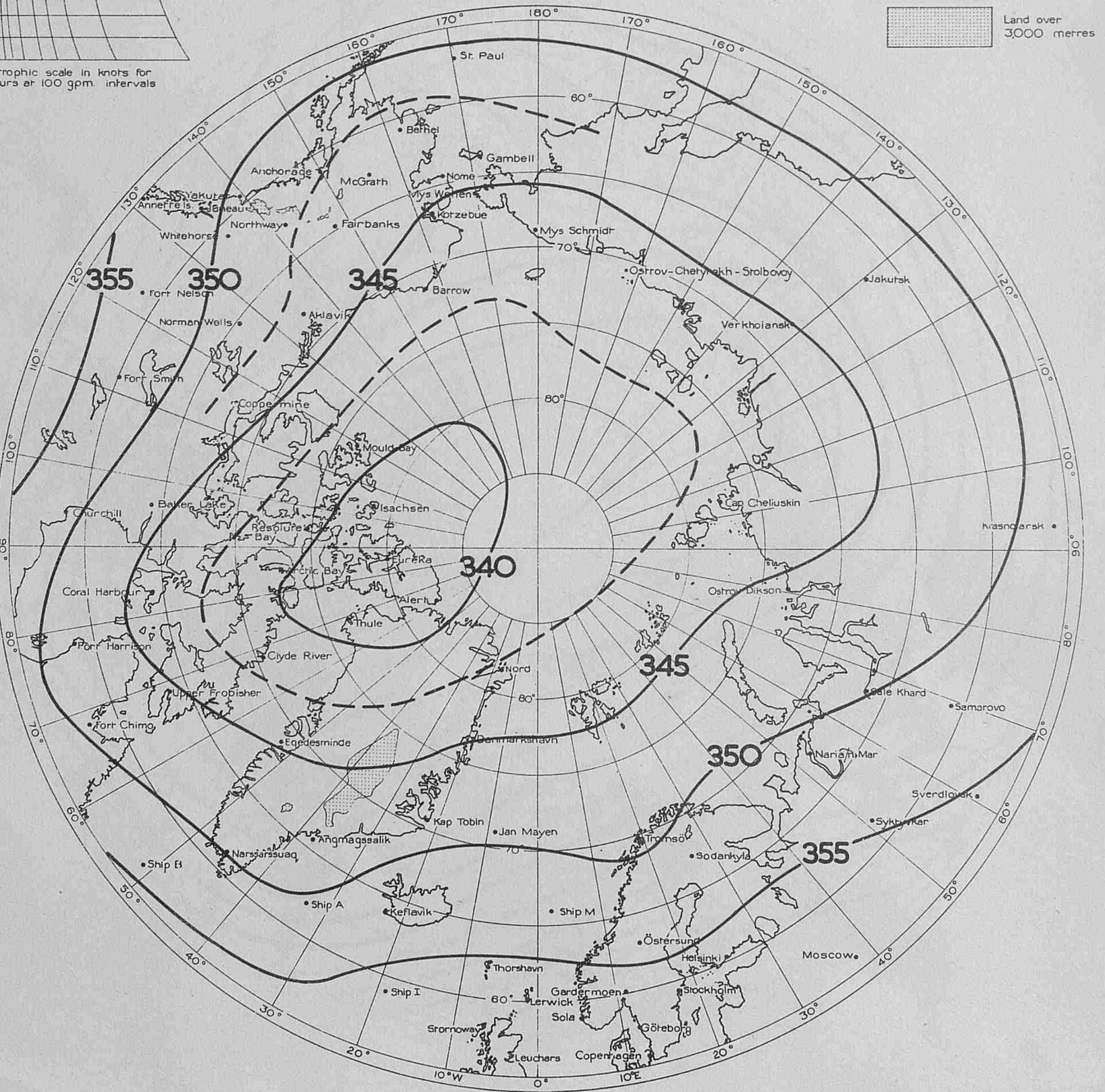
Land over 3,000 metres
180°
170°
160°
150°
140°
130°
120°
110°
100°
90°
80°
70°
60°
50°
40°
30°
20°
10°W
0°
10°E
60°
70°
80°
355
350
345
340
St. Paul
Bethel
Gambell
Anchorage
McGrath
Nome
Mys Wellen
Kotzebue
Yakutat
Annette Is.
Juneau
Northway
Fairbanks
Whitehorse
Mys Schmidt
Ostrov-Chetyrekh-Stolbovoy
Jakutsk
Barrow
Fort Nelson
Aklavik
Norman Wells
Verkhoiansk
Fort Smith
Coppermine
Mould Bay
Isachsen
Cap Cheliuskin
Baker Lake
Churchill
Resolute Bay
Eureka
Arctic Bay
Alert
Thule
Krasnoiarsk
Ostrov Dikson
Coral Harbour
Port Harrison
Clyde River
Nord
Upper Frobisher
Sale Khard
Samarovo
Fort Chimo
Egedesminde
Danmarkshavn
Narian Mar
Sverdlovsk
Syktyvkar
Kap Tobin
Jan Mayen
Tromsö
Sodankylä
Angmagssalik
Narssarssuaq
Ship B
Ship A
Keflavik
Ship M
Östersund
Helsinki
Moscow
Thorshavn
Ship I
Gardermoen
Lerwick
Sola
Stockholm
Stornoway
Göteborg
Leuchars
Copenhagen

Height in dekametres

Upper Air Branch (M.O.23)

AVERAGE 300 mb. CONTOURS

OCTOBER 1949 – 53

GEOSTROPHIC WIND SCALE

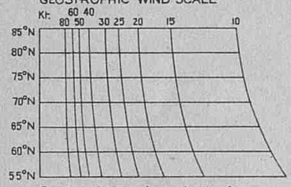

Geostrophic scale in knots for contours at 100 gpm. intervals

▨ Land over 3,000 metres

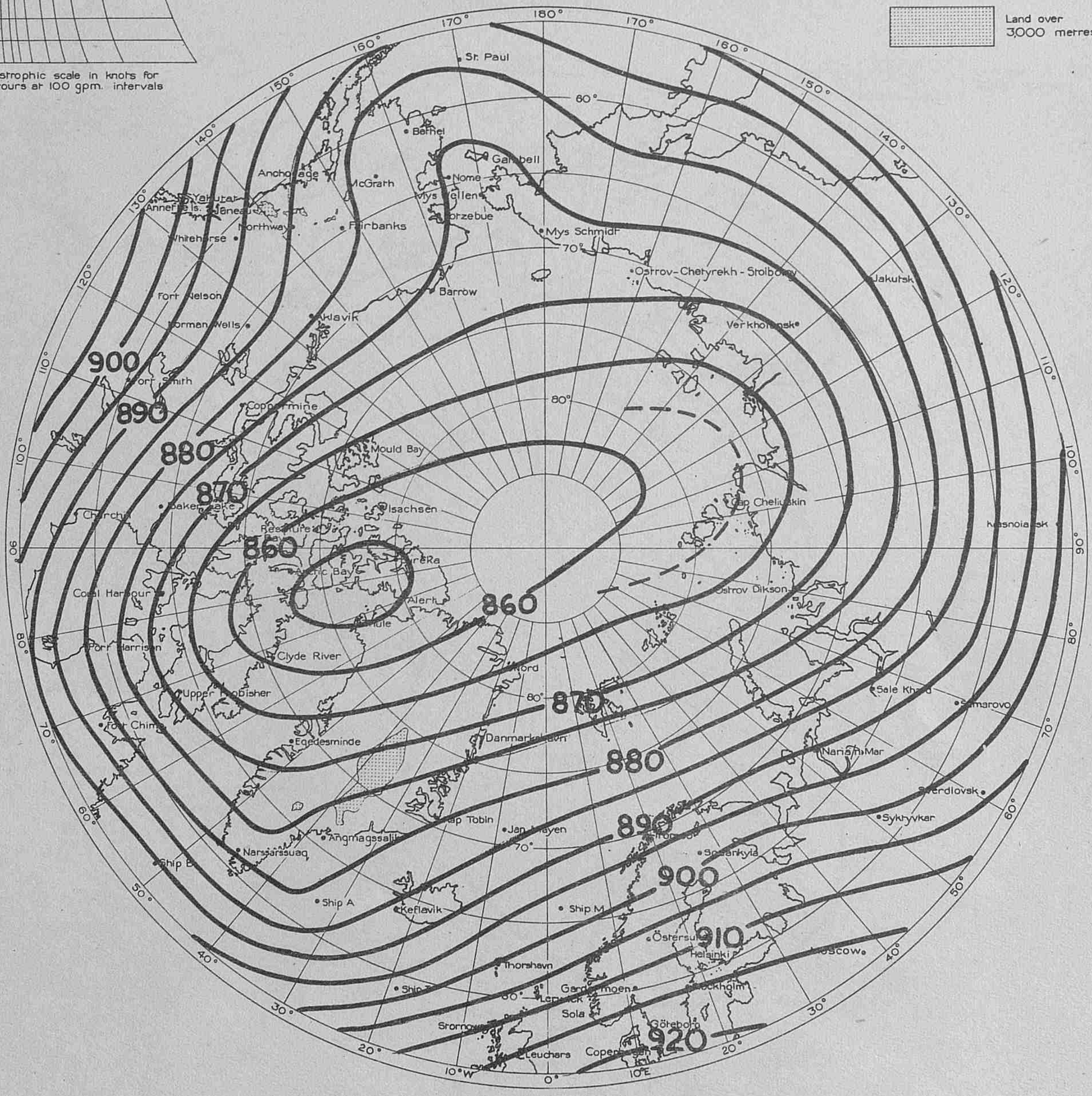
900
890
880
870
860
860
870
880
890
900
910
920
180°
170°
160°
150°
140°
130°
120°
110°
100°
90°
80°
70°
60°
50°
40°
30°
20°
10°W
0°
10°E
80°
70°
60°
St. Paul
Bethel
Gambell
Nome
Mys Wellen
Kotzebue
McGrath
Anchorage
Fairbanks
Yakutat
Annette Is.
Juneau
Northway
Whitehorse
Fort Nelson
Norman Wells
Fort Smith
Aklavik
Barrow
Mys Schmidt
Ostrov-Chetyrekh-Stolbovoy
Jakutsk
Verkhoyansk
Coppermine
Mould Bay
Isachsen
Resolute
Eureka
Alert
Thule
Baker Lake
Churchill
Coral Harbour
Port Harrison
Clyde River
Upper Frobisher
Fort Chimo
Egedesminde
Danmarkshavn
Nord
Cap Chelyuskin
Ostrov Dikson
Krasnoiarsk
Sale Khard
Samarovo
Nar'yan Mar
Sverdlovsk
Syktyvkar
Sodankyla
Östersund
Helsinki
Moscow
Stockholm
Gardermoen
Lerwick
Sola
Thorshavn
Göteborg
Copenhagen
Leuchars
Stornoway
Ship I
Ship M
Ship A
Ship B
Keflavik
Jan Mayen
Cap Tobin
Angmagssalik
Narssarssuaq

Height in dekametres

Upper Air Branch (M.O.23)

M.R.P. 1020

300-200 mb. THICKNESS

OCTOBER 1949-53

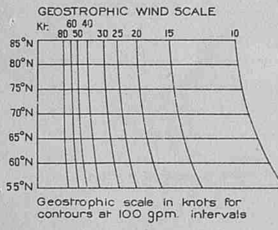

Geostrophic scale in knots for contours at 100 gpm. intervals

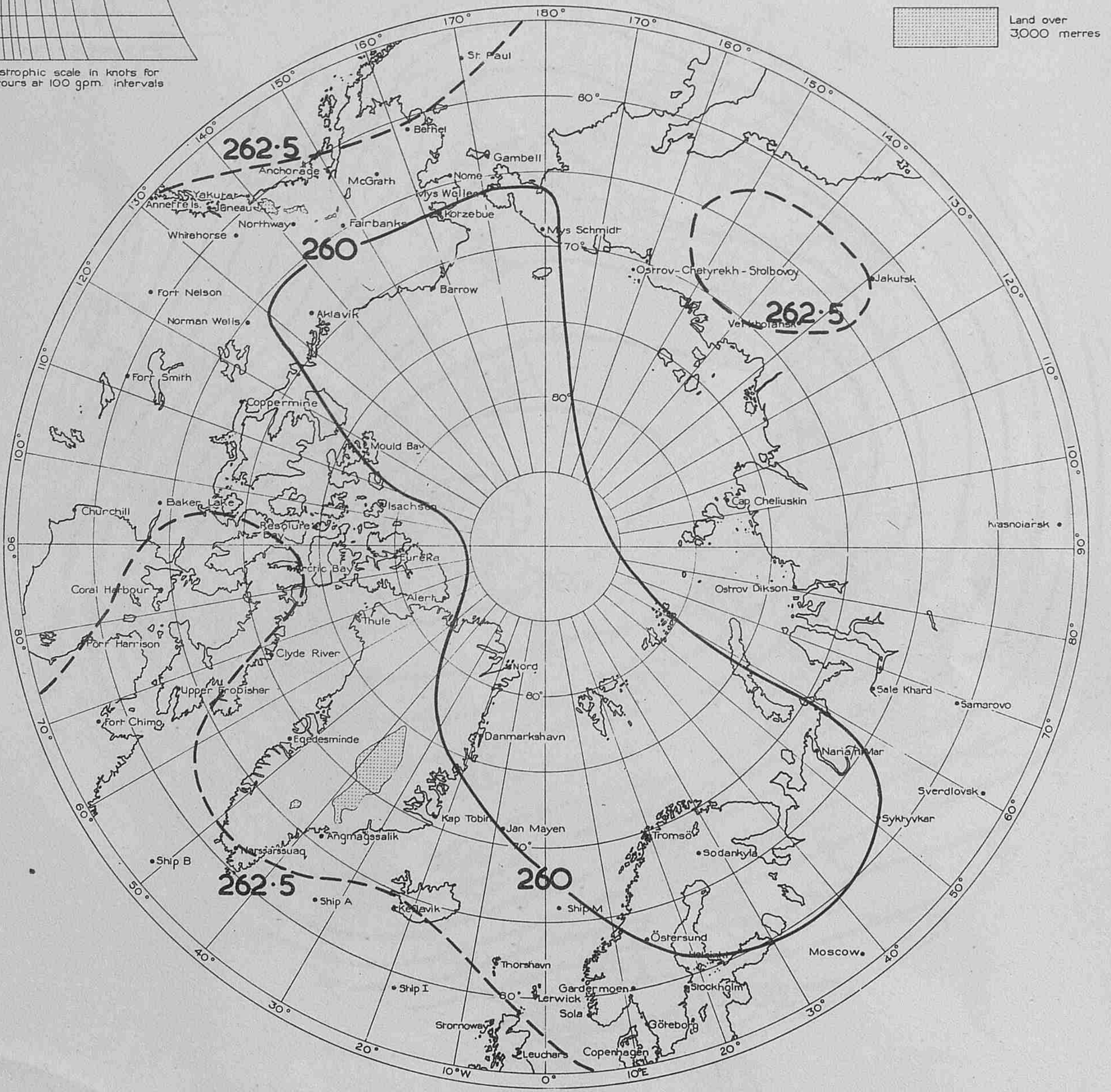
Land over 3,000 metres
262·5
260
262·5
262·5
260
180°
170°
160°
150°
140°
130°
120°
110°
100°
90°
80°
70°
60°
50°
40°
30°
20°
10°W
0°
10°E
60°
70°
80°
St. Paul
Bethel
Gambell
Nome
McGrath
Mys Wellen
Korzebue
Anchorage
Yakutat
Annette Is.
Juneau
Northway
Fairbanks
Whitehorse
Mys Schmidt
Ostrov-Chetyrekh-Stolbovoy
Jakutsk
Verkhoiansk
Barrow
Fort Nelson
Norman Wells
Aklavik
Fort Smith
Coppermine
Mould Bay
Isachsen
Cap Cheliuskin
Krasnoiarsk
Churchill
Baker Lake
Resolute Bay
Eureka
Arctic Bay
Alert
Ostrov Dikson
Coral Harbour
Thule
Port Harrison
Clyde River
Nord
Sale Khard
Samarovo
Upper Frobisher
Fort Chimo
Egedesminde
Danmarkshavn
Narian Mar
Sverdlovsk
Sykhyvkar
Kap Tobin
Jan Mayen
Angmagssalik
Tromsö
Sodankyla
Narssarssuaq
Ship B
Ship A
Keflavik
Ship M
Östersund
Helsinki
Moscow
Thorshavn
Ship I
Lerwick
Gardermoen
Stockholm
Sola
Stornoway
Göteborg
Leuchars
Copenhagen

Height in dekametres

Upper Air Branch (M.O.23)

AVERAGE 200 mb. CONTOURS

OCTOBER 1949-53

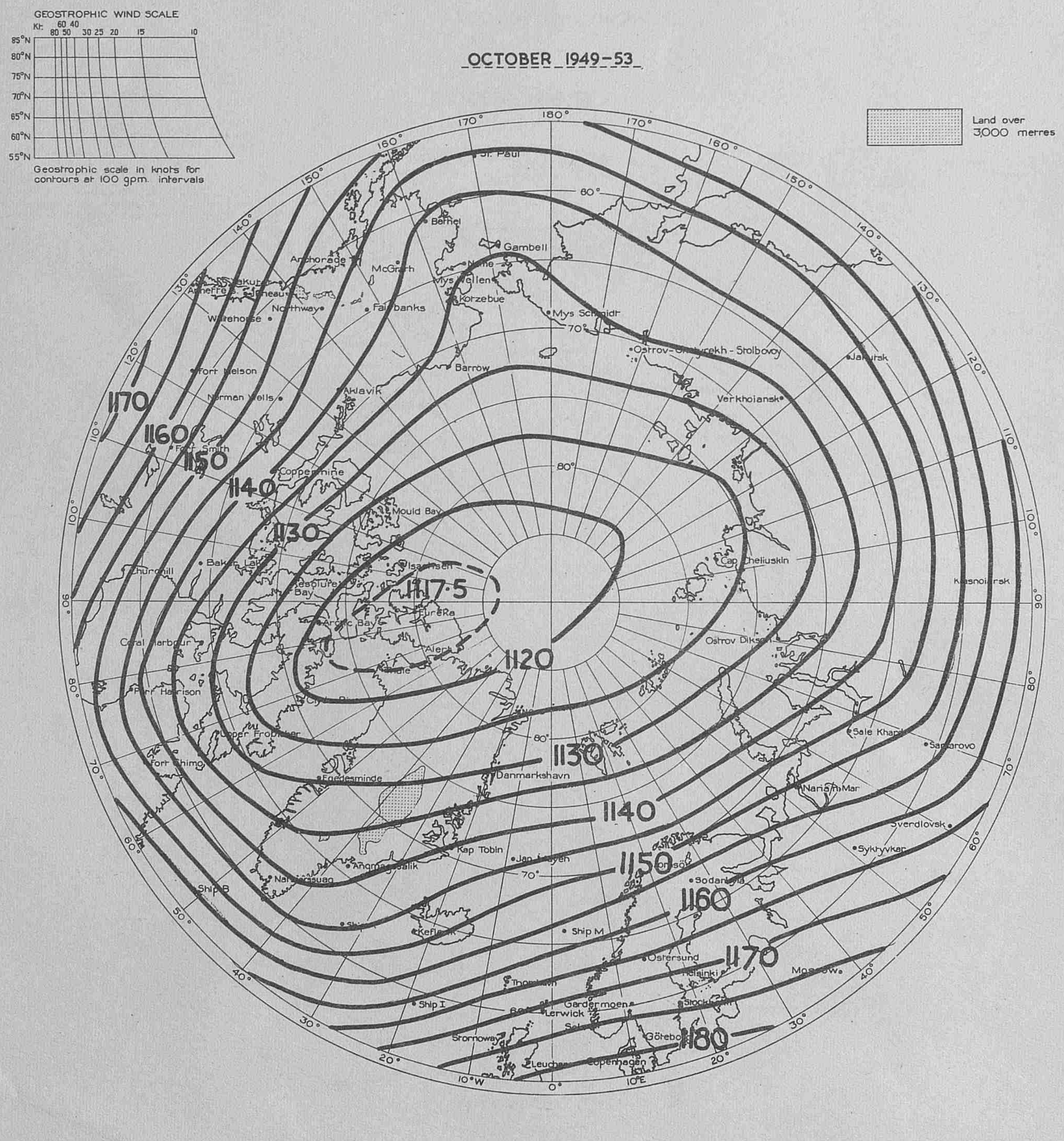
GEOSTROPHIC WIND SCALE
Kt. 80 60 50 40 30 25 20 15 10
85°N
80°N
75°N
70°N
65°N
60°N
55°N
Geostrophic scale in knots for contours at 100 gpm. intervals
Land over 3,000 metres
1117·5
1120
1130
1140
1150
1160
1170
1180
180°
170°
160°
150°
140°
130°
120°
110°
100°
90°
80°
70°
60°
50°
40°
30°
20°
10°W
0°
10°E
St. Paul
Bethel
Gambell
Anchorage
McGrath
Nome
Mys Wellen
Kotzebue
Fairbanks
Yakutat
Annette
Juneau
Northway
Whitehorse
Mys Schmidt
Ostrov-Chetyrekh-Stolbovoy
Jakutsk
Barrow
Fort Nelson
Aklavik
Norman Wells
Verkhoiansk
Fort Smith
Coppermine
Mould Bay
Isachsen
Resolute Bay
Eureka
Arctic Bay
Alert
Thule
Clyde
Cap Cheliuskin
Krasnoiarsk
Baker Lake
Churchill
Coral Harbour
Ostrov Dikson
Port Harrison
Upper Frobisher
Fort Chimo
Sale Khard
Saharovo
Danmarkshavn
Faeringehavn
Narsarssuaq
Angmagssalik
Kap Tobin
Jan Mayen
Naryan Mar
Sverdlovsk
Sykhyvkar
Bodø
Sodankyla
Ship B
Ship
Keflavik
Ship M
Ostersund
Helsinki
Moscow
Thorshavn
Ship I
Gardermoen
Lerwick
Stockholm
Stornoway
Göteborg
Leuchars
Copenhagen

Height in dekametres

Upper Air Branch (M.O.23)

200-150 mb. THICKNESS

OCTOBER 1949-53

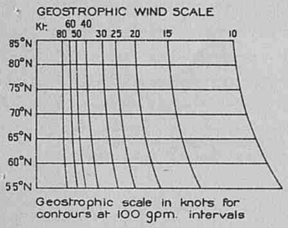

▨ Land over 3,000 metres

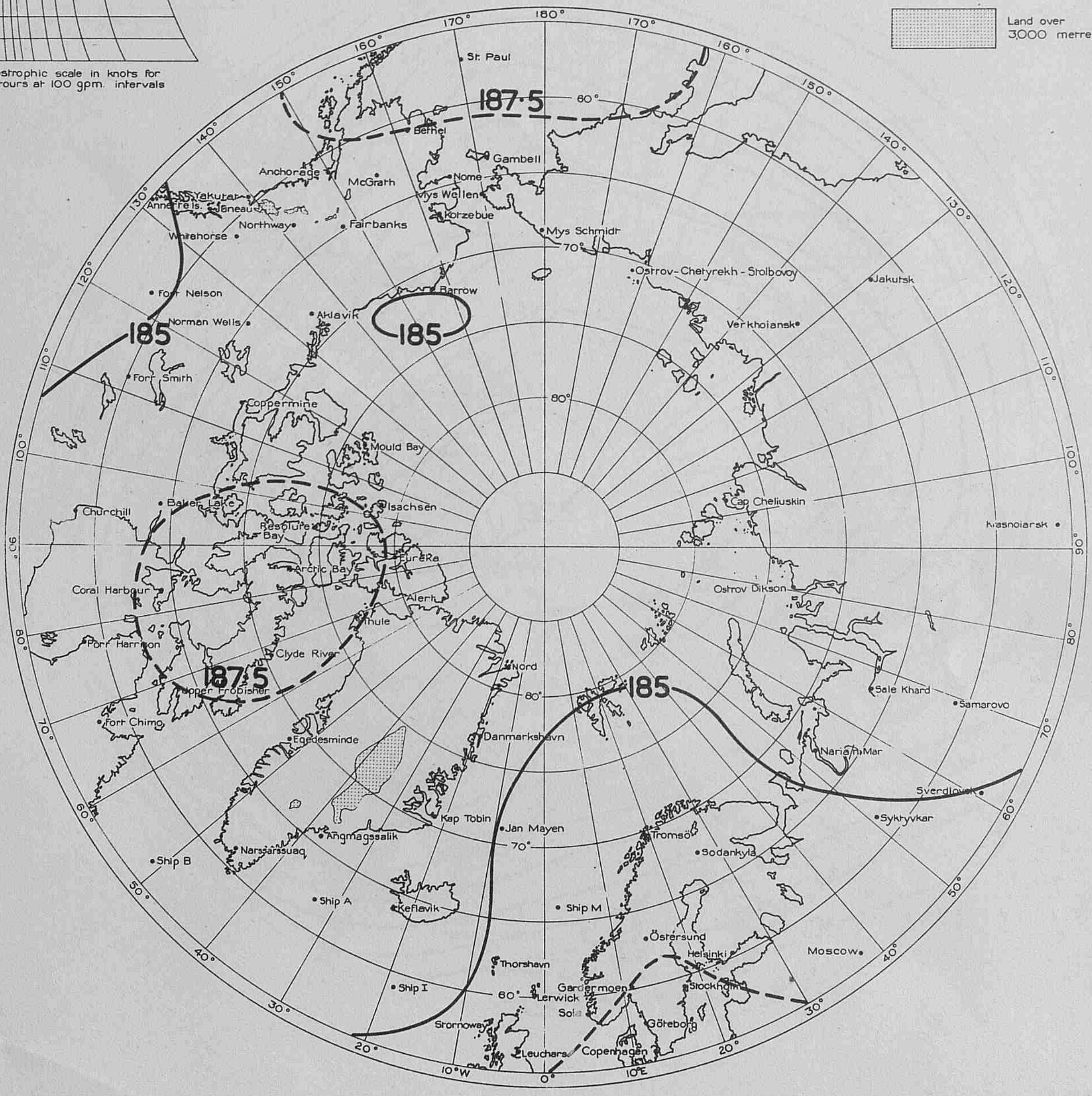
180°
170°
160°
150°
140°
130°
120°
110°
100°
90°
80°
70°
60°
50°
40°
30°
20°
10°W
0°
10°E
80°
70°
60°
187·5
185
185
185
187·5
185
St. Paul
Bethel
Gambell
Anchorage
McGrath
Nome
Mys Wellen
Kotzebue
Yakutat
Annette Is.
Juneau
Northway
Fairbanks
Whitehorse
Mys Schmidt
Ostrov-Chetyrekh-Stolbovoy
Jakutsk
Barrow
Fort Nelson
Aklavik
Norman Wells
Verkhoiansk
Fort Smith
Coppermine
Mould Bay
Cap Cheliuskin
Baker Lake
Isachsen
Churchill
Resolute Bay
Eureka
Krasnoiarsk
Arctic Bay
Coral Harbour
Ostrov Dikson
Alert
Thule
Port Harrison
Clyde River
Nord
Upper Frobisher
Sale Khard
Samarovo
Fort Chimo
Egedesminde
Danmarkshavn
Narian Mar
Sverdlovsk
Kap Tobin
Jan Mayen
Syktyvkar
Tromsö
Angmagssalik
Narssarssuaq
Sodankylä
Ship B
Ship A
Keflavik
Ship M
Östersund
Moscow
Helsinki
Thorshavn
Stockholm
Ship I
Gardermoen
Lerwick
Sola
Stornoway
Göteborg
Leuchars
Copenhagen

Height in dekametres

Upper Air Branch (M.O.23)

AVERAGE 150 mb. CONTOURS

OCTOBER 1949-53

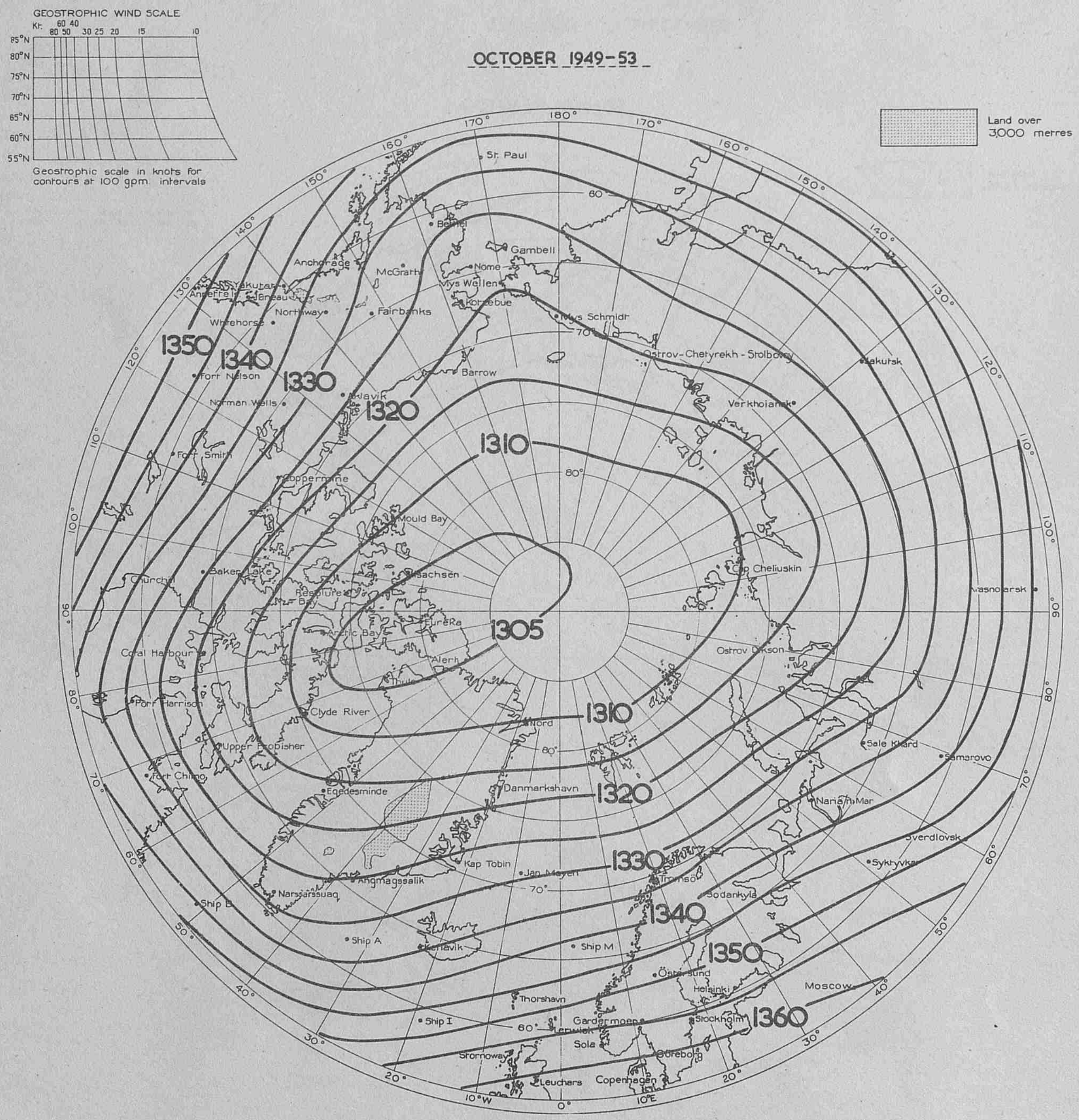
GEOSTROPHIC WIND SCALE
Kt. 60 40
80 50 30 25 20 15 10
85°N
80°N
75°N
70°N
65°N
60°N
55°N
Geostrophic scale in knots for contours at 100 gpm. intervals
Land over 3,000 metres
1305
1310
1320
1330
1340
1350
1360
180°
170°
160°
150°
140°
130°
120°
110°
100°
90°
80°
70°
60°
50°
40°
30°
20°
10°W
0°
10°E
St. Paul
Bethel
Gambell
Nome
McGrath
Mys Wellen
Kotzebue
Anchorage
Yakutat
Annette
Juneau
Northway
Fairbanks
Whitehorse
Mys Schmidt
Barrow
Fort Nelson
Aklavik
Norman Wells
Ostrov-Chetyrekh-Stolbovoy
Yakutsk
Verkhoiansk
Fort Smith
Coppermine
Mould Bay
Isachsen
Baker Lake
Resolute Bay
Churchill
Eureka
Arctic Bay
Alert
Thule
Cap Cheliuskin
Krasnoiarsk
Ostrov Dikson
Coral Harbour
Port Harrison
Clyde River
Nord
Upper Frobisher
Fort Chimo
Egedesminde
Danmarkshavn
Sale Khard
Samarovo
Narian Mar
Sverdlovsk
Syktyvkar
Kap Tobin
Jan Mayen
Angmagssalik
Narssarssuaq
Tromso
Sodankyla
Ship B
Ship A
Keflavik
Ship M
Ostersund
Helsinki
Moscow
Thorshavn
Ship I
Lerwick
Gardermoen
Stockholm
Sola
Stornoway
Orebro
Leuchars
Copenhagen

Height in dekametres

Upper Air Branch (M.O.23)

150-100 mb. THICKNESS

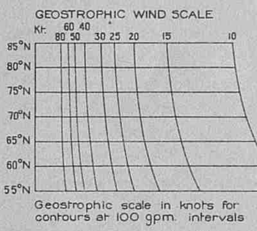

OCTOBER 1949-53

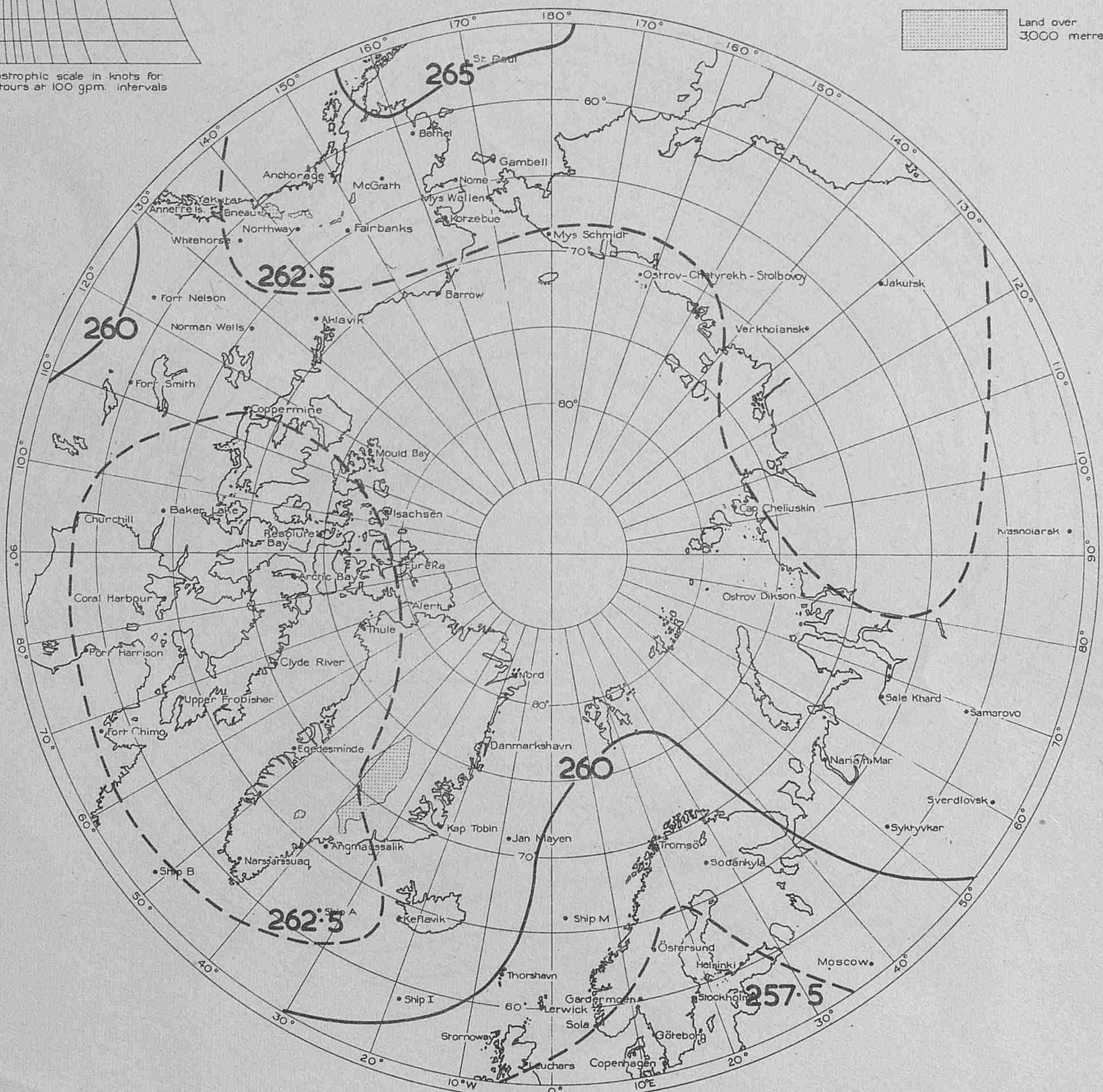
Land over 3000 metres
265
262·5
260
260
262·5
257·5
180°
170°
170°
160°
160°
150°
150°
140°
140°
130°
130°
120°
120°
110°
110°
100°
100°
90°
90°
80°
80°
70°
70°
60°
60°
50°
50°
40°
40°
30°
30°
20°
20°
10°W
0°
10°E
60°
70°
80°
St. Paul
Bethel
Gambell
Nome
Mys Wellen
Kotzebue
McGrath
Anchorage
Yakutat
Annette Is.
Sneau
Northway
Fairbanks
Whitehorse
Mys Schmidt
Barrow
Ostrov-Chetyrekh-Stolbovoy
Jakutsk
Verkhoiansk
Fort Nelson
Norman Wells
Aklavik
Fort Smith
Coppermine
Mould Bay
Isachsen
Cap Cheliuskin
Krasnoiarsk
Churchill
Baker Lake
Resolute Bay
Eureka
Arctic Bay
Ostrov Dikson
Coral Harbour
Alert
Thule
Port Harrison
Clyde River
Nord
Sale Khard
Samarovo
Upper Frobisher
Fort Chimo
Egedesminde
Danmarkshavn
Narian Mar
Sverdlovsk
Kap Tobin
Jan Mayen
Sykyvkar
Tromso
Sodankyla
Angmagssalik
Narssarssuaq
Ship B
Ship A
Keflavik
Ship M
Ösrersund
Helsinki
Moscow
Thorshavn
Ship I
Gardermoen
Lerwick
Sola
Stockholm
Stornoway
Göteborg
Leuchars
Copenhagen

Height in dekametres

Upper Air Branch (M.O.23)

AVERAGE 100 mb. CONTOURS

OCTOBER 1949-53

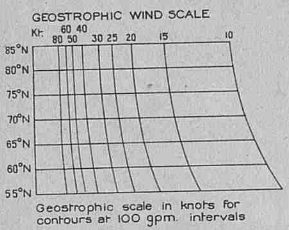

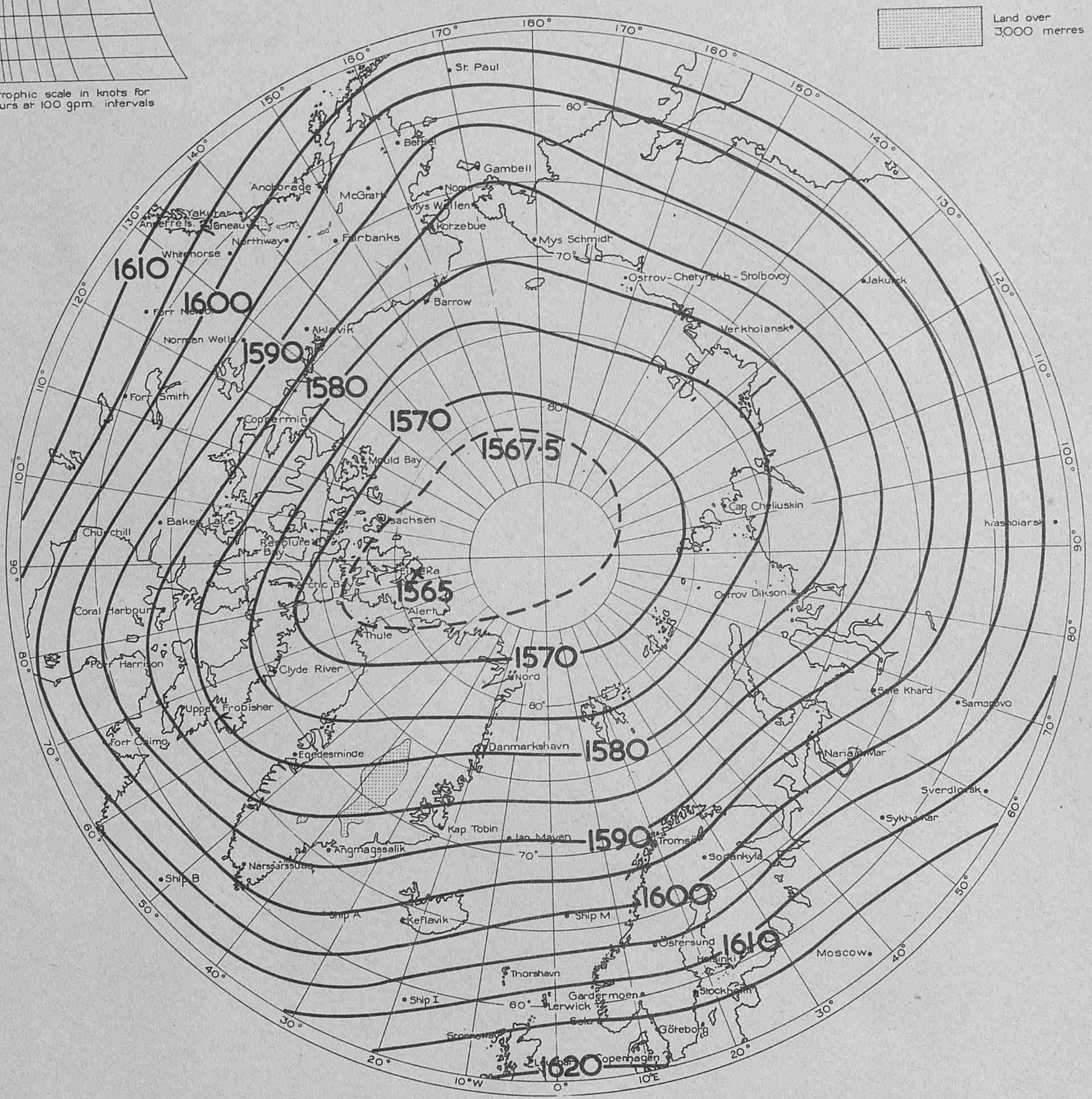
Land over 3000 metres
1610
1600
1590
1580
1570
1567·5
1565
1570
1580
1590
1600
1610
1620
180°
170°
160°
150°
140°
130°
120°
110°
100°
90°
80°
70°
60°
50°
40°
30°
20°
10°W
0°
10°E
St. Paul
Bethel
Gambell
Nome
McGrath
Mys Wellen
Kotzebue
Anchorage
Yakutat
Annette Is.
Juneau
Northway
Fairbanks
Mys Schmidt
Whitehorse
Ostrov-Chetyrekh-Stolbovoy
Jakutsk
Barrow
Fort Nelson
Aklavik
Verkhoiansk
Norman Wells
Fort Smith
Coppermine
Mould Bay
Cap Cheliuskin
Baker Lake
Isachsen
Krasnoiarsk
Churchill
Resolute Bay
Eureka
Arctic Bay
Alert
Ostrov Dikson
Coral Harbour
Thule
Port Harrison
Clyde River
Nord
Salekhard
Samarovo
Upper Frobisher
Fort Chimo
Egedesminde
Danmarkshavn
Narian Mar
Sverdlovsk
Sykhtyvkar
Kap Tobin
Jan Mayen
Tromsö
Angmagssalik
Narssarssuaq
Sodankylä
Ship B
Ship A
Keflavik
Ship M
Östersund
Helsinki
Moscow
Thorshavn
Ship I
Gardermoen
Lerwick
Stockholm
Sola
Göteborg
Stornoway
Copenhagen
80°
70°
60°

Height in dekametres

Upper Air Branch (M.O.23)

AD No 139540

M.R.P. 1021
S.C.I/121
31st December, 1956.

Radio refraction in the free atmosphere.

by

A.H. Hooper and A.P. Taylor.

(Meteorological Office)

AIR MINISTRY

METEOROLOGICAL RESEARCH COMMITTEE

At the time of issue this report has not been published. Any author desiring to quote this paper should refer to it as "A paper of the Meteorological Research Committee (London), M.R.P. No. 1021 by Messrs. A.H. Hooper and A.P. Taylor
A copy is available in the Library of the Meteorological Office."

M.R.P. 1021
S.C.I./121
31st December, 1956

AIR MINISTRY

METEOROLOGICAL RESEARCH COMMITTEE

Radio refraction in the free atmosphere

by

A.H. Hooper and A.P. Taylor (Meteorological Office)

Summary

The effect of refraction on the height of an object calculated from radar measurements of slant range and elevation is determined, with particular reference to the reflectors carried by free balloons used for wind finding by the Meteorological Office. The true height of an object is expressed as a function of its angle of elevation as observed from a point on the ray path and numerical solutions are obtained for a particular distribution of refractive index. The effects of departures from this refractive index structure are discussed and the conclusion is reached that a set of standard corrections is probably adequate for meteorological purposes.

The fundamental relationship

The path of a ray travelling through an atmosphere whose refractive index varies with height above the earth's surface is determined by

$$\mu r \cos\phi = \text{a constant} = \mu_0 r_0 \cos\phi_0 \text{ (say)} \qquad (1)$$

where μ is the refractive index, r is the distance from the centre of curvature of the surface of the point considered, ϕ is the angle between the tangent to the ray and the tangent to a circle through the point and concentric with the earth, and μ_0, r_0 and ϕ_0 are the corresponding values where the ray intersects the surface of the earth. See Fig.1.

If the path of the ray is specified in polar co-ordinates with the centre of the earth as origin we have

$$\text{Tan}\,\phi = \frac{dr}{r\,d\theta}$$

Thus $$\mu r \cos\phi = \mu r \sqrt{\frac{1}{1+\left(\frac{1}{r}\frac{dr}{d\theta}\right)^2}}$$

$$= \frac{\mu r^2 \frac{d\theta}{dr}}{\sqrt{1+r^2\left(\frac{d\theta}{dr}\right)^2}} = \mu_0 r_0 \cos\phi_0$$

$$\mu_0^2 r_0^2 \cos^2\phi_0 \left[1 + r^2\left(\frac{d\theta}{dr}\right)^2\right] = \mu^2 r^4 \left(\frac{d\theta}{dr}\right)^2$$

G.1565/JEK/12/56/50

$$\therefore \quad r^2\left(\frac{d\theta}{dr}\right)^2\left[\mu^2 r^2 - \mu_0^2 r_0^2 \cos^2\phi_0\right] = \mu_0^2 r_0^2 \cos^2\phi_0$$

$$\frac{d\theta}{dr} = \frac{\mu_0 r_0 \cos\phi_0}{r\sqrt{\mu^2 r^2 - \mu_0^2 r_0^2 \cos^2\phi_0}}$$

$$\int d\theta = \int \frac{\cos\phi_0 \, . \, dr}{r\sqrt{\left(\frac{\mu r}{\mu_0 r_0}\right)^2 - \cos^2\phi_0}} \quad \ldots\ldots\ldots\ldots (2)$$

Before the expression on the right-hand side can be integrated it is necessary to express μ as a function of r.

Refractive index structure of the atmosphere

The radio refractive index μ at a point in the atmosphere is given by the expression

$$(\mu - 1)\, 10^6 = \frac{79}{T}\left(P - \frac{e}{7} + \frac{4800\, e}{T}\right)$$

where P is the total atmospheric pressure (mb), e is the partial pressure of water vapour (mb) and T is the air temperature (°A). The refractive index can be expressed as a function of height if T and e are similarly specified.

The I.C.A.N. standard atmosphere specifies a relationship between pressure, temperature and height which is generally acceptable as representative of average conditions but no such standard has been accepted with regard to the moisture structure. Values of $(\mu - 1) \times 10^6$ were therefore calculated both for the I.C.A.N. atmosphere and for an atmosphere comprising the I.C.A.N. values together with a moisture structure in which the relative humidity decreases from 80% at the surface to 10% at 300 mb and is zero thereafter. These atmospheres are referred to respectively as "ICAN dry" and "ICAN moist", and a selection of values is given in Table I.

TABLE I

Height above earth's surface (thousands of feet)		0	4	8	12	16	20	30	36.09	40	50	60	80	100
$(\mu - 1) \times 10^6$	ICAN moist	342.0	282.0	236.0	200.6	172.8	149.5	102.8	81.4	67.5	41.7	25.9	9.3	3.6
	ICAN dry	278.3	247.1	218.8	192.9	169.6	148.2	102.8	81.4	67.5	41.7	25.9	9.3	3.6

Effect of an "ICAN moist" refractive structure

It has been suggested (1) that radio refractive index can best be represented

/as

as a logarithmic function of height. It was found that the equation

$$\frac{\mu r}{\mu_0 r_0} = 1 + A \log \frac{r}{r_0} + B\left(\log \frac{r}{r_0}\right)^2 \quad \ldots\ldots \quad (3)$$

closely represented the values of Table I providing that the atmosphere was treated in a series of layers and appropriate values of A and B chosen for each. This formula was also convenient for the integration of Equation (2). Values of the constants and of the layers for the "ICAN moist" atmosphere are given in Table II.

TABLE II

Layer (feet)	0 - 20,000	20,000-50,000	50,000-80,000	80,000-100,000
Value of A	0.672 728 676	0.885 230 233	0.964 899 698	0.992 113 907
constant B	132.072 415 0	28.035 019 5	4.642 535 83	2.490 555 066
Height	4,000 feet 15,000 feet	40,000 feet	70,000 feet	
Error (μ -1) x 10^6	5 4	2	2	

From equation (3)

$$\left(\frac{\mu r}{\mu_0 r_0}\right)^2 = 1 + 2A \log \frac{r}{r_0} + (A^2+2B)\left(\log \frac{r}{r_0}\right)^2 + 2AB\left(\log \frac{r}{r_0}\right)^3 + B^2\left(\log \frac{r}{r_0}\right)^4$$

$\log \frac{r}{r_0}$ is small and terms of higher order than the squares may be neglected.

$$\therefore \left(\frac{\mu r}{\mu_0 r_0}\right)^2 = \left(\alpha \log \frac{r}{r_0} + \beta\right)^2 + 1 - \beta^2 \quad \ldots\ldots \quad (3(a))$$

where $\alpha = (A^2+2B)^{\frac{1}{2}}$

and $\beta = A(A^2+2B)^{-\frac{1}{2}}$

Substituting in Equation (2)

$$d\theta = \int \frac{\cos \phi_0 \, dr}{r\left\{\left(\alpha \log \frac{r}{r_0} + \beta\right)^2 + 1 - \beta^2 - \cos^2 \phi_0\right\}^{\frac{1}{2}}}$$

$$= \frac{\cos \phi_0}{\alpha} \int (X^2 - C^2)^{-\frac{1}{2}} \, dX$$

where $X = \left(\alpha \log \frac{r}{r_0} + \beta\right)$ and $C^2 = \beta^2 - \sin^2 \phi_0$

Thus if $\theta = 0$ and $X = X_0$ when $r = r_0$ we have on integration

$$\frac{\alpha\theta}{\cos\phi_0} = \cosh^{-1}\frac{X}{c} - \cosh^{-1}\frac{X_0}{c}$$

$$= \cosh^{-1}\left\{\frac{\alpha\log\frac{r}{r_0}+\beta}{(\beta^2-\sin^2\phi_0)^{\frac{1}{2}}}\right\} - \cosh^{-1}\left\{\frac{\beta}{(\beta^2-\sin^2\phi_0)^{\frac{1}{2}}}\right\}$$

whence

$$\alpha\log\frac{r}{r_0}+\beta = (\beta^2-\sin^2\phi_0)^{\frac{1}{2}}\left[\frac{\beta\cosh(\alpha\theta\sec\phi_0)}{(\beta^2-\sin^2\phi_0)^{\frac{1}{2}}} + \sinh(\alpha\theta\sec\phi_0)\left(\frac{\beta^2}{\beta^2-\sin^2\phi_0}-1\right)^{\frac{1}{2}}\right]$$

$$= \beta\cosh(\alpha\theta\sec\phi_0) + \sin\phi_0\sinh(\alpha\theta\sec\phi_0) \quad \text{.........} \quad (4)$$

Values of r were then obtained from Equation (4) for a series of values of ϕ_0 and θ. The calculations had to be carried out in steps corresponding to the layers in Table II but the ϕ_0 for each layer were calculated from Equation (1) to correspond with the series of ϕ_0 at the surface used in the lowest layer. Thus values of r and θ were obtained for each of a series of rays arriving at the surface at selected angles of elevation.

The quantity $r - r_0 = h$ is the true height of a target which would be observed by radar to have an angle of elevation ϕ_0 and a slant range of say R. The height of the target for routine work is computed with allowance for curvature of the earth from the formula:

$$h' = R\sin\phi_0 + \frac{(R\cos\phi_0)^2}{2r_0} \quad \text{.........} \quad (5)$$

In order to compare the apparent height (h') with the true height (h) it was necessary to find R. The observed slant range is in fact half the time taken for a pulse to travel from the radar to the target and back multiplied by an assumed velocity of propagation, say V. Thus

$$\frac{R}{V} = \int_0^s \frac{\mu}{v_0}\,ds$$

where v_0 is the velocity of electromagnetic waves in vacuo and s is the distance measured along the path of the ray to the target. It can be demonstrated that the measured slant range does not differ significantly, for the present purpose, from the straight line distance (R') between the radar equipment and the target. Advantage has been taken of this in order to reduce the amount of calculation. Values of R' were computed for the same series of values of r and θ as obtained from Equation (4). Using these values of R' in Equation (5) corrections were obtained which could be applied to the apparent heights (h') to give true heights (h). Graphs of these corrections are given in Fig.2, which is set out in a form convenient for wind-finding work.

Departures from "ICAN moist" conditions

1. A dry atmosphere

Since this computation was carried out for a standard atmosphere it was necessary to ascertain the effect of departures from this condition. Table III compares for various elevation angles the correction for the "ICAN moist" atmosphere with the corresponding correction for the "ICAN dry" atmosphere. The differences are due to the presence of water vapour.

TABLE III

Local height (feet)		50,000				20,000		
Elevation Angle (°)		7°	10°	14°	20°	7°	10°	14°
Refraction correction in feet for	ICAN moist	-605	-320	-168	-92	-150	-80	-39
	ICAN dry	-430	-216	-117	-58	-89	-46	-23

In that refraction of light and radio waves is practically the same for dry air the result for the "ICAN dry" atmosphere has an application in theodolite work.

2. A low level European moisture discontinuity

The error caused by a given angular amount of refraction (Equation (1)) will be greatest when the refraction is concentrated at a single, very low, level. In the European region the effect is greatest in subsidence conditions where warm moist air of sub-tropical origin is present in the lowest layers with dry air overlying. A computation was carried out for two examples of this condition for differing heights of the subsidence layer.

The extreme condition of a constant mixing ratio of 15 g/Kg and temperature of 68°F extending from surface to 1,500 feet, with dry air superimposed, was selected. The true correction at a height of 50,000 feet with an elevation angle of 20° was found to be -92 feet whereas the corresponding "ICAN moist" correction was -90 feet.

The second example was for a change from moist to dry air at 500 feet and otherwise similar conditions. The true correction was found to be -102 feet compared with the "ICAN moist" correction of -90 feet.

The assumption of wholly dry air above the discontinuity is slightly unrealistic. An examination of examples has shown that the effect of small quantities of water vapour in this region will be to reduce the true correction required, as the effect of reduced refraction at a low discontinuity more than balances the increased refraction above due to the increased moisture lapse above. It is possible, therefore, on a given occasion, for the "standard" value either to under-correct within the order of the limit indicated above or to over-correct within the limits of Table III. Reference to M.O.555 part 1 suggests that during the years 1948 to 1950 over Larkhill excess corrections of more than half this range were rarely encountered.

3. A low level sub-tropical discontinuity

The extreme case of high moisture content in the surface layers followed by an abrupt decrease to normal values aloft is a regular summertime feature at Bahrain where dry desert air flows out over the Persian Gulf. Table IV below gives values obtained from a summer-time ascent selected at random.

TABLE IV

Pressure (mb)	996	985	972	960	950	900	850	800
Temperature (°F)	95	97	99	100	99	93	85	77
Mixing Ratio (g/Kg)	29.6	21.4	5.7	5.9	6.2	6.2	5.3	5.0
$(\mu - 1) \times 10^6$	446	387	283	280	279	269	252	239

It will be noted that above 972 mb the μ structure closely approximates to European conditions. The true correction at 50,000 feet with an elevation of 20° was found to be -110 feet compared with an "ICAN moist" correction of -93 feet.

Conclusion

The G.L.III equipment used by the Meteorological Office for wind-finding purposes gives heights which are in error due to refraction approximately by the magnitudes of Fig.2.

Heights are used, as a routine, for assigning mean winds measured over layers of 2,500 to 3,500 feet to standard height levels. In this application the effect of refraction appears insignificant.

The equipment is used also, by comparison with heights computed by radio-sonde data, to assess the systematic errors of the radio-sonde. The probable error at 50,000 feet and elevation 20° of an individual radar height determination is 250 feet and it is necessary to use averages. It is apparent that refraction introduces a systematic error into such differences and that correction for this effect is necessary before radio-sonde performance can be assessed.

The authors wish to acknowledge the very considerable assistance given by Mr. J.A. Smith, of the Meteorological Office, in performing the extensive series of computations embodied in Fig. 2 of this paper.

Reference

1. Stickland, A.C. - "Refraction in the lower atmosphere and its applications to the propagation of radio waves" at a conference of the Physical Society and the Royal Meteorological Society - April, 1946.

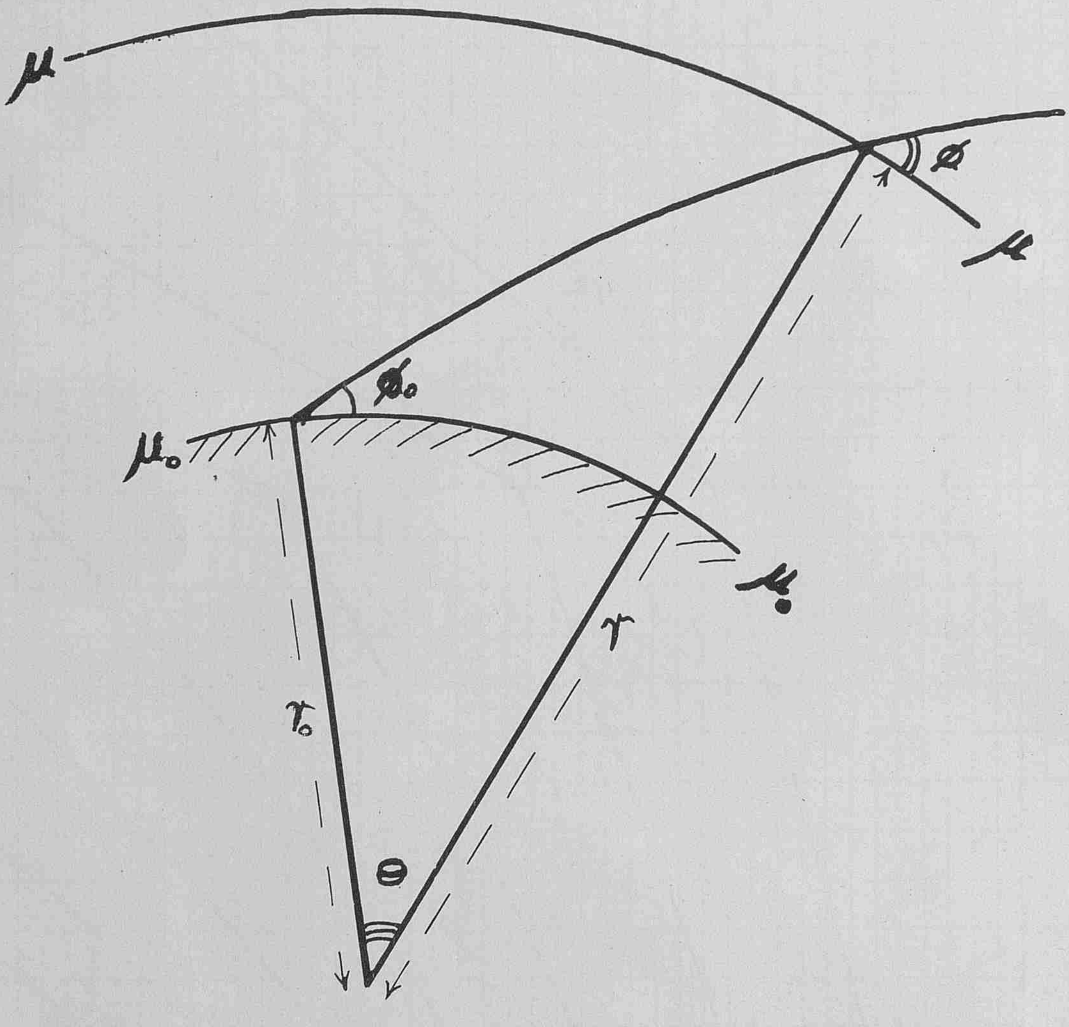
μ
ϕ
μ
ϕ_0
μ_0
μ_0
r
r_0
θ

FIG. 1.

FIG. 2.

CORRECTION FOR REFRACTION

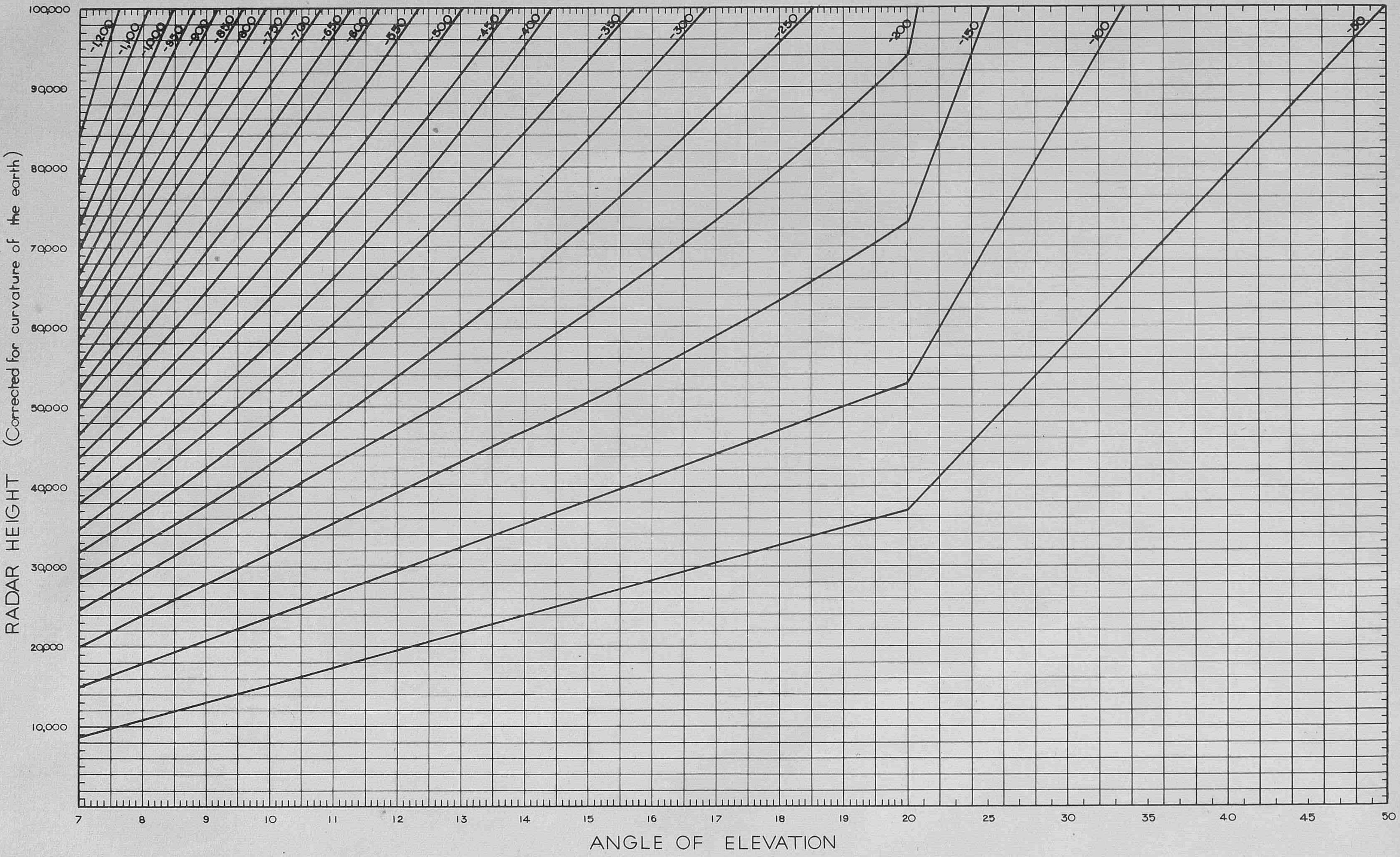

AD216263

M.R.P. 1022
S.C. II/224
S.C. III/225
17th December, 1956

AD216263

The movement of precipitation belts as observed by radar

by

W. G. Harper and J. G. D. Beimers

(Meteorological Office)

AIR MINISTRY

METEOROLOGICAL RESEARCH COMMITTEE

At the time of issue this report has not
been published. Any author desiring to
quote this paper should refer to it as "A
paper of the Meteorological Research
Committee (London),
M.R.P. No. 1022 by Messrs. W.G. Harper
and J.G.D. Beimers
A copy is available in the Library of
the Meteorological Office."

M.R.P. 1022
S.C. II/224
S.C. III/225
17th December, 1956

AIR MINISTRY

METEOROLOGICAL RESEARCH COMMITTEE

The movement of precipitation belts as observed by radar

by

W.G. Harper and J.G.D. Beimers (Meteorological Office)

Summary

The movement of 103 belts of precipitation over Southeast England, mostly associated with cold fronts and cold occlusions, ~~have~~ were been measured from radar records and compared with upper winds at each 50 mb level from 950 to 500 mb.

A correlation in excess of 0.9 is found with the mean winds across the belts at the 700 mb level. Even at 650 and 750 mb the correlations are significantly lower, while at 950 mb (roughly the level of the gradient wind above the friction layer) the correlation is little more than 0.6. The mean of the wind components at 700 mb is in close agreement with the speed of the belts.

No significant variation in correlation level was found despite subdivision of the material either (a) on the basis of frontal types, or (b) on the basis of the height ranges of observed echo.

Strong support is found for the forecasting rule that cold fronts and cold occlusions move at a speed that is equal to the average component of the wind across the frontal surface at the 700 mb level.

A similar comparison has not been possible in the case of warm fronts because of the absence of well-defined edges of echo in them.

1. Introduction

In forecasting the movement of fronts the forecaster usually moves surface fronts on with the geostrophic wind scale, conveniently obtaining the component of the geostrophic wind normal to the front by laying the scale along the front of the surface chart. The rules he employs are largely empirical, but in general warm fronts are moved on at about 70 per cent of the speed of the geostrophic wind, cold fronts at between 80 and 100 per cent of the geostrophic wind or even more, allowance being made where possible for isallobaric effects and for curvature of the isobars (cf. Petterssen's (1) forecasting rules). The method is not entirely satisfactory, and occasional serious errors occur.

Ligda, (2) however, in America has compared the movement of small precipitation areas as observed by radar with winds scaled from upper air charts at the three levels 850, 700 and 500 mb, and found that the correlation in both speed and direction was better at 700 mb than at either of the other levels. The present paper attempts a more detailed comparison in the case of belts of precipitation.

2. Method adopted

Belts of precipitation are frequently observed on radar to have clearly defined edges of echo. Their direction and speed of movement can be rapidly and accurately determined from the PPI display over the limited area observed.

Many of these belts are identifiable with the passage of fronts. A clear distinction must be drawn here between the direction and speed of movement of the belt (which is measured perpendicular to its length), and the movement of the individual echoes of which it is composed, for these will normally have a component of motion along the belt which may or may not be obvious from radar. On some occasions there may also be a continuous process of development and dissipation, precipitation forming at one side of a belt, moving through and dissipating at the other, as in orographic rainfall. The present observations were taken over Southeast England, where orographic effects are negligible, and it is reasonable to assume that the belt movement as measured from radar was that of its associated front.

Reference has been made to the limited area of the normal radar display, and it is obvious that a single radar station cannot measure movement at widely spaced points along a frontal belt; but for the present study radar scores heavily in being able to define a movement accurately at one point in a belt from observations covering perhaps half an hour. In contrast, even a close network of weather reports allows considerable latitude in placing fronts, and their movement is often hard to define from synoptic charts, especially when they are slow-moving.

Comparison has been made with components of measured values of wind from the British radar-wind network. This had two main advantages over the use of geostrophic winds measured from upper air charts, namely that radar winds were available (a) every 6 hr as against the 12-hr spacing of the upper air charts, and (b) at each 50-mb level against upper air charts at 700 and 500 mb only.

3. Nature of radar material

Photographic records taken at East Hill on a 500-Kw 10-cm plan-position radar in the five-year period 1947-52 were found to include 103 belts of precipitation whose movement could be clearly defined. The average duration of the measurements on these belts was 67 minutes. They were usually recorded for longer, but outside the period of measurement were more ill-defined.

51 of the belts (50 per cent) could be identified with the passage of cold fronts shown on the Daily Weather Report, or were reasonable extrapolations of such fronts. 31 (30 per cent) could be identified similarly with the passage of occlusions. In the remaining 21 cases (20 per cent) no fronts were shown in the Daily Weather Report, and the precipitation consisted mainly of ordered collections of showers in a persistent belt. Some of these may well have been associated with minor cold fronts not regarded as essential to the synoptic analysis, and in any case no sound reason was seen for excluding them.

Measurements have not been possible on warm fronts as the radar echoes from warm-front precipitation are usually very diffuse, and no persistent edge of echo can be defined.

4. Analysis of radar material

Isochrones of a clearly-defined edge of echo were drawn for each belt of precipitation by projection of the 35-mm plan-position photographs. Slight adjustment of magnification was usually necessary from frame to frame to allow for variations in the voltage of the mains supply. No single adjustment of magnification in the projection process can eliminate a slight non-uniformity in the range scale across the display. This is inherent in any cathode-ray tube presentation. The residual error can be greatly reduced however by scaling off echo movements against their own sections of the radial range scale, and is negligible for the present purpose.

An actual plotting is shown at Fig. 1. This is of precipitation associated with a well-defined but weak cold-front passage, selected because it has enabled the echo pattern at each time to be shown. Observations in this case covered a period of 80 min, and included seven positions of the trailing edge. It can be seen that the precipitation belt is nowhere more than 3 mi in width and would probably not have given more than 10 min of rain in passing.

/A

A point that is clearly shown in Fig. 1 is the difficulty in following individual echo sequences even in as clearly defined a belt as this. The general impression of the individual movement is clear, e.g. CD in Fig. 1, but for very few could a direction and speed be given with confidence. In any case there was often a broader belt of continuous precipitation in which identification of individual echoes was impossible.

The movement of the belts was measured perpendicular to the echo-edge, e.g. along AB in Fig. 1. A single value for the speed of movement was determined graphically by plotting the intercepts measured along AB against time, and taking the slope of the mean line. This gave equal weight to each plotting, and minimized the effect of local irregularities. It might be claimed that the placing of the line AB is rather arbitrary, but the variability of measured speed due to this cause is usually less than the probable error in the measured winds. Not all the belts were as smooth as this one, and in general some degree of smoothing of slight protuberances and indentations in the echo edge has been necessary.

5. Comparison with upper winds

The advantages of comparison with measured wind components over values scaled from upper-air charts are given in para. 2. Two radar-wind ascents were used for each belt, one to represent the winds ahead, the other the winds behind the belt, the choice being affected by the orientation of the belt. Whenever possible one ascent was chosen downwind and one upwind from the area in which the belt movement was measured, but it was not possible to hold rigorously to this because of the more limited choice of ascents to the south and east of East Hill. On average the soundings used were 40 mi ahead and 100 mi behind the belts, and as close as possible in time. Those used for the belt shown in Fig. 1 were Liverpool and Larkhill at 0800 G.M.T.

6. Results

The results are presented graphically. The upper curves of Fig. 2 are the correlations with the mean wind components for the full 103 belts and with the wind components ahead of and behind the belts, while the wind components themselves are plotted against the scale of knots at the right-hand edge of the diagram (lower curves), with the mean speed of the belts indicated for comparison.

The striking features are

(a) that the correlations have a well-defined maximum of high significance at 700 mb

(b) that the correlations are much lower at 950 mb (which roughly represents the gradient wind at 2,000 ft) and at 500 mb

It is of interest to compare this with the correlations found by Ligda (2) for the movement of small precipitation areas. He compared both the direction and speed of movement of 90 storms with geostrophic winds scaled from upper air charts at the three levels 850, 700 and 500 mb, and obtained the following correlations:-

Pressure, mb	850	700	500
Direction	0.73	0.96	0.87
Speed	0.49	0.81	0.58

The variation in speed correlation is in excellent agreement with the form of the curve of Fig. 2

(c) that the best level of agreement of mean belt speed with mean wind components is also close to 700 mb

/(d)

(d) that the correlations are higher for the mean winds at all levels than for those ahead of or behind the belts

(e) that the mean wind components behind the belts are stronger than those ahead at all levels.

Fig. 3 is a scatter diagram of the belt movements at the 700 mb level, with belt speed plotted against the mean of the wind components. The mean belt speed was 19.3 kt, and the extreme speed is seen to be 45 kt. An explanation of the negative and zero values is desirable. The direction of movement of the belt on the radar display was always taken as positive. If the mean wind component turned out negative this of course adversely affected the correlation at the level concerned. There are two such cases at 700 mb, but the negative components are small. In the three cases of zero belt speed, although there was no detectable movement of the belt where the echo edge was well-defined, there was a small movement one way or the other in the less well-defined parts of the display, and this was taken as positive. A wind component opposed to it was counted negative.

To allay any suspicion that features of Fig. 2 may have been fortuitous, correlations and wind components have been evaluated separately for the 51 cold fronts and for the 31 occlusions. These are presented in Fig. 4 and 5. The main features to which attention has already been drawn are present in both. There is the same rapid improvement in correlation from 950 to 800 mb, and the highest correlation in both is at the 700 mb level, although for the cold fronts the correlation remains high between 750 and 550 mb. The best agreement between the actual values of belt-movement and wind component lies within 50 mb of the 700 mb level in each case.

For the sake of completeness Fig. 6 presents curves derived from the 21 belts of showers. Even here the same broad features exist, but there is no well-defined maximum in the correlation curves. The fairly uniform correlation from 900 to 600 mb (curve C) may be due to the fact that occasions suitable for convective development are usually characterised by small variations of wind with height, and it is probable that the winds themselves are more highly correlated than usual. The rapid fall-off in correlation from 0.82 at 550 mb to 0.51 at 500 mb in curve A appeared suspicious, and the individual wind values were closely examined. It was found that on one ascent a completely different wind regime had set in above 550 mb, associated with a pronounced upper trough. From 295 deg/29 kt at 550 mb the wind backed to 240 deg/64 kt at 500 mb. This was clearly unrelated to the shower development in the northwesterly airstream. Exclusion of this belt would have raised the correlation coefficient for the remaining 20 shower belts from 0.51 to 0.69 at 500 mb while leaving that at 550 mb practically unchanged. This draws attention to the inadequacy of these 21 cases as a statistical sample. The effect of excluding this one belt from the main correlation for the 103 belts is however almost negligible.

The correlation coefficients and wind components are given as a table (Table 1).

7. Separation into height ranges of echo top

A further test of the validity of the 700 mb correlation has been applied by separating the material into ranges on the basis of the heights of the observed radar echo tops. These classes have been correlated separately. Range-height information was available for 77 of the 82 belts associated with cold fronts and occlusions. In most cases precipitation was continuous from echo top level to the ground, either as diffuse echo, or with some column structure; in a few cases the echo top was associated with an upper layer-type echo which may or may not have been related to the rain reaching the ground. No attempt has been made to discriminate between these types.

The heights of maximum echo top have been analysed into various height ranges in Table 2. It is of interest that only 7 of the 77 belts have a maximum echo top at 10,000 ft (700 mb) or below.

Table 2. Numbers of occasions of maximum echo tops associated with cold fronts and occlusions falling in the given ranges.

Height range 10^3 ft	Cold fronts	Occlusions	Total
0 - 5	0	0	0
6 - 10	3	4	7
11 - 15	15	8	23
16 - 20	11	9	20
21 - 25	12	4	16
26 - 30	3	3	6
31 - 35	2	2	4
36 - 40	0	1	1
Total	46	31	77

There were roughly equal numbers of cases above and below 18,000 ft, and the wind components for these classes have been correlated and meaned separately to see if any variation in correlation level could be related to the radar appearance, for the 46 cold fronts (Fig. 7), for the 31 occlusions (Fig. 8), and for the whole 77 fronts (Fig. 9).

Only in the cold fronts is there any difference in level of best correlation. The 24 with echo tops above 18,000 ft have their maximum at 650 mb (0.93), while the 22 with tops below 18,000 ft have a broader maximum from 750 to 700 mb (0.94 to 0.95). The wind components at 700 mb for the former agree closely with the speed of the belts, but for the latter are almost 2 kt greater and are nearly constant from 800 to 650 mb. In both Fig. 8 and 9 the best correlations are at 700 mb, and the mean wind components are within 1 kt of the mean belt velocities. The numbers of cases in the correlations of Fig. 7 and 8 are of course rather small. The results are not very conclusive, but indicate that no variation of 'steering level' with height is deducible from radar.

8. Discussion

The wind components measured behind the belts of precipitation were on average stronger at all levels than those measured ahead of the belts (para. 6(e)). This is clearly shown in Fig. 2. It represents an inflow of air consistent with the frontal character of the belts, but an independent check of the reasonableness of the winds is desirable.

The excess of the wind component normal to a cold front surface in the cold air over that in the warm air is related to the upglide of the warm air relative to the cold. An average vertical velocity could be derived if we knew the average frontal slope, but we are not on firm ground in assuming a frontal slope. We think it preferable to assess roughly the weight of air lifted and from suitable environmental conditions to derive the average rainfall from the belt.

It is assumed that there was on average no uplift in the cold air. This is supported by Fig. 2. The wind normal to the belt in the cold air was less than the belt speed below 850 mb, and the effective excess at levels above 850 mb must have been carried downwards in order to make up the large deficit of air below 850 mb and so maintain the identity of the frontal surface. We have therefore limited the computation to the warm air ahead of the belts, and have assumed that all the overtaken air between 1,000 and 650 mb (the level at which the warm air wind component equalled the mean belt speed) must have been lifted to the higher level or have displaced an equivalent amount of air to that level, which is the same for present purposes. This lifting must occur if there is no acceleration of air parallel to the belt. The lapse of air temperature assumed for the lifting and for the environment was the saturated adiabatic through 10°C at 1,000 mb. This implies a freezing level at 800 mb and a temperature of -11°C at 650 mb, reasonable values for Southern England.

Considering a column of air of cross-section 1 cm^2, the weight of air in any 50-mb layer will be roughly 0.05 kg. From the tephigram we find that the 50-mb layer from 950 to 900 mb will have a humidity mixing ratio for saturated air of 6.5 g/kg before lifting, but only 2.5 g/kg at 650 mb. A small part of the excess will probably be lost by evaporation in falling through cold air but as a first approximation we shall neglect this and assume that the balance of 4.0 g/kg will ultimately be made available as precipitation at the ground. This unit column contributes a quantity 'm' of water, in this case 0.20 g. We can extract values of 'm' for each 50-mb layer from the tephigram.

We see that $m(v_f - v_a)$ is the weight of water released in unit time along unit length of the belt due to the lifting of the air in this layer, where v_a is the wind component in the warm air, and v_f is the mean belt speed. But in this time the belt has moved a distance v_f, and assuming uniform precipitation in time we see that the contribution ΔR to the rainfall on unit area due to this layer is $m(v_f - v_a)/v_f$. The contributions from the various layers are given in the following table:-

Table 3. Computation of average belt rainfall.

Layer mb	m gm	$\frac{v_f - v_a}{v_f}$	ΔR mm
1,000-950	0.24	0.57	1.36
950-900	0.20	0.38	0.76
900-850	0.17	0.23	0.39
850-800	0.13	0.17	0.22
800-750	0.09	0.13	0.12
750-700	0.05	0.08	0.04
700-650	0.02	0.04	0.01
		Total	2.90

A slight extrapolation of the v_a curve has been necessary to give a value to $(v_f - v_a)$ for the 1,000 to 950 mb layer, and it is worth noticing that this layer makes the largest contribution to the rainfall total of 2.9 mm.

We assumed for simplicity that lifting took place to 650 mb, but the lifted air could not all have been disposed of at that level. Lifting must have continued into the layers just above 650 mb where $v_a > v_f$. This is supported by the echo top evidence of Table 2 which suggests that some lifting took place on average to 18,000 ft (500 mb). The computed rainfall is not in fact greatly increased by this additional lifting because of the much slower rate of change of humidity mixing ratio of saturated air with height at these levels. A computation similar to Table 3 for lifting to 500 mb gives an average belt rainfall of 4.0 mm.

Rainfall between 2.9 and 4.0 mm is very reasonable for cold-front type belts of precipitation, and this gives us added confidence in the validity of the measured wind components and in their correlation with belt speed.

The high correlation at 700 mb can only be regarded as empirical. It is not possible from this limited study to attribute it to any physical cause. It seems quite possible that fronts which give no precipitation at all also move on average with the 700 mb wind, although none were of course included in our radar studies. This might be inferred from the results of para. 7. The subdivision on the basis of height of echo tops was, one must suppose, a rough separation of the more active from the less active fronts, yet no substantial difference in correlation level was found. The extrapolation to rainless fronts is not such a great step. It must be remembered that the forecaster is often more interested in the movement of fronts because of the changes of airmass involved than with the weather along them.

If the data of Fig. 2 had had submerged in them a significant number of belt speeds which correlated at levels substantially different from 700 mb an over-all correlation as high as 0.93 would surely have been impossible, and we think there is strong support from the present paper for the forecasting rule:- "Cold fronts and cold occlusions move with a speed equal to the component of the wind across the front at the 700 mb level."

9. References

1. Petterssen, S. 1940 "Weather analysis and forecasting". McGraw-Hill, New York.

2. Ligda, M.G.H. 1953 "The horizontal motion of small precipitation areas as observed by radar". Tech. Rep. No. 21, Dept. of Met., M.I.T., Cambridge, Mass.

NOTE

Some of the belts of precipitation discussed in this paper were not associated with easily identifiable fronts on the relevant synoptic charts. This should be borne in mind by the reader and the paper should be regarded as referring to belts of precipitation and not necessarily to the movement of cold fronts or occlusions.

Table 1. Correlation of upper wind components V (kt) at various pressure levels with the speed of movement of precipitation belts V'. The highest correlation in each column is underlined.

		COLD FRONTS			OCCLUSIONS			SHOWER BELTS			ALL BELTS				
P mb		Winds ahead	Winds behind	Mean winds	Winds ahead	Winds behind	Mean winds	Winds ahead	Winds behind	Mean winds	Winds ahead	Winds behind	Mean winds		P mb
950	r	.521	.553	.603	.551	.582	.599	.755	.679	.747	.599	.604	.647	r	950
	V	10.6	15.0	12.8	7.1	10.6	8.9	14.5	18.8	16.7	10.3	14.5	12.4	V	
900	r	.662	.685	.751	.543	.693	.658	.854	.773	.840	.681	.721	.754	r	900
	V	14.9	18.6	16.8	9.4	13.0	11.2	18.1	21.2	19.6	13.9	17.4	15.7	V	
850	r	.736	.804	.835	.689	.785	.791	.882	.777	.865	.769	.806	.838	r	850
	V	17.5	21.2	19.4	9.9	15.2	12.5	18.9	23.2	21.1	15.5	19.8	17.7	V	
800	r	.761	.802	.869	.764	.850	.866	.810	.781	.833	.787	.824	.864	r	800
	V	17.9	22.5	20.2	10.9	15.2	13.0	20.1	23.6	21.9	16.2	20.5	18.4	V	
750	r	.836	.824	.898	.835	.875	.910	.799	.799	.842	.839	.842	.895	r	750
	V	18.9	22.6	20.8	12.5	16.0	14.2	20.1	23.7	21.9	17.2	20.9	19.0	V	
700	r	.842	.875	.934	.899	.885	.944	.888	.804	.884	.875	.862	.928	r	700
	V	19.9	23.3	21.6	13.3	17.9	15.6	20.3	24.3	22.3	18.0	21.9	19.9	V	
650	r	.847	.869	.919	.843	.830	.880	.877	.799	.881	.862	.845	.902	r	650
	V	21.3	23.9	22.6	13.5	17.7	15.6	22.3	26.0	24.2	19.2	22.5	20.8	V	
600	r	.848	.862	.910	.817	.803	.858	.831	.733	.847	.842	.817	.884	r	600
	V	24.0	25.0	24.5	13.7	16.9	15.3	22.4	26.8	24.6	20.6	22.9	21.8	V	
550	r	.814	.823	.893	.808	.762	.858	.822	.647	.804	.825	.759	.868	r	550
	V	26.0	26.5	26.2	15.4	17.8	16.6	24.7	29.7	27.2	22.5	24.5	23.5	V	
500	r	.773	.769	.856	.805	.780	.852	.510	.583	.653	.735	.727	.814	r	500
	V	27.6	28.7	28.2	16.2	17.4	16.8	25.0	31.3	28.1	23.7	25.8	24.7	V	
V' kt		20.7			15.5			21.5			19.3			V' kt	
No.		51			31			21			103			No.	

FIG. 1

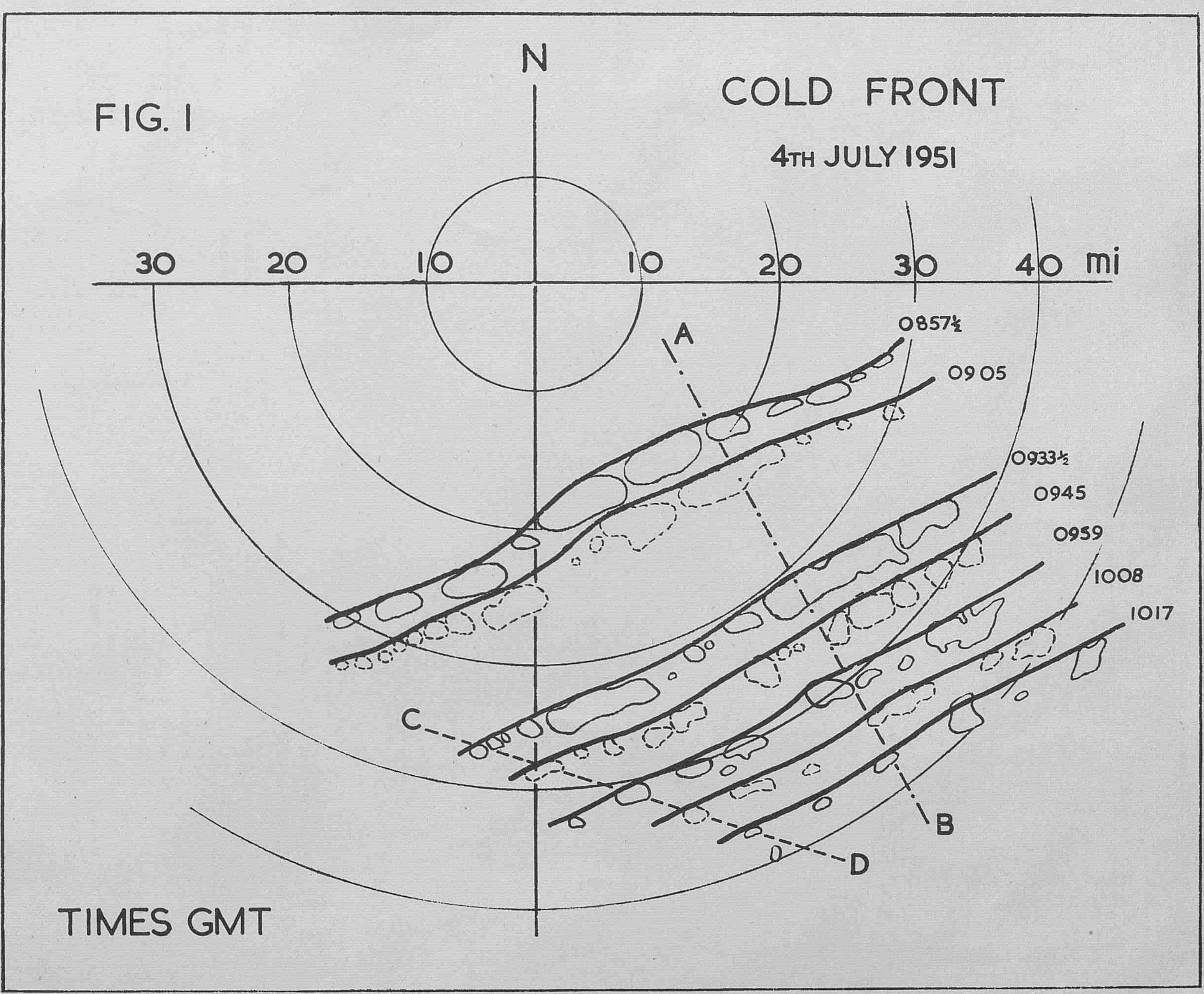

COLD FRONT

4TH JULY 1951

TIMES GMT

N
30
20
10
10
20
30
40
mi
0857¼
0905
0933½
0945
0959
1008
1017
A
B
C
D

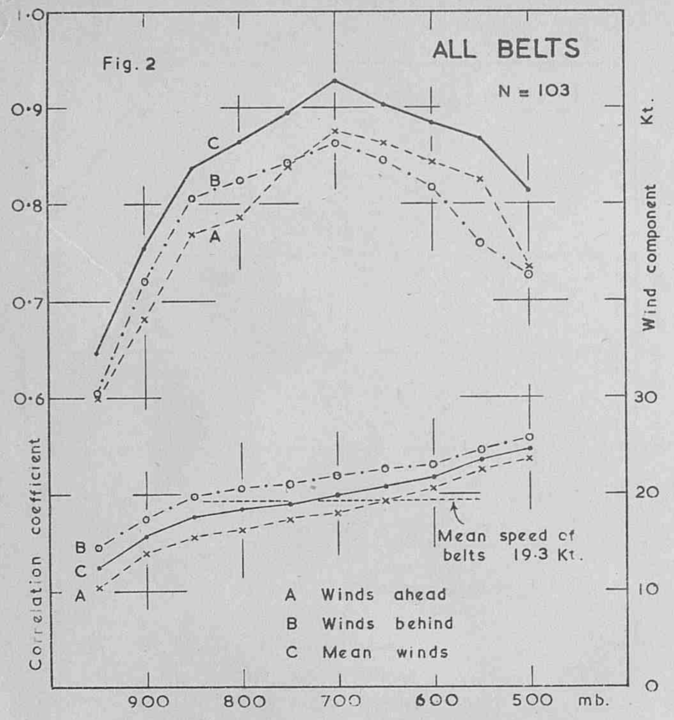

Correlation of movement of precipitation belts with measured upper winds

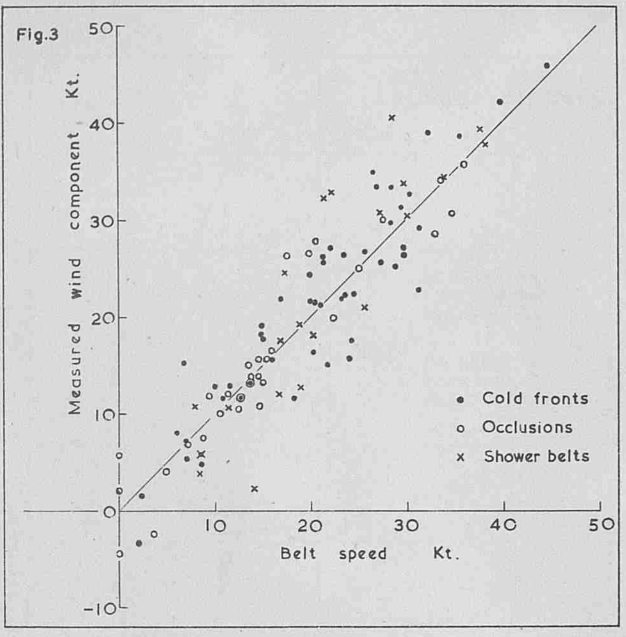

Scatter diagram of 700 mb wind components against precipitation belt speed

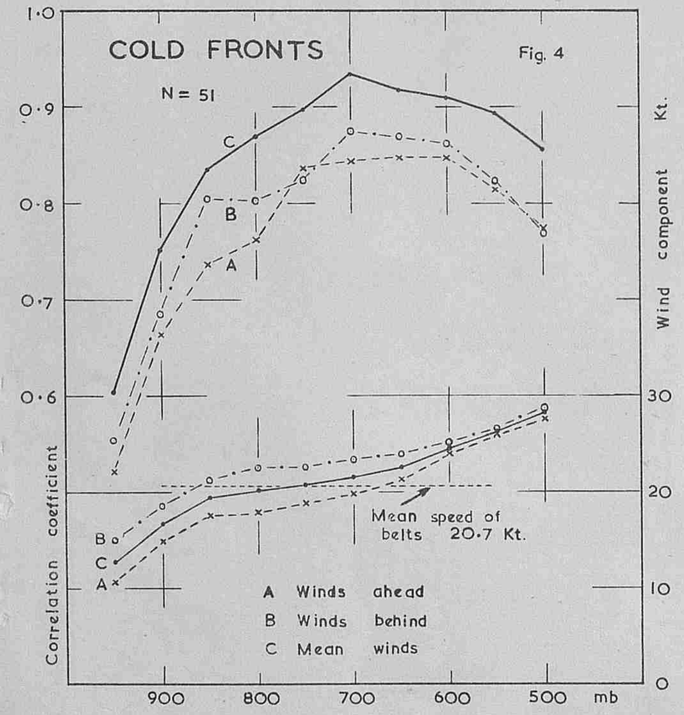

Correlation of movement of precipitation belts with measured upper winds

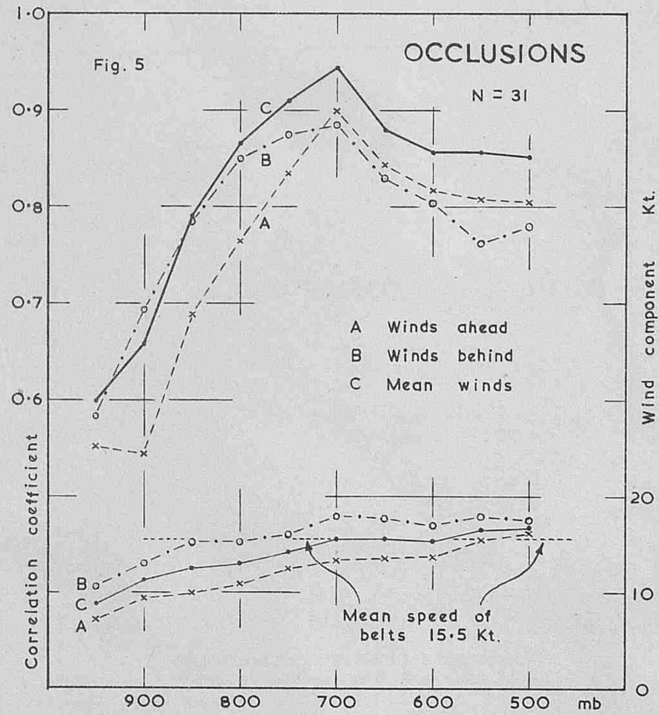

Correlation of movement of precipitation belts with measured upper winds

Correlation of movement of precipitation belts with measured upper winds

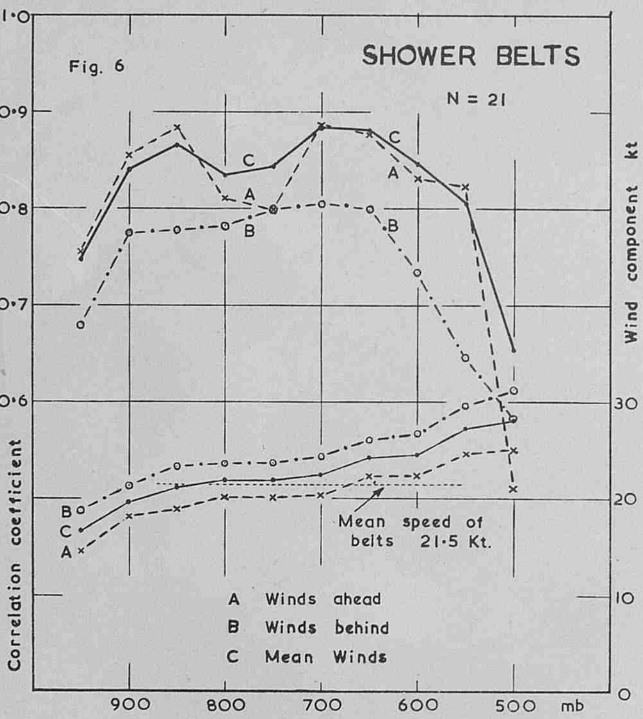
Fig. 6

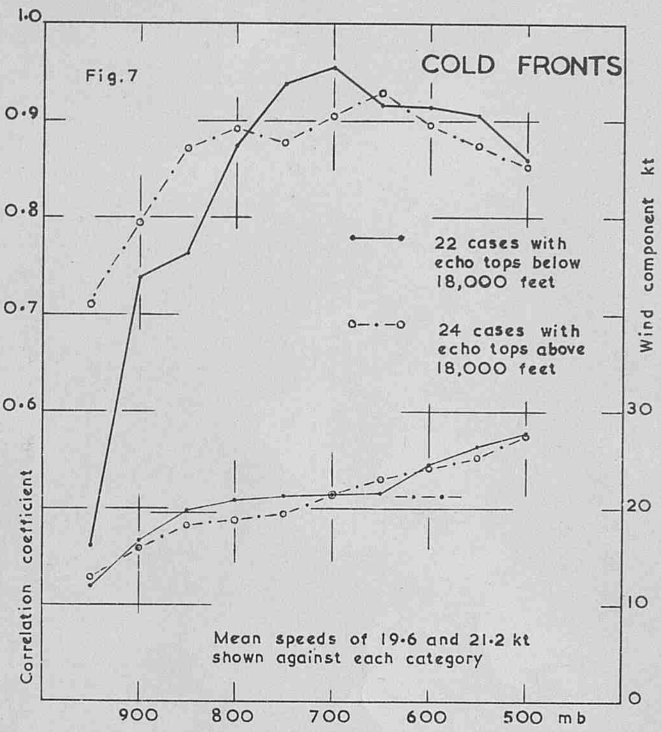
Fig. 7

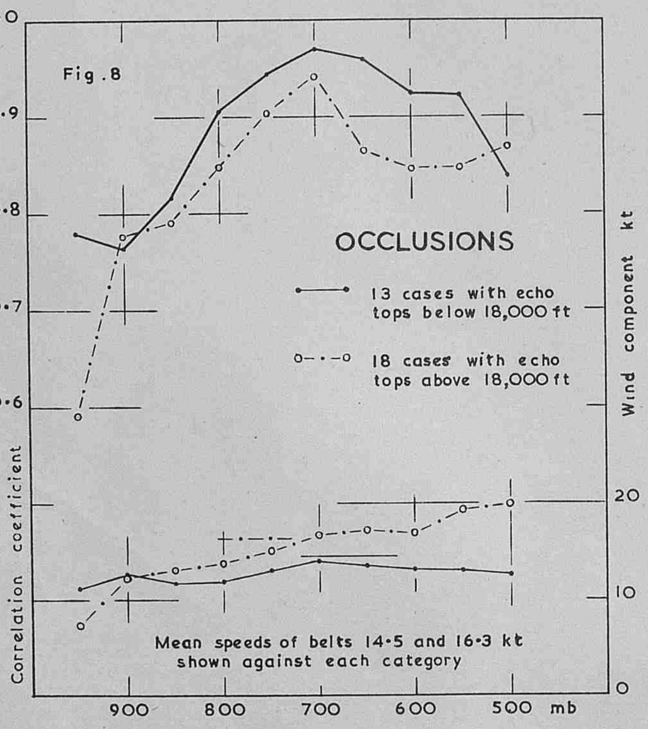
Fig. 8

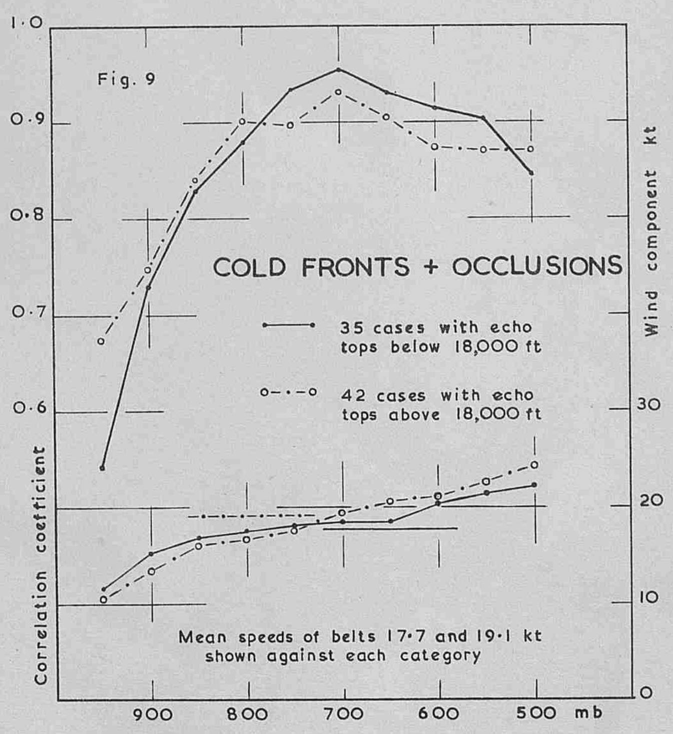
Fig. 9

M.R.P. 1023
S.C. 11/225
31st December, 1956

The serial correlations of daily mean temperatures at Kew Observatory

by

J. M. Craddock

(Meteorological Office)

AIR MINISTRY

METEOROLOGICAL RESEARCH COMMITTEE

At the time of issue this report has not been published. Any author desiring to quote this paper should refer to it as "A paper of the Meteorological Research Committee (London), M.R.P. No. 1023 by Mr. J. M. Craddock A copy is available in the Library of the Meteorological Office."

M.R.P.1023
S.C.II/225
31st December, 1956

AIR MINISTRY

METEOROLOGICAL RESEARCH COMMITTEE

The serial correlations of daily mean temperatures at Kew Observatory

by

J. M. Craddock (Meteorological Office)

Summary

A study is made of the correlation between the daily mean temperature at Kew on each calendar day of the year with the temperature on each of the seven following days. It appears that the level of the correlations varies with the time of year. For any particular season the correlation decreases as the separation between the dates is increased, but generally remains positive for separations of up to seven days. The correlations are used to suggest a division of the year into natural seasons. Regression equations are given to enable the temperature on any day to be predicted in terms of those of the preceding days.

1. Introduction

It is well known that the mean daily air temperature near the earth's surface shows coherent departure from normal over periods of days or weeks. The present paper sets out to measure this coherence numerically. The direct and obvious method of doing so is to find the serial correlations of a series of daily mean temperature anomalies covering at least 50 to 100 consecutive days. This is open to the objection that data will extend over a considerable part of a year, while the correlations we are trying to measure may themselves have an annual variation.

The method actually used is to take a very long series of daily temperature anomalies (18,615 terms, covering 51 years) and to perform a separate analysis for each calendar day of the year. For example, for January 1, we find the mean temperature and standard deviation for the 51 years 1900 to 1950 and the serial correlations r_1 up to r_7 between the temperature on January 1 and that on each succeeding day up to January 8. A similar analysis is repeated every day of the year.

A computation of this size could not be carried out in a reasonable time without high speed computing facilities and the main part was done by punched card methods, using the Hollerith installation at Rothamsted Experimental Station by the courtesy of Dr. F. Yates.

2. Data and computation

Kew Meteorological Observatory is a station representative of much of South-East England at which meteorological observations of high quality have been maintained over many years. The data used covering the period 1900-1950 were taken from manuscript tabulations made at the observatory, giving separately for each day of each year the daily maximum and minimum temperature. These values were punched direct from the source documents on to Hollerith cards. The daily mean temperatures, the sums required to find mean values and the sums of squares and products required to give variances and covariances were all found mechanically using the Hollerith Tabulator without any further manual transcription. The final calculations to give means, standard deviations and correlation coefficients were carried out by hand and checked by repetition. A detailed description of the calculations and the steps taken to minimize the risk of errors is given in Appendix A.

It should be mentioned that the daily mean temperature was estimated as $\frac{1}{2}$(max. + min.). While this method of estimation has its disadvantages as pointed out, for example, by Hoblyn (1928) it is still probably the best for general use, taking into account questions such as the availability of printed tabulations, and the time which would otherwise be spent on averaging data taken from original records. It is most unlikely that any of the main results of this paper would have been different had some other estimate of the daily mean temperature been used.

3. Results

The standard deviation of the daily mean temperature for each day of the year, and the correlation between the mean temperature on that day and the temperature on each of the seven following days, is shown diagrammatically in Fig.1. The results which number 2920 are rather numerous to present in tabular form, but can be made available to any investigator who wishes to use them. The salient features may be summarised as follows:-

3.1. The standard deviation of daily mean temperature

Considering first the lowest graph in Fig.1 it appears that besides a rather irregular fluctuation in value between one day and the next, this quantity shows a slow variation throughout the year. During the winter period from about November 20 to February 20 its average value is about 3.3°C, after which it falls to a value during March and April of about 2.7°C. From about May 8 to June 5 the value rises to about 3.0°C after which it falls to about 2.2°C during early August, and then rises steadily till it reaches its winter value in late November.

There is little doubt that these broad features are genuine, and not due to any accident of the statistics, but we cannot by elementary arguments assess the significance of the finer detail, such as the minor peak in mid-April, or the trough centred on December 24. To give the broad outlines concisely, the monthly mean values are given in Table 1.

It is hoped to carry out a more elaborate statistical analysis in another paper.

3.2. The variation of the serial correlations from month to month

If the remaining graphs in Figure 1 are considered in ascending order, they seem to differ more and more from what would be expected if the values of the serial correlations were independent of the time of year. We may put this impression into numerical form by using these data to estimate monthly values of the various coefficients.

The statistical distribution of a correlation coefficient departs a good deal from the normal, so that it is undesirable to average them as they stand. Instead each value in Figure 1 was converted into the z-statistic which is almost normally distributed and with 51 pairs of observations has variance 1/48. The monthly mean values of z are given in Table 2 and the corresponding values of r in Table 3.

We have to decide whether any of the monthly values of z in Table 2 depart significantly from the appropriate annual average. If consecutive values of z (or r) were independent, then the monthly mean value of z would have variance 1/48m where m is the number of days in the month. However, Figure 1 appears to confirm what mathematical reasoning would suggest, namely, that consecutive values of r are not independent. This fact reduces the number of degrees of freedom of the estimate of each monthly mean value of z, and we have to decide by how much. The adjustment has been discussed by, inter alia, Brooks (1948) and by Lewis and McIntosh (1952) and the latter authors give a formula for correcting m in terms of the serial correlations of the data in question. The calculation of several serial correlation coefficients for each set of 365 values of z would, however, have considerably increased the work put into this already laborious research so a simpler and cruder method of estimation was used, which is probably quite good enough for the purpose.

When consecutive terms of a series are positively correlated, the expectation that a given term is followed by another which departs from normal in the same direction will be greater than it would be in a series of independent terms. The expectation of finding a long run of consecutive departures in the same sense will be greater, and hence the average length of run. Conversely, by finding the average length of runs of terms departing from normal in the same direction, we should be able to estimate the first serial correlation. The question has been discussed by Ogawara and others (1955) and his diagram for the estimation of r_1 is given with full working directions in Appendix B.

This method is very quick in use since the only operation required on the data is that of counting the runs of consecutive above or below normal values. The first serial correlation was estimated in this way for each of the sets of 365 values of z_1 up to z_7, the values being given in the last line but one of Table 2. On the further assumption that for these series the consecutive serial correlations are in geometrical progression we arrive at the values of the reducing factor E (given in Table 2) by which the actual number of observations in each sample are to be multiplied to find the number of effectively independent observations.

Using these values of E, and allowing for the months having 28, 30 or 31 days, the coefficients underlined in Table 3 appear to differ significantly at the 5 per cent level from the annual mean values.

All the February values are significantly higher than the annual mean, while all but one of those for November are significantly lower; and while the values of r_1 and r_2 for May differ little from the annual mean values, the May values of r_4 to r_7 are significantly below the annual values. While the statistical procedure used is only approximate, the consistency of the results makes it extremely probable that the observed variations between months are real and not due to any accident of the statistics. To give a numerical measure to this probability would mean much extra work which at this stage hardly seems justified.

In every month the serial correlations decrease as the interval between the days correlated is increased, but the monthly averages are still all positive for dates seven days apart.

4. The division of the year into "natural seasons"

Further examination of Figure 1 prompts the enquiry whether the calendar months are really the most natural way of subdividing the year. On a date for which values of r_1 to r_7 are comparatively high the temperature departure is more likely to persist than it is on dates with lower values of r_1 to r_7. A trough in the values of r_1 indicates a date or period when temperature anomalies are relatively unstable. We may distinguish seasons with undisturbed temperature regimes from others with more disturbed regimes and a break between two periods with high values of $\underline{r}$ is an obvious choice for the end of a "natural season". Lamb (1950) has made a similar subdivision but based on the persistence of weather types rather than that of temperature anomalies. Looking at the upper curves in Figure 1, for which the variations are more marked, and starting with the summer, the first real break covers the period September 14 to September 22. There is then a short relatively undisturbed spell until October 9 and then a disturbed temperature regime until December 3. Then, apart from short breaks about December 10, December 22 and January 9 the type remains relatively undisturbed till about March 12. The curve then shows an oscillation with seven peaks and six troughs in the 95 days until June 15 after which the temperature regime becomes progressively less disturbed, without major breaks until early September.

This subdivision may be compared with that devised by Lamb (1950) who divided the year into five seasons, the terminal dates being September 9, November 19, January 19, March 29 and June 17. Two of these dates, September 9 and June 17, agree fairly well with the division suggested above while a third, March 29, coincides with a well marked trough in the correlation graphs. The other dividing dates, November 19 and January 19, do not agree with any discernible features of the correlation graphs. From the present data it would be more natural to consider autumn as running from September 15 to December 3, and winter as continuing from December 4 to March 12. Spring will then run from March 13 to June 15, and summer from June 16 to September 14.

5. Statistical forecasts

Given the correlations between the temperature anomaly on a particular day and those on several preceding days, a multiple regression equation can be found to give the best statistical forecast of the temperature in terms of the earlier days. This is an application of the method of Wiener (1950) but can readily be justified from first principles.

Suppose T_n' is the temperature anomaly on day n, and $T_n''(K)$ is the best possible forecast of T_n' obtainable as a linear combination of the anomalies for the K preceding days.

Let
$$T_n''(K) = a_1 T_{n-1}' + a_2 T_{n-2}' \text{ - - - - - - - } + a_K T_{n-K}' \tag{1}$$
and
$$T_n' - T_n''(K) < \epsilon_n(K) \tag{2}$$
Then the problem is to choose a_1 - - - - a_K to make the general run of values of $\epsilon_n(K)$ as small as possible: to do this we impose the condition that $\overline{\epsilon_n^2(K)}$ should be a minimum.

If the values of a_1 - - - a_K have been chosen to make $\epsilon_n(K)$ minimum, then $\epsilon_n(K)$ must be uncorrelated with T_{n-1}', T_{n-2}' - - - - T_{n-K}' because if it were correlated, positively or negatively, another set of values of a_1 - - - a_K could be found, allowing for the correlation which would have a lower mean value for $\epsilon_n^2(K)$.

Thus $\overline{\epsilon_n(K)T_{n-1}'}$, $\overline{\epsilon_n(K)T_{n-2}'}$ - - - - - - $\overline{\epsilon_n(K)T_{n-K}'}$

all tend to zero if summed over many cases.

But
$$\epsilon_n(K) = T_n' - a_1 T_{n-1}' - a_2 T_{n-2}' \text{ - - - - - - - - } - a_n T_{n-K}' \tag{3}$$
so that multiplying in turn by T_{n-1}', T_{n-2}' - - - T_{n-K}', summing over many cases, and dividing by $\sigma_{T'}^2$
$$\begin{aligned}
r_1 &= a_1 + a_2 r_1 + a_3 r_2 \text{ - - - - - - - - - - - - - - - - } + a_K r_{K-1} \\
r_2 &= a_1 r_1 + a_2 + a_3 r_1 \text{ - - - - - - - - - - - - - - - - } + a_K r_{K-2} \\
r_3 &= a_1 r_2 + a_2 r_1 + a_3 + a_4 r_1 \text{ - - - - - - - - - - - - - - } + a_K r_{K-3} \\
r_K &= a_1 r_{K-1} + a_2 r_{K-2} \text{ - - - - - - - - - - - - - - - - - - } + a_K
\end{aligned} \tag{4}$$
Thus, given the values of r_1 - - - - - r_K we can find the corresponding values of a_1 - - - - a_K by means of equations (4)

Further $\epsilon_n^2 = (T_n' - a_1 T_{n-1}' \text{ - - - - - - - - - - - } - a_K T_{n-K}')^2$

and, when mean values are taken and equations (4) used, this becomes
$$\overline{\epsilon_n^2} = \overline{T_n'(T_n' - a_1 T_{n-1}' \text{ - - - - - - } - a_n T_{n-K}')} \tag{5}$$
so that the relative residual error E_K is given by
$$E_K = \frac{\overline{\epsilon_n^2(K)}}{\sigma_{T'}^2} = (1 - a_1 r_1 - a_2 r_2 \text{ - - - - - } - a_K r_K) \tag{6}$$
This enables us to estimate the proportional error remaining after the regression equation has been used and hence the value of the statistical forecast.

For large values of K the equations (4) can be solved by relaxation, or by the method described by Levinson (see Wiener (1950), Appendix B).

For K = 2, 3 or 4 the algebraic solutions are simple enough to be useful, and are given in Table 4.

The choice of data on which to apply these equations deserves some consideration. If we work on correlation coefficients calculated for one particular day, we have the difficulties that the coefficients are subject to substantial sampling errors and that the relation between these errors and the sampling errors of the resulting regression coefficients is far from obvious. If we average values of $\underline{z}$ over a period, then the corresponding values of $\underline{r}$ will be statistically more stable, but will refer to the average conditions during the period which, unless we are careful in choosing the period, may differ considerably from the conditions on a particular day. We might try to set up some theoretical criterion to help us decide what to do, but it is probably more informative to see the results of the analysis of values of $\underline{r}$ relating to different trial periods.

First we consider the analysis of the values of $\underline{r}$ obtained from averaging $\underline{z}$ throughout the year, which statistically are the most stable obtainable from these data. The results are given in Table 5.

It appears that if the simplest formula is used (K = 1) the unpredicted variance amounts to $41\frac{1}{2}$ per cent of the original value, while by using the 3-term regression equation (K = 3) the percentage residual variance is reduced to 41. The use of the 7-term formula, entailing much more work in calculation and in use produces a further improvement of 0.1 per cent. To put the matter differently, if we seek to forecast tomorrow's temperature by formulae applicable at all times of year, the mean square errors will have the values given in Table 6.

This shows that if we want a statistical formula to work all the year round, then the simple formula $T''_n = 0.7641\, T'_{n-1}$ is as good as anything more complicated. Incidentally, the standard of accuracy, as measured by the mean square error, is not very impressive. A synoptic forecaster using conventional methods might expect to do better.

Similar regression formulae may be based on the values of the serial correlations appropriate to each month of the year, and are given in Tables 7 to 18.

The regression equations take account of from one up to four consecutive terms, and it seems that, compared with the formulae based on annual values, the earlier terms may contribute a little more compared with the latest. Nevertheless, the improvement is not enough to suggest that the inclusion of still more terms is likely to justify the additional work of calculation. The use in forecasting routine of a statistical forecast obtained in this way is not likely to commend itself to synoptic meteorologists who would expect to do better by the exercise of personal skill. Nevertheless the statistical forecast may have value as a yardstick for research purposes, since it is objective and can be calculated quickly from past data, whereas the conditions under which a synoptic forecast is made cannot be reproduced properly after the event. For use as a yardstick the one-term regression formulae given in Tables 7 to 18 are probably as good as any others. Whatever formulae are used, the degree of success as measured by the E-value varies appreciably with the time of year.

6. It may of course be argued that rather than averaging the correlations, regression formulae should be calculated for each individual day and the significance of the regression coefficients judged from their stability from one day to the next. Whatever the theoretical advantages of this approach, it would involve more computation than could be undertaken at present, and the large sampling errors of the correlation coefficients might present a serious obstacle to the interpretation of the results. However, in Table 19 are given the correlations appropriate to non-overlapping 5-day periods covering the year. These should show the result of fairly short term variations in the coherence level while not being unduly affected by sampling errors.

Examples of the analysis of these data are given in Tables 20 and 21. The period was chosen because r_1 was low and the simple one-term prediction formula was expected to be below the general level.

It appears that the improvement in E-value obtained by using a four-term regression formula is much larger than in the cases examined before. It is hard to say how much of this apparent improvement is due to the 5-day mean coefficients having larger sampling errors than the monthly, and the examples are given mainly to help other investigators to form their own judgments whether the use of more complicated regression equations is likely to produce any worthwhile increase in accuracy of prediction. My own view is that none of the more complicated formulae show enough improvement on the simple one-term formulae to justify their adoption.

Acknowledgments

Acknowledgments are due to Dr. Yates of the Statistical Department of Rothamsted Experimental Station for permission to use the Hollerith installation there, to Mr. M. J. R. Healy and Miss S. Cohen for advice and assistance in using it, and to Mrs. D. Gaskin and Miss N. P. Roberts who carried out most of the hand calculations.

References

Brooks, C.E.P. (1948) Met. Mag., London, Vol. 77, 1948, p.283.

Hoblyn, T.N. (1928) Quart.J.R. Met.Soc., Vol.54, 1928, p.183.

Lamb, H.H. (1950) Quart.J.R.Met.Soc., Vol.76, 1950, p.393.

Lewis, R.P.W. and McIntosh, D.H, (1952) Met.Mag., London, Vol.81, 1952, p.242.

Ogawara, M. and others (1955) Pap. Met. Geoph., Tokyo, Vol.VI, No.1, p.87.

Wiener, N. (1950) Extrapolation, Interpolation and Smoothing of Stationary Time Series, New York. (John Wiley & Sons).

/Tables

TABLES

Table 1. Mean monthly values of variance $(^{\circ}C)^2$ and standard deviation $(^{\circ}C)$

	Variance	S.D.
January	11.56	3.40
February	10.80	3.29
March	8.03	2.83
April	7.60	2.76
May	8.40	2.90
June	7.06	2.66
July	6.61	2.57
August	5.42	2.33
September	6.64	2.58
October	7.65	2.77
November	9.43	3.07
December	10.89	3.30
Annual	8.328	2.886

Table 2. Monthly averages of z

	z_1	z_2	z_3	z_4	z_5	z_6	z_7
January	1.0474	0.6287	0.4974	0.3835	0.3042	0.2455	0.2032
February	1.1604	0.7771	0.6154	0.5063	0.4386	0.3775	0.3254
March	1.0077	0.6410	0.4548	0.3384	0.2890	0.2455	0.2213
April	1.0183	0.6020	0.3957	0.2823	0.2037	0.1273	0.1067
May	1.0455	0.6052	0.3694	0.2287	0.1290	0.0516	0.0126
June	1.0033	0.5947	0.4003	0.2907	0.2113	0.1707	0.1483
July	0.9900	0.6123	0.4223	0.3194	0.2606	0.2348	0.2348
August	0.9955	0.6232	0.4690	0.3974	0.3474	0.3250	0.3127
September	0.9490	0.5563	0.4107	0.3343	0.2783	0.2470	0.2050
October	0.9329	0.5426	0.3903	0.2945	0.2281	0.1752	0.1310
November	0.9180	0.5030	0.3320	0.2183	0.1500	0.1053	0.0743
December	1.0119	0.5919	0.4261	0.3381	0.2852	0.2552	0.2400
Ann. mean	1.0058	0.6056	0.4310	0.3253	0.2595	0.2117	0.1832
First serial correlation of series of z values	0.227	0.535	0.573	0.564	0.641	0.705	0.627
Reducing factor E	0.6774	0.3341	0.3014	0.3089	0.2467	0.1994	0.2575

Table 3. Monthly mean values of r

	r_1	r_2	r_3	r_4	r_5	r_6	r_7
January	0.7806	0.5574	0.4598	0.3653	0.2950	0.2402	0.2003
February	0.8210	0.6510	0.5476	0.4668	0.4128	0.3601	0.3140
March	0.7649	0.5656	0.4260	0.3257	0.2812	0.2402	0.2175
April	0.7691	0.5385	0.3765	0.2748	0.2012	0.1263	0.1066
May	0.7799	0.5406	0.3531	0.2251	0.1283	0.0520	0.0130
June	0.7629	0.5335	0.3799	0.2831	0.2079	0.1694	0.1469
July	0.7574	0.5455	0.3986	0.3086	0.2552	0.2308	0.2308
August	0.7595	0.5532	0.4374	0.3774	0.3337	0.3140	0.3032
September	0.7393	0.5050	0.3893	0.3221	0.2711	0.2421	0.2022
October	0.7320	0.4953	0.3714	0.2867	0.2241	0.1732	0.1303
November	0.7249	0.4645	0.3203	0.2146	0.1489	0.1046	0.0730
December	0.7666	0.5313	0.4020	0.3257	0.2775	0.2496	0.2355
Ann. mean	0.7641	0.5413	0.4062	0.3140	0.2534	0.2089	0.1810

/Table 4.

Table 4. Algebraic solutions for regression coefficients

<table>
<tr><th>$K = 2$</th><th>$K = 3$</th></tr>
<tr><td>$a_1 = r_1(1-a_2) = \frac{r_1(1-r_2)}{1 - r_1^2}$
$a_2 = \frac{r_2 - r_1^2}{1 - r_1^2}$</td><td>$a_1 + a_3 = \frac{r_1 + r_3 - 2r_1r_2}{1 + r_2 - 2 r_1^2}$
$a_1 - a_3 = \frac{r_1 - r_3}{1 - r_2}$
$a_2 = \frac{r_2(1+r_2)-r_1(r_1 + r_3)}{1 + r_2 - 2 r_1^2}$</td></tr>
<tr><td colspan="2">$K = 4$</td></tr>
<tr><td colspan="2">$a_1 + a_4 = \frac{(r_2 + r_3)(r_1 + r_2) - (r_1 + r_4)(1 + r_1)}{(r_1 + r_2)^2 - (1 + r_1)(1 + r_3)}$
$a_1 - a_4 = \frac{(r_2 - r_3)(r_1 - r_2) - (r_1 - r_4)(1 - r_1)}{(r_1 - r_2)^2 - (1 - r_1)(1 - r_3)}$
$a_2 + a_3 = \frac{(r_1 + r_4)(r_1 + r_2) - (r_2 + r_3)(1 + r_3)}{(r_1 + r_2)^2 - (1 + r_1)(1 + r_3)}$
$a_2 - a_3 = \frac{(r_1 - r_4)(r_1 - r_2) - (r_2 - r_3)(1 - r_3)}{(r_1 - r_2)^2 - (1 - r_1)(1 - r_3)}$</td></tr>
</table>

Table 5. Prediction formulae based on annual mean values of r_1, r_2 -- r_7

K	Formula	E
1	$T''_n = 0.7641\, T'_{n-1}$	0.4162
2	$T''_n = 0.8421\, T'_{n-1} - 0.1021\, T'_{n-2}$	0.4119
3	$T''_n = 0.8491\, T'_{n-1} - 0.1603\, T'_{n-2} + 0.0689\, T'_{n-3}$	0.4100
4	$T''_n = 0.8486\, T'_{n-1} - 0.1593\, T'_{n-2} + 0.0627\, T'_{n-3} + 0.0077\, T'_{n-4}$	0.4099
7	$T''_n = 0.8479\, T'_{n-1} - 0.1615\, T'_{n-2} + 0.0673\, T'_{n-3} - 0.0186\, T'_{n-4}$ $+ 0.0245\, T'_{n-5} - 0.0130\, T'_{n-6} + 0.0272\, T'_{n-7}$	0.4094

/Table 6.

Table 6. Mean square errors of various statistical forecasts applicable throughout the year

Basis of forecast	σ_E (°C)
Climatic normal: $T''_n = 0$	2.89
$K = 1$: $T''_n = 0.7641\ T'_{n-1}$	1.87
$K = 7$: $T''_n = 0.8479\ T'_{n-1} - 0.1615\ T'_{n-2} + 0.0673\ T'_{n-3} - 0.0186\ T'_{n-4} + 0.0245\ T'_{n-5} - 0.0130\ T'_{n-6} + 0.0272\ T'_{n-7}$	1.86

Table 7. Prediction formulae based on January mean values of r_1 to r_7

K	Formula	E
1	$T''_n = 0.7806\ T'_{n-1}$	0.3907
2	$T''_n = 0.8843\ T'_{n-1} - 0.1328\ T'_{n-2}$	0.3837
3	$T''_n = 0.9087\ T'_{n-1} - 0.2957\ T'_{n-2} + 0.1839\ T'_{n-3}$	0.3709
4	$T''_n = 0.9242\ T'_{n-1} - 0.3209\ T'_{n-2} + 0.2613\ T'_{n-3} - 0.0845\ T'_{n-4}$	0.3683

Table 8. Prediction formulae based on February mean values of r_1 to r_7

K	Formula	E
1	$T''_n = 0.8210\ T'_{n-1}$	0.3260
2	$T''_n = 0.8788\ T'_{n-1} - 0.0706\ T'_{n-2}$	0.3245
3	$T''_n = 0.8861\ T'_{n-1} - 0.1611\ T'_{n-2} + 0.1027\ T'_{n-3}$	0.3212
4	$T''_n = 0.8853\ T'_{n-1} - 0.1597\ T'_{n-2} + 0.0975\ T'_{n-3} + 0.0063\ T'_{n-4}$	0.3209

Table 9. Prediction formulae based on March mean value of r_1 to r_7

K	Formula	E
1	$T''_n = 0.7649\ T'_{n-1}$	0.4149
2	$T''_n = 0.8009\ T'_{n-1} - 0.0470\ T'_{n-2}$	0.4140
3	$T''_n = 0.8019\ T'_{n-1} - 0.0642\ T'_{n-2} + 0.0217\ T'_{n-3}$	0.4137
4	$T''_n = 0.8018\ T'_{n-1} - 0.0638\ T'_{n-2} + 0.0140\ T'_{n-3} + 0.0095\ T'_{n-4}$	0.4137

/Table 10.

Table 10. Prediction formulae based on April mean values of r_1 to r_7

K	Formula	E
1	$T''_n = 0.7691\, T'_{n-1}$	0.4085
2	$T''_n = 0.8688\, T'_{n-1} - 0.1297\, T'_{n-2}$	0.4016
3	$T''_n = 0.8716\, T'_{n-1} - 0.1480\, T'_{n-2} + 0.0209\, T'_{n-3}$	0.4015
4	$T''_n = 0.8706\, T'_{n-1} - 0.1443\, T'_{n-2} + 0.0011\, T'_{n-3} + 0.0259\, T'_{n-4}$	0.4014

Table 11. Prediction formulae based on May mean values of r_1 to r_7

K	Formula	E
1	$T''_n = 0.7799\, T'_{n-1}$	0.3918
2	$T''_n = 0.9144\, T'_{n-1} - 0.1725\, T'_{n-2}$	0.3802
3	$T''_n = 0.9115\, T'_{n-1} - 0.1567\, T'_{n-2} - 0.0175\, T'_{n-3}$	0.3800
4	$T''_n = 0.9115\, T'_{n-1} - 0.1561\, T'_{n-2} - 0.0211\, T'_{n-3} + 0.0043\, T'_{n-4}$	0.3800

Table 12. Prediction formulae based on June mean values of r_1 to r_7

K	Formula	E
1	$T''_n = 0.7629\, T'_{n-1}$	0.4180
2	$T''_n = 0.8514\, T'_{n-1} - 0.1160\, T'_{n-2}$	0.4124
3	$T''_n = 0.8555\, T'_{n-1} - 0.1453\, T'_{n-2} + 0.0345\, T'_{n-3}$	0.4117
4	$T''_n = 0.8551\, T'_{n-1} - 0.1425\, T'_{n-2} + 0.0153\, T'_{n-3} + 0.0225\, T'_{n-4}$	0.4114

Table 13. Prediction formulae based on July mean values of r_1 to r_7

K	Formula	E
1	$T''_n = 0.7574\, T'_{n-1}$	0.4263
2	$T''_n = 0.8075\, T'_{n-1} - 0.0662\, T'_{n-2}$	0.4245
3	$T''_n = 0.8087\, T'_{n-1} - 0.0816\, T'_{n-2} + 0.0193\, T'_{n-3}$	0.4243
4	$T''_n = 0.8081\, T'_{n-1} - 0.0787\, T'_{n-2} + 0.0114\, T'_{n-3} + 0.0379\, T'_{n-4}$	0.4236

/Table 14.

Table 14. Prediction formulae based on August mean values of r_1 to r_7

K	Formula	E
1	$T''_n = 0.7595\ T'_{n-1}$	0.4232
2	$T''_n = 0.8019\ T'_{n-1} - 0.0558\ T'_{n-2}$	0.4219
3	$T''_n = 0.8067\ T'_{n-1} - 0.1247\ T'_{n-2} + 0.0859\ T'_{n-3}$	0.4187
4	$T''_n = 0.8011\ T'_{n-1} - 0.1163\ T'_{n-2} + 0.0313\ T'_{n-3} + 0.0675\ T'_{n-4}$	0.4167

Table 15. Prediction formulae based on September mean values of r_1 to r_7

K	Formula	E
1	$T''_n = 0.7393\ T'_{n-1}$	0.4534
2	$T''_n = 0.8072\ T'_{n-1} - 0.0918\ T'_{n-2}$	0.4496
3	$T''_n = 0.8173\ T'_{n-1} - 0.1807\ T'_{n-2} + 0.1101\ T'_{n-3}$	0.4442
4	$T''_n = 0.8140\ T'_{n-1} - 0.1745\ T'_{n-2} + 0.0844\ T'_{n-3} + 0.0307\ T'_{n-4}$	0.4435

Table 16. Prediction formulae based on October mean values of r_1 to r_7

K	Formula	E
1	$T''_n = 0.7320\ T'_{n-1}$	0.4642
2	$T''_n = 0.7958\ T'_{n-1} - 0.0872\ T'_{n-2}$	0.4607
3	$T''_n = 0.8037\ T'_{n-1} - 0.1584\ T'_{n-2} + 0.0891\ T'_{n-3}$	0.4571
4	$T''_n = 0.8031\ T'_{n-1} - 0.1577\ T'_{n-2} + 0.0867\ T'_{n-3} + 0.0031\ T'_{n-4}$	0.4571

Table 17. Prediction formulae based on November mean values of r_1 to r_7

K	Formula	E
1	$T''_n = 0.7249\ T'_{n-1}$	0.4745
2	$T''_n = 0.8181\ T'_{n-1} - 0.1286\ T'_{n-2}$	0.4667
3	$T''_n = 0.8274\ T'_{n-1} - 0.1872\ T'_{n-2} + 0.0718\ T'_{n-3}$	0.4642
4	$T''_n = 0.8299\ T'_{n-1} - 0.1935\ T'_{n-2} + 0.0993\ T'_{n-3} - 0.0335\ T'_{n-4}$	0.4637

Table 18. Prediction formulae based on December mean values of r_1 to r_7

K	Formula	E
1	$T''_n = 0.7666\ T'_{n-1}$	0.4123
2	$T''_n = 0.8715\ T'_{n-1} - 0.1368\ T'_{n-2}$	0.4046
3	$T''_n = 0.8861\ T'_{n-1} - 0.2309\ T'_{n-2} + 0.1083\ T'_{n-3}$	0.3999
4	$T''_n = 0.8839\ T'_{n-1} - 0.2257\ T'_{n-2} + 0.0897\ T'_{n-3} + 0.0229\ T'_{n-4}$	0.3995

Table 20. Prediction formulae based on mean values of r_1 to r_7 for the 5 days January 5 - 9

K	Formula	E
1	$T''_n = 0.6973\ T'_{n-1}$	0.5138
2	$T''_n = 0.7692\ T'_{n-1} - 0.1030\ T'_{n-2}$	0.5082
3	$T''_n = 0.7973\ T'_{n-1} - 0.3133\ T'_{n-2} + 0.2732\ T'_{n-3}$	0.4704
4	$T''_n = 0.8010\ T'_{n-1} - 0.3174\ T'_{n-2} + 0.2837\ T'_{n-3} - 0.0130\ T'_{n-4}$	0.4701

Table 21. Prediction formulae based on mean values of r_1 to r_7 for the 5 days January 10 - 14

K	Formula	E
1	$T''_n = 0.7192\ T'_{n-1}$	0.4828
2	$T''_n = 0.9186\ T'_{n-1} - 0.2771\ T'_{n-2}$	0.4455
3	$T''_n = 0.9605\ T'_{n-1} - 0.4163\ T'_{n-2} + 0.1515\ T'_{n-3}$	0.4354
4	$T''_n = 0.9825\ T'_{n-1} - 0.4749\ T'_{n-2} + 0.2865\ T'_{n-3} - 0.1411\ T'_{n-4}$	0.4265

/Table 19.

Table 19. Correlations and corresponding z values for 5-day periods

Period	z_1	r_1	z_2	r_2	z_3	r_3	z_4	r_4	z_5	r_5	z_6	r_6	z_7	r_7
1	.862	.697	.464	.433	.424	.400	.386	.368	.280	.273	.262	.256	.370	.354
2	.906	.719	.404	.383	.224	.220	.100	.100	.066	.066	.136	.135	.176	.174
3	1.032	.775	.656	.576	.516	.475	.448	.420	.404	.383	.296	.288	.182	.180
4	1.124	.809	.750	.635	.552	.573	.534	.488	.374	.357	.266	.260	.152	.151
5	1.246	.847	.768	.646	.570	.515	.478	.445	.396	.377	.300	.291	.300	.291
6	1.088	.796	.694	.601	.612	.546	.402	.382	.284	.277	.214	.211	.148	.147
7	1.180	.827	.744	.632	.542	.495	.438	.412	.398	.378	.368	.352	.314	.304
8	1.272	.854	.960	.744	.754	.638	.544	.496	.484	.449	.436	.410	.380	.363
9	1.190	.831	.820	.675	.682	.593	.616	.548	.484	.449	.404	.383	.334	.322
10	1.182	.828	.712	.612	.500	.462	.394	.375	.334	.322	.278	.271	.216	.213
11	1.052	.783	.710	.611	.584	.526	.480	.446	.422	.399	.354	.340	.294	.286
12	1.100	.800	.822	.676	.728	.622	.624	.554	.548	.499	.442	.415	.396	.377
13	1.016	.768	.610	.544	.386	.368	.356	.342	.356	.342	.306	.297	.264	.258
14	.792	.660	.420	.397	.302	.293	.204	.201	.230	.226	.236	.232	.238	.234
15	.924	.728	.536	.490	.294	.286	.108	.108	.092	.092	.052	.052	.012	.012
16	1.052	.783	.672	.586	.516	.475	.428	.404	.282	.275	.192	.190	.164	.163
17	1.124	.809	.814	.672	.594	.533	.488	.453	.462	.432	.496	.459	.512	.472
18	1.034	.776	.678	.590	.454	.425	.292	.284	.238	.234	.216	.213	.216	.213
19	.912	.722	.482	.448	.358	.343	.312	.302	.244	.239	.156	.155	.142	.141
20	.952	.741	.514	.473	.298	.289	.180	.178	.086	.086	.122	.121	.172	.170
21	1.232	.843	.802	.665	.622	.553	.518	.476	.460	.430	.314	.304	.114	.114
22	1.020	.770	.580	.523	.392	.373	.306	.297	.234	.230	.166	.164	.208	.205
23	1.006	.764	.588	.528	.342	.329	.174	.172	.036	.036	.008	.008	-.040	-.040
24	.904	.718	.462	.432	.250	.245	.182	.180	.162	.161	.062	.062	.042	.042
25	.980	.753	.608	.543	.348	.335	.142	.141	-.014	-.014	-.080	-.080	-.022	-.022
26	.986	.756	.510	.470	.328	.317	.238	.234	.136	.135	.002	.002	-.098	-.098
27	1.218	.839	.804	.666	.532	.487	.360	.345	.278	.271	.144	143	.074	.074
28	1.042	.779	.528	.484	.276	.269	.140	.139	.020	.020	.022	.022	.040	.040
29	1.136	.813	.690	.598	.394	.375	.164	.163	.020	.020	-.096	-.096	-.184	-.182
30	1.000	.762	.630	.558	.420	.397	.356	.342	.312	.302	.280	.273	.290	.282

/31

Table 19. (Continued)

Period	z_1	r_1	z_2	r_2	z_3	r_3	z_4	r_4	z_5	r_5	z_6	r_6	z_7	r_7
31	1.056	.784	.642	.566	.426	.402	.262	.256	.122	.121	.014	.014	.030	.030
32	1.082	.794	.636	.562	.464	.433	.344	.331	.252	.247	.218	.215	.122	.121
33	.988	.757	.546	.498	.390	.371	.296	.288	.226	.222	.224	.220	.208	.205
34	.950	.740	.588	.528	.334	.322	.218	.215	.106	.106	.058	.058	.070	.070
35	.920	.726	.540	.493	.372	.356	.264	.258	.226	.222	.150	.149	.142	.141
36	.990	.757	.610	.544	.460	.430	.360	.345	.320	.310	.276	.269	.256	.251
37	.962	.745	.558	.506	.362	.347	.276	.269	.252	.247	.236	.232	.236	.232
38	1.108	.803	.676	.589	.412	.390	.338	.326	.308	.299	.282	.275	.236	.232
39	.878	.705	.518	.476	.368	.352	.250	.245	.190	.188	.186	.184	.148	.147
40	.942	.736	.570	.515	.338	.326	.308	.299	.286	.278	.290	.282	.302	.293
41	1.104	.802	.766	.645	.586	.527	.404	.383	.264	.258	.208	.205	.234	.230
42	.962	.745	.574	.518	.456	.427	.360	.345	.284	.277	.234	.230	.234	.230
43	1.008	.765	.660	.578	.404	.383	.306	.297	.292	.284	.252	.247	.200	.197
44	1.016	.768	.704	.607	.566	.512	.504	.465	.376	.359	.370	.354	.320	.310
45	.988	.757	.594	.533	.460	.430	.386	.368	.394	.375	.328	.317	.298	.289
46	1.010	.766	.638	.564	.498	.461	.414	.392	.310	.300	.290	.282	.324	.313
47	.964	.746	.512	.472	.370	.354	.358	.343	.342	.329	.284	.277	.280	.273
48	1.010	.766	.664	.581	.500	.462	.374	.357	.322	.311	.336	.324	.338	.326
49	1.004	.763	.668	.584	.546	.498	.430	.405	.346	.333	.352	.338	.330	.319
50	.986	.756	.612	.546	.494	.457	.470	.438	.508	.468	.500	.462	.418	.395
51	.882	.707	.496	.459	.390	.371	.388	.370	.376	.359	.342	.329	.304	.295
52	.920	.726	.438	.412	.278	.271	.204	.201	.130	.129	.116	.115	.160	.159
53	.920	.726	.516	.475	.340	.327	.214	.211	.094	.094	.044	.044	-.034	-.034
54	.972	.750	.608	.543	.462	.432	.342	.329	.260	.254	.202	.199	.136	.135
55	1.002	.762	.666	.582	.442	.415	.298	.289	.244	.239	.246	.241	.246	.241
56	.960	.744	.596	.534	.584	.526	.544	.496	.460	.430	.368	.352	.262	.256
57	.868	.700	.424	.400	.256	.251	.228	.224	.258	.252	.268	.262	.232	.228
58	.944	.737	.484	.449	.308	.299	.232	.228	.172	.170	.072	.072	.038	.038
59	.844	.688	.444	.417	.290	.282	.242	.237	.254	.249	.248	.243	.190	.188
60	.976	.751	.618	.550	.468	.437	.278	.271	.090	.090	-.006	-.006	-.034	-.034

/61

Table 19. (Continued)

Period	z_1	r_1	z_2	r_2	z_3	r_3	z_4	r_4	z_5	r_5	z_6	r_6	z_7	r_7
61	.914	.723	.514	.473	.298	.289	.190	.188	.144	.143	.100	.100	.128	.127
62	.826	.678	.436	.410	.264	.258	.112	.112	.026	.026	.016	.016	-.010	-.010
63	.924	.728	.574	.518	.358	.343	.270	.264	.186	.184	.148	.147	.174	.172
64	.946	.738	.450	.422	.298	.289	.202	.199	.152	.151	.106	.106	.068	.068
65	.926	.729	.508	.468	.332	.320	.218	.215	.140	.139	.090	.090	.008	.008
66	.972	.750	.564	.511	.432	.407	.336	.324	.266	.260	.162	.161	.100	.100
67	.958	.743	.552	.502	.338	.326	.186	.184	.086	.086	.110	.110	.126	.125
68	.918	.725	.478	.445	.354	.340	.268	.262	.190	.188	.096	.096	.016	.016
69	1.036	.776	.666	.582	.542	.495	.450	.422	.370	.354	.392	.373	.348	.335
70	1.166	.823	.730	.623	.522	.479	.374	.357	.298	.289	.224	.220	.104	.104
71	.904	.718	.456	.427	.366	.350	.312	.302	.256	.251	.184	.182	.168	.166
72	1.096	.799	.650	.572	.410	.388	.286	.278	.226	.222	.134	.133	.084	.084
73	1.054	.783	.630	.558	.428	.404	.360	.345	.434	.409	.302	.293	.486	.451

Appendix A

Data and computation

The original tabulations made at Kew Observatory gave separately for each day of each year from 1900 to 1950 the daily maximum and minimum temperature. These were given in degrees Absolute to the nearest tenth of a degree.

Each temperature (omitting the initial figure, nearly always 2) formed a 3-figure group. The maxima were punched on one pack of Hollerith cards and the minima in corresponding positions on another. In each pack, data for the first 16 days of each month are on one card and those for the rest of the month on another, so that each of the two packs covering the 51 years contains 1224 cards. The punching was verified by the normal Hollerith procedure and finally the entire contents of each card were listed, using the Hollerith Tabulator, and the printed version was checked back against the source documents. There is no reasonable doubt that the data punched on the cards which form the basis of all the calculations are accurately copied from the record made at the Observatory.

These two packs of Hollerith cards bear in corresponding positions the maximum and minimum temperatures for the same day. The packs were interleaved and the temperatures added on a Hollerith Tabulator, with a break of control after every second card, the totals being summary punched into corresponding positions on a blank pack of cards. This third pack effectively gives the daily mean temperature in units of $\frac{1}{2}$ degree Absolute. February 29 was ignored when it occurred.

Most of the work in finding variances and correlations consists in finding the sums of squares and products. If the daily mean temperatures are denoted by T_1, T_2, etc., then the sums $\sum T_1^2$ and products $\sum T_1 T_2$, $\sum T_1 T_3$ up to $\sum T_1 T_7$ were found on the Hollerith Tabulator by progressive digiting. Here T_1 is supposed to represent the temperature on any particular calendar date, and the summations to extend over the 51 years 1900-1950. In the progressive digiting each 'summation' such as $\sum T_1 T_2$ is obtained in two different ways and thus checked for accuracy, but the sums of squares are not so checked. However, on account of the way the calculation was arranged each result had a large non-significant constant added to it, such that any mistakes in the non-significant digits would probably be obvious. Apart from known machine failures no mistakes seem to have occurred in the non-significant digits so that the number of mistakes among the significant figures is probably very small.

From each printed result the constant (3,511,485) was subtracted, and the variances, covariances and serial correlations were found by the formulae

$$V(T_1) = \frac{n\sum T_1^2 - (\sum T_1)^2}{n(n-1)}$$

$$\operatorname{cov}(T_1 T_2) = \frac{n\sum T_1 T_2 - (\sum T_1)(\sum T_2)}{n(n-1)}$$

$$r_k(T_1) = \frac{\operatorname{cov} T_1 T_{1+k}}{\sqrt{V(T_1)\,V(T_{1+k})}}$$

These steps were done on a hand or electric calculating machine, the results being checked by repetition. In three cases out of 2455, the final calculation gave a value of r exceeding unity. It was confirmed that no error had occurred in the hand part of the calculation, so that the inconsistency must be present in the printed figures output from the Tabulator. At first sight the fault is more likely to arise in the sums of squares which are unchecked, rather than in the sums of products which are checked, but it seems very unlikely that an error in a sum of squares should produce an impossible

/value

value for only one of the fourteen correlations into which it enters. The checking of the sums of products is by comparing two columns of printed figures, and perhaps the most likely explanation is that in these three cases a discrepancy escaped the notice of the scrutineer. These errors were only discovered months after the completion of the Hollerith part of the calculation, and it would have been quite awkward to have recomputed the values, so the mean values for the appropriate month have been used in Fig. 1 instead.

Appendix B

A diagram for simple estimation of a correlation coefficient

If two variables are positively correlated we would expect that the number of cases in which the signs of corresponding deviations agree would exceed the number in which the signs disagree. The relation between the correlation coefficient r and the proportion of cases with like signs p is discussed by Ogawara and others (1955) on the assumption that both the variables are normally distributed. Fig. 2 is a simplified version of the diagram given by Ogawara, showing the unique relation between p and r when the sample considered is infinitely large, and the limits within which r is expected to lie (at the 10 per cent confidence level) if p is found from a sample of 500, 100 or 20 pairs.

In dealing with one autocorrelated series let p be the probability that a term which departs from normal in one direction is followed by another which departs in the same direction. p is assumed not to depend on whether the departure is positive or negative or on the sequence of previous anomalies. Then the probability that a chosen term is followed by exactly n more with anomalies of the same sign is $p^n (1-p)$, and the probability that it is preceded by exactly m terms of like sign is $p^m (1-p)$. Thus the probability that a chosen term belongs to a run of exactly k terms is $kp^{k-1} (1-p)^2$. Hence in a large sample, if N is the total number of terms and R the total number of runs

$$\begin{aligned} R &= \sum_{k=1}^{\infty} N p^{k-1} (1-p)^2 \\ &= N(1-p) \\ \therefore p &= 1 - \frac{R}{N} \end{aligned}$$

The investigator intending to use this method should therefore:-

(i) satisfy himself that the distribution of the series studied does not depart seriously from normal

(ii) find the mean and then R and hence p by the above equation and

(iii) look up the corresponding value of r in Fig. 2.

FIG I. STANDARD DEVIATION OF THE MEAN DAILY TEMPERATURE AT KEW FOR EACH DAY OF THE YEAR (IN DEGREES CELSIUS) AND SERIAL CORRELATIONS BETWEEN THE TEMPERATURE ON EACH CALENDAR DAY AND THOSE OF THE SEVEN SUCCEEDING DAYS.

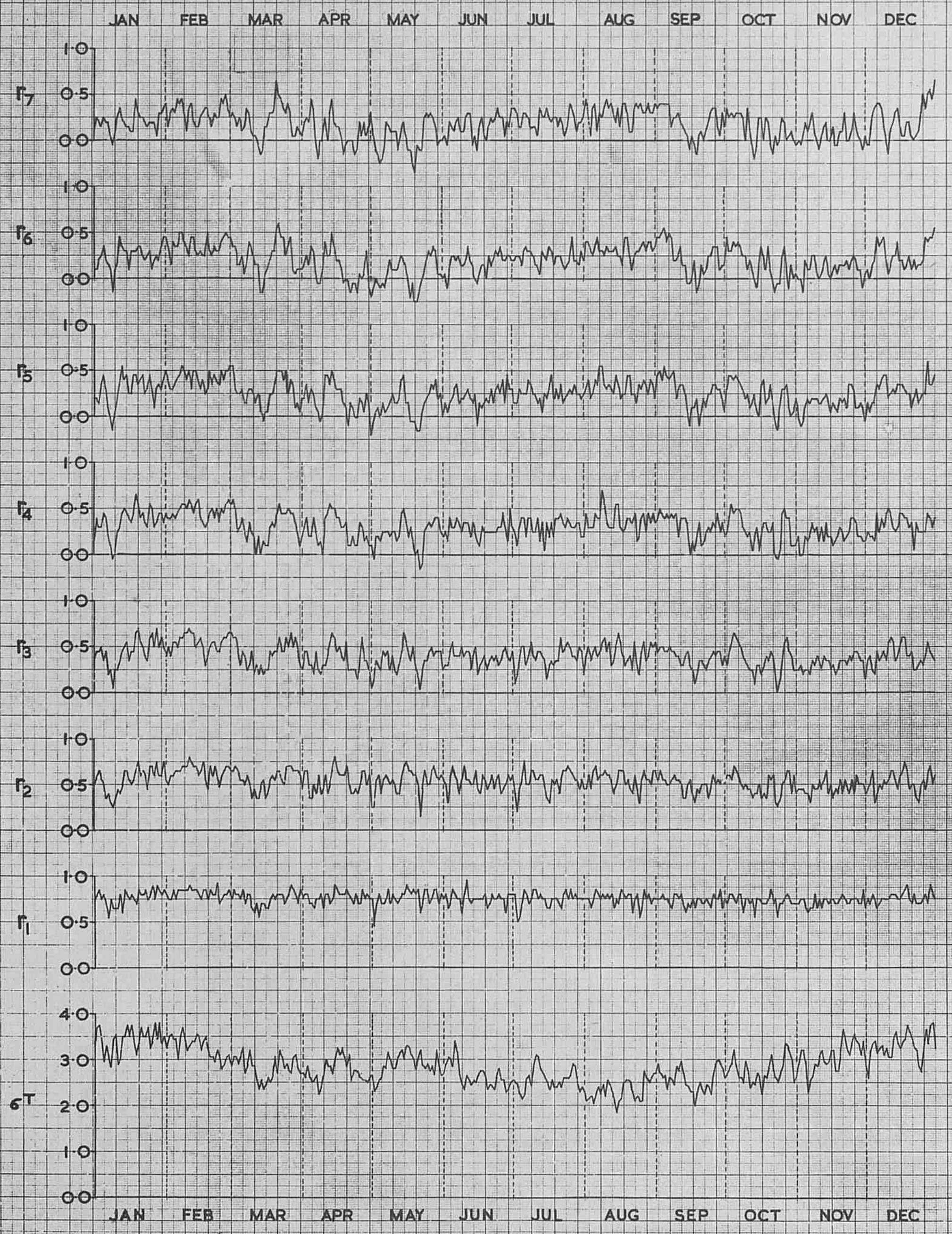

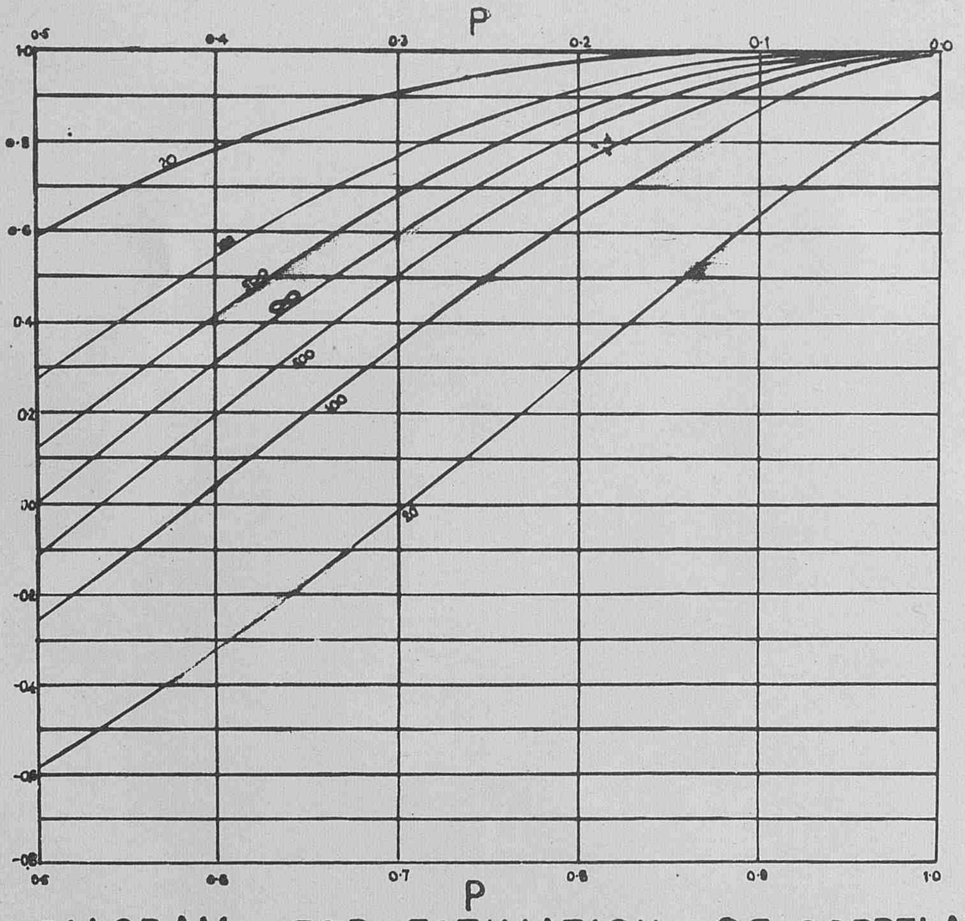

DIAGRAM FOR ESTIMATION OF CORRELATION COEFFICIENT WITH CONFIDENCE LIMITS

M.R.P. 1024
S.C.III/226
12th April, 1957

RECD
27 MAR 1958

Observations of humidity, temperature and wind at Idris 23rd May - 2nd June, 1956

by

N. C. Helliwell and J. K. Mackenzie

(Meteorological Office)

AIR MINISTRY

METEOROLOGICAL RESEARCH COMMITTEE

At the time of issue this report has not been published. Any author desiring to quote this paper should refer to it as "A paper of the Meteorological Research Committee (London),
M.R.P. No. 1024 by Mr. N.C. Helliwell and Mr. J.K. Mackenzie

A copy is available in the Library of the Meteorological Office."

M.R.P. 1024
S.C.III/226
12th April, 1957

AIR MINISTRY
METEOROLOGICAL RESEARCH COMMITTEE

Observations of humidity, temperature and wind at Idris 23rd May-2nd June, 1956

by

N.C. Helliwell and J.K. Mackenzie (Meteorological Office)

1. Summary

Seventeen flights were made from 23rd May to 2nd June, 1956 to investigate the humidity of the atmosphere at altitude over Idris in Tripolitania. Two types of flight were made: those over the desert to the south at heights between 35,000 and 48,000 ft. and ascents over Idris in which measurements were made at selected levels up to 48,000 ft.

The first type of flight is treated synoptically and an attempt is made to explain the values of frost point found. The second type of flight is also treated synoptically. Over some eight or nine observations during the period, the mean frost point at 48,000 ft. over Idris was found to be -82.6°C compared to -82°C over Southern England, but the mean values over Idris show more moisture at all lower altitudes than do the means over Southern England for 1954 and 1955.

2. Introduction

It was decided in April, 1956 that Canberra W.J.582 of the Meteorological Research Flight should go to R.A.F. Station, Idris (32°40'N., 13°10'E.) to be used for measurements of humidity, temperature and wind. It was also intended to measure the ozone content of the air at altitude, but the results were so anomalous that they have been made the subject of a separate report which also assesses the value of all the measurements made by the Flight this year, using the same apparatus abroad and at home.

Alongside Fig. 10 of this report there are a number of conversion tables, scales, etc., which are useful in reading the text.

3. Flight planning

The plan of the flights was to make measurements of humidity, temperature, ozone and wind

(1) during ascents over Idris to 48,000 ft. or maximum altitude

(2) during flights to the south of Idris, outbound leg at varying levels, inbound leg at maximum altitude

(3) during flights to the north similar to those to the south but with shorter legs at four different altitudes.

/Owing

Owing to the fact that most of the stand-by equipment carried to Idris by R.A.F. Transport Command was not unloaded at Idris, the flight plan was modified and on the first few flights humidity, temperature and wind measurements only were made. The hygrometer became unserviceable on three occasions due to the high temperature reached in the aircraft cabin on the ground and the consequent breaking of the pressure-seals. The flights were as listed below in Table 1.

Table 1. Flights from R.A.F. Idris

Date	Type of flight	No. of flight	Observations taken and remarks
23rd May	Odiham to Idris	1	Frost points, wind, temperature
a.m. 24th May	High level ascent over Idris	2	Frost points, wind, temperature
p.m. 24th May	"	3	Two values of frost points. Hygrometer unserviceable
a.m. 25th May	"	4	Hygrometer unserviceable. Temperature to 46,000 ft.
p.m. 25th May	"	5	Frost points, wind and temperature to 48,000 ft.
a.m. 26th May	Flight to the south of Idris	6	Hygrometer unserviceable. Some winds and temperatures
p.m. 26th May	High level ascent over Idris	7	Frost points, wind and temperature
a.m. 27th May	Flight to 24°N. and return to Idris	8	Frost points, wind and temperature
p.m. 27th May	High level ascent over Idris	9	Frost points, wind and temperature
a.m. 29th May	Flight to 23°N. and return to Idris	10	Frost points, ozone, wind and temperature
p.m. 29th May	High level ascent over Idris	11	Frost points, wind and temperature
a.m. and p.m.) 30th May)	"	12 13	Frost points, wind and temperature
a.m. and p.m.) 31st May)	"	14 15	Ozone was measured on the morning flights
a.m. 1st June	Flight to 23°N. and return	16	Wind, temperature and ozone
a.m. 2nd June	Idris to Tangmere	17	Wind and temperature

4. Instruments

Frost point was measured by the Dobson-Brewer pressurised frost point hygrometer. Temperature was measured by flat-plate thermometer and standard Meteorological Office balanced bridge. The results are presented here in comparison with winds found by the radio sonde at Wheelus Field, some 17 miles NNE. of Idris. All readings of height, airspeed and course were taken from the standard aircraft altimeter, airspeed meter and gyrocompass.

/5.

5. High level ascents only

Mean temperatures and frost points

Fig. 1 and Table 2 compare mean temperatures, mean frost points and relative humidities derived from them, found at Idris during May, 1956 with the overall means for the two years 1954 and 1955 over Southern England (2) and with the means for those ascents over Southern England which showed a tropopause at 38,000 ft. or above.

Table 2. Mean temperatures and frost points (degrees C)

Height ft.	No. of cases at Idris	Mean temperature May, 1956 Idris	1954-55 England	1954-55 High trop. England	No. of cases at Idris	Frost points May, 1956 Idris	1954-55 England	1954-55 High trop. England	Relative humidity % May, 1956 Idris	1954-55 England
5,000	4	+24.8	+ 1.4	-	3	- 5.8	- 8.5	-	12.5	45
10,000	11	+ 9.8	- 6.4	-	7	-10.6	-14.7	-	22	49
15,000	6	- 4.1	-15.6	-	3	-13.5	-29.5	-	46	26
20,000	12	-15.95	-25.8	-22.6	9	-30.6	-37.1	-31.9	25	31
25,000	11	-27.1	-37.3	-33.9	9	-41.6	-47.6	-43.8	31.5	30
30,000	12	-39.6	-47.4	-46.7	9	-46.2	-56.6	-53.5	46	32
34,000	9	-49.5	-54.9	-55.7	9	-55.0	-64.6	-60.6	51	27
36,000	7	-54.2	-56.1	-59.7	7	-59.0	-67.6	-64.8	50	20
40,000	12	-59.3	-55.2	-63.4	10	-71.1	-75.4	-72.9	18.8	5.4
44,000	10	-61.3	-53.4	-58.0	8	-78.6	-80.3	-80.8	8.8	2.3
46,000	9	-63.8	-52.8	-57.5	7	-80.4	-81.4	-82.3	8	1.8
48,000	11	-65.9	-53.1	-56.8	8	-82.6	-82.0	-83.0	4.7	1.6

From Fig.1 it can be seen that the mean temperature difference between Idris and the south of England falls from 25°C at 5,000 ft. to almost zero at 38,000 ft. At Idris the mean height of the tropopause is 38,600 ft., and there is a cooling above 44,000 ft. presumably towards the tropical tropopause which is believed to lie between 50,000 and 55,000 ft., whereas over Southern England the temperature, in the two-year mean, rises slightly in the stratosphere between 38,000 ft. and 50,000 ft.

Table 3 shows the heights of clouds and haze observed during the ascents.

Table 3

Cirrus, altocumulus and haze tops and bases, with tropopause height on high level ascents over Idris

Date	Flight no.	Haze top	Altocumulus base	Altocumulus top	Cirrus base	Cirrus top	Tropopause ht. (ft.) 1st	Tropopause ht. (ft.) 2nd
a.m. 24th May	2	18,000	18,000	22,000	34,000	34,200	38,000	-
p.m. 24th May	3	17,000	16,500	19,000	33,500	34,000	-	-
a.m. 25th May	4	-	-	-	33,500	34,000	-	-
p.m. 25th May	5	19,000	-	-	31,500	34,000	36,000	-
a.m. 26th May	6	14,000	-	-	31,500	-	-	-
p.m. 26th May	7	20,000	-	-	27,000	38,500	38,000	-
a.m. 27th May	8	15,000	-	-	-	-	-	-
p.m. 27th May	9	18,500	16,000	18,500	-	-	38,000	42,000
a.m. 29th May	10	19,500	-	-	-	-	-	-
p.m. 29th May	11	19,500	-	-	-	-	42,000	-
a.m. 30th May	12	19,500	-	-	30,000	-	40,000	-
p.m. 30th May	13	18,000	-	-	30,000	-	39,000	-
a.m. 31st May	14	18,000	-	-	30,000	38,000	38,000	-
p.m. 31st May	15	21,500	-	-	30,000	42,000	38,000	-
	Mean	18,300	-	-			38,600	

The mixing ratio as indicated by the frost point decreases only slightly with increasing height up to 15,000 ft., but at 20,000 ft. it has fallen to about a quarter of the value at 15,000 ft. This decrease is no doubt associated with the haze top, the mean height of which is 18,000 ft. The air remains dry from 20,000 to 30,000 ft., as shown by the absence of cloud and the low frost points. Above 30,000 ft., however, cirrus cloud is reported on 10 of the 14 flights and this is reflected in the mean frost point and relative humidity figures between 30,000 and 38,000 ft. where there is a layer of high relative humidity. Above 40,000 ft. the frost point falls somewhat less rapidly and in the mean reaches a value of -82.6°C at 48,000 ft.

Although the humidity structure of the stratosphere at Idris resembles that over Southern England the amount of moisture in gm/kgm is a little greater at Idris and the relative humidity is three or more times as great.

A complete list of the ascents and the observations obtained are given in Table 4 and the observations are plotted in Fig. 2 to 10. Each of the long flights at fixed levels to examine humidity variation in the horizontal is described in a later section.

5.1 Notes on individual ascents

Flight 2. As can be seen from Fig. 2 there is fairly close agreement in the lower layers between the aircraft ascent and the radio sonde ascent made some seven hours earlier. Between 30,000 ft. and 40,000 ft. the frost points and the thin layer of cirrus are mutually consistent. At the tropopause (38,000 ft.) there is a relative humidity of 50 per cent but above this level it falls sharply to about 15 per cent and remains at this value to 46,000 ft. although the frost point continues to decrease at about 1°C per 1,000 ft. At 48,000 ft. the relative humidity is about 10 per cent and the frost point appears to have decreased sharply although small (1°C) errors at 46,000 ft. and 48,000 ft. may have accentuated the sharpness of the fall off.

There is quite close agreement between the radio sonde winds and those obtained by the observer in the aircraft, the general wind direction in the stratosphere being south-west.

Flights 5, 7 and 9 are shown in Fig. 3, 4 and 5. They generally show the same type of air mass in the stratosphere as Flight 2. The agreement with the radio sonde data is generally close except, in some cases, for the frost points.

Flight 11. In Fig. 6 the measurements of humidity, temperature and wind made by the aircraft are compared with those made by radio sonde. Once again there is quite close agreement in the lower levels, but above 20,000 ft. there is a difference between the temperatures, not very large but remarkably constant. The high relative humidities, the presence of cirrus, and the low thermal stability, suggest that some ascent was taking place in the upper troposphere. The same inference can be drawn from a consideration of the changes in temperature and frost point which will result from raising the air between 250 and 150 mb. - as represented by Fig. 5 - through 20 mb., when it will be found that the new curves approximate very closely to those of Fig. 6. The north-west winds shown by the aircraft ascent are consistent with the winds found by radio sonde methods.

Fig. 7 shows the newly formed high tropopause and Fig. 8-10 show a gradual decrease in its height.

6. Long flights at constant altitude and weather sequence during the period

6.1 Flight 1. Odiham to Idris 23rd May, 1956

The flight was made at 40,000 ft. rising to 42,000 ft. to the south, and the details can be found on Fig. 12.

The general synoptic situation at 0900 G.M.T. (Fig. 11) showed a strong ridge over Norway and a weak col over Southern England ahead of an eastward moving frontal system. There was a shallow depression over Germany and Italy and a depression off the coast of Spain was moving east. Associated with each of these depressions was a cold front and both these fronts were moving along the North African coast, one in the vicinity of Algiers, the other near Tunis. Observations from the Sahara indicate the seasonal low pressure area to the south of Idris. Outbreaks of rain were reported over Southern France. Weather over England on take-off was fine but hazy, with some small cumulus, and at Idris the weather was fine with 3/8 of cirrus and altocumulus.

At 0300 G.M.T. the 200 mb. flow shown in Fig. 12 was divided, with a strong south-westerly flow to the north of the British Isles and a strong west-south-westerly flow over the Southern Mediterranean and North Africa. From 5°W. to 15°E. and roughly between 55°N. and 40°N. there was a weak sinusoidal flow with the principal trough-axis at about 2°W. and the ridge between 5 and 10°E.

The 200 mb. flow is superimposed on the same map as the flight observations in Fig. 12 which shows the variation of wind field very clearly, with light winds in the north changing to strong westerlies in the south. These strong winds in the south are probably associated with the sub-tropical jet stream. South of 45°N. there is very close agreement between the observed winds of the flight and those shown by the contour chart. Presumably the differences between the observed winds in the north and those shown on the contour chart are due to the movement of the trough at 2°W. to a position further east during the five hours between the observations on the chart and those taken in the aeroplane: they may also be due to the difference between the wind at the height of the contour map and the wind at the height of the aircraft.

At 40,000 to 42,000 ft. temperatures gradually decreased southwards from -50°C at 40°N. to -60°C at 34°N., but it would seem that the tropopause was never crossed during the flight (except on ascent and descent) although it is possible that some form of discontinuity was encountered between 0945 and 1000 G.M.T. at 42,000 ft. where there is a sharp change of temperature. The tropopause chart for 1500 G.M.T. published in the Daily Aerological Report likewise suggests that the tropopause was not crossed in level flight.

Frost points remained generally steady at -77°C until 40°N. was reached and then there was a gradual increase to -73°C at 35°N. The inaccuracy of the measurements at this altitude makes it extremely difficult to state whether this increase is real or not. However, the variation of frost point with latitude seems to have been rather small on this day and the pattern obtained in the south conforms generally with previous analyses by Murray (5) on the variation of frost point in the vicinity of jet streams.

Cloud conditions on the flight showed much stratocumulus over Northern France and a general increase in the height of cloud tops southwards with broken cirrus layers over the south of France and over the Mediterranean. The cirrus persisted and at 34°N. the top of the thin layer of cirrus was 34,000 ft. with 3/8 of altocumulus below, between 22,000 ft. and 18,000 ft.

6.2 Weather 23rd May-27th May at Idris

During the day of 23rd May the depression off the Spanish coast moved east and the area of low pressure over the Sahara extended to the east and north. By 0600 G.M.T. on 24th May both these depressions were ill-defined but a weak frontal system was moving east over Algeria. The cirrus cloud increased to 5/8 at Idris but cleared by nightfall. The 200 mb. flow remained south-westerly over Tripolitania with ridging to the east which resulted in north-westerly winds over Cyrenaica. The flows at 700, 500 and 300 mb. were similar in character to this with high contours over the Sahara. The upper ridge moved slowly westwards and although there are south-westerly winds at 200 mb. at 0300 G.M.T. on 27th May the flow at lower levels became west to north-west.

The synoptic situation at the surface during this period was fairly stable with a ridge established over Algeria in the rear of a depression which moved eastward from the Spanish coast (Fig. 4). This ridge moved east and by 0600 G.M.T. on the 26th was east of Idris with a depression over Algeria and a general area of lower pressure to the south over the Sahara. This situation was substantially unchanged for Flight 8 on 27th May but before detail is given of this flight it is perhaps relevant to remark that the three successful aircraft ascents made during this period (Fig. 2, 3, 4) show similar features of structure. The progressive slow ascent at levels between 300 mb. and the tropopause can be quite easily followed in successive soundings and there is a suggestion of subsidence occurring in the lower stratosphere at the same time. By the afternoon of 27th May the character of the ascent had changed and there was no longer the very high humidity at the tropopause. The wind direction was westerly at all the levels for which charts are drawn, showing a distinct veer from the previous day's soundings: these facts suggest that the steady type of flow which persisted during the preceding four days was being destroyed and a different flow was about to be established.

6.3 Flight 8 to 24°N. from Idris 27th May, 1956

This flight was made due south from Idris at 35,000 ft. to 24°N. and returned at 45,000 ft., slowly climbing to 48,000 ft. at 33°N. over Idris. The results are presented diagrammatically in Fig. 13 and complete tabulations are made in Table 5. (In Fig. 13, 15 and 20 winds are plotted in the usual way with North at the top of the page).

At 0600 G.M.T. there was a depression over north-west Spain and an associated cold front in the vicinity of Algiers with a trough over Tunisia and a slight ridge over Libya. The weather at Idris was fine with 1/8 of cirrus during the day.

The flow at 0300 G.M.T. at 200 mb. is shown in Fig. 14. There was a jet stream from west-south-west, 45 kt., over Morocco. These winds became westerly during the course of the day. The flow pattern at 0300 G.M.T. for the 700, 500 and 300 mb. contour surfaces was anticyclonic with light or moderate winds. This is borne out by the data obtained by the aircraft during the climb. To the south of Idris there was light westerly flow with anticyclonic curvature at 200 mb. although no wind sounding was available at 0300 G.M.T. to confirm this.

The wind field obtained during the flight suggests that the eastern edge of an anticyclonic circulation was encountered to 26°N., but that south of this there was a recurrence of north-westerly winds. However, these winds are all in the range 10 to 20 kt. and such low speeds are difficult to measure by observations made in a fast-moving aircraft.

The flow in the high troposphere (and possibly in the inter-tropopause regions) between 45,000 and 48,000 ft. is south-westerly and the winds strengthen from about 20 kt. at 23°N. to 40 to 50 kt. at 30°N.

The temperature at 35,000 ft. increases southwards. Between 45,000 and 48,000 ft. there is little or no change of temperature, which suggests an isothermal layer, and the increase in wind at 45,000 ft. over that at 35,000 ft. suggests a warmer layer of air to the south-east between these levels.

At 35,000 ft. there is a fairly uniform frost point of -68°C between 27°N. and 23°N. but there is a gradient of frost point from -62°C at 32°N. to -68°C at 27°N.

At 45,000 ft. the frost point is -80°C at 26°N., and at 28°N. the frost point at 46,000 ft. is -76°C. This is a surprising increase of about 4°C., since it would be expected that the frost point at 46,000 ft. would be the same as or slightly lower than at 45,000 ft. This apparent jump of frost point is confirmed by the next observation of -74°C at 29°N. The frost point was steady at -73°C for three successive observations and then decreased to a value of -85°C at

/31°N.

31°N. Although these observations were not made in level flight it is reasonable to suppose that between 27°N. and 30°N. there was a great current of moister air which was moving north-east.

6.4 Weather 27th May to 29th May at Idris

The depression over Algeria on 27th May developed during the course of the day and a ridge extending southwards from an area of high pressure over Sicily was maintained over Tripoli. By 1800 G.M.T. on 28th May the ridge progressed to the east and during the night a trough moved steadily eastwards and began to affect the Idris area by 0600 G.M.T. on 29th May. The weather at Idris was fine on 27th but the trough caused dense cirrus by 0001 G.M.T. on the 29th May.

The upper flow at Idris was westerly at all levels and wind speeds were 10 to 20 kt. at lower levels. The sub-tropical jet stream was south-westerly and located over Morocco and a ridge formed at all levels at about 10°E. during the night 27th-28th causing a north-westerly flow to persist at all levels until the 31st May. Winds reached 50 to 60 kt. at 200 mb. but generally at higher pressures (300, 500, 700 mb.) winds of 20 to 40 kt. were predominant. In the air to the east of the ridge the ascents show marked differences from those ascents found in the south-westerly flow and this is probably best illustrated by Fig. 5 and 6. Above 40,000 ft. the temperature was 5°C colder in the north-westerly airstream than in the south-westerly and frost points were 3° to 5°C higher.

6.5 Flight 10. Idris to 23°N. and return 29th May, 1956

Fig. 15 shows graphically the flight made to 23°N. at 40,000 ft. with the return at 45,000 ft. to 48,000 ft. and the results are tabulated in Table 6.

The synoptic situation at 0600 G.M.T. showed a surface depression at 25°N. 5°E. with a shallow trough extending northwards over Algeria and into the Mediterranean (Fig. 17). The 700, 500, 300 and 200 mb. flows show a ridge near 10°E. Over Morocco and Spain there was a south-westerly jet stream, and over Cyrenaica north-westerly winds. No wind information is available over the Sahara but at 200 mb. the contours (Fig. 16) suggest lighter winds with anticyclonic circulation at 10°E. between 30°N. and 25°N.

The winds observed at 40,000 ft. (Fig. 15) confirm the flow-pattern deduced from synoptic data. There were uniform northerly winds at 30°N. but these became north-easterly at 24°N. At higher altitudes the north-westerly winds persisted with speeds of 20 to 30 kt. except for a band at 45,000 ft. at 25°N. and 26°N. where the speeds were about 5 kt. Temperature was steady throughout the flight at about -60°C at 40,000 ft. but rose to -57°C at 23°N. The return flight was carried out in more or less isothermal conditions with temperatures between -64°C and -66°C.

The frost point at 40,000 ft. was constant at about -74°C although one observation at 24°N. was 4°C warmer: the exact cause of this is unknown. On the return journey frost points were 1°C or 2°C higher than those found later in the day over Idris but are sufficiently near to the values to suggest that the air was homogeneous (with respect to its water content) from 33°N. to 23°N.

6.6 Weather 29th May to 2nd June

At 0600 G.M.T. on 29th May there was a depression over the Sahara at 10°E. and a weak ridge to the north-east of Idris. This ridge became dominant, the depression moved slowly southwards, and by 0600 G.M.T. on May 31st the trough, which had been over Algeria on the 29th (para. 6.5), had moved east bringing fresh to moderate winds over Tripolitania and much cirrus during the day. The trough receded quickly during the night and in association with a depression over Italy a cold front moved east across Tunisia, a strong ridge developing to the west over Algeria. During the next 48 hours this ridge extended eastwards to affect the whole of North Africa to Cyrenaica by the 1st June.

The upper flow became westerly as the high contour cells over the Sahara at 700, 500 and 300 mb. moved east and a trough moved from the Atlantic with a cut-off low at these levels moving across the central Mediterranean. At 200 mb. the sub-tropical jet stream gradually backed to west over Morocco and extended along the coast of North Africa with the ridge at 10°E. receding southwards.

During this period four ascents were made. All these ascents show similar characteristics and are described in another section. The last of the series of flights to 24°N. was made on 1st June and it was possible to measure only temperature and wind. By this time the 200 mb. flow was westerly and the surface trough extending to the north-east over Idris had begun to recede. (Fig. 18 and 19.) Measurements were taken at two-minute intervals and are tabulated in Table 7. Fig. 20 is a diagrammatic representation of a selection of the observations. At 40,000 ft. winds gradually backed from west-north-west (20 kt.) to become light (5 kt.) and variable and although there is a suggestion of a circulation in the more detailed observations, winds became south-west to west at about 20 kt. in the extreme south at $22\frac{1}{2}$°N. On the return journey at 44,000 to 48,000 ft. winds were generally south-west to west at 20 to 30 kt. in the south strengthening to 70 kt. at 31°N. at 48,000 ft. At least three of the winds on this return journey are suspect. These are the ones taken at 0720, 0722 and 0728 G.M.T.

Temperature remained steady at -55°C to -57°C throughout the flight at 42,000 ft. and at 45,000 ft. there was little change of temperature. However, values of temperature were obtained at 46,000 to 48,000 ft. and it is probable that these temperatures were taken in the region where the temperature begins to fall with height until the tropical tropopause is reached.

The lack of data over the Sahara at this period makes synoptic comparison impossible but it is suggested by the observations that there was a slow westerly flow at altitude and this is consistent with the mean circulation pattern obtained at lower altitudes.

6.7 Flight 17. 2nd June, 1956. Idris to Odiham

The data obtained on this flight can be seen in Table 8 and a diagrammatic representation of the observations is given in Fig. 21. The contours for the 200 mb. surface at 0300 G.M.T. on the same day are also superimposed on Fig.21. Fig. 22 is a synoptic chart for 0900 G.M.T.

At 0900 G.M.T. (Fig. 22) a shallow depression existed over Southern Italy and Greece and a ridge extended eastwards along the North African coast from the Azores anticyclone. A second ridge from the anticyclone was over the Low Countries and Germany. A vigorous depression centred to the north of Scotland was moving eastwards and the associated cold front was moving east across Wales and Northern England. Weather at Idris was fine with some altocumulus and there was much cirrus and medium cloud over the Mediterranean clearing at the French coast to 3 to 5 oktas. Variable stratocumulus sheets covered most of France breaking to small amounts to the north, but multilayered cloud associated with the warm sector conditions over England penetrated into the extreme north of France.

The 700, 500, 300 and 200 mb. contour maps show similar features and a description of the 200 mb. contour surface will suffice to describe the general upper flow pattern. A cut-off low in the 200 mb. contours was over Italy and Yugoslavia with a strong flow to the west and south and this was the dominant feature of the chart. North of 55°N. the flow was mainly westerly and so the effect of this cut-off low was to divide the flow, the division occurring over Southern England and Northern France.

The winds obtained during the flight at 40,000 ft. rising to 42,000 ft. show reasonably good agreement with the 200 mb. contour pattern as regards direction, although the speeds obtained during the flight are somewhat lighter than those obtained six hours earlier at 0300 G.M.T. by radio sonde. It is possible that the cut-off low had edged south-west during the period or that the centre had begun to fill and that the discrepancy of wind is principally due to time lag.

Temperature at 40,000 ft. was -52°C over Tunisia and rose to -48°C towards the centre of the cut-off low but subsequently fell to reach a value of -54°C at the French coast. A further decrease to -56°C was obtained over Southern France but the aircraft climbed to 42,000 ft. before the temperature had steadied. At 42,000 ft. over France the temperature was -59°C to -60°C.

The cloud notes obtained during flight agreed generally with the surface observations of weather taken from synoptic charts.

The supply of liquid nitrogen was limited and there was none available for 1st and 2nd June so that humidities were not measured on these two days.

7. General discussion

The well-marked increase of frost point associated with decreasing temperature and increasing wind in Flight 1 is typical of the features of the cold-air side of jet streams in England investigated by Murray (3) and the observations of temperature and wind on Flight 17 have the same characteristics. Hence it would appear that, as far as this evidence goes, the sub-tropical jet stream is similar in structure to jet streams found in association with extra-tropical cyclones. The position of the jet stream relative to Idris (i.e. near or to the north) would suggest that the ascents at Idris resembled those over Southern England in anticyclonic (high tropopause) conditions. Hence in Table 2 the means for England when the tropopause is at 38,000 ft. or above should be more comparable with those for Idris than the overall means for England. This is indeed found to be so up to 40,000 ft. but above this level there is a drier stratosphere over anticyclones in England than during this period over Idris. The mean humidity of this series of flights at Idris between 30,000 and 40,000 ft. is greater than the two-year mean over England when air masses with high tropopauses alone are considered and this higher humidity is accompanied by cirrus layers over Idris at these levels.

In the main, however, it appears that the frost point between 40,000 and 50,000 ft. over Idris differs only slightly from that found over Southern England. Local variations (including the influx of moist air from the south at levels near or just above 40,000 ft.) are well within the variations of frost point found over Southern England. The higher relative humidities are almost entirely an effect of the lower temperatures.

Little can be deduced from the three flights over the desert. The wind flow in the upper air at this season is believed to be predominantly westerly, and to be modified by the passage of troughs and ridges in much the same way as in temperate latitudes. The observations made on these flights are compatible with this view. At 35,000 and 40,000 ft. the temperatures increased towards the south, but at 46,000-48,000 ft. there was little variation. It is noticeable that at 35,000 ft., on the 27th, the frost point fell towards the south, whereas at 40,000 ft. on the 29th there was no such variation. The one striking anomaly was the narrow band of higher frost points and slightly lower temperatures encountered in 29-30°N. at 46,000, 48,000 ft. on May 27th: but it is impossible to assess the significance of this, on the evidence available.

/8.

8. References

1.	Helliwell, N.C. and Mackenzie, J.K.	1956	Meteorological Research Papers, Air Ministry London, No. 979.
2.	Helliwell, N.C., Mackenzie, J.K. and Kerley, M.J.	1956	Meteorological Research Papers, Air Ministry, London, No. 976.
3.	Murray, R.	1956	Geophysical Memoirs No. 97. Air Ministry, London.

Table 4

High level ascents over Idris 23rd May, 1956 - 1st June, 1956

Height ft.	ICAN Press. mb.	Temp. °C	Frost Point °C	Wind Dirn. deg.	Wind Speed kt.	Temp. °C	Frost Point °C	Wind Dirn. deg.	Wind Speed kt.
Date			24th May, 1956				24th May, 1956		
Flight No.			2				3		
Time G.M.T.	-		0638-0845				1335-1410		
5,000	843	+23.6	-12.5	228	23	-	-	-	-
10,000	697	+10.2	-14.5	215	27	+9.0	-11.5	214	25
15,000	572	-3.3	-10.5	214	36	-	-	-	-
20,000	465	-17.8	-28.0	235	25	-16.0	-31.0	231	29
25,000	376	-27.5	-38.0	246	37	-	-	-	-
30,000	301	-39.8	-48.5	244	33	-	-	-	-
32,000	274	-45.3	-54.0	233	51	-	-	-	-
34,000	250	-48.9	-49.5	241	50	-	-	-	-
36,000	227	-52.0	-59.0	259	60	-	-	-	-
38,000	206	-57.2	-62.0	259	67	-	-	-	-
40,000	187	-58.9	-72.0	255	71	-	-	-	-
42,000	170	-59.8	-75.5	267	56	-	-	-	-
44,000	155	-62.6	-77.5	245	55	-	-	-	-
46,000	140	-65.0	-78.0	246	60	-	-	-	-
48,000	127	-67.3	-83.0	233	60	-	-	-	-

Height ft.	ICAN Press. mb.	Temp. °C	Frost Point °C	Wind Dirn. deg.	Wind Speed kt.	Temp. °C	Frost Point °C	Wind Dirn. deg.	Wind Speed kt.
Date			25th May, 1956				25th May, 1956		
Flight No.			4				5		
Time G.M.T.			0620-0735				1250-1450		
5,000	843	-	-	-	-	-	-	-	-
10,000	697	+7.9	-	199	48	+8.7	-24.0	204	25
15,000	572	-	-	-	-	-	-	-	-
20,000	465	-17.0	-	228	40	-17.4	-39.0	-	-
25,000	376	-	-	-	-	-25.2	-47.0	235	45
30,000	301	-38.9	-	-	-	-39.5	-46.0	245	53
32,000	274	-	-	-	-	-44.2	-46.0	227	62
34,000	250	-	-	-	-	-49.2	-52.0	246	70
36,000	227	-	-	-	-	-53.9	-58.5	248	60
38,000	206	-	-	-	-	-55.5	-69.0	244	78
40,000	187	-57.7	-	251	56	-57.4	-73.0	239	60
42,000	170	-59.6	-	-	-	-59.8	-76.0	239	65
44,000	155	-60.1	-	-	-	-60.5	-83.0	257	53
46,000	140	-62.4	-	239	67	-64.6	-	248	50
48,000	127	-	-	-	-	-65.7	-	260	35

Height ft.	ICAN Press. mb.	Temp. °C	Frost Point °C	Wind Dirn. deg.	Wind Speed kt.	Temp. °C	Frost Point °C	Wind Dirn. deg.	Wind Speed kt.
Date			26th May, 1956				26th May, 1956		
Flight No.			6						
Time G.M.T.			0608-0700				1239-1403		
5,000	843	-	-	-	-	-	-	-	-
10,000	697	+9.6	-	225	21	+9.1	-7.5	195	21
15,000	572	-	-	-	-	-	-	-	-
20,000	465	-14.5	-	-	-	-14.4	-42.0	230	20
25,000	376	-26.4	-	234	37	-28.1	-43.5	279	19
30,000	301	-40.2	-	228	30	-40.0	-46.5	217	37
32,000	274	-	-	-	-	-	-	-	-
34,000	250	-	-	-	-	-48.4	-54.5	229	40
36,000	227	-	-	-	-	-	-	-	-
38,000	206	-	-	-	-	-60.7	-60.5	248	40
40,000	187	-	-	-	-	-55.9	-72.5	-	-
42,000	170	-	-	-	-	-59.5	-75.5	246	54
44,000	155	-	-	-	-	-60.9	-78.5	224	42
46,000	140	-	-	-	-	-64.2	-81.5	237	47
48,000	127	-	-	-	-	-66.6	-83.0	239	50

Table 4

Height ft.	ICAN Press. mb.	Temp. °C	Frost Point °C	Wind Dirn. deg.	Wind Speed ft.	Temp. °C	Frost Point °C	Wind Dirn. deg.	Wind Speed ft.
Date			27th May, 1956				29th May, 1956		
Flight No.			9				11		
Time G.M.T.			1235-1351				1240-1420		
5,000	843	-	-	-	-	+25.2	-2.0	229	07
10,000	697	+9.5	-4.5	212	24	+12.4	-6.0	303	12
15,000	572	-	-	-	-	-4.2	-18.0	348	25
20,000	465	-17.2	-32.0	065	06	-16.4	-21.0	334	23
25,000	376	-26.9	-49.5	037	05	-26.5	-41.5	300	32
30,000	301	-39.5	-46.0	293	15	-39.8	-43.0	327	47
32,000	274	-45.4	-50.0	294	28	-44.2	-47.0	313	42
34,000	250	-49.8	-60.0	315	25	-49.8	-54.5	329	29
36,000	227	-55.0	-62.0	344	32	-54.1	-62.5	311	37
38,000	206	-58.8	-68.5	307	19	-59.5	-64.0	316	38
40,000	187	-58.7	-73.5	329	20	-62.7	-67.0	314	31
42,000	170	-61.6	-75.5	238	22	-65.0	-71.0	303	33
44,000	155	-58.6	-79.5	269	33	-65.4	-73.5	310	37
46,000	140	-62.8	-81.0	254	43	-65.8	-77.5	320	57
48,000	127	-65.8	-82.0	272	28	-66.5	-79.5	329	40
Date			30th May, 1956				30th May, 1956		
Flight No.			12				13		
Time G.M.T.			0542-0750				0900-1050		
5,000	843	-	-	-	-	+24	-3.0	315	15
10,000	697	+10.3	-	333	11	+10.9	-6.0	317	07
15,000	572	-	-	-	-	-4.2	-12.0	303	22
20,000	465	-15.6	-23.0	317	12	-15.5	-27.5	332	16
25,000	376	-26.9	-39.0	313	20	-26.5	-37.5	286	20
30,000	301	-39.6	-48.0	326	49	-39.2	-48.0	319	47
32,000	274	-44.4	-52.0	324	55	-43.6	-	-	-
34,000	250	-49.2	-57.0	312	52	-49.7	-55.0	317	49
36,000	227	-54.7	-59.5	318	53	-54.6	-	-	-
38,000	206	-58.8	-62.5	318	57	-59.3	-62.5	316	53
40,000	187	-63.3	-66.5	323	48	-61.6	-69.0	308	49
42,000	170	-61.4	-76.0	328	43	-61.0	-74.0	309	40
44,000	155	-61.7	-78.0	321	46	-61.1	-79.0	301	49
46,000	140	-62.3	-82.5	310	61	-64.3	-81.0	303	50
48,000	127	-65.6	-83.5	332	38	-67.4	-83.5	329	30
Date			31st May, 1956				31st May, 1956		
Flight No.			14				15		
Time G.M.T.			0530-0700				0900-1000		
5,000	843	-	-	-	-	-	-	-	-
10,000	697	-	-	-	-	-	-	-	-
15,000	572	-	-	-	-	-	-	-	-
20,000	465	-16.7	-31.5	324	42	-	-	-	-
25,000	376	-26.1	-38.0	292	42	-26.4	-40.5	-	-
30,000	301	-39.9	-43.0	310	40	-39.8	-47.0	303	41
32,000	274	-44.6	-	-	-	-43.5	-	-	-
34,000	250	-50.2	-56.5	304	55	-50.1	-56.0	300	54
36,000	227	-55.2	-58.0	314	48	-54.5	-	-	-
38,000	206	-59.2	-64.5	301	60	-58.5	-69.0	297	50
40,000	187	-59.7	-70.5	322	45	-58.4	-73.0	312	43
42,000	170	-59.8	-76.5	287	47	-59.8	-76.0	267	52
44,000	155	-60.0	-	281	35	-62.3	-79.5	285	50
46,000	140	-62.9	-81.5	273	53	-	-	-	-
48,000	127	-65.3	-	291	41	-	-	-	-

Table 5

Flight 8. 27th May, 1956

Idris to 24°N. and return. Longitude 13°E.±15'

Time G.M.T.	Height ft.	Pressure mb.	Temp. °C	Frost Point °C	Wind		Remarks
					Dirn. deg.	Speed kt.	
0543	Surface	-	+19.5	-	-	-	Taxying
	1,000	978	+26.4				Climb to 35,000 ft. No cloud. Haze top 15,000 ft. with very patchy A.c. and Ci. to the east
	2,000	942	+30.9				
	3,000	908	+30.8				
	5,000	843	+26.4				
	6,000	812	+22.8				
	7,000	782	+20.6				
	13,000	619	+ 0.1				
	15,000	572	- 6.0		165	11	
	20,000	465	-12.9		270	05	
	25,000	376	-31.2		227	12	
	30,000	301	-38.9		290	20	
0616	35,000	238	-52.0		264	17	Much Ci. and As. to E. and N. at these levels
0620	35,100	238	-50.8	-62.0	273	08	
0625	35,100	238	-50.8	-61.0	273	08	
0630	35,200	238	-49.2	-65.0	324	06	
0638	35,200	238	-47.8	-68.0	321	08	Ci. bands have receded
0645	35,100	238	-45.8	-68.0	351	14	
0650	35,200	238	-45.7	-68.0	050	14	
0658	35,250	237	-44.9	-67.0	282	18	
0702	35,100	238	-44.1	-66.0	297	19	
0707	35,100	238	-43.7	-	254	20	
0717	40,200	187	-55.7	-76.0	233	31	) Turning back at
0726	45,400	144	-65.4	-	270	07	) 600 mi. south
0739	45,400	144	-64.4	-	228	23	Southern edge of Ci. which is to N. and E.
0749	45,400	144	-63.4	-80.0	227	35	
0752	45,400	144	-62.7	-	220	39	
0802	46,400	137	-65.7	-76.0	239	30	
0812	46,450	137	-64.6	-74.0	235	50	
0817	46,450	137	-64.8	-73.0	235	53	
0819	47,000	133	-64.5	-73.0	210	44	
0821	48,250	126	-65.8	-73.0	230	38	
0831	48,600	123	-65.5	-85.0	222	41	
0841	48,600	123	-63.7	-85.0	228	45	

Table 6

Flight 10. 29th May, 1956. 0550 to 0905 G.M.T.

Idris to 600 miles south of Idris and return. Longitude 13°E.±15'

Time G.M.T.	Height ft.	Pressure mb.	Temp. °C	Frost Point °C	Wind		Remarks
					Dirn. deg.	Speed kt.	
0613	40,000	187	-61.4	-74.0	344	37	Haze top 18,500 ft.
0616	40,000	187	-60.8	-74.0	344	37	
0624	40,000	187	-60.5	-75.0	355	33	
0634	40,000	187	-60.0	-74.0	357	41	
0637	40,000	187	-60.1	-74.0	357	40	
0645	40,000	187	-60.5	-74.0	003	43	
0650	40,000	187	-60.4	-74.0	021	42	
0659	40,000	187	-60.0	-74.5	026	35	
0703	40,000	187	-59.8	-71.0	022	42	
0707	40,000	187					Slight clear air turbulence
0710	40,000	187	-57.1	-73.0			
	(41,000	179	-58.8				) Turning back at
0712	(42,000	170	-60.3				) 600 miles south.
to	(43,000	162	-61.7				) Climbing 40,000
0722	(44,000	155	-63.0				) to 45,000 ft.
	(45,000	147	-65.1				)
0728	45,000	147	-66.3	-78.0	322	23	
0730	45,000	147	-65.3	-78.5	334	05	
0734	45,000	147	-64.6	-78.0	297	03	
0743	45,000	147	-64.2		326	06	
0751	45,500	144	-65.3	-78.0	330	27	Cirrus on horizon to NW.
0759	46,000	140	-65.4	-80.0	320	21	
0803	46,000	140	-65.8	-80.0	332	32	
0814	46,500	136	-67.4				
0815	47,000	133	-67.3				
0817	47,500	130	-65.9				
0819	48,000	127	-66.2	-83.5	332	21	
0828	48,000	127	-66.9	-82.5	334	25	
0839	48,000	127	-66.6	-81.5	319	38	
0845							Rapid descent. Ci. tops 35,000 ft. base 32,000 ft.

Table 7 Part I

Flight 16. 1st June, 1956. 0530 to 0840 G.M.T.

Idris to 600 n.miles south of Idris and return. Longitude 13°E.±15'

Time G.M.T.	Height ft.	Pressure mb.	Temp. °C	Wind Dirn. deg.	Wind Speed kt.	Remarks
0557	40,200	186	-56.1	283	38	$\frac{3}{8}$-$\frac{5}{8}$ Cu. base 12,000 ft.
0559	40,100	187	-55.9	273	32	Isolated tops 21,500 ft.
0601	40,000	187	-55.7	284	22	$\frac{1}{8}$ Ci. to east on climb.
0603	40,200	186	-56.8	282	22	No cloud at 120 mi. south of
0605	40,200	186	-57.3	281	22	Idris at 0557 G.M.T.
0608	40,000	187	-57.4	285	20	
0610	40,100	187	-57.5	299	21	
0612	40,200	186	-56.4	300	25	
0614	40,280	185	-57.5	295	20	
0616	40,200	186	-56.5	308	20	
0618	40,200	186	-57.3	286	23	
0620	40,200	186	-57.4	278	15	
0622	40,220	186	-56.8	297	17	
0624	40,200	186	-55.4	301	12	
0626	40,200	186	-56.5	274	20	
0628	40,200	186	-57.1	278	26	
0630	40,100	187	-58.8	260	04	
0632	40,200	186	-58.2	331	08	
0634	40,000	187	-57.8	271	04	
0636	40,000	187	-57.6	327	07	
0638	40,200	186	-57.5	290	11	
0640	40,200	186	-57.5	151	05	
0642	40,200	186	-56.7	051	06	
0644	40,200	186	-57.4	312	05	
0646	40,200	186	-57.6	004	02	
0648	40,200	186	-57.2	032	06	
0650	40,200	186	-56.7	005	06	
0652	40,400	184	-57.2	326	12	Slight clear air turbulence
0654	40,200	186	-57.0	280	11	
0656	40,000	187	-57.9	245	18	
0658	40,000	187	-57.4	223	11	
0700	40,000	187	-57.9	287	15	
0702	40,000	187	-57.7	282	11	
0705	42,000	170	-60.9	253	23	

Table 7 Part II

Flight 16. 1st June, 1956. 0530 to 0840 G.M.T.

Idris to 600 n.mi. south of Idris and return. Longitude 13°E±15'

Time G.M.T.	Height ft.	Pressure mb.	Temp. °C	Wind		Remarks
				Dirn. deg.	Speed kt.	
0708	44,000	155	-62.0	250	27	
0712	45,300	146	-64.9	242	29	
0714	45,200	146	-64.3	246	29	
0716	45,400	145	-64.6	265	11	
0718	45,250	146	-64.2	210	20	
0720	45,250	146	-64.1	178	13	
0722	45,400	145	-64.2	198	13	
0724	45,200	146	-63.8	249	10	
0726	45,200	146	-63.5	255	13	
0728	45,200	146	-63.1	178	12	
0730	45,400	145	-62.7	242	21	
0732	45,100	147	-63.1	230	15	
0734	45,100	147	-62.1	242	20	
0736	45,200	146	-62.6	255	23	
0738	45,300	146	-63.1	267	25	
0740	45,400	145	-63.0	255	22	
0742	45,450	145	-62.8	268	38	
0744	45,200	146	-63.0	269	18	
0746	45,250	146	-63.0	275	29	
0750	46,700	133	-66.6	257	30	
0755	47,600	131	-64.8	240	42	
0757	48,000	127	-65.7	245	32	
0759	48,400	125	-67.7	281	33	
0801	48,400	125	-66.5	249	37	
0803	48,450	125	-66.2	264	49	
0805	48,500	124	-66.5	256	43	
0807	48,400	125	-67.0	247	51	
0809	48,400	125	-66.5	260	55	
0811	48,400	125	-66.0	278	61	
0813	48,400	125	-65.0	267	62	
0815	48,400	125	-65.0	263	63	
0817	48,400	125	-64.7	262	71	
0830	21,500	Descent				135 mi. south of Idris edge of cloud. Top 21,500 ft. Haze top at 21,500 ft.

Table 8 Part I

Flight 17. 2nd June, 1956. 0830 to 1150 G.M.T.

Idris to Tangmere

Time G.M.T.	Height ft.	Pressure mb.	Temp. °C	Wind Dirn. deg.	Wind Speed kt.	Remarks
0857	40,200	185	-52.4	249	82	3/8 cirrus base 28,000 ft. top 35,000 ft. in layers
0859	40,200	185	-52.4	246	85	
0901	41,000	186	-50.3	240	85	
0903	40,250	185	-49.6	233	80	
0905	40,250	185	-51.0	241	64	
0907	40,200	185	-50.0	244	58	
0909	40,200	185	-47.1	247	63	
0911	40,000	187	-50.5	253	48	
0913	40,200	185	-50.8	258	51	
0915	40,400	183	-48.0	265	50	
0917	40,400	183	-48.6	253	42	
0919	40,200	185	-48.6	260	39	
0921	40,400	183	-49.6	259	37	
0923	40,200	185	-49.5	262	31	
0925	40,200	185	-49.0	246	49	
0927	40,200	185	-49.2	255	29	
0929	40,100	186	-49.0	243	39	
0931	40,200	185	-48.5	253	36	Slight clear air turbulence
0933	40,200	185	-48.2	265	21	Slight clear air turbulence
0935	40,200	185	-48.1	261	39	
0937	40,200	185	-48.0	286	25	
0939	40,200	185	-48.5	296	21	
0941	40,200	185	-48.8	271	33	
0943	40,100	186	-50.0	272	24	
0945	40,200	185	-49.5	280	15	
0947	40,000	187	-49.0	329	08	
0949	40,200	185	-48.8	294	18	
0951	40,200	185	-49.6	318	14	
0953	40,200	185	-51.1	303	13	
0955	40,200	185	-51.3	325	25	
0957	40,200	185	-51.3	344	18	
0959	40,200	185	-51.2	350	13	
1001	40,200	185	-52.2	349	15	
1003	40,000	187	-51.5	334	15	
1005	40,100	186	-52.3	356	30	

Table 8 Part II

Flight 17. 2nd June, 1956. 0830 G.M.T.

Idris to Tangmere

Time G.M.T.	Height ft.	Pressure mb.	Temp. °C	Wind Dirn. deg.	Wind Speed kt.	Remarks
1007	40,100	186	-52.4	004	17	
1009	40,000	187	-54.2	319	17	
1011	40,200	185	-53.1	333	15	
1013	40,200	185	-53.4	352	13	
1015	40,100	186	-55.5	013	19	
1017	40,100	186	-54.4	334	06	
1019	40,200	186	-54.0	350	14	Over Marseilles
1021	40,200	185	-53.8	351	14	
1023	40,200	185	-54.2	358	19	
1025	40,200	185	-53.9	006	16	
1027	40,200	185	-56.7	346	27	
1029	40,200	185	-57.6	353	31	
1031	40,200	185	-57.5	013	23	
1033	40,400	184	-55.9	025	06	
1035	40,700	182	-58.5	008	21	
1037	41,300	176	-54.5	345	21	
1039	41,400	175	-55.8	326	20	
1041	41,900	171	-56.6	009	21	
1043	42,200	169	-56.3	319	13	
1045	42,200	169	-56.7	323	19	
1047	42,300	168	-56.8	323	19	
1049	42,300	168	-57.3	323	19	
1051	42,200	169	-61.0	299	11	
1053	42,200	169	-60.4	334	03	
1055	42,000	170	-59.4	-	0	
1057	42,200	169	-59.8	318	12	
1059	42,000	170	-60.1	334	02	
1101	42,000	170	-60.4	299	12	
1103	42,000	170	-59.4	203	07	Cirrus ahead
1105	42,000	170	-59.8	302	08	
1107	41,700	173	-59.5	286	09	
1109	41,700	173	-60.2	286	10	
1111	42,100	170	-60.6	280	23	
1113	42,100	170	-59.3	278	14	
1115	42,000	170	-58.7	282	28	
1117	42,000	170	-57.6	239	16	

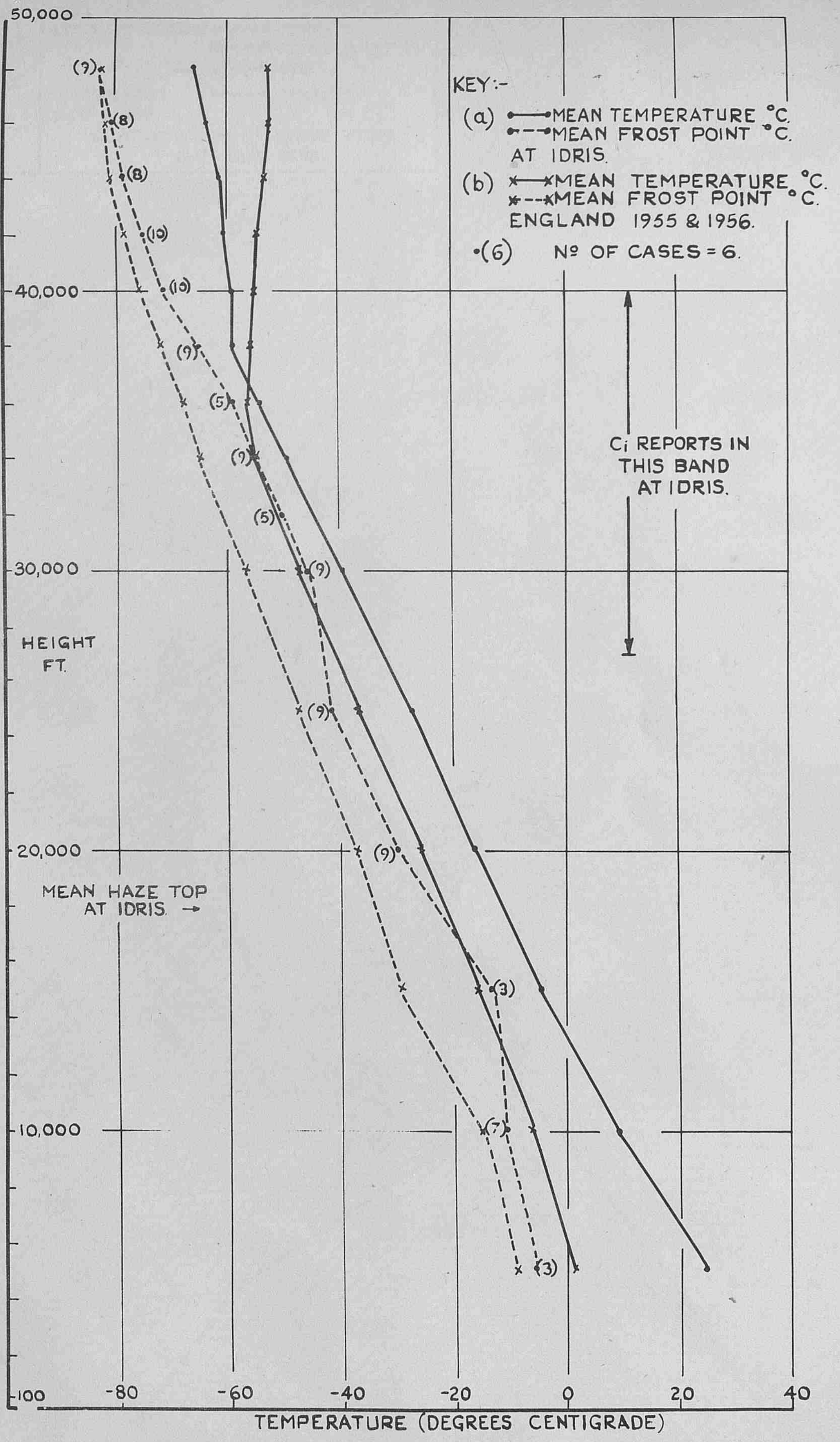

FIG. I. MEAN TEMPERATURE °C AND FROST POINTS.

(a) OVER IDRIS 23RD MAY TO 2ND JUNE 1956.

(b) OVER ENGLAND 1954 AND 1955.

FIG.2

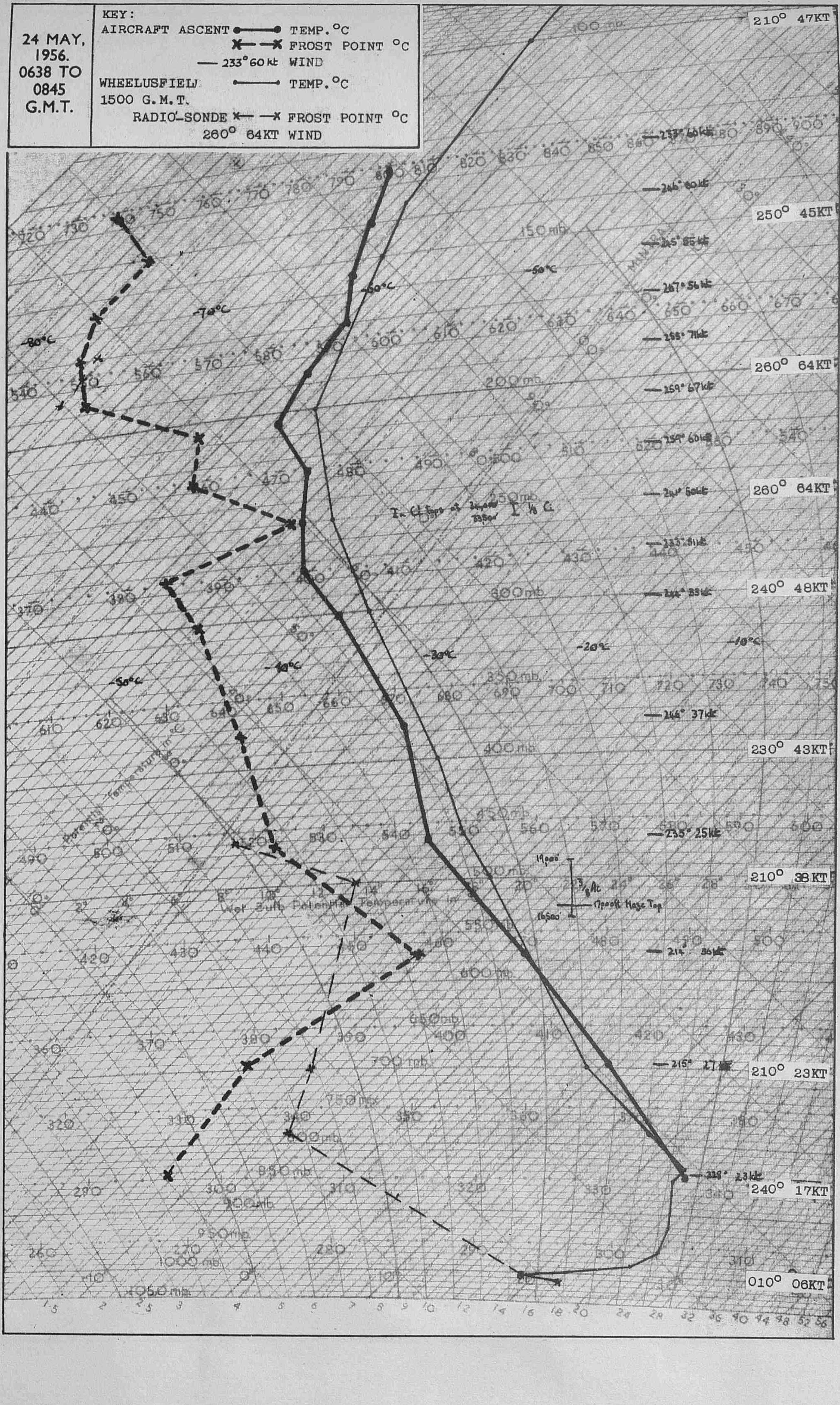

R.A.E. 129165 57

FIG.3

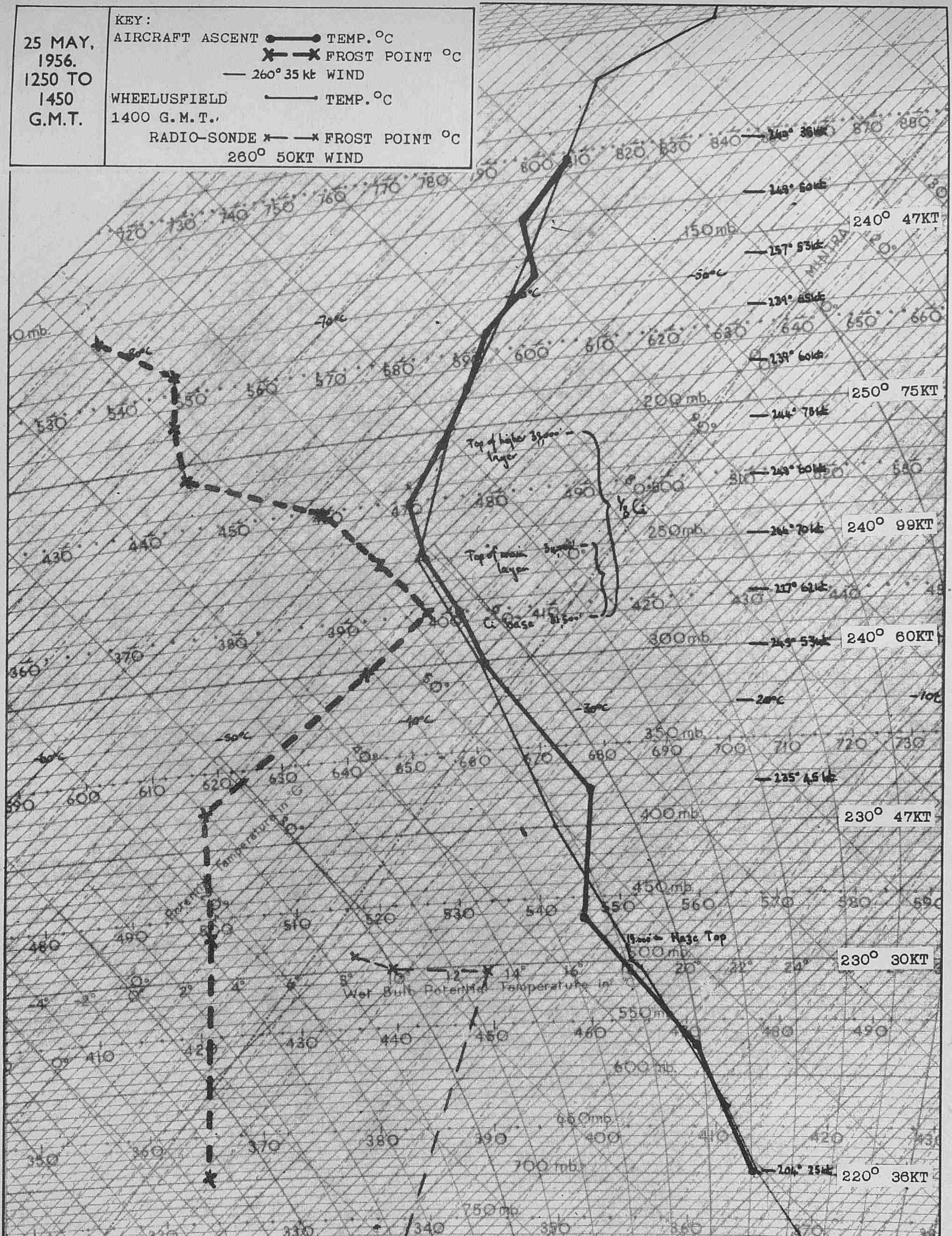
25 MAY, 1956. 1250 TO 1450 G.M.T.
KEY:
AIRCRAFT ASCENT — TEMP. °C
FROST POINT °C
260° 35 kt WIND
WHEELUSFIELD 1400 G.M.T.
TEMP. °C
RADIO-SONDE FROST POINT °C
260° 50KT WIND
240° 47KT
250° 75KT
240° 99KT
240° 60KT
230° 47KT
230° 30KT
220° 36KT
010° 14KT
240° 36kt
248° 60kt
257° 53kt
239° 65kt
239° 60kt
244° 78kt
248° 60kt
246° 70kt
227° 62kt
243° 53kt
235° 45kt
204° 25kt
Top of higher 38,000' layer
1/8 Ci
Top of main layer 34,000'
Ci base 31,500'
19,000' Haze Top
2500' 2300' 1/8 Sc
Potential Temperature in °C
Wet Bulb Potential Temperature in °C
150mb
200mb
250mb
300mb
350mb
400mb
450mb
500mb
550mb
600mb
650mb
700mb
750mb
800mb
850mb
900mb
950mb
1000mb
1050mb

FIG.4

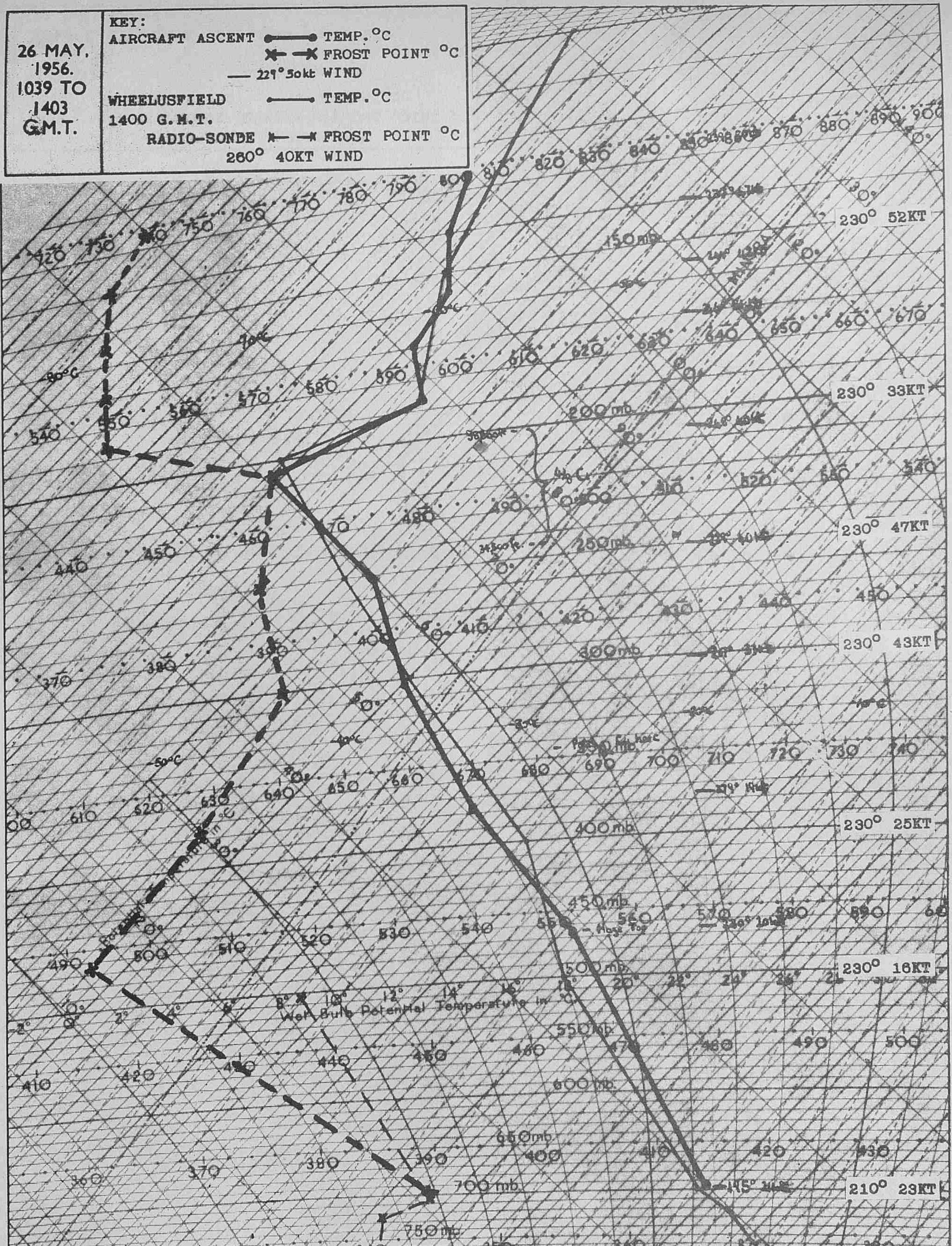

R.A.E. 129167 57

FIG.5

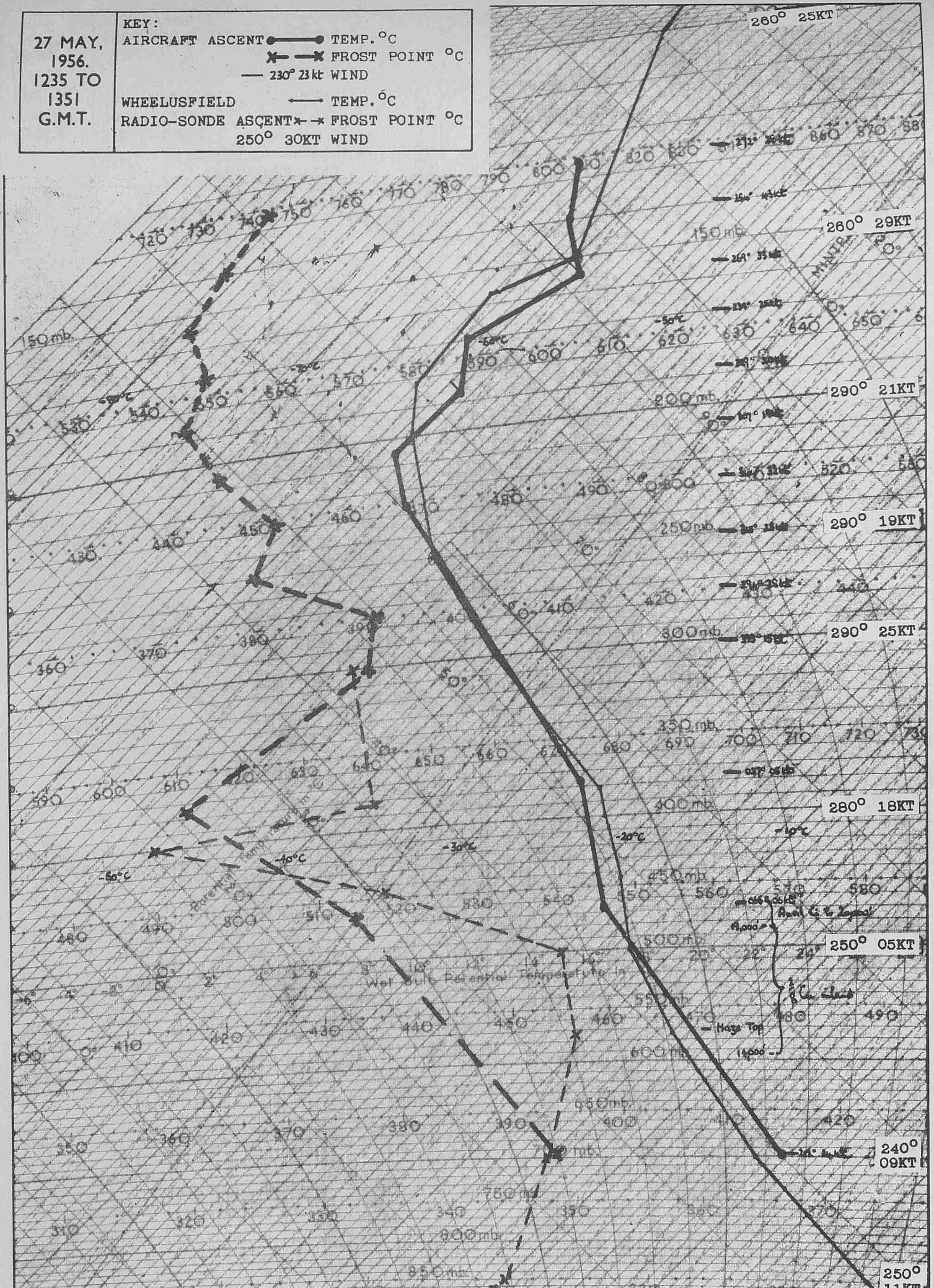

R.A.E. 129168 57

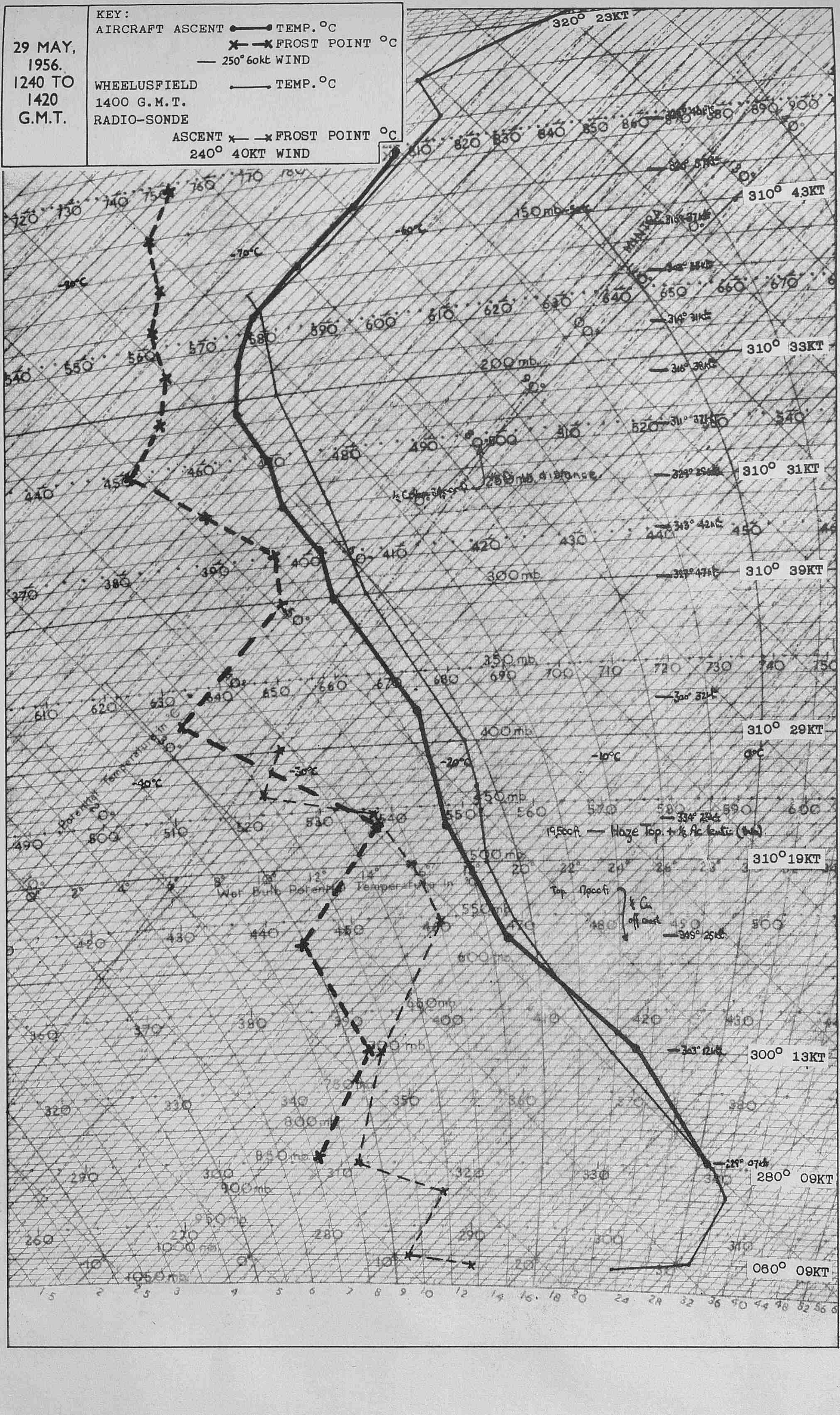
29 MAY, 1956. 1240 TO 1420 G.M.T.
KEY:
AIRCRAFT ASCENT ●—● TEMP. °C
✕— —✕ FROST POINT °C
— 250° 60kt WIND
WHEELUSFIELD 1400 G.M.T. RADIO-SONDE ASCENT
—— TEMP. °C
×— —× FROST POINT °C
240° 40KT WIND
320° 23KT
310° 43KT
310° 33KT
310° 31KT
310° 39KT
310° 29KT
310° 19KT
300° 13KT
280° 09KT
060° 09KT
150 mb
200 mb
250 mb
300 mb
350 mb
400 mb
450 mb
500 mb
550 mb
600 mb
650 mb
700 mb
750 mb
800 mb
850 mb
900 mb
950 mb
1000 mb
1050 mb
-70°C
-60°C
-50°C
-40°C
-30°C
-20°C
-10°C
0°C
Wet Bulb Potential Temperature in °C
Potential Temperature in °C
19,500ft — Haze Top + 1/8 Ac lentic
Top
1/8 Cu off coast

FIG.7

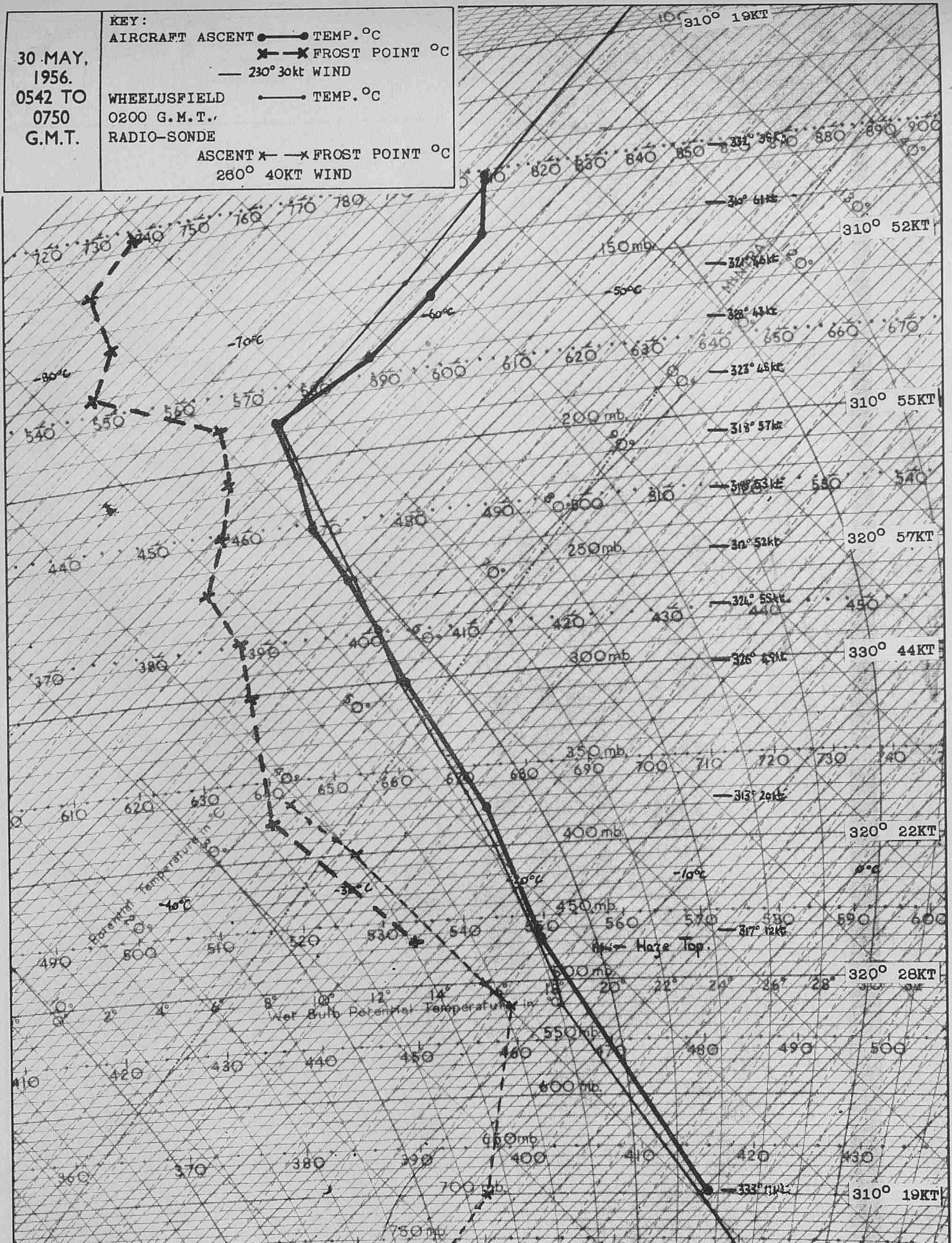

R.A.E. 129170 57

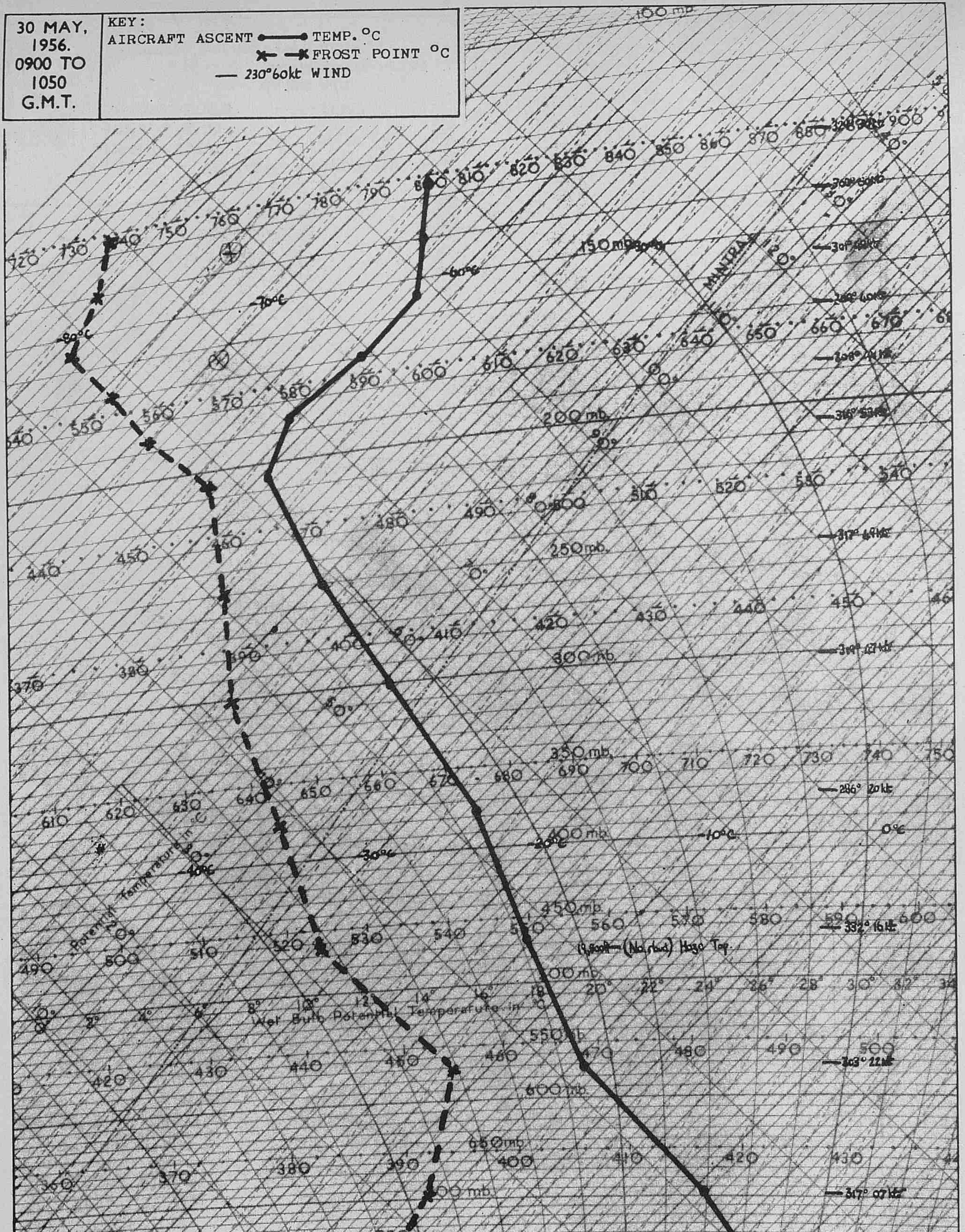

30 MAY, 1956. 0900 TO 1050 G.M.T.

R.A.E. 129171 57

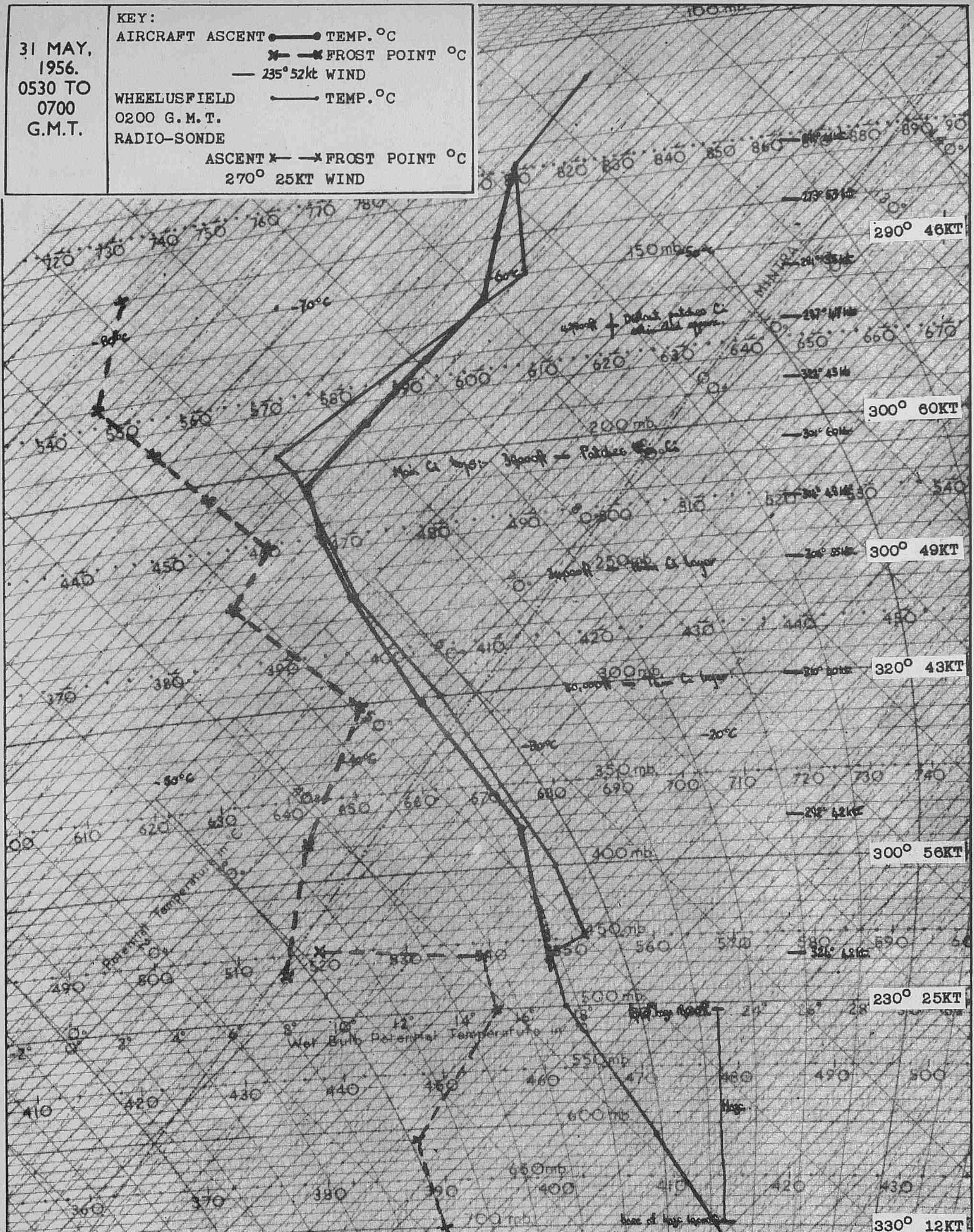
31 MAY, 1956. 0530 TO 0700 G.M.T.
KEY:
AIRCRAFT ASCENT ●—● TEMP. °C
✱— —✱ FROST POINT °C
— 235° 52kt WIND
WHEELUSFIELD 0200 G.M.T. RADIO-SONDE ASCENT —— TEMP. °C
✕— —✕ FROST POINT °C
270° 25KT WIND
290° 46KT
300° 60KT
300° 49KT
320° 43KT
300° 56KT
230° 25KT
330° 12KT
030° 12KT
010° 16KT
100 mb
150 mb
200 mb
250 mb
300 mb
350 mb
400 mb
450 mb
500 mb
550 mb
600 mb
650 mb
700 mb
750 mb
800 mb
850 mb
900 mb
950
1000 mb
1050 mb
-80°C
-70°C
-60°C
-50°C
-40°C
-30°C
-20°C
Potential Temperature in °C
Wet Bulb Potential Temperature in °C
MINTRA
Cirrus layer
Base of haze layer
Haze
0
1.5
2
2.5
3
4
5
6
7
8
9
10
12
14
16
18
20
24
28
32
36
40
44
48

FIG.10

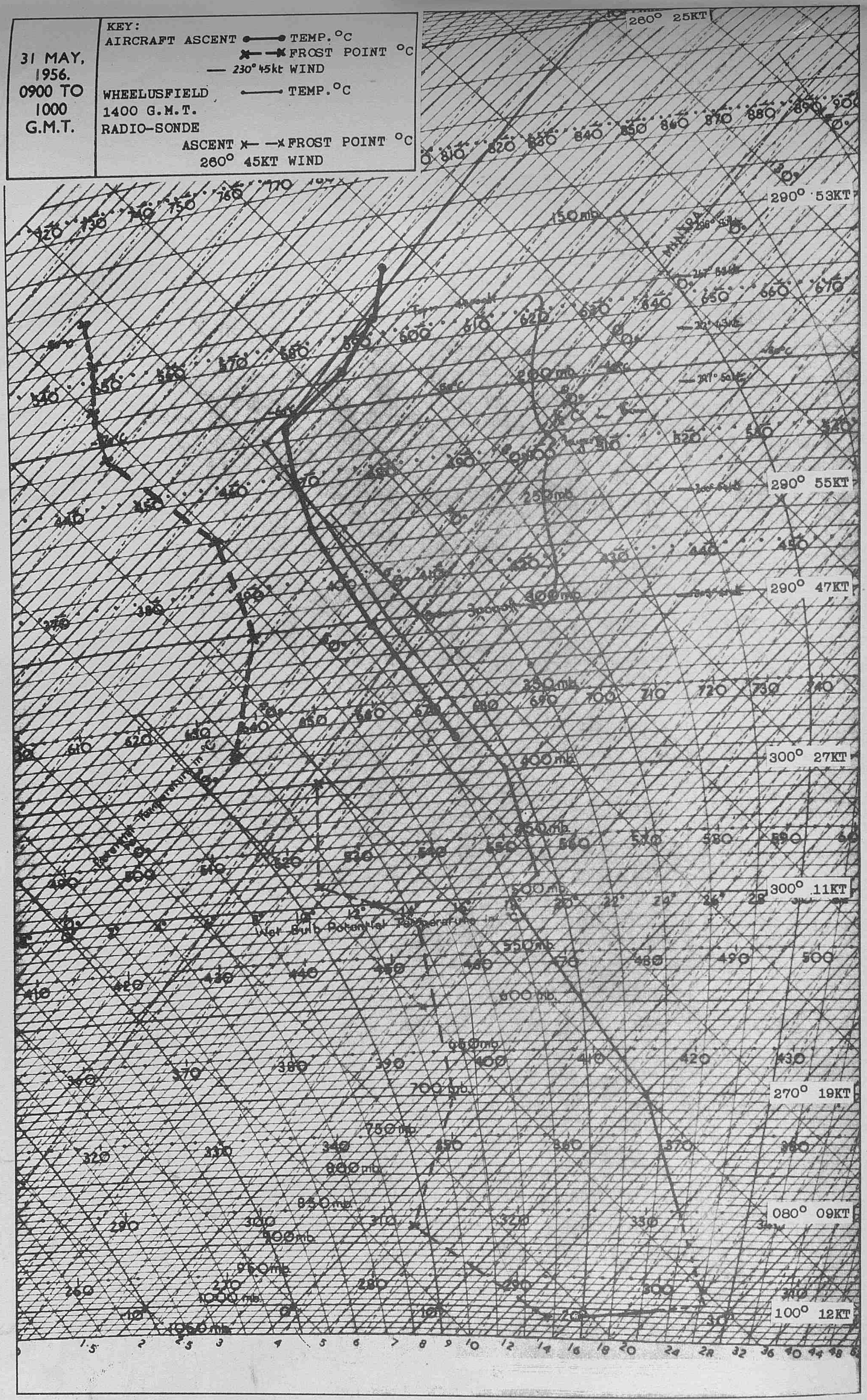

SOME USEFUL DATA

MIXING RATIO IN GM/KG

ICAN HEIGHT FEET	PRESSURE Mb	FROST POINT, DEGREES CENTIGRADE -10	-20	-30	-40	-50	-60	-70	-77.5	-80	-82.5
10,000	697	3.1	1.2	0.55	0.17	-	-	-	-	-	-
15,000	572	3.2	1.4	0.55	0.21	0.05	-	-	-	-	-
20,000	465	3.8	1.7	0.67	0.25	0.06	-	-	-	-	-
25,000	376	4.8	2.1	0.85	0.31	0.10	0.019	-	-	-	-
30,000	301	-	-	1.1	0.4	0.14	0.025	0.006	-	-	-
32,000	274	-	-	1.2	0.43	0.15	0.026	0.007	-	-	-
34,000	250	-	-	1.3	0.48	0.16	0.027	0.007	-	-	-
36,000	227	-	-	1.4	0.53	0.17	0.029	0.008	-	-	-
38,000	206	-	-	-	0.58	0.18	0.032	0.0085	-	-	-
40,000	187	-	-	-	0.62	0.19	0.034	0.009	0.003	0.00195	-
42,000	170	-	-	-	-	0.20	0.039	0.0097	0.0035	0.002	0.00135
44,000	155	-	-	-	-	-	0.044	0.0105	0.0037	0.0022	0.0016
46,000	140	-	-	-	-	-	-	0.0110	0.0040	0.0028	0.0017
48,000	127	-	-	-	-	-	-	0.0120	0.0044	0.0030	0.0019

RELATIVE HUMIDITY % WITH RESPECT TO ICE

TEMP. °C	DEPRESSION OF FROST POINT, DEGREES CENTIGRADE 0	1	2	5	10	20	30
+10	100	95	88	73	50	22.0	8.7
+10	100	95	85	68	44	18.0	6.8
-10	100	94	83	63	39	15.5	5.0
-20	100	90	83	62	37	12.8	4.0
-30	100	90	80	58	33	10.2	2.8
-40	100	90	78	55	30	8.5	2.0
-50	100	90	78	53	28	6.5	1.6
-60	100	88	75	50	25	5.8	1.3
-70	100	85	74	48	25	5.3	-

Geostrophic Wind Scale for Charts at 40°N.

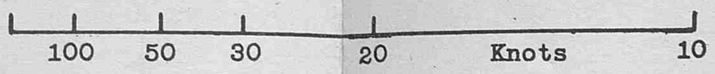

R.A.E. 129173 57

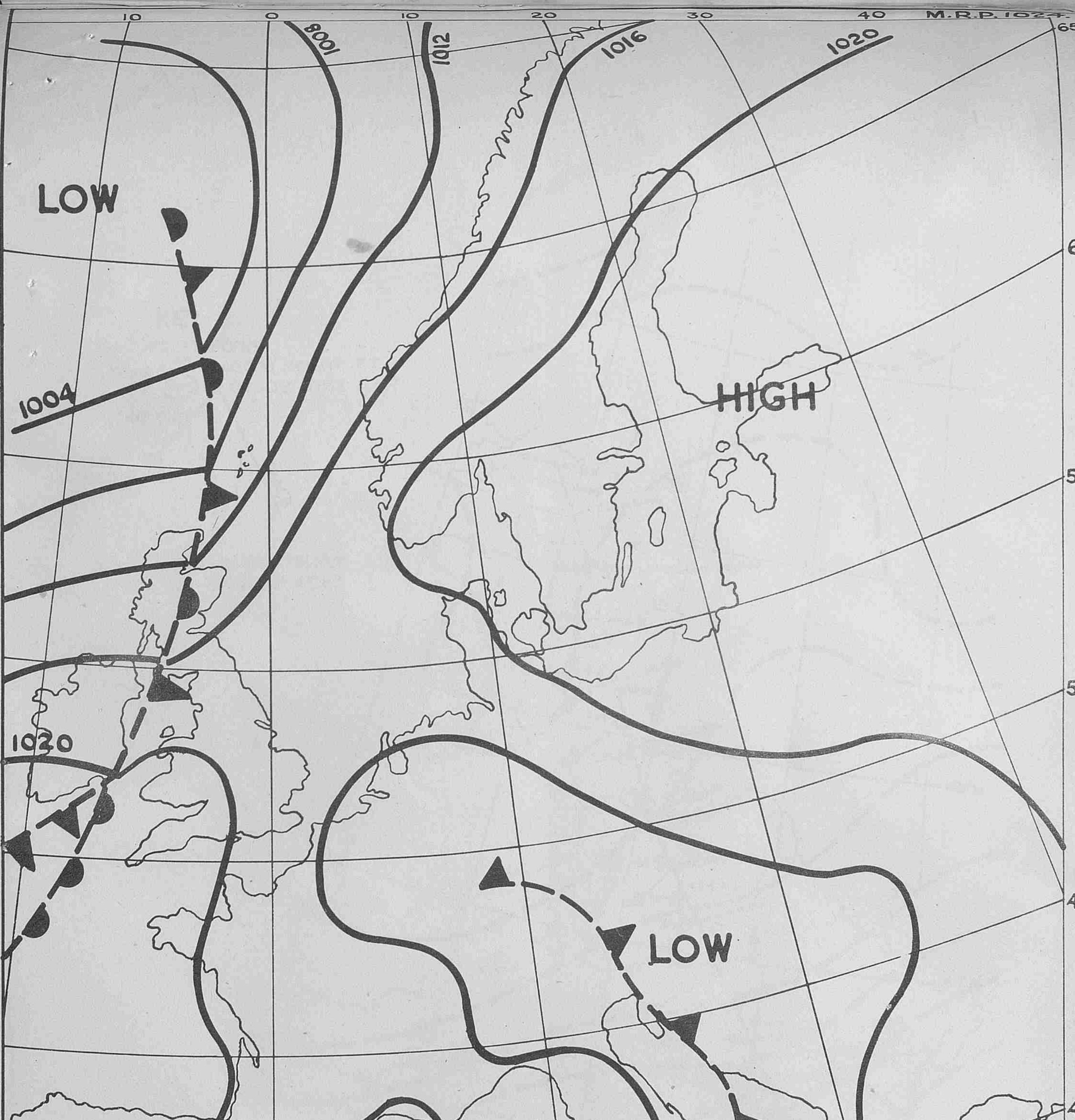
M.R.P. 1024
10
0
10
20
30
40
65
60
55
50
45
40
35
30
LOW
1004
1008
1012
1016
1020
HIGH
1020
LOW
LOW
1012
1016
1020
1016
1012
0
10
20

FIG. 11. SYNOPTIC CHART AT 0900Z ON 23RD MAY 1956.

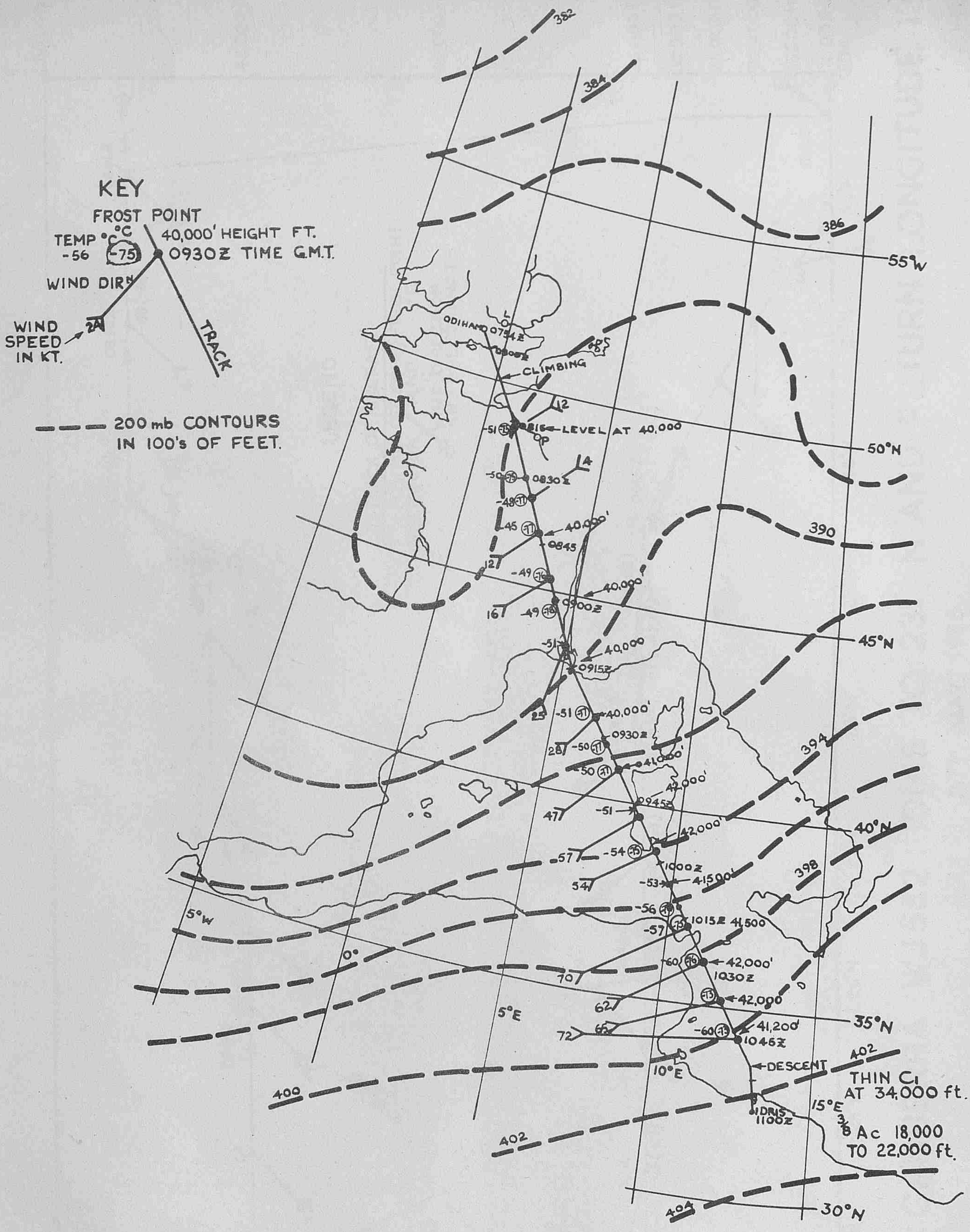
KEY
FROST POINT
TEMP °C °C
-56
-75
40,000' HEIGHT FT.
0930Z TIME G.M.T.
WIND DIRN
WIND SPEED IN KT.
24
TRACK
200 mb CONTOURS IN 100's OF FEET.
382
384
386
390
394
398
400
402
402
404
55°N
50°N
45°N
40°N
35°N
30°N
5°W
0°
5°E
10°E
15°E
ODIHAM 0754Z
L
0800Z
CLIMBING
P
12
-51
-75
BIS
LEVEL AT 40,000
P
4
-50
-75
0830Z
-48
-77
-45
-77
40,000'
0845
12
-49
-76
40,000
16
-49
-78
0900Z
-51
40,000
0915Z
25
-51
-77
40,000'
0930Z
28
-50
-77
-50
-77
41,000'
42,000'
0945Z
47
-51
42,000'
-57
-54
-75
1000Z
54
-53
41,500'
-56
-76
-57
-75
1015Z 41,500
-60
-76
42,000'
1030Z
70
-73
42,000
62
65
72
-60
-73
41,200'
1046Z
DESCENT
IDRIS 1100Z
THIN Ci AT 34,000 ft.
3/8 Ac 18,000 TO 22,000 ft.

FIG. 12. FLIGHT 1 ODIHAM TO IDRIS: 23RD MAY 1956.

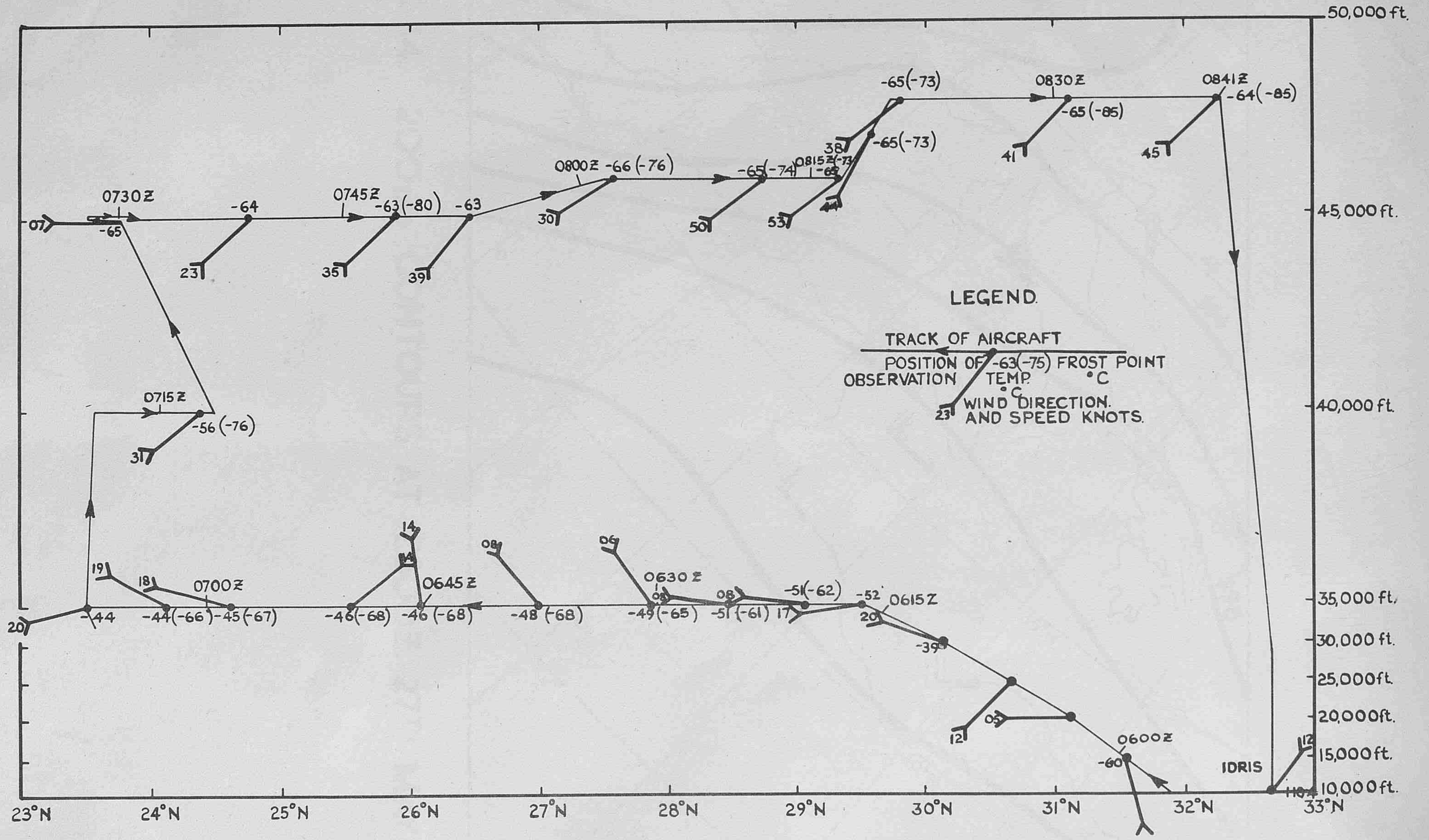

FIG. 13. FLIGHT 8: CANBERRA WJ582: IDRIS TO 23½° N AND RETURN LONGITUDE 13°E ±15'.

27TH MAY. 1956.

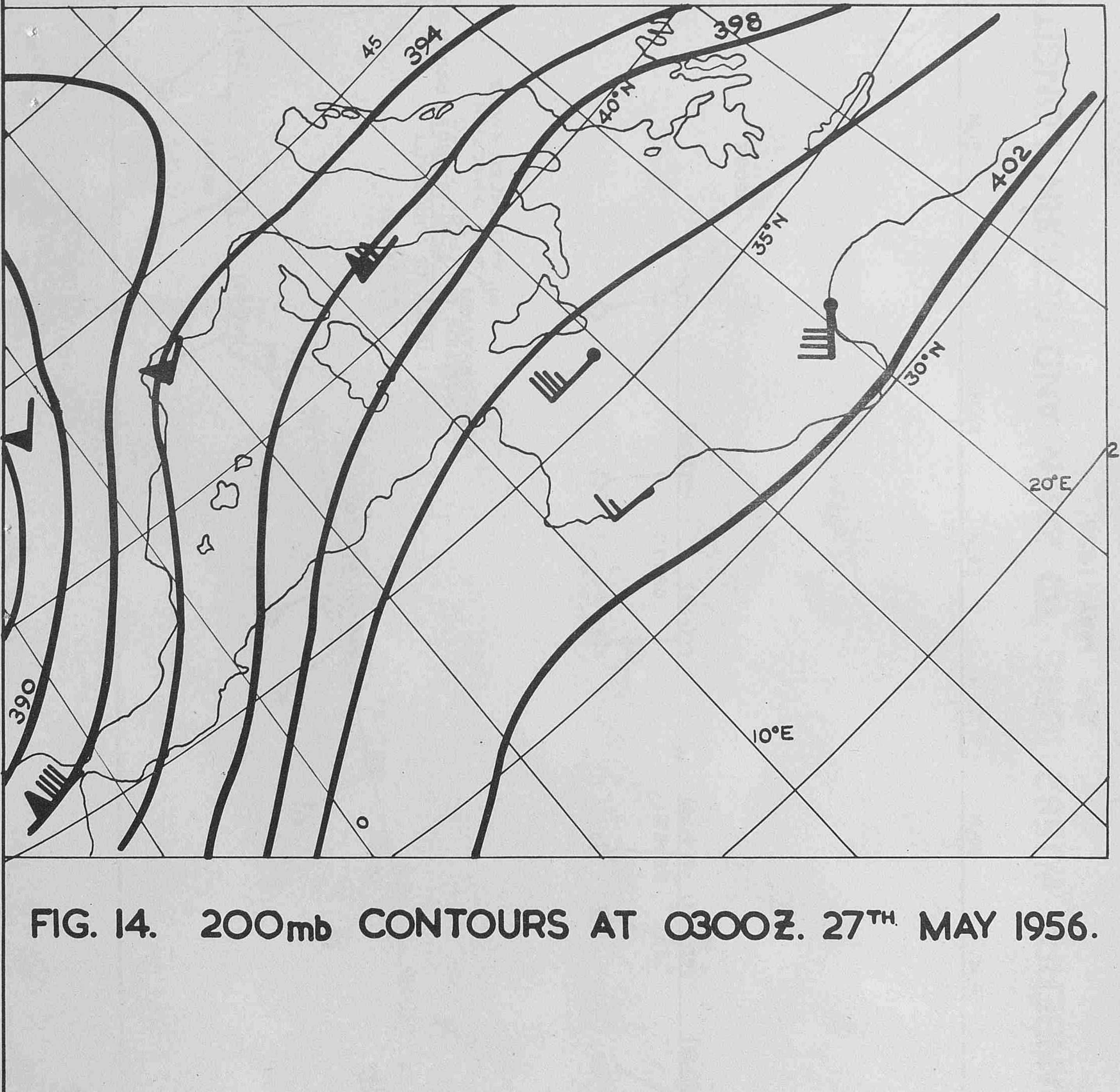
45
394
398
40°N
35°N
30°N
402
390
25
20°E
10°E

FIG. 14. 200mb CONTOURS AT 0300Z. 27TH. MAY 1956.

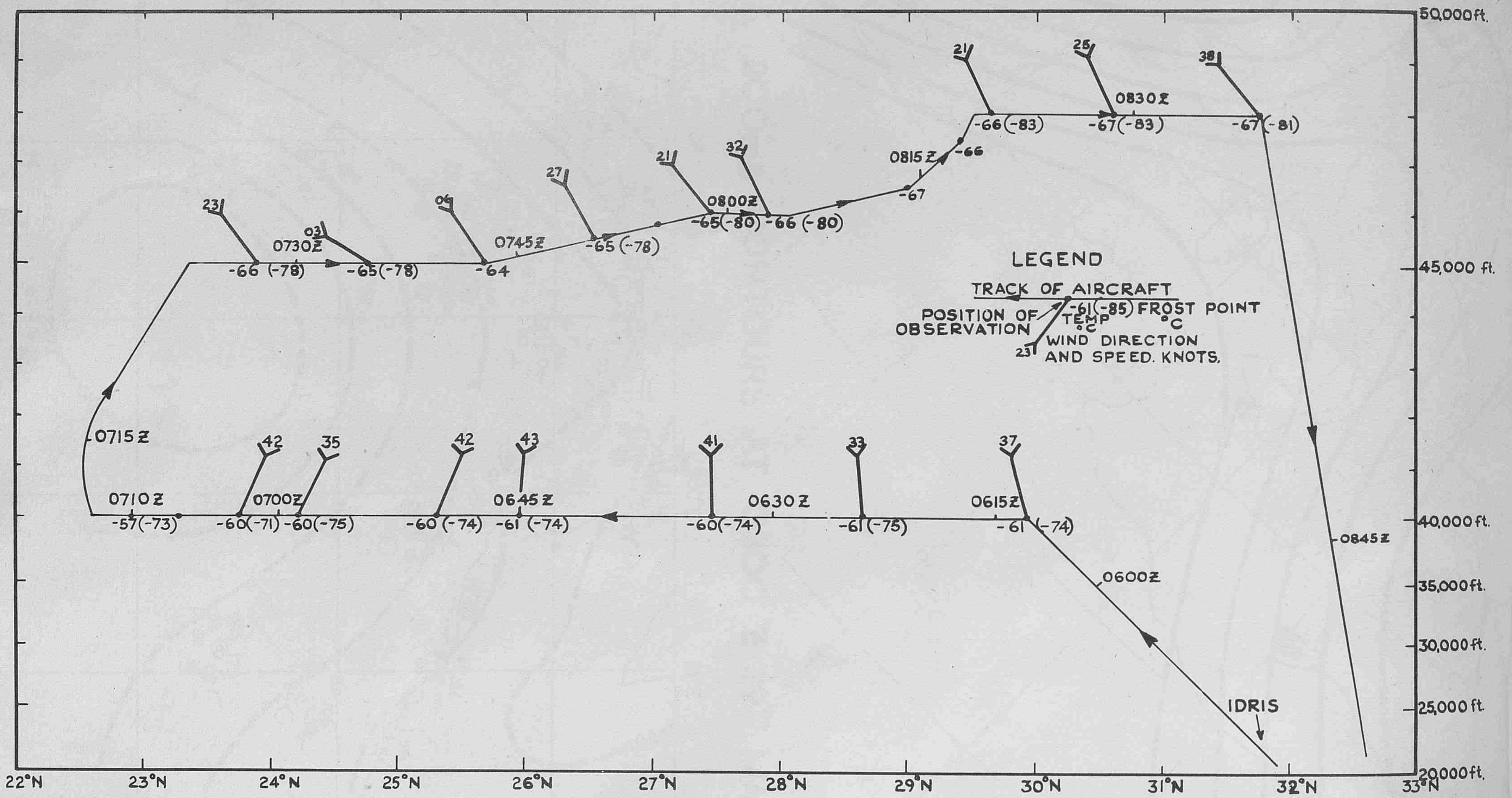

FIG. 15. FLIGHT 10: CANBERRA WJ582: IDRIS TO 22½°N AND RETURN: LONGITUDE 13°E ± 15'.
29TH MAY. 1956.

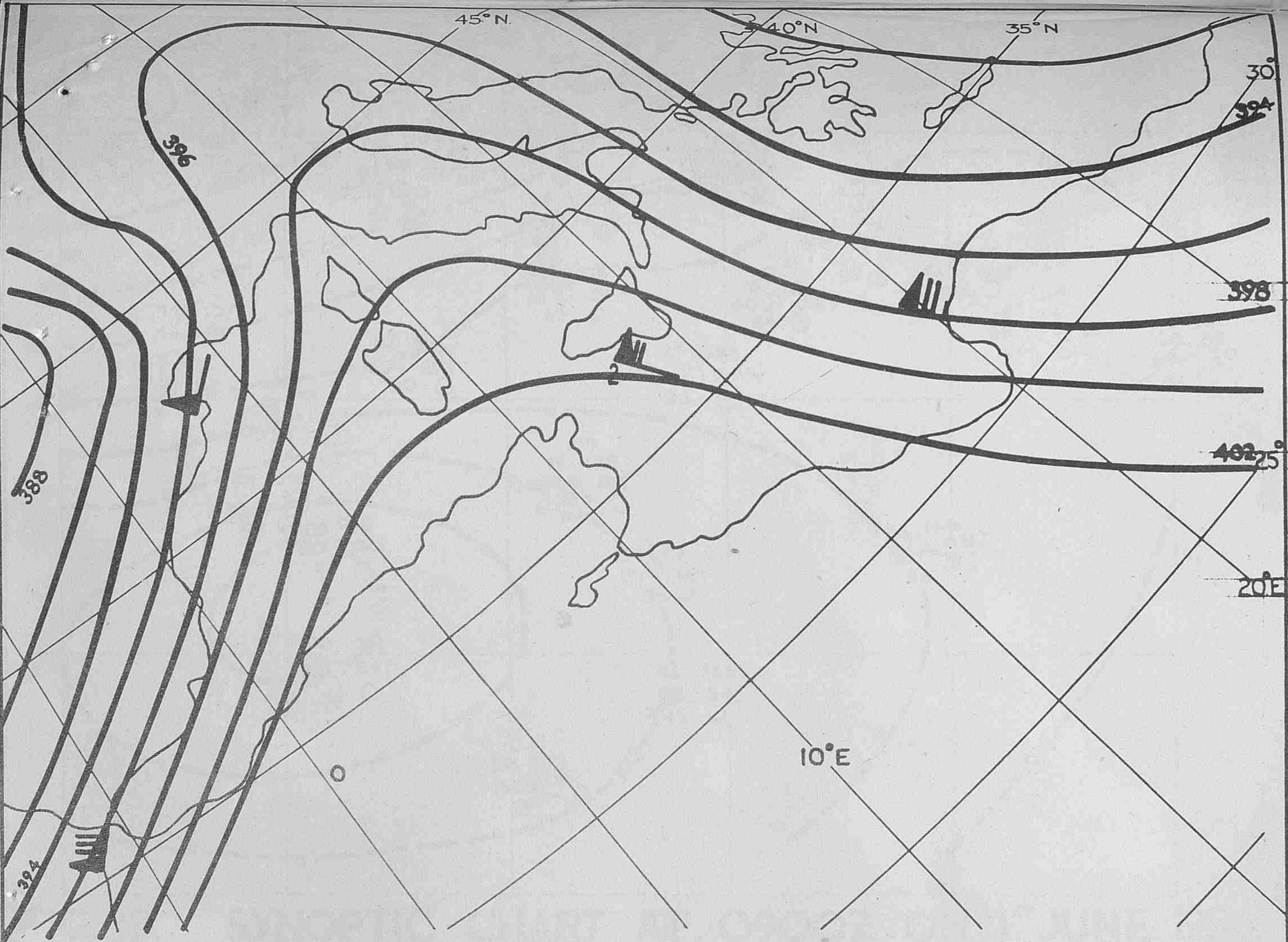
45°N.
40°N
35°N
30°
394
396
398
402
25°
20°E
388
10°E
0
394

FIG. 16. 200mb CONTOURS AT 0300 Z 29TH. MAY 1956.

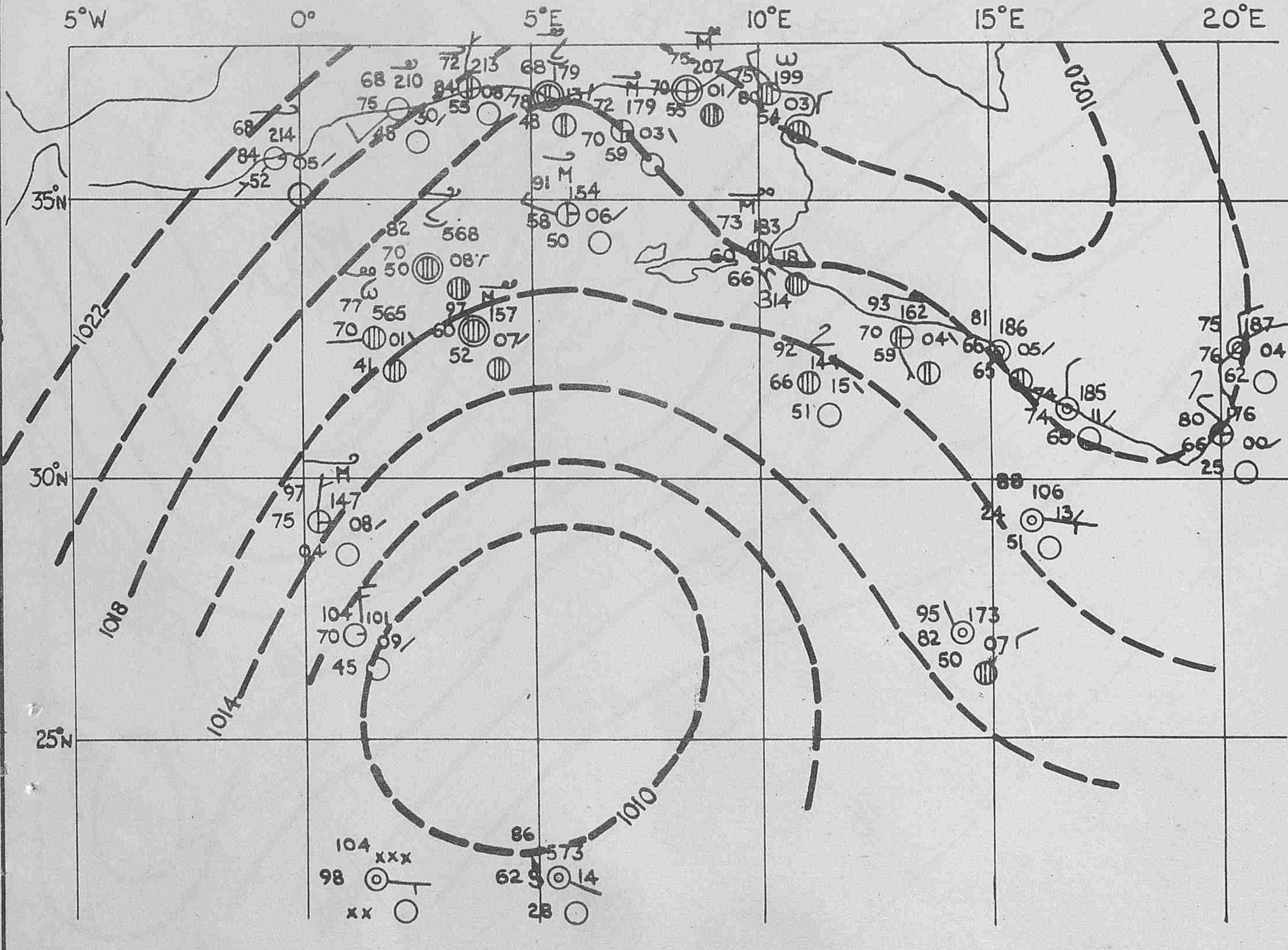
5°W
0°
5°E
10°E
15°E
20°E
35°N
30°N
25°N
1022
1018
1014
1010
1020

FIG. 17. SYNOPTIC CHART AT 0900Z ON TUES. 29TH. MAY 1956

M.R.P. 1024.

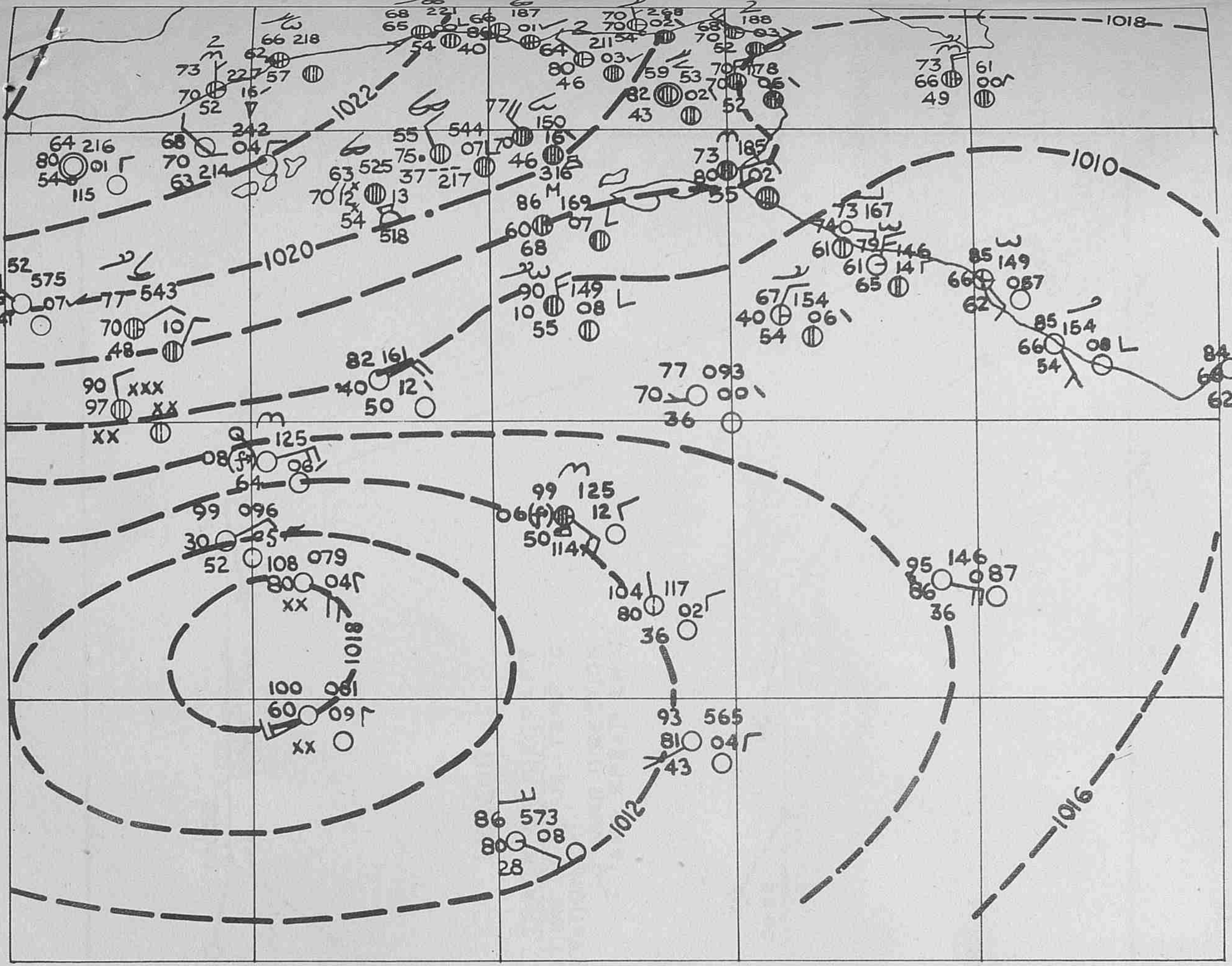
1018
1022
1020
1010
1018
1012
1016

FIG. 18. SYNOPTIC CHART AT 0900Z ON 1st JUNE 1956.

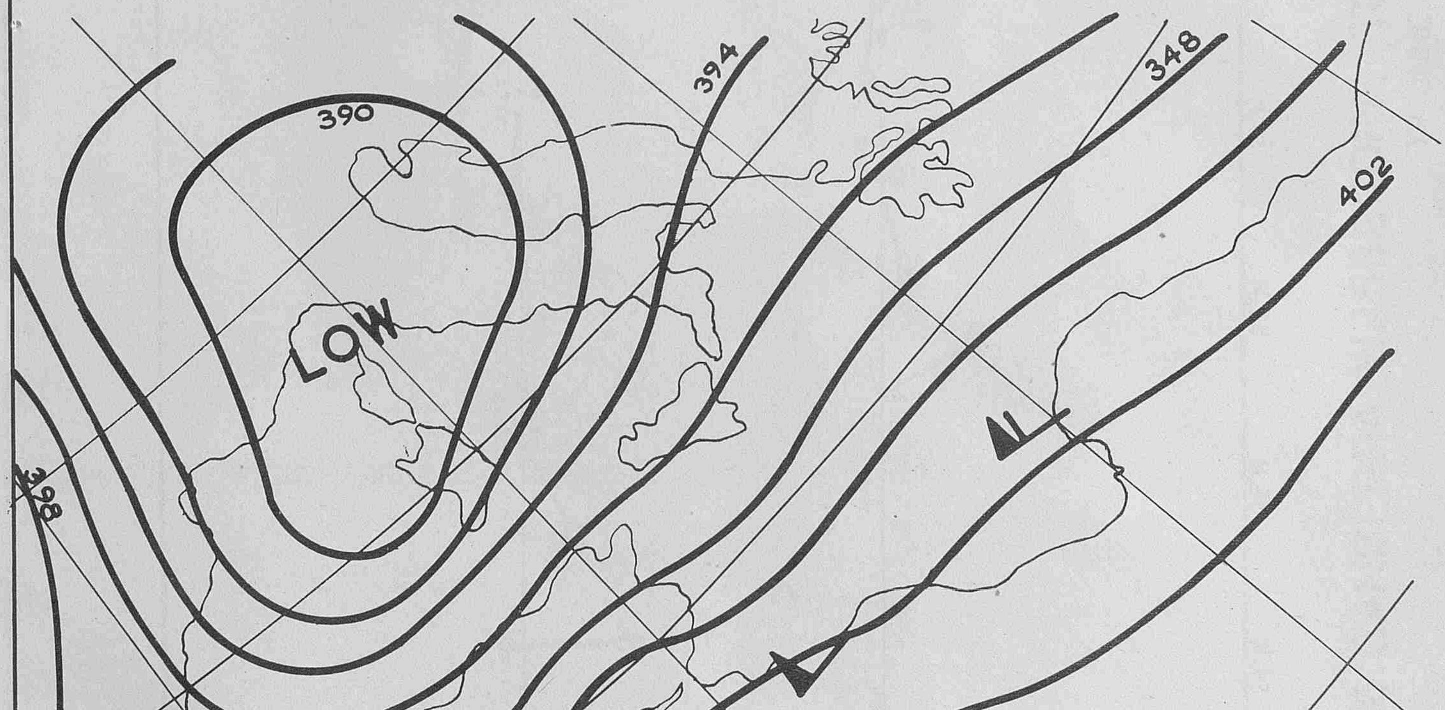
390
394
348
402
LOW
398
402

FIG. 19. 200mb CONTOURS AT 1400Z 1st JUNE 1956.

M.R.P. 1024.

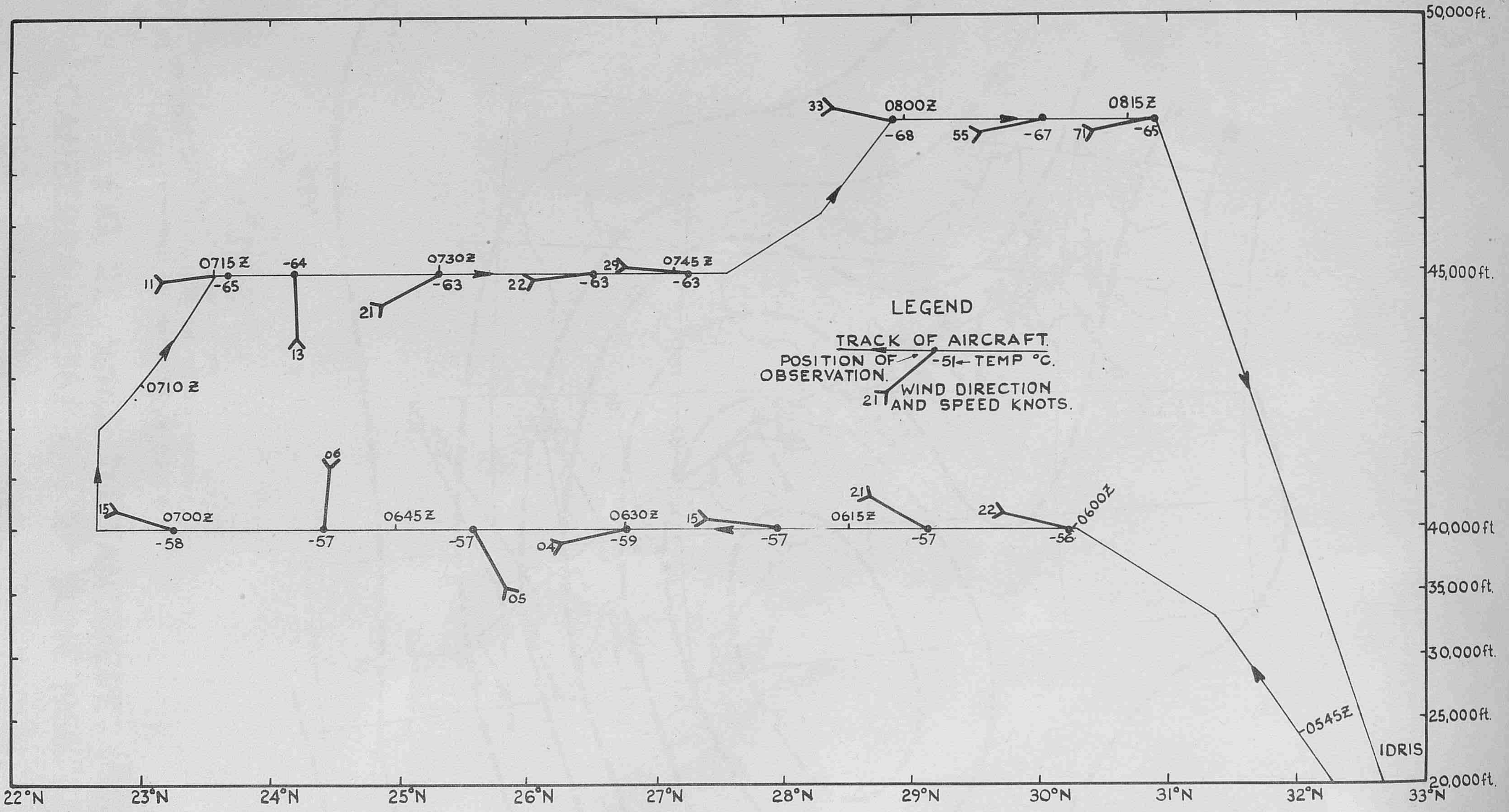

FIG. 20. FLIGHT 16: CANBERRA WJ582: IDRIS TO 22 °N AND RETURN: LONGITUDE 13°E ± 15′.

1ST JUNE. 1956.

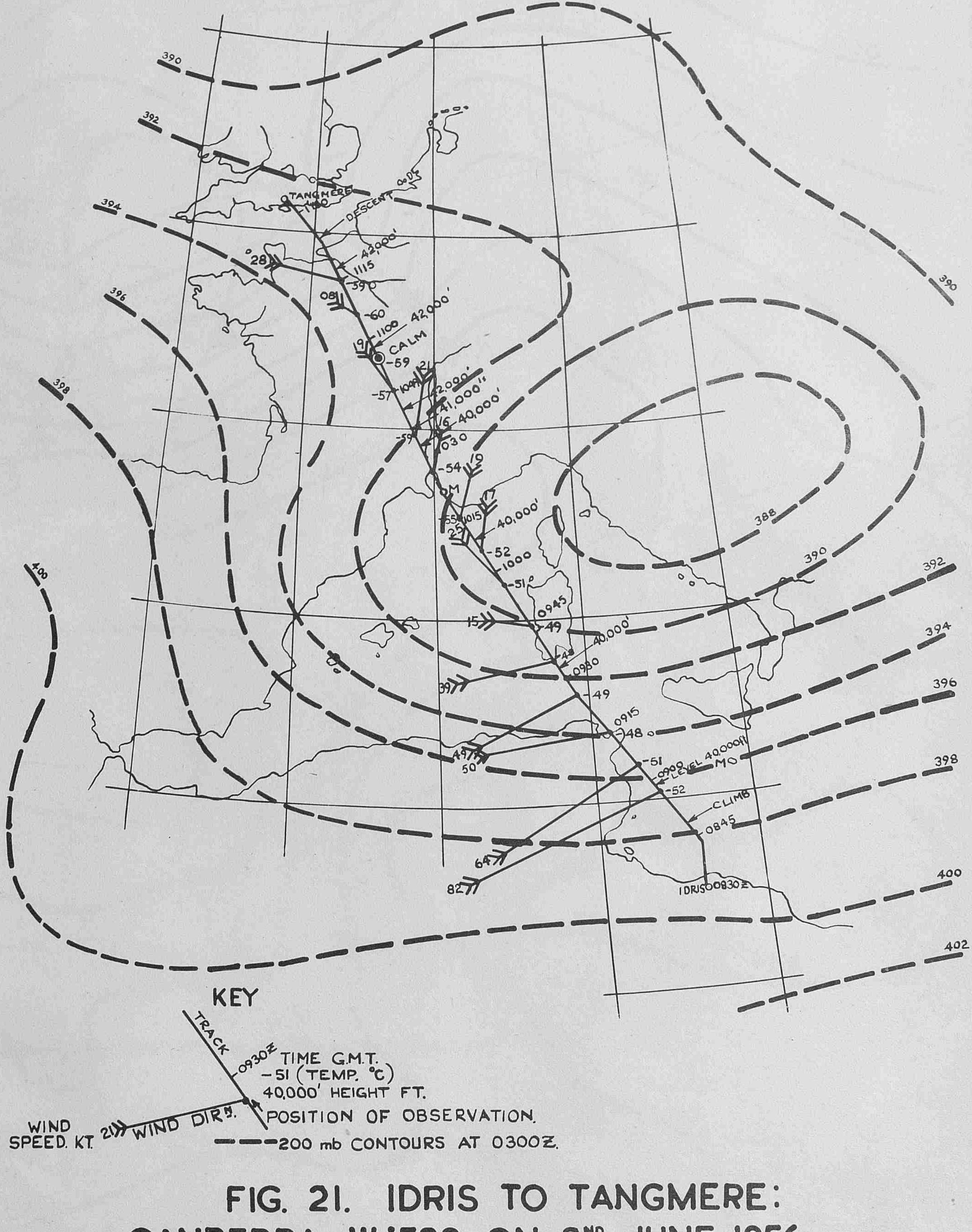
390
392
394
396
398
400
402
388
TANGMERE
1130
DESCENT
42,000'
1115
28
-59
08
-60
1100
42,000'
19
CALM
-59
21
1049
-57
42,000'
41,000'
40,000'
16
-59
1030
19
-54
DM
17
-55
1015
40,000'
25
-52
1000
-51
0945
15
-49
40,000'
48
0930
39
-49
0915
-48
49
50
-51
0900
LEVEL 40,000 FT
MO
-52
CLIMB
0845
64
82
IDRIS 0830Z
KEY
TRACK
0930Z TIME G.M.T.
-51 (TEMP. °C)
40,000' HEIGHT FT.
POSITION OF OBSERVATION.
WIND SPEED. KT.
21
WIND DIRN.
200 mb CONTOURS AT 0300Z.

FIG. 21. IDRIS TO TANGMERE: CANBERRA WJ582 ON 2ND JUNE 1956.

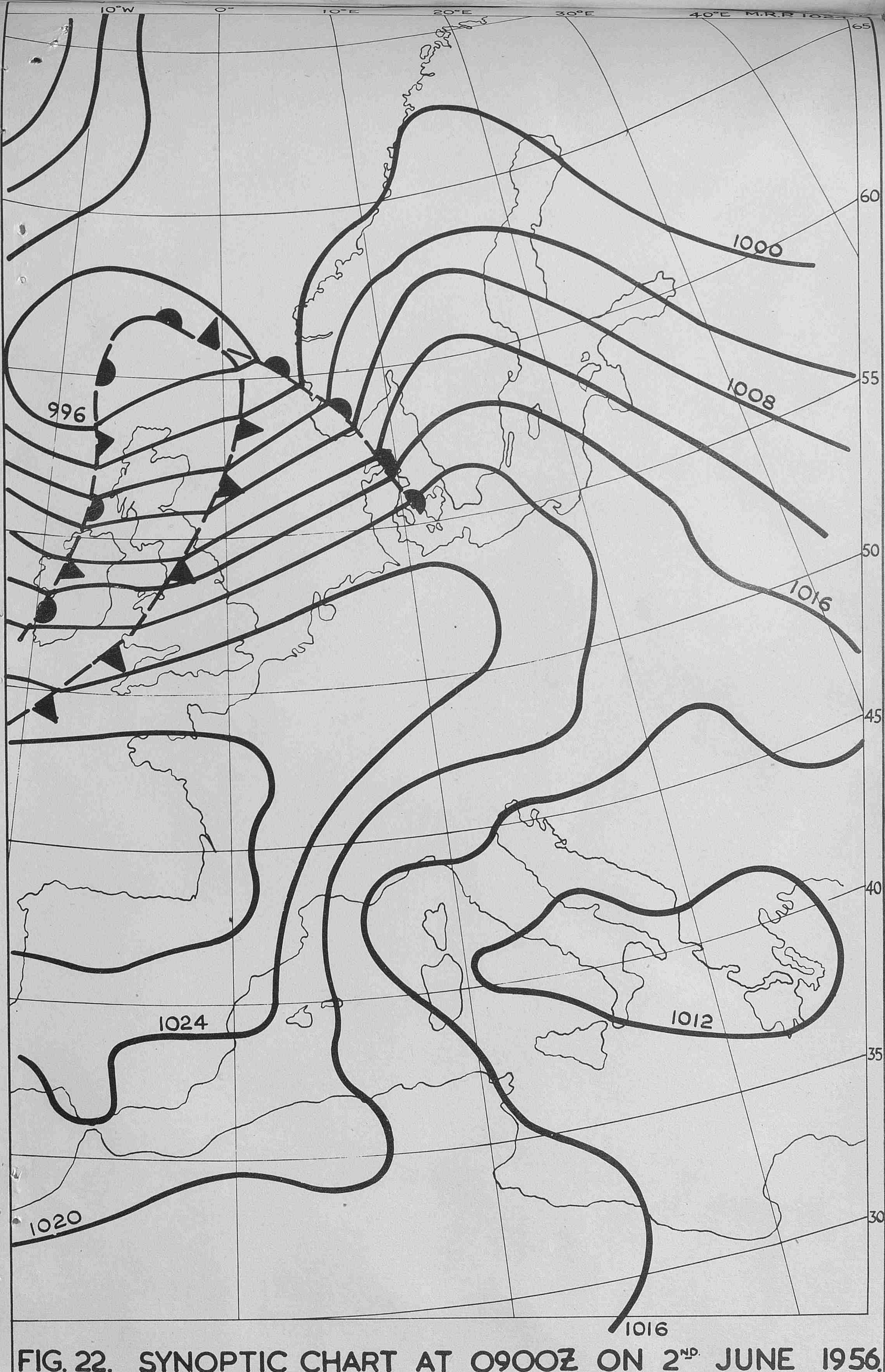
10°W
0°
10°E
20°E
30°E
40°E
M.R.P. 102
65
60
55
50
45
40
35
30
1000
1008
1016
996
1012
1024
1020
1016

FIG. 22. SYNOPTIC CHART AT 0900Z ON 2ND. JUNE 1956.

M.R.P. 1025
S.C. 11/226
2nd January, 1957

AD223131

A numerical study of the wavelength and amplitude of lee waves

by

C.E. Wallington and Janet Portnall

(Meteorological Office)

AIR MINISTRY

METEOROLOGICAL RESEARCH COMMITTEE

At the time of issue this report has not been published. Any author desiring to quote this paper should refer to it as "A paper of the Meteorological Research Committee (London),
M.R.P. No. 1025 by C.E. Wallington
and Janet Portnall.
A copy is available in the Library of the Meteorological Office."

M.R.P.1025
S.C.II/226
2nd January, 1957

AIR MINISTRY

METEOROLOGICAL RESEARCH COMMITTEE

A numerical study of the wavelength and amplitude of lee waves

by

C.E. Wallington and Janet Portnall (Meteorological Office)

Introduction

In a number of papers Scorer (1949 and 1953) has discussed the occurrence of lee waves in the atmosphere and has shown how the values of possible wavelengths may be calculated for an airstream which can be divided into two or more layers each with constant value of a parameter depending on wind and temperature structure. The calculations become rather lengthy if the number of layers exceeds four and it is not clear how much the criteria for lee waves and their wavelength is dependent upon the rather artificial division of the atmosphere into only a few discrete layers.

It is therefore of interest to calculate the wavelength of lee waves in a manner which is convenient for high speed computing and which includes a more detailed treatment of the wind and temperature structure of any given airstream.

As the temperature and wind at great heights are not normally known it is necessary to make some artificial boundary assumptions at the upper limit of the atmospheric layer considered. Our main object in this investigation is to study the effect of these assumptions on the computed wave flow and to test the general applicability of the method by comparing observed and computed lee wavelengths.

The equation of flow

We shall regard the flow as represented by small stationary disturbance imposed on a steady, horizontally uniform stream. Treating the flow as two-dimensional in a vertical plane, an equation can be formed to determine the pressure disturbance, p , at any point on any streamline. Then assuming that hydrostatic equilibrium is maintained, a differential equation defining the flow pattern can be obtained.

For continuity along a stream tube the horizontal velocity component, u, is related to its undisturbed value, U, by the equation

$$u = U\left(1 + \partial p/\partial P\right)^{-1} \qquad (1)$$

where P is pressure on the streamline in an undisturbed part of the flow.

The equation of continuity enables the vertical velocity component, w , to be given by the equation

G.1792/JB/1/57/50

$$\rho g w = -U \cdot \frac{\partial p}{\partial x}\left(1 + \frac{\partial p}{\partial P}\right)^{-1} \qquad (2)$$

where ρ denotes the density,

g denotes acceleration due to gravity,

and x is the horizontal co-ordinate.

From the vertical component of the equation of motion we can derive the equation

$$\frac{\partial z}{\partial P} = -\frac{1}{\rho}\left(1 + \frac{\partial p}{\partial P}\right)\left(g + u\frac{\partial w}{\partial x}\right)^{-1} \qquad (3)$$

z being the height.

The second term in the denominator of the right hand side of this equation represents the vertical acceleration of the air and is very small compared with g. Therefore an approximate form of the equation is

$$\frac{\partial z}{\partial P} = -\frac{1}{\rho g^2}\left(1 + \frac{\partial p}{\partial P}\right)\left(g - u\frac{\partial w}{\partial x}\right) \qquad (4)$$

For adiabatic flow of unsaturated air, scalar multiplication of the vector equation of motion by the velocity vector leads to Bernouilli's equation which may be expressed as

$$\rho g z + \frac{1}{2}\rho(u^2 + w^2) - \frac{\gamma}{\gamma - 1}(P + p) = \rho\psi \qquad (5)$$

γ being the ratio of the specific heat of dry air at constant pressure to that at constant volume and ψ being a function of P only.

Differentiating Eq.(5) with respect to P and introducing the potential temperature, θ, referred to a standard pressure level, P_0, we get

$$\frac{1}{2}\rho\frac{\partial}{\partial P}\left(u^2 + w^2\right) + \frac{\gamma}{\gamma - 1}\,\frac{P + p}{\theta}\,\frac{\partial\theta}{\partial P} + \frac{u}{g}\left(1 + \frac{\partial p}{\partial P}\right)\frac{\partial w}{\partial x} = \rho\frac{\partial\psi}{\partial P} \qquad (6)$$

Equations (1) and (2) may be used to eliminate u and w from Eq.(6) and, for small disturbances only, terms involving powers of p higher than the first may be neglected. Thus after some manipulation Eq.(6) becomes

$$\frac{\partial^2 p}{\partial P^2} + \frac{2}{U}\frac{\partial U}{\partial P}\frac{\partial \rho}{\partial P} + \left(\frac{R\theta P_0^{\frac{1-\gamma}{\gamma}}}{g P^{\frac{1}{\gamma}}}\right)\frac{\partial^2 p}{\partial x^2} - \frac{R P_0^{\frac{1-\gamma}{\gamma}}}{P^{1/\gamma} U^2}\, p\,\frac{\partial\theta}{\partial P} = 0 \qquad (7)$$

where R is the gas constant.

/Method

Method of computation

In order to seek solutions of Eq.(7) which are sinusoidal in the x direction we substitute p = the real part of $f e^{ikx}$, where f is a function of P only, $i = \sqrt{-1}$, and k is a number to be determined. Eq.(7) may then be written in the form

$$\frac{\partial^2 f}{\partial P^2} + 2C \frac{\partial f}{\partial P} + (B - A k^2) f = 0 \qquad (8)$$

where A, B and C are functions of P only.

The problem of determining the existence and wavelength of lee waves now becomes one of finding values of k (= K, say) which permit solutions of Eq.(8) satisfying appropriate boundary conditions. For numerical integration of the equation it is convenient to deal with its finite difference approximation which, after some rearrangement of terms, may be written

$$f_{p+1} = \left[(n^2 A_p k^2 - n^2 B_p + 2) f_p + (n C_p - 1) f_{p-1} \right] (n C_p + 1)^{-1} \qquad (9)$$

where the suffixes refer to pressure levels, n being the pressure interval between successive levels.

The lower boundary condition is taken to be $f = 0$ at the 1000 mb pressure level, but it is difficult to justify a definite assumption for the pressure disturbance at some upper boundary. Therefore we take as the upper boundary conditions a unit pressure disturbance at the 200 mb level and make arbitrary trial assumptions of the value of f at 150 mb. Since we do not, at this stage, define a unit pressure disturbance, these assumptions involve only the ratio of the pressure disturbance at 150 mb to that at 200 mb. We shall denote this ratio by ϕ

In the present series of computations n was given the constant value of 50 mb and the coefficients A_P, B_P and C_P were calculated for 50 mb pressure intervals centred at 200, 250, 300, ... 950 mb.

For each assumed value of ϕ and for values of k = 0, 0.0625, 0.125, 0.1875 .... 8.0 nautical miles^{-1}, Eq.(9) was used to compute f at 50 mb steps from 250 mb down to the 1000 mb level. Changes of sign for successively computed values of f at 1000 mb showed where to intensify the search for wave numbers which allowed $f = 0$ at 1000 mb. These wave numbers were then calculated to within 6 x 10^{-6} n.mi.$^{-1}$. The search for values of K was not extended to wave numbers greater than 8 n.mi.$^{-1}$ since experience and theory suggest that short lee waves are usually of small amplitude.

Having computed values of K and corresponding profiles of f it was desirable to assign realistic magnitudes to the pressure disturbance.

Scorer (1949) has derived an expression for the lee wave flow downwind of an 'idealized' two-dimensional ridge whose height, h, at a horizontal distance x from the crest is given by

$$h = \frac{H b^2}{b^2 + x^2} \qquad (10)$$

where H is the height of the ridge and b is a width parameter. Adapting his method to this study we can determine the flow pattern through lee waves induced by such a ridge. The vertical displacement, ζ_z, of a streamline from its undisturbed level at height z is given by the equations

$$\begin{aligned} \zeta_z &= -Hbe^{-Kb}\,\xi_z \sin Kx \\ \xi_z &= 2\pi\left(\frac{\rho_0}{\rho_z}\right) f_z \left(\frac{\partial f}{\partial K}\right)_0^{-1} \end{aligned} \qquad (11)$$

where the suffix 0 refers to the lower boundary level. Values of the lee wave amplitude factor, ξ_z, have been computed and are discussed in the following section.

Discussion of results

The data chosen for numerical study comprised 19 sets of Leuchars radio-sonde ascents in which Corby (1956) had already detected the effect of pronounced lee waves.

Fig. 1 typifies many of the results obtained. Distributions of ξ with height are shown for four of the assumed upper boundary conditions. The full lines show that with $\phi = 0$ two values of K were obtained; the corresponding wavelengths ($2\pi/K$) are given in the figure. For a wavelength of 5·384 n.mi. the amplitude factor, ξ, attains a maximum of 1·05 n.mi.$^{-1}$ in the middle of the stable layer indicated by the observed temperature profile. The longer wavelength of 11·935 n.mi. appears to be associated with a significant lee wave which has a nodal surface at 610 mb. The remaining three pairs of curves relate to $\phi = 1$, 8, and 16. A feature of the ξ curves and the computed wavelengths is that, for the short wavelength, they change only slightly with the upper boundary variation, whereas the long wave value and its amplitude curve were much more sensitive to the choice of ϕ. Particular attention is called to this feature since most of the computed profiles could be classified into two distinct groups: either they varied quickly with variations of the upper boundary assumption or they appeared to change very slowly through a wide (though not unlimited) range of values of ϕ.

Another feature of the plotted curves is that the compact groups such as the short wavelength group of Fig. 1 usually portray waves whose amplitude factors attain only one or two maxima in the troposphere and, apart from a few exceptions, these waves tend to become small near the tropopause. The broad groups on the other hand are usually associated with amplitude curves which vary much more rapidly with height especially in the upper troposphere.

An example of this feature is illustrated in Fig. 2 which shows two compact groups of curves for wavelengths of 2.4 and 4.8 n.mi. and a broad group comprising a set of longer computed wavelengths. The two short waves are confined to the troposphere and it is encouraging to note that Corby detected a wavelength of 4.8 n.mi. for this particular case. The shorter 2.4 n.mi. wavelength was not apparent in his study but inspection of the topography upwind of Leuchars suggests that if this short wave did exist then its maximum vertical velocity would have been smaller than that of the 4.8 n.mi. wave and may therefore have escaped detection. The presence of the broad group of computed longer waves also requires some explanation, for there is no evidence of their actual existence at Leuchars at 04 GMT on 20 November, 1953.

Since the computed values of K and the amplitude of the calculated waves differ greatly according to the choice of upper boundary conditions, there is no reason to think that these solutions correspond to any real dynamical property of the air-stream. If any waves do exist in this band of wavelength, they are inadequately treated by this method, either because they depend on conditions at higher levels or because of inaccuracies in the method.

Some computing tests have shown that truncation errors may be appreciable for the amplitude curves which exhibit large values of $\partial^2\xi/\partial P^2$ at high levels, but it is not yet possible to make a general statement on the effect of these errors. Until more exhaustive tests have been carried out we must be wary of attaching undue significance to curves of this type.

Thus the compact groups of ξ curves may be subdivided into two categories according to whether they have large or small values of $\partial^2\xi/\partial P^2$ at high levels. The significance of the first category is doubtful but the compact groups of curves without large curvature at high levels may legitimately be interpreted as real waves whose wavelength and amplitude are almost independent of conditions in the high stratosphere. Of the 19 cases examined 13 yielded curves which could be included in this latter category. The observed and computed wavelengths for these cases are listed below.

Date and time	Observed wavelength (n.mi.)	Computed wavelength (n.mi.)
4/11/53 14 GMT	7.2	7.9
18/11/53 14 GMT	7.2	8.1
20/11/53 14 GMT	4.8	4.8 & 2.4
21/12/53 14 GMT	5.4	7.0
3/1/54 03 GMT	10.0	9.2
3/1/54 14 GMT	10.0	9.7
4/1/54 02 GMT	5.6	5.4

Date and time	Observed wavelength (n.mi.)	Computed wavelength (n.mi.)
11/1/54 14 GMT	3.2	4.1
12/1/54 16 GMT	4.8	6.0
23/1/54 14 GMT	3.0	3.1
11/4/54 14 GMT	4.7	4.2
15/4/54 02 GMT	10.1	12.6
15/4/54 14 GMT	7.8	6.2

Two of the remaining six cases produced compact groups of curves with large values of $\partial^2\xi/\partial P^2$ at high levels while the four other cases revealed no definitely compact groups. The nature of the curves obtained in these four cases may be illustrated by reference to Fig. 3. On this occasion $\phi = 4$, 8 and 16 led to a compact group of curves with wavelengths close to 9.7 n.mi. but $\phi = 1$ failed to produce a curve in this group; instead of one significant curve we obtained two, both of which vary quickly with changes of ϕ. This illustrates the fact that although we may derive the wavelength of about 9.7 n.mi. by making only an approximate guess at the appropriate value of ϕ, our guess must at least be within some wide range. In the four unsolved cases it appeared that none of the trial values of ϕ was within an appropriate range: the ξ profiles comprised only chaotic sets of curves which could not be analysed into compact groups. It was impractical in these four cases to extend the search for suitable values of ϕ, especially since the high level conditions tended to amplify inaccuracies in the method of computation. These inaccuracies are mainly due to the coarseness of the finite difference interval of 50 mb at high levels. It is intended to reduce this interval in future numerical work.

As a further guide to the realism of the computed amplitude factors a comparison between the vertical motion anomalies of the radio-sondes and the calculated vertical speeds was attempted. Usually it was difficult to assess the values of H and l applicable to the upwind terrain. Nevertheless, estimates made showed the computed ξ curves with their mean maxima of 1.6 n.mi.$^{-1}$ at an average level of 780 mb to be reasonably consistent with the general magnitude and distribution of the observed vertical speeds.

In one case it was feasible to analyse the high ground profile in detail sufficiently far upwind of Leuchars to include the most effective topographical features. At 1415 GMT on 21 December, 1953 an airstream, whose temperature and wind structure are shown in Fig. 4, blew from about 290° across the Sidlaws to Leuchars. Upwind of Leuchars the high ground profile could be considered as a synthesis of six "ideal" ridges as far as the Tay valley. For some considerable distance further upwind the topographical features did not appear suitable for setting off lee waves on this occasion. Fig. 4 shows the computed vertical motion field in the lee wave over and downwind of Leuchars. Comparison of the observed and computed vertical motion anomalies of the radio-sonde shows that the computations yield vertical speeds of approximately correct magnitudes. There does appear to be a phase difference between the observed and computed wave but this appears to arise from the two-dimensional treatment of two of the "ideal" ridges; the 290° airstream crossed these two ridges close to their northeastern ends and the associated lee wave amplitudes may not therefore have attained their full two-dimensional values.

Conclusion

Comparison of computed lee-wavelengths with those estimated by Corby from the rate of ascent of the radio-sonde balloon, indicate a reasonable accuracy in the computed wavelengths.

The method of calculation as adopted in the present experiment is likely to be inaccurate for lee-waves which have a significant amplitude in the stratosphere. It is not known whether the failure to determine the wavelength satisfactorily in 4 out of the 19 cases is for this reason.

References

Corby, G.A.	1956	Meteorological Research Papers, Air Ministry, London, No. 985.
Scorer, R.S.	1949	Quart.J.R..Met.Soc., 75, p.41.
	1953	Ibid., 79, p.70.

Appendix

Observed and computed wavelengths

In the table below each line of wavelengths is associated with ξ -curves which have similar characteristics or which fall into compact groups.

Wavelengths are given in nautical miles.

Date and time	Observed wavelength	Computed wavelengths for various values of ϕ				Character of ξ curves
14 GMT 4/11/53	7.2	ϕ = 0	1	4	16	
		7.9	7.9	7.9	7.8	C
		5.7	5.3	4.9	4.7	n
		3.7	-	2.5	1.5	n
14 GMT 18/11/53	7.2	ϕ = 0	1	4	16	
		12.0				
			8.2	8.1	8.1	C
		8.0				
			6.2	3.0	1.4	n
14 GMT 20/11/53	4.8	ϕ = 0	1	8	16	
		10.3	6.1	25.5	24.0	X
		4.8	4.8	4.8	4.8	C
		2.4	2.4	2.4	2.4	C
				2.0	1.4	n
02 GMT 30/11/53	14.4	ϕ = 0	1	4	16	
		11.2	33.2	21.2	20.2	
			7.0	3.4	1.6	n
14 GMT 21/12/53	5.4	ϕ = -4	1	4	8	
		34.2				X
		7.0	7.0	7.0	7.0	C
			5.5	3.3	2.3	n
03 GMT 3/1/54	10.0	ϕ = 0	1	4	16	
			9.4			X
		9.1		9.2	9.2	C
			7.9			X
				3.2	1.4	n
14 GMT 3/1/54	10.0	ϕ = 1	4	8	16	
		11.5				
			9.7	9.6	9.6	C
		9.0				
					1.5	n
02 GMT 4/1/54	5.6	ϕ = 0	1	8	16	
		11.9	10.1	7.9	7.6	X
		5.4	5.4	5.4	5.4	C
		3.5	3.1	1.9	1.4	n
02 GMT 11/1/54	6.5	ϕ = 0	1	8	16	
		8.9	8.4	8.1	8.1	CX
		5.7	5.4	5.3	5.2	CX
		4.9	4.8	4.8	4.8	CX
		3.9	2.9	1.3		n
14 GMT 11/1/54	3.2	ϕ = 0	1	4		
		6.5	6.5	6.5		CX
		4.1	4.1	4.1		C
16 GMT 12/1/54	4.8	ϕ = -16	0	16		
		10.1	16.7	10.9		X
		5.9	6.1	5.9		C
			4.6	1.4		n
02 GMT 14/1/54	5.6	ϕ = 0	1	8	32	
		17.5	11.5	10.1	9.6	X
		8.7	8.0	7.2	7.2	X
		5.4	4.4			n
				1.9	1.0	n
14 GMT 23/1/54	3.0	ϕ = 0	1	4	16	
		11.0	11.1	11.1	11.0	CX
		4.5	4.5	4.5	4.5	CX
		4.0	4.0	4.0	4.0	CX
		3.1	3.1	3.1	3.1	C
		1.3	1.3	1.3	1.2	n
14 GMT 24/1/54	2.6	ϕ = 0	1	4	16	
		6.4	6.4	6.4	6.4	CX
		4.9	4.9	4.9	4.9	CX
		3.1	3.1	3.1	3.1	n
		1.9	1.8	1.5	1.0	n
02 GMT 21/3/54	4.7	ϕ = 0	1	8	32	
		20.4	14.1	11.5	11.5	X
		9.9	9.3	7.6	7.1	
		4.0	3.6	2.1	1.1	n
14 GMT 11/4/54	4.7	ϕ = 0	1	8	16	
				18.7	15.7	
		6.1	5.9	5.5	5.5	CX
		4.2	4.2	4.2	4.2	C
		3.7	3.3	1.9	1.4	n
15 GMT 14/4/54	13.0	ϕ = 0	1	4	16	
			42.3			X
		12.0		13.0	12.7	
			11.0			
				3.9	1.6	n
02 GMT 15/4/54	10.1	ϕ = 1	8	16	32	
		14.2				
			12.8	12.6	12.6	C
		6.7				
			2.6	1.8	1.3	n
14 GMT 15/4/54	7.8	ϕ = 0	4	16		
		10.0				n
		6.2	6.2	6.2		C
			3.5	1.7		n

Characteristics of ξ -curves -
C = Compact group
X = Accuracy doubtful
n = Almost negligible values

LEUCHARS, 0200 G.M.T. 4:1:54

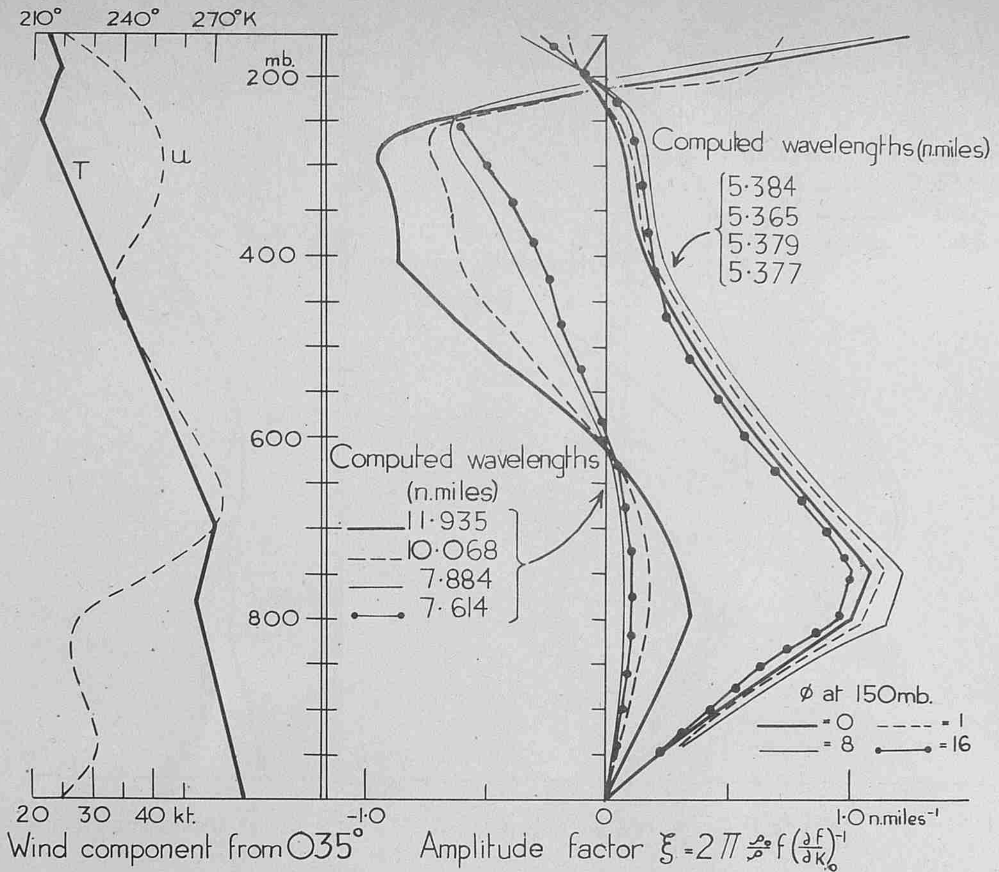

Observed wavelength = 5·6 n.miles

Fig. 1

LEUCHARS, 0400 G.M.T. 20:11:53

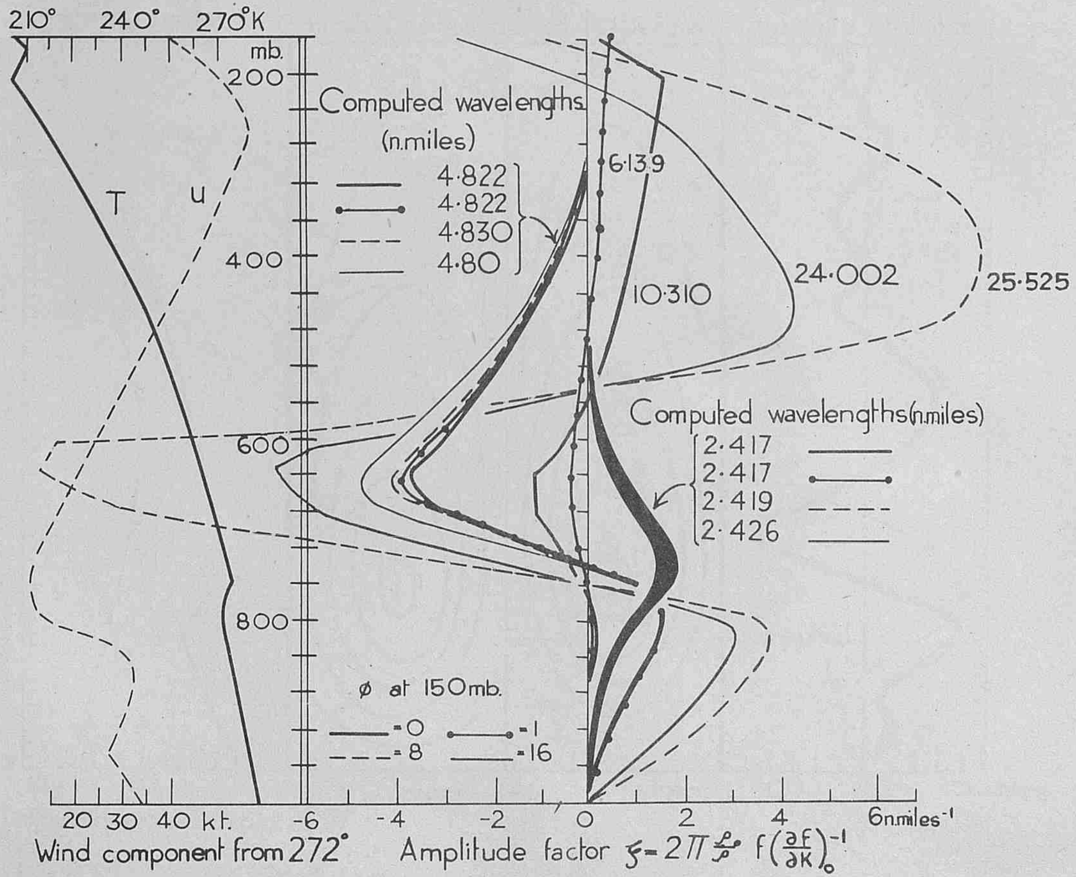

Observed wavelength = 4·8 n.miles

Fig. 2

Figs. 1, 2 and 3. Wind and temperature distribution with height is indicated in the left of the figures. ξ -curves and their associated wavelengths for several values of ϕ are shown on the right. The observed wavelengths were measured by Corby (1956).

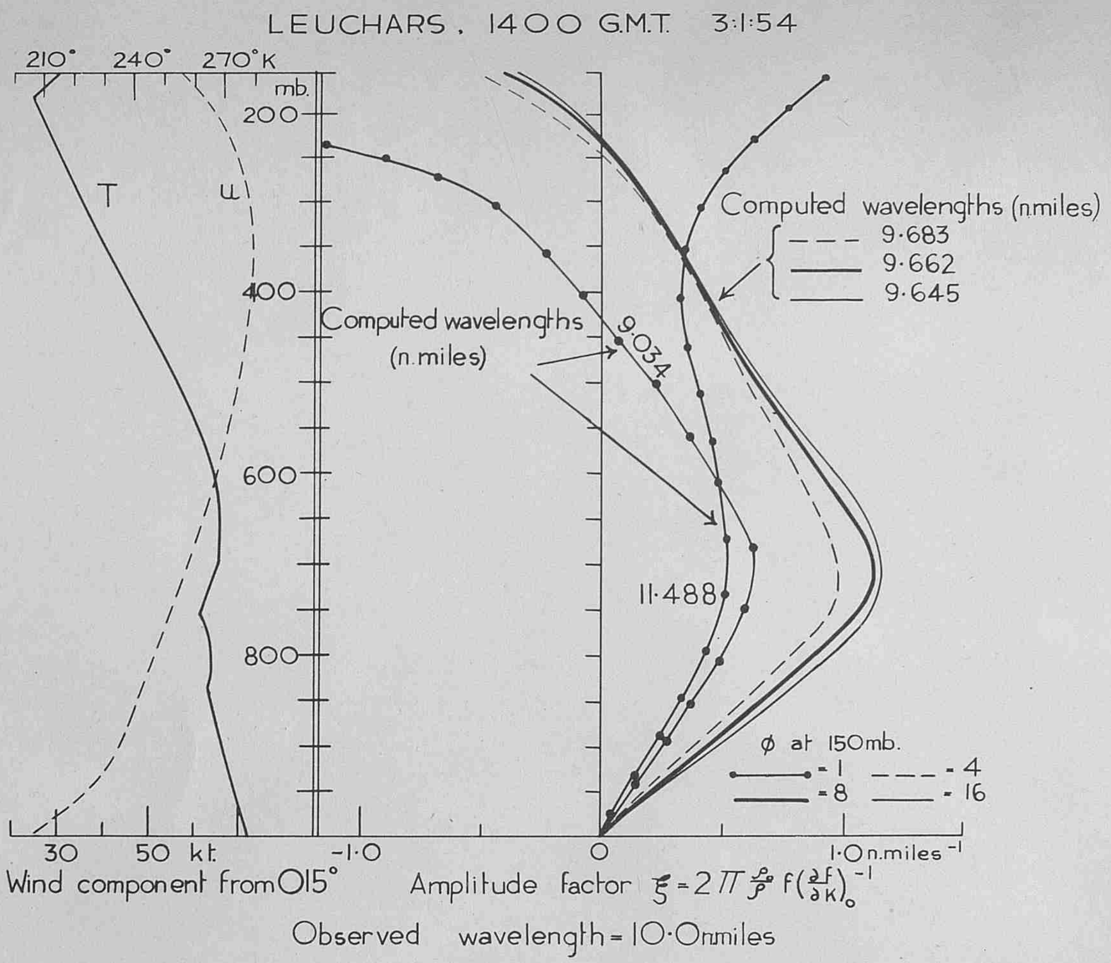

Fig. 3

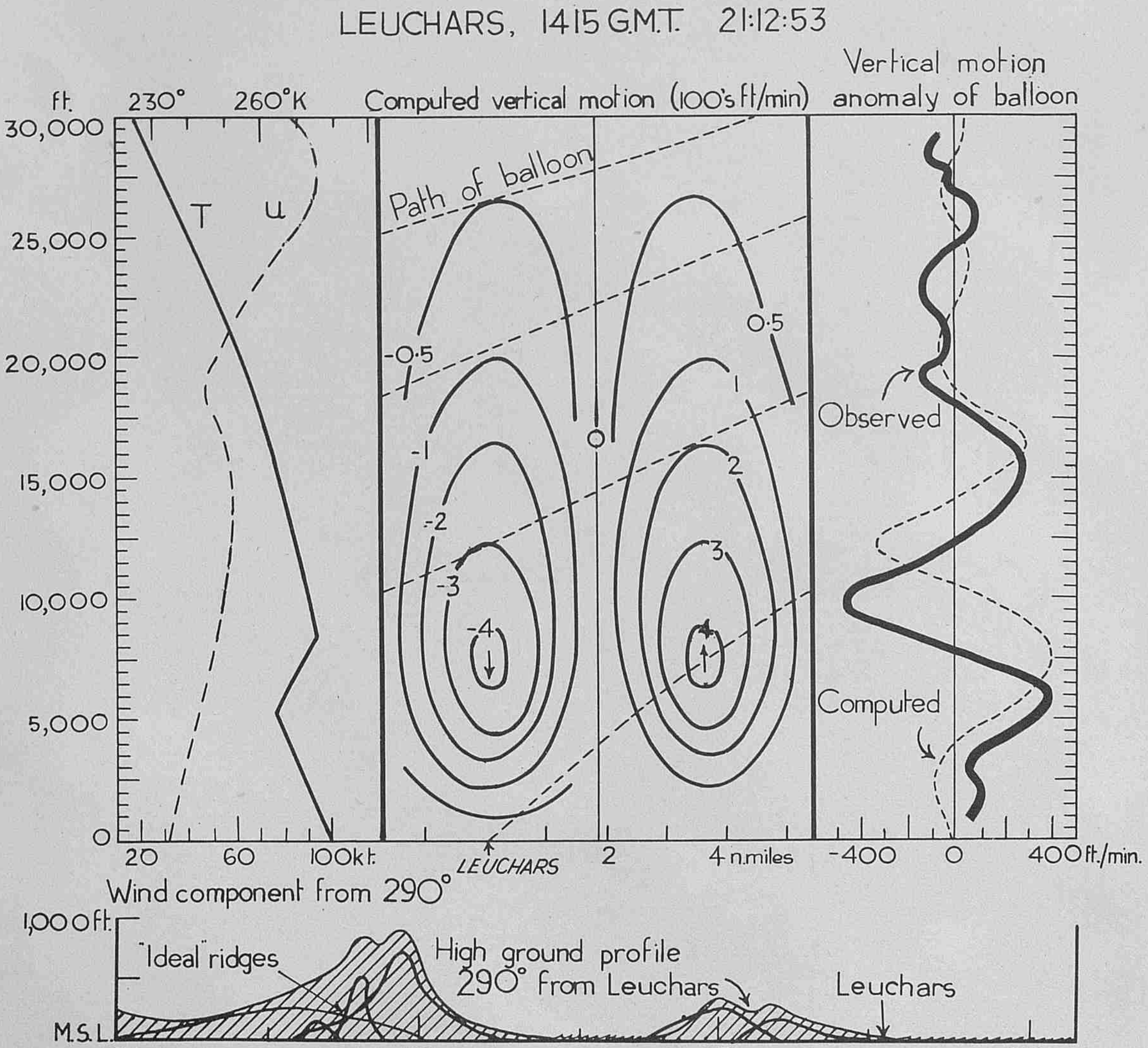

Fig.4

Fig. 4. The topography upwind of Leuchars may be analysed into the seven 'ideal' ridges shown. The central section of the figure shows the computed vertical motion field over and downwind of Leuchars. The pattern is repeated through each wavelength; the passage of the radio-sonde has therefore been adjusted to save space.

mats

M.R.P. 1032
S.C. I/124
25th January, 1957

AD 141027

Response characteristics of the sensitive cup anemometer Type IV

by

A.G.A. Rae

(Meteorological Office)

AWSSS
ROUTING SLIP

FILE	INFO	ACTION			
	6		DIRECTOR		
	5		DEP DIRECTOR		
	4		ASST TO DIRECTOR		
	2		CONSULTANTS		
		1	TRSO	CHF	
				TSS	
				RRB	
				EDB	
				SEC	
			EDD	CHF	
				HLFB	
				STB	
				SPFB	
				CU	
				SEC	
	3		TIPD	CHF	
				PUE	
				TECH INFO	
				SEC	

AIR MINISTRY

METEOROLOGICAL RESEARCH COMMITTEE

57-667

At the time of issue this report has not been published. Any author desiring to quote this paper should refer to it as "A paper of the Meteorological Research Committee (London), M.R.P. No. 1032 by Mr. A.G.A. Rae
A copy is available in the Library of the Meteorological Office."

M.R.P. 1032
S.C.I/124
25th January, 1957

AIR MINISTRY

METEOROLOGICAL RESEARCH COMMITTEE

Response characteristics of the sensitive cup anemometer Type IV

by

A.G.A. Rae (Meteorological Office)

Summary

Wind tunnel investigations into the variation of response of the sensitive cup anemometer Type IV (Plate 1), as made by Casella, with orientation relative to the wind have confirmed the existence of variations amounting to some 2 per cent of the response. Further variations due to the effect of the supporting mast normally used in fieldwork are shown to be of similar magnitude. Means of achieving greater accuracy are discussed.

Introduction

In the course of accurate measurements of wind gradient near the surface, where errors of 1 per cent or less become significant, a number of workers have noticed that the response of the sensitive cup anemometer is not constant at constant wind speed. In particular, N.E. Rider, School of Agriculture, Cambridge University, has observed anomalous points on his wind profiles which he ascribes to the fact that the corresponding anemometers were supported on the opposite side of the mast to the remainder.

There are three distinct effects which may occur: variation of response due to (1) varying the orientation of the contact housing relative to the wind direction; (2) varying the orientation of the supporting arm relative to the wind; (3) varying the distance of the anemometer from the mast. These will hereafter be referred to as effects (1), (2) and (3). In the field, of course, the three effects will be combined.

It was thought desirable to investigate the magnitude of these effects under controlled conditions in the wind tunnel and, in particular, to find out whether there is any way of using the instrument so as to reduce the errors to an acceptable level.

A number of experiments have been performed at Harrow to this end. Part I of this report deals with effect (1); the remaining effects are dealt with in Part II.

Part I - The effect of the contact housing

Experimental method

Two slightly different methods have been used, both employing an electrical contact anemometer (Crawford (1951)) and an open circuit wind tunnel whose working section has dimensions approximately $2\frac{1}{2}$ metres x $1\frac{1}{2}$ metres x 1 metre. Owing to the difficulty of maintaining a constant wind speed in the tunnel it was necessary to use a control instrument to monitor the wind speeds.

In the first series of experiments, a sensitive cup anemometer of the dial reading type was used for this purpose, the two instruments being placed

57-667

in line abreast at equal distances (30 cm) from the side of the tunnel. A pitot-static tube was used to obtain rough adjustments of the wind speed, and series of readings were taken at eight different orientations of the test instruments, and at several wind speeds. On reversing the relative positions of the anemometers the results obtained were of the same type as before.

Unfortunately it transpired that the anemometer under test possessed a time lag: it sometimes required a period of up to 20 minutes to settle down to a steady reading after re-orientation. This fault was ascribed to mechanical imperfections and was not found in five other anemometers tested.

For this and other reasons the first results were not considered reliable and a second series of tests was made, this time with a mechanically sound anemometer, calibrated in 1953. The instrument was supported in the centre of the working space and a N.P.L. calibrated airmeter was used as the monitor. The latter was supported in a position approximately 40 cm to one side and 15 to 20 cm to leeward of the anemometer.

In the main two wind speeds were used, 3 and 6 metres per second, but some observations at 9 and 12 metres per second gave almost identical results to those at 6 metres per second.

It was felt that the appropriate unit in which to express the response was that of counts per minute. For this purpose and to compensate for the variations of airspeed in the tunnel two observations were sufficient, namely (a) the number of counts made by the anemometer in the time required for the airmeter to complete a fixed run and (b) the amount of this time as measured by a stopwatch. These data were used to compute the number of counts per minute which would be registered by the anemometer at some convenient standard airspeed (very close to the nominal airspeed). The normal time for a run was about 8 minutes.

Results

The resulting response was plotted against the orientation expressed as one of sixteen points of the compass. Typical curves are shown in Fig.1. It was thought that the rather marked asymmetry shown in the 6 metre per second curves might be due to the influence of the anemometer on the airmeter readings, so the airmeter was moved to a similar position on the other side of the tunnel and further readings taken. No significant change in the shape of the curve was obtained, although its absolute value changed by about 0.3 per cent.

The observational uncertainty in each reading may be taken as about 0.2 per cent at 6 metres per second and about 0.3 per cent at 3 metres per second, and systematic errors of a similar magnitude may be present owing to the various tunnel effects. The latter, however, are unlikely to affect the actual shape of the curves.

Further tests with an anemometer supplied by N.E. Rider give closely similar results, though rather more asymmetry was observed at 3 metres per second and the variation of response with orientation was 0.5 per cent greater. This agrees approximately with Rider's own estimate.

As a control experiment a cylindrically symmetrical cover was made, of the minimum size, and placed over the anemometer housing. No significant variation of response with orientation could then be observed.

Discussion

Let us consider in turn the two main aims of the investigation.

(a) Determination of the magnitude of the errors. It can be said with some confidence that, on the average, effect (1) gives rise to a range of response of about 2 per cent over the 360° range of orientation. But this figure will vary, certainly by 0.5 per cent and possibly by more, from anemometer to anemometer and wind speed to wind speed.

It is clear, however, that in the field, with a fixed length of supporting arm, effects (1) and (2) will combine, and not necessarily in a simple manner. It is possible (see Part II) that the combined error could in some cases reach as much as 4 per cent.

(b) Methods of reducing errors to an acceptable level. Considering effect (1) alone, the only hope of using the present type of anemometer successfully for highly accurate work in the field would be to use it in the orientation for which it was calibrated and to choose this orientation to lie on a sufficiently flat part of the response curve. Whether this is possible in a particular case will, of course, depend on the degree of accuracy desired and on the nature of the response curve. The other alternative is to redesign the anemometer so as to be cylindrically symmetrical. It should then be possible to apply an independent correction for the combined effects (2) and (3) or to make them small by using a somewhat longer supporting arm than is the custom at present (see Part II).

The ideal solution would be to have the cup assembly rotating about the mast itself, but this would appear to be impractical owing to excessive friction in the bearings.

Part II - The effect of the supporting mast

Experimental method

An open-circuit wind tunnel and an electrically indicating anemometer were used, with an airmeter to monitor the airspeed. The anemometer under test was supported throughout in the centre of the working space to minimise uncertainties due to wall-effects.

Effect (2). In order to simulate as far as possible the effect likely to be obtained with a symmetrically designed anemometer, a large circular disc was placed horizontally just above the dial housing as indicated in Fig.2.

Eight positions of the mast relative to the wind were used, numbered as in Fig.2(b). When the mast was in one of the positions 3, 4, 5, 6 or 7 the airmeter was placed as shown in Fig.2(b). For positions 7, 8, 1, 2, and 3 it was placed correspondingly on the opposite side of the system. Thus two readings in each of positions 3 and 7 were obtained and the (small) difference could be taken into account in setting out the response curves.

The quantity actually observed was the number of counts made by the anemometer in the time required for the airmeter to complete a fixed run (in feet of air). The latter was chosen so as to give between 600 and 700 anemometer counts at each of three wind speeds, and was 5,000 ft in each case.

As a rough check on the results obtained by this method, a similar experiment was carried out in the absence of the large disc, using positions 1, 3, 5 and 7 of the mast, but still keeping the anemometer contact housing fixed in the upwind direction. The same type of variation was obtained as with the disc, though the actual number of counts per run was increased.

By fixing the standard ten-inch supporting arm just below the anemometer and removing the mast, it was shown that no part of effect (2) was due to the supporting arm. That is, the response showed no measurable variation with orientation of the supporting arm in the absence of the mast.

Effect (3). This effect was investigated only for orientations 1 and 5 of the mast. The horizontal disc was not used, and the anemometer itself was kept pointing upwind. The only variable was the distance of the mast from the anemometer which ranged from six inches to twenty inches.

3, 6 and 9 m/s were the wind-speeds used, and the method of observation was that described above.

/Results

Results

The magnitude of effect (2) is shown graphically in Fig.3 for wind speeds of 3, 6 and 9 m/s. Instead of expressing the results in counts per minute at a standard airspeed, the actual number of counts made during a fixed airmeter run was plotted as a measure of the response. The latter quantity is directly proportional to the former within the experimental error.

The pecked base-lines represent the response obtained with the disc in place but without the mast.

The observational error may be taken as 0.2 per cent, but the errors due to tunnel effects, position of airmeter, etc. are probably rather larger than this (0.3 per cent to 0.8 per cent) and impossible to assess accurately. Consequently the curves are to be regarded as giving a reliable qualitative picture of the effect, though only an approximate quantitative picture. It is encouraging to note that this picture is in good agreement with some observations made by Rider using a different experimental arrangement.

Fig.4 illustrates the third effect. Over much of the range the 6 m/s and 9 m/s curves were practically identical and are shown for convenience as one curve. Response, as measured by the number of counts per fixed airmeter run, is plotted against distance of the anemometer from the mast in inches. For ease of comparison the curves have been plotted relative to a common baseline representing the response of the anemometer in the absence of the mast.

The experimental error in this case may be taken as about 0.3 per cent.

Discussion

In Part I it was suggested that the only satisfactory solution to the problem of effect (1) was to redesign the instrument to be cylindrically symmetrical. It was also pointed out that effect (2) might be made small by increasing the length of the supporting arm, that is by making use of effect (3).

The results of the present investigation, as far as they go, show that there is every hope that this should be possible. It would seem that the supporting arm would need to be of the order of 18 inches in length for a mast of 1 inch thickness. More detailed wind tunnel experiments, using a redesigned anemometer, would be necessary to confirm this point.

Reference

Crawford, S.G. J. Scient. Instr., 28, p.36, 1951.

"A simple form of sensitive electric contact cup anemometer".

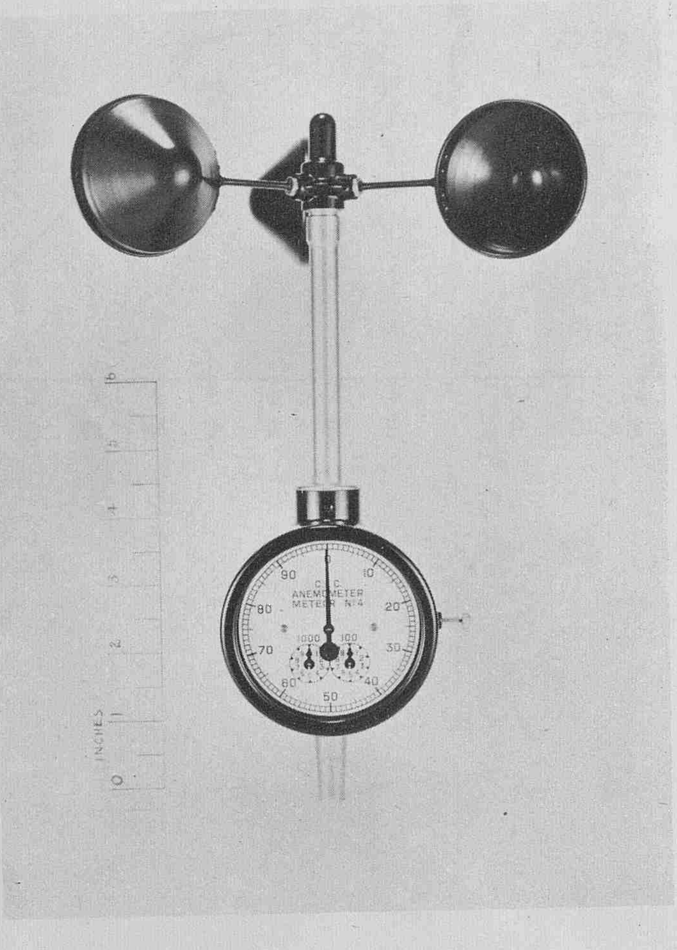

Plate I. Sensitive cup anemometer Type IV

FIGURE I. RESPONSE CURVES OF ANEMOMETER M.O. No. 46

(a) WIND SPEED 6 M/SEC. (b) WIND SPEED 3 M/SEC.

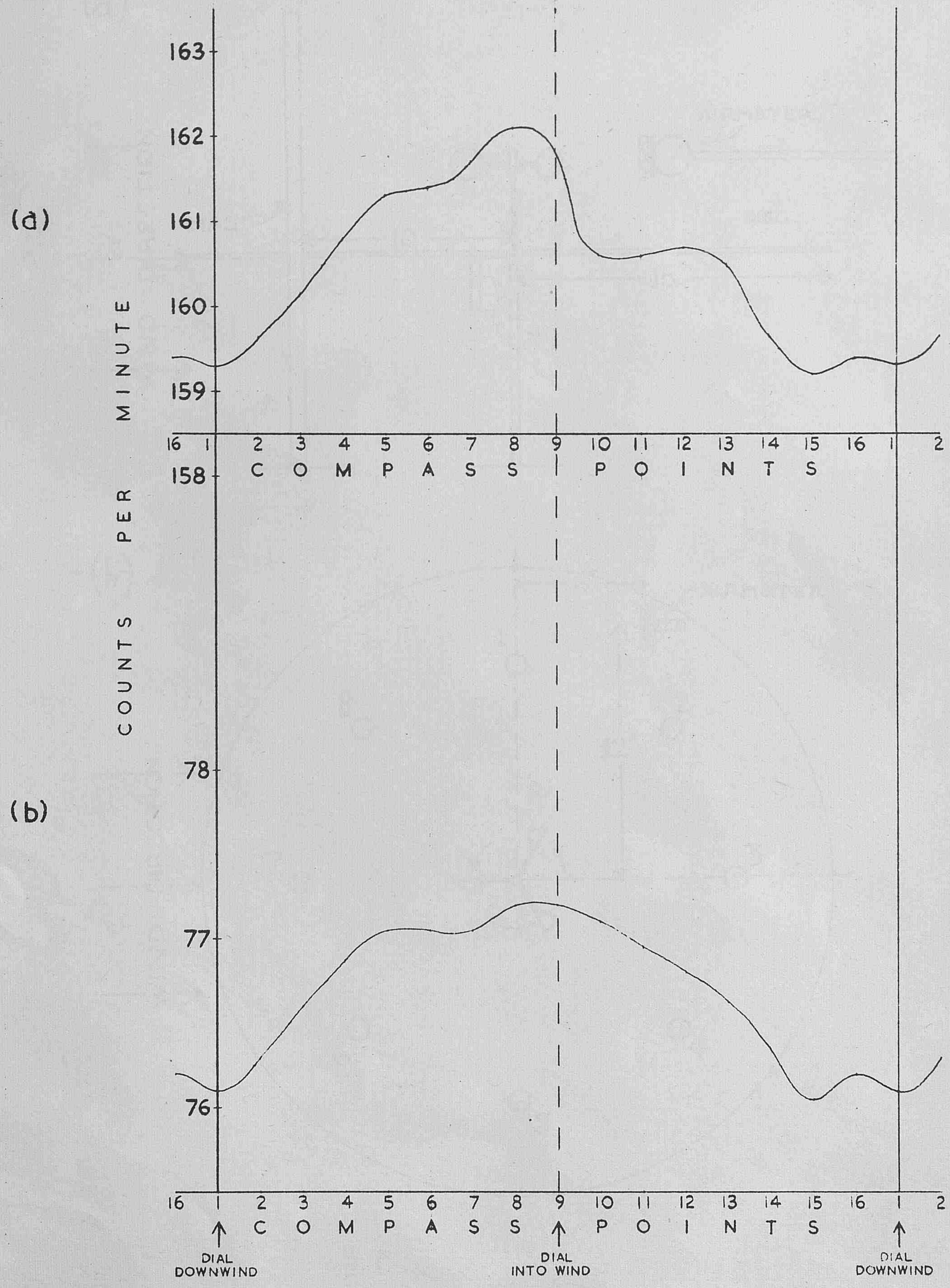

DIAL ROTATED CLOCKWISE FROM ABOVE

FIGURE 2 For explanation see text, Part II.

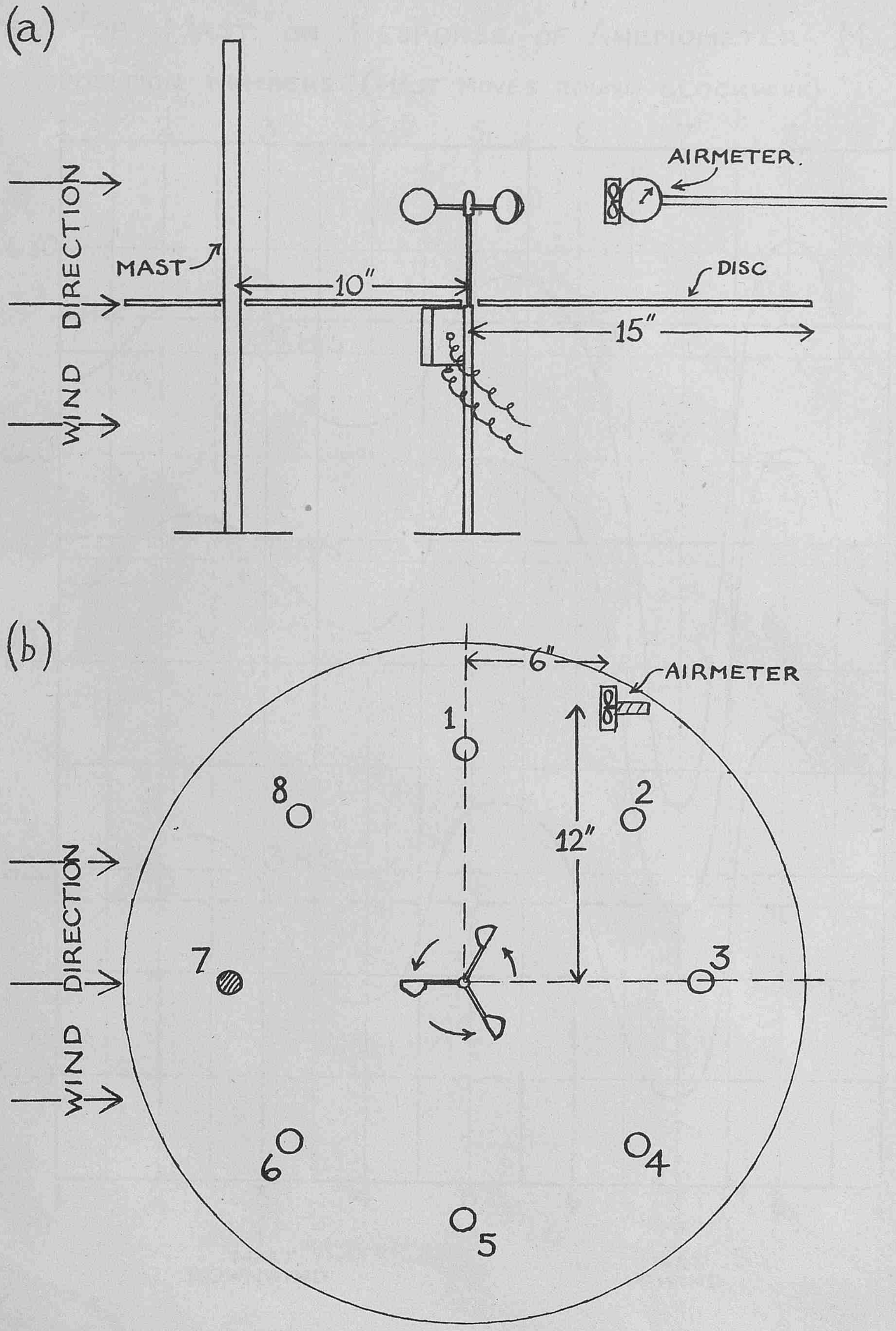
(a)
WIND DIRECTION
MAST
10"
DISC
15"
AIRMETER.
(b)
6"
AIRMETER
1
2
3
4
5
6
7
8
12"
WIND DIRECTION

FIGURE 3.

EFFECT OF MAST ON RESPONSE OF ANEMOMETER M.O.46.

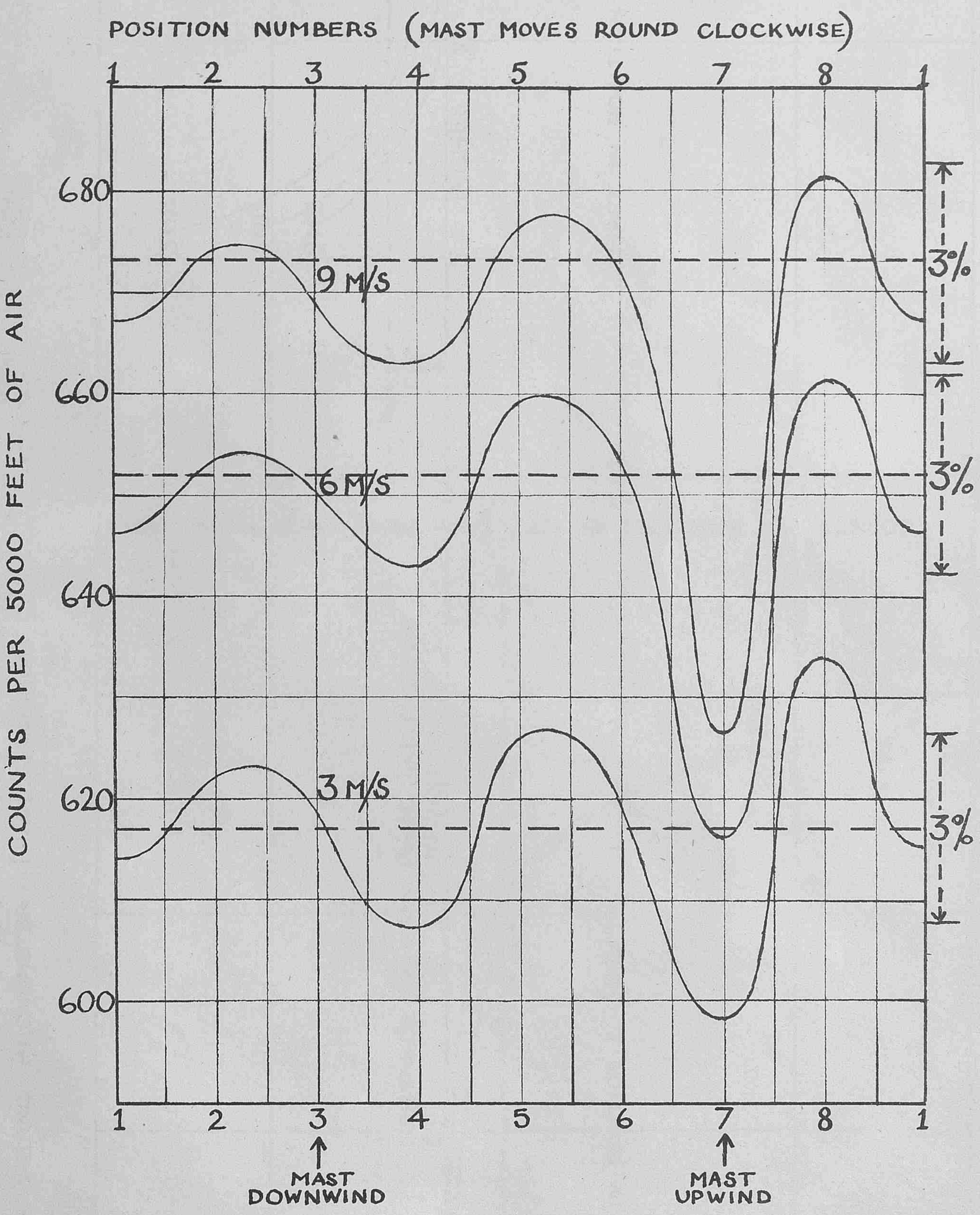

FIGURE 4.

EFFECT OF VARYING ANEMOMETER — MAST DISTANCE.

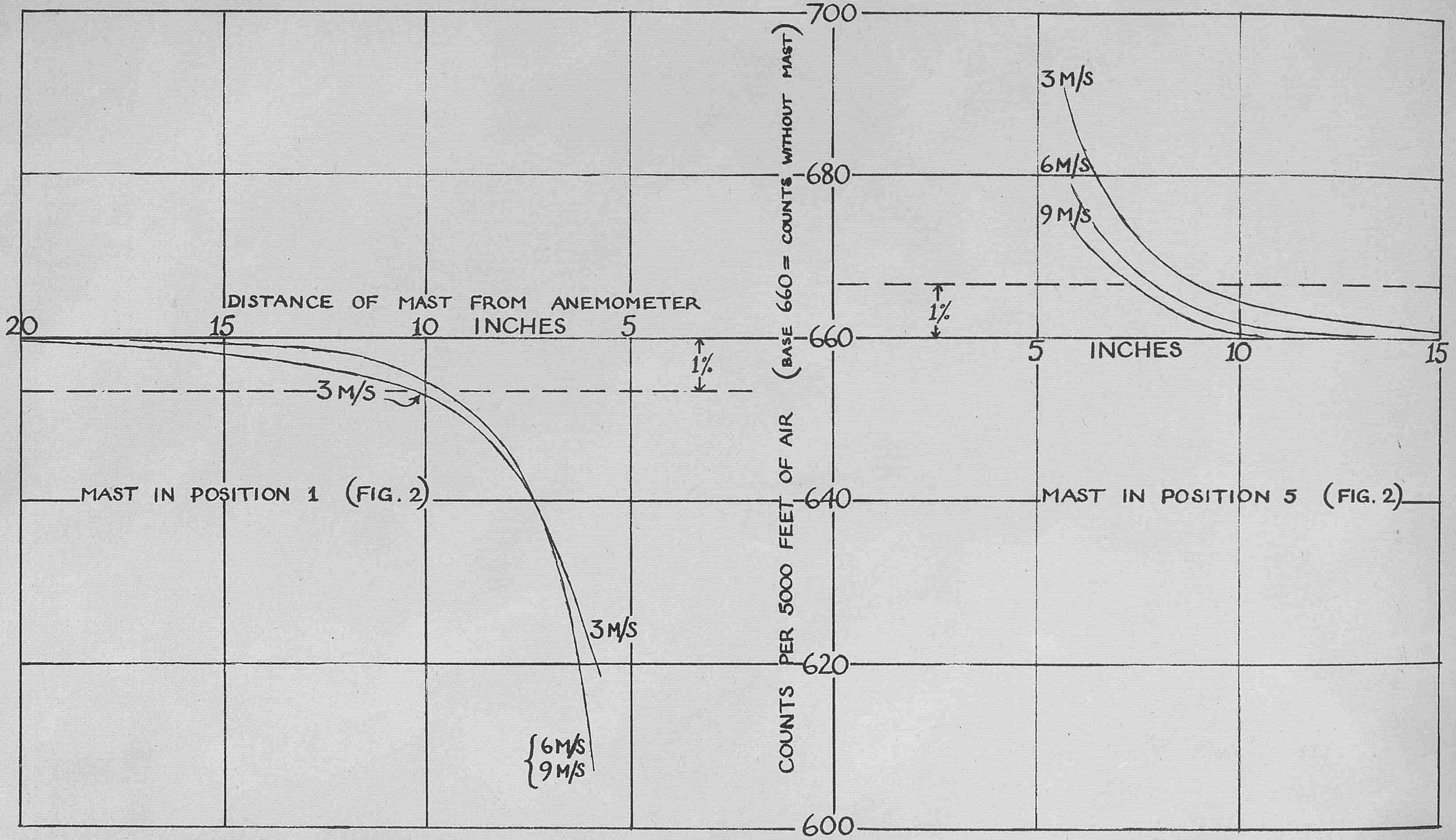

Mats

M.R.P. 1033

S.C. 1/125

18th January, 1957

AD 141 026

Photo-electric visibility meter Mk. II

by

J R. Bibby

(Meteorological Office)

AWSSS

ROUTING SLIP

FILE	INFO	ACTION				
	6		DIRECTOR			
	5		DEP DIRECTOR			
	4		ASST TO DIRECTOR			
	2		CONSULTANTS			
		1	TRSD	✓	CHF hws	
					TSS	
				✓	RRB	
				✓	CDB	
					SEC	
			EDD		CHF	
					HLFB	
					STB	
					SPFB	
					CU	
					SEC	
			TIPD		CHF	
					PUE	
	3				TECH INFO	
					SEC	

AIR MINISTRY

METEOROLOGICAL RESEARCH COMMITTEE

57-670

At the time of issue this report has not been published. Any author desiring to quote this paper should refer to it as "A paper of the Meteorological Research Committee (London), M.R.P. No. 1033 by Mr. J.R. Bibby
A copy is available in the Library of the Meteorological Office."

M.R.P. 1033
S.C.I/125
18th January, 1957

AIR MINISTRY
METEOROLOGICAL RESEARCH COMMITTEE

Photo-electric visibility meter Mk.II

by

J. R. Bibby (Meteorological Office)

1. Historical

The development of photo-electric equipment for measuring visibility began in 1943, with the object of obtaining more accurate information on the distance at which runway lights would be visible to an aircraft about to land. Early work is described by Atkins (1943, 1945) and Bibby (1945), and led to the manufacture of twenty photo-electric visibility meters (Mark I). Trials of these at 15 stations during 1949 showed various ways in which improvements could be made. These were discussed at a meeting called by D.M.O. on 9th February, 1950, when the urgent need of a reliable instrument for use on airfields was stressed. A re-designed instrument (Mark II) was installed at London Airport in March, 1951, and has been operating ever since. Several others have been made in the Instrument Division workshop for fog investigations, chiefly at Cardington.

2. Description

The principle used is to measure the attenuation of a horizontal beam of light over a distance of about 300 yards. The beam is formed by a small projector, adapted from a Naval signalling lamp (Fig.1). It has a parabolic mirror $5\frac{1}{2}$ in. diameter, $2\frac{1}{2}$ in. focal length. A "solid source" lamp (24 volts 240 watts) is used to give a beam which is sensibly uniform over several degrees, so that very accurate alignment on the receiver is not necessary. The projector is mounted on an adjustable base, and is fitted with a hood to keep rain off the front glass. Power for the lamp is provided by a transformer giving a nominal 24 volts; its primary is supplied from A.C. mains through a "Variac", by means of which the voltage applied to the lamp can be varied.

At a point about 300 yards from the lamp, the intensity of the beam is measured by means of a photocell (selenium barrier layer type, 25 mm diameter). It is at one end of a long cylindrical housing (Fig.2) behind a screen in which is a hole 3/16 in. diameter. This hole is at the focus of a convex lens (5 in. diameter, 31 in. focal length) at the other end of the housing. This arrangement ensures that very little daylight reaches the photocell. To keep the lens dry, a rain shield is fitted in front of it, and also a small electric heater consisting of lengths of fine wire stretched across the lens a little way behind it. A silica-gel drier is placed in the housing, at the photocell end. The housing is mounted on adjusting screws for accurate alignment on the projector. To facilitate this, the photocell can be moved to one side, allowing observation through a small lens, which forms a telescope with the main lens.

The photocell current could be measured by a simple mirror galvanometer, but it is more convenient to use a recorder. That at London Airport is a Cambridge thread recorder (full scale deflection $5\,\mu A$, resistance 2000 ohms). It makes a dot each minute, and works on a four minute cycle as follows:-

1st and 2nd minute: photocell current with projector lamp off (this is to give a correction for any daylight which may reach the photocell).

57-670

3rd minute: photocell current with projector switched on (by an automatic switch in the recorder).

4th minute: record of mains voltage, obtained via a small transformer, rectifier, and resistance network - including a variable resistance for adjusting the record as required.

A typical record is shown in Fig.3. The lowest trace is the effect of daylight, which is always very small. The middle trace is the photocell current with projector on, and is adjusted (by means of the Variac) so that it reads 45 on the scale in extremely good visibility. The top trace shows variations in mains voltage, and should be set (by means of the variable resistance) so that it reads exactly 50 when the mains voltage has its normal value.

3. Interpretation of the records

The middle trace on the record indicates the visibility, but it must be corrected as follows:-

(a) If the lowest trace is not zero, its value is deducted from the middle trace.

(b) If the top trace is not on the 50 line, the middle trace is increased (decreased) by 6 per cent for every unit by which the voltage trace is below (above) 50. This is based on the experimental finding that the lamp brightness varies approximately as the cube of the voltage.

The corrected value of the middle trace is then used to obtain the visibility from a table, of which an abridged version is given in Table 1.

Table 1

Galvanometer	1	5	10	15	20	25	30	35	40	44
Visibility	280	480	700	950	1300	1750	2600 yards	2¼	4½	20 miles

The basis of this table is as follows. The extinction coefficient of the air, σ, is given by

$$I = I_o e^{-\sigma d}$$

where I is the galvanometer reading (i.e., the middle trace, corrected); I_o the reading if the atmosphere was perfectly transparent, which is taken as 45 on the charts used at London Airport; d is the distance between projector and photocell unit, 280 yards at London Airport.

The visibility V is then obtained from Koschmieder's equation

$$\sigma V = - \log_e E$$

where E is the threshold contrast which the eye can just perceive in daylight. E has usually been taken as 0.02, whence $\sigma V = 3.91$; but as this applies to completely black objects, the table is based on $\sigma V = 3.75$, as it was expected that this would give better agreement with the visibility of ordinary objects.

4. Results obtained at London Airport

Two years' records (1954-55) have been analysed to find out how closely the meter readings agree with the visibility as ordinarily observed. Hourly observations, during daylight only, were used. A correction was first applied to the readings, however, for the following reason: as indicated above, slow changes in lamp brightness and photocell sensitivity can be allowed for by adjusting the Variac to bring the middle trace to the right visibility reading, then adjusting the variable resistance to bring the voltage reading to the 50 line. Ideally this should be done on every occasion of good visibility, but was actually only done fairly infrequently (because the instrument is useful more as indicating changes of visibility than absolute values).

A retrospective adjustment was therefore made as follows: on each occasion of visibility 10 miles or more, a factor was calculated, by which the galvanometer reading should be multiplied to bring it to the correct reading for the observed visibility. The average of these factors obtained for any particular day was used to multiply the readings for subsequent days, until another day of good visibility enabled another factor to be obtained. The factors were mostly between 0.95 and 1.15, and it was unusual for successive factors to differ by more than 0.1. A few exceptionally large changes occurred, some of which were probably due to adjustments of the controls or replacement of the lamp, but no complete record of these has been kept. As an example, the factors for the second half of 1954 are shown in Fig.4.

Whenever the observed visibility was 3000 yards or less, the meter reading was multiplied by the factor, as indicated above, the corresponding visibility determined, and plotted on a graph of measured visibility against observed visibility. The part of the graph for observed visibilities below 1000 yards is shown in Fig.5. These observations have been considered separately, for the following reasons:-

(a) They cover the range of greatest importance to aviation.

(b) Variations of lamp brightness and photocell sensitivity (i.e., uncertainty in the correction factor) have relatively little effect in this visibility range, as can be seen from Table 1.

(c) The 280 yard path sampled by the instrument is more likely to be representative of the atmosphere observed visually.

Only 70 useful observations below 1000 yards occurred in the two years. This is partly because those below about 250 yards give zero reading on the recorder and partly because many occasions with visibility in the required range occurred during the onset or clearance of fog, when visibility was varying so rapidly that comparisons would be misleading because of possible timing errors.

The 70 observations are shown on Fig.5, the co-ordinates being on logarithmic scales. The diagonal full line indicates equality between measured and observed visibility, and the broken lines indicate differences between measured and observed visibility of ± 25 per cent and ± 50 per cent. The percentage of the observations with differences in each category is shown on the first line of Table 2. In the last three columns of the table the positive and negative differences are combined.

It is clear from Fig.5 that in most cases the meter indicates a visibility greater than is observed by eye. An improvement would result if the meter visibilities were all reduced in the same proportion. To give equal numbers of positive and negative differences a reduction of 14 per cent is needed, and the result of doing this is shown in the second line of Table 2.

The third line of Table 2 gives the result of a similar analysis of the 279 readings when the observed visibility was from 1000 to 3000 yards inclusive. (All higher visibilities were ignored, as small changes in lamp brightness, etc., would have a big effect on the accuracy of the meter). Again it is seen that positive differences predominate, and a reduction of 12 per cent was needed to equalise the number of positive and negative ones. The result of doing this is given in the fourth line of the table.

/5.

5. Discussion of results

Table 2 confirms the expectation that meter readings would show better agreement with observed visibility below 1000 yards.

In considering the figures it must be remembered that eye estimates of visibility are hardly accurate to better than 15 per cent even in good conditions, and that differences of about 10 per cent in the visibility in different directions are probably quite common. Thus even if the visibility meter was perfect, differences from the observed visibility of up to 25 per cent would be commonplace. If corrections are applied as indicated above, differences are less than 25 per cent in 79 per cent of occasions with visibility below 1000 yards, and 61 per cent of occasions between 1000 and 3000 yards. The performance of the instrument can be considered satisfactory in these cases, inasmuch as a perfect instrument would show equally large differences.

Differences over 25 per cent may be due to instrument errors, or to exceptionally large errors of observation by eye, or exceptionally large variations of visibility over short distances. The relative importance of these can only be conjectured, but several reasons suggest that large instrumental errors are infrequent.

First, the largest differences amount to a factor of about two below 1000 yards, and about three in the range 1000 to 3000 yards. These roughly correspond to the galvanometer reading being wrong by a factor of two. But Fig.4 shows the general consistency of the galvanometer readings, amd makes such large errors appear unlikely.

As a check on this point, two visibility meters were set up side by side at Harrow and compared over a month. The ratio of their readings only varied by ±6 per cent.

Finally, in the majority of cases of large discrepancies the visibility meter gives the higher value, whereas the more obvious instrumental defects would make it read too low.

Occasional gross errors of observing may be possible, not only through carelessness, but also because of the small size and light colour of some of the visibility objects, probably made worse at times by uneven illumination, e.g., in partly cloudy conditions. But atmospheric inhomogeneity may well account for most of the big differences, even though one end of the instrument light path is near the observation point. There are several large buildings just to one side of the light path, which might be expected to change the extinction coefficient of the adjacent air on occasions.

6. Conclusions

(1) This instrument is capable of continuous operation by persons without special experience of instruments (the need for repairs or adjustment by the Instruments Branch has not occurred oftener than once or twice a year).

(2) The table for converting meter readings to visibility should be revised, reducing the visibilities by 13 per cent (the mean of the two values in Table 2). This is equivalent to using the equation $\sigma V = 3.25$ instead of 3.75, and corresponds to a contrast threshold of 0.039 instead of 0.02 previously assumed. (It may be noted that the World Meteorological Organization has recommended that a contrast threshold of 0.05 should be adopted).

(3) Provided the proper adjustments are made on every occasion of good visibility, the readings should be within 25 per cent of eye estimates made nearby on about 80 per cent of occasions with visibility below 1000 yards, and about 60 per cent of occasions with visibility between 1000 and 3000 yards.

(4) Most cases of lower accuracy can probably be accounted for by atmospheric inhomogeneity. This points to the need for installing the instrument at the exact place where the visibility is required, rather than improvements in the instrument itself.

(5) It would probably be worth the extra expense to provide a voltage stabiliser for the projector lamp. This should eliminate the voltage correction and allow the charts to show the visibility directly.

7. References

Atkins, W.R.G. 1943 Meteorological Research Papers, Air Ministry, London, No. 157.

Atkins, W.R.G. 1945 Meteorological Research Papers, Air Ministry, London, No. 226.

Bibby, J.R. 1945 Meteorological Research Papers, Air Ministry, London, No. 236.

Visibility range	Percentage of readings differing the observed visibility by the fo amounts (in per cent)				
	more than -50	-50 to -25	-25 to 0	0 to +25	+25 to +50
Less than 1000 yards (70 readings)	0	1	17	44	24
As above, but meter visibilities reduced by 14 per cent.	0	4	46	33	11
1000-3000 yards inclusive (279 readings)	2	6	23	33	17
As above, but meter visibilities reduced by 12 per cent.	3	13	33	28	11

at Harrow and compared over a month. The ratio of their readings only varied by ±6 per cent.

Finally, in the majority of cases of large discrepancies the visibility meter gives the higher value, whereas the more obvious instrumental defects would make it read too low.

Occasional gross errors of observing may be possible, not only through carelessness, but also because of the small size and light colour of some of the visibility objects, probably made worse at times by uneven illumination, e.g., in partly cloudy conditions. But atmospheric inhomogeneity may well account for most of the big differences, even though one end of the instrument light path is near the observation point. There are several large buildings just to one side of the light path, which might be expected to change the extinction coefficient of the adjacent air on occasions.

6. Conclusions

(1) This instrument is capable of continuous operation by persons without special experience of instruments (the need for repairs or adjustment by the Instruments Branch has not occurred oftener than once or twice a year).

(2) The table for converting meter readings to visibility should be revised, reducing the visibilities by 13 per cent (the mean of the two values in Table 2). This is equivalent to using the equation $\sigma V = 3.25$ instead of 3.75, and corresponds to a contrast threshold of 0.039 instead of 0.02 previously assumed. (It may be noted that the World Meteorological Organization has recommended that a contrast threshold of 0.05 should be adopted).

(3) Provided the proper adjustments are made on every occasion of good visibility, the readings should be within 25 per cent of eye estimates made nearby on about 80 per cent of occasions with visibility below 1000 yards, and about 60 per cent of occasions with visibility between 1000 and 3000 yards.

Table 2

Visibility range	Percentage of readings differing from the observed visibility by the following amounts (in per cent)								
	more than -50	-50 to -25	-25 to 0	0 to +25	+25 to +50	more than +50	differences less than ±25 per cent	differences ±25 to ±50 per cent	differences over ±50 per cent
Less than 1000 yards (70 readings)	0	1	17	44	24	13	61	25	13
As above, but meter visibilities reduced by 14 per cent.	0	4	46	33	11	6	79	15	6
1000-3000 yards inclusive (279 readings)	2	6	23	33	17	20	56	23	22
As above, but meter visibilities reduced by 12 per cent.	3	13	33	28	11	12	61	24	15

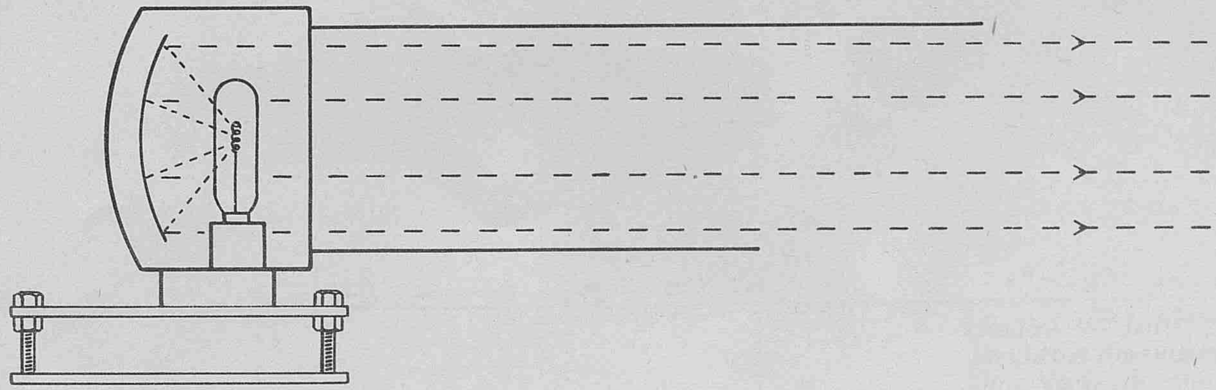

FIG. 1.

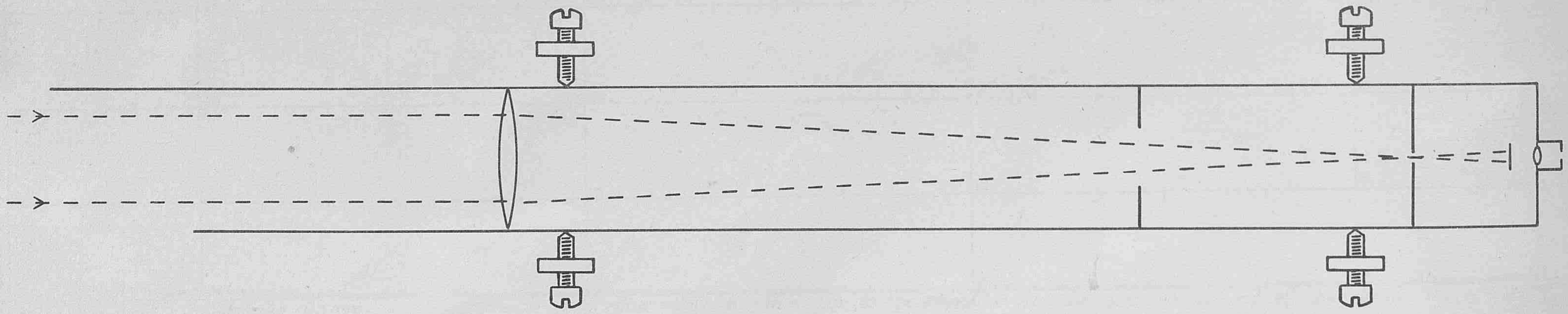

FIG. 2.

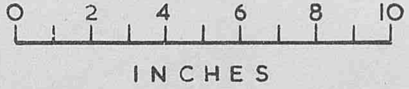

0
2
4
6
8
10
INCHES

M.R.P. 1033

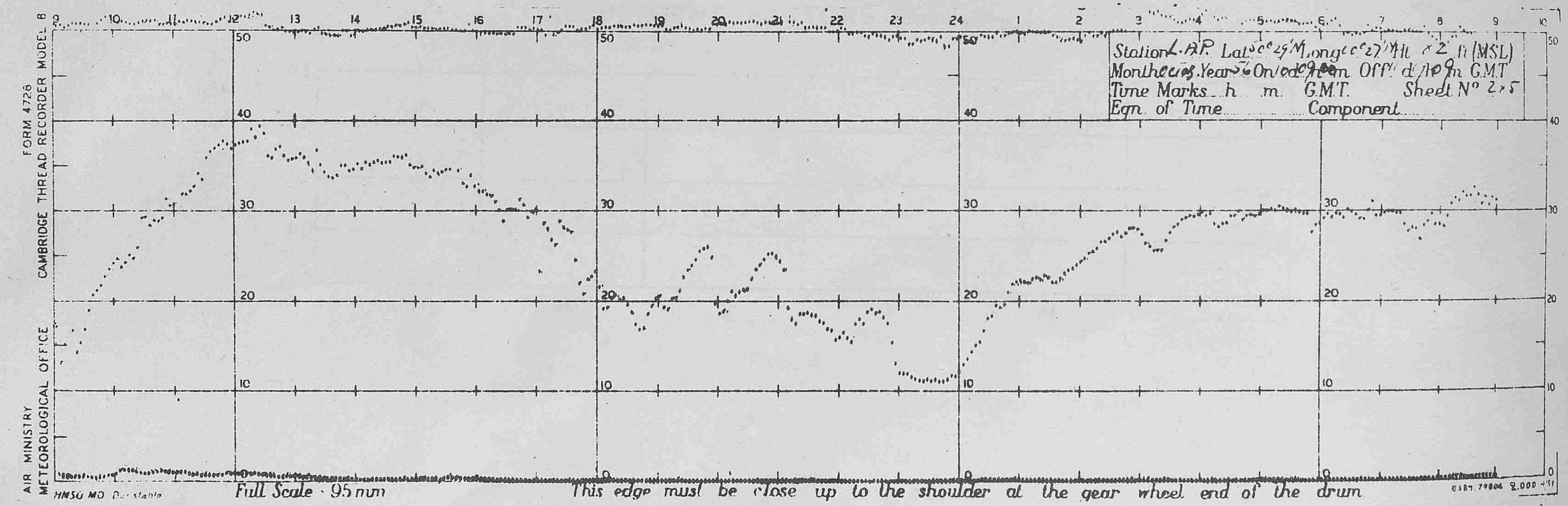

FIG. 3.

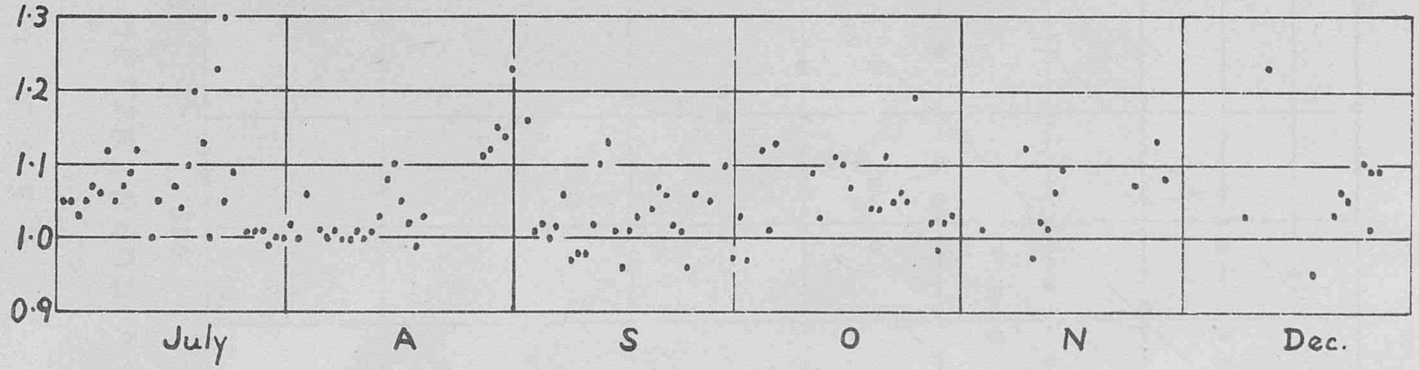
ADJUSTMENT FACTORS (See para. 4)

FIG. 4.

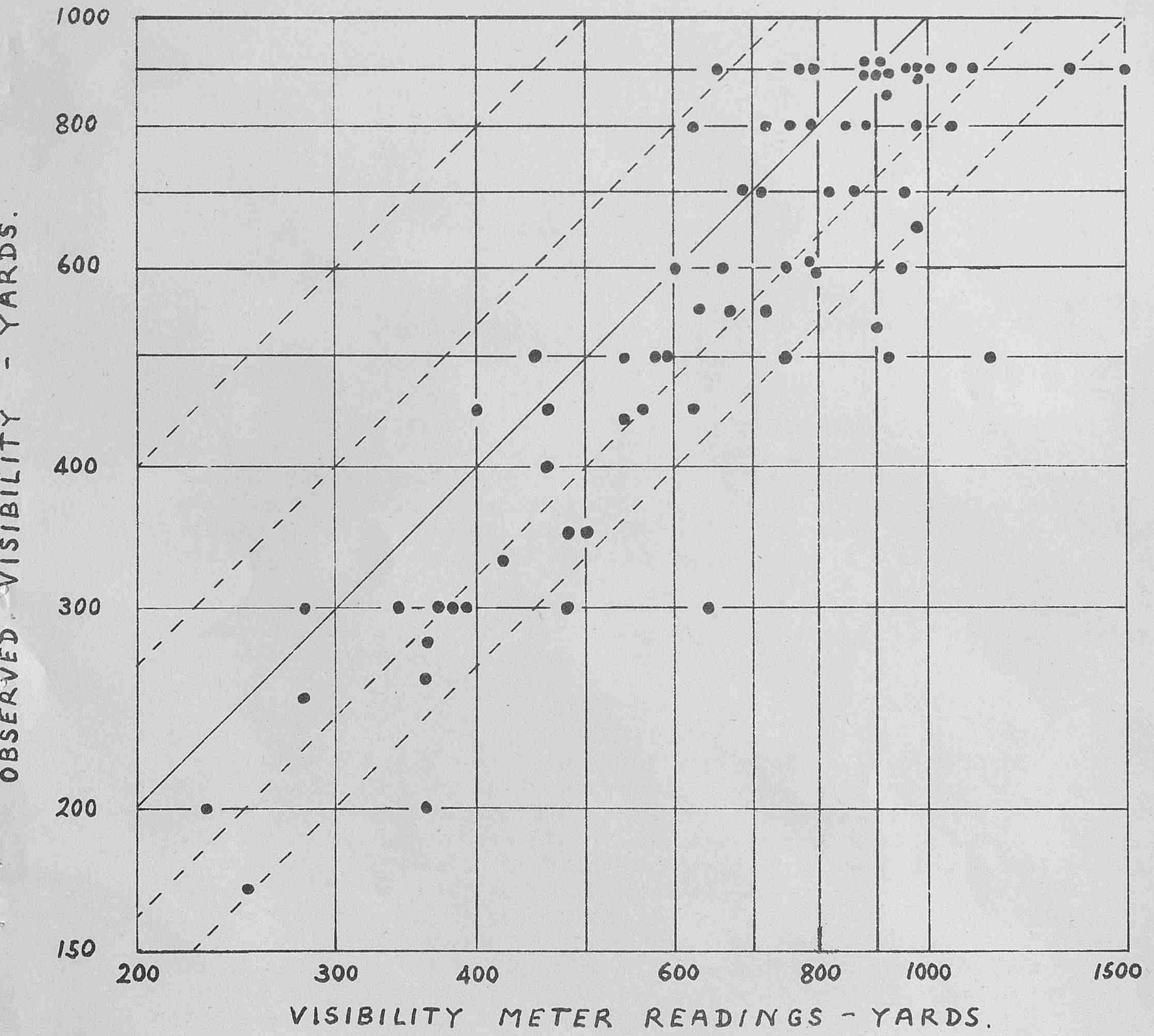
OBSERVED VISIBILITY - YARDS.
1000
800
600
400
300
200
150
200
300
400
600
800
1000
1500
VISIBILITY METER READINGS - YARDS.

FIG. 5.

At the time of issue this report has not
been published. Any person desiring to
[illegible]
[illegible]
[illegible]
M.R.P. No. 1038 by Messrs. J.I.P. Jones
and H.E. Butler.
A copy is available in the Library of
the Meteorological Office."

M.R.P. 1038
S.C. [illegible]
[illegible] February, 1957

Also issued as
Porton Techn. Paper #574
(same date)

AIR MINISTRY
METEOROLOGICAL RESEARCH COMMITTEE

Studies of eddy structure in the first few thousand feet of the atmosphere

Part 1. Measurements of the vertical and horizontal (longitudinal) components

by

J.I.P. Jones and H.E. Butler (Meteorological Office)

SUMMARY

Details are given of modifications to the instrument, previously described in M.R.P.974, for measuring vertical gustiness in the form of inclination and mean speed of the wind. A description is also given of an adaption of a sensitive airmeter for recording fluctuations of total wind speed. Both instruments, which have good response at periods down to about one second, are designed for mounting on the cable of a captive balloon.

A brief account is given of some recent observations made up to a maximum height of 7000 ft. at Cardington. Some examples of records covering a variety of meteorological conditions are presented.

1. INTRODUCTION

During the past year experimental equipment has been developed at C.D.E.E. for the study of the vertical component of turbulence at heights beyond the reach of towers and masts. In the first instance attention was concentrated on measurements of the fluctuations of wind inclination only, since it seemed probable that for many purposes an acceptable approximation to the fluctuations of the actual vertical component of velocity would then follow from a knowledge of the mean horizontal wind speed. The apparatus developed for this purpose, for use from a position on a captive balloon cable, was described in M.R.P.974. Since then minor modifications have been made to the apparatus and a more extensive study has been made of its response, and these features are discussed in Section 2(a) of this paper.

When it is required to deduce accurate values of the vertical component from the measurements of inclination, it is of course necessary to measure the fluctuation of horizontal or total wind speed. An Ower vane anemometer has recently been adapted for this purpose and the design and performance of the instrument are described in Section 2(b). Apparatus for measuring mean air temperature from the captive balloon cable has also been assembled and is described in Section 2(c).

At the time of issue this report has not been published. Any author desiring to quote this paper should refer to it as "A paper of the Meteorological Research Committee (London), M.R.P. No. 1038 by Messrs. J.I.P. Jones and H.E. Butler. A copy is available in the Library of the Meteorological Office."

M.R.P. 1038
S.C.III/229
7th February, 1957

Also issued as
Porton Techn. Paper #574
(same date)

AIR MINISTRY
METEOROLOGICAL RESEARCH COMMITTEE

Studies of eddy structure in the first few thousand feet of the atmosphere

Part 1. Measurements of the vertical and horizontal (longitudinal) components

by

J.I.P. Jones and H.E. Butler (Meteorological Office)

SUMMARY

Details are given of modifications to the instrument, previously described in M.R.P.974, for measuring vertical gustiness in the form of inclination and mean speed of the wind. A description is also given of an adaption of a sensitive airmeter for recording fluctuations of total wind speed. Both instruments, which have good response at periods down to about one second, are designed for mounting on the cable of a captive balloon.

A brief account is given of some recent observations made up to a maximum height of 7000 ft. at Cardington. Some examples of records covering a variety of meteorological conditions are presented.

1. INTRODUCTION

During the past year experimental equipment has been developed at C.D.E.E. for the study of the vertical component of turbulence at heights beyond the reach of towers and masts. In the first instance attention was concentrated on measurements of the fluctuations of wind inclination only, since it seemed probable that for many purposes an acceptable approximation to the fluctuations of the actual vertical component of velocity would then follow from a knowledge of the mean horizontal wind speed. The apparatus developed for this purpose, for use from a position on a captive balloon cable, was described in M.R.P.974. Since then minor modifications have been made to the apparatus and a more extensive study has been made of its response, and these features are discussed in Section 2(a) of this paper.

When it is required to deduce accurate values of the vertical component from the measurements of inclination, it is of course necessary to measure the fluctuation of horizontal or total wind speed. An Ower vane anemometer has recently been adapted for this purpose and the design and performance of the instrument are described in Section 2(b). Apparatus for measuring mean air temperature from the captive balloon cable has also been assembled and is described in Section 2(c).

It is now proposed to use the above equipment in carrying out two types of observations of eddy structure in the first few thousand feet of the atmosphere. In the first type attention will be confined to wind inclination (and mean wind speed) measurements, the aim being to accumulate statistics on the broad variations of vertical gustiness with height, time and synoptic conditions. The second type will be concerned with obtaining a more detailed description of the turbulent structure, in the form of the scale and energy

/spectrum

spectrum of the vertical component and the horizontal shearing stress. These observations will involve measurements of the fluctuations of both wind inclination and total speed, with corrections for the movements of the instrument supports, and will be carried out on a less regular basis than the first type of observation. A number of observations of both types have already been made, using captive balloon facilities at the Balloon Development Establishment, Cardington, Bedfordshire. The analysis of the results, especially those of the more elaborate observations, has yet to be completed, and various aspects of these will be discussed in subsequent papers of the present series. However, in view of the novel nature of the data which are being accumulated it was thought appropriate to give in Sections 3(a) and (b) of the present paper a description of the procedure and examples of the raw data, with some approximate root mean square values of wind inclination.

2. INSTRUMENTAL DETAILS

(a) Fluctuation of wind inclination

The principle of operation of the three instruments used for measuring wind inclination is similar to that described in M.R.P.974, with minor modifications in design (see Fig.1(a)). Components of the electrical bridge circuit were housed inside the lower part of the control fin, A, and the overall length of the instrument was reduced by 6 inches to $31\frac{1}{2}$ inches. Wind tunnel tests were made to select the minimum clearance, B, for the inclination vane which gave free exposure with inclinations within the range +40° to -30°, and as a result the support, C, for the potentiometer was increased in length, by $2\frac{1}{2}$ in. to 8 in., from its fulcrum, D. The air meter, E, at the lower end of this support was of standard pattern (by Negretti and Zambra), but modified to operate an electrical changeover switch at approximately every 1000 ft. of airflow. The weight of the airmeter and the additional streamlined weight, F, maintained the support arm vertical in wind speeds up to 13 m/sec. The natural period of the pendulum was 0.9 sec. while critical damping by piston, G, prevented oscillatory motion. Fig. 2 shows the effect of initially deflecting the pendulum 20°, without and with the damper connected.

A counter-balance weight, H, restored loss of balance due to the small ($\frac{7}{8}$") off-setting of the main support arm from the balloon cable, and the addition of a hook, I, at the tail, provided an initial support for the electric cable (see Fig.5) and a fixing point for cables leading from instruments at a higher level.

The dimensions of the inclination vane remained 6" x 3" but the new models were lighter and weighed 0.16 oz. ($4\frac{1}{2}$ g.) including a 6" shaft, but not including the pivoted support and the counter-balance weight. Starting torque of the vane bearing (plain) and potentiometer was 0.055 oz. in. (4 g.cm.) and frictional effects, though adverse at very low wind speed, were not much in evidence at normal working speeds. Response tests were carried out at various wind speeds in a tunnel, by displacing the vane with a fine thread, to +30° relative to the air stream and releasing it instantaneously. Fig.3 shows the nature of the record obtained for six wind speeds over a range 6.6 to 0.8 m/s, and, for comparison, the response of the recorder alone. Though the vane was not dead-beat above about 3 m/s, over-shoot was not registered, owing to the slower response time of the recorder. Under usual working conditions (5 m/sec. or greater), the effective time of response was thus governed by that of the recorder (0.2 sec.), but at 2 m/s it increased to about 0.5 sec. The modified vertical gustiness meters were considered suitable for use in wind speeds within the range approximately 3 to 12 m/sec., the lower limit being governed by the inadequate response of the control fin, and the upper limit by vibrations of the balloon cable which occurred at times in high wind speeds.

In order to economise in electric connecting cable, the balloon tethering cable was used as a common conductor from the three vertical gustiness meters, and from a thermistor circuit for measuring mean air temperature. The remaining conductors were brought to a junction near the lowest instrument and from there formed the four conductors of a 5000 ft. length of light-weight cable. See Fig.6(b).

Records of gustiness were made on a three-channel ink recorder, (Everett Edgcumbe) with a chart width of 6.7 cm. per channel. Full scale deflection from the centre zero was $2\frac{1}{2}$ mA and the coil resistance was 600 ohms. The three direct-coupled amplifiers required to drive the recorder were built on the lines described in M.R.P.974, but were supplied with a stabilised high tension voltage of 250 V, and 6.3 V unstabilised AC for the valve heaters. However, with the use of the common conductor, and since all amplifiers were provided with power by the same supply, it was necessary to make "single ended" connections at the input end.

A three-pole switch, S_2 Fig.6(c), at the input to the amplifiers allowed recordings to be made of either inclination of each of the three vanes or the difference in the inclination of pairs of vanes. When S_2 was switched to the left the inclinations ϕ_1, ϕ_2 and ϕ_3 were recorded on the corresponding channels of the recorder, and when S_2 was right, while channel 1 remained unchanged, channel 2 recorded $\phi_2 - \phi_1$ and channel 3 gave $\phi_3 - \phi_2$. In these cases the required equality of the output voltage for a given inclination could be observed by comparing reference pulse heights on the same amplifier-recorder channel. Furthermore the balance of each amplifier was checked when S_2 was in the mid-position with S_1 closed. Under these conditions, when the same signal voltage was applied to both input terminals, a dynamically balanced amplifier would produce no output.

(b) Fluctuations of total wind speed

The function of the anemometer in the gustiness meter was firstly to provide reference pulses for the setting of sensitivity, and secondly to give wind speeds. The minimum period over which mean speeds could be measured was inversely proportional to wind speed and at 5 m/sec. was about 1 min. For shorter period fluctuations, a separate anemometer (shown in Fig.1(b)) was used. This was an Ower (see Ower, 1949, p.150) airmeter, K, with the gear train and dial removed, and with a miniature switch, L, fitted on the spindle of the rotor. Four contacts per revolution of the rotor were made, and the electric pulses produced were "counted" electrically over $2\frac{1}{2}$ sec. sequential periods and recorded as amplitudes. Provision was also made for continuously recording the pulse rate so that periods of shorter duration could be examined.

The performance of the anemometer was investigated in a wind tunnel, with various angles of pitch of the vanes, and its time of response measured on a high speed recorder. The pitch of 30° (relative to the airflow) which was finally chosen gave a response time (90%) from zero of 0.3 sec., and a rotational speed of approximately 12/sec. in a wind speed of 5 m/sec. Linearity of the calibration curve remained unchanged over a calibrated range of 1 to 10 m/sec., and the pulse rate (four times the rotational speed) varied from about 10/sec. at 1 m/sec. to 100/sec. at 10 m/sec.

Tests of the anemometer to a fluctuating speed were carried out in the tunnel by moving it to and fro at a controlled rate. The anemometer, guided by a rail, was moved along the airstream with approximately sinusoidal motion. This was effected with a 20 ft. length of string attached to the rotating arm of a constant speed motor, and an elastic return cord. Tests at two frequencies were made, by altering the gear ratio of the motor, and peak speeds of 1.0 m/sec. were used in both cases by adjusting the effective length of the rotating arm. Tracings of the records produced with a chart speed of 12 in./min. are shown in Figs. 4(a) and (b). In a mean wind speed of 5 m/sec. a peak-to-peak response of 90% was obtained with a period of 2.4 sec. and just over 70% when the period was 1.0 sec.

For operation on the balloon cable, the anemometer support was carried on double bearings, M, which allowed it to be freely directed into the mean wind under the action of a cylindrical fin, N. The total wind speed was thus measured, corrections being unnecessary for large excursions of the wind inclination from the horizontal (see Ower, 1949, page 152 for effect of yaw). The anemometer was connected to the ground equipment with a separate light-weight twin-core cable.

The electronic integrator (see Fig.7) consisted of a high speed relay, a storage and switching unit and a d-c amplifier. The relay, operated by an 18 V power supply and the anemometer switch, charged one of three equal condensers C_1 from a constant voltage supply, E, by step-transfer of charge via a small condenser C_2. The ratio of C_1 to C_2 was large (2000 : 1) so that the charging rate of C_1 was almost linear over a large range. Connections to the condensers C_1 were made through a 3-pole "snail" cam switch S_1, driven continuously by a mains synchronous motor at 1 revolution in $7\frac{1}{2}$ sec. Contacts 'a', 'b' and 'c' of this switch dropped from segment to segment in sequence, but separated in time by only about 1/100 sec. In the position shown in Fig.7 one of the $2\mu F$ condensers C_1 was being charged through contact 'b', another was registering its voltage on the recorder through contact 'c' and the d-c amplifier, while the third had been discharged through 'a'.

Every $2\frac{1}{2}$ sec., 'a' dropped first, started discharge of the registering condenser and time marked the recorder. Contact 'b' followed and transferred charging to the newly discharged condenser, and finally contact 'c' operated, registering the voltage which the condenser under charge had acquired during the previous $2\frac{1}{2}$ sec. A manually operated switch S_2 allowed a negative bias to be applied to the condensers C_1, so that the full range of the recorder (centre zero) could be used on a scale of 0-10 m/sec. For a continuous registration of wind speed, within the limits of the anemometer response, condensers C_1 were replaced by a leaking condenser circuit, R_1 C_3, by means of switch S_3. Setting up and checking procedure included the operation of the relay at 50 c/s from a biased AC supply, with switch S_4. This allowed the short-term stability of the mains frequency to be checked, and adjustment of sensitivity to be made by altering the input voltage, E, to the integrator with potentiometer P.

(c) Mean air temperatures

A thermistor (Stantel type K 2361/120), mounted in a bakelite tube, J, (Fig.1(a)) was fitted in the upper part of the control fin of one of the instruments, for the measurement of air temperature. To make effective use of natural ventilation a low operating current was used, and the insulating mounting tube ($1\frac{1}{4}$ in. internal diameter, 6 in. long) and aluminium sides of the fin were utilised as radiation shields. At first the resistance of the thermistor was measured with a "Wheatstone's Bridge", and after deduction of the known cable resistance, converted to temperature from a laboratory calibration of the thermistor. This method of observing temperature was later changed to a direct reading method, with a bridge circuit mounted in the fin of the instrument, where the supply battery of the gustiness instrument was used for power. Components were arranged so that the out-of-balance current of the bridge had a near-linear relationship with temperature and gave full-scale deflection on a 20-0-20 μA meter over a temperature range of +30°F to +70°F. Fig. 6 shows the connection of the thermistor into the circuit. When switch S_1 is open, the output current Im passing through the meter M is given by the equation

$$Im = \frac{V(Rt - R_3)}{(Rt + R_3)(2Rm + R_4) + 2RtR_3}$$

where V = supply voltage to the bridge

Rt = resistance of thermistor

and Rm = total resistance in the external (meter) circuit.

R_3, (wire wound Eureka) was adjusted to balance the bridge at 50°F so that any error introduced by a change of V ($Im \propto V$) was reduced to a percentage of the meter deflection from the centre of the scale. Thus a change in V from 3.0 to 2.9 would cause an error of -2/3 at 70, -1/3 at 60, 0 at 50, +1/3 at 40 and +2/3°F at 30°F. In practice it was evident from changes in the height of the reference pulse of the gustiness recorder that voltage changes of this order did not occur. Variation in the resistance of the balloon cable from 0 to 5000 ft. was only 0.12% of Rm and could be ignored. The "live" conductor from bridge to meter (0.9% of Rm) was always in circuit and its resistance was taken into account when evaluating R_5, while variations due to its temperature coefficient of resistance were negligible in this circuit. An absolute accuracy of $\pm \frac{1}{2}$°F was achieved without the application of corrections, and changes of 0.1°F could be measured. With this direct reading method it was possible to raise the instruments with little delay while making temperature readings at frequent intervals during the ascent, it being necessary to wait only about 1 min. for the thermistor to acquire ambient temperature.

(d) Movement of the balloon

A movement of the balloon, and hence of the instrument support, introduces errors into the recorded values of gustiness. The effect of the changing angle of the tethering cable due to this movement was eliminated from vertical gustiness measurements through the principle of operation of the instrument, while for total speed fluctuations the operation of the anemometer was independent of the cable angle. Errors caused by the bodily transfer of the instruments through the air were, however, present in the recordings from both instruments whenever significant movement of the balloon took place.

To minimise the effects of movements, and to enable approximate measurement of their value to be made easily, it was necessary to use a balloon which provided a substantial residual lift when at operating height. The tethering cable was thus maintained sensibly straight and calculations of the height of instruments could be made from a knowledge of the cable length and its angle, θ , from the vertical.

During experiments carried out at Cardington, a record of movement was made with the aid of a theodolite with a potentiometer coupled to its telescope, erected near the tethering point of the cable, (a power driven winch). A point on the cable, usually one of the instruments, was "followed" continuously when recordings of gustiness were being made. For measurement of height, a cosine potentiometer was used and cos θ was recorded on a linear scale over a range 0.9 to 1.0. The full scale represented a height range of 10% of the distance, l, of an instrument from the winch (taken to be the length of cable) and a close approximation to height changes was given from changes in l cos θ . When total speed measurements were made the cosine potentiometer was replaced by a linear one, and the cable angle was recorded.

As would be expected, the effects of movement were smallest in the absence of large-scale turbulence at the balloon height. In conditions where there was little or no measurable vertical component of wind near the balloon, movement of the instruments was correspondingly small and in general no corrections were necessary for accurate interpretations of the records. This presented the best method of obtaining error-free measurements in turbulent air, i.e. by flying the balloon where possible in relatively stable air above the turbulent region, with the instruments attached to the cable at selected heights above the ground.

3. RECENT OBSERVATIONS

(a) Procedure

Observations have been carried out during the three periods 8th to 15th May, 26th to 30th June and 12th to 17th September, 1956. A van was adapted as a mobile laboratory in which all the equipment could be conveyed to a site at Cardington and in which the ground instruments could be operated. A mains supply of 240 volts A.C. was available to provide the electronic equipment with power.

For the first two periods a modified Mk. 10 kite balloon was provided by the Balloon Development Establishment. This balloon had a capacity of 24,000 cu. ft. and a lift of about 7 cwt. near the ground. The tethering cable was of stranded steel with a breaking strain of $3\frac{1}{4}$ tons and weighing 100 lb. per 1000 ft. For the third period a Mk. 11 balloon was used. This was larger than the modified Mk. 10 and gave a lift of about 15 cwt. near the ground. Using similar cable the residual lift at 5000 ft. was about 10 cwt.

Three gustiness meters were attached to the balloon cable usually at spacings of 1000 ft. for recording actual wind inclinations, and at spacings of up to 400 ft. for recording the differences between the inclinations. Recordings were made at various heights up to a maximum of 7000 ft. The electric cable from a junction at the lowest gustiness meter to the ground was 5000 ft. long, and was stored on a drum with its inner end accessible. Connection to ground equipment could thus be made after any length had been paid out. During the second and third periods the highest gustiness meter was fitted with the thermistor for measuring temperatures. Generally, readings of temperature were taken every 250 ft. and the temperature structure was sampled at the rate of 1000 ft. in about 10 minutes. The total wind speed anemometer, described in 2(b), was available for the third period and was attached to the balloon cable just below the lowest gustiness meter. Two three-channel clockwork driven recorders and one single-channel recorder with an A.C. synchronous motor drive (Everett Edgcumbe) were used in various combinations to obtain the recordings.

The modified theodolite was set up conveniently near the balloon winch and was used to obtain a continuous recording of either the height or elevation of one gustiness meter.

In order to specify the meteorological conditions near the ground, temperature difference was measured with aspirated thermistors (Stantel type K 2361/120) between $\frac{1}{2}$ metre and 4 metres above the ground, the indicating meter and remote control of the aspirating motors being housed in the mobile laboratory. Total radiation flux was measured during the third period, using a radiometer built to the design described by J.MacDowall (1954), and at the same time readings of surface wind speed were taken using an electric cup anemometer.

(b) Examples of data and accuracy of records

Samples of some of the records taken in various meteorological conditions are shown in Figures 8 to 18, with additional meteorological information opposite each figure. This information includes a temperature sounding (dry bulb) plotted on a graph where the dry adiabatic lapse rate is indicated by a pecked line. For all examples, except the first, local temperature data from measurements with a thermistor, or from the Cardington "BALTHUM" sounding are used and are plotted against the length of cable from the winch. The heights quoted on the gustiness records are also cable-lengths, but can be regarded as the height above ground to within 3%. Accuracy of the gustiness records is governed by the degree of balloon movement which took place during the recordings. In some cases (Figures 14, 15 and 16) the recorded elevation of the instruments is shown, and an approximation of errors included in the gustiness traces may be deduced by assuming that the instruments always move in an arc centred at the winch and in the vertical plane of the mean wind direction. The correction, C_ϕ, to inclination will then be given by

$$C_\phi = \tan^{-1}\left[\frac{\pm S \sin(\theta+\phi)}{V \pm S\cos(\theta+\phi)}\right]$$

and the corrected total speed V_t by

$$V_t = \sqrt{V^2 + S^2 \pm 2VS\cos(\theta+\phi)}$$

/where

where ϕ and V are respectively the apparent inclination and total speed of the wind, $(90-\theta)$ is the elevation of the instrument and S is the tangential speed of the instrument, approximately equal to $l\,d\theta/dt$ (l = cable length). The negative sign is used for decreasing θ.

In Figure 14, $d\theta/dt$ is a maximum at about 1638¼ B.S.T. and the correction to speed and inclination deduced from the above formulae is - 1.1 m/s and $< 1^\circ$ respectively. Thus whereas correction for the movement of the instrument in this instance caused a marked levelling of the recorded total wind speed, there was little effect on the inclination record. Similar considerations apply to Figure 16. On the other hand, from Figure 15 it is evident from the record of the instrument movement that little or no correction is necessary to either inclination or speed traces. It will be noted that total speed records in both Figures 14 and 15 are in histogram form, the height of each pulse representing the mean speed for the previous 2½ sec., whereas for the record of Figure 16 the storage circuit (Section 2(b)) has been switched out and the higher frequencies are apparent.

Recordings of instrument elevation were also made with the other examples of gustiness shown (Figures 8 to 13, 17 and 18), but are not given in this paper. It will, however, frequently be evident from the nature of the inclination records themselves that the general trend, as well as the higher frequency component, is reasonably true, as the three gustiness meters were always mounted on the same cable. Each would therefore be affected in a similar manner by a movement of the balloon, though to a degree in proportion to its height. Thus, there can be little doubt as to the reality of the convective turbulence indicated in Figure 8 at 3000 and 4000 ft. The long period (approx.7 min.) wave motion at 5000 ft. is also believed to be genuine as this cannot be accounted for by the effects of a balloon movement. The positive "bump" between 1207 and 1208 B.S.T. would however be flattened out and the mean after 1208¾ raised to about + 2°.

Figures 9 and 10 are samples taken from records made on one day, the former illustrating a period of well developed convection up to 3000 ft. at about noon and the latter, in two 6-min. periods, the results of decayed convection up to 6000 ft. in the evening. In Figure 9 the corrections for movement are such as to increase the positive inclination (balloon rising) by a few degrees for about 1 min. around 1141½ B.S.T. and to reduce the inclination for a period of ¾ min. around 1145. The steady downward component at 4000, 5000 and 6000 ft. in Figure 10 is also regarded as real and corrections would increase this component slightly as the balloon was falling steadily throughout the period. In contrast to the convective conditions of Figure 9, Figures 11 and 12 illustrate the low degree of turbulence recorded up to 3000 ft. in approaching warm front conditions during the night. No measurable error due to balloon movement was evident during these runs. R.M.S. values of wind inclination at 1000, 2000 and 3000 ft. for 20-min. periods during the day are given opposite Figure 9, and for comparison some R.M.S. values are shown opposite Figure 12 for the following early morning.

Differences of inclination between pairs of vanes are shown in Figure 13, together with the inclination at 2000 ft. In this case the three instruments were suspended one above the other at 2000, 2100 and 2150 ft., and differences over 100 and 50 ft. height intervals were recorded. During this sample period, the corrections to inclination for instrument movement are, in general, small, but rise to a peak of about -4° at 1126.8 B.S.T. For the records of differences, it is assumed that as the three instruments were closely spaced, the effects of movement would be roughly the same on all three when the differences of inclination are small, and that errors due to movement need not be taken into account. The results obtained on this occasion are the subject of a more detailed analysis in a separate report (M.R.P.1044). The remaining two figures given in this paper (Figures 17 and 18) are examples of vertical gustiness below and above a subsidence inversion of base around 3000 ft. and top 4000 ft. In this case the balloon was flying in stable air and recorded movement was small, giving maximum corrections of about 1°. It is noteworthy that the tension of the cable at ground level was still about 4 cwt. with the balloon flying at 7000 ft. and the angle of the tethering cable lay within 6° of the vertical. Figure 17 shows a moderate degree of turbulence at 2000 ft. decreasing somewhat near the inversion base at 3000 ft. and damped out almost entirely at the inversion top at 4000 ft. A slow undulating motion with a period of about 5 min. is shown in Figure 18 at 5000 ft. with practically no vertical component above at 6000 ft. and very little at 7000 ft.

Acknowledgements

The instruments used in this investigation were made or adapted by Mr. H. Scamell and Mr. R. Penny. Acknowledgement is made to Mr. L.A. Speed and Mr. J. Long, of the Balloon Development Establishment, Cardington, for provision of balloon facilities.

References

E. Ower	1949	The measurement of air flow	
J. MacDowall	1954	A total radiation fluxmeter	Meteorological Research Papers, Air Ministry, London, No. 858.

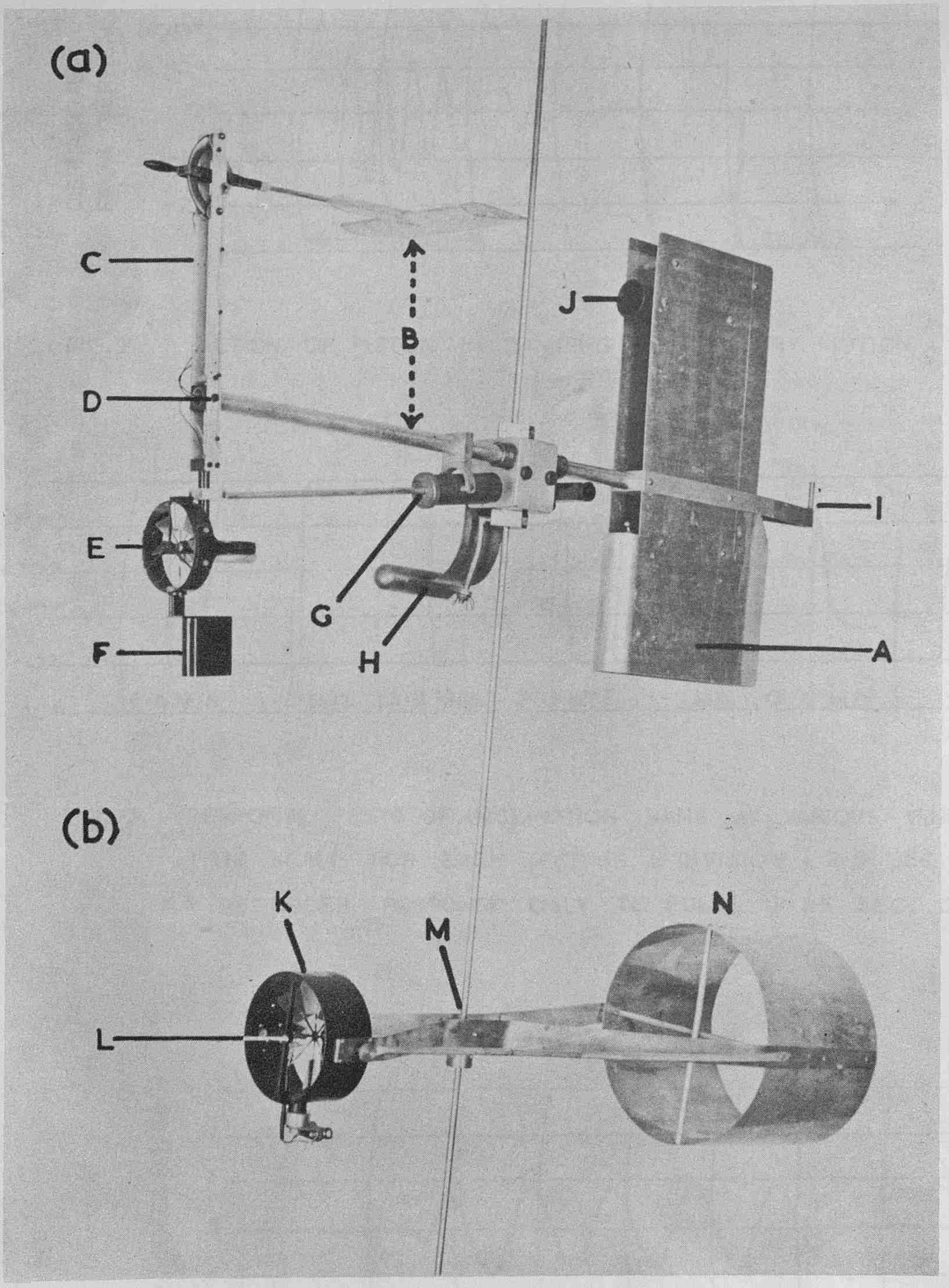
(a)
C
D
E
F
G
H
B
J
I
A
(b)
K
M
N
L

FIG. 1. (a) & (b)

T.1355.

MODIFIED GUSTINESS METER (TOP) AND "TOTAL SPEED" ANEMOMETER ON STEEL ROD TO RESEMBLE MOUNTING ON BALLOON CABLE.

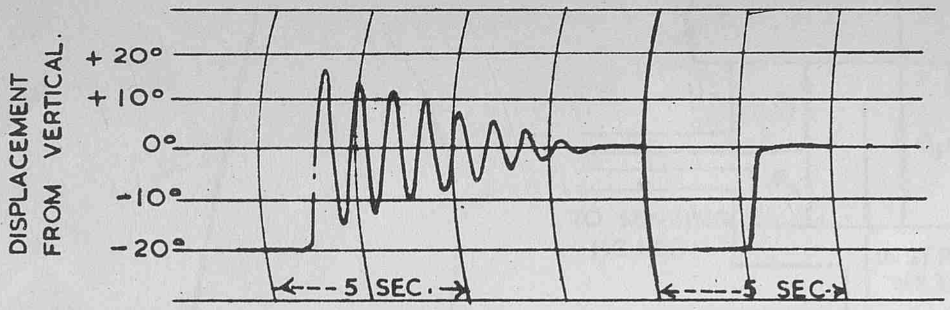

FIG. 2. ACTION OF PISTON IN DAMPING OSCILLATORY MOTION.

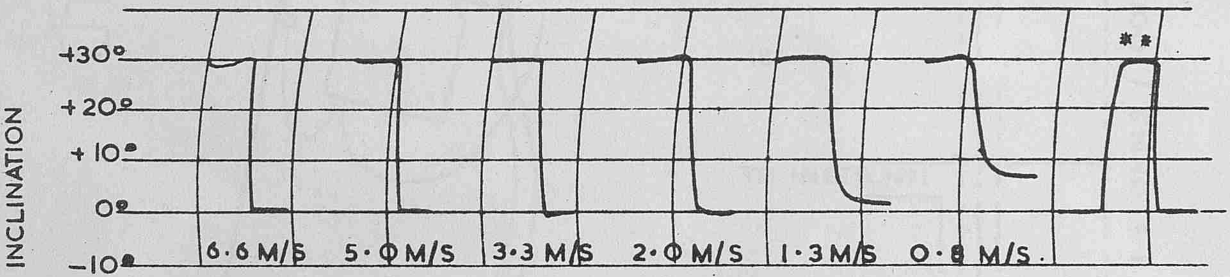

FIG. 3. RESPONSE TESTS OF INCLINATION VANE AT VARIOUS WIND SPEEDS.
TIME SCALE FOR EACH TEST IS 1 DIVISION = 2·5 SEC.
** RECORDER RESPONSE ONLY TO PULSE 1·25 SEC. DURATION.

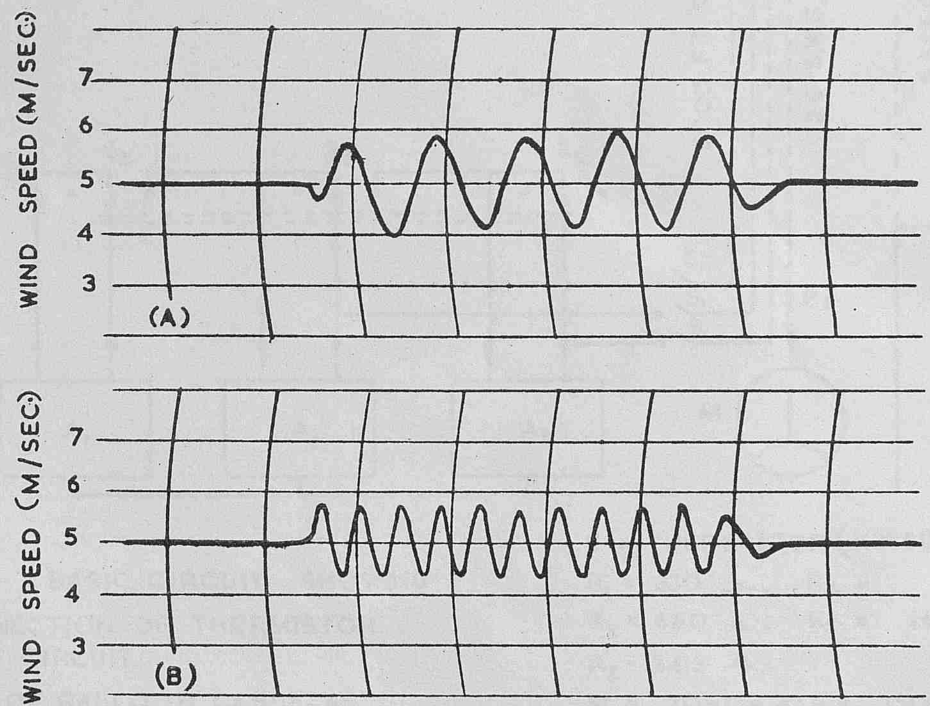

FIG 4 (A) AND (B). RECORD OF ANEMOMETER RESPONSE TO APPROXIMATELY SINUSOIDAL FLUCTUATIONS OF 2 M/SEC PEAK-TO-PEAK AMPLITUDE.
(A) PERIOD OF FLUCTUATION = 2·4 SEC.
(B) PERIOD OF FLUCTUATION = 1·0 SEC.

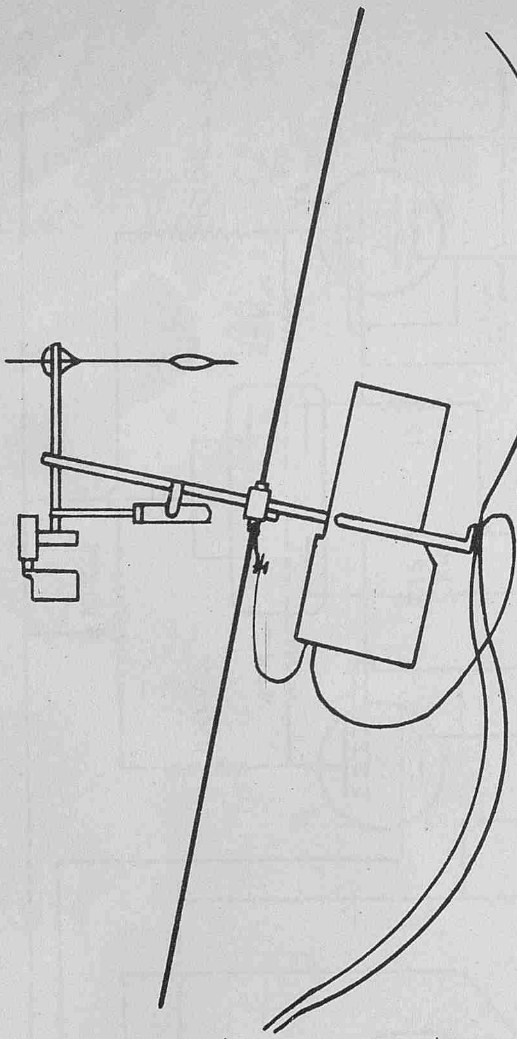

FIG 5. GUSTINESS METER No 2 MOUNTED ON BALLOON CABLE.

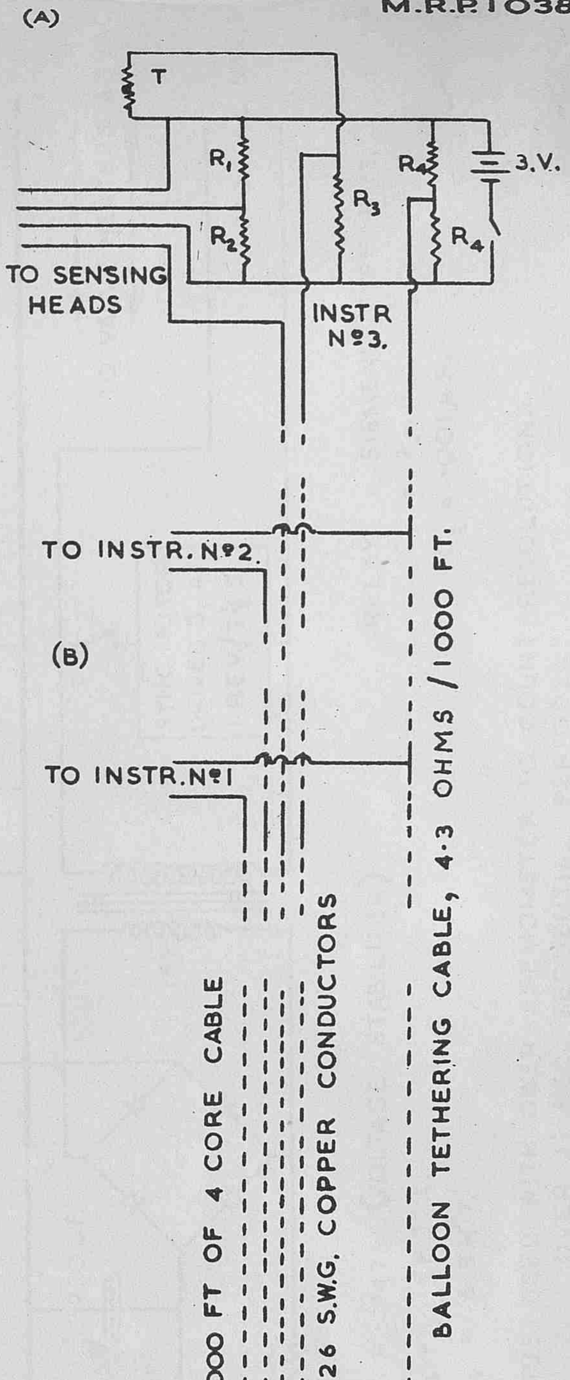
(A)
T
R1
R2
R3
R4
R4
3.V.
TO SENSING HEADS
INSTR No 3.
TO INSTR. No 2.
(B)
TO INSTR. No 1
5000 FT OF 4 CORE CABLE
26 S.W.G. COPPER CONDUCTORS
BALLOON TETHERING CABLE, 4·3 OHMS / 1000 FT.

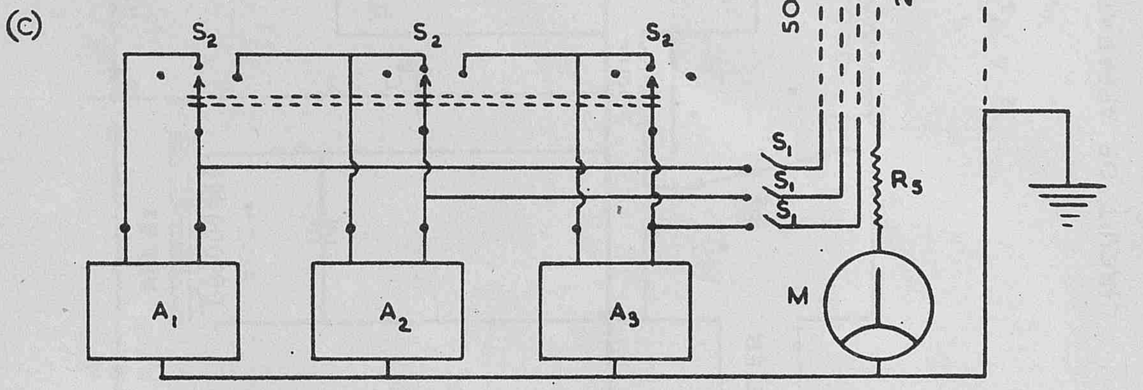
(C)
S2
S2
S2
S1
S1
S1
R5
M
A1
A2
A3

FIG 6. BASIC CIRCUIT SHOWING

(A) CONNECTION OF THERMISTOR INTO CIRCUIT.

(B) USE OF BALLOON CABLE AS COMMON CONDUCTOR.

(C) SWITCHING ARRANGEMENT FOR RECORDING INCLINATION DIFFERENCES.

T = THERMISTOR (K2361/120)

R_1 = 330 Ω. R_4 = 200 Ω.

R_2 = 680 Ω. R_5 = 16280 Ω.

R_3 = 3413 Ω.

M = 20-0-20 μA 1500 Ω.

A_1, A_2, A_3 = AMPLIFIERS.

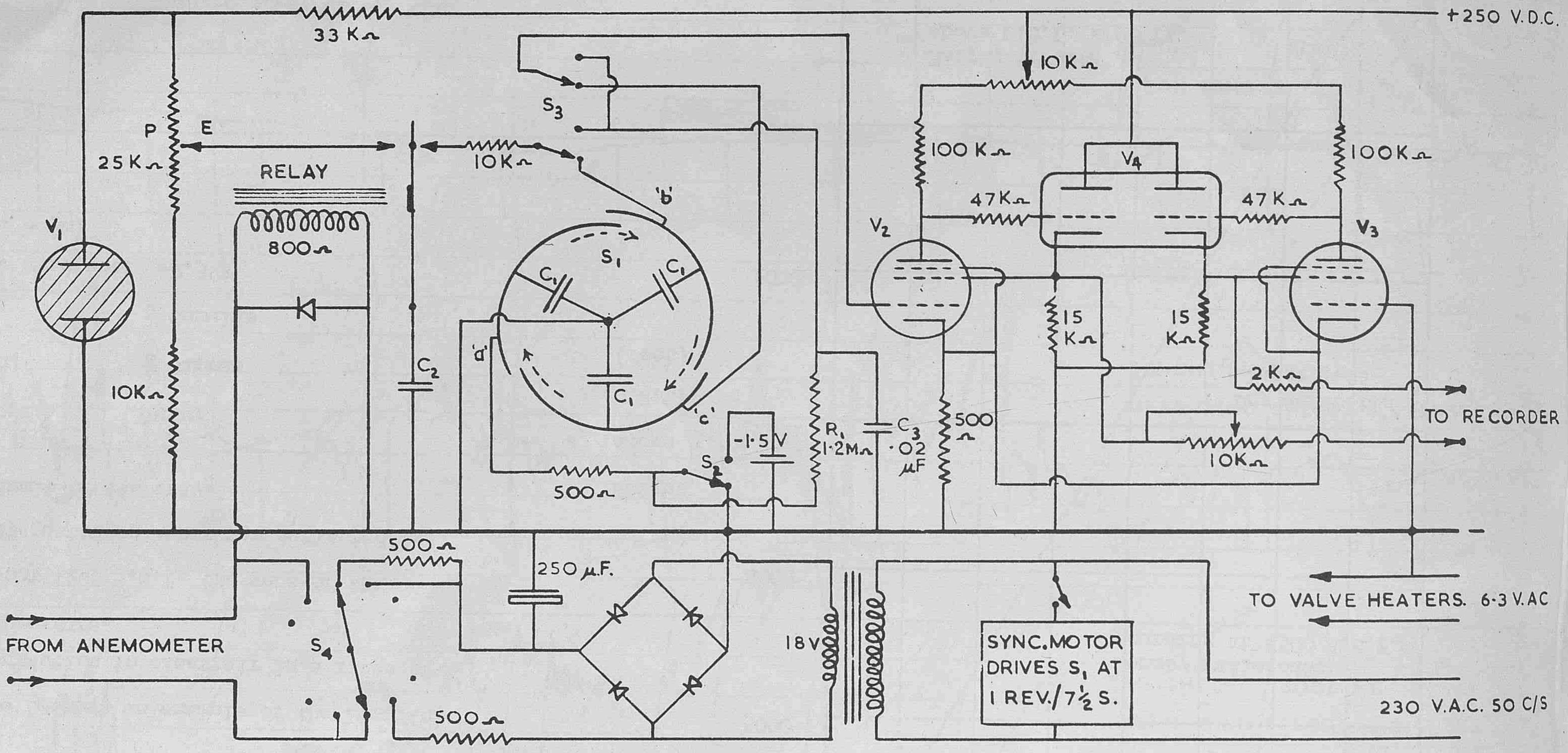
+250 V.D.C.
33 KΩ
10 KΩ
S₃
P
E
25 KΩ
10 KΩ
'b'
RELAY
800Ω
V₁
S₁
C₁
C₁
C₁
C₂
'd'
'c'
10KΩ
-1·5 V
S₂
500Ω
R₁ 1·2MΩ
C₃ ·02 μF
500 Ω
100 KΩ
100 KΩ
V₄
47KΩ
47 KΩ
V₂
V₃
15 KΩ
15 KΩ
2 KΩ
10KΩ
TO RECORDER
500Ω
250 μF.
FROM ANEMOMETER
S₄
500Ω
18V
SYNC. MOTOR DRIVES S₁ AT 1 REV./7½ S.
TO VALVE HEATERS. 6·3 V.AC
230 V.A.C. 50 C/S

V_1 = 7475. (VOLTAGE STABILIZER)

V_2 & V_3 = EF 37A.

V_4 = 6 SN 7.

RELAY = SIEMENS TYPE H 73.

$C_1 = 2\mu F$

$C_2 = \cdot 001 \mu F$.

FIG: 7

CIRCUIT OF APPARATUS USED WITH OWER ANEMOMETER TO COUNT REVOLUTIONS OVER 2½ SEC. SEQUENTIAL PERIODS.

Figure 8 shows an example of the limiting of convection in clear air in a ridge of high pressure.

At about 1205 B.S.T. the vane of the lowest gustiness meter was deflected to the limit of its travel.

Weather: Sunny

Cloud: $\frac{1}{8}$ Cirrus

$\frac{1}{8}$ Cumulus

Temp. gradient: -2.3°F

(4m. $- \frac{1}{2}$m)

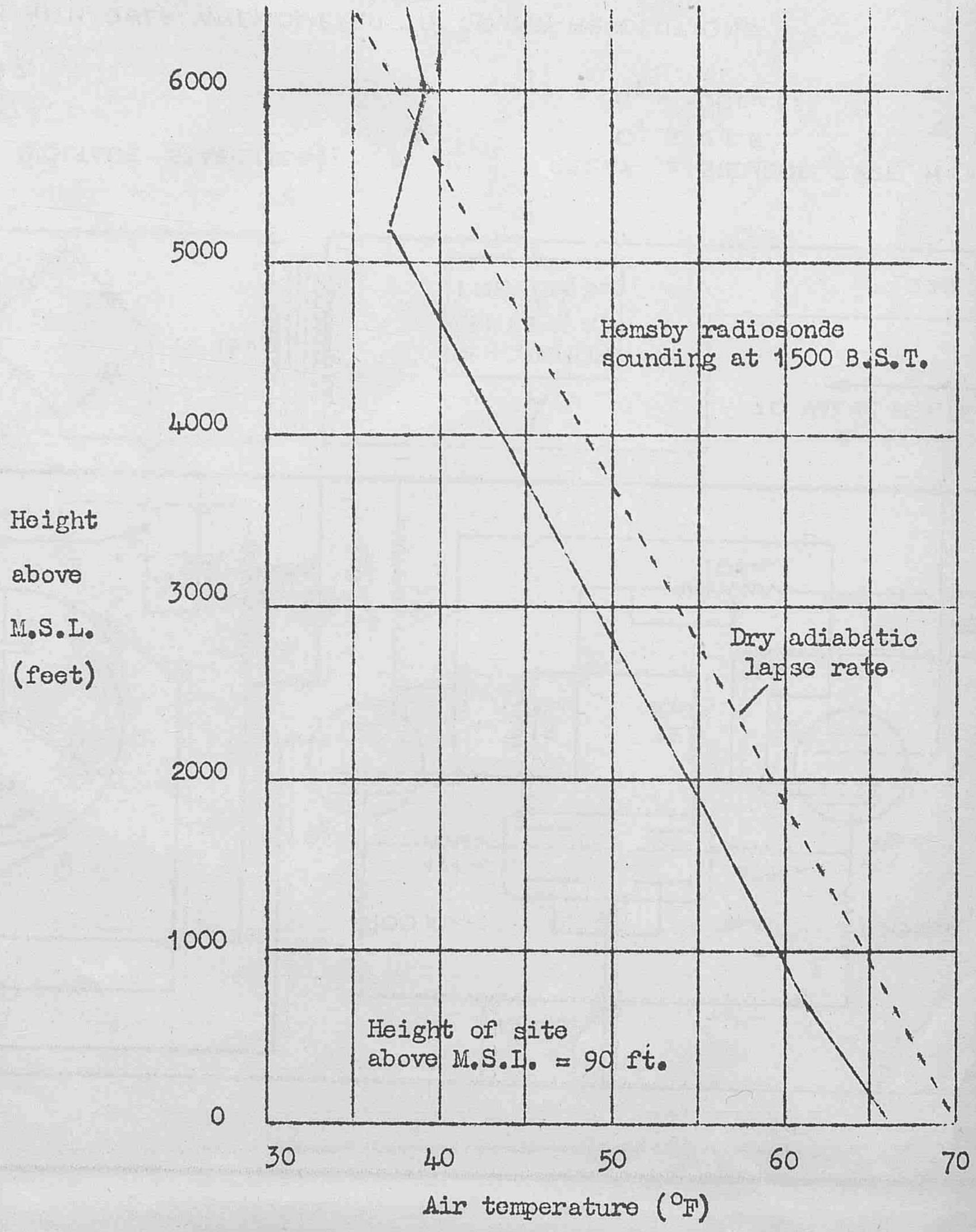

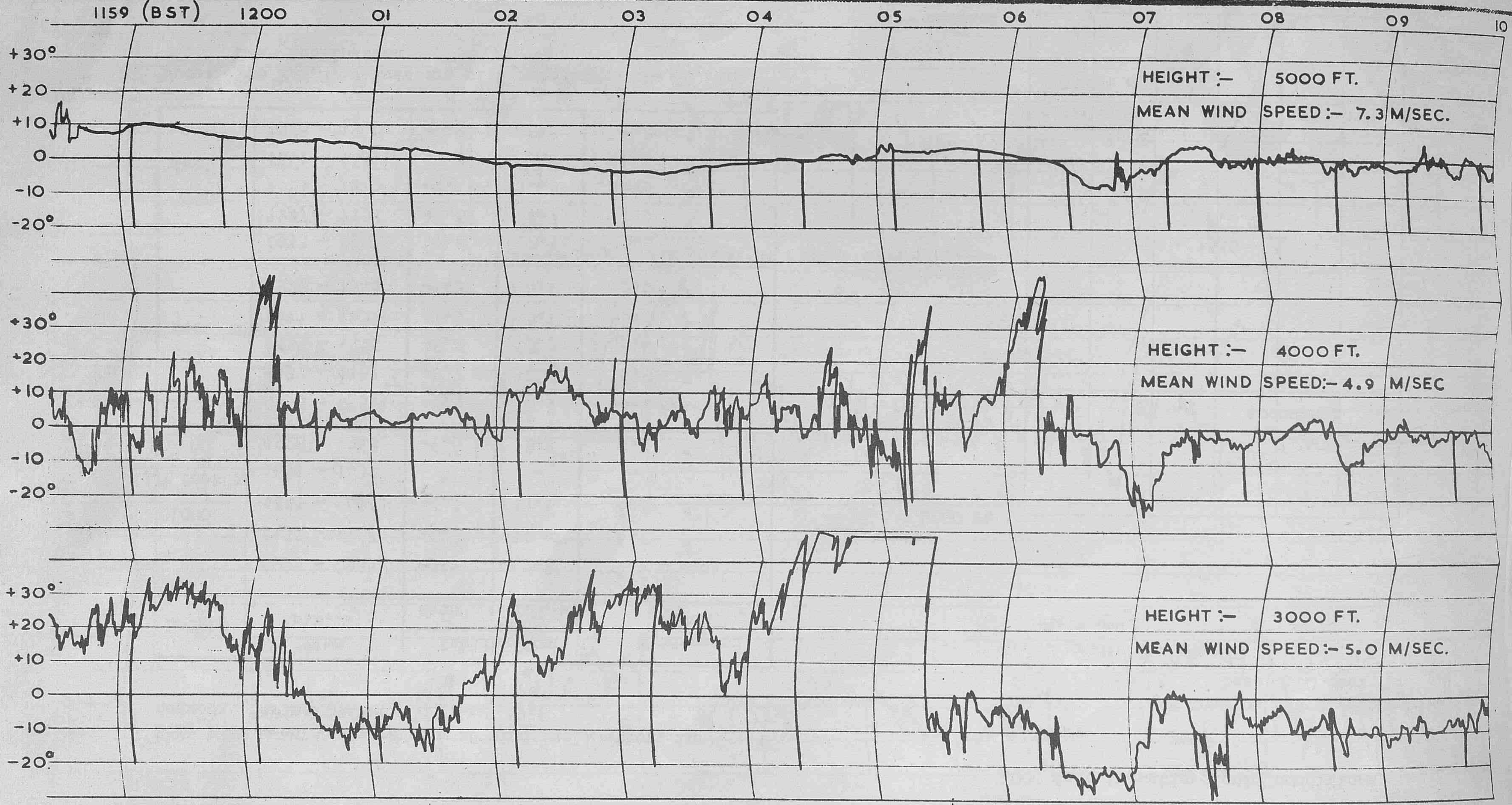

SAMPLE RECORD OF WIND INCLINATION AT 3000, 4000 AND 5000 FEET AT CARDINGTON ON 15 MAY 1956.

FIG: 8

Some root mean square values of wind inclination, in degrees, during the day 27 June 1956

Height	Time B.S.T.	Inclination		Wind speed mean
		Mean	R.M.S.	
1000 feet	0933 - 0953	-3.9	5.2	6.6 m/sec.
	1137 - 1157	+0.7	10.4	6.5 "
	1353 - 1413	-5.3	11.6	6.3 "
	1611 - 1631	-	-	-
	1928 - 1948	-1.5	8.9	1.7 "
2000 feet	0933 - 0953	+0.5	5.3	6.4 m/sec
	1137 - 1157	+0.7	10.6	6.5 "
	1353 - 1413	-8.2	13.9	6.4 "
	1611 - 1631	+1.5	5.1	5.2 "
	1928 - 1948	+1.2	4.1	3.8 "
3000 feet	0933 - 0953	+7.6	5.3	5.0 "
	1137 - 1157	+3.5	8.7	6.3 "
	1353 - 1413	-6.1	10.5	6.3 "
	1611 - 1631	+0.8	5.6	4.4 "
	1928 - 1948	-0.9	2.8	5.8 "

Note: The R.M.S. values are with respect to the 20 min. mean inclination

Figure 9 shows strong convection up to at least 3000 feet in anticyclonic conditions

Weather: Fine

Cloud: 4/8 Cumulus and Stratocumulus base 2500 feet

Temp. gradient: $-1.2^{\circ}F$
($4m. - \frac{1}{2}m.$)

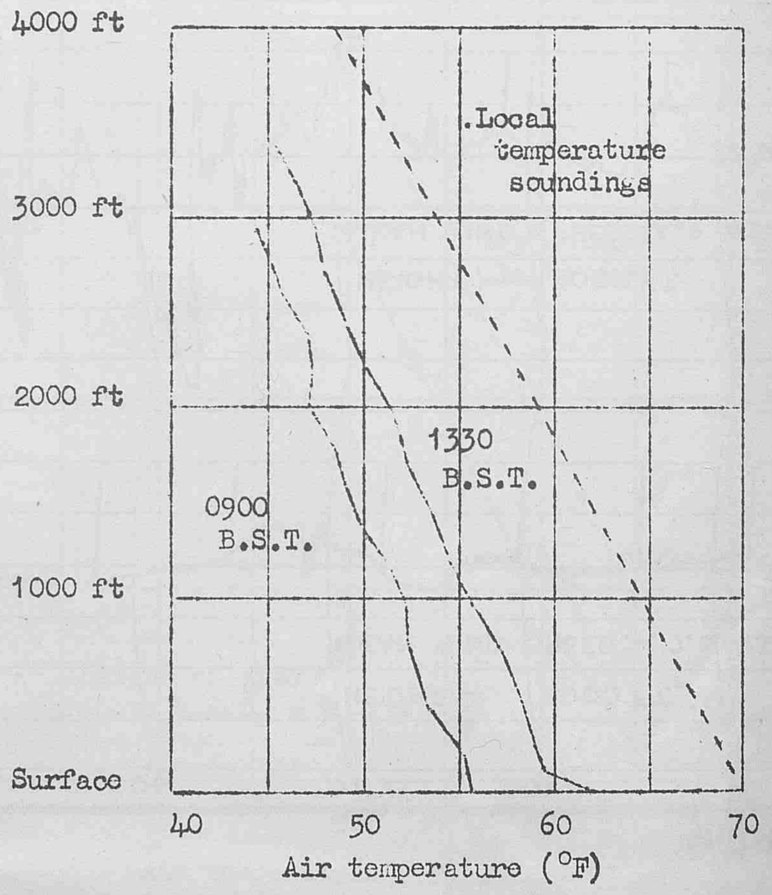

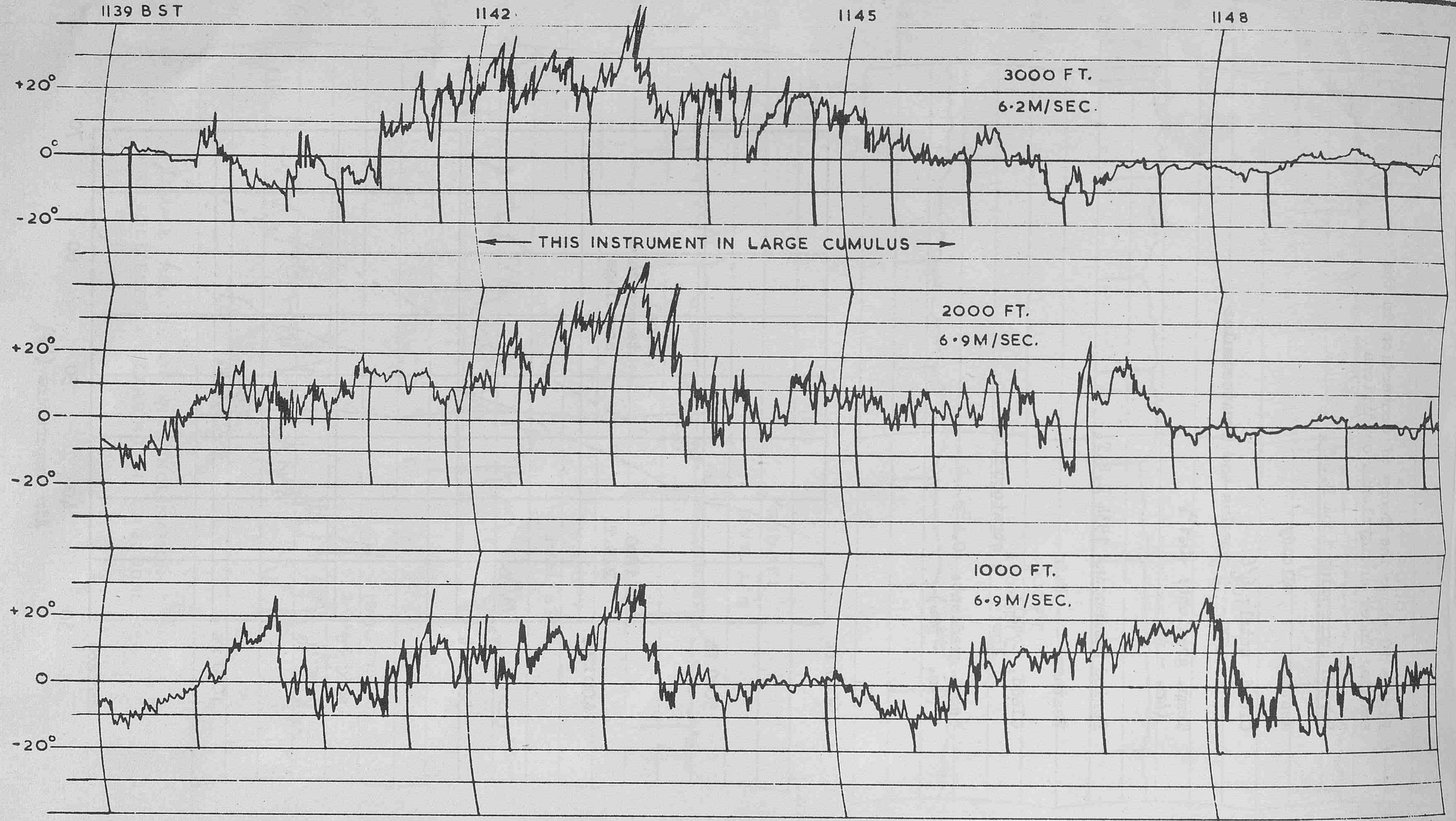

FIG 9. SAMPLE RECORD OF WIND INCLINATION AT 1000, 2000 AND 3000 FEET AT CARDINGTON ON 27 JUNE 1956.

Figure 10 shows the decay of convection in the evening under anticyclonic conditions

Period commencing 1854 B.S.T.

Weather: Cloudy

Cloud, total: 6/8
low: $\frac{3}{8}$ cumulus and stratocumulus

Temp. gradient: +0.1°F
(4m. - ½m)

Period commencing 1934 B.S.T.

Weather: Fair

Cloud, total: $\frac{3}{8}$
low: $\frac{1}{8}$ stratocumulus

Temp. gradient: +0.4°F
(4m. - ½m.)

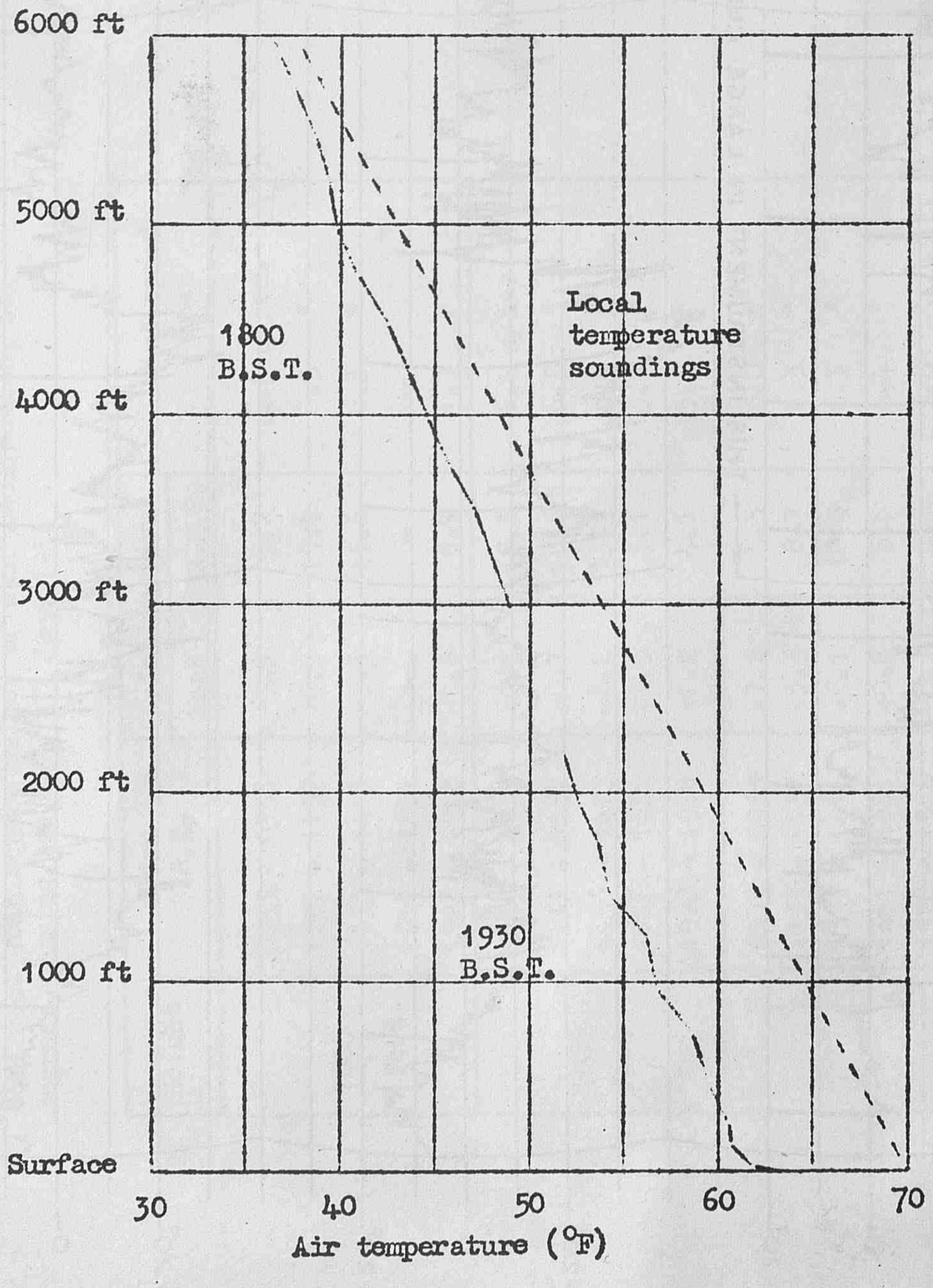

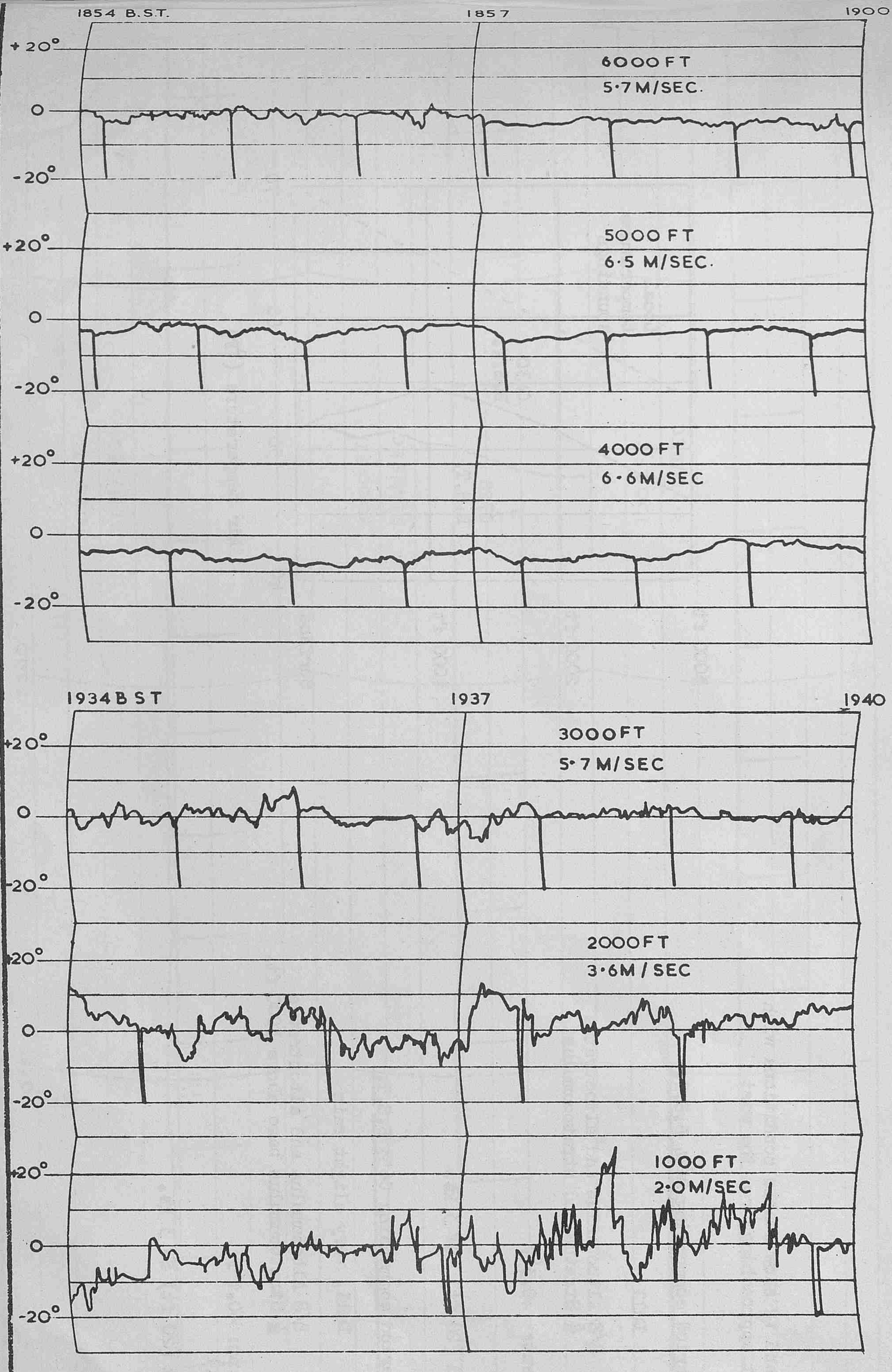

FIG 10. SAMPLE RECORD OF WIND INCLINATION TO 6000 FEET AT CARDINGTON ON 27 JUNE 1956.

Figures 11 and 12 show stable conditions with a warm front approaching from the west

Fig. 11 Period commencing 0454 B.S.T.

Weather: Dull

Cloud: 8/8 Altocumulus and altostratus
$\frac{5}{8}$ Stratus and stratocumulus

Temp: gradient: +0.3 °F
($4\text{m.} - \frac{1}{2}\text{m.}$)

Surface wind (20 ft) SW 3 kt.

Fig. 12 Period commencing 0653 B.S.T.

Weather: Dull, very slight rain

Cloud: 8/8 Altocumulus and altostratus
$\frac{7}{8}$ Stratocumulus base above 3000 ft.

Temp. gradient: –0.1 °F
($4\text{ m.} - \frac{1}{2}\text{m.}$)

Surface wind (20 ft) SW 3 kt.

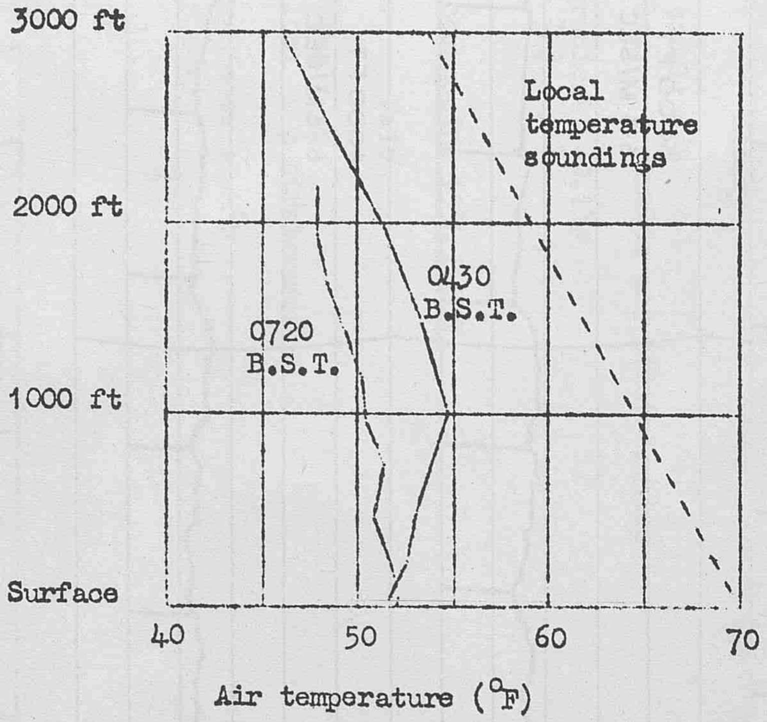

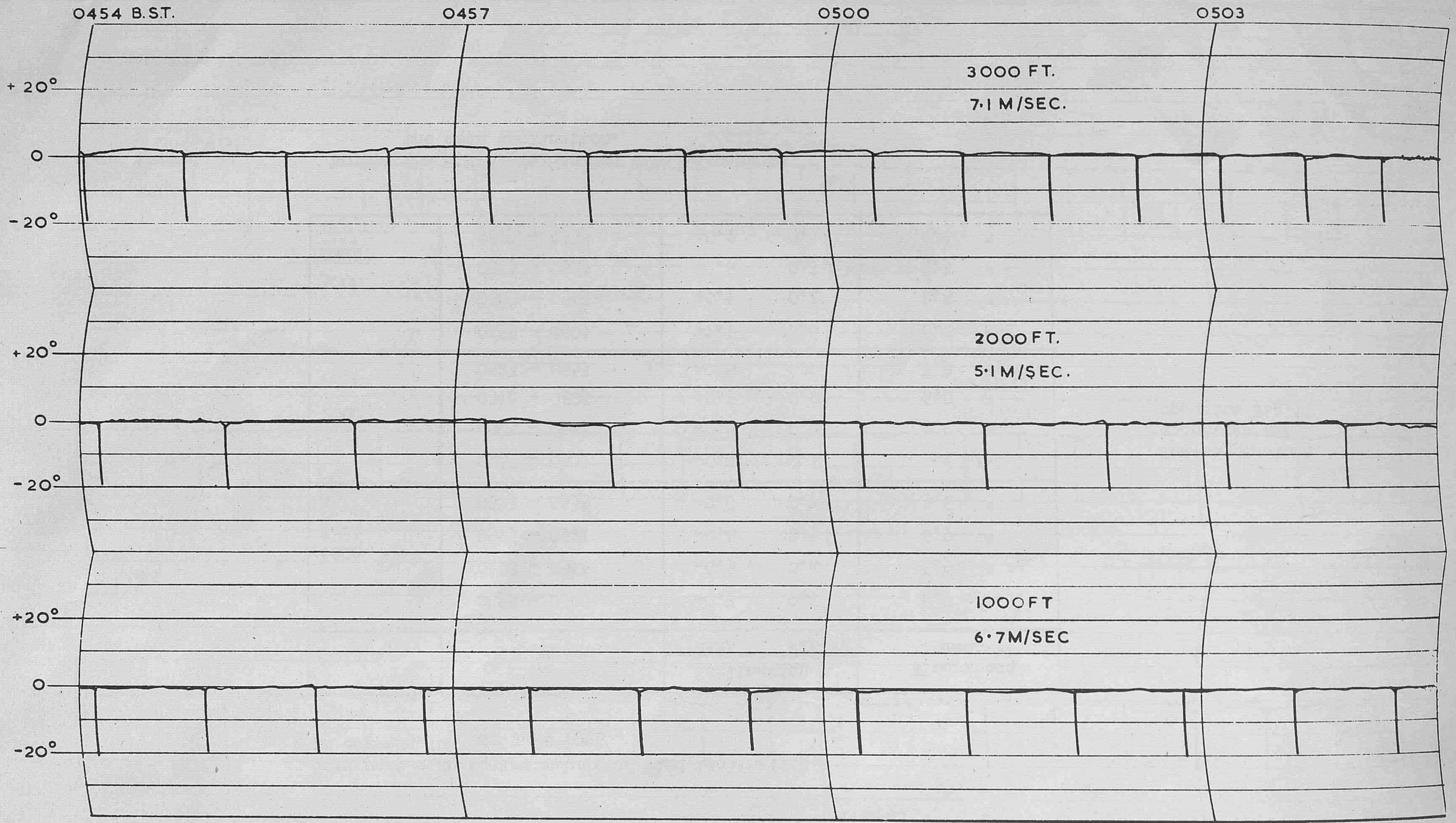

FIG 11. SAMPLE RECORD OF WIND INCLINATION AT 1000, 2000 AND 3000 FEET AT CARDINGTON ON 28 JUNE 1956.

Some root mean square values of wind inclination, in degrees, on 27 June 1956

Height	Time B.S.T.	Inclination		Wind speed mean
		Mean	R.M.S.	
1000 feet	0453 - 0503	-0.7	0.4	6.7 m/sec.
	0503 - 0513	-0.5	0.4	6.9 "
	0513 - 0523	-0.4	0.5	6.9 "
	0523 - 0533	-0.6	0.7	5.6 "
2000 feet	0453 - 0503	-0.4	0.3	5.1 m/sec
	0503 - 0513	-0.8	0.9	5.4 "
	0513 - 0523	-0.3	0.2	6.0 "
	0523 - 0533	-0.8	1.1	7.5 "
3000 feet	0453 - 0503	+1.1	0.6	6.8 m/sec
	0503 - 0513	+0.1	0.2	8.5 "
	0513 - 0523	+0.6	0.3	9.3 "
	0523 - 0533	+0.2	0.4	10.1 "

For temperature soundings see opposite Fig.11

Note: The R.M.S. values are with respect to the mean inclination.

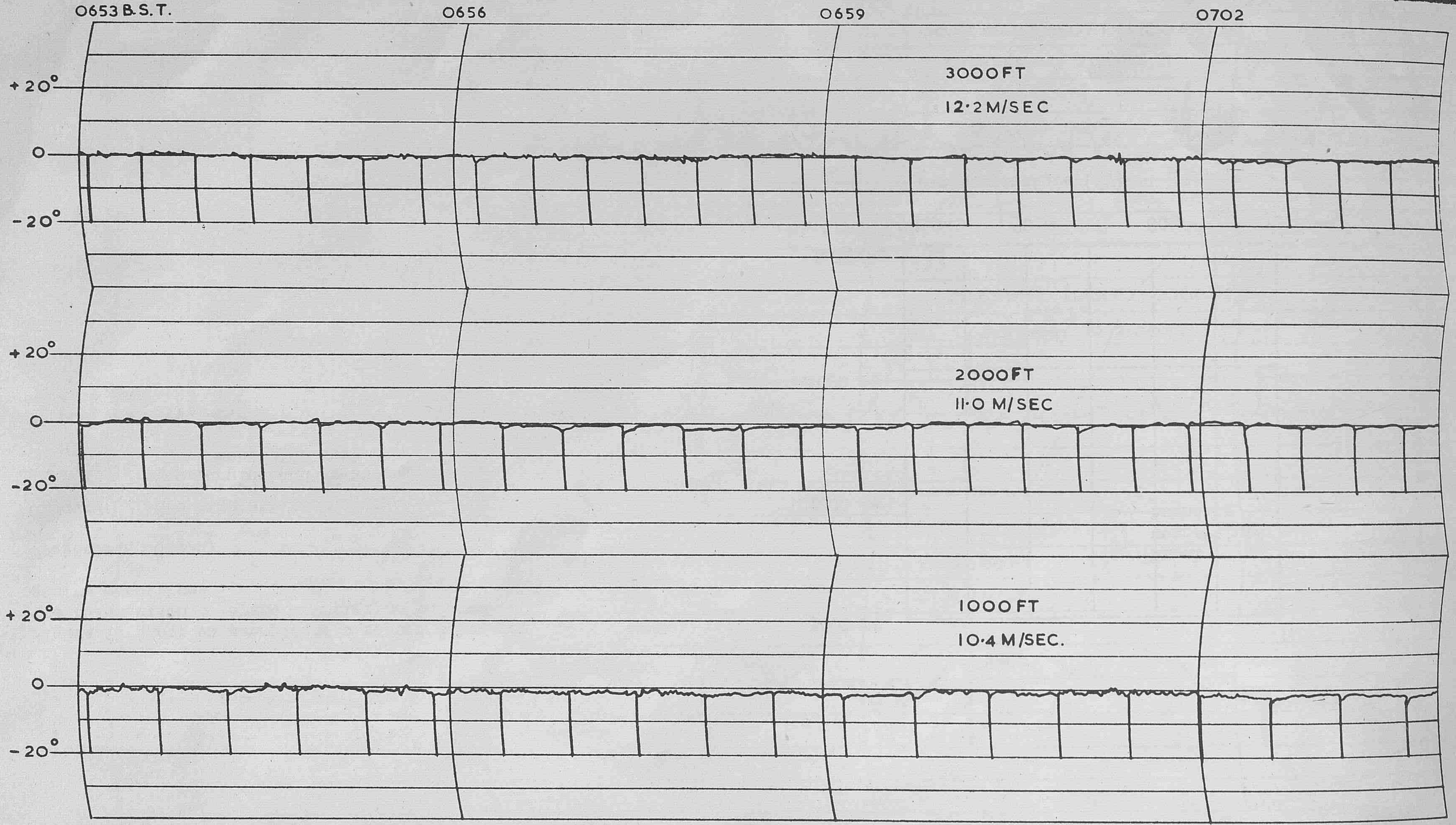

FIG 12. SAMPLE RECORD OF WIND INCLINATION AT 1000, 2000 AND 3000 FEET AT CARDINGTON ON 28 JUNE 1956.

Figure 13 shows an example of a record taken for the calculation of space correlation in warm sector conditions

Weather: Cloudy

Cloud: 8/8 high stratocumulus

4/8 Cumulus and Fractocumulus base 2500 feet

Temp. gradient: $-0.5^{\circ}F$
$(4m. - \frac{1}{2}m.)$

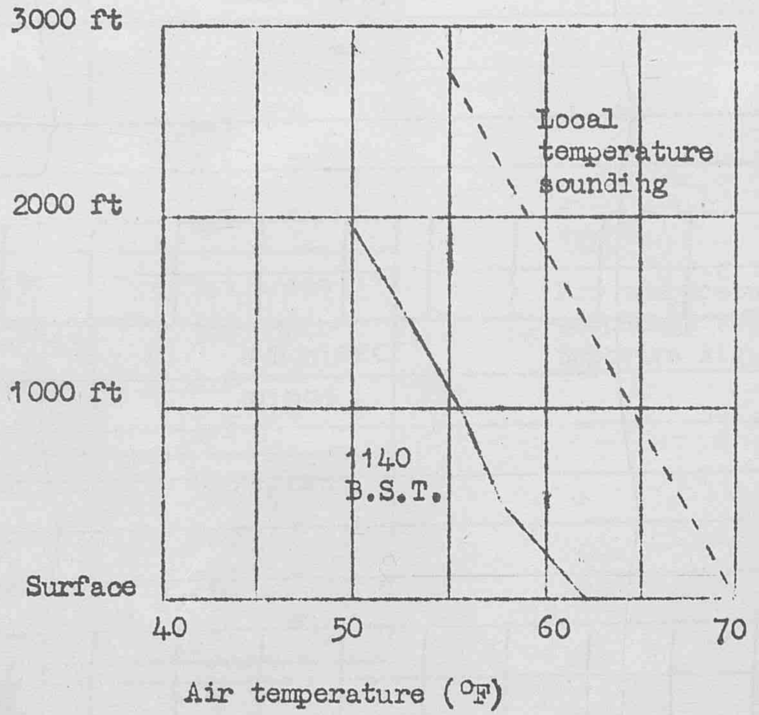

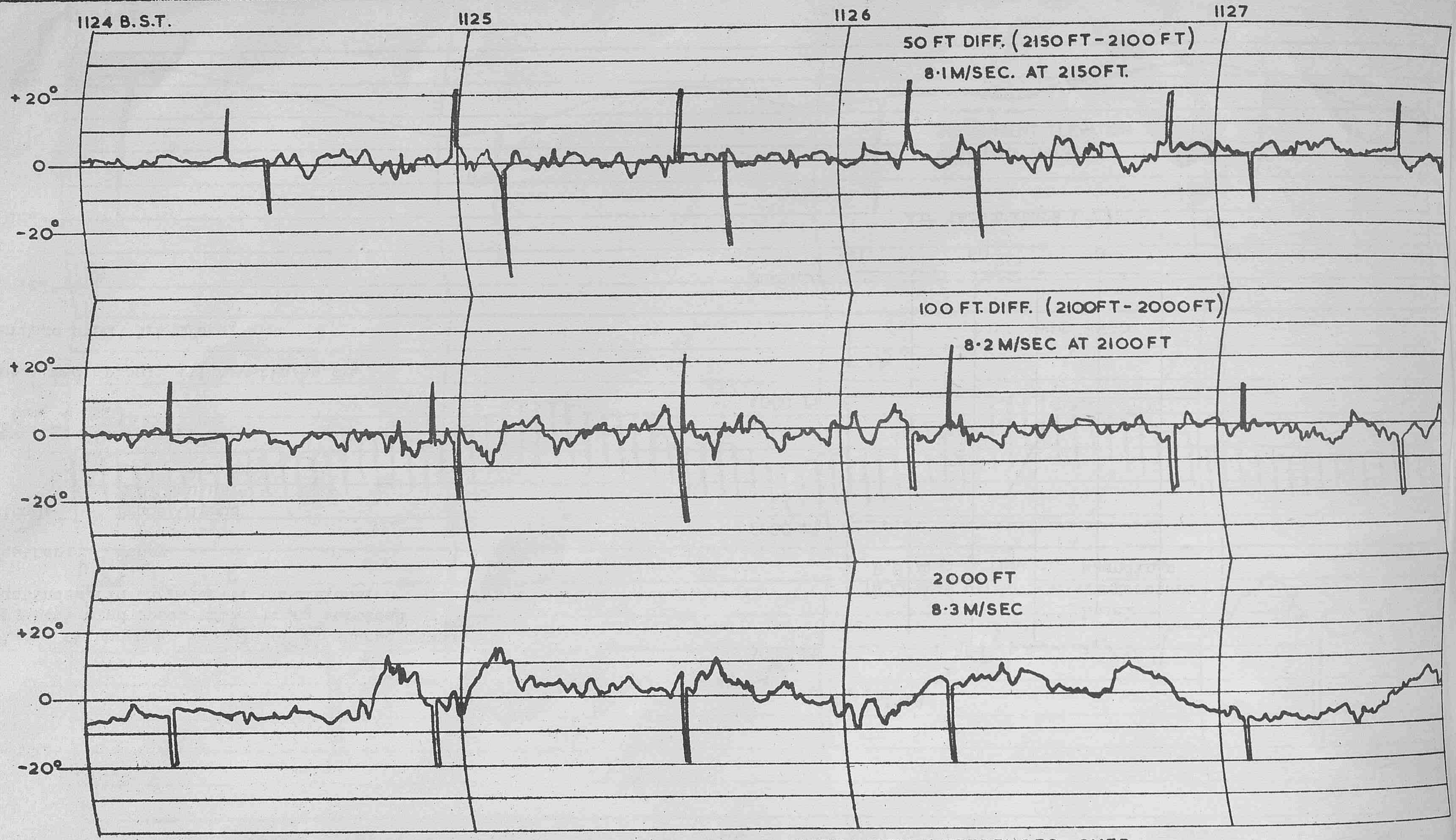

FIG 13.

SAMPLE RECORD OF WIND INCLINATION AT 2000 FEET WITH DIFFERENCES OVER 50 AND 100 FEET AT CARDINGTON ON 30 JUNE 1956.

Figure 14 shows an example of 2½ second means of total wind speed with strong vertical gustiness, in warm sector conditions.

Weather: Sunny

Cloud: Trace Cirrus
2/8 Cumulus

Temp. gradient: +0.1°F
($4m. - \frac{1}{2}m.$)

Total radiation: +11 m.watts/sq.cm.

Surface wind 3.4 m/sec.

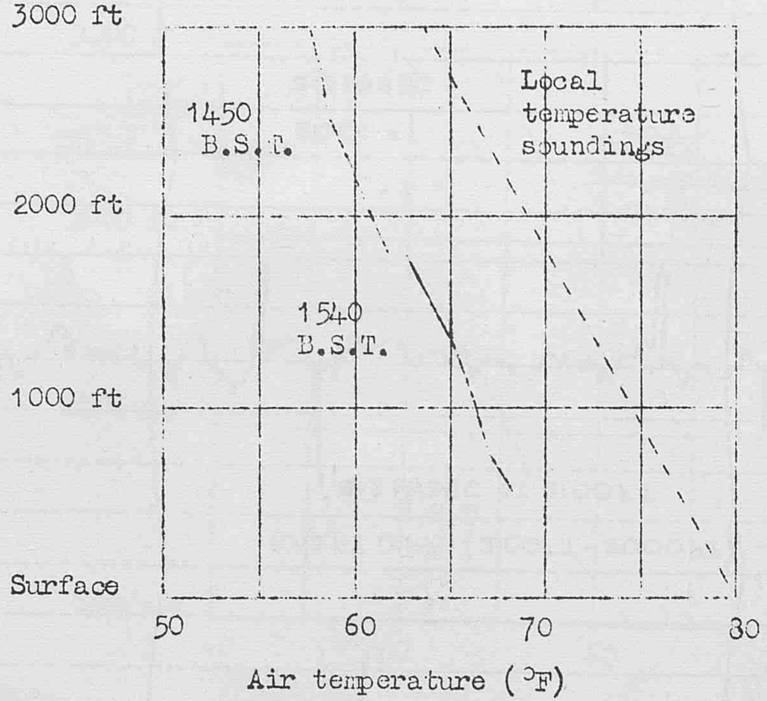

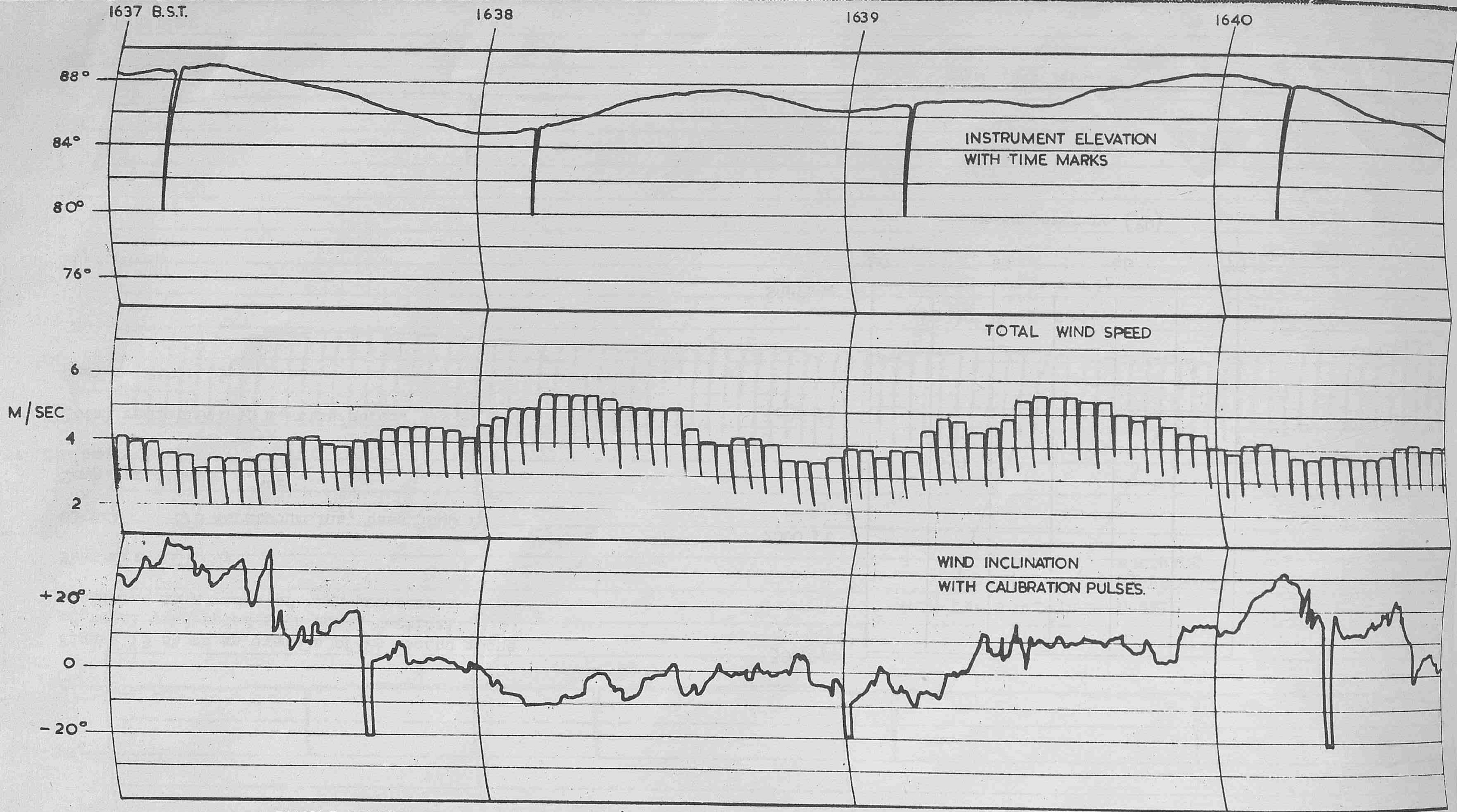

FIG. 14. SAMPLE RECORD OF WIND INCLINATION, 2½ SECOND MEANS OF TOTAL WIND SPEED, AND ELEVATION OF INSTRUMENT, AT 1500 FEET AT CARDINGTON 13 SEPTEMBER 1956.

Figure 15 shows an example of $2\frac{1}{2}$ second means of total wind speed with small vertical gustiness in a ridge of high pressure

Weather: Cloudy

Cloud: 8/8 Stratocumulus, base 3000 ft

Temp. gradient: 0.0°F
($4m. - \frac{1}{2}m.$)

Total radiation: +3 m.watts/sq.cm.

Surface wind: 5.2 m/sec.

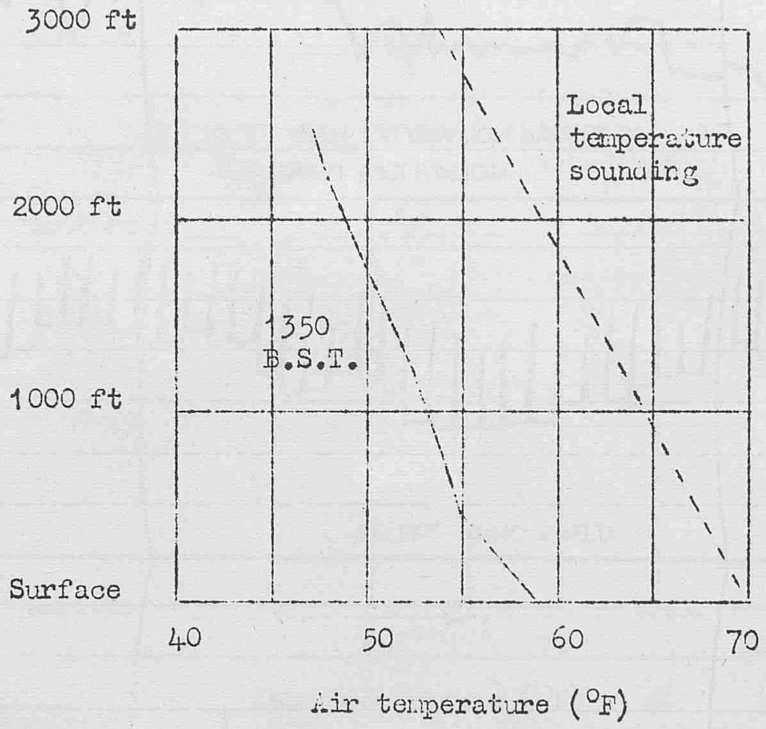

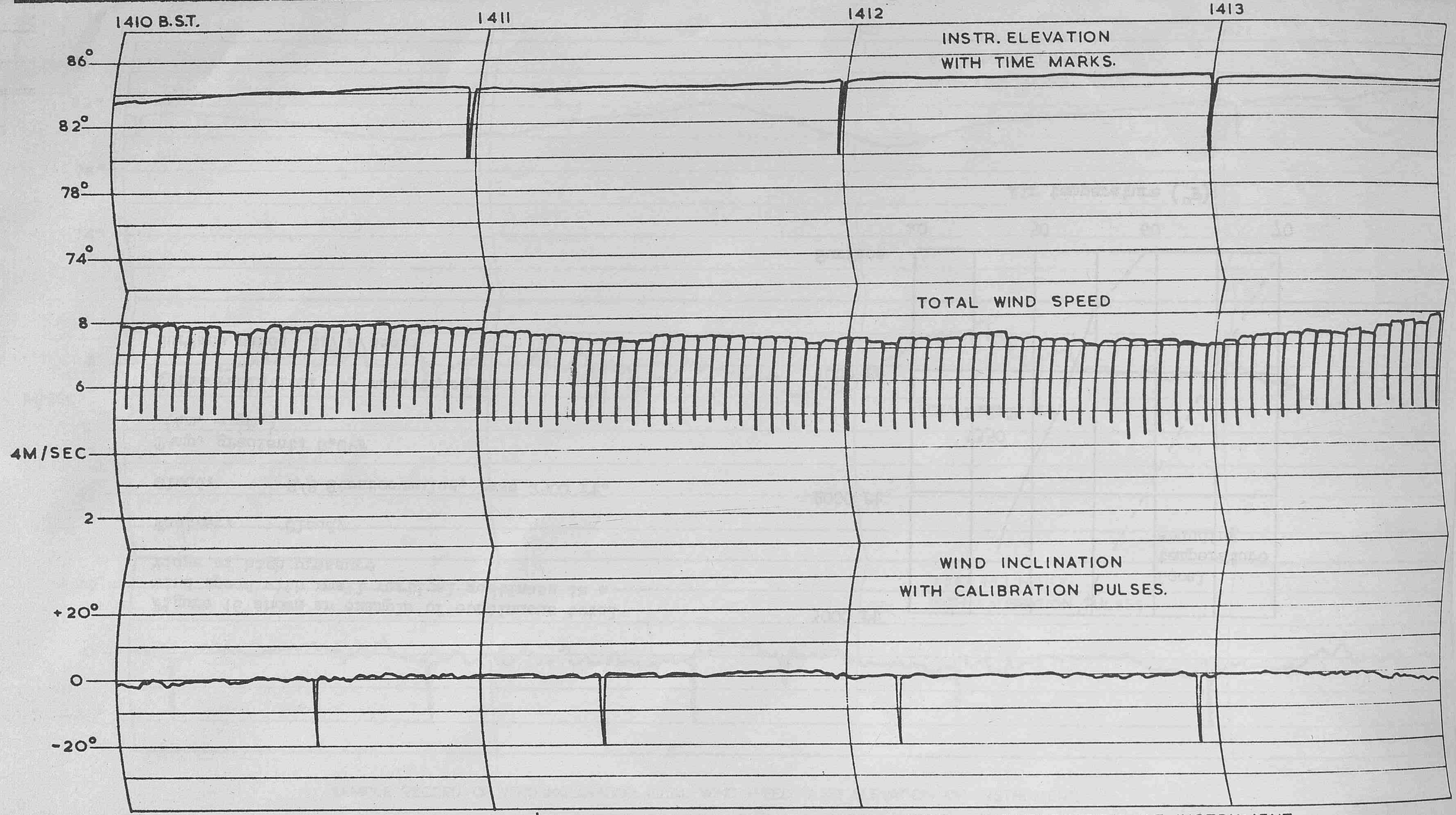

FIG.15. SAMPLE RECORD OF WIND INCLINATION, $2\frac{1}{2}$ SECOND MEANS OF TOTAL WIND SPEED, AND ELEVATION OF INSTRUMENT, AT CARDINGTON ON 16 SEPTEMBER 1956. (AT 2000 FT.)

Figure 16 shows an example of continuous total wind speed with small vertical gustiness in a ridge of high pressure

Weather: Cloudy

Cloud: 8/8 Stratocumulus, base 2500 ft.

Temp. gradient: 0.0°F
(4m. - $\frac{1}{2}$m.)

Total radiation: +3 m.watts/sq.cm.

Surface wind: 5.7 m/sec.

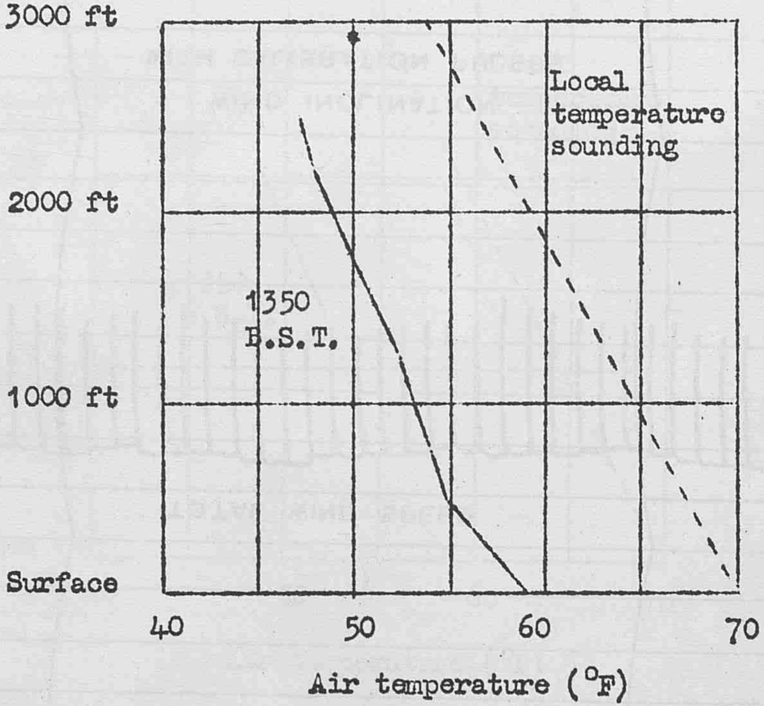

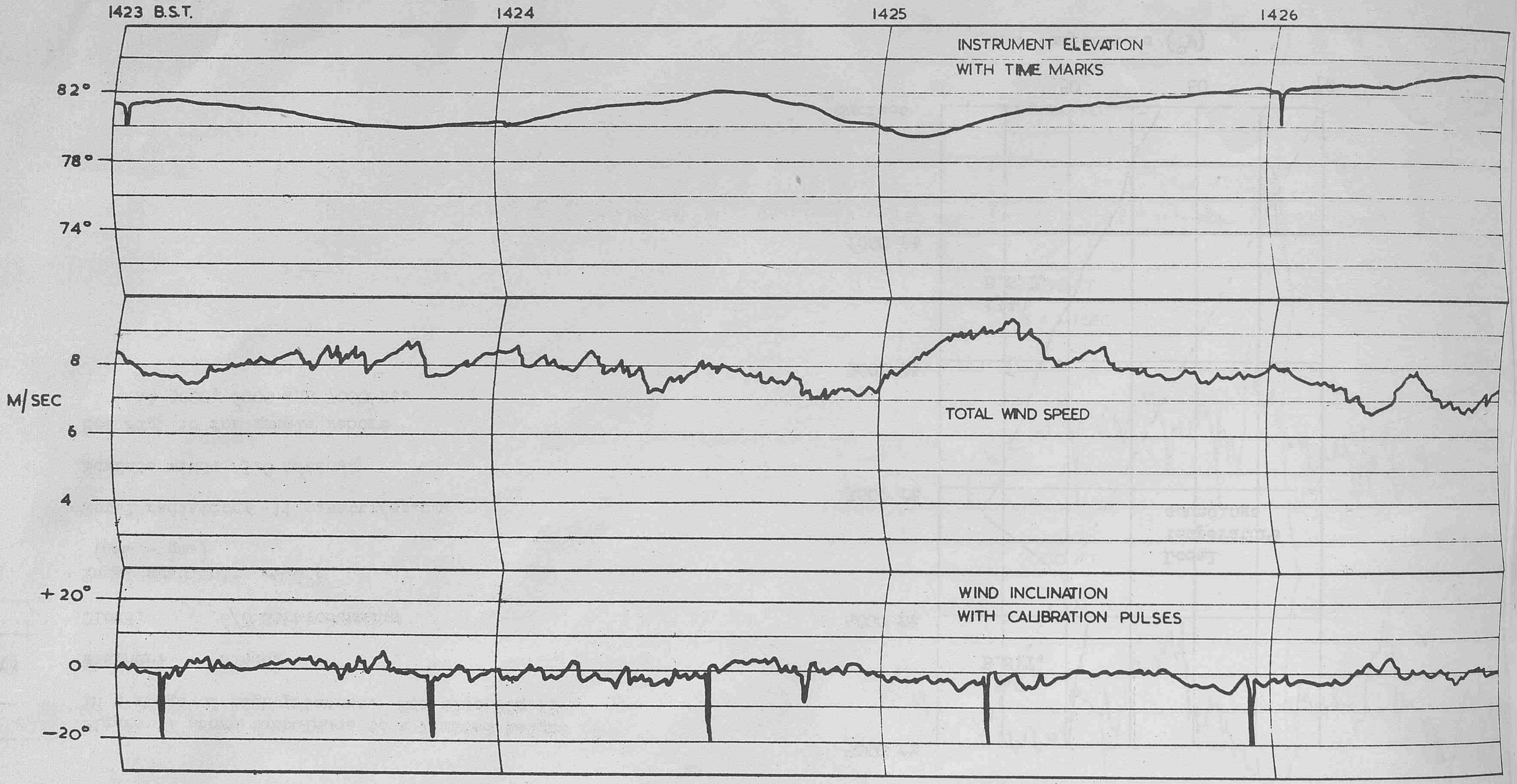

FIG. 16

SAMPLE RECORD OF WIND INCLINATION, TOTAL WIND SPEED, AND ELEVATION OF INSTRUMENT,
AT 2,000 FEET AT CARDINGTON ON 16 SEPTEMBER 1956

Figure 17 shows turbulence to a limited height in a ridge of high pressure. See also Fig.18

Weather: Cloudy

Cloud: 6/8 Stratocumulus

Temp. gradient: −0.6°F
(4m. − ½m.)

Total radiation: 11 m.watts/sq.cm.

Surface wind: 3.6 m/sec.

See Fig. 18 for sample record
at 5000, 6000 and 7000 ft.

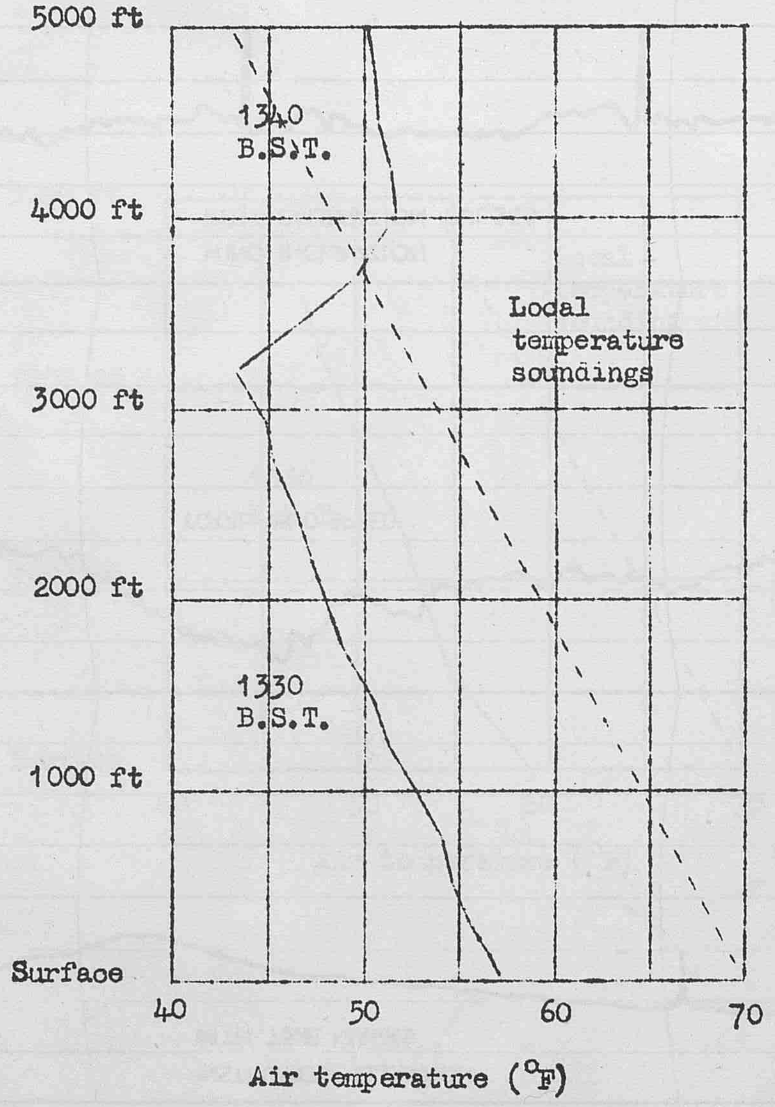

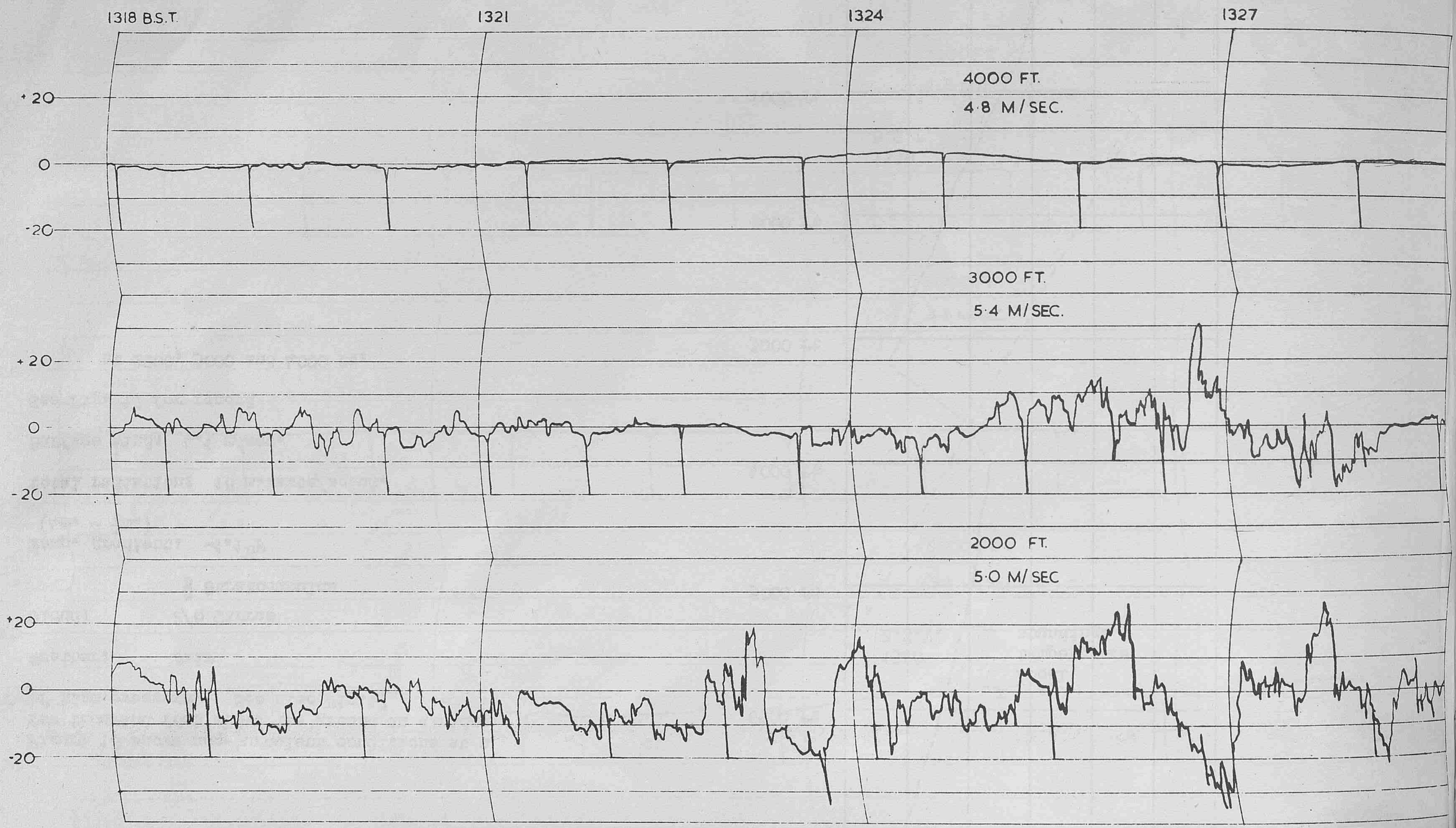

FIG.17 SAMPLE RECORD OF WIND INCLINATION AT 2000, 3000 AND 4000FT. AT CARDINGTON ON SEPT. 17TH. 1956

Figure 18 shows non-turbulent conditions at a few thousand feet above the ground in a ridge of high pressure.   See also Fig.17

Weather: Fair

Cloud: 2/8 Cirrus
$\frac{3}{8}$ Stratocumulus

Temp. gradient: -1.1 °F
(4m. - $\frac{1}{2}$m.)

Total radiation: 18 m.watts/sq.cm.

Surface wind: 4.1 m/sec.

See Fig. 17 for record

at 2000, 3000 and 4000 ft.

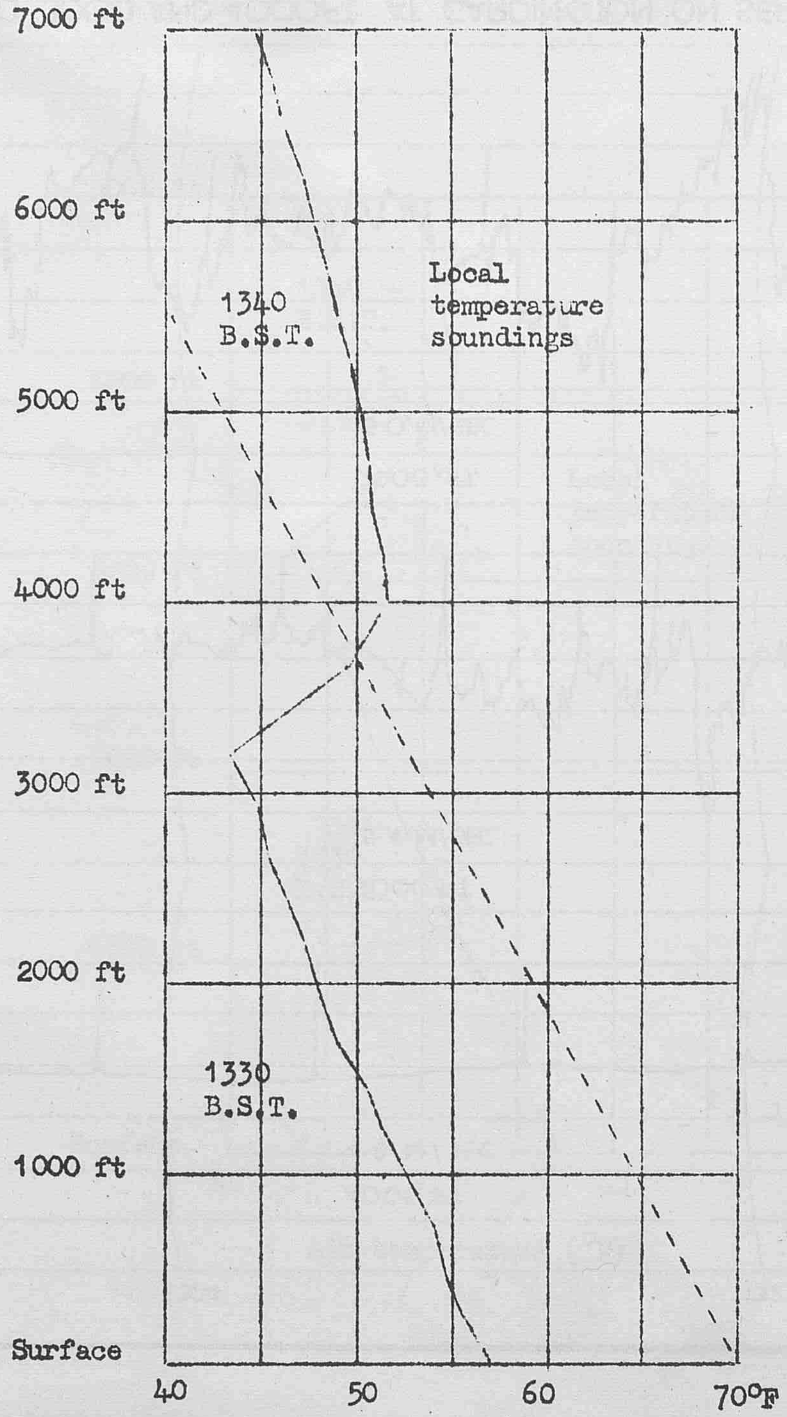

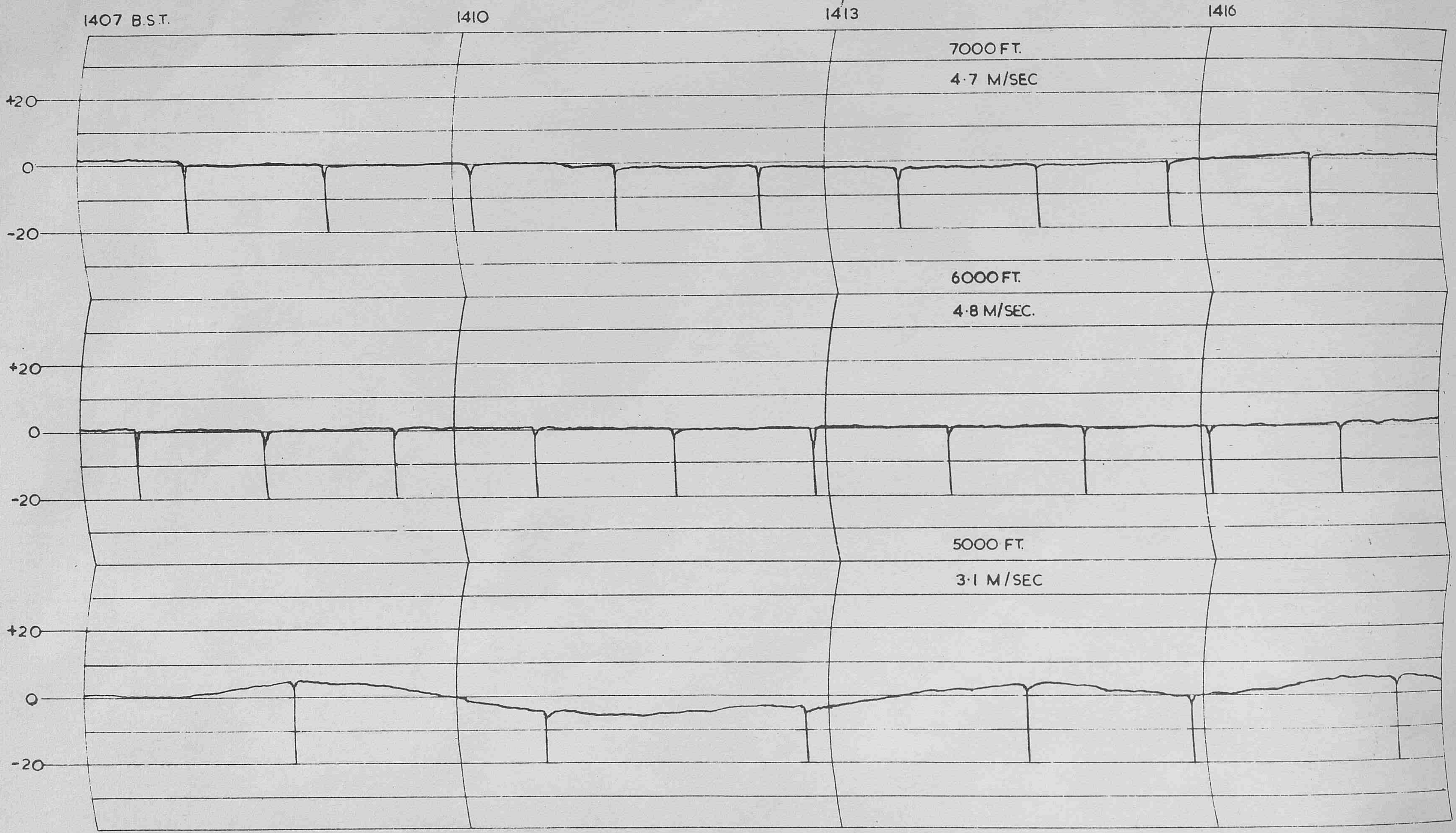

FIG. 18 SAMPLE RECORD OF WIND INCLINATION AT 5000, 6000 AND 7000 FT. AT CARDINGTON ON SEPT. 17 1956

M.R.P. 1039
S.C. III/230
18th February, 1957

A study of the average distribution of pollution around Staythorpe

by

P. J. Meade and F. Pasquill

(Meteorological Office)

AWSSS
ROUTING SLIP

FILE	INFO	ACTION			
	4.1		DIRECTOR		
			DEP DIRECTOR		
	3		ASST TO DIRECTOR		
	1		CONSULTANTS		
	2		TRSD	CHF	
				TSS	
				RRB nil	
				EDB	
				SEC	
	4		EDD	CHF	
				HLFB	
				STB	
				SPFB	
				CU	
				SEC	
6	5		TIPD	CHF	
				PUE	
				TECH INFO	
				SEC	

4.2 AWSCL

AIR MINISTRY

METEOROLOGICAL RESEARCH COMMITTEE

At the time of issue this report has not been published. Any author desiring to quote this paper should refer to it as "A paper of the Meteorological Research Committee (London), M.R.P. No. 1039 by Messrs. P.J. Meade and F. Pasquill
A copy is available in the Library of the Meteorological Office."

M.R.P. 1039
S.C.III/230
18th February, 1957

AIR MINISTRY

METEOROLOGICAL RESEARCH COMMITTEE

A study of the average distribution of pollution around Staythorpe

by

P. J. Meade and F. Pasquill (Meteorological Office)

Summary

An examination has been made of the average distribution of sulphur pollution around Staythorpe power station in relation to sulphur output and wind statistics during the period November, 1951 to September, 1954.

The data for winter and summer half-years separately are shown to support a relation, which follows from conventional treatment of diffusion from a point source, of the form

$$p = a + b\frac{f(\theta)S}{\bar{u}}$$

In this relation p is the observed pollution for the half-year, at a distance of 1,500 yards and averaged over an octant about the power station, $f(\theta)$ is the percentage frequency of occurrence of wind directions in the corresponding octant, $\bar{u}$ is the corresponding mean wind speed, and S is the average monthly output of sulphur dioxide during the half-year.

The quantity " a ", logically a "background" pollution, has values which are close to the winter and summer pollution existing immediately before the power station was commissioned. The magnitude of the coefficient " b " is shown to be consistent with previous ideas and other recent data on the vertical diffusion from an elevated point source.

1. Introduction

Over a number of years surveys of sulphur dioxide pollution around power stations have been carried out by the Central Electricity Authority and by the Fuel Research Station of the Department of Scientific and Industrial Research. Analysis of the observational data thus obtained has hitherto generally failed to reveal any significant correlation between the amount of coal consumed at a station and the average sulphur dioxide pollution as measured at a number of sites surrounding the station. It has proved difficult to account for this absence of correlation, and a number of possibilities, mainly concerned with variations in meteorological conditions from one period to another, have been suggested.

With the object of studying in more detail the meteorological effects involved and at the invitation of the Atmospheric Pollution Research Committee, the authors have examined the reports of pollution surveys round a number of power stations. The analysis of observations described in these reports consisted mainly of a direct comparison between coal consumption or sulphur dioxide output and the average values of the pollution measured at all the observing sites around each power station. It appeared, however, that such a procedure was not sufficiently detailed to permit any correlation, if one existed, to emerge.

/It

G.5914/IKW/3/57/50

It was decided therefore to examine the observations of sulphur dioxide pollution as measured at the individual sites around a power station. In this manner the pattern of pollution instead of its overall average became the main subject of investigation and the objective was to ascertain whether this pattern could be explained in terms of the total sulphur dioxide output and the local distribution of wind speed and wind direction. An investigation on these lines concerned with one power station, that at Staythorpe in Lincolnshire, is described in the present paper. Staythorpe is a country district, remote from such complicating factors as built-up areas and industrial plants, and its power station was therefore considered the most appropriate for a first or pilot investigation of this kind. Observations made before the power station was commissioned had shown a uniform distribution of sulphur dioxide pollution in the area. In the following sections the results obtained from an analysis of the Staythorpe data for the three winters and three summers from November, 1951 to September, 1954 are described.

2. The data available

In the absence of wind records for Staythorpe itself, those for the nearest meteorological station, Swinderby, were used. Staythorpe lies about 10 miles to the southwest of Swinderby and it seems highly probable that the wind conditions at the two places are closely similar.

Figure 1 shows the average SO_2 pollution around Staythorpe for each season from the summer of 1948 to the summer of 1954 and also the total coal consumption each season from the time of commissioning the power station in the summer of 1950. Thus the data in this figure, although going back well beyond the period with which the present investigation is concerned, show usefully the seasonal trend in average SO_2 pollution both before and after the power station came into operation. It will be noted from Figure 1 that each season consists of five months, the summer extending from May to September and the winter from November to March.

Table 1, which is supplementary to Figure 1, gives for each season the coal consumption and sulphur dioxide emission expressed in thousands of tons per month and in tons per month respectively.

Table 1

Fuel Consumption and Sulphur Dioxide Emission - Staythorpe

Season	Fuel consumed thousand tons/month	SO_2 emission tons/month
Winter 1951-52	25.2	273
Summer 1952	34.0	536
Winter 1952-53	49.9	881
Summer 1953	38.2	706
Winter 1953-54	51.6	1050
Summer 1954	55.3	1210

At Staythorpe concentrations of sulphur dioxide in the air are measured (Meetham, 1956) by the "lead peroxide" method. A glass or porcelain cylinder is coated with lead peroxide paste and exposed in a louvered box which ensures protection from rain while permitting the free access of air. The paste absorbs sulphur dioxide from the air to form lead sulphate. After exposure for one calendar month the cylinder is removed and analysis of the paste then gives the amount of sulphur dioxide absorbed. This quantity is expressed as milligrammes of SO_3 per day per 100 cm^2.

In Figure 2 the 14 observing sites round the power station at Staythorpe are indicated by means of small circles. The figures within the circles are the measured concentrations (in mg of SO_3/day 100 cm^2) for the winter period November, 1951 to March, 1952. Contours have been drawn to represent

/concentrations

concentrations of 0.9 and 1.0 in these units. Corresponding diagrams for the other five seasons are not reproduced but estimated concentrations derived from them are given in Tables 4 and 5. In Figure 1 the average values of pollution plotted for each season are the means of the observations recorded at all 14 sites.

The percentage frequency of winds in each octant and the weighted mean speed for each octant for the three winters and three summers respectively at Swinderby are shown in Tables 2 and 3 below. The raw data showed for each octant the total times during which the wind speed fell within the ranges 1-3, 4-6, 7-10, etc., knots and for reasons which will appear later the mean wind speed was derived from the reciprocal of the speed in the middle of each range weighted according to the given time. After the mean speeds had been calculated, the percentage of calms in a season was distributed uniformly among the eight octants which in Tables 2 and 3 are shown in clockwise order from the north.

Table 2

Swinderby Wind Distribution - Winter Seasons

	Winter 1951-52		Winter 1952-53		Winter 1953-54	
Octant	percentage frequency	mean speed (kt)	percentage frequency	mean speed (kt)	percentage frequency	mean speed (kt)
0 - 45°	4.2	5.4	10.4	7.0	6.9	6.9
45 - 90°	5.1	5.4	7.0	6.1	11.0	6.7
90 - 135°	7.4	5.4	4.1	5.1	11.2	7.6
135 - 180°	13.5	7.0	7.8	4.5	17.3	8.1
180 - 225°	21.7	9.7	24.4	7.5	26.7	9.0
225 - 270°	23.9	11.3	15.2	8.4	11.6	9.7
270 - 315°	12.7	9.5	8.1	8.3	5.8	8.8
315 - 360°	11.5	7.8	23.0	8.5	9.5	8.0

Table 3

Swinderby Wind Distribution - Summer Seasons

	Summer 1952		Summer 1953		Summer 1954	
Octant	percentage frequency	mean speed (kt)	percentage frequency	mean speed (kt)	percentage frequency	mean speed (kt)
0 - 45°	9.2	6.9	9.4	6.9	8.7	8.0
45 - 90°	6.8	5.7	6.2	5.8	2.3	4.6
90 - 135°	4.5	3.1	6.4	5.5	2.7	5.0
135 - 180°	8.2	5.3	10.6	7.3	11.0	7.2
180 - 225°	17.7	7.1	25.0	9.3	25.3	9.6
225 - 270°	24.1	9.3	21.2	9.6	22.0	10.0
270 - 315°	16.8	8.3	11.5	9.4	13.5	8.9
315 - 360°	12.7	7.1	9.7	6.6	14.5	8.3

3. Analysis procedure

In the present analysis we shall be concerned with the ground level concentration over a circle of radius x from a point source of strength Q units per second at height h. If the cloud is instantaneously narrow in the lateral (crosswind) direction, a condition which will normally hold, the integrated concentration around the circle may be taken to be equal to the concentration at distance x from an infinite crosswind line source of strength Q units/cm sec. at the same height. It then follows that the average concentration in any octant of the circle must be of the form

$$\frac{f(\theta)}{12.5} \; \frac{1}{2\pi x} \; g(h, x) \; \frac{Q}{\bar{u}} \qquad (1)$$

where: $\bar{u}$ = mean wind speed assumed constant with height
$f(\theta)$ = percentage frequency of wind directions in the corresponding octant
$g(h,x)$ = function of the vertical shape and size of the cloud. If, for example, the vertical distribution is Gaussian with standard deviation σ, the wind velocity is constant with height and the cloud is simply reflected from the ground -

$$g(h, x) = \frac{2}{\sqrt{2\pi}\,\sigma} \exp\left(-h^2/2\sigma^2\right) \qquad (2)$$

(This expression follows immediately from a crosswind integration of the point source formula deduced by Sutton (1947, equation (6), p.429) and the substitution of the form

$$\sigma^2 = \frac{1}{2} C_z^2 \, x^{2-n}$$

The pollution at Staythorpe will also include a "background" contribution, a, due to distant sources, and the total average value, p, over any octant may then be written

$$p = a + b \, \frac{f(\theta)\, S}{\bar{u}} \qquad (3)$$

where, if p and a are in units* of mg SO_3/day 100 cm², S is the number of tons of sulphur dioxide discharged per month in a particular season, and if $\bar{u}$ and x are expressed in knots and yards respectively,

$$b = 8.511 \times 10^3 \, g(h, x) \qquad (4)$$

In equation (4), $g(h, x)$ is still in c.g.s. units.

The extent to which the relation (3) is supported by the data is examined below, firstly with regard to the functional form and secondly with regard to the absolute magnitude of the quantity $g(h, x)$.

We proceeded in the following manner:-

(a) a circle was drawn round the power station on each pollution diagram (see Figure 2) to represent a distance of 1,500 yards from the station. Radial lines were also drawn in order to indicate the octants and to divide the circle into eight equal arcs.

(b) the quantity $f(\theta)S/\bar{u}$ in respect of each octant was calculated for the three winters and three summers, an allowance being made for the percentage of calms that occurred in each season.

(c) from each pollution diagram the actual seasonal concentration in each octant at a distance of 1,500 yards from the power station was estimated.

---

* For the conversion involved here a relation was supplied by the Fuel Research Station in the form: "concentration in parts per 100 million of sulphur dioxide = 4.2 x pollution in mg SO_3 /day 100 cm²".

Taking the seasons separately, the data formed 24 pairs of values of the quantity $f(\theta)\,S/\bar{u}$ and of the corresponding estimated actual concentration, the latter representing p on the left hand side of equation (3). The next stage was therefore to ascertain whether there existed between the two parameters a functional relationship of the form shown in this equation. This part of the investigation is described in the following two sections.

4. Winter pollution

The values of p and $f(\theta)S/\bar{u}$ that were tested for relationship are given in the following Table 4.

Table 4

Octant	1951-52		1952-53		1953-54	
	$\frac{f(\theta)S}{\bar{u}}$	p	$\frac{f(\theta)S}{\bar{u}}$	p	$\frac{f(\theta)S}{\bar{u}}$	p
0 - 45°	$2.12\text{x}10^2$	.80	$13.09\text{x}10^2$	.97	$10.50\text{x}10^2$	1.00
45 - 90°	2.58	.76	10.11	.97	17.24	.92
90 - 135°	3.74	.94	7.08	.98	15.47	1.10
135 - 180°	5.27	.89	15.27	1.04	22.43	1.28
180 - 225°	6.11	.95	28.66	1.12	31.16	1.35
225 - 270°	5.77	.97	15.94	1.10	12.56	1.32
270 - 315°	3.65	.96	8.60	1.00	6.92	1.29
315 - 360°	4.03	.88	23.84	.94	12.47	1.10

NOTE: The values of p (observed concentration) have been rotated through 180° in order to correspond with the wind distribution.

By the method of least squares the best straight line to fit these pairs of values of p and $f(\theta)S/\bar{u}$ was found to be:-

$$p = 0{\cdot}89 + 1{\cdot}16 \times 10^{-4}\,\frac{f(\theta)S}{\bar{u}} \qquad (5)$$

The closeness of fit may be judged from Figure 3 in which are shown the straight line given by the above equation together with a plot of all the points listed in Table 3. It will be seen that for most of the points the straight line provides a good representation. However, it seemed desirable to apply some quantitative criterion in order to estimate the extent to which the straight line does adequately represent the observations.

The most suitable index is the correlation coefficient, R, between the observed values of p and the corresponding values computed from equation (5) above. The value of R is given by

$$R = 1 - \Sigma\,\epsilon^2 / \Sigma\,p_d^2$$

where
ϵ = observed p - calculated p
p_d = observed p - $\bar{p}$
$\bar{p}$ = mean value of observed ps

Applied to the above observations and the straight line, the value of R was found to be 0.604. In the "Handbook of Statistical Methods of Meteorology", Brooks and Carruthers give, for the conditions of this problem, a value 0.404 for the 5 per cent point of R and a value 0.515 for the one per cent point of R.

The computed value of R , i.e., 0.604, is considerably better than the one per cent point and for the winter season, therefore, we may attribute some significance to the relationship,

$$p = 0\cdot 89 + 1\cdot 16 \times 10^{-4} \frac{f(\theta) S}{\bar{u}}$$

between the observed pollution at Staythorpe and a quantity based on the wind distribution and the output of sulphur dioxide at the power station.

A feature of this result is worthy of special comment. The value of the constant term (0.89) can be seen by reference to Figure 1 to approximate closely to the average pollution which existed before the power station was commissioned, i.e., when S in the above equation was zero. The fact that this constant term is so nearly equal to the original background pollution lends support to the significance of the equation.

5. Summer pollution

For the summer seasons, the values of p and $f(\theta) S/\bar{u}$ that were tested for relationship are given in Table 5.

Table 5

Octant	1952		1953		1954	
	$\frac{f(\theta)S}{\bar{u}}$	p	$\frac{f(\theta)S}{\bar{u}}$	p	$\frac{f(\theta)S}{\bar{u}}$	p
0 - 45°	7.15x10^2	.27	9.62x10^2	.42	13.16x10^2	.58
45 - 90°	6.39	.26	7.54	.36	6.05	.44
90 - 135°	7.78	.37	8.21	.47	6.53	.46
135 - 180°	8.29	.35	10.25	.54	18.49	.44
180 - 225°	13.37	.42	18.98	.72	31.88	.78
225 - 270°	13.89	.40	15.59	.67	26.62	.74
270 - 315°	10.85	.34	8.64	.56	18.35	.63
315 - 360°	9.59	.28	10.38	.50	21.13	.64

NOTE: The values of p (observed concentration) have been rotated through 180° in order to correspond with the wind distribution.

As for the winter data, the method of least squares was again used and gave the following straight line equation:-

$$p = 0\cdot 26 + 1\cdot 78 \times 10^{-4} \frac{f(\theta) S}{\bar{u}} \qquad (6)$$

This line is shown in Figure 4 where the points of Table 5 are also plotted and can be seen to conform reasonably well with the straight line.

The correlation coefficient R, computed in the manner described in the proceding section, was found to be 0.804, i.e., a value considerably better than the one per cent point of R (0.515) and therefore significant. The constant term (0.26) can be seen from Figure 1 to be approximately equal to the summer background pollution before the power station began to function, a result which corresponds with that found in the winter analysis.

6. The magnitude of $g(h, x)$ and associated diffusion parameters

Our analysis has so far been confined to the functional form of the relationship between pollution and the conditions of output and wind distribution. We now seek to extend the analysis in a more explicit way, by examining the absolute values of the coefficient b in equation (3). From equations (2), (3) and (4) and from the values of b contained in equations (5) and (6), we may derive values of σ, the 'standard deviation' of the vertical distribution which the cloud must possess (apart from the effect of the boundary) in order to explain the observed pollution at ground level.

We need first to assign a value to h, the effective height of the source. This is equal to the height of the chimney added to the vertical distance by which the discharged gases are raised in consequence of their initial buoyancy and upward velocity. Several formulae are available for calculating the effective height in problems of this nature and we selected the Oakridge formula which is simple to apply and which was recommended by the Beaver Committee (1954). This formula is:-

$$uz = 1{\cdot}5\, v d + 0{\cdot}4\, Q_H \qquad \text{(c.g.s. units)}$$

where u is the wind velocity, v is the velocity of efflux of the gases, d is the chimney diameter, Q_H is the heat output in calories/sec., z is the height reached by the gases measured from the mouth of the chimney, so the effective height h is equal to z plus the chimney height.

If the air temperature is $T_1\,{}^\circ A$ and the gases are discharged at a temperature $(T_1+\Delta)^\circ A$, then assuming the gases have the same specific heat c_p and, at $T_1\,{}^\circ A$, the same density as the air,

$$Q_H = \frac{\pi}{4} d^2 v \left(\frac{T_1}{T_1+\Delta}\right) \rho\, c_p\, \Delta$$

hence

$$uz = Q_H \left\{ 0{\cdot}4 + \frac{6}{\pi}\, \frac{(T_1+\Delta)}{T_1 \rho\, c_p\, \Delta d} \right\}$$

For Staythorpe $T_1+\Delta$ = 419°A, the chimney diameter is 20 feet and Q_H is obtained from the coal consumption, each pound of coal burnt yielding 153 cu. ft. of gas at N.T.P. With these data combined with mean wind velocities for each season, an average effective height for the six seasons was derived. The value obtained for h was 504 feet and this was approximated to 500 feet for further calculations on the magnitude of $g(h,x)$ and thence of σ.

Comparisons between equations (3), (4) and (5) and between equations (3), (4) and (6) permit the following values to be derived for $g(h,x)$, for h = 500 ft and x = 1,500 yd:-

Winter $g(h,x) = 2.05 \times 10^{-5}\,\text{cm}^{-1}$

Summer $g(h,x) = 3.14 \times 10^{-5}\,\text{cm}^{-1}$

From Figure 5, a graph showing the variation of g with σ for h = 500 feet, the values of σ corresponding to these values $g(h,x)$ can be determined and are seen to be

Winter σ = 90 or 390 yards

Summer σ = 150 or 180 yards

It is common experience that the vertical component of turbulence is greater in the summer than in the winter months and as a general rule we should therefore expect the summer value of σ to be greater than the winter value. We therefore reject the value of 390 yards for winter and conclude that the true values of σ are approximately 90 yards for the winter and between 150 and 180 yards for the summer.

The results for σ refer to a distance of 1,500 yards from the source and can be converted approximately to an angular deviation given by $\tan^{-1} \sigma/1500$. The values obtained are 3.5° for the winter and between 5.7° and 6.8° for the summer months. These figures appear reasonable as regards order of magnitude and can be compared with some results recently obtained by Hay and Pasquill (1956) and reported to the Meteorological Research Committee. Their experiments, which were conducted at Porton in the early autumn, included the measurement of the vertical distribution of airborne particles released mainly at a height of 500 feet and sampled at downwind distances up to 500 metres. The results indicated that the vertical spread of the cloud of particles varied approximately linearly with the distance of travel, and the corresponding standard (angular) deviations fell in the range 1.7° to 6.0°. These values are very similar to those derived above from the Staythorpe data.

Another parameter which can be evaluated is the vertical diffusion coefficient, C_z, which occurs in Sutton's treatment of diffusion and is given by

$$C_z = \sigma \left(\frac{2}{x^{2-n}} \right)^{\frac{1}{2}}$$

Taking $n = 0.25$, $x = 1{,}500$ yards and the winter and summer values of σ in turn and working in c.g.s. units, we find

Winter $C_z = 0.37 \text{ cm}^{\frac{1}{8}} = 0.21 \text{ m}^{\frac{1}{8}}$

Summer $C_z = 0.49 \text{ to } 0.75 \text{ cm}^{\frac{1}{8}} = 0.35 \text{ to } 0.42 \text{ m}^{\frac{1}{8}}$

These values for C_z may be compared with those obtained by Stewart, Gale and Crooks (1954) from measurements of the diffusion of the gases discharged from the Harwell Pile. For distances up to 800 metres they found the following mean values of C_z

Inversion conditions	$.11 \text{ m}^{\frac{1}{8}}$
Adiabatic "	$.20 \text{ m}^{\frac{1}{8}}$
Lapse "	$.25 \text{ m}^{\frac{1}{8}}$

At greater distances, up to 1,050 metres, Stewart et al report values of $0.32 \text{ m}^{\frac{1}{8}}$ for C_z in lapse and adiabatic conditions.

The present results are thus obviously consistent with two independent experimental studies of the vertical diffusion from an elevated source. Moreover, it might even be argued that the rather greater degree of vertical diffusion implied by the present results is in keeping with the fact that they represent an average over several months whereas the results with which they are compared represent averages over the order of one hour. On the other hand it should be remembered that the treatment applied here is only approximate, especially in the sense that the influence of the variation of output and wind speed on the effective height of the source are neglected. The detailed agreement obtained is therefore to be regarded as fortuitous to some extent.

7. Concluding discussion

It has been shown that for the three winter and three summer seasons that have formed the period of this investigation, the distribution of sulphur dioxide pollution around Staythorpe was significantly related to a parameter incorporating in a simple fashion the sulphur emission at the power station and the distribution of wind speed and direction near the site. In addition, the relationship found has provided values of diffusion parameters which compare reasonably with the values obtained experimentally by other workers.

In the present analysis we have not attempted to examine the separate effects of output and wind conditions. However, from an inspection of Figures 3 and 4, bearing in mind the variation in output from year to year (see Table 1), it is fairly evident that the relation between p and $f(\theta)/\bar{u}$ alone would be less systematic than that between p and $f(\theta)S/\bar{u}$.

This investigation, which has been based on a detailed study of the pattern of pollution around a power station, has led to conclusions which could not have been drawn from a consideration of the average pollution in the area. Our results therefore suggest that the average pollution, which is commonly used in studies of this kind and is in fact the unweighted mean of readings taken at various distances from a power station, may prove misleading both for year by year comparisons at one power station and for comparisons between different power stations. Consideration might well be given to devising a system of weighting the individual observations in accordance with the wind distribution and the distance from the source before local averages are worked out.

8. Acknowledgement

We are glad to acknowledge the assistance of the Central Electricity Authority and of the Fuel Research Station for providing much of the data used in this investigation.

References

1. Meetham, A.R. Atmospheric Pollution (Pergamon Press, 1956) p.167.
2. Sutton, O.G. 1947 Quart J. R. Met. Soc., London, 73, pp.426-436.
3. Final Report of Government Committee on Air Pollution. Cmd.9322 (H.M. Stationery Office, 1954).
4. Hay, J.S. and Pasquill, F. 1956 Measurements of the short range diffusion of airborne particles at a height of a few hundred feet in the atmosphere. Meteorological Research Papers, Air Ministry, London, No. 1006.
5. Stewart, N.G., Gale, H.J. and Crooks, R.N. 1954 The atmospheric diffusion of gases discharged from the chimney of the Harwell Pile (BEPO). A.E.R.E. Report HP/R.1452.

M.R.P. 1039

STAYTHORPE POWER STATION

Seasonal Coal Consumption and Pollution Averages

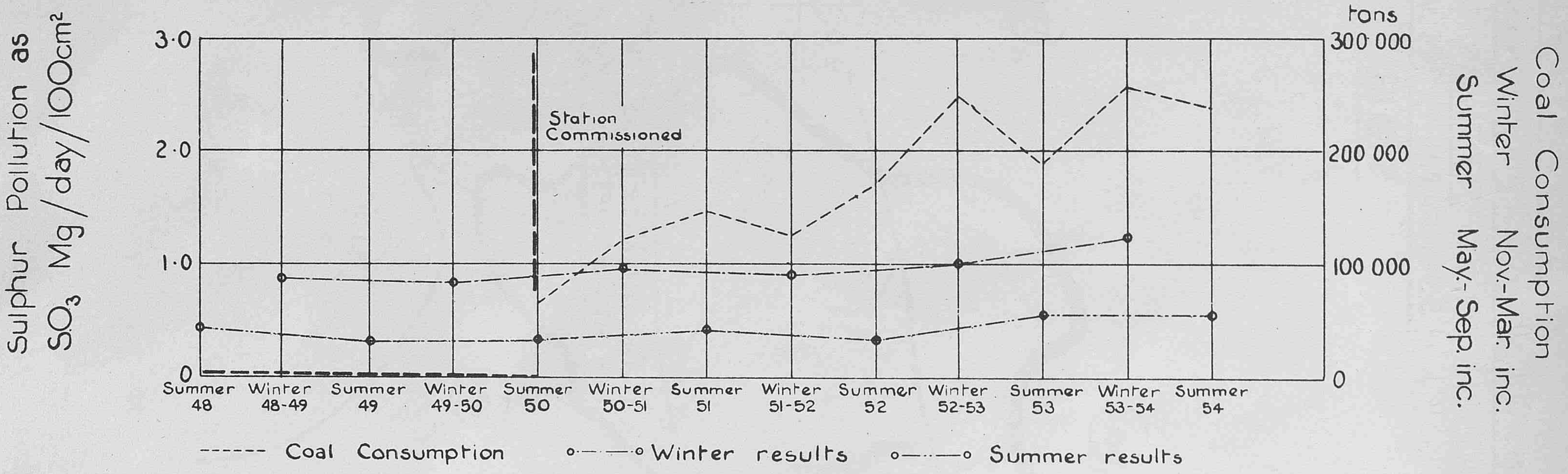

Figure 1.

M.R.P. 1039

STAYTHORPE

Sulphur Dioxide as mg. SO_3/day/100 cm.^{2}

WINTER

Nov. 1951 – Mar. 1952

FIG. 2.

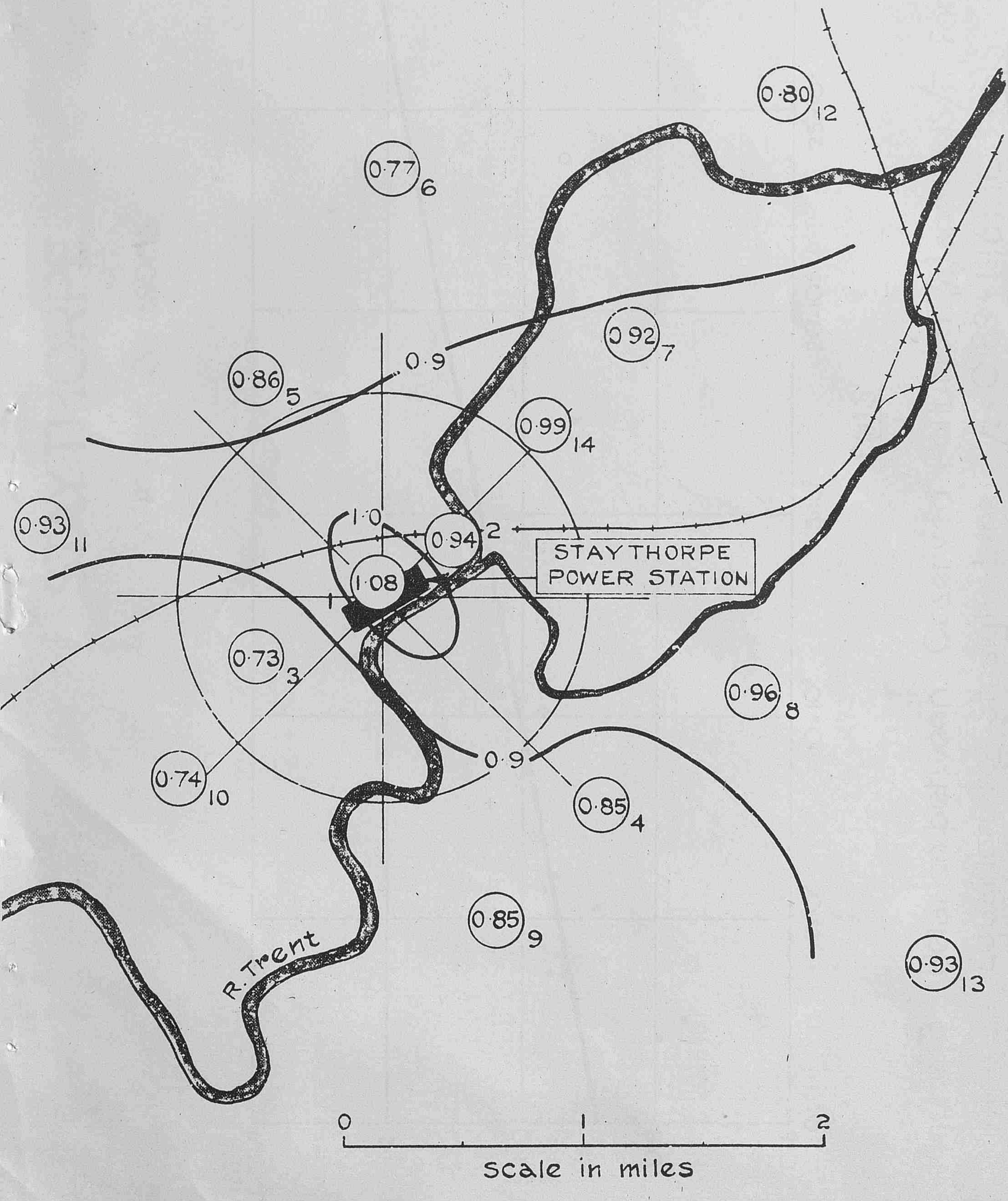

0·80 12
0·77 6
0·92 7
0·9
0·86 5
0·99 14
0·93 11
1·0
0·94 2
STAYTHORPE POWER STATION
1·08
1
0·73 3
0·96 8
0·9
0·74 10
0·85 4
0·85 9
R. Trent
0·93 13
0
1
2
scale in miles

STAYTHORPE

Winter Seasons

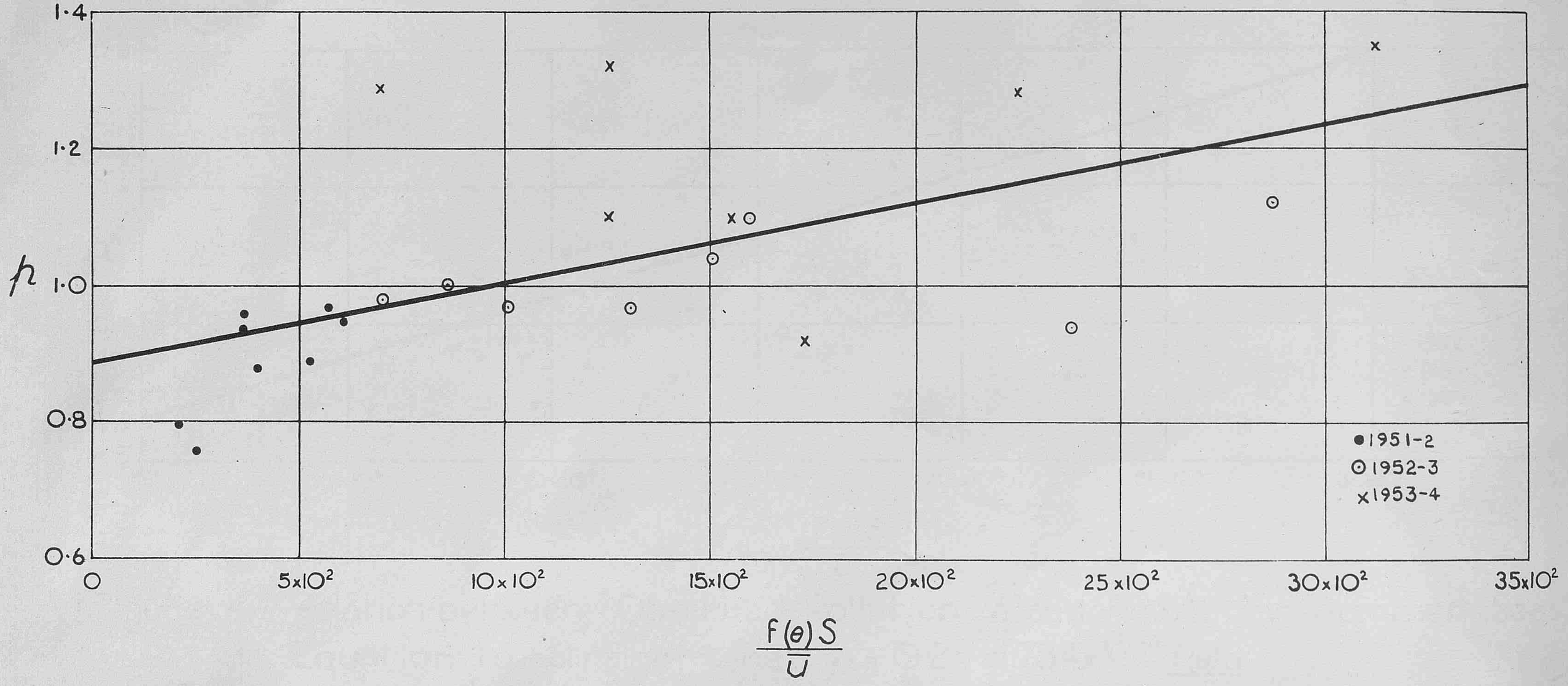

Figure 3 Relation between Observed Pollution (h) and $f(\theta)S/\bar{u}$ for Winter Seasons
Equation to Straight Line $h = 0{\cdot}89 + 1{\cdot}16 \times 10^{-4} \frac{f(\theta)S}{\bar{u}}$

STAYTHORPE

Summer Seasons

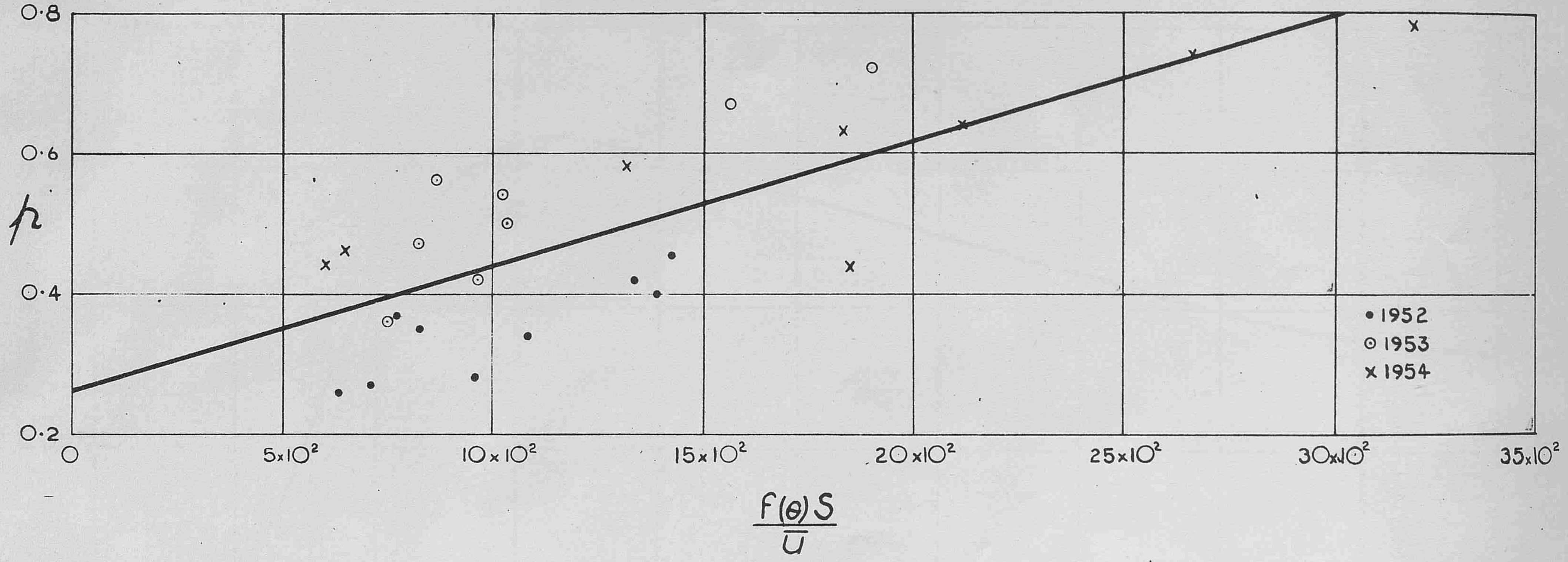

Figure 4. Relation between Observed Pollution (h) and $f(\theta)S/\bar{u}$ for Summer Seasons.
Equation to Straight Line $h = 0{\cdot}26 + 1{\cdot}784 \times 10^{-4} \frac{f(\theta)S}{\bar{u}}$

$$g = \frac{2}{\sqrt{2\pi}\,\sigma} e^{-\frac{h^2}{2\sigma^2}} \text{ in c.g.s. units}$$

$$g = \frac{8{\cdot}75 \times 10^{-3}}{\sigma} e^{-\frac{h^2}{18\sigma^2}}$$

h in feet
σ in yards

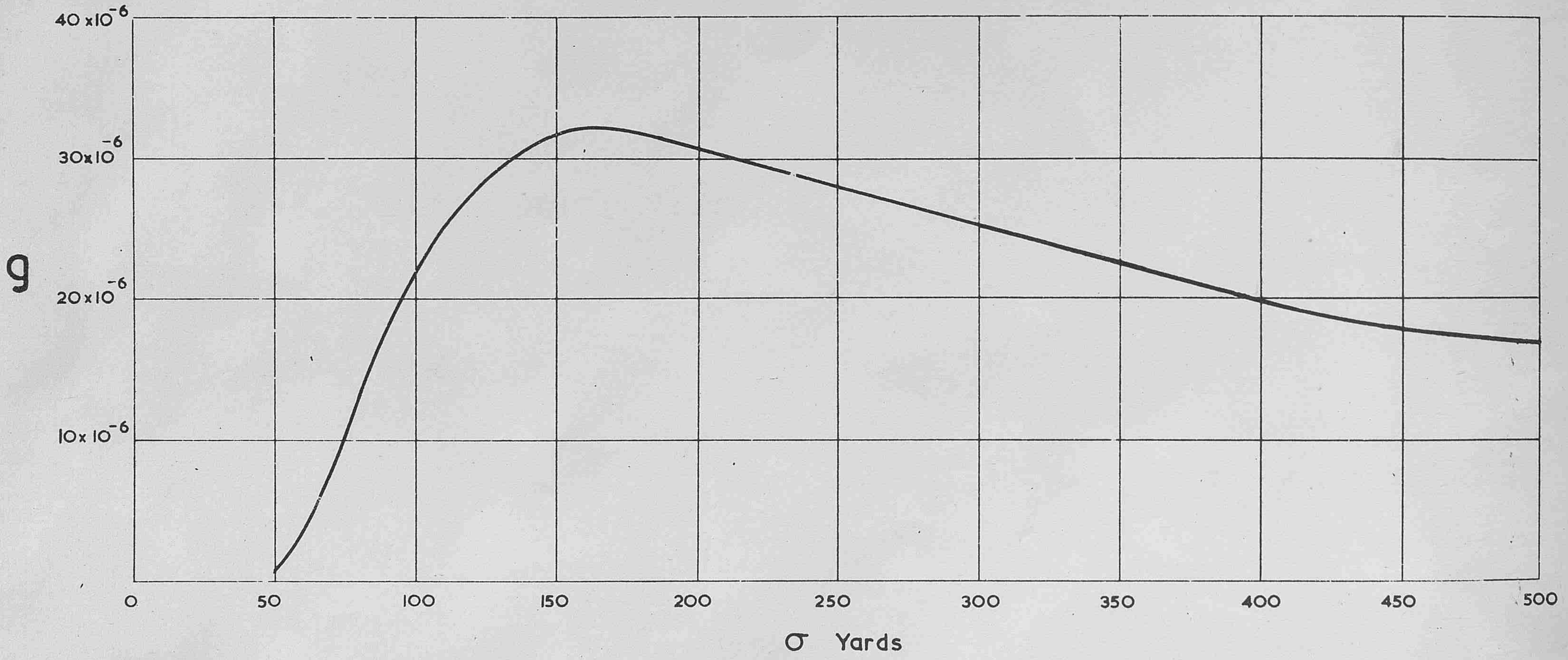

FIGURE 5 Variation of g with standard deviation, σ for h = 500 feet.

AD No, 139541

M.R P. 1040
S.C. 11/230
19th February, 1957

AD 139541

The representation of circumpolar 500 mb charts by a series of spherical harmonics

by

A. Gilchrist

(Meteorological Office)

AIR MINISTRY

METEOROLOGICAL RESEARCH COMMITTEE

At the time of issue this report has not been published. Any author desiring to quote this paper should refer to it as "A paper of the Meteorological Research Committee (London), M.R.P. No. 1040 by Mr. A. Gilchrist. A copy is available in the Library of the Meteorological Office."

M.R.P. 1040
S.C.II/230
19th February, 1957

AIR MINISTRY

METEOROLOGICAL RESEARCH COMMITTEE

The representation of circumpolar 500 mb charts by a series of spherical harmonics

by

A. Gilchrist (Meteorological Office)

1. Introduction

Though it was intended to use the results to investigate the feasibility of making a numerical index of charts, the mathematical representation of 500 mb charts was undertaken mainly with a view to using the representations in numerical forecasting. It is hoped that this will reduce the number of variables that have to be dealt with (as compared with finite difference methods of integrating the dynamical equations), and thus lead to a method applicable to medium range forecasting. The representations have been made in terms of surface spherical harmonics, because, being functions of co-latitude and longitude only on a sphere, they are naturally suited to the purpose, and because both the derivation of the geostrophic vorticity from the height field and the reverse process are then comparatively simple. Previous work on the use of spherical harmonics to represent meteorological charts has been reported by Haurwitz and Craig (1952) and Blinova (1943).

2. Surface spherical harmonics

Surface spherical harmonics Y_n^m of integral degree n, and order m satisfy the equation,

$$\nabla_S^2 Y_n^m + \frac{n(n+1)}{R^2} Y_n^m = 0 \qquad \text{----- (1)}$$

where ∇_S^2 is the Laplacian operator on the surface of the sphere of radius R, and we take m to be a positive integer less than or equal to n (a positive integer), or zero.

The usual form taken for the Y_n^m's is

$$P_n^m(\cos\theta)\left\{a_n^m \cos m\phi + b_n^m \sin m\phi\right\}$$

where θ is the co-latitude, ϕ is the longitude and a_n^m and b_n^m are arbitrary constants. $P_n^m(\cos\theta)$ is the Associated Legendre Function of degree n and order m. We shall deal throughout with the semi-normalised functions which are such that the mean value of $\left\{P_n^m(\cos\theta) \begin{matrix}\sin m\phi \\ \cos m\phi\end{matrix}\right\}^2$ over the unit sphere is $\frac{1}{2n+1}$. These functions have been tabulated to P_6^6 by Schmidt (1935). For the present investigation the tables were extended to P_{12}^{12} using the coefficients calculated by Doodson (1936). They were evaluated on the Manchester University Electronic Computer.

It may be helpful to recall briefly the form of the function

$$P_n^m(\cos\theta)\left\{a_n^m\cos m\phi + b_n^m\sin m\phi\right\}$$

It vanishes along ($n-m$) circles of latitude, symmetrically placed with respect to the equator, and if $m \neq 0$, its value at the poles is also zero; also along m great circles through the poles, the angle between any two consecutive great circles being π/m. If $m = 0$, the function is called a zonal harmonic, and the value along any line of latitude is constant. If $m = n$, there are no zeros along lines of latitude, and the function is called a sectorial harmonic. Otherwise the function is called a tesseral harmonic. For illustration Fig.1 shows $P_8^2 \sin 2\phi$ drawn on a circumpolar chart.

Spherical harmonics are orthogonal and have the property that in fitting a completely defined function, the coefficient of a harmonic found by least squares does not depend on the number of harmonics used to fit the function. This is true for instance also in ordinary Fourier analysis where if $f(\theta)$ is perfectly represented by the infinite series

$$a_0 + \sum_{r=1}^{\infty}\left(a_r\cos r\theta + b_r\sin r\theta\right)$$

and is approximated by a series containing ($2s + 1$) coefficients which are determined by least squares so that

$$f(\theta) \doteqdot a_0' + \sum_{r=1}^{s}\left(a_r\cos r\theta + b_r\sin r\theta\right)$$

then $$a_0 = a_0', \quad a_r = a_r', \quad b_r = b_r'$$

For ordinary Fourier analysis this is also true when the initial function is not known everywhere, but only at equally spaced values of θ. However, it is not true in this case for spherical harmonics; if a function is known at a network of points over a sphere the values of the coefficients found by the least squares criterion are dependent on the number of harmonics.

The method of spherical harmonic analysis used in the cases so far considered is that due to Schuster (1902). It involves the following steps

(1) plain harmonic analysis of the contour heights around lines of latitude, giving coefficients $a_m(\theta_\ell)$, $b_m(\theta_\ell)$ where θ_ℓ denotes the particular line of latitude, and m the order of the harmonic

(2) a modified harmonic analysis of corresponding harmonic coefficients $a_m(\theta_1)$, $a_m(\theta_2)$ -- or $b_m(\theta_1)$, $b_m(\theta_2)$ --- given by (1); if m is even the analysis being carried out in sines only, if odd in cosines only

(3) the use of Schuster's coefficients, which effectively substitute for $\cos r\theta$ or $\sin r\theta$ in terms of Associated Legendre Polynomials of any given order. Schuster gives the coefficients necessary to determine the coefficients up to P_{12}^{12}. His method is not a least squares method. The coefficients obtained by it do not depend on the number of harmonics used in the representation and are, in general, not the best possible ones. However it was considered that in the first stages of this investigation, flexibility and ease of fitting were more important than best possible fit, and Schuster's method has just these advantages.

The harmonic coefficients a_n^m, b_n^m given by Schuster's method depend only on the values of the $a_m(\theta)$ and $b_m(\theta)$ of stage (1).

/That is

That is, $\{A_m(\theta)\cos m\phi + B_m(\theta)\sin m\phi\}$ is fitted by

$$\left\{a_m^m P_m^m + a_{m+2}^m P_{m+2}^m + \dots\right\}\cos m\phi + \left\{b_m^m P_m^m + b_{m+2}^m P_{m+2}^m + \dots\right\}\sin m\phi$$

where $\sum_{m=0}^{\infty}\{A_m(\theta)\cos m\phi + B_m(\theta)\sin m\phi\}$ defines the initial function completely. For this reason, when considering the goodness of fit, it is convenient to treat each order m separately.

3. The representations

Four 500 mb hemispherical charts have been analysed, viz., those for

I 0300Z 28th January, 1953 II 0300Z 9th November, 1953
III 0300Z 27th February, 1953 IV 0300Z 29th June, 1953.

These data were analysed because they had previously been subjected to plane harmonic analysis along lines of latitude. Initially the values of the 500 mb heights were read off at 5° intervals of latitude and longitude from circumpolar charts. Near the equator, where no values were given on the charts, convenient values were supplied. It was assumed that the Southern Hemisphere pattern was a mirror image of the Northern Hemisphere one, and so the representations involve only even spherical harmonics (i.e., $n - m$ is even). The fitting of the four cases was carried out on the Manchester University Electronic Computer; a programme which synthesised the charts, given the spherical harmonic coefficients, was also operated.

Fig. 2, 5, 8, 11 show the circumpolar charts which were represented; Fig. 3, 6, 9, 12 the representations with harmonics up to P_{12}^{12} (91 coefficients); Fig. 4, 7, 10, 13 the representations with harmonics up to P_8^8 (45 coefficients). The fitting is considerably more successful in cases I and III than in II and especially IV. Case IV is a summer situation and in summer the average wavelength between troughs is less than in other seasons. Generally, short wavelength features are absent from or only inadequately represented on the reconstructed charts. To fit them adequately would require the inclusion of higher harmonics, though a better method of fitting (e.g., a least squares method with some weighting towards middle latitudes) should be able to include more of them without an increase in the number of coefficients.

It is usual in measuring the adequacy of a fit by ordinary harmonic analysis to make use of the theorem that, if x_i are $(2n+1)$ equally spaced values, $\bar{x}$ is their mean, and A_i, B_i are the harmonic coefficients of order i derived by least squares then

$$\sum_{i=0}^{2n}(x_i - \bar{x})^2 = \sum_{i=1}^{n}(A_i^2 + B_i^2)$$

There is an equivalent integral theorem for surface spherical harmonics; this is

$$\int_S f^2\,ds = (a_0^0)^2 + \sum_{n=1}^{\infty}\sum_{m=0}^{n}\left\{(a_n^m)^2 + (b_n^m)^2\right\}$$

where the integral of f^2 is taken over the surface of the sphere and a_p^q, b_p^q are the coefficients of the normalised spherical harmonics of order q and degree p fitted by least squares.

The corresponding equation for discrete values of the function f is not strictly true, and, further, does not hold in the present examples because Schuster's method is not a least squares one. However it has been assumed to hold sufficiently nearly to provide a reasonable method of judging goodness of fit when used comparatively; for instance, from it we can obtain information about whether one order is fitted more closely than another; but, on the other hand, it would be wrong to assume that if, for example, the sum of the squares of the normalised harmonic coefficients came to 99 per cent of the initial total variance, then only 1 per cent remained to be fitted.

Tables I–IV summarise the variances and residual variances for the four cases.

Table I – The variance of the initial function over the sphere omitting that due to the variation of mean height in the N.–S. direction

	Case I	Case II	Case III	Case IV	
V_T(Total variance)	117,347	96,884	129,844	38,968	
V_{12}(Variance up to harmonic 12)	116,583	95,928	128,702	38,626	
V_{12}/V_T x 100	99.35%	99.01%	99.12%	99.12%	Units (ft)^2
V_8 (Variance up to harmonic 8)	114,984	94,802	127,394	36,961	
V_2/V_T x 100	97.99%	97.85%	98.11%	94.85%	

These variances have been derived from the plane harmonic analysis along lines of latitude.

$$V_T = \frac{\sum_\theta V_\theta \sin\theta}{\sum_\theta \sin\theta} = \frac{\sum_\theta \sum_n \left\{ a_n^2(\theta) + b_n^2(\theta) \right\} \sin\theta}{\sum_\theta \sin\theta}$$

where θ is the co-latitude and V_θ is the total variance along the line of latitude defined by θ = const. V_{12} and V_8 are derived in the same way, but using the variance accounted for by harmonics 0–12 and 0–8 respectively, in the initial plane harmonic analysis.

Table II – Variance due to the N.–S. variation of mean 500 mb height averaged around a line of latitude

	Case I	Case II	Case III	Case IV	
V_T (Total variance)	1170510	1066409	1536725	174411	
V_{12}	1129	1232	452	49	Units (ft)^2
V_8	3399	3129	132	255	

These variances were derived giving equal weight to each line of latitude

$$\text{i.e.,}\quad V_T = \frac{1}{n}\sum_{\theta}\left\{\bar{h}_\theta - \frac{\sum_{\theta}\bar{h}_\theta}{n}\right\}^2$$

where n is the number of lines of latitude considered and $\bar{h}_\theta$ is the mean height around the line of latitude θ = constant. V_{12} and V_8 are the variances not accounted for by the zonal harmonics 0-12 and 0-8 respectively,

$$\text{i.e.,}\quad V_{12} = \frac{1}{n}\sum\left(\bar{h}_\theta - \sum_{0}^{12} a_n P_n^0\right)^2$$

/Table III

Table III - The variance associated with the separate orders in the plane harmonic analysis, and the amount not accounted for in the spherical harmonic analysis (neglecting N.-S. variation of mean 500 mb height)

		Case I		Case II		Case III		Case IV	
		variance	% of total	variance	% of total	variance	% of total	variance	% of total
	V_{T1} x 100	54621	46.55	42192	43.55	22246	17.13	92244	23.67
Order 1	V_{12}	555	.46	612	.63	142	.11	318	1.59
	V_8	2669	2.27	3597	3.71	3758	2.89	1658	4.25
	V_{T2}	19969	17.02	19350	19.97	61097	47.05	7634	19.59
	V_{12} x 100	1079	.92	1227	1.27	179	.14	1280	3.28
2	V_8	1206	1.03	1447	1.49	356	.27	1520	3.90
		17868	15.23	6502	6.71	32313	24.89	7359	18.88
		858	.73	1307	1.35	510	.39	372	.97
3		3031	2.58	2583	2.67	1294	1.00	1308	3.35
		12211	10.41	5563	5.74	1810	1.39	8211	21.07
		394	.34	14	.01	430	.33	227	.58
4		2536	2.16	3556	3.67	910	.70	1923	4.93
		3175	2.71	9264	9.56	4361	3.36	1610	4.13
		279	.24	1344	1.39	382	.29	840	2.18
5		2994	2.55	6084	6.28	2059	1.59	1444	3.71
		3352	2.86	1365	1.41	3503	2.70	968	2.48
		208	.18	163	.17	826	.64	207	.53
6		1332	1.14	507	.52	1998	1.54	406	1.04
		2788	2.38	9365	9.67	1209	.93	1536	3.94
		1185	1.01	1755	1.81	902	.69	248	.64
7		2671	2.28	8615	8.89	1124	.87	1485	3.81
		1021	.87	1053	1.09	851	.66	399	1.02
		592	.50	678	.70	714	.55	239	.61
8		882	.75	1035	1.07	849	.65	381	.98
		520	.44	504	.52	745	.57	1196	3.07
		134	.11	421	.43	471	.36	803	2.06
9		520	.44	504	.52	745	.57	1196	3.07
		513	.44	488	.50	312	.24	216	.55
		460	.39	425	.44	201	.15	179	.46
10		513	.44	488	.50	312	.24	216	.55
		349	.30	181	.19	167	.13	65	.17
		342	.29	178	.18	165	.13	63	.16
11		349	.30	181	.19	167	.13	65	.17
		222	.19	168	.17	80	.06	189	.48
		215	.18	166	.17	70	.06	189	.48
12		222	.19	168	.17	80	.06	189	.48

Units $(ft)^2$

% of total variance accounted for using harmonics up to 12	92.7	90.4	95.3	86.3

$$V_{T_m} = \frac{\sum_\theta V_{\theta m} \sin\theta}{\sum_\theta \sin\theta} = \frac{\sum_\theta \{a_m^2(\theta) + b_m^2(\theta)\} \sin\theta}{\sum_\theta \sin\theta}$$

where $V_{\theta m}$ is the variance around line of latitude θ = constant due to the mth harmonic.

$$(V_{12})_m = V_{T_m} - \sum_{n=m}^{12} \frac{\{(a_n^m)^2 + (b_n^m)^2\}}{2n+1}$$

$$(V_8)_m = V_{T_m} - \sum_{n=m}^{8} \frac{\{(a_n^m)^2 + (b_n^m)^2\}}{2n+1}$$

Table IV shows the average and the maximum percentage (over the 4 cases) of the total variance still to be accounted for in the various orders after fitting with harmonics up to P_{12}^{12}.

Table IV - Percentage variance in each order not accounted for in the fitting

Order	1	2	3	4	5	6	7	8	9	10	11	12
Average	.70	1.40	.86	.32	1.0	.38	1.04	.59	.74	.36	.19	.22
Maximum	1.59	3.28	1.35	.58	2.18	.64	1.81	.70	2.06	.46	.29	.48
No. of harmonics	6	6	5	5	4	4	3	3	2	2	1	1

It is seen that the greatest average percentages occur for orders 2,3, 5 and 7. The increase between 6 and 7 is shown by all four cases, and presumably arises because of the decrease from 4 to 3 in the number of harmonics. For order 7 there are only harmonics P_7^7, P_9^7, P_{11}^7 and of these, as explained below, P_7^7 makes a negligible contribution. The maximum for order 9 is for case IV, the only summer situation represented. In summer a larger number of troughs is likely to appear in the hemispherical pattern than at other periods of the year, and this must lead to an increased prominence of the higher harmonics.

It is notable how small a part the sectorial harmonics play in the representations. This is not surprising in view of their form over the sphere. Table V shows the average and maximum contribution of the sectorial harmonics to the total variance.

Table V - Contribution of sectorial harmonics to the total variance

Order	1	2	3	4	5	6	7	8	9	10	11	12
Average	4.6%	1.8%	2.2	.3	.2	.2	.3	0	.1	0	0	0
Maximum	12.2	4.6	3.6	.6	.4	.3	.8	.1	.1	0	0	0

The contribution becomes negligible after the third or fourth harmonic, and we could clearly omit most of the sectorial harmonics without significant loss.

In judging the adequacy of the representations, it has to be remembered that when using them to provide numerical forecasts, it is necessary to derive the vorticity field from the height field. The variance contribution of a particular harmonic to the vorticity field is $\{n(n+1)\}^2$ times its contribution to the height field, where n is the degree of the harmonic, so that terms whose numerical values are small may be important in the vorticity field if they are associated with a large n. In practice, it might be expedient to use different numbers of harmonics for the height and vorticity fields in the forecasting problem. We would then attempt to include a small wavelength feature in the vorticity field, while omitting it from the wind field.

4. Use of spherical harmonic representations

The representations might be used to select circumpolar charts which have basic similarities, possibly for use in some form of analogue forecasting. The spherical harmonic coefficients a_n^m, b_n^m would then form the basis of a numerical index, and analogous charts would be found by considering the magnitudes of corresponding coefficients.

It is intended to use the representations to solve the barotropic equation for the hemisphere. The equation which will be dealt with is

$$\nabla^2 \frac{\partial h}{\partial t} = -\frac{f}{g} J(h, \nabla_s^2 h) - J(h, f)$$

when h is the contour height and f the Coriolis parameter.

If h has been expressed in terms of spherical harmonics, $\nabla_s^2 h$ is easily obtained from equation (1). The right hand side then contains products of spherical harmonics; with suitable 'interaction' coefficients it may be expressed as a sum of spherical harmonics. Then using the integral form of equation (1)

$$\frac{1}{\nabla_s^2} Y_n^m = \frac{R^2}{n(n+1)} Y_n^m + F, \quad \text{where } \nabla^2 F = 0$$

$\partial h/\partial t$ can be found. The success of the method depends upon obtaining a sufficiently accurate initial representation without the number of 'interaction' coefficients becoming prohibitively large.

5. Conclusions

By using the even spherical harmonics up to P_8^8 and P_{12}^{12}, adequate representation of the largest features of the 500 mb hemispherical flow have been obtained, but even in the representations using harmonics to P_{12}^{12}, some features which appear to be important synoptically are not reproduced in the representations.

Further investigations using more harmonics, and better methods of fitting are needed.

Acknowledgement

The author is indebted to Miss M. K. Hinds and Mr. F. H. Bushby for help in preparing and testing the electronic computer programmes.

/References

References

Blinova	1943	"A hydrodynamical theory of pressure and temperature waves and of centres of action." C.R. Acad.Sci., U.R.S.S., 39, 257.
Doodson	1936	Phil. Trans. Roy. Soc., Series A, Vol.235, p.338.
Haurwitz and Craig	1952	"Atmospheric flow patterns and their representation by spherical surface harmonics." Geophysical Research Paper No. 14, Cambridge, Mass.
Schmidt	1935	"Tafeln der Normierten Kugelfunktionen, Goth, Engelhard-Reyher.
Schuster	1902	"On some definite integrals, and a new method of reducing a function of spherical coordinates to a series of spherical harmonics." Phil.Trans.Roy.Soc., Series A, Vol. 200, p.181.

M.R.P. 1040

obtained from equation
with suitable 'interaction' coefficients it may be expressed

Fig. 1

DIAGRAM OF $P_8^2 \sin 2\Phi$

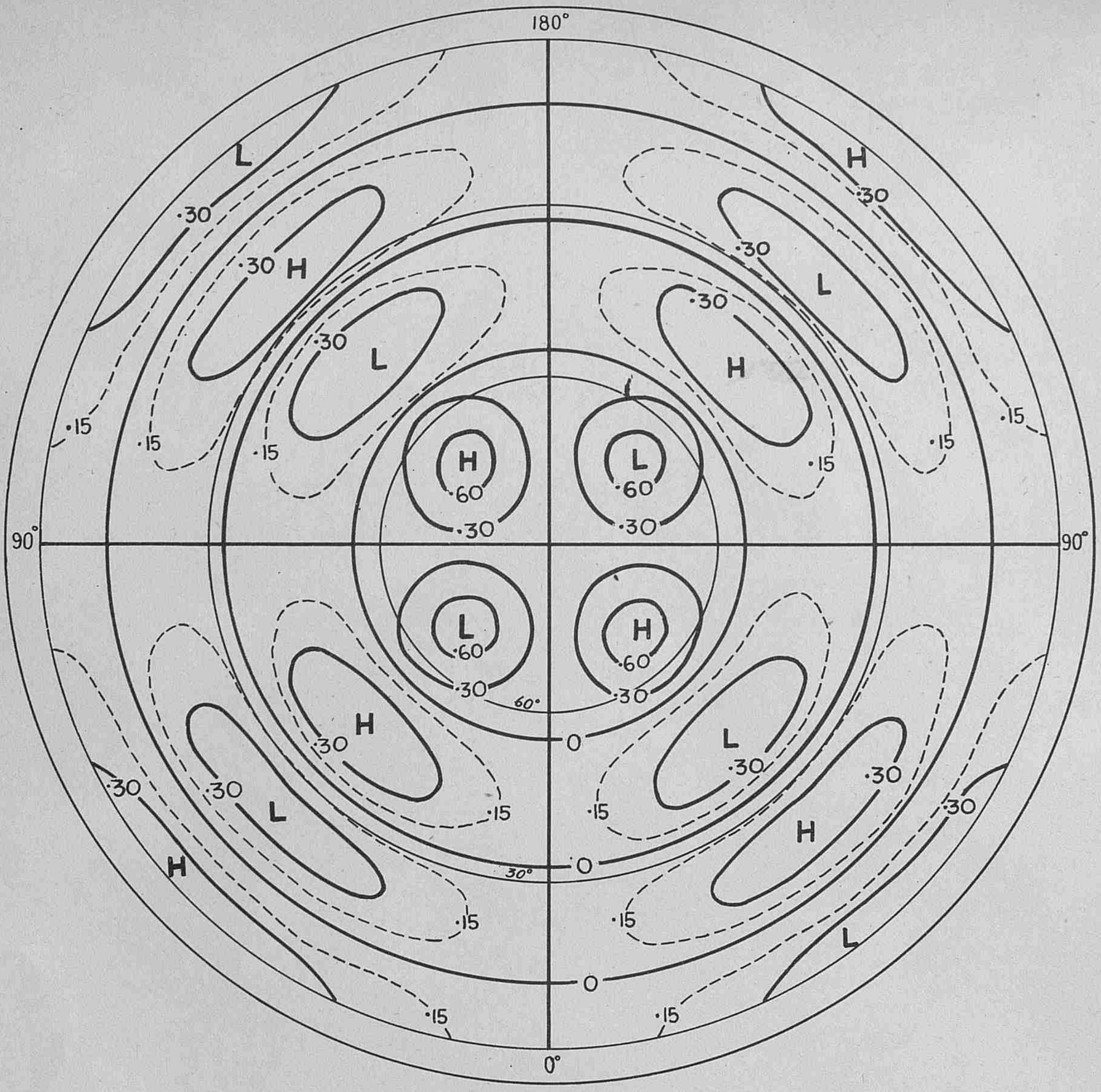
180°
L
·30
·30 H
·30
L
H
·30
·30
L
·30
H
·15
·15
·15
H
·60
·30
L
·60
·30
·15
·15
·15
90°
90°
L
·60
·30
H
·60
·30
60°
0
·30 H
L
·30
·30
·30
L
·30
·30
H
·15
·15
H
30°
0
L
·15
·15
0
·15
·15
0°

FIG. 2 500mb. 0300Z 28:1:53

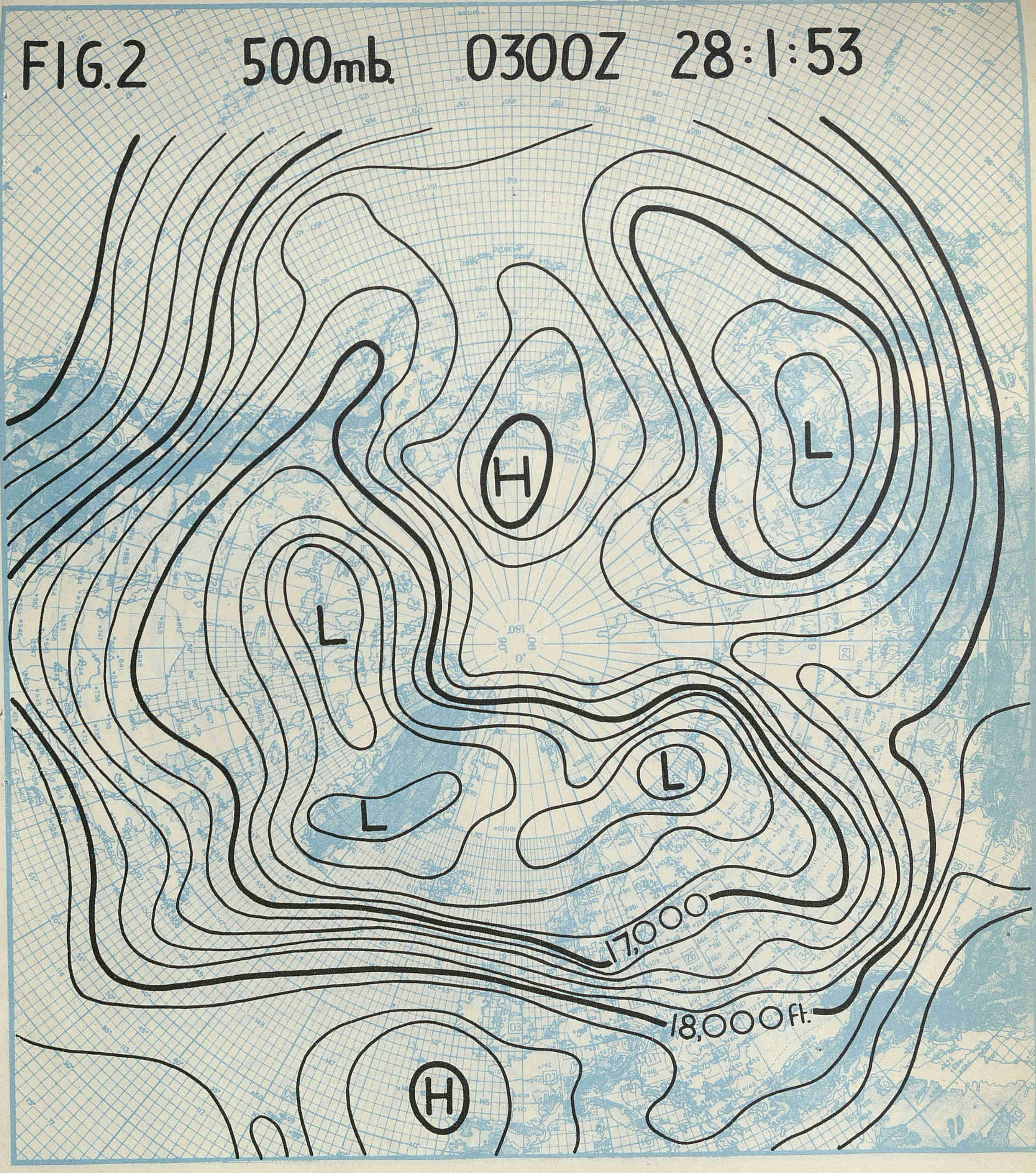
H
L
L
L
L
H
L
17,000
18,000 ft.

FIG. 3 500mb. 0300Z 28:1:53

SPHERICAL HARMONIC REPRESENTATION n,m,≤12

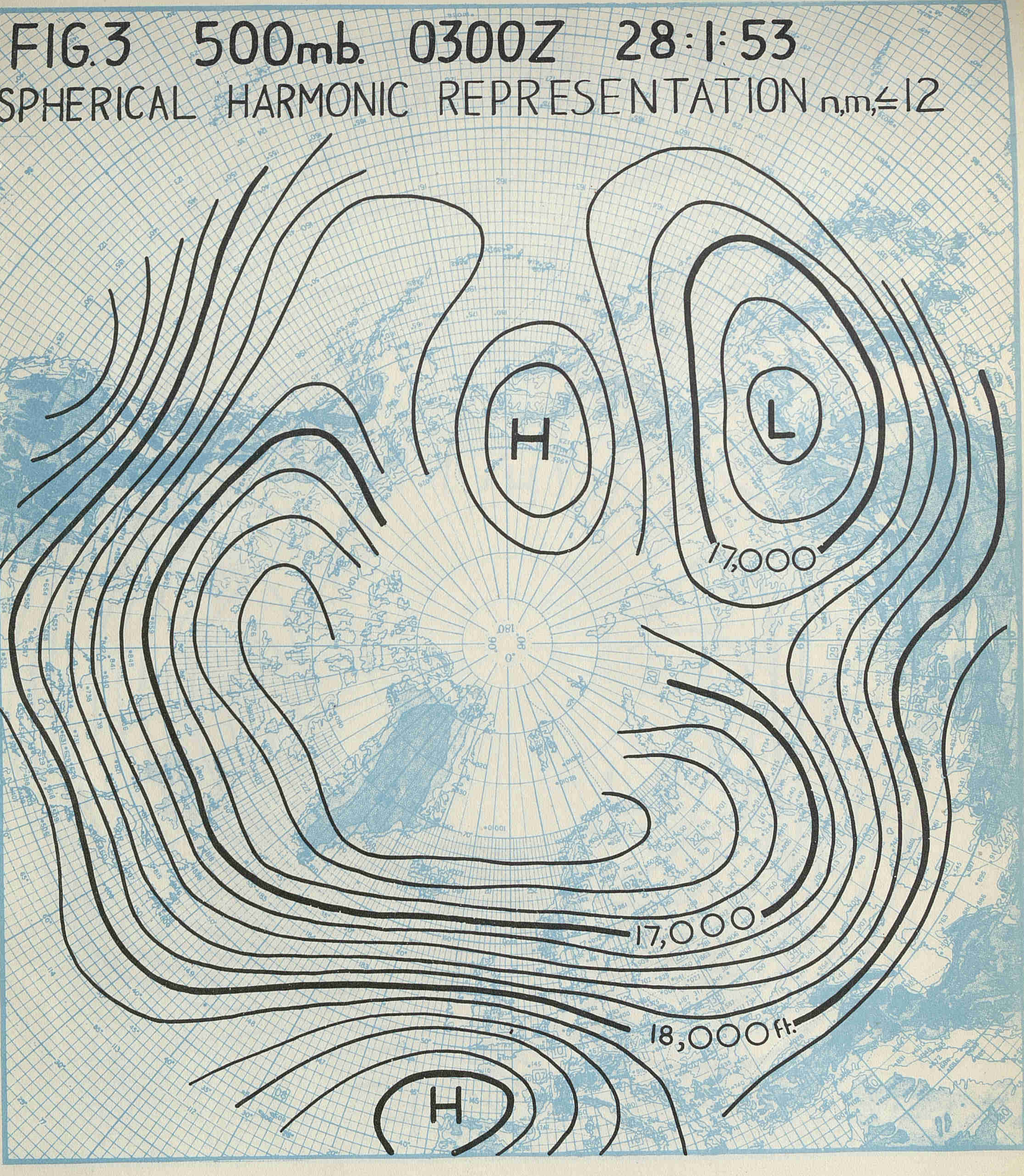
H
L
17,000
17,000
18,000 ft.
H

FIG.4 500mb. 0300Z 28:1:53

SPHERICAL HARMONIC REPRESENTATION n,m,≤8

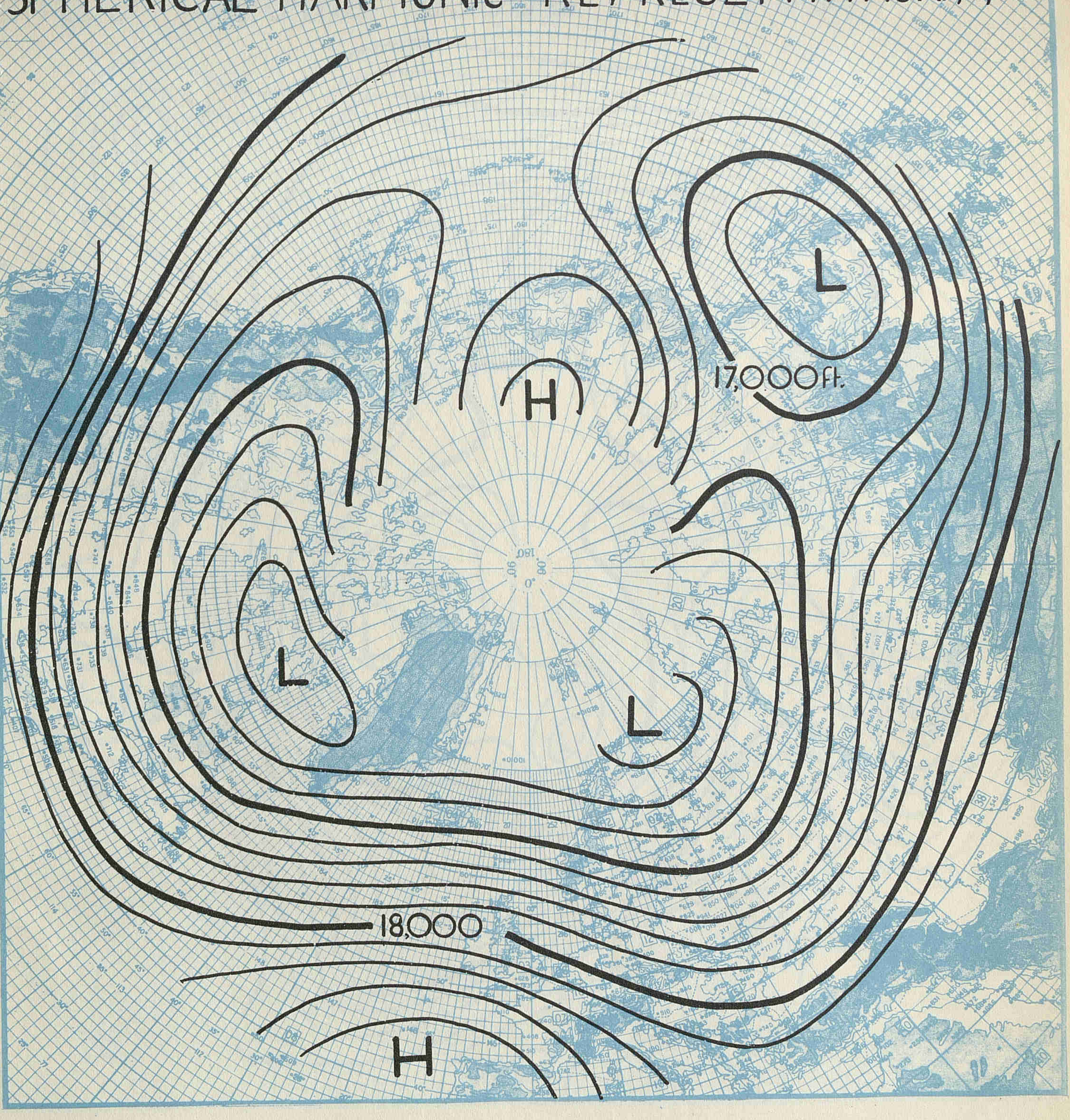

L
H
17,000 ft.
L
L
18,000
H

FIG. 5 500 mb. 0300Z 9:11:53

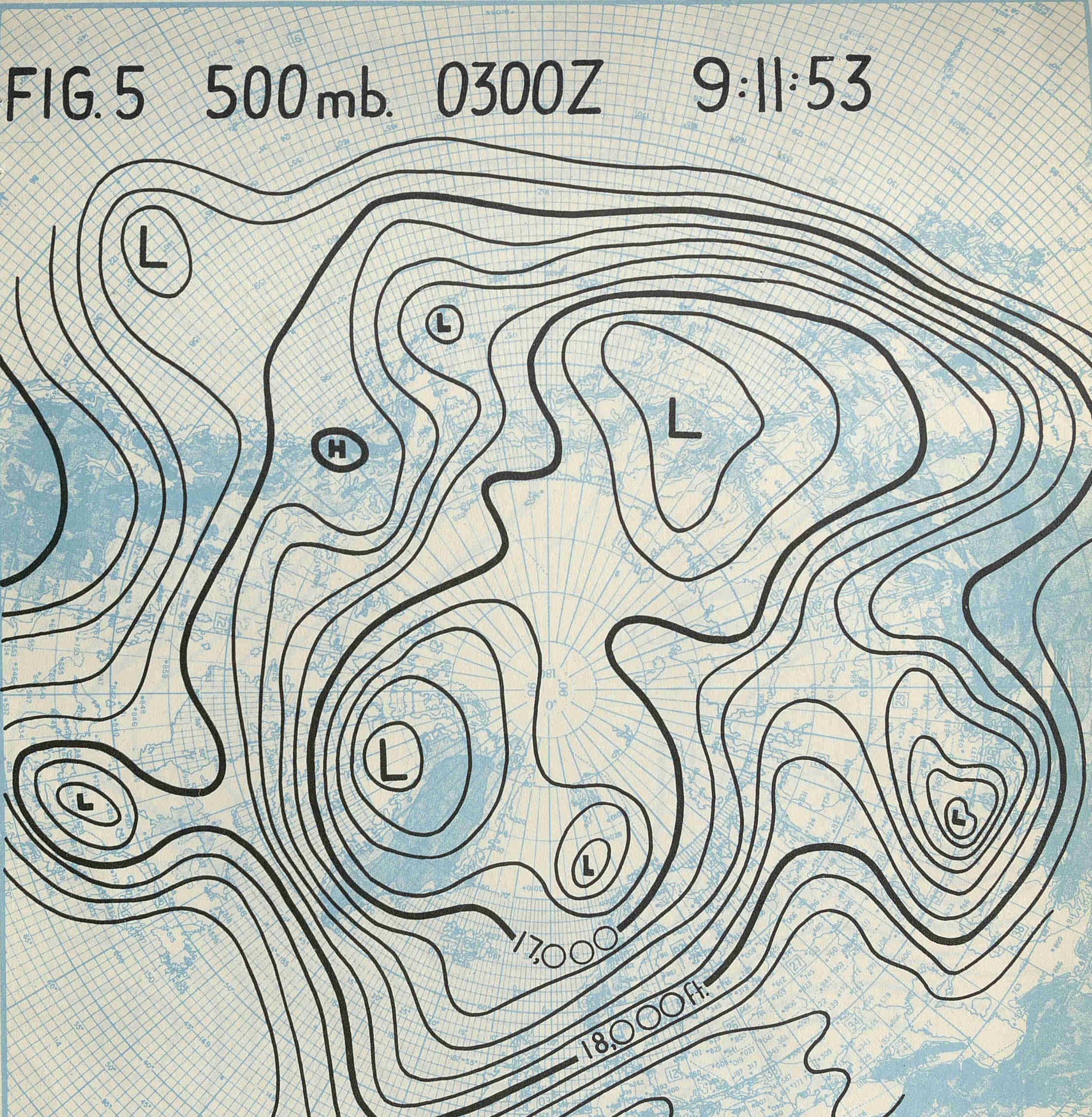
L
L
L
H
L
L
L
L
L
H
17,000
18,000 ft.

FIG. 6 500mb. 0300Z 9:11:53

SPHERICAL HARMONIC REPRESENTATION $n, m, \leq 12$

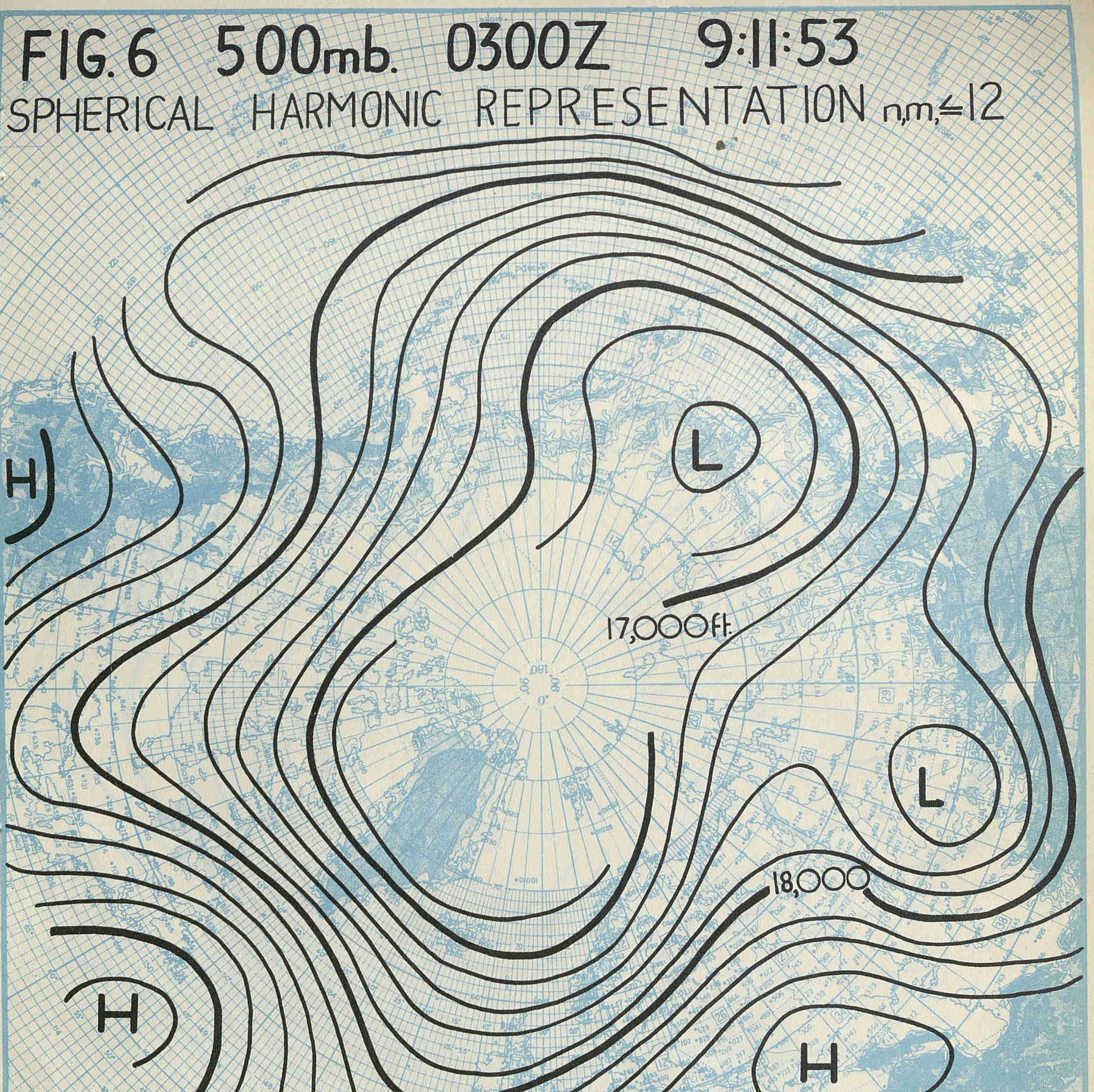
H
L
17,000ft.
L
18,000
H
H
H
L

FIG.7 500mb. 0300Z 9:11:53

SPHERICAL HARMONIC REPRESENTATION n,m,≤8

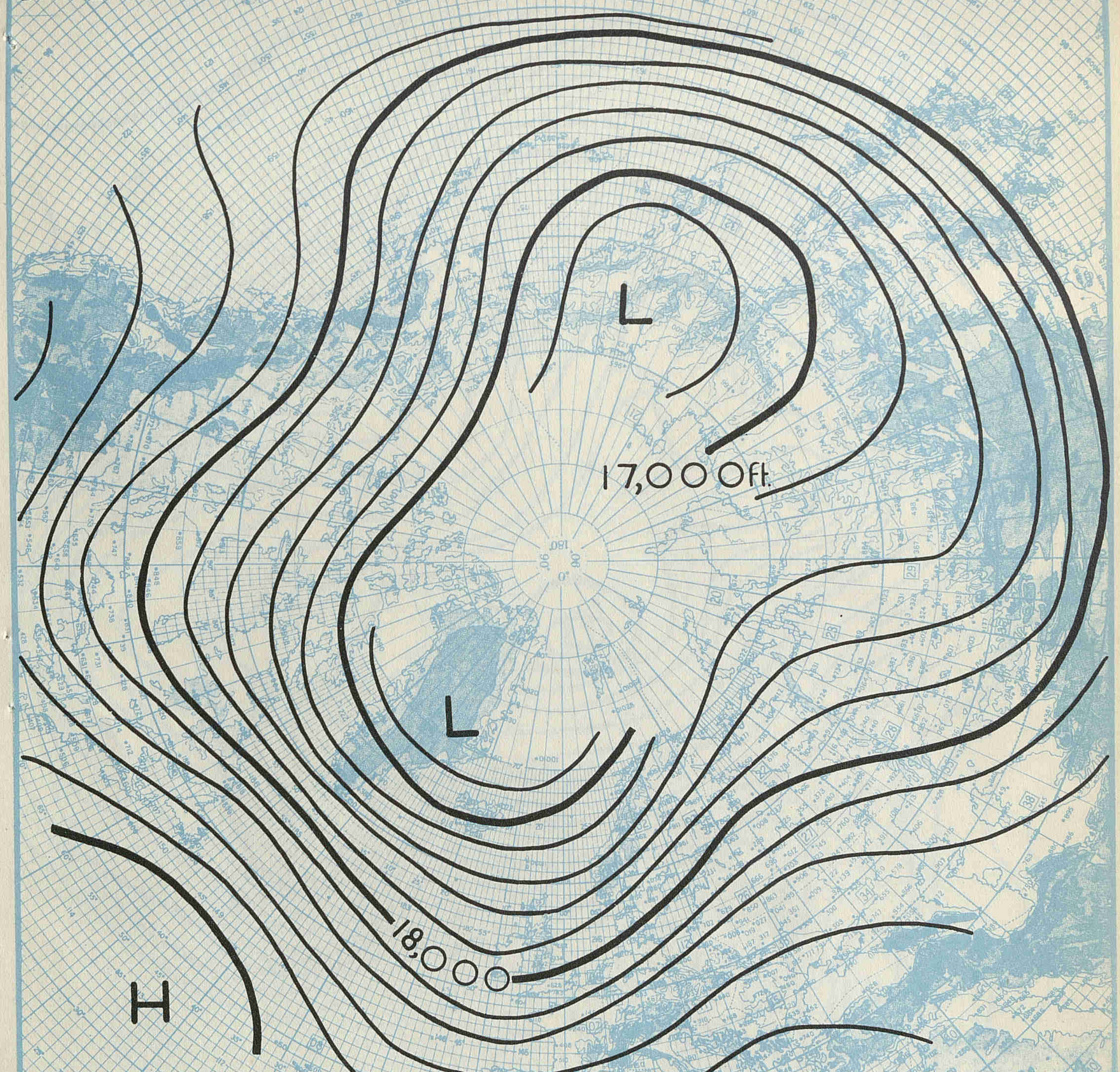
L
L
H
17,000ft.
18,000

FIG. 8 500 mb. 0300Z 27:2:53

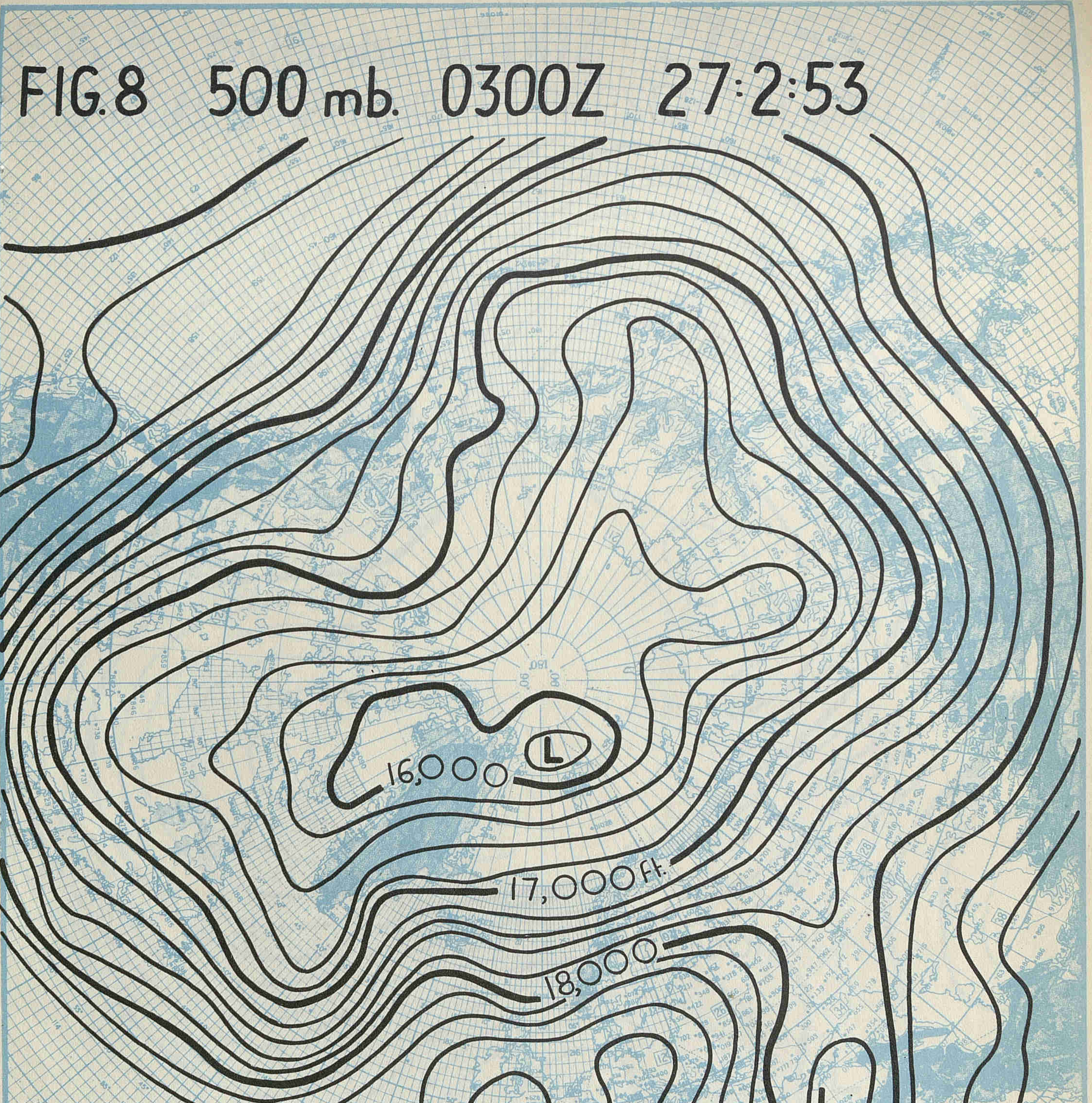
16,000
L
17,000 Ft.
18,000
H
L

FIG. 9 500mb. 0300Z 27:2:53

SPHERICAL HARMONIC REPRESENTATION n,m,≦12

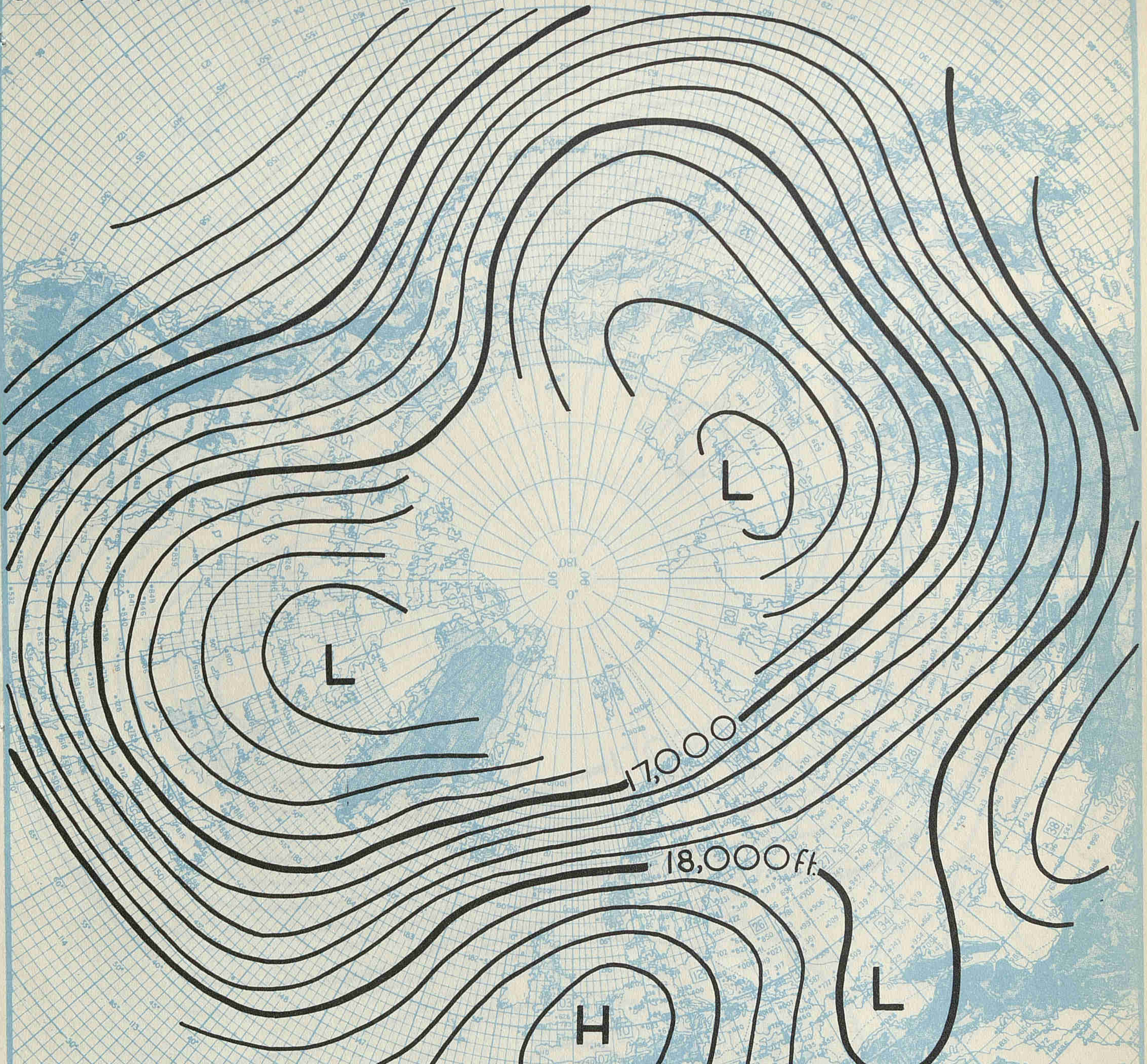
L
L
17,000
18,000 ft.
H
L

FIG. 10 500 mb. 0300Z 27:2:53

SPHERICAL HARMONIC REPRESENTATION $n,m \leq 8$

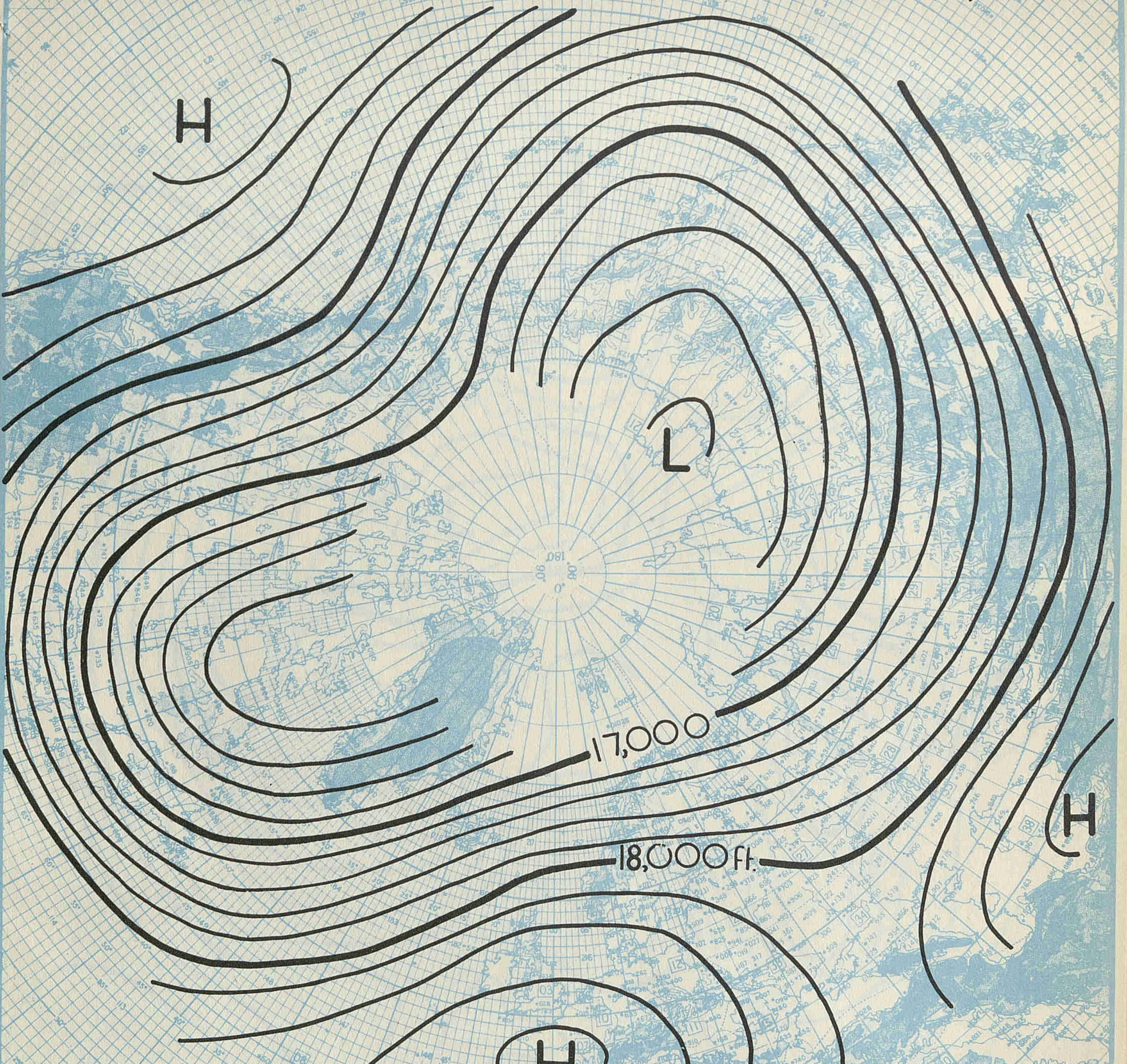
H
L
H
H
17,000
18,000 ft.

FIG. 11 500mb. 0300Z 29:6:53

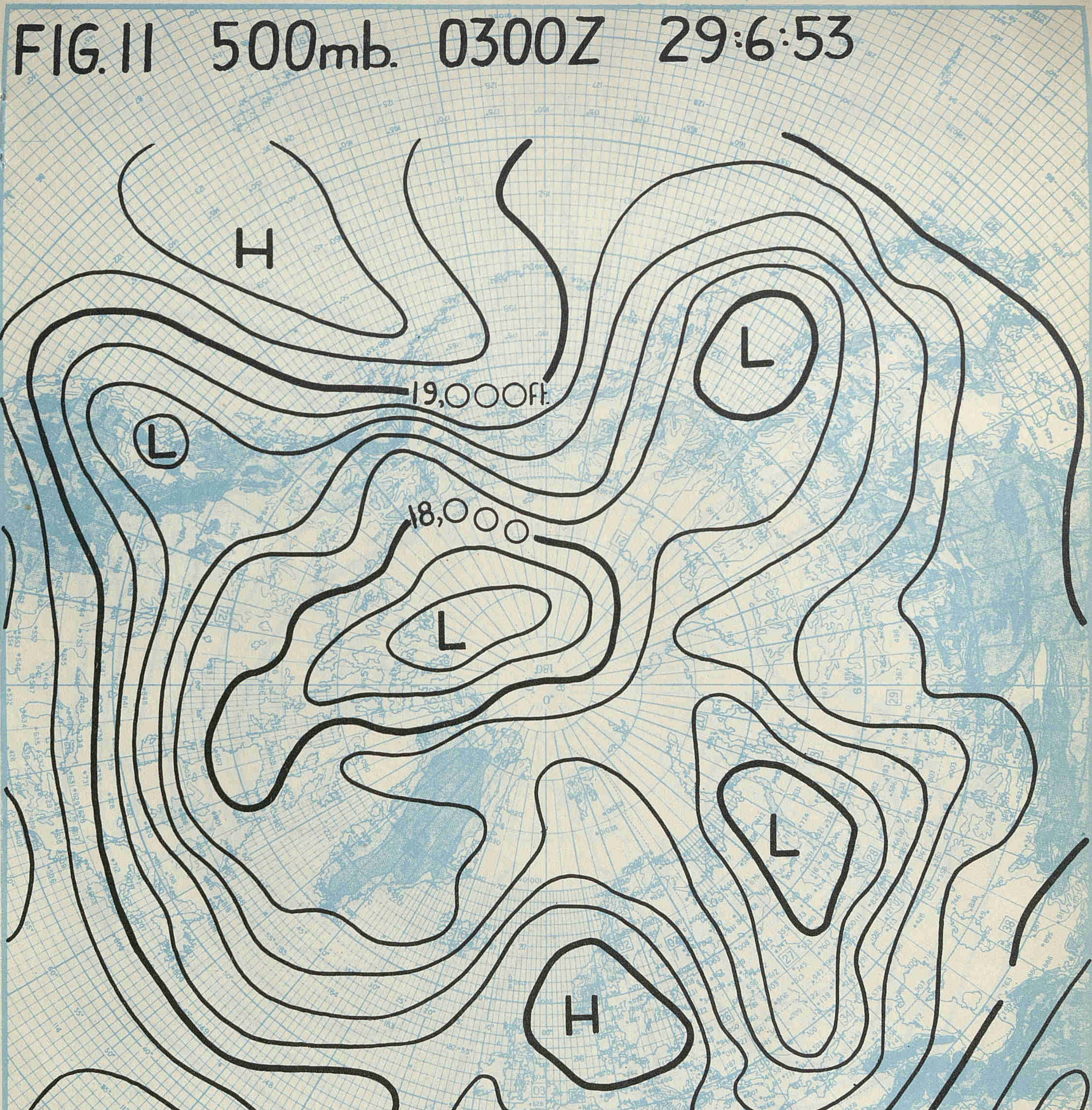
H
L
19,000ft.
18,000
L
L
L
L
H
L

FIG. 12 500mb. 0300Z 29:6:53

SPHERICAL HARMONIC REPRESENTATION n,m,≤12

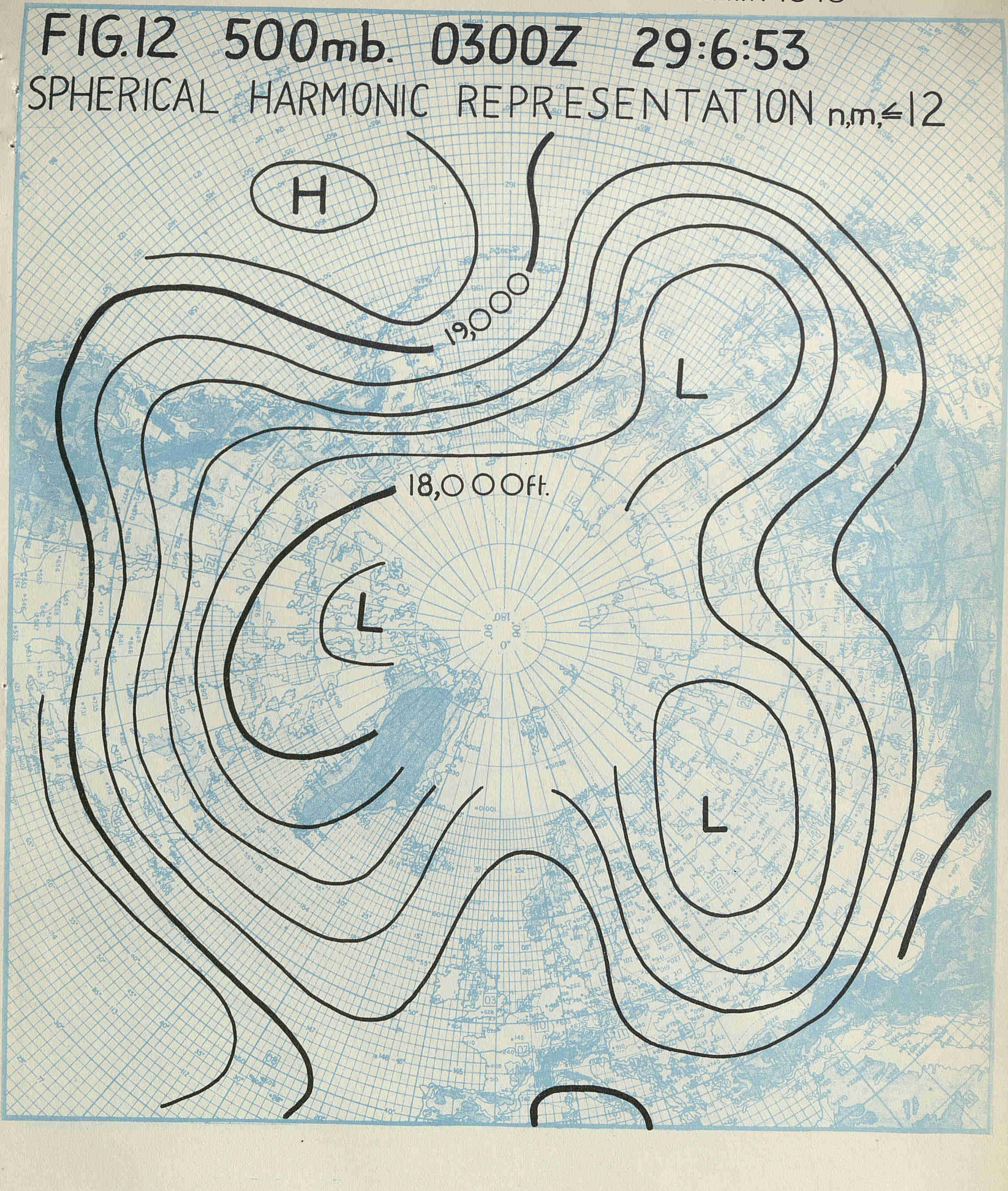
H
L
L
L
19,000
18,000ft.

FIG.13 500 mb. 0300Z 28:6:53

SPHERICAL HARMONIC REPRESENTATION n,m, ≤ 8

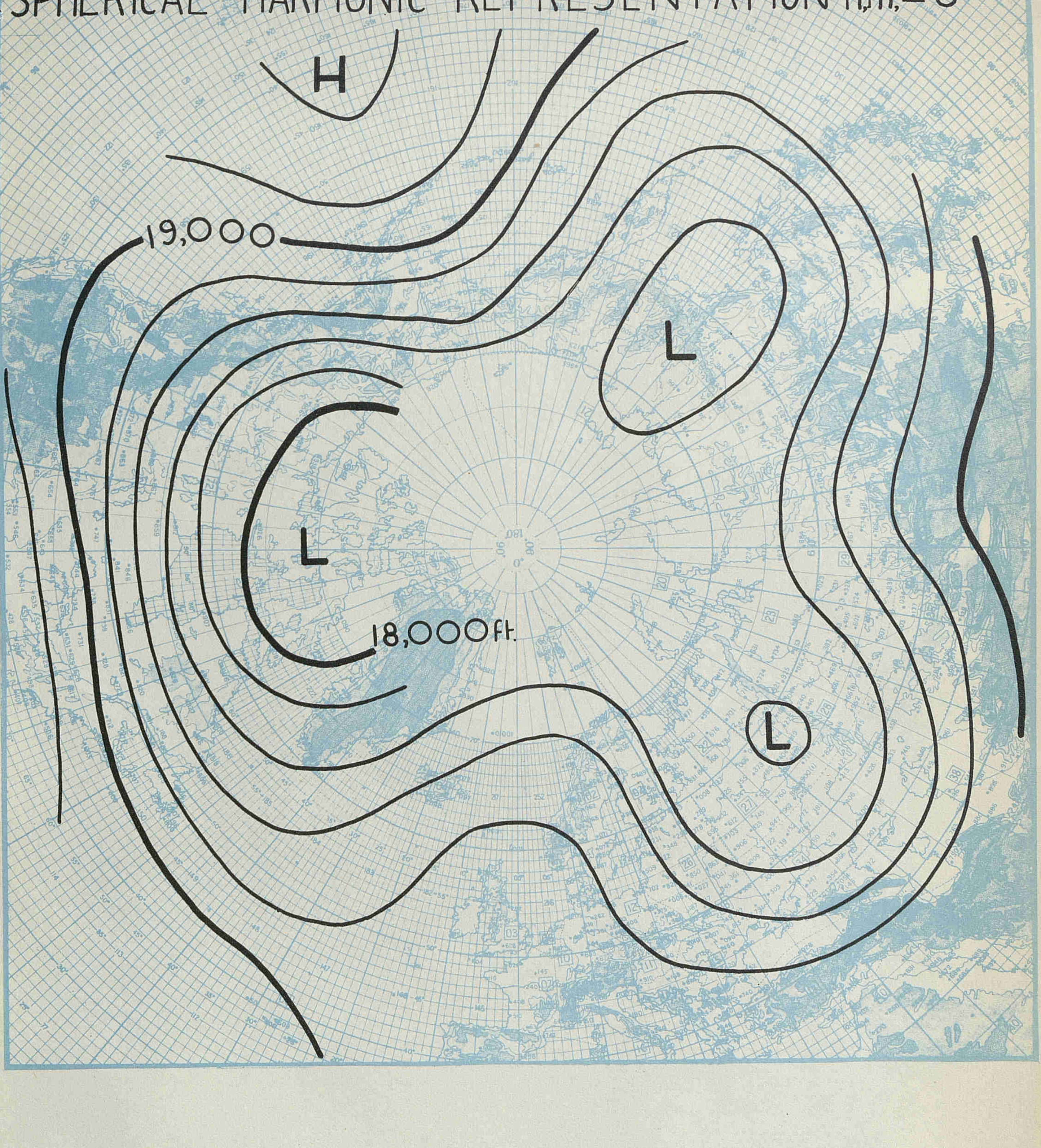
H
19,000
L
L
18,000 ft.
L

MATS

M.R.P. 1041
S.C. 11/231
26th February, 1957

AD 223132

Numerical calculations of the airflow over a ridge for small amplitudes

by

J. S. Sawyer and M. K. Hinds

(Meteorological Office)

AWSSS
ROUTING SLIP

FILE	INFO	ACTION				
			DIRECTOR			
			DEP DIRECTOR			
	4		ASST TO DIRECTOR			
	5		CONSULTANTS		lws [illegible]	[illegible]
			TRSD ✓		CHF	
					TSS	
	1				RRB Milo X	
					EDB	
					SEC	
			EDD		CHF G	
					HLFB	
	3			✓	GSB McClain LNC	
					SPFB	
					CU	
					SEC	
6	2		TIPD	✓	CHF	RAf
					PUE	
					TECH INFO	
					SEC	

AIR MINISTRY

METEOROLOGICAL RESEARCH COMMITTEE

57-912

2 verifax copies

METEOROLOGICAL OFFICE, AIR MINISTRY

CORRIGENDUM

Meteorological Research Paper 1041 - Numerical calculations of the airflow over a ridge for small amplitudes, by J. S. Sawyer and M. K. Hinds.

Later studies have revealed that the calculations in this paper contain large errors due to the finite difference method used (truncation errors). The results should not therefore be quoted.

HWL Absalom
Secretary

Meteorological Research Committee

18th March, 1958

Distribution

To all recipients of M.R.P.1041.

G.H19129/RMH/3/58/270

, 1957

plitudes

Office)

y country has
tics tractable,
he mathematical
implifications
:-

h

ation.

It is not known how far such restrictions imposed on the mathematical problem will preclude direct comparison between calculated airflow and that observed in the atmosphere; nor is it clear which is the most important restriction to lift if any more complicated mathematical formulation of the problem is to be attempted.

The earlier work of Lyra (1943) and Queney (1947) was restricted to currents in which the static stability and wind speed in the basic current were the same at all levels. However the treatment given by Scorer (1949) clearly shows that the vertical variation of both the stability and the wind speed can have very large effects on the pattern of air motion over a barrier. There have been a number of published discussions of the flow in air streams in which either wind, stability or both varies with height but, in order to keep the mathematical analysis within bounds, the authors have been restricted to simple and often highly artificial air currents. Probably the most realistic formulation for which a solution has been obtained is that used by Scorer (1954) and Wallington (1955) in which the atmosphere is divided into three layers each with a constant value of Scorer's parameter "ℓ".

It seems unlikely that any much more complicated variation of wind speed or stability with height could be treated conveniently by analytical methods, and the present paper treats the problem by the methods of numerical analysis and finite differences. This has the advantage that more complex vertical variations of wind and stability can be used; it also permits a realistic representation of the ground profile without undue complication. The equations have been

/linearised

At the time of issue this report has not been published. Any author desiring to quote this paper should refer to it as "A paper of the Meteorological Research Committee (London), M.R.P. No. 1041 by J.S. Sawyer and M.K. Hinds. A copy is available in the Library of the Meteorological Office."

M.R.P. 1041
S.C.II/231
26th February, 1957

AIR MINISTRY

METEOROLOGICAL RESEARCH COMMITTEE

Numerical calculations of the airflow over a ridge for small amplitudes

by

J. S. Sawyer and M. K. Hinds (Meteorological Office)

1. Introduction

The mathematical problem of determining the airflow over hilly country has been considered by several authors. In order to make the mathematics tractable, some simplifying assumptions and approximations must be made, or the mathematical treatment must be limited to special cases. The more important simplifications which have commonly been made in the treatment of this problem are:-

(a) steady, non-turbulent flow
(b) neglect of viscous forces
(c) adiabatic conditions (without condensation effects)
(d) two-dimensional motion (i.e., motion over a ridge)
(e) no separation of the flow from the ground
(f) small amplitude disturbances (permitting the neglect of non-linear terms in the governing equations)
(g) specially simple variation of the wind and stability with height in the basic air stream
(h) horizontal scale small enough to neglect the earth's rotation.

It is not known how far such restrictions imposed on the mathematical problem will preclude direct comparison between calculated airflow and that observed in the atmosphere; nor is it clear which is the most important restriction to lift if any more complicated mathematical formulation of the problem is to be attempted.

The earlier work of Lyra (1943) and Queney (1947) was restricted to currents in which the static stability and wind speed in the basic current were the same at all levels. However the treatment given by Scorer (1949) clearly shows that the vertical variation of both the stability and the wind speed can have very large effects on the pattern of air motion over a barrier. There have been a number of published discussions of the flow in air streams in which either wind, stability or both varies with height but, in order to keep the mathematical analysis within bounds, the authors have been restricted to simple and often highly artificial air currents. Probably the most realistic formulation for which a solution has been obtained is that used by Scorer (1954) and Wallington (1955) in which the atmosphere is divided into three layers each with a constant value of Scorer's parameter "ℓ".

It seems unlikely that any much more complicated variation of wind speed or stability with height could be treated conveniently by analytical methods, and the present paper treats the problem by the methods of numerical analysis and finite differences. This has the advantage that more complex vertical variations of wind and stability can be used; it also permits a realistic representation of the ground profile without undue complication. The equations have been

/linearised

57 - 912

linearised so that the results still apply only to small amplitude disturbances, but it seems likely that finite difference methods will also be required if any attempt is made to calculate the form of finite amplitude disturbances, and the present calculations provide indications of some of the problems which will arise.

2. The differential equation governing the motion

The appropriate perturbation equation governing the two-dimensional motion of a stably-stratified air stream on a scale appropriate to the meteorological problem has been derived in various forms, differing slightly according to the assumptions and simplifications made.

Scorer (1955) gives (his equation 7.5)

$$\frac{\partial^2 w}{\partial z^2} + \frac{\partial^2 w}{\partial x^2} + \left(\frac{g\beta}{U^2} - \frac{\partial^2 U/\partial z^2}{U} \right) w = 0 \qquad (1)$$

where x and z are the horizontal and vertical coordinates,
w is the vertical velocity,
U is the horizontal velocity in the undisturbed stream,
$\beta = \theta^{-1}\, \partial\theta/\partial z$ is a measure of stability (θ = potential temperature).

The basic equation used in the present work has essentially the same form. When numerical constants have been inserted to make the equation convenient for numerical manipulation, it is

$$\frac{\partial^2 \phi}{\partial p^2} + A \frac{\partial^2 \phi}{\partial x^2} + B\phi = 0 \qquad (2)$$

where $A = 2{\cdot}2811 \times 10^{-4}\, \theta^2 / p^{1/\gamma}$

$$B = -\left\{ \frac{148{\cdot}16\, [\partial\theta/\partial p]_0}{U^2 p^{1/\gamma}} + \frac{\partial^2 U/\partial p^2}{U} \right\}$$

In this formulation of the problem, p (= pressure) is used as a vertical coordinate and the flow is defined by a stream function ψ such that $u = \partial\psi/\partial p$ and $\tilde{w} \equiv dp/dt = -\partial\psi/\partial x$, ϕ, which has to be determined from equation (2), is the departure of the stream function ψ from its value at the same pressure level in the undisturbed stream.

In deriving the numerical constants the unit of horizontal distance has been taken as 1 Km, and the unit of pressure 100 mb. U is expressed in m/s and θ in °A, the differentiation $[\partial\theta/\partial p]_0$ being carried out in the undisturbed stream. (Since $\partial\theta/\partial p < 0$, B is normally positive).

The derivation of equation (2) is given in Appendix I. The most important assumptions which have been made are:-

(a) steady, frictionless, adiabatic flow
(b) horizontal scale small enough to neglect the earth's **rotation** (i.e., less than 50 Km)
(c) accelerations small compared with gravity
(d) amplitude small enough to permit neglect of non-linear terms.

3. Boundary conditions

In order to carry out the solution of equation (2) it is necessary to specify adequate "boundary conditions" to render the solution unique. In the numerical solution of equations such as (2), it is usually possible to specify conditions based on the physical formulation of the problems which apply at its boundaries of the area of integration. This is not possible in the present problem because no real physical boundaries exist except at the ground.

In order to obtain unique solutions of (2) the following conditions have been applied:-

(1) The disturbance of the stream function, $\phi \to 0$ as $x \to -\infty$. The flow is assumed to be in the positive direction of x and this condition implies that the disturbance dies away upstream from the ridge.
(2) The disturbance of the stream function should remain finite as $x \to +\infty$ (i.e., downstream from the ridge).
(3) The lowest stream line should follow the ground contour.
(4) The disturbance of the stream function vanishes (i.e., $\phi = 0$) at some specified level which is the upper boundary of the area of integration.

Requirements (1) and (2) are clearly plausible, although since the equations do not apply to disturbances of large amplitude a solution which appeared to grow indefinitely downstream might not in fact do so if the full non-linear equation could be solved.

Assumption (3) rules out any separation of the flow from the surface or any special consideration of a turbulent boundary layer. Nevertheless consideration of flow in which the flow follows the lower boundary without friction is a necessary preliminary to any more complex treatment of the lower boundary. As in the present report we are concerned only with small amplitude disturbances of the flow, at the lower boundary, p = 10 (1000 mb), we can write the boundary condition as

$$\phi = - g \rho U H(x)$$

where H(x) is the height of the lower boundary above its level at a distance up or downstream.

Assumption (4), which is equivalent to imposing a rigid upper lid on the atmosphere, is the most difficult to justify. Corby and Sawyer (1956) have shown that, if such a rigid lid is imposed and then withdrawn to infinity, the solution tends to a limit which is, presumably, the solution appropriate to the atmosphere. However, it appears that for a close approach to this limit, the boundary must be at a considerable height in the stratosphere - too great a height to provide a practical limit for numerical integration.

It is also apparent from Corby and Sawyer's treatment that the introduction of a "rigid lid" at a level in the upper troposphere may make possible lee-wave oscillations which would not be possible if stability conditions characteristic of the troposphere extended to an indefinite height. On the other hand, rather similar oscillations to those arising with a "rigid lid" are possible if the existence of a highly stable stratosphere is taken into account. In other words the tropopause acts in some degree like a rigid lid, so that the flow patterns calculated with boundary assumption (4) above may be reasonably indicative of the behaviour of the atmosphere, provided that the upper boundary is chosen to coincide with the tropopause. The significance of the oscillations arising from the upper boundary condition is further discussed in Appendix II.

4. Method of solution of the differential equation

In order to perform the numerical solution of equation (2) the problem is transformed to one of finite differences by replacing the differential coefficients by their finite-difference approximations, using a rectangular lattice with mesh length δx and δp for this purpose.

The finite difference equation to be satisfied at each point of the lattice is then

$$\phi_{r,s+1} + \phi_{r,s-1} + A_s \frac{(\delta p)^2}{(\delta x)^2} \left\{ \phi_{r+1,s} + \phi_{r-1,s} \right\} - \left\{ 2 + 2 A_s \frac{(\delta p)^2}{(\delta x)^2} - B_s (\delta p)^2 \right\} \phi_{r,s} = 0 \quad (3)$$

where $\varphi_{r,s}$ is the value of φ at the rth point in the sth row of the lattice. The scale factors in equation (2) have been chosen so that it is convenient to use a lattice for which $\delta x = \delta p = 1$ and equation (3) can then be rewritten

$$\varphi_{r,s+1} + \varphi_{r,s-1} + A_s\left(\varphi_{r+1,s} + \varphi_{r-1,s}\right) - C_s\,\varphi_{r,s} = 0 \tag{4}$$

For simplicity all further equations will be written for such a lattice. (Here A_s and B_s are the values of A and B applying to row s of the lattice and $C_s = 2 + 2A_s - B_s$). It may be noted that equation (4) determines a single value in row s + 1 in terms of values of φ in lower rows; thus

$$\varphi_{r,s+1} = -\varphi_{r,s-1} - A_s\left(\varphi_{r+1,s} + \varphi_{r-1,s}\right) + C_s\,\varphi_{r,s} \tag{5}$$

Although (2) is an elliptic partial differential equation, numerical solution by relaxation methods is not practical for two reasons:- namely, (a) because $B > 0$ so that if equation (4) is used to reduce the residual at point (r,s) the sum of the residuals at the surrounding points will be increased by a greater amount than the residual at (r,s) is reduced, and (b) because no boundaries can be introduced at finite distances along the x-axis without materially altering the problem (i.e., if such boundaries are introduced the solution will not satisfy the specified boundary conditions (1) and (2)).

Consequently the following method has been devised to determine the values of $\varphi_{r,1}$, that is the values of φ on the lowest row of points above the boundary. Once these values are determined the complete field of φ can be determined by applying equation (5) first to determine each point of row 2 from values in row 1 and row 0 (the lower boundary), and subsequently to determine φ in row 3 from values in row 2 and 1 and so on.

Reference to Fig. 1 shows that application of equation (5) determines φ at point A in terms of the values of φ at C, B, D and E. Further application of the equation will express these latter values of φ in terms of φ on lower rows, so that φ_A can be expressed as a linear function of the values of φ on row 1 from point X to Y together with the values specified on the lower boundary from U to V. Similarly, the value at G, on the upper boundary, is a linear combination of the 2n + 1 values on row 1 from X to Z. (The grid is assumed to have n rows excluding upper and lower boundaries). Application of the upper boundary condition ($\varphi = 0$) at each point of the upper boundary thus provides a linear equation relating 2n + 1 values of $\varphi_{r,1}$.

Outside a limited range, representing the ridge over which the flow takes place (LM in Fig. 1), the boundary condition at the lower boundary is given by $\varphi_{r,0} = 0$. It is easily seen therefore that the linear equation obtained by applying the upper boundary condition at all points outside the range OP has the same form, namely:

$$a_0\varphi_{r,1} + a_1\varphi_{r+1,1} + \cdots + a_{n-1}\varphi_{r+n-1,1} + a_n\varphi_{r+n,1} + a_{n-1}\varphi_{r+n+1,1} \cdots + a_0\varphi_{r+2n,1} = 0 \tag{6}$$

Only 2n linearly independent solutions are possible, and we seek solutions of the form $\varphi_{1,s} = Dt^s$.

Equation (6) then provides an equation of order 2n, the roots of which are the possible values of t.

$$a_0t^{2n} + a_1t^{2n-1} + \cdots + a_nt^n + a_{n-1}t^{n-1} + \cdots + a_1t + a_0 = 0 \tag{7}$$

The method used to obtain the roots of this equation numerically is described in Appendix III.

The roots occur in pairs which are of the form
either (a) t_r and t_r^{-1} for t_r real or complex, $|t_r| \neq 1$,

or (b) t_r and conjugate complex of t_r for $|t_r| = 1$.

The former type of solution increases in magnitude indefinitely either upstream or downstream, whereas the latter type (b) are oscillatory and remain finite as x tends to infinity.

Boundary condition (1) can therefore be satisfied by requiring that the solution to the left of OL (Fig. 1) should be formed of a linear combination of those solutions of type (a) corresponding values of $\phi_{r,1}$ increasing in magnitude with x increasing. Boundary condition (2) can be satisfied if the solution to the right of MP (Fig. 1) is formed of a linear combination of the remaining solutions i.e., those of type (a) decreasing with x increasing, and those of type (b) (oscillatory solutions).

It is therefore possible to define the field of ϕ in terms of 2n + m - 2 unknowns, where m is the number of lattice columns over which the "ridge" extends in the lower boundary. These unknowns are the 2n unknown multipliers of the solutions corresponding to the 2n values of t (these solutions applying outside and on the dotted lines OL and PM in Fig. 1), together with the m - 2 unknown values of ϕ_1 lying between L and M. Application of the upper boundary condition at the 2n + m - 2 points between O and P provides 2n + m - 2 linear equations for these unknowns.

In order to simplify the algebra, the present calculations have been made in the first instance for a "ridge" represented by a non-zero value of $\phi_{r,0}$ at only a single point of the lower boundary. In this case there are 2n unknowns, n - 1 equations are given by the upper boundary condition and one is given the fact that ϕ_1 at the point immediately above the "ridge" must be compatible with both the upstream and downstream solutions. The solution for a ridge with any arbitrary profile is easily formed from the combination of solutions appropriate to a series of "ridges" each consisting of a displacement at single point. This is possible because the basic equation (2) is linear.

More complete details of the mathematical procedure are contained in Appendix III.

Although the solution determined by the method outlined is unique, difficulties arise in the computation because of the very high accuracy which must be maintained in certain stages of the calculation, if a satisfactory accuracy is to be achieved in the final answer. There are two main reasons for this:-

(a) The coefficients in equations (6) appropriate to a natural air-stream are large. Consequently, if when the solution at all lattice points is built up from the values of $\phi_{r,1}$, the upper boundary condition $\phi_{n+1} = 0$ is to be satisfied with an error not greater than ϵ, the values of $\phi_{r,1}$ must be known with an error not exceeding

$$\epsilon \left\{ |a_n| + 2|a_{n-1}| + 2|a_{n-2}| + \cdots + 2|a_0| \right\}^{-1}$$

In a typical case with n = 7 this requires an error in $\phi_{r,1}$ of the order of only 3×10^{-7} times the error which can be tolerated in ϕ_{n+1}, (i.e., in the fitting of the upper boundary condition).

(b) The equations given by the upper boundary condition for the 2n unknown coefficients of the fundamental solutions appear to form an "ill-conditioned" set. Thus the accuracy achieved in the solutions of these equations is much less than that of the calculated coefficients.

5. Results

Calculations by the method outlined have been carried out on the electronic computer at Manchester University. A programme was written by Miss M. K. Hinds to calculate the flow over a symmetrical ridge with an otherwise arbitrary profile. It was intended to use a lattice with up to 10 rows intermediate between the boundaries, but for the reasons indicated in the preceding section, it was found that insufficient accuracy was being achieved when the lattice included more than 6 intermediate rows.

The calculations have been carried out for a number of different sets of values of A and B representing the distribution of potential temperature and wind in typical air streams. One of these examples (Fig. 8) was made to represent the temperature and wind sounding on an occasion when gravity waves were known to have been widespread. The others were devised to illustrate the effect of various variations of stability with height, and for convenience the wind velocity in these cases was assumed to be the same at all levels.

Six intermediate rows were used in the lattice and in all cases the boundary condition $\phi_7 = 0$ was applied at the level equivalent to a pressure of 300 mb. The lower boundary of the undisturbed stream was assumed to be at 1000 mb.

The results are displayed in Figs. 2 to 10. In these diagrams the vertical displacements are plotted for stream lines at 100 mb intervals, together with the assumed ground profile. The displacements have been calculated from the relation

$$\Delta z = \frac{U_{10}\,\rho}{U\,\rho_{10}}\,\phi$$

where U_{10} and ρ_{10} are the velocity and density at 1000 mb. (No attempt has been made to space the individual stream lines in Figs. 2 to 10 at intervals appropriate to a linear scale of height).

The distribution of stability is indicated with each diagram by a tephigram on which the assumed vertical distribution of temperature is plotted. The assumed wind distribution is also given. For convenience in comparison with results given by Scorer (1954) the variation of $g^2\rho^2 B^2$ with pressure is also given. $g^2\rho^2 B^2$ is equivalent to Scorer's parameter ℓ^2 defined by

$$\ell^2 = \frac{g\beta}{U^2} - \frac{\partial^2 U/\partial z^2}{U}$$

In several papers Scorer has drawn attention to the lee-waves which can form if the vertical distribution of temperature and wind is such that the parameter ℓ^2 takes a larger value in the lower troposphere than in the upper troposphere. It is characteristic of such waves that they have their greatest amplitude in the lower region of large ℓ and that they decrease in amplitude rapidly with height at higher levels; their wavelength L is such that $2\pi/L$ lies between the maximum and minimum values of ℓ. Corby and Sawyer (1956) have shown that the calculated amplitude and wavelengths of such waves are very little affected by the assumption of a rigid upper boundary. "Scorer waves" of this type appear in Figs. 5, 6, 7, 8 and 10, and in Figs. 7, 8 and 10 they dominate the flow pattern to the lee of the ridge in the layers near the ground.

As indicated in section 3, waves can also appear in the solution as a direct result of the upper boundary condition. Corresponding waves can be expected to appear in the atmosphere only in so far as the tropopause acts as a rigid lid. This requires $2\pi/L$ much less than ℓ in the stratosphere where L is the wavelength of the wave. It is characteristic of these wave solutions that they maintain their amplitude through much of the troposphere, and often tend to have greater amplitude in the upper rather than the lower troposphere. They may have one or more nodal surface and their wavelength is such that $2\pi/L$ is less than ℓ through most of the troposphere. Their wavelength is therefore greater than any "Scorer waves" which may be present.

Such "tropopause waves" are present in Figs. 2, 3, 5, 6, 7, 9 and 10. The possible number of such waves increases as B, or ℓ, increases (i.e., as the stability increases or the wind speed decreases). In Fig. 4 no lee-waves are possible because the wind speed is too high, leading to a value of B which is too small for waves. Slight reduction in the wind speed with no change in the vertical stability introduces one lee-wave of long wavelength (Fig. 3). Further reduction of wind speed or increase of stability introduces a second wave with one nodal surface, and if continued a third wave with two nodal surfaces and so on. Fig. 2 which illustrates the same stability profile as Figs. 3 and 4 but a much lower wind speed contains three superposed waves.

In Figs. 2, 3 and 4 there are no large variations of ℓ^2 with height and only "tropopause type" waves are present. On the other hand in Figs. 5, 6, 7 and 8 there is a substantial decrease of ℓ^2 with height and "Scorer waves" are present. In Figs. 5, 6 and 7 both types of wave solution are present but in case 8 the "Scorer wave" occurs alone.

Figs. 9 and 10 are interesting as illustrating more complicated ℓ^2 profiles. Both have an elevated layer of high stability, but that in Fig. 9 is more shallow than that of Fig. 10. The calculated stream lines, both of which contain waves, show how critically the amplitude of the calculated flow pattern may depend on the detail of the ℓ^2 profile. This has already been pointed out by Corby and Wallington (1955).

Comment and conclusion

In interpreting the results of the present calculations in terms of atmospheric motion the restrictive assumptions must be recalled; in particular the restriction to small amplitude disturbances, and the conditions applied at the upper and lower boundaries. Formation of a turbulent layer near the ground and the formation of standing eddies is likely to make the effective profile of the ground smoother than it is in fact, and the calculated disturbance at higher levels is probably greater than that actually occurring.

The most artificial assumption is, no doubt, that of a rigid upper boundary, but it seems probable (Appendix II) that the tropopause will act in approximately the same fashion except for very short wavelength disturbances. Thus we may reasonably expect to find natural lee-waves with the same general form as those illustrated in Figs. 2 to 10.

The results illustrated in Figs. 2 to 10 can therefore be regarded as suggestive of the naturally occurring flow patterns.

Some of the features which may be expected to have counterparts in the atmosphere are:-

(a) Small values of Scorer's ℓ throughout the atmosphere:- absence of lee-waves and approximately symmetrical hill disturbance. Disturbance decreases with height and may reverse in sign.

(b) Larger values of ℓ (exceeding about 0.6 Km^{-1}) but without great variation with height:- lee-waves may occur owing to the effect of the tropopause; these have maximum amplitude in middle or upper troposphere; disturbance near the hill is slightly asymmetric with downward motion above the ridge line and intensified downward flow on the lee side.

(c) Large values of ℓ in lower troposphere with small values aloft:- "Scorer" lee-waves occur; these have maximum amplitude in lower troposphere; flow over the ridge is markedly asymmetric with downward flow over the ridge line and intensified downdraft in lee of hill; "Scorer" waves may occur together with waves resulting from the tropopause and interference between wave systems may result in locally intensified up and down currents in mid-troposphere.

References

Aitken, A. C.	1951	"On the factorisation of polynomials by iterative methods." Proc. Roy. Soc., Edinburgh, Vol. 63, Part II, p.174.
Corby, G. A. and J. S. Sawyer	1956	"The airflow over a ridge - the effects of the upper boundary and high level conditions." Meteorological Research Papers, Air Ministry, London, No. 1015.
Corby, G. A. and C. E. Wallington	1955	"Airflow over mountains - the lee-wave amplitude". Meteorological Research Papers, Air Ministry, London, No. 939.
Lamb, H.	1916	Hydrodynamics (4th edition), Cambridge, p.388 et seq.
Lyra, G.	1943	"Theorie der stationaren Leewellenstromung in frier Atmosphäre, Z. a Math., Mech., Berlin, Volume 23, p.1.
Olver, F. W. J.	1951-2	"The evaluation of zeros of high degree polynomials." Phil. Trans. Roy. Soc., Ser. A, Vol. 244, p.385.
Queney, P.	1947	"Theory of perturbations in stratified currents with applications to airflow over mountain barriers." Dept. Met., Chicago University, Misc. Rep. No. 23.
Scorer, R. S.	1949	"Theory of waves in the lee of mountains." Quart.J. Roy. Met. Soc., Vol. 75, p.41.
	1954	"Theory of airflow over mountains III - airstream characteristics." Ibid, Vol. 80, p.417.
	1955	"Theory of non-horizontal adiabatic flow in the atmosphere." Ibid, Vol. 81, p.551.
Wallington, C. E.	1955	"Lee-waves ahead of a warm front." Ibid, Vol. 81, p.251.

Appendix I - Derivation of a differential equation for the stream lines in two-dimensional motion over a ridge using pressure as the vertical coordinate

The problem is treated as one of steady, adiabatic, inviscid flow in the x, z plane. The following notation is used:-

x, z horizontal and vertical coordinates
u, w velocities in the x and z directions
p, ρ, θ pressure, density and potential temperature
h (p) height of the isobaric surface (pressure = p)
$\tilde{\omega} \equiv dp/dt$

The equations of motion in the x and z directions are:-

$$u\frac{\partial u}{\partial x} + w\frac{\partial u}{\partial z} = -\frac{1}{\rho}\frac{\partial p}{\partial x} \tag{8}$$

$$u\frac{\partial w}{\partial x} + w\frac{\partial w}{\partial z} = -g - \frac{1}{\rho}\frac{\partial p}{\partial z} \tag{9}$$

In most meteorological problems it is possible to assume that the atmosphere is in hydrostatic equilibrium. This is not possible in studying vertical air motions with a horizontal scale of a few kilometres, because the vertical acceleration of the air may be comparable in magnitude with its horizontal acceleration and an important contribution to the motion will arise from the oscillations of the stably stratified air column under gravity. However, it remains true in the motions which we wish to study that the pressure at any point is very close to that which would be calculated on a hydrostatic basis, and although the differences from hydrostatic pressure may not be neglected in determining the small horizontal pressure differences involved in the value of $\partial p/\partial x$ in equation (8), nevertheless it seems justifiable to use the hydrostatic approximation except in the elimination of p from equation (8). This elimination will be carried out using the exact equation (9).

If we allow the hydrostatic approximation and use isobaric coordinates, it becomes possible to express the motion in terms of a stream function, ψ, because the equation of continuity has the form,

$$\left(\frac{\partial u}{\partial x}\right)_p + \frac{\partial \tilde{\omega}}{\partial p} = 0 \tag{10}$$

Thus we write

$$u = \frac{\partial \psi}{\partial p}, \qquad \tilde{\omega} = -\frac{\partial \psi}{\partial x} \tag{11}$$

Since the motion is treated as steady, the potential temperature is constant along a stream line and θ is a function of ψ only. Moreover from the gas equation

$$\rho = \frac{p^{\frac{1}{\gamma}}\, p_0^{\frac{\gamma-1}{\gamma}}}{\theta\, R} \tag{12}$$

where p_0 = 1000 mb.

The vertical velocity, w, and $\tilde{\omega}$ are related by the following equation

$$w = \frac{dz}{dt} = u\left(\frac{\partial h}{\partial x}\right)_p + \tilde{\omega}\frac{\partial z}{\partial p} \tag{13}$$

/However

However, we shall ignore the slope of the isobaric surfaces and use the hydrostatic relation here, so that

$$w = -\tilde{\varpi}/g\rho \qquad (14)$$

If the left hand sides of equations (8) and (9) are rewritten in isobaric coordinates and substitution for w made from (14) we have

$$u\left(\frac{\partial u}{\partial x}\right)_p + \tilde{\varpi}\left(\frac{\partial u}{\partial p}\right) = -\frac{1}{\rho}\frac{\partial p}{\partial x} = -g\left(\frac{\partial h}{\partial x}\right)_p \qquad (15)$$

and $$-\frac{1}{g}\left\{u\frac{\partial}{\partial x}\left(\frac{\tilde{\varpi}}{\rho}\right) + \tilde{\varpi}\frac{\partial}{\partial p}\left(\frac{\tilde{\varpi}}{\rho}\right)\right\} = -g - \frac{1}{\rho}\frac{\partial p}{\partial z} \qquad (16)$$

From (12) $$\frac{1}{\rho}\frac{\partial \rho}{\partial p} = \frac{1}{\gamma p} - \frac{1}{\theta}\frac{\partial \theta}{\partial \psi}\frac{\partial \psi}{\partial p}$$

Thus from (16)

$$\frac{\partial h}{\partial p} = \frac{1}{-g\rho + \frac{1}{g}\left\{u\frac{\partial \tilde{\varpi}}{\partial x} + \tilde{\varpi}\frac{\partial \tilde{\varpi}}{\partial p} - \frac{\tilde{\varpi}^2}{\gamma p} + \frac{\tilde{\varpi}^2}{\theta}\frac{\partial \theta}{\partial \psi}\frac{\partial \psi}{\partial p}\right\}} \qquad (17)$$

(In evaluating the small terms involving $\frac{\partial}{\partial x}\left(\frac{\tilde{\varpi}}{\rho}\right)$ the horizontal variations of density have been ignored).

Differentiation of (15) with respect to p and (17) with respect to x, and elimination of $\partial^2 h/\partial x\,\partial p$ leads to

$$u\frac{\partial^2 u}{\partial x\partial p} + \frac{\partial u}{\partial p}\frac{\partial u}{\partial x} + \tilde{\varpi}\frac{\partial^2 u}{\partial p^2} + \frac{\partial \tilde{\varpi}}{\partial p}\frac{\partial u}{\partial p} =$$

$$\frac{g\left\{-g\frac{\partial \rho}{\partial x} + \frac{1}{g}\frac{\partial}{\partial x}\left(u\frac{\partial \tilde{\varpi}}{\partial x} + \tilde{\varpi}\frac{\partial \tilde{\varpi}}{\partial p} - \frac{\tilde{\varpi}}{\gamma p} + \frac{\tilde{\varpi}^2}{\theta}\frac{\partial \theta}{\partial \psi}\frac{\partial \psi}{\partial p}\right)\right\}}{\left\{-g\rho + \frac{1}{g}\left(u\frac{\partial \tilde{\varpi}}{\partial x} + \tilde{\varpi}\frac{\partial \tilde{\varpi}}{\partial p} - \frac{\tilde{\varpi}^2}{\gamma p} + \frac{\tilde{\varpi}^2}{\theta}\frac{\partial \theta}{\partial \psi}\frac{\partial \psi}{\partial p}\right\}^2}$$

We may neglect all terms except $g^2\rho^2$ in the denominator - this is equivalent to making the hydrostatic approximation. Moreover if the vertical scale of the disturbances is small compared with the height of the 300 mb surface the last two terms in the bracket in the numerator are also smaller than the immediately preceding term which will itself be neglected when conditions appropriate to small perturbations are introduced. Making these approximations and substituting from (11) we have

$$\frac{\partial \psi}{\partial p}\frac{\partial^3 \psi}{\partial x\partial p^2} - \frac{\partial \psi}{\partial x}\frac{\partial^3 \psi}{\partial p^3} = -\frac{1}{\rho^2}\frac{\partial \rho}{\partial x} - \frac{1}{\rho^2 g^2}\left\{\frac{\partial \psi}{\partial p}\frac{\partial^3 \psi}{\partial x^3} - \frac{\partial \psi}{\partial x}\frac{\partial^3 \psi}{\partial x^2\partial p}\right\} \qquad (18)$$

Substituting from (12)

$$\frac{\partial \psi}{\partial p}\frac{\partial^3 \psi}{\partial x\partial p^2} - \frac{\partial \psi}{\partial x}\frac{\partial^3 \psi}{\partial p^3} = \frac{R}{p^{\frac{1}{\gamma}}p_0^{\frac{\gamma-1}{\gamma}}}\frac{\partial \theta}{\partial \psi}\frac{\partial \psi}{\partial x} - \left\{\frac{R\theta}{g p^{\frac{1}{\gamma}} p_0^{\frac{\gamma-1}{\gamma}}}\right\}^2\left\{\frac{\partial \psi}{\partial p}\frac{\partial^3 \psi}{\partial x^3} - \frac{\partial \psi}{\partial x}\frac{\partial^3 \psi}{\partial x^2\partial p}\right\} \qquad (19)$$

If we now restrict our study to small disturbances of a uniform flow, write $\psi = \psi_0 + \phi$ and neglect terms of the second order in ϕ

equation (19) becomes

$$\frac{\partial \psi_0}{\partial p}\frac{\partial^3 \phi}{\partial x\,\partial p^2} - \frac{\partial^3 \psi_0}{\partial p^3}\frac{\partial \phi}{\partial x} = \frac{R}{p^{\frac{1}{\gamma}} p_0^{\frac{\gamma-1}{\gamma}}}\frac{\partial \theta}{\partial \psi_0}\frac{\partial \phi}{\partial x} - \left\{\frac{R\theta}{g p^{\frac{1}{\gamma}} p_0^{\frac{\gamma-1}{\gamma}}}\right\}\left\{\frac{\partial \psi_0}{\partial p}\frac{\partial^3 \phi}{\partial x^3}\right\} \quad (20)$$

This equation may be integrated with respect to x, so that making use of the fact that $\phi \rightarrow 0$ as $x \rightarrow -\infty$ i.e., upstream in the undisturbed stream, we have

$$\frac{\partial^2 \phi}{\partial p^2} + A\,\frac{\partial^2 \phi}{\partial x^2} + B\phi = 0$$

where $$A = \left\{\frac{R\theta}{g p^{\frac{1}{\gamma}} p_0^{\frac{\gamma-1}{\gamma}}}\right\}^2$$

$$B = -\left\{\frac{R}{U^2 p^{\frac{1}{\gamma}} p_0^{\frac{\gamma-1}{\gamma}}}\left[\frac{\partial \theta}{\partial p}\right]_0 + \frac{\partial^2 U/\partial p^2}{U}\right\}$$

and $U = \left[\frac{\partial \psi}{\partial p}\right]_0$ = velocity in the undisturbed stream.

For the purposes of numerical solution, it is convenient to use units for x and p comparable with the mesh length of the grid upon which (21) is to be solved. A convenient choice of unit for x is 1 Km and for p_0, 100 mb. With these units the expressions for A and B become

$$A = 2{\cdot}2811 \times 10^{-4}\ \theta^2 p^{-\frac{1}{\gamma}}$$

$$B = -\left\{\frac{148{\cdot}16}{U^2 p^{\frac{1}{\gamma}}}\left[\frac{\partial \theta}{\partial p}\right]_0 + \frac{\partial^2 U/\partial p^2}{U}\right\}$$

where θ is expressed in °A and U in m/s.

Appendix II - Lee-waves arising from the presence of a stable stratosphere

It has been mentioned that solutions of equation (1) or (2) based on the presence of a rigid upper boundary can contain oscillations corresponding to lee-waves. In the atmosphere no rigid upper boundary exists, but a marked change of stability is usually present at the tropopause, and it is the purpose of this appendix to show that the existence of a stable stratosphere can lead to wave motions very similar to those arising from the imposition of a rigid upper boundary.

It is convenient to return to Scorer's formulation of the problem, and to consider the amplitude, ζ, of a simple harmonic oscillation of the form $w = \zeta e^{ikx}$. Substitution in equation (1) leads to

$$\frac{\partial^2 \zeta^2}{\partial z^2} + (\ell^2 - k^2)\zeta = 0 \qquad (22)$$

where $\ell^2 = \frac{g}{U^2\Theta}\frac{\partial\Theta}{\partial z} - \frac{1}{U}\frac{\partial^2 U}{\partial z^2}$

If the shape of the ridge over which the flow is required is represented by a Fourier integral

$$H(x) = \text{real part of} \int_0^\infty \zeta_0(k) e^{ikx}\, dk$$

then the lower boundary condition for the solution of (22) is

$$\zeta = \zeta_0 \text{ at } z = 0.$$

We seek solutions of the form

$$\zeta = \int_0^\infty \zeta(k) e^{ikx}\, dk \qquad (23)$$

In order to compare the effect of a stable stratosphere with that of a rigid lid, it is convenient to consider the simplified problem in which the stability parameter ℓ is constant in both troposphere and stratosphere. We may then compare the solution for this case with a single layer representation in which a rigid lid is imposed at the tropopause. The two models of the atmosphere which are to be compared are then:-

Rigid lid: $\ell = \ell_1$, boundary condition $\zeta = 0$ at $z = a$

Two-layer $\ell = \ell_1$ in the lower layer, $z < a$
$\ell = \ell_2$ in the upper layer, $z > a$
$\ell_2 > \ell_1$.

Following Corby and Sawyer (1956) an appropriate upper boundary condition in the two-layer model is obtained by requiring that in the upper layer $\zeta(k)$ should have the form $\zeta(k) = A e^{i\nu_2 z}$ where $\nu_2^2 = \ell_2^2 - k^2$.
In the case of the rigid lid it is easily shown that

$$\zeta(k) = \zeta_0(k)\left\{\cos \nu_1 z - \frac{1}{t_1}\sin \nu_1 z\right\} \qquad (24)$$

where $t_1 = \tan a\nu_1$ and $\nu_1^2 = \ell_1^2 - k^2$.

However when an attempt is made to reconstruct the flow by carrying out the integration $\zeta = \int_0^\infty \zeta(k) e^{ikx} dk$ difficulty arises because the integral is indeterminate around the singularities of $\xi(k)$ which arise where $\tan a\nu_1 = 0$. This difficulty is resolved by Lamb (1916) in a similar problem by introducing internal friction into the controlling equation, and thereby displacing the poles of $\xi(k)$ slightly off the real axis in the complex k-plane towards the positive imaginary side.

Scorer (1949) adopts a solution which is equivalent to Lamb's with the result that the integral $\int_{-\infty}^{\infty} \xi(k) e^{ikx}\, dk$ can be evaluated by integrating in the complex k-plane along a path following the real axis but passing just on the negative imaginary side of any poles of $\xi(k)$, (Fig.11(a)). The integral may be approximated by completing the contour by means of an arc of the circle at infinity and a convenient radius. For $x > 0$ the contour must be completed on the positive imaginary side of the real axis and for $x < 0$ on the negative imaginary side so that the factor $e^{ikx} \to 0$ on the circle at infinity in both cases. As a result the solutions for positive and negative x differ by an amount given approximately by $2\pi i \times$(sum of the residues at the poles of $\xi(k)$.

This part of the solution is identified as the lee-waves and appears as an infinite **train of harmonic oscillations** on the downstream side of the ridge ($x > 0$). The remaining part of the solution is approximately symmetrical about $x = 0$ and decreases to zero as x increases.

In the particular case of a stream with constant l flowing beneath a rigid lid, the lee-wave part of the solution is $2\pi i \times$ (residue of

$$\xi_0(k)\left\{\cos\nu_1 z - \frac{1}{t_1}\sin\nu_1 z\right\} e^{ikx} \text{ at its poles)}$$

$$= -\sum \frac{2\pi \xi_0 \nu_1}{a k_0} \sin\nu_1 z(\sin k_0 x - i\cos k_0 x)$$

(the summation being over all poles).

We are interested only in the real part of the solution which represents a lee-wave train with amplitude $\frac{2\pi \xi_0 \nu_1 \sin\nu_1 z}{a k_0}$ corresponding to each k_0 which satisfies $\tan a\nu_1 = 0$.

Turning now to the two-layer model, conditions of continuity at the interface lead to an equation corresponding to (24), namely:-

$$\xi(k) = \xi_0(k)\left\{\cos\nu_1 z + \frac{\nu_1 t_1 + i\nu_2}{\nu_1 - i\nu_2 t_1}\sin\nu_1 z\right\} \qquad (25)$$

The lee-waves will be discussed as though only one set of lee-waves were present in the corresponding model with a lid (i.e., $\tan a\nu_1 = 0$ had only one solution), but the treatment is essentially the same if more than one lee-wavelength is possible.

The right hand side of equation (25) has no poles on the real axis, but if $\nu_2 \gg \nu_1$, for each pole in the single layer case with a lid there is a corresponding pole at a neighbouring position for which $t_1 = -i\nu_1/\nu_2$ (approx.).

If k_0 is the value of k which results in lee-waves in the "lid-model", the corresponding value of $t_1 = 0$.

Moreover for small increments,

$$\delta t_1 = a\sec^2\nu_1\,\delta\nu_1 = -\frac{a\sec^2\nu_1\; k\,\delta k}{\nu_1} \qquad (26)$$

Thus, since ν_1/ν_2 is supposed to be small, the value of k corresponding to the pole in the two-layer model is approximately

$$k_0 + (i\nu_1^2/a\,\nu_2 k_0)$$

where k_0 is the value of k for the pole in the model with a lid.

In the neighbourhood of this pole the expression (25) becomes large, and there is thus a small range of k with width of the order ν_1/ν_2 for which the integrand in (23) is large, and makes a contribution to the integral comparable with that from the remainder of the range of integration. The contribution from the small range of integration near the pole corresponds to the lee-wave component in the model with a lid which arises in a similar way. This can be made clearer by an examination of the integral by contour integration methods.

The integral (23) has to be evaluated along OX in the complex k-plane. In order to examine the integral over a small section A B from $k = k_0 - \epsilon$ to $k = k_0 + \epsilon$, the line A B is replaced by the line A C parallel to the imaginary axis, the line C D at infinity and D B also parallel to the imaginary axis (see Fig.11(b)). If C D is chosen on the positive side of the real axis for $x > 0$ and on the negative side for $x < 0$ (e.g., C'D' in Fig.11(b)), then the factor e^{ikx} introduces a factor into the integrand which decreases exponentially with the imaginary part of k. The contribution to the integral from C D or C'D' can therefore be neglected.

If we write $k = k_1 + i\,k_2$, $k_1 = k_0 - \epsilon$ on A C and $k_1 = k_0 + \epsilon$ on D B the contribution from the integrals along A C and D B can be evaluated as follows

$$\int_A^C \zeta(k)\, e^{ikx}\,dk - \int_B^D \zeta(k)\, e^{ikx}\,dk$$

$$= \int_0^\infty dk_2 \left\{ \left[\zeta_0(k) \frac{\nu_1 t_1 + i\nu_2}{\nu_1 - i\nu_2 t_1} \sin\nu_1 z\, e^{ikz} \right]_{k_0 - \epsilon + ik_2} - \left[\zeta_0(k) \frac{\nu_1 t_1 + i\nu_2}{\nu_1 - i\nu_2 t_1} \sin\nu_1 z\, e^{ikx} \right]_{k_0 + \epsilon + ik_2} \right\}$$

$$= 2\epsilon \int_0^\infty dk_2 \frac{\partial}{\partial k_1} \left\{ \zeta_0(k) \frac{\nu_1 t_1 + i\nu_2}{\nu_1 - i\nu_2 t_1} \sin\nu_1 z\, e^{ikx} \right\}$$

$$= 2\epsilon \int_0^\infty \left[\frac{\partial}{\partial k_1} \left\{ \zeta_0(k) \frac{\nu_1 t_1 + i\nu_2}{\nu_1 - i\nu_2 t_1} \sin\nu_1 z \right\} e^{ik_1 x} + ix\,\zeta_0(k) \frac{\nu_1 t_1 + i\nu_2}{\nu_1 - i\nu_2 t_1} \sin\nu_1 z\, e^{ik_1 x} \right] e^{-k_2 x}\,dk_2$$

Since ϵ can be chosen so that $|\nu_1 - i\nu_2 t|$ does not approach zero on A C or D B the preceding integral is less than $2\epsilon M e^{-k_2 x}/x$ where M is the upper bound of the modulus of the expression enclosed by square brackets within the integral, showing that the integral along A C D B makes a contribution to the integral which varies with ϵ and is of the same order of magnitude as the contribution from other parts of the range of integration outside A B.

Thus we have:-

for $x > 0$ $\displaystyle\int_0^x \zeta(k)\, e^{ikx}\,dk = \int_{OACDBX} \zeta(k)\, e^{ikx}\,dk + 2\pi i$ (residue at pole) (27)

for $x < 0$ $\displaystyle\int_0^x \zeta(k)\, e^{ikx}\,dk = \int_{OAC'D'BX} \zeta(k)\, e^{ikx}\,dk$ (28)

In the first integral on the right hand side of these equations no special contribution arises from any part of the range of integration and since the contribution from the section A B is essentially proportional to ϵ , it is small compared with the remainder of the integral.

The second term on the right of (27) can be identified with the lee-wave component. As a result of the adoption of solutions of the form $\xi(k) = Ae^{i\nu_2 z}$ in the upper layer, the lee-waves occur only on the downstream side of the ridge.

In evaluating the residue at the pole we recall that

$$\frac{\partial}{\partial k}(\nu_1 - i\nu_2 t) = -\frac{k}{\nu_1} + i\frac{kt_1}{\nu_2} + i\frac{\nu_2 ak}{\nu_1}$$

$$= \frac{i\nu_2 ak}{\nu_1} \quad \text{(approx.) since } \nu_2/\nu_1 \text{ is large.}$$

Thus, the lee-wave component in (27) has the approximate form

$$\frac{2\pi\xi_0\nu_1}{ak_0}\sin\nu_1 z\, e^{ik_0x}\, e^{-\frac{x\nu_1^2}{a\nu_2 k_0}}$$

This is the same as the form obtained in the model with the rigid lid except for the factor $e^{\frac{-x\nu_1^2}{a\nu_2 k_0}}$ which indicates an exponential decrease with x. Thus in the two-layer atmosphere lee-waves occur with amplitude near the mountain and wavelength similar to those computed with the artificial boundary condition represented by the rigid lid. However the waves decay downstream and are reduced to about half their original amplitude after a distance $x = \frac{a\nu_2}{\nu_1^2} k_0 \log_e 2$ or after a number of lee-waves equal to $\frac{\log_e 2\; a\; \nu_2 k_0^2}{2\pi\nu_1^2}$

Although the preceding theory has been developed on the assumption that l_2 is much greater than l_1 , there is little reason to doubt that some similar form of lee-waves will exist when l_2 and l_1 have values typical of the stratosphere and troposphere respectively. Typical values would be $l_1^2 = 0.89$ Km^{-2} and $l_2^2 = 6.75$ Km^{-2} leading to $\nu_1 = 0.63$ Km^{-1}, $\nu_2 = 2.5$ Km^{-1} for k = 0.7 Km^{-1} and a = 10 Km. The above analysis then suggests that the amplitude of the lee-wave train falls to half its original value after three oscillations.

Appendix III - Notes on mathematical technique

1. Method of obtaining values of t corresponding to possible solutions of the form $\phi_{s,1} = Dt^s$ at a distance from the ridge

In section 4 of the present paper it has been shown that with a lower boundary condition $\phi_0 = 0$ and $\phi_{s,1} = Dt^s$ at points on the lowest internal line of the grid, the upper boundary condition $\phi_{n+1} = 0$ applied at the n + 1th row of the grid leads to an equation for t of the form:-

$$a_0 t^{2n} + a_1 t^{2n-1} + \text{-----------} + a_n t^n + a_{n-1} t^{n-1} + \text{------------} + a_1 t + a_0 = 0 \quad (7)$$

This equation has roots in pairs of the form t_r, $1/t_r$ and in order to obtain these it is convenient to transform the equation to one with x as variable, where

$$x = t + \frac{1}{t}$$

and the roots t_r, $1/t_r$ are obtained as roots of the quadratic equation

$t^2 - xt + 1 = 0.$

As explained in section 4 the value of $\phi_{r,s}$, the disturbance of the stream function at a point in the sth internal row of the grid can be expressed as a linear function of the values $\phi_{j,1}$ in row 1 symmetrical about the point (r,1). For any solution which has the form $\phi_{j,1} = Dt^j$ corresponding values spaced equally on either side of $\phi_{r,1}$ are respectively $t^m \phi_{r,1}$ and $t^{-m} \phi_{r,1}$, so that $\phi_{r,s}$ can be expressed as $\phi_{r,1}$ multiplied by a polynomial in x of degree s - 1. A recurrence relation which enables the coefficients of the polynomial to be calculated is obtained from the finite difference form of the equation governing the flow (4), namely:-

$$\phi_{r,s+1} + \phi_{r,s-1} + A_s \left(\phi_{r+1,s} + \phi_{r-1,s} \right) - C_s \phi_{r,s} = 0 \qquad (4)$$

If we suppose $\phi_{r,s} = \phi_{r,1} \left\{ \sum_{i=0}^{s-1} b_{i,s} x^i \right\}$ substitution in (4)

gives

$$\sum_{i=0}^{s} b_{i,s+1} x^i + \sum_{i=0}^{s-2} b_{i,s-1} x^i + A \left\{ t \sum_{i=0}^{s-1} b_{i,s} x^i + \frac{1}{t} \sum_{i=0}^{s-1} b_{i,s} x^i \right\} - C_s \sum_{i=0}^{s-1} b_{i,s} x^i = 0$$

Equating coefficients

$$b_{i,s+1} = C_s b_{i,s} - A_s b_{i-1,s} - b_{i,s-1} \qquad i \neq 0 \qquad (29)$$

This relation also applies for i = 0 provided $b_{i,s}$ is treated as zero for negative i.

Commencing with $b_{i,0} = 0$ for all i and $b_{0,1} = 1$, $b_{i,1} = 0$ i $\neq$ 0, the coefficients $b_{i,s}$ can be calculated for any row s from the recurrence relation (29). The upper boundary condition $\phi_{r,n+1} = 0$ then yields the equation

$$\sum_{i=0}^{n} b_{i,n+1} \, x^{n} = 0 \qquad (30)$$

In the numerical treatment of the problem the coefficients $b_{i,n+1}$ are first calculated by means of the recurrence relations (29). Equation (30) was then solved for x. Since allowance had to be made for the possible existence of imaginary roots, the equation was first made of even degree by multiplying by x, if necessary. The quadratic factors were then evaluated numerically. To determine each factor 10 iterations were carried out by the "penultimate remainder method" (Aitken, 1951). Subsequently the iteration was continued by "Blairstow method" (Olver, 1951), because this appeared to converge more rapidly in the later stages. Iteration was continued until the change in the coefficients was less than 10^{-6}, the equation was then divided through by the quadratic factor and a further factor sought. Each quadratic factor was tested against the full equation (30) and further iterations carried out by Blairstow method, if necessary, to maintain the specified accuracy.

The values of x and the corresponding values of t were obtained by solving for x the quadratic equations provided by each factor, and then solving the equation

$$t^2 - x\,t + 1 = 0$$

for t.

The solutions for t were sorted into those corresponding to solutions for $\phi_{r,s}$ which increase or decrease indefinitely downstream, namely those for which $|t| \neq 1$ (that is x real and $|x| > 2$ or x complex) on the one hand, and those for which $\phi_{r,s}$ oscillates but remains finite, namely those for which $|t| = 1$ (that is x real and $|x| \leq 2$) on the other. In the following paragraphs the former solutions will be denoted by t_p and the latter by t_q.

2. Determination of the field of $\phi_{r,s}$

The next stage was to determine the disturbance upstream and downstream of a ridge represented by a non-zero value of ϕ at only a single point of the lower boundary, namely the origin (0, 0). As indicated in section 4 the appropriate solutions on the lowest internal row of the grid can be represented by

$$\phi_{r,1} = \sum_p P'_p \, t_p^{r} \qquad \text{for } r < 0$$

$$\phi_{r,1} = \sum_p P_p \, t_p^{-r} + \sum_q \left(Q_q t_q^{-r} - Q'_q t_q^{r} \right) \qquad \text{for } r > 0$$

Now it has been seen (equation (6)) that the upper boundary condition applied at a single point of the boundary provides a linear equation relating $\phi_{r,1}$ at 2n +1 points of row 1.

If we write S_s for either P_p or Q_q, so that summation can be carried out over both sets of coefficients, it is easily seen that applying the upper boundary condition at the point (-n+1, n+1) and making use of the fact that t_s satisfies equation (7), leads to the equation

$$\sum_s a_0 \left(S_s t_s^{-1} - S'_s t_s \right) + \epsilon_1 = 0 \qquad (31)$$

where ϵ_1 is the value of ϕ at this boundary point if $\phi_{i,1}$ = 0 for all i, $\phi_{0,0}$ = 1 and $\phi_{j,0}$ = 0 for j ≠ 0.

Application of the boundary condition successively at points (-n+2, n+1) (-n+3, n+1) and so on, leads to equations

$$\left.\begin{array}{l} \sum_s a_0 \left(S_s t_s^{-2} - S'_s t_s^{2} \right) + \sum_s a_1 \left(S_s t_s^{-1} - S'_s t_s \right) + \epsilon_2 = 0 \\ \sum_s a_0 \left(S_s t_s^{-3} - S'_s t_s^{3} \right) + \sum_s a_1 \left(S_s t_s^{-2} - S'_s t_s^{2} \right) + \sum_s a_2 \left(S_s t_s^{-1} + S'_s t_s \right) + \epsilon_3 = 0 \\ - - - - - - - - - + - - - - - - - - - + - - - - - - + - - - \end{array}\right\} \quad (32)$$

n such equations can be formed.

Application of the boundary condition at the points (n-1, n+1), (n - 2, n + 1) (n - 3, n + 1) etc. leads to a similar set of equations in which the position of S, and S′ are reversed.

Since the values of ϵ_r are symmetrical about the point (0, n + 1) subtraction of these sets of equations in pairs gives a set of n independent equations for $S_s - S'_s$ namely

$$\sum_s \left(S_s - S'_s \right) a_0 \left(t_s^{-1} - t_s \right) = 0$$

$$\sum_s \left(S_s - S'_s \right) \left\{ a_0 \left(t_s^{-2} - t_s^{2} \right) + a_1 \left(t_s^{-1} - t_s \right) \right\} = 0$$

$$\sum_s \left(S_s - S'_s \right) \left\{ a_0 \left(t_s^{-3} - t_s^{3} \right) + a_1 \left(t_s^{-2} - t_s^{2} \right) + a_2 \left(t_s^{-1} - t_s \right) \right\} = 0$$

etc., etc..

These can only be satisfied if $S_s = S'_s$ for all s and the preceding equations

/(32)

(32) reduce to

$$\left.\begin{aligned}
&\sum_s S_s a_0 \left\{ t_s - t_s^{-1} \right\} &&= \epsilon_1 \\
&\sum_s S_s \left\{ a_0 (t_s^2 - t_s^{-2}) + a_1 (t_s - t_s^{-1}) \right\} &&= \epsilon_2 \\
&\sum_s S_s \left\{ a_0 (t_s^3 - t_s^{-3}) + a_1 (t_s^2 - t_s^{-2}) + a_2 (t_s - t_s^{-1}) \right\} &&= \epsilon_3 \\
&\qquad \text{etc.,} \qquad\qquad \text{etc,}
\end{aligned}\right\} \quad (33)$$

For convenience in manipulation these equations can be rewritten

$$\sum_s S_s (t_s^r - t_s^{-r}) = F(r) \qquad r = 1, 2, 3 \dots n \qquad (34)$$

where F(r) is obtained from the recurrence relation

$$\left.\begin{aligned}
F(r) &= a_0^{-1} \left\{ \epsilon_r - \sum_{i=1}^{r-1} a_{r-i} F(i) \right\} \\
F(1) &= a_0^{-1} \epsilon_1
\end{aligned}\right\} \quad (35)$$

The values of a_r, and ϵ_r required to calculate F(i) from equations (35) can themselves be derived from the finite difference equation (4). If we denote by a_{rs} and ϵ_{rs} the values of a_r and ϵ_r appropriate to an upper boundary at the Sth row of the grid then equation (4) leads directly to the recurrence formulae

$$\left.\begin{aligned}
a_{r,s+1} &= C_s a_{r,s} - A_s (a_{r-1,s} + a_{r+1,s}) - a_{r,s-1} \\
\epsilon_{r,s+1} &= C_s \epsilon_{r,s} - A_s (\epsilon_{r-1,s} + \epsilon_{r+1,s}) - \epsilon_{r,s-1}
\end{aligned}\right\} \quad (36)$$

with the starting conditions

$$\left.\begin{aligned}
&a_{r,0} = 0 \text{ for all r,} \\
&a_{0,1} = 1 \qquad a_{r,1} = 0 \qquad r \neq 0 \\
&\epsilon_{0,0} = 1 \qquad \epsilon_{r,0} = 0 \qquad r \neq 0 \\
&\epsilon_{r,1} = 0 \quad \text{for all r.}
\end{aligned}\right\} \quad (37)$$

The relations (36) and (37) were used to calculate a_r and ϵ_r and from these equations (35) were used to calculate the constant terms in equations (34). This set of n linear equations was then solved for the coefficients S_s and, using these, the solutions on the lowest row of the grid, $\phi_{r,1}$ could be obtained.

The solution appropriate to a ridge represented by non-zero values of the stream-function at more than one point of the lower boundary was then derived by superposition of appropriate multiples of the solution obtained for the case of a single non-zero value. Subsequently the solution for the whole field was reconstructed using the finite difference equation (4).

A check on the accuracy of the procedure should have been provided by the vanishing of $\phi_{r,n+1}$ on the upper boundary. However as noted in section 4 of the paper a very high degree of accuracy is needed in intermediate stages of the calculation if this condition is to be satisfied. In the calculations now reported adequate accuracy could not be achieved with n = 7 and even with n = 6 no satisfactory check at the upper boundary was achieved in all cases. (The individual diagrams illustrate the stream lines computed at the upper boundary which should have been straight and horizontal.)

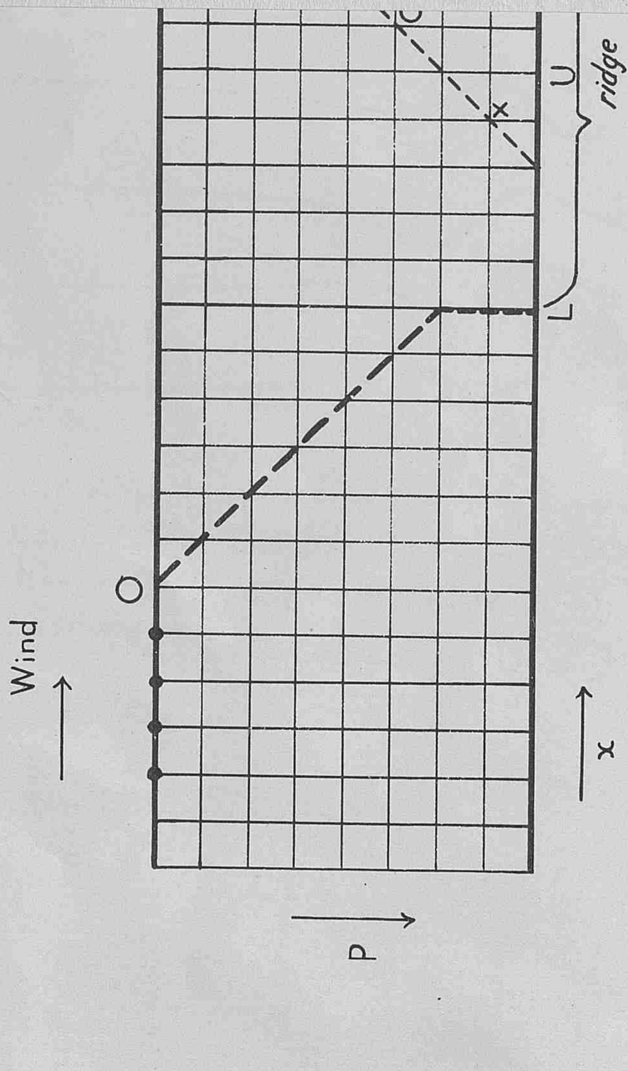

Fig. I

$$\left.\begin{aligned} F(r) &= a_0^{-1}\left\{\epsilon_r - \sum_{i=1}^{r-1} a_{r-i}\, F(i)\right\} \\ F(1) &= a_0^{-1}\,\epsilon_1 \end{aligned}\right\} \quad (35)$$

The values of a_r, and ϵ_r required to calculate F(i) from equations (35) can themselves be derived from the finite difference equation (4). If we denote by a_{rs} and ϵ_{rs} the values of a_r and ϵ_r appropriate to an upper boundary at the Sth row of the grid then equation (4) leads directly to the recurrence formulae

$$\left.\begin{aligned} a_{r,s+1} &= C_s\, a_{r,s} - A_s\left(a_{r-1,s} + a_{r+1,s}\right) - a_{r,s-1} \\ \epsilon_{r,s+1} &= C_s\, \epsilon_{r,s} - A_s\left(\epsilon_{r-1,s} + \epsilon_{r+1,s}\right) - \epsilon_{r,s-1} \end{aligned}\right\} \quad (36)$$

with the starting conditions

$$\left.\begin{array}{llll} a_{r,0} = 0 \text{ for all } r, & & & \\ a_{0,1} = 1 & a_{r,1} = 0 & & r \neq 0 \\ \epsilon_{0,0} = 1 & \epsilon_{r,0} = 0 & & r \neq 0 \\ \epsilon_{r,1} = 0 & \text{for all } r. & & \end{array}\right\} \quad (37)$$

The relations (36) and (37) were used to calculate a_r and ϵ_r and from these equations (35) were used to calculate the constant terms in equations (34). This set of n linear equations was then solved for the coefficients S_s and, using these, the solutions on the lowest row of the grid, $\phi_{r,1}$ could be obtained.

/The

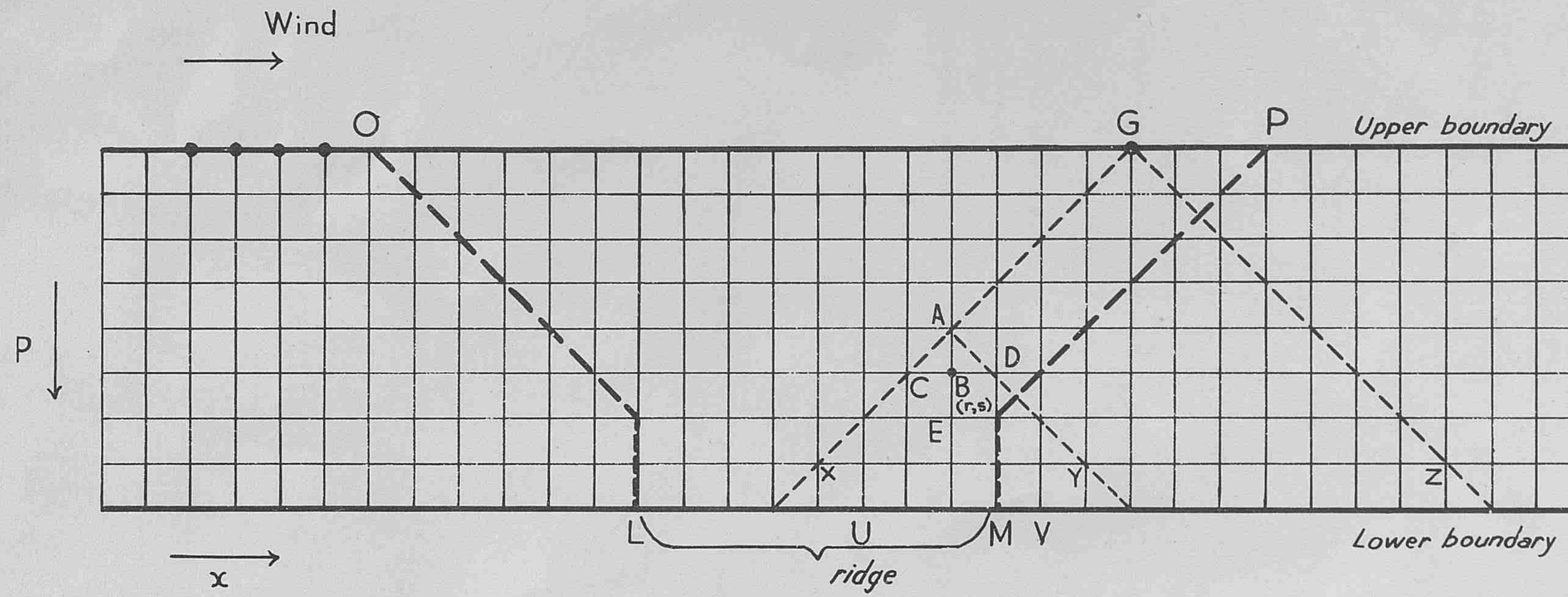
Wind
O
G
P
Upper boundary
P
A
D
C
B
(r,s)
E
x
Y
Z
L
U
M
V
Lower boundary
x
ridge

Fig. 1

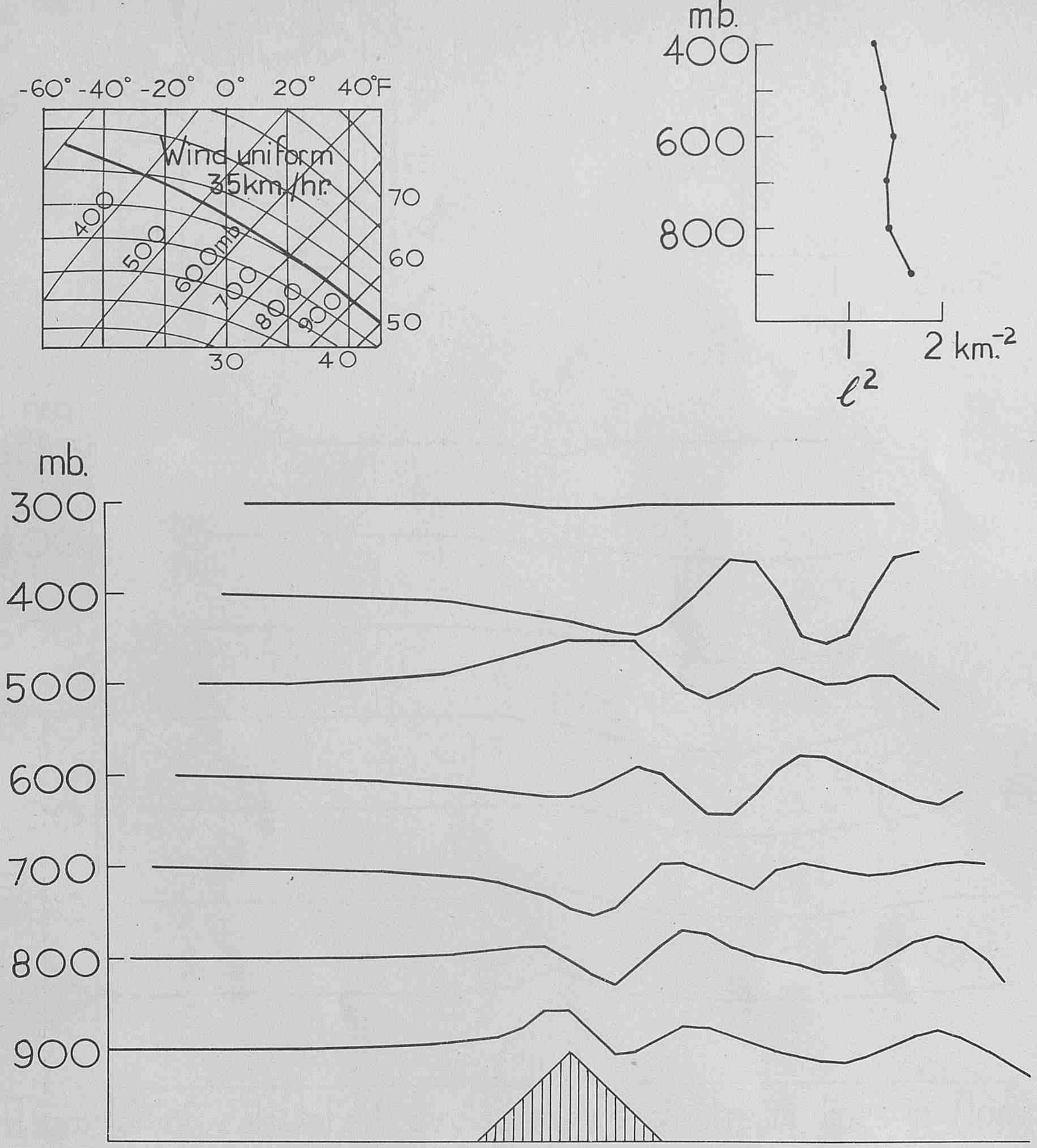

Example of calculated displacements of stream lines in flow over a ridge

Fig. 2

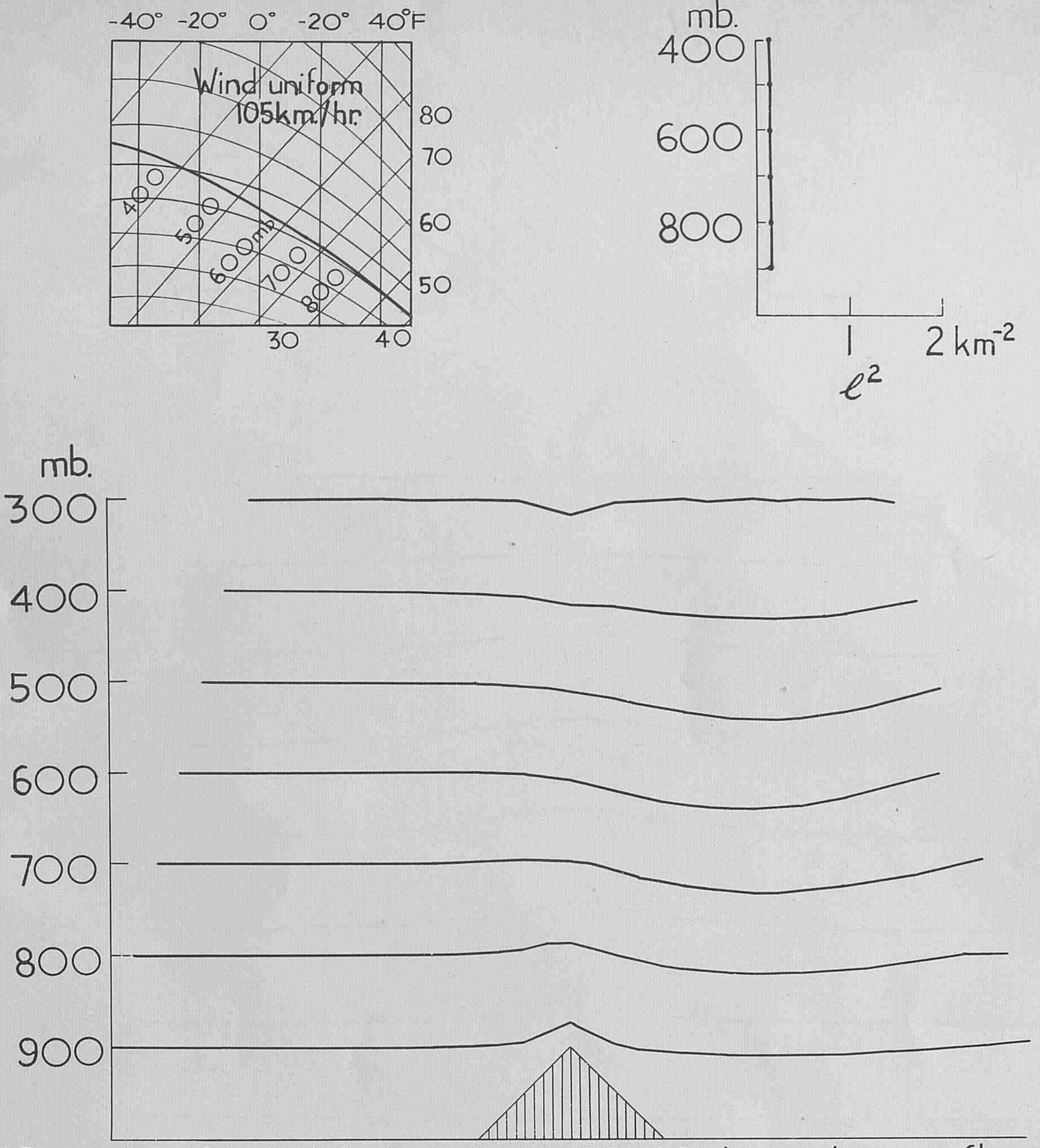

Example of calculated displacements of stream lines in flow over a ridge

Fig. 3

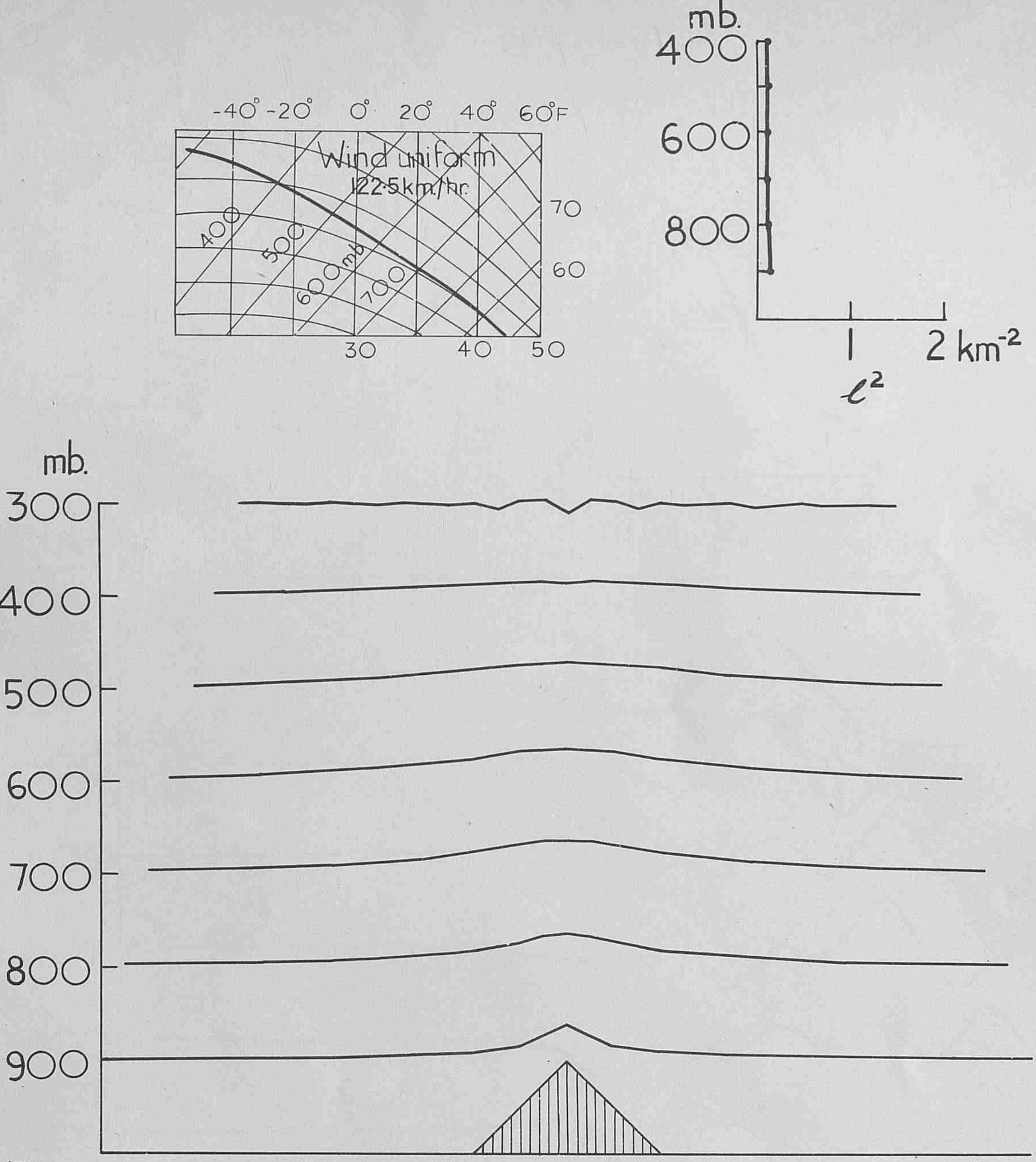

Example of calculated displacements of stream lines in flow over a ridge

Fig. 4

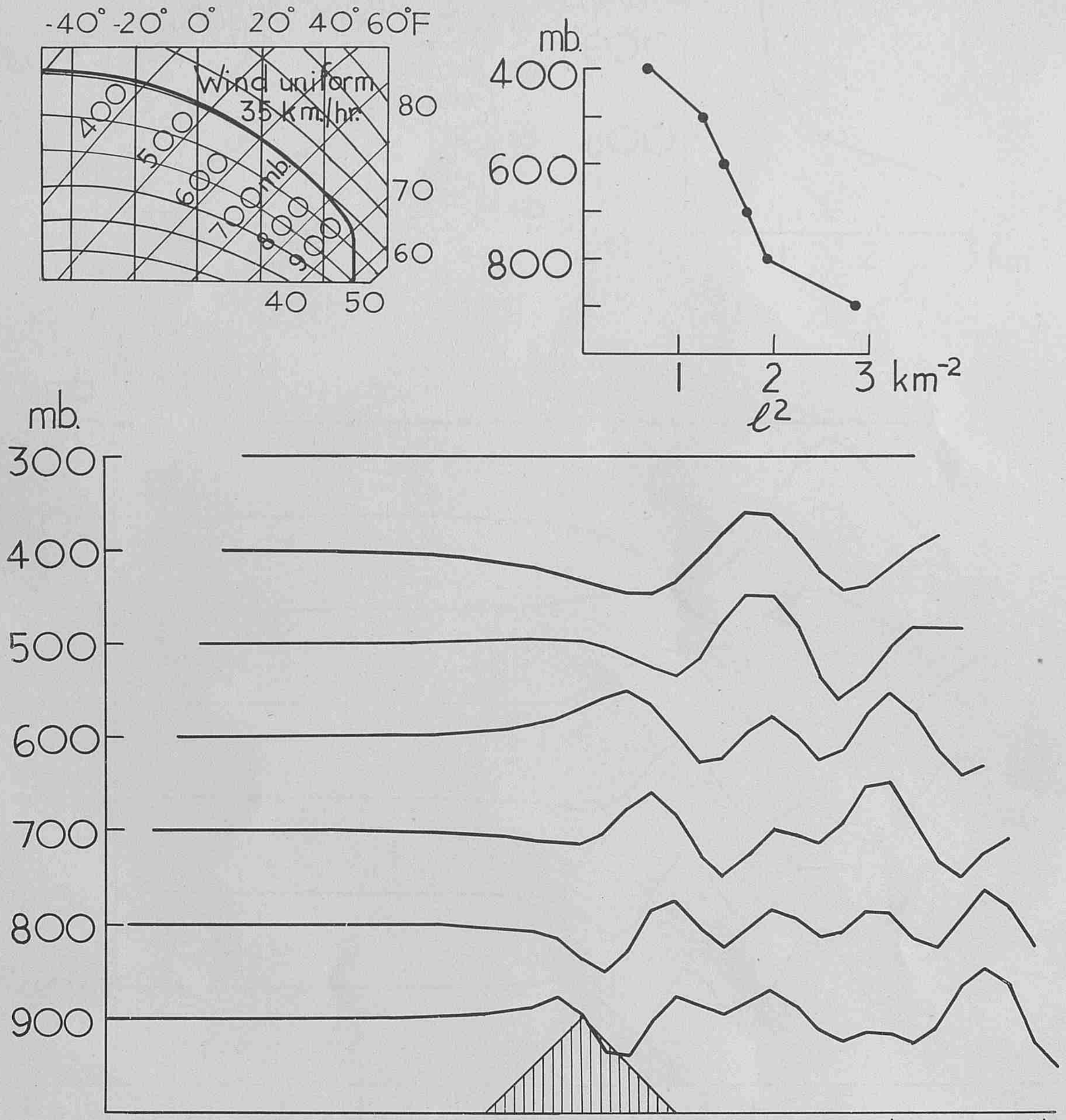

Example of calculated displacements of stream lines in flow over a ridge
Fig. 5

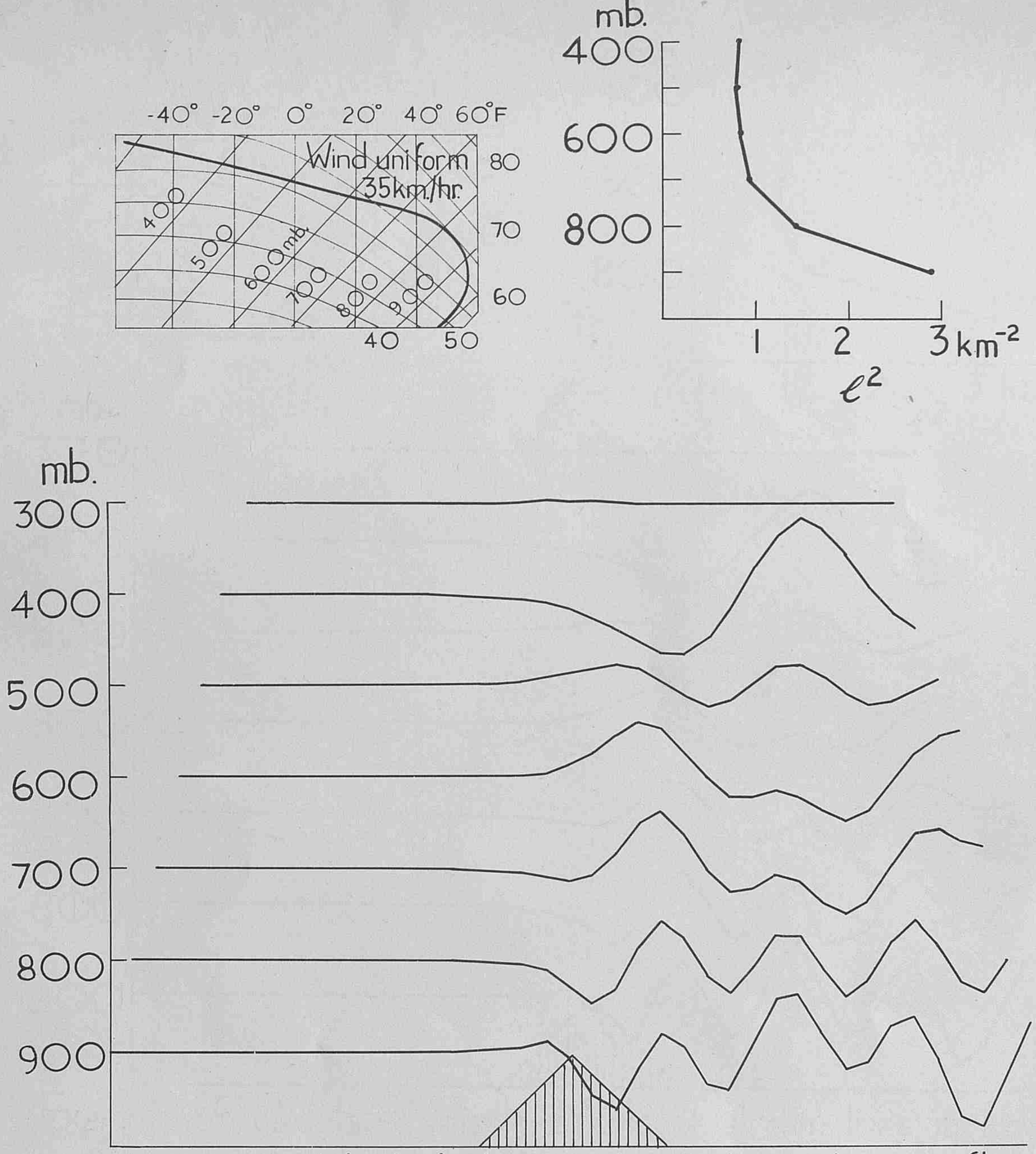

Example of calculated displacements of stream lines in flow over a ridge

Fig. 6

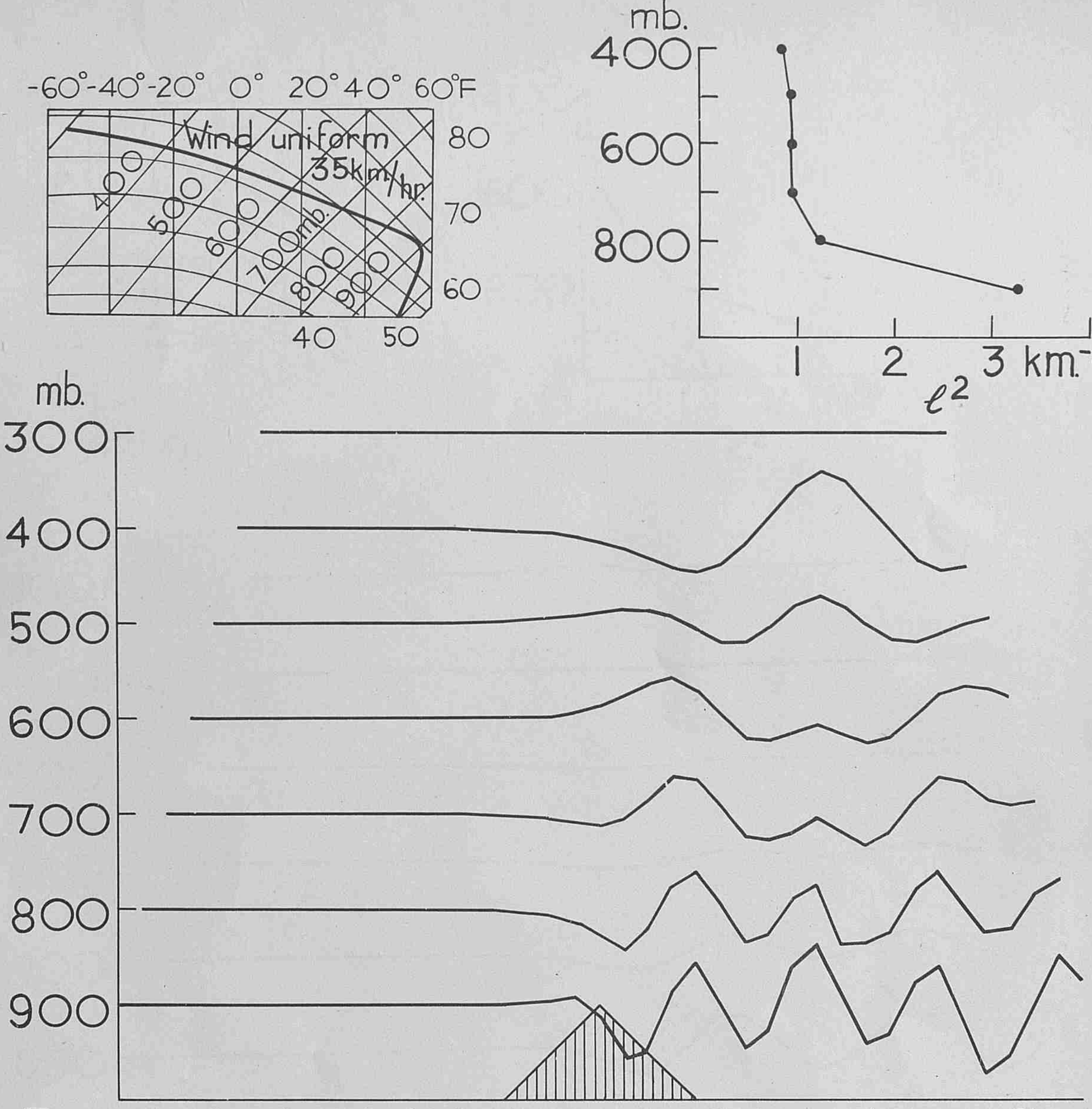

Example of calculated displacements of stream lines in flow over a ridge

Fig. 7

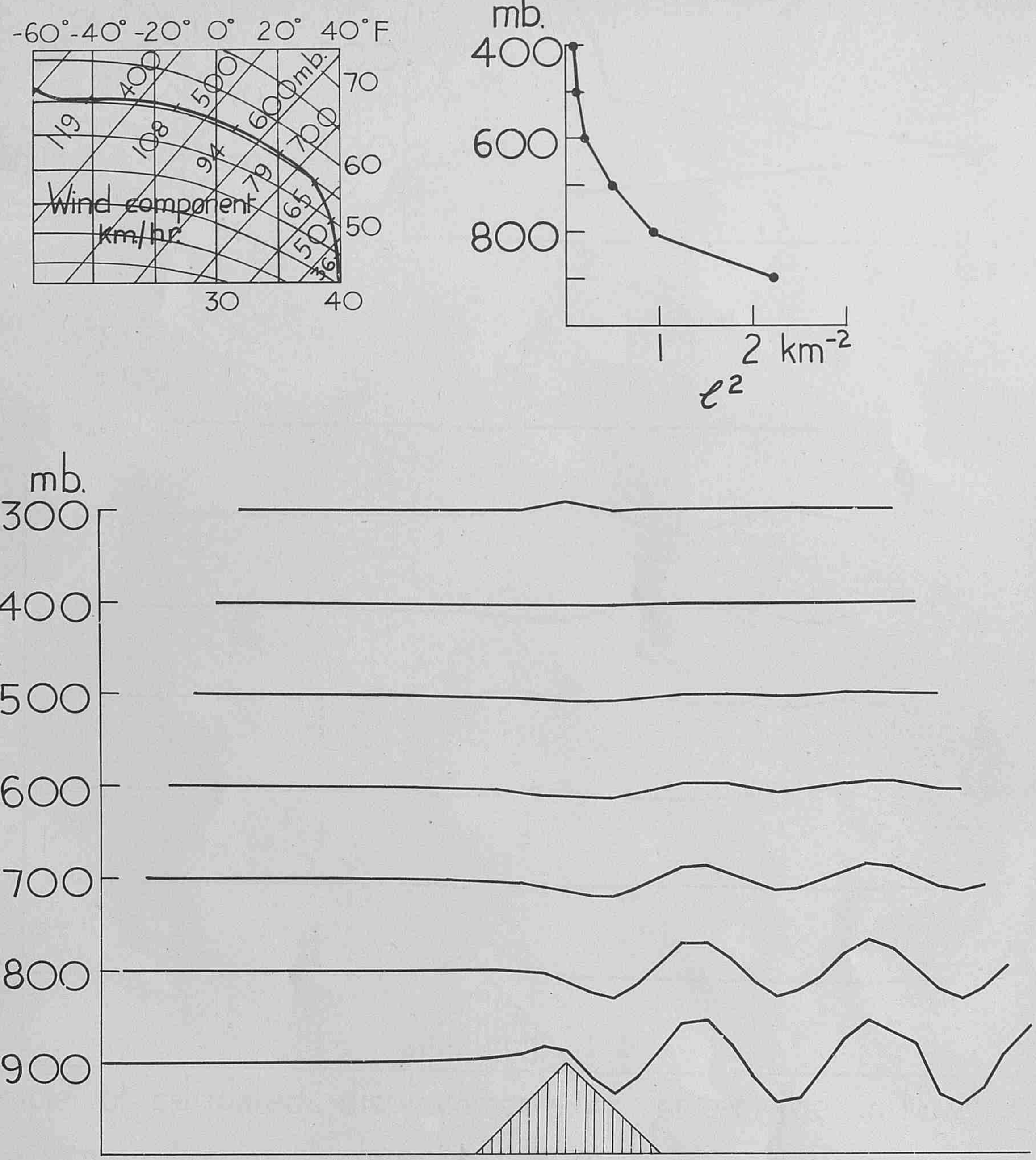

Example of calculated displacements of stream lines in flow over a ridge

Fig. 8

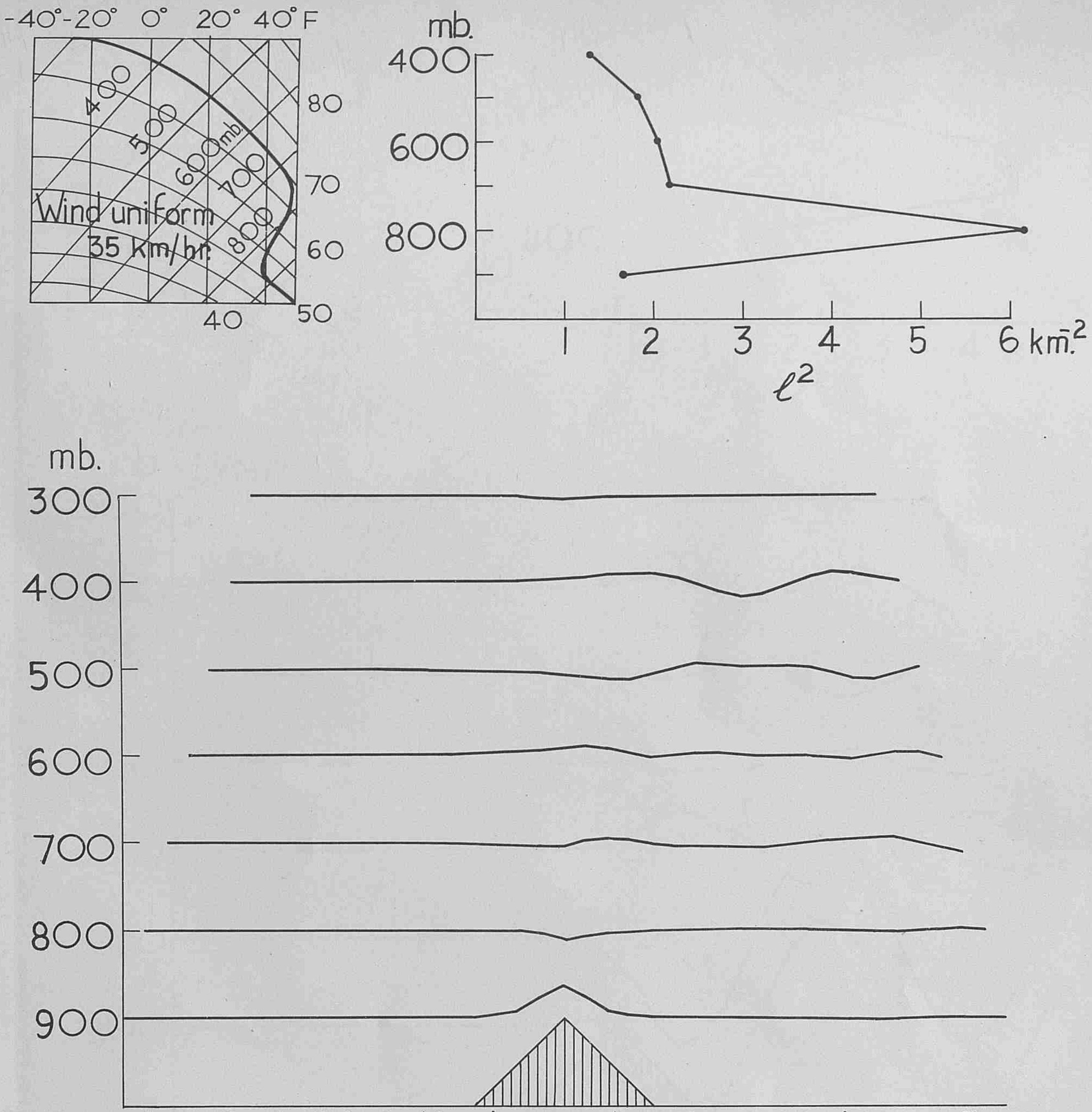

Example of calculated displacements of stream lines in flow over a ridge

Fig. 9

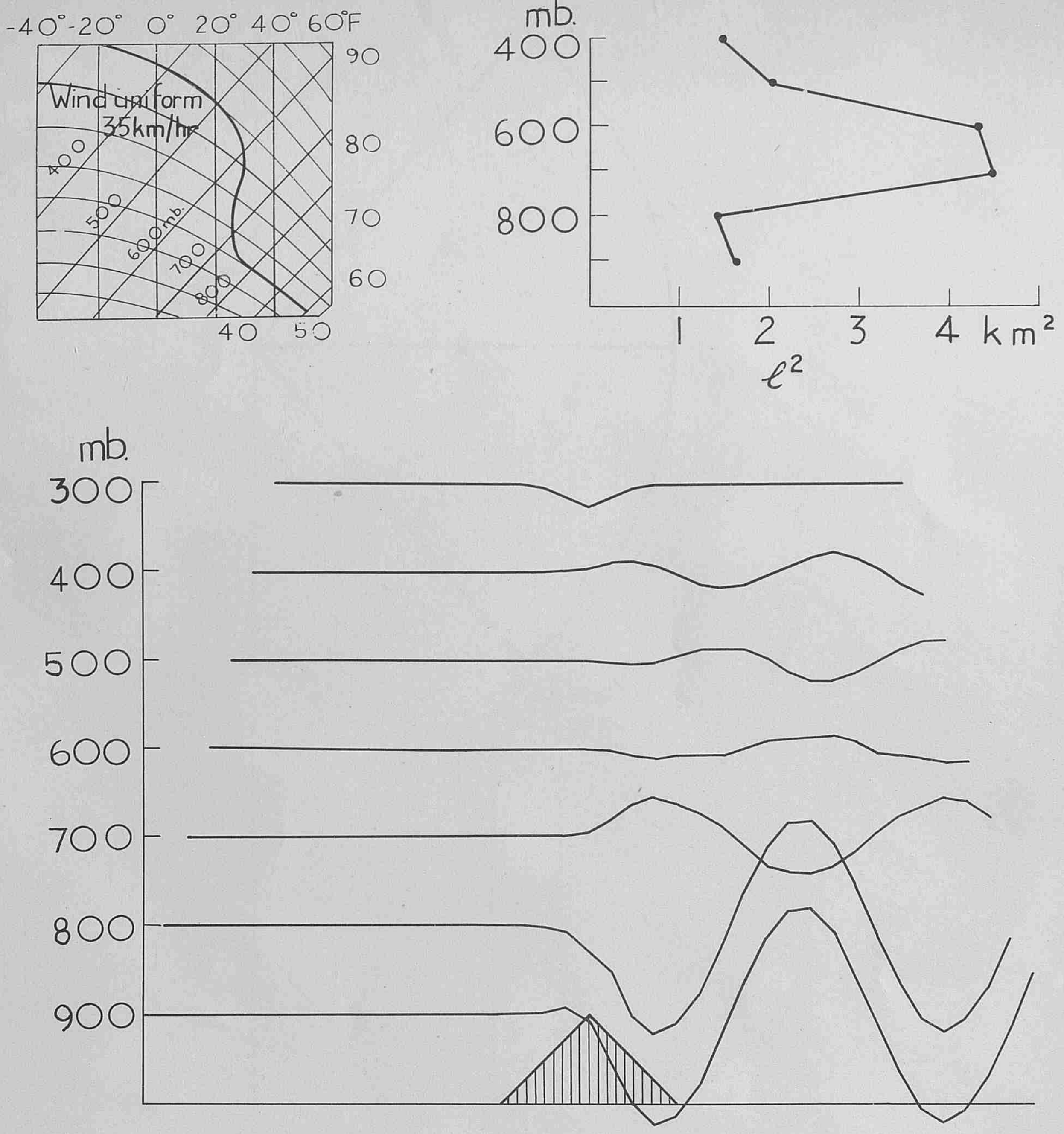

Example of calculated displacements of stream lines in flow over a ridge

Fig. 10

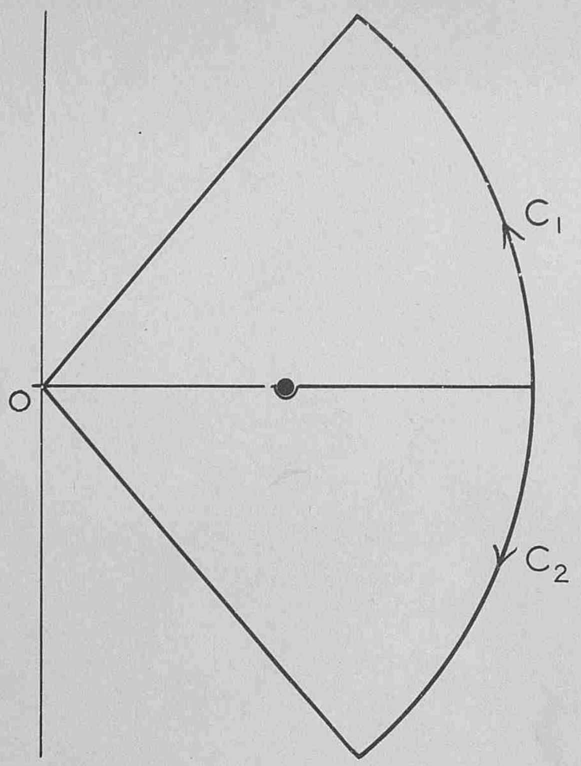

Fig. 11(a)

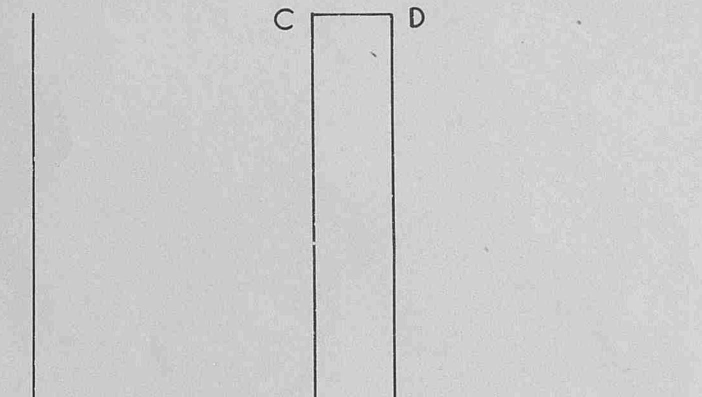
C
D
Pole
ν1/ν2
ε
ε
O
A
B
X
K = k0
C1
D1

Fig. 11(b)

M.R.P. 1043 MAY

M.R.P. 1043
S.C.I/126
12th March, 1957

1043

MAY 1958

Report on flight tests of a prototype conical head aircraft thermometer

by

C. H. Hinkel

(Meteorological Office)

AIR MINISTRY

METEOROLOGICAL RESEARCH COMMITTEE

MASTER FILE COPY
NOT TO BE REMOVED
FROM AWS TECH FILES

At the time of issue this report has not been published. Any author desiring to quote this paper should refer to it as "A paper of the Meteorological Research Committee (London), M.R.P. No. 1043 by Mr. C.H. Hinkel. A copy is available in the Library of the Meteorological Office."

M.R.P. 1043
S.C.I/126
12th March, 1957

AIR MINISTRY
METEOROLOGICAL RESEARCH COMMITTEE

Report on flight tests of a prototype conical head aircraft thermometer

by

C.H. Hinkel (Meteorological Office)

1. Introduction

In a recent paper Clark (1956) describes an aircraft thermometer which on theoretical considerations has a sensibly constant recovery factor. Confirmation of the theory was obtained by wind tunnel testing, but as there is often a considerable difference between tunnel and flight conditions it was decided to test the thermometer in free flight. The details of these tests and the results obtained are set out below.

2. Construction and mounting

The thermometer was mounted on a hollow metal rod attached to the port wing tip of Canberra aircraft No. W.J.582 of the Meteorological Research Flight at Farnborough. The rod projects forward a distance of about 3 feet ahead of the leading edge of the wing in order that the thermometer element may be in airflow unaffected by the wing surfaces and tips. Photographs of the mounting are shown in Fig. 1 and 2.

The thermometer was made to the specification and drawings set out by Clark (1956) with one slight alteration. The metal former upon which the resistance element is wound was made of dural instead of thermo-pure aluminium, since the latter was found to be almost impossible to machine to the required standard of accuracy. This change could not in any way affect the aerodynamic performance of the thermometer and laboratory tests failed to show any significant increase in the lag. A close-up of the completed instrument is shown in Fig. 3.

3. Instrumentation

The element was used in conjunction with a standard Meteorological Office Mk. 2(b) balanced bridge indicator mounted in the observer's compartment. The thermometer and bridge were calibrated both before and after the flights in order that any drift or other errors might be detected. The aircraft also carried a flat-plate thermometer mounted under the nose (see Fig. 2) and connected to a balanced bridge indicator in the observer's compartment. The readings of this thermometer were used as a check on those of the conical head.

4. Flight procedure

On each flight readings of conical head, flat plate and I.C.A.N. altimeter were taken simultaneously by the observer every half minute, while at the same time the aircraft navigator read the radar altimeter and airspeed indicator.

The speed runs were carried out on the lines of those done by Durbin (1955) and consisted of five-minute runs on two reciprocal bearings, one at low speed (about 160 kt indicated airspeed at all heights) and the other at as high a speed as possible (420 kt I.A.S. at 10,000 ft decreasing to 230 kt I.A.S.

at 40,000 ft). Ten sets of runs were made altogether at heights of 10,000 ft, 20,000 ft and thereafter at 5,000 ft intervals to 40,000 ft. In addition a set of runs was made at 10,000 ft indicated height in which the speed of each run was increased by 30 kt to cover the speed range from 160 kt to 420 kt indicated airspeed. These latter runs were all done on one flight.

5. Data

Corrections for instrumental error were applied to all the instruments except the radar altimeter, which was only used as a check on the I.C.A.N. altimeter readings. The airspeed indicator and altimeter readings were corrected for position and compressibility errors.

The values of the recovery factor (λ) were computed from the equation given in the Appendix, which is very similar to that used by Durbin (1955). The values of the temperature increment δT due to the difference in the pressure heights of the fast and slow runs were obtained from representative radio sonde ascents for the day and time of the flight. The differences so obtained did not affect the values of the recovery factor by more than 2 per cent on any individual value. The values of the specific heat at constant pressure used were those given by Clark (1951). Finally the recovery factors were recomputed after an attempt had been made to correct the thermometer readings for radiation errors on the basis of Clark's figures ((1956) Table 5), assuming the emissivity to be 0.15.

6. Results

The results of the flights for both conical head and the flat-plate thermometer are set out in Table 1 below as mean values for each level:-

Table 1

Height (1,000 ft)	No. of obs.	Flat plate		Conical head			
				No radiation correction		Radiation correction applied	
		λ	σ	λ	σ	λ	σ
10	8	.76	.022	.88	.030	.88	.026
20	9	.78	.026	.86	.027	.87	.015
25	7	.81	.028	.87	.017	.88	.025
30	9	.84	.017	.87	.024	.87	.025
35	8	.88	.063	.90	.063	.91	.065
40	10	.85	.057	.87	.050	.89	.047
Mean		.822	.035	.88	.035	.88	.034
Mean all values		.823	.058	.88	.041	.88	.026

In this table λ = recovery factor, σ = standard deviation.

The results of the second flight series are shown in Fig. 4 as a graph of indicated temperature against (equivalent airspeed)^2/ pressure, and the values of the recovery factors computed for this flight are

Conical head $\lambda = 0.87$
Flat plate $\lambda = 0.75$

/7.

7. Discussion

An examination of the values of the recovery factor λ obtained shows that for the conical head they remain sensibly constant up to 30,000 ft but that there is an increase above this height especially when radiation corrections were applied. Above 30,000 ft the standard deviation was more than doubled. This last result is also apparent in the standard deviations for the flat plate and is noted by Durbin (1955). The flat plate shows a fairly steady increase in recovery factor up to 35,000 ft and then a decrease. Pairs of values of λ for each thermometer were next tested for significant difference using Student's t-test (Fisher (1946)) as follows. The mean value of λ for 10,000 ft for the conical head was tested with that for 20,000 ft and the probability that the two arose from the same population determined and the determination was then repeated for all possible combinations. The probabilities obtained were not less than 0.15 for any pair. Thus it is reasonable to conclude that the recovery factor of the conical head can be regarded as sensibly constant. Similar tests were applied to the flat-plate thermometer and the probability varied from 0.6 to 0.01, being largest where the two levels were adjacent and least where they were furthest apart, as might be expected from the values obtained. In this case the assumption of a constant recovery factor does not seem justified. Graphs of recovery factor against height for the two thermometers are shown in Fig. 5.

As a further comparison the mean values for each level were correlated with height and regression lines obtained. The values are set out in Table 2. The correlation coefficients were tested for significant difference from zero. In tests of this type a low probability is associated with a highly significant difference and vice versa. The low correlation coefficient for the conical head, especially when no correction for radiation errors is made, points to the non-dependence of the recovery factor upon height, and this is reflected in the slope of the regression line. Furthermore, it suggests that the radiation correction applied is too large and that the true correction is of such small proportions that for practical purposes it can be ignored.

Table 2

	Conical head		Flat plate
	No radiation correction	Radiation correction applied	
Correlation coefficient (r)	0.118	0.504	0.924
Probability of significant difference from zero	0.82	0.25	0.01
Regression line (h = ht. x 10^{-4})	$0.873 + 0.0014h$	$0.865 + 0.006h$	$0.718 + 0.039h$

The increased variances at above 35,000 ft require some explanation. They can arise from four causes:

(i) change of airflow over the entire aircraft causing fluctuations in λ

(ii) the generation of shock waves on the thermometer elements

(iii) changes of airflow over the thermometers due to a turbulent boundary layer causing fluctuations in the values of λ

(iv) instrumental errors in the airspeed indicator and altimeter at high altitudes and high Mach numbers.

The first of these can be ruled out on the grounds that it would seriously impair the performance of the aircraft and lead to stalling. The stalling speed of a Canberra is about 110 kt indicated airspeed at all heights or about 50 kt less than the speed of the slow runs.

The formation of shock waves would affect the flow over the thermometers if such a wave occurred near or in contact with them. The faster of the two runs was carried out at approximately Mach number 0.81 and the occurrence of shock waves is therefore not unlikely. The conical head thermometer has a shock wave attached to the apex of the cone at speeds approaching that of sound other than about $M = 0.95$ to $M = 1.046$ in which range it is slightly ahead of the apex (Taylor and McColl (1933)). There is also another at the point where the slant of the cone curves round to fit into its holder. Neither of these would affect the element. However, any irregularities in the join between the metal element cover and the paxolin body of the cone would generate further shock waves which would be in contact with the thermometer element itself and would therefore affect its readings. The flat plate is somewhat different in that there will certainly be a shock wave at the leading edge of the plate and also at each of the leading edges of the radiation shield. The line of these last two might well intersect the thermometer element and cause additional interference. Failure of these to affect the behaviour of the thermometer below 35,000 ft can be ascribed to the fact that only at the highest two levels was Mach number 0.81 exceeded and for $M < 0.80$ the intensity of the shocks is likely to be small. An examination of the individual values of λ for the two levels concerned shows that there are three anomalous values at 35,000 ft and two at 40,000 ft, all of which are considerably larger than the rest. This applies to both thermometers and the anomalous values all occurred on the same flights. The correlation between the anomalous values and the Mach number of the corresponding high-speed runs is -0.67 for the conical head and -0.66 for the flat plate. These are significant at the 20 per cent level. The number of observations in the sample is only five, and much stress cannot therefore be laid upon this result. It does, however, indicate a possible source of variation, although the fact that the anomalous values occur always on the same flights for both thermometers points more strongly to some other cause extraneous to the thermometers themselves.

The third possible source of the large scatter, namely, change of character of the airflow over the thermometers, is not thought likely to provide anomalies of the sort found. For if following Clark (1952) a change of boundary layer flow from laminar to turbulent at Reynolds numbers 0.5×10^5 (unit of length = 1 cm throughout) is postulated, then theoretical considerations require that the change of flow is in fact from a turbulent to a laminar boundary layer in order to be consistent with the values of recovery factor obtained for the lower levels. At the highest two levels the speed runs are done at Reynolds numbers less than 0.5×10^5, and the anomalous values must therefore be due to laminar boundary flow for which the recovery factor is less than that for turbulent flow. If we assume that the change, contrary to considerations of Reynolds number, does take place from laminar to turbulent boundary and substitute the appropriate values in the expression given by Clark (1951) for the recovery factor, only about half the difference between the two sets of values can be explained. Furthermore the simultaneous occurrence of the anomalies with both thermometers would imply that the boundary layer changes occur together over each thermometer and in view of their different geometrical shapes this seems most unlikely to occur.

Finally the fact that the fluctuations occur at the same time for each thermometer suggests that their cause is unconnected with the thermometers themselves or the airflow over them. A further pointer in favour of this is the two different positions of mounting, one at the wing tip and the other at the nose. An extraneous source of error can arise from only two instruments, the altimeter and the airspeed indicator. It seems likely therefore that irregularities in the behaviour of either or both of these instruments at high altitude or Mach number are the sources of the large variances.

The single flight at 10,000 ft with increasing speeds for each run provides a slight measure of confirmation of this last suggestion. The top speed reached on this run was $M = 0.76$ so that the conditions of the runs above 30,000 ft do not obtain and in addition the range of Reynolds numbers covered (0.5×10^5 to 1.27×10^5) precludes extrapolation to the higher levels at which the highest Reynolds number was $Re = .67 \times 10^5$ for the fast runs at 35,000 ft, all other runs being at $Re < 0.5 \times 10^5$. However, the two graphs do indicate a recovery factor for each thermometer which shows little evidence of change with speed and the values obtained (0.87 for the conical head and 0.75 for the flat plate) agree well with the corresponding values obtained by the previous method.

8. Conclusions

It would appear that the conical head thermometer does have a sensibly constant recovery factor within the limitations of speed and height ranges covered by the above flights. The increased scatter at high altitude of the values of the recovery factor when speeds in excess of $M = 0.80$ are reached stresses the need for a very smooth surface of the instrument especially at the joins of the outer thermometer element and the cone itself, since it is at these points that irregularities giving rise to shock waves can affect the recovery factor. Photographs taken in a wind tunnel at appropriate Mach numbers and corresponding Reynolds number should reveal such effects. The introduction of a radiation correction makes only about a one per cent difference in the results and from a practical point of view seems scarcely worth while at subsonic speeds.

The flat-plate thermometer shows generally an increasing value of recovery factor with height, but little variation with speed at least up to Mach number 0.80 and similar remarks apply to the scatter of the values at high level. The increase in recovery factor is the opposite of that obtained by Shellard (1949) who found a decrease with altitude. This is probably due to the differing angles of attack of the thermometers and also to the angles of attack of the aircraft themselves at high level. It is not clear, however, that the scatter is due to the thermometers. As pointed out in the text it could well be caused by errors in the other instruments involved, namely the airspeed indicator or the altimeter.

The scatter imposes limits upon the accuracy of the measurement of the true air temperature. Taking σ as 0.03 for heights up to 30,000 ft the error in the true air temperature is less than 1°C at true airspeeds less than 500 kt but above this height taking $\sigma = 0.06$ the error is only less than 1°C up to 300 kt T.A.S. and is 1-2°C between 300 and 500 kt. The conclusion already reached that the error is not due to the thermometers implies that the development of the latter has reached the limit of its useful accuracy when used with present equipment for measuring altitude and airspeed. A similar conclusion was reached by Durbin (2).

9. Acknowledgements

In writing this report I very gratefully acknowledge the work done by the Meteorological Research Flight who arranged for the mounting of the thermometer and did all the flying involved. I have also pleasure in acknowledging the skill of Mr. B.T. Quilter who made and calibrated the thermometer.

/10.

10. References

Clark, D.D. 1951 An assessment of the probable causes of variation of the speed correction coefficient of aircraft thermometers. Meteorological Research Papers, Air Ministry, London, No. 677.

Clark, D.D. 1952 Wind tunnel tests of the M.O. flat-plate thermometer. Meteorological Research Papers, Air Ministry, London, No. 744.

Clark, D.D. 1956 Development of thermometers for high-speed aircraft. Meteorological Research Papers, Air Ministry, London, No. 960.

Durbin, W.G. 1955 Some further determinations made by the M.R.F. of the speed correction coefficients of aircraft thermometers. Meteorological Research Papers, Air Ministry, London, No. 930.

Fisher, R.A. 1946 Statistical methods for research workers. Oliver and Boyd.

Shellard, H.C. 1949 Variation with altitude of the speed correction coefficients of aircraft thermometers. Meteorological Research Papers, Air Ministry, London, No. 527.

Taylor, G.I. and McColl, J.W. 1933 The air pressure on a cone moving at high speeds. Proc. Roy. Soc., (A), Vol. 139, p. 278.

Appendix

Determination of the recovery factor

The recovery factor is given by

$$T = T_i \Big/ \left(1 + \frac{\gamma-1}{2}\lambda M^2\right) \tag{1}$$

in which T is the true air temperature, T_i = indicated temperature, λ = recovery factor $(0 < \lambda \leq 1)$, γ = the ratio of the specific heats of air, M = Mach number.

Using suffix 'L' to denote values relating to the low speed run and suffix 'H' for the high speed run and assuming both runs are done at the same height

$$\frac{T_L}{1 + \frac{\gamma-1}{2}\lambda M_L^2} = \frac{T_H}{1 + \frac{\gamma-1}{2}\lambda M_H^2} \tag{2}$$

In practice, due to errors in the airspeed indicator, it is not feasible to do both runs at the same height. Suppose then that the temperature at the height of the slow run is T and that at the height of the fast run T+ δT then

$$T = \frac{T_L}{1 + \frac{\gamma-1}{2}\lambda M_L^2} \qquad \text{and} \qquad T + \delta T = \frac{T_H}{1 + \frac{\gamma-1}{2}\lambda M_H^2}$$

whence

$$\frac{T_L}{1 + \frac{\gamma-1}{2}\lambda M_L^2} + \delta T = \frac{T_H}{1 + \frac{\gamma-1}{2}\lambda M_H^2}$$

from which

$$T_H - T_L - \delta T = \lambda \frac{\gamma-1}{2}\left\{T_L M_H^2 - T_H M_L^2\right\} - \lambda\frac{\gamma-1}{2}\delta T\left(M_L^2 + M_H^2\right) - \left\{\frac{\lambda(\gamma-1)}{2}\right\}^2 M_L^2 M_H^2 \delta T \tag{3}$$

Now $0 < \lambda \leq 1$ and δT did not amount to more than $\frac{1}{2}$°C. and $M_L^2 + M_H^2$ was always < 1. The ratio of the first and second terms on the R.H.S. is therefore not greater than 1/180 and of the first and third terms not greater than 1/1,000. Thus by ignoring the last two terms on the R.H.S. the error in the determination is certainly not greater than one per cent.

Equation (3) then becomes

$$T_H - T_L - \delta T = \lambda\frac{\gamma-1}{2}\left(T_L M_H^2 - T_H M_L^2\right) \tag{4}$$

Let suffix zero refer to standard I.C.A.N. values of the variables at M.S.L. Let a be the speed of sound, p be the pressure at the levels concerned and v the equivalent airspeed then with a little manipulation

$$M^2 = k v^2 / p \qquad (k = p_0 / a_0^2) \tag{5}$$

Substituting for M^2 in (4) and solving for λ

$$\lambda = \frac{2\left(T_H - T_L - \delta T\right)}{(\gamma-1)k\left\{\frac{T_L v_H^2}{p_H} - \frac{T_H v_L^2}{p_L}\right\}} \qquad (6)$$

This equation, which is substantially the same as that given by Durbin (1955), was used for the determination of the recovery factor.

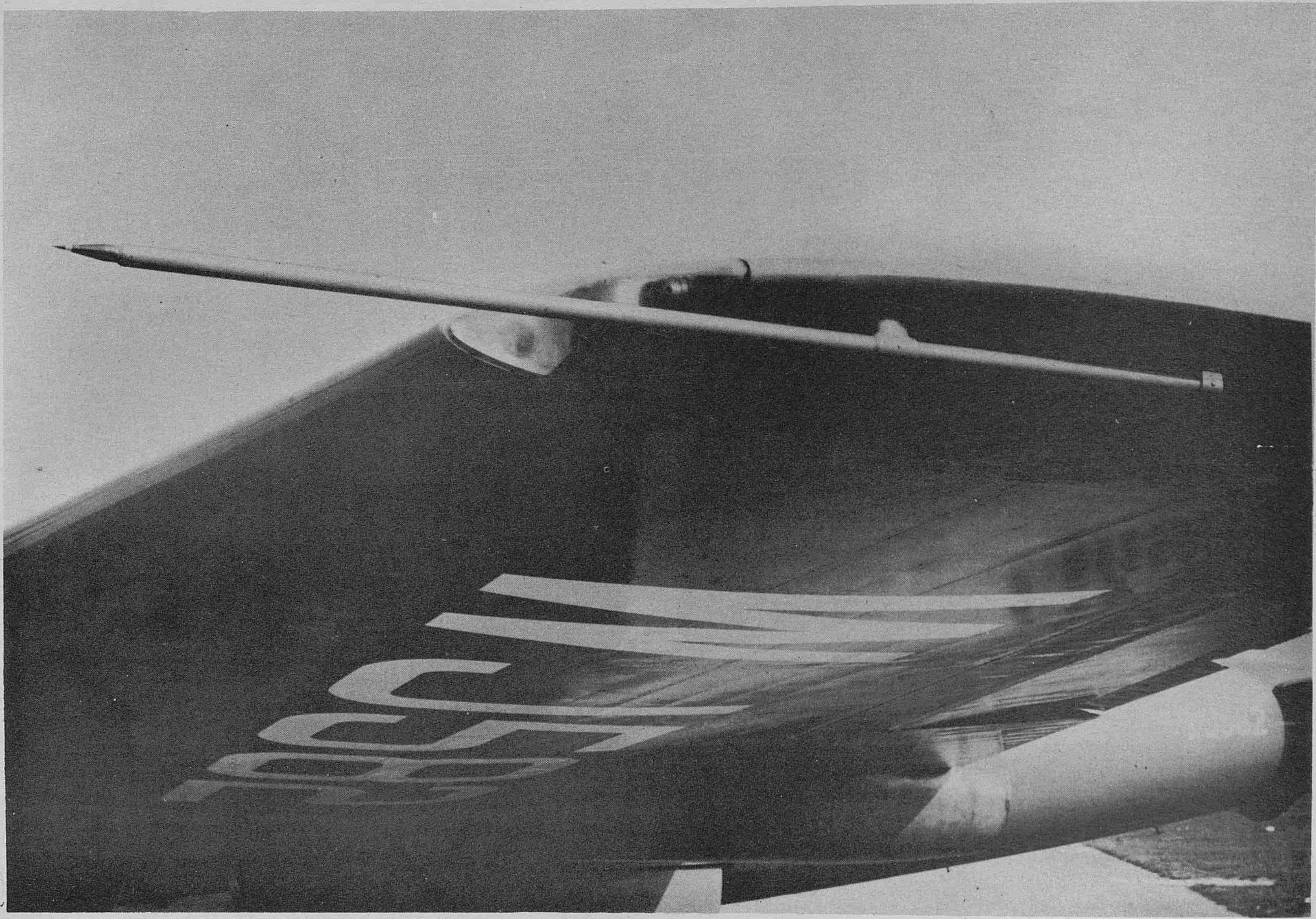

FIG. 1

CLOSE-UP OF THERMOMETER MOUNTED ON WING-TIP OF CANBERRA AIRCRAFT

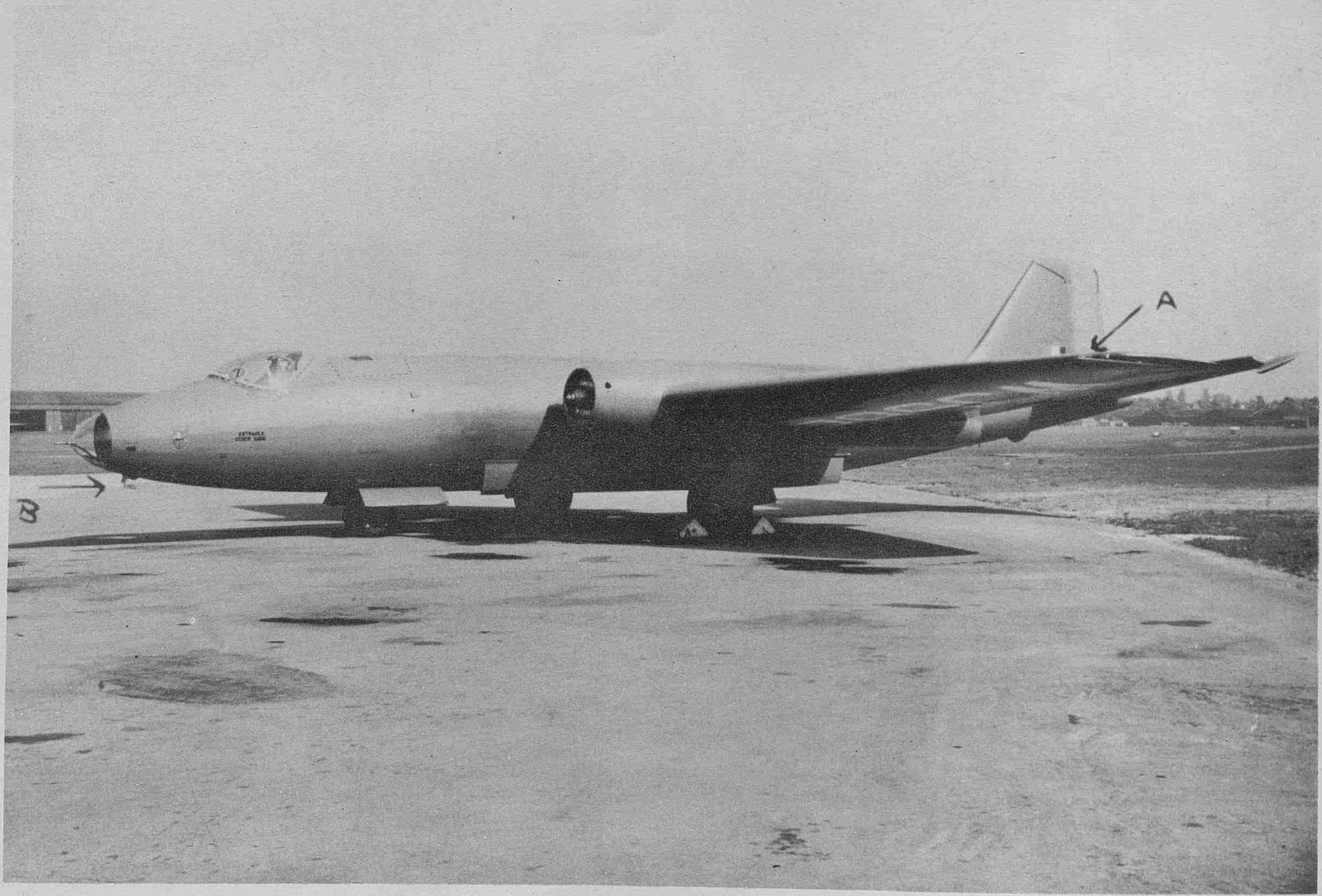

FIG. 2

CANBERRA WJ582

SHOWING (A) CONICAL HEAD THERMOMETER & (B) FLAT PLATE THERMOMETER

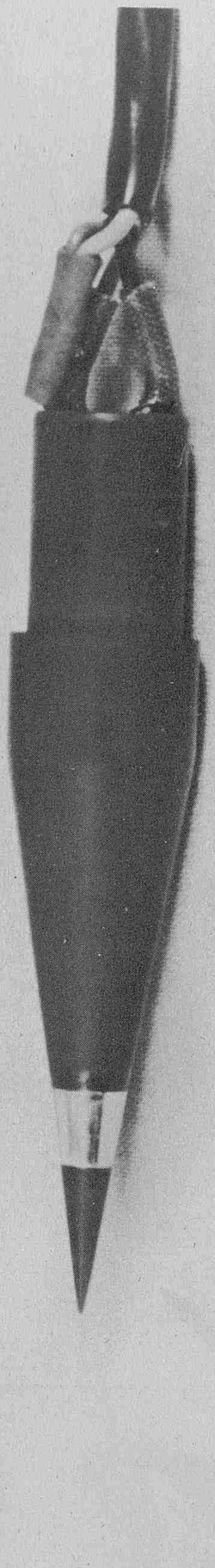

FIG. 3

CONICAL HEAD THERMOMETER

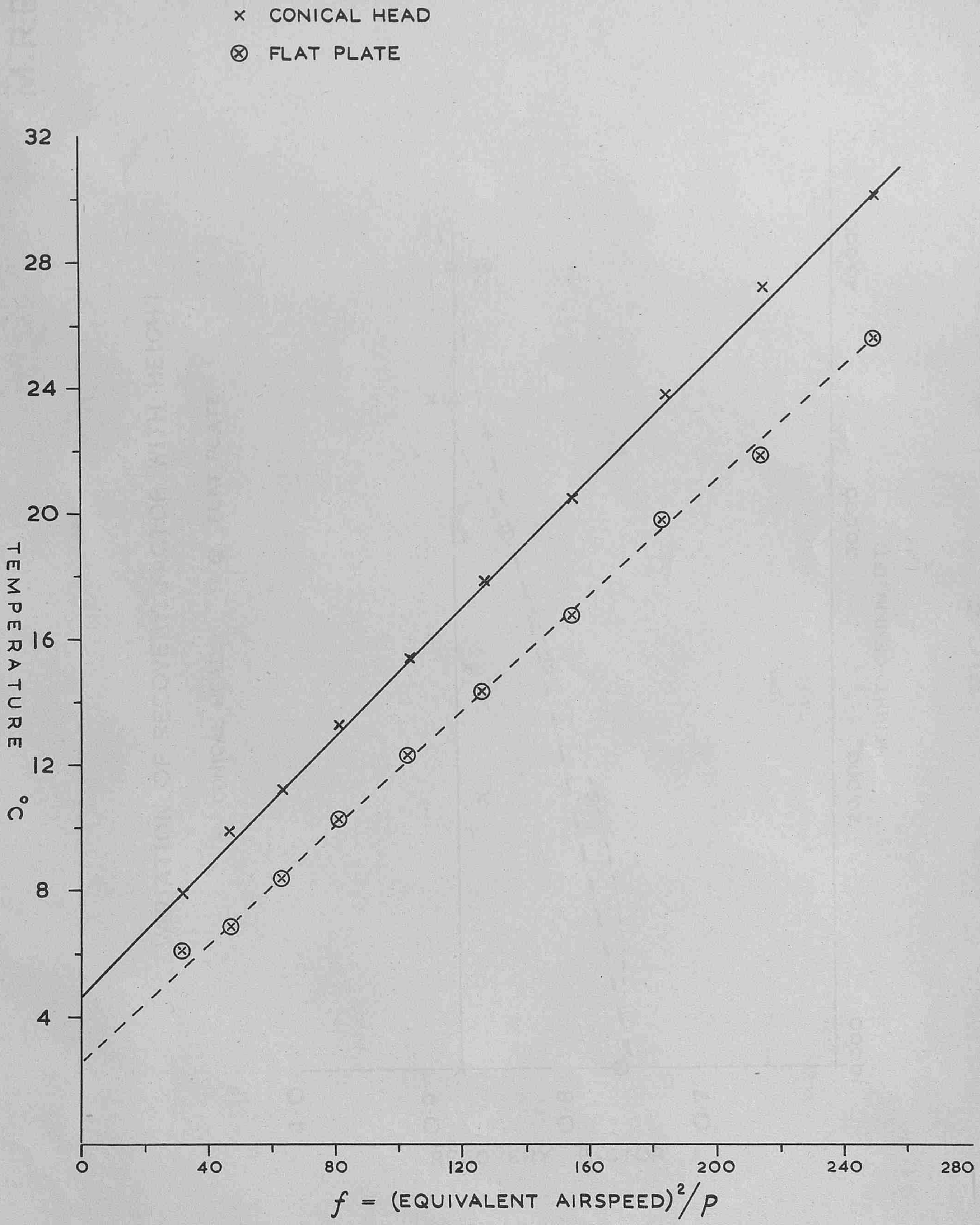
× CONICAL HEAD
⊗ FLAT PLATE
TEMPERATURE °C
32
28
24
20
16
12
8
4
0
40
80
120
160
200
240
280
f = (EQUIVALENT AIRSPEED)²/p

FIG. 4

VARIATION OF RECOVERY FACTOR WITH HEIGHT

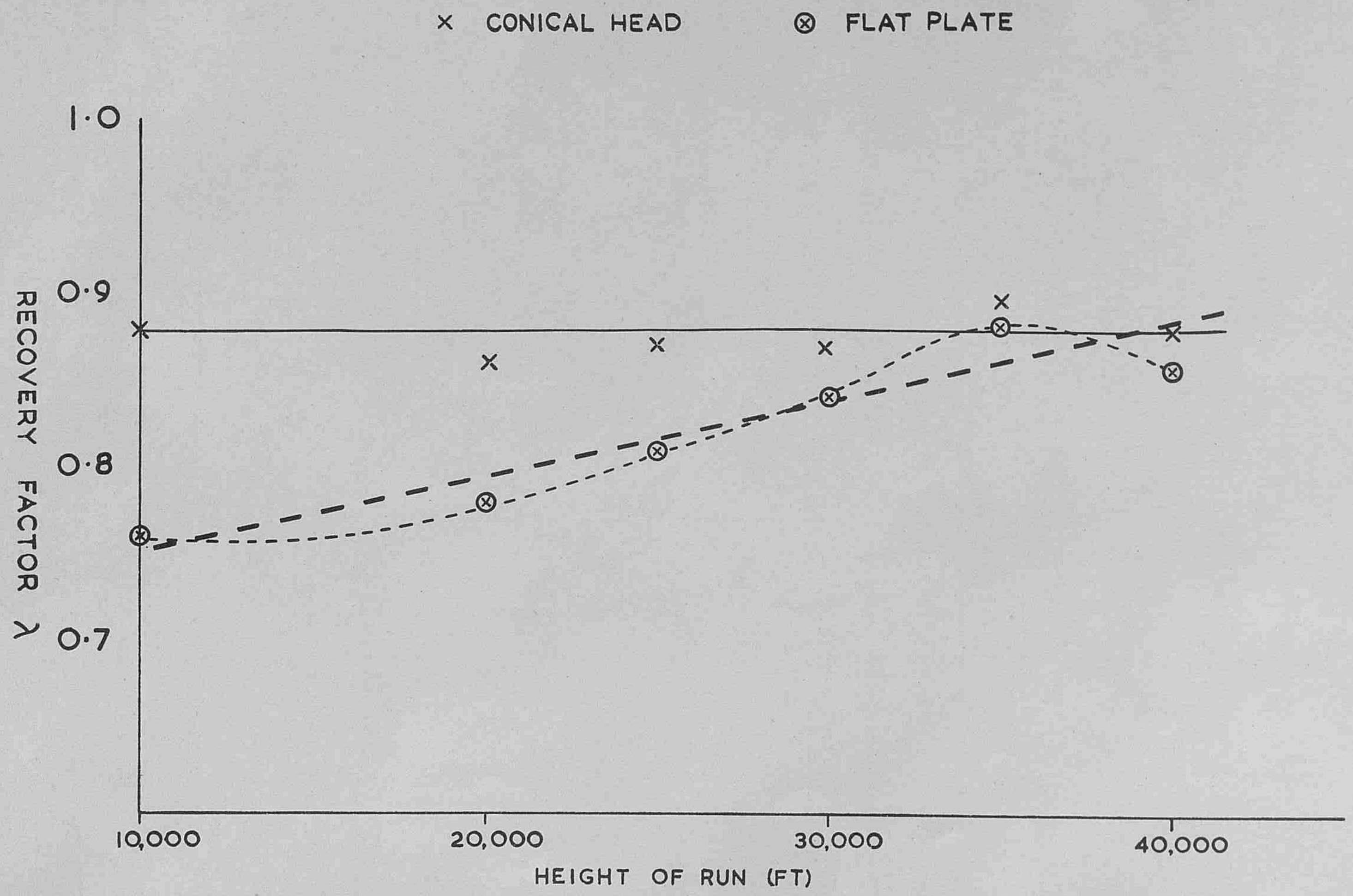

FIG. 5

M.R.P. 1044
S.C. 111/231
26th February, 1957

Studies of eddy structure in the first few thousand feet of the atmosphere

Part 2. A preliminary examination of the spectrum and scale of the vertical component at 2,000 feet.

by

R. A. Jones

(Meteorological Office)

AWSSS
ROUTING SLIP

FILE	INFO	ACTION				
	4.1		DIRECTOR			
			DEP DIRECTOR			
	3	3	ASST TO DIRECTOR			
	1	1	CONSULTANTS		lws	
	2	2	[illegible]		CHF	
				✓	SS	RKW
					RB	Mls
					[illegible]	
					[illegible]	
	4	4		✓	[illegible]	G
					[illegible]	
			EDD	✓	[illegible]	
					SPFB	
					CU	
					SEC	
6	5		TIPD		CHF	
					PUE	
					TECH INFO	
					SEC	

AIR MINISTRY

METEOROLOGICAL RESEARCH COMMITTEE

At the time of issue this report has not been published. Any author desiring to quote this paper should refer to it as "A paper of the Meteorological Research Committee (London), M.R.P. No. 1044 by Mr. R.A. Jones. A copy is available in the Library of the Meteorological Office."

M.R.P. 1044
S.C.III/231
26th February, 1957

AIR MINISTRY
METEOROLOGICAL RESEARCH COMMITTEE

Studies of eddy structure in the first few thousand feet of the atmosphere

Part 2. A preliminary examination of the spectrum and scale of the vertical component at 2,000 feet

by

R.A. Jones (Meteorological Office)

SUMMARY

A preliminary calculation of the energy spectrum for the vertical component of eddy motion over the frequency range $\left(\frac{1}{75} - \frac{1}{5}\right)$ cycles per sec. has been made, using observations of wind inclination at 2,000 feet over Cardington under near neutral conditions. The description of this calculation is preceded by a brief review of the principles of the various methods available for computing energy spectra, including the Fourier-transform method as developed and modified by Tukey (1950), the practical details of which are given in the appendices. Graphs and tables show the effect of the modifications on the resulting energy spectrum, and it is seen that the spectral curves decrease rapidly with increasing frequency over the greater part of the frequency range investigated. This variation with frequency agrees well with that deduced from measurements at similar heights from aircraft, and is broadly consistent with with the predictions of similarity theory.

An attempt was also made to investigate the vertical scale of turbulence around 2,000 feet through the Eulerian space-correlation coefficients, but the vertical space separations then attainable (up to 150 feet) were insufficient for a full specification of the correlation curve.

INTRODUCTION

In the study of atmospheric turbulence and diffusion it is desirable to estimate the turbulent energy of the various velocity components, and also to investigate the scale of turbulence as a means of assessing the magnitude of the eddies taking part in the turbulent motion. The total energy of the motion represents fluctuations in a wide range of frequencies (reciprocal of the period), and a more detailed knowledge of the eddy structure can be obtained if the fractions of the energy which are associated with the various frequencies are known. Published work to date on the evaluation of "energy spectra" (for example Panofsky and McCormick 1954, Webb 1955, and Panofsky and Van der Hoven 1956) and of the scale of turbulence (Howcroft 1956, MacCready 1953 and Gerhardt et alia 1952) is largely confined to the lower layers of the atmosphere. This paper describes a preliminary calculation of the energy spectrum and the scale of turbulence for the vertical velocity component, using some recent data on wind inclination at 2,000 feet. Discussion of the data and the calculation is preceded by a brief review of the principles of the various numerical methods available for computing energy spectra of velocity fluctuations, including the Fourier-transform method used here. The practical details of the method used are presented in appendices.

/I.

I. METHODS OF COMPUTING ENERGY SPECTRA

1. Moving averages

It is possible to get an idea of the energy distribution in turbulent motion by the crude method of forming a succession of moving averages of the original data with different periods (Panofsky and Singer 1951). The averaging process cuts out the shorter period fluctuations more or less effectively, leaving the longer period fluctuations. Hence, by choosing a succession of averaging periods, one can separate to some extent by subtraction the energy contributions possessed by eddies of a particular frequency range.

Given a sequence of observations X_i for i = 1, 2 ...... N, individual values of which are short-period means over δT sec., the simplest procedure is to form another sequence of running means Y_i of period T sec. (where T is some multiple of δT). Then $(X_i - Y_i)$ contains the contribution from the eddies with periods T to δT sec. or in the frequency range $1/\delta T$ to 1/T cycles per sec. This process can be repeated as often as desired, subject to limitation by the original period δT sec. and the number of observations N. It should be noted that the mean values of the parameter $(X_i - Y_i)$ in the separate sequences are not strictly zero, since in forming the mean of Y_i the end values of the original series have less weight than the remaining values. This is overcome by considering the energy to be contributed by fluctuations from the mean $\overline{(X_i - Y_i)}$ in each sequence. The energy contribution to the total energy of the motion from the respective frequency ranges is then determined by the mean square of the fluctuations from that mean.

The most important defect is that a moving average does not have a sharp energy cut-off, so that some of the energy assigned to a particular frequency range is actually contributed by fluctuations outside that range. This can be eliminated to some extent by forming weighted moving averages from the original series X_i, thereby sharpening the cut-off property in the frequency ranges. This modification is mentioned by Tukey (1951) in an unpublished paper, but has not been widely used by workers on energy spectra.

2. Fourier-transform method

Spectral analysis by this method is based on the theorem (Wiener 1930) that the cosine-transform of the autocorrelation function of a time-series is essentially equal to the spectrum of the original series. In the classical form (Priestley and Sheppard 1952)

$$F(n) = 4\int_0^\infty R(t).\cos 2\pi nt.\,dt; \qquad \int_0^\infty F(n)dn = 1 \qquad (1)$$

where R(t) is the autocorrelation coefficient after a time t, F(n)dn is the contribution to the energy present between the frequencies n and (n + dn) cycles per unit time. This transformation can be applied to a finite period T provided the period is taken sufficiently long for R(t) to become insignificant at all times greater than T. The accuracy of the results will increase with increasing length of the given series.

Assuming a continuous curve for the correlogram, energy spectra can be computed from equation (1) to varying degrees of approximation by the following three methods:-

(a) graphical integration of the product of the assumed correlation curve with a succession of cosine functions of known periods,

(b) the use of an appropriate integral approximation formula (e.g. Webb 1955),

(c) approximating the correlation function R(t) to a standard decay function (Webb 1955), evaluating the spectral estimates analytically, and subsequently applying a correction for the residue using a planimetric method (Crease and Tucker 1954).

The extreme range of frequencies over which spectral estimates can be obtained is $\left[\frac{1}{N\delta t} - \frac{1}{2\delta t}\right]$ cycles per sec. It has a lower bound at the low frequency end of the spectrum determined by the total length of the original record, and an upper bound at the high frequency end of the spectrum governed by the time interval δt between successive observations of the original data. Spectral analysis by Fourier-transform methods has a two-fold advantage over a straightforward Fourier analysis of the original data. Firstly, the computational time is shorter. Secondly, the correlation method gives the average power or energy over a range of frequency, in contrast to the energy present in each separate harmonic of Fourier analysis, with the result that it yields a 'smoothed' form of spectrum which is reproducible from a statistically similar set of data.

Tukey (1950) has presented a computational technique for evaluating the energy spectrum through equation (1) in a more realistic manner, which

(1) recognises the discontinuous nature of the correlogram,

(2) automatically limits the extreme frequency range which can be investigated,

(3) enables the statistical accuracy of the resultant spectral estimates to be determined,

(4) ultimately gives 'smoothed' spectral estimates representing average values over small finite frequency bands, and

(5) presents modifications to eliminate certain sources of error, dealt with in Appendix II under "aliasing", "prewhitening", and "averaging".

This method has been widely used by American workers (e.g. Panofsky and Van der Hoven 1954) and is used in the calculations in Part II of this paper. The computational procedure, together with the smoothing and correcting processes, are set out in some detail in the appendices.

Essentially the method consists firstly of forming values of the lag-products Q_k (lagged covariance) of the velocity fluctuations from the overall long-term mean values, thus

$$Q_k = \frac{1}{N-k}\left\{\sum_{i=1}^{N-k} x_i x_{i+k} - \frac{1}{N-k}\sum_{i=1}^{N-k} x_i \sum_{i=1}^{N-k} x_{i+k}\right\}; \quad k=0,1\cdots m \qquad (2)$$

for successive values of the lag-time $k, \delta t$. Covariances are used instead of correlation coefficients as in equation (1), since Wiener's original transformation is in terms of covariances. Thus, complications due to the variance altering with the lag-number k (i.e. changing with time) do not arise.

The number of lags, m, should be chosen with care. An estimate of the best value of m can be obtained from 'sampling theory' (Tukey 1950) by the use of the formula

$$f = \text{number of degrees of freedom} = \frac{2(N - m/4)}{m} \qquad (3)$$

the reliability of the spectral estimates increasing with increasing number of degrees of freedom. However, if m is too large the computational work involved becomes prohibitive; also the estimates of spectral energy obtained are uncertain due to the low value of f resulting for a fixed number of observations N. If m is too small the resolution of spectral estimates at low frequencies is poor. The number of degrees of freedom, through m, imposes a further restriction upon the lowest frequency at which reasonably accurate spectral estimates are possible. Thus the extreme range of frequencies over which spectral estimates are obtainable becomes limited to $\left[\frac{1}{2m\delta t} - \frac{1}{2\delta t}\right]$ cycles per sec. Values recommended by American workers in this field are $6 \leqslant m \leqslant 30$ and $f > 30$.

Subjecting the lagged covariances Q_k to harmonic analysis finally yields values of the 'smoothed' spectral estimates U_h, for h = 0, 1..... m, which are related to the classical theory's energy densities through the equation

$$U_h \equiv F(n) . \Delta n . Q_0 \qquad (4)$$

where Q_o = total variance, $n = h/2m\delta t$ and $\Delta n \equiv 1/2m\delta t$. The 'smoothed' spectral estimate U_h represents an average total energy contribution over the frequency range $(h-1)/2m\delta t \leqslant n \leqslant (h+1)/2m\delta t$ for h = 1, 2 .... (m - 1), while U_o and U_m are separately defined as the average energy contributions over the ranges $0 < n \leqslant 1/2m\delta t$ and $(m - 1)/2m\delta t \leqslant n \leqslant 1/2\delta t$ respectively. The process of smoothing must inevitably lead to some distortion near h = 0 and m.

The values of U_h^*, corrected for averaging of the original data (see Appendix II), when plotted as a function of the frequency represent the energy spectrum curve, which has the property that the area beneath the curve, between any two frequencies, is a measure of the contribution to the total variance from that frequency range; and the total area bounded by the curve when extended to infinity represents the total variance. In order to examine very large ranges of frequency the spectral estimates can be conveniently plotted against abscissae of logarithm of frequency; if the spectral estimates are themselves multiplied by their representative frequencies, then the same relationship exists between the area under the curve and the variance contribution.

The final result U_h^* represents an estimate of the average energy over a finite frequency range obtained from a certain finite sample of data X_i (i = 1, ... N), and the result will vary from sample to sample under given external conditions. However, it is possible to determine the statistical reliability of U_h^*. Assuming that the original data X_i are normally distributed, the spectral estimates U_h^* from different samples (containing the same number of observations) will have a χ^2/f - distribution for f degrees of freedom given by equation (3) (Tukey 1950). Hence given the value of f, the range of variability of the estimate U_h^* in each frequency band, for desired confidence limits, can be determined by means of the usual Tables of the χ^2 - distribution found in any book on statistics. It should be noted that the number of degrees of freedom corresponding to the end estimates U_o, U_m are f/2 since the estimates are here only averages over half the previous frequency range.

3. Squared difference method

The method above is an exact one, involving a great deal of computation depending upon the number, m, of lagged products desired. Although the analysis can often be accomplished with desk calculating machines, for very large m the use of electronic computers becomes necessary. A simpler method suggested by Tukey (Cramer 1955) of obtaining rough spectral estimates of the energy contained within various frequency bands, is that of deriving a sequence of squared differences between successive observations. The method gives very limited resolution, especially at low frequencies.

Given the set of consecutive data in a time series X_i for i = 1, 2..... N, with a time-lag δt sec. between successive values, the procedure is to form the sequences of squared differences of consecutive values of the sum of 2^{p-1} non-overlapping terms for p = 1, 2, ..., thus

$$\left[d_i(1)\right]^2 = \left[X_{2i} - X_{2i-1}\right]^2$$

$$\left[d_i(2)\right]^2 = \left[\left\{X_{2^2 i} + X_{2^2 i-1}\right\} - \left\{X_{2^2 i-2} + X_{2^2 i-3}\right\}\right]^2 \qquad (5)$$

$$\left[d_i(p)\right]^2 = \left[\left\{X_{2^p i} + \text{-----} + X_{2^p i-(2^{p-1}-1)}\right\} - \left\{X_{2^p i-2^{p-1}} + \cdots + X_{2^p i-(2^p-1)}\right\}\right]^2$$

for i = 1, 2, ... $\frac{N}{2^p}$, N being an integral power of 2.

It can be shown (Cramer 1955) that mean spectral density

$$= \frac{1}{N} \sum_{i=1}^{N/2^p} \left[d_i(p) \right]^2, \quad \text{for } p = 1, 2 \text{ ----} \tag{6}$$

representing rough estimates over the frequency intervals $\left[\frac{1}{2^p \delta t} - \frac{1}{2^{p+1} \delta t} \right]$ cycles per sec., but the cut-off property between the various frequency bands is not sharply defined and thus results in limited resolution.

This method is subject to the same sources of error, "aliasing" and "averaging", as the Fourier-transform method, but to a greater degree; however it involves less computation. At low frequencies the minimum confidence limits, assuming a χ^2-distribution for maximum number of degrees of freedom (which equals the total number of i's), become very wide for a large p due to the small number of degrees of freedom. Thus for $N = 512$, one must have $p<9$ for reasonable accuracy of spectral estimates at the lower frequencies.

4. Composite spectra

It is possible to increase the extreme frequency range over which the energy spectrum is obtained (Griffith et alia 1956) without increasing the computational work prohibitively, by forming several sequences composed of various short-period non-overlapping mean values of the original data X_i. Thus originally the frequency range is $[1/2m\delta t - 1/2\delta t]$ cycles per sec. for m lags, N observations and f degrees of freedom. Forming the non-overlapping means over $q\delta T$ sec., the spectral estimates for the range $\left[\frac{1}{2mq\delta T} - \frac{1}{2q\delta T} \right]$ cycles per sec. can be calculated. The value of m, upon which the increased frequency range depends, can be chosen subject to variation in f or the length of the original data X_i. This process can be repeated for different values of q. When combining the separate portions into a composite spectrum it is essential that the correction for the different averaging periods $q\delta T$ sec. in the various sequences is applied (see Appendix II). It is also important to note that the highest frequency estimates in each sequence are of doubtful accuracy due to "aliasing", but this can be overcome by choosing q so that the various frequency ranges overlap sufficiently to obviate the spurious values.

5. Estimation of the remaining energy from very high frequencies

The computed energy spectrum is limited at the high frequency end by the interval δt sec. between successive observations, the highest available frequency being $n_1 = 1/2\delta t$ cycles per sec. An estimate of the remaining energy contained in the frequency range from n_1 cycles per sec. to infinity can be obtained by extrapolation of the spectral curve to higher frequencies. It is usually found that a 'power-law' relation holds for that part of the spectral curve which decreases continuously with increasing frequency, resulting in a form

$$U(n) = An^{-\beta} \tag{7}$$

where $A, \beta > 0$, are constants.

Then

$$\text{energy remainder} \quad U(n) = \int_{n_1}^{\infty} An^{-\beta} dn = \frac{An_1^{-\beta+1}}{1-\beta} \quad \text{provided } \beta > 1 \tag{8}$$

Spectral curves of the form of equation (7) have been found with values of $\beta = 5/3$ (MacCready 1953) and $\beta = 2$ (Robinson 1953); and it should be noted that similarity theory for homogeneous turbulence predicts $\beta = 2$ for the inertial subrange of frequencies (Priestley and Sheppard 1952).

/II

II. CALCULATIONS OF ENERGY SPECTRA AND SCALE OF TURBULENCE

The experimental data consist of consecutive observations of wind inclination at a height of about 2,000 feet over Cardington on 30th June, 1956. They are used in the present analysis to determine the Eulerian correlation coefficients, both with respect to time and to space (vertically), and partly in a trial computation of energy spectra using the Fourier-transform method developed and modified by Tukey. Although the results refer strictly to fluctuations of wind inclination, they are considered approximately applicable to the vertical component of eddy motion.

The observations were obtained from a vertical array of three wind vanes A, B, C attached to the cable of a tethered balloon, using a technique which is described in detail in a separate report (Jones and Butler, 1956). Defining the apparent wind inclinations at the heights of the instruments by ϕ_A, ϕ_B, ϕ_C respectively, the data were in the form of three synchronous continuous records of the variates ϕ_A, $\phi_B - \phi_A$, $\phi_C - \phi_B$ (+ve in this sense); and a continuous record of the vertical movement of the balloon was also obtained.

Three 10-minute periods were chosen for analysis and are listed below with the corresponding instrument spacing (the instrument A being in each case at a height of 2,000 feet).

Run	Period (B.S.T.)	Distances (feet)		
		AB	BC	CA
1	1017 - 1027	5	50	-
2	1128 - 1138	100	50	150
3	$1222\frac{1}{2}$ - $1232\frac{1}{2}$	20	50	70

Over the entire period of the three runs, the external meteorological conditions remained similar with 7/8 - 8/8 high stratocumulus with 4/8 shallow cumulus cloud beneath, a slight lapse rate (surface lapse between 4 metres and $\frac{1}{2}$ metre of 0.5 - 1.0°F), and a mean wind speed of approximately 8 metres per sec. at 2,000 feet.

Successive non-overlapping $2\frac{1}{2}$ sec. mean values of the variates ϕ_A, $\phi_B - \phi_A$, $\phi_C - \phi_B$, were extracted in each case, so providing sequences of 240 values. At the wind speeds obtaining the total response-time of instrument and recorder is governed by the response-time of the recorder and is approximately 0.2 sec., so that the use of $2\frac{1}{2}$ sec. mean values eliminates any errors due to instrumental time-lag. Approximate corrections for the spurious component arising due to the movement of the balloon were applied individually to the extracted values ϕ_A. It was not possible to apply a complete correction for balloon movement, because no data of fluctuations in the horizontal wind speed were available. However, it is believed that the error in not applying the full correction will be very small. In any case it is reasonable to assume that the corrections to $\phi_B - \phi_A$ and $\phi_C - \phi_B$ due to balloon movement are zero, since the distance involved between the instruments is at most 150 feet.

1. Energy spectrum

Run (2) was chosen for the computation of the energy spectrum of wind inclination at 2,000 feet because the autocorrelation coefficient decreased most rapidly in this case, becoming + 0.06 after a total time-lag of $37\frac{1}{2}$ sec. (i.e. m = 15) (Fig. I). 'Sampling theory' gives through equation (3) that f = number of degrees of freedom $\bumpeq 30$, so that m = 15 gives reasonably reliable estimates of the energy contributions from the respective frequency bands. The resolution is limited to a total frequency range of (1/75 - 1/5) cycles per sec.

The procedure of Appendix I is now followed, forming the lagged covariances Q_k (k = 0, 1 ...., 15) and thence obtaining for h = 0, 1, ... 15 the 'apparent line powers' L_h, the 'smoothed' spectral estimates U_h, and the spectral estimates U_h^* corrected for 'averaging' (see Appendix II). The correction for averaging affects the spectral estimates at all frequencies, but is most marked at the highest frequencies. The individual values, related to a total variance or total energy of unity from all frequencies, are given in Table II. Spectral curves (Fig. II) are given with abscissae the logarithm of frequency and ordinates the spectral estimates (as a fraction of the total energy) multiplied by their respective frequencies in 1/75 cycles per sec., i.e. the ordinates are nF(n). In this manner the area under the curve between any two frequencies represents directly the fraction of the variance, or energy, contributed by the frequencies in that interval. The 'smoothing' process eliminates the pronounced peak which occurs near the frequency of 1/15 cycles per sec.

The original data were next subjected to the "prewhitening" process of Appendix II with b = 0.75, and Fig.I shows the effect of this transformation on the correlation curve. The computational analysis was then repeated with the transformed data and the true spectral estimates L_h, U_h recovered by the application of equation (2) of Appendix II. These were again corrected for 'averaging' by equation (3) of Appendix II. The results are given in Table II and the spectral curve of 'corrected' U_h^*, plotted as a function of the logarithm of frequency, is shown in the same manner as before (Fig. II). As expected, the 'prewhitening' process does not appreciably alter the spectral estimates except at the lowest frequencies.

The spectral curves decrease rapidly with increasing frequency over the greater part of the frequency range investigated. The 'corrected' U_h^* values for the 'unprewhitened' case are found to fit a 'power law' of the frequency of the form

$$U^*(n) \propto n^{-\beta}$$

where $\beta = 1.59 \pm 0.20$ for the frequency range (1/75 - 15/75) cycles per sec., $\beta = 1.62 \pm 0.32$ for the frequency range (2/75 - 15/75) cycles per sec., and $\beta = 1.86 \pm 0.32$ for the frequency range (1/75 - 9/75) cycles per sec., representing 95% confidence limits in each case. These values show reasonable agreement with the inverse 'square law' predicted by the similarity theory of homogeneous turbulence for the 'inertial subrange' of frequencies (Priestley and Sheppard 1952).

It is interesting to note that data have recently been obtained (Crane and Chilton 1956) for the vertical component of eddy motion from an aeroplane flying at 1,700 feet in clear air with moderate turbulence (the measured apparent variance for the vertical component being 25 (feet per sec.)^2). Fig. III compares these results, extracted from graphs of two overlapping portions of the energy spectrum, with the Cardington results using the linear transformation $n = \bar{u}k$, where $\bar{u}$ is the mean wind speed at 2,000 feet (about 25 feet per sec.) and k is the wave-number (cycles per foot). The log-log plots of spectral density (cycles per foot)$^{-1}$ referred to a total variance of unity (i.e. the energy per unit interval of wave-number per unit variance) against wave-number show fairly good agreement.

2. Scale of turbulence

The investigation into the scale of turbulence was made through the spatial correlation function, characterised by the vertical separation between the instruments measuring the turbulent fluctuations.

The spatial correlation coefficients R(z) were evaluated as cross-correlation coefficients between two sequences of wind inclination observations recorded simultaneously at two fixed points distance z apart, and for each of the separation distances z = 5, 20, 50, 70, 100, 150 feet, using the equalities listed below:-

$$\overline{\phi_A\phi_B} = \overline{\phi_A\cdot(\phi_B-\phi_A)} + \overline{\phi_A^{\,2}}$$

$$\overline{\phi_B\phi_C} = \overline{(\phi_B-\phi_A)\cdot(\phi_C-\phi_B)} + \overline{\phi_A\cdot(\phi_C-\phi_B)} + 2\overline{\phi_A\cdot(\phi_B-\phi_A)} + \overline{(\phi_B-\phi_A)^2} + \overline{\phi_A^{\,2}}$$

$$\overline{\phi_C\phi_A} = \overline{(\phi_C-\phi_B)\cdot\phi_A} + \overline{(\phi_B-\phi_A)\cdot\phi_A} + \overline{\phi_A^{\,2}}$$

$$\overline{\phi_B^{\,2}} = \overline{(\phi_B-\phi_A)^2} + \overline{2(\phi_B-\phi_A)\cdot\phi_A} + \overline{\phi_A^{\,2}}$$

$$\overline{\phi_C^{\,2}} = \overline{2(\phi_C-\phi_B)\cdot(\phi_B-\phi_A)} + \overline{2(\phi_C-\phi_B)\cdot\phi_A} + \overline{2(\phi_B-\phi_A)\cdot\phi_A} + \overline{(\phi_C-\phi_B)^2} + \overline{(\phi_B-\phi_A)^2} + \overline{\phi_A^{\,2}}$$

and hence $R(z) = R(AB) = (\overline{\phi_A\phi_B}-\overline{\phi_A}\,\overline{\phi_B})/(\overline{\phi_A^{\,2}}-(\overline{\phi_A})^2)^{\frac{1}{2}}(\overline{\phi_B^{\,2}}-(\overline{\phi_B})^2)^{\frac{1}{2}}$

the bars denoting temporal mean values.

The autocorrelation coefficients R(t) as a function of the lag-time t were also evaluated for the three runs separately (Fig. I), from the values of the inclination ϕ_A at 2,000 feet, and the individual values are given in Table I. Assuming the turbulence is isotropic and that the velocity fluctuations are small compared with the resultant mean velocity $\bar{u}$ at 2,000 feet, the transformation $z' = \bar{u}t$ can be used to convert the Eulerian time-correlation R(t) into the equivalent Eulerian space-correlation R(z'). The values of R(z) and ratios of R(z) to R(z') are shown below.

	Run 1		Run 2			Run 3		
z feet	5	50	50	100	150	20	50	70
R(z)	0.99	0.90	0.94	0.86	0.78	0.98	0.96	0.94
R(z)/R(z')	1.01	1.07	1.01	1.09	1.15	1.00	1.04	1.01

It is seen that the actual Eulerian space-correlation coefficient R(z) is always greater than the corresponding derived correlation coefficient R(z'). This could arise because the Lagrangian time-correlation coefficient over a distance of travel equal to z is less than unity, or because the turbulence is non-isotropic, or to a combination of both. However, the distances involved in the experiment (z ≤ 150 feet) provide correlation coefficients falling only to 0.78 and correspond to time-lags of less than 6 sec. in wind speeds of about 8 metres per second, so that the ratios can be obtained for only a small portion of the auto-correlation curve. In order, therefore, to assess fully the scale of turbulence, distances much greater than 150 feet need to be considered.

Appendix I to M.R.P. 1044

Computation of energy spectra by the Fourier-transform method (after Tukey)

This represents a technique, recommended by Tukey (1950), for the computation of the energy spectrum of a finite series of observations. The original data are a series of consecutive observations of wind velocity X_i for $i = 1, 2 \ldots\ldots N$, which may be instantaneous values or short-period mean values, with successive observations separated by a time interval δt sec. The procedure is to form values of the lag-products Q_k (covariances) of the fluctuations from the overall long-term mean value, thus

$$Q_k = \frac{1}{N-k}\left\{\sum_{i=1}^{N-k} X_i X_{i+k} - \frac{1}{N-k}\sum_{i=1}^{N-k} X_i \sum_{i=1}^{N-k} X_{i+k}\right\} \qquad k = 0, 1 \cdots m \qquad (1)$$

for successive values of the lag-time $k\delta t$.

The chosen number of lags, m, is fairly critical. An estimate of m can be obtained from the 'sampling theory' (Tukey 1950) by the use of the formula

$$f = \text{number of degrees of freedom} = \frac{2(N - \frac{m}{4})}{m} \qquad (2)$$

the reliability of the spectral estimates increasing with increasing number of degrees of freedom. However, if m is too large the computational work becomes prohibitive; also the estimates of the spectral energy obtained are uncertain due to the low value of f resulting for a fixed number of observations N. If m is too small the resolution of spectral estimates at low frequencies is poor. The extreme range of frequencies over which reasonably accurate spectral estimates are obtainable is $\left(\frac{1}{2m\delta t} - \frac{1}{2\delta t}\right)$ cycles per sec. Values recommended by American workers in this field are $6 \leqslant m \leqslant 30$ and $f > 30$.

The covariance function $Q(t)$ is an even function of the time-lag t, and values Q_k are known at the (m+1) equally spaced points $0 \leqslant k \leqslant m$. For the finite range $0 \leqslant t \leqslant m\,\delta t$, harmonic analysis determines the values of $Q(t)$ at the given (m+1) points, exactly in the form of the cosine series

$$Q(t) = \sum_{h=0}^{m} L_h \cos\frac{\pi h t}{m\delta t} \qquad (3)$$

where L_h are the contributions at equally spaced frequency bands centred at $n = 0, \frac{1}{2m\delta t}, \cdots\cdots \frac{1}{2\delta t}$; and

$$\left.\begin{aligned} L_0 &= \frac{1}{2m}(Q_0 + Q_m) + \frac{1}{m}\sum_{k=1}^{m-1} Q_k \\ L_h &= \frac{1}{m}Q_0 + \frac{2}{m}\sum_{k=1}^{m-1} Q_k \cos\frac{kh\pi}{m} + \frac{1}{m}Q_m \cos\pi h\ ; \quad h = 1, 2 \cdots (m-1) \\ L_m &= \frac{1}{2m}\left(Q_0 + (-1)^m Q_m\right) + \frac{1}{m}\sum_{k=1}^{m-1} (-1)^k Q_k \end{aligned}\right\} \quad (4)$$

and it is implicit that $Q_0 = \text{total variance} = \sum_{h=0}^{m} L_h$. The quantities L_h

are termed "apparent line powers" and are discussed below.

In this way no assumption is made about the shape of the covariance curve, only those values of Q_k actually obtained by computation being used. The analysis leads to more accurate spectral estimates the greater the range of n, i.e. the greater the value of m.

If P(n) is the energy density at a frequency n, i.e. the energy contribution per unit frequency, and Q_k is the covariance, then the inverse Fourier-cosine transformation (Wiener 1930) gives

$$Q_k = \int_0^\infty \cos 2\pi n k \delta t . P(n) . dn \qquad (5)$$

$$\equiv \sum_n \cos 2\pi n k \delta t . P(n) . \Delta n$$

Substituting the values for Q_k from (5), into equations (4) for the 'line powers' L_h, give

$$L_h = \int_0^\infty l_h(n) . P(n)\, dn \qquad \text{for } h = 0, 1 - - - m \qquad (6)$$

$$\equiv \sum_n l_h(n) . P(n) . \Delta n$$

where $$l_h(n) = \frac{1}{m} + \frac{2}{m} \sum_{k=1}^{m-1} \cos \frac{kh\pi}{m} . \cos 2\pi k n . \delta t + \frac{1}{m} \cos h\pi \cos 2\pi m n \delta t.$$

Thus the 'apparent line power' L_h represents the energy weighted according to the function $l_h(n)$, which has the values of near unity at $n = \frac{h}{2m\delta t}$ and near zero elsewhere over the frequency range n; and so L_h can be considered an average estimate over the range $(h-\frac{1}{2})/2m\delta t \leqslant n \leqslant (h+\frac{1}{2})/2m\delta t$; except for the 'end values' L_o and L_m which are averages over the frequency ranges $0 \leqslant n \leqslant \frac{1}{4m\delta t}$ and $(m-\frac{1}{2})/2m\delta t \leqslant n \quad \frac{1}{2\delta t}$ respectively.

In terms of the classical theory, the 'line powers' are effectively equivalent to

$$L_h \equiv F(n) . \Delta n . Q_o \qquad \text{where} \quad n = \frac{h}{2m\delta t} \qquad (7)$$

The curve of 'apparent line power' as a function of frequency oscillates considerably from point to point. An averaging process is, therefore, employed in which irregularities of the spectral curve, which occur due to the use of a finite instead of an infinite set of data, are 'smoothed' but the smoothing occurs at the expense of resolution in all the frequency bands. Experience has shown that the best results are given by the following 3-term weighted average:

$$\left.\begin{aligned} U_o &= 0{\cdot}54\, L_o && + 0{\cdot}46\, L_1 \\ U_h &= 0{\cdot}54\, L_h && + 0{\cdot}23(L_{h-1} + L_{h+1}) \text{ for } h = 1, 2 - - - (m-1) \\ U_m &= 0{\cdot}54\, L_m && + 0{\cdot}46\, L_{m-1} \end{aligned}\right\} \qquad (8)$$

U_h represents the average total energy contribution over the frequency range $(h-1)/2m\,\delta t \leqslant n \leqslant (h+1)/2m\,\delta t$; except the end values U_o and U_m which are averages over the frequency ranges

$$0 < n \leqslant \frac{1}{2m\,\delta t} \quad \text{and} \quad (m-1)\,\frac{1}{2m\,\delta t} \leqslant n < \frac{1}{2\,\delta t} \quad \text{respectively.}$$

---

spectral estimates at high frequencies. It is rectified by a process called "prewhitening" (Panofsky 1954) which entails forming a new series with a spectrum in which high frequency fluctuations are emphasised relative to the low frequency fluctuations. In practice a new series of consecutive observations is derived from the original one by means of the linear transformation

$$Y_i = X_i - bX_{i-1} \qquad \text{where } 0 < b \leqslant 1 \qquad (1)$$

$$\text{for } i = 1,\ 2\ \ldots\ldots.\ N$$

The constant b = 0.75 is usually chosen, and it is assumed that $\overline{\overline{X}}_i = \overline{\overline{X}}_{i-1}$ where bars denote overall long-term mean values. The whole computational procedure is now carried out with the new series Y_i, forming lagged covariances and ultimately obtaining 'prewhitened' spectral estimates V_h. The true spectral estimates, U_h, are then recovered, using the transformation

$$U_h = \frac{V_h}{1 + b^2 - 2b\cos\frac{\pi h}{m}} \qquad (2)$$

$$= \frac{V_h}{1{\cdot}5625 - 1{\cdot}5\cos\frac{\pi h}{m}} \qquad \text{for } b = 0.75.$$

(c) Averaging

An error is introduced into the spectral estimates when the original velocity data extracted from continuous records are mean values over a certain finite period δT sec. instead of instantaneous values. This causes the

/effective

where $\ell_h(n) = \frac{1}{m} + \frac{2}{m} \sum_{k=1}^{m-1}{}' \cos \frac{kh\pi}{m} . \cos 2\pi kn.\delta t + \frac{1}{m} \cos h\pi \cos 2\pi mn\delta t.$

Thus the 'apparent line power' L_h represents the energy weighted according to the function $l_h(n)$, which has the values of near unity at $n = \frac{h}{2m\delta t}$ and near zero elsewhere over the frequency range n; and so L_h can be considered an average estimate over the range $(h-\frac{1}{2})/2m\delta t \leqslant n \leqslant (h+\frac{1}{2})/2m\delta t$; except for the 'end values' L_o and L_m which are averages over the frequency ranges $0 \leqslant n \leqslant \frac{1}{4m\delta t}$ and $(m-\frac{1}{2})/2m\delta t \leqslant n \quad \frac{1}{2\delta t}$ respectively.

In terms of the classical theory, the 'line powers' are effectively equivalent to

$$L_h \equiv F(n).\,\Delta n.\,Q_o \quad \text{where} \quad n = \frac{h}{2m\delta t} \tag{7}$$

The curve of 'apparent line power' as a function of frequency oscillates considerably from point to point. An averaging process is, therefore, employed in which irregularities of the spectral curve, which occur due to the use of a finite instead of an infinite set of data, are 'smoothed' but the smoothing occurs at the expense of resolution in all the frequency bands. Experience has shown that the best results are given by the following 3-term weighted average:

$$\left.\begin{aligned} U_o &= 0{\cdot}54\,L_o && + 0{\cdot}46\,L_1 \\ U_h &= 0{\cdot}54\,L_h && + 0{\cdot}23(L_{h-1} + L_{h+1}) \text{ for } h = 1, 2 --- (m-1) \\ U_m &= 0{\cdot}54\,L_m && + 0{\cdot}46\,L_{m-1} \end{aligned}\right\} \tag{8}$$

Errors and modifications of the Fourier-transform method

(a) Aliasing

The effect known as 'aliasing' has been mentioned rather vaguely in a number of papers, and refers to the fact that there is present at the relatively lower frequencies 'apparent energy' which is really due to oscillations of frequency greater than $\frac{1}{2\delta t}$ cycles per sec. The time-interval δt sec. between consecutive observations determines the resolution of the spectrum and the highest frequency at which reasonably accurate estimates can be obtained. Although the error due to 'aliasing' cannot be wholly eliminated it can be minimised by making the time-interval δt as small as possible, its limiting value being the short-term averaging period δT of the original observations. The averaging period δT sec. also has a lower bound, since $2\delta T$ must not be less than the natural period (or not less than approximately five times the response time) of the instrument measuring the observations, in order to eliminate high frequency oscillations which are not faithfully recorded by the instrument.

For a given spectrum the error due to 'aliasing' increases with increasing frequency, and so it is current practice to discard the spectral estimates at the highest frequencies. This source of error is not so important in spectra of horizontal wind components, since most of the energy in this case is contained in the low frequency or long period eddies.

(b) Prewhitening

When the spectrum varies rapidly as a function of the frequency, spectral analysis by the Fourier-transform method yields poor estimates of the spectral energy contributions. This is particularly serious in the case of spectra of horizontal velocity components, the computations often resulting in negative spectral estimates at high frequencies. It is rectified by a process called "prewhitening" (Panofsky 1954) which entails forming a new series with a spectrum in which high frequency fluctuations are emphasised relative to the low frequency fluctuations. In practice a new series of consecutive observations is derived from the original one by means of the linear transformation

$$Y_i = X_i - bX_{i-1} \quad \text{where } 0 < b \leq 1 \qquad (1)$$

$$\text{for } i = 1, 2 \ldots\ldots N$$

The constant b = 0.75 is usually chosen, and it is assumed that $\bar{X}_i = \bar{X}_{i-1}$ where bars denote overall long-term mean values. The whole computational procedure is now carried out with the new series Y_i, forming lagged covariances and ultimately obtaining 'prewhitened' spectral estimates V_h. The true spectral estimates, U_h, are then recovered, using the transformation

$$U_h = \frac{V_h}{1 + b^2 - 2b\cos\frac{\pi h}{m}} \qquad (2)$$

$$= \frac{V_h}{1\cdot5625 - 1\cdot5\cos\frac{\pi h}{m}} \qquad \text{for } b = 0.75.$$

(c) Averaging

An error is introduced into the spectral estimates when the original velocity data extracted from continuous records are mean values over a certain finite period δT sec. instead of instantaneous values. This causes the effective amplitudes of the high frequency oscillations to be partially suppressed to an extent which depends upon the relation between the averaging period δT sec. and the actual period of oscillation under consideration. For example, the apparent velocity amplitude is damped to 0.64 of its true value when the averaging period δT is half the period of oscillation. In general the velocity field can be represented by the expression

$$V(t) = \int_{-\infty}^{\infty} s(n).e^{2\pi int}\, dn ,$$ where n is the frequency of the harmonic oscillations

into which the record is resolved and s(n) is the amplitude at frequency n. The effect of using average values over a finite time δT sec. is, therefore, to suppress the amplitude s(n) by a factor

$$\frac{1}{\delta T}\int_{-\frac{\delta T}{2}}^{\frac{\delta T}{2}} e^{2\pi int}\, dt = \frac{\sin n\pi\delta T}{n\pi\delta T} .$$

Hence the resolved spectral estimates, which depend upon the square of the velocity amplitudes, are corrected for 'averaging' according to the equation

$$\underset{\text{corrected}}{U^{*}(n)} = \underset{\text{average}}{U(n)} \times \left(\frac{n\pi\delta T}{\sin n\pi\delta T}\right)^{2} \qquad (3)$$

BIBLIOGRAPHY

Cramer, H.E. and Record, F.A.	1955	J.Met., Vol.12, No.2, p.146.
Crane, H.L. and Chilton, R.G.	1956	N.A.C.A. Tech. Note, No.3702(27).
Crease, J. and Tucker, M.J.	1954	Brit.J.Appl.Phys., 5, p.143.
Gerhardt, J.R., Crain, C.M. and Smith, H.W.	1952	J.Met., Vol.9, No.5, p.229.
Griffith, H.L., Panofsky, H.A. and Van der Hoven, I.	1956	J.Met., Vol.13, No.3, p.279.
Howcroft, J.G. and Smith, J.R.	1956	J.Met., Vol.13, No. 1, p.75.
Jones, J.I.P. and Butler, H.E.	1956	Meteorological Research Papers, Air Ministry, London, No. 1038.
MacCready, P.B.	1953	J.Met., Vol.10, p.325.
MacCready, P.B.	1953	J.Met., Vol. 10, p.434.
Panofsky, H.A. and McCormick, R.A.	1954	Q.J.Roy.Met.S., Vol.80, No.346, p.546.
Panofsky, H.A. and Singer, I.A.	1951	U.S. Atomic Energy Comm., Ann. Prog. Rep. NYO-1559 T.I.S., Oak Ridge, Tenn.
Panofsky, H.A. and Van der Hoven, I.	1954	Final Rpt., Penns. State Univ., AFCRC Con. AF. 19 (604)-166.

/Panofsky

BIBLIOGRAPHY (Contd.)

Panofsky, H.A. and Van der Hoven, I.	1956	Scientific Rep. No.1, Penns. State Univ., AFCRC Con.AF.19 (604)-1027.
Priestley, C.H.B. and Sheppard, P.A.	1952	Q.J.Roy.Met.S., Vol. 78, No.338.
Robinson, G.D.	1953	Meteorological Research Papers, Air Ministry, London, No.808.
Tukey, J.W.	1950	Symposium on 'Applications of autocorrelation analysis to physical problems'. O.N.R., Washington, D.C. NAVEXOS.
Tukey, J.W.	1951	Unpublished - Bell Telephone Lab.Inc.
Webb, E.K.	1955	C.S.I.R.O., Australia, Techn. Pap. 5.
Wiener, N.	1930 4	Acta Math., 55.

TABLE I

Eulerian-time correlation coefficients (autocorrelations) $R(t)$ for wind inclination at 2,000 feet

Run	Period (B.S.T.) \ Lag number k	0	1	2	3	4	5	6	7	8	9	10	11	12	13	14	15	16
1	1017 – 1027	1.0	.79	.58	.46	.40	.33	.30	.32	.33	.32	.28						
2	1128 – 1138	1.0	.88	.72	.58	.47	.41	.32	.25	.18	.14	.13	.13	.13	.11	.09	.06	.03
3	1222½ – 1232½	1.0	.93	.87	.81	.77	.70	.62	.55	.51	.47	.42						
	Arithmetic mean	1.0	.87	.72	.62	.55	.48	.41	.37	.34	.31	.28						

(Time-interval for 1 lag = 2½ sec.)

TABLE II

Spectral analysis for run 2 (see App. I for meaning of symbols)

h	Frequency n cycles/hr.	Average spectral estimates (fraction of total variance)			hU_h^* $\equiv nF(n)$	Prewhitened process			hU_h^* $\equiv nF(n)$
						Average spectral estimates			
		L_h	U_h	corrected U_h^*		L_h	U_h	U_h^*	
0	0	.3331	.3369	.3240	0	.3403	.4006	.3873	0
1	48	.3432	.2942	.2855	.2855	.3341	.2915	.2844	.2844
2	96	.1435	.1688	.1639	.3278	.1564	.1374	.1343	.2686
3	144	.0559	.0693	.0689	.2067	.0501	.0559	.0558	.1674
4	192	.0277	.0365	.0372	.1488	.0313	.0341	.0350	.1400
5	240	.0381	.0304	.0321	.1605	.0345	.0273	.0290	.1450
6	288	.0154	.0193	.0211	.1266	.0158	.0160	.0177	.1062
7	336	.0097	.0097	.0112	.0784	.0080	.0080	.0093	.0651
8	384	.0039	.0053	.0065	.0520	.0043	.0044	.0054	.0432
9	432	.0042	.0045	.0059	.0531	.0028	.0035	.0045	.0405
10	480	.0060	.0052	.0073	.0730	.0049	.0040	.0057	.0570
11	528	.0045	.0050	.0076	.0836	.0039	.0043	.0065	.0715
12	576	.0053	.0050	.0084	.1008	.0052	.0045	.0076	.0912
13	624	.0049	.0046	.0085	.1105	.0043	.0040	.0074	.0962
14	672	.0031	.0031	.0066	.0924	.0028	.0027	.0056	.0784
15	720	.0014	.0022	.0052	.0780	.0014	.0019	.0045	.0675

Total variance = Q_o = 29.1 (degrees)^2

FIG: I.

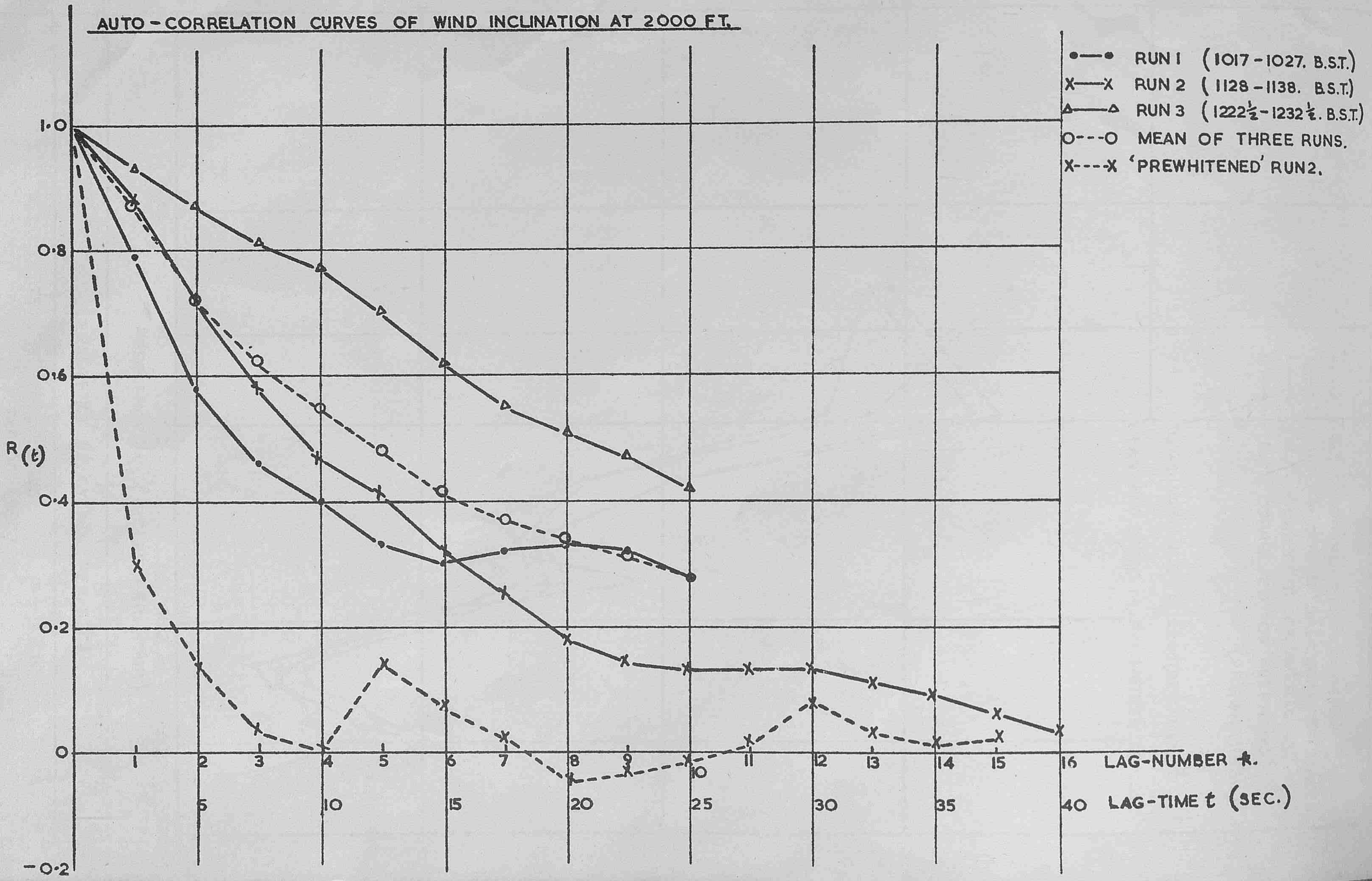

AUTO-CORRELATION CURVES OF WIND INCLINATION AT 2000 FT.

M RP 1044

ENERGY SPECTRA COMPUTED FOR RUN 2.

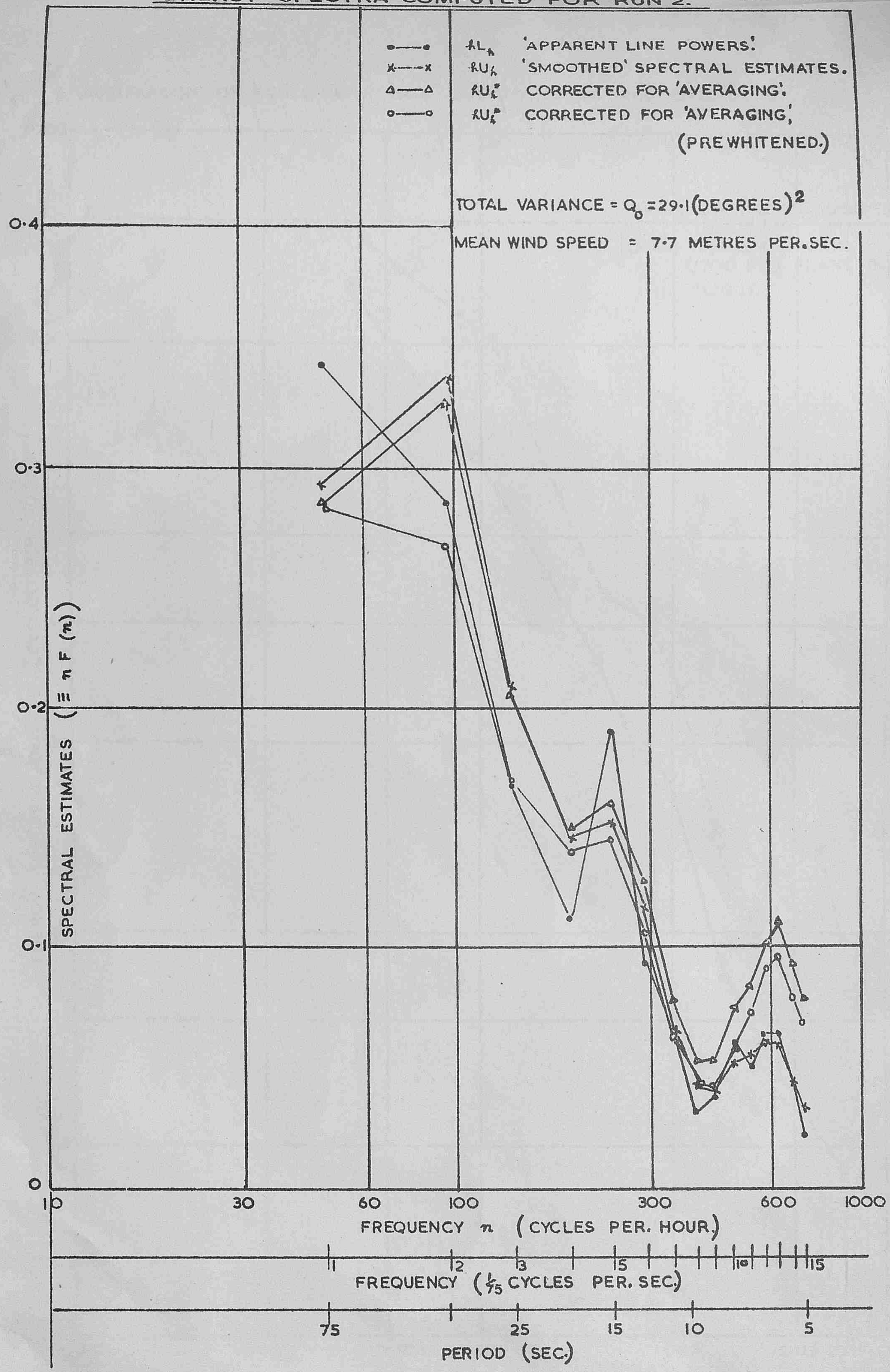

FIG II.

COMPARISON OF RUN 2 WITH DATA DUE TO CRANE AND CHILTON

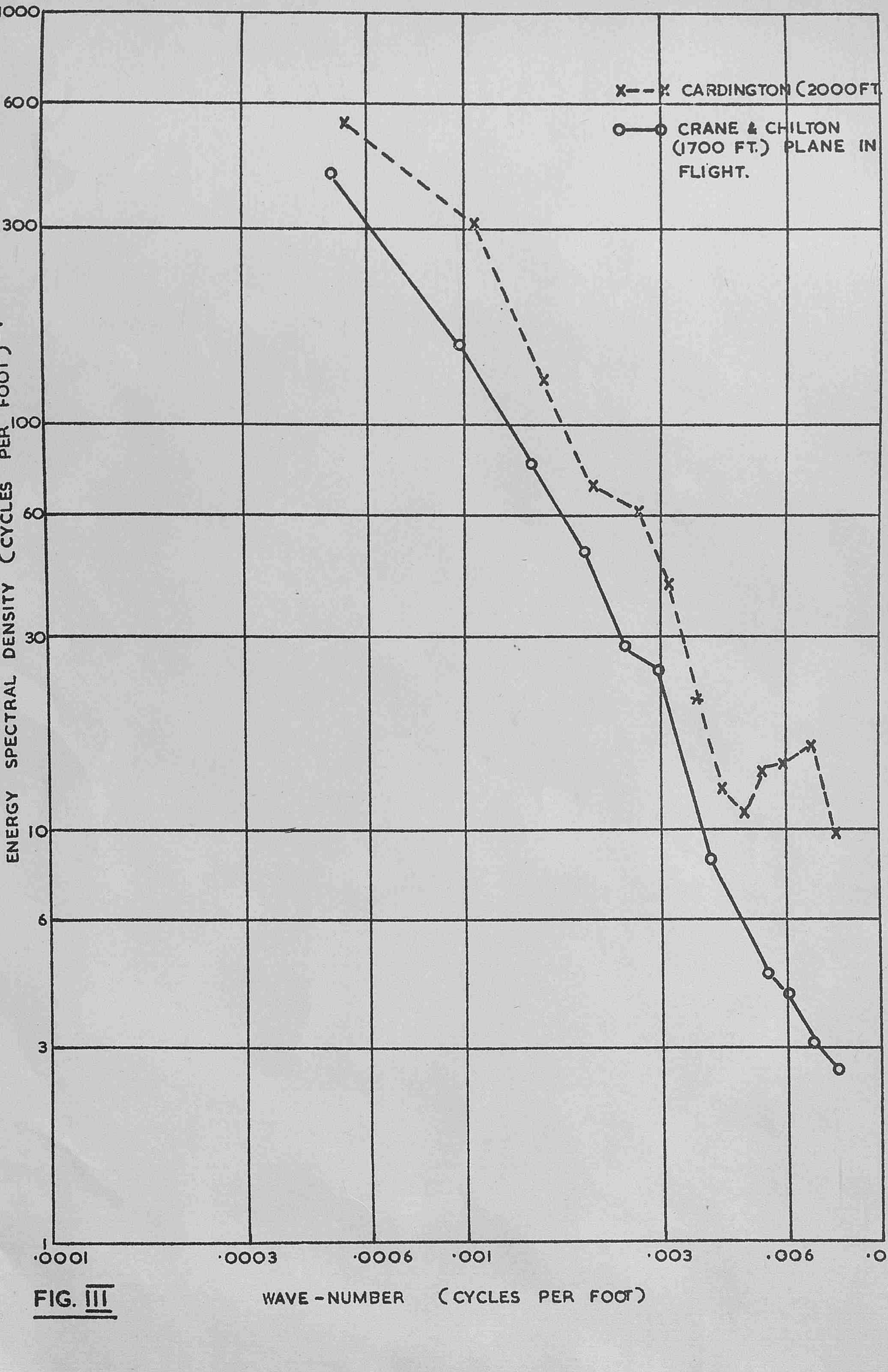

FIG. III

WAVE-NUMBER (CYCLES PER FOOT)

M.R.P. 1045
S.C. 11/233
28th March, 1957

24 S

Average height of the standard isobaric surfaces over the temperate and tropical regions in January

by

H. Heastie

(Meteorological Office)

[illegible]
ROUTING SLIP

FILE	INFO	ACTION				
	6		DIRECTOR			RV
	5		DEP DIRECTOR		B	
	4		ASST TO DIRECTOR			
	1		CONSULTANTS		WS, E.A.F.	
	2		TR&D	CHF	JS	
				TSS	R.H.H. K	
				RRB		
				PDB		
				SEC		
	3		EDD	CHF		G
				ELFB		
				STB		
				SPFB		
				CU		
				SEC		
8	7		TIPD	CHF		
				PUE		
				TECH INFO		
				SEC		

(Cl. ?)
[illegible] ?

AIR MINISTRY

METEOROLOGICAL RESEARCH COMMITTEE

At the time of issue this report has not been published. Any author desiring to quote this paper should refer to it as "A paper of the Meteorological Research Committee (London), M.R.P. No. 1045 by Mr. H. Heastie. A copy is available in the Library of the Meteorological Office."

M.R.P. 1045
S.C.II/233
28th March, 1957

AIR MINISTRY
METEOROLOGICAL RESEARCH COMMITTEE

Average height of the standard isobaric surfaces over the temperate and tropical regions in January

by

H. Heastie (Meteorological Office)

1. Introduction

This paper is a further step in the revision of Geophysical Memoir 85 - Upper Winds over the World. In three earlier papers (1, 2, 3), the contours of the standard isobaric surfaces were mapped over an area from the North Pole to 55° N. for the four mid-season months January, April, July and October and this paper extends the mapping, for the month of January, down to 60°S. on a Mercator projection. It was not considered feasible to extend the charts any further south owing to the extreme scarcity of upper air data from Antarctica.

2. The data

Data for the same period 1949-53 were used. The main sources were manuscript data, the Climat Temp reports and the tabulations in U.S.W.B. Daily Series Synoptic Weather Maps, together with daily, monthly and annual publications of various countries. Further details are given in the appendix. The daily synoptic charts from Central Forecasting Office, Dunstable were used to supplement data in the Atlantic, European and North African regions of the chart. At some stations the hour of the observation varied during the period and the hour was not the same at all stations. Whenever available, data from ascents made in darkness were used in order to minimise errors due to solar radiation. As, further, the type of instrument varied from station to station, no attempt was made to apply radiation corrections systematically. An exception was made over stations in South Africa where a Canadian type of instrument was in use and corrections for radiation were made based on a paper by Henry (4) comparing the Canadian and American types of radiosonde. For Nairobi, Aden, Bahrein and Hong Kong a correction was made to the 100 mb temperature. For most of the period, at these stations the correction curves for the effect of temperature on the pressure element of the radiosonde were incorrectly extrapolated for temperatures below -90°F and, in consequence, the temperature reading at 100 mb was from 1°C to 3°C too high. Wind data, which were readily available for British overseas stations and Hong Kong, were used. The period of these data was 1948-53 in general, though shorter periods only were available for some stations.

3. Method of constructing the charts

(1) General. In constructing the circumpolar charts it was found necessary to draw a separate set of charts for each year. This necessity arose from the great variability of the pattern from year to year together with the fact that data from few stations were available with equal reliability for all five years. The drawing of five sets of charts naturally delays the production of of the average charts and an attempt was made to draw the average circumpolar charts for one month (July) directly from the data meaned over the five years. From this test it was decided that the drawing of yearly circumpolar charts was justified but that this procedure might not be necessary for the Mercator charts. A large part of the region between 55°N. and 60°S. lies in the

tropics and subtropics where the changes in contour height from year to year are comparatively small. In the zones from 55°N. to 30°N. and from 30°S. to 60°S. such data as there are are fairly complete for the whole five years. In consequence it has proved unnecessary to draw charts for each year and the charts submitted in this paper were drawn from data meaned over the five year period.

(2) 700 mb chart. Where available the data were fairly complete and mean values were acceptable. There were however large areas with no available data. To obtain a pattern over these areas grid values of 700 mb contour height were evaluated as follows. A chart of M.S.L. pressure in the southern hemisphere was constructed using grid values of mean pressure for the period 1949-53 (5). This chart was extended to about 20°N. with the aid of a chart of average M.S.L. pressure obtained from the World Climatology Branch of the Meteorological Office. From this chart and values of M.S.L. temperature supplied by the Marine Division of the Meteorological Office, grid values of 1,000 mb contour height were evaluated. These were added to values of 1,000-700 mb thickness evaluated from M.S.L. temperature and 700 mb temperature read off the average temperature chart in the memoir on upper air temperature (6) to obtain grid values of 700 mb contour height, a correction for humidity being first applied to the thickness values. A 700 mb contour chart was sketched from these grid values; the final 700 mb contour chart was then drawn, primarily from the actual data, but using the sketched map as a guide.

(3) 500 mb and 300 mb charts. A map of 700-500 mb thickness was sketched from grid values derived from the charts of average 700 mb and 500 mb temperature in the memoir (6). The 700-500 mb thickness chart was then drawn from the data with the aid of the sketched map. Grid values of 500 mb height were evaluated by adding 700 mb contour to 700-500 mb thickness values and the 500 mb contour chart drawn from the data with the aid of these grid values. Minor adjustments were then made between the three charts to make them consistent. The 500-300 mb thickness and the 300 mb contour charts were then drawn in a similar manner.

(4) 200 mb, 150 mb and 100 mb charts. Above 300 mb the data from an increasing number of stations became more and more unreliable owing to a loss of observations with height. Charts of 300 mb temperature and of lapse of temperature from 300 to 200 mb were therefore drawn, primarily from the data, but with the aid of the average temperature charts in the memoir (6). From these two charts a chart of 200 mb temperature was drawn. Some adjustment was then made to the three charts to remove minor irregularities arising from the gridding technique. The charts of 300 mb and 200 mb temperature were then used in conjunction with the charts of average temperature and pressure at the tropopause (6) to evaluate grid values of "correction for tropopause" (1) for the lower tropopause in the relevant areas of both hemispheres. Values so obtained for the southern hemisphere did not lead to a reasonable pattern and a new set was evaluated based on analogy with the values in the northern hemisphere and on values obtained from Australian and New Zealand data. Grid values of 300-200 mb thickness were then evaluated from values of 300 mb and 200 mb temperature and of "correction for tropopause". The 300-200 mb thickness chart was drawn from the data and with the assistance of these grid values. Finally, to remove minor irregularities, slight adjustments were made between the charts of 300 mb and 200 mb temperature, the chart of temperature lapse from 300 to 200 mb and the 300-200 mb thickness chart. Values of 300-200 mb thickness were then added to those of 300 mb contour height to obtain values of 200 mb contour height and the 200 mb contour chart was drawn from the data and these grid values. The charts of 200-150 mb and 150-100 mb thickness and of 150 mb and 100 mb contour height were drawn in a similar manner, though without the complication of a "correction for tropopause". The upper tropopause is generally above the 100 mb surface, but does fall to 115-120 mb over Tasmania and New Zealand, and perhaps elsewhere, though data are lacking. However, no correction on account of the upper tropopause was made because a check, using values from the New Zealand data, suggested that the requisite correction was probably less than 10 metres everywhere. The 100 mb chart showed some irregularities and these were removed by making minor adjustments to the charts as a whole. Finally a few minor amendments were made along the 55°N. parallel to improve the fit between the circumpolar and Mercator charts.

/4.

4. The charts

It should be noted that, on the contour charts, the isopleth interval is 100 geopotential metres while, on the thickness charts, the interval is 50 geopotential metres. North of 55°N. the charts are merely the redrawing of the circumpolar charts on the Mercator projection apart from some very minor amendments along the 55°N. parallel.

In the tropics the contours bear little relation to the actual flow, but in extratropical regions a mainly westerly flow is shown in both hemispheres, with much greater meridional components in the northern hemisphere. There the main troughs occur at 80°W. and 140°E. in association with the cold lows over northern Canada and Siberia. The main ridges are at 160°W. and 0°W. with a weak trough-ridge pattern over eastern Europe and Russia. The axis of the ridge at 0°W. is more tilted in a SSW.-NNE. direction than are the other features and there is a pronounced trough over the western Sahara. In the southern hemisphere troughs and ridges are much less pronounced. The main trough appears to be at about 40°E. with a subsidiary trough at 40°W. though in the lower layers there is a more pronounced trough in subtropical latitudes at 180°E. The troughs at 40°E. and 40°W. reflect the surface pattern (5) and there is some suggestion that both may form part of a wave train set up by the Andes.

Average contour charts tend to smooth out the jet streams which appear on the daily charts, but at 300 mb two strong wind belts can be noted over the North Atlantic. These are associated with the polar and subtropical jet streams. The more southerly one can be seen to link up across the Sahara with the strong wind belt of the Middle East which in turn extends across India to form part of the very strong belt over and south of Japan. The more northerly one becomes diffuse towards Europe and it is not possible to identify two separate streams elsewhere on the chart. These features are also distinguishable on the 200, 150 and 100 mb charts. In the southern hemisphere the data are too sparse to provide much detail. The strongest wind belt appears to lie between 45° and 50°S., though there is some suggestion that in the sector south of Africa it swings north to about 40° to 45°S. In the Australia - New Zealand sector there is a further wind maximum at 30° to 35°S. on the 200 mb and 150 mb contour charts. Hutchings (7) has drawn a southern hemisphere cross-section along the 170°E. meridian which shows wind maxima, at about 200 mb, of 60 kt. at 47°S. and 50 kt. at 32°S. The present charts show wind maxima at the same latitudes, but with the stronger wind at the lower latitude. Another cross-section along the 150°E. meridian has been drawn by Gibbs (8), who shows two wind maxima, one of 50 kt. at 200 mb at 32°S. and the second of 40 kt. at 320 mb at 62°S. The first agrees very well with the present charts, which, however, show the second maximum at 200 mb and at about 47°S. It is, of course, possible to make only a rough comparison without drawing actual cross-sections from the charts.

References

(1) Heastie, H. Average height of the standard isobaric surfaces over the area from the North Pole to 55°N. in January. Meteorological Research Papers, Air Ministry, London, No. 918, 1955.

(2) Heastie, H. Average height of the standard isobaric surfaces over the area from the North Pole to 55°N. in July. Meteorological Research Papers, Air Ministry, London, No. 981, 1956.

(3) Heastie, H. Average height of the standard isobaric surfaces over the area from the North Pole to 55°N. in April and October. Meteorological Research Papers, Air Ministry, London, No. 1020, 1957.

(4) Henry, T. J. G. A comparison of mean temperatures obtained with Canadian and American types of radiosonde. Department of Transport, Meteorological Division, Toronto, Circular 2041, 1951.

(5) Pretoria, South African Weather Bureau. Notos, Vol. 4, No. 1, 1955.

(6) Goldie, N., Moore, J. G. and Austin, E. E. Upper air temperatures over the world. Geophys. Mem. No. 101, London (in the press).

(7) Hutchings, J. W. A meridional atmospheric cross-section for an oceanic region. J. Met., Vol. 7, p. 94.

(8) Gibbs, W. J. A comparison of hemispheric circulations with particular reference to the western Pacific. Quart. J. R. Met. Soc., 79, p. 121, 1953.

Appendix

1. Climat Temp data were used where available and the countries for which various sources of data, other than Climat, were used are listed below.

(a) Manuscript data

Australia
British East Africa
Canada
Ceylon
Eire
Falkland Islands
Germany (British Zone)
Hong Kong
New Zealand
Nigeria
Portuguese East Africa
Sudan
Thailand
United Kingdom (including overseas stations)
Weather ships

(b) Micro-film

Pacific Islands
Panama
Philippines
Weather ships

(c) Data tabulations from U.S.W.B. Daily Series Synoptic Weather Maps

Austria
Azores
Bermuda
Czechoslovakia
France
French North Africa
French Sahara
Greece
Italy
Mexico
Nicaragua
Pacific Islands
Philippines
Poland
Roumania
Turkey
U.S.S.R.
West Indies
Wheelus Field

(d) Daily weather reports

Czechoslovakia
Egypt
Germany
Greece
Holland
India
Portugal (including islands)

(f) Monthly publications

Belgian Congo
Belgium
Cocos Island
French Equatorial Africa
India
Indo-China
Japan, Japanese Islands and Weather ships
Korea
Madagascar and Amsterdam Island
Mexico
Spain
United States of America and American Pacific Islands
West Indies

(g) Annual reports

Angola
Holland
Hong Kong
Hungary
Switzerland
Union of South Africa
Venezuela

/2.

2. Special publications

Presentation of meteorological data for the North American sector for the year 1949. Final Report, Vol. II. Johns Hopkins University, Baltimore

Weather ships N and P

Australian National Antarctic Research Expedition. Series D, Meteorology

Heard Island
Macquarie Island

Les Observations Météorologiques de Port-Martin en Terre Adélie, Fasc. III

Adélie Land

Aerological Data for Southern Canada

Canada

This list refers to data for stations south of 55°N.

M.R.P. 1045

Average 700 mb. Contours

JANUARY 1949-1953

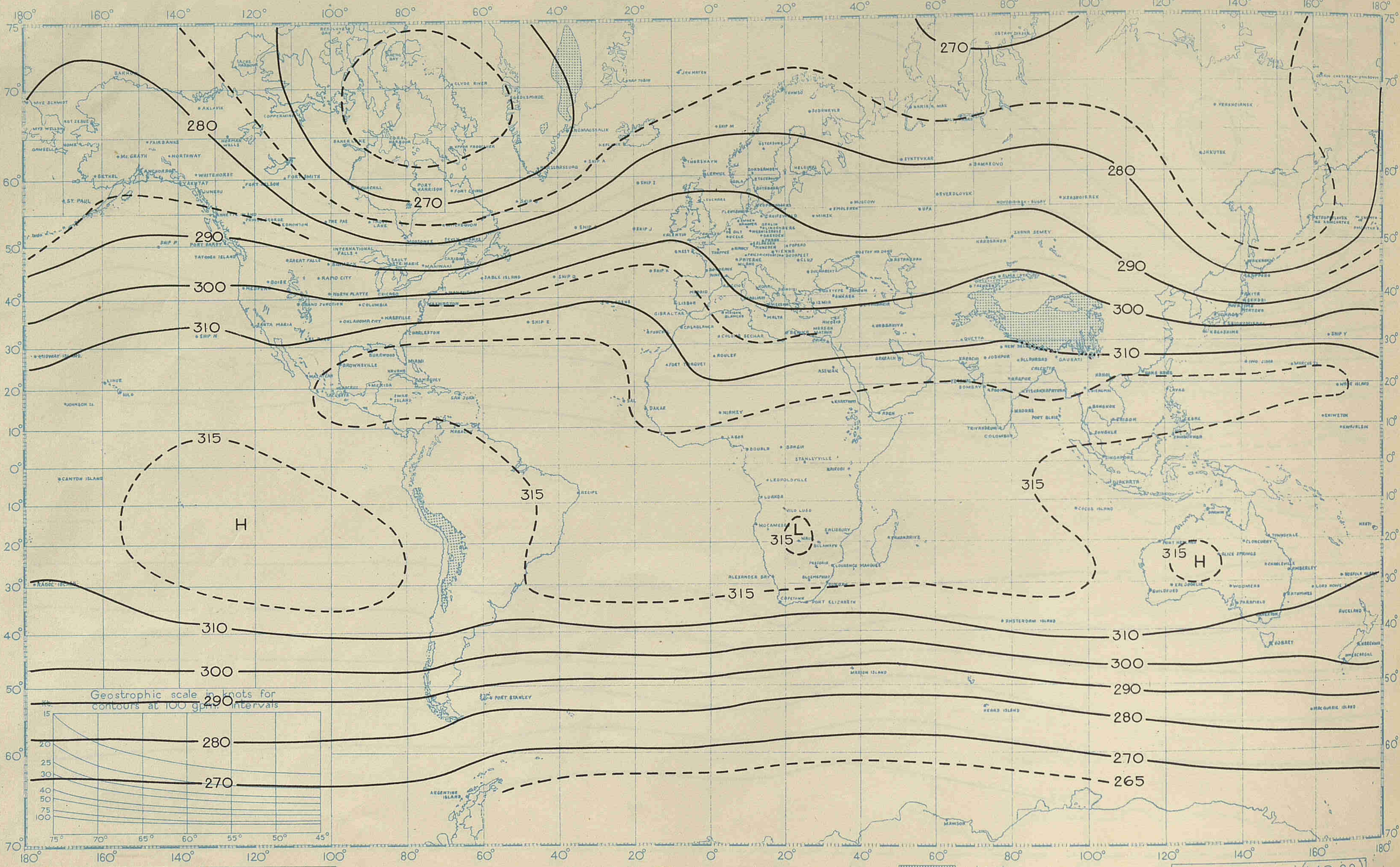

180° 160° 140° 120° 100° 80° 60° 40° 20° 0° 20° 40° 60° 80° 100° 120° 140° 160° 180°
75° 70° 60° 50° 40° 30° 20° 10° 0° 10° 20° 30° 40° 50° 60° 70°
270
280
290
300
310
315
265
H
L
Geostrophic scale in knots for contours at 100 gpm. intervals
Kt.
15
20
25
30
40
50
75
100
75° 70° 65° 60° 55° 50° 45°

Temperature in °C. | Height in dekametres

Revised to May 1955

▨ Land over 3,000 metres

Upper Air Branch (M.O.23)

M.R.P. 1045

Average 700-500 mb. Thickness

JANUARY 1949-1953

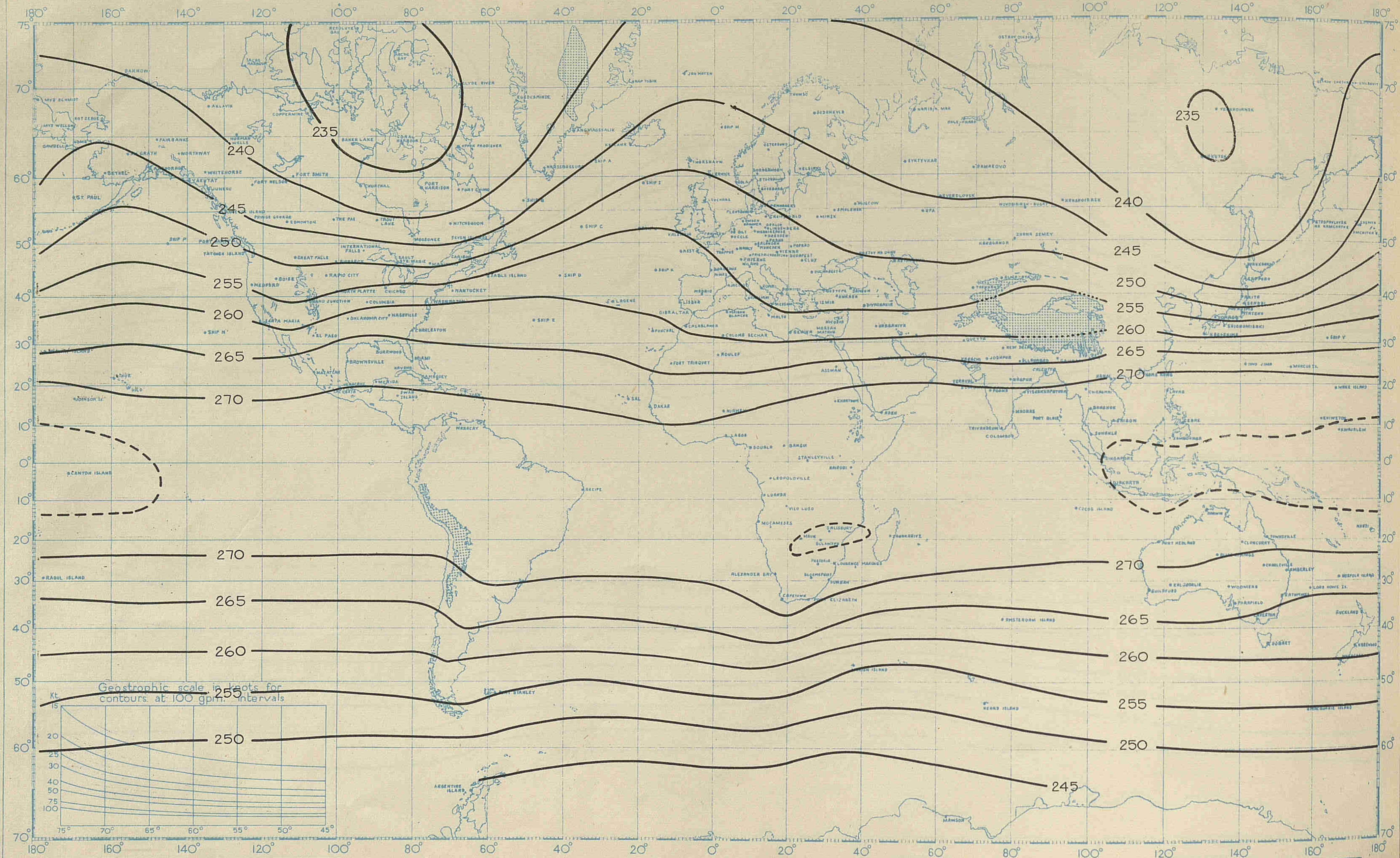

180° 160° 140° 120° 100° 80° 60° 40° 20° 0° 20° 40° 60° 80° 100° 120° 140° 160° 180°
75° 70° 60° 50° 40° 30° 20° 10° 0° 10° 20° 30° 40° 50° 60° 70°
235
240
245
250
255
260
265
270
Geostrophic scale in knots for contours at 100 gpm. intervals
Kt.
15 20 25 30 40 50 75 100
75° 70° 65° 60° 55° 50° 45°

Temperature in °C. | Height in dekametres

Revised to May 1955

▨ Land over 3,000 metres

Upper Air Branch (M.O.23)

M.R.P. 1045

Average 500 mb. Contours

JANUARY 1949-1953

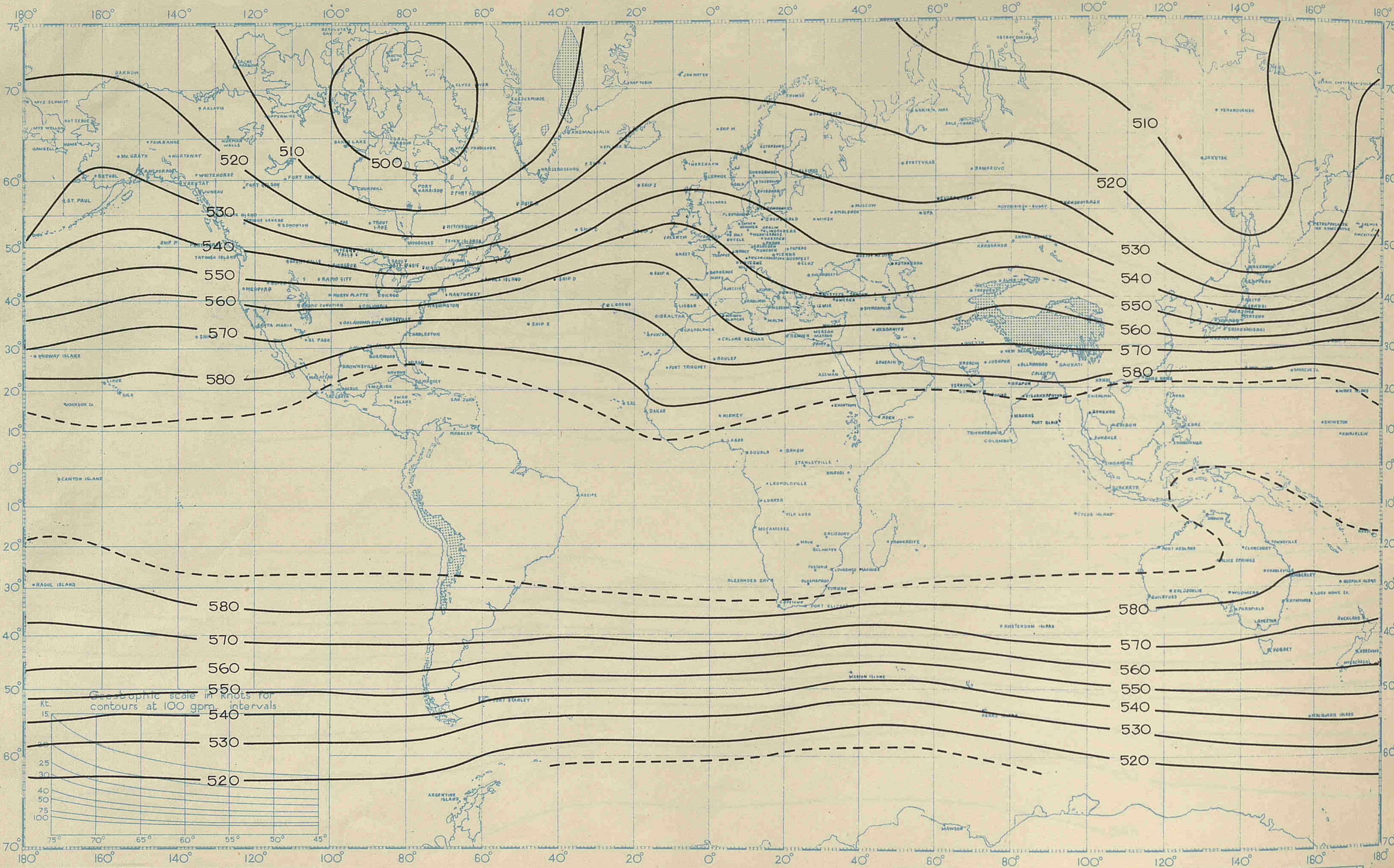

180°
160°
140°
120°
100°
80°
60°
40°
20°
0°
75°
70°
60°
50°
40°
30°
20°
10°
0°
500
510
520
530
540
550
560
570
580
Geostrophic scale in knots for contours at 100 gpm. intervals
Kt.
15
20
25
30
40
50
75
100
75°
70°
65°
60°
55°
50°
45°

Temperature in °C.

Height in dekametres

Revised to May 1955

▨ Land over 3,000 metres

Upper Air Branch (M.O.23)

M.R.P. 1045

Average 500-300 Thickness

JANUARY 1949-1953

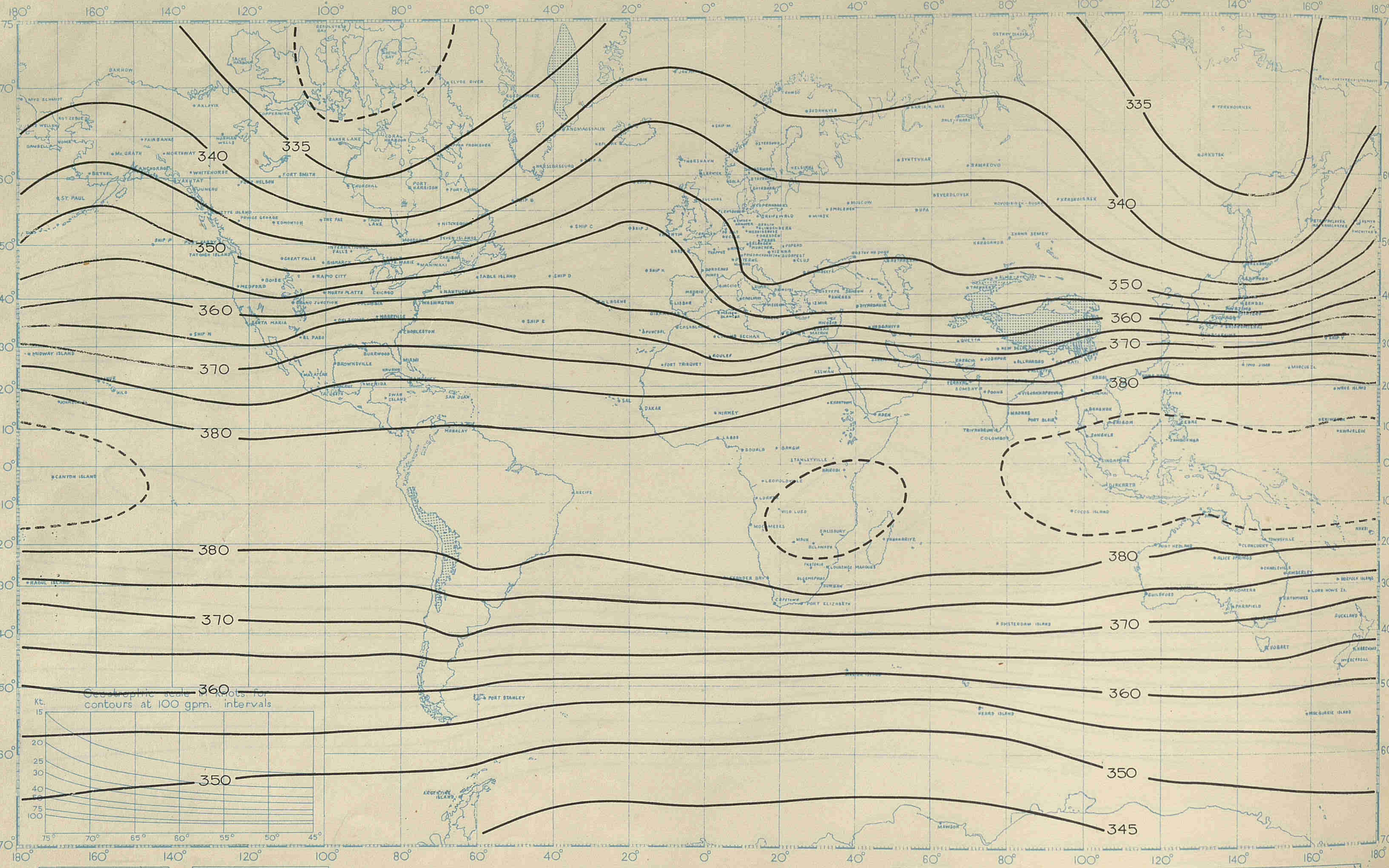
335
335
340
340
350
350
360
360
370
370
380
380
380
380
370
370
360
360
350
350
345
Geostrophic scale in knots for contours at 100 gpm. intervals
Kt.
15
20
25
30
40
50
75
100
75°
70°
65°
60°
55°
50°
45°
180°
160°
140°
120°
100°
80°
60°
40°
20°
0°
75°
70°
60°
50°
40°
30°
20°
10°

Temperature in °C.

Height in dekametres

Revised to May 1955

▨ Land over 3,000 metres

Upper Air Branch (M.O.23)

M.R.P. 1045

Average 300 mb. Contours

JANUARY 1949-1953

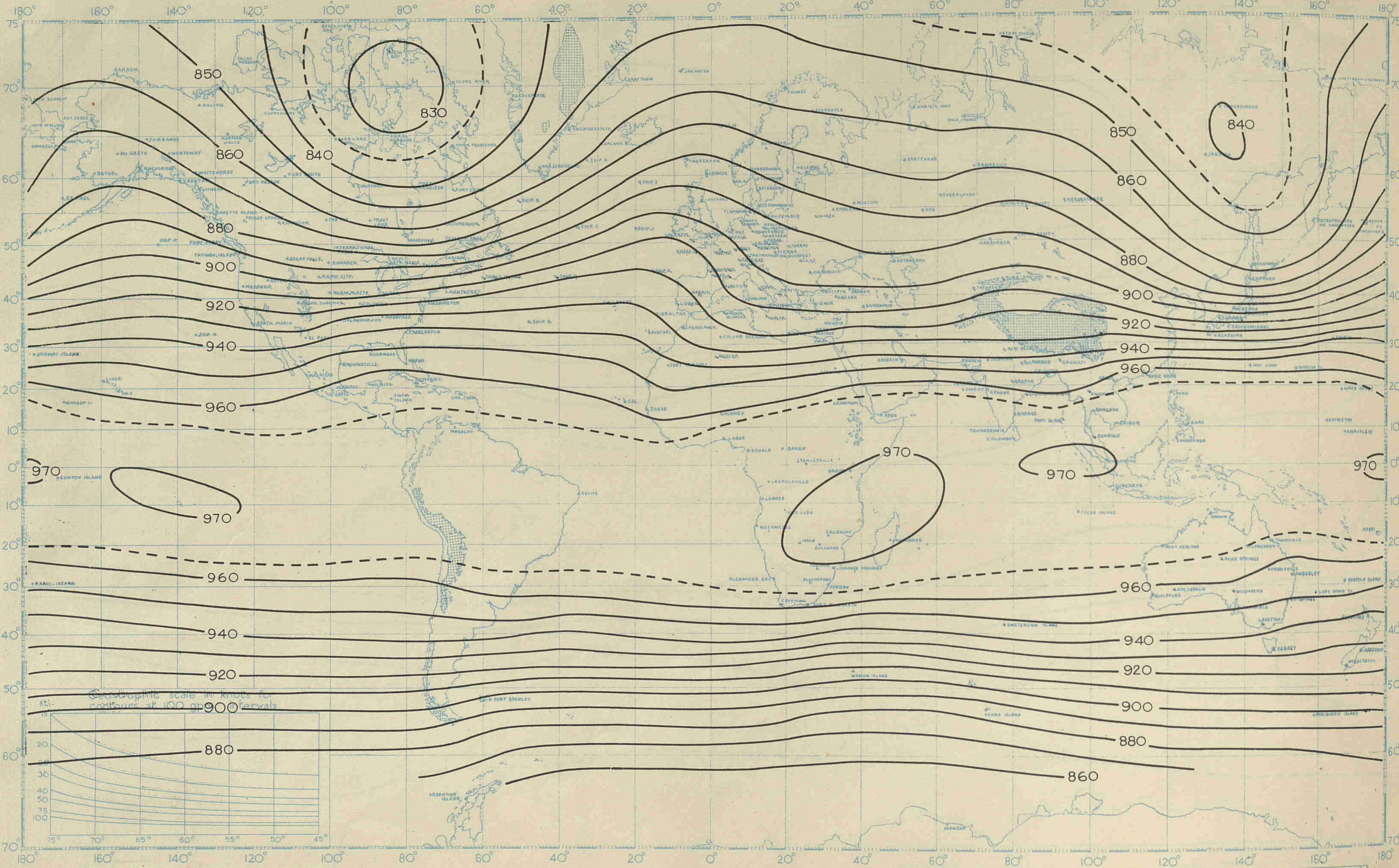
830
840
850
860
880
900
920
940
960
970
Geostrophic scale in knots for contours at 100 gpm intervals
Kts.
15
20
25
30
40
50
75
100
75°
70°
65°
60°
55°
50°
45°
180°
160°
140°
120°
100°
80°
60°
40°
20°
0°
75°
70°
60°
50°
40°
30°
20°
10°

Temperature in °C.

Height in dekametres

Revised to May 1955.

▨ Land over 3,000 metres

Upper Air Branch (M.O.23)

M.R.P. 1045

Average 300-200 mb. Thickness

JANUARY 1949-1953

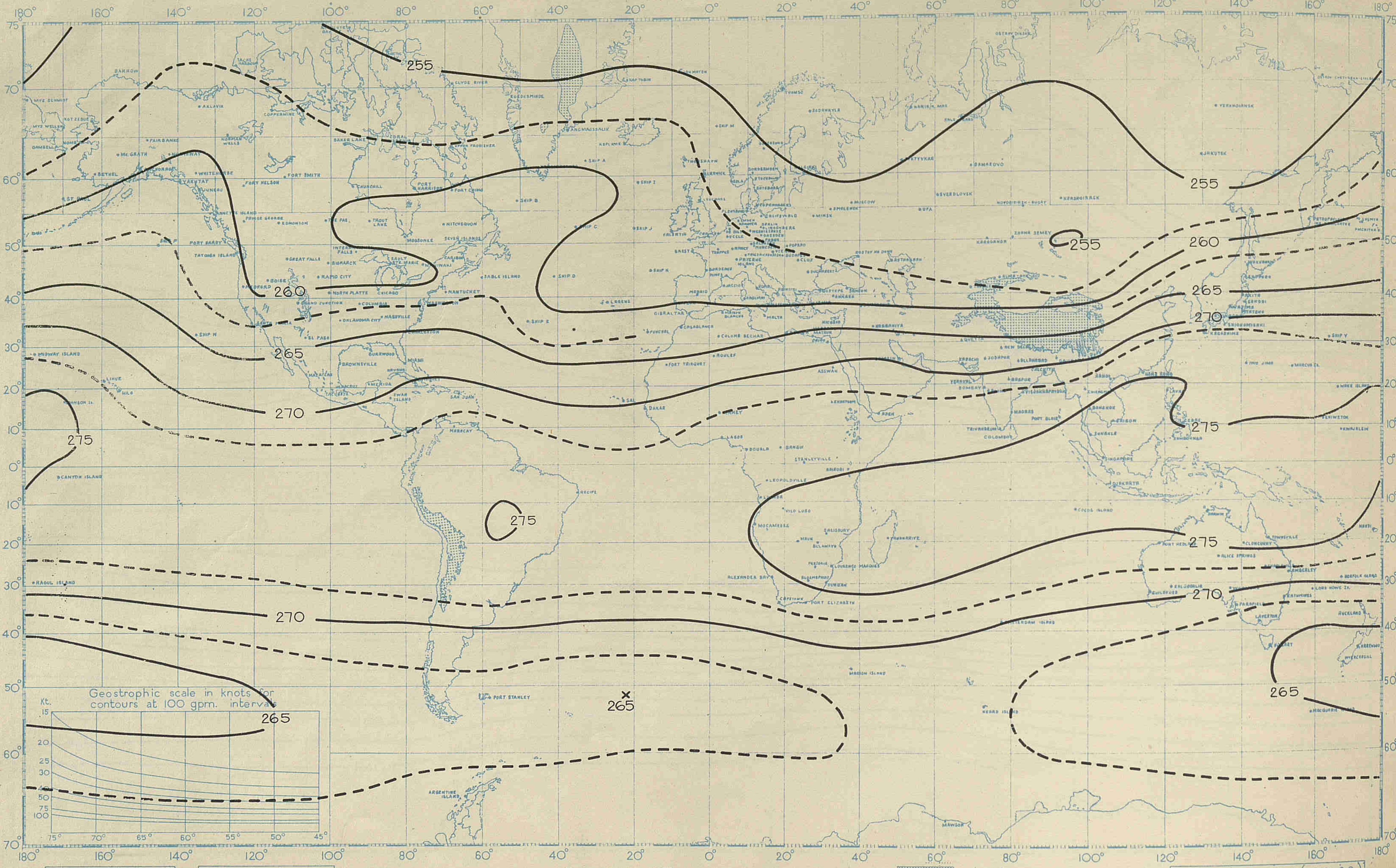
255
255
255
260
260
265
265
270
270
275
275
275
275
270
270
265
265
265
Geostrophic scale in knots for contours at 100 gpm. interval
Kt.
15
20
25
30
40
50
75
100
75°
70°
65°
60°
55°
50°
45°

Temperature in °C.

Height in dekametres

Revised to May 1955

▨ Land over 3,000 metres

Upper Air Branch (M.O.23)

M.R.P. 1045

Average 200 mb. Contours

JANUARY 1949-1953

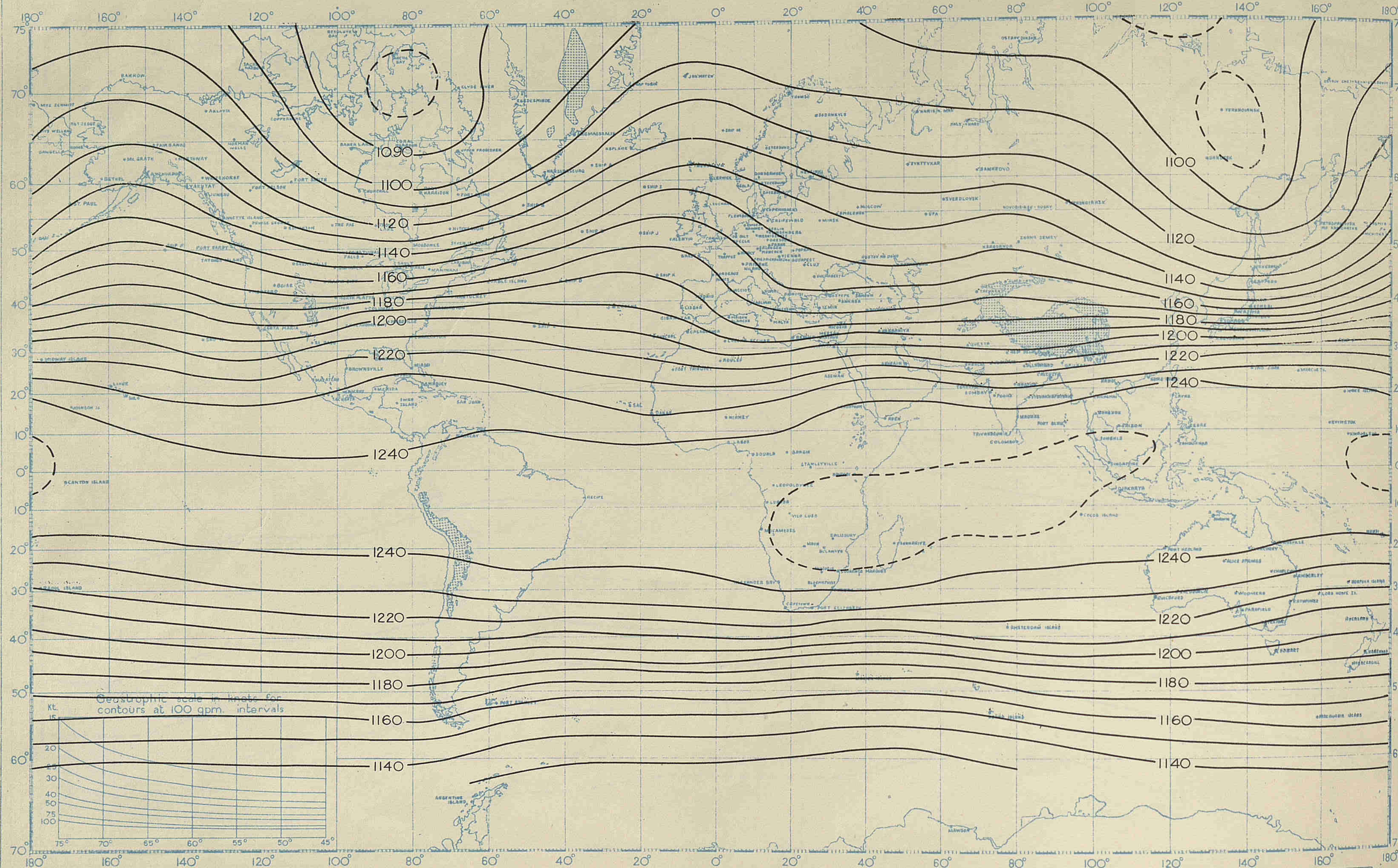
1090
1100
1120
1140
1160
1180
1200
1220
1240
Geostrophic scale in knots for contours at 100 gpm. intervals
Kt.
15
20
25
30
40
50
75
100
75°
70°
65°
60°
55°
50°
45°
180°
160°
140°
120°
100°
80°
60°
40°
20°
0°
75°
70°
60°
50°
40°
30°
20°
10°

Temperature in °C.

Height in dekametres

Revised to May 1955

▨ Land over 3,000 metres

Upper Air Branch (M.O.23).

M.R.P. 1045

Average 200-150 mb. Thickness

JANUARY 1949-1953

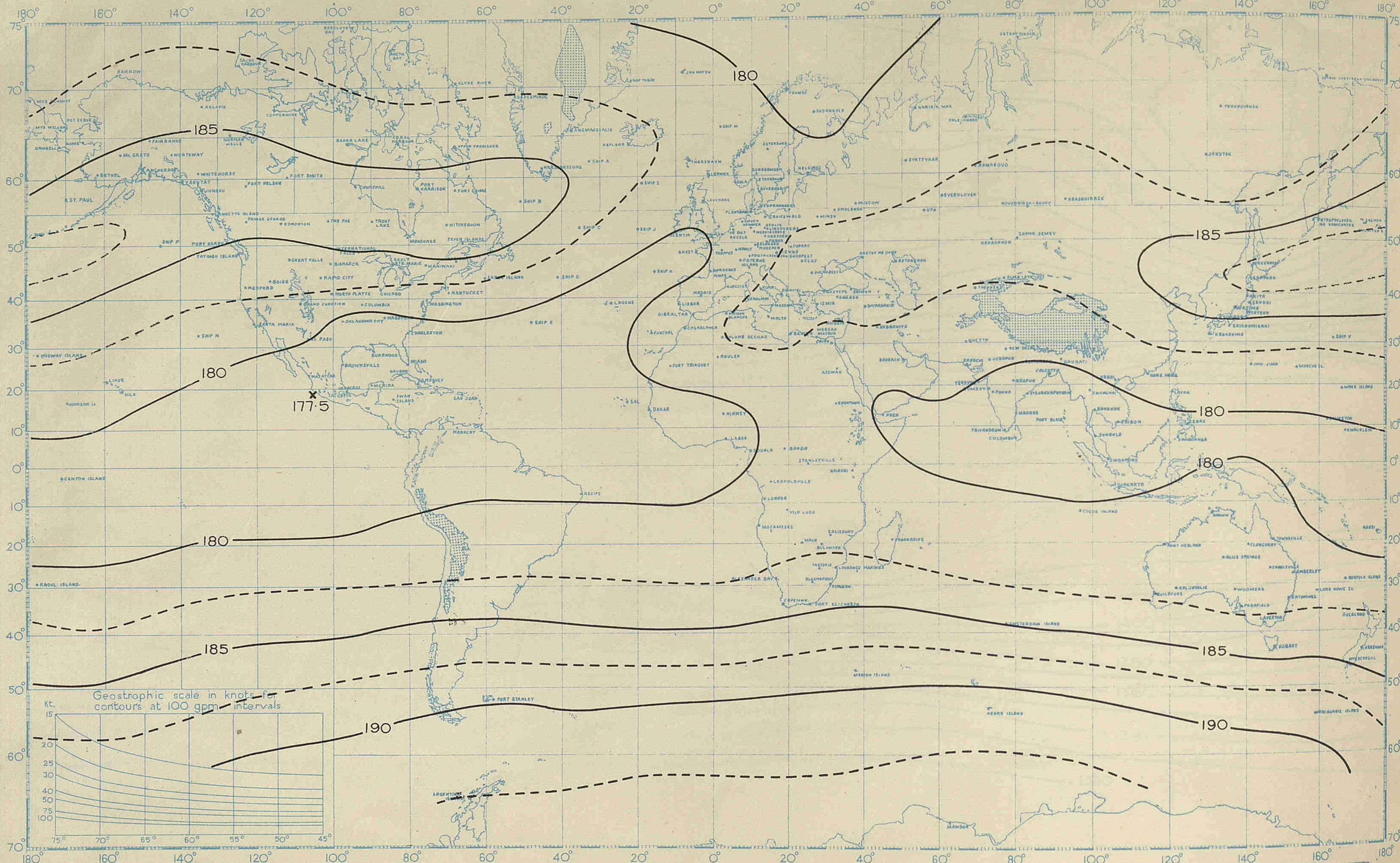
180°
160°
140°
120°
100°
80°
60°
40°
20°
0°
20°
40°
60°
80°
100°
120°
140°
160°
180°
75°
70°
60°
50°
40°
30°
20°
10°
0°
10°
20°
30°
40°
50°
60°
70°
180
185
180
177·5
180
185
180
180
180
185
185
190
190
Geostrophic scale in knots for contours at 100 gpm intervals
Kt.
15
20
25
30
40
50
75
100
75°
70°
65°
60°
55°
50°
45°

Temperature in °C.

Height in dekametres

Revised to May 1955

▨ Land over 3,000 metres

Upper Air Branch (M.O.23)

M.R.P. 1045

Average 150 mb. Contours

JANUARY 1949 - 1953.

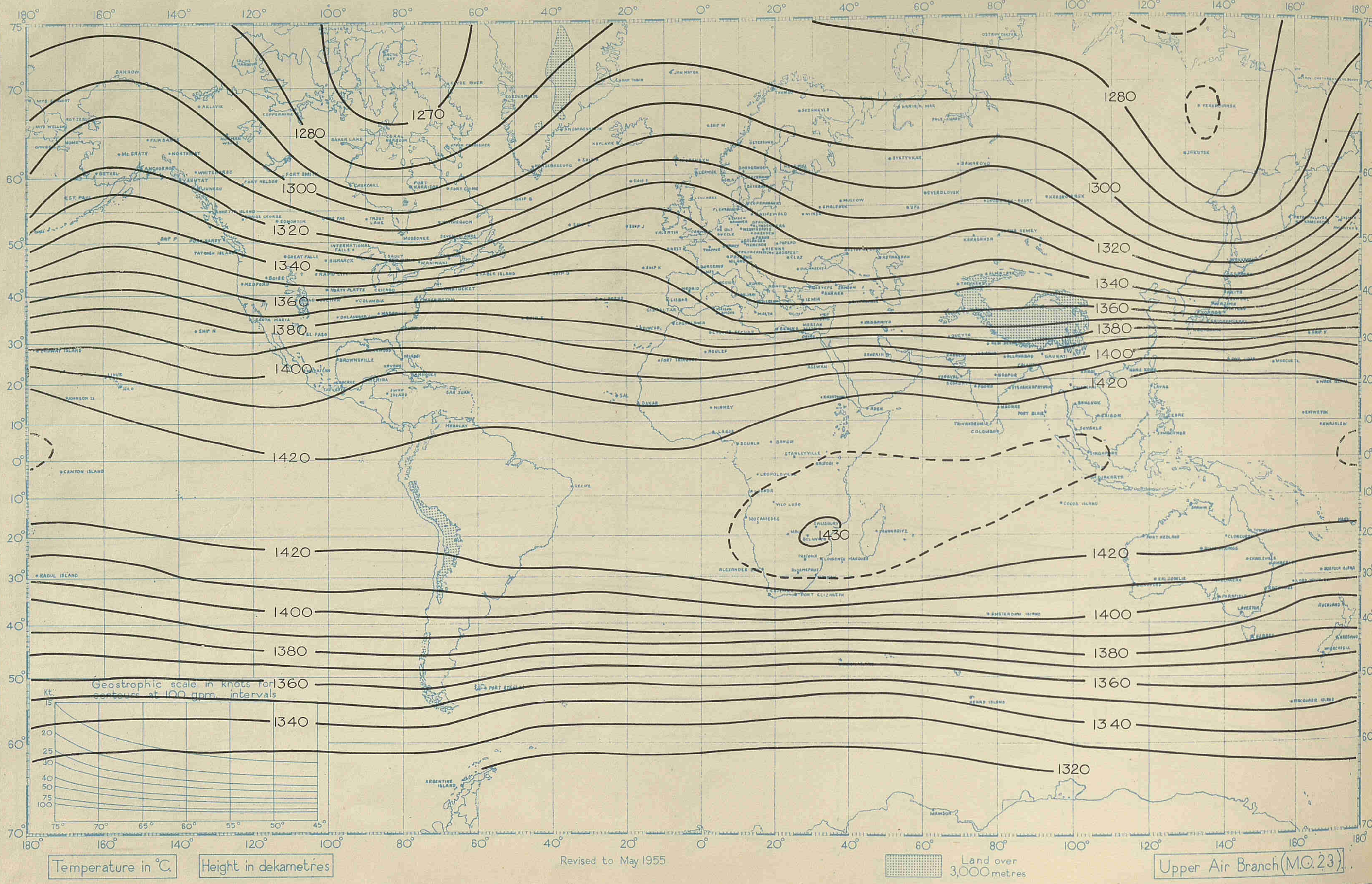

1270
1280
1300
1320
1340
1360
1380
1400
1420
1430
Geostrophic scale in knots for contours at 100 gpm. intervals
Kt.
15
20
25
30
40
50
75
100
75°
70°
65°
60°
55°
50°
45°
Temperature in °C.
Height in dekametres
Land over 3,000 metres
Upper Air Branch (M.O.23)

Revised to May 1955

M.R.P. 1045

Average 150-100 mb. Thickness

JANUARY 1949-1953

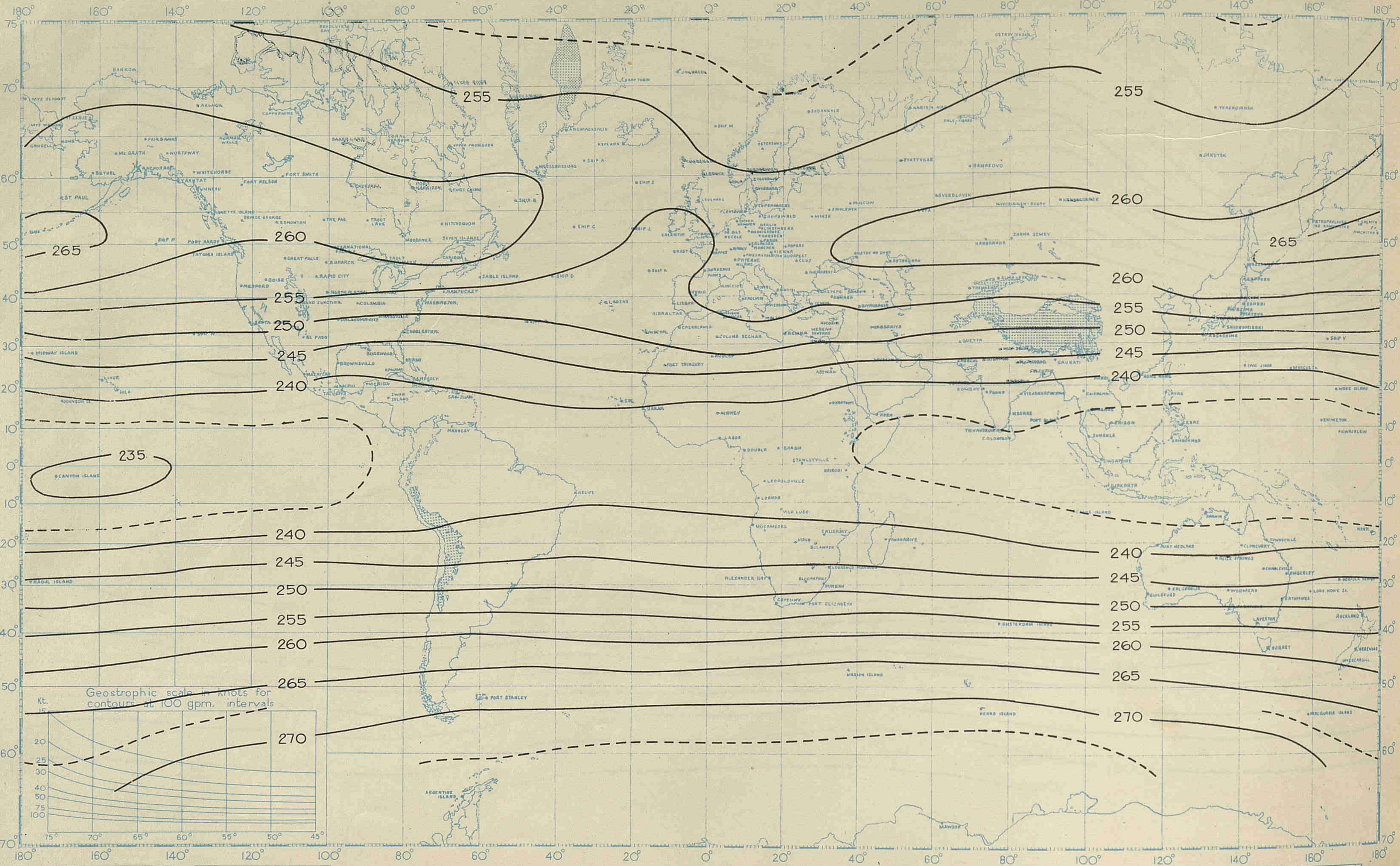
255
260
265
255
250
245
240
235
240
245
250
255
260
265
270
Geostrophic scale in knots for contours at 100 gpm. intervals
Kt.
15
20
25
30
40
50
75
100
75°
70°
65°
60°
55°
50°
45°
180°
160°
140°
120°
100°
80°
60°
40°
20°
0°
75°
70°
60°
50°
40°
30°
20°
10°

Temperature in °C.

Height in dekametres

Revised to May 1955

▨ Land over 3,000 metres

Upper Air Branch (M.O.23)

M.R.P. 1045

Average 100 mb. Contours

JANUARY 1949-1953

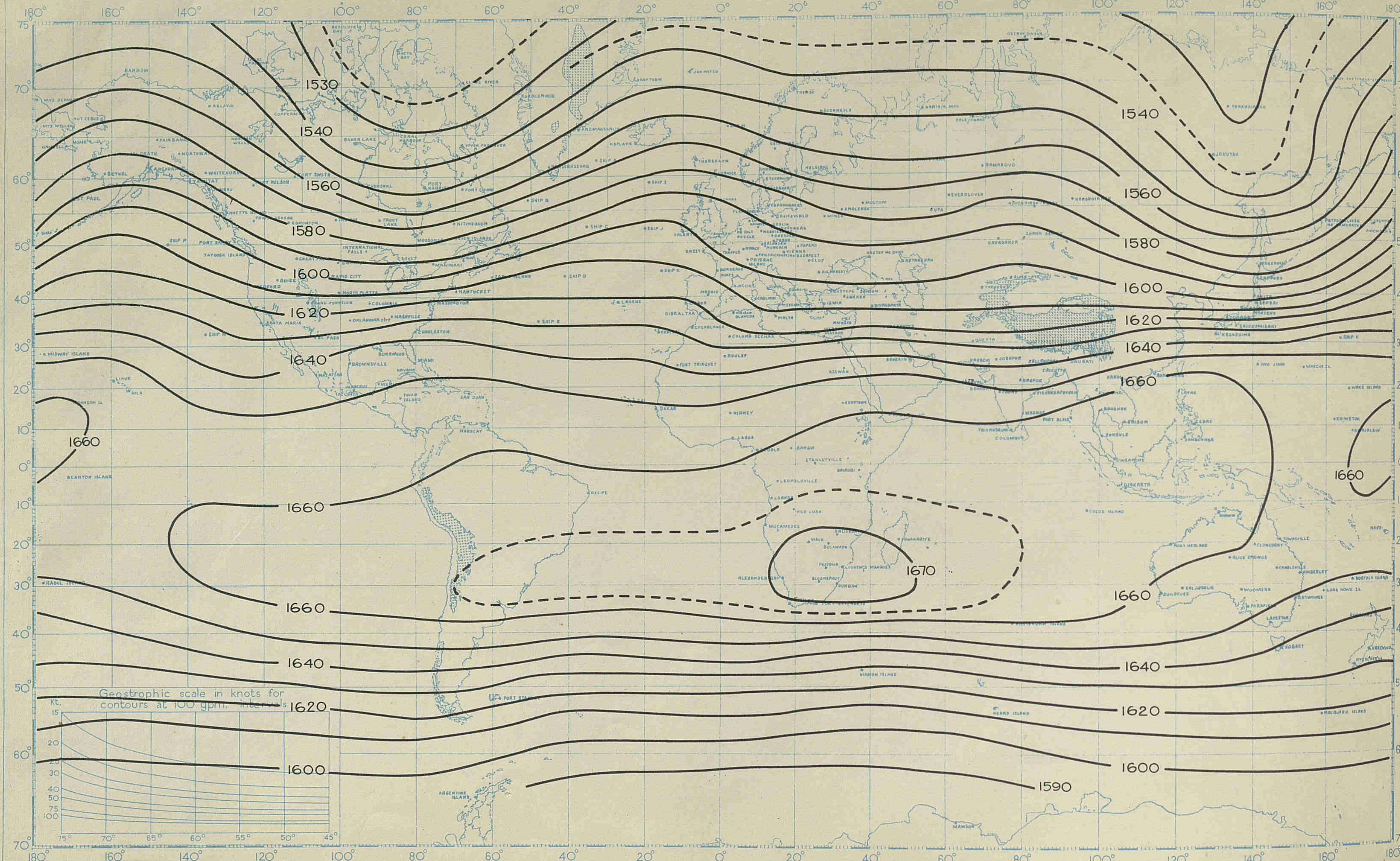
1530
1540
1560
1580
1600
1620
1640
1660
1670
1590
Geostrophic scale in knots for contours at 100 gpm. intervals
Kt.
15
20
25
30
40
50
75
100
75°
70°
65°
60°
55°
50°
45°
180°
160°
140°
120°
100°
80°
60°
40°
20°
0°
75°
70°
60°
50°
40°
30°
20°
10°

Temperature in °C.

Height in dekametres

Revised to May 1955

Land over 3,000 metres

Upper Air Branch (M.O.23)

AD216262

M.R.P. 1046
S.C. 111/232
3rd April, 1957

AD216 262

An approximate relation between slant visibility and horizontal visibility at ground level

by

K. H. Stewart

(Meteorological Office)

AIR MINISTRY

METEOROLOGICAL RESEARCH COMMITTEE

At the time of issue this report has not been published. Any author desiring to quote this paper should refer to it as "A paper of the Meteorological Research Committee (London), M.R.P. No. 1046 by Dr. K.H. Stewart
A copy is available in the Library of the Meteorological Office."

M.R.P. 1046
S.C.III/232
3rd April, 1957

AIR MINISTRY

METEOROLOGICAL RESEARCH COMMITTEE

An approximate relation between slant visibility and horizontal visibility at ground level

by
K. H. Stewart (Meteorological Office)

Preface

A method for calculating the variation of visibility with height in a fog was suggested some years ago (Stewart, 1955, App. VI). It was not extended to give estimates of slant visibility at that time because it was hoped on the one hand that observations on the composition of fog would soon be available to verify the model on which the calculations were based, and on the other hand that direct observations of slant visibility would be made on a fairly wide scale and would make indirect estimates unnecessary. Neither of these things has happened, and in view of the continuing interest in problems of slant visibility it has seemed worth while to extend the previous calculations to give values of slant visibility (instead of horizontal visibility at different levels) and at the same time to test the theoretical values as fully as possible against existing data. The data used for testing are observations of slant visibility at Cardington and of vertical visibility at London Airport. It is shown that both sets of observations can be fitted, within broad limits, by a single curve, which represents the best estimate of slant visibility that can be made from surface observations at the present time.

1. Introduction

The temperature gradient in a well developed fog is usually found to be close to the saturated adiabatic value (Dines 1930, Stewart 1955, Urfer 1956), as would be expected from the fact that fogs lose heat by long wave radiation from their upper surfaces and gain heat from the ground surface; the heat is presumably transferred upwards by convection currents. If it is assumed that the water condensed in rising air currents is all deposited on existing droplets and also, for simplicity, that all the droplets at a given level are of the same size, then the way in which opacity varies with height can readily be calculated. For most practical purposes the opacity at a given height is not of great interest, but it is not difficult to extend the calculations to give the more interesting quantity "slant visibility".

2. Definition of slant visibility

The visual range of an object to a given observer depends on illumination, contrast and eyesight as well as on the state of the atmosphere, but it is convenient to define "visibility", V, as the range of a standard object to a standard observer in standard conditions of illumination. If the standards are suitably specified, the visibility becomes a function only of the atmospheric attenuation coefficient for visible light, σ , given by Koschmieder's equation, $V\sigma = 3.91$, if the fog is uniform, or its extension, $\int_0^V \sigma \, dx = 3.91$, if σ varies along the line of sight. This definition can, of course, be applied to slant visibility from a height h (i.e., the visibility along a path from this height to the ground) as well as to horizontal visibility, and it will be used here. It should be noted, however, that the correspondence between visibility and visual range may be much less close for slant observations than it is for normal horizontal ones, because the conditions of observation are more likely to depart widely from the standard conditions used in the definition of visibility.

3. Relation between slant visibility and attenuation coefficient

The slant visibility, S, from height h_1 is given by

$$\int_0^S \sigma \, dx = 3\cdot 91$$

where the path of integration (the line of sight) extends from h_1 to ground level at an angle with the horizontal whose sine is h_1/S. If we assume that σ depends only on height, h, i.e., that the fog is uniform in the horizontal, we can rewrite the equation as

$$\frac{S}{h_1} \int_0^{h_1} \sigma \, dh = 3.91 \qquad (1)$$

or, approximately,

$$S = 4h_1 \Big/ \int_0^{h_1} \sigma \, dh \qquad (2)$$

4. Variation of attenuation coefficient with height

The attenuation coefficient of a cloud containing n drops per unit volume, of radius r, is

$$\sigma = K n \pi r^2 \qquad (3)$$

or $$\sigma = K \left(\frac{9\pi}{16}\right)^{\frac{1}{3}} n^{\frac{1}{3}} m^{\frac{2}{3}} \qquad (4)$$

where m is the mass of liquid water (of unit density) per unit volume and K is the "scattering area ratio" which, for drops larger than a few microns, can be taken as equal to 2.0 (Middleton, 1952).

The attenuation coefficient at height h is therefore

$$\sigma = \sigma_0 \left(1 + \frac{\delta m}{m_0}\right)^{\frac{2}{3}} \qquad (5)$$

where σ_0 is the coefficient at ground level, m_0 the liquid water content and δm the extra water condensed by adiabatic ascent to height h, which we may write as

$$\delta m = \Gamma_w \frac{dw}{dT} h$$

where Γ_w is the saturated adiabatic lapse rate and $\frac{dw}{dT}$ the rate of change of vapour density with temperature. σ_0 can be expressed in terms of the horizontal visibility at ground level, H, by the equation $\sigma_0 = 3.91/H$, which will be taken, exactly enough, as $\sigma_0 = 4/H$; m_0 can then be obtained from (4).

We can therefore write (5) as

$$\sigma = \frac{4}{H}\left(1 + \frac{\Gamma_w \frac{dw}{dT} . h}{\frac{8}{H^{\frac{3}{2}}}\left(\frac{2}{9\pi n}\right)^{\frac{1}{2}}}\right)^{\frac{2}{3}}$$

$$= \frac{4}{H}\left(1 + A H^{\frac{3}{2}} h\right)^{\frac{2}{3}} \qquad (6)$$

where $A = \sqrt{\frac{9\pi}{128}} \sqrt{n} . \Gamma_w \frac{dw}{dT}$

5. Variation of slant visibility with height

The slant visibility can be obtained by integrating (6) with respect to h and substituting in (2), which gives

$$\frac{S}{H} = \frac{5}{3} \frac{A H^{\frac{3}{2}} h_1}{(1 + A H^{3/2} h_1)^{5/3} - 1} \qquad (7)$$

We have thus obtained an expression for the slant visibility, S, in terms of the horizontal visibility at ground level, H, the height of observation, h_1, and a constant A which depends on temperature and on the number of fog drops per unit volume. The expression indicates, of course, that slant visibility is always less than horizontal and that its relative variation with height is greater the greater the horizontal visibility. It will be valid only when all observations are made within a large-drop water-fog; it cannot be used when the horizontal visibility at ground level, H, depends on "smoke" or "nuclei" rather than on water droplets (i.e., roughly speaking, when H is greater than about 800 yards or when relative humidity is appreciably below 100 per cent), nor does it give directly the slant visibility from heights above a fog layer.

6. Testing of the relation

Equation (7) is based on assumptions about the nature and behaviour of fogs which are probably not exactly fulfilled in practice. In the absence of reliable measurements of drop size and concentration at different levels in fog, it is impossible to test the assumptions directly. Direct comparison of equation (7) with visibility observations is also impossible, because the constant A is unknown. We can, however, draw curves of S/H as a function of $h.H^{3/2}$ for various values of A. Observations on any one occasion should lie on one of these curves and to the extent that observations on different occasions lie on a common curve, we can say that A has the same value in all fogs.

Two sets of observations and curves for two values of A have been plotted in Fig. 1. The first set of observations contains measurements of the slant visual range of a small lamp made at Cardington in 1953 and briefly reported by Stewart (1955). The visual ranges have been converted into "equivalent daylight visibilities" by the methods described in the "Observers Handbook" and should therefore correspond fairly closely to the slant visibility as defined in para. 2. Horizontal visibility was measured simultaneously by a photoelectric meter or by visual estimation. It ranged from 30 to 250 yards in the observations plotted, while slant measurements were made up to the height at which the light disappeared, from 300-500 ft.

The second set of observations contains daylight observations of "vertical visibility" made at London Airport by noting the time for a small balloon, filled to ascend at a known rate, to disappear from view. It was assumed that the height at which the balloon disappeared was equal to the slant visibility from that height, so that each balloon ascent gave a single measurement of slant visibility. In these observations the standard conditions for visibility observations were reasonably well fulfilled, though appreciable errors may have arisen from the small size and pale colour of the balloon and from its drifting in the wind.

Fig. 1 shows that within a rather wide margin of error the majority of observations, both at Cardington and London Airport, lie on the curve with $A = 1.15 \times 10^{-6} (ft)^{-5/2}$ (corresponding to 300 droplets/c.c. at 40°F). The fit for the Cardington observations is not greatly improved if A is varied to give the best fit for each occasion separately.

The departures of the observed points from the mean curve may be due to a variety of causes, other than over-simplification of the model on which the theoretical curve is based. The observations themselves are not very accurate; at Cardington, errors of 20 per cent in both slant and horizontal visibility are quite possible and at London Airport even greater errors may be expected in vertical visibility. (Vertical visibility is, in any case, usually only reported in hundreds of feet, rounding off to the lower hundred; in these cases the observations have been plotted as if they were fifty feet higher than the reported values.) Points above the mean curve may represent observations made above the fog top, in the early stages of a fog before convective equilibrium has been established, in fogs uniformly polluted by smoke or in fogs where, for some reason, the number of droplets is unusually small. Points below the curve may represent conditions of low cloud or "lifted fog" with visibility at the ground restricted by smoke rather than water drops; fogs with smoke concentration increasing upwards; fogs in which the size of droplets near the ground is unusually small, or fogs with unusually large numbers of droplets.

It is clear that equation (7) cannot be used to find accurate values of S on individual occasions, but it probably does give the best available representation of the average behaviour of the type of fog considered - certainly much better than the assumption that fogs are uniform with height, equivalent to $S/H = 1$. It would, no doubt, be possible to improve the fit between theory and observation by introducing further variables such as the spread of the drop size distribution or the degree of convection in the fog, but there seems little point in doing so unless these variables can be measured.

7. Estimation of slant visibility

Equation (7) and fig. 1 do not give estimates of S in the most convenient form. Fig. 2 gives values of S at different heights, in terms of H, as derived from equation (7) with $A = 1.15 \times 10^{-6} (ft)^{-5/2}$. It represents the best estimate of slant visibility that can be made at present from surface observations alone and it is hoped that it may be of some value in connection with aircraft landing problems. As a guide to the accuracy that may be expected, the Cardington observations for $h = 300$ ft have been plotted on fig. 2.

Fig. 2 should be used with the following limitations in mind:

(a) It gives the most likely value of slant visibility, on average, but quite large differences may occur on some occasions.

(b) It gives visibility not visual range; by day the visual range is likely to be less than the visibility, because of poor contrast and uneven lighting; by night the range of the usual bright approach and runway lights may be several times the "visibility". Visual range can easily be calculated from visibility, if the necessary data are available.

(c) It cannot be used when H is seriously affected by smoke.

(d) It applies only to "mature" fogs, in which convection is active; as a rough guide, it should apply to fogs with "sky invisible" but not to those with "sky visible".

(e) It does not apply to heights above the fog top, though if the height of fog top is known calculations to cover this case can be made.

(f) It has been plotted using values of constants found appropriate at Cardington and London Airport. The curves may require modification for use at other stations, though they are likely to be roughly correct for all low-level inland stations in SE. England.

8. References

Dines, L. H. G.	1930	Met. Mag., 65, p. 277.
Middleton, W. E. K.	1952	Vision throughout the Atmosphere. Toronto University Press, p. 29.
Stewart, K. H.	1955	Meteorological Research Papers, Air Ministry, London, No. 912.
Urfer, A.	1956	Geof. Pura e Applicata, 34, p. 231.

G.17351/PAG/4/57/50

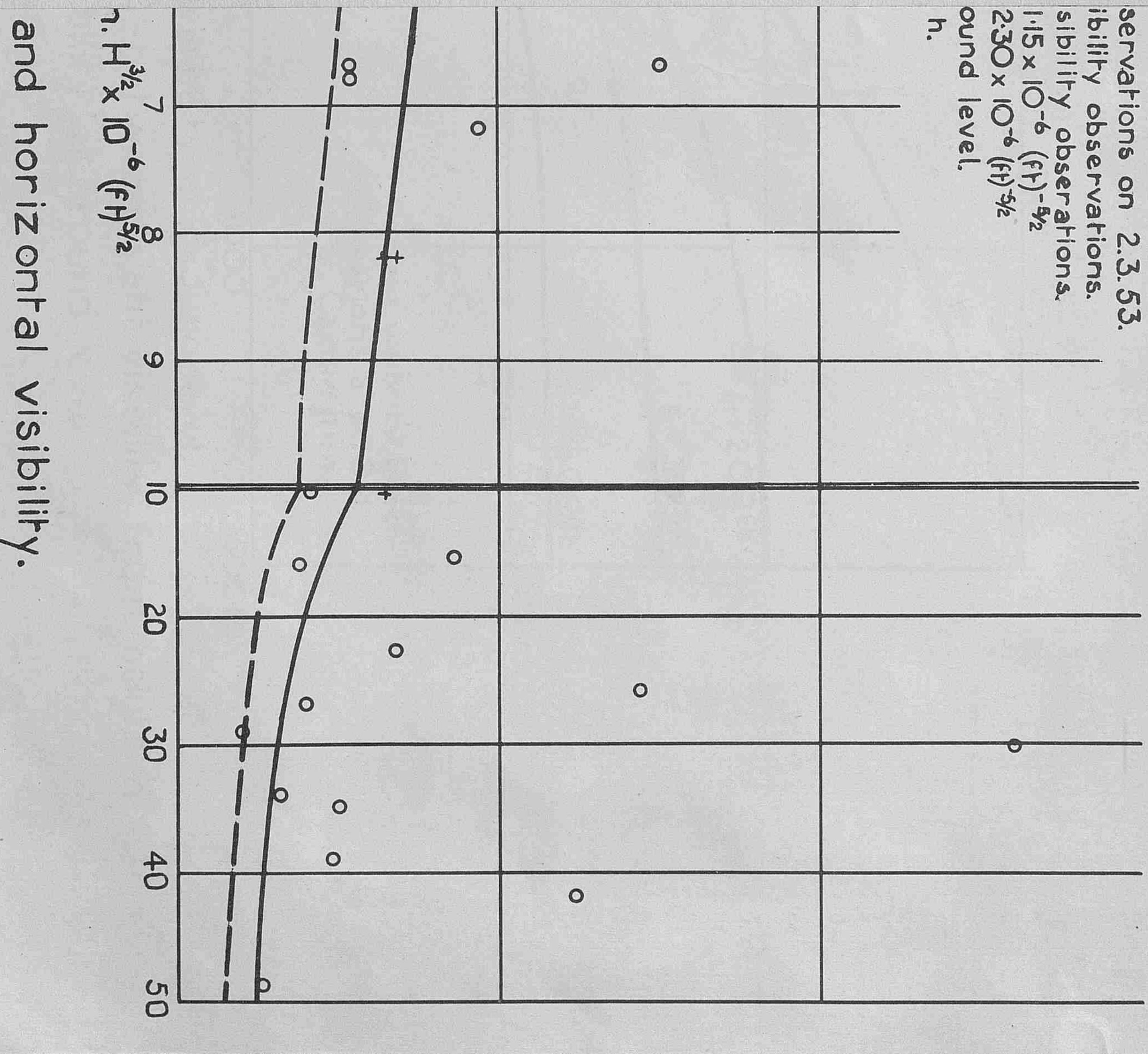

tration increasing upwards, fogs in which the
is unusually small, or fogs with unusually large numbers of droplets.

It is clear that equation (7) cannot be used to find accurate values of S on individual occasions, but it probably does give the best available representation of the average behaviour of the type of fog considered - certainly much better than the assumption that fogs are uniform with height, equivalent to $S/H = 1$. It would, no doubt, be possible to improve the fit between theory and observation by introducing further variables such as the spread of the drop size distribution or the degree of convection in the fog, but there seems little point in doing so unless these variables can be measured.

7. Estimation of slant visibility

Equation (7) and fig. 1 do not give estimates of S in the most convenient form. Fig. 2 gives values of S at different heights, in terms of H, as derived from equation (7) with $A = 1.15 \times 10^{-6}\ (\text{ft})^{-5/2}$. It represents the best estimate of slant visibility that can be made at present from surface observations alone and it is hoped that it may be of some value in connection with aircraft landing problems. As a guide to the accuracy that may be expected, the Cardington observations for $h = 300$ ft have been plotted on fig. 2.

Fig. 2 should be used with the following limitations in mind:

(a) It gives the most likely value of slant visibility, on average, but quite large differences may occur on some occasions.

(b) It gives visibility not visual range; by day the visual range is likely to be less than the visibility, because of poor contrast and uneven lighting; by night the range of the usual bright approach and runway lights may be several times the "visibility". Visual range can easily be calculated from visibility, if the necessary data are available.

(c) It cannot be used when H is seriously affected by smoke.

(d) It applies only to "mature" fogs, in which convection is active; as a

/rough

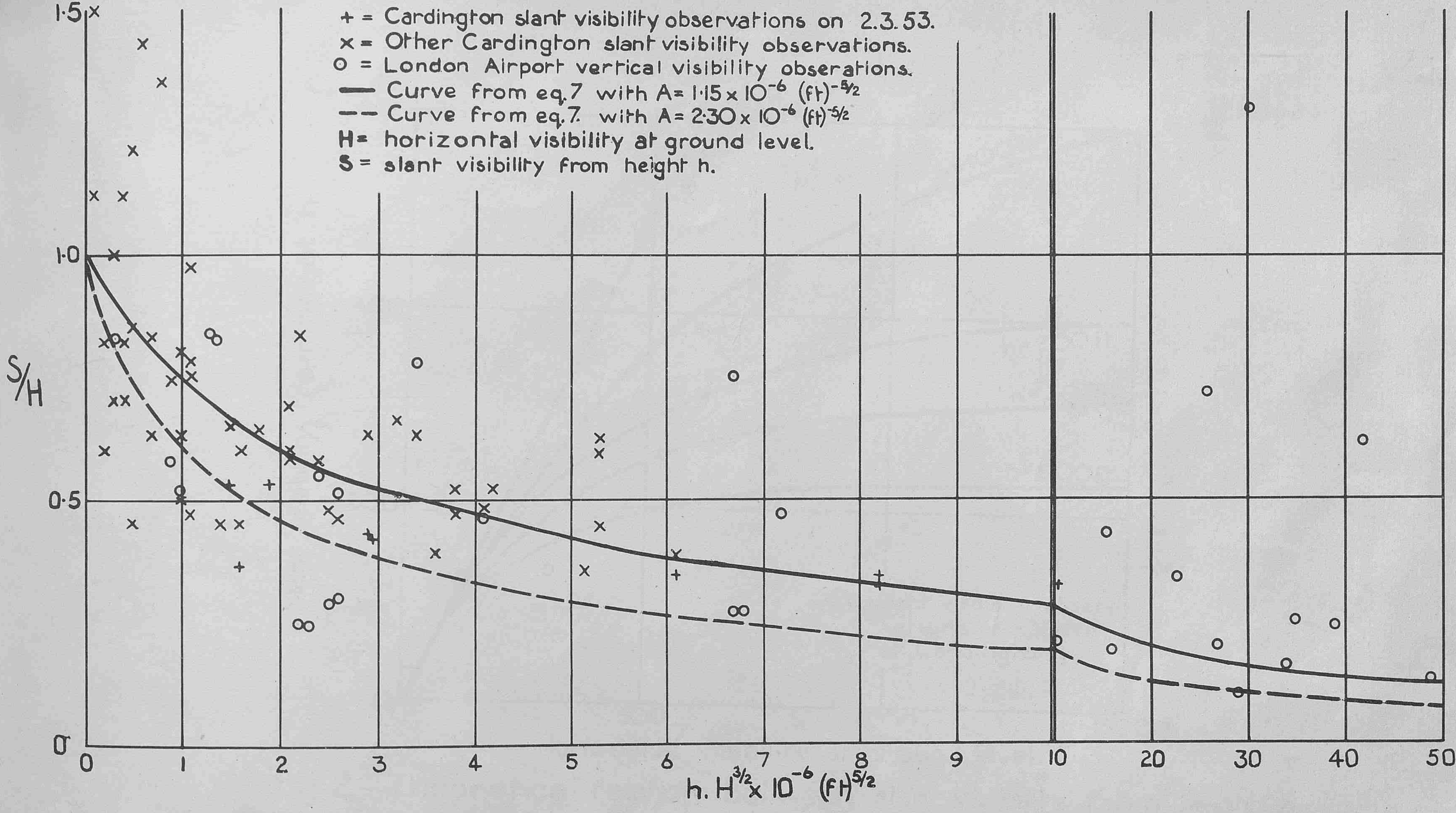

Fig 1. Relation between slant and horizontal visibility.

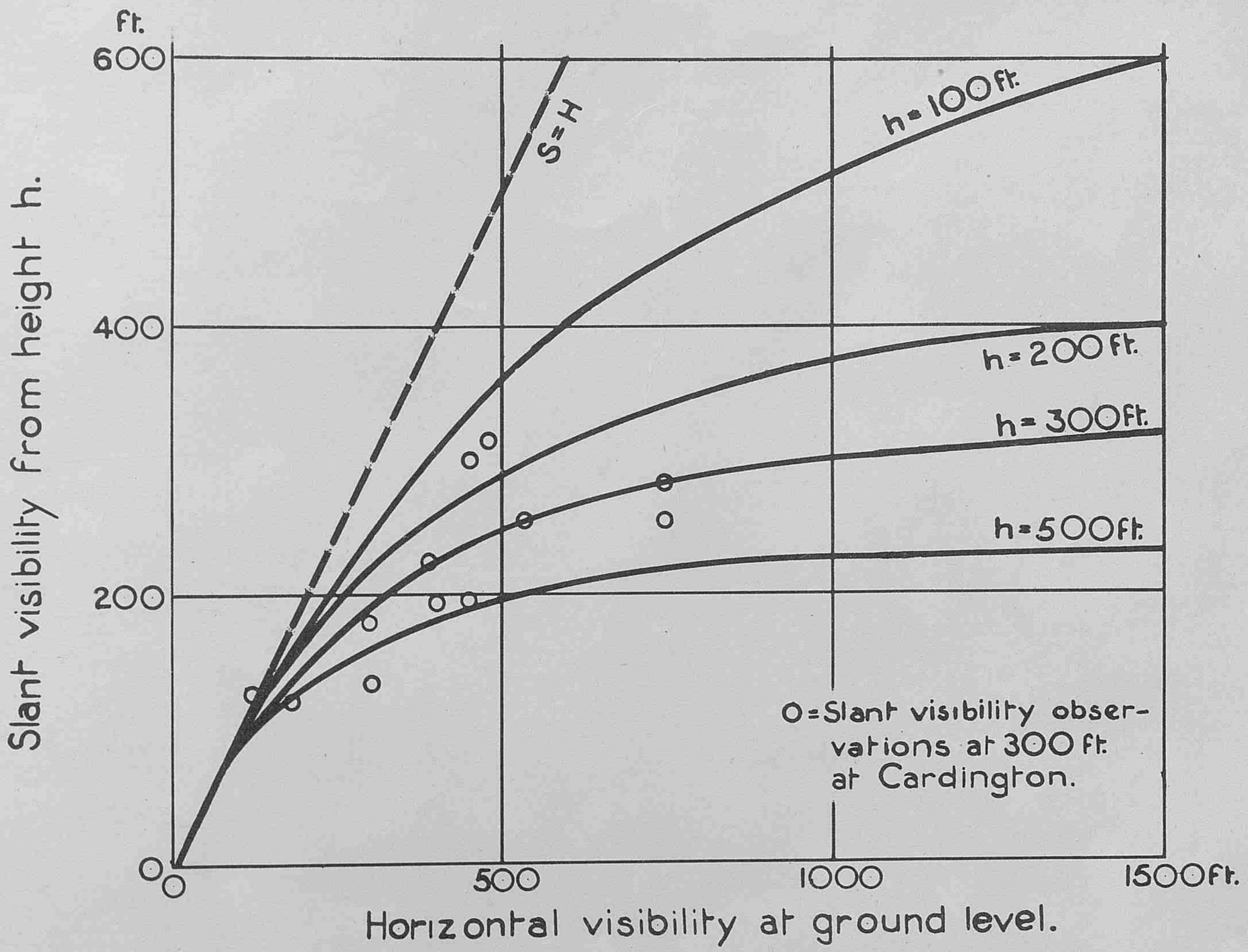

Fig. 2. Theoretical relation between slant visibility from height h and horizontal visibility at ground level.

MATS

AD208932.

M.R.P. 1047
S.C. 111/233
3rd April, 1957

AD 208932

A method for assessing the frequency of dangerous visibility conditions

by

K. H. Stewart

(Meteorological Office)

AIR MINISTRY

METEOROLOGICAL RESEARCH COMMITTEE

57-1115

At the time of issue this report has not been published. Any author desiring to quote this paper should refer to it as "A paper of the Meteorological Research Committee (London), M.R.P. No. 1047 by Dr. K. H. Stewart A copy is available in the Library of the Meteorological Office."

M.R.P. 1047
S.C.III/233
3rd April, 1957

AIR MINISTRY
METEOROLOGICAL RESEARCH COMMITTEE

A method for assessing the frequency of dangerous visibility conditions

by

K. H. Stewart (Meteorological Office)

1. Introduction

It has long been recognised that the visibility from a few hundred feet above ground level in fog may be very different from that observed at ground level. There has been considerable discussion of the possible dangers that this may involve for aircraft trying to land in fog, but much of the discussion has been vague because of our lack of knowledge of visibility at different levels in fog. The plans for observing "slant visibility" that have been in operation for the last few years have produced very meagre results; it is hoped that the new plans now being put into force will be more productive, but the accumulation of data will be a slow process at best. It therefore seems worth while, even on the basis of our present very slender knowledge of slant visibility, attempting to assess how frequently dangerous conditions are likely to arise. The attempt should show what quantities have to be considered in practical problems, and may give some guide to the best method of analysing data obtained in the future. Most important, it can give a factual basis for a decision whether or not to proceed urgently with the development of devices suitable for the routine observation of slant visibility at airfields.

2. Representation of fogs

It has been shown (Stewart, 1957) that in the great majority of cases at Cardington and London Airport there is a simple approximate relation between the slant visibility from a given height in a fog and the horizontal visibility at ground level, the slant visibility decreasing with increasing height. For observations from above the top of the fog, the slant visibility as defined (Stewart, 1957) increases with height and is simply proportional to height above ground, as can be seen by considering that objects at the limit of visibility must always be seen through the same amount of fog.

The variation of slant visibility with height in and above a fog layer is therefore as shown schematically in fig. 1. The line ABC represents a thick shallow fog, DEF a thinner deeper one. Lines BC and EF are simply straight lines from the origin drawn through points B and E, representing slant visibilities at the fog tops. AB and DE are drawn from the equation already derived relating slant and horizontal visibilities.

Each curve is uniquely determined by the point (B or E) representing height of fog top and slant visibility from fog top; these two quantities can therefore be used to specify completely the visibility conditions in a fog, and fogs can conveniently be represented by single points such as B and E on diagrams like fig. 1, rather than by drawing the complete slant visibility curves. It will be seen later that this representation is of some value even when the visibility curve below the fog top does not follow the theoretical model exactly.

57-1115

/3.

3. Data on fogs at Cardington

Measurements of slant visibility have so far been made on relatively few occasions and they give no reliable information on the frequency of occurrence of different visibility conditions. However, the height of fog top can be estimated fairly accurately from almost all of the numerous temperature and humidity soundings that have been made in fog at Cardington, and in each case the slant visibility from this height can be deduced from the observed horizontal visibility at ground level, as previously shown (Stewart, 1957). We can thus obtain the set of points in fig. 2, representing the visibility conditions in a more or less random selection of fogs at Cardington in the past few years. The points come partly from a series of special ascents made at two- or three-hourly intervals in the fogs of 1951-53 and partly from the routine ascents made at 0730 (since 1956 at 0600), 1200, 1800 and (since 1956) 2400 hr. The times of these routine ascents may tend to exclude newly formed fogs but it is not thought that this possible bias will have any very serious effect on the representativeness of fig. 2 as a sample of all Cardington fogs (the points from frequent soundings throughout the periods of fog do not seem to differ much from the points corresponding to the more widely spaced routine ascents).

The number of points included in fig. 2, in relation to the period and frequency of the observations, is such that each point corresponds to a time of about six hours per year, i.e., the conditions represented by each point may be expected to exist for about six hours in each year.

4. Conditions dangerous to aircraft

Fig. 2 contains the meteorological data required for assessing the frequency of dangerous visibility conditions at Cardington. ("Dangerous conditions" is used here in a restricted sense; the only danger considered is that arising directly from the vertical structure of the fog, other possible dangers such as horizontal patchiness or the glare of a low sun on the fog top being left for separate consideration). Any specification of the visibility conditions that actually constitute a danger can be expressed as an area on fig. 2 and the number of points falling within this area indicates the time per year for which the danger is to be expected. The specification of dangerous conditions is a matter for aviation experts and the tentative specifications put forward here are intended only to provide an illustration of how the meteorological data can be used.

The normal landing procedure in fog is for a pilot to descend to a predetermined "critical height" (which will be taken, for illustration, as 200 ft) and then to decide whether or not to complete his landing. His decision is based on his own impression of visibility conditions from critical height - he would obviously not continue unless he could already see the ground lights or markings well enough to steer by - and on the report he receives of visibility at ground level on the runway. With this procedure it is clear that poor visibility at and above critical height or at ground level does not constitute a danger; dangerous conditions arise only when, with adequate visibility at critical height and on the runway, visibility is markedly worse from some intermediate height. This may happen, according to the scheme of fig. 1, when the fog top is below critical height and when the visibilities have certain values.

For a concrete example we consider landings made at night at London Airport. The approach lighting system has "crossbars" of 10,000 c.p. lights at 500 ft intervals. Simple geometrical calculations show that to be certain of seeing at least one crossbar from about 200 ft the pilot must be able to see the lights at a slant range of 1300 ft. The visibility required to see a light of 10,000 c.p. at this range is 400 ft. The line OA in fig. 3 drawn from the origin through the point representing slant visibility of 400 ft from height 200 ft will therefore separate the representative points of fogs in which the pilot will have adequate visibility at critical height from those with inadequate visibility. Points above the line represent "safe" conditions (because the pilot will realise at critical height that conditions are too bad, and will not continue his approach); points below the line may represent dangerous conditions.

Below critical height, if we continue to use the criterion of "at least one crossbar visible", the required slant visibility decreases steadily to a value of 130 ft at ground level and we can therefore draw the line AB in fig. 3 with "safe" conditions to the right and "unsafe" to the left. The lower part of this line is unrealistic because close to the ground the pilot ceases to see the approach light crossbars and begins to use the runway lights for guidance; the effects of this change could be shown by appropriate changes in AB, if the lighting and guidance requirements were known.

We are left, therefore, with the narrow area OAB within which points represent dangerous visibility conditions. The area can be still further restricted by bringing in the condition that no attempt at landing will be made unless visibility at ground level (the "runway visual range") is adequate. If we take the limiting condition that 800 ft of runway lighting must be visible and assume lights of 1000 c.p. we find visibility at ground level must exceed 270 ft. With this ground visibility, the slant visibility varies with height as shown by CD in fig. 3. Points to the left of this line represent "safe" conditions - landing will not be attempted - but points to the right may represent unsafe conditions. We are left finally with the shaded area of fig. 3 to represent truly dangerous conditions in which neither the pilot's own observations nor reports from the ground will warn him that if he descends below critical height (and therefore becomes committed to land) he will, for a time, lose the guidance he needs.

The shaded area of fig. 3 has been redrawn on fig. 2 and we can estimate that it contains 1.2 of the representative points, each corresponding to six hours per year. It appears, therefore, that if all our assumptions about fog structure and about visibility requirements are correct, "dangerous conditions" occur at Cardington for about 7 hours per year.

5. Discussion

The estimate of the frequency of dangerous conditions is based on two main assumptions, that the relation between slant visibility and height is given by the theoretical equation in all fogs and that the criteria for adequate visibility are those used in the last section.

The theoretical equation is not applicable to all types of fog, but in practice, at Cardington and London Airport serious departures from it seem relatively rare, with a more or less random sample of fogs. Small random departures from the theoretical relation will not affect the frequency of dangerous conditions greatly; they will tend to remove as many occasions from the danger class as they bring into it. Large departures are rare and will therefore have a small effect on the frequency except when it is extremely small or zero. Our estimate is therefore a lower limit to the frequency of dangerous conditions, but the possibility of freak conditions must be allowed for in addition.

Changes in the criteria for adequate visibility can obviously have a very big effect on our estimate, by changing the position of the lines in fig. 3. As illustrations we may consider the effect of plausible changes of two different types. In the first, we make a numerical change in one of the limiting quantities, the runway visual range limit. If this is varied from the rather low figure of 800 ft to the more usual one of 1500 ft the line CD of fig. 3 is moved so far to the right that the shaded area vanishes altogether. In the second illustration we change the criterion for "adequate guidance" from critical height downwards; instead of supposing that the pilot must be able to see a minimum length of the lighting pattern (500 ft in our previous discussion) we suppose that he must be able to see a minimum angular amount of the lighting pattern, i.e., that the angle subtended at his eye by the length of pattern he can see must remain above some minimum value (which we take to be equal to the angle subtended by 500 ft of lighting when he is at critical height). In fig. 3 this has the effect of turning the line AB until it coincides with AO - and again the shaded area vanishes.

It appears, then, that the greatest uncertainty in our estimate of the frequency of dangerous conditions arises from uncertainty in the criteria for adequate visual guidance. Using what are thought to be fairly realistic criteria we find the frequency to be very low - so low that the chance of making measurements in such conditions in any one year is very small. It also seems likely, with this very low frequency of dangerous conditions, that the dangers arising from horizontal variations in fog density and from time variations are more serious than those due to variations in the vertical, which have been considered here.

6. Conclusions

(a) We cannot decide - even approximately - the frequency of dangerous visibility conditions without a precise statement of what pilots require to see; small changes in requirements produce very big changes in frequency.

(b) Given such a precise statement we can estimate the frequency of dangerous conditions, probably within a factor of two or three, from existing data for SE. England.

(c) A very long programme of measurements will be required to produce any appreciable improvement in the accuracy of this estimate.

(d) Estimates based on present data seem precise enough to permit a decision on the need for the routine operational measurement of slant visibility at airfields.

(e) It seems likely that visibility variations in the horizontal and in time may be a more important source of danger than the vertical variations which have been considered here.

7. Reference

Stewart, K. H. 1957 Meteorological Research Papers, Air Ministry, London, No. 1046.

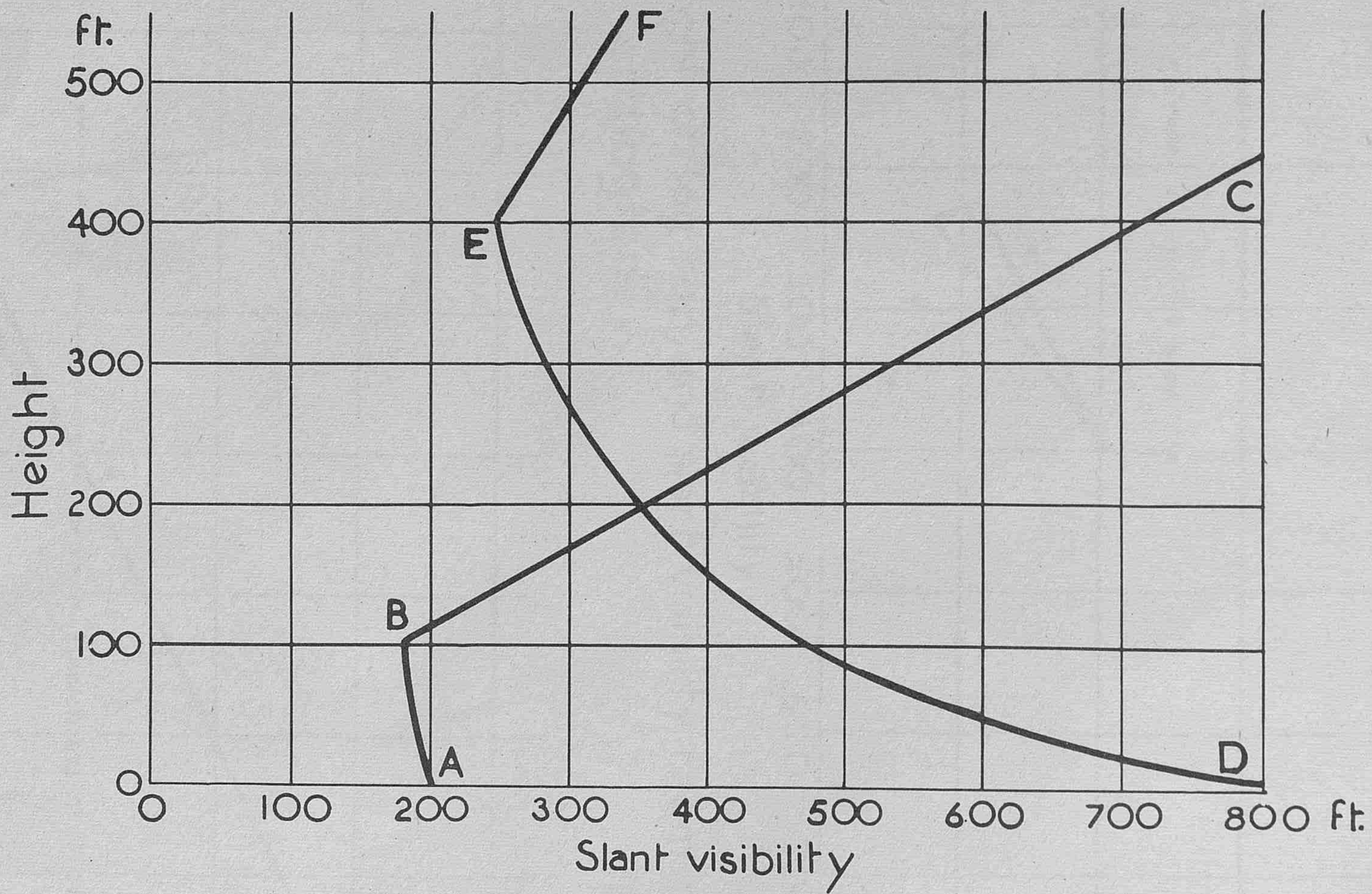

Fig I. Variation of slant visibility with height in and above two typical fogs.

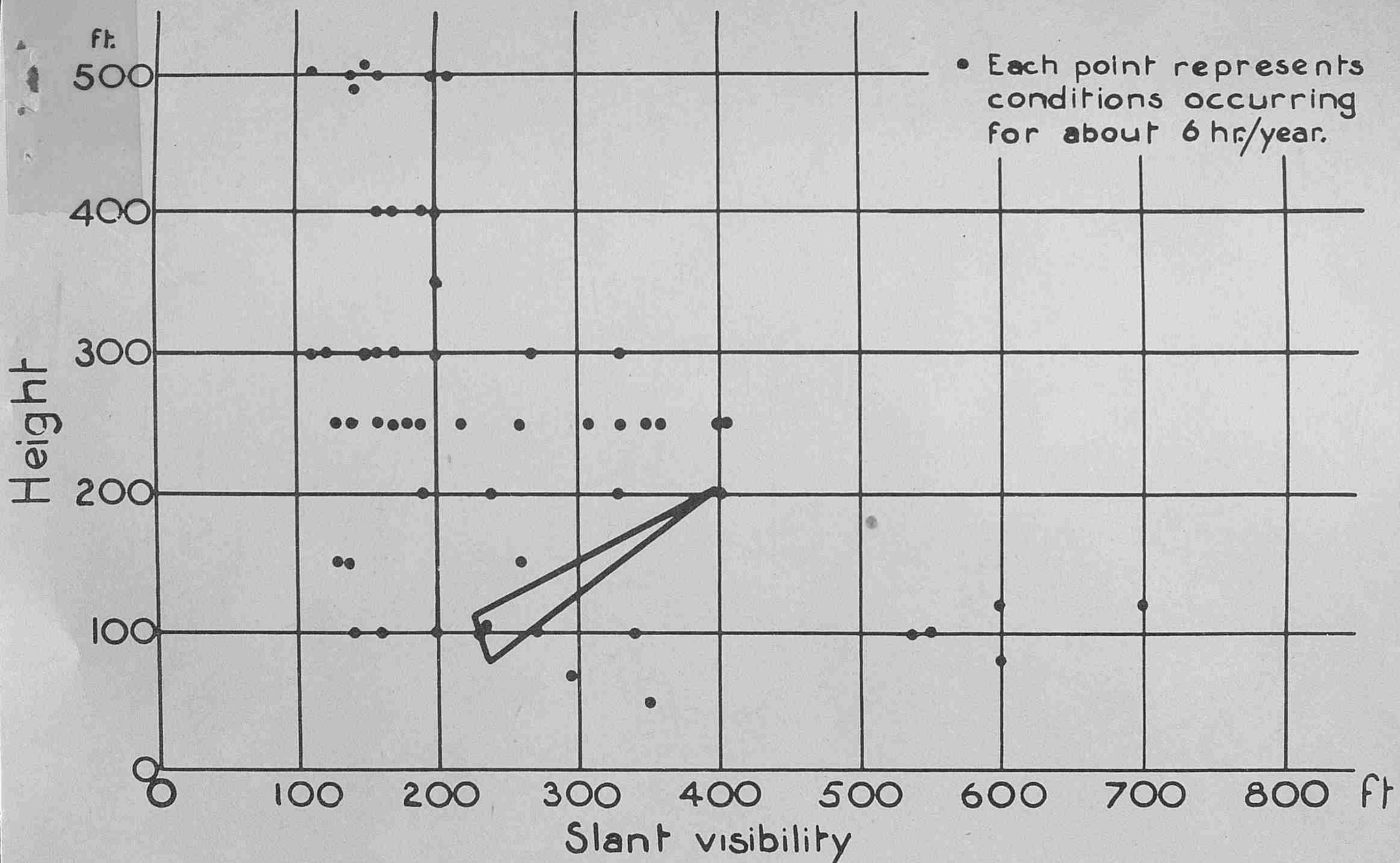

Fig 2. Height of fog top, and slant visibility from fog top at Cardington.

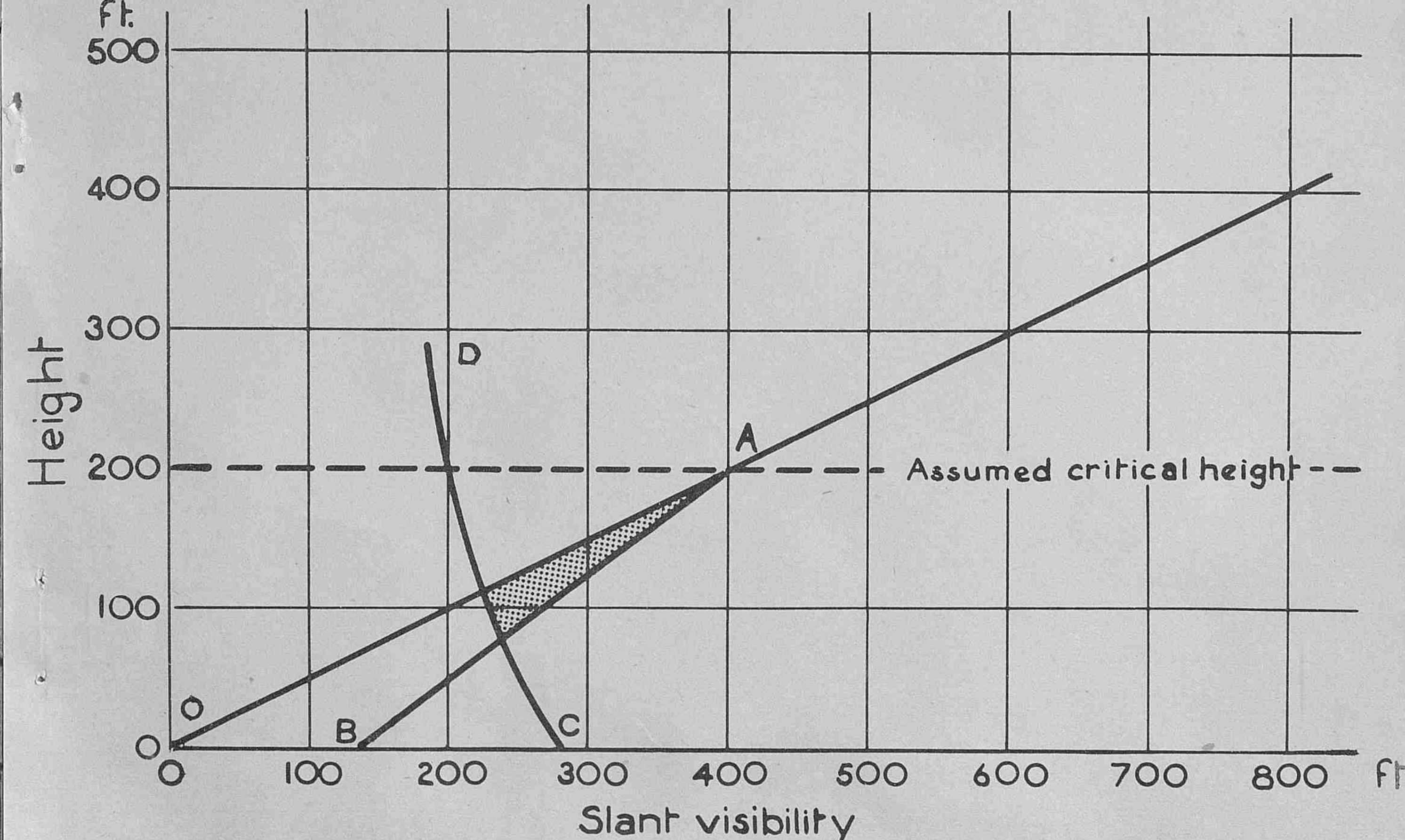

Fig 3. Boundaries of "safe" and "unsafe" areas on slant visibility diagram.

AD216261

M.R.P. 1048
S.C. III/234
28th March, 1957

AD216261

Convection - diffusion processes below a stable layer

by

F.B. Smith

(Meteorological Office)

AIR MINISTRY

METEOROLOGICAL RESEARCH COMMITTEE

At the time of issue this report has not been published. Any author desiring to quote this paper should refer to it as "A paper of the Meteorological Research Committee (London), M.R.P. No. 1048 by Dr. F.B. Smith. A copy is available in the Library of the Meteorological Office."

M.R.P. 1048
S.C. III/234
28th March, 1957

AIR MINISTRY
METEOROLOGICAL RESEARCH COMMITTEE

Convection - diffusion processes below a stable layer

by

F.B. Smith

SUMMARY

Solutions are obtained for the mean concentrations of an emittant dispersed from a cross-wind line source into a turbulent layer of finite depth. Turbulent mixing, represented qualitatively by an eddy diffusivity coefficient K(z), is one of the dominant causes of the dispersion. Unlike most previous solutions based on turbulent diffusion alone, the present ones are derived using diffusivity coefficients all of which fall to zero, either smoothly or sharply, at the top of the finite turbulent layer (as, for example, might happen at the base of a strong inversion).

A further important dispersion effect which also may occur is that of convective transfer. An idealized model, retaining only the dominant features of the convection process, is proposed. The natural diffusion process is augmented by the transport of the emittant, at ground level concentrations, to the top of the layer by thermally generated bubbles or streams rising from the ground. This is in contrast to the conventional method in which the convective transfer is represented by an enhanced value of K(z). In the present model, the convection is balanced by a uniform subsidence throughout the layer. It is assumed that, as the bubbles or streams rise, no mixing takes place with the surrounding atmosphere, that the concept of an eddy diffusivity coefficient can be retained to represent the dispersive processes other than that of free convection and that this coefficient, as without convection, falls smoothly to zero at the inter-surface between the turbulent and stable layers.

The method used in these solutions is that of Heaviside Calculus. One specific case of the convection - diffusion model is evaluated, and is compared with the solution of equal K(z) when convection is absent. The important role of convection is demonstrated.

I. INTRODUCTION TO THE SIMPLE DIFFUSION MODEL

Most of the present formulae for the vertical distribution of concentration of non-buoyant matter emitted from sources and dispersed by simple diffusion are likely to fail at moderately large distances downstream of the source because of variations aloft in the functional form of the eddy diffusivity coefficient, K(z), not accounted for in the initial assumptions. This is particularly true in cases when a turbulent layer adjacent to the ground has above it a stable layer in which turbulent mixing is virtually non-existent. The diffusion will then take place in a region of limited depth and be equivalent to diffusion between parallel planes in which the eddy diffusivity coefficient may take a variety of forms. These coefficients will be characterized by falling to zero at the upper plane.

The height of the inter-surface between two such layers introduces a length scale into the problem, otherwise absent, which not only implies that the concentration will eventually become uniform in the lower layer, but also that dimensional arguments could give a measure of the distance X downstream at which this uniformity is achieved.

A further phenomenon which can lead to important differences in the distribution of concentration is that of convection. The convection concerned will not be the kind arising out of the inherent buoyancy in hot plumes relative to their environment, but rather from the usual type of convection arising from solar heating of the ground and, as such, will be independent of the source. It is clearly desirable to make some attempt to represent statistically the effect of free convection in transporting matter; in particular in its effect in taking the emittant from a layer near the ground up to the inter-surface between the turbulent and stable layers. This effect will be in addition diffusive processes. The nature and effect of convection will be further dealt with in II.

The object of this paper is to account for the above; namely, the limitation in depth of the layer through which the emittant will be distributed and the augmentative effect of free convection on the rate at which the emittant is spread throughout the layer. The approach will be to produce analytic results by attempting to make a compromise between the complex physical phenomena and the mathematics.

The effect of free convection will most readily be appreciated by comparison with the corresponding result when convection is absent but in which all other factors are the same. A comparison between two such models is made in VII. The paper will tend to divide itself into two parts; a discussion of the problem of simple diffusion between parallel planes (without convection) for several functional forms of the eddy diffusivity coefficient and a more restricted examination of the diffusion-convection problem in which the dominant features of the process are described. What remains of this section and III, IV and V will be devoted to the former type problem and II and VI to the latter. These parts will be linked by the comparison in VII.

In the case of simple diffusion, the mathematical problem consists of finding the solution of the diffusion equation with variable eddy diffusivity coefficient K(z) and mean wind velocity u(z), between two parallel planes across which there can be no transport of the emittant. These two planes represent the ground and the inter-surface. The source of the emittant is elevated at a height h (which may be zero). Where exact solutions cannot be determined, asymptotic solutions for small distances downstream (compared with X) will be of interest.

On the assumption that u(z) and K(z) may be represented as powers of the height (measured from any prescribed origin), a transformation of the independent variables x and z (Sutton 1943) changes the diffusion equation to one which represents conditions in an atmosphere of constant wind velocity. Hence, in this paper, the wind velocity will without loss of generality be considered constant with height.

Moreover we shall restrict ourselves to the problem of a continuous infinite line source, not only because in present-day application this is of primary interest but also because the point source solutions may be derived as an extension of the present solutions by the method used in an earlier paper (Smith 1957).

Two alternative approaches have been suggested for the solution of the two-dimensional mathematical problem. They are in many ways very similar, but in actual handling each offers its own particular difficulties. However as far as obtaining actual results is concerned, where these exist, the two methods are equally effective; where a solution can be found by one, it is invariably found that the other will also produce the result. The first method suggested by Sutton (1943) consists of obtaining a set of fundamental solutions involving a parameter; this parameter being restricted to a sequence of eigenvalues determined by the boundary conditions. Which set of fundamental solutions is chosen, also depends on the nature of the boundaries. It is therefore analogous to the method of solving the wave equation in acoustic problems by representing the solution as a series of orthogonal functions each satisfying the wave equation: in the one-dimensional case, as a Fourier Series. The fundamental difficulty of this method is the problem of obtaining the optimum set of fundamental solutions which will satisfy the boundary conditions. In the present problem of diffusion between parallel planes, the set has been found. Certain of the results given below have already been determined by this method by Rounds (1955). (Indication of these solutions will be given in the appropriate section). In order to demonstrate this method, the first of the two problems in V is treated in this way.

The alternative approach, being the one otherwise used here, is that of Heaviside Operational calculus. This method has been used successfully in other diffusion problems, its chief merit being that it rids the problem of any kind of apparent arbitrariness in the determination of the solution (for example, the difficulty mentioned above in Sutton's approach). In the Heaviside method, the solution in terms of x and z is related to the solution in operational form by the well-known integral relationship. When exact solutions are not to be found by either method it is usually true that this is because in the Heaviside method, the operational solution has one or more branch points. The occurrence of these branch points is not always an unsurmountable difficulty but generally one is forced to be satisfied with asymptotic solutions. Goldstein's interpretation formulae (Jeffreys) are often an invaluable aid in dealing with branch points and several more complex forms have been solved, apart from the usual standard results. At any rate, the fact that asymptotic solutions can invariably be found by this method appears to be an obvious advantage over the other method where no such opportunities present themselves. In the present problem of the diffusion between parallel planes the above difficulty will, in the simpler cases, not arise; the operational solutions have poles but no branch points.

The restriction to obtaining a complete solution for every occasion arises from the necessity of being able to represent K(z) by a simple function of z. If sufficient simplicity is achieved, solutions in the operational form can be found and the boundary conditions applied. When the co-ordinates are as shown in figure (i), solutions have been found with:

(i) $K = \text{constant}.$

(ii) $K = kz^{\alpha} \qquad 0 \leqslant z \leqslant H$

(iii) $K = k(H - z)^{\alpha} \qquad 0 \leqslant z \leqslant H$

and in two further cases. Generally it can be assumed that under such conditions as we are trying to represent, the eddy diffusivity would increase with height from zero at the ground to some maximum before falling away to zero again at the base of the stable layer. The following models, representative of this behaviour, have been solved

(iv) $K = kz(H - z) \qquad 0 \leqslant z \leqslant H$

(v) $K = kz \qquad 0 \leqslant z \leqslant \frac{1}{2}H$

$\quad = k(H - z) \qquad \frac{1}{2}H \leqslant z \leqslant H$

Since the source can be at any height, it is clear that solutions (ii) and (iii) are mathematically identical. Consequently only the solution of (iii) will be given in any detail. Details of the solutions of (i), (iii), are given in III and IV respectively, (iv) and (v) in V and the result only of (ii) in IV.

II. INTRODUCTION TO THE CONVECTION-DIFFUSION MODEL

The diffusion of the emittant is aided by the presence of free thermal convection. Prolonged heating of the ground by solar radiation results in very complex motion of the air in the adjacent layer. Precisely what this behaviour is, is still not fully understood, but very broadly the picture would seem to be this: in the lowest layer of the air (depth of the order of 100 ft.), the air is very unstable and mechanical turbulence, arising from the break down of the velocity shear and the surface roughness, together with forced convection, consisting of small irregular bubbles and jets of hot air rising from thermal sources at the ground, results in a random but quasi-continuous flux of heat away from the surface. The energy spectrum of this turbulence will have its largest components in the moderately high wave numbers.

Above this region is a more stable layer, perhaps several thousand feet thick, with nearly zero lapse conditions, in which there will be very little mechanical turbulence. The transitional zone between these two layers appears to be fairly thin and for some purposes might be considered to be a surface of discontinuity. As this inter-surface is unstable to large perturbations received from below, a succession of discrete bubbles will break away from the lower layer and rise through the quasi-adiabatic layer. In its ascent a bubble will entrain air from the surrounding atmosphere and will consequently grow in size and slow down. In consequence, the magnitude of the energy spectrum of the velocity perturbations in this upper layer is very small at the high frequency end, whereas the larger low frequency components will correspond to the motion resulting from the penetrative convection process. Recordings of temperature fluctuations (James 1953) confirm this. This picture is based on the work by Scorer (1954). It is also confirmed by Priestley's work (1955) in which he shows that for small negative values of the Richardson number (Ri) (i.e. near the ground, since (Ri) increases with height) the vertical flux of heat depends on the Richardson number and thus on the mechanical turbulence and forced convection, whereas for larger values of (Ri) (i.e. at larger heights) a relatively sharp transition takes place to the state in which the flux of heat is independent of Ri. This may be interpreted as flux by free convection. Similar confirmation comes from other workers.

The model presented in this paper is a first attempt to represent the main effects of the diffusion-convection processes on the dispersal of an emittant. In the future, it is hoped to improve the model so that it may be more consistent with the physical realities. In the present model, we are concerned with dispersal in a layer of finite depth; that is, the stability increases above the quasi-adiabatic layer so rapidly that no penetration occurs through the boundary. Also we shall neglect any effects due to the condensation of water vapour. Our model, which is designed to give statistical representation of the phenomena rather than to deal with the fine detail of the process, is then this: the dispersion may be separated into two distinct processes, firstly that of mechanical turbulence and forced convection which we shall assume can be represented by a coefficient of eddy diffusivity $K(z)$, (this will be large near the ground and will fall off to zero at the top of the layer), and secondly, that of free convection consisting of a succession of discrete bubbles typical of conditions at the ground rising to the top of the layer where they diffuse out mixing with the local atmosphere. The concept of discrete bubbles is not universally accepted as the complete representation of the free convection process although it has much support. However it is not essential to the model since this is to be a statistical approach, but on the other hand it is convenient to the description. As these bubbles rise they may slow down and they may grow laterally but it is to be assumed that no intermixing takes place between the bubbles and the surrounding atmosphere. This is clearly one of the points in which an improvement is to be sought in any future model. The convection process, in effect, amounts to a sink on the ground, $z = 0$ (to account for the disappearance of matter carried away by the bubbles) and an equivalent source at the top of the layer (to account for the appearance of this matter carried up to the inversion by the bubbles), together with a continuous subsidence throughout the layer to balance the effect of the transfer (air as well as the emittant is transfered). The effect is most pronounced when the source is at the ground or very close to it. We shall therefore put $h = 0$: the source at ground level. Then the source-centred plume will neither be as dense nor as deep as without convection, on account of the sink action on $z = 0$. At the top of the layer, the convected emittant which has been removed from the source-centred plume, will remain fairly concentrated at first; the diffusive effect will initially be small on account of the increase of stability as the stable layer is reached. However as the emittant subsides with the arrival of fresh bubbles, it is increasingly influenced by diffusion, it spreads out more rapidly and eventually recombines with the plume spreading up from the ground.

The nature of the eddy diffusivity coefficient has already been discussed. We shall take $K(z)$ to decrease linearly to zero $K = K_0\ (H - z)$ except that, in order to avoid mathematical difficulties arising from the unrealistic discontinuity in dK/dz at $z = H$ (the inter-surface), we shall assume that very near to this inter-surface, K departs from the linear law and goes smoothly to zero (i.e. dK/dz continuous across $z = H$) (see figure (ii)). Alternatively it may reasonably be supposed that the bubbles slightly overshoot the inter-surface due to their upward momentum and mix in a very thin layer just above the inter-surface. Mathematically, this produces the same result. This representation for $K(z)$ does not fully take into account the rapid change in turbulence across the transitional zone described above, but it seems to be otherwise satisfactory. The equation of dispersion, representing the expectation concentration of the emittant, is derived in VI and is

$$u_o \frac{\partial C}{\partial x} = K_o \frac{\partial}{\partial z} (H - z) \frac{\partial C}{\partial z} + \lambda \frac{\partial C}{\partial z} \qquad (1)$$

where λ is a measure of the flux of matter from the ground to the inter-surface by convection and is most easily defined as the average velocity of subsidence of the atmosphere needed to balance the sink-source action of the convection process. λ is, under the assumptions made above, constant with height, and when the convection is at all appreciable it will be of the order of 1 cm/sec. or more. For such values of λ, the comparison between the equivalent problems, one with convection, the other without, shows very markedly the effect of convection. In the solution the strength of the convection is represented by the parameter $\beta = \lambda/K_o$. Now if H is about $O(10^5)$ and K at the ground, enhanced by forced convection, is about $O(10^5)$, then $K_o = \frac{K}{H} = O(1)$ and thus β will also be $O(1)$. In fact the comparison is made for $\beta = \frac{1}{2}$, since this makes the computation particularly simple. The result is that the convection aids the diffusion process to such an extent that the emittant is, to all intents and purposes, uniformly distributed across the layer at a distance much less than half that in which uniformity is achieved without convection. This is clearly demonstrated in the corresponding figures (vii) and (viii).

This is indeed fortunate because a complete solution has not been obtained, only an asymptotic solution. But this approximation is so good that it holds throughout the whole region of interest, as these solutions confirm.

Two small corrections may be applied to the result if desired. In fact, if they were applied to figure (viii) very little difference would be observed at all; but for very small x they would be of importance. Firstly, the bubbles take a finite time to rise. Their terminal velocity v is presumably of the order of metres/sec. This means that the first term $\tilde{C}(x,z)$ (see VI), which represents the contribution from the convected emittant, should be 'displaced' that is, it should be replaced by a term $\tilde{C}\left(x - \frac{Hu_o}{v}, z\right) H\left(x - \frac{Hu_o}{v}\right)$. This displacement is $O(10^{-3})$ compared with X_c (the distance in which uniformity is achieved). Secondly any recording instrument measuring the concentration of the emittant will not only record the concentration due to the surrounding subsiding atmosphere, but also occasionally it will record values corresponding to bubbles which are rising past it. Near the source this may well be important. Now the statistical proportion of the atmosphere filled with bubbles is $\frac{\lambda}{v}$ of the whole and at any position (x,z) in the field, the bubbles passing the point will have originated from the ground at a position $x_o = x - \frac{u_o z}{v}$. Thus to correct for this effect we can add on an extra term $\frac{\lambda}{v} C_o \left(x - \frac{u_o z}{v}\right)$ where C_o is the ground level concentration (see figure (iii)).

III. DIFFUSION MODEL WITH CONSTANT DIFFUSIVITY

Consider case (i): $u = 1,\ K = 1,\ H = 1,\ h = 0 \qquad (2)$

obtained from the general case by making the transformation:

$$z \longrightarrow \bar{z}H, \quad x \longrightarrow \frac{\bar{x}u_oH}{K}, \qquad Q \longrightarrow u_oH\,\bar{Q}$$

Now drop the bars. The equation of diffusion is

$$\frac{\partial C}{\partial x} = \frac{\partial^2 C}{\partial z^2} \tag{3}$$

with boundary conditions $\dfrac{\partial C}{\partial z} = 0$ on $z = 1$

$$\int_0^1 C\,dz = Q \qquad \text{independent of } x. \tag{4}$$

In operational form (3) becomes

$$\frac{\partial^2 C}{\partial z^2} - pC = -\,pQ\,\delta(z) \tag{5}$$

the solution of which is

$$C = A(p)\,e^{\sqrt{p}z} + B(p)\,e^{-\sqrt{p}z} \tag{6}$$

where $A(p)$ and $B(p)$ are determined by (4):

$$B(p) = A(p)\,e^{2\sqrt{p}}$$

$$B(p) = A(p) + Q\sqrt{p}$$

$$\text{Thus } C(p,z) = \frac{Q\sqrt{p}}{e^{\sqrt{p}} - e^{-\sqrt{p}}}\left(e^{-\sqrt{p}(1-z)} + e^{+\sqrt{p}(1-z)} \right) \tag{7}$$

$$\text{i.e. } C(x,z) = \frac{Q}{2\pi i}\int_{C-i\infty}^{C+i\infty} \frac{\cosh\sqrt{p}(1-z)}{\sqrt{p}\,\sinh\sqrt{p}}\,e^{px}\,dp \tag{8}$$

This is an even function of $\sqrt{p}$. Therefore there are no branch points. The contributions come from the residues at the poles (i.e. the zeros of $\sqrt{p}\,\sinh\sqrt{p}$) These are at $p = -n^2\pi^2$ $(n = 1,2,3, \ldots\ldots\ldots)$ and at $p = 0$.

The residue at $p = 0$ is Q; at $-n^2\pi^2$ it is $2Q(-1)^n \cos n\pi(1-z)\,e^{-n^2\pi^2x}$

$$\text{Thus } C(x,z) = Q\left\{1 + 2\sum_{n=1}^{\infty} (-1)^n \cos n\pi(1-z)\,e^{-n^2\pi^2x}\right\} \tag{9}$$

valid for all x, z.
It is worth noting that this is very rapidly convergent except for very small x.

IV. DIFFUSION MODEL WITH $K = K_o\,(H - z)^{\alpha}$: ELEVATED LINE SOURCE

This example refers to case (iii) of the introduction. By obvious transformation of x and z, take

$u = 1$
$K = (H - z)^{\alpha}$
$h = 1.$

In operational form the diffusion equation is

$$\frac{\partial}{\partial z}\left\{(H - z)^{\alpha}\ \frac{\partial C}{\partial z}\right\} - pC = - pQ\ \delta(z-1) \qquad (10)$$

Put $H - z = t,\ n = \frac{1-\alpha}{2-\alpha}\ ,\ r = \frac{2}{2-\alpha}\ \sqrt{p}\,t^{1-\frac{\alpha}{2}}$ (11)

Then the solution of (10) is

$C_1 = A(p)\ r^n I_n\ (r) + D(p)\ r^n I_{-n}\ (r)$, in (1) (i.e. $0 \leqslant z \leqslant 1$) (12)

$C_2 = B(p)\ r^n I_{-n}\ (r)$, in (2): $1 \leqslant z \leqslant H$

(satisfying the boundary condition at $z = H$, $K\frac{\partial C}{\partial z} = 0$)

On $z = 0$; let $r = \rho$. Then since $K\frac{\partial C}{\partial z} = 0$ there, we have

$A\ I_{n-1}\ (\rho) = - D\ I_{1-n}\ (\rho)$ (13)

Also on $z = 1$ we have $C_1 = C_2$. Let $r = q$ on $z = 1$, then

$A\ I_n\ (q) + D\ I_{-n}\ (q) = B\ I_{-n}\ (q)$ (14)

Finally, we must apply the flux condition $Q = \int_0^H C\ dz$

$$Q = \frac{1}{p}\ \frac{(2-\alpha)^{1-2n}}{(2\sqrt{p})}\ \left\{\int_0^q B(p)\ r^{1-n} I_{-n}(r)\ dr + \right.$$

$$\left.\int_q^{\rho}\left\{A(p)\ r^{1-n}\ I_n(r) + D(p)\ r^{1-n}\ I_{-n}(r)\right\}dr\right\} \qquad (15)$$

which by (13), (14) and the Wronskian relationship reduces to

$$Q = \frac{1}{p}\ \frac{(2\sqrt{p})^n}{(2-\alpha)}\ \frac{A(p)}{I_{-n}(q)}\ \frac{2}{\pi q}\ \sin n\pi \qquad (16)$$

$$\therefore\ A(p) = -\frac{\pi}{2}\ Q\sqrt{p}\ \frac{(2\sqrt{p})^{1-n}}{(2-\alpha)}\ \operatorname{cosec} n\pi\ \ I_{-n}(q)$$

$$D(p) = \frac{\pi}{2}\ Q\ \operatorname{cosec} n\pi\ \frac{(2\sqrt{p})^{1-n}}{(2-\alpha)}\ \sqrt{p}\ I_{-n}(q)\ \frac{I_{n-1}(\rho)}{I_{1-n}(\rho)}$$

and $$B(p) = \frac{\pi}{2}\ Q\ \operatorname{cosec} n\pi\ \frac{(2\sqrt{p})^{1-n}}{(2-\alpha)}\sqrt{p}\ \left\{ I_{-n}(q)\ \frac{I_{n-1}(\rho)}{I_{1-n}(\rho)} - I_n(q)\right\} \qquad (17)$$

Consider $C_1 = A(p)\ r^n\ I_n(r) + D(p)\ r^n\ I_{-n}(r)$

The first term has no poles or branch points, and therefore has no contribution. The second term has no branch points but gives a contribution from the residues at the poles.

For both regions (1) and (2)

$$C = \frac{\pi}{2-\alpha} \; Q \operatorname{cosec} n\pi \; t^{\frac{1-\alpha}{2}} \; p \, I_{-n}(q) \, \frac{I_{n-1}(\rho)}{I_{1-n}(\rho)} \; I_{-n}(r) \tag{18}$$

At $p = 0$ the contribution is $\frac{Q}{H}$

If s_i are the roots of $J_{1-n}(s) = 0$ then (18) has poles at $p = -\, s_i^2/a^2$

where $a = \frac{2}{2-\alpha} \; H^{1-\frac{\alpha}{2}}$. The sum of the residues gives the result:

$$C = \frac{Q}{H} \left\{ 1 + \frac{2-\alpha}{2} \pi \operatorname{cosec} n\pi \frac{(H-z)^{\frac{1-\alpha}{2}}}{H^{1-\alpha}} \sum_{i=1}^{\infty} s_i \, \frac{J_{-n}(H^{\frac{\alpha-2}{2}} s_i) J_{n-1}(s_i) J_{-n}((\frac{t}{H})^{\frac{2-\alpha}{2}} s_i)}{J_{-n}(s_i)} \; e^{-s_i^2 x/a^2} \right\} \tag{19}$$

These solutions have been obtained by Rounds using Sutton's method. In the special case of $h = 0$, $H = 1$, $K = 1 - z$, equation (19) reduces to the following form:

$$C = Q \left\{ 1 + \sum_{i=1}^{\infty} \frac{J_0(s_i\sqrt{t})}{J_0(s_i)} \; e^{-s_i^2 x/4} \right\} \tag{20}$$

where s_i are the zeros of $J_1(s)$

This is the solution which will be used in the comparison in VII. The more general form than this when $h = 0$, $H = 1$, $K = (1 - z)^{\alpha}$ is

$$C = Q \left\{ 1 + (2-\alpha) t^{\frac{1-\alpha}{2}} \sum_{i=1}^{\infty} \frac{J_{-n}(s_i t^{1-\frac{\alpha}{2}})}{J_{-n}(s_i)} \; e^{-s_i^2 x/a^2} \right\} \tag{21}$$

where $a = \frac{2}{2-\alpha}$, s_i are the zeros of $J_{1-n}(s)$

The solution to problem (ii) of the introduction: $u = 1$, $K = z^{\alpha}$, $h = 0$, $H = 1$; can be deduced from (19).

$$\text{It is } C = Q \left\{ 1 + (n-1)! \; z^{\frac{1-\alpha}{2}} \sum_{i=1}^{\infty} s_i^{1-n} \; \frac{J_{n-1}(s_i) J_{-n}(z^{1-\frac{\alpha}{2}} s_i)}{J_{-n}(s_i)} \; e^{-s_1^2 x/a^2} \right\} \tag{22}$$

In the special case of $\alpha = 1$, $n = 0$ we obtain the solution by a limiting process This gives

$$C = Q \left\{ 1 - \frac{\pi}{2} \sum_{i=1}^{\infty} s_i \; \frac{Y_1(s_i) J_0(s_i\sqrt{z})}{J_0(s_i)} \; e^{-s_i^2 x/4} \right\} \tag{23}$$

All these series are rapidly convergent and the Bessel functions are tabulated for a selection of values of n in Watson's "Theory of Bessel Functions". The result (20) is shown graphically in the comparison (figure (vii)).

V. THREE-REGION DIFFUSION MODEL (CASE (v)) AND CASE (iv): $K = z(1 - z)$

This section deals with cases in which K is zero at both the ground ($z = 0$) and the upper surface.

Firstly, case (iv) of the introduction, with the source elevated at height h and

$$u = 1$$
$$K = z(1 - z) \tag{24}$$

For purposes of illustration we shall treat this problem using Sutton's approach, although it may equally be done using operational methods.

The equation of diffusion is

$$\frac{\partial C}{\partial x} = \frac{\partial}{\partial z}\left\{ z(1-z)\frac{\partial C}{\partial z} \right\} \tag{25}$$

Separate the variables. Put $C = X(x)\, Z(z)$

Then $X(x) = A\, e^{-\sigma x}$ (26)

where σ is some constant to be determined.

$Z(z)$ satisfied $\frac{\partial}{\partial z}\left\{z(1-z)\frac{\partial Z}{\partial z}\right\} + \sigma Z = 0$ (27)

Solutions satisfying the boundary conditions on $z = 0$ and $z = 1$ are obtained by putting $\sigma = n(n + 1)$ with n integer, when the solutions are Legendre Polynomials:

$$C = A(n)\, e^{-n(n+1)x}\, P_n(y) \qquad \text{when } y = 2z - 1 \tag{28}$$

Now on $x = 0$: $C = Q\,\delta(z-h)$ in delta function notation

$$\therefore \sum_{n=0}^{\infty} A(n)\, P_n(y) = Q\,\delta(z-h) \tag{29}$$

Multiply both sides by $P_m(y)$ and integrate with respect to y between $(-1, 1)$

$$\begin{aligned} \frac{2}{2m+1} A(m) &= \int_{-1}^{1} P_m(y)\, Q\, \delta(\tfrac{1}{2}(1+y)-h)\, dy \\ &= 2Q\, P_m(2h-1) \end{aligned} \tag{30}$$

Thus the solution is

$$C = Q \left\{ 1 + \sum_{n=1}^{\infty} (2n+1)\, P_n(2h-1)\, P_n(2z-1)\, e^{-n(n+1)x} \right\} \tag{31}$$

where the first few of the Legendre Polynomials are

$P_0(z) = 1$, $P_1(z) = z$, $P_2(z) = \frac{1}{2}(3z^2 - 1)$, $P_3(z) = \frac{1}{2}(5z^3 - 3z)$.

The second example, namely case (v) of the introduction is the three-region diffusion model. Transform the variables (as in IV) so that

$$
\begin{aligned}
u &= 1 \\
K &= z \text{ for } 0 \leqslant z \leqslant 1 \qquad \text{(region 1)} \\
&= 2 - z \text{ for } 1 \leqslant z \leqslant 2 \quad \text{(region 2)} \\
&= 0 \text{ for } z \leqslant 2 \\
&\text{(see figure (v))}
\end{aligned}
\tag{32}
$$

In the upper region put $2 - z = t$.

Then the solution in operation form, valid in this region, and satisfying the boundary conditions of zero flux at $z = 2$ is

$$C_2 = B(p)\, I_0(2\sqrt{pt}) \tag{33}$$

In the lower region the solution is

$$C_1 = E(p)\, I_0(2\sqrt{pz}) + D(p)\, K_0(2\sqrt{pz}) \tag{34}$$

The three unknown functions of p are determined from the boundary conditions

(a) $C_1 = C_2$ on $z = 1$

(b) $\dfrac{\partial C_1}{\partial z} = \dfrac{\partial C_2}{\partial z}$ on $z = 1$

(c) Flux condition $Q = \displaystyle\int_0^1 C_1\, dz + \int_0^1 C_2\, dt.$

By (c) we deduce $D = 2pQ$, and by the Wronskian relationship, (a) and (b) give

$$B = p\,\frac{Q}{2}\,\frac{1}{I_0(2\sqrt{p})I_1(2\sqrt{p})}\,, \qquad E = Qp\,\frac{K_1(2\sqrt{p})I_0(2\sqrt{p}) - K_0(2\sqrt{p})I_1(2\sqrt{p})}{I_0(2\sqrt{p})I_1(2\sqrt{p})}$$

Thus the solution in the upper region is

$$C_2(x,z) = \frac{1}{2\pi i}\int_{C-i\infty}^{C+i\infty} \frac{Q\, I_0(2\sqrt{pt})}{2\sqrt{p}\, I_0(2\sqrt{p})I_1(2\sqrt{p})}\, e^{px}\, dp \tag{35}$$

The integrand is an even function of $\sqrt{p}$ and therefore has no branch points. Its value comes from the residues at the zeros of $I_1(2\sqrt{p})$ and $I_0(2\sqrt{p})$. If s_i is a root of $J_1(s) = 0$ and r_i a root of $J_0(r) = 0$ then we obtain

$$C_2(x,z) = \frac{Q}{2}\left\{ 1 + \sum_{i=1}^{\infty} \frac{J_0(\sqrt{2-z}\, s_i)}{J_0^2(s_i)}\, e^{-s_i^2 x/4} - \sum_{i=1}^{\infty} \frac{J_0(\sqrt{2-z}\, r_i)}{J_1^2(r_i)}\, e^{-r_i^2 x/4} \right\} \tag{36}$$

In the lower region

$$C_1(p,z) = \frac{Q/\sqrt{p}\; I_0(2\sqrt{pz})}{2I_0(2\sqrt{p})I_1(2\sqrt{p})} - 2Qp\,\frac{K_0(2\sqrt{p})}{I_0(2\sqrt{p})}\, I_0(2\sqrt{pz}) + 2Qp\, K_0(2\sqrt{pz}) \tag{37}$$

The first term is identical to $C_2(p,z)$ and has the same interpretation. The interpretation of the other two terms is best obtained by a limiting process

$$p \left\{ - \frac{K_o(a\sqrt{p})}{I_o(a\sqrt{p})} I_o(b\sqrt{p}) + K_o(b\sqrt{p}) \right\}$$

$$= \lim_{n \to 0} \left\{ - \frac{K_n(a\sqrt{p})}{I_{-n}(a\sqrt{p})} I_{-n}(b\sqrt{p}) + K_n(b\sqrt{p}) \right\} p^{1-\frac{n}{2}}$$

$$= \lim_{n \to 0} p^{1-\frac{n}{2}} \frac{\pi}{2} \operatorname{cosec} n\pi \left\{ \frac{I_n(a\sqrt{p})}{I_{-n}(a\sqrt{p})} I_{-n}(b\sqrt{p}) - I_n(b\sqrt{p}) \right\} \qquad (38)$$

The second of these terms has neither branch points nor poles. The first term has poles, with residues

$$= \frac{\pi}{2} \operatorname{cosec} n\pi \, \frac{2}{a} \left(\frac{r_i}{a}\right)^{1-n} \frac{J_n(r_i) J_{-n}(\frac{b}{a} r_i)}{J_{1-n}(r_i)} e^{-r_i^2 x/a^2}$$

at $p = - r_i^2/a^2$ where r_i is the ith zero of $J_{-n}(r)$

As $n \longrightarrow 0$ we have $\operatorname{cosec} n\pi \; J_n(r_i) = Y_o(r_i)$

Hence the interpretation of equation (37) is

$$C_1(x_1 z) = \frac{Q}{2} \left\{ 1 + \sum_{i=1}^{\infty} \frac{J_o(\sqrt{z}\, s_i)}{J_o^2(s_i)} e^{-s_i^2 x/4} + \sum_{i=1}^{\infty} \left(\pi r_i \frac{Y_o(r_i)}{J_1(r_i)} J_o(\sqrt{z}\, r_i) - \frac{J_o(\sqrt{z}\, r_i)}{J_1^2(r_i)} \right) e^{-r_i^2 x/4} \right\} \qquad (39)$$

It is clear that $C_1 = C_2$ on $z = 1$, as indeed it must do, since $J_o(r_i) = 0$. The extension of this model to more general initial data seems to be extremely difficult, except possibly in a few cases, on account of the introduction of branch points into the operational solutions.

VI. DIFFUSION AIDED BY CONVECTION

The theoretical aspects of this model have been discussed in II. It remains to specify the boundary conditions more precisely and to solve the mathematical equations.

Firstly, we must consider the boundary condition at the top of the layer. Considering a small element ABCD (see figure (vi)) at the inter-surface, then, with assumptions made, the rate of change of concentration in the element is

$$\frac{\partial C}{\partial t} \, dx \, dz = 0 = u_o C(x) dz - u_o C(x + dx) dz + \lambda \, dz \, dx \, (C_o(x) - C(x))$$

where C (x) is the ground level concentration of which the bubbles are typical.

λ is the velocity of subsidence.

Hence $\quad u_o \dfrac{\partial C}{\partial x} = \lambda \left\{ C_o(x) - C(x) \right\}$ (40)

We are neglecting the refinements suggested in II. If required, the necessary alterations are easily made.

The equation of diffusion is

$$u_o \frac{\partial C}{\partial x} = K_o \frac{\partial}{\partial z} (H - z) \frac{\partial C}{\partial z} + \lambda \frac{\partial C}{\partial z} \qquad (41)$$

Put $z = H\bar{z}$, $1 - \bar{z} = t$, $\quad x = \dfrac{u_o H}{K_o} \bar{x}$, $\quad \dfrac{\lambda}{K_o} = \beta$ (42)

where $K_o = 0\ (1)$

Dropping the bar on $\bar{x}$ we obtain

$$\frac{\partial C}{\partial x} = \frac{\partial}{\partial t} \left(t \frac{\partial C}{\partial t}\right) - \beta \frac{\partial C}{\partial t} \qquad (43)$$

with boundary conditions

$$\frac{\partial C}{\partial x} = \beta H \left\{ C_o(x) - C(x) \right\} \quad \text{on } t = 0$$

$$\frac{Q}{u_o H} = \int_0^1 C \, dt \qquad (44)$$

Putting (43) into operational form, the solution is

$$C = A(p)\, r^{\beta} K_{\beta}(r) + B(p)\, r^{\beta} I_{\beta}(r) \qquad (45)$$

where $2\sqrt{pt} = r$

Applying the boundary conditions (44):

$$\text{On } r = 0: \quad A(p) \frac{\pi}{2} \frac{\operatorname{cosec} \beta\pi}{(-\beta)!} 2^{\beta} = \frac{\beta H}{p + \beta H} \left\{ A(p)\, (2\sqrt{p})^{\beta} K_{\beta}(2\sqrt{p}) + B(p)\, (2\sqrt{p})^{\beta} I_{\beta}(2\sqrt{p}) \right\} \qquad (46)$$

Now βH is a large quantity and except for very small x (large p) it will dominate the denominator on the right-hand side. When x is other than very small, the solution is of most interest: this will be represented by solutions (a). Solutions (b) and (c) refer to very small x and to the solution on r = 0 for all x, respectively.

The flux condition gives, for $x < 1$, large p:

$$\text{(a)}: \quad 2p \frac{Q}{u_o H} = \frac{\Lambda}{\beta H} \frac{\pi}{2} \operatorname{cosec} (1 + \beta)\pi \frac{2^{1+\beta}}{(-1-\beta)!} p^{-\frac{1}{4}+\frac{\beta}{2}} e^{2\sqrt{p}} B(p) +$$

$$B(p)\, (2\sqrt{p})^{1+\beta} \frac{e^{2\sqrt{p}}}{2\sqrt{\pi} p^{\frac{1}{4}}} \qquad (47)$$

where $\Lambda = \dfrac{\sin \beta\pi}{\pi^{3/2}} (-\beta)!\ \beta H$

and similarly for (b) and (c). Taking the second term, which is dominant, we obtain B(p). Substitution into (46) gives A(p).

B(p) is independent of whether case (a), (b) or (c) is being considered.

Thus

$$C(p_1 z) = 2^{1-\beta} \frac{Q}{u_o H} \sqrt{\pi}\, p^{\frac{3}{4}-\frac{\beta}{2}} e^{-2\sqrt{p}} r^{\beta} I_{\beta}(r) + \begin{cases} \dfrac{Q}{u_o H} \wedge \dfrac{\sqrt{\pi}}{\beta H}\, 2^{1-\beta}\, p^{\frac{1}{2}}\, r^{\beta} K_{\beta}(r) \; \ldots\ldots\ldots \; \text{(a)} \\[2ex] \dfrac{Q}{u_o H} \wedge 2^{1-\beta} \sqrt{\pi}\, p^{-\frac{1}{2}}\, r^{\beta} K_{\beta}(r) \; \ldots\ldots\ldots \; \text{(b)} \\[2ex] \dfrac{Q}{u_o H} \wedge 2\sqrt{\pi}\, \dfrac{p^{\frac{1}{2}}}{p+\beta H}\, \dfrac{\pi}{2} \dfrac{\operatorname{cosec} \beta\pi}{(-\beta)!} \; \ldots\ldots \; \text{(c)} \end{cases} \tag{48}$$

The first of these terms we denote by $\tilde{\tilde{C}}(p,z)$ and the second by $\tilde{C}(p,z)$. This solution is valid for moderately small x:

$$\tilde{\tilde{C}}(p,z) \simeq 2^{1-\beta} \frac{Q}{u_o H} \quad (2\sqrt{t})^{\beta}\; 2p\; K_{\beta}(2\sqrt{p})\; I_{\beta}(2\sqrt{t}\,\sqrt{p}) \qquad \text{since p is large.}$$

Putting 2 = b, $2\sqrt{t}$ = a the interpretation of $pK_{\beta}(2\sqrt{p})I_{\beta}(2\sqrt{pt})$ is

$$I = \frac{1}{2\pi i} \int_{C-i\infty}^{C+i\infty} I_{\beta}(a\sqrt{p})\, K_{\beta}(b\sqrt{p})\, e^{px}\, dp \tag{49}$$

Following the method of § 2, (Smith 1957) we obtain, by deforming the contour to a loop round the negative real axis,

$$\tilde{\tilde{C}}(x,z) = 2 \frac{Q}{u_o H} \frac{t^{\beta/2}}{x} e^{-\frac{1+t}{x}} I_{\beta}\left(\frac{2\sqrt{t}}{x}\right) \tag{50}$$

valid for all z and moderately small x.

$\tilde{\tilde{C}}(x,z)$ represents the concentration derived from the source-centred plume whereas $\tilde{C}(x,z)$ gives the concentration due to the emittant which has been convected to the top of the layer.

C(p,z) (a) and (b) can be interpreted using Goldstein's interpretation formulae for Bessel Functions. C(p,z) (c) with r = 0 is also a standard form given in "Tables of Integral Transforms": Bateman Manuscript Project, C.I.T.

The results can be summarized as follows:

$$\tilde{C}(x,z)\ \text{(c)} = 2\frac{Q}{u_o H} \wedge \frac{\sqrt{\pi}}{(-\beta)!}\ \frac{\pi}{2} \operatorname{cosec} \beta\pi \frac{1}{\beta H} f(\beta H x) \tag{51}$$

where $f(S^2) = \frac{2}{\pi} e^{S^2} \int_0^S e^{t^2}\, dt$, tabulated in Jahnke-Emde

$$\tilde{C}(x,z)\ \text{(b)} = \frac{Q}{\sqrt{\pi}\, u_o} x^{\frac{1}{2}} e^{-t/x} \left\{ {}_1F_1\left(\tfrac{3}{2}-\beta;\ 1-\beta; \tfrac{t}{x}\right) - \frac{(-\frac{1}{2})!\,(-\beta)!}{(\frac{1}{2}-\beta)!\ \beta!} \left(\frac{t}{x}\right)^{\beta}\ {}_1F_1\left(\tfrac{3}{2};\ 1+\beta; \tfrac{t}{x}\right) \right\} \tag{52}$$

valid for very small x.

$$\tilde{C}(x,z)\ (a) = \frac{Q}{u_o H(\beta-1)!}\ x^{-\frac{1}{2}}\ e^{t/x}\ U(\tfrac{1}{2}-\beta;\ 1-\beta;\ \tfrac{t}{x}) \tag{53}$$

It is equation (53) which is of primary importance, being valid over practically all the range of x and z in which we are interested.

The final solution is thus

$$C(x,z) = \tilde{C}(x,z) + \tilde{\tilde{C}}(x,z) \tag{54}$$

How effective and realistic these results are, is best shown by evaluating a specific example. The next section deals with a comparison between a diffusion model and a diffusion-convection model. It is seen that the picture provided by these formulae is consistent with what one would expect from the physical assumptions.

VII. EVALUATION AND COMPARISON

To determine the effect of convection on the diffusion process is most easily accomplished by comparing the results of the last section, with specific values of the parameter involved, with the results obtained by evaluating the corresponding simple-diffusion solution (20) of IV.

Inspection of these solutions shows that for purposes of comparison only one parameter has to be chosen. That is the convection parameter β. It has already been shown that β is of order one. Therefore, with an eye to simplifying the calculations as much as possible, we shall take $\beta = \frac{1}{2}$. This, as will be seen, gives results which bring out the effect of convection very clearly without swamping the natural diffusion processes.

Equation (54) becomes, with $\beta = \frac{1}{2}$,

$$\frac{u_o H}{Q} C = \frac{1}{\sqrt{\pi x}} \left\{ e^{-t/x} + e^{-\frac{1+t}{x}} \left\{ e^{\frac{2\sqrt{t}}{x}} - e^{-\frac{2\sqrt{t}}{x}} \right\} \right\} \tag{55}$$

Equation (20) becomes

$$\frac{u_o H}{Q} C = 1 + \sum_{i=1}^{\infty} \frac{J_o(s_i\sqrt{t})}{J_o(s_i)}\ e^{-s_i^2 x/4} \tag{56}$$

The results are shown graphically where they may best be compared. (See figures (vii) and (viii)). One important feature, which justifies the assumption, made in the previous section, about having x small, is that with convection, uniformity is achieved in under half the distance that is required without the convection.

ACKNOWLEDGEMENTS

Thanks are due to Dr. Scorer for a discussion and for his advice.

REFERENCES

Bateman Manuscript Project (C.I.T.)		Tables of Integral Transforms, McGraw-Hill Book Co.
James, D.G.	1953	Q.J.R. Met.Soc., 79, p.425.
Jeffreys, H. and Jeffreys, B.S.	1956	Methods of Mathematical Physics, p.612, Cambridge University Press.
Priestley, C.H.B.	1955	Q.J.R. Met.Soc., 81, p.139.
Rounds, W.	1955	Trans. Amer. Geophysical Union, Vol. 36, No. 2, p.395.
Scorer, R.S.	1954	Met. Mag., 83, p.202.
Smith, F.B.	1957	J. of Fluid Mechanics, Vol. 2, Pt.1, p.49.
Sutton, W.G.L.	1943	Proc. Roy. Soc., A.182, p.48.
Watson, G.N.		Theory of Bessel Functions, Cambridge University Press.

TABLE OF NOTATION *

C	expectation concentration (statistical mean).
h	height of source above ground.
H	height of inversion base.
$K(z)$	eddy diffusivity coefficient.
k, K_0	constant multipliers involved in $K(z)$, e.g. $K(z) = kz(H - z)$.
Q	flux of emittant.
u, u_0	constant velocity in x direction.
v	velocity of ascent of the bubbles.
x	distance downstream.
z	height above ground.
λ	velocity of subsidence of the environment.
$\beta = \frac{\lambda}{K_0}$	convection parameter; a measure of the respective importance of convection to diffusion.
$H(\xi) = 1$ if $\xi > 0$ $= 0$ if $\xi < 0$	Heaviside step function.
${}_1F_1(a; b; \xi)$, $U(a; b; \xi)$	confluent hypergeometric functions.
$I_n(\xi)$, $K_n(\xi)$, $J_n(\xi)$, $Y_n(\xi)$	Bessel functions.
$P_n(z)$	Legendre polynomials.

---

* Other notation used only in a limited part of the text is defined on introduction.

FIGURES

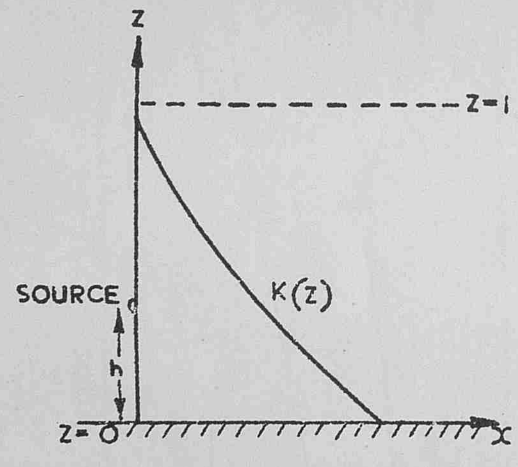
Z
Z=1
SOURCE
h
K(Z)
Z=0
x

FIGURE (i)
THE DIFFUSION MODEL

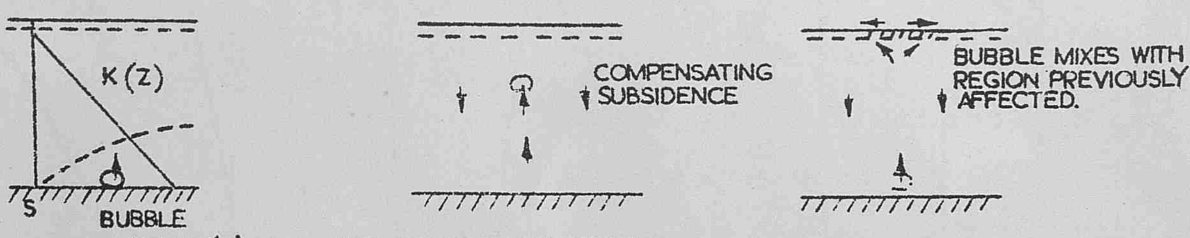
K(Z)
S
BUBBLE
COMPENSATING SUBSIDENCE
BUBBLE MIXES WITH REGION PREVIOUSLY AFFECTED.

FIGURE(ii) THE CONVECTION MODEL

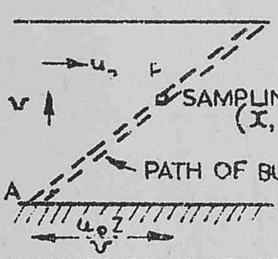
u₀
P
v
SAMPLING POINT (x, z)
PATH OF BUBBLE
A
u₀Z/v

FIGURE(iii) BUBBLES RISING FROM A ARE RECORDED IN THE 'CATCH' AT P

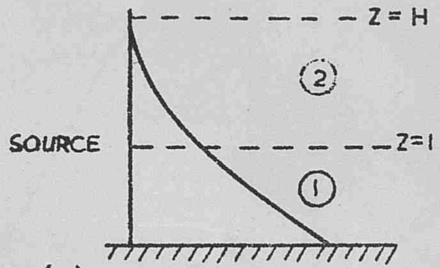
Z = H
②
SOURCE
Z=1
①

FIGURE(iv) REGIME FOR ELEVATED SOURCE WITH SIMPLE DIFFUSION

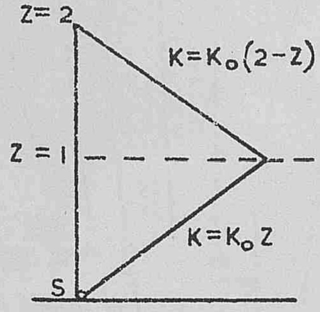
Z= 2
K=K₀(2-Z)
Z = 1
K=K₀ Z
S

FIGURE (v)
THE THREE-REGION DIFFUSION MODEL

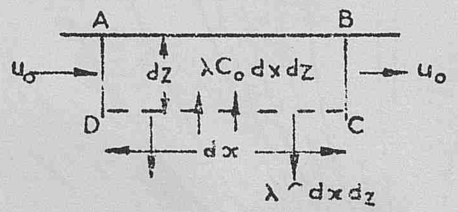
A
B
u₀
dz
λC₀ dx dz
u₀
D
C
dx
λ ⌢ dx dz

FIGURE (vi)
THE ELEMENT ABCD AT THE INTERSURFACE BETWEEN THE TURBULENT AND STABLE LAYERS.

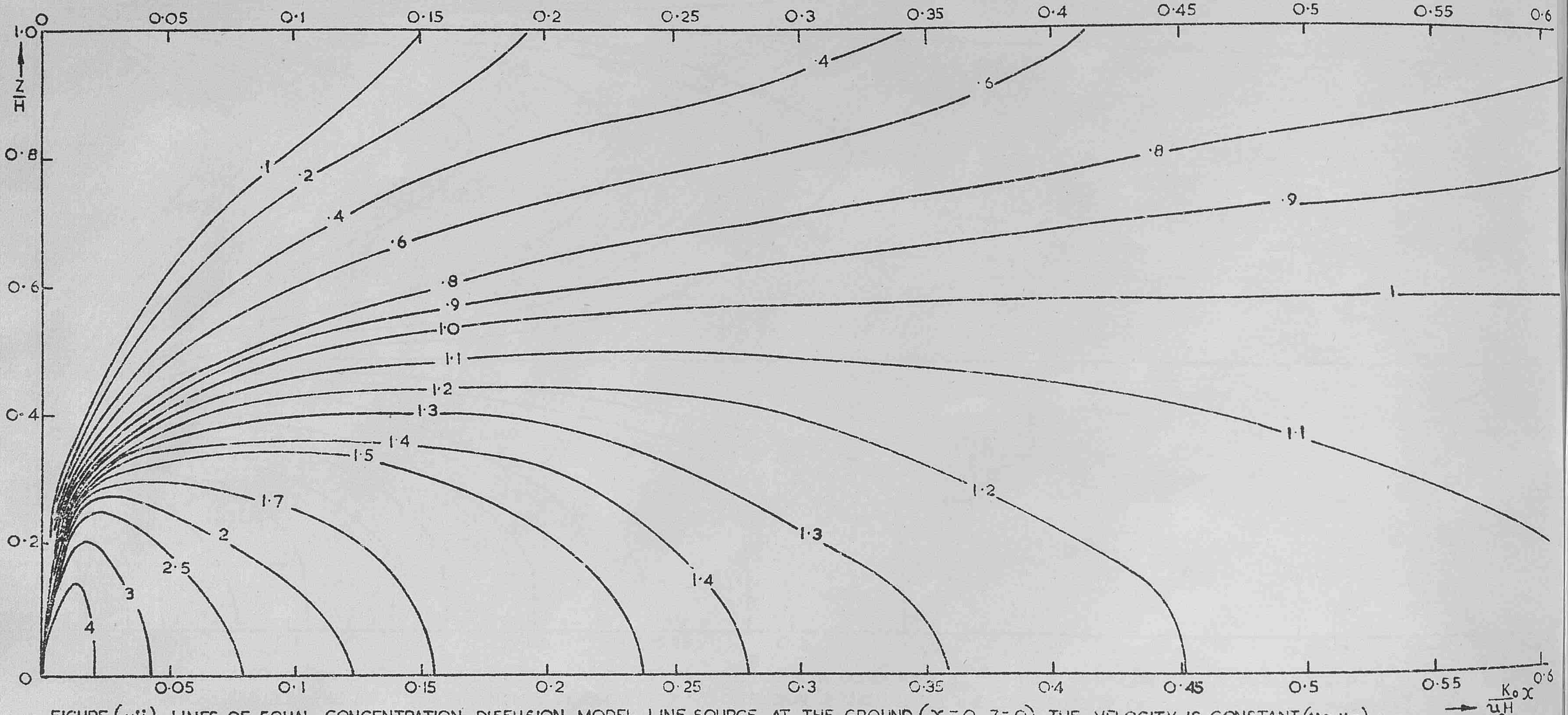

FIGURE (vII) LINES OF EQUAL CONCENTRATION. DIFFUSION MODEL, LINE SOURCE AT THE GROUND ($x = 0$, $Z = 0$). THE VELOCITY IS CONSTANT ($u = u_o$) AND THE EDDY DIFFUSIVITY COEFFICIENT DECREASES LINEARLY WITH HEIGHT $K = K_o(H - Z)$. CONCENTRATION IS PLOTTED AS MULTIPLES OF THE FINAL UNIFORM CONCENTRATION $\frac{Q}{u_o H}$

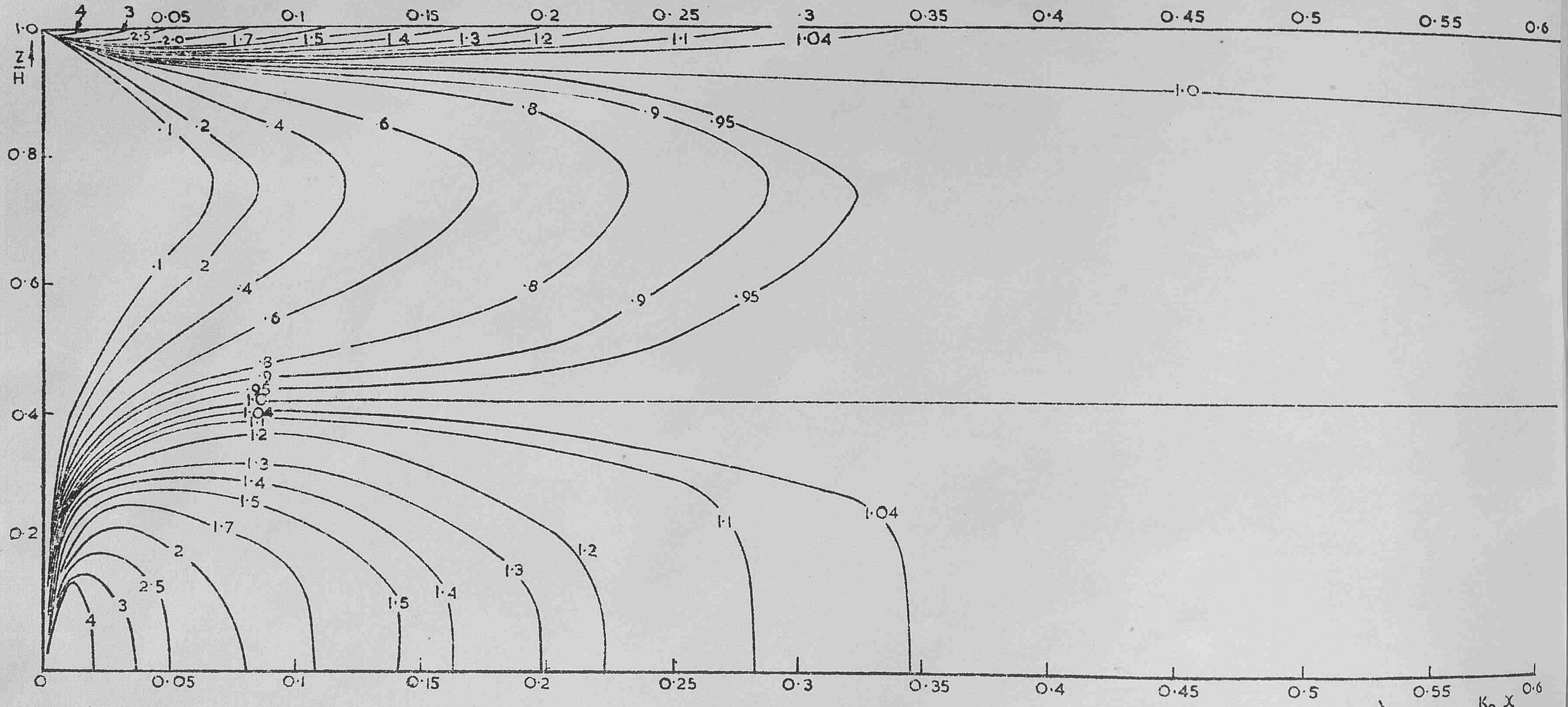

FIGURE(viii) LINES OF EQUAL CONCENTRATION. CONVECTION-AIDED DIFFUSION MODEL WITH CONDITIONS AS IN FIGURE(vii). CONVECTION PARAMETER $\beta = \frac{\lambda}{K_o}$ WHICH MEASURES THE RELATIVE IMPORTANCE OF CONVECTION TO DIFFUSION, IS TAKEN AS $\frac{1}{2}$ (λ IS THE VELOCITY OF COMPENSATING SUBSIDENCE).

THE CORRECTION TERM $\frac{\lambda}{v} C \left(x - \frac{uz}{v}\right)$, WHICH SHOULD BE INCLUDED IN THE SOLUTION SINCE A MEASURING INSTRUMENT WOULD PERIODICALLY BE TAKING SAMPLES FROM THE ASCENDING BUBBLES THEMSELVES, IS NOT INCLUDED IN THIS FIGURE. THIS IS BECAUSE NOT ONLY IN GENERAL WILL IT BE SMALL BUT ALSO IT DEPENDS ON A FURTHER PARAMETER v (THE VELOCITY OF ASCENT OF THE BUBBLE). THIS FIGURE, THEREFORE, GIVES THE MEAN CONCENTRATION OF THE ENVIRONMENT.

M.R.P. 1049
S.C. III/235
8th April, 1957

AD223144

Problems of surface air-flow and related phenomena in agriculture, horticulture and forestry

by

R. W. Gloyne

(Meteorological Office)

AIR MINISTRY

METEOROLOGICAL RESEARCH COMMITTEE

been published. Any author desiring to
quote this paper should refer to it as "A
paper of the Meteorological Research
Committee (London),
M.R.P. No. 1049 by Mr. R.W. Gloyne
A copy is available in the Library of
the Meteorological Office."

M.R.P. 1049
S.C. III/235
8th April, 1957

AIR MINISTRY

METEOROLOGICAL RESEARCH COMMITTEE

Problems of surface air-flow and related phenomena in agriculture, horticulture and forestry

by

R.W. Gloyne (Meteorological Office)

1. Introduction

The aim of this paper is first, to survey some eight years' experience in providing information on surface air-flow and related phenomena to workers in agriculture, horticulture and forestry, and second to set out for consideration suggestions as to future work on the problems. As may be anticipated, the particular needs of the inquirers have imposed a form and content upon the advice given, not necessarily the same as would have been adopted had the problems been viewed in purely meteorological terms. It is perhaps pertinent to emphasise that in spite of inadequate knowledge and data, we are increasingly pressed by many authorities to make some contribution towards the solution of certain problems, e.g., those which arise from the apparently conflicting claims of forestry and agriculture for extensive areas of hilly country, particularly in Scotland and Wales. The economic importance of the problem may be judged from the fact that some £25 million has been set aside under the Hill Farming (1946) and Livestock Rearing (1951) Acts, to meet 50 per cent of the cost to the farmer of a comprehensive scheme for improvement - in which the provision of shelter-belts may be included. The Forestry Commission will also grant up to £17 per acre for the planting of small areas (not less than two acres). In addition it was recommended by the Committee on Hedgerow and Farm Timber (1955) that grants should be available for approved schemes not covered by the above provision, whilst the recent Crofting Commission urged the extension of afforestation near townships - although their motive was not directly one of climatic amelioration. The value of wind-protection for horticultural crops is now being assessed (see 2a), and this promises to be substantial.

In Section 2 the various problems are set out and analysed with notes on work on hand and progress made. Section 3 deals with some of the ideas and data which have been used to clarify and partially to solve the various questions posed, and in Section 4 suggestions on future work are offered for consideration.

2. Statement and classification of problems: account of work completed or in progress

(a) Horticulture: glasshouses; farm buildings

(i) What is the distribution of wind at a given place up to the height of the building with respect to speed, direction and season: sub-classified according to temperature, precipitation and humidity, etc.?

To what extent would a wind-break of given type reduce the wind speed from some particular direction to below some stated limit? Alternatively, what type of wind-break would be required to effect a given speed reduction?

What consequential effects as a result of shading would there be on received radiation, on humidity, on dew deposition. What effect will there be on temperature especially with regard to the risk of frost?

/(ii)

G.17407/JIJ/4/57/50.

(ii) Given that a certain reduction in wind speed is desirable to reduce heat loss from a glasshouse at some particular time of year, what design of wind-break would be selected, bearing in mind the need not to intercept low altitude winter and spring sunshine?

What effects, if any, will such a wind-break have upon the ventilation of such a structure?

(iii) What information is there on the frequency and seasonal incidence of winds considered sufficient to cause damage to low glass structures?

In view of a given degree of danger, what measures might be taken to reduce the damage, e.g., by screening, by more secure anchorage, etc.?

The extensive literature on interrupted flow on this scale has been summarised, e.g., Gloyne (1955) and the data and concepts so assimilated as to permit an approximate answer to be given to questions posed. Complete answers are handicapped by inadequacies in the network of reporting stations of various categories in some areas of horticultural importance, e.g., as in Mid and Upper Clyde Valley, Strathmore, E. Lothian in Scotland; much of Somerset amongst other west and midland areas in England, and the potentially important areas in the west coast of the British Isles (of which many in Wales have been recently surveyed by the Agricultural Land Service of the Ministry of Agriculture, Fisheries and Food). There is also a relative lack of analysed and consolidated data on wind, and little on wind in association with other elements - the adoption of machine processing now envisaged should help materially in this respect.

Lack of knowledge of the effect of topography on air-flow handicaps progress in all fields of agricultural application, but possibly least so in horticulture.

It is not yet possible to advise confidently on the major decision as to whether additional shelter would be beneficial in any given instance. The main unsolved problems concern the best design and layout of shelter units for a particular case in the light of the cropping programme and the management policy, the economics of shelter in relation to the seasonal wind risk, the higher yield and the better and earlier produce frequently associated with the successful use of shelter. Field investigations on these topics have been carried out for three seasons jointly by the Senior Meteorological Officer at Bristol and four of the Experimental Horticultural Stations of the M.A.F.F. Provisional results for 1953-55 are now available and those for the whole series are being consolidated.

There is still much to be learnt regarding the effect of wind-breaks upon the ventilation of protected structures but this is mainly the responsibility of engineers. Extensive wind-tunnel work has brought out the main features of the problem, but the transition to full-scale phenomena with an air-flow fluctuating in speed and direction introduces new and only partially solved complications.

(b) Forestry

(i) Given a tract of country:

What are the wind hazards to forestry? What are the probabilities of an "exceptional" gale from a given direction occurring in n years?

What is the effect of topography in such gales?

(ii) How may we describe quantitatively the "climate" in those areas known to be unsuitable for trees of a given species; further how may this quantitative description be employed to identify such areas and be used in framing future policy?

(iii) What is known of the climate in the vicinity of the forest margin?

Gales such as that of January, 1951 lend urgency to questions as posed in (i). Gale damage is reported on a minor scale every year, but major "blows" force attention to questions of policy. The forester's interest is two-fold: he wishes to assess the "calculated" risk of planting up a certain area; and secondly wishes to plan the layout of his plantation - tree species, location of roadways etc. - so as to reduce, or confine, the liability to subsequent gale damage. There are two basic requirements, first an adequate network of meteorological stations and secondly an appropriate statistical analysis of the data (not, of course, a purely meteorological responsibility). Shellard, H.C. (1956) is a valuable first step.

The quantitative description of climate - usually that of remote areas - required by (ii) suffers both from lack of data, and of appropriate methods of analysis. Some progress is being made by examining a few case histories but one of the most promising approaches appears to be on ecological lines. The general question of excessive "exposure" is certainly not a matter of wind alone precipitation and temperature are involved and it is possible that more attention should be paid to the dry intervals between successive rains or periods of high humidity but firm criteria have yet to be devised. However advances might be hoped for as data accumulate on the rate of "tattering" (i.e., of deterioration) of flags of standard size and material now being collected at a large number of Forestry Commission Sites. So far the data collected and any appropriate wind records as are available are not inconsistent.

Question (iii) above is practically the same, meteorologically speaking, when considering air-flow in its agricultural context. A reasonably coherent picture of some aspects of the climate of the forest margin is now emerging due mainly to recent work in Germany, Switzerland and to a small degree in the U.K. The extensive work originating from U.S.A. and the U.S.S.R. is not directly relevant to conditions in the British Isles. The question of the definition, in simple geometrical terms, of the total obstruction due to a given assemblage of trees has yet to be solved, although it is being tackled.

(c) Agriculture

The problems arising in arable areas have strong affinities with those dealt with in horticulture, those in livestock areas with forestry.

(i) What climatic hazards are there to agricultural enterprises (especially to livestock farming) in a particular area?

(ii) What will be the effect of a given disposition of obstacles - natural topographical features, boulders, forest plantations of more or less irregular geometrical outline, narrow belts - in reducing the damage due to wind, either alone or in association with other meteorological elements?

The importance of shelter on any particular property will vary with the extent of the vulnerability of farm stock and farm operations to wind and weather "stress". Obviously then little can be done in meteorological terms alone in relation to a particular problem until some criteria are forthcoming from the agriculturalists: progress can however be reported.

More generally, and for application in fields other than agriculture etc., there is an acute need for more knowledge, suitably codified and presented, on the character of air-flow:

(α) over hilly, much dissected, countryside - the problem of "canalisation" arises here;

(β) over horizontal surfaces with roughness elements of various types (crops, trees, rocks, houses, hedges, etc.) disposed in various patterns;

(γ) over terrain such as indicated in (α) with the addition of irregularly spaced trees or blocks of trees, rocks and boulders.

In its general form, the problem may well be insoluble; what might however be reasonably sought for are some empirical solutions for certain typical, but idealised, cases in those weather situations where wind is believed to constitute a limiting factor to agricultural protection. "In toto" a considerable amount of work has been done especially on (β) but the data need further reduction and analysis and more appropriate methods of presentation before results can be directly applied to agricultural needs.

(d) Phenomena involving air-borne material (including snow)

The questions come from three main groups of workers; viz., plant pathologists, entomologists and to some extent veterinary surgeons, on the dispersal and interception of spores and pollens, insects and smokes, gases and dusts from definite sources; horticultural engineers on the drift of spray particles; agriculturalists, road engineers and others on snow deposition and drifting.

Questions take the form:-

(i) What is the risk of smoke or dust deposit at a given place, due to the presence of a source at a given distance and bearing: alternatively, could a given case of damage by pollution be due to any particular source?

(ii) How far from an infected plant(s) will the concentration of disease spores fall below a stated limit: what, if anything, can be done to intercept or filter out possible disease-bearing material?

(iii) How will the natural air-flow interfere with the distribution of spray droplets or dust particles of a given size?

(iv) What information is there on wind speed and gustiness within an orchard, and how may these elements be measured?

(v) What is known relative to the interception of wind-borne material by obstacles, leaf surfaces, twigs?

(vi) What is the frequency of snow-falls in association with winds of particular strengths and directions at any given place at stated times of the year?

Recent work on turbulent diffusion and on the collection and interception of particles is sufficient to give, at any rate, a provisional answer to questions such as (i) to (iv), providing the information is expressed in an appropriate form. Inability to certify whether or not a given source was responsible for a given deposit stems mainly from insufficient information on wind distribution at the time, i.e., from data on "local" climate.

Regarding the control of snow drifts, a good deal of knowledge is well-known to both the Meteorological Office and civil engineers. The inability to utilise this knowledge for carrying out the protection of roads etc. again lies in lack of sufficient knowledge of the incidence and intensity of snow-fall and the associated wind distribution occurring in the (often remote) hilly areas where the need for economical preventative measures is most pressing.

(e) General comment

As will be apparent from the phraseology adopted in setting out the type of inquiry posed, problems under (a) and (d) are much more clearly formulated than those under (b) and (c). In respect of the former considerable progress has been made notably by civil engineers: the contribution from the Meteorological Office has varied widely from case to case, but it is not unreasonable to suppose that this contribution will gradually decrease with time.

The situation is very different in regard to (b) and (c), and cases have arisen in which even the initial working criteria have been suggested by the meteorologist.

In broad terms the "field" of wind is required:

(i) on a regional scale;

(ii) on a medium, e.g., county, scale, down to that involving identifiable topographical units such as a range of hills;

(iii) on a local scale, e.g., the estate or farm.

It is required to identify, define and measure the role of topography; of general surface roughness due to boulders etc.; and of specific features which admit of geometrical definition - such as belts of trees and hedges.

In many cases it is not wind alone which needs to be considered (gale damage to forests is an important exception), but a complex of meteorological factors which, as far as possible, should be expressed in a few empirical relationships. From the investigational point of view the distinction mentioned above is important: air-flow can be studied with hope of success in the wind-tunnel, but the effect of a complex of obstructions on climate as a whole requires field work.

3. Notes on the sources and types of relevant information

(a) Basic climatological data. The most immediately useful tools for general advice have been:

(i) maps of mean wind speed as given in the Climatological Atlas and other material in the Meteorological Office (M.O.3) supplemented by

(ii) results of wind surveys carried out by the Electrical Research Association, and their experiences in attempting to find suitable sites for wind-engines;

(iii) the increasing amount of data on "run-of-wind" at 2m. now coming to hand (mainly from Crop Weather Stations).

(b) Ecological data. An independent source of information stems from broad ecological criteria.

(i) Certain species of trees grown in windy spots exhibit distortion or "flagging", the crown being cut back to windward, but extended down-wind.

(ii) Low vegetation such as heather will assume a similar profile whilst the gradual decrease in the height and girth of trees, bushes, enclosed pastures and houses with increase of elevation and nearness to the sea is also broadly associated with increasing "exposure" - but probably not to wind alone. Botanically, the phenomena are considered as the variation in the position of the "moorland edge".

(iii) In recent years a third approach has been explored by the Forestry Commission, viz., "the tattering of flags" mentioned earlier under 2(b).

(iv) Evidence of "exposure" is also implicit in many farming practices, in the layout of buildings, the size and disposition of fields and hedges. Obviously such evidence must be treated with the greatest reserve, but there can be no doubt that, e.g., the very small fields in the Scilly Islands, and the high hedges of Devonshire are a consequence of coming to terms with the climate.

/(v)

(v) Semi-quantitative work has been done in Japan whereby the air-flow in selected hilly areas has been plotted by reference to the asymmetry of plant growth. The prevailing wind at different seasons could be plotted by examining the shape of different plants which were wind-sensitive at different seasons of the year.

A distinction which is of importance is between the prevailing wind and that which has been termed the "dominant" wind. On the north-east coast of England for example we find trees "flagging" towards the west: presumably therefore:-

either when the trees are particularly wind-sensitive the prevailing direction is easterly;

or only the easterly winds are associated with other factors which lead to a depression in growth.

An analogous case arises with young livestock, especially sheep, for when these are most vulnerable to "wind stress" the wind is frequently from the east and associated with a low temperature.

(vi) Evidence of the canalisation of wind can be derived from these ecological observations. A study of the distribution of the extensive damage to forests in Scotland in the north-westerly gale of January 31st, 1953 provides some pointers.

(vii) Observational studies on the grazing behaviour, posture etc. of farm livestock are being made in increasing numbers. When analysed in association with parallel weather records it is anticipated that certain broad associations will become evident relating behaviour etc. and subsequent productivity to climatic "stress".

Experience suggests that whenever the mean annual wind speed is 15 m.p.h. or more at 10 metres, as given by climatological maps, phenomena mentioned in (b)(i) are evident and that when favoured by topography similar phenomena will be found in the areas experiencing a mean speed of 10-15 m.p.h.: indeed cases are coming to hand of obvious "wind stress" inland where the general speed is less than 10 m.p.h.

The "run-of-wind" data at 2m. now available from Experimental Establishments of the M.A.F.F. are in general confirming earlier judgments of the wind hazard arrived at before the instruments were installed: the exceptions are mainly cases where relatively high rates of flow have been recorded at sites where this was not expected from climatological maps and where sufficient ecological evidence did not exist.

(c) "Canalisation"

For guidance on the presence or not of this phenomenon attention is paid to:-

(i) ecological evidence as mentioned in 3(b);

(ii) evidence implicit in the "wind roses" when available;

(iii) some findings noted in sections 3(d) below.

It has been difficult to codify observations on "canalisation" - it apparently may not occur in situations where topography leads us to suppose otherwise and contrariwise. There is, for example, clear evidence of the deflection and concentration of flow in a shallow east-west valley at Long Ashton, near Bristol, yet there are unexpectedly few observations of strong north-westerly winds, from a station at the south-east end of the deep, well-defined valley of Loch Maree in Wester Ross. It appears that "canalisation" may be an attribute of open undulating country rather than of highly dissected country with narrow, boulder strewn, or partially forested valleys - although striking cases (as judged by gale damage to forests in 1953) have occurred in such conditions.

/(d)

(d) "Break-away" of flow

Whether or not, and if so in what circumstances, flow ceases to follow the ground contours is necessary information.

Here we have been guided mainly by:-

(i) wind-tunnel studies;

(ii) the results from small scale field experiments;

(iii) field observations - mainly arising from studies in the control of snow drifting;

(iv) information from large scale field studies carried out by the Electrical Research Association and similar bodies.

Wind-tunnel work (e.g., Irminger and Noddentved (1936), Serra, L. (1951)) supplemented by small scale tests in the open (e.g., Pugh, H.Ll. (1950)) have indicated the factors likely to be of importance. The information, linked to field work on the larger scale (e.g., Pugh, H.Ll. (1950), Seligman (1936)) and taken in conjunction with evidence of the type given by Scrase (1930, page 7), on the lack of an effect on gustiness due to a smoothly contoured ridge about 30H upwind (H = height of ridge), allows the construction of a coherent picture.

It seems that "break-away" does not occur so readily in Nature as might be gleaned from wind-tunnel tests where "similarity" is judged in terms of the Reynolds number. This finding - supported by Scorer's theoretical work (Scorer (1953)) - has been further confirmed by the tank tests carried out by the Electrical Research Association (1951). Field observations, e.g., the deposition patterns of snow in railway cuttings (Anon. (1950)) and of airborne insects (Slater (1945)) and related evidence Idrac, P. (1923)), add confirmation to a rough generalisation that in circumstances of practical importance the boundary layer does not break away from windward slopes of less than 1 in 2 nor from lee slopes less than 1 in 5.

The fact that thermal stability and the speed of the "free" wind must be taken into account in the general case is rendered a little less troublesome in practice, as we are particularly concerned with wind speeds greater than 10 m.p.h. generally associated with an adiabatic lapse rate in the lowest few hundred feet.

(e) Topographic parameters

Concepts relating to up-wind ruggedness, such as "relief intensity" and "effective distance", are frequently associated with reductions in wind speed. Both these ideas are expressible in a numerical form, although whether in a relevant form remains to be seen (Conrad (1946, p. 171), Thomas, D. (1957)).

(f) Single cross-wind barriers

A great deal is known of the effect of a barrier of simple geometrical design on a normally incident wind, but there are serious gaps in our knowledge of what happens when the wind fluctuates widely in direction and when it approaches the barrier obliquely.

Furthermore conflicting accounts are given of the effect of a barrier with considerable thickness, i.e., down-wind dimension.

(g) Multiple obstructions; macro-roughness

Although there appears no evidence that a succession of widely spaced barriers (i.e., at distances apart of 25-30H or more) exert a cumulative effect on wind speed as measured and assessed by the customary techniques, it is incontestable that the totality of roughness elements on a tract of country will exert a drag on the flow which will increase up to a point, as the number of roughness elements increase.

The effect of this "macro-roughness" may be expressible by empirical rules giving the relationship of the surface flow over land, sea, islands etc. and the geostrophic speed (Carruthers (1943) quoting Brooks; Shaw (1931)).

There can be no doubt that if land is progressively denuded of natural features such as trees, hedges, woods etc. there comes a point when the lack of "roughness" results in a reduction in the productivity of the area and where some sort of shelter must be re-established if the area is to be successfully rehabilitated.

In certain circumstances wind erosion of soil (a "saltation" process rather than a strictly aereal one) can commence at "blowing foci" and increase unchecked to disastrous proportions if the soil surface is left bare and uninterrupted.

It is difficult to map this "roughness" in meteorological terms, but relevant information is given by:-

(i) wind profiles over various types of terrain, including built-up areas (made in, and on the margin of, such areas);

(ii) estimates of the shearing stress or of C_D (the coefficient of resistance) of isolated obstacles, of different surfaces etc.;

(iii) the variation of wind direction with height and the approach to the geostrophic wind (Ekman spiral).

Important recent work has been carried out in Denmark by M. Jensen (1954) who attempted to express the changes in wind speed which took place when a given incident wind passed simultaneously over two nearby tracts of country - one bare of natural obstructions and the other carrying a relatively dense assemblage of trees, hedges, etc.

To date the information above has been used more as "background" material than as a precise guide, but it is hoped to try and consolidate these ideas into an appropriate form.

(h) Irregular obstructions

The effect on air-flow of a block of trees, of a copse (often found in association with topographical irregularities) cannot yet be expressed in any quantitative fashion and little in the way of advice has been possible.

As such obstructions are the rule rather than the exception in those parts of the country where the problem of shelter occurs most acutely, it is obvious that urgent attempts must be made to devise suitable parameters.

(i) The zone of influence of a shelter system

In principle the definition of zone of influence in terms of wind speed, or percentage reduction of wind speed, sub-divided if necessary into seasons and direction, would appear tractable. In practice however such a division may have limited relevance to a particular shelter problem: for in actual cases we are usually concerned with a complex of events in relation to a more or less vulnerable object. Thus we require preliminary information on the susceptibility of the object to be protected before much progress can be made; work is proceeding on this.

/4.

4. Programme of Investigations

(N.B. Those investigations, related to the several problems, in the current Meteorological Research Programme (M.R.P. 1034A) are noted in brackets.

It is recognised that, in essence, some of the information sought already exists, although widely scattered throughout the literature. A systematic re-analysis and re-appraisal of existing data will almost certainly lead to many results sufficiently accurate for present needs, but it is equally certain that a number of important gaps in our knowledge requiring both theoretical and practical study will be revealed.)

(a) The general field of wind over the British Isles

(i) The representativeness and reliability of existing data

Study of records from, and siting of, existing P.T. anemometers to assess the significance of the data in the light of any peculiarities of the site. (Items I.3.(a); II.4.(d); M.R.P. 989.)

(ii) Adequacy of the present anemometric network

Although the fundamental network is under constant review, the need for a supplementary one, using a form of integrating anemometer, would seem to require further consideration.

(iii) Statistical investigations of the general wind-field

The current (March, 1957) programme of M.O.3 appears to cover most requirements, providing studies of directional distribution and of sequences receive sufficient attention.

(b) Topographical influences on air-flow

(i) Gross effect of mountains and hill ranges on flow

The forestry/agricultural interest in work on this current PX problem might well be covered if due attention were paid to:

(α) the expression of results in terms of the geometry of the area;

(β) the use of parameters such as the standard vector distribution of winds (e.g., see G.M. No. 85, p. 21 on the relative values of this quantity over the sea and over mountainous country);

(γ) the interpretation of wind-tunnel studies, bearing in mind that immediate needs would largely be met by good qualitative agreement between tunnel and field patterns of flow.

(ii) Effect of particular topographic features on air-flow

Study by surveys, field work and possibly models of the effect on flow of obstructions recognisable on the scale of miles or tens of miles. Emphasis initially upon the interpolation "in the horizontal" and upon "canalisation".

(α) Preliminary analysis of records from sites known to be influenced by a definable topographic feature: provisional classification of sites according to degree of obstruction to wind (as revealed by characteristics of the record).

(β) Field work at selected sites. Basic instrumental requirement: either continuous recording of wind speed and direction, or "run-of-wind" according to direction (8 points). A measure of "gustiness" may become necessary later (Items III.1.(b)(c); III.3.(b)(d)(f)(g)(h): also Gold, 1936.)

Sites and some observational assistance may be reasonably expected from interested authorities (Forestry Commission, Nature Conservancy, Hill Farming Research Organization and Universities of Durham, Edinburgh, Wales).

(γ) Surveys of selected areas using either or both of short period runs of meteorological observations and any biological criteria which may emerge.

(δ) Study, by models, is envisaged on the lines of the apparently successful methods adopted by the German Meteorological Service centered at Geissen.

(c) Effect on air-flow of specific types of roughness elements

(i) It is required to establish the broad features of the disturbance to flow by built-up areas, woods on horizontal terrain, scrubland, orchards and parkland (Jensen (1954), Carruthers (1943, p. 289); item III.3.).

(ii) On simple two-dimensional obstructions (tree belts, fences, hedges) relevant work at the Experimental Horticultural Stations (2a) and by Department of Forestry, University of Edinburgh, is reasonably adequate providing the study includes the effect of barriers on winds oblique to them.

(d) Investigations relating to the definition, measurement and distribution in space and time of "exposure"

(N.B. In the final analysis "exposure" is intelligible only in relation to the effect of various meteorological elements and combination of elements upon some body which is responsive to those elements.) Work with a high degree of priority is proceeding (Universities of Wales, Durham, Oxford) with regard to plants and animals.

In the meantime enough is known of certain of the parameters to justify limited effort on the physical aspects.)

(i) Specification of the geometry of an area with respect to "exposure"

In progress at the University of Wales. Topic is related to one being considered by W.M.O. Working Party (W.M.O. No. 48, Rc. 10. 2.2.2.2. on "Station Network").

(ii) Development of field techniques for assessing "exposure" as variously defined.

/References

References

Anon, 1950 Snow Fences - placing them to get maximum protection. Rly. Engng. Maint. Chicago, 46, p. 1132.

Carruthers, N. 1943 Quart. Jour. Roy. Met. Soc., London, Vol. 69, No. 302, p. 289.

Conrad, V. 1946 Methods in Climatology. Camb. (Mass).

Elec. Res. Ass. 1951 O.E.E.C. Wind Power Group. Rep. of Meetings, p. 105.

Gloyne, R.W. 1955 Meteorological Magazine, London, Vol. 84, p. 272.

Gold, E. 1936 Quart. Jour. Roy. Met. Soc., London, Vol. 62, No. 264, p. 186.

Idrac, P. 1923 Mémor Off. nat. mét. Fr. Paris, No. 7.

Irminger, J.O.V. and Noddentved, C. 1936 Ingen Vidensk. Skr., Copenhagen, Ser. A, No. 42.

Jensen, M. 1954 Shelter Effect. Danish Tech. Press, Copenhagen.

Pugh, H.Ll. 1950 Road Res. Tech. Paper, No. 19, London.

Seligman, G. 1936 Snow Structure and Skifields, London.

Serra, L. 1951 O.E.E.C. Wind Power Group. Rep. of Meetings, p.101.

Scorer, R.S. 1953 Met. Mag., Vol. 82, p. 23.

Scrase, F.J. 1930 Geophys. Mem., No. 52.

Shellard, H.C. 1956 Climat. Branch Memo., No. 6.

Slater, A.E. 1945 Quart. Jour. Roy. Met. Soc., Vol. 71, p. 223.

Thomas, D. 1957 Private Communication.

M.R.P. 1050
S.C.111/236
9th April, 1957

27 MAR RECD
27 MAR 1958

Recent developments in the measurement of precipitation elements from aircraft

by

M. P. Garrod

(Meteorological Office)

AIR MINISTRY

METEOROLOGICAL RESEARCH COMMITTEE

At the time of issue this report has not been published. Any author desiring to quote this paper should refer to it as "A paper of the Meteorological Research Committee (London),

M.R.P. No. 1050 by Mr. M. P. Garrod

A copy is available in the Library of the Meteorological Office."

M.R.P. 1050
S.C. III/236
9th April, 1957

AIR MINISTRY
METEOROLOGICAL RESEARCH COMMITTEE

Recent developments in the measurement of precipitation elements from aircraft

by

M.P. Garrod (Meteorological Office)

1. Introduction

During the last few years the Meteorological Research Flight, for the purpose of cloud physics studies, has attempted to make measurements of many cloud parameters. Results up to 1955 have been reviewed in (1). Little progress in making one of the most important measurements, that of raindrop and precipitation elements (greater than 100 μ diameter), had been made previous to this time. It is the purpose of this report to describe the development of instruments for this purpose during the last two years and to present some preliminary results.

The instrumental development has now reached a stage where considerable data can be obtained very rapidly, and it is hoped later to produce more detailed studies of the various aspects outlined here.

For meteorological purposes, measurements of the development of precipitation elements, both solid and liquid, are important for the study of rainfall mechanisms and of the constitution of radar precipitation echoes. For aeronautical purposes a knowledge of the size, concentration and constitution of precipitation elements is important in studies of rain erosion, visibility in precipitation and airframe and engine icing, and the problem has therefore also received considerable attention from the Mechanical Engineering Department at the Royal Aircraft Establishment, Farnborough, with which close co-operation has been maintained in this work. The results of the Mechanical Engineering Department's laboratory studies have been described in (2).

2. Experiments with sooted screen techniques

2.1. From the outset several techniques, normally applicable for use at ground level, were considered for use in an aircraft. Many of these required complex equipment, e.g., those counting particles by electronic and optical methods required complex equipment which is difficult to install. Others, though simple, would provide only limited data after long periods in the air. The most promising method, and the simplest to install, was the sooted mesh screen technique described by Blanchard (3) which also included a method for calibration on the ground.

In this method a wire mesh, coated with soot produced by acetylene gas, is exposed horizontally in rain. A raindrop striking the gauze will not splash as if striking an impenetrable surface, but will break up after passing through the mesh, taking with it a small quantity of soot. As a result, a visible circular impression is left which bears a certain relation to drop size and velocity.

/2.2

2.2. Before attempting any airborne trials it was necessary to establish what type of mesh was to be used, and the best form of soot coating. This was investigated by trying various combinations in a wind tunnel, and the final choice was a white silver plated mesh screen (80 strands per inch) and a coating of paraffin soot. No suitable coating was found for airspeeds exceeding 150 knots, but this, fortunately, was not a serious disadvantage. Incidentally, as a result of these experiments an excellent method for ground measurements was evolved, employing a screen with a first coating of magnesium oxide and a second of paraffin soot. A drop striking the screen completely removed the black soot, leaving the white magnesium oxide exposed in brilliant contrast to its surrounds.

2.3. A simple instrument was designed and constructed for use in the Hastings aircraft of the Meteorological Research Flight. (Fig.1) This instrument consisted of a tube four feet long and two inches in diameter. To one end was attached a screen holder and shutter mechanism operated by a Bowden cable. The tube could be clamped to an existing trolley, normally used for other sampling experiments, which was situated on the wireless operator's table. With the instrument fully extended the screen was exposed to an unobstructed airstream at about two feet from the skin of the aircraft. The complete installation for various samplers of this type has been described in (4).

2.4. A number of trial flights were made during the summer of 1955 to establish the capabilities and limitations of the sooted screen technique. In the first instance sampling was carried out in rain beneath cloud with varying airspeeds and rain intensity. It was found that the necessary exposure time, to obtain a good sample at 150 knots was five seconds or less, depending on rain intensity. Provided the airspeed did not exceed 150 knots the contrast obtained on the screen was sufficient for visual measurements, with the exception of marks less than 1 mm. diameter, the coarseness of the screen being too great for clear impressions. Examples are shown in Fig. 2a, 2b which indicate the clarity of the records for a considerable range of drop size.

A second series of flights was then made in rain-producing clouds. Results obtained were rather variable depending on cloud density and the quantity of rain. In many cases clarity of the record was lost, presumably due to cloud particles striking the screen in large numbers and partially removing the soot coating over the whole surface. However, this rarely caused complete loss of the record. Examples of screens exposed in cloud are shown in Fig. 2c, 2d. Rough outlines of snow and large ice crystals have also been detected by this method. (Fig. 2e, 2f)

2.5. The minimum size of impression on a screen for accurate measurements was about 1 mm., and this consequently limited the range of size measureable. To record drops of smaller diameter it was suggested that a sooted plate might be tried, as it was unlikely that much splashing would occur. A number of plates were exposed in very light rain, and the results were satisfactory. Some impressions were clearly visible having a diameter of about 250 microns, which suggested a true drop size less than this value. Above some unknown size splashing was occurring. Examples are shown in Fig. 2g, 2h of sooted plates exposed to varying drop sizes.

2.6. Before any research was possible using the sooted screen method it was necessary to obtain a calibration. This work was carried out by the Mechanical Engineering Department at Farnborough using a method similar to that described by Blanchard (2) known as the whirling arm. Sooted screens were firmly attached at each end of a horizontal rod four feet long, and rotated at the required airspeed by a 6 h.p. electric motor. The speed of the screens was obtained by means of a stroboscope. Drops of known size, calibrated by means of filter papers dusted with Rhodamine dye, were allowed to fall in the path of the screens until sufficient hits were made. The calibrations obtained for sooted screens and plates are given in Fig.3.

/3.

3. The aluminium foil technique

3.1. During the process of calibration the opportunity was taken by the Mechanical Engineering Department to test several other ideas which might be an advance on the sooted screen. It was found that if a thin aluminium foil was placed in front of a wire mesh screen, a raindrop hitting it at 100 knots or more left a circular indent and an inner circle formed by impressions of the gauze behind the foil. This inner circle had a diameter proportional to the true drop size.

It was at once apparent that a method had been evolved from which a continuous raindrop recorder could be designed, basically consisting of a continuous metal tape passing over a wire mesh screen behind an aperture. Provided the tape could be sufficiently long for several minutes running time, then it would show a vast improvement in sampling quantity as compared with sooted screens, apart from being a cleaner and more permanent record.

3.2. An impactor was designed and built late in 1955 at the Meteorological Research Flight (Fig.4). Other impactors based on the same principle have also been used in the Mechanical Engineering Department's aircraft, and also for experimental work with Bristol Britannia airliners. The basic design of the Meteorological Research Flight's instrument was similar to that used for the original sooted screen type. The instrument was operated automatically by a 24 volt electric motor, and the impactor head, shown also in Fig.4, contained two spools. The feed spool held about 20 feet of aluminium tape, 0.002 inch in thickness and one inch wide, one end of which was fed round rollers past an aperture to the second spool actuated by the electric motor. Behind the aperture a wire mesh screen was firmly soldered to a brass plate. The instrument was capable of giving a continuous running period of three minutes.

3.3. Calibration of the aluminium foil was carried out by the Mechanical Engineering Department at Farnborough, using the whirling arm method. The maximum speed attainable was about 150 knots, and a second method was used for higher speeds. This employed an aluminium bullet, the nose holding a small screen covered by the aluminium foil, which was fired by a compressed air gun at a drop suspended on a fine web (6). The bullet was decelerated by a succession of aluminium rings, clamped in a trough, whose internal diameter was slightly smaller than the outside diameter of the bullet. The sample obtained was undamaged by this process.

Calibration, using the gun, was carried out for speeds up to 300 knots. Fig.5 (inner circle diameter plotted against raindrop diameter) shows relevant calibration data for the Hastings aircraft, which normally flies at speeds of 150-200 knots.

3.4. During the first six months of 1956 a number of flights were carried out using this instrument. As a result, minor modifications were carried out, as follows:-

(a) The record on 0.002 inch thick tape was not very clear. 0.001 inch tape was substituted. (The Bristol Britannia instrument utilised tape 0.0005 inch thick.)

(b) It was found difficult to reload the instrument in flight, and the head was redesigned so that the spools could be easily separated from the instrument. The rollers, illustrated in Fig.4, were replaced by a smoothly curved brass plate, as the tape was breaking frequently, owing to sudden changes of direction round the rollers.

(c) The existing one-inch square aperture was too large for heavy precipitation conditions. This was reduced by a half, and the tape speed increased from about one inch per second to three inches per second.

/3.5.

3.5. During the latter half of 1956 further flights were made to investigate rain in and out of cloud, and also to record sizes and distribution of ice particles. Impressions obtained of small ice crystals were better than those of raindrops of similar size, but those of snowflakes were rather blurred. Examples of drizzle, moderate rain, and mixed snow and rain are shown in Fig.6. The apparent decrease in numbers of impressions across the tape record is due to a graded aperture used temporarily to establish the best width.

4. Preliminary results of flights during 1956 using the aluminium tape recorder

4.1. During 1956 records were obtained in about 50 flights concerned with large droplet content of cumulus and stratocumulus cloud, rain and snow particles in frontal cloud, coalescence rainfall and precipitation elements in cumulonimbus cloud. Each of these is a very large subject and it will only be possible here to present a brief summary of the preliminary measurements.

4.2. The distribution of large cloud droplets in cumulus and stratocumulus clouds

4.2.1. During traverses of non-precipitating clouds a number of drop impressions were found on the tape record which indicated the presence of drops considerably less than 500 microns, but probably more than 100 microns in diameter and therefore representative of the early stage of rain formation. To establish the lower limit of sizes recorded an experiment was set up in a wind tunnel. It was found possible to produce marks on a tape similar to those found in cumulus clouds. By comparing the tape record with a series of droplet samples, collected on oiled slides, it was evident that the smallest size causing a visible mark on the tape record was around 80-100 microns at 180 knots airspeed. As drop sizes of 500 microns were known to cause a very much larger impression, the size range of large drops recorded in cumulus and stratocumulus clouds was estimated to be between 100 and 250 microns. Droplets less than 80 microns diameter do not mark the foil used (0.001 inch thick). It may be possible to detect smaller sizes when thinner foil is used, and further work on these lines is contemplated.

4.2.2. A number of flights were carried out through convection clouds, and in all cases so far examined these drops were found at some levels. Further flights were made in stratocumulus layers, and examples are illustrated in Fig. 7. As far as can be concluded from the 15 flights so far made it appears that:-

(a) In Southern England, cumulus clouds having a depth of 1,000 feet to 3,000 feet can be expected to have mean concentrations of these larger droplets in the body of the cloud which may be as great as 1,000 per cubic metre but are usually less than 500. There is a distinct tendency for the base of the cloud to consist entirely of drops less than 80 microns diameter, while the top often shows the greatest number of drops in the 100-250 micron range.

(b) Active cumulus cloud having a depth of 4,000 feet to 6,000 feet, whether extending above the freezing level or not, show values up to 7,000 drops per cubic metre in the 100-250 micron range, and may include a few isolated 500 micron drops.

(c) Stratocumulus clouds having a depth of 1,000 to 3,000 feet give values up to 1,500 drops per cubic metre in the 100 to 250 micron range. Stratus cloud of this depth shows fewer, and sometimes none at all, greater than 80 microns. For thicker layers (i.e., 3,000 feet and over) the number of large droplets increases considerably.

As a rule the "concentrations" referred to above were the means over a flight path of about 1,000 feet, the starting point being chosen at random within the cloud. However, with some small cumulus clouds the whole width was sampled. This applies also to the concentrations shown in Fig.7.

/4.2.3.

4.2.3. A comparison is possible between these and the results on cumulus cloud sampling by the Meteorological Research Flight using the magnesium oxide technique (5). On these latter flights it was found that the average total number of cloud droplets per c.c. was about 100 to 300, with a maximum of 1,000 per c.c., or 10^9 per cubic metre. The maximum value so far found for drops in the 100-250 micron range by the aluminium foil method is 7×10^3 per cubic metre. Hence, for every drop exceeding 100 microns it appears that there are about 10^5 to 10^6 drops less than 100 microns in a medium sized non-precipitating cumulus cloud. It is also apparent that the chances of impacting a large drop in a cumulus cloud, using the magnesium oxide or oiled slide method (which samples only a few c.c. of air) is very remote, unless several hundred samples are taken. However, a few drops exceeding 100 microns were caught during the series of 150 magnesium oxide shots which were reported in (5). This report also pointed out that the drop size tends to increase with height in a cumulus cloud. Although this comment referred to sizes below 50 microns, it suggests a correlation with the increase in numbers of 100 to 250 micron drops with height found with the aluminium tape instrument.

4.3 The distribution of rain and snow particles in frontal cloud

The amount of data obtained so far on this subject is limited, and investigations of complete frontal systems have not yet been attempted. Sampling has been carried out on different occasions in various types of cloud associated with fronts, and to illustrate the type of information now obtainable abbreviated results of four of these are shown in Fig.8 and summarised below:-

(a) Nimbostratus. 23.1.56. In the zone sampled above the freezing level a considerable decrease in both sizes and numbers of snow particles occurred with increase in height, the greatest diameters, about 3 mm., being found at the freezing level. (The term diameter is used here to mean the estimated diameter of a circle having the same area as the impression of the ice crystal on the tape record. It is not known precisely how this is related to the dimensions of the crystal.)

Below the freezing level there is evidence of coalescence taking place, the maximum drop-diameter increasing from 1½ mm. at 4,000 feet to 2½ mm. at 2,000 feet. However, as samples were taken at random positions in an area 5 to 10 miles wide, variations at any level are inevitable over such distances. Consequently, comparison of one level with another for purposes of mathematical analysis should be made with caution.

(b) Nimbostratus. 11.12.56. No sampling was carried out above 6,500 feet on this flight. The figures suggest that in the zone below the freezing level some coalescence was occurring, the maximum drop-diameter increasing from 1½ mm. at 5,000 feet to 2 mm. at 2,000 feet, while the numbers of all the remaining drops decreased substantially with decrease in height. These results are comparable with those of the previous case, showing a little less weight of precipitation at all three levels.

(c) Altostratus. 14.12.56. The figures obtained for the two levels sampled show an increase in the sizes of the ice particles with decrease in height, the total numbers at both levels being almost similar at around 5,000 per cubic metre. The largest size found was 1 mm. in diameter.

(d) Cirrostratus. 12.12.56. On this flight a predominance of very small ice crystals was found, but with small numbers with diameters of 250 microns. (Several of these crystals were caught and preserved on the aluminium foil owing to the very low temperature. Visual observation confirmed the estimate of the crystal size from the record.)

/4.4

4.4. The vertical distribution of drizzle and rain formed by the coalescence process

Two comprehensive flights have been carried out on occasions when rain was falling from cloud entirely below the freezing level. These are described separately below:-

4.4.1. 1.8.56. Cloud was solid from 1,500 to 7,500 feet, and the freezing level 10,000 feet, The aircraft climbed and descended twice through the cloud, and the mean values of drop counts calculated for each level are shown in Fig.9. No drops greater than 250 microns diameter were found, and there was a marked decrease in numbers with height from 16,000 to 1,000 per cubic metre.

4.4.2. 20.7.56. Drop sampling was carried out during the morning and the afternoon, one ascent being illustrated in Fig.10 which is somewhat similar to the three others which were obtained. The freezing level was 10,000 feet.

Drops in the 100-250 micron range decreased sharply with height from 6,000/cu.m. at 2,000 feet to less than 100 per cu.m. at 5,000 feet and above. Drops from $\frac{1}{2}$ mm. to $1\frac{1}{2}$ mm. were found at 2,000 feet, but were not found at all above 3,000 feet.

A comparison between these results and those of the cumulus cloud series shows an apparent reversal of the height distribution of 100-250 micron drops. Actual numbers are somewhat similar, but the greatest numbers are towards the top in a cumulus cloud, and at the bottom in a layered precipitating cloud. This aspect will be investigated further as data accumulate.

4.5. The distribution of rain and snow in cumulonimbus clouds

Five detailed flights have been made in cumulonimbus clouds, all in connection with the "Britannia" icing problem late in 1956. On these flights sampling was carried out every 500 feet over cloud depths of 10,000 feet or less, and it has been necessary to abbreviate these results to make a comprehensive picture. Owing to the rapid development of these clouds in space and time, samples at the same level varied considerably. The quoted values are those of the greatest concentrations encountered.

Considerable difficulty has been encountered in the analysis of the records for occasions of heavy snow. Figures quoted should be taken with some reserve, a factor of 2 being the probable error in the number of snowflakes per cubic metre. Where snow particles do not exceed 1 mm. in diameter the results are of greater accuracy.

The results of these flights are illustrated in Fig.11, which shows clouds in three different states. Each one is discussed separately below:-

4.5.1. Small cumulonimbus. Three flights have been made through cumulonimbus clouds with tops at or below 15,000 feet. Mean maximum values are shown of snow or supercooled drops between 5,000 and 12,500 feet. Snowflakes were found with diameters up to 3 mm. at the lower levels, while 2 mm. ones were found throughout the cloud. Supercooled drops of 1 mm. diameter were found in one case up to 7,500 feet (-10°C). Maximum numbers of small ice crystals were about 20,000 per cubic metre at 10,000 feet, with considerably smaller values at lower levels.

4.5.2. Large cumulonimbus. Only one flight has been carried out through a cumulonimbus of great vertical extent. In this case, on 4.10.56, the top was 25,000 feet or more and sampling was restricted to levels between 12,500 and 20,000 feet. Snowflakes of 2 mm. diameter were found at all levels, but none greater. On several runs at around 17,000 and 18,000 feet (-30°C) impressions were found on the tape record which were similar to those made by raindrops of about 1 mm. diameter. As considerable turbulence and vertical motion were experienced in the cloud, it is reasonable to assume these were supercooled drops. Ice crystals in the 100-250 micron range showed a maximum at 20,000 feet of 45,000 per cubic metre, by far the most as yet encountered, and generally the numbers throughout the levels examined were much more than has been found in any other cloud type.

4.5.3. Old cumulonimbus anvil. One example only is available, which was recorded on 4.10.56. The cloud had probably been in existence for several hours, and at the time of sampling extended from 12,000 to 20,000 feet, over a wide area. The largest ice crystals (aggregates) were about 500 microns in diameter at 15,000 feet, and at 19,000 feet only the smallest ice crystals were evident. This is somewhat similar to the results for frontal cloud, except that 1 mm. snowflakes were not evident, presumably having fallen out earlier during the decaying stage of the main bulk of the cumulonimbus cloud.

5. Conclusions

An instrument has been developed for continuously recording in an aircraft the size distribution of raindrops. It has also been established that it can be used for determining the distribution and size of ice particles in the atmosphere, and the calibration for this purpose is now almost complete.

This instrument can be used in research into many aspects of cloud physics which have until now been insufficiently studied, such as the variation of rain and snow spectra in frontal and shower clouds, and their relation to radar echoes. Measurement of diameters of cloud drops at the higher end of the spectrum is possible, and perhaps with certain improvements smaller cloud drops may be included.

Acknowledgments

To the Mechanical Engineering Department at Farnborough for carrying out almost all the calibration work, and for general co-operation in development of the instruments. To Mr. F. A. Gordon for the construction and maintenance of equipment.

References

1. Murgatroyd, R.J.	Cloud physics at the Meteorological Research Flight.	Archiv für Meteorologie, Geophysik und Bioklimatologie. Serie A: Band 8,3. Heft, 1955.
2. Bigg, F.J., McNaughton, I.I. and Methven, T.J.	The measurement of rain from an aircraft in flight.	R.A.E. Tech. Note Mech. Eng. 223. Min. of Supply.
3. Blanchard, D.C.	The use of sooted screens for determining raindrop size and distribution.	General Electric Research Lab. Occ. Report No. 16. Project Cirrus.
4. Murgatroyd, R.J.	Meteorological Research in aircraft.	Meteorological Research Papers, Air Ministry, London, No. 995.
5. Durbin, W.G.	Droplet sampling in cumulus clouds.	Meteorological Research Papers, Air Ministry, London, No. 991.

6. Jenkins, D.C. Interim note on the design and development of a laboratory apparatus to study the high speed impact between a liquid drop and a surface. R.A.E. Tech. Note Mech. Eng., 193, 1954.

G.17610/PVC/5/57/50

FIG. 1

SOOTED SCREEN TYPE RAINDROP IMPACTOR.

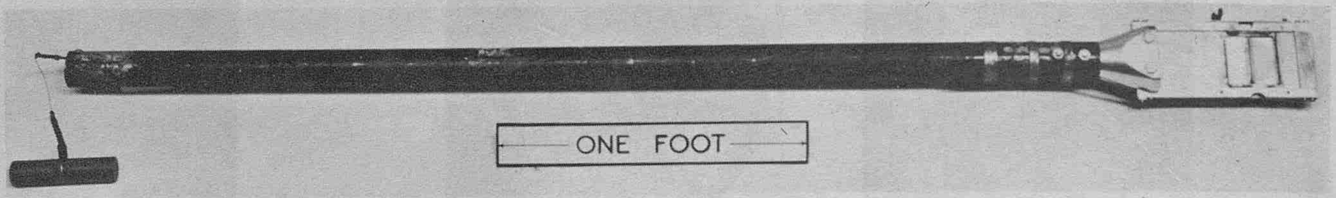

IMPACTOR HEAD AND SCREEN.

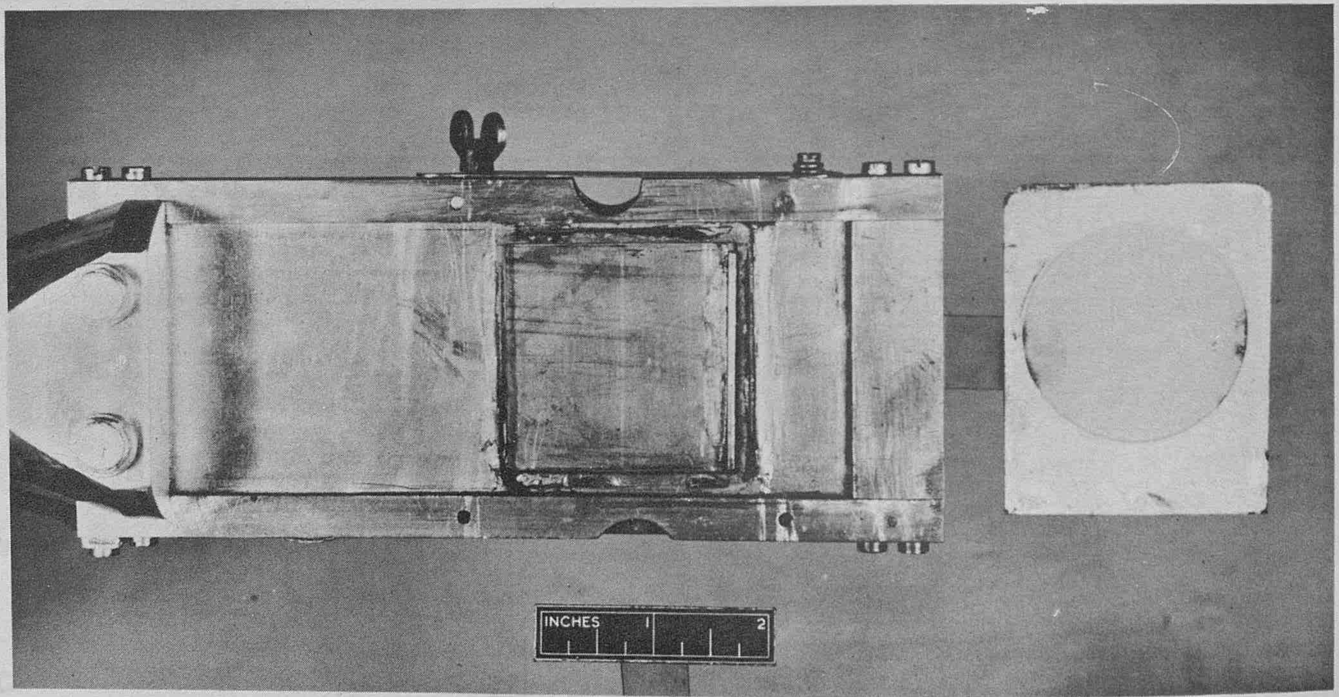

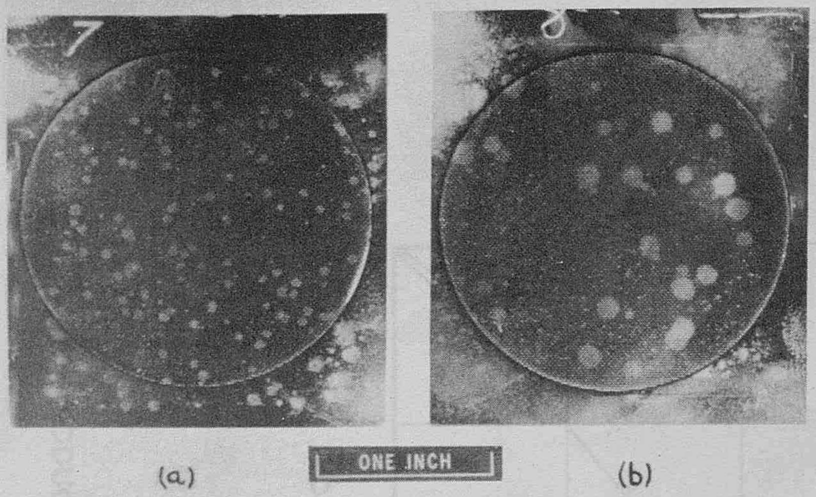
7
8
(a)
ONE INCH
(b)

RAIN SAMPLES IN CLEAR AIR

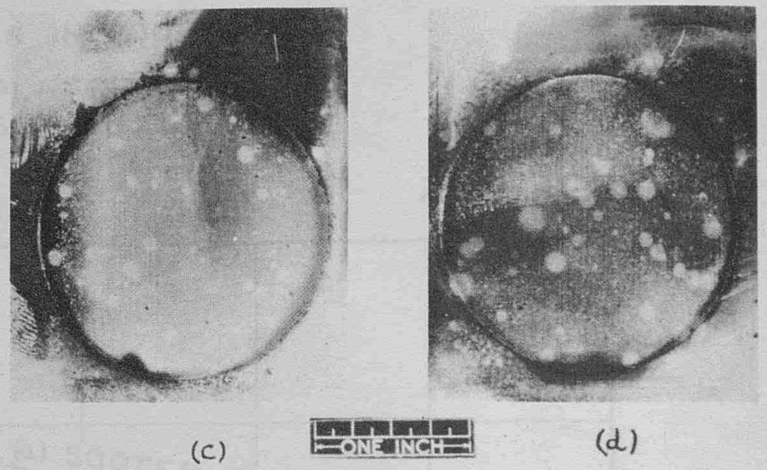

RAIN SAMPLES IN CLOUD

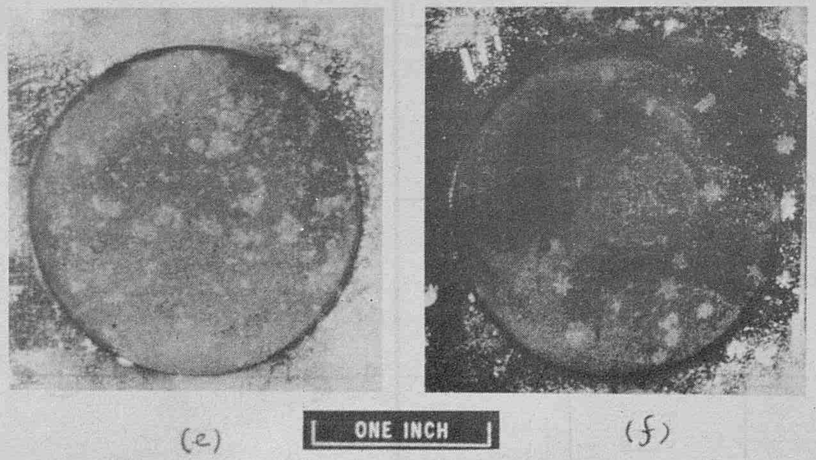

SNOW SAMPLES IN CLOUD

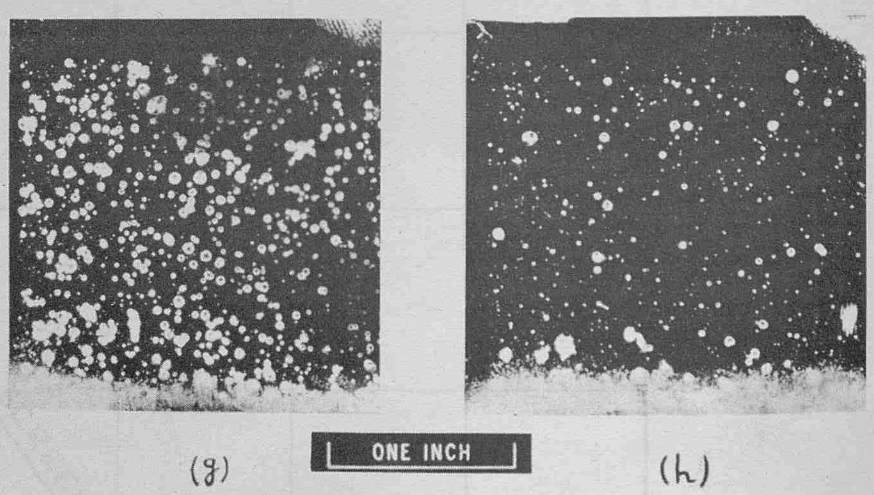

SAMPLES OF LIGHT RAIN ON SOOTED PLATES

FIG. 2

Nº MET. RES. FLT.
DR.
TR. JS. 29·1·57
CH.
APP.

M.R.P. 1050

FIG. 3.

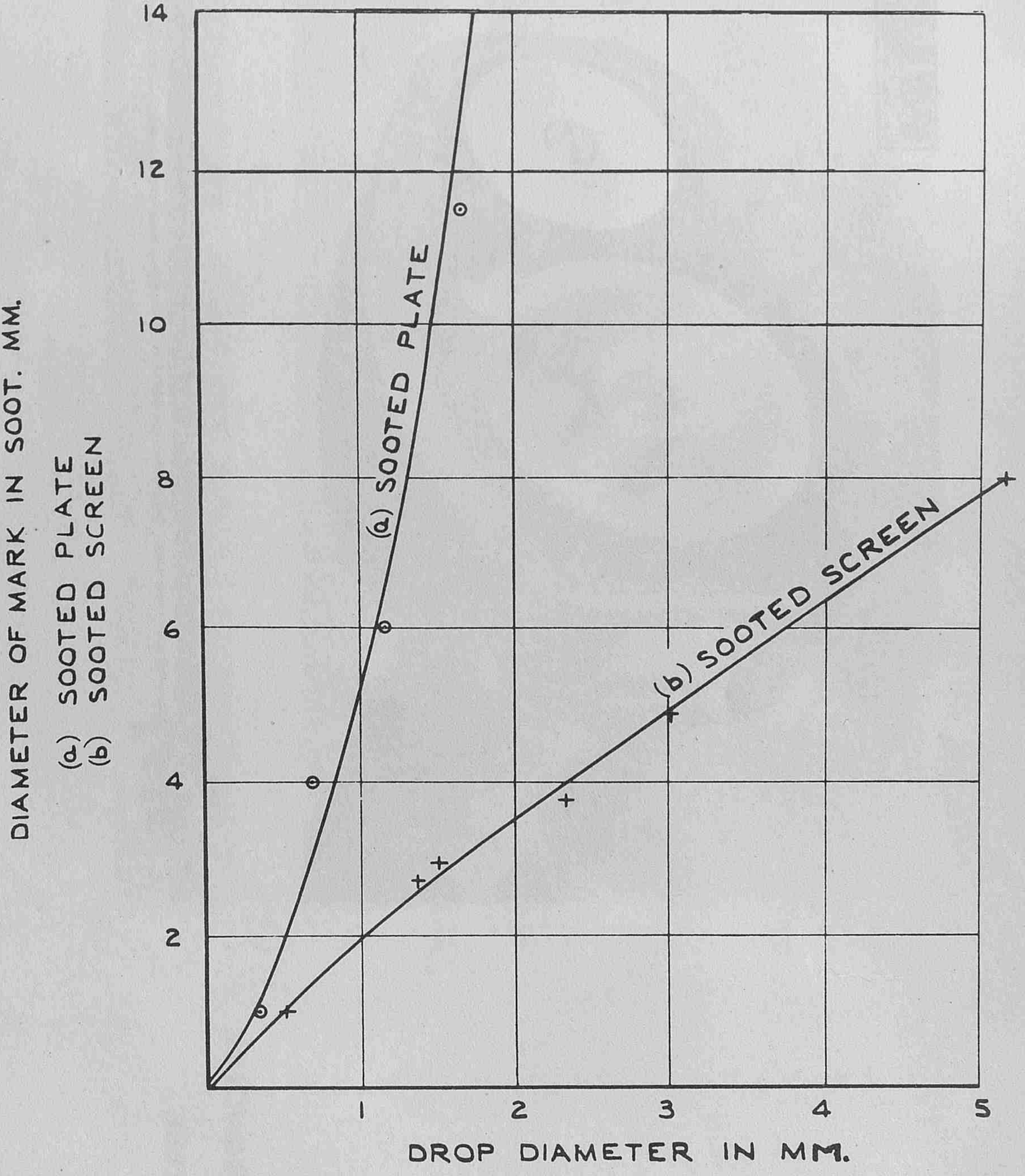

(REPRODUCED FROM T.N. M.E. 223.)

FIG. 3. CALIBRATION CURVES FOR SOOTED SCREEN AND PLATE AT 130 KNOTS.

FIG. 4

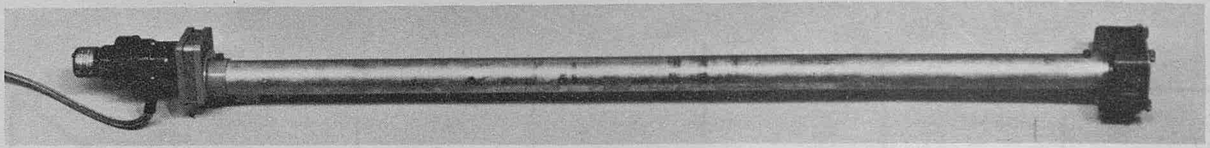

ALUMINIUM TAPE
RAINDROP IMPACTOR

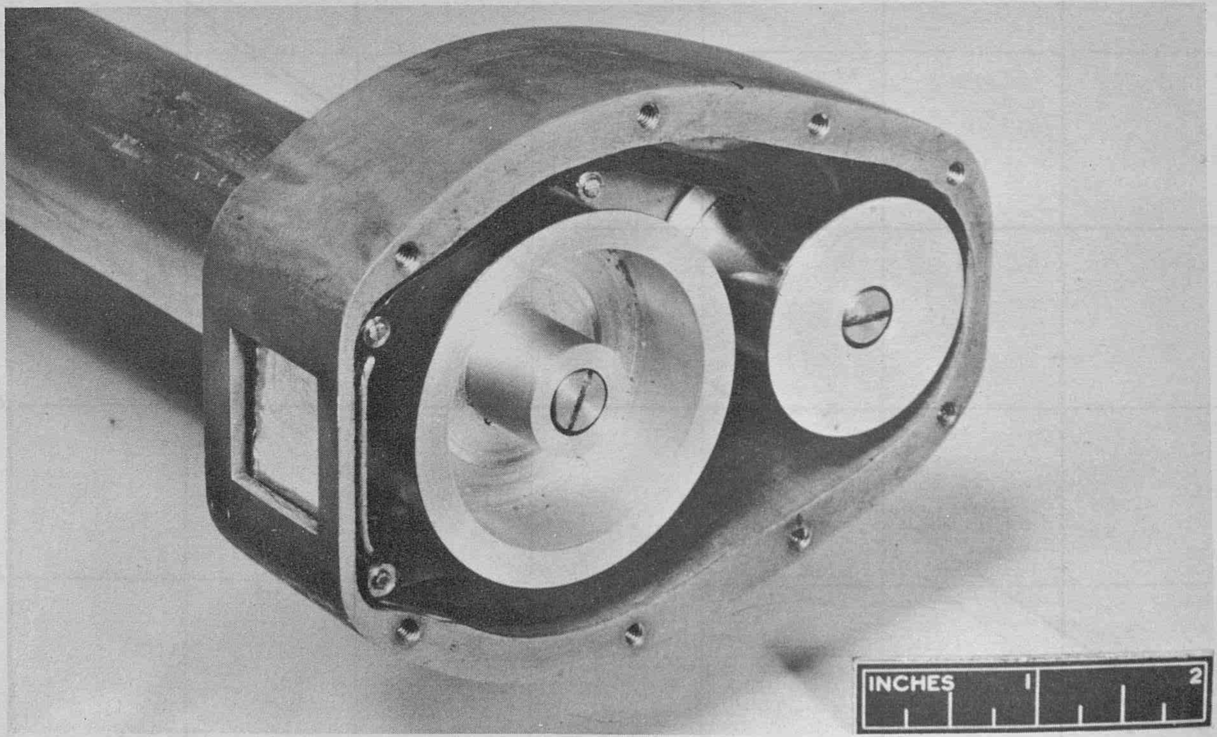

EXPOSED HEAD.

Nº MET. RES. FLT.
DR.
TR. J.S. 29·1·57
CH.
APR.

FIG.5

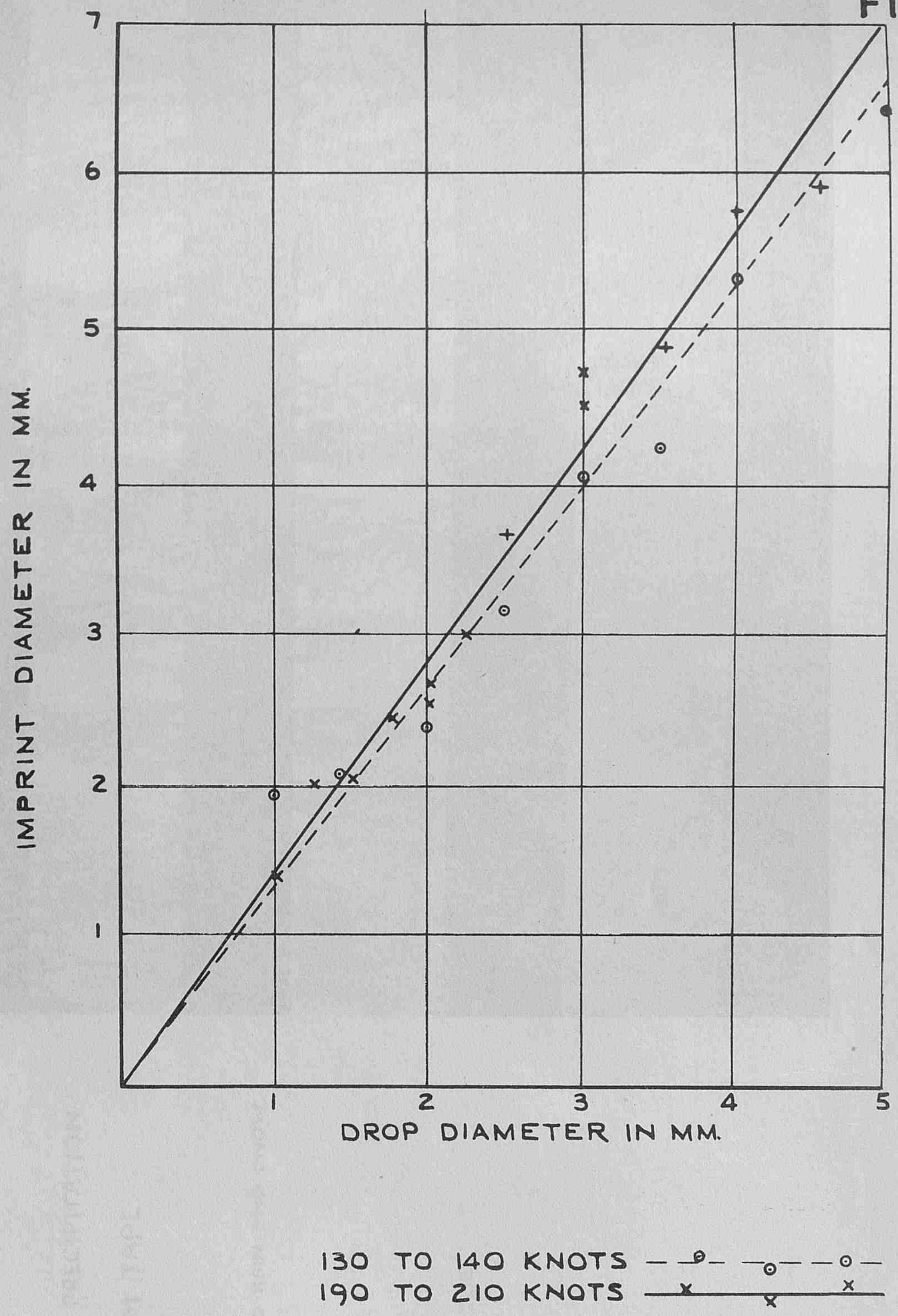

(REPRODUCED FROM T.N. M.E. 223.)

FIG. 5. CALIBRATION CURVE FOR ALUMINIUM FOIL (RAIN IMPACTOR GUN TESTS.)

FIG. 6

EXAMPLES OF PRECIPITATION ON ALUMINIUM TAPE.

TOP MIXED RAIN AND SNOW.

CENTRE. RAIN.

BOTTOM. DRIZZLE.

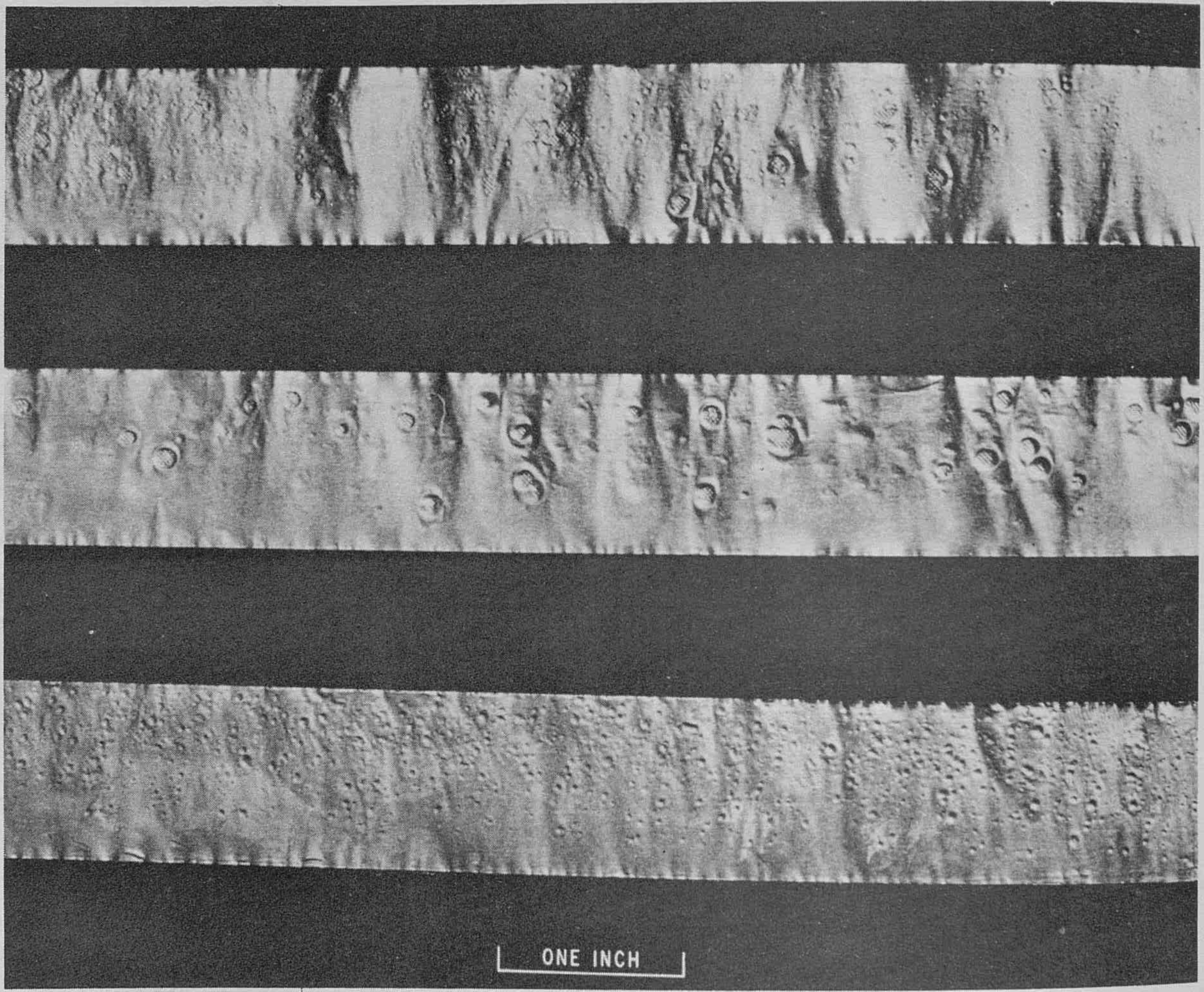

Nº MET. RES. FLT.
DR.
TR J.S. 1·2·57
CH.
APP.

FIG.7.

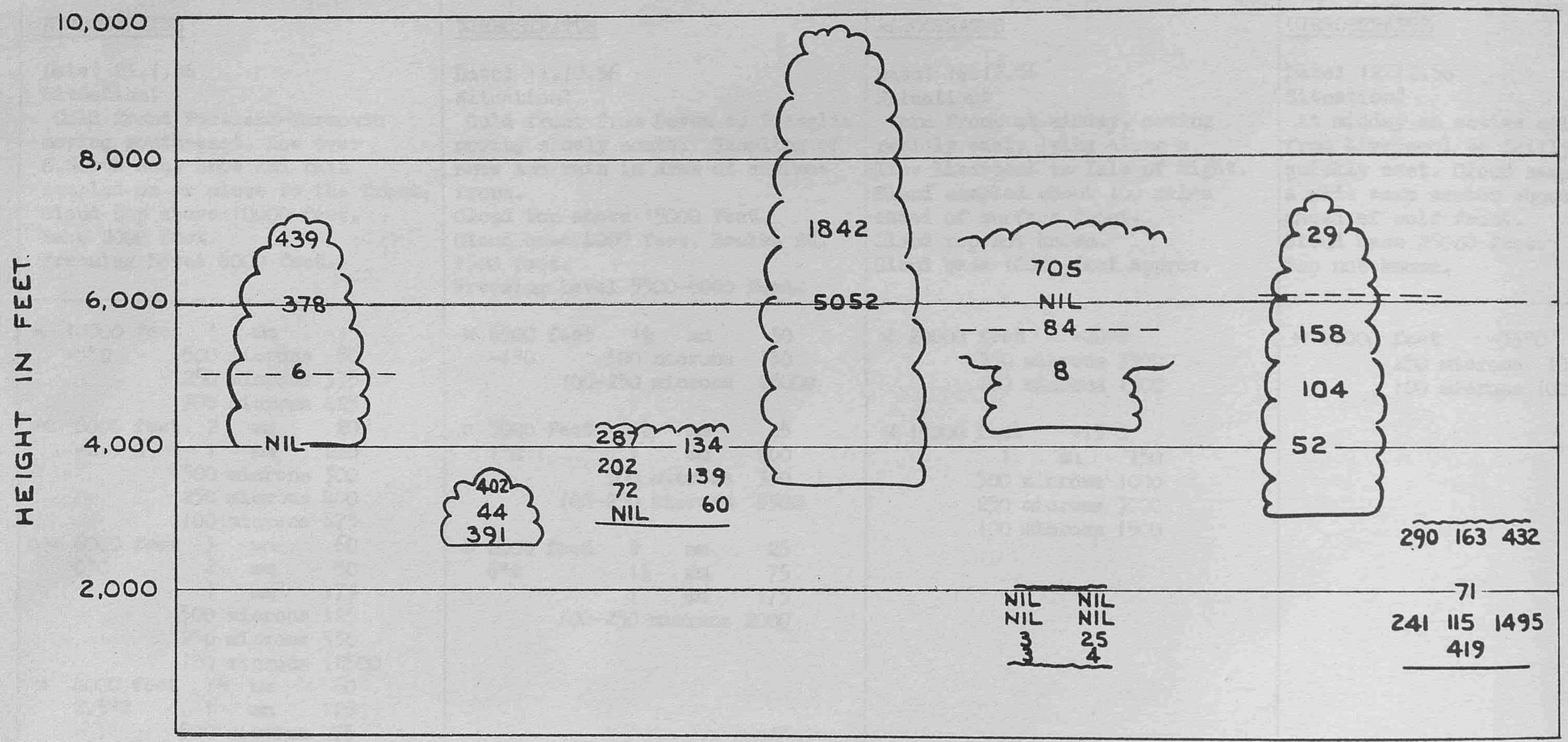

FIG. 7. EXAMPLES OF 100-250 MICRON DROP CONCENTRATIONS IN CUMULUS AND STRATOCUMULUS CLOUDS.
FIGURES GIVEN ARE NUMBERS PER CUBIC METRE.
FREEZING LEVEL DENOTED BY PECKED LINE WHERE APPLICABLE.

NIMBOSTRATUS	NIMBOSTRATUS	ALTOSTRATUS	CIRROSTRATUS
Date: 23.1.56 Situation: Cold front Portland-Yarmouth moving south-east. Low over S.North sea. Snow and rain sampled on or close to the front. Cloud top above 10000 feet. Base 2000 feet. Freezing Level 6000 feet.	Date: 11.12.56 Situation: Cold front from Devon to E.Anglia moving slowly south. Sampling of snow and rain in area of surface front. Cloud top above 15000 feet. Cloud base 4000 feet. Broken St. 1500 feet. Freezing Level 5500-6000 feet.	Date: 14.12.56 Situation: Warm front at midday, moving rapidly east, lying along a line Liverpool to Isle of Wight. Cloud sampled about 100 miles ahead of surface front. Cloud top not known. Cloud base 12000 feet approx.	Date: 12.12.56 Situation: At midday an active cold front from Liverpool to Scilly moving quickly east. Cloud sampled in a wide warm sector about 100 miles ahead of cold front. Cloud base 25000 feet. Top not known.
* 10000 feet -5°C 1 mm 15 500 microns 80 250 microns 375 100 microns 425 * 8000 feet -2.5°C 2 mm 20 1 mm 200 500 microns 300 250 microns 400 100 microns 475 o* 6000 feet 0°C 3 mm 60 2 mm 50 1 mm 175 500 microns 125 250 microns 350 100 microns 12500 o 4000 feet 2.5°C 1½ mm 60 1 mm 125 500 microns 75 100-250 microns 75 o 2000 feet 6°C 2½ mm 7 2 mm 25 1½ mm 40 1 mm 80 500 microns 50 100-250 microns 150	* 6500 feet -1°C 1½ mm 30 500 microns 150 100-250 microns 25000 o 5000 feet 1°C 1½ mm 25 1 mm 200 500 microns 350 100-250 microns 5500 o 2000 feet 6°C 2 mm 25 1½ mm 75 1 mm 175 100-250 microns 2000	* 20000 feet -20°C 250 microns 3500 100 microns 1500 * 15000 feet -15°C 1 mm 150 500 microns 1000 250 microns 3000 100 microns 1500	* 26000 feet -35°C 250 microns 1000 100 microns 10000

FIG. 8. EXAMPLES OF SNOW AND RAIN IN LAYER CLOUDS.

* Snow o* Sleet o Rain

Sizes quoted are diameters in millimetres or microns
Figures quoted are numbers per cubic metre

Nº MET. RES. FLT.
DR.
TR. J.S. 4·2·57
CH.
APP.

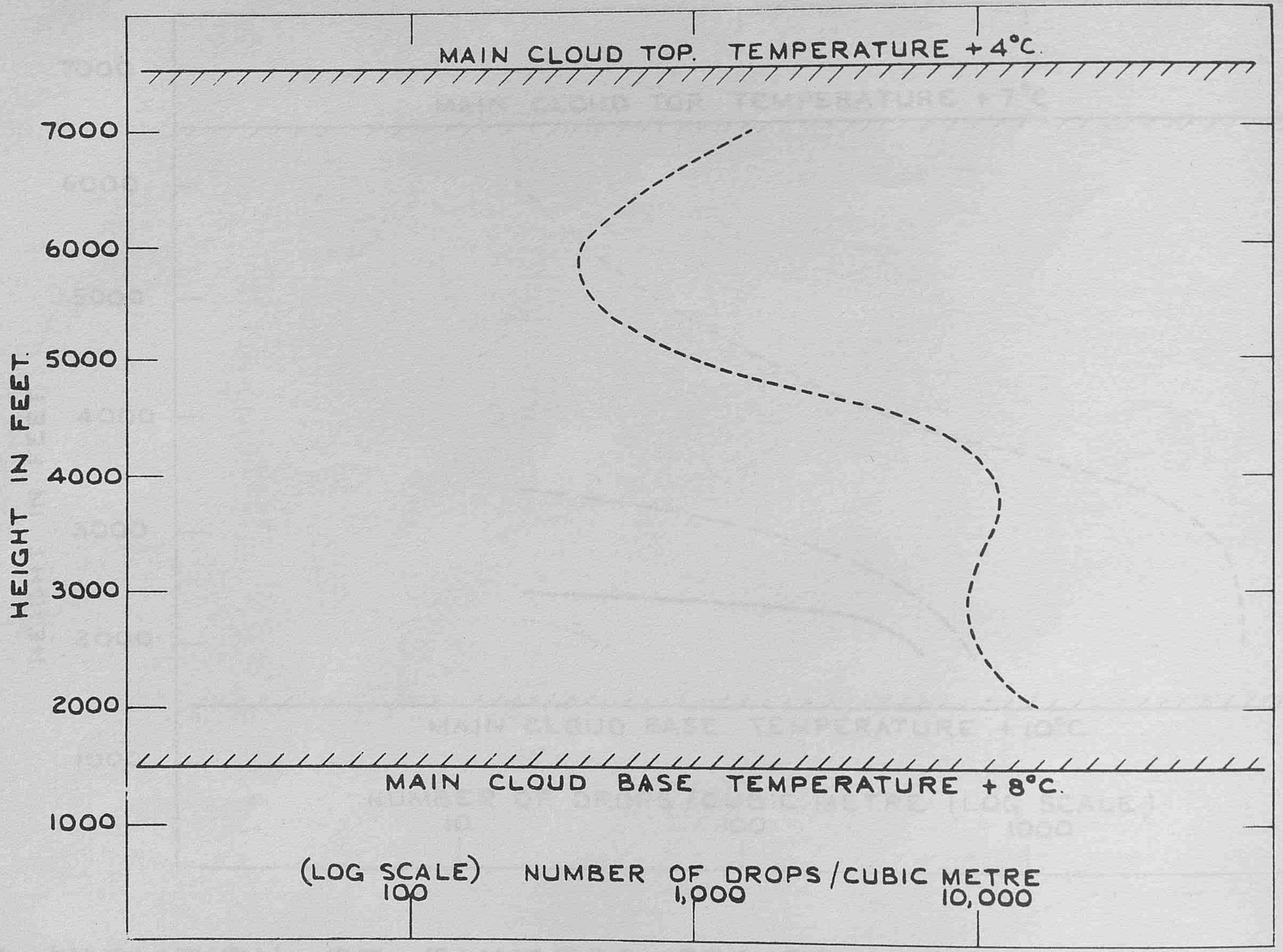

FIG. 9. VARIATION OF 100-250 MICRON DROPS WITH HEIGHT.

FARNBOROUGH. 1ST. AUGUST 1956.

M.R.P. 1050

Nº MET. RES. FLT.
DR.
TR. J.S. 4.2.57
CH.
APR.

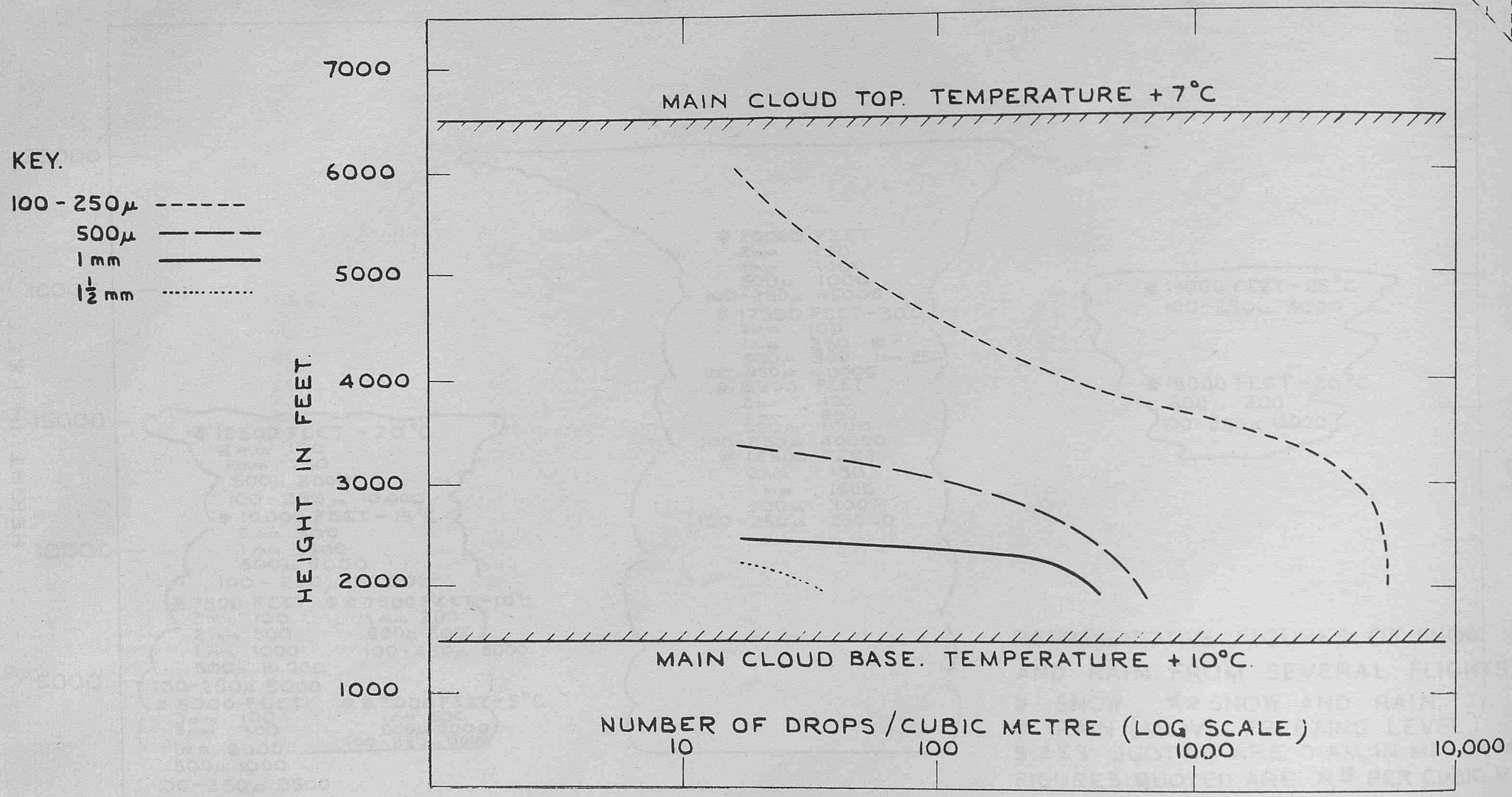

FIG. 10. VARIATION OF RAINDROP SPECTRUM WITH HEIGHT.

FARNBOROUGH 20th JULY 1956.

FIG. 10.

R

M.R.P. 1050

Nº MET. RES. FLT.
DR.
TR. J.S. 4.2.57.
CH.
APR.

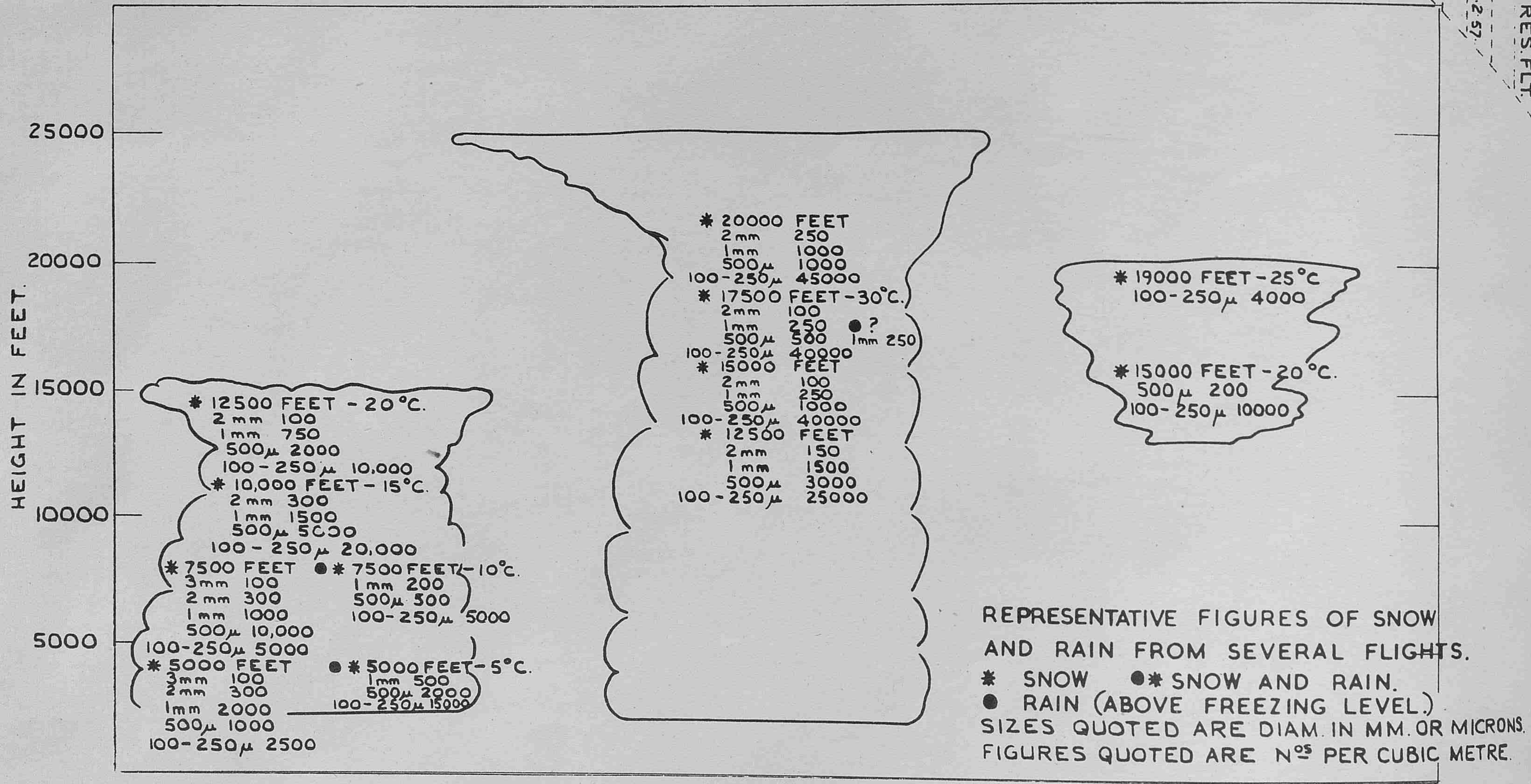
HEIGHT IN FEET.
25000
20000
15000
10000
5000
* 12500 FEET - 20°C.
2 mm 100
1 mm 750
500µ 2000
100 - 250µ 10,000
* 10,000 FEET - 15°C.
2 mm 300
1 mm 1500
500µ 5000
100 - 250µ 20,000
* 7500 FEET
3mm 100
2 mm 300
1 mm 1000
500µ 10,000
100-250µ 5000
● * 7500 FEET - 10°C.
1 mm 200
500µ 500
100-250µ 5000
* 5000 FEET
3mm 100
2mm 300
1mm 2000
500µ 1000
100-250µ 2500
● * 5000 FEET - 5°C.
1mm 500
500µ 2000
100-250µ 15000
* 20000 FEET
2mm 250
1mm 1000
500µ 1000
100-250µ 45000
* 17500 FEET - 30°C.
2mm 100
1mm 250
500µ 500
100-250µ 40000
● ?
1mm 250
* 15000 FEET
2mm 100
1mm 250
500µ 1000
100-250µ 40000
* 12500 FEET
2mm 150
1mm 1500
500µ 3000
100-250µ 25000
* 19000 FEET - 25°C
100-250µ 4000
* 15000 FEET - 20°C.
500µ 200
100-250µ 10000
REPRESENTATIVE FIGURES OF SNOW AND RAIN FROM SEVERAL FLIGHTS.
* SNOW
●* SNOW AND RAIN.
● RAIN (ABOVE FREEZING LEVEL.)
SIZES QUOTED ARE DIAM. IN MM. OR MICRONS.
FIGURES QUOTED ARE Nºs PER CUBIC METRE.

FIG. II. CUMULONIMBUS CLOUD.

FIG. II.

M.R.P. 1051
S.C. 11/234
6th May, 1957

A contribution to the study of Meteorological Time Series

by

J. M. Craddock

(Meteorological Office)

AIR MINISTRY

METEOROLOGICAL RESEARCH COMMITTEE

At the time of issue this report has not been published. Any author desiring to quote this paper should refer to it as "A paper of the Meteorological Research Committee (London), M.R.P. No. 1051 by Mr. J.M. Craddock. A copy is available in the Library of the Meteorological Office."

M.R.P. 1051
S.C.II/234
6th May, 1957

AIR MINISTRY

METEOROLOGICAL RESEARCH COMMITTEE

A contribution to the study of Meteorological Time Series

by

J. M. Craddock (Meteorological Office)

Summary

An account is given of the numerical analysis of meteorological time series by means of mutually exclusive band pass filters. It gives methods for producing efficient filters and for the statistical interpretation of the results. Practical examples are given, including an analysis of the slower temperature variations at Kew Observatory, covering the range of periods from 2 days up to about 50 years.

Background

1. This work was undertaken to help to provide a firm statistical foundation to the work of the synoptic meteorologist and the climatologist, so I have given most attention to the features which are important in dealing with the slower atmospheric fluctuations. Nevertheless, the method developed is of far wider application and could be used, for example, in the study of atmospheric turbulence or of tidal series or for the analysis of data regularly distributed in space instead of time.

The outstanding characteristic of the slower atmospheric fluctuations (excluding the strictly periodic ones, based on the day or the year) is their lack of regularity. An oscillation after persisting for several wavelengths may cease abruptly and be followed by another of different period, amplitude and duration. Any method of analysis, such as periodogram or correlogram analysis, which assumes that the series to be analysed preserves its general character throughout a considerable time interval is likely to prove unrewarding when applied to these data, if the statistical properties vary from one part of the series to another. This may happen if the variable is subject to fluctuations with periods as long as or longer than the time covered by the series, or if there are more or less irregular changes in the character of the physical processes producing the observed variations.

The intractability of the material, and the difficulty of assembling and processing the data on the scale necessary to obtain worthwhile results, has meant that very few hard facts have been established about the slower atmospheric fluctuations. Hence the present work has novelty both in the method and in the results. However, the analysis of Kew temperatures though interesting in itself is only one example of many possible applications of a versatile technique.

2. Our problem is parallel to that facing a radio engineer who wishes to design a radio receiver to accept signals from a particular station while excluding signals from other stations, and unorganised noises which may be incident on the aerial at the same time. We can look on our time series as composed of a number of sine waves spread over a particular range of frequencies, but unlike the radio engineer, we do not know initially what part of the range, if any, is likely to

prove interesting. Our method of analysis consists in splitting the original signal into mutually exclusive components each limited to one section of the original wave band, and measuring the power (or variance) of each component series to find which are the most important. The question whether the power of one component series is significantly greater than that of another is settled by means of Snedecor's F-test.

The actual analysis of the original series is carried out with linear operators, or filters, each of which is designed to pass all oscillations lying in a particular wave band with their original amplitudes and phase relationships, while all oscillations lying outside the band are reduced or annulled altogether. The design of filters is a matter for compromise based on practical experience, since the requirements of efficiency in discrimination and of ability to follow the changes of a non-stationary time series conflict with one another. The filters used here are suitable enough for experimental work, but could be elaborated with advantage when the work is extended.

3. Suppose now that we have a time series $x_1\ x_2\ x_3 \ldots x_N$ relating to times $\alpha\ 2\alpha\ 3\alpha \ldots N\alpha$ (N is assumed to be even). Let us carry out a harmonic analysis with basic period $N\alpha$. Then if a_K, b_K are the components of the Kth harmonic

$$a_K = \frac{2}{N}\sum_{j=1}^{N} x_j \cos\frac{2\pi jK}{N} \qquad (1)$$

$$b_K = \frac{2}{N}\sum_{j=1}^{N} x_j \sin\frac{2\pi jK}{N} \qquad (2)$$

Any selection of harmonics will give a "least squares" fit to the original data, but if we take all harmonics from $K=1$ to $K=N/2$ then the number of harmonic coefficients will equal the number of data, and the fit will be exact. The frequencies of these harmonics (i.e., the number of cycles per unit time) are $1/N\alpha,\ 2/N\alpha,\ 3/N\alpha\ \frac{N/2}{N\alpha}$ i.e., they divide the interval $(0, \frac{1}{2\alpha})$ into N/2 equal parts. Thus any time series of N terms at time intervals α can be represented uniquely as the sum of N/2 harmonics equally dividing the interval $(0, \frac{1}{2\alpha})$. This interval does not depend on the number of terms in the series, but only on the time interval between one term and the next, and the higher limit $\frac{1}{2\alpha}$ may be called the cut-off frequency.

Suppose now that the terms of the x series are completely uncorrelated with one another, and that the series is obtained by random drawings from a normal distribution. From equation (1)

$$a_K^2 = \frac{4}{N^2}\left(\sum_{j=1}^{N} x_j \cos\frac{2\pi jK}{N}\right)^2 \qquad (3)$$

and if this is summed over a large number of samples, M

$$\frac{1}{M}\sum^{M} a_K^2 = \frac{4}{N^2}\frac{1}{M}\sum^{M}\left(\sum_{j=1}^{N} x_j \cos\frac{2\pi jK}{N}\right)^2 \qquad (4)$$

Now if the R.H.S. of (4) is expanded, and the order of the summations reversed, expressions such as $\frac{1}{M}\sum^{M} x_i x_j$ will vanish in the limit, so that

$$\frac{1}{M}\sum^{M} a_K^2 = \frac{4}{N^2}\sum_{j=1}^{N}\frac{1}{M}\sum^{M} x_j^2 \cos^2\frac{2\pi jK}{N} \qquad (5)$$

and writing $V(x)$ for the variance of x_1 etc.

$$V(a_K) = \frac{4}{N^2} V(x) \sum_{j=1}^{N} \cos^2 \frac{2\pi j K}{N} \tag{6}$$

$$= \frac{2}{N} V(x) \tag{7}$$

The cos or sin component of the Kth harmonic, say $a_K \cos \frac{2\pi K t}{N\alpha}$ has variance

$$\frac{a_K^2}{2} = \frac{1}{N} V(x) \tag{8}$$

Thus the average amplitude of any harmonic component obtained by the analysis of a random series of N terms is 1/N times the variance of the original series. Thus while any series of N terms can be represented uniquely by the sum of N harmonic components with equally spaced frequencies $\left(\frac{1}{N\alpha}, \frac{2}{N\alpha} \cdots \frac{1}{2\alpha}\right)$ if the series consists of random terms drawn from a normal distribution the amplitudes of all the harmonics are, on average, equal.

Reverting to our radio illustration it appears that a series which is random, and of which the values of individual terms are therefore wholly unpredictable, appears as a "noise" spread evenly over the whole frequency band. Such a noise cannot be eliminated totally by any method of discrimination between frequencies, whereas it is possible to eliminate unwanted oscillations if these are confined to a band of frequencies which does not overlap the band which interests us. To eliminate an unwanted oscillation we need not reduce its amplitude precisely to zero; it is enough to ensure that the remaining amplitude falls well below the general noise level. This fact reduces the difficulties of filter design mentioned in Section 9.

When a signal is analysed into a series of frequency bands covering the range $\left(0, \frac{1}{2\alpha}\right)$ we must expect it to show significant peaks of power in certain frequency bands rising above a uniform noise level. Conversely, if we have several estimates of the power in different wavebands, all estimates statistically compatible with the lowest estimate of all may be pooled to get an improved estimate of the noise level.

4. All meteorological series contain a random, or noise, component and it is worthwhile considering how this arises. The part which is derived from instrumental errors, or errors involved in rounding observed values to a fixed number of decimal places is truly random, but there is another source which is far more important. To take an example, in Section 15 it is shown that the noise in a long series of Kew daily mean temperatures has variance almost exactly equal to 1°C^2. In Section 17 the noise variance in Kew monthly mean temperatures is found to be 1.50°C^2. Of this only about 0.03°C^2 can originate from the noise of the daily temperatures, averaged in groups of 30, so we have to account for the other 1.47°C^2.

Now, as shown in Section 3, any series of monthly mean temperatures can be represented as the sum of sine waves of period 2 months (= 60 days) or more, while to represent daily mean temperatures we have to use waves of period 2 days and upwards. Suppose the daily temperatures are represented in this way, and consider the effect of averaging in groups of 30 on the individual sine waves. Waves of period less than 60 days disappear entirely. and are replaced by contributions to longer wavelengths: waves of period somewhat greater than 60 days survive but with reduced amplitudes while waves of period much more than 60 days are hardly affected. The net result is to inflate the noise component in the series of monthly data. In fact, as the figures above show, the noise element in the monthly mean temperatures is nearly all due to the operation of averaging over monthly intervals, which randomises oscillations with frequencies near the cut-off frequency. It follows that if we find that the series we are examining has an objectionably high noise level, we may be able to reduce the noise level by using the same data but with observations taken at a much shorter time interval and then filtering out the unwanted high frequency variations which before were randomised by the averaging. An example of this is given in Section 24.

5. It may seem artificial to some readers to pay so much attention to the noise component when we know that this is not essentially random at all, but is due to physical processes just as much as the variations we wish to study. However, the noise component, which is unpredictable, and can only be treated statistically, is the price we pay for condensing a multitude of raw data into a far smaller number of averaged data which are easier to handle and to understand. If we overdo the averaging and find that the noise level is objectionably high, we can always go back and use data averaged over shorter time intervals.

The practical design of filters

6. The idea of filtering time series is not new and has been discussed by the Labroustes (1936) who were concerned with filters suitable for use by hand computers, and by Vercelli (1940) who had a mechanical analyser. Unlike these authors, we have electronic computing facilities, and can consider simply what it is worthwhile to do without having to tailor our methods to fit the means of execution. More or less efficient filters have been used by many authors for specific purposes. For example, the ordinary 30-year running mean is a smoothing filter, while Carruthers' periodoscope (1944) is a band pass filter.

7. The operation of filtering, which a radio engineer carries out by means of a tuned circuit, is performed on a time series by means of a moving weighted average. Symmetric filters are additive, in the sense that the sum of the output series from two symmetric filters is exactly equal to the output from the sum of the two filters. This is a great convenience in designing filters, since it enables us to modify an experimental filter progressively towards a desired form, so this paper deals only with symmetric filters.

Let $x_1\ x_2 \ldots x_N$ be our time series and $(w_0, w_1, w_2 \ldots w_K)$ a symmetric filter. Then the operation of generating a new series by the relation

$$y_n = \sum_{j=0}^{K} \frac{1}{2} w_j \left(x_{n-j} + x_{n+j}\right) \tag{9}$$

is called filtering the x-series with the filter $(w_0, w_1 \ldots w_K)$ and the y-series is the output series. The y-series is shorter than the x-series both at the beginning and the end by K terms. This loss is inherent in the use of symmetric filters, but it may be inconvenient if for example the intention is to predict the extension of the x-series. In this important but rather specialised application, it may be preferable to use asymmetric filters.

8. Consider now the periodic function

$$x = A\cos(2\pi f t + \phi) \tag{10}$$

for which
$$x_n = A\cos(2\pi f n\alpha + \phi) \tag{11}$$

Operating on this with the symmetric filter $(w_0, w_1 \ldots w_K)$ gives

$$y_n = \sum_{j=0}^{K} \frac{1}{2} w_j \left\{ A\cos(2\pi f\, \overline{n-j}\, \alpha + \phi) + A\cos(2\pi f\, \overline{n+j}\, \alpha + \phi) \right\} \tag{12}$$

$$= A\cos(2\pi f n\alpha + \phi) \sum_{j=0}^{K} w_j \cos 2\pi f j\alpha \tag{13}$$

Thus the effect of filtering is to leave unchanged the period and phase of the original oscillation, and to multiply the amplitude by a factor

$$M(f) = \sum_{j=0}^{K} w_j \cos 2\pi f j \alpha \qquad (14)$$

As shown already, any series with terms at a time interval α can be represented by the sum of harmonics with frequencies not exceeding $\frac{1}{2\alpha}$ so that we need only examine the variations of $M(f)$ for $(0 \leqslant f \leqslant \frac{1}{2\alpha})$. Further, we can usually choose our time unit to be unity, and then we have to study the variations of

$$M(f) = \sum_{j=0}^{K} w_j \cos 2\pi j f \qquad (15)$$

$$\text{for } (0 \leqslant f \leqslant \tfrac{1}{2})$$

9. To produce a perfect filter, which passes all waves in a particular frequency band with their true amplitudes and completely eliminates waves of any other frequency we require that M(f) should take specified values at every point of the range $(0 \leqslant f \leqslant \frac{1}{2})$. Since the symmetric filter $(w_0 . w_1 . . . . w_K)$ contains only K + 1 arbitrary constants we cannot satisfy this requirement exactly, but if we choose a reasonable value of K and require M(f) to take the intended value at K + 1 suitably chosen frequencies, we can arrive at a satisfactory approximation.

What I did was to choose a value of K (namely, 6) and then select my K + 1 fitting frequencies spread over the range (0,1/2). Then I considered the K + 1 elementary filters (1, 0, 0 - ---- 0), (0, 1, 0 - ----- 0) .... (0, 0, --- 0,1) and for each of these wrote down the magnification factor at each of the fitting frequencies. Then I found the K + 1 linear combinations of these elementary filters each of which gives a magnification factor of unity at one of the fitting points and zero at all the others. These combinations (of which Filters No. 71 ----76 and 92 are an example, see Table 2 or 3 or Fig. 9) form a set in which each member passes a rather narrow frequency band and has zero acceptance at the peak frequencies of all the other bands. The output series from any two of the set are almost confined to different frequency bands and are almost uncorrelated, while the sum of the output series from all filters in the set is algebraically equal to the original series. Filters having the property that when applied to a random series they produce uncorrelated output series may be termed orthogonal.

Once we have produced such a set, which represents the maximum resolving power possible with the chosen value of K, the members can be added to produce a filter passing a broader frequency band.

Within limits, the investigator can choose the fitting points to preserve or annul harmonic components known to be present. For example, Filters No. 17 and 117, which annul the 12-term periodicity, are more suitable for use in climatic studies based on monthly mean data than is Filter No. 92 which resembles them except that it annuls the 10-term periodicity.

Finally, if one filter is applied to the output series of another, then the magnification factor for the resultant is equal to the product of those of the two filters. This fact can be used to modify imperfect filters by introducing extra zeros and affords a method of building up complicated filters from simple ones which is less laborious for large values of K than the direct method I have described.

However, I had to remember that the time series I was studying might not be statistically stationary, and decided that the 13-point filters I had produced directly (which are listed in the Appendix) were neither too long nor too short for exploratory work. The frequency response curves for ten typical filters are given in Fig. 9.

/The

The statistical analysis of filtered series

10. Our statistical treatment starts from the null hypothesis that the original series shows nothing but noise and is composed in fact of random drawings from a normal distribution. If then we apply in turn a number of mutually orthogonal filters, each filter will give us an independent estimate of the noise variance, and these estimates may be compared by means of Snedecor's F-test as described, for example, by Brooks and Carruthers (1953).

If $V(x)$, $V_w(y)$ are the variances of the original data assumed to be random and of the M terms of the output series from the filter $(w_0, w_1 \cdots w_K)$ (see equation (9)) then

$$V_w(y) = \frac{1}{M}\sum_{j=1}^{M} y_n^2 \tag{16}$$

$$= \frac{1}{M}\sum_{j=1}^{M}\left(\tfrac{1}{2}x_{n-K}w_K \cdots + \tfrac{1}{2}x_{n-1}w_1 + x_n w_0 + \tfrac{1}{2}x_{n+1}w_1 \cdots + \tfrac{1}{2}x_{n+K}w_K\right)^2$$

$$= V(x)\left\{w_0^2 + \tfrac{1}{2}\sum_{j=1}^{K} w_j^2\right\} \tag{17}$$

Thus if we put $P(w) = \left\{w_0^2 + \tfrac{1}{2}\sum_{j=1}^{K} w_j^2\right\}$

and call it the filter factor

then $$V(x) = \frac{V_w(y)}{P(w)} \tag{18}$$

Thus we obtain an estimate of the variance of the original series on the null hypothesis by measuring the variance of the output series and dividing by the filter factor: this will be called the normalised variance of the filtered series.

11. To compare two such estimates by means of the F-test, we must attach to each the appropriate number of degrees of freedom.

Now a series $x_1\, x_2\, x_3 \cdots x_N$ derived by random drawings from a normal distribution must have N degrees of freedom. If this series is broken up by a set of orthogonal filters into uncorrelated components which when summed add up to the original series, then the N degrees of freedom must be distributed among the component series,

$$N = N_1 + N_2 \cdots \tag{19}$$

where the ratio N_1/N is determined only by the weights $(w_0 \cdots w_K)$ of the first filter, the ratio N_2/N by those of the second, and so on.

Now we can look on the N degrees of freedom as being attached not to the terms of the series, but equally well to the N harmonic components by which the series can be uniquely represented: and on the null hypothesis these harmonics are on average of equal amplitude. If now we have a perfect filter, which preserves N_1 of these harmonics while suppressing the remainder, then it seems to me beyond doubt that the number of degrees of freedom of the filtered series is N_1, the number of independent harmonics which enter into it. Our problem, therefore, is to relate N_1 to the weighting coefficients which make up the filter.

Now for a perfect filter, M(f) is unity for frequencies within the band passed by the filter, and zero elsewhere, and since the harmonics are spaced equally in the frequency range $(0, \frac{1}{2})$

$$\frac{N_1}{N} = \frac{\int_0^{\frac{1}{2}} M(f)\,df}{\int_0^{\frac{1}{2}} 1.\,df} \tag{20}$$

and
$$\frac{N_1}{N} = \frac{\int_0^{\frac{1}{2}} (M(f))^2\,df}{\int_0^{\frac{1}{2}} 1.\,df} \tag{21}$$

Both these expressions give the right answer for a perfect filter, and we have to decide which is right when our filter is not perfect. Bearing in mind that the larger the number of degrees of freedom the larger the expected variance, and that a negative value of M(f), implying a phase reversal at the frequency in question, will still represent a positive contribution to the variance, I think that equation (21) which in these conditions gives a positive contribution to the number of degrees of freedom, must be the correct form.

Thus by equation (15)

$$\frac{N_1}{N} = 2\int_0^{\frac{1}{2}} \left(\sum_{j=0}^{K} w_j \cos 2\pi j f\right)^2 df \tag{22}$$

$$= P(w) \tag{23}$$

so that $N_1 = N.P(w)$ (24)

This derivation may not seem entirely convincing, but there is no doubt that the problem posed by equation (19) must have a solution, and it is hard to see what the solution can be, other than this.

At any rate, the conclusion leads to sensible results in practice, and the margin of uncertainty, which is present only with imperfect filters, can be reduced by improving the filters. In the present work many of the variance ratios we wish to test range from 5 to over 100, so that a small uncertainty about numbers of degrees of freedom does not matter much.

12. We are now able to split a series up into components which on the null hypothesis are uncorrelated, and to attach the appropriate number of degrees of freedom to each filtered component. This opens the way to the solution of an unsolved problem of great importance in meteorology, namely, that of judging the significance of the correlation between two time series which are themselves autocorrelated. If the original series are analysed by a set of orthogonal filters, and are represented as the algebraic sum of uncorrelated components, then, since it is impossible for an oscillation in one frequency band to be correlated with an oscillation in any other band, the original covariance must be due to a correlation between one or more of the corresponding pairs of components passed by the same filter. It may even happen that the correlation is positive in certain wavebands and negative in others, and that the overall correlation appears to be small although one series is in fact highly dependent on the other.

In any case, the argument of Section 11 enables us to attach a number of degrees of freedom to and hence to judge the significance of the correlation between the output series obtained by the use of the same filter.

Practical examples

13. In the next sections, the methods already described will be applied mainly on meteorological data. The actual operation of filtering is laborious to carry out by hand, since a separate calculation consisting of multiplication with summation has to be done to get each term of the filtered series. However, it is very easy to carry out electronically, and all the results given were obtained on the Elliott Bros. 401 Computer operated at the Rothamsted Experimental Station. The machine was programmed to accept a data tape followed by a filter, and to output the filtered series followed by its mean, variance and standard deviation, the estimated variance on the null hypothesis given by equation (20), and the appropriate number of degrees of freedom given by equation (24).

The electronic computation was entirely unchecked, and any machine failure would be liable to affect the results. This risk was taken to save time, since previous work had shown this machine to be extremely reliable. Further, each filtered series has a recognisable character, while the results themselves can be roughly tested by eye. Apart from results affected by known punching errors or vitiated, for example, through the capacity of the machine having been exceeded, none of the output figures gave any suggestion of serious machine failure. I think that there is only the smallest chance that any of the results mentioned here should be misleading owing to an undetected machine fault.

14. The first data consisted of a series of 112 random numbers drawn from an effectively normal distribution. In fact they were made on the Manchester University Mark 1 Electronic Computer, by producing groups of 400 random binary digits from the random number generator, and counting the number of unit digits among them. These numbers should be distributed about a mean of 200 with standard deviation of 10. The details of the analysis are given in Table 1.

Table 1. Filter analysis of random numbers drawn from a normal distribution

Filter no.	Peak frequency	Filter factor	Normalised variance $^\circ C^2$	Degrees of freedom
17	0	.0798	8.5	8
31	1/12	.1527	10.5	15
21	1/6	.1528	6.3	15
35	$\frac{1}{4}$	.1528	12.2	15
14	1/3	.1528	10.8	15
33	5/12	.1527	13.8	15
24	$\frac{1}{2}$	.0798	14.1	8

It will be seen that none of the normalised variances differs significantly from the expected value, 10, nor does the ratio of any one to any other exceed even the 5 per cent significance level. This analysis gives no ground whatever for doubting the null hypothesis that the original series is as random as it was intended to be. The original series and the filtered series are plotted out in Fig. 1 to give an impression of the appearance of series covering these particular wavebands. The series passed by Filter No. 24 shows curious variations in amplitude suggesting a real wave with period nearly equal to twice the interval between the terms. However, all series passed by this filter have this appearance, which must be mathematical in origin and cannot be taken as evidence of the physical existence of such a wave.

15. An analysis was made of daily mean temperature anomalies at Kew. 377 daily values were taken, each the mean of 24 hourly observations, covering the year 1955 with six extra terms at each end, so that the filtered series should cover the calendar year. The annual and semi-annual variations were removed by subtracting daily normals obtained by fitting a two term harmonic form to mean temperatures averaged over the 50 years 1901-1950. This should not affect the frequencies studied in the present analysis, of which details are given in Table 2.

/Table 2.

Table 2. Filter analysis of Kew daily mean temperatures for 1954

Filter no.	Peak frequency	Filter factor	Normalised variance $^{\circ}\mathrm{C}^2$	Degrees of freedom
71	$\frac{1}{2}$	.0852	0.95	31
72	$^{2}/_{5}$	.1493	1.03	54
73	$^{1}/_{3}$	.1516	1.64	55
74	$\frac{1}{4}$	.1502	2.49	55
75	$^{1}/_{6}$	.1516	5.39	55
76	$^{1}/_{10}$	.1493	13.63	54
92	0	.0852	46.59	31

The normalised variances strongly contradict the null hypothesis, in that while the outputs for the higher frequencies are mutually compatible, those for all longer periods are not. They show that significant atmospheric fluctuations exist with peak frequency $^{1}/_{10}$ or less (i.e., with period 10 days or more).

The output from Filters No. 71 and 72 can be pooled to give an estimate of the noise variance of Kew daily mean temperatures of 1.00$^{\circ}\mathrm{C}^2$, based on 85 degrees of freedom. Sections of some of the filtered series are plotted out in Fig. 2.

16. The next stage was to analyse Kew temperatures averaged over non-overlapping periods of 5 days. Again, a series of 377 terms was used, covering the five years 1946-50 with six extra terms at each end. The daily values were estimated as $\frac{\max + \min}{2}$ and the annual and semi-annual variations were removed as before. Details of the analysis are given in Table 3, and sections of the filtered series are given in Fig. 3.

Table 3. Filter analysis of Kew 5-day mean temperatures for 1946-1950

Filter no.	Peak frequency	Filter factor	Normalised variance $^{\circ}\mathrm{C}^2$	Degrees of freedom
71	$\frac{1}{2}$	.0852	2.79	31
72	$^{2}/_{5}$	.1493	2.15	54
73	$^{1}/_{3}$	.1516	3.27	55
74	$\frac{1}{4}$	.1502	4.31	55
75	$^{1}/_{6}$	.1516	7.92	55
76	$^{1}/_{10}$	.1493	10.55	54
92	0	.0852	20.48	31

These variances again contradict the null hypothesis and show that there are significant atmospheric fluctuations with periods of 30 to 50 days or more.

17. The analysis is continued on Kew monthly mean temperatures for the years 1921-50 given by Marshall (1952), and is summarised in Table 4.

Table 4. Filter analysis of Kew monthly mean temperatures for 1921-1950

Filter no.	Peak frequency	Filter factor	Normalised variance $^{\circ}\mathrm{C}^2$	Degrees of freedom
24	$\frac{1}{2}$	.0798	1.35	28
33	$^{5}/_{12}$	.1527	1.43	53
14	$^{1}/_{3}$	.1528	1.63	53
35	$\frac{1}{4}$	.1528	1.53	53
21	$^{1}/_{6}$	.1528	3.69	53
31	$^{1}/_{12}$	.1527	151.7	53
17	0	.0798	3.21	28

It appears that the variance in the bands centred on periods of 2, 2.4, 3 and 4 months are compatible, and can be pooled, giving a joint estimate of the variance of the random component of Kew monthly mean temperature, based on 187 degrees of freedom of 1.502°C².

The 6-monthly component, the semi-annual variation is significantly greater than this (at the 1 per cent level) while the annual variation is much greater still. The components of longer period passed by Filter No. 92, which may be termed the interannual variations, are also significantly larger than expectation, in about the same ratio as the semi-annual variation.

18. Kew monthly temperatures for the 86 years 1871-1956 taken from Marshall (1952) were averaged over 3-monthly periods to give the next series for analysis, of which the results are summarised in Table 5.

Table 5. Filter analysis of Kew 3-monthly mean temperatures for the years 1871-1956

Filter no.	Peak frequencies	Filter factor	Normalised variance °C²	Degrees of freedom
40	$\frac{1}{2}$, $\frac{1}{4}$	.2465	77.00	81
41	5/12, 1/3	.3334	.75	110
21	1/6	.1528	.91	50
31	1/12	.1527	.99	50

The special Filter No. 40 used on 3-monthly data passes the annual and semi-annual variation with their true amplitudes. Filter No. 41 passes a band of periods between about 7 and 9 months, which is very hard to examine because of its proximity to two much larger oscillations. However, it does not appear to have significantly greater power than the bands centred around 18 months or 36 months and these estimates can be pooled to give one estimate of the variance of 3-monthly mean temperatures at Kew of 0.843°C² based on 210 degrees of freedom.

19. Finally, the analysis was applied to the annual mean temperatures for Central England for the years 1698-1952 as estimated by Manley (1953). Manley's data were used instead of the shorter series of annual mean temperatures at Kew, because by making the numbers of degrees of freedom as large as possible the maximum resolution is obtained among the fluctuations on the longer time scales. Details are given in Table 6.

Table 6. Filter analysis of annual mean temperatures estimated by Manley (1953) for Central England for the years 1698-1952

Filter no.	Peak frequency	Filter factor	Normalised variance °C²	Degrees of freedom
24	$\frac{1}{2}$	.0798	.421	19
33	5/12	.1527	.244	37
14	1/3	.1528	.288	37
35	$\frac{1}{4}$	.1528	.239	37
21	1/6	.1528	.299	37
31	1/12	.1527	.415	37
17	0	.0798	.601	19

The second to fifth variances are obviously compatible, and when pooled these give an estimate of the variance of the random element in the annual mean temperatures of 0.267°C² based on 148 degrees of freedom. The output of Filter No. 24 has a ratio to this estimate of 1.58 which is about on the 5 per cent level for significance. The output of Filter No. 31 has a ratio of 1.55 which is significant at a level between 5 and 1 per cent. The output of Filter No. 17 has a ratio of 2.25 which is significant at the 1 per cent level.

These annual data thus provide three features of interest, namely

(1) a tendency for alternation of years. This is only just significant,

and, until supporting evidence is produced, it would be as well to treat it with reserve

(2) significant oscillations are passed by Filter No. 31 which has peak frequency at $^1/12$, and zeros at $^1/6$ and 0. If there were significant temperature oscillations related to the 11-year sunspot fluctuation, they would certainly show up in this frequency band, but it would be unjustifiable at this stage to assume the existence of a causal relationship; the question can be tested by finding the correlation between this filtered series and a similar series of filtered sunspot numbers and judging its significance as suggested in Section 12

(3) there is a significant variation on the longest time scale, passed by Filter No. 17, which may reasonably be regarded as climatic change. The non-normalised variance passed by this filter is only $0.048^\circ C^2$, so that the climatic change is not very impressive in magnitude.

20. The variations of Kew temperatures have been discussed for several different wavebands, and I will now try to fit them all together. It is not difficult to show that a 13-point filter with factor P acting on m-day mean data produces the same variance as a 13m-point filter with factor P/m acting on daily data; thus all the estimates of variance can be rendered comparable by multiplying them by the appropriate value of m.

These estimates can generally be plotted against the peak frequency of the filter which relates to them, but it will be seen that since, for example, Filter No. 21 which has peak frequency $^1/6$ will pass half or more of any oscillation in the frequency range (1/5, 1/10) there is a margin of uncertainty as to what really produces the variance in question. Also, as regards the lowest frequencies of all, the output of Filter No. 17 which passes the oscillations with period much exceeding 12 years must be allotted to some frequency within the range which can be resolved by a series of data covering no more than 255 years. In all cases, uncertainty about the details of the oscillations producing any estimate of variance can be removed by simply plotting the filtered series.

The normalised variances vary in the range of 1 to 250, while the interesting variations are all at the low frequency end of the spectrum. Consequently, a plot of log V_n against log f displays the information more clearly than would a linear plot, and is used in Fig. 4.

Of the 28 points, 25 lie very nearly on a smooth curve. The other three give the familiar annual and semi-annual variation, and the biennial variation mentioned in Section 21. If this biennial variation were spurious, due to the randomising of higher frequency variations in forming the annual means, then the adjacent points on the curve would be affected in the same way, whereas in fact they agree among themselves on a lower value of the variance in this region, so with some hesitation I am inclined to regard the biennial variation as real.

If a series of random numbers was analysed in the same way the resulting graph would be horizontal, so that the presence of horizontal stretches in the graph in Fig. 4 would indicate the existence of frequency bands not characterising the operation of any specific physical processes, i.e., bands in which the variations were due entirely to the chance superposition of oscillations of higher frequency. In fact the graph does not encourage us to think that there are any such flat regions, but suggests that positive contributions to variation are occurring on every possible time scale.

21. While Fig. 4 is convenient for showing variances on every time scale, it does not show them in true relation of magnitude. To do this we plot V_n against log f and obtain an "equal area" graph in the sense that frequency bands enclosing equal areas under the curve will correspond to oscillations of equal amplitude. This is done in Fig. 5. This shows quite clearly that the most important temperature fluctuations at Kew lie in the middle band of frequencies, in the range of periods from about 5 to 60 days. The smooth curve drawn among the points is obtained by transforming that in Fig. 4. Apart from the annual, semi-annual and biennial components mentioned already, the smooth curve gives a fairly good

fit to the wings of the curve, but near the peak it gives values which differ considerably from those observed. It is difficult to avoid the conclusion that the power spectrum at Kew has two peaks centred about periods of 10 and 35 days. The dotted curve drawn freehand to follow the observations is probably nearer to the truth. It is clear in any event that the peak is a fairly broad one, and that (excluding the astronomical components) perhaps two thirds of the variance of atmospheric temperature fluctuations at Kew is associated with periods of between 5 and 60 days.

The lower peak at about 10 days may depend on the movement of long waves in the westerlies. As regards the peak at 35 days, it appears from work by Craddock and Lowndes (1956) that fluctuations on about this time scale are large in amplitude and in geographical extent over the greater part of the Northern Hemisphere, and that they appear to be associated with abnormalities in the general circulation of the westerlies. There is thus a presumption that at Kew apart from the annual and semi-annual variations the largest fluctuations to which the atmosphere is subject are associated with two types of variation in the general circulation.

22. It is interesting to compare Fig. 5 with a very similar graph published by Griffith, Panofsky and van der Hoven (1956) based on data for University Park, Pennsylvania. Their graph shows peaks at about 12, 38 and 900 days of which the first two probably correspond to our peaks at 10 and 35 days.

The peak at 900 days is not beyond doubt, because the American low frequency values are based on data for a much shorter period of years than ours, and are subject to wider sampling fluctuations. However, it may correspond to our peak at about 730 days.

The American results also give a very pronounced peak at about 4 days of which there is no sign in Fig. 5. This is not due to any fault in the present calculation because, as Fig. 2 shows, the filtered series show that at Kew there is no peak amplitude at this frequency. Also comparing the peaks near 10 and 35 days, the second is relatively larger at Kew than it is in Pennsylvania.

These differences point to deep seated differences between the workings of the atmospheric heat engine at the two places which, in view of the differences in latitude and geographical situation, is not really surprising.

23. To finish this discussion of Kew temperatures Fig. 6 and 7 show the actual course of the fluctuations in the wave bands which are most interesting. Bearing in mind that the fluctuations must lie within certain limits to be passed by the filter at all, they show almost as much irregularity as it is possible to imagine. There is no consistency either in period or amplitude, although on average the amplitudes are so large that it is impossible for any meteorologist to ignore them.

The prediction of the course of such intractable series is bound to be difficult, whether looked at from the physical or the statistical standpoint, but is made somewhat less formidable by the fact that the longer of these oscillations are so slow that a forecast covering no more than a single wavelength would have practical value. This topic, however, is outside the scope of the present paper.

24. A final example shows the value of filtering analysis in the study of climatic change. The basic data are monthly mean temperatures for Bear Island for the years 1923-June, 1941. These observations cover only 18½ years and if annual averages are taken only 18 degrees of freedom will be left, far too few for us to be able to find anything of interest. However, we filter the monthly mean temperatures for the 18½ years with three filters, one passing waves of period up to four months, the next the semi-annual and the annual period and the third only the waves of period exceeding 12 months. In the first and last the annual and semi-annual waves are annulled entirely. The results are given in Table 7, and the series are displayed in Fig. 8.

/Table 7.

Table 7. Filter analysis of Bear Island monthly mean temperatures to show inter-annual variations

Filter no.	Peak frequencies	Filter factor	Normalised variance $^{\circ}C^2$	Degrees of freedom
115	$\frac{1}{2}$, $2/5$, $\frac{1}{2}$, $\frac{1}{4}$	.5879	3.52	123
114	$1/6$, $1/12$	.3334	58.85	70
117	0	.0797	15.60	17

It appears that the variance in the longer wavelengths is decisively larger than the chance expectation, so that we have evidence of significant inter-annual temperature variations. There is a minimum in the late 1920's and a maximum in the late 1930's followed by a sharp fall. There is also a strong suggestion of an oscillation of smaller amplitude of period 3 to 4 years.

These features deserve further study but need not delay us here: the important fact is that it has been possible to identify them at all in data covering so short a period.

Conclusion

25. The main object of this work has been to describe a method of analysis applicable to a very wide range of meteorological time series without assuming the series to be stationary in the statistical sense. The features for which novelty is claimed are

(1) the use of orthogonal filters covering the whole range of possible frequencies,

(2) the comparison of the variance of the output from different filters by means of the variance ratio test, and

(3) the use of comparatively short filters to avoid obscuring the transient features of a non-stationary time series.

The literature shows a dearth of worthwhile analyses of meteorological data and the whole project, both theoretical and practical, had to be planned with very little prior knowledge of the probable outcome. Nevertheless, the results though intended primarily to indicate the flexibility of the method are of considerable practical importance.

To the meteorologist they indicate the time scales on which long range forecasting research is most likely to yield worthwhile returns, while they show the statistician that the mass of statistical theory concerned with stationary time series is not readily applicable to the main problems of synoptic meteorology.

Acknowledgments

Acknowledgments are due to Messrs. M. J. R. Healy and Mr. D. Rees of Rothamsted Experimental Station for assistance in getting the electronic programmes to work and in carrying out the machine calculations.

References

Brooks and Carruthers	1953	Handbook of Statistical Methods to Meteorology, M.O.538 H.M.Stationery Office, London, 1953
Carruthers, N.	1944	Quart. J. R. Met. Soc., London, Vol. 70, p.141
Craddock and Lowndes	1956	Meteorological Research Papers, Air Ministry, London, No. 994
Griffith, Panofsky and van der Hoven	1956	J. Met., Lancaster, Pennsylvania, Vol.13, pp. 279-282
Labrouste, H. and Mrs.	1938	Terr.Mag., London, Vol.XLI, pp.15-28 & 105-126
Manley, G.	1953	Quart. J. R. Met. Soc., London, Vol.79, pp.242-26
Marshall	1952	A Century of London Weather
Vercelli, F.	1940	R. Comitato Talassografico Italiano, Venezia, Memoria 285

Appendix. Sets of 13-point band pass filters used in the analysis

Each of these sets has the following properties

(1) when any two of the set are applied in turn to a series obtained by random drawings from a normal distribution the two output series are almost uncorrelated (i.e., the members of the set are mutually almost orthogonal)

(2) each filter has zero acceptance at the peak frequencies of all other members of the set and unit acceptance at its peak frequencies and

(3) when all members of the set are applied to one data series in turn, the algebraic sum of all the output series is equal to the original series.

Set 1

Filter refce. number	Coefficients							Peak frequency	Filter factor
71	.1063	-.2127	.1897	-.1667	.1437	-.1206	.0603	½	.0852
72	.1708	-.2764	.1708	0	-.1708	.2764	-.1708	2/5	.1493
73	.1273	-.1273	-.2060	.3333	-.1273	-.2060	.2060	1/3	.1516
74	.1910	0	-.3090	0	.3090	0	-.1910	¼	.1502
75	.1173	.1273	-.2060	-.3333	-.1273	.2060	.2060	1/6	.1516
76	.1708	.2764	.1708	0	-.1708	-.2764	-.1708	1/10	.1493
92	.1065	.2127	.1897	.1667	.1435	.1206	.0603	0	.0852

Set 2

Filter refce. number	Coefficients							Peak frequency	Filter factor
24	.0833	-.1667	.1667	-.1667	.1667	-.1667	.0833	½	.0798
33	.1667	-.2887	.1667		-.1667	.2887	-.1667	5/12	.1527
14	.1667	-.1667	-.1667	.3333	-.1667	-.1667	.1667	1/3	.1528
35	.1667	0	-.3333	0	.3333	0	-.1667	¼	.1528
21	.1667	.1667	-.1667	-.3333	-.1667	.1667	.1667	1/6	.1528
31	.1667	.2887	.1667	0	-.1667	-.2887	-.1667	1/12	.1527
17	.0833	.1667	.1667	.1667	.1667	.1667	.0833	0	.0798

Set 3

Filter refce. number	Coefficients							Peak frequency	Filter factor
40	.2500	-.1667	-.1667	-.1667	.5000	-.1667	-.0833	¼, ½	.2465
41	.3333	-.4553	0	.3333	-.3333	.1220	0	1/3, 5/12	.3334

These two filters form an orthogonal set with Nos. 21, 31 and 17 of Set 2.

Set 4

Filter refce. number	Coefficients							Peak frequency	Filter factor
114	.3317	.4581	-.0016	-.3333	-.3317	-.1248	.0016	1/6, 1/12	.3334
115	.5874	-.6293	-.1625	.1666	.1626	-.0373	-.0875	½, 2/5, 1/3, ¼	.5879
117	.0809	.1712	.1641	.1667	.1691	.1621	.0859	0	.0797

Notation and Definitions

If $x_1, x_2 \cdots\cdots x_n \cdots\cdots$ is any time series and $(w_0\, w_1 \cdots\cdots w_K)$ is a filter, then the series $y_1\, y_2 \cdots\cdots y_n \cdots$ defined by the equation

$$y_n = \sum_{j=0}^{K} \tfrac{1}{2} w_j (x_{n-j} + x_{n+j}) \quad \cdots\cdots ①$$

is the output from the series $x_1, x_2 \cdots\cdots x_n \cdots\cdots$ from the filter $(w_0\, w_1 \cdots\cdots w_K)$.

If the x-series is strictly periodic, so that

$$x = A\cos(2\pi f t + \phi)$$

then

$$y_n = x_n . M(f)$$

where

$$M(f) = \sum_{j=0}^{K} w_j \cos 2\pi j f \quad \cdots\cdots ④$$

$M(f)$ is called the magnification factor of the filter $(w_0, w_1, \cdots\cdots w_K)$ and $M(f)$ plotted against f for $(0 \le f \le \frac{1}{2})$ is called the response curve of the filter.

If $V(x)$, $V_w(y)$ are the variances of the original data, (assumed to be a series of random numbers), and of the output series from filter $(w_0, w_1 \cdots\cdots w_K)$, then

$$V_w(y) = V(x) . P(w)$$

where

$$P(w) = \left\{ w_0^2 + \frac{1}{2}\sum_{j=1}^{K} w_j^2 \right\} \quad \cdots\cdots ⑤$$

and

$$V(x) = \frac{V_w(y)}{P(w)} \quad \cdots\cdots\cdots\cdots ⑥$$

$P(w)$ is called the filter factor and $V(x)$ estimated in this way is the normalised variance of the output series.

When a data series is operated on in turn by each of several mutually exclusive filters, then on the null hypothesis the various normalised variances are independent estimates of the same thing.

Statistical Problems

If we have N terms of the output series from filters $(\varpi_0, \varpi_1, \ldots \varpi_k)$ and the variance measured from these has N_1 degrees of freedom, how do we express N_1 as a function of N and $(\varpi_0 \varpi_1 \ldots \varpi_k)$?

I suggest that

$$\frac{N_1}{N} = 2\int_0^{\frac{1}{2}} (M(f))^2 \, df$$

which gives

$$N_1 = N.P(\varpi) \quad \cdots\cdots\cdots \quad (10)$$

This seems to be right if we have perfect filters. I assume without proof that it holds also for imperfect filters. We can, however, design filters to approach perfection as nearly as we please by taking enough trouble.

Is any adjustment necessary because to get N terms of filtered series we require N+2K terms of original data?

The null hypothesis is that the original data were obtained by random drawings from a normal distribution. How should we modify the analysis if the frequency distribution of the values making up the time series is not even approximately normal?

Daily rainfall or sunshine totals and daily or yearly totals of sunspot numbers form series of this type.

What features do we expect the power spectrum to show if the original data are drawn at random from a distribution which is not normal?

FIG. I A SERIES OF NUMBERS DRAWN AT RANDOM FROM NORMAL DISTRIBUTION ANALYSIS WITH FILTERS NOS. 24, 33, ~~14,~~ 35, 21, 31 & 17.

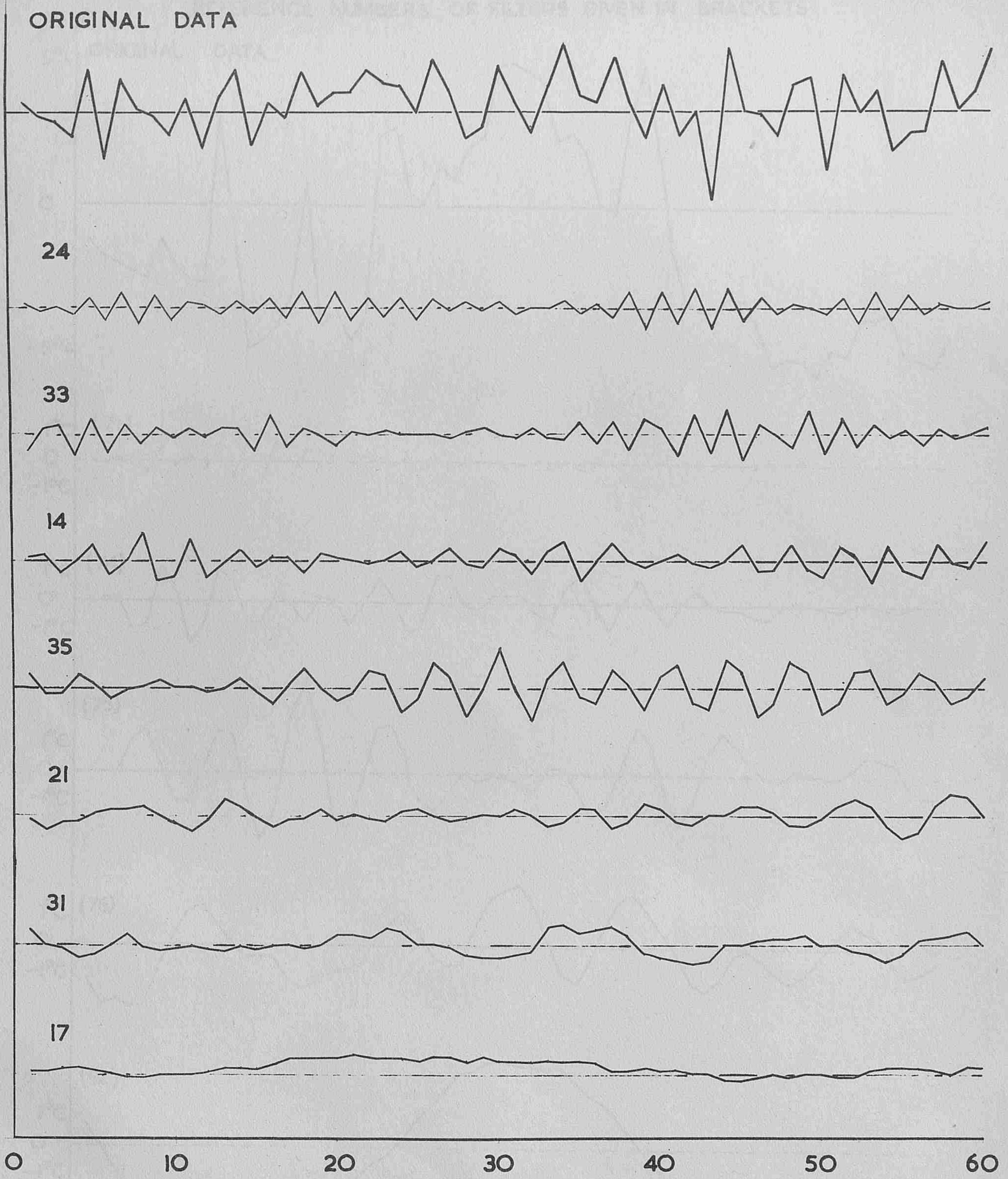

FIG. 2. FILTER ANALYSIS OF KEW DAILY MEAN TEMPERATURES FOR JANUARY AND FEBRUARY 1955. REFERENCE NUMBERS OF FILTERS GIVEN IN BRACKETS.

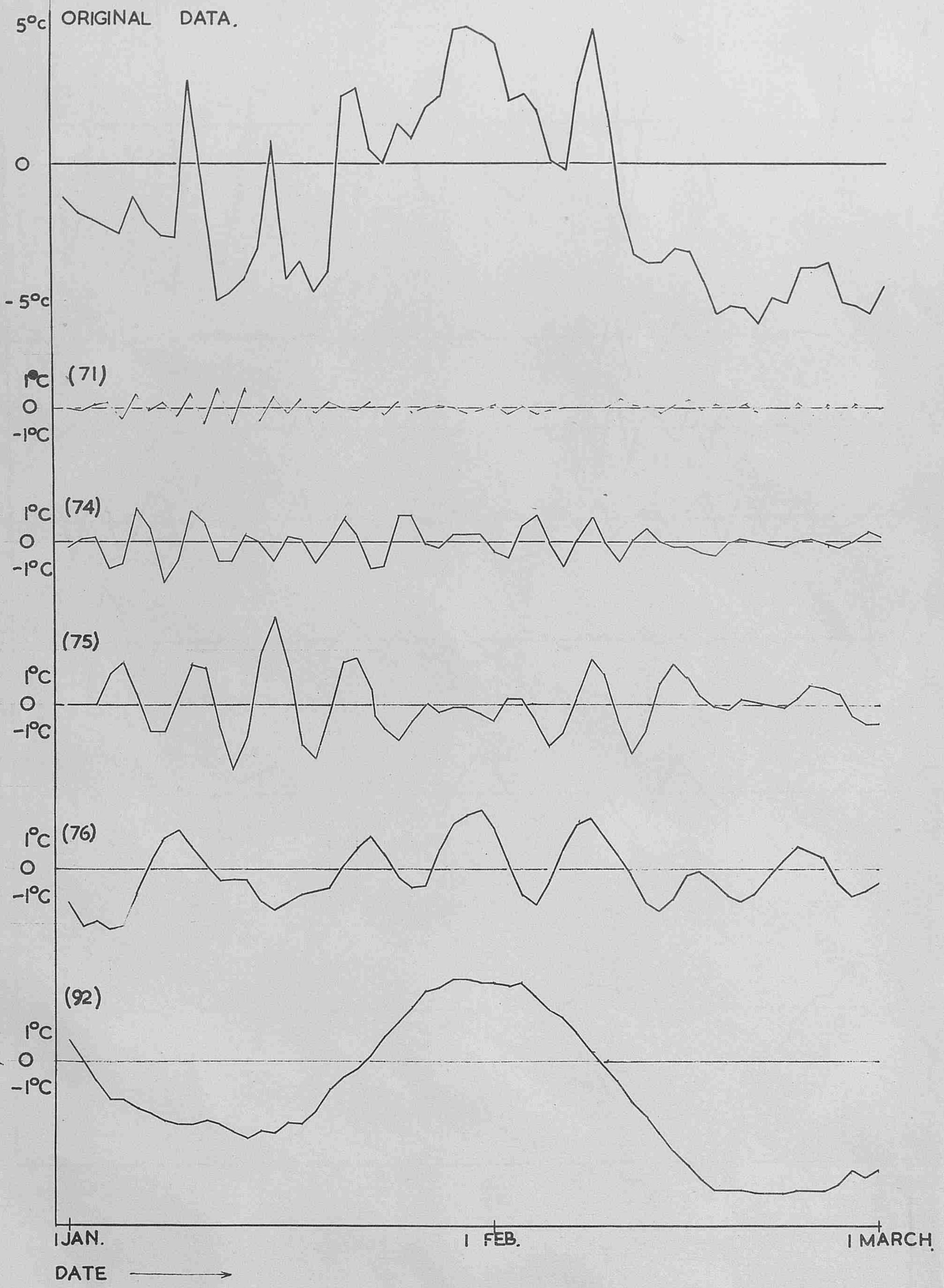

Fig 3. Filter Analysis of Kew 5-day mean temperatures for Jan-Oct 1946
Filter numbers given in margin.

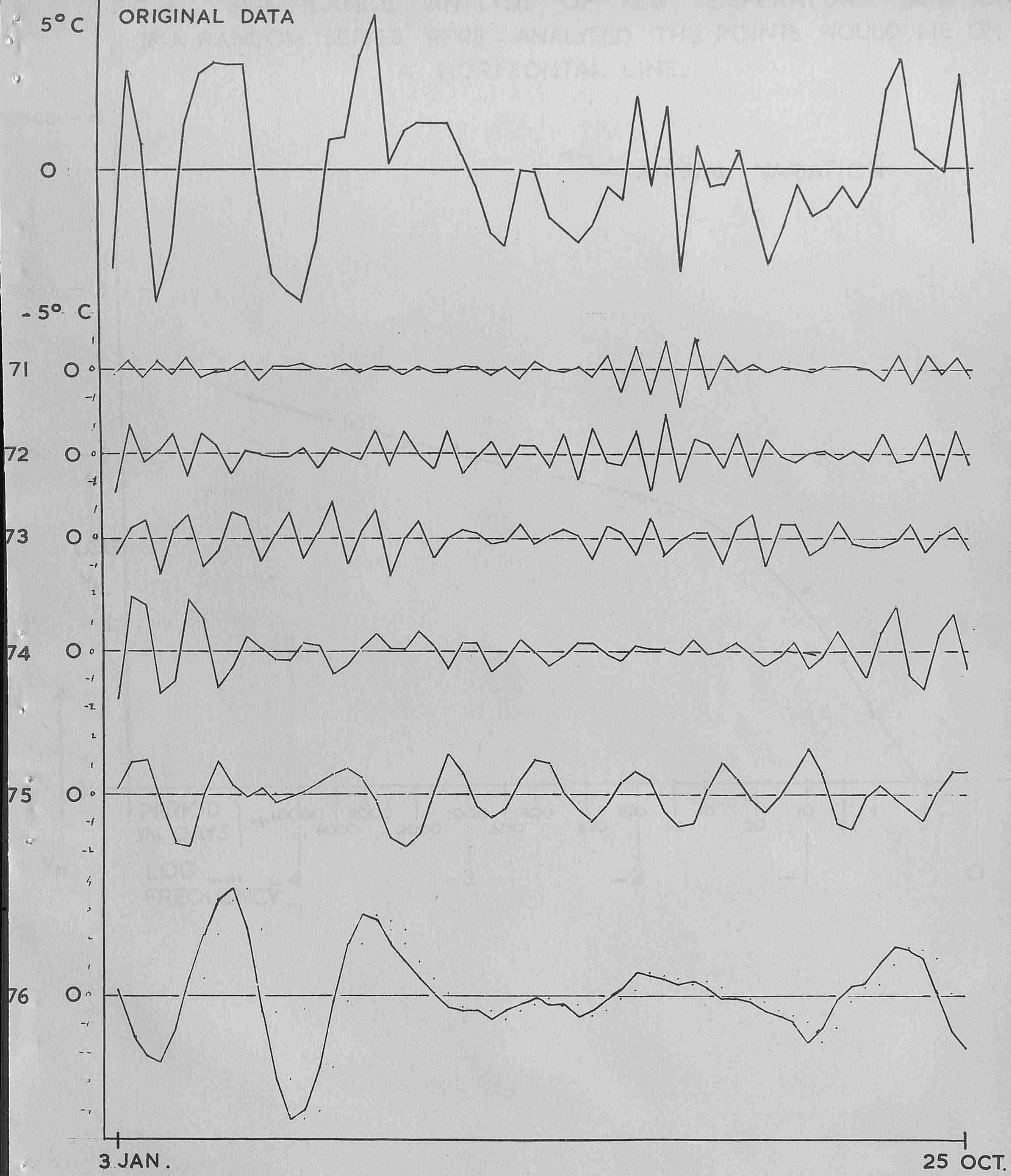

FIG. 4. SIGNIFICANCE ANALYSIS OF KEW TEMPERATURE VARIATIONS
IF A RANDOM SERIES WERE ANALYSED THE POINTS WOULD LIE ON
A HORIZONTAL LINE.

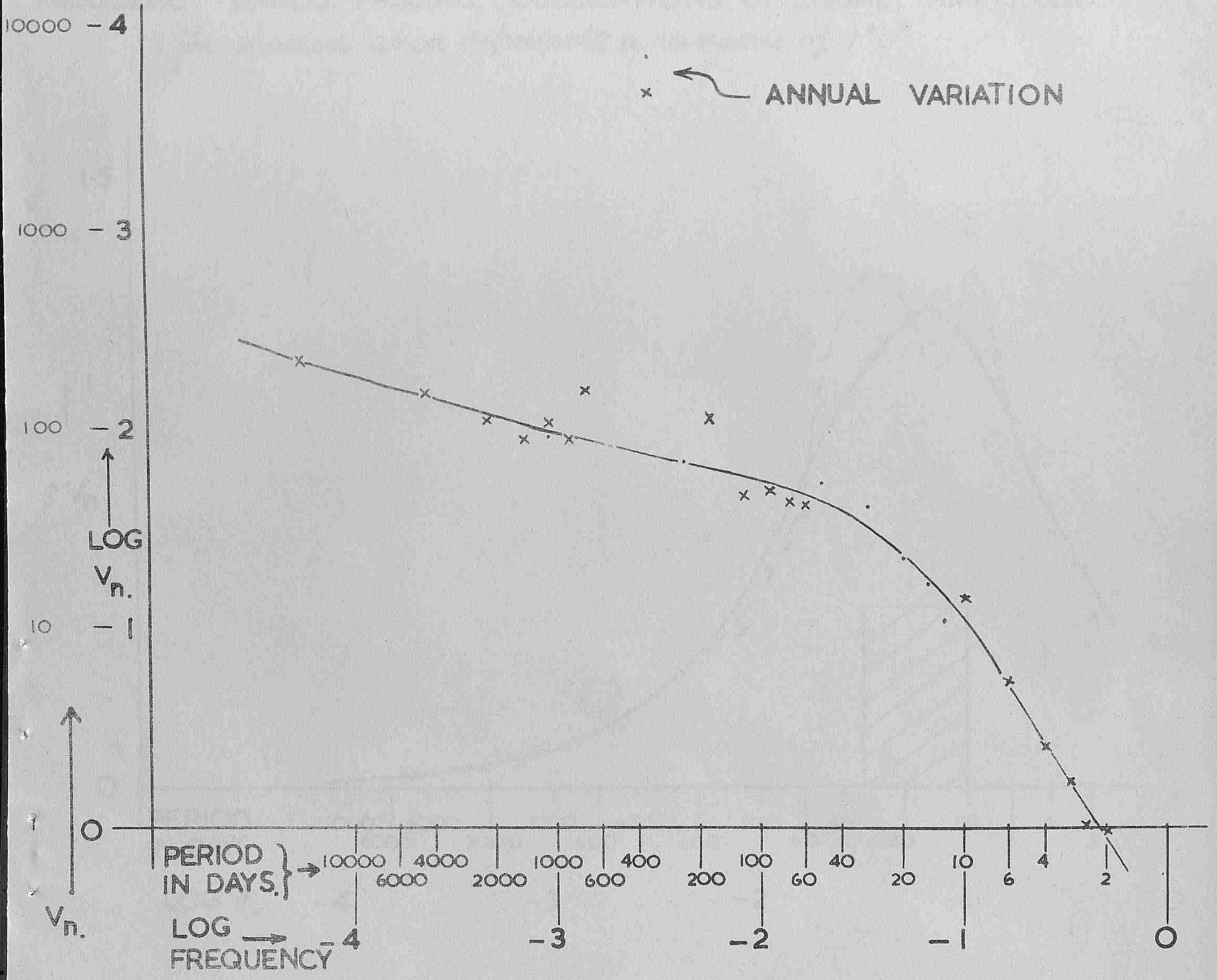

FIG. 5. POWER SPECTRUM ANALYSIS FOR KEW TEMPERATURES. ORDINATES ENCLOSING EQUAL AREAS UNDER THE GRAPH INCLUDE FREQUENCY BANDS PASSING OSCILLATIONS OF EQUAL AMPLITUDE.

The shaded area represents a variance of $1°C^2$

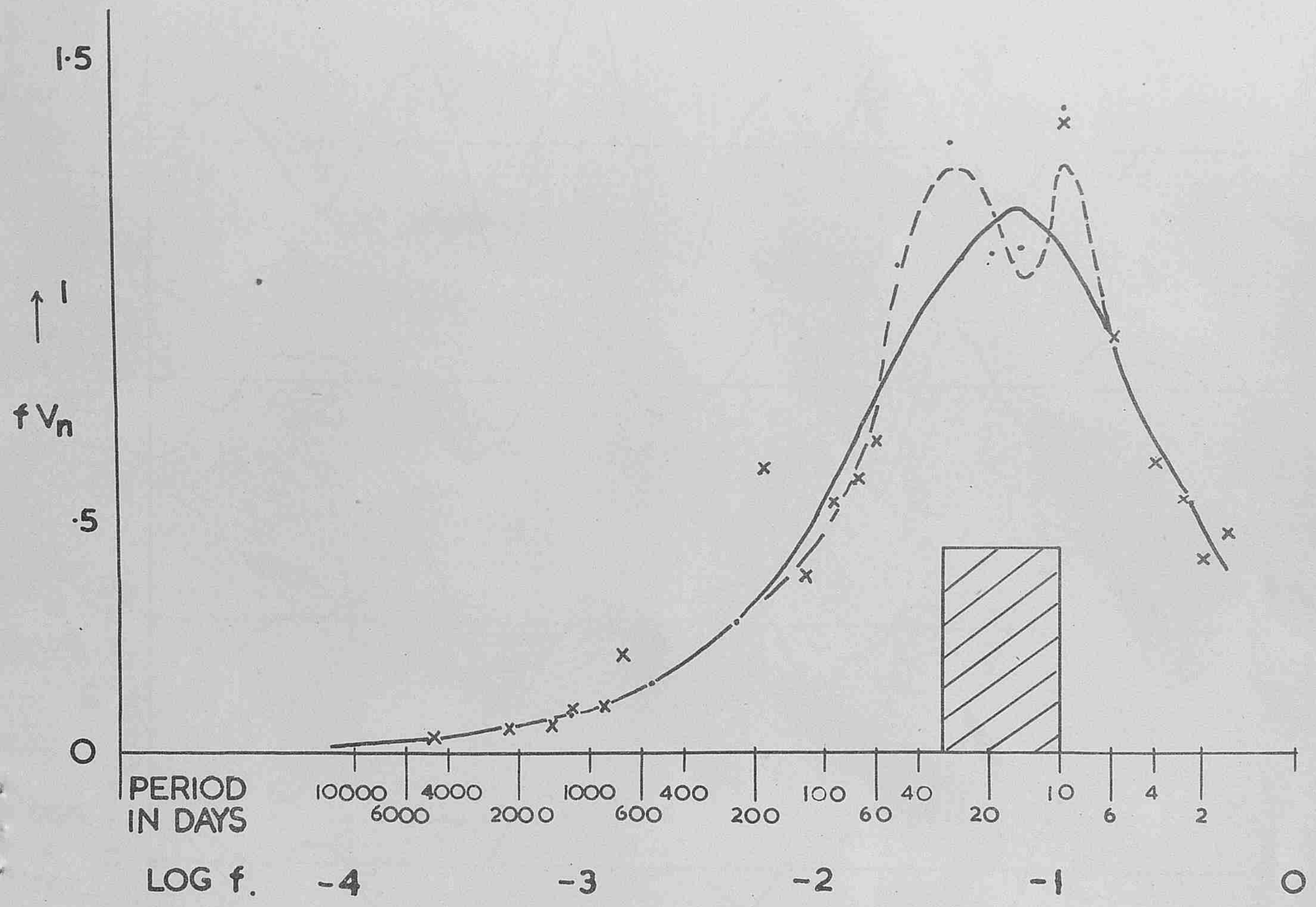

FIG. 6. KEW DAILY TEMPERATURES FOR 1955 AFTER FILTERING TO RETAIN ONLY A FREQUENCY BAND CENTRED ABOUT 1/10 (I.E. A PERIOD OF 10 DAYS)

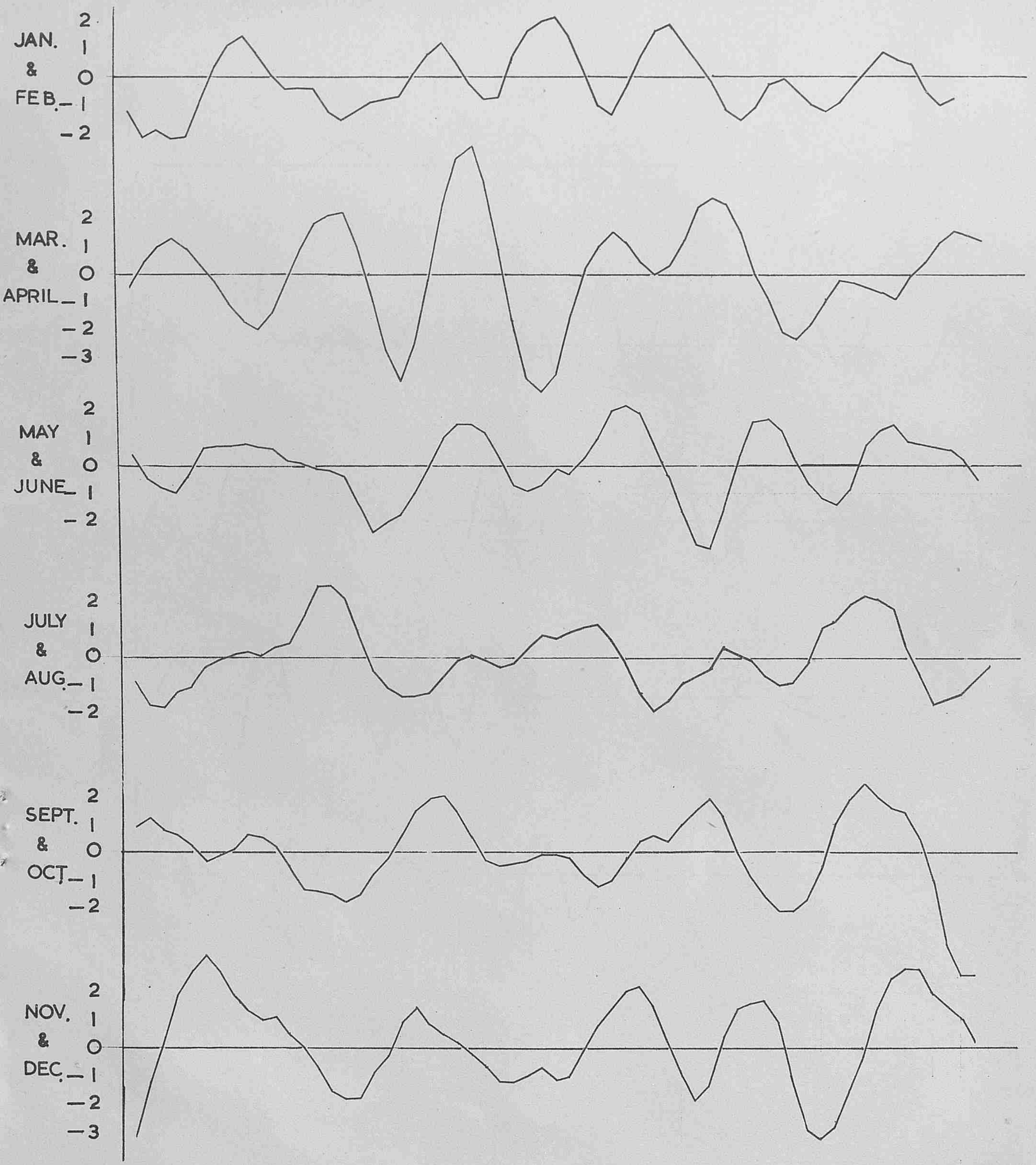

FIG. 7 KEW 5 - DAY MEAN TEMPERATURES FOR 1946 - 1950 FILTERED TO SHOW THE 30- DAY WAVE IN ITS TRUE PHASE AND AMPLITUDE.

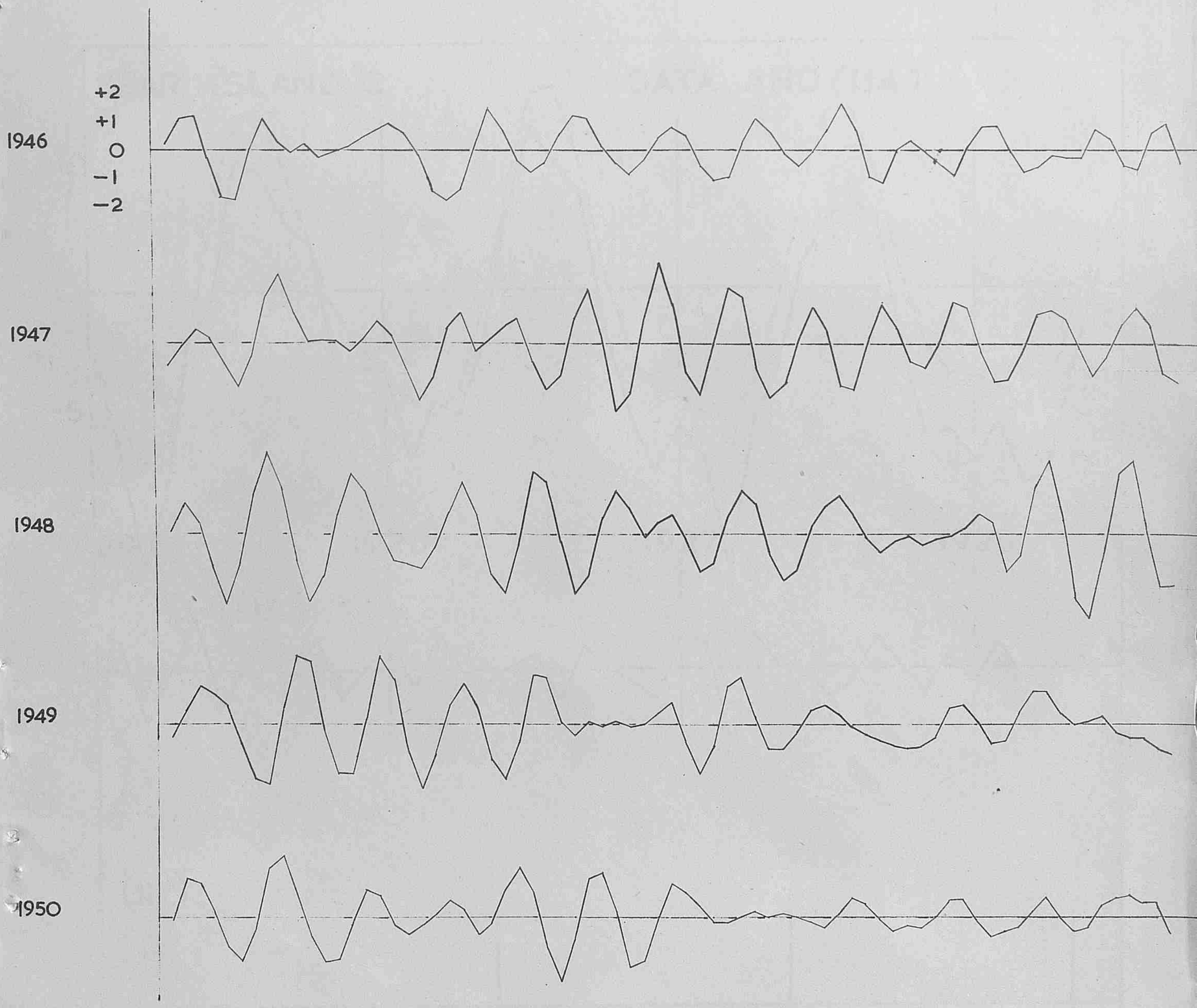

FIG. 8 BEAR ISLAND MONTHLY TEMPERATURE FILTERED TO SHOW INTER-ANNUAL VARIATIONS

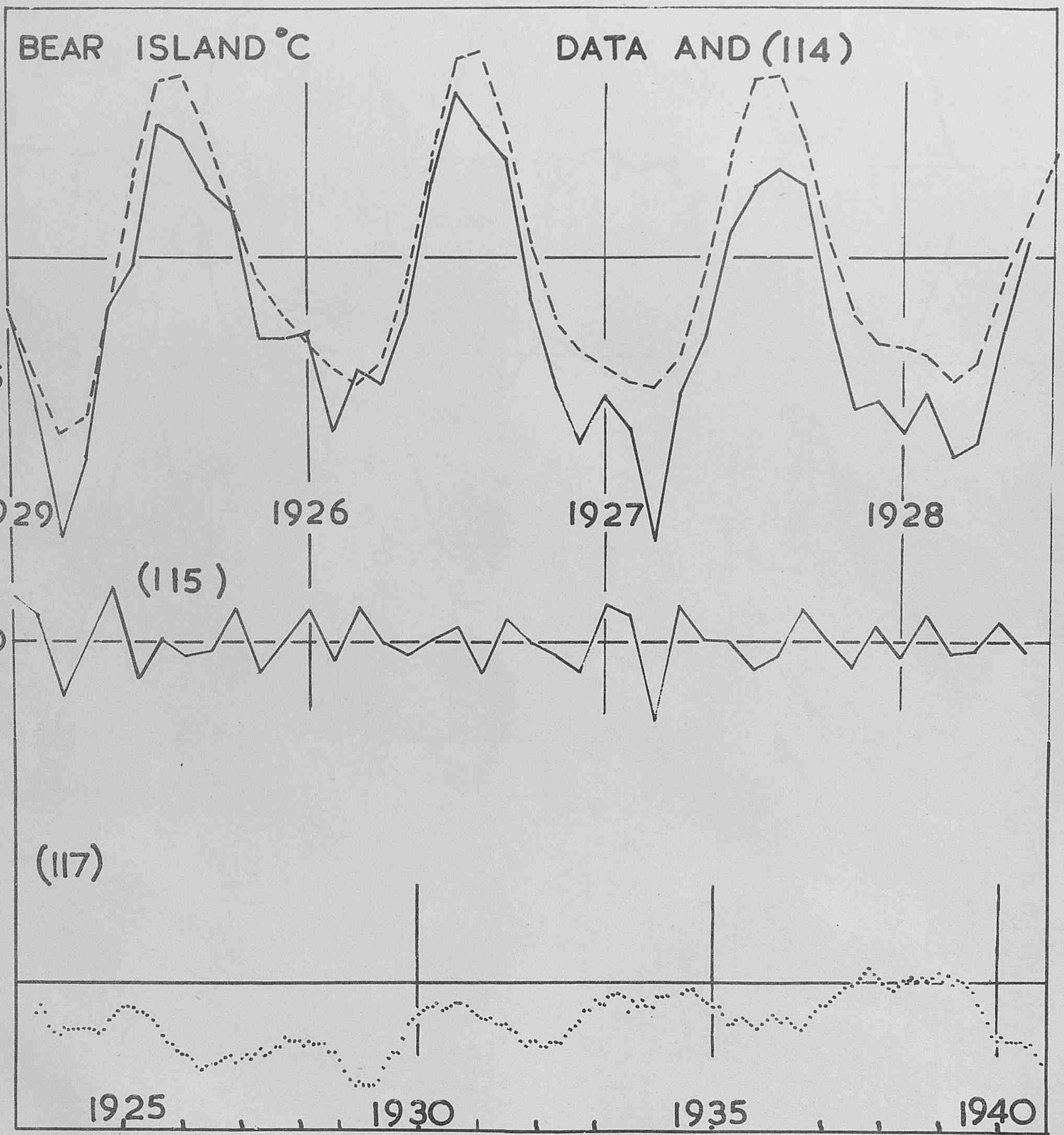

Fig. 9

Response curves of typical filters. Filter numbers are bracketed. In all the graphs "f" is abscissa and "M(f)" ordinate

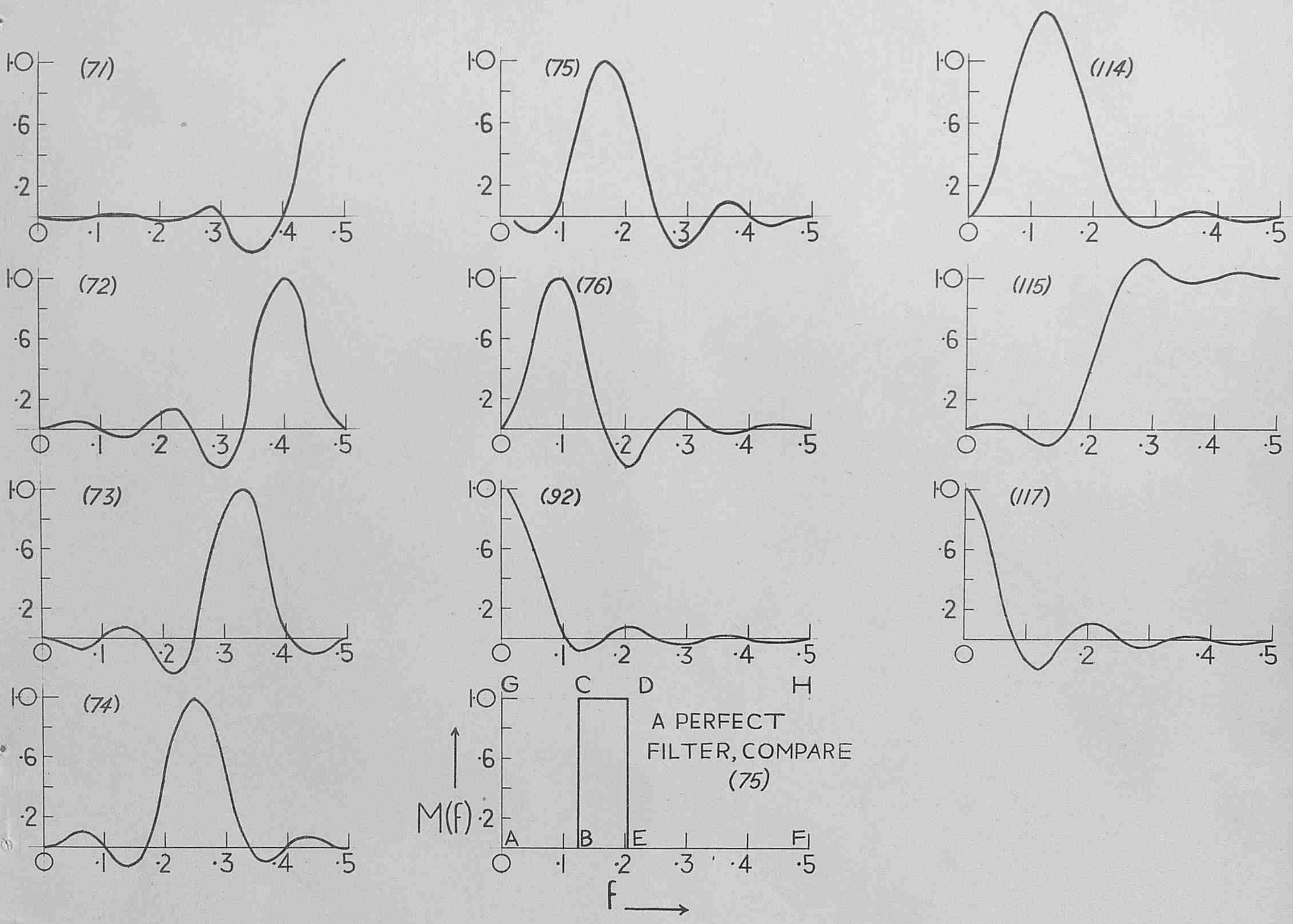

M.R.P. 1052
S.C.II/235
9th May, 1957

AD 223145

An analysis of humidity measurements in the upper troposphere and lower stratosphere over Southern England

by

G. B. Tucker

(Meteorological Office)

AIR MINISTRY

METEOROLOGICAL RESEARCH COMMITTEE

58-94

At the time of issue this report has not been published. Any author desiring to quote this paper should refer to it as "A paper of the Meteorological Research Committee (London), M.R.P. No. 1052 by Dr. G.B. Tucker. A copy is available in the Library of the Meteorological Office."

M.R.P.1052
S.C.II/235
9th May, 1957

AIR MINISTRY

METEOROLOGICAL RESEARCH COMMITTEE

An analysis of humidity measurements in the upper troposphere and lower stratosphere over Southern England

by

G. B. Tucker (Meteorological Office)

Summary

399 high altitude ascents measuring temperature and frostpoint, made by aircraft of the Meteorological Research Flight, are analysed and the results compared with previous conclusions. Before 1954 observations were made from a Mosquito aircraft and ascents seldom exceeded the 200 mb level; from 1954 onwards a Canberra aircraft was used and the 125 mb level was regularly attained.

Little systematic difference is detected between the mean of the Canberra ascents and that of other aircraft. The extreme dryness of the stratosphere is a feature of all seasons, but summer is the most moist season (in terms of water content) in the stratosphere as well as in the troposphere. Above about 500 mb the humidity mixing ratio lapse decreases with height, and above 150 mb the humidity mixing ratio levels out to about .002 g/Kg. The tropopause does not coincide with any marked discontinuity in frostpoint or humidity mixing ratio. An attempt to represent the observed distribution of water vapour in the vertical as a balance between vertical eddy diffusion and vertical motion is found to be inadequate. An earlier suggestion (1) - that at any fixed level above or below the tropopause the frostpoint is lower if the tropopause is low - is confirmed. A graphical method is devised to show the inter-relationships between season and the temperature, frostpoint and pressure at the tropopause. Finally an attempt to relate the frostpoint to the jet-stream proves to be largely unsuccessful.

1. Introduction

At the end of 1955 observations of temperature and frostpoint had been made on 399 high altitude ascents (begun in 1943) over Southern England by aircraft of the Meteorological Research Flight. The earlier ascents (130, up to June, 1950) have been analysed by Bannon, Frith and Shellard (1). This paper is a continuation of that work using all 399 ascents. The following analysis is not as exhaustive as (1) and, although an essentially similar method of processing observations is involved, in some cases the material has been handled differently.

The type and method of observation together with the instrumentation and estimates of accuracy have been dealt with elsewhere (1, 2, 3). Murgatroyd, Goldsmith and Hollings (2) have also analysed the first 21 flights (begun in 1954) by a Canberra aircraft, while Helliwell, Mackenzie and Kerley (4) have made a similar analysis of 46 such ascents in 1955. The Canberra soundings have usually attained 48,500 ft (125 mb): of the 399 ascents considered below, 85 Canberra soundings are included. Earlier Mosquito flights did not exceed 38,600 ft (200 mb).

The analysis is divided into five sections:-

(i) ascents are presented in chronological order and the preliminary processing of individual soundings is described;

(ii) mean seasonal and annual values of temperature, frostpoint and humidity mixing ratio are evaluated at standard pressure levels; Canberra and other aircraft observations are distinguished for comparison;

(iii) a discussion of the vertical distribution of frostpoint relative to the tropopause;

(iv) an attempt to relate the seasonal variations of frostpoint, temperature and pressure at the tropopause;

(v) the vertical structure of frostpoint is considered in relation to the jet-stream.

2. Data

From the original ascent curves, values of temperature (T) and frostpoint (F) at standard pressure levels (700, 500, 400, 300, 250, 200, 150 and 125 mb) were extracted and tabulated in chronological order (Table 1), together with the selection of tropopause for each ascent. These were done partly by the Upper Air Climatology Branch and partly by the Meteorological Research Flight. These data are recorded on punched Hollerith cards, one card for each ascent. Much of the sorting and tabulating was done mechanically. The soundings prior to July, 1950 have been published previously (1) and only values for July, 1950 to December, 1955 are given in Table 1. Although the approximate position of the ascent is quoted it has been decided to regard these figures as appertaining to 'Southern England' because the area over which the atmosphere is sampled, especially since the use of the Canberra aircraft, is so large. The observations were classified according to air mass and circulation (as in Geophysical Memoir No. 88 (1)) by the Upper Air Climatology Branch and, although not analysed below, these classifications are included in Table 1.

The recommended international classification of 'tropopause' was used:- ≠

(i) the "first tropopause" is defined as the lowest level at which the lapse rate decreases to 2°C/Km or less, provided also that the average lapse rate between this level and all higher levels within 2 Km does not exceed 2°C/Km;

(ii) when, above the first tropopause, the average lapse rate between any level and all higher levels within 1 Km exceeds 3°C/Km, then a "second tropopause" can occur and is defined by the same criteria as in para. (i). This tropopause can either be above or within the 1 Km layer;

(iii) further tropopauses are defined at higher levels by the same criteria as in para. (ii).

For the sake of continuity and to afford comparison the seasons are defined as in G.M.88 (1):-

Winter - January, February, March.
Spring - April, May, June.
Summer - July, August, September.
Autumn - October, November, December.

/3.

≠ Resolution 42 of E.C. IV of W.M.O.

3. Seasonal and annual mean values of temperature and frostpoint at standard pressure levels

Observations at the 150 and 125 mb levels began with Canberra aircraft in January, 1954. It was necessary to determine whether the discrepancy suggested by Murgatroyd et al. (2) between the first observations made by Canberra aircraft and those given in Geophysical Memoir No.88 (1) is also a feature of subsequent Canberra observations. (Murgatroyd et al. found frostpoints considerably lower than those given in Geophysical Memoir No.88, above a level with a pressure 50 mb less than the tropopause pressure. They suggested that this may be due to an instrumental error in the earlier observations).

Table II presents the mean seasonal values of T and F at standard pressure levels together with the number of observations. The differences between Canberra and pre-Canberra means are shown graphically in Figure 1. No systematic differences occur apart from:-

(i) the lower levels in spring where the negative anomalies of both T and F coupled with the small number of observations suggested that a difference in sampling is the reason;

(ii) the highest levels where the pre-Canberra soundings record slightly warmer (autumn and winter) and moister (all seasons) conditions in the stratosphere.

The mean seasonal curves are shown in Figure 2 with the number of observations entered at each point. (The curves are not drawn through the points representing the mean values for the tropopause; these points are obtained by averaging pressures and temperatures at the tropopause and would not necessarily be expected to lie on the true mean curves of temperature against pressure. See, e.g., the winter curves where the mean pressure of the tropopause is near 250 mb). Values for 200, 250 and 300 mb from Geophysical Memoir No.88 are shown and, with the exception of autumn, when relatively few observations were made (in G.M.88), the agreement is good. The divergence of the curves above the tropopause proves to be a feature of the mean values as well as of the individual ascents, and the mean frostpoint shows a tendency to become asymptotic to about -120°F. with increasing height - agreeing with the results of (2) and (4). These features are also characteristic of the mean annual curve, Figure 3.

An interesting seasonal feature is revealed when the frostpoint differences between summer and winter are plotted (Figure 4); they show that the atmosphere in summer is moister* than in winter in the lower stratosphere as well as the troposphere; the summer-winter amplitude of F is 15 to 20°F in the troposphere but however only 0 to 5°F in the stratosphere. The frostpoint depressions in Figure 5 also show that while the stratosphere in summer is systematically of lower relative humidity, the seasonal difference in frostpoint depression is only about 10°F, compared with actual frostpoint depressions of 40 or 50°F. These points are better illustrated in Table III which gives the mean seasonal and annual relative humidities and humidity mixing ratios at standard pressure levels. The lower stratosphere although having a higher moisture content in summer has a lower relative humidity. It should be noted however that although summer is moister than winter, both spring and autumn are drier than winter. Any definite seasonal trend in water content is masked by the variations in the average tropopause pressures (Table III) which may not be representative of the seasons. The humidity mixing ratios for winter, summer and the year have been plotted logarithmically against a linear height scale in Figures 6A, B and C together with values obtained by Barrett (5) from three single soundings. Barrett's figures which refer to ascents over Central North America are shown to be very different from mean conditions in the lower stratosphere over England.

/4.

---

* 'moister' here and throughout the analysis refers to water content and not to relative humidity.

4. Temperature and frostpoint in relation to the tropopause

The aircraft soundings were too spasmodic in time for unweighted means of T and F at various pressures above and below the tropopause to be representative of mean conditions. To overcome this ascents were grouped according to tropopause height, each group covering a range of 2000 ft on the I.C.A.N. scale, as in the following table.

Tropopause groups	Pressure range in mb (pressure at tropopause)	Height range in 1000 ft I.C.A.N.
1	less than 147	greater than 45
2	162-148	45-43
3	179-163	43-41
4	197-180	41-39
5	216-198	39-37
6	238-217	37-35
7	262-239	35-33
8	287-263	33-31
9	315-288	31-29
10	344-316	29-27
11	376-345	27-25
12	410-377	25-23

Mean values of T and F at 25 mb intervals above and below the tropopause in each group were extracted and weighted according to the frequency of tropopause height over Larkhill for the whole year and for the four seasons separately for the period 1946-1950 (6). Only rough weighting factors were considered necessary for the accuracy required; they are given in the following table.

Weighting factor

Tropopause group	1	2	3	4	5	6	7	8	9	10	11	12
Winter	0	1	3	6	7	5	4	3	2	1	0	0
Spring	0	1	2	5	7	6	5	3	2	1	1	0
Summer	0	1	2	6	8	7	5	2	1	0	0	0
Autumn	1	2	3	5	6	5	4	3	2	1	1	0
Annual	1	4	10	23	27	24	18	11	6	3	2	1

Because the soundings in each season for tropopauses outside the range of groups 3 to 9 are so few they may not represent average high and low tropopause conditions; this together with their low weighting factor has led to their omission in the calculation of seasonal mean values. The weighted means are presented in Table IV and graphed in Figures 7A to 7E. For the annual means, values for Canberra ascents alone (similarly weighted) have been included. The curve of summer minus winter frostpoint differences (Figure 8A) shows the same features as Figure 4 except that at very high levels the winter stratosphere tends to be slightly moister than summer. However summer and winter frostpoint depression curves (Figure 8B) show similar values in the troposphere but in the lower stratosphere the summer depressions are some 10 to 15°F greater than in winter.

The dryness of the air in the lower stratosphere has been appreciated for some years and Brewer (7) suggests that this dryness is maintained by a large scale meridional circulation. By neglecting horizontal advection, considering a steady state and utilizing the concept of a vertical eddy diffusion coefficient

/embracing

embracing the whole of the turbulence spectrum, Brewer develops an equation -

$$K \frac{\partial^2 r}{\partial z^2} + w \frac{\partial r}{\partial z} = 0$$

where K is the eddy diffusion coefficient,

r is the humidity mixing ratio,

w is the vertical velocity downwards,

z is height above the tropopause.

The solution is $r = r_o + (r_t - r_o) \exp - wz/K$; the suffix 'o' refers to dry air aloft and suffix 't' to the tropopause value. Fitting curves to 16 early ascents into the stratosphere, and taking $K = 10^3$, he obtains a value for w of about 25 m/day (corresponding to a necessary cooling by radiation of 0.25°C/day).

Recently acquired knowledge of the lower stratosphere maintains the importance of horizontal advection, and the use of a K to embrace all eddy sizes smaller than the meridional circulation may not be realistic. Notwithstanding this, it is interesting to fit curves, similar to Brewer's, (Figure 9A, B, C and D) to values of humidity mixing ratio obtained from values of T and F in Table IV, and to compare the values of w thus derived with those of Brewer (using his value $K = 10^3$). The observed and theoretical values of humidity mixing ratio are given in Table V; the height scale in Figure 9 assumes an isothermal stratosphere. The values of w/K are derived from estimated values of r_o and F as in the following table:-

	Winter	Spring	Summer	Autumn	
r_o	.00250	.00210	.00251	.00250	g/Kg
F	-115.5	-117.4	-115.5	-115.5	°F
w/K	1.1	1.3	1.5	1.2	($\times 10^{-5}$c.g.s.)

(Estimated r_o was the lowest value obtained, and F was estimated by assuming r_o to apply at 100 mb.)

These values are roughly one-half of those of Brewer, and correspond to a downward vertical velocity of about 10-15 m/day and require a radiative cooling of about 0.1-0.15 °C/day. The actual mean seasonal radiative cooling is estimated to be an order of magnitude higher (8) - which serves to indicate the inadequacy of this explanation.

Early sampling of the lower stratosphere has been criticised because of selectivity in favour of low tropopauses. The mean profiles of T and F for the ranges of tropopause-height (grouped as in the table on p.4) were calculated and the annual values are plotted in Figure 10. For clarity only the even numbered groups are plotted for about 150 mb above and below the tropopause. The conclusions of a similar but less detailed analysis in Geophysical Memoir No.88 are borne out, namely:-

(i) the higher the mean tropopause the lower the air temperature at the tropopause;

(ii) the higher the mean tropopause the lower the frostpoint at the tropopause;

(iii) at any specified pressure interval above or below the tropopause, the frostpoint is low if the temperature is low.

The variation with height of any frostpoint discontinuity occurring at the tropopause was investigated by calculating the values of $\partial F/\partial z$ in the 25 mb interval above and below the tropopause for each seasonal/tropopause height group (Table VI). These results show that no definite relationship exists between $\partial F/\partial z$ and the tropopause pressure in this series of observations.

5. Frostpoint and temperature at the tropopause

It was interesting to investigate the relation between the variation with season of temperature (T_c), frostpoint (F_c) and pressure (P_c) at the tropopause. Correlation coefficients for two such relationships were calculated in Geophysical Memoir No.88 (1); they were

	Correlation coefficient	No. of pairs
$T_c : P_c$	+.77	106
$F_c : P_c$	+.51	106

There appears to be no reason why the relationship should be linear, and before resorting to any more complex statistical analysis a graphical relationship has been attempted with dot diagrams to illustrate qualitatively the reliability of the results. The basis of this study was the grouping into tropopause pressures for each season (Section 3), and from this:-

(i) the mean tropopause temperature, frostpoint and pressure in each group were calculated;

(ii) a diagram was drawn showing the variation of T_c and P_c with season (Figure 11); along each seasonal ordinate the mean tropopause temperature (T_c) in each of the tropopause groups 3 to 9 is plotted at the mean pressure (P_c) of the group;

(iii) a similar diagram for F_c and P_c is given in Figure 12;

(iv) Figure 13 shows the variation of F_c and T_c with season; along each seasonal ordinate the mean tropopause frostpoint (F_c) in each tropopause group is represented as a function of the mean temperature (T_c) of the group. This was done by combining the smoothed values of T_c as a function of P_c (Figure 11) and F_c as a function of P_c (Figure 12) along each seasonal ordinate to produce F_c as a function of T_c - with the implicit assumption that F_c is a single valued function of T_c.

(N.B. The tropopause pressure groupings afford a graphical means of drawing a mean curve to represent F_c as a function of T_c without assuming linearity as would a regression equation.)

In order to obtain an estimate of the deviation of individual observations from the means expressed in Figures 11, 12 and 13, dot diagrams of individual values of T_c and F_c were drawn up for each tropopause pressure group for each season (Figure 14). The points $\bar{T}_c$, $\bar{F}_c$ are indicated by crosses and are consistent with Figure 13. The deviations of individual points from this value in the vertical represent the scatter about the mean values plotted in the $\bar{F}_c$ ($\bar{P}_c$, season) diagram, Figure 12, the deviations in the horizontal similarly represent the scatter for the T_c ($\bar{P}_c$, season) diagram, Figure 11.

The dot diagram proves interesting in its own right, e.g., illustrating the proximity of each cluster to saturation (the 100 and 50 per cent relative humidity lines have been drawn in each case). The three ascents showing supersaturation have been plotted (Figure 15): the 1950 and 1952 values appear realistic and saturation was reported in a cirrus environment; but the earlier (1948) ascent must be treated with scepticism.

/6.

6. Frostpoint and the jet-stream

Circulations in the vertical plane at right angles to the jet axis have been the subject of several recent investigations (9, 10, 11). An attempt was made to utilize these frostpoint measurements to obtain the humidity distribution about the jet axis and to use it as a tracer element to deduce vertical motion. This was not successful but the method of approach and one result are described briefly below.

The 300 mb charts in the Daily Aerological Record were used to determine the distance from a jet axis of each ascent (a jet-stream was defined as a stream in which the wind speed exceeded 85 kt at 300 mb). If the ascent was within 500 miles of a jet axis it was included in one of five 200-mile range-groups (i.e., 500 to 300, 300 to 100, +100 to -100 etc. miles relative to the axis). Entrances, centres and exits of jet-streams were studied individually making fifteen groups in all. The mean ascent for each group was then calculated and the mean tropopause height, H, was noted. This mean ascent was then compared with a 'weighted average'+ ascent obtained by compounding the average seasonal ascents for the tropopause height H, obtained from Table I, weighted according to the total number of ascents in each season.

Three attempts were made to classify into range-groups according to distance from the jet-stream axis:

(i) by referring each ascent to the current synoptic situation,

(ii) by taking the mean over the preceding 12 hours of the position of the air relative to the jet-stream by drawing trajectories at 300 mb,

(iii) by choosing examples of well-defined jet-streams from (ii).

Of these three attempts the answers of the last were most coherent but even these have little significance. They are expressed in the form of a diagrammatic table (Figure 16). The 'classical' circulation at the jet entrance below the tropopause (9) can be distinguished, as can a reverse circulation at the exit. Elsewhere there is no systematic trend except a possible indication that in the lower stratosphere ascent occurs south of the entrance and north of the exit with a general subsidence at the centre (Figure 17). However it is obvious that little reliance can be based on the above conclusions, and that this method cannot compare with Murray's analysis (11) of observations obtained on special horizontal traverses of jet-streams.

+The 'weighted average'

It will be recalled that in Section 3 the ascents analysed in the paper were divided into the four seasons. The ascents in each season were grouped according to their tropopause height. Each of these tropopause height groups covered a range of 2,000 ft on the I.C.A.N. scale. The means of these groups were then obtained, arriving at a series of mean ascents which are effectively average seasonal ascents for various tropopause heights.

Reverting to the jet-stream analysis, the representative (mean) ascent within a certain distance of the jet axis must be compared with some sort of standard ascent purporting to represent the atmosphere undisturbed by jet-stream effects: the 'weighted average' ascent was chosen as the standard.

It is appreciated that this ignores the fact that the height of the tropopause may well be partially a result of the existence of the jet-stream.

Bibliography

1. Bannon, J.K., Frith, R. and Shellard, H.C. Humidity of the upper troposphere and lower stratosphere over Southern England. Geophysical Memoirs, London, No. 88, 1952.

2. Murgatroyd, R.J., Goldsmith P. and Hollings, W.E.H. An interim report on measurements of humidity from aircraft to heights of about 50,000 feet over Southern England. Meteorological Research Papers, Air Ministry, London, No. 877, 1954.

3. Durbin, G. Some further determinations made by the M.R.F. of the speed correction coefficients of aircraft thermometers. Meteorological Research Papers, Air Ministry, London, No. 930, 1955.

4. Helliwell, N.C., Mackenzie, J.K. and Kerley, M.J. Further observations of humidity up to 50,000 feet made from an aircraft of the Meteorological Research Flight in 1955. Meteorological Research Papers, Air Ministry, London, No. 976, 1956.

5. Barrett, E.W. Some measurements of the distribution of water vapour in the stratosphere. Tellus, 2, 1950.

6. M.O.555, Part I Upper Air Data - Larkhill. Air Ministry, London.

7. Brewer, A.W. Evidence for a world circulation provided by measurements of Helium and Water Vapour distribution in the stratosphere. Quart. J.R. Met. Soc., 75, 1949.

8. London, J. The distribution of infra-red cooling in the atmosphere for Winter and Summer seasons. Proc. Toronto Met. Conf., 1953.

9. Sawyer, J. The vertical circulation at meteorological fronts and its relation to frontogenesis. Proc. Roy. Soc., A.234, 1956, p.346.

10. Murray, R. and Daniels, S.M. Transverse flow at entrance and exit to jet-streams. Quart. J.R. Met. Soc., 79, 1953.

11. Murray, R. Some features of jet-streams as shown by aircraft observations. Geophysical Memoirs, London, No.97, 1956.

M.R.P. 1052

TABLE 1

Values of temperature and frostpoint at standard pressure levels, as obtained from aircraft soundings

(Listed in chronological order)

Date			Approximate position		Tropopause			Standard pressure levels														
								700 mb		500 mb		400 mb		300 mb		250 mb		200 mb		150 mb		125 mb		
Year	Month	Day	Latitude (°N)	Longitude (°W except where otherwise stated)	Pressure (mb)	Temperature (°F)	Frostpoint (°F)	Temperature (°F)	Frostpoint (°F)	Temperature (°F)	Frostpoint (°F)	Temperature (°F)	Frostpoint (°F)	Temperature (°F)	Frostpoint (°F)	Temperature (°F)	Frostpoint (°F)	Temperature (°F)	Frostpoint (°F)	Temperature (°F)	Frostpoint (°F)	Temperature (°F)	Frostpoint (°F)	Air mass classification
50	07	14	51	02	300	-44	-82	+27		- 7		-27	-60	-44	-32	-42	-115							1
50	07	18	51	02	216	-67	-84	+39	+15	+ 8	+ 7	-13	-19	-40	-50	-57	-71	-64	-94					4
50	07	19	51	02	205	-70	-87	+37	+34	+10	-38	-10	-53	-38	-40	-56	-68	-68	-93					4
50	07	24	51	02	205	-64	-93	+34	-17	+12	- 6	- 6	-22	-35	-42	-51	-67	-65	-94					8
50	07	25	51	02	239	-60	-80	+35	+26	+ 5	-51	-16	-61	-42	-72	-56	-77	-57	-99					8
50	07	28	51	02	228	-65	-80	+33	+19	+ 4	-39	-15	-41	-44	-60	-60	-73							8
50	07	31	51	02	227	-63	-87	+29	+18	+ 2	-26	-19	-44	-48	-72	-60	-82	-56	-100					8
50	08	01	51	01	238	-63	-91					-20	-21	-44	-50	-59	-90							1
50	08	02	51	02	330	-50	-69	+21	+13	-12	-33	-34	-45	-51	-79	-44	-101							1
50	08	03	51	02	238	-57	-71	+34	+12	- 3	-40	-26	-55	-39	-61	-55	-70	-52	- 72					6
50	08	08	51	02	200	-68		+35	+35	+11	+10	- 7	-11	-35	-37	-49	-66	-68	- 98					7
50	08	09	51	02	205	-66	-81	+37	-16	- 7	-31	-13	-59	-34	-44	-51	-64	-66	- 85					8
50	08	10	51	02	262	-53	-84									-53	-89	-55	-109					6
50	08	14	51	02	228	-71	-72	+34	+ 4	+ 6	-30	-15	-44	-44	-45	-63	-63	-58	- 90					8
50	08	14	51	02	228	-71	-72	+34	+ 3	+ 5	-30	-16	-45	-44	-45	-61	-61	-56	-105					8
50	08	18	51	02	286	-59	-67	+22	+14	- 7	-11	-28	-28	-55	-60	-57	-83							1
50	08	21	51	02	215	-66	-86					-18	-61	-43	-75	-59	-77	-66	- 96					7
50	08	22	51	02	179			+35		+ 8	-20	-15	-18	-42	-50	-59	-68	-74	- 88					2
50	08	29	51	02	262	-61	-76	+22	+17	- 5	-28	-25	-50	-51	-62	-61	-80	-54	-104					2
50	08	30	51	02	237	-70	-77							-53	-57	-68	-77	-56	- 92					4
50	09	04	51	02	183			+44		+12		- 7	-42	-35	-55	-52	-76	-71	- 83					4
50	09	05	51	02	262	-63	-58	+34	-42	+ 5	-47	-22	-57	-47	-54	-64	-73	-65	-100					8
50	09	15	51	02	301	-61	-65	+22		- 9	- 1	-32	-37	-61	-65	-45	-104							1
50	09	18	51	02	250	-59	-90	+22	-22	+ 3	-55	-15	-26	-43	-55	-58	-90	-55	-108					6
50	09	19	51	02	287	-53	-75	+29			-18	-22	-64	-48	-70	-55	-85	-54	- 97					2
50	09	25	51	02	301	-51	-76	+22	+13	-12	-20	-34	-47	-51	-77	-46	-103							1
50	09	26	51	00	250	-55	-101	+21		- 8		-30		-47	-82	-55	-101	-56	-112					8
50	09	29	51	02	190			+33	+29	+ 8	- 3	-12	-26	-35	-66	-53	-76	-71	- 94					4
50	10	10	51	02	250	-61	-72	+21	+14	- 8	-12	-25	-42	-49	-64	-61	-72	-59	- 76					8
50	10	11	51	02	180			+26	+10	+ 5	- 2	-15	-27	-42	-49	-57	-64	-74	- 85					7
50	10	12	51	02	191	-78	-88	+38	+ 6	+ 9	-49	-13	-42	-39	-58	-55	-70	-76	- 81					4
50	10	17	51	02	159			+36	+30	+10	- 1	-11	-20	-37		-55		-76						4
50	10	17	53	00	188			+35	+ 1	+11	- 1	-13		-39		-57		-74						8
50	10	18	51	02	123			+36	+ 4	+ 8	-32	-14	-44	-40	-71	-53	-80	-69	- 92					4
50	10	19	51	02	175			+39	+18	+ 9	- 7	-14	-30	-39	-63	-56	-77	-75	- 81					4
50	10	19	53	00	178			+38	+34	+ 7	- 3	-17	-30	-39	-68	-56	-74	-75	- 87					4
50	10	21	51	01	205	-79	-86	+35	+20	+ 1	- 3	-19	-25	-48	-59	-65	-68	-79	- 87					8
50	10	22	51	01	228	-75	-83	+29	+15	- 4	-11	-26	-32	-51	-59	-67	-75	-72	- 95					8
50	10	24	51	02	205	-78	-92	+29	+17	- 2	-21	-22	-42	-51	-60	-67	-83	-76	- 98					1
50	10	24	53	00	227	-74	-86	+31	+11	0	-31	-24	-47	-60	-72	-66	-85	-77	- 88					1
50	10	25	53	00	238	-73	-89	+27		+ 7		-29		-52		-67	-82	-73	- 89					1
50	10	25	51	02	250	-69	-75	+31	-38	+ 4	-59	-26	-67	-53	-69	-69	-75							1
50	10	26	51	01	207	-72	-93	+26	-51	- 6	-42	-28	-76	-48	-66	-60	-76	-72	- 97					1
50	10	26	51	01	228	-71	-82	+23	-39	- 7	-35	-27	-67	-46	-58	-59	-70	-75	- 93					1
50	11	14	51	02	315	-52	-86	+ 9	- 2	-20	-52	-40	-66	-53	-88	-54	-102							1
50	11	17	51	01	315	-58	-73	+10	-31	-15	-43	-35	-49	-49	-82	-59	-97	-55	-109					1
50	11	28	51	02	288	-58	-76	+23	-12	- 6	-51	-29	-62	-56	-68	-59	-97	-63	-113					8
50	11	29	51	02	343	-51	-65	+12	+ 7	-18	-25	-39	-51	-56	-92	-55	-95							1
50	12	07	51	02	238	-70	-95	+11	-24	- 6	-56	-27	-50	-50	-70	-64	-87	-67	-111					6
50	12	08	51	02	158			+23	+ 6	- 2	-16	-23	-61	-50	-68	-65	-82	-81	- 94					7
50	12	11	51	02	345	-58	-72	+ 5	-13	-28	-35	-48	-54	-54	-84	-53	-106	-57	-112					1
51	01	12	51	02	344	-65	-68	+ 9	-14	-27	-40	-51	-51	-57	-91	-51	-106							1
51	01	24	51	02	273	-75	-85	+15		-17		-40		-69	-70	-69	-93	-64	-119					7
51	02	07	51	02	300	-55	-82	+10	-11	-15	-34	-34	-45	-55	-82	-53	-89	-52	- 90					1
51	02	15	51	02	286	-67	-75	+ 8	0	-22	-36	-41	-47	-64	-72	-60	-97	-53	-102					6
51	02	19	51	02	376	-53	-63	+ 9	-11	-26	-37	-48	-49	-60	-85	-50	-88	-46	-106					1
51	02	23	51	02	314	-62	-76	+ 6	- 6	-22	-48	-40	-64	-61	-83	-60	-91	-61	- 96					1
51	03	01	51	02	239	-77	-83	+25	- 5	- 7	-19	-29	-37	-57	-65	-74	-79	-75	- 96					7
51	03	09	51	02	215	-83	-91	+19	- 2	-11	-33	-32	-42	-60	-72	-75	-86	-76	- 98					3
51	03	14	51	02	330	-53	-83	+13	-22	-20	-39	-41	-55	-56	-88	-54	-93	-59	- 93					1
51	03	15	51	02	228	-72	-87	+20	-21	-12	-29	-34	-47	-54	-73	-67	-84	-71	- 93					6
51	03	17	51	02	315	-57	-82	+19	+ 5	-18	-26	-40	-51	-56	-85	-60	-93	-62	- 91					4
51	03	19	51	02	329	-65	-70	+11		-22	-36	-45		-58	-91	-52	-91	-53	- 90					1
51	04	05	51	01	228	-79	-86	+21		- 7	-49	-29	-48	-58	-58	-72	-79	-72	-102					8
51	04	10	51	02	315	-61	-78	+ 7		-24		-43	-60	-60	-87	-51	-108							1

M.R.P. 1052

Date			Approximate position		Tropopause			Standard pressure levels																Air mass classification
								700 mb		500 mb		400 mb		300 mb		250 mb		200 mb		150 mb		125 mb		
Year	Month	Day	Latitude (°N)	Longitude (°W except where otherwise stated)	Pressure (mb)	Temperature (°F)	Frostpoint (°F)	Temperature (°F)	Frostpoint (°F)	Temperature (°F)	Frostpoint (°F)	Temperature (°F)	Frostpoint (°F)	Temperature (°F)	Frostpoint (°F)	Temperature (°F)	Frostpoint (°F)	Temperature (°F)	Frostpoint (°F)	Temperature (°F)	Frostpoint (°F)	Temperature (°F)	Frostpoint (°F)	
51	04	13	55	02	344	-56	-76	+6		-29	-41	-46	-71	-52	-95	-49	-105							1
51	04	17	51	02	206	-82	-93	+24	-31	-6	-24	-27	-37	-54	-59	-71	-77	-83	-95					6
51	04	18	51	02	216	-80	-89	+24	+24	-6	-10	-25	-32	-54	-60	-71	-77	-79	-95					6
51	04	19	51	02	217	-82	-87	+25	+20	-5	-26	-22	-62	-53	-71	-71	-74	-80	-96					6
51	04	23	51	02	164			+32	-6	+5	-18	-20	-45	-49	-52	-63	-79	-81	-92					8
51	04	24	51	02	173			+33	+5	+4	-35	-19	-48	-47	-66	-63	-79	-80	-86					4
51	05	07	51	02	262	-69	-81	+22	0	-10	-38	-33	-56	-61	-68	-68	-84	-60	-113					1
51	05	08	51	02	315	-55	-77	+7		-18		-37	-61	-54	-90	-54	-98	-52	-110					1
51	05	15	51	02	238	-74	-76	+24	+16	-6	-12	-27	-34	-52		-69	-74	-69	-93					4
51	05	25	51	02	261	-67	-72	+24	+14	-4	-47	-27	-31	-55	-56	-66	-88	-59	-109					2
51	05	28	51	02	300	-53	-85	+21	+16	-8	-20	-30	-44	-53	-85	-53	-102							2
51	06	08	51	02	216	-73	-79	+31	-1	0	-5	-19	-54	-45	-48	-61	-71	-68	-90					6
51	06	11	51	02	227	-67	-73	+33	+27	-4	-37	-18	-45	-45	-54	-62	-62	-66	-78					4
51	06	20	51	02	228	-71	-82	+28	-8	-1	-18	-22	-42	-49	-69	-64	-78	-67	-95					2
51	06	28	51	02	238	-67	-77	+29	-18	+3	-48	-18	-40	-48	-55	-66	-70	-61	-107					8
51	06	29	51	02	250	-59	-84	+20		+3	-10	-20	-37	-48	-69	-59	-84							8
51	09	04	51	02	170			+49	+2	+18	-30	-3	-29	-30	-49	-49	-56							4
51	09	21	51	02	165			+40	+1	+10	-19	-14	-37	-40	-54	-56	-68	-72	-84					2
51	09	26	51	02	194							-20	-33	-45	-54	-57	-77							7
51	11	07	51	02	273	-68	-79	+25	+8	-8	-26	-32	-47	-59	-63	-66	-100	-65	-103					2
51	11	12	51	02	272	-58	-67	+25	-4	-10	-28	-31	-56	-51	-64	-59	-83	-59	-103					2
51	11	26	51	02	227	-76	-82	+20		-11		-33		-54	-64	-68	-74							7
51	11	26	51	02	215	-80	-99	+21	-14	-9	-28	-30	-44	-51	-73	-70	-91							7
51	11	26	51	02	190			+21	-12	-10	-34	-30	-50	-55	-71	-70	-88	-87	-95					7
51	11	29	52	03	115									-50	-79	-65		-87	-108					4
51	11	30	51	02	150			+31	+2	0	-24	-20	-46	-46	-70	-65	-78	-84	-100					4
51	12	11	51	02	193			+27	-21	-6	-24	-28	-39	-57		-71		-83						6
51	12	12	51	02	216	-75	-90	+27	-18	-8	-17	-32	-37	-53	-72	-67	-79	-75	-92					6
51	12	17	51	02	200			+33	+4	-1	-27	-24	-51	-53	-69	-63	-80	-71	-93					4
51	12	18	51	01	220							-20	-27	-50	-61									4
52	01	01	51	02	250	-73	-100	+7	-18	-27	-42	-43	-63	-59	-84	-73	-100	-69	-103					6
52	01	14	51	02	189			+23	-42	-2	-9	-19	-29	-49	-54	-62	-69	-77	-86					8
52	01	25	51	02	261	-79	-89	+3	-6	-28	-42	-47	-56	-71	-79	-79	-91	-73	-114					
52	02	13	51	02	273	-74	-81	+4	-21	-23	-34	-42	-45	-69	-69	-75	-93	-75	-104					5
52	02	19	51	02	216	-81	-94	+17		-9		-32	-68	-59	-90	-75	-95	-79	-102					2
52	02	29	51	02	180			+26	+20	0	-6	-21	-26	-49	-53	-67		-89						4
52	03	04	51	02	315	-56	-83							-54	-90	-46	-102							1
52	03	11	52	04	223									-56	-68	-73	-80							8
52	03	18	51	01	328	-51	-85	+15		-20	-34	-40	-66	-53	-92	-56	-93	-57	-97					2
52	04	01	53	02	360	-52	-65	+2		-24	-36	-42	-57	-55	-73	-52	-73							1
52	04	02	51	01	360	-56	-72	+2	-16	-27	-50	-46	-62	-54	-88	-43	-93							1
52	04	04	51	02	228	-76	-95	+22	-30	-13	-55	-34	-67	-61	-82	-73	-92							2
52	04	22	51	02	344	-55						-41		-53	-88	-45	-99							1
52	04	23	51	02	392	-44	-54	+10	-4	-23	-43	-42	-53	-41	-77	-45	-78							1
52	05	06	51	01	287	-61	-66	+21		-9		-33	-43	-59	-69	-55	-80							1
52	05	07	51	04	282	-50	-73	+12		-20		-36		-47		-47	-78							1
52	05	16	51	01	180									-47	-77	-63	-84	-82	-94					2
52	05	20	51	01	250	-72	-75	+26	-20	-3	-8	-25	-29	-54	-57	-72	-75	-66	-99					2
52	05	21	52	01	227	-75	-81	+27		-3	-30	-24	-50	-53	-59	-70	-74	-70	-96					2
52	06	16	51	02	198			+30	-14	+7	-6	-15	-19	-41	-47	-60	-65	-77	-79					6
52	06	19	53	02	250	-66	-72							-52	-61									1
52	07	01	51	02	205	-66	-78	+44		+10	-9	-11	-21	-39	-45	-56	-72							4
52	07	03	51	01	215	-70	-76	+28		+5		-16		-39	-46	-59	-62	-64						7
52	07	04	51	02	185			+42	+25	+12	-9	-8	-34	-34	-45	-54	-63							7
52	07	10	52	01	185			+35		+10		-12		-35		-51	-72							4
52	07	23	51	01	180			+39	+12	+11	-27	-6	-37	-35	-51	-51	-67							4
52	08	29	51	02	190			+44	+12	+12	-14	-7	-24	-34	-38	-52	-52							4
52	09	09	51	02	330	-54	-63	+19		-11		-34		-46	-83	-39	-97							6
52	09	15	51	02	227	-69	-84	+34	-36	+2	-38	-20	-56	-46	-67	-61	-76	-66	-87					2
52	09	22	51	01	175			+37	+17	+10	-26	-11	-36											8
52	10	06	53	03	197			+33	-17	+5	-14	-14	-30	-41	-60	-57	-70	-74	-78					7
52	10	08	51	01	160			+37	+10	+3	-21	-19	-43	-48	-57	-65	-67							6
52	10	10	51	01	301	-54	-72			-10	-49	-30	-59	-54	-72	-56	-77							1
52	10	17	51	01E	216	-80	-79	+34	0	+3	-22	-20	-42	-51	-61	-69	-69	-76	-85					2
52	10	21	51	02	268			+27	-8	-3	-35	-27	-50	-53	-62									6
52	10	24	51	01	289	-42	-76							-41	-73	-43	-78							2
52	10	29	51	02	349	-52	-62					-39	-52	-48	-81									2
52	10	30	51	01	300	-51	-76					-41	-47	-51	-76	-51	-84							1
52	11	10	51	02	228	-75	-94	+29	+9	-1	-27	-25	-33	-53	-57	-69	-78	-74	-80					2
52	11	12	53	02E	262	-69	-71	+19		-9		-27	-32	-56	-66	-70	-77	-69						7
52	11	13	51	02	228	-75	-96	+15	-4	-12	-22	-29	-41	-57	-77	-70	-82							7
52	11	20	51	01	360	-47	-81							-46	-95	-49	-98							2
52	11	24	53	02E	287	-63	-73	+9		-11	-30	-30	-45	-60	-70	-66	-86							8
52	11	25	51	02	239	-68	-72	+25		-7		-29	-39	-55	-56	-66	-66							8

BC

M.R.P. 1052

Date			Approximate position		Tropopause			Standard pressure levels																
								700 mb.		500 mb.		400 mb.		300 mb.		250 mb.		200 mb.		150 mb.		125 mb.		
Year	Month	Day	Latitude (°N)	Longitude (°W except where otherwise stated)	Pressure (mb.)	Temperature (°F)	Frostpoint (°F)	Temperature (°F)	Frostpoint (°F)	Temperature (°F)	Frostpoint (°F)	Temperature (°F)	Frostpoint (°F)	Temperature (°F)	Frostpoint (°F)	Temperature (°F)	Frostpoint (°F)	Temperature (°F)	Frostpoint (°F)	Temperature (°F)	Frostpoint (°F)	Temperature (°F)	Frostpoint (°F)	Air mass classification
52	12	03	51	00	262	-60	-85	+19		-13		-35		-51	-76	-60	-88	-62	-102					6
52	12	17	51	02	345	-52	-66	+ 5	-11	-30	-55	-47	-67	-53	-76	-57	-84							1
52	12	19	51	01	280	-63	-69	+22		-10		-33		-59	-67	-60	-85							2
53	01	05	51	00	210			+20	-35	- 9	-42	-31	-50	-59	-60	-76	-77							6
53	01	20	51	02	200			+21	+ 2	-10	-37	-30	-60	-59	-64	-73	-79							4
53	01	22	51	02	231									-61	-66	-75	-77							4
53	02	02	51	02	238	-79	-92	+13		-15		-37		-64		-76	-87	-69						1
53	02	04	51	01	200			+19	-12	-12	-43	-35	-47	-60	-67									2
53	02	04	51	02	200			+16		- 9		-32		-61		-78	-78							2
53	02	06	51	02	239	-77	-93			-21	-45	-44	-57	-65	-83	-76	-93	-70	-106					1
53	02	13	51	02	261	-81	-104	+10		-17		-38		-68		-80	-108	-72	-133					6
53	02	16	51	01	238	-81	-87	+23	- 1	-11	-28	-30	-60	-59	-75	-76	-78	-82	-101					6
53	03	11	51	01	216	-83	-86	+19		- 7		-28		-55		-75	-75	-82	-92					6
53	03	13	51	01	206	-85	-90	+23	-10	- 8	-52	-29	-60	-57	-75	-72	-81	-83	-92					2
53	03	17	51	02	250	-76	-85	+20	-45	-16	-39	-37	-59	-64	-70	-76	-85	-74	-101					3
53	04	10	51	02	238	-76	-87	+16	-17	-12	-46	-33		-61	-76	-73	-83	-75	-103					6
53	04	14	51	02	300	-55	-79	+ 3	-28	-21	-62	-34	-67	-55	-79	-60	-90							1
53	04	17	51	02	274	-66	-77	+17	- 3	-11	-49	-32	-52	-60	-66	-62	-91							1
53	04	20	51	02	228	-74	-79	+25	- 1	- 8	-29	-30	-58	-55	-65	-67	-73	-69	-89					3
53	04	21	51	02	238	-73	-85	+28	- 4	- 7	-41	-29	-54	-56	-67	-71	-81	-66	-104					3
53	04	22	51	02	238	-71	-85	+26	+ 3	- 9	-27	-31	-50	-58	-73	-70	-82	-66	-100					3
53	04	23	52	01	262	-70	-75	+27	-20	- 9	-44	-30	-54	-59	-61	-70	-79	-65	-91					3
53	04	28	51	02	360	-57	-57	+12	+ 9	-21	-28	-44	-48	-52	-78	-47	-84							1
53	05	05	51	02	206	-82	-85	+29	+11	- 1	-21	-21	-41	-50	-65	-68	-75	-82	-87					4
53	05	06	52	01	213			+28	-23	0	-33	-22	-52	-50	-69	-68	-78							4
53	05	11	52	01	238	-73	-88	+25	- 6	- 7	-40	-29	-57	-55	-77	-70	-84	-66	-96					1
53	05	12	52	01	250	-73	-80	+23	+ 2	- 6	-34	-30	-47	-57	-69	-73	-80	-67	-102					1
53	05	19	51	02	239	-65	-75	+29	+11	- 4	-21	-24	-41	-52	-70	-63	-76							2
53	05	21	51	02	228	-75	-75	+30	+19	0	- 9	-20	-32	-49	-50	-67	-67	-66	-86					2
53	05	29	51	01	173			+32		+ 5	+ 3	-14	-15	-39	-39	-56	-57	-72	-101					7
53	06	09	51	01	238	-63	-83			- 4		-16		-45	-68	-60	-76	-66						1
53	06	10	51	01	238	-64	-82	+32	- 7	-12	-36	-14	-42	-45	-59	-59	-73	-62	-84					1
53	06	17	51	01	288	-60	-64			- 7	- 5	-30	-30	-58	-62	-49	-79	-46						1
53	06	18	51	01	300	-54	-71			- 7	-16	-30	-46	-54	-71	-51	-90	-47	-102					1
53	06	22	51	01	279			+29	+ 7	- 3	-30	-26	-36											2
53	06	22	51	01	330	-44	-56			- 3	-30	-25	-32	-43	-85	-42								2
53	06	23	51	01	260	-60	-68	+26	+26	+ 2	- 4	-19	-30	-48	-52	-56	-76							2
53	06	23	51	01	254			+29	+17	+ 1	-30	-20	-40	-49	-56									2
53	07	30	51	01	236	-62	-68	+26	+11	0	-20	-16	-18	-42		-57	-62							7
53	08	07	51	01	228	-61	-62	+43	+ 9	+ 7	- 6	-12	-34	-34	-49	-52	-53	-61	-93					4
53	08	07	51	01	228							-10	-30	-36	-49	-54	-57							4
53	08	11	51	01	200			+43	- 6	+10	-47	-11	-51	-39	-56	-58	-73							2
53	08	13	51	01	206	-70	-83	+39	-12	+ 9	-17	- 9	-18	-37	-40	-53	-57	-68	-83					2
53	08	18	51	01	182			+27	-18	+ 6	-30	-14	-30	-41	-56	-56	-77							7
53	08	19	51	01	198			+33	+ 3	+ 5	- 2	-12	-22	-41	-62	-60	-74	-76						7
53	09	04	51	01	227	-61	-81	+37	+30	+ 9	-28	-11	-45	-41	-72	-58	-77							7
54	01	12	51	01	207	-86		+19	-48	-15	-17	-37	-37	-62	-62	-78	-81	-86						2
54	01	19	51	01	206	-82	-90	+34	+10	+ 4	-38	-18	-58	-50	-64	-70	-78	-82	-93	-72	-123	-72	-120	4
54	02	04	51	01	275			+ 8	-57	-19	-47	-40	-57	-63	-82									3
54	02	22	51	01	205	-84	-87	+33	+12	- 1	-24	-23	-54	-50	-58	-69	-74	-84	-88	-66	-106	-67	-107	4
54	02	23	51	02	262	-70	-87	+ 8	- 4	-18	-29	-40	-47	-65	-77	-69	-89	-64	-96					2
54	02	24	51	01	262	-62	-90	+17	+ 4	-18	-35	-40	-59	-54	-88	-62	-93	-60	-104	-58	-115	-58	-113	2
54	02	25	51	01	250	-60	-92	+12	- 4	-14	-60	-28	-69	-53	-81	-60	-92	-51	-109	-55	-117	-52	-118	1
54	03	05	51	01	237	-71	-97	+10	-29	-22	-67	-43	-68	-58	-77	-69	-93	-63	-110	-60	-115	-62	-117	1
54	03	10	51	01	227	-69	-89	+22	-25	- 8	-38	-29	-59	-52	-74	-65	-83	-69	-99	-63	-116	-61	-120	2
54	03	11	51	01	250	-60	-91	+24	+ 2	- 6	-40	-26	-58	-50	-81	-60	-91	-58	-111	-60	-120	-66	-122	2
54	03	22	51	02	228	-69	-79	+33	- 2	0	-26	-20	-25	-52	-53	-66	-73	-71	-88	-58	-110	-56	-117	4
54	03	23	51	02	301	-57	-82	+27	-37	-10	-47	-32	-57	-57	-82	-55	-99	-53	-109	-51	-118	-53	-121	2
54	04	06	51	01	227	-74	-86	+ 6	-36	-17	-57	-36	-62	-58	-65	-70	-81	-67	-94					1
54	05	13	51	01	206	-77	-88	+31	+25	0	- 6	-20	-30	-49	-63	-64	-71	-77	-92					2
54	05	25	51	01	227	-67	-86	+25	+12	+ 1	- 2	-20	-21	-48	-49	-64	-76	-61	-93	-54	-118			2
54	05	28	51	01	186	-71	-91	+34	+25	+ 4	+ 3	-16	-29	-41	-46	-57	-62	-66	-87					2
54	06	10	51	01	265									-51	-74	-49	-88	-47	-107	-45	-116	-45	-118	1
54	06	11	51	01	275									-54	-74	-51	-97	-46	-112	-47	-119	-48	-121	1
54	06	16	51	01	238	-67	-78	+38	+25	+10	- 3	-13	-29	-42	-58	-62	-74	-59	-97	-60	-110	-58	-110	7
54	06	24	51	01	188	-76	-90							-39	-48	-56	-63	-72	-84	-61	-113	-60	-118	6
54	06	28	51	01	275									-52	-65	-53	-89	-45	-105	-45	-111			1
54	06	29	51	01	250	-57	-84	+33	+12	+ 2	-23	-19	-44	-47	-63	-57	-84	-46	-109	-45	-120	-45	-120	1
54	07	01	51	01	238	-60	-79							-45	-45	-57	-72	-56	-102	-52	-116	-52	-119	2
54	07	05	51	01	300									-45	-85	-42	-100	-42	-109	-43	-116	-47	-118	1
54	07	06	51	01	300	-49	-83	+18	- 3	-15	-35	-35	-52	-49	-83	-43	-98	-42	-109	-43	-113	-47	-116	1
54	07	14	51	01	227	-64	-69	+33	-11	+ 4	-51	-13	-41	-39	-56	-57	-62	-66	-94	-54	-117	-56	-119	7
54	08	04	51	01	227	-61	-83	+40	+11	+ 9	-10	-14	-30	-44	-57	-57	-74	-51	-95	-57	-111	-59	-119	2
54	08	05	51	01	228	-65	-75							-35	-52	-57	-69	-67	-86	-67	-90	-65	-94	2

BC

M.R.P. 1052

Date			Approximate position		Tropopause			Standard pressure levels																Air mass classification	Circulation
								700 mb.		500 mb.		400 mb.		300 mb.		250 mb.		200 mb.		150 mb.		125 mb			
Year	Month	Day	Latitude (°N)	Longitude (°W. except where otherwise stated)	Pressure (mb)	Temperature (°F)	Frostpoint (°F)	Temperature (°F)	Frostpoint (°F)	Temperature (°F)	Frostpoint (°F)	Temperature (°F)	Frostpoint (°F)	Temperature (°F)	Frostpoint (°F)	Temperature (°F)	Frostpoint (°F)	Temperature (°F)	Frostpoint (°F)	Temperature (°F)	Frostpoint (°F)	Temperature (°F)	Frostpoint (°F)		
54	08	10	51	01	252	-58	-75	+26	+17	- 1	-30	-24	-54	-51	-59	-55	-79	-45	-94	-49	-109	-49	-117	1	2
54	08	11	51	01	262	-53	-80	+30	-12	+ 1	-19	-20	-25	-47	-53	-51	-84	-51	-97	-55	-113	-56	-118	6	2
54	08	17	51	01	227	-61	-84	+39	+27	+ 7	- 4	-11	-28	-42	-67	-58	-70	-57	-97	-59	-114	-61	-119	8	5
54	08	23	51	01	261	-57	-86	+27	+ 8	- 5	-28	-25	-42	-50	-77	-56	-90	-49	-101	-47	-111	-52	-104	2	3
54	08	26	51	01	228	-66	-73	+36	+13	+11	-30	- 9	-36	-39	-61	-59	-68	-66	-82	-60	-107	-66	-112	7	6
54	12	09	51	01	300									-67	-81	-65	-101	-68	-112					1	3
54	12	10	51	01	328	-70	-83	+ 8	-26	-28	-43	-53	-55	-67	-93	-68	-110	-69	-117	-72	-122	-76	-122	1	3
54	12	13	51	01	226	-72	-86			- 5	-20	-26	-36	-51	-59	-67	-82	-69	-100	-69	-113	-74	-116	7	
54	12	14	51	01	205	-82	-91	+31	-37	0	- 5	-24	-32	-48	-64	-66	-71	-80	-95	-74	-120	-76	-123	4	
54	12	20	51	01	205	-81	-98	+27	0	- 1	-49	-27	-55	-57	-77	-73	-84	-80	-100	-77	-114	-73	-117	7	
54	12	21	51	01	187	-95	-98	+24	+18	+ 1	-44	-20	-44	-45	-68	-65	-71	-88	-91	-83	-110			7	
54	12	22	51	01	170	-97	-109	+27	+15	- 4	-13	-21	-35	-49	-63	-66	-75	-86	-93	-84	-115	-76	-117	7	
55	02	03	51	00	301	-55	-94	+ 8	-23	-26	-43	-40	-73	-55	-94	-52	-99	-50	-114	-53		-62		2	
55	02	04	50	00	301	-62	-82	+12	-17	-18	-32	-39	-54	-62	-82	-65	-95	-58	-110	-57	-115			2	
55	02	07	51	02	235	-73	-77	+24	+ 8	- 3	-22	-24	-38	-53	-66	-69	-75	-74						4	
55	02	08	51	02	225	-79	-79	+19	- 4	- 4	-14	-24	-40	-54	-73	-71	-75	-81	-96	-73	-116	-70	-118	7	
55	02	08	51	02	250	-69	-77	+16	-33	- 7	-18	-26	-35	-52	-68	-69	-77	-73	-101	-68	-117	-66	-119	7	
55	02	09	51	00	301	-61	-82	+15	0	-19	-43	-38	-77	-61	-82	-64	-93	-62	-108	-60	-112	-68		2	
55	02	11	51	02	370	-58	-72	+ 1	-49	-28	-38	-50	-63	-62	-93	-61	-101	-59	-110	-61	-113	-63	-118	0	
55	02	14	51	02	275	-69	-91	+11	-55	-21		-41		-63	-81	-70	-93	-70	-102	-60	-109	-61	-111	2	
55	02	15	51	02	235	-69	-103	+ 7		-23		-42		-60	-78	-67	-98	-63	-111	-66	-115	-63	-119	5	
55	02	16	51	00	301	-62	-81	+ 7	- 8	-17	-48	-37	-64	-62	-81	-67	-95	-65	-109	-59	-117	-70	-120	1	
55	02	28	51	01	187	-87	-97	+19		- 5		-23	-32	-53	-68	-71	-75	-84	-92	-78	-114	-79	-118	9	
55	03	01	51	01	187	-92	-101							-54	-67	-73	-78	-89	-96	-80	-117			9	
55	03	02	51	01	187	-94	-100							-57	-69	-76	-85	-91	-99	-80	-114	-76	-117	3	
55	03	03	51	02	187	-88	-100	+23	- 2	- 5	-27	-29	-49	-59	-73	-70	-88	-84	-98	-79	-113			3	
55	03	04	51	01	206	-91	-97	+22		- 9		-32		-61	-70	-77	-81	-89	-97	-75	-113	-72	-117	1	
55	03	09	51	02	275	-70	-75	+ 4		-22		-41		-64	-73	-68	-83	-67	-91	-64	-90	-64	-91	6	
55	03	10	51	01	228															-71	-109	-68	-111	6	
55	03	10	51	02	285	-67	-73					-37		-63	-69	-74	-84	-76	-95	-70	-105	-74	-102	6	
55	03	11	51	01	227	-83	-89					-30		-60	-70	-75	-83	-84	-93	-73	-101	-71	-108	6	
55	03	14	51	01	187	-98	-106					-30		-59	-65	-73	-84	-92	-102	-82	-116	-74	-118	2	
55	03	15	51	01	175									-62	-71	-77	-81	-89	-93					2	
55	03	16	51	01	215									-64		-79	-85	-89	-94					2	
55	03	18	51	02	275	-70	-83	+13	-11	-17	-42	-37	-63	-63	-77	-72	-92	-77	-100	-74	-116	-70	-118	1	
55	03	18	51	01	301	-64	-73			-15		-38		-64	-73	-74	-92	-75	-103					1	
55	03	21	51	00	250	-75	-91	+12	-14	-14	-47	-35	-64	-61	-81	-75	-91	-70	-109	-62	-117	-61	-117	1	
55	03	28	51	01	274	-73	-77					-40	-52	-67	-71	-69	-93							1	
55	08	30	51	02	215	-65	-91	+34	+17	+ 6	-19	-17	-25	-43	-74	-59	-83	-62	-99	-61	-115	-67	-117	2	
55	08	31	51	02	250	-63	-77	+28	+19	0	-17	-20	-51	-47	-67	-63	-77	-61	-104	-63	-117	-60	-118	2	
55	09	29	52	01E	178	-84	-92							-40	-59	-58	-70	-75	-87	-83	-108	-88	-115	7	
55	10	04	51	01	250	-67	-81							-56	-75	-67	-81	-65	-98	-65	-115	-67	-118	7	
55	10	12	51	01	197	-77	-92	+28	+14	0	8	-20	-19	-49	-52	-63	-73	-75	-88	-72				4	
55	10	17	51	01	238	-74	-89	+13	-22	- 9		-33		-54		-69	-85	-70	-100					6	
55	10	18	51	01	301	-65	-67	+10	-25	-16	-23	-36	-38	-65	-67	-68	-92	-61	-108					6	
55	10	18	51	01	287	-68	-72					-34	-48	-63	-68	-68	-93	-64	-108	-61	-113	-64	-114	6	
55	10	20	51	01	287	-60	-76	+20	-18	-13	-22	-32	-52	-56	-72	-51	-95	-48	-106	-57	-110	-63	-112	6	
55	10	26	51	01	206	-84	-88	+29		- 4		-23		-48	-62	-68	-73	-82						4	
55	10	28	51	00	287	-63	-83	+10	-13	-15	-54	-34	-62	-59	-78	-65	-92	-69	-102	-66	-115	-66	-117	1	
55	10	31	51	00	206	-85	-90	+20	0	- 9	-23	-31	-46	-59	-71	-75	-86	-80	-94	-73	-113	-72	-116	6	
55	11	01	51	00	238	-75	-90	+19	- 7	-12	-22	-35	-46	-61	-81	-72	-85	-71	-104	-71	-113	-70	-116	4	
55	11	08	51	00	262	-71	-74	+22	+19	-10	-40	-34	-52	-61	-72	-70	-80	-67	-103	-64	-112	-66	-115	2	
55	11	11	51	02	238	-82	-86	+25		- 6		-27		-59	-67	-78	-83	-75	-104					7	
55	11	22	51	00	227	-73	-93	+15	-13	-10	-39	-29	-52	-50	-77	-63	-89	-75	-100	-78	-113	-79	-112	2	
55	11	28	51	00	227	-79	-85	+26		- 7		-29		-59		-74	-81	-79	-94	-74	-113	-75	-117	2	
55	11	29	50	05	206	-72	-95	+25		- 7		-23		-50	-82	-64	-90	-72.	-97	-74	-114	-76	-117	2	
55	12	01	52	02	227	-64	-99					-36		-55	-84	-62	-92	-65	-107	-69	-115	-70	-120	2	

Air mass classification key

Code	Type
0	Arctic
1	Polar
2	Polar Maritime
3	Polar Continental
4	Tropical
5	Polar/Arctic
6	Polar Maritime/Polar
7	Tropical/Polar Maritime
8	Tropical/Polar
9	Tropical/Polar Continental

Circulation classification key

Code	Type
1	Anticyclonic
2	Intermediate
3	Cyclonic
4	Intermediate/Cyclonic
5	Cyclonic/Intermediate
6	Intermediate/Anticyclonic
7	Cyclonic/Anticyclonic
8	Anticyclonic/Intermediate
9	Anticyclonic/Cyclonic

In the compound classifications, the first named refers to the upper level, about 300 mb - e.g., Polar/Arctic indicates polar air overlying arctic air; and Cyclonic/Anticyclonic indicates the circulation at 300 mb is cyclonic while that at the surface is anticyclonic.

BC

M.R.P. 1052

Date			Approximate position		Tropopause			Standard pressure levels																	
								700 mb.		500 mb.		400 mb.		300 mb.		250 mb.		200 mb.		150 mb.		125 mb			
Year	Month	Day	Latitude (°N)	Longitude (°W except where otherwise stated)	Pressure (mb)	Temperature (°F)	Frostpoint (°F)	Temperature (°F)	Frostpoint (°F)	Temperature (°F)	Frostpoint (°F)	Temperature (°F)	Frostpoint (°F)	Temperature (°F)	Frostpoint (°F)	Temperature (°F)	Frostpoint (°F)	Temperature (°F)	Frostpoint (°F)	Temperature (°F)	Frostpoint (°F)	Temperature (°F)	Frostpoint (°F)	Air mass classification	
54	08	10	51	01	252	-58	-75	+26	+17	-1	-30	-24	-54	-51	-59	-55	-79	-45	-94	-49	-109	-49	-117	1	
54	08	11	51	01	262	-53	-80	+30	-12	+1	-19	-20	-25	-47	-53	-51	-84	-51	-97	-55	-113	-56	-118	6	
54	08	17	51	01	227	-61	-84	+39	+27	+7	-4	-11	-28	-42	-67	-58	-70	-57	-97	-59	-114	-61	-119	8	
54	08	23	51	01	261	-57	-86	+27	+8	-5	-28	-25	-42	-50	-77	-56	-90	-49	-101	-47	-111	-52	-104	2	
54	08	26	51	01	228	-66	-73	+36	-13	+11	-30	-9	-36	-39	-61	-59	-68	-66	-82	-60	-107	-66	-112	7	
54	12	09	51	01	300									-67	-81	-65	-101	-68	-112					1	
54	12	10	51	01	328	-70	-83	+8	-26	-28	-43	-53	-55	-67	-93	-68	-110	-69	-117	-72	-122	-76	-122	1	
54	12	13	51	01	226	-72	-86			-5	-20	-26	-36	-51	-59	-67	-82	-69	-100	-69	-113	-74	-116	7	
54	12	14	51	01	205	-82	-91	+31	-37	0	-5	-24	-32	-48	-64	-66	-71	-80	-95	-74	-120	-76	-123	4	
54	12	20	51	01	205	-81	-98	+27	0	-1	-49	-27	-55	-57	-77	-73	-84	-80	-100	-77	-114	-73	-117	7	
54	12	21	51	01	187	-95	-98	+24	+18	+1	-44	-20	-44	-45	-68	-65	-71	-88	-91	-83	-110			7	
54	12	22	51	01	170	-97	-109	+27	+15	-4	-13	-21	-35	-49	-63	-66	-75	-86	-93	-84	-115	-76	-117	7	
55	02	03	51	00	301	-55	-94	+8	-23	-26	-43	-40	-73	-55	-94	-52	-99	-50	-114	-53		-62		2	
55	02	04	50	00	301	-62	-82	+12	-17	-18	-32	-39	-54	-62	-82	-65	-95	-58	-110	-57	-115			2	
55	02	07	51	02	235	-73	-77	+24	+8	-3	-22	-24	-38	-53	-66	-69	-75	-74						4	
55	02	08	51	02	225	-79	-79	+19	-4	-4	-14	-24	-40	-54	-73	-71	-75	-81	-96	-73	-116	-70	-118	7	
55	02	08	51	02	250	-69	-77	+16	-33	-7	-18	-26	-35	-52	-68	-69	-77	-73	-101	-68	-117	-66	-119	7	
55	02	09	51	00	301	-61	-82	+15	0	-19	-43	-38	-77	-61	-82	-64	-93	-62	-108	-60	-112	-68		2	
55	02	11	51	02	370	-58	-72	+1	-49	-28	-38	-50	-63	-62	-93	-61	-101	-59	-110	-61	-113	-63	-118	0	
55	02	14	51	02	275	-69	-91	+11	-55	-21		-41		-63	-81	-70	-93	-70	-102	-60	-109	-61	-111	2	
55	02	15	51	02	235	-69	-103	+7		-23		-42		-60	-78	-67	-98	-63	-111	-66	-115	-63	-119	5	
55	02	16	51	00	301	-62	-81	+7	-8	-17	-48	-37	-64	-62	-81	-67	-95	-65	-109	-59	-117	-70	-120	1	
55	02	28	51	01	187	-87	-97	+19		-5		-23	-32	-53	-68	-71	-75	-84	-92	-78	-114	-79	-118	9	
55	03	01	51	01	187	-92	-101							-54	-67	-73	-78	-89	-96	-80	-117			9	
55	03	02	51	01	187	-94	-100							-57	-69	-76	-85	-91	-99	-80	-114	-76	-117	3	
55	03	03	51	02	187	-88	-100	+23	-2	-5	-27	-29	-49	-59	-73	-70	-88	-84	-98	-79	-113			3	
55	03	04	51	01	206	-91	-97	+22		-9		-32		-61	-70	-77	-81	-89	-97	-75	-113	-72	-117	1	
55	03	09	51	02	275	-70	-75	+4		-22		-41		-64	-73	-68	-83	-67	-91	-64	-90	-64	-91	6	
55	03	10	51	01	228															-71	-109	-68	-111	6	
55	03	10	51	02	285	-67	-73					-37		-63	-69	-74	-84	-76	-95	-70	-105	-74	-102	6	
55	03	11	51	01	227	-83	-89					-30		-60	-70	-75	-83	-84	-93	-73	-101	-71	-108	6	
55	03	14	51	01	187	-98	-106					-30		-59	-65	-73	-84	-92	-102	-82	-116	-74	-118	2	
55	03	15	51	01	175									-62	-71	-77	-81	-89	-93					2	
55	03	16	51	01	215									-64		-79	-85	-89	-94					2	
55	03	18	51	02	275	-70	-83	+13	-11	-17	-42	-37	-63	-63	-77	-72	-92	-77	-100	-74	-116	-70	-118	1	
55	03	18	51	01	301	-64	-73			-15		-38		-64	-73	-74	-92	-75	-103					1	
55	03	21	51	00	250	-75	-91	+12	-14	-14	-47	-35	-64	-61	-81	-75	-91	-70	-109	-62	-117	-61	-117	1	
55	03	28	51	01	274	-73	-77					-40	-52	-67	-71	-69	-93							1	
55	08	30	51	02	215	-65	-91	+34	+17	+6	-19	-17	-25	-43	-74	-59	-83	-62	-99	-61	-115	-67	-117	2	
55	08	31	51	02	250	-63	-77	+28	+19	0	-17	-20	-51	-47	-67	-63	-77	-61	-104	-63	-117	-60	-118	2	
55	09	29	52	01E	178	-84	-92							-40	-59	-58	-70	-75	-87	-83	-108	-88	-115	7	
55	10	04	51	01	250	-67	-81							-56	-75	-67	-81	-65	-98	-65	-115	-67	-118	7	
55	10	12	51	01	197	-77	-92	+28	+14	0	8	-20	-19	-49	-52	-63	-73	-75	-88	-72				4	
55	10	17	51	01	238	-74	-89	+13	-22	-9		-33		-54		-69	-85	-70	-100					6	
55	10	18	51	01	301	-65	-67	+10	-25	-16	-23	-36	-38	-65	-67	-68	-92	-61	-108					6	
55	10	18	51	01	287	-68	-72					-34	-48	-63	-68	-68	-93	-64	-108	-61	-113	-64	-114	6	
55	10	20	51	01	287	-60	-76	+20	-18	-13	-22	-32	-52	-56	-72	-51	-95	-48	-106	-57	-110	-63	-112	6	
55	10	26	51	01	206	-84	-88	+29		-4		-23		-48	-62	-68	-73	-82						4	
55	10	28	51	00	287	-63	-83	+10	-13	-15	-54	-34	-62	-59	-78	-65	-92	-69	-102	-66	-115	-66	-117	1	
55	10	31	51	00	206	-85	-90	+20	0	-9	-23	-31	-46	-59	-71	-75	-86	-80	-94	-73	-113	-72	-116	6	
55	11	01	51	00	238	-75	-90	+19	-7	-12	-22	-35	-46	-61	-81	-72	-85	-71	-104	-71	-113	-70	-116	4	
55	11	08	51	00	262	-71	-74	+22	+19	-10	-40	-34	-52	-61	-72	-70	-80	-67	-103	-64	-112	-66	-115	2	
55	11	11	51	02	238	-82	-86	+25		-6		-27		-59	-67	-78	-83	-75	-104					7	
55	11	22	51	00	227	-73	-93	+15	-13	-10	-39	-29	-52	-50	-77	-63	-89	-75	-100	-78	-113	-79	-112	2	
55	11	28	51	00	227	-79	-85	+26		-7		-29		-59		-74	-81	-79	-94	-74	-113	-75	-117	2	
55	11	29	50	05	206	-72	-95	+25		-7		-23		-50	-82	-64	-90	-72	-97	-74	-114	-76	-117	2	
55	12	01	52	02	227	-64	-99					-36		-55	-84	-62	-92	-65	-107	-69	-115	-70	-120	2	

Air mass classification key

Code	Type
0	Arctic
1	Polar
2	Polar Maritime
3	Polar Continental
4	Tropical
5	Polar/Arctic
6	Polar Maritime/Polar
7	Tropical/Polar Maritime
8	Tropical/Polar
9	Tropical/Polar Continental

Circulation classification key

Code	Type
1	Anticyclonic
2	Intermediate
3	Cyclonic
4	Intermediate/Cyclonic
5	Cyclonic/Intermediate
6	Intermediate/Anticyclonic
7	Cyclonic/Anticyclonic
8	Anticyclonic/Intermediate
9	Anticyclonic/Cyclonic

In the compound classifications, the first named refers to the upper level, about 300 mb - e.g., Polar/Arctic indicates polar air overlying arcti air; and Cyclonic/Anticyclonic indicates the circulation at 300 mb is cyclonic while that at the surface is anticyclonic.

Mean seasonal values of temperature (T) and frostpoint (F) at standard pressure levels

		Winter						Spring						Summer						Autumn					
		Canberra		Pre-Canberra		All observations		Canberra		Pre-Canberra		All observations		Canberra		Pre-Canberra		All observations		Canberra		Pre-Canberra		All observations	
			No. of obs.		No. of obs.		No. of obs.		No. of obs.		No. of obs.		No. of obs.		No. of obs.		No. of obs.		No. of obs.		No. of obs.		No. of obs.		No. of obs.
Tropopause	P_c mb	246.0	38	250.3	68	248.7	106	233.7	10	247.5	107	246.3	117	242.4	14	224.1	81	226.7	95	239.3	23	240.8	58	243.8	81
	T_c °F	-72.9	34	-71.9	55	-72.3	89	-69.9	7	-66.4	91	-66.7	98	-62.0	13	-62.8	59	-62.7	72	-75.3	22	-65.0	41	-68.6	63
	F_c °F	-87.4	33	-86.3	54	-86.7	87	-86.1	7	-79.4	90	-79.9	97	-80.5	13	-77.6	58	-78.1	71	-87.5	22	-80.0	41	-82.6	63
700 mb	T °F	+16.4	28	+15.2	29	+15.8	57	+27.8	6	+23.9	43	+24.4	49	+31.1	10	+33.2	42	+32.8	52	+21.1	18	+24.8	45	+23.7	63
	F °F	-16.8	23	-12.7	20	-14.9	43	+10.5	6	- 1.3	32	+ 0.6	38	+ 6.0	10	+ 7.7	32	+ 7.3	42	- 4.5	13	- 1.1	35	- 2.0	48
500 mb	T °F	-13.9	27	-13.5	65	-13.6	92	0	5	- 6.9	99	- 6.6	104	+ 1.7	10	+ 4.3	71	+ 4.0	81	- 9.1	17	- 5.3	51	- 6.0	68
	F °F	-36.6	23	-36.8	45	-36.7	68	-14.7	6	-27.2	92	-26.4	98	-24.3	10	-19.5	67	-20.1	77	-28.9	14	-27.6	43	-27.9	57
400 mb	T °F	-33.9	32	-33.7	60	-33.8	92	-20.7	6	-25.7	104	-25.4	110	-18.8	10	-15.9	79	-16.3	89	-29.9	21	-27.4	55	-28.1	76
	F °F	-55.0	24	-52.2	53	-51.7	77	-35.8	6	-46.8	100	-46.2	106	-38.4	10	-36.5	75	-36.7	85	-44.8	15	-46.4	50	-46.0	65
300 mb	T °F	-58.6	36	-56.9	68	-57.5	104	-48.1	10	-50.7	106	-50.5	116	-44.0	14	-42.2	79	-42.4	93	-56.0	23	-50.6	58	-52.1	81
	F °F	-74.5	35	-75.7	64	-75.3	99	-60.5	10	-68.1	104	-67.5	114	-63.9	14	-56.5	77	-57.7	91	-72.0	21	-69.9	54	-70.5	75
250 mb	T °F	-68.1	36	-66.5	67	-67.0	103	-58.3	10	-61.3	103	-61.0	113	-55.1	14	-55.5	80	-55.4	94	-67.3	23	-61.0	55	-62.9	78
	F °F	-86.7	36	-87.8	66	-87.5	102	-78.5	10	-81.1	102	-80.8	112	-78.3	14	-73.4	80	-74.1	94	-85.4	23	-82.7	51	-83.5	74
200 mb	T °F	-72.9	35	-71.7	51	-72.2	86	-58.6	10	-67.0	80	-66.0	90	-56.4	14	-62.2	58	-61.4	72	-72.1	23	-70.9	37	-71.4	60
	F °F	-100.9	33	-97.5	49	-98.9	82	-98.0	10	-96.8	78	-96.9	88	-96.9	14	-93.1	56	-93.8	70	-101.0	22	-95.1	33	-97.1	55
150 mb	T °F	-66.3	30	-	-	-66.3	30	-51.0	7	-	-	-51.0	7	-56.6	14	-	-	-56.6	14	-71.3	18	-	-	-71.3	18
	F °F	-113.1	24	-	-	-113.1	24	-115.3	7	-	-	-115.3	7	-111.2	14	-	-	-111.2	14	-114.1	17	-	-	-114.1	17
125 mb	T °F	-65.9	27	-	-	-65.9	27	-51.2	5	-	-	-51.2	5	-58.9	14	-	-	-58.9	14	-71.4	16	-	-	-71.4	16
	F °F	-115.1	25	-	-	-115.1	25	-117.4	5	-	-	-117.4	5	-114.7	14	-	-	-114.7	14	-116.8	16	-	-	-116.8	16

TABLE III

Mean relative humidity (R.H., %) and humidity mixing ratio (r, g/Kg)

Tropopause pressure (mb) / Level (mb)	Winter			Spring			Summer			Autumn			Year	
	248.7			246.3			226.7			243.8			241.4	
	R.H.	r	n	R.H.	r	n	R.H.	r	n	R.H.	r	n	R.H.	r
Tropopause	33.2	.0118	87	37.6	.0203	97	32.4	.0253	71	35.0	.0166	63	34.6	.0179
700	20.0	.5052	43	30.7	1.1687	38	29.4	1.6504	42	27.6	1.0194	48	26.6	1.0035
500	25.8	.1961	68	32.7	.3654	98	27.0	.5273	77	29.0	.3343	57	28.4	.3363
400	31.9	.0936	77	27.7	.1343	106	30.0	.2452	85	33.0	.1361	65	30.7	.1443
300	28.0	.0236	99	31.0	.0419	114	36.4	.0832	91	27.7	.0337	75	30.7	.0413
250	21.1	.0110	102	23.5	.0187	112	26.5	.0310	94	21.7	.0151	74	23.2	.0177
200	12.1	.0054	82	9.1	.0064	88	8.5	.0083	70	13.3	.0063	55	10.5	.0065
150	2.2	.0021	29	0.6	.0017	7	1.4	.0024	14	2.9	.0019	17	1.5	.0020
125	1.9	.0019	25	0.5	.0016	5	1.2	.0021	14	2.3	.0017	16	1.3	.0019

n denotes the number of observations. Values for the year were derived by giving equal weight to seasonal values of temperature and frostpoint.

G.17898/(c)/JEK/5/57/50

TABLE IV

Weighted mean seasonal and annual temperatures and frostpoints: datum level the tropopause

'n' indicates the number of 'tropopause pressure groups' used to derive the mean

Level	Winter			Spring			Summer			Autumn			Annual				
													All obs.			Canberra obs.	
	T(-°F)	F(-°F)	n	T(-°F)	F(-°F)	n	T(-°F)	F(-°F)	n	T(-°F)	F(-°F)	n	T(-°F)	F(-°F)	n	F(-°F)	n
P_c-150 mb	66.5	105.5	1	50.3	117.4	2	44.0	114.5	1	66.0	114.0	1	59.2	110.9	5	112.9	3
P_c-125 mb	61.1	111.9	2	46.7	116.3	3	52.7	113.3	2	63.9	114.3	2	56.9	111.5	6	112.9	4
P_c-100 mb	63.0	111.2	4	47.6	113.1	3	56.2	112.6	3	59.0	111.9	4	56.5	108.3	6	111.5	5
P_c-75 mb	71.1	110.5	6	55.9	111.2	5	57.2	109.2	5	65.1	108.7	5	62.5	107.8	7	106.4	6
P_c-50 mb	71.0	104.5	6	59.5	103.9	5	59.2	103.5	6	70.4	103.1	6	67.3	105.7	12	104.6	12
P_c-25 mb	74.6	98.2	6	63.6	93.4	5	61.2	93.8	6	72.4	95.9	7	70.1	96.9	12	101.4	12
P_c mb	77.9	90.6	6	70.0	83.0	6	66.6	79.8	7	74.7	87.6	7	73.1	85.7	12	88.6	12
P_c+25 mb	72.7	85.2	7	63.2	75.8	7	59.2	72.6	7	65.7	79.0	7	65.7	77.9	12		
P_c+50 mb	66.3	78.3	7	56.1	69.1	7	51.6	67.5	7	59.1	72.8	7	58.3	71.1	12		
P_c+75 mb	59.2	72.6	7	48.5	63.0	7	43.4	58.6	7	51.4	66.0	7	50.7	64.2	12		
P_c+100 mb	51.8	65.8	7	41.5	58.1	7	35.7	52.7	7	44.1	59.6	7	43.6	58.8	12		
P_c+125 mb	44.8	61.2	7	34.7	52.9	7	28.8	46.4	6	37.2	53.5	7	36.3	53.1	12		
P_c+150 mb	36.5	55.5	7	27.9	47.4	7	22.3	41.8	6	30.8	48.2	7	30.3	47.4	12		

TABLE V

A

The evaluation of $r = r_0 + (r_t - r_0) \exp - wz/K$

(which is the solution to Brewer's eqn. $K \frac{\partial^2 r}{\partial z^2} + w \frac{\partial r}{\partial z} = 0$)

z is the height above the tropopause

Computed values of r (g/Kg)

w/K	1.0	1.5	1.0	1.5	1.0	1.5	1.0	1.5	x 10^{-5} c.g.s. units
	Winter		Spring		Summer		Autumn		
	r_o = .00250		r_o = .00210		r_o = .00251		r_o = .00250		g/Kg
z	r_t = .00939		r_t = .01685		r_t = .02328		r_t = .01389		g/Kg
5 Km	.00255	.00250	.00220	.00211	.00265	.00252	.00258	.00251	
4 Km	.00263	.00252	.00237	.00214	.00289	.00256	.00271	.00253	
3 Km	.00284	.00258	.00283	.00226	.00354	.00274	.00307	.00263	
2 Km	.00343	.00284	.00409	.00283	.00531	.00354	.00404	.00307	
1 Km	.00504	.00404	.00753	.00539	.01015	.00714	.00669	.00504	
0.5 Km	.00668	.00576	.01105	.00908	.01512	.01233	.00941	.00789	
0	.00939	.00939	.01685	.01685	.02328	.02328	.01389	.01389	

B Observed mean humidity mixing ratio (datum level the tropopause)

	Winter			Spring			Summer			Autumn		
	F(°C)	e_s(mb)	r(g/Kg)	F	e_s	r	F	e_s	r	F	e_s	r
(P_c-150)*	-80.5	.000504	.00395	-	-	-	-83.2	.000321	.00263	-82.4	.000367	.00279
P_c-150	-76.4	.000979	.00767	-83.0	.000332	.00249	-81.4	.000434	.00356	-81.1	.000456	.00346
P_c-125	-79.9	.000556	.00331	-82.4	.000367	.00211	-80.7	.000487	.00300	-81.3	.000441	.00257
P_c-100	-79.6	.000584	.00281	-80.6	.000496	.00232	-80.3	.000521	.00258	-79.9	.000556	.00262
P_c -75	-79.2	.000624	.00251	-79.6	.000584	.00230	-78.4	.000710	.00293	-78.2	.000734	.00291
P_c -50	-75.8	.001076	.00373	-75.5	.001128	.00383	-74.7	.001279	.00453	-74.3	.001360	.00465
P_c -25	-72.3	.001850	.00563	-69.7	.002734	.00817	-69.1	.002988	.00925	-70.3	.002501	.00752
P_c	-68.1	.003460	.00939	-63.9	.006313	.01685	-61.8	.008452	.02328	-65.3	.005180	.01389
Tropopause height (P_c)	229.4 mb			233.0 mb			225.8 mb			231.9 mb		

In three seasons, only one tropopause group extends to P_c-150 mb, (P_c-150)* represents the value computed by applying the lapse of this group to the mean value at P_c-125 mb.

e_s is the saturation vapour pressure.

F(°F) at these levels are given in Table IV, °C are used here so that all units in this table are in the c.g.s. system.

TABLE VI

Ratio of frostpoint lapse ($\delta F/\delta z$) above and below the tropopause

(based on 25 mb finite difference)

Suffix A refers to above the tropopause, and suffix B to below

Pressure Group	Winter			Spring			Summer			Autumn			Annual		
	$\frac{\partial F}{\delta z}/A$	$\frac{\partial F}{\delta z}/B$	Ratio $^A/_B$	$\frac{\partial F}{\delta z}/A$	$\frac{\partial F}{\delta z}/B$	Ratio $^A/_B$	$\frac{\partial F}{\delta z}/A$	$\frac{\partial F}{\delta z}/B$	Ratio $^A/_B$	$\frac{\partial F}{\delta z}/A$	$\frac{\partial F}{\delta z}/B$	Ratio $^A/_B$	$\frac{\partial F}{\partial z}/A$	$\frac{\partial F}{\partial z}/B$	Ratio
4	2.1	1.9	1.1	3.0	1.7	1.8	-	-	-	1.9	2.8	.7	2.7	1.9	1.4
5	1.4	2.1	.6	-	-	-	3.7	2.9	1.3	2.2	2.3	1.0	2.7	2.6	1.0
6	1.5	2.0	.8	2.7	2.6	1.0	3.5	2.9	1.2	1.7	2.6	.7	2.6	2.3	1.1
7	2.2	1.9	1.1	3.3	3.1	1.1	3.3	4.0	.8	2.0	1.9	1.0	3.2	2.7	1.2
8	2.6	1.6	1.7	3.6	2.5	1.4	2.9	2.9	1.0	4.0	2.7	1.5	3.8	3.1	1.2
9	1.6	2.9	.6	3.4	3.3	1.0	4.1	2.6	1.5	2.9	2.6	1.1	2.5	3.3	.8
10	-	-	-	-	-	-	-	-	-	-	-	-	2.2	3.3	.7
11	-	-	-	-	-	-	-	-	-	-	-	-	1.7	3.5	.5
12	-	-	-	-	-	-	-	-	-	-	-	-	1.6	2.2	.7

$\frac{\partial F}{\delta z}$ in units of 10^{-2} °Fm^{-1}

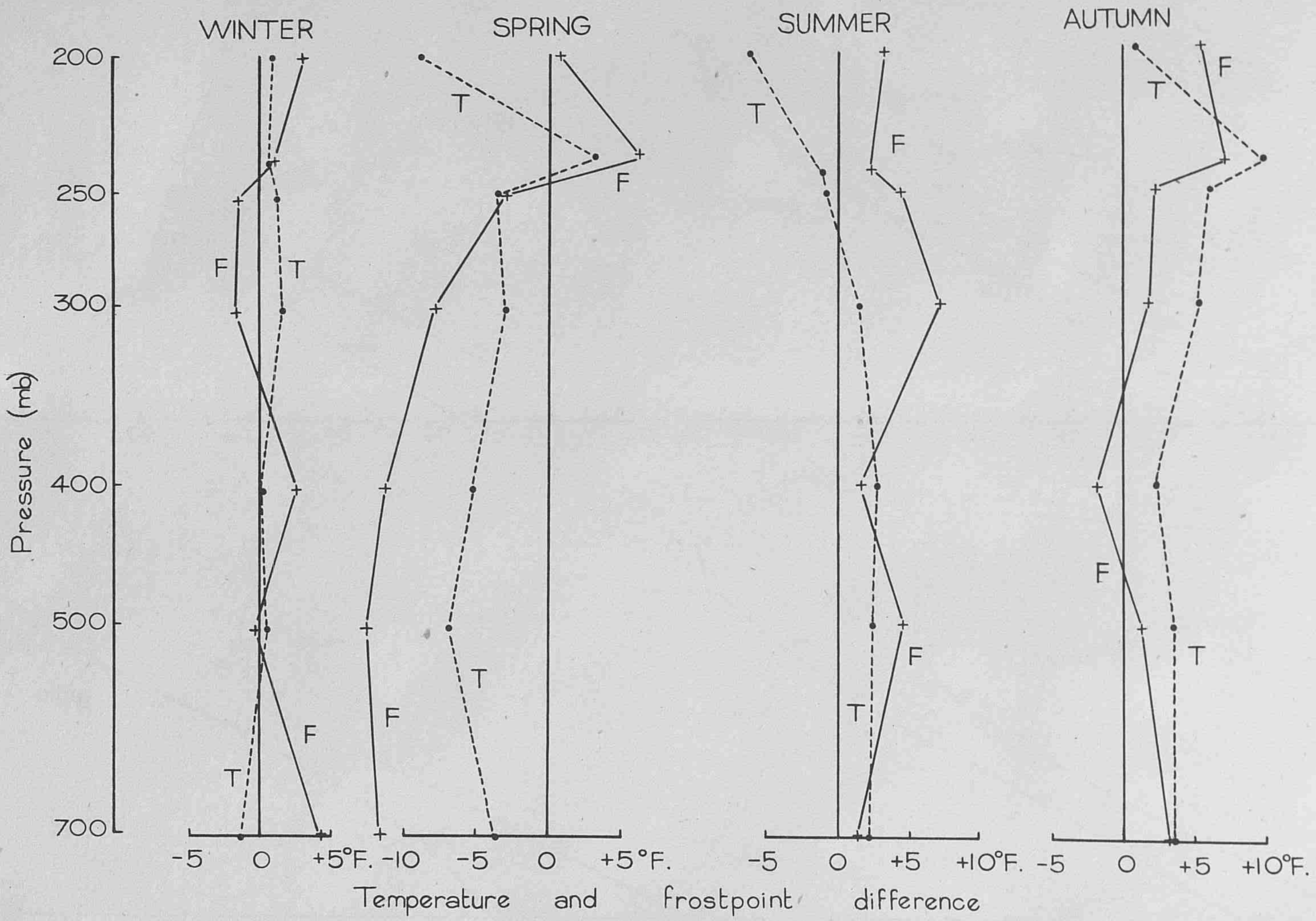

Fig. 1. Difference between Pre-Canberra and Canberra mean values of temperature (T.) and frostpoint (F.) Where the Pre-Canberra value is warmer, the difference is designated positive.

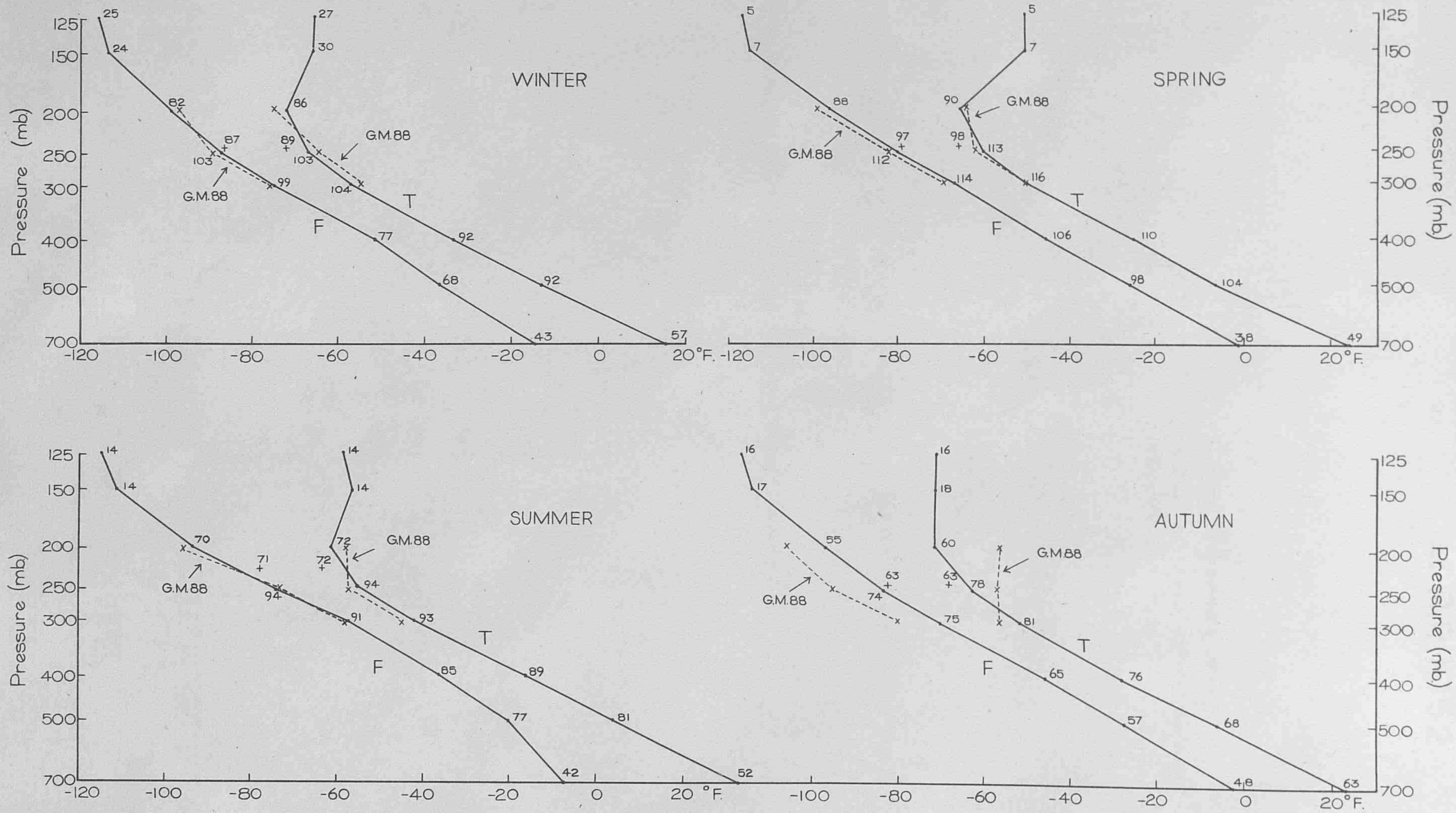

Fig. 2. MEAN SEASONAL VALUES OF TEMPERATURE (T.) AND FROSTPOINT (F.) AT STANDARD PRESSURE LEVELS
+ marks mean tropopause values. Number of observations is entered alongside points. x marks G.M.88 values.

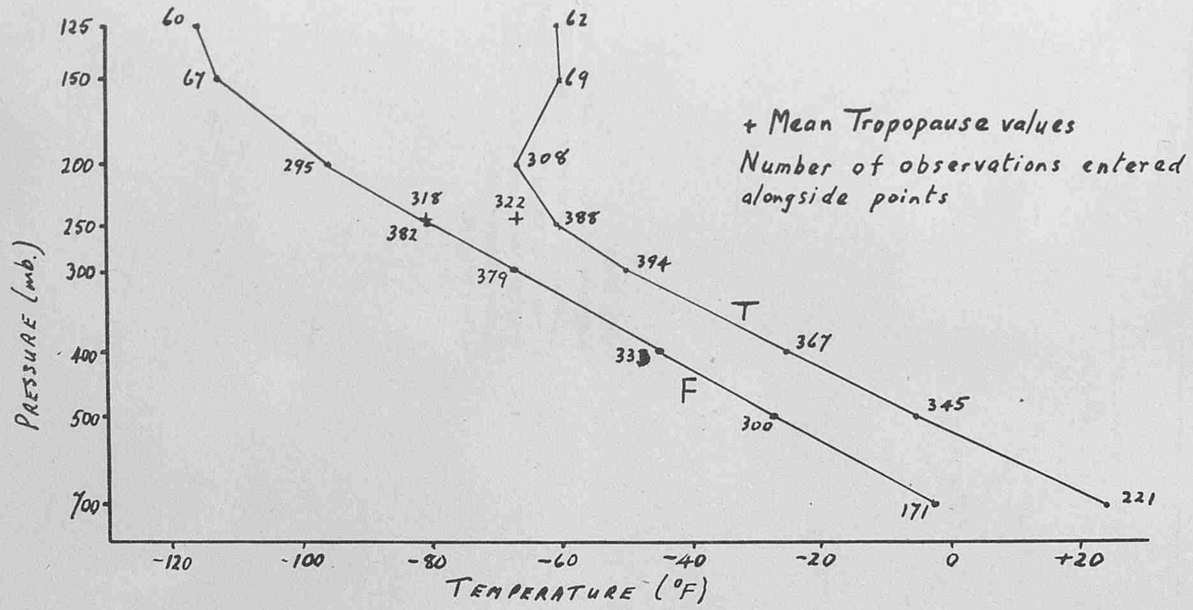

FIGURE 3

MEAN ANNUAL TEMPERATURE (T) AND FROSTPOINT (F).

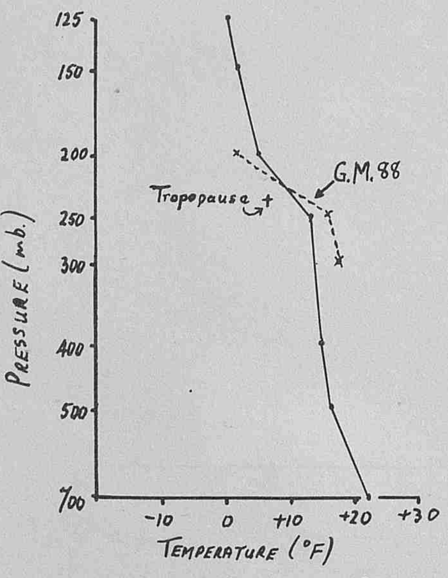

FIGURE 4

FROSTPOINT DIFFERENCES
SUMMER MINUS WINTER

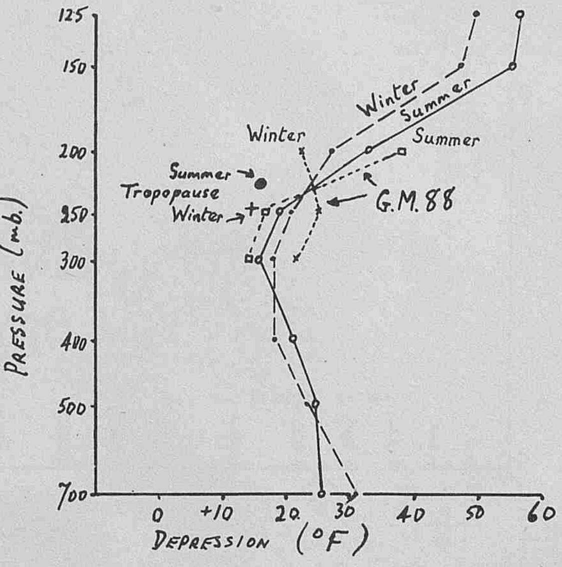

FIGURE 5

FROSTPOINT DEPRESSION

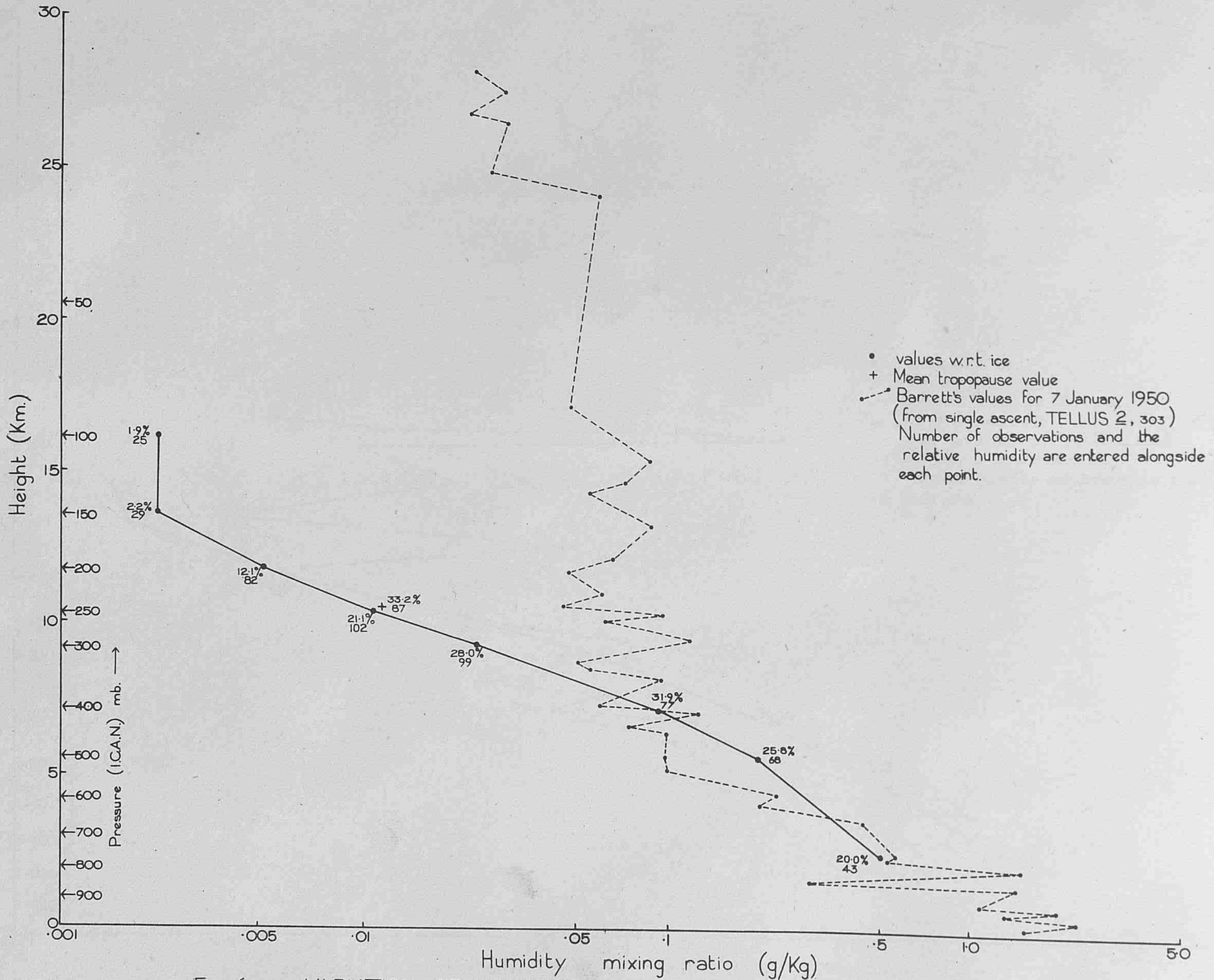

Fig. 6a. VARIATION OF HUMIDITY MIXING RATIO WITH HEIGHT IN THE TROPOSPHERE AND LOWER STRATOSPHERE IN WINTER.

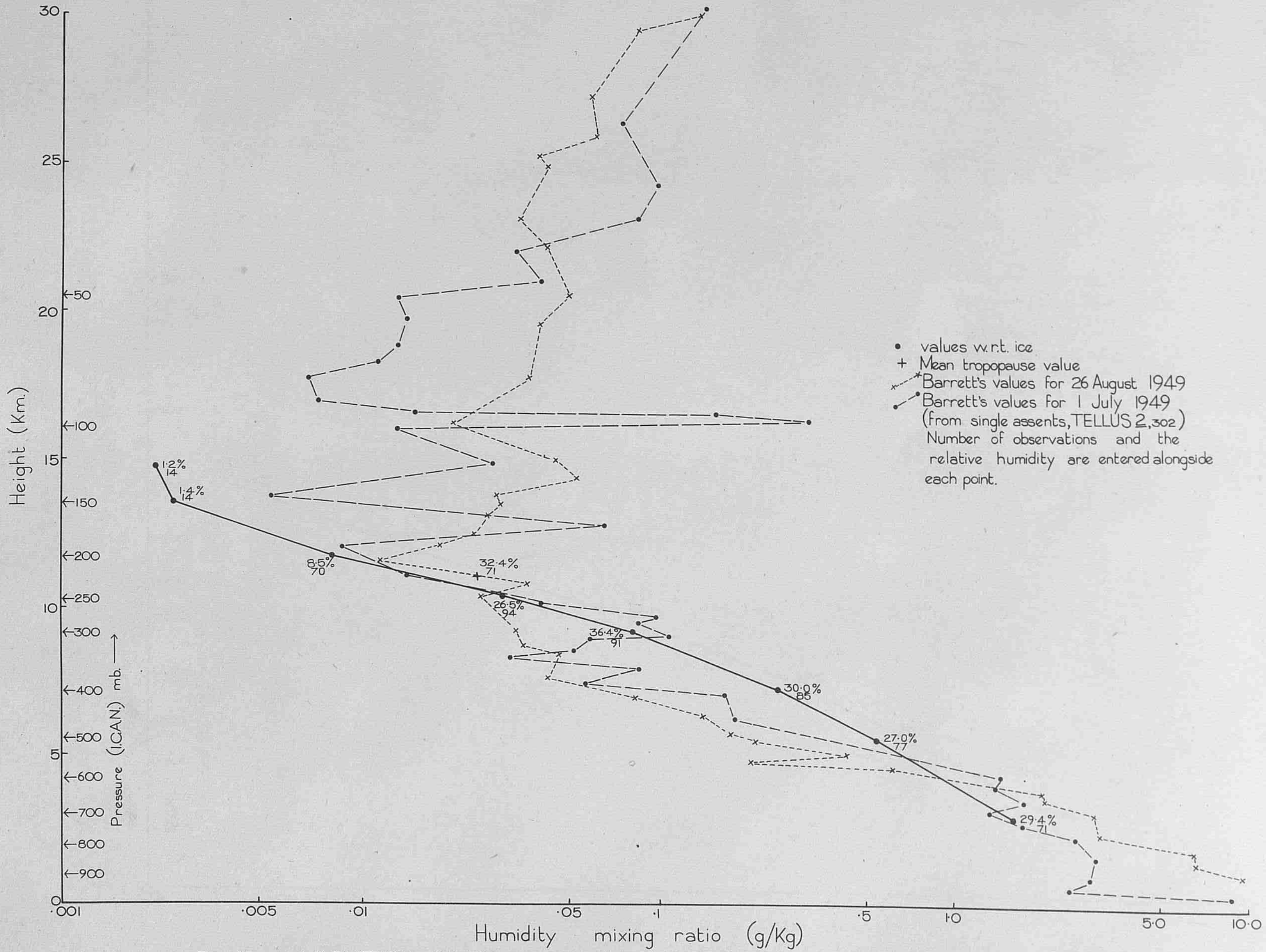

Fig. 6b. VARIATION OF HUMIDITY MIXING RATIO WITH HEIGHT IN THE TROPOSPHERE AND LOWER STRATOSPHERE IN SUMMER.

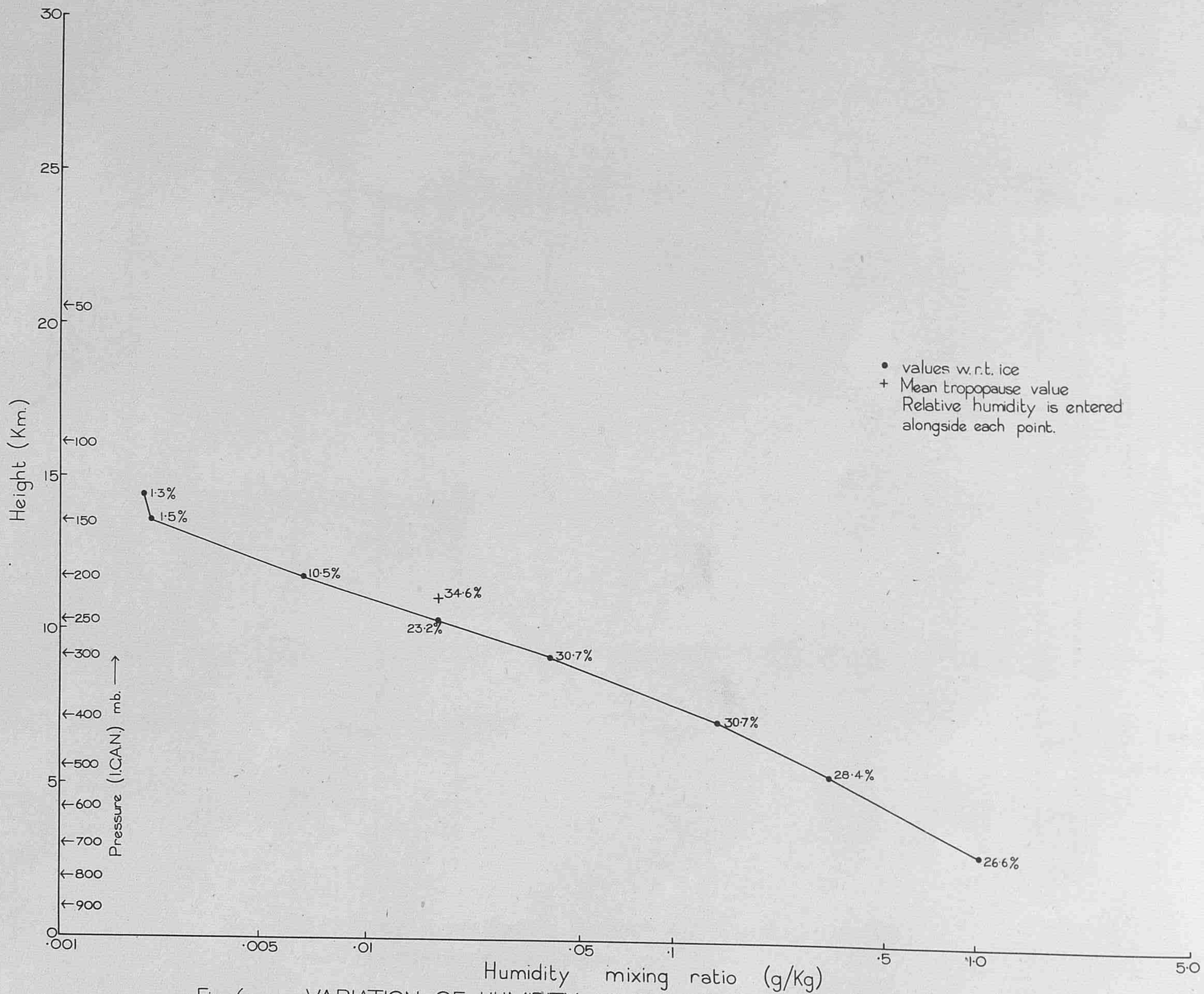

Fig. 6c. VARIATION OF HUMIDITY MIXING RATIO WITH HEIGHT IN THE TROPOSPHERE AND LOWER STRATOSPHERE: ANNUAL MEAN

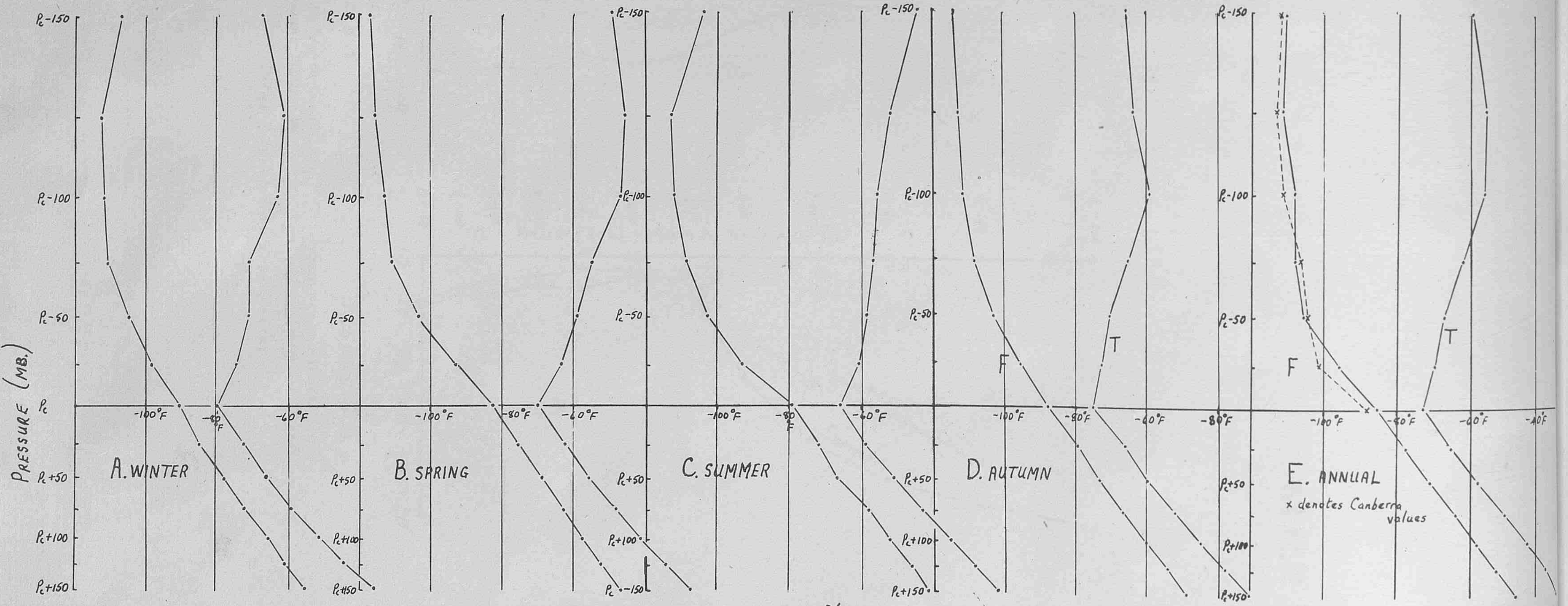

FIGURE 7.
MEAN SEASONAL AND ANNUAL TEMPERATURE (T) AND FROSTPOINT (F) USING THE TROPOPAUSE AS A DATUM LEVEL.

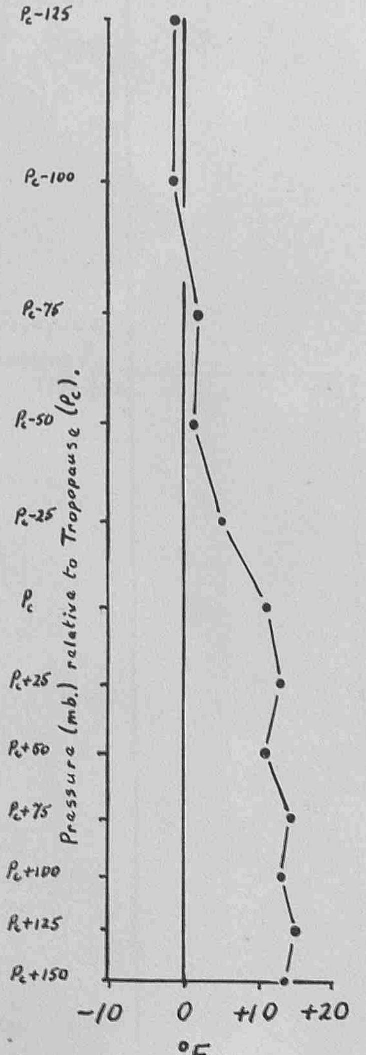

FIGURE 8 A

Summer minus Winter
Frostpoint Difference.

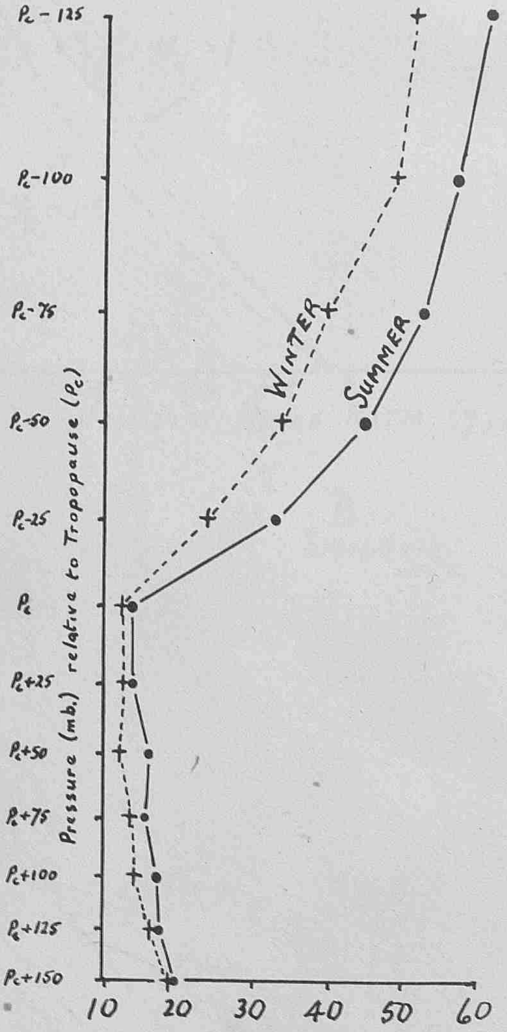

FIGURE 8 B

Summer and Winter
Frostpoint Depression.

Datum Level the Tropopause.

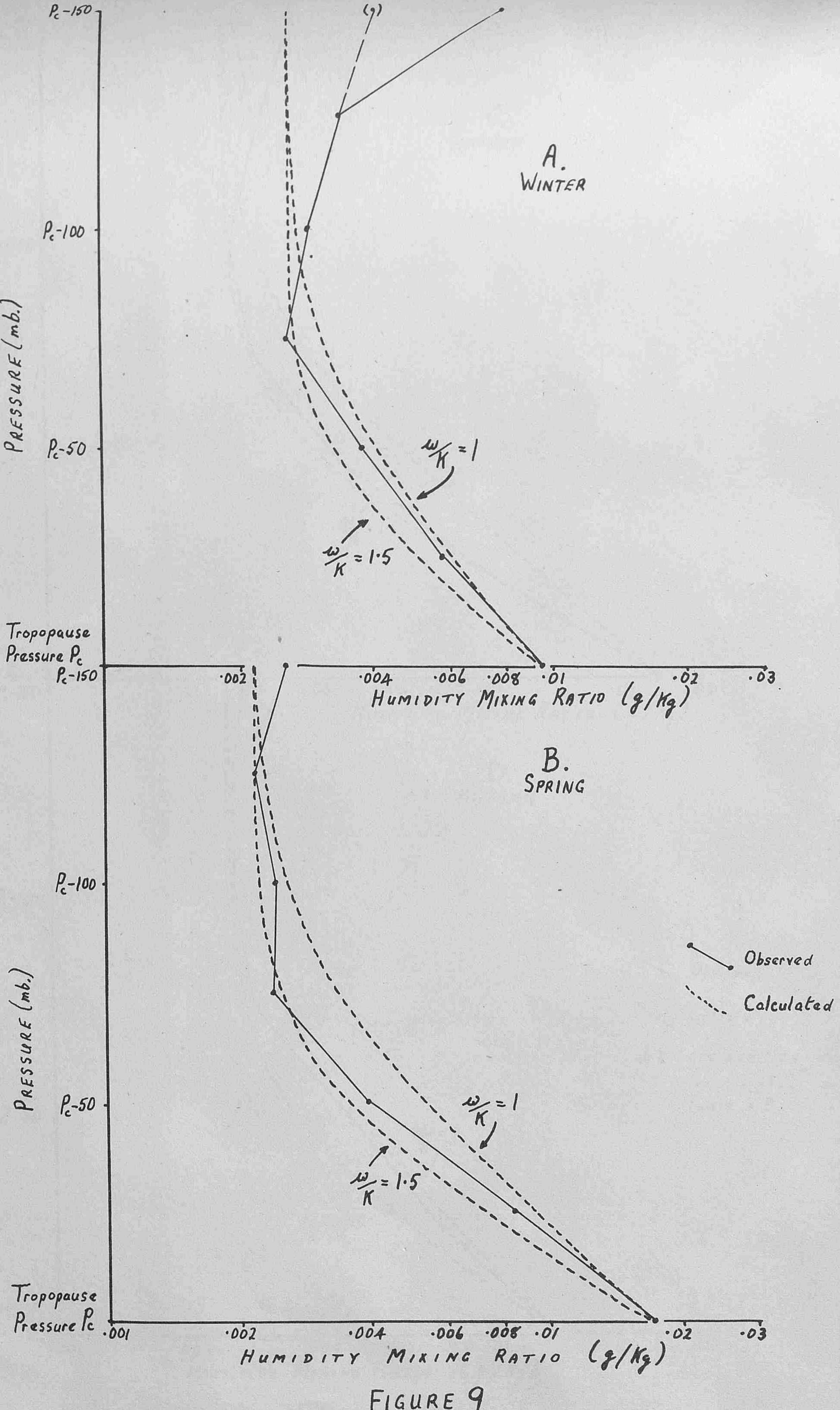

FIGURE 9

MEAN HUMIDITY MIXING RATIO (g/Kg) USING TROPOPAUSE AS DATUM LEVEL.

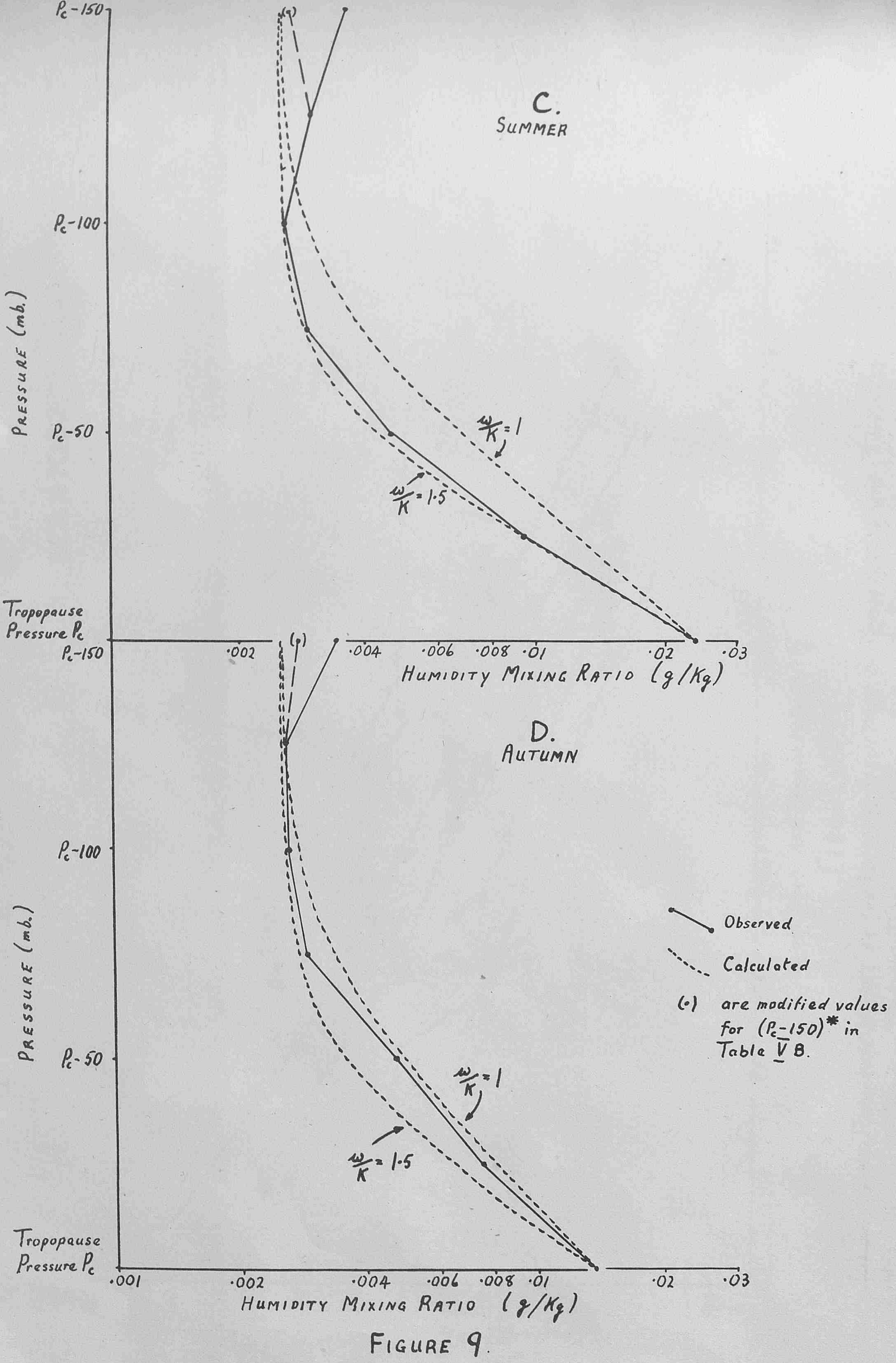

FIGURE 9.

MEAN HUMIDITY MIXING RATIO (g/Kg) USING TROPOPAUSE AS DATUM LEVEL.

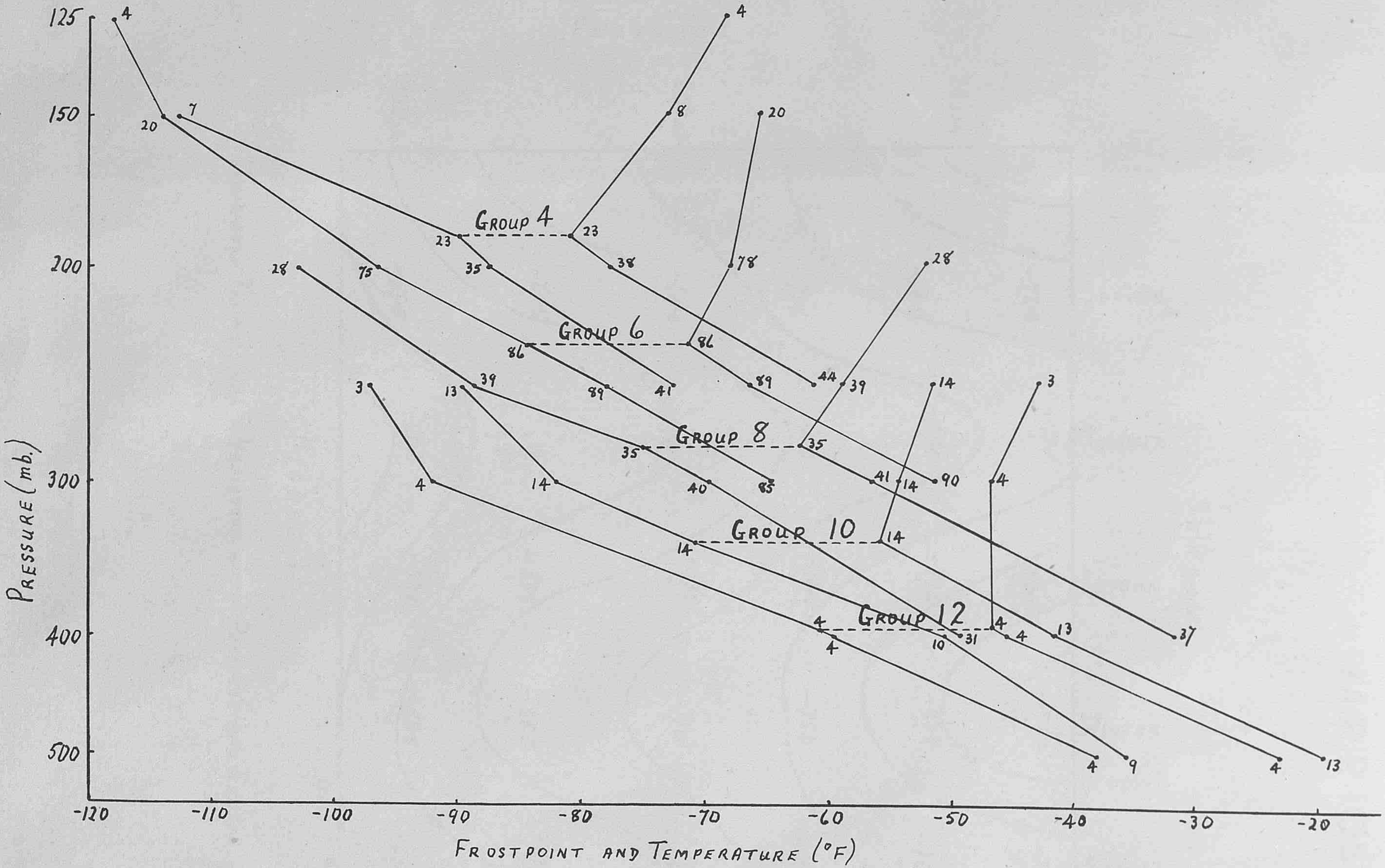

FIGURE 10.

THE EFFECT OF TROPOPAUSE HEIGHT ON THE VERTICAL STRUCTURE OF TEMPERATURE AND FROSTPOINT.
MEAN ANNUAL CURVES FOR VARIOUS TROPOPAUSE PRESSURE GROUPS. (Number of observations entered alongside points).

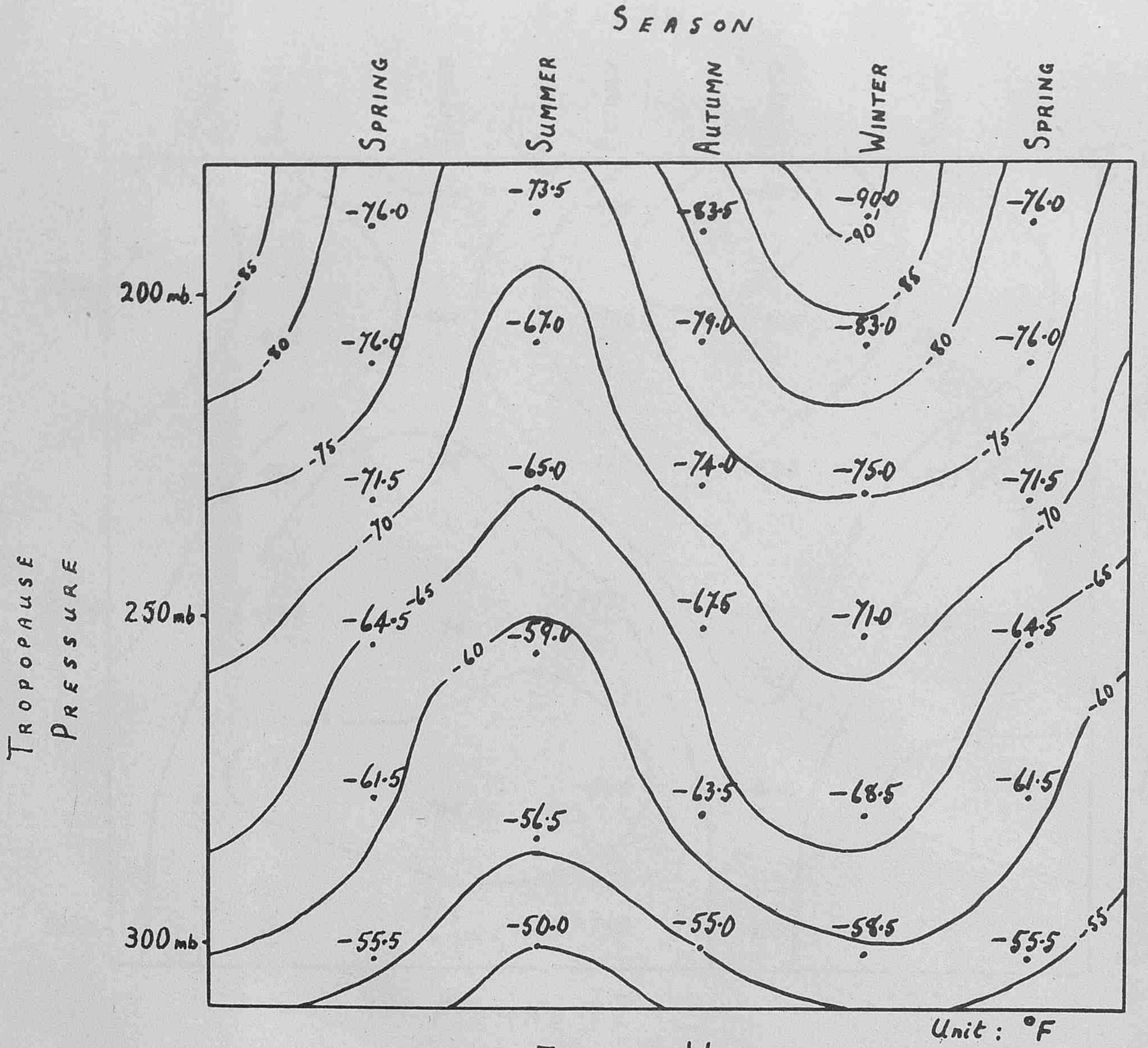

FIGURE 11.

TROPOPAUSE TEMPERATURE : VARIATION WITH PRESSURE AND SEASON.

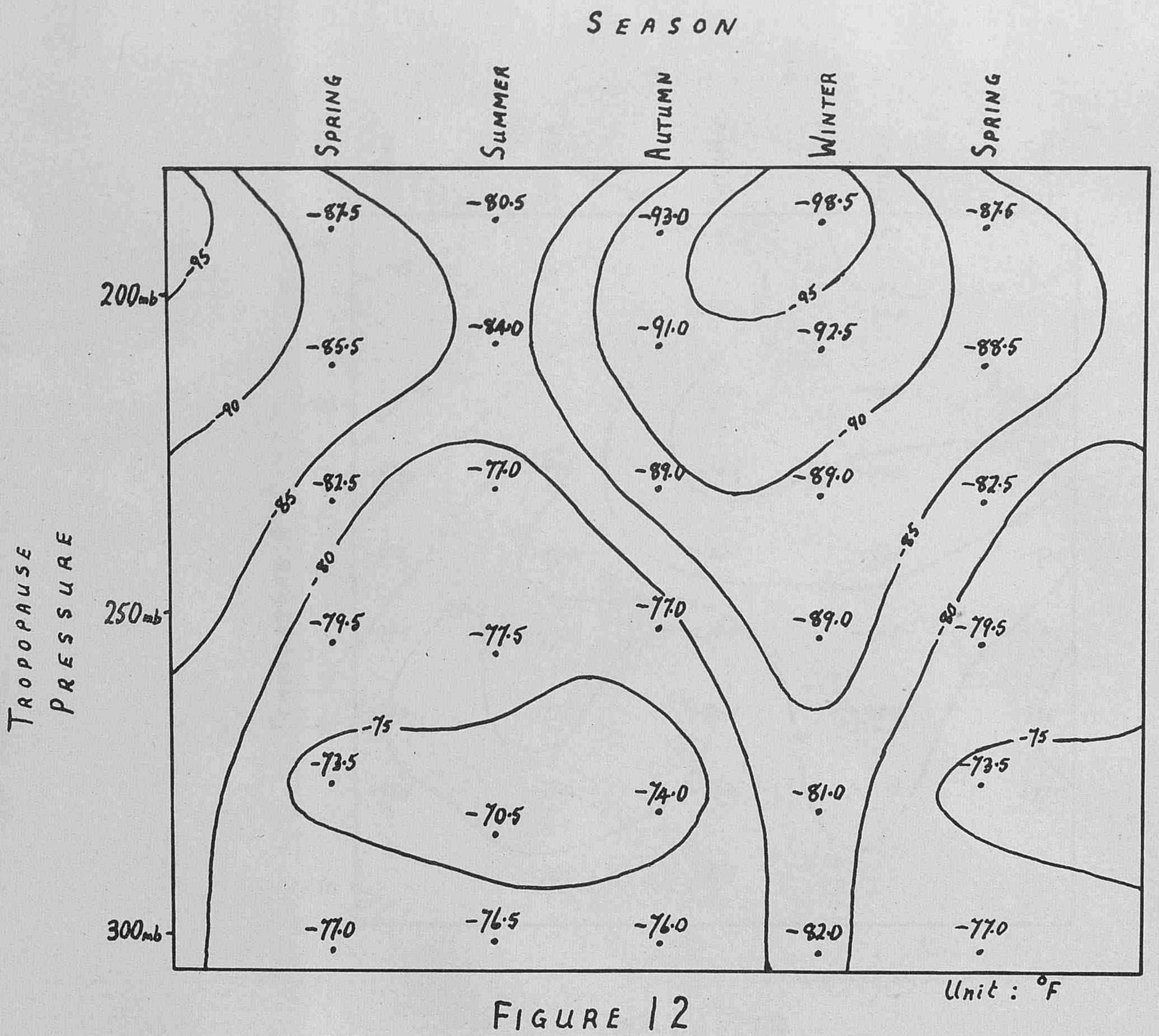

FIGURE 12

TROPOPAUSE FROSTPOINT : VARIATION WITH PRESSURE AND SEASON.

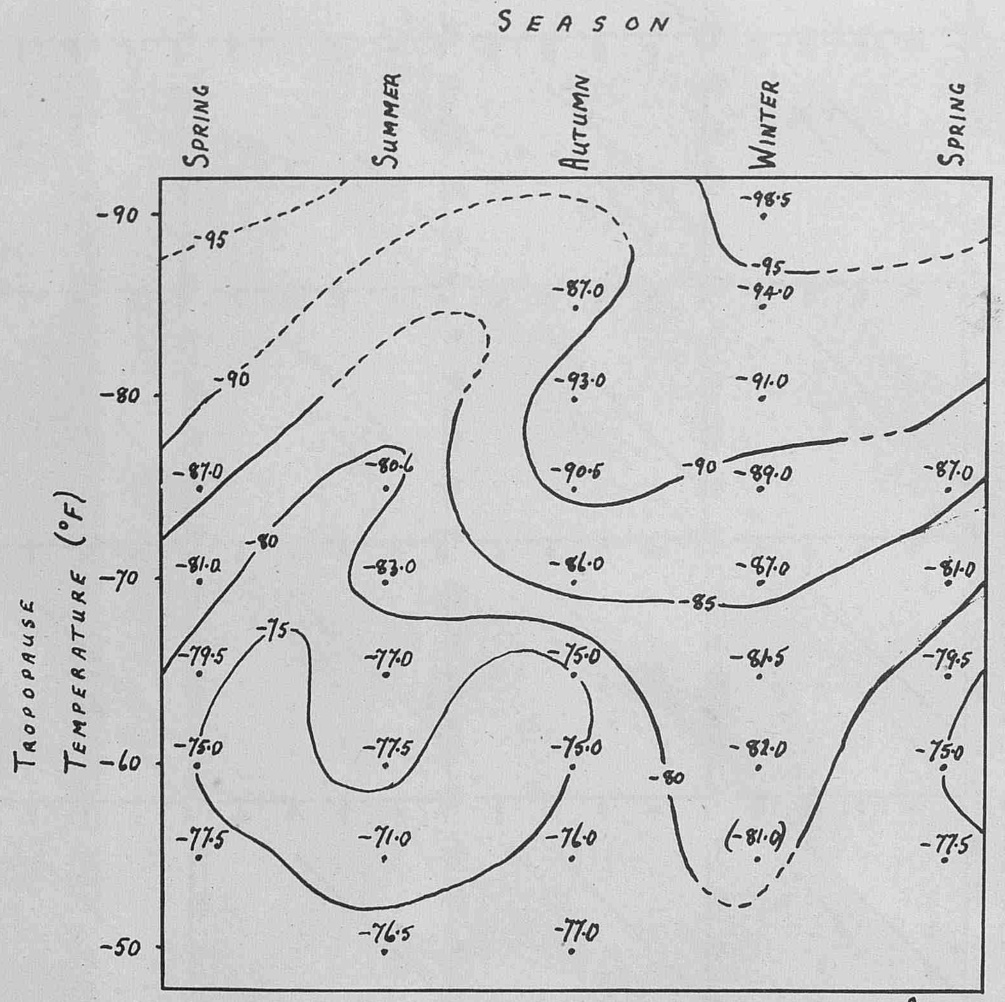

Unit : °F
Extrapolated value in brackets

FIGURE 13

TROPOPAUSE FROSTPOINT : VARIATION WITH TEMPERATURE AND SEASON.

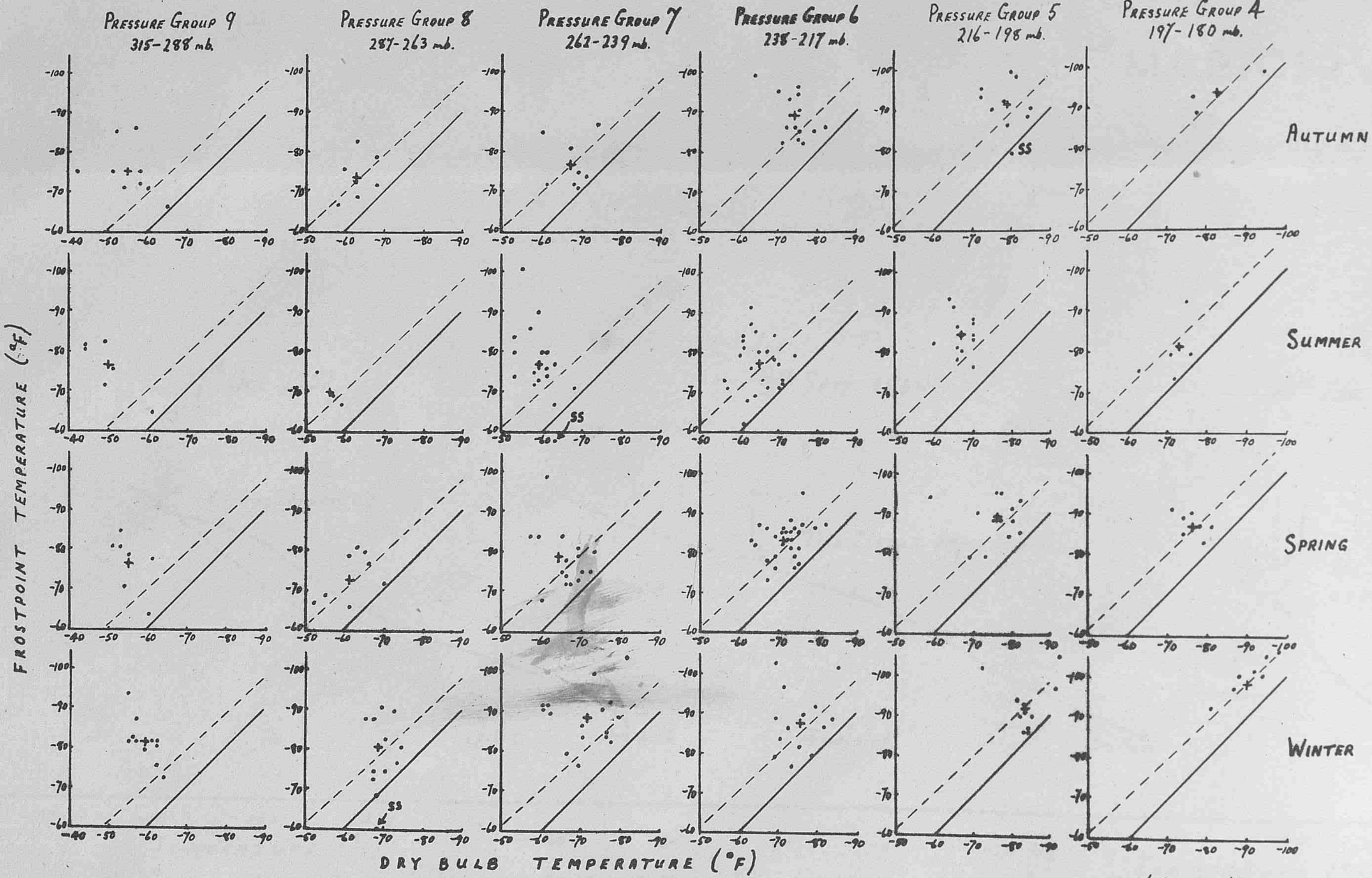

FIGURE 14.

FROSTPOINT AND TEMPERATURE AT THE TROPOPAUSE IN TROPOPAUSE PRESSURE/SEASON GROUPINGS.

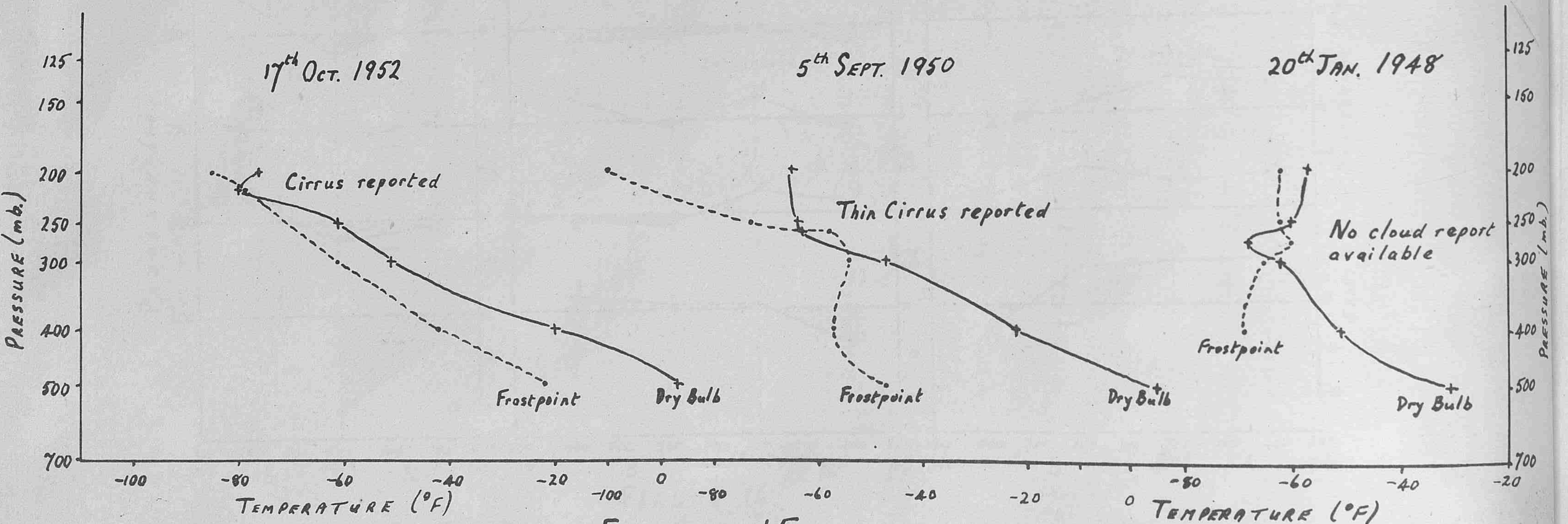

FIGURE 15

ASCENTS WHERE SUPERSATURATION AT THE TROPOPAUSE WAS REPORTED.

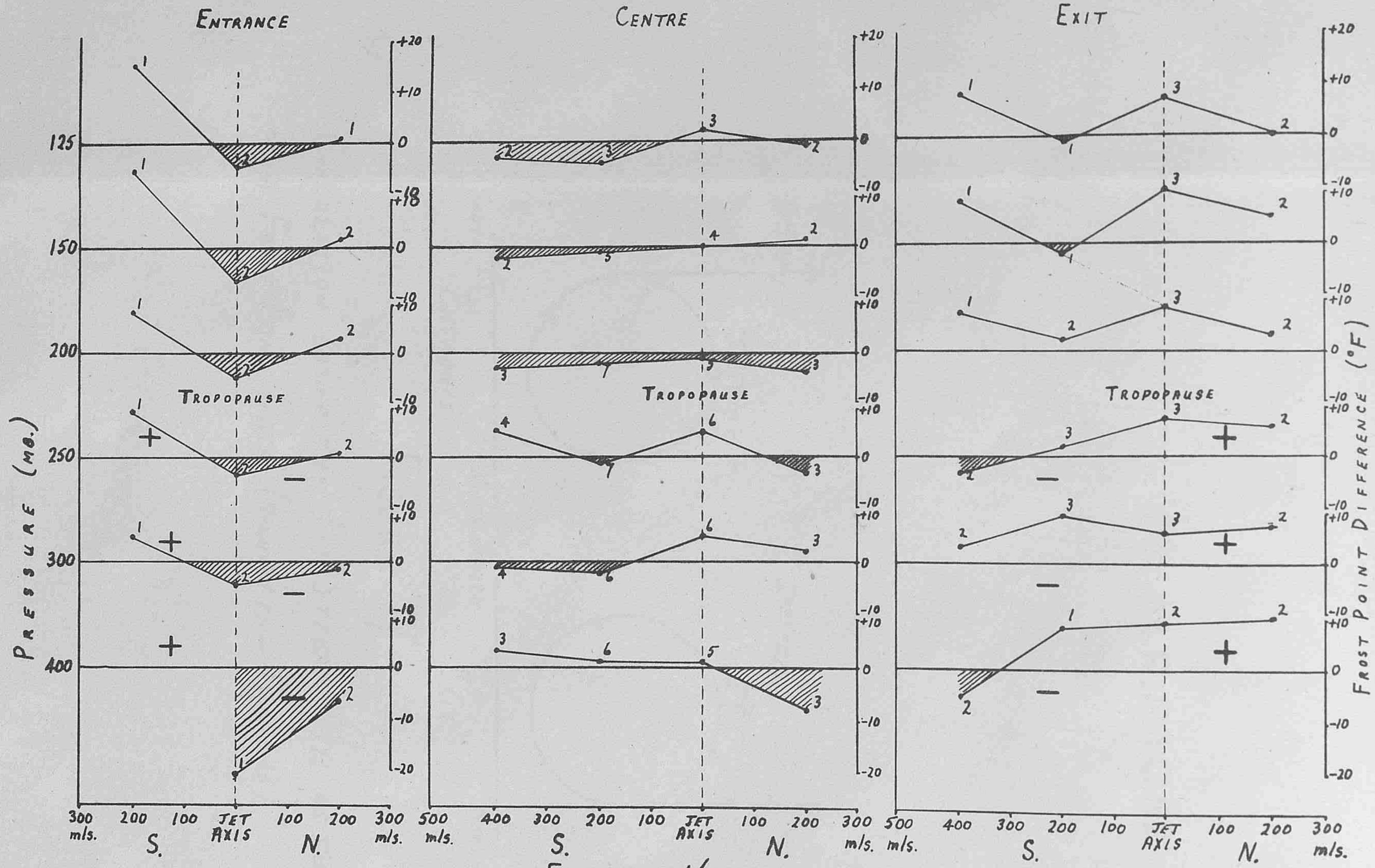

FIGURE 16.

Frost Point Differences from "Average" about the Jet Stream.

Negative (shaded) values refer to a lower frost point than average (i.e. drier) and suggest downward vertical motion. Positive values suggest upward motion. Figures alongside points indicate the number of cases considered. Signs indicate the "classical" picture of vertical motion (see text). Position in relation to the 300 mb. Jet Axis is the abscissae.

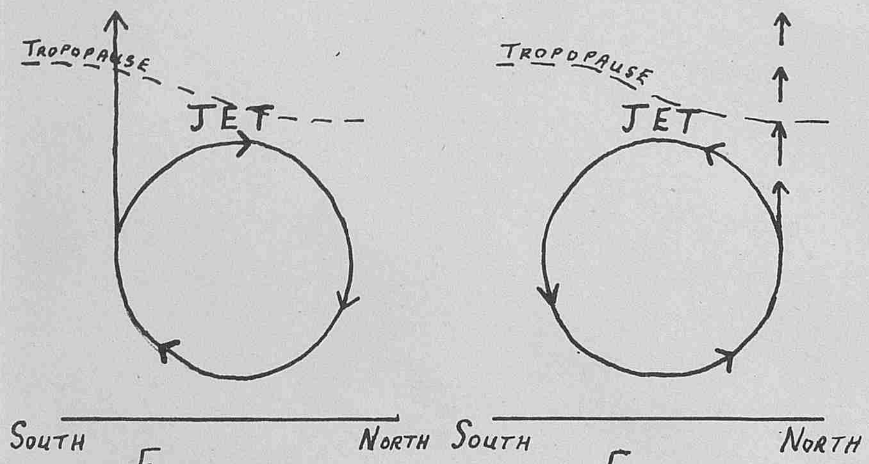
Tropopause
Jet
South
North
Tropopause
Jet
South
North

Entrance

Exit

Figure 17

Circulation about the Jet Stream Axis as suggested from Frost Point Data (Deduced from Figure 13).

M.R.P. 1054

28th August, 1957

5544

Index of M. R. Ps. Approved for General Distribution
Appendix 17 of M. R. P. 200

AIR MINISTRY

METEOROLOGICAL RESEARCH COMMITTEE

57-1407

MATS ①

54
st, 1957

Addendum to M.R.P. 1054

M.R.P.	Title	Author
1024	Observations of humidity, temperature and wind at Idris 23rd May - 2nd June, 1956	N.C. Helliwell J.K. Mackenzie
1043	Report on flight tests of a prototype conical head aircraft thermometer	C.H. Hinkel
1050	Recent developments in the measurement of precipitation elements from aircraft	M.P. Garrod
1052	An analysis of humidity measurements in the upper troposphere and lower stratosphere over Southern England	G.B. Tucker

1054 (3cp) cancelled 3 Sep 92

File

G.19757/AKH/5/58/300(a)

OR
ting
ting
ghton
ill
per
artley
idie
idie

1015	The air flow over a ridge - the effects of the upper boundary and high-level conditions	G.A. Corby J.S. Sawyer
1016	Numerical forecasts based on objectively analysed data	Vera M. Huckle
1017	Analysis of reports of ice accretion on aircraft	R.F. Jones
1018	Numerical experiments in the integration of the meteorological equations of motion	E. Knighting D.E. Jones Mavis K. Hinds
1019	Preliminary report on cumulus investigations, East Hill, June-August, 1956 and on plans for future similar work	W.G. Harper F.H. Ludlam P. Saunders
1020	Average height of the standard isobaric surfaces over the area from the North Pole to 55°N. in April and October	H. Heastie

/1021

G.24265/PO/9/57/340

57-1407

At the time of issue this report has not been published. Any author desiring to quote this paper should refer to it as "A paper of the Meteorological Research Committee (London),
M.R.P. No. 1054.
A copy is available in the Library of the Meteorological Office."

M.R.P. 1054
28th August, 1957

AIR MINISTRY
METEOROLOGICAL RESEARCH COMMITTEE

Index of M.R.Ps. Approved for General Distribution
Appendix 17 of M.R.P. 200

M.R.P.	TITLE	AUTHOR
1001	Index of M.R.Ps. approved for general distribution (Appendix 16 of M.R.P. 200)	-
1002	An atmospheric model for numerical integration including the tropopause effects	E. Knighting
1003	A non-geostrophic extension of the Sawyer-Bushby model of the atmosphere suitable for numerical integration	E. Knighting
1005	Heat Sources and Sinks at the Earth's Surface	D.M. Houghton
1006	Measurements of short range diffusion of airborne particles at a height of a few hundred feet in the atmosphere (Porton Technical Paper No. 561)	J.S. Hay F. Pasquill
1009	A survey of the facilities and research programme of the Radar Research Station	W.G. Harper
1010	Wind recording apparatus for the new Ballistic Range at Shoeburyness	G.E.W. Hartley
1012	Atmospheric Nuclei. An estimate of the value and practicability of routine measurements	B.C.V. Oddie
1014	A note on the published results of studies in atmospheric chemistry	B.C.V. Oddie
1015	The air flow over a ridge - the effects of the upper boundary and high-level conditions	G.A. Corby J.S. Sawyer
1016	Numerical forecasts based on objectively analysed data	Vera M. Huckle
1017	Analysis of reports of ice accretion on aircraft	R.F. Jones
1018	Numerical experiments in the integration of the meteorological equations of motion	E. Knighting D.E. Jones Mavis K. Hinds
1019	Preliminary report on cumulus investigations, East Hill, June-August, 1956 and on plans for future similar work	W.G. Harper F.H. Ludlam P. Saunders
1020	Average height of the standard isobaric surfaces over the area from the North Pole to 55°N. in April and October	H. Heastie

/1021

57-1407

M.R.P.	TITLE	AUTHOR
1021	Radio refraction in the free atmosphere	A.H. Hooper A.P. Taylor
1022	The movement of precipitation belts as observed by radar	W.G. Harper J.G.D. Beimers
1023	The serial correlations of daily mean temperatures at Kew Observatory	J.M. Craddock
1024	Obs. of Humidity, Temp. and wind at IDRIS 23rd May - 2d June 1956	NC Helliwell JK Mackenzie
1025	A numerical study of the wavelength and amplitude of lee waves	C.E. Wallington Janet Portnall
1032	Response characteristics of the sensitive cup anemometer Type IV	A.G.A. Rae
1033	Photo-electric visibility meter Mk. II	J.R. Bibby
1038	Studies of eddy structure in the first few thousand feet of the atmosphere. Part 1. Measurements of the vertical and horizontal (longitudinal) components. (Porton Technical Paper No. 574)	J.I.P. Jones H.E. Butler
1039	A study of the average distribution of pollution around Staythorpe	P.J. Meade F. Pasquill
1040	The representation of circumpolar 500 mb charts by a series of spherical harmonics	A. Gilchrist
1041	Numerical calculations of the airflow over a ridge for small amplitudes	J.S. Sawyer M.K. Hinds
1043	Rpt. on Flight Tests of a Prototype conical head acft. thermometer	CH HINKEL
1044	Studies of eddy structure in the first few thousand feet of the atmosphere. Part 2. A preliminary examination of the spectrum and scale of the vertical component at 2000 feet. (Porton Technical Paper No. 588)	R.A. Jones
1045	Average height of the standard isobaric surfaces over the temperate and tropical regions in January	H. Heastie
1046	An approximate relation between slant visibility and horizontal visibility at ground level	K.H. Stewart
1047	A method for assessing the frequency of dangerous visibility conditions	K.H. Stewart
1048	Convection - diffusion processes below a stable layer (Porton Technical Paper No. 584)	F.B. Smith
1049	Problems of surface air-flow and related phenomena in agriculture, horticulture and forestry	R.W. Gloyne
1050	Recent Developments in the Measurement of Precip. Elements from Aircraft	M P GARROD
1051	A contribution to the study of Meteorological Time Series	J.M. Craddock
1052	An analysis of humidity measurements in the upper troposphere and lower stratosphere over Southern England	G B Tucker